



UGR

Universidad
de Granada

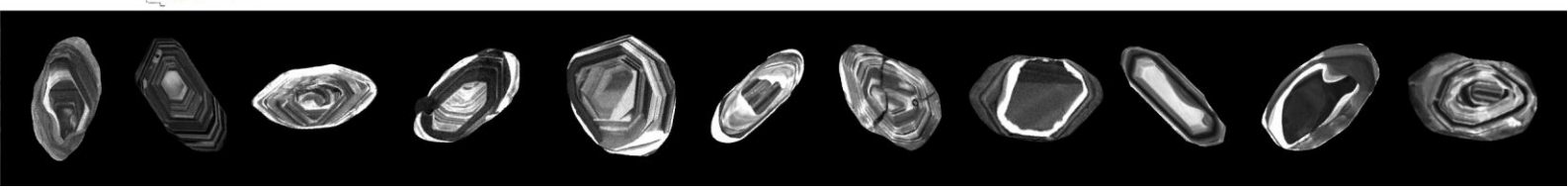
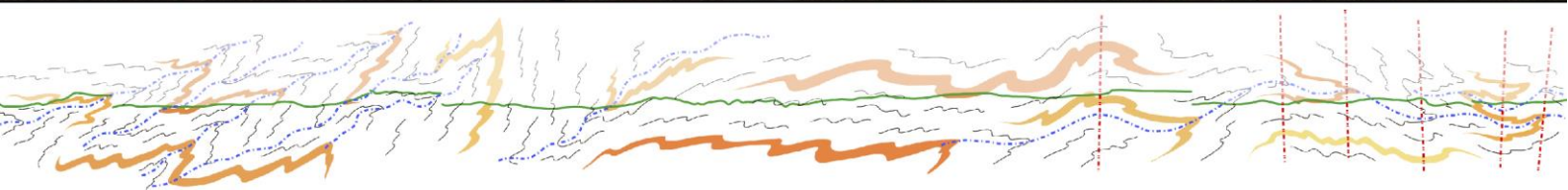
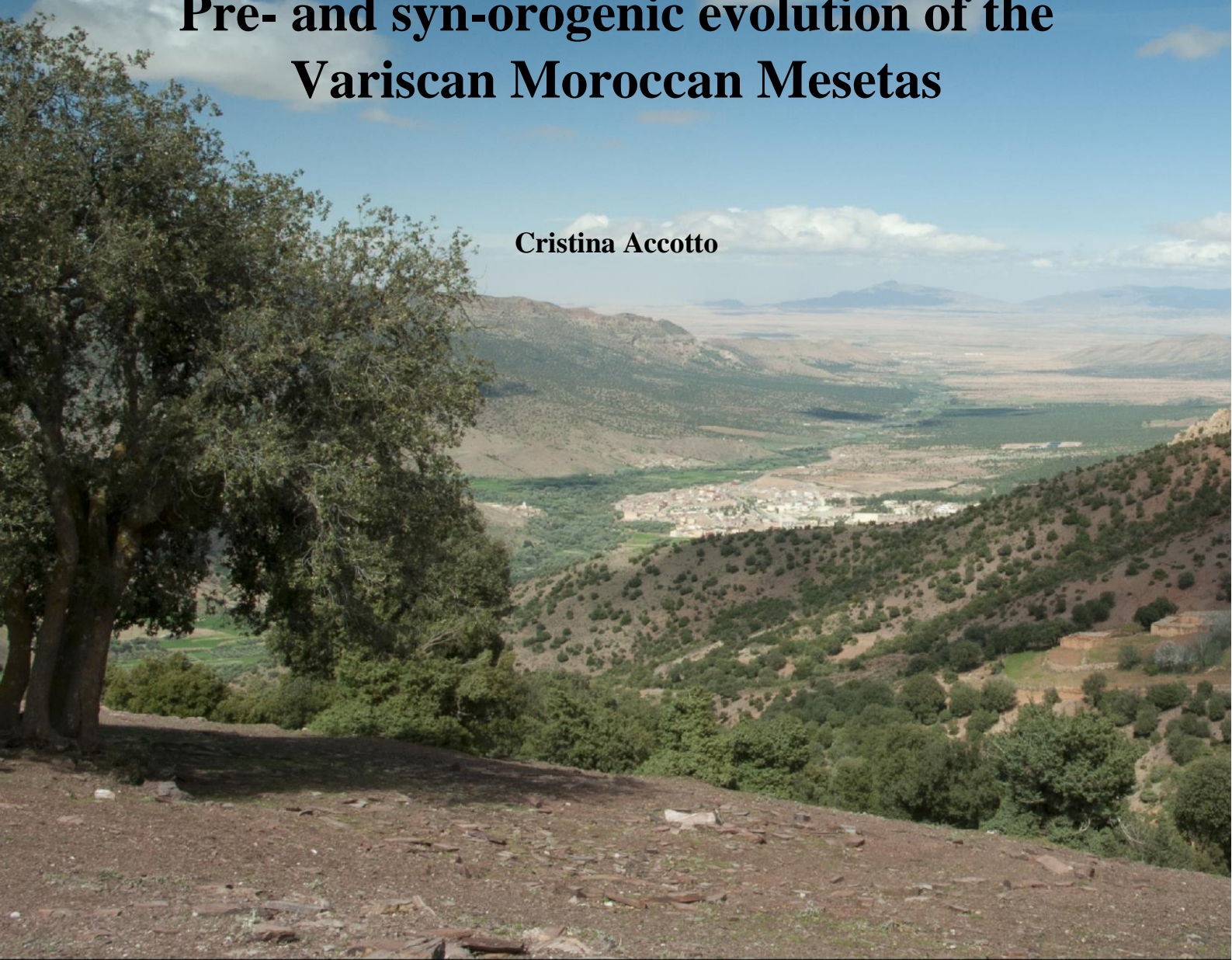


Programa Doctorado
Ciencias de la Tierra

Ph.D. Thesis 2021

Pre- and syn-orogenic evolution of the Variscan Moroccan Mesetas

Cristina Accotto



Editor: Universidad de Granada. Tesis Doctorales
Autor: Cristina Accotto
ISBN: 978-84-1117-029-1
URI: <http://hdl.handle.net/10481/70718>

*La pietra antica non emette suono
Ma parla come il mondo e come il sole
Parole troppo grandi per un uomo.*

Francesco GUCCINI

Radici

*Saper leggere il libro del mondo
Con parole cangianti e nessuna scrittura*

Fabrizio DE ANDRÈ

Khorakhané (a forza di essere vento)

Index

	Page
Acknowledgments	v
Abstract	ix
Resumen	xi
Chapter I: Introduction	1
1. Geographic location	2
2. The Variscan-Appalachian belt	3
3. The northern Moroccan Variscides	5
3.1. <i>The Western Moroccan Meseta</i>	7
3.1.1. <u>The Coastal Block</u>	7
3.1.2. <u>The Central Zone</u>	8
3.1.3. <u>The Nappe Zone</u>	10
3.2. <i>The Eastern Moroccan Meseta</i>	11
4. Aims and structure of the Ph.D. Thesis	12
5. Methodology	13
References	16
Chapter II: The pre-orogenic evolution of the Moroccan Mesetas	25
Section II.1	26
1. Introduction	28
2. Geological setting	31
2.1. <i>Oujda area</i>	33
2.2. <i>Tazekka area</i>	33
2.3. <i>Azrou area</i>	34
3. Samples and methods	34
4. Results	36
4.1. <i>Oujda area</i>	36
4.2. <i>Tazekka area</i>	39
4.3. <i>Azrou area</i>	41
5. Discussion	44
5.1. <i>Maximum depositional ages and stratigraphic attributions</i>	44

5.2. <i>West African Craton provenance</i>	44
5.3. <i>Tonian-Stenian population</i>	46
5.4. <i>Cambro-Ordovician rifting in northern Gondwana</i>	48
6. Conclusion	49
References	50
Section II.2	60
1. Introduction	61
2. Geological setting	62
2.1. <i>Stratigraphy of the Beni Mellala inlier</i>	63
3. Samples and methods	65
4. Results	67
5. Discussion	70
5.1. <i>Detrital zircon-derived maximum depositional ages versus true depositional ages</i>	70
5.2. <i>Stable detrital zircon sources throughout the Ordovician in the northern Moroccan Variscides</i>	73
5.3. <i>Paleogeography of the northern Moroccan Variscides and correlation with European counterparts</i>	76
6. Conclusions	77
References	78
Section II.3	92
1. Introduction	93
2. Geological setting	97
2.1. <i>The Western Moroccan Meseta</i>	97
2.1.1. <u>The Coastal Block</u>	97
2.1.2. <u>The Central Zone</u>	98
2.1.3. <u>The Nappe Zone</u>	98
2.2. <i>The Eastern Moroccan Meseta</i>	100
3. Samples and results	100
3.1. <i>U-Pb analyses</i>	101
3.2. <i>Hf isotopes analyses</i>	103
4. Results	103
<u>El Mansouria area</u>	103
<u>Oued Akreuch area</u>	104
<u>Ezzhiliga area</u>	105
<u>Oulmes area</u>	107
<u>Khenifra area</u>	108
<u>Azrou area</u>	110
<u>Zekkara area</u>	111

5. Discussion	114
5.1. <i>Maximum depositional ages</i>	114
5.2. <i>Main sediment source: West African Craton affinity</i>	114
5.3. <i>Discriminating between Pan-African and Cadomian sources</i>	116
5.4. <i>Minor detrital zircon populations and secondary sediment sources</i>	118
5.4.1. <u>Cambrian-Ordovician magmatism</u>	118
5.4.2. <u>Stenian-early Tonian detrital zircon ages</u>	120
5.4.3. <u>Orosirian-Statherian detrital zircon ages</u>	122
5.5. <i>Relevance of the tectonic boundaries within the Moroccan Mesetas</i>	123
6. Conclusions	123
References	124
Chapter III: Tectonic evolution of the Eastern Moroccan Meseta during the Eovariscan phase	139
1. Introduction	141
2. Geological setting	144
2.1. <i>The Debdou-Mekkam massifs</i>	145
3. Detrital zircon geochronology	147
3.1. <i>U-Pb analyses</i>	147
3.1.1. <u>Results</u>	148
3.2. <i>Hf isotope analyses</i>	151
3.2.1. <u>Results</u>	152
4. Structural analysis	154
4.1. <i>Main tectonic fabrics</i>	154
4.1.1. <u>Early fabric</u>	154
4.1.2. <u>Late fabric</u>	156
4.2. <i>The Debdou inlier</i>	157
4.3. <i>The Lalla Mimouna-Oued Awam inliers</i>	159
4.4. <i>The Mekkam inlier</i>	160
4.5. <i>Building up a composite cross-section of the Debdou-Mekkam region</i>	163
5. Discussion	165
5.1. <i>Age of the Debdou-Mekkam Metasediments</i>	165
5.2. <i>Detrital zircon provenance in the Debdou-Mekkam Metasediments</i>	166
5.3. <i>Original vergence of D1 folds</i>	170
5.4. <i>Proposing a large-scale tectonic scenario</i>	170
6. Conclusions	174

References	175
Chapter IV: Evolution of the sedimentary sources during the Eovariscan phase in the Moroccan Mesetas	185
1. Introduction	188
2. Geological setting	188
2.1. <i>Ben Slimane area</i>	190
2.2. <i>Sidi Bettache area</i>	191
2.3. <i>Oulmes area</i>	193
2.4. <i>Tiflet area</i>	193
2.5. <i>Jerada area</i>	194
3. Samples and methods	194
4. Results	197
4.1. <i>Ben Slimane area</i>	197
4.2. <i>Sidi Bettache area</i>	199
4.3. <i>Oulmes area</i>	200
4.4. <i>Tiflet area</i>	200
4.5. <i>Jerada area</i>	201
5. Discussion	203
5.1. <i>Maximum depositional ages</i>	203
5.2. <i>Provenance of pre-Devonian detrital zircon grains</i>	205
5.3. <i>Source evolution during Late Devonian-Carboniferous time</i>	206
6. Conclusions	210
References	211
Chapter V: Conclusions	221
Open issues	224
References	226
Appendix	229
A. Analytical methods (all the chapter)	230
B. Description of the zircon grains (Chapter II, Section II.1)	236
C. Cathodoluminescence images (Chapter II, Section II.3; Chapter III; Chapter IV)	239
D. Results of the U-Pb analyses (all the chapters) – Only in the digital version of this Ph.D. Thesis	
E. Results of the He analyses (Chapter II, Section II.3; Chapter III; Chapter IV) – Only in the digital version of this Ph.D. Thesis	

Acknowledgments

This Ph.D. Thesis is the result of the work I carried out during the last four years. When I look back at the first paper we published I can see how much I have evolved as a geologist, and many (and from many countries) are the people I want to acknowledge for helping me in this process and allowing me to grow professionally and as a person.

En primer lugar, agradezco a mi director, David Martínez Poyatos, la confianza que depositó en mí en el momento en el que me concedió esta plaza; gracias por ser paciente conmigo, por explicarme las cosas miles de veces, por apoyarme y aguantarme. Igualmente, gracias a Antonio Azor Pérez quien, pese a no haber sido formalmente reconocido como codirector, siempre me ha apoyado y ayudado como si lo fuese.

Asimismo, quiero agradecer a Antonio Jabaloy Sánchez su ayuda en el laboratorio, en el campo y en la interpretación de los datos. Gracias también a Irene Pérez Cáceres, que fue mi primer contacto en Granada y me enseñó a separar circones detríticos.

Gracias a Montse Nosty Priede, pues sin ella no habría sabido de la convocatoria de esta beca, me habría costado mucho más entenderla y, al final, habría perdido la oportunidad. Gracias por todo esto y por mucho más.

Quiero agradecer también a todo el Departamento de Geodinámica de la Universidad de Granada, aunque no os voy a citar a todos, cada uno de vosotras y vosotros ha tenido su parte durante esta experiencia. No obstante, quiero dedicar un agradecimiento especial a Ángel Perandrés Villegas por su disponibilidad y trabajos de laboratorio, y a José Fernando Simancas Cabrera que, a pesar de no trabajar directamente conmigo, ha sido siempre muy atento y ha seguido de cerca la evolución de esta tesis.

Obviamente, no puede faltar un enorme agradecimiento a todos los que han pasado por ese «mundo» peculiar que es la becaría. Gracias a los becarios con los que he compartido solo una parte de ese camino: Irene, Manuel, Ángel, Asier, Luis, Mayte... Seguro que me olvido algún nombre, pero os agradezco igualmente el granito de arena que habéis aportado. El agradecimiento más especial, sin embargo, es para los que más han compartido conmigo, dentro y fuera de la becaría: Ángela, Víctor, Cristina y Alejandro (¡y sus respectivas parejas!). Gracias por las discusiones, los cotilleos, las cervezas, las excursiones, las correcciones de español... Habéis sido como una familia y me habéis regalado los mejores momentos de mi estancia en Granada. Una última mención especial para Lourdes, por su ala protectora, con la que nos cuida como buena mamá, por sus consejos y todos los vicios y mimos que nos dedica.

Fuera de las paredes de la UGR, quiero agradecer a la Asociación Cultural Ante Bellum las tardes pasadas a golpes de espadas y bastones (o juegos de mesas y de rol): Pedro, Isidro, «Antoñico», Antonio, Rafa, Fernando, Manu, Philippos, y todos los demás que han coincidido conmigo con menos regularidad.

Finalmente, gracias también a mis vecinas Quica y Maribel, que con sus ricos platos y su fruta del huerto me han hecho sentir menos sola durante este último año de confinamientos y terremotos.

This Thesis is based on a huge number of U-Pb geochronological analyses. I never worked with this kind of data before and I have to give a special thanks to Dr. Cristina Talavera and Dr. Noreen J. Evans for carrying out the analyses, helping me to understand the data, explaining them to me time after time, and for being extremely patient with me.

My sincere thanks goes to Dr. Yvette D. Kuiper for receive me at the Colorado School of Mines for my internship and for all our constructive discussions about the evolution of the Variscan/Appalachian orogeny that continued even after my time there. Thank you also to Allison Severson and Sonia Ellison for guiding me in this new (for me) American world and for sharing information, knowledge, stress, and beers with me.

Thank you to Sheila and Ken Urban, who hosted me in their house in Golden and made me feel at home in every moment. Thank you to Judy and Marlan Grisby, who became my grandparents on the other side of the “pond”; to Ann Ross, who accompanied me to unforgettable concerts and many walks to discover Colorado; to Diane Gebetsberger Lowry, who received and hosted me during my very first days in the US, and was always kind and helpful.

Je dois une particulière reconnaissance à Professeur Hassan El Hadi pour sa gentillesse, sa coopération et son aide précieuse au cours de mon stage au sein de la faculté des Sciences Ben m'sik, Université Hassan II Casablanca et lors des missions faites sur les terrains de la Meseta Marocaine. Je saisis cette occasion pour remercier aussi Professeur Saida Alikouss, directrice du Laboratoire de Géodynamique des Chaines Anciennes pour son accueil chaleureux.

Mes remerciements sincères vont également à Professeur Abdelfatah Tahiri (Institut Scientifique de Rabat et spécialiste de la chaine hercynienne) et Professeur Ali Azdimousa (Faculté Polydisciplinaire de Nador, Université Mohammed I d'Oujda) pour le temps qu'ils m'ont accordé, la documentation sur la géologie du Maroc qu'ils ont mis à ma disposition et pour m'avoir assuré les autorisations des missions de terrains sur le territoire marocain.

Je désire en outre remercier mes chères copines Hind El Haibi et Sakina Mehdioui pour leurs amitiés, sympathies, disponibilité, les moments agréables partagés et pour me faire découvrir leur culture. J'adresse contentement mes remerciements les plus vifs et sincères à la famille de Hind (Mina, Aomar et Sanaâ) pour l'accueil qu'ils m'ont réservé le long de mon séjour au Maroc. Une pensée va également à sa grand-mère avec qui je passais des moments réjouissants malgré les problèmes linguistiques qu'on a rencontrés.

امينه ، سناء و عمار لقد كنتم مميزين معي لكم مني جزيل الشكر لكل ما قدمتموه لاجلي. شكري لجدتي الثانيه بالمغرب رغم مشكل اللغه بيننا الا اننا تمكنا من التواصل طوال فتره اقامتي بالمغرب مع عائلتي الثانيه.

Infine un ringraziamento speciale lo vorrei dedicare ai miei genitori, Anna e Guido, che mi hanno sempre appoggiato e, sebbene a volte non sia stato facile, mi hanno sempre assecondata nella ricerca del mio cammino. Mi hanno cresciuta cittadina del mondo, mi hanno insegnato a rispettare e conoscere altre culture e, anche se per questioni logistiche sono finiti alla fine di questi ringraziamenti, sono stati i primi ad insegnarmi ad essere curiosa, osservare ed interpretare.

Grazie a Lorenzo, pilastro che sempre mi accompagna: grazie per correggermi pazientemente l'inglese ma soprattutto per essere sempre al mio lato, seguirmi in questa avventura spagnola, e trovare sempre un modo per farmi ridere. Non so dove finiremo dopo, ma non mi importa perché so che non sarò sola. Grazie ad Anna e Giovanni Valetti, per il loro supporto... e per i pacchi di parmigiano, carburante indispensabile per finire la Tesi! Grazie anche alla nonna Rosina, che mi vede poco e ne soffre molto, per sopportare questa nipote che non può starsene ferma in Italia.

Grazie a Giulio Roffino per i contatti a Granada, a Cristina Bona per i contatti a Denver (ed in tutti gli altri posti che si sono susseguiti negli anni), agli amici che sono riusciti a venirmi a trovare e quelli che avrebbero voluto ma (per il momento) non ci sono riusciti.

Esta Tesis Doctoral ha sido financiada por la beca predoctoral BES-2016-078168 concedida por el Ministerio de Ciencia, Innovación y Universidades del Gobierno de España, proyecto de investigación CGL2015-71692-P (Ministerio de Ciencia, Innovación y Universidades), por el Departamento de Geodinámica de la Universidad de Granada y por el grupo RNM-148 Geología Estructural y Tectónica (Junta de Andalucía).

Abstract

The Rheic Ocean was formed by the early Paleozoic drifting of Avalonian (Amazonian-type) terranes from northwest Gondwana. These terranes docked with Laurentia and Baltica during middle Paleozoic time (Acadian/Caledonian orogeny) forming Laurussia. The late Paleozoic Variscan/Alleghanian orogeny resulted from the closure of the Rheic Ocean and the subsequent collision among Laurussia, Gondwana and a number of peri-Gondwanan terranes. In the European portion of the Variscan belt, the Rheic suture is considered to run from Poland to SW Iberia, separating Avalonian terranes to the west from Gondwanan terranes to the east, although true Rheic Ocean ophiolites have not been found yet. To the south, the Rheic suture might reappear in the Mauritanides. In between, the northern Moroccan Variscides, which include the Moroccan Mesetas, are considered part of the northern Gondwana margin involved in the Variscan orogeny, although the trace of the Rheic suture is uncertain or even nonexistent.

This Ph.D. Thesis investigates the Paleozoic Moroccan Mesetas, with focus on: (i) sediment provenance according to U-Pb and Hf isotopic analyses on detrital zircon grains, and (ii) the Variscan evolution based on detailed structural analysis of selected areas. The obtained results shed light on: (i) the pre- and syn-orogenic Paleozoic paleogeography, (ii) the Eo-Variscan tectonics, and (iii) the possible location of the Rheic suture.

Detrital zircon grains from the pre-orogenic Cambrian-Devonian succession show the predominance of two populations peaked at c. 700-550 Ma (Cadoimian/Pan-African orogenies) and c. 2.1 Ga (Eburnean orogeny) ages, and a general lack of Mesoproterozoic and late-Paleoproterozoic (c. 1.8-1.1 Ga) ages. These features are distinctive of the West African Craton (WAC), which therefore can be considered the main sediment source during early-middle Paleozoic time. A Stenian-Tonian (c. 1.0 Ga) detrital zircon population is locally present and points to distant and intermittent NE African sources (*e.g.*, Sahara Metacraton, Arabian-Nubian Shield). Finally, rift-related Cambrian-Ordovician volcanism provided locally abundant zircon grains in the Cambrian-Lower Ordovician succession. Altogether, these data suggest that the entire region belonged to the northern Gondwana passive margin, with paleogeographic continuity among the subdomains that are traditionally described within the Moroccan Mesetas.

The flysch-like Famennian-Tournaisian successions from the Tiflet (northern Western Moroccan Meseta) and Debdou-Mekkam (Eastern Moroccan Meseta) inliers show the presence of a Late Devonian (c. 370 Ma) detrital zircon population, accompanied by a noticeable number of Mesoproterozoic-late Paleoproterozoic (c. 1.8-1.1 Ga) grains. These ages, unknown in the WAC, could have been provided by an active Avalonian (Amazonian-type) arc approaching the northern Gondwana margin during the Rheic Ocean closure.

The appearance of these exotic detrital zircon populations was immediately followed by an Eo-Variscan intense deformational phase that has been studied in the Debdou-Mekkam region. In these inliers, a thick Famennian-Tournaisian succession is strongly deformed by folds that are tight to isoclinal, overturned to recumbent, have SE regional vergence, and are associated with axial-planar cleavage. The reconstructed folded structure implies an important NW-SE shortening, which is interpreted as the result of a frontal SE-directed push of the Avalonian promontory. Accordingly, the Rheic suture would be concealed in between this Avalonian promontory and the Gondwanan margin. Lateral correlatives of the suture are likely found (i) to the north at the boundary between the Ossa-Morena and South Portuguese Zones, and (ii) to the west in the late Variscan thrust which superposed the Caledonian Sehoul Block onto the Western Moroccan Meseta.

The post-Eo-Variscan succession also shows a WAC affinity, with variable record of NE African and Avalonian sources and local Variscan granitoids sources.

Resumen

El Océano Rheico se formó por la separación de terrenos Avalonianos (de tipo Amazónico) del borde noroeste del continente Gondwana. Tales terrenos colisionaron con Laurentia y Báltica durante el Paleozoico medio dando lugar a la orogenia Acadiense/Caledoniana y a la formación del continente Laurrusia. Durante el Paleozoico superior, el cierre del Océano Rheico y posterior colisión entre Laurrusia, Gondwana y una serie de fragmentos peri-Gondwánicos formó el orógeno Varisco/Apalachiano. En la parte europea de la cadena Varisca, la sutura Rheica discurre probablemente desde Polonia hasta el sudoeste de Iberia, separando terrenos Avalonianos al oeste y terrenos Gondwánicos al este, si bien no se conocen ofiolitas verdaderamente Rheicas. Más al sur, la sutura Rheica podría localizarse de nuevo en los Mauritánides. Entre ambas regiones, se sitúan los macizos Variscos del norte de Marruecos (incluyendo la Meseta Marroquí), que se interpretan como parte del margen septentrional de Gondwana involucrado en la orogenia Varisca, y donde se desconoce, si es que existe, la posición de la sutura Rheica.

La presente Tesis Doctoral investiga el Paleozoico de la Meseta Marroquí, prestando especial atención a: (i) la procedencia de sedimentos mediante el análisis sistemático de los isotopos de U-Pb y Hf de poblaciones de circones detríticos, y (ii) la evolución Varisca mediante el estudio estructural detallado de algunos sectores clave. Los resultados obtenidos constituyen un avance importante en el conocimiento de: (i) la paleogeografía Paleozoica pre- y sin-orogénica, (ii) la tectónica Eo-Varisca, y (iii) la posible situación de la sutura Rheica.

Los circones detríticos de la sucesión pre-orogénica (Cámbrico-Devónico) se agrupan en dos poblaciones principales con edades de c. 700-550 Ma (orogenia Cadomiense/Pan-Africana) y c. 2.1 Ga (orogenia Eburniense), y no existen apenas circones Mesoproterozoicos o tardi-Paleoproterozoicos (c. 1.8-1.1 Ga). Tal distribución de edades es representativa del Cratón Africano Occidental, el cual sería por tanto la fuente principal de sedimentos en la Meseta Marroquí durante del Paleozoico inferior y medio. Además, algunas muestras tienen una población variable de edad c. 1.0 Ga (Esténico-Tónico inferior), cuya fuente, relativamente lejana y con aportes detríticos intermitentes, puede estar en los cratones del noreste de Africa (Metacratón del Sáhara, Escudo de Arabia-Nubia). Por último, circones detríticos de edad Cambro-Ordovícico inferior constituyen poblaciones significativas en algunas muestras de esa misma edad, y se relacionan con la existencia de actividad volcánica local durante un episodio de rifting continental. En conjunto, todos los datos disponibles sugieren que la Meseta Marroquí formó parte de un único margen continental pasivo desarrollado en el norte de Gondwana, habiendo existido continuidad paleogeográfica entre los distintos sub-dominios en los que tradicionalmente se ha subdividido la Meseta Marroquí.

La sucesión Fameniense-Tournaisiense de Tiflet (borde septentrional de la Meseta Occidental Marroquí) y Debdou-Mekkam (Meseta Oriental Marroquí) incluye, además de las dos poblaciones dominantes en las sucesión Cambro-Devónica, circones detríticos del Devónico superior (c. 370 Ma, con valores de ϵ_{HF} positivos) y del Mesoproterozoico-Paleoproterozoico superior (c. 1.8-1.1 Ma). Tales edades se desconocen en el Cratón Africano Occidental. Estos circones exóticos podrían provenir de la erosión de un arco magmático Devónico desarrollado sobre un basamento Avaloniano, durante su aproximación al margen de Gondwana al final del cierre del Océano Rheico.

Tras el cierre del Océano Rheico, tuvo lugar un episodio de intensa deformación Eo-Varisca, que ha sido estudiada en la región de Debdou-Mekkam. Aquí, la sucesión Fameniense-Tournaisiense, de gran espesor y carácter flyschoides, está deformada por pliegues con foliación de plano-axial, cuya vergencia regional es hacia el sudeste y sus geometrías isoclinales, volcadas y recumbentes. El tren de pliegues reconstruido implica un importante acortamiento de orientación NO-SE, que se interpreta como el resultado del empuje frontal hacia el sudeste de un promontorio Avaloniano. Por tanto, la sutura Rheica se localizaría de manera críptica entre este promontorio avaloniano y el margen de Gondwana. La sutura continuaría hacia el norte a lo largo del límite entre la Zonas de Ossa-Morena y Sud-Portuguesa, y hacia el oeste estaría oculta bajo el cabalgamiento que superpuso el Bloque Caledoniano de Sehouf sobre La Meseta Occidental Marroquí.

Los circones detríticos de la sucesión post-Eo-Varisca de la Meseta Marroquí también muestran afinidad con el Cratón Africano Occidental, más un registro variable procedente de fuentes Avalonianas y de granitos Variscos.

Chapter I

Introduction

1. Geographic location

The region that is the focus of this Ph.D. Thesis is located in the Moroccan Mesetas, northern Morocco, and consists of a roughly ENE-WSW elongated sector between the cities of Rabat (to the west), Khenifra (to the south), and Oujda (to the northeast; Figure 1.1). To the north, the Betic-Rif Alpine orogenic system separates the Moroccan Mesetas from the Variscan Iberian Massif; to the south, the High Atlas Alpine mountain range separates the Moroccan Mesetas from the Anti-Atlas region. The Moroccan Mesetas can be subdivided into two territories (Western and Eastern), separated by the moderately uplifted NE-SW trending Middle Atlas range that runs between the cities of Taza, to the NE, and Khenifra, to the SW.

The Eastern Moroccan Meseta extends from the Middle Atlas to Oujda, and is characterized by a wide plateau (c. 600 m a.s.l.) crosscut by the rivers Za and Moulouya, both draining toward the Mediterranean Sea. This plateau is locally interrupted by isolated massifs that can reach c. 1600 m a.s.l.

The Western Moroccan Meseta extends from the Middle Atlas to the Rabat-Casablanca Atlantic coast, with catchments draining westwards. It is characterized by moderately and variably elevated landscapes that gradually lose altitude westwards and are bounded to the north by the Fes-Rabat plain.



Figure 1.1. Approximate location of the studied region (red square). Satellite image: Landsat/Copernicus 2020 from Google Earth.

2. The Variscan-Appalachian belt

At the end of the Neoproterozoic era, the global geodynamic scenario included three main continents: Laurentia and Baltica, separated from Gondwana by the Iapetus and Tornquist Oceans, respectively (Figure 1.2a). Previously, the northern part of Gondwana was involved in the collisional Pan-African (Cryogenian-Ediacaran) and in the Cadomian Andean-type (Ediacaran) orogenies. After the cessation of the Cadomian subduction, an Early Paleozoic continental rift affected the northern margin of Gondwana. This rift culminated in the diachronous opening of the Rheic Ocean at Late Cambrian-Early Ordovician time (Nance et al., 2010, 2012), and in the drifting of a number of ribbon-like microcontinents, collectively referred to as peri-Gondwanan terranes. Some of these terranes drifted far away (e.g., Avalonian terrane, derived from northwestern Gondwana; Figure 1.2b; e.g., Nance et al., 2002); other terranes seem to have remained close to Gondwana (e.g., Ossa-Morena, Armorica, Saxo-Thuringia terranes, derived from northwestern Gondwana), separated by minor oceanic realms.

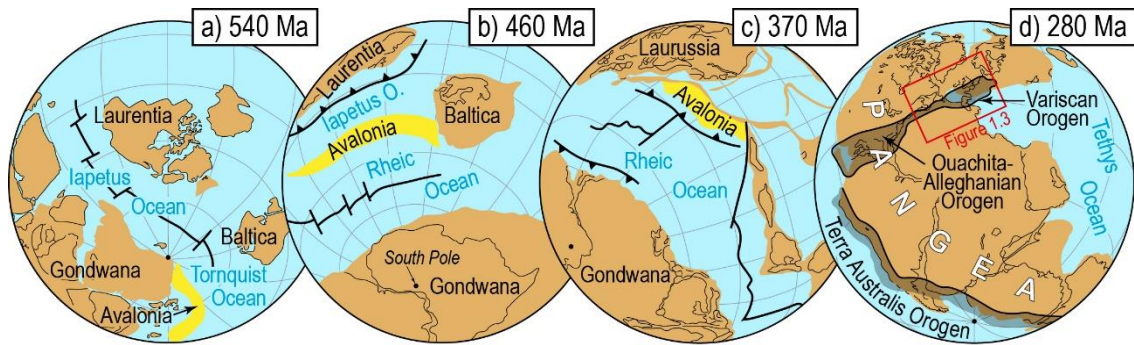


Figure 1.2. Paleogeographic reconstruction showing the opening and closure of the Rheic Ocean. Modified from Nance et al. (2010 and references therein).

The Early Paleozoic opening of the Rheic Ocean was coeval to the closure of the Iapetus Ocean (e.g., Franke et al., 2017 and references therein; Nance et al., 2012 and references therein) which, in turn, resulted in the Silurian-Early Devonian collision between Avalonia, Baltica and Laurentia (Caledonian-Acadian orogeny). This collision also triggered the diachronous closure of the Rheic Ocean (Figure 1.2c; e.g., Nance et al., 2010; 2012) that ended with the continental collision of northern Laurussia with northern Gondwana at Late Devonian-Early Carboniferous time (Variscan orogeny; e.g., Kroner et al., 2007; Matte, 2001) and southern Laurussia with western Gondwana at Late Carboniferous-Permian time (Alleghanian orogeny; e.g., Nance et al., 2012; Sacks and Secor, 1990). The final result was the formation of a huge orogenic belt and the assemblage of the supercontinent Pangea (Figure 1.2d and 1.3).

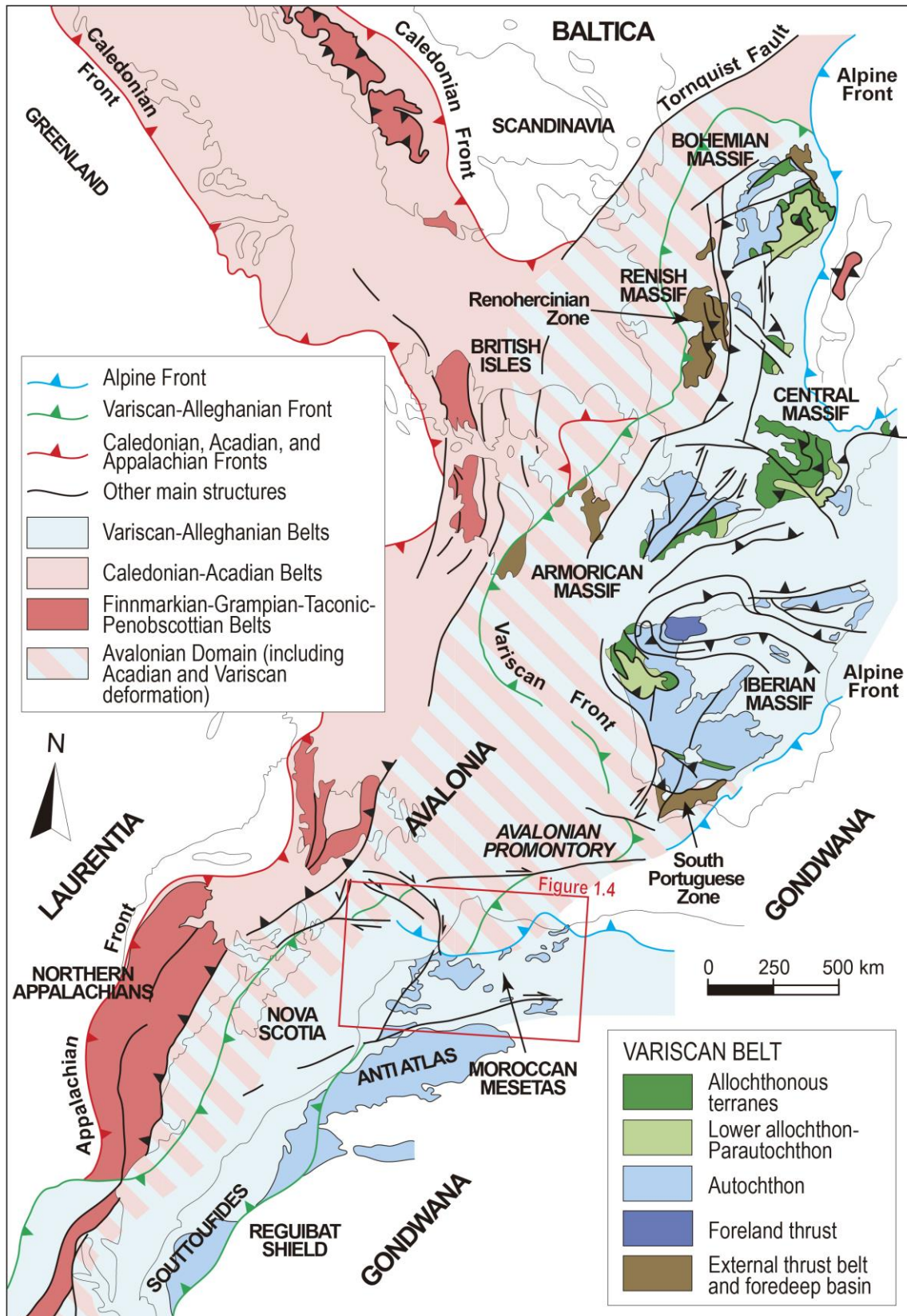


Figure 1.3. Large-scale reconstruction of the Variscan-Alleghanian and Caledonian belts at the end of the Paleozoic (modified from Martínez Catalán et al., 2002; Michard et al., 2010b; Simancas et al., 2009).

The paleogeographic and paleotectonic reconstructions of such a large and complex orogenic belt are still far from being well constrained, due to the uncertainty of correlating

the many continental pieces and ophiolitic/high-pressure units involved. The Variscan part of the belt, namely Variscides, extends from Central Europe to Morocco through Iberia (Figure 1.3). The northwestern orogenic front (the Laurussian foreland) is well defined from England to Germany, while the southeastern one (the Gondwanan foreland) is mostly obscured due to Alpine reworking, except in Morocco where it is exposed in the Anti-Atlas region.

In Europe, there is agreement on the Avalonian affinity of the Rheno-Hercynian and South Portuguese terranes (*e.g.*, Franke and Dulce, 2017; Linnemann et al., 2012; Pérez-Cáceres et al., 2017). The remaining Gondwana-derived continental pieces involved in the Variscan orogeny would have never drifted far away from Gondwana, having evolved either as ribbon microcontinents separated by minor oceanic realms from the mainland, or as aborted rifts and passive margins attached to it. The primary Rheic ocean suture should be located between the Avalonian and other peri-Gondwanan terranes, but it appears concealed by a superimposed and protracted Variscan tectonometamorphic imprint (*e.g.*, Franke et al., 2017; Pérez-Cáceres et al., 2017).

The continuation of the Rheic suture in the Moroccan Variscides is unclear and based on indirect data. This Ph.D. Thesis provides additional information with which to constrain the possible location of this suture in northern Morocco. Between the southwestern Iberian Variscides and the Mauritanides (located just to the south of the Souttouflides shown in Figure 1.3) there is no evidence of ophiolitic rocks and/or high-pressure metamorphic units, which would suggest the presence of the Rheic suture. However, several pieces of evidence suggest that an exotic (probably Avalonian) basement occurs to the north and west of the Moroccan Mesetas. To the north, the Sehouf Block (Figure 1.4; see below) recorded a Caledonian deformation (Tahiri et al., 2010) not recognized in the remaining Moroccan Mesetas. To the west, some Mesoproterozoic (c. 1.45-1.18 Ga) and late Paleoproterozoic (c. 1.95-1.65 Ga) zircon and monazite grains were recently reported (El Haibi et al., 2020; Kuiper et al., 2019) in igneous rocks from the offshore Mazagan escarpment and the El Jadida coastal locality (Figure 1.4). To the south, Caledonian zircon populations were found (Bea et al., 2020; Gärtner et al., 2013) in the Souttouf massif (Figure 1.3). Finally, ophiolitic rocks (Villeneuve, 2008 and references therein) and Carboniferous eclogitic facies rocks (Le Goff et al., 2001) were described in the Mauritanides.

3. The northern Moroccan Variscides

In northern Morocco, the Paleozoic sequence affected by the Variscan orogeny (Moroccan Variscides) crops out in different domains (Figure 1.4) limited by fault zones, whose paleogeographic and tectonic importance is still a matter of debate (*e.g.*, Hoepffner et al., 2006; Michard et al., 2010a, 2010b; Simancas et al., 2009, 2010).

To the northwest, the Rabat-Tiflet Fault Zone (RTFZ) separates the Sehouf Block from the remaining Moroccan Mesetas. The Sehouf Block (in lilac in Figure 1.4) contains a

lower-middle Cambrian sequence of phyllites and metaquartzites strongly foliated at low-grade metamorphic conditions. The sequence is intruded by undeformed Late Devonian (c. 367 Ma) granitoids (Tahiri et al., 2010) which suggests a middle Paleozoic age, likely Caledonian (Silurian-Early Devonian), for the foliation. This deformation has not been observed in any other part of the northern Moroccan Variscides and, hence, the Sehoul Block is considered to be part of an exotic terrane (*i.e.*, Avalonian promontory; *e.g.*, Simancas et al., 2005) accreted to the northern Gondwanan margin during the Variscan orogeny (*e.g.*, Michard et al., 2010b and references therein; Tahiri et al., 2010).

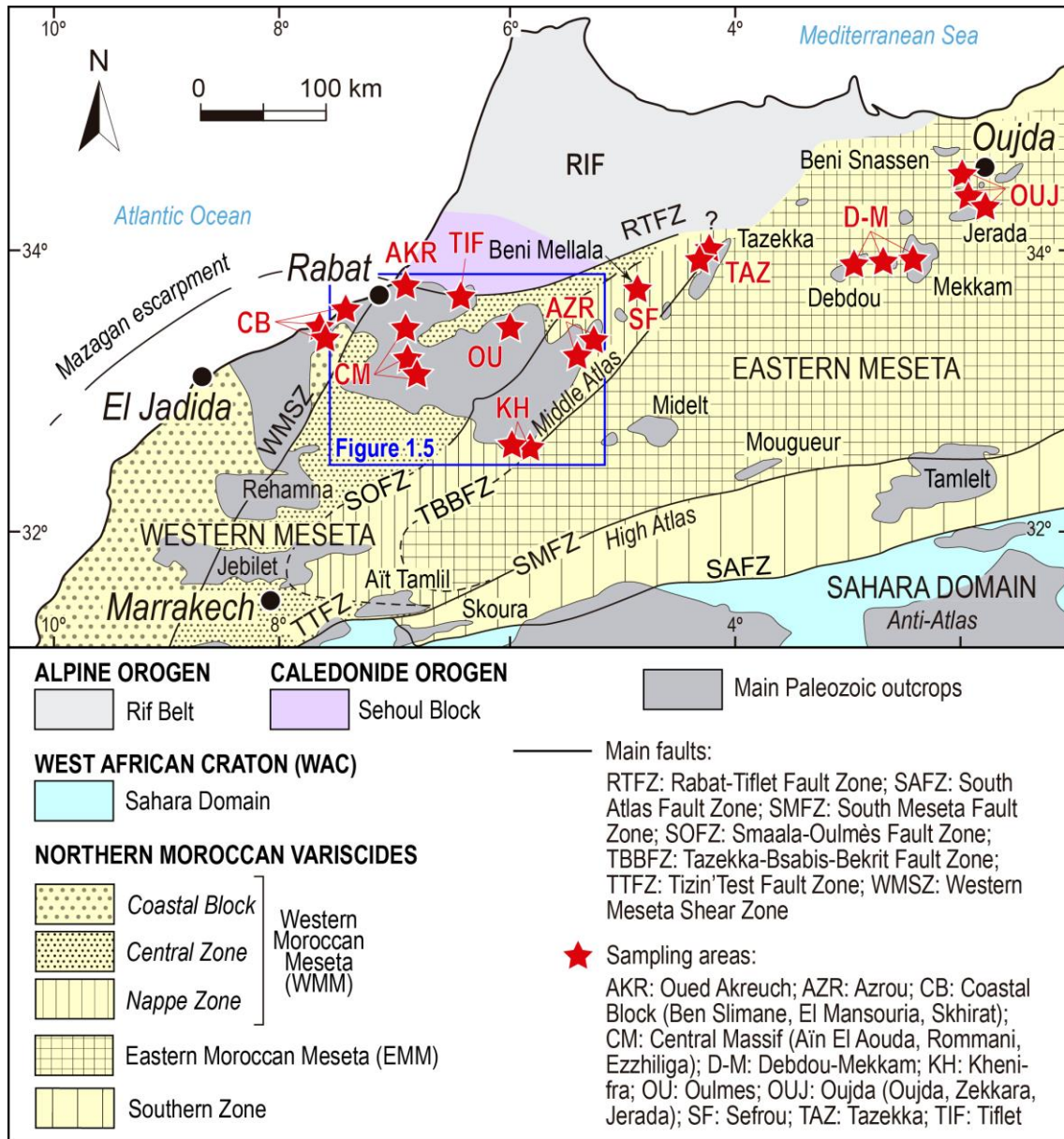


Figure 1.4. Map of the main structural domains and Paleozoic inliers in northern Morocco (modified from Hoepffner et al., 2006; Michard et al., 2010b).

The region that extends between the RTFZ to the north, and the South Meseta (SMFZ) and Tizin'Test (TTFZ) Fault Zones to the south corresponds to the Moroccan Mesetas

(Western and Eastern Mesetas; in yellow in Figure 1.4). These are the focus of this Ph.D. Thesis and are described in detail in the following subsections.

The SMFZ represents the northern limit of the Southern Zone (in yellow in Figure 1.4) which extends southwards up to the South Atlas Fault Zone (SAFZ). The Southern zone is made up of a Cambrian-Devonian siliciclastic and carbonatic platform sequence overlying a volcanic and volcanoclastic Neoproterozoic basement (Hoepffner et al., 2005 and references therein). During the Carboniferous, the sedimentation was turbiditic (Izart et al., 1989; Michard et al., 1982; Soualhine et al., 2003). There is no evidence of Variscan magmatism. The Variscan Pennsylvanian deformation formed E-W trending S-vergent folds and thrusts (Houari and Hoepffner, 2000, 2003). The metamorphism was of low- or very low-grade (Hoepffner et al., 2005).

The Sahara domain (in light blue in Figure 1.4), and in particular the Anti-Atlas, extends to the south of the TTFZ and SAFZ. On top of the Paleoproterozoic-Neoproterozoic basement, the metasedimentary sequence of this domain shows the passage from an Early Cambrian carbonatic platform to a more detrital shallow and epicontinental Early Ordovician platform. The Late Ordovician is marked by the deposition of glaciogenic deposits followed by Silurian transgressive black shales and carbonate platform deposits during the Early Devonian. The Late Devonian-Pennsylvanian period is characterized by mainly detrital sedimentation (Hoepffner et al., 2005 and references therein; Michard et al., 2010b and references therein). The Variscan structure consists of SW-NE to W-E trending upright open folds with no associated foliation. The intensity of the deformation gradually decreases southwards until the undeformed Tindouf Basin (Hoepffner et al., 2005; Michard et al., 2010b). Due to the style of the Variscan deformation, the Anti-Atlas is considered to represent the foreland of the Variscan belt.

3.1. The Western Moroccan Meseta

The Western Moroccan Meseta (WMM) extends from the Tazekka-Bsabis-Bekrit Fault Zone (TBBFZ) to the east, to the Atlantic coast to the west, and is bounded by the RTFZ to the north and the TTFZ and SMFZ, to the south. Within the WMM, three sub-domains were traditionally differentiated (Figure 1.4; Hoepffner et al., 2005 and references therein; Michard et al., 2010b and references therein): the Coastal Block, the Central Zone, and the Nappe Zone, separated by the Western Meseta Shear Zone (WMSZ) and the Smaala-Oulmes Fault Zone (SOFZ), respectively.

3.1.1. The Coastal Block

The Coastal Block is the westernmost sub-domain of the WMM and it is characterized by a Cambrian-Mississippian sedimentary sequence overlying a Precambrian basement. The latter is found in small outcrops of by Paleoproterozoic Eburnean rhyolites and rhyolitic porphyroids exposed in western Rehamna (Pereira et al., 2015), and

Neoproterozoic Cadomian rhyolites cropping out in El Jadida (El Haïbi et al., 2020; El Houicha et al., 2018; Hoepffner et al., 2005 and references therein).

The base of the Paleozoic sequence is represented by lower Cambrian limestones. The carbonatic platform was interrupted during the middle Cambrian by the opening of a NNE-SSW oriented graben filled by a thick siliciclastic sequence that locally intercalates basaltic flows. This graben is the expression of an aborted rift branch associated with the opening of the Rheic Ocean (Bernardin et al., 1988; Ouali et al., 2003; Piqué, 2003, 1979; Piqué et al., 1995; Piqué and Michard, 1989). Two middle-late Cambrian volcanic centers are located in the El Jadida (Sidi Saïd Maâchou; Mohsine, 2002; Remmal et al., 2009) and the Ben Slimane (Oued Rhebar; El Attari et al., 2019; El Hadi et al., 2006b) areas.

The Early-Middle Ordovician detrital sedimentation returned to shallow platform conditions (Hammoumi, 1988), followed by Late Ordovician glacial deposits (Destombe and Jeannette, 1966). With the withdrawal of the glacial sheet during the Silurian period, the sedimentation in all the Moroccan Variscides became pelitic and represented by a sequence of black shales with graptolites. In the Coastal Block, these black shales are interbedded with Late Silurian carbonatic levels and, locally, basalt flows (Cornée et al., 1985; El Kamel et al., 1998).

The amount of limestones increased during Early Devonian with the establishment of a carbonatic platform that emerged during Middle-Late Devonian (Zahraoui, 1991). Finally, siliciclastic sedimentation resumed in new depocenters during the Famennian-Visean (Zahraoui, 1991). Postorogenic Triassic rocks (red shales and basalts) lie unconformably over the previous Paleozoic succession.

The Coastal Block is affected by weak Variscan deformation characterized by NNE-SSW trending upright folds, slaty cleavage, and weak metamorphism, which increases eastwards (*e.g.*, Hoepffner et al., 2005, 2006; Michard et al., 2010b; Piqué et al., 1980).

3.1.2. The Central Zone

The Ediacaran Cadomian basement of the Central Zone crops out locally in the Tiflet (El Haïbi et al., 2021; Tahiri et al., 2010), central Rehamna (Figure 1.4; Baudin et al., 2003; Pereira et al., 2015 and references therein), and Marrakech (Eddif, 2002) areas. On top of this basement, the Paleozoic sedimentary sequence starts with Cambrian limestones and slates, followed by a Tremadocian *hiatus*. The Ordovician sequence is very similar to the one on the Coastal Block, with shallow platform siliciclastic sediments followed by glaciogenic deposits. To the north, in the area adjacent to the Sehoul Block (Rabat-Tiflet, or Bou Regreg corridor; Figure 1.5), the Early-Middle Ordovician sedimentation is made up of shales with interbedded basalt flows and cross-cut by doleritic dykes; Late Ordovician rocks are missing (Piqué, 1979).

During the early Silurian, black shales with graptolites deposited, passing upwards to carbonatic facies at late Silurian time. In the Rabat-Tiflet area, the lower Silurian shales

are lacking and the upper Silurian limestones directly overlie the Middle Ordovician rocks.

The Devonian sedimentation in the Central Zone is mainly siliciclastic, and marked by a basin instability event (Cornée, 1989; Cornée et al., 1987a, 1987b; Hollard et al., 1982; Mayol and Muller, 1985) that ended with the development of the Ben Slimane and Sidi Bettache depocenters in the Late Devonian (Figure 1.5). These basins are filled with Famennian-Tournaisian coarse deposits (olistostromes) that laterally grade to sandstones and shales (El Hassani, 1990; Fadli, 1990; Izart et al., 2001; Piqué, 1979; Tahiri, 1991; Tahiri and Hoepffner, 1988).

The terrigenous sedimentation continued during the Visean-Serpukhovian, with the deposition of turbiditic shales, sandstones and greywackes with some conglomerate and limestone intercalations (Izart, 1991; Piqué, 1979). Moscovian alternation of lacustrine conglomerates and black limestones are found in some areas (eg. Sidi Bettache; Piqué, 1979), as well as unconformable Permian red conglomerates and volcanic rocks (Sidi Bettache and Oulmes areas; (Cailleux et al., 1986; El Wartiti, 1990; El Wartiti et al., 1990; Youbi et al., 1995). Finally, Triassic red shales and basaltic lavas unconformably overlie the previous successions (Destombe, 1987).

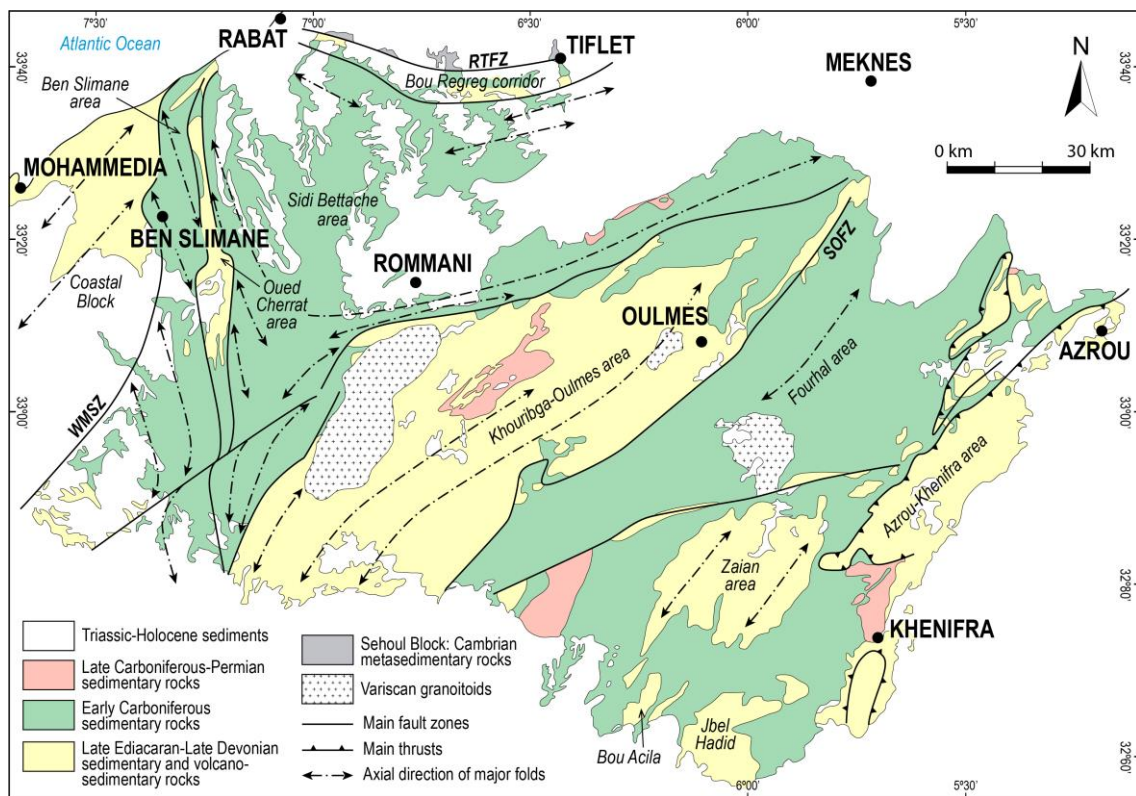


Figure 1.5. Simplified geological map of the Rabat-Khenifra region from the Coastal Block to the Nappe Zone (northern Western Moroccan Meseta). Modified from Becker and El Hassani (2020); RTFZ: Rabat-Tiflet Fault Zone; SOFZ: Smaala-Oulmes Fault Zone; WMSZ: Western Meseta Shear Zone.

The main Variscan deformation in the Central Zone took place during the Pennsylvanian/early Permian and developed variably oriented (polyphasic?) fold trains

(Figure 1.5; (Hoepffner et al., 2006, 2005). The attitudes of the axial planes in folds varies from mostly upright to moderate vergent towards diverse directions, and have associated slaty cleavage and very low- to low-grade regional metamorphism. K-Ar dating on neoformed mica grains yielded ages varying from 300 to 290 Ma (Huon et al., 1987).

A number of granitic bodies were also emplaced during the Late Carboniferous-Permian (El Hadi et al., 2006a and references therein). An exception to the moderate folding intensity and related weak metamorphism described above is found in the Rehamna and Jebilet massifs (Figure 1.4). In these massifs, a late- (post-?) Variscan medium-grade thermal imprint and intense ductile deformation were recognized and described (Chopin et al., 2014; Delchini et al., 2018; Wernert et al., 2016).

3.1.3. The Nappe Zone

The Nappe Zone is the easternmost sub-domain of the WMM, located between the SOFZ and the TBBFZ (Figure 1.4; Hoepffner et al., 2005). Most of the zone shares the features of the Central Zone, and only in the eastern part (Azrou-Khenifra) a remarkable west-directed thrust tectonics has been recognized (Figure 1.5; Ben Abbou et al., 2001; Michard et al., 2010b).

The Cadomian basement in the Nappe Zone crops out in small inliers located to the west of Khenifra: Bou Acila, Jebel Hadid, and Goaïda (Ouabid et al., 2017; Ouali et al., 2003), and is represented by granitoids and metavolcanic rocks with Ediacaran ages (U-Pb on magmatic zircons; Letsch et al., 2018; Ouabid et al., 2017). The Ediacaran basement is covered by lower Cambrian carbonatic levels that in Bou Acila are followed by a volcano-sedimentary sequence ascribed to the lower Cambrian (Ouali et al., 2003). In Goaïda, rift-related bimodal magmatic rocks (gabbros and rhyolites) that cross-cut the Ediacaran and Cambrian succession yielded ages varying from c. 519 to c. 479 Ma (U-Pb on magmatic zircons; Ouabid et al., 2020).

The Ordovician-Silurian metasedimentary sequence of the Nappe Zone is similar to the one described in the other sub-domains of the WMM, although more distal and deeper facies (shales and turbiditic deposits) are common here.

The Early Devonian time is characterized by an open carbonatic marine shelf (Chakiri, 2002; Piqué, 1979; Tahiri, 1991; Termier, 1936). In the autochthonous and para-autochthonous nappes, the Late Devonian sequence is representative of a shelf environment with gravitational deposits; the allochthonous sequence presents more distal turbiditic facies (Allary et al., 1976; Bouabdelli, 1989).

The Viséan-Serpukhovian sequence unconformably overlies the previous ones (Bouabdelli, 1989). The latter is made up of shales and sandy or calci-turbidites with conglomeratic and olistrostromic deposits (Lahfid et al., 2019 and references therein), which mark an increase of the tectonic activity in the region. Synorogenic flysch sedimentation continued up to the Moscovian at the front of the nappes in the Azrou-Khenifra area (Ben Abbou et al., 2001).

Finally, during the Late Carboniferous, the Nappe Zone was deformed by NE-SW trending, upright to west-vergent folds in a similar way to the deformation in the Central Zone (Hoepffner et al., 2005, 2006). Neoformed mica grains yielded c. 330-320 Ma K-Ar ages (Huon et al., 1987). Furthermore, a pre-Visean (Eo-Variscan) folding event was recently described in the Zaian anticline located west of Khenifra (Lahfid et al., 2019). It consists of NW-SE to N-S trending upright to recumbent folds with related slaty cleavage formed at c. 300-350 °C, while the late Carboniferous folds only developed spaced cleavage formed at c. 150-250 °C (Lahfid et al., 2019).

3.2. *The Eastern Moroccan Meseta*

In the Eastern Moroccan Meseta (EMM; Figure 1.4) the outcrops of Paleozoic rocks are relatively small (not more than c. 1200 km²) and isolated by the overlying Mesozoic-Cenozoic cover, which complicates the reconstruction of the pre-Mesozoic geology.

The Precambrian basement is not exposed in the EMM, where the oldest rocks are shales and greywackes attributed to the Cambrian based on their similarities with the Cambrian succession of the WMM (Hoepffner, 1987). Evidence of Cambrian magmatism is absent, except in Midelt (Figure 1.4) where outcropping amphibolites were interpreted as intraplate alkaline basalts (Ouali et al., 2000).

During Early-Middle Ordovician time (Hoepffner, 1977; Rauscher et al., 1982; Torbi, 1996), sandy pelitic rocks were deposited in a shallow marine environment, followed by Late Ordovician sandstones and quartzites, and by a Silurian pelitic succession of phanites and black shales with graptolites (Hoepffner, 1987).

The late Silurian carbonatic levels and Early Devonian platform limestones, common in the WMM, are completely absent in the EMM. The Devonian sequence here is characterized by sandstones and shales, followed by a thick sequence of turbiditic shales and greywackes that crops out in the Debdou and Mekkam and eastern Tazekka (to the east of the TBBFZ) inliers (Hoepffner et al., 2005). Attempts to date these turbidites yielded Middle Devonian (palynomorphs; Marhoumi, 1984; Marhoumi et al., 1983) and Tournaisian-Visean (fragments of fossil plants; Médioni, 1980) ages.

A horizon of conglomerates unconformably overlies the Devonian (-Early Carboniferous?) turbiditic sequence, followed by Late Visean limestones (Berkhli et al., 1999; Huvelin and Mamet, 1989; Médioni, 1980). At late Visean-Serpukhovian time, a succession of olistotromic deposits made up of blocks of the lower-middle Paleozoic sequence (El Ghazi and Huvelin, 1981; Huvelin, 1986; Torbi, 1996), and a thick volcano-sedimentary sequence were put in place (Chalot-Prat, 1990; Hoepffner, 1981; Huvelin, 1986), the latter containing ignimbrites and andesitic, dacitic, and rhyolitic flows.

Finally, late Serpukhovian-early Kasimovian sedimentation is recorded only in the easternmost areas of the EMM, where shales and greywackes are found (Desteucq et al., 1988; Essamoud and Courel, 1998; Izart, 1991; Torbi, 1996). Triassic red shales and basalts unconformably overlie the Late Carboniferous succession.

At least two folding events were described in the EMM: Eo-Variscan (Late Devonian-early Carboniferous) and Variscan (late Pennsylvanian). In the Tazekka area, a Visean deformational event was also recognized (Hoepffner et al., 2005, 2006; Michard et al., 2010b and references therein).

The Eo-Variscan phase is characterized by intense folding and the development of pervasive slaty cleavage particularly well defined in the Midelt, Debdou-Mekkam, and eastern Tazekka inliers. Hoepffner (1987) described these structures as west-vergent, although structural maps and cross-sections were not provided. The metamorphism associated with these structures was generally of low-grade, except in Midelt where it reached greenschist to amphibolite grade conditions (Hoepffner et al., 2005, 2006; Michard et al., 2010b and references therein). The Late Devonian age of the Eo-Variscan phase was determined in Midelt as being c. 366 Ma (Rb-Sr; Clauer et al., 1980), while in the Tazekka area (to the east of the TBBFZ) the slaty cleavage formed at low-grade metamorphic conditions dated c. 330 Ma (K-Ar; Huon et al., 1987). In the Debdou-Mekkam inliers (Figure 1.4) K-Ar analyses on neoformed mica grains gave ages ranging from c. 372 and c. 368 Ma (Huon et al., 1987). This Ph.D. Thesis provides new structural maps and cross-sections which support a re-interpretation of the structure of this region.

The Variscan event deformed the Cambrian-Carboniferous succession with NE-SW to E-W trending open folds, described as north-vergent (Erraji, 1997; Hoepffner, 1987; Hoepffner et al., 2005, 2006), and associated with spaced cleavage and very low- to low-grade metamorphism dated c. 300 Ma (K-Ar; Huon et al., 1987). Numerous granitoid bodies were emplaced from Visean to Permian times (El Hadi et al., 2006a and references therein).

4. Aims and structure of the Ph.D. Thesis

The northern Moroccan Variscides have been extensively studied in terms of stratigraphy and classical igneous petrology. Modern structural and geochronological studies are scarce and mainly focused on discrete areas of the WMM (*e.g.*, Rehamna, Jebilet, Göaida). As for U-Pb detrital zircon geochronology, the beginning of this work coincided with the first published studies on early Paleozoic rocks of the WMM (El Houicha et al., 2018; Ghienne et al., 2018; Letsch et al., 2018; Pérez-Cáceres et al., 2017).

This work is organized as a compendium of papers focused on the detrital zircon provenance analysis and paleogeographic reconstruction of the northern margin of Gondwana in the Moroccan Mesetas at pre-Variscan (Chapter II; Accotto et al., 2019, in press, submitted) and syn-/post-Variscan (Chapters III and IV; Accotto et al., 2020, 2021) times.

From a tectonic point of view, the Variscan structure of the WMM is relatively well known (although still far from fully understood) and seems to be rather simple. On the contrary, similar studies focused on the EMM are very scarce in comparison (Hoepffner, 1989, 1987). In particular, some inliers of the EMM record a clear polyphasic Variscan

evolution (*e.g.*, Debdou-Mekkam, Tazekka, Midelt), evidenced by a refolded Eo-Variscan pervasive foliation, that had not been previously investigated using modern structural approaches. Chapter III of this Thesis contains new structural data collected in the Debdou-Mekkam inliers. In this latter area, an extensive structural field work was carried out, complemented with detrital zircon geochronology, which allowed for the formulation of a new proposed tectonic evolution of the region (Accotto et al., 2020).

Finally, Chapter V summarizes the conclusions obtained in this Thesis and makes references to a few main issues suitable for future research in the Moroccan Mesetas.

Supplementary materials cited in this work are collected in the Appendix.

5. Methodologies

In order to achieve the aims described in the previous section, the following methodologies were applied:

- Detailed field structural work, including observations at the microscale (thin sections).
- U-Pb geochronology on detrital zircon grains from 46 samples (Table 1.1) of the Cambrian-Carboniferous succession of the Moroccan Mesetas (Figure 1.4). Zircon grains were extracted and imaged by standard procedures. Most of the analyses were carried out using laser ablation inductively coupled plasma mass spectrometry (LA-ICPMS) in the laboratory of the John de Laeter Centre (JdLC) of the Curtin University (Perth, Australia). Nevertheless, many detrital zircon grains were too small to be analyzed with this technique, therefore they were studied using sensitive high-resolution ion microprobe (SHRIMP; JdLC, Curtin University) or secondary ion mass spectrometry (SIMS; University of Edinburgh, UK).
- Hf analyses on selected samples characterized by peculiar detrital zircon populations; these analyses were carried out in the JdLC of the Curtin University.

Furthermore, part of this Thesis was carried out during two internships in foreign institutions:

- *Laboratoire de Géodynamique des Chaînes Anciennes*, Department of Geology of the Faculty of Science Ben M'sik, University Hassan II of Casablanca (Morocco).
- Colorado School of Mines, Golden (Colorado, USA).

The interaction with experts of these two institutions working on the tectonic evolution of the Variscan/Appalachian belt has been significant for the development of the interpretations proposed in this Ph.D. Thesis.

Table 1.1. List of the samples.

Sample	IGSN (IEACC)	Location (UTM, NDAS 83)			Lithology	Stratigraphic age	Analyses	
		Zone	Lat. (m N)	Long. (m E)			U-Pb	Hf
COASTAL BLOCK (CB in Figure 1.4; see chapters II.3 and IV)								
SKH1	0011	29S	3748316	678921	Quartzitic sandstone	Visean	LA-ICPMS and SHRIMP	X
BES1	0009	29S	3720500	674467	Quartzitic sandstone	Visean	LA-ICPMS	X
BES2	0010	29S	3724273	671847	Quartzitic sandstone	Famennian	LA-ICPMS	-
MAN1	0040	29S	3735681	3735681	Quartzitic sandstone	Early Ordovician	LA-ICPMS	-
TIFLET AREA (TIF in Figure 1.4; see chapter IV)								
TIF1	0016	29S	3752612	750380	Sandstone	Tournaisian	LA-ICPMS	X
TIF2	0017	29S	3752611	750354	Sandstone	Tournaisian	LA-ICPMS	X
OUED AKREUCH AREA (AKR in Figure 1.4; see chapter II.3)								
AKR1	0038	29S	3757672	704231	Quartzitic sandstone	Late Ordovician	LA-ICPMS	-
AKR2	0039	29S	3757780	704321	Quartzitic sandstone	Early Ordovician	LA-ICPMS	-
CENTRAL MASSIF (CM in Figure 1.4; see chapters II.3 and IV)								
ROM1	0012	29S	37122830	719745	Sandstone	Visean	LA-ICPMS and SHRIMP	-
AOU1	0013	29S	3736131	708680	Sandstone	Visean	LA-ICPMS and SIMS	-
EZ7	0037	29S	3683869	735286	Quartzitic sandstone	Early Devonian	LA-ICPMS and SIMS	-
EZ1	0032	29S	3682713	733796	Quartzitic sandstone	Late Ordovician	LA-ICPMS and SHRIMP	-
EZ2	0033	29S	3682624	733776	Quartzitic sandstone	Late Ordovician	LA-ICPMS	-
EZ5	0035	29S	3682849	737554	Quartzitic sandstone	Late Ordovician	LA-ICPMS	-
EZ6	0036	29S	3684150	739164	Quartzitic sandstone	Late Ordovician	LA-ICPMS	-
EZ4	0034	29S	3682341	737693	Quartzitic sandstone	Late-Mid. Ordovician	LA-ICPMS	-
OULMES AREA (OU in Figure 1.4; see chapters II.3 and IV)								
OU1	0014	30S	3731845	244382	Sandy shale	Late Visean	LA-ICPMS	-
OU4	0015	29S	3716170	777438	Quartzitic sandstone	Famennian	LA-ICPMS	-
OU5	0031	29S	3715910	777396	Sandstone	Early Devonian	LA-ICPMS	-
KHENIFRA AREA (KH in Figure 1.4; see chapter II.3)								
AZR10	0029	30S	3633628	233758	Quartzitic sandstone	Early-Mid. Ordovician	LA-ICPMS	X
AZR11	0030	30S	3643326	252046	Sandstone	Cambrian-Ordovician	LA-ICPMS and SIMS	-
AZROU AREA (AZR in Figure 1.4; see chapters II.1 and II.3)								
AZR7	0028	30S	3695342	271772	Quartzitic sandstone	Early Devonian	LA-ICPMS	-
AZR6	0027	30S	269001	3690998	Quartzitic sandstone	Devonian	LA-ICPMS	-

Table 1.1 (continues).

Sample	IGSN (IEACC)	Location (UTM, NDAS 83)			Lithology	Stratigraphic age	Analyses	
		Zone	Lat. (m N)	Long. (m E)			U-Pb	Hf
AZROU AREA (AZR in Figure 1.4; see chapters II.1 and II.3)								
AZR5	0026	30S	268951	3692089	Quartzitic sandstone	Devonian	LA-ICPMS	-
AZR4	0025	30S	267866	3692882	Quartzitic sandstone	Devonian	LA-ICPMS	-
AZR2	0024	30S	296820	3705220	Quartzitic sandstone	Late Ordovician	LA-ICPMS	-
AZR1	0023	30S	3821747	574362	Quartzitic sandstone	Late Ordovician	LA-ICPMS and SIMS	-
SEFROU AREA (SF in Figure 1.4; see chapter II.2)								
SF1	0006	30S	321855	3746816	Quartzitic sandstone	Late Ordovician	LA-ICPMS	-
SF2	0007	30S	321334	3747211	Quartzitic sandstone	Early-Mid. Ordovician	LA-ICPMS and SIMS	-
SF3	0008	30S	320976	3747518	Quartzitic sandstone	Early-Mid. Ordovician	LA-ICPMS and SHRIMP	-
TAZEKKA AREA (TAZ in Figure 1.4; see chapter II.1)								
TAZ6	0044	30S	373058	3765756	Quartzitic sandstone	Silurian	LA-ICPMS	-
TAZ5	0043	30S	373058	3765756	Quartzitic sandstone	Silurian	LA-ICPMS	-
TAZ3	0042	30S	381775	3773906	Sandstone	Late Ordovician	LA-ICPMS and SHRIMP	-
TAZ2	0041	30S	380945	3774869	Sandstone	Late Ordovician	LA-ICPMS and SHRIMP	-
DEBDOU-MEKKAM AREA (D-M in Figure 1.4; see chapter III)								
MIM2	0004	30S	3763408	509359	Quartzitic sandstone	Famennian-Tournaisian	LA-ICPMS	-
DEB2	0005	30S	3754573	486535	Greywacke	Famennian-Tournaisian	LA-ICPMS	X
OUI13	0003	30S	3775692	533485	Quartzitic sandstone	Famennian-Tournaisian	LA-ICPMS	X
OUI11	0002	30S	3764944	536550	Arkose	Famennian-Tournaisian	LA-ICPMS	X
OUI10	0001	30S	3764944	536550	Arkose	Famennian-Tournaisian	LA-ICPMS	X
OUJDA AREA (OUJ in Figure 1.4; see chapters II.1, II.3, III, and IV)								
OUI18	0019	30S	3796505	587288	Sandstone	Late Carbonif.	LA-ICPMS and SIMS	X
OUI19	0020	30S	3796474	587262	Sandstone	Late Carbonif.	LA-ICPMS	X
OUI16	0018	30S	3796135	587342	Sandstone	Middle Carbonif.	LA-ICPMS	X
OUI2	0045	30S	582303	3834439	Quartzitic sandstone	Late Ordovician	LA-ICPMS	-
OUI3	0046	30S	582303	3834439	Arkose	Late Ordovician	LA-ICPMS	-
OUI5	0021	30S	3821747	574362	Greywacke	Early-Mid. Ordovician	LA-ICPMS	-
OUI6	0022	30S	3821747	574362	Greywacke	Early-Mid. Ordovician	LA-ICPMS	-

References

- Accotto, C., Martínez Poyatos, D., Azor, A., Jabaloy-Sánchez, A., Talavera, C., Evans, N.J., Azdimousa, A., 2020. Tectonic Evolution of the Eastern Moroccan Meseta: From Late Devonian Forearc Sedimentation to Early Carboniferous Collision of an Avalonian Promontory. *Tectonics* 39, 1–29. doi:10.1029/2019TC005976
- Accotto, C., Martínez Poyatos, D., Azor, A., Talavera, C., Evans, N.J., Jabaloy-Sánchez, A., Azdimousa, A., Tahiri, A., El Hadi, H., 2021. Syn-collisional detrital zircon source evolution in the northern Moroccan Variscides. *Gondwana Res.* 93, 73–88. doi:10.1016/j.gr.2021.02.001
- Accotto, C., Martínez Poyatos, D., Azor, A., Talavera, C., Evans, N.J., Jabaloy-Sánchez, A., El Hadi, H., Tahiri, A. (in press). Detrital zircon sources in the Ordovician metasedimentary rocks of the Moroccan Meseta: inferences for northern Gondwanan passive margin paleogeography. In: Kuiper, Y., Murphy, J.B., Nance, R.D., Strachan, R.A., Thompson, M.D. (Eds.), *New developments in the Appalachian-Caledonian-Variscan orogen*, GSA books, Special Publication
- Accotto, C., Martínez Poyatos, D., Azor, A., Talavera, C., Evans, N.J., Jabaloy-Sánchez, A., El Hadi, H., Tahiri, A., Azdimousa, A. (submitted). Systematics of detrital zircon grains from Cambrian-Lower Devonian rocks of the Moroccan Mesetas. *Earth Science Reviews*
- Accotto, C., Martínez Poyatos, D.J., Azor, A., Talavera, C., Evans, N.J., Jabaloy-Sánchez, A., Azdimousa, A., Tahiri, A., El Hadi, H., 2019. Mixed and recycled detrital zircons in the Paleozoic rocks of the Eastern Moroccan Meseta: Paleogeographic inferences. *Lithos* 338–339, 73–86. doi:10.1016/j.lithos.2019.04.011
- Allary, A., Lavenue, A., Ribeyrolles, M., 1976. Étude tectonique et microtectonique d'un segment de chaîne hercynienne dans la partie sud-orientale du Maroc central. *Notes du Serv. géologique du Maroc* 261, 169.
- Baudin, T., Chèvremont, P., Razin, P., Youbi, N., Andries, D., Hoepffner, C., Thiéblemont, D., Chihani, E.M., Tegye, M., 2003. Carte géologique du Maroc 1/50.000, feuille 435bis Skhour des Rehamna. *Mémoire explicatif. Notes Mem. du Serv. Géologique du Maroc.*
- Bea, F., Montero, P., Haissen, F., Molina, J.F., Lodeiro, F.G., Mouttaqi, A., Kuiper, Y.D., Chaib, M., 2020. The Archean to Late-Paleozoic architecture of the Oulad Dlim Massif, the main Gondwanan indenter during the collision with Laurentia. *Earth-Science Rev.* 103273. doi:10.1016/j.earscirev.2020.103273
- Becker, R.T., El Hassani, A., 2020. Devonian to Lower Carboniferous stratigraphy and facies of the Moroccan Meseta: implications for palaeogeography and structural Interpretation - a project outline. *Front. Sci. Eng.* 10, 9–25.
- Ben Abbou, M., Soula, J.-C., Brusset, S., Roddaz, M., N'Tarmouchant, A., Driouch, Y., Christophoul, F., Bouadbelli, M., Majesté-Menjoulas, C., Béziat, D., Debat, P., Déramond, J., 2001. Contrôle tectonique de la sédimentation dans le système de bassins d'avant-pays de la Meseta marocaine. *Comptes Rendus l'Académie des Sci. - Ser. IIA - Earth Planet. Sci.* 332, 703–709. doi:10.1016/S1251-8050(01)01590-7

- Berkhli, M., Vachard, D., Paicheler, J.-C., Tahiri, A., 1999. Séries volcano-sédimentaires du Carbonifère inférieur du Maroc oriental: datation, composition et implication structurale. *Comptes Rendus l'Académie des Sci. - Ser. IIA - Earth Planet. Sci.* 329, 89–94. doi:10.1016/S1251-8050(99)80209-2
- Bernardin, C., Cornée, J.J., Corsini, M., Mayol, S., Muller, J., Tayebi, M., 1988. Variations d'épaisseur du Cambrien moyen en Meseta marocaine occidentale: signification géodynamique des données de surface et de subsurface. *Can. J. Earth Sci.* 25, 2104–2117.
- Bouabdelli, M., 1989. Tectonique et sédimentation dans un bassin orogénique: le sillon viséen d'Azrou-Khenifra (Est du Massif Hercynien Central du Maroc). U.E.R. de Sciences de la vie et de la Terre, Strasbourg, France.
- Cailleux, Y., Deloche, C., Gonord, H., Zouine, E.M., 1986. Synthèse sur le volcanisme permien du Maroc. Son insertion dans le contexte géodynamique Ouest Méditerranéen, in: 111ème Congrès Des Sociétés Savantes. Poitiers, pp. 221–235.
- Chakiri, S., 2002. Sédimentologie et géodynamique du Maroc central hercynien pendant le Dévonien. State Thesis, University of Kénitra, Morocco.
- Chalot-Prat, F., 1990. Pétrogénèse d'un volcanisme intracontinental tardi-orogénique hercynien. Étude du complexe volcanique du Tazzeke et des zones volcaniques comparables dans le Mekkam et la région de Jerada (Maroc oriental). Université Paris-6.
- Chopin, F., Corsini, M., Schulmann, K., El Houicha, M., Ghienne, J.-F., Edel, J.-B., 2014. Tectonic evolution of the Rehamna metamorphic dome (Morocco) in the context of the Alleghanian-Variscan orogeny. *Tectonics* 33, 1154–1177. doi:10.1002/2014TC003539
- Clauer, N., Jeannette, D., Tisserant, D., 1980. Datation isotopique des cristallisations successives d'un socle cristallin et cristallophyllien (Haute Moulouya, Moyen Maroc). *Geol. Rundschau* 69, 63–83. doi:10.1007/BF01869024
- Cornée, J.J., 1989. Le Haut Atlas occidental paléozoïque: un reflet de l'histoire hercynienne du Maroc occidental. State Thesis, University of Marseille, France.
- Cornée, J.J., Costagliola, C., Leglise, H., Willefert, S., Destombe, J., 1985. Précisions stratigraphiques sur l'Ordovicien supérieur et le Silurien d'Oulad Abbou (Meseta marocaine occidentale). Manifestations volcaniques au Silurien. *Ann. la Société Géologique du Nord. Lille CIV*, 141–146.
- Cornée, J.J., Destombe, J., Willefert, S., 1987a. Stratigraphie du Paléozoïque de l'extrémité nord-ouest du Haut Atlas occidental (Maroc hercynien); interprétation du cadre sédimentaire du Maroc occidental. *Bull. la Soc. Géologique Fr.* 2, 327–335.
- Cornée, J.J., Ferrandini, J., Muller, J., Simon, B., 1987b. Le Haut Atlas occidental paléozoïque: un graben cambrien moyen entre deux décrochements dextres N60oE hercyniens (Maroc). *Comptes Rendus l'Académie des Sci. Paris* 305, 499–503.
- Delchini, S., Lahfid, A., Lacroix, B., Baudin, T., Hoepffner, C., Guerrot, C., Lach, P., Saddiqi, O., Ramboz, C., 2018. The Geological Evolution of the Variscan Jebilet Massif, Morocco, Inferred From New Structural and Geochronological Analyses.

- Desteucq, C., Izart, A., Potherat, P., 1988. Étude sédimentologique du Carbonifère du bassin de Jerada (Maroc oriental). *Ann. la Société Géologique du Nord. Lille CVII*, 203–210.
- Destombe, J., 1987. Carte géologique du Maroc No350: Casablanca-Mohammedia - Echelle 1/100.000. Roy. du Maroc, Ministère l’Energie des Mines du Développement Durable.
- Destombe, J., Jeannette, A., 1966. Mémoire explicatif de la carte géotechnique de la Meseta côtière à l’Est de Casablanca. Régions de Mohammedia, Bouznika et Ben Slimane. *Notes Mem. du Serv. Géologique du Maroc* 180, 104.
- Eddif, A., 2002. Géochronologie, pétrologie, géochimie et structure des intrusions tardi panafricaines de Wirane et de leur couverture néoprotérozoïque à paléozoïque (Haut Atlas occidental, Maroc). Ph.D. Thesis, University of Rabat, Morocco.
- El Attari, A., Pereira, M.F., Ezzouhairi, H., El Houicha, M., Jouhari, A., Berrada, I., Fekkak, A., Ennih, N., Hoepffner, C.H., Gama, C., Silva, J.B., 2019. Zircon U-Pb geochronology and geochemistry of Cambrian magmatism in the Coastal Block (Oued Rhebar volcanic complex, Moroccan Meseta): Implications for the geodynamic evolutionary model of North-Gondwana. *J. African Earth Sci.* 160, 103598. doi:10.1016/j.jafrearsci.2019.103598
- El Ghazi, O., Huvelin, P., 1981. Présence d’un olistostrome dans le Viséen supérieur volcano-sédimentaire de Tannecherfi (Maroc oriental). Simultanéité de la resédimentation et de l’activité volcanique. *Comptes Rendus l’Académie des Sci. Paris* 292, 91–96.
- El Hadi, H., Simancas, J.F., Tahiri, A., González-Lodeiro, F., Azor, A., Martínez-Poyatos, D., 2006a. Comparative review of the Variscan granitoids of Morocco and Iberia: Proposal of a broad zonation. *Geodin. Acta* 19, 103–116. doi:10.3166/ga.19.103-116
- El Hadi, H., Tahiri, A., Simancas Cabrera, F., González Lodeiro, F., Azor Pérez, A., Jesús Martínez Poyatos, D., 2006b. An example of calc-alkaline, orogenic-type volcanism emplaced in a rift setting (Cambrian of Oued Rhebar, western Meseta, Morocco). *Comptes Rendus - Geosci.* 338, 229–236. doi:10.1016/j.crte.2005.12.006
- El Haïbi, H., El Hadi, H., Pesquera, A., Tahiri, A., Martínez Poyatos, D., Zahour, G., Mehdioui, S., Tahiri, M., 2021. Geochemical and Sr–Nd isotopic constraints on the petrogenesis of the Tiflet granitoids (Northwestern Moroccan Meseta): geological implications. *J. Iber. Geol.* doi:10.1007/s41513-020-00156-7
- El Haïbi, H., El Hadi, H., Tahiri, A., Martínez Poyatos, D., Gasquet, D., Pérez-Cáceres, I., González Lodeiro, F., Mehdioui, S., 2020. Geochronology and isotopic geochemistry of Ediacaran high-K calc-alkaline felsic volcanism: An example of a Moroccan perigondwanan (Avalonian?) remnant in the El Jadida horst (Mazagonia). *J. African Earth Sci.* 163, 103669. doi:10.1016/j.jafrearsci.2019.103669
- El Hassani, A., 1990. La bordure nord de la chaîne hercynienne du Maroc: la chaîne “calédonienne” des Sehoul et plate-forme nord mésétienne. State Thesis,

University of Strasbourg, France.

- El Houicha, M., Pereira, M.F., Jouhari, A., Gama, C., Ennih, N., Fekkak, A., Ezzouhairi, H., El Attari, A., Silva, J.B., 2018. Recycling of the Proterozoic crystalline basement in the Coastal Block (Moroccan Meseta): New insights for understanding the geodynamic evolution of the northern peri-Gondwanan realm. *Precambrian Res.* 306, 129–154. doi:10.1016/j.precamres.2017.12.039
- El Kamel, F., Remmal, T., Mohsine, A., 1998. Mise en évidence d'un magmatisme alcalin d'intraplaque post-calédonien dans le bassin silurien des Ouled Abbou (Meseta côtière, Maroc). *Comptes Rendus l'Académie des Sci. Paris, Earth Planet. Sci.* 327, 309–314.
- El Wartiti, M., 1990. Le Permien du Maroc mésétien: étude géologique et implications paléogéographiques. Ph.D. Thesis, Université Mohammed V, Rabat.
- El Wartiti, M., Broutin, J., Freytet, P., Larhrib, M., Toutin-Morin, N., 1990. Continental deposits in Permian basins of the Mesetian Morocco, geodynamic history. *J. African Earth Sci. (and Middle East)* 10, 361–368. doi:10.1016/0899-5362(90)90067-O
- Erraji, A., 1997. Analyse des terrains carbonifères de la région de Jerada (Maroc oriental) à partir des données de terrain, de forage et de sismique réflexion. 3rd cycle Thesis, Univeristy of Rabat, Morocco.
- Essamoud, R., Courel, L., 1998. Séries charbonneuses dans des séquences rétrogradantes: cas du bassin houiller paraliqwestphalien de Jérada (Maroc). *Comptes Rendus l'Académie des Sci. - Ser. IIA - Earth Planet. Sci.* 326, 885–892. doi:10.1016/S1251-8050(98)80028-1
- Fadli, D., 1990. Evolution sédimentaire et structurale des massifs de Mdakra et du Khatouat: deux segments hercyniens de la Meseta marocaine nord-occidentale. Ph.D. Thesis, Université Mohammed V, Rabat.
- Franke, W., Cocks, L.R.M., Torsvik, T.H., 2017. The Palaeozoic Variscan oceans revisited. *Gondwana Res.* 48, 257–284. doi:10.1016/j.gr.2017.03.005
- Franke, W., Dulce, J.-C., 2017. Back to sender: tectonic accretion and recycling of Baltica-derived Devonian clastic sediments in the Rheno-Hercynian Variscides. *Int. J. Earth Sci.* 106, 377–386. doi:10.1007/s00531-016-1408-y
- Gärtner, A., Villeneuve, M., Linnemann, U., El Archi, A., Bellon, H., 2013. An exotic terrane of Laurussian affinity in the Mauritanides and Souttoufides (Moroccan Sahara). *Gondwana Res.* 24, 687–699. doi:10.1016/j.gr.2012.12.019
- Ghienne, J.F., Benvenuti, A., El Houicha, M., Girard, F., Kali, E., Khoukhi, Y., Langbour, C., Magna, T., Míková, J., Moscariello, A., Schulmann, K., 2018. The impact of the end-Ordovician glaciation on sediment routing systems: A case study from the Meseta (northern Morocco). *Gondwana Res.* 63, 169–178. doi:10.1016/j.gr.2018.07.001
- Hoepffner, C., 1977. Données nouvelles sur le Paléozoïques de la bordure occidentale du massif du Tazekka. *Comptes Rendus l'Académie des Sci. Paris* 284, 1635–1637.
- Hoepffner, C., 1981. Le complexe volcano-sédimentaire d'âge carbonifère dans le

- massif du Tazekka, sa place dans l'évolution hercynienne de la Méséta marocaine orientale. *Sci. Géologiques, Bull. mémoires* 34, 97–106.
- Hoepffner, C., 1987. La tectonique hercynienne dans l'Est du Maroc. Université Louis Pasteur, Strasbourg.
- Hammoumi, N., 1988. La plate-forme ordovicienne du Maroc; dynamique des ensembles sédimentaires. State Thesis, University of Strasbourg, France.
- Hoepffner, C., 1989. L'évolution structurale hercynienne de la Méséta marocain orientale. Essai de mise au point. Notes Mem. du Serv. Géologique du Maroc.
- Hoepffner, C., Houari, M.R., Bouabdelli, M., 2006. Tectonics of the North African Variscides (Morocco, western Algeria): An outline. *Comptes Rendus - Geosci.* 338, 25–40. doi:10.1016/j.crte.2005.11.003
- Hoepffner, C., Soulaïmani, A., Piqué, A., 2005. The Moroccan Hercynides. *J. African Earth Sci.* 43, 144–165. doi:10.1016/j.jafrearsci.2005.09.002
- Hollard, H., Michard, A., Jenny, P., Hoepffner, C., Willefert, S., 1982. Stratigraphie du Primaire de Mechraa ben Abbou (Rehamna). Notes Mem. du Serv. Géologique du Maroc 303, 13–34.
- Houari, M.R., Hoepffner, C., 2000. Structures des terrains paléozoïques à la limite sud de la chaîne hercynienne du Maroc: Haut Atlas oriental. *Africa Geosci. Rev.* 7, 39–53.
- Houari, M.R., Hoepffner, C., 2003. Late Carboniferous dextral wrench-dominated transpression along the North African craton margin (Eastern High-Atlas, Morocco). *J. African Earth Sci.* 37, 11–24. doi:10.1016/S0899-5362(03)00085-X
- Huon, S., Piqué, A., Clauer, N., 1987. Étude de l'orogénèse hercynienne au Maroc par la datation K-Ar de l'évolution métamorphique de schistes ardoisiers. *Sci. Géol. Bull.* 40, 273–284.
- Huvelin, P., 1986. Le Carbonifère du massif du Tazekka (Maroc): volcanisme et phénomènes de resédimentation. *Comptes Rendus l'Académie des Sci. Paris* 303, 1483–1488.
- Huvelin, P., Mamet, B., 1989. Essai de datation des transgressions et des phénomènes de resédimentation dans le Viséen supérieur-Namurien du Maroc oriental. *Ann. la Société Géologique du Nord. Lille CVIII*, 59–67.
- Izart, A., 1991. Les bassins carbonifères de la Méséta marocaine, étude sédimentologique et approche du contexte structural. Part de la tectonique et de l'eustatisme. *Géologie Méditerranéenne* 18, 61–72. doi:10.3406/geolm.1991.1452
- Izart, A., Poty, E., Vieslet, J.L., 1989. Le Viséen de la boutonnière de Skoura. Notes Mem. du Serv. Géologique du Maroc 335, 67–76.
- Izart, A., Tahiri, A., El Boursoumi, A., Chevremont, P., 2001. Carte géologique du Maroc no 411: Bouqachmir - échelle 1/50.000. Roy. du Maroc, Ministère l'Energie des Mines du Développement Durable.
- Kroner, U., Hahn, T., Romer, R.L., Linnemann, U., 2007. The Variscan orogeny in the Saxo-Thuringian Zone -heterogenous overprint of Cadomian/Palaeozoic Peri-Gondwana crust, in: Linnemann, U., Nance, R.D., Kraft, P., Zulauf, G. (Eds.), *The*

Evolution of the Rheic Ocean: From Avaloniane-Cadomian Active Margin to Alleghenian-Variscan Collision. Geological Society of America, Special Paper, 423, pp. 153–172.

- Kuiper, Y.D., Michard, A., Ruellan, E., Holm-Denoma, C., Crowley, J.L., 2019. U-Pb zircon and monazite results from granite and charnockite from the Mazagan escarpment, offshore Morocco, in: GSA Abstracts with Programs, Vol. 51, No. 2.
- Lahfid, A., Baidder, L., Ouanaimi, H., Soulaïmani, A., Hoepffner, C., Farah, A., Saddiqi, O., Michard, A., 2019. From extension to compression: high geothermal gradient during the earliest Variscan phase of the Moroccan Meseta; a first structural and RSCM thermometric study. *Eur. J. Mineral.* 31, 695–713.
doi:10.1127/ejm/2019/0031-2882
- Le Goff, É., Guerrot, C., Maurin, G., Johan, V., Tegye, M., Ben Zerga, M., 2001. Découverte d'éclogites hercyniennes dans la chaîne septentrionale des Mauritanides (Afrique de l'Ouest). *Comptes Rendus l'Académie des Sci. - Ser. IIA - Earth Planet. Sci.* 333, 711–718. doi:10.1016/S1251-8050(01)01694-9
- Letsch, D., El Houicha, M., von Quadt, A., Winkler, W., 2018. A missing link in the peri-Gondwanan terrane collage: The Precambrian basement of the Moroccan Meseta and its lower Paleozoic cover. *Can. J. Earth Sci.* 55, 33–51.
doi:10.1139/cjes-2017-0086
- Linnemann, U., Herbosch, A., Liégeois, J.P., Pin, C., Gärtner, A., Hofmann, M., 2012. The Cambrian to Devonian odyssey of the Brabant Massif within Avalonia: A review with new zircon ages, geochemistry, Sm-Nd isotopes, stratigraphy and palaeogeography. *Earth-Science Rev.* 112, 126–154.
doi:10.1016/j.earscirev.2012.02.007
- Marhoumi, M.R., 1984. Etude palynologique des séries dinantiennes de la Méséta marocaine. Conséquences stratigraphiques et structurales. Université Louis Pasteur, Strasbourg.
- Marhoumi, M.R., Hoepffner, C., Doubinger, J., Rauscher, R., 1983. Données nouvelles sur l'histoire hercynienne de la Meseta orientale au Maroc: l'âge dévonien des schistes de Debdou et du Mekkam. *Comptes Rendus l'Académie des Sci. Paris* 297, 69–72.
- Martínez Catalán, J.R., Díaz García, F., Arenas, R., Abati, J., Castiñeiras, P., González Cuadra, P., Gómez Barreiro, J., Rubio Pascual, F., 2002. Thrust and Detachment systems in the Ordenes Complex (northwestern Spain): implications for the Variscan-Appalachian geodynamics, in: Martínez Catalán, J.R., Hatcher Jr., R.D., Arenas, R., Díaz García, F. (Eds.), *Variscan-Appalachian Dynamics: The Building of the Late Paleozoic Basement*. Geological Society of America, Special Paper 364, pp. 163–182.
- Matte, P., 2001. The Variscan collage and orogeny (480-290 Ma) and the tectonic definition of the Armorica microplate: a review. *Terra Nov.* 13, 122–128.
doi:10.1046/j.1365-3121.2001.00327.x
- Mayol, S., Muller, J., 1985. Mise en évidence d'une unité allochtone hercynienne précoce (antéschisteuse) dans les Jebilet occidentales (Maroc). *Comptes Rendus l'Académie des Sci. Paris* 300, 369–372.

- Médioni, R., 1980. Mise au point stratigraphique sur les terrains carbonifères de la bordure septentrionale des Hauts-Plateaux marocains (Massif de Debdou, boutonnières de Lalla-Mimouna et du Mekam). Notes du Serv. géologique du Maroc 285, 25–37.
- Michard, A., Ouanaimi, H., Hoepffner, C., Soulaïmani, A., Baidder, L., 2010a. Comment on Tectonic relationships of Southwest Iberia with the allochthons of Northwest Iberia and the Moroccan Variscides by J.F. Simancas et al. [C. R. Geoscience 341 (2009) 103-113]. Comptes Rendus - Geosci. 342, 170–174. doi:10.1016/j.crte.2010.01.008
- Michard, A., Soulaïmani, A., Hoepffner, C., Ouanaimi, H., Baidder, L., Rjimati, E.C., Saddiqi, O., 2010b. The South-Western Branch of the Variscan Belt: evidence from Morocco. Tectonophysics 492, 1–24. doi:10.1016/j.tecto.2010.05.021
- Michard, A., Yazidi, A., Benziane, F., Willefert, S., 1982. Foreland thrusts and olistromes on the pre-Sahara margin of the Variscan orogen, Morocco. Geology 10, 253–256. doi:10.1130/0091-7613(1982)10<253:FTAOOT>2.0.CO;2
- Mohsine, A., 2002. L'évolution volcano-tectonique dans le Paléozoïque de la Meseta côtière et des Rehamna. L'exemple du bassin cambro-ordovicien de Sidi Saïd Maâchou, du bassin silurien des Oulad Abbou et du bassin viséen de Mechraâ Ben Abbou. Approche pétrographique, géoqu. Ph.D. Thesis, Université Mohammed V de Rabat.
- Nance, R.D., Gutiérrez-Alonso, G., Keppie, J.D., Linnemann, U., Murphy, J.B., Quesada, C., Strachan, R.A., Woodcock, N.H., 2012. A brief history of the Rheic Ocean. Geosci. Front. 3, 125–135. doi:10.1016/j.gsf.2011.11.008
- Nance, R.D., Gutiérrez-Alonso, G., Keppie, J.D., Linnemann, U., Murphy, J.B., Quesada, C., Strachan, R.A., Woodcock, N.H., 2010. Evolution of the Rheic Ocean. Gondwana Res. 17, 194–222. doi:10.1016/j.gr.2009.08.001
- Nance, R.D., Murphy, J.B., Keppie, J.D., 2002. A Cordilleran model for the evolution of Avalonia. Tectonophysics 352, 11–31. doi:10.1016/S0040-1951(02)00187-7
- Ouabid, M., Garrido, C.J., Ouali, H., Harvey, J., Hidas, K., Marchesi, C., Acosta-Vigil, A., Dautria, J., El Messbahi, H., Román-Alpiste, M.J., 2020. Late Cadomian rifting of the NW Gondwana margin and the reworking of Precambrian crust – evidence from bimodal magmatism in the early Paleozoic Moroccan Meseta. Int. Geol. Rev. 00, 1–24. doi:10.1080/00206814.2020.1818301
- Ouabid, M., Ouali, H., Garrido, C.J., Acosta-Vigil, A., Román-Alpiste, M.J., Dautria, J.M., Marchesi, C., Hidas, K., 2017. Neoproterozoic granitoids in the basement of the Moroccan Central Meseta: Correlation with the Anti-Atlas at the NW paleo-margin of Gondwana. Precambrian Res. 299, 34–57. doi:10.1016/j.precamres.2017.07.007
- Ouali, H., Briand, B., Bouchardon, J.-L., Capiez, P., 2003. Le volcanisme cambrien du Maroc central: implications géodynamiques. Comptes Rendus Geosci. 335, 425–433. doi:10.1016/S1631-0713(03)00064-6
- Ouali, H., Briand, B., Bouchardon, J.-L., El Maâtaoui, M., 2000. Mise en évidence d'un volcanisme alcalin intraplaque d'âge Acadien dans la Meseta nord-occidentale (Maroc). Comptes Rendus l'Académie des Sci. - Ser. IIA - Earth Planet. Sci. 330,

611–616. doi:10.1016/S1251-8050(00)00166-X

- Pereira, M.F., El Houicha, M., Chichorro, M., Armstrong, R., Jouhari, A., El Attari, A., Ennih, N., Silva, J.B., 2015. Evidence of a Paleoproterozoic basement in the Moroccan Variscan Belt (Rehamna Massif, Western Meseta). *Precambrian Res.* 268, 61–73. doi:10.1016/j.precamres.2015.07.010
- Pérez-Cáceres, I., Martínez Poyatos, D., Simancas, J.F., Azor, A., 2017. Testing the Avalonian affinity of the South Portuguese Zone and the Neoproterozoic evolution of SW Iberia through detrital zircon populations. *Gondwana Res.* 42, 177–192. doi:10.1016/j.gr.2016.10.010
- Piqué, A., 1979. Évolution structurale d'un segment de la chaîne hercynienne: la Meseta marocaine nord-occidentale. Ph.D. Thesis, Université de Strasbourg.
- Piqué, A., 2003. Evidence for an important extensional event during the Latest Proterozoic and Earliest Paleozoic in Morocco. *Comptes Rendus Geosci.* 335, 865–868. doi:10.1016/j.crte.2003.08.005
- Piqué, A., Bouabdelli, M., Darboux, J.-R., 1995. Le rift cambrien du Maroc occidental. *Comptes Rendus l'Académie des Sci. - Ser. IIA - Earth Planet. Sci.* 320, 1017–1024.
- Piqué, A., Jeannette, D., Michard, A., 1980. The Western Meseta Shear Zone, a major and permanent feature of the Hercynian belt of Morocco. *J. Struct. Geol.* 2, 55–61.
- Piqué, A., Michard, A., 1989. Moroccan Hercynides: a synopsis. The Paleozoic sedimentary and tectonic evolution at the northern margin of West Africa. *Am. J. Sci.* 289, 286–330.
- Rauscher, R., Marhoumi, M.R., Vanguetaine, M., Hoepffner, C., 1982. Datation palynologique des schistes du Tazekka au Maroc. Hypothèse structurale sur la socle hercynien de la Meseta orientale. *Comptes Rendus l'Académie des Sci. Paris* 294, 1203–1206.
- Remmal, T., Mohsine, A., El Hatimi, N., 2009. Mise en évidence de téphrites à néphéline syntectoniques dans le bassin cambrien de Sidi Saïd Maâchou (Meseta côtière, Maroc); signification géodynamique. *Estud. Geológicas* 65, 147–156. doi:10.3989/egol.39519.042
- Sacks, P.E., Secor, D.T., 1990. Kinematics of Late Paleozoic continental collision between Laurentia and Gondwana. *Science* (80-.). 250, 1702–1705. doi:10.1126/science.250.4988.1702
- Simancas, J.F., Azor, A., Martínez-Poyatos, D., Tahiri, A., El Hadi, H., González-Lodeiro, F., Pérez-Estaún, A., Carbonell, R., 2009. Tectonic relationships of Southwest Iberia with the allochthons of Northwest Iberia and the Moroccan Variscides. *Comptes Rendus Geosci.* 341, 103–113. doi:10.1016/j.crte.2008.11.003
- Simancas, J.F., Azor, A., Martínez-Poyatos, D., Tahiri, A., Hadi, H. El, González-Lodeiro, F., Pérez-Estaún, A., Carbonell, R., 2010. Reply to the comment by Michard et al. on “Tectonic relationships of Southwest Iberia with the allochthons of Northwest Iberia and the Moroccan Variscides.” *Comptes Rendus - Geosci.* 342, 175–177. doi:10.1016/j.crte.2010.01.007
- Simancas, J.F., Tahiri, A., Azor, A., Lodeiro, F.G., Martínez Poyatos, D.J., El Hadi, H.,

2005. The tectonic frame of the Variscan–Alleghanian orogen in Southern Europe and Northern Africa. *Tectonophysics* 398, 181–198.
doi:10.1016/j.tecto.2005.02.006
- Soualhine, S., Tejera de León, J., Hoepffner, C., 2003. Les faciès sédimentaires carbonifères de Tisdafine (Anti-Atlas oriental): remplissage deltaïque d'un bassin en "pull-apart" sur la bordure méridionale de l'Accident sud-atlasique. *Bull. l'Institut Sci. Rabat, Sect. Sci. la Terre* 25, 31–41.
- Tahiri, A., 1991. Le Maroc central septentrional: stratigraphie, sédimentologie et tectonique du Paléozoïque; un exemple de passage des zones internes aux zones externes de la chaîne Hercynienne du Maroc. Ph.D. Thesis, Université de Bretagne Occidentale, Brest, France.
- Tahiri, A., Hoepffner, C., 1988. Importance des mouvements distensifs au Dévonien supérieur en Meseta nord-occidentale (Maroc); les calcaires démantelés de Tiliouine et la ride d'Oulmès, prolongement oriental de la ride des Zaer. *Comptes Rendus l'Académie des Sci. Paris* 306, 223–226.
- Tahiri, A., Montero, P., El Hadi, H., Martínez Poyatos, D., Azor, A., Bea, F., Simancas, J.F., González Lodeiro, F., 2010. Geochronological data on the Rabat-Tiflet granitoids: their bearing on the tectonics of the Moroccan Variscides. *J. African Earth Sci.* 57, 1–13. doi:10.1016/j.jafrearsci.2009.07.005
- Termier, H., 1936. Etude géologique sur le Maroc central et le Moyen Atlas septentrional. *Notes Mem. du Serv. Géologique du Maroc* 33, 1566.
- Torbi, A., 1996. Stratigraphie et évolution structurale paléozoïque d'un segment de la Meseta orientale marocaine (Monts du Sud-Est d'Oujda): rôle des décrochements dans la formation de l'olistostrome intraviséen et le plutonisme tardi-hercynien. *J. African Earth Sci.* 22, 549–563. doi:10.1016/0899-5362(96)00036-X
- Villeneuve, M., 2008. Review of the orogenic belts on the western side of the West African craton: The Bassarides, Rokelides and Mauritanides. *Geol. Soc. Spec. Publ.* 297, 169–201. doi:10.1144/SP297.8
- Wernert, P., Schulmann, K., Chopin, F., Štípská, P., Bosch, D., El Houicha, M., 2016. Tectonometamorphic evolution of an intracontinental orogeny inferred from P-T-t-d paths of the metapelites from the Rehamna massif (Morocco). *J. Metamorph. Geol.* 34, 917–940. doi:10.1111/jmg.12214
- Youbi, N., Cabanis, B., Chalot-Prat, F., Cailleux, Y., 1995. Histoire volcano-tectonique du massif permien de Khénifra (Sud-Est du Maroc Central). *Geodin. Acta* 8, 158–172. doi:10.1080/09853111.1995.11105387
- Zahraoui, M., 1991. La plate-forme carbonatée dévonienne du Maroc occidentale et sa dislocation hercynienne. UBO, Brest, France.

Chapter II

The pre-orogenic evolution of the Moroccan Mesetas

This chapter is focused on the geochronological analyses on detrital zircon grains from Cambrian-Early Devonian rocks of the Moroccan Meseta. This aim was achieved in three papers focused on (i) the first data from the Eastern Moroccan Meseta, (ii) the Ordovician evolution of sources in the Nappe Zone (Western Moroccan Meseta), and (iii) an extensive comparison of data from the two Mesetas showing the evolution of the sources since Late Cambrian to Early Devonian.

Section II.1

Mixed and recycled detrital zircons in the Paleozoic rocks of the Eastern Moroccan Meseta: paleogeographic inferences

Cristina Accotto¹, David Martínez Poyatos¹, Antonio Azor¹, Cristina Talavera^{2,3},
Noreen J. Evans^{3,4}, Antonio Jabaloy-Sánchez¹, Ali Azdimousa⁵, Abdelfatah Tahiri⁶,
Hassan El Hadi⁷

Published on:

Lithos, 2019

Volume 338-339, Pages 73-86

doi: 10.1016/j.lithos.2019.04.011

(Received: 22 January 2019; Accepted: 10 April 2019; Available online: 16 April 2019)

¹ Department of Geodynamics, University of Granada, Granada, Spain

² School of Geosciences, University of Edinburgh, Edinburgh, UK

³ John de Laeter Centre, Curtin University, Bentley, Australia

⁴ School of Earth and Planetary Science, John the Laeter Centre, Curtin University,
Perth, Australia

⁵ Faculté Pluridisciplinaire de Nador et Laboratoire des Géosciences Appliquées,
Faculté des Sciences, Université Mohammed I, Oujda, Morocco

⁶ Laboratoire Géo-biodiversité et Patrimoine Naturel (GEOBIO), Institut scientifique;
Geophysics, Natural Patrimony and Green ChemistResearch Center (GEOPAC),
Université Mohammed V, Rabat, Morocco

⁷ Faculté des Sciences Ben M'Sik, Université Hassan II, Casablanca, Morocco

Abstract

The paleogeographic evolution of the Moroccan Variscides has been a matter of discussion for several decades, with current theories mostly based on classical geological correlations. In this regard, the scarce number of studies devoted to U-Pb geochronological analyses of detrital zircon populations is particularly limiting when trying to ascribe the different domains to a single continental piece either derived from the West African Craton or to different sources, with some located in the Nubian Shield or the Saharan Metacraton. In this work, detrital zircon grains from 10 samples of sandstones from the Paleozoic (Ordovician to Devonian) sequence of the Eastern Meseta and Middle Atlas were dated in order to identify possible sediment sources and elucidate the paleogeography of this easternmost portion of the Moroccan Variscides. The main detrital zircon populations have Ediacaran-Cryogenian ages (610-670 Ma, related to the Cadomian and/or Pan-African orogeny) and middle Paleoproterozoic ages (1980-2080 Ma, related to the Eburnean orogeny), which are in agreement with previous data from the Western Meseta, suggesting similarity between both Mesetas, and strong West African Craton affinity. Such an affinity verifies the most accepted paleogeographic interpretation considering that the Moroccan Mesetas remained attached to northern Gondwana during the entire Paleozoic period. The main differences between our samples and those from the Western Meseta concern the minor detrital zircon populations, such as the Cambro-Ordovician and the Tonian-Stenian ones. In particular, Eastern Meseta and Middle Atlas samples lack a Cambro-Ordovician detrital zircon population, usually interpreted as related to the rifting that opened the Rheic Ocean. This population is locally reported in the Western Meseta and widely described in southwestern Europe, where magmatism of this age is well known. Furthermore, the most northeastern samples are also characterized by a Tonian-Stenian detrital zircon population (up to 30% of the data), which might imply northeastern African sources (Saharan Metacraton and/or Arabian-Nubian Shield).

Keywords

Eastern Moroccan Meseta, Paleozoic paleogeography, West African Craton, U-Pb geochronology, Zircon provenance

Highlights

- Ordovician-Devonian samples from Eastern Meseta and Middle Atlas were studied
- The main detrital zircon populations are Ediacaran-Cryogenian and Paleoproterozoic
- These detrital zircon populations suggest WAC affinity for the studied area
- The minor Tonian-Stenian population might be sourced in north-eastern Africa
- There is no evidence of the Cambro-Ordovician rifting in the studied region

1. Introduction

Zircon is a very common accessory mineral, formed in a wide range of magmatic and metamorphic rocks in orogenic crustal growth areas, and very commonly present in sedimentary detrital rocks, which combined with its strong physical and chemical endurance, make it a valuable tool for geochronological and paleogeographic studies (*e.g.*, Avigad et al., 2003; Fernández-Suárez et al., 2002; Linnemann et al., 2004). Detrital zircon grains in sedimentary rocks might have survived a number of sedimentary cycles, preserving primary source signatures. In addition, technological improvements in analytical methods (*e.g.*, LA-ICPMS, SHRIMP) have permitted a wide application of detrital zircon geochronology in paleogeographic and geodynamic reconstructions (*e.g.*, Fedo et al., 2003), carried out by comparing statistically meaningful detrital zircon age populations with those of possible source areas. This technique has been widely applied to Variscan terranes in central and southern Europe (*e.g.*, Braid et al., 2011; Fernández-Suárez et al., 2014; Linnemann et al., 2004, 2008; Pereira et al., 2017; Pérez-Cáceres et al., 2017; Shaw et al., 2014), but only a few works have focused on the Moroccan Meseta Variscides (ensemble of the Variscan domains cropping out in Morocco; *e.g.*, El Houicha et al., 2018; Ghienne et al., 2018; Letsch et al., 2018; Pérez-Cáceres et al., 2017).

A magmatic arc was active in the northern margin of the Gondwanan continent during Ediacaran times (*i.e.* Cadomian orogeny). Later, a new Wilson cycle began with the fragmentation of Gondwana during the Cambro-Ordovician rifting that preceded the opening of the Rheic Ocean and the drifting of Gondwana-derived terranes (Franke et al., 2017; Matte, 2001; Murphy et al., 2004; Nance et al., 2012). During the Devonian, subduction narrowed the Rheic Ocean, culminating in continental collision during Carboniferous times (Variscan-Alleghanian orogeny). On a broad scale, this collision involved the northern margin of Gondwana and the southern margin of Laurussia (already docked Gondwana-derived terranes, Laurentia and Baltica), leading to the assembly of the Pangea supercontinent (Franke et al., 2017; Matte, 2001; Nance et al., 2012).

The northwestern African Variscides are considered the southern termination of the Variscan Belt (Matte, 2001), and usually divided into six structural domains (Figure 2.1A; Hoepffner et al., 2006): (i) the Sehoul Block, or Caledonian block, characterized by a Caledonian tectonothermal imprint (Michard et al., 2010b; Simancas et al., 2005; Tahiri et al., 2010) and juxtaposed with the Moroccan Meseta domains along the Late-Variscan Rabat-Tiflet Fault Zone; (ii) the Coastal Block (considered the western part of the Western Meseta *s.l.*; Michard et al., 2010b), weakly deformed by the Variscan orogeny and limited to the east by the Western Meseta Shear Zone; (iii) the Central zone of the Western Meseta, deformed by fold and thrusts and bounded to the east by the so-called Nappe Zone and the Tazekka-Bsabis-Bekrit Fault Zone (TBBFZ), located in the Middle Atlas (Michard et al., 2010b); (iv) the Eastern Meseta domain, characterized by small and variably deformed Paleozoic outcrops; (v) the Southern Zone (Hoepffner et al., 2006; Michard et al. 2008), bounded to the north by the Atlas Paleozoic Transform Zone (APTZ) and to the south by the South Moroccan Variscan Front (SMF), which separates the Variscan domains from the almost undeformed Anti-Atlas foreland (Figure 2.1A);

and (vi) the Mauritanides belt (Villeneuve, 2008), located west of the West African Craton (WAC) and extending from southern Morocco to Senegal (not represented in Figure 2.1A).

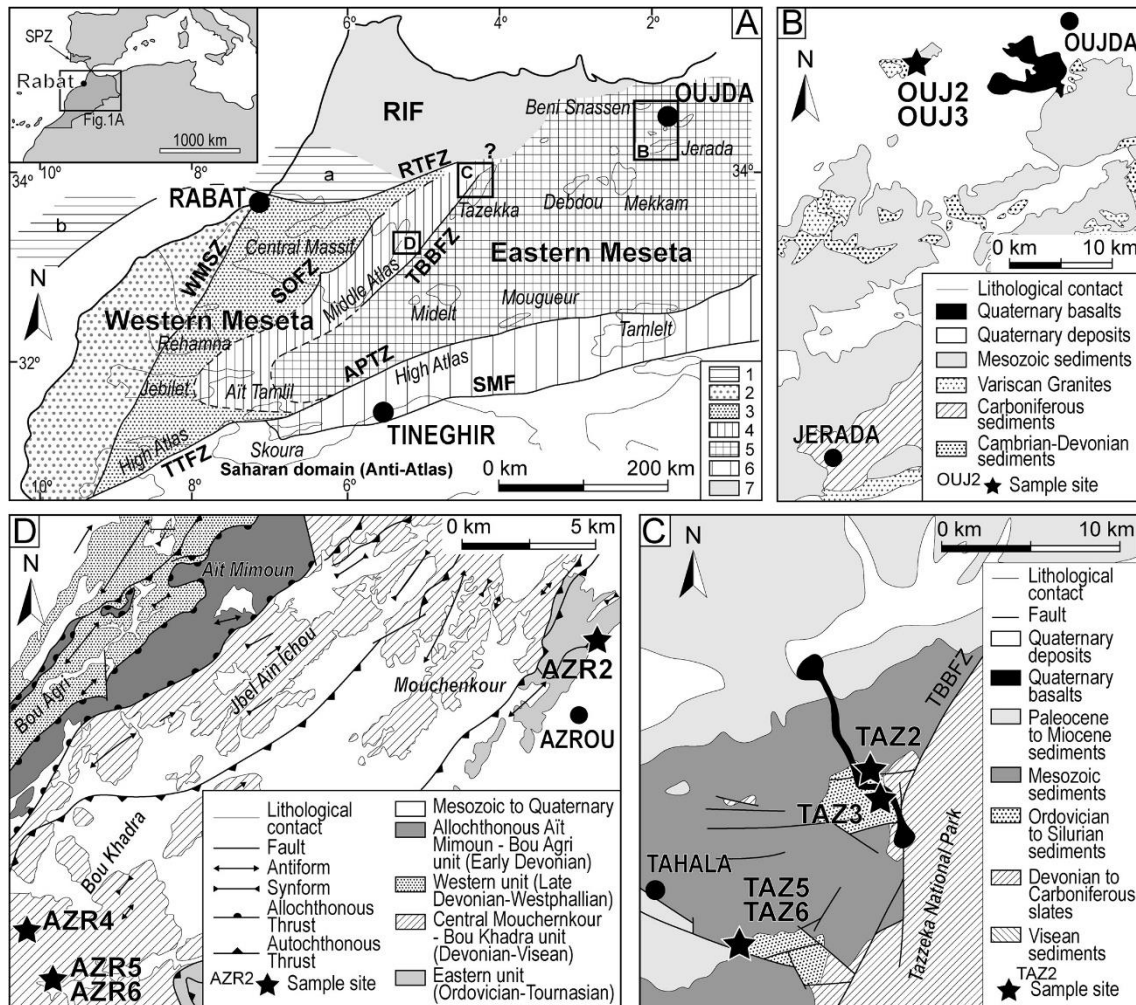


Figure 2.1. Geological maps of the northwestern African Variscides with sampling areas. (A) Structural domains (modified from Hoepffner et al., 2006; Michard et al., 2010b). 1: Sehou Block (a) and Mazagan escarpment (b); 2: Coastal Block; 3: Central zone; 4: Nappe Zone; 5: Eastern Meseta; 6: Southern Zone; 7: Rif Belt. Main structural features: Rabat-Tiflet Fault Zone (RTFZ); Western Meseta Shear Zone (WMSZ); Smaala-Oulmès Fault Zone (SOFZ); Tazekka-Bsabis-Bekrit Fault Zone (TBBFZ); Atlas Paleozoic Transform Zone (APTZ); South Moroccan Front (SMF); Tizin'Test Fault Zone (TTFZ); SPZ: South Portuguese Zone. Black boxes refer to the detailed geological sketches of the sampling areas: (B) Oujda area (after Kharbouch et al., 1989); (C) Tazekka area (after Vidal and Hoepffner, 1979); (D) Azrou area (after Bouabdelli et al., 1989).

The pre-Variscan paleogeographic evolution of the Moroccan Mesetas was studied by several authors (*e.g.*, El Hassani et al., 2003; Hoepffner et al., 2006; Michard, 1976; Michard et al., 1989, 2010a, 2010b; Piqué, 2001; Piqué and Michard, 1981, 1989; Simancas et al., 2005, 2009; Walliser et al. 1995, 2000), who suggested that they were part of the northern margin of Gondwana because of the stratigraphic similarity that they share with other autochthonous Gondwanan domains (*e.g.*, Anti-Atlas Variscan foreland; Figure 2.1A). Further evidence supporting this paleogeographic attribution is the absence of Variscan ophiolitic and/or high-pressure metamorphic rocks indicating the presence of

suture zones separating the Moroccan Meseta domains and the foreland (Michard et al., 2010a, 2010b; Simancas et al., 2009). From Cambrian to Devonian times, the entire region was a passive margin (Hoepffner et al., 2005, 2006; Michard et al., 2010b; Piqué, 2001) characterized, from a stratigraphic point of view, by mainly Cambrian-Silurian detrital sequences with some hiatuses, *e.g.*, the regression tied to the Late Ordovician glaciation (Le Heron, 2007; Le Heron et al., 2009). The stratigraphic sequences of the Moroccan Meseta domains began to differentiate during the Devonian, which is characterized by reefal platform facies in the Western Meseta, and by more basinal facies in the Eastern Meseta (Hoepffner et al., 2005, 2006; Michard et al., 2010b; Piqué, 2001). From a structural point of view and according to Michard et al. (2010b), the Moroccan Meseta domains were originally separated by narrow Early Paleozoic thinned-crust zones, probably related to incipient intra-continental rifting, which were later reactivated as shear zones during the Variscan orogeny. To the south, the Moroccan Meseta domains were separated from the Anti-Atlas foreland by a major intra-continental fault corresponding to the SMF, a polyphasic crustal-scale flower-structure characterized by dextral transpressive kinematics (Houari and Hoepffner, 2003) with a minimum offset of tens of kilometers (Michard et al., 2010b).

In this context where different domains are recognized, detrital zircon dates become a helpful tool to identify the main source areas of the sediments and, therefore, their paleogeographic affinities. In particular, the WAC affinity is usually characterized by Ediacaran-Cryogenian and Paleoproterozoic peaks, as well as a general Mesoproterozoic gap in the age distribution pattern. However, it must be noticed that detrital zircon populations of this age (1.0-1.5 Ga) were locally described by Bradley et al. (2015) in the Ediacaran clastic sequences unconformably overlying the western part of the WAC basement in Mauritania. The source of these Mesoproterozoic detrital zircons is unlikely the WAC basement, since primary sources of that age are unknown in the WAC, and relevant Mesoproterozoic detrital zircon populations have not been detected in Ediacaran/Paleozoic sediments located to the North of the WAC and derived from it (see below). Therefore, suitable sources for these Mesoproterozoic zircons could be the Amazonian basements adjoining western Gondwana at Ediacaran time.

In the Moroccan Variscides north of the WAC, most of the previous detrital zircon studies focused on Cambro-Ordovician and Precambrian sedimentary sequences from the Anti-Atlas (Abati et al., 2010; Avigad et al., 2012), Middle Atlas, Western Meseta and Coastal Block (El Houicha et al., 2018; Ghienne et al., 2018; Letsch et al., 2018), all of them having highlighted a strong WAC affinity. Very similar results were obtained on Triassic sandstones and siltstones of the High Atlas (Domènech et al., 2018; Marzoli et al., 2017) and Middle Atlas (Pratt et al., 2015). Furthermore, Avigad et al. (2012), Marzoli et al. (2017), and Ghienne et al. (2018) also identified, on Middle Cambrian sandstones and siltstones (Anti-Atlas), Late Triassic siltstones (High Atlas), and Late Ordovician sandstones (Middle Atlas) respectively, a minor 1.1-0.9 Ga detrital zircon population that they attributed to distal north-eastern African sources, probably located in the Precambrian basement of the Saharan Metacraton or the Arabian-Nubian Shield (Bea et al., 2010; Linnemann et al., 2011). In the Central zone of the Western Moroccan Meseta

(Figure 2.1A), an unimodal detrital zircon population centered around 488 Ma was recognized in a Lower Paleozoic greywacke (Letsch et al., 2018), and Late Cambrian granite boulders in a Devonian conglomerate were dated by Tahiri et al. (2017). These pieces of evidence suggest the presence of a nearby and unknown igneous Late Cambrian source. A few Cambro-Ordovician detrital zircon grains were also found in the Middle Atlas in Late Ordovician sandstones of the Tifarouine Formation (Ghienne et al., 2018) and in Middle Jurassic sandstones of the Bou Rached Formation (Pratt et al., 2015). These Cambro-Ordovician ages have been interpreted as evidence of magmatism related to the continental rifting that preceded the opening of the Rheic Ocean (*e.g.*, Cambeses et al., 2017; Nance et al., 2010, 2012). Finally, U-Pb zircon ages from Cambrian sandstones of the Sehoul Block (Pérez-Cáceres et al., 2017) also show main Ediacaran and Paleoproterozoic peaks, together with a very minor 1.1-0.9 Ga population and scattered Archean data, suggesting that this terrane was close to the Gondwana margin at Cambrian time.

Despite the new advances, the paleogeographic interpretation of the Moroccan Variscides is still a matter of debate and lacks data, in particular from the Paleozoic sedimentary sequences of the Eastern Meseta. In this paper we present the first U-Pb detrital zircon ages for Ordovician sedimentary rocks from the Eastern Meseta (Oujda area; Figure 2.1B) and new data from the Ordovician to Devonian sequence cropping out at the boundary between the Eastern and Western Mesetas (Middle Atlas: Tazekka and Azrou massifs; Figures 2.1C and D).

2. Geological setting

The Moroccan Mesetas (Figure 2.1A; Hoepffner et al., 2006) include scarce outcrops of Precambrian basement (mainly igneous Cadomian rocks) unconformably overlain by Cambro-Devonian sedimentary rocks (Chopin et al., 2014; El Houicha et al., 2018; Hoepffner et al., 2005; Letsch et al., 2018; Michard et al., 2008, 2010b; Ouabid et al., 2017; Pereira et al., 2015). The Precambrian basement does not crop out in the Eastern Meseta domain, where the Paleozoic sequence seems to be continuous from Late Cambrian to Devonian time, being unconformably overlaid by a Visean to Westphalian flysch with limestones and volcanic rocks (Hoepffner, 1987; Michard et al., 2010b). Several Variscan and post-Variscan (330-250 Ma) granitic plutons outcrop in the Moroccan Meseta domains, intruding the Paleozoic sequences (El Hadi et al., 2006 and references therein).

The Variscan deformation that characterizes the Eastern Meseta domain is variable in style and intensity and occurred under very low- to low-grade metamorphic conditions (Hoepffner et al., 2006 and references therein). According to these authors, the deformation is generally expressed by one or more folding phases associated with a cleavage that can be penetrative or locally spaced and poorly defined. Late Variscan fault zones delineate the current boundaries between the different domains of the Moroccan Mesetas.

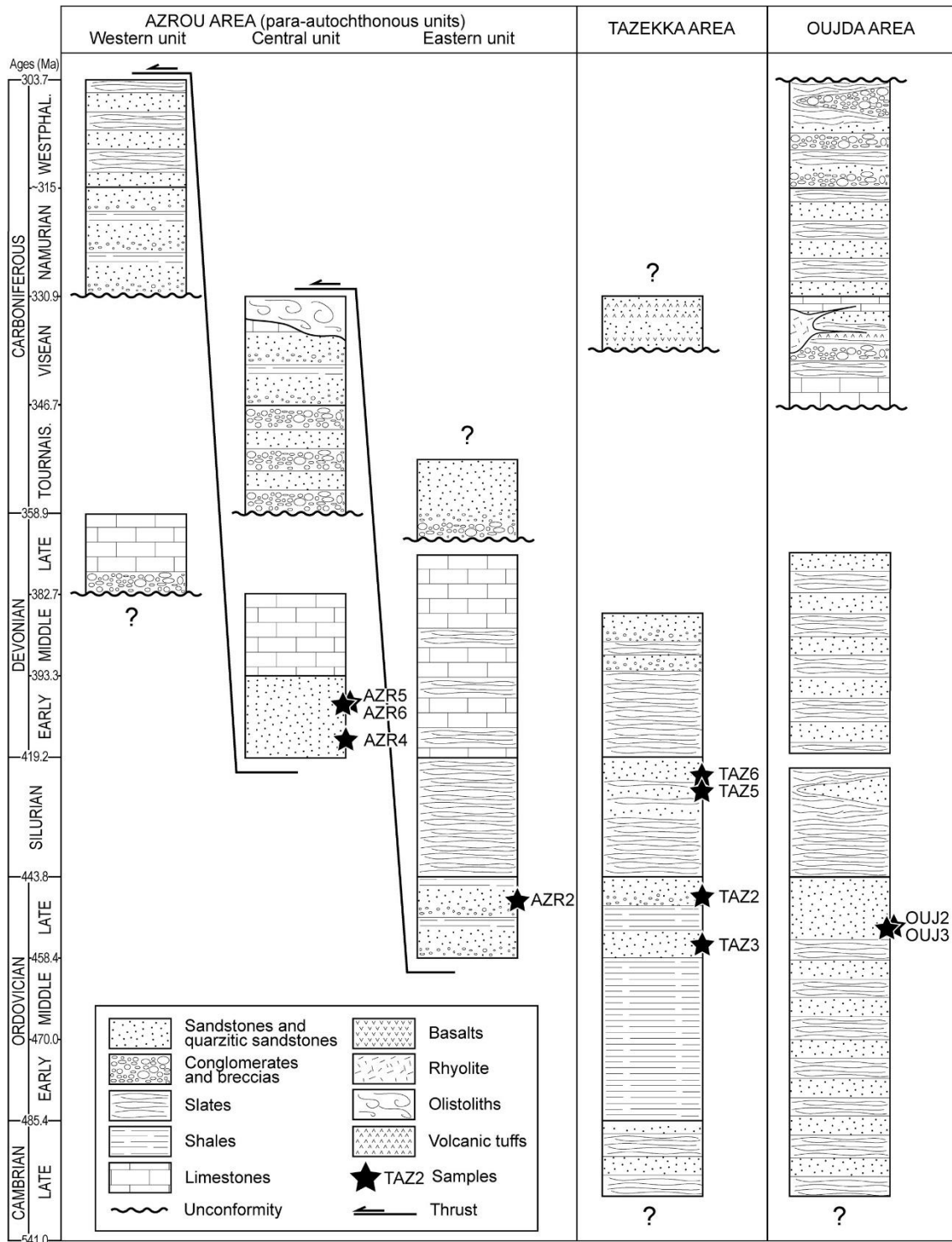


Figure 2.2. Schematic correlation of the stratigraphic columns from different Paleozoic outcrops of the Eastern Meseta and Middle Atlas (not to scale): Azrou area (Bouabdelli et al., 1989 and references therein), Tazekka area (Marhoumi et al., 1989 and references therein; Vidal and Hoepffner, 1979), and Oujda area (Choubert et al., 1978; Hoepffner, 1989; Horon, 1952; Marhoumi et al., 1989).

In the three sampled areas, the general Variscan structure consists on low- to moderate-dipping beds as a result of N-S (with variations from NW to NE) oriented upright folding and related rough axial-planar cleavage.

2.1. *Oujda area*

The Paleozoic sequence of the Eastern Meseta domain crops out in several relatively small areas in the Oujda region (Figures 2.1B and 2.2), where it is characterized by Cambro-Ordovician shales, slates, minor greywackes and quartzites, dated by stratigraphic correlations with neighboring regions (Huvelin, 1970; Valin, 1979). The Silurian is characterized by black shales with Graptolites and few intercalations of thin layers of fine-grained black sandstones (Horon, 1952). The upper limit of the Silurian is not exposed in this area. The Devonian sequence is an alternation of slates, greywackes and sandstones, dated as Emsian-Frasnian with palynomorphs (Marhoumi et al., 1983). The whole Cambrian-Devonian sequence attests a general subsidence episode which was interrupted by a Late Devonian-Early Carboniferous initial Variscan deformation phase responsible for the exhumation of at least part of the Moroccan Meseta (Hoepffner, 1989). The Viséan sedimentation is represented by turbidites associated with volcanic rocks (Hoepffner, 1989), whose age was assigned by facies analogy with similar deposits cropping out in the Debdou-Mekkam area palaeontologically dated by Marie (1931) and Marhoumi (1984).

2.2. *Tazekka area*

The Tazekka area is located in the northern part of the Middle Atlas, at the boundary between Eastern and Western Mesetas, corresponding with the TBBFZ (Figure 2.1C). The stratigraphic sequence outcropping east of the TBBFZ is characterized by homogeneous, low-grade, intensively deformed schists (Tazekka Schists), attributed to the Devonian-Carboniferous (Hoepffner, 1987 and references therein) by facies comparison with the Debdou-Mekkam area (Mekkam Schists), where they were dated with palynomorph (Medioni, 1980) and plant fragments (Marhoumi and Rauscher, 1984). West of the TBBFZ, a less deformed and less metamorphosed Late Cambrian to Middle Devonian detrital sequence that resembles the Oujda sequence crops out (Figure 2.2; Hoepffner, 1987). The sequence begins with Cambro-Ordovician slates and greywackes (dated by facies comparison with the Cambrian Paradoxides Shales of the Coastal Block; Hoepffner, 1987 and references therein), which turns upward into a thick sequence of green shales and slates dated as Lower-Middle Ordovician with fossils and palynolomorphs (Desteucq and Fournier-Vinas, 1981; Hoepffner, 1977; Rauscher et al., 1982). The Late Ordovician is characterized by sandy shales interbedded with quartzites (Tifarouine Fm.; Hoepffner, 1987; Huvelin, 1970; Khoukhi and Hamoumi, 2001; Valin, 1979), interpreted as glacial deposits (Le Heron, 2007). Similar to most of the Moroccan Variscides outcrops, the Silurian is represented by black shales with Graptolites (Destombe, 1971), and coarser beds in the upper part of the sequence (Hoepffner, 1977), gradually passing upwards to Devonian sandstones dated with palynomorphs (Marhoumi et al., 1983).

The sedimentation appears to have been interrupted during a Late Devonian-Tournaisian tectonic phase, and then started again during the Viséan, with a volcano-sedimentary succession; the age of these rocks was established by facies comparison with

similar rocks cropping out in the Debdou-Mekkam area and dated by palynology (Hoepffner, 1981; Marhoumi, 1984).

2.3. Azrou area

The Azrou area (Figure 2.1D) is located in the Middle Atlas, and it is characterized by the tectonic imbrication of three para-autochthonous units (Figure 2.2) and an allochthonous one (Bouabdelli et al., 1989). The age of the stratigraphic sequences cropping out in these units (Ordovician to Early Carboniferous) was established by means of palynomorphs and fossil micro- and macrofaunas (Bouabdelli, 1989 and references therein).

The eastern sector corresponds to the oldest and structurally highest para-autochthonous unit, and it is characterized by a stratigraphic sequence that includes Late Ordovician sandy sediments, rarely interbedded with shales (Bouabdelli, 1982), which passes upwards to the Silurian black shales with graptolites. The Devonian sequence is characterized by alternating slates and fossiliferous Late Devonian limestones. Tournaisian quartzitic deposits lay unconformably onto the Devonian limestones.

In the central sector, the sequence is detached at the level of the Silurian shales, which are overlain by Early Devonian quartzitic and sandy slates and Middle to Upper Devonian limestones (Walliser et al., 2000; Lazreq, 1999). The sedimentation was interrupted during Late Devonian time and started again at Early Carboniferous time with the deposition of quartzitic and conglomeratic beds, passing upwards to turbiditic and gravitational deposits (Bouabdelli et al., 1989; Berkhli, 1999; Berkhli et al., 2000).

In the western sector of the Azrou area, the structurally lowest para-autochthonous unit crops out, constituted by a basal conglomerate followed by Late Devonian limestones. A Middle Carboniferous flysch and limestones with crinoids (Bouabdelli et al., 1989; Dir. Geol. Maroc, 2005; Wollen, 1974) unconformably overlay the Late Devonian succession.

The allochthonous Aït Mimoun-Bou Agri unit of Early Devonian age is characterized by turbidites passing upwards to calcarenites and calcareous reef breccias with abundant fossiliferous material (Bouabdelli et al., 1989; Dir. Geol. Maroc, 2005; Said et al., 2010).

3. Samples and methods

This study is based on the results obtained on 10 samples collected in the Late Ordovician-Early Devonian siliciclastic rocks of the Oujda, Tazekka and Azrou areas. The geographic, geological and stratigraphic locations of each sample are shown in Figures 2.1 and 2.2, and Table 2.1.

OUI2 and OUI3 were collected 20 km westward from Oujda and they correspond to quartzites sampled in the upper part of the Ordovician sequence, just below Silurian beds of fine-grained black quartzites (according to the “Oujda” geological map scale 1:500.000; Choubert et al., 1978).

Table 2.1. Details of the analyses carried out on the zircon grains separated from the studied samples; (*) UTM coordinates, WGS84 system, zone 30 S; (**) total analyses carried out and total concordant results (bold numbers).

Area	Sample	Location*		Lithology	Age	Zircon grains	Type of analyses	Number analyses**
		X	Y					
Oujda	OIJ2	582303	3834439	Quartzite	Ordovician	123	LA-ICPMS	150/ 126
	OIJ3	582303	3834439	Arkose	Ordovician	124	LA-ICPMS	150/ 135
Tazekka	TAZ2	380945	3774869	Sandstone	Ordovician	79	LA-ICPMS SHRIMP	30/ 21 56/ 44
	TAZ3	381775	3773906	Sandstone	Ordovician	92	LA-ICPMS SHRIMP	54/ 45 48/ 41
	TAZ5	373058	3765756	Quartzite	Silurian	114	LA-ICPMS	150/ 136
	TAZ6	373058	3765756	Quartzite	Silurian	126	LA-ICPMS	150/ 115
Azrou	AZR2	296820	3705220	Quartzite	Late Ordovician	125	LA-ICPMS	150/ 131
	AZR4	267866	3692882	Quartzite	Devonian	121	LA-ICPMS	150/ 140
	AZR5	268951	3692089	Quartzite	Devonian	129	LA-ICPMS	149/ 143
	AZR6	269001	3690998	Quartzite	Devonian	131	LA-ICPMS	150/ 137

Four samples were collected close to the Tazekka National Park (Geological map "Tahala", scale 1:50.000; Vidal and Hoepffner, 1979) in the western block of the TBBFZ. Based on this geological map, samples TAZ2 and TAZ3 from Ahel Boudriss are Late Ordovician quartzites, while samples TAZ5 and TAZ6, collected 5 km south-east of Tahala, are Silurian quartzites.

Three samples (AZR4, AZR5 and AZR6) were collected 25 km south-west of Azrou, in the Sidi Bel Khair area. Based on the Geological map "Azrou" (Dir. Geol. Maroc, 2005), all of them correspond to Early Devonian quartzitic sandstones from the central para-autochthonous unit (Bouabdelli et al., 1989). Sample AZR2 was collected 5 km north-east of Azrou from the quartzitic beds of the Late Ordovician Kaâorana Formation, dated with fossiliferous material (eastern para-autochthonous unit of Bouabdelli et al., 1989; Geological map "Azrou", scale 1:50.000; Dir. Geol. Maroc, 2005).

About four kilograms of rock were collected for each sample and processed in the laboratories at the University of Granada (Spain). Samples were mechanically smashed in a jaw-crusher and sorted by sieving. A heavy mineral concentrate was obtained by manual panning. Magnetic minerals were removed from the concentrate material using a Nd magnet and, finally, about 120-160 zircon grains were separated by handpicking under a binocular microscope.

The selected zircon grains were mounted in epoxy rounds and imaged by cathodoluminescence (Figure 2.3) to reveal internal structures using a Mira3 FESEM instrument at the Microscopy and Microanalysis Facility of the John de Laeter Centre (JdLC, Curtin University, Perth, Australia).

Most of the zircon grains were large enough to be analyzed with Laser Ablation Inductively Coupled Plasma Mass Spectrometry (LA-ICPMS). Where possible, 150 analyses were performed per sample in order to obtain representative and statistically significant age populations after discordant analyses were removed (Vermeesch, 2004). Fifty-six zircon grains from sample TAZ2 and 48 from TAZ3 were too small to be analyzed with LA-ICPMS, and were analyzed using the Sensitive High-Resolution Ion Microprobe (SHRIMP II) at the JdLC. Detailed analytical methods are described in the supplementary material (Appendix A).

Data with $> \pm 10\%$ discordance and/or $> 1\%$ $^{206}\text{Pb}/^{206}\text{Pbc}$ were not taken into account for results interpretation. Furthermore, SHRIMP data were processed using the software package SQUID, which calculates the discordance percentage based on the $^{207}\text{Pb}/^{206}\text{Pb}$ and the $^{206}\text{Pb}/^{238}\text{U}$ ages corrected for common Pb. For young zircon ages, the uncertainty of $^{207}\text{Pb}/^{206}\text{Pb}$ ages is bigger due to the low content of ^{207}Pb and may produce data with high discordance level. However, when these high discordant data are plotted in a concordia diagram, they are actually concordant. $^{206}\text{Pb}/^{238}\text{U}$ dates were used to characterize zircon grains younger than 1500 Ma, and $^{207}\text{Pb}/^{206}\text{Pb}$ dates were utilized for older zircon grains. The data were plotted as combined histograms and Kernel Density Estimates (KDE) using DensityPlotter 8.4 (Vermeesch, 2012) and applying an adaptive bandwidth of 40 Ma for the KDE and a bin width of 40 Ma for the histograms (Figures 2.4, 2.5, and 2.6). Detrital zircon populations were defined using the mixture modeling tool of DensityPlotter 8.4, while the mean square weighted deviation (MSWD) of the youngest populations was calculated with IsoplotR online (Vermeesch, 2018).

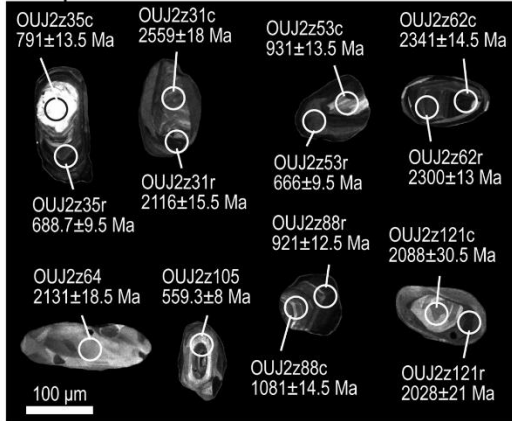
4. Results

A synthesis of the U-Pb analyses and estimated ages is provided in Tables 2.1 and 2.2 (the detailed analytical dataset is given in the supplementary material as Appendix D, tables D.1 to D.10). Distribution histograms and KDE diagrams for each sample are reported in Figures 2.4, 2.5, and 2.6. A description of the zircon grains of each sample (size, color, morphology, internal structure) has been included in the supplementary material as Appendix B. Because of the size of the zircon grains and/or their continuous oscillatory zoning (Figure 2.3), most of the analyses were carried out only in the core of the detrital zircons; nevertheless, in some cases it was possible to analyze both the core and the rim of the grains. Errors are expressed at the 1σ level.

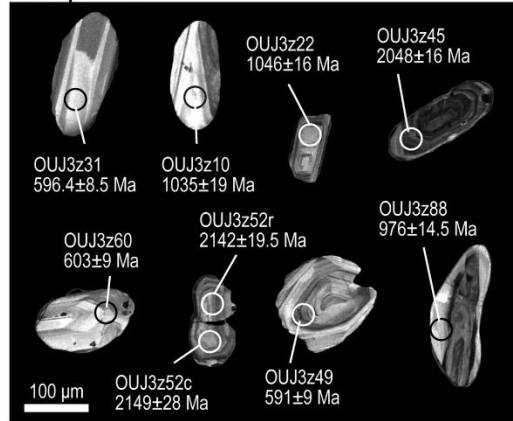
4.1. Oujda area

From the two samples of the Oujda area (OUJ2 and OUJ3, of Late Ordovician age), a total of 247 zircon grains were selected and 300 analyses were carried out yielding 261 concordant results.

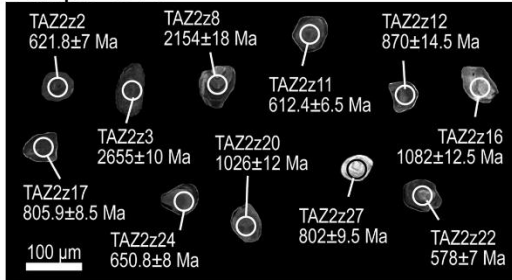
Sample OUIJ2



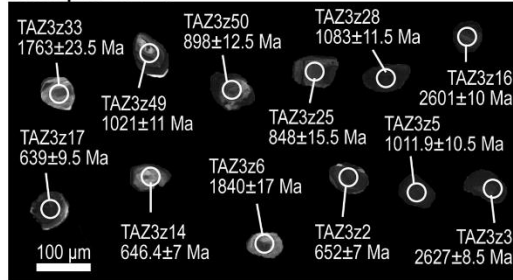
Sample OUIJ3



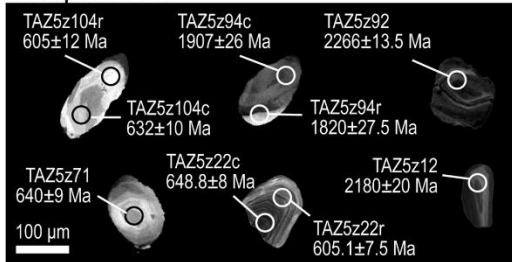
Sample TAZ2



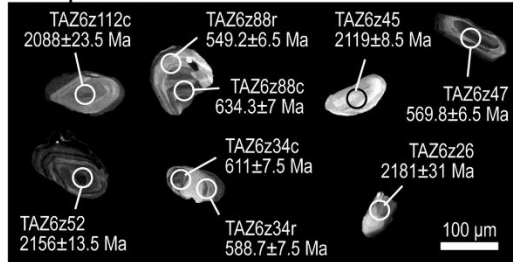
Sample TAZ3



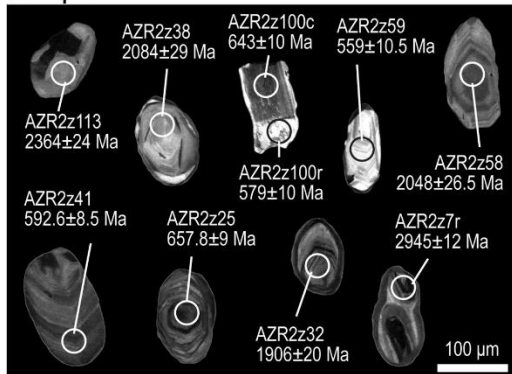
Sample TAZ5



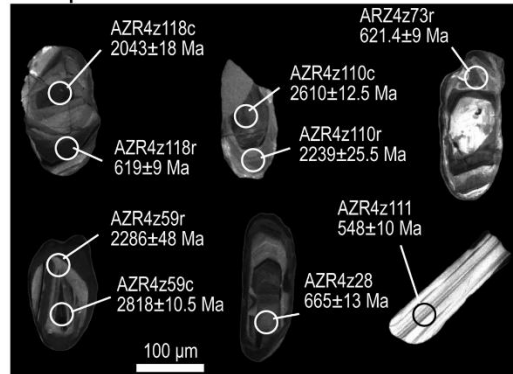
Sample TAZ6



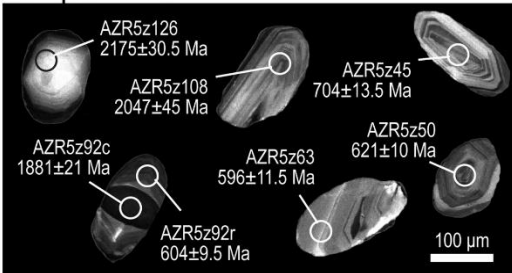
Sample AZR2



Sample AZR4



Sample AZR5



Sample AZR6



Figure 2.3 (previous page). Cathodoluminescence images of selected detrital zircon grains; darker zones correspond to high-U sectors and brighter zones to low-U sectors.

The OUI2 sample is a medium-grained quartzite, with muscovite and iron oxides. From this sample, 150 analyses were carried out on 123 detrital zircon grains, yielding 126 concordant data (Figure 2.4A). Two main detrital zircon populations were obtained, of 529-791 Ma (Ediacaran mean age of 621.5 ± 1.1 Ma, 57.9%) and 1781-2215 Ma (Paleoproterozoic mean age of 2037.6 ± 3.9 Ma, 23.8%) ages. A few dates can be grouped into two minor and not well defined peaks: 921-1081 Ma (Tonian mean age of 975.6 ± 5.3 Ma, 5.6%) and 2300-2743 Ma (Neoproterozoic mean age of 2523.7 ± 4.7 Ma, 8.7%). Four scattered Mesoproterozoic data (1207-1461 Ma) cannot be grouped in a significant population. The youngest detrital zircon population, comprising 4 analyses, yielded an age of 537.5 ± 3.9 Ma (MSWD = 0.66), thus indicating an earliest Cambrian maximum depositional age.

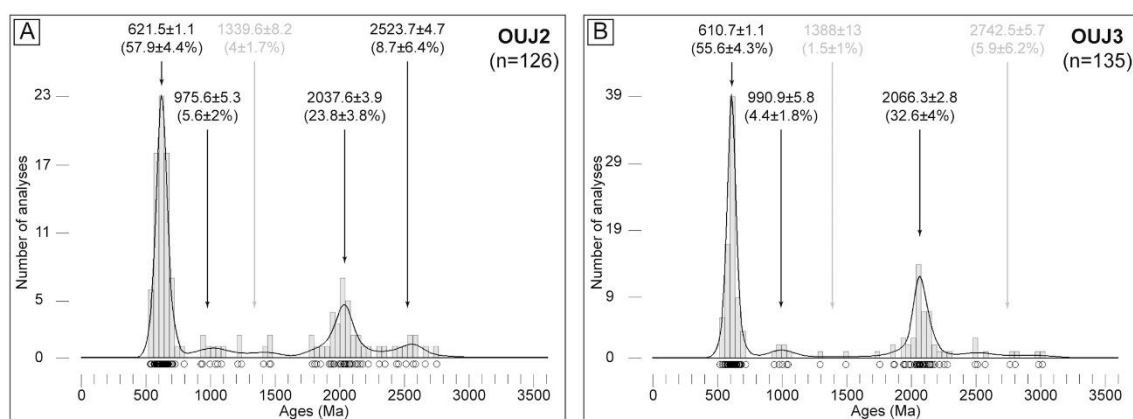


Figure 2.4. Kernel Density Estimates (black lines) combined with distribution histograms (grey bars) showing the detrital zircon ages ($^{206}\text{Pb}/^{238}\text{U}$ for dates $<1500\text{Ma}$; $^{207}\text{Pb}/^{206}\text{U}$ for dates $>1500\text{Ma}$) obtained from the samples of the Oujda area. Errors are expressed at the 1σ level and data with a discordance level $>10\%$ and/or $>1\%$ ^{206}Pb were discarded. The circles in the lowest part of the diagrams show the single analyses. The arrows indicate the main detrital zircon populations estimated using the mixture modeling tool in DensityPlotter 8.4 (Vermeesch, 2012). Grey text identifies the populations comprising scattered dates with no geological meaning. These populations were not considered in the interpretation.

The sample OUI3 is a fine-grained quartzite with a faint planar fabric marked by quartz grains and opaque minerals. One hundred twenty-four detrital zircon grains were separated from this sample and a total of 150 analyses were carried out, 135 of which were concordant (Figure 2.4B). The two main detrital zircon populations identified are 520-717 Ma (Ediacaran mean age of 610.7 ± 1.1 Ma, 55.6%) and 1754-2281 Ma (Paleoproterozoic mean age of 2066.3 ± 2.8 Ma, 32.6%). A few grains (941-1046 Ma) correspond to a Tonian minor peak (mean age 990.9 ± 5.8 Ma, 4.4%). A few data yield Mesoproterozoic (1293-1493 Ma) and Archean (2495-3013 Ma) ages, but they are too scattered to characterize minor populations. The youngest detrital zircon population, made up of 5 data, yielded an age of 545.3 ± 3.7 Ma (MSWD = 1.28), indicating a Late Ediacaran maximum depositional age.

In summary, detrital zircon populations of both Oujda samples are very similar and show an important Ediacaran detrital zircon population at ≈ 610 - 620 Ma, which represents ≈ 55 - 60% of the analyses. A second main peak corresponds to a Paleoproterozoic population (≈ 2030 - 2070 Ma), which represents ≈ 25 - 35% of the data. Minor detrital zircon populations yielded Tonian (≈ 975 - 990 Ma, $\approx 5\%$) and Archean (≈ 2520 Ma, $\approx 10\%$) ages. The maximum depositional age for both samples is Late Ediacaran - Early Cambrian (≈ 540 Ma).

4.2. Tazekka area

A total of 411 zircon grains were isolated from the 4 samples of the Tazekka area: TAZ2 and TAZ3, of Late Ordovician age, and TAZ5 and TAZ6, of Silurian age. A total of 488 analyses were carried out (104 with SHRIMP in samples TAZ2 and TAZ3) yielding 402 concordant results (86 with SHRIMP in samples TAZ2 and TAZ3).

Sample TAZ2 is a very fine-grained quartzite with some detrital micas. From this sample, 79 zircon grains were separated and 86 analyses were carried out, 65 of which gave concordant ages (21 LA-ICPMS and 44 SHRIMP analyses, see Tables D.3a and D.3b in Appendix D). Concordant LA-ICPMS and SHRIMP data were then combined to create the histogram and KDE shown in Figure 2.5A. The main detrital zircon populations are 480-674 Ma (Ediacaran mean age of 613 ± 1.4 Ma, 47.7%) and 731-1082 Ma (Tonian mean age of 914.1 ± 2.6 Ma, 30.8%). Minor populations in this sample are 1908-2154 Ma (Paleoproterozoic mean age of 1999.5 ± 7.7 Ma, 6.2%) and 2369-3012 Ma (Archean mean age of 2639.6 ± 3 Ma, 12.3%). Two data yield Mesoproterozoic ages (1373-1425 Ma). The youngest detrital zircon population, made up of 8 grains, gave an age of 581.4 ± 2.8 Ma (MSWD = 0.53), indicating a Late Ediacaran maximum depositional age.

Sample TAZ3 corresponds to a quartzitic sandstone. Its grain size is very fine and homogeneous, quartz crystals being rounded and with no preferential orientation. 92 grains were separated from sample TAZ3, and 102 analyses were carried out yielding 86 concordant dates (45 LA-ICPMS and 41 SHRIMP analyses, see Tables D.4a and D.4b in Appendix D). Concordant SHRIMP and LA-ICPMS data were used to generate the histogram and the KDE curve showed in Figure 2.5B. The main detrital zircon populations are 547-803 Ma (Cryogenian mean age of 668.5 ± 1.5 Ma, 34.9%) and 813-1146 Ma (Tonian mean age of 972.1 ± 2.4 Ma, 32.6%). Paleoproterozoic (1746-2211 Ma, mean age 1982.4 ± 3.2 Ma, 20.9%) and Archean (2583-2851 Ma, mean age 2689.3 ± 4.1 Ma, 8.1%) peaks represent minor populations. Three scattered data gave Late Silurian-Devonian ages (426, 399, and 359 Ma), which will not be considered to establish the maximum depositional age. Thus, the youngest detrital zircon population, composed of 4 concordant analyses, yielded an age of 607.6 ± 3.5 Ma (MSWD = 0.34), indicating an Ediacaran maximum depositional age.

Sample TAZ5 is a medium- to coarse-grained quartzite. The quartz grains are rounded and do not show any preferential shape orientation. From this sample 114 zircon grains were handpicked and a total of 150 analyses were performed, yielding 136 concordant

results (Figure 2.5C). The main detrital zircon population is 488-750 Ma (Ediacaran mean age of 612 ± 0.87 Ma, 57.4%); a Paleoproterozoic (1702-2316 Ma, mean age 2055.6 ± 2.4 Ma, 25.7%) peak represents a minor detrital zircon population. Scattered data gave Tonian (782-977 Ma), Mesoproterozoic (1231-1513 Ma) and Siderian-Archean ages (2460-3407 Ma). The youngest population, comprising 5 grains, yielded an age of 554.2 ± 3 Ma (MSWD = 0.77), indicating a Late Ediacaran maximum depositional age.

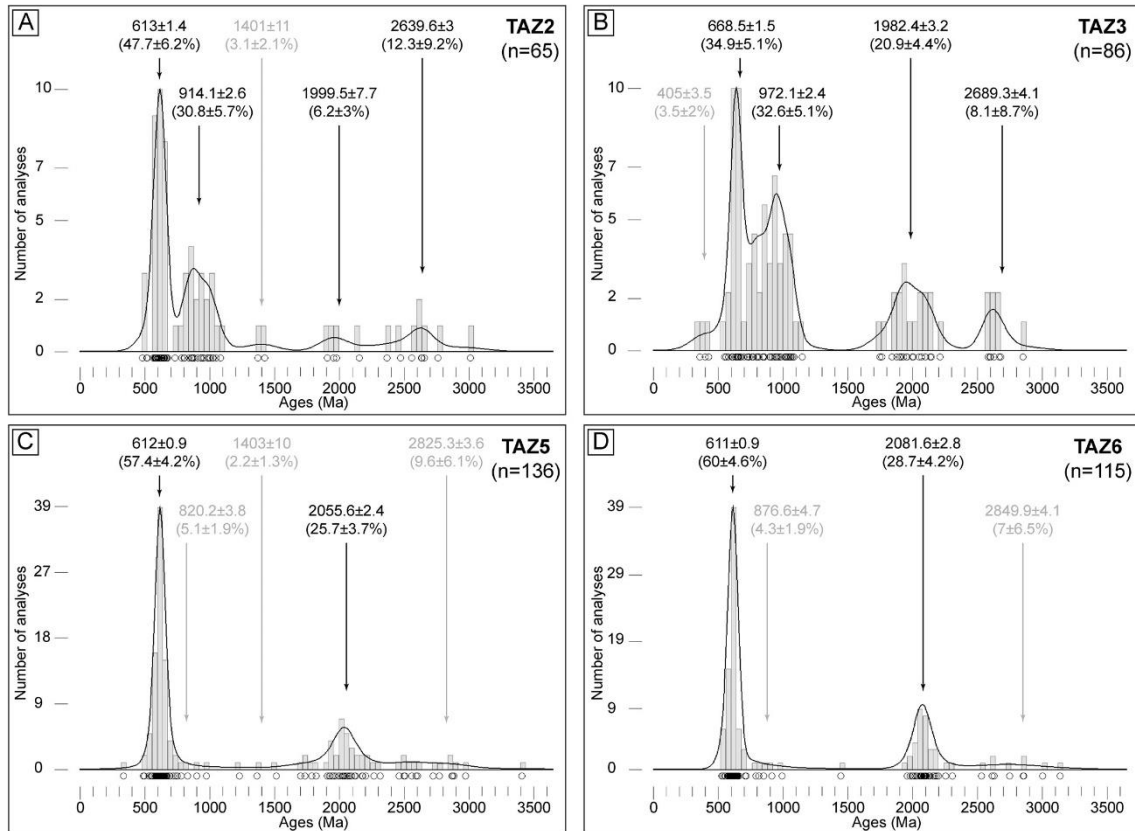


Figure 2.5. Kernel Density Estimates (black lines) combined with distribution histograms (grey bars) showing the detrital zircon ages ($^{206}\text{Pb}/^{238}\text{U}$ for dates <1500Ma; $^{207}\text{Pb}/^{206}\text{U}$ for dates >1500Ma) obtained from the samples of the Tazekka area. Errors are expressed at the 1σ level and data with a discordance level >10% and/or >1% ^{206}Pbc were discarded. The circles in the lowest part of the diagrams show the single analyses. The arrows indicate the main detrital zircon populations estimated using the mixture modeling tool in DensityPlotter 8.4 (Vermeesch, 2012). Grey text identifies the populations comprising scattered dates with no geological meaning. These populations were not considered in the interpretation.

Sample TAZ6 is a medium-grained quartzite with equidimensional quartz grains and some small mica grains. 126 zircons were separated from this sample and 150 analyses were carried out, yielding 115 concordant ages (Figure 2.5D). The two main detrital zircon populations are 527-714 Ma (Ediacaran mean age of 611.04 ± 0.92 Ma, 60%) and 1955-2304 Ma (Paleoproterozoic mean age of 2081.6 ± 2.8 Ma, 28.7%). A few, very scattered data yielded Tonian (787-992 Ma), Mesoproterozoic (1442 ± 17.5 Ma), and Archean (2528-3135 Ma) ages. The youngest detrital zircon population, made up of 10 analyses, yielded an age of 579.7 ± 2.3 Ma (MSWD = 0.95), indicating a Late Ediacaran maximum depositional age.

To sum up, all samples from the Tazzeka area are characterized by a main Ediacaran-Cryogenian detrital zircon population (≈ 610 - 670 Ma, ≈ 35 - 60%) and a minor Paleoproterozoic peak (≈ 1980 - 2080 Ma, ≈ 5 - 30%). Nevertheless, in samples TAZ2 and TAZ3 an important Tonian population (≈ 915 - 975 Ma, $\approx 30\%$) and a secondary Archean peak (≈ 2640 - 2690 Ma, ≈ 10 - 15%) are observed. The maximum depositional ages are Ediacaran (≈ 555 - 605 Ma).

4.3. Azrou area

Of the 506 zircon grains isolated from the 4 samples of the Azrou area (AZR2, Late Ordovician age; AZR4, AZR5, and AZR6, Early Devonian age), a total of 597 analyses were carried out, yielding 555 concordant ages.

Sample AZR2 is a medium- to fine-grained quartzite with rare detrital micas and a very faint preferential shape orientation of the quartz grains. From this sample 125 zircon grains were separated and 150 analyses yielded 131 concordant dates (Figure 2.6A). The main detrital zircon populations are 511-725 Ma (Ediacaran mean age of 618.1 ± 1.3 Ma, 42.7%) and 1906-2273 Ma (Paleoproterozoic mean age of 2068.9 ± 2.7 Ma, 38.9%), while ages in the range 2364-2966 Ma (Archean mean age of 2753.1 ± 4.4 Ma, 7.6%) represent a third minor population. A few scattered data yielded Tonian-Stenian (769-1154 Ma) and Mesoproterozoic (1253-1756 Ma) ages. The youngest detrital zircon population, made up of 8 analyses, yielded an age of 570 ± 3.5 Ma (MSWD = 1.10), indicating a Late Ediacaran maximum depositional age.

Sample AZR4 corresponds to a medium-grained quartzite with rounded grains that do not define any planar fabric. A total of 150 analyses were carried out on 121 zircon grains separated from this sample. One hundred and forty of the analyses gave concordant results (Figure 2.6B). A 548-733 Ma population (Ediacaran mean age of 620 ± 1.2 Ma, 47.9%) marks the principal peak in this sample; minor populations yielded 1762-2358 Ma (Paleoproterozoic mean age of 2050.4 ± 2.8 Ma, 36.4%) and 2441-2838 Ma (Archean mean age of 2622.7 ± 4 Ma, 11.4%) ages. A few data, too scattered to be considered as minor populations, gave Mesoproterozoic (1012-1500 Ma) and Paleoarchean (3325 ± 12 Ma) ages. The youngest detrital zircon population, made up of 21 analyses, yielded an age of 591 ± 2 Ma (MSWD = 1.03), indicating an Ediacaran maximum depositional age.

Sample AZR5 is a homogeneous medium-grained quartzite, with a few opaque minerals filling fractures and very scarce micas. From this sample 129 zircon grains were handpicked, 149 analyses were performed, yielding 143 concordant ages (Figure 2.6C). Fifty-five percent of the data correspond to the age range 532-716 Ma (Ediacaran mean age of 625.5 ± 1.1 Ma), while 32.9% define a Paleoproterozoic age (1793-2267 Ma, mean age 2054.4 ± 3 Ma). A few scattered data yielded Tonian (786-926 Ma), Mesoproterozoic (1374-1517 Ma), and Archean (2367-3225 Ma) ages. The youngest zircon population, made up of 41 data, gave an age of 612 ± 2 Ma (MSWD = 1.3), indicating an Ediacaran maximum depositional age.

Finally, sample AZR6 is a quartzite very similar to samples AZR4 and AZR5. The grain size is medium and homogeneous and there is no evidence of preferential shape quartz orientation. 131 zircon grains were separated from this sample and 150 analyses were carried out, yielding 137 concordant dates (Figure 2.6D). The 545-726 Ma detrital zircon population (Ediacaran mean age of 620.5 ± 1.2 Ma, 46%) represents the highest peak in this sample; a second population yielded a Paleoproterozoic age (1729-2308 Ma, mean age 2073.3 ± 2.9 Ma, 32.1%), while a third minor peak represents a Siderian population (2395-2572 Ma, mean age 2481.9 ± 5.1 Ma, 8%). A few scattered data yielded Tonian (798-910 Ma), Mesoproterozoic (1389-1424 Ma), and Archean (2699-3029 Ma) ages. The youngest population, composed of 4 analyses, gave an age of 577 ± 8 Ma (MSWD = 1.3), indicating a Late Ediacaran maximum depositional age.

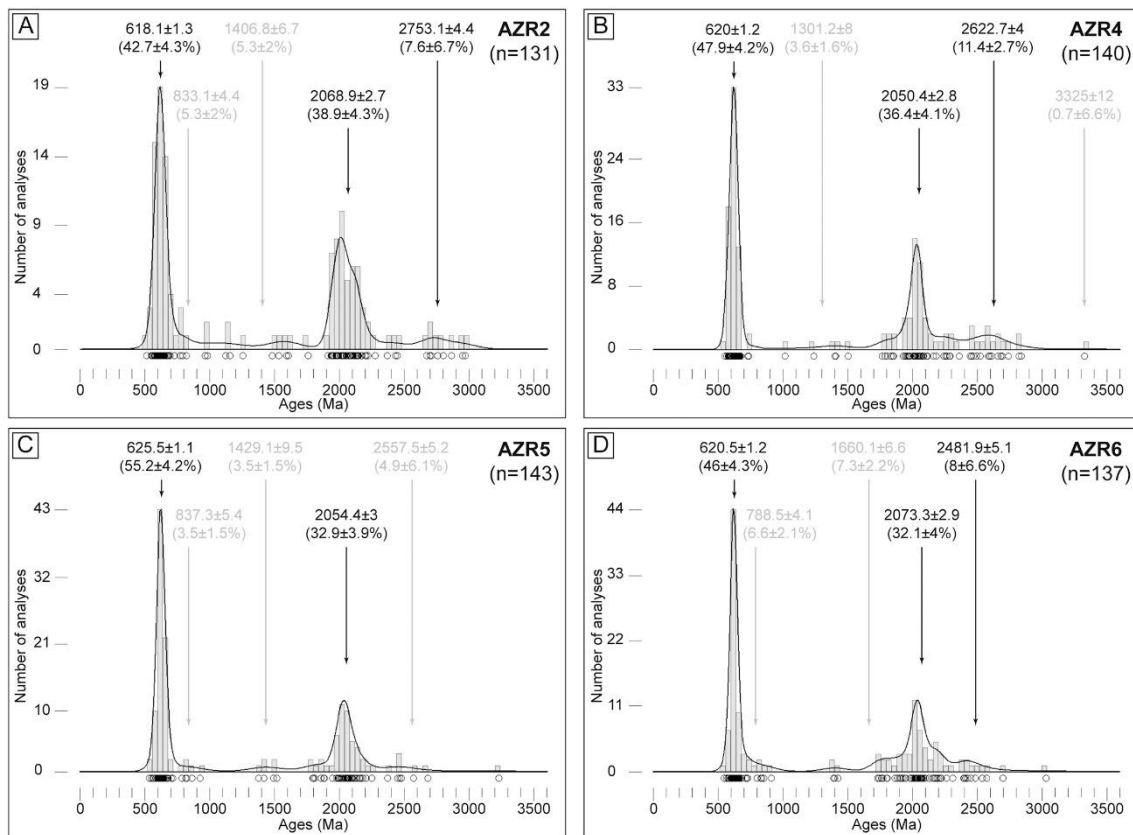


Figure 2.6. Kernel Density Estimates (black lines) combined with distribution histograms (grey bars) showing the detrital zircon ages ($^{206}\text{Pb}/^{238}\text{U}$ for dates $<1500\text{Ma}$; $^{207}\text{Pb}/^{206}\text{U}$ for dates $>1500\text{Ma}$) obtained from the samples of the Azrou areas. Errors are expressed at the 1σ level and data with a discordance level $>10\%$ and/or $>1\%$ ^{206}Pb were discarded. The circles in the lowest part of the diagrams show the single analyses. The arrows indicate the main detrital zircon populations estimated using the mixture modeling tool in DensityPlotter 8.4 (Vermeesch, 2012). Grey text identifies the populations comprising scattered dates with no geological meaning. These populations were not considered in the interpretation.

In summary, the most prominent feature of the Azrou samples is the Ediacaran peak at ≈ 620 Ma, which represents the $\approx 40\text{-}55\%$ of the results. The Paleoproterozoic population ($\approx 2050\text{-}2080$ Ma) is well defined and represents $\approx 30\text{-}40\%$ of the data. A third minor peak ($\approx 5\text{-}10\%$) corresponds to an Archean population at $\approx 2480\text{-}2750$ Ma. The maximum depositional age for these samples is Ediacaran ($\approx 570\text{-}615$ Ma).

Table 2.2. Details of the different detrital zircon populations in the analyzed samples; errors are expressed at the 1σ level; N°: number of grains in the youngest population.

Area	Sample	Youngest zircon population		Youngest zircon age (Ma)	Ediacaran-Cryogenian		Tonian-Stenian		Paleoproterozoic		Archean	
		age (Ma)	N°		Age (Ma)	Prob. (%)	Age (Ma)	Prob. (%)	Age (Ma)	Prob. (%)	Age (Ma)	Prob. (%)
Oujda	OUI2	537.5 ± 3.9	4	529 ± 8.5	621.5 ± 1.1	57.9	975.6 ± 5.3	5.6	2037.6 ± 3.9	23.8	2523.7 ± 4.7	8.7
	OUI3	545.3 ± 3.7	5	520 ± 10	610.7 ± 1.1	55.6	990.9 ± 5.8	4.4	2066.3 ± 2.8	32.6	-	-
Tazekka	TAZ2	581.4 ± 2.8	8	480 ± 6	613 ± 1.4	47.7	914.1 ± 2.6	30.8	1999.5 ± 7.7	6.2	2639.6 ± 3	12.3
	TAZ3	607.5 ± 3.5	4	339 ± 6	668.5 ± 1.5	34.9	972.1 ± 2.4	32.6	1982.4 ± 3.2	20.9	2689.3 ± 4.1	8.1
	TAZ5	554.2 ± 3	5	336 ± 5.5	612 ± 0.9	57.4	-	-	2055.6 ± 2.4	25.7	-	-
	TAZ6	579.7 ± 2.3	10	527.4 ± 7	611 ± 0.9	60	-	-	2081.6 ± 2.8	28.7	-	-
Azrou	AZR2	570 ± 3.5	8	511.8 ± 7.5	618.1 ± 1.3	42.7	-	-	2068.9 ± 2.7	38.9	2753.1 ± 4.4	7.6
	AZR4	591 ± 2	21	548 ± 10	620 ± 1.2	47.9	-	-	2050.4 ± 2.8	36.4	2622.7 ± 4	11.4
	AZR5	612 ± 2	41	532 ± 8.5	625.5 ± 1.1	55.2	-	-	2054.4 ± 3	32.9	-	-
	AZR6	577 ± 8	4	545.3 ± 8	620.5 ± 1.2	46	-	-	2073.3 ± 2.9	32.1	2481.9 ± 5.1	8

5. Discussion

5.1. Maximum depositional ages and stratigraphic attributions

The age of the youngest detrital zircon population is often used to constrain the maximum depositional age of the sample. In this study, all the samples yielded (earliest Cambrian-) Ediacaran ages for the youngest zircon populations (Table 2.2). Specifically, the Ordovician samples OUI2 and OUI3 from the Oujda area gave a youngest detrital zircon population age of ≈ 540 Ma, while the Late Ordovician-Devonian samples from Azrou area yielded youngest zircon populations with variable ages between ≈ 570 and 610 Ma; finally, the samples from the Tazekka area (TAZ2 and TAZ3, Ordovician; TAZ5 and TAZ6, Silurian) gave maximum depositional ages of ≈ 555 -605 Ma. Therefore, our data are compatible with the previous stratigraphic attribution of these samples, since the maximum depositional age is in all cases older than the putative stratigraphic age. Regarding the reliability of the stratigraphic ages of the different formations sampled in this work, it must be noticed that in a few cases those ages are based on previously reported fossiliferous content, though in most cases they rely on regional stratigraphic correlations of analogous passive margin sequences (see section 2). Furthermore, an Ediacaran age attribution can be discarded by considering that the rocks of that age locally cropping out in the Moroccan Meseta are quite different from the Paleozoic rocks: they consist on felsic volcanic and volcanoclastic rocks with granitoids, all of them probably attesting a Cadomian magmatic arc bordering northern Gondwana at that time (Eddif et al., 2007; El Houicha et al., 2018; Letsch et al., 2018; Ouabid et al., 2017; Tahiri et al., 2010). The consistent Ediacaran maximum depositional age of our samples simply reflects that the magmatism of that age generated the youngest zircons incorporated as detrital material into these Ordovician to Devonian rocks (see next subsections).

5.2. West African Craton provenance

Most of the U-Pb geochronological results published so far in detrital rocks from the Moroccan Variscides (*e.g.*, Abati et al., 2010; Avigad et al., 2012; Domènech et al., 2018; El Houicha et al., 2018; Ghienne et al., 2018; Letsch et al., 2018; Marzoli et al., 2017; Pérez-Cáceres et al., 2017; Pratt et al., 2015) are characterized by Ediacaran-Cryogenian and Paleoproterozoic detrital zircon populations, with a significant gap at Mesoproterozoic ages. Such characteristics are considered the typical signature of WAC affinity (Figure 2.7), the main detrital zircon populations being attributed to the Cadomian and/or Pan-African (Ediacaran-Cryogenian) and Eburnean (Paleoproterozoic) orogenies (Nance et al., 2008 and references therein). An Archean population, possibly attributed to the Liberian orogeny (Nance et al., 2008 and references therein), is often present but at very scarce percentages. The absence of relevant Mesoproterozoic populations strongly suggests that the source of the zircons of that age described by Bradley et al. (2015) in

Ediacaran samples directly overlying the western WAC in Mauritania should be located in a more western area, *i.e.* an Amazonian basement.

All the samples described in this work include the above-mentioned WAC-diagnostic three detrital zircon populations (Ediacaran-Cryogenian, Paleoproterozoic, and Archean). In particular, the Late Ordovician-Early Devonian samples from the Azrou area (AZR2, AZR4, AZR5, and AZR6) and the two Silurian samples from the Tazekka area (TAZ5 and TAZ6) are characterized by a strong WAC affinity, their detrital zircon content being comparable with previously published studies in the region (*e.g.*, Abati et al., 2010; Avigad et al., 2012; Domènech et al., 2018; El Houicha et al., 2018; Ghienne et al., 2018; Letsch et al., 2018; Marzoli et al., 2017; Pérez-Cáceres et al., 2017; Pratt et al., 2015). For this reason, and because of the similarities in the Early Paleozoic stratigraphic record within the Moroccan Variscides (Michard et al., 2010b and references therein), it seems plausible that the Moroccan Meseta domains were all part of the same continental margin located to the north of the WAC (*i.e.* at the northern margin of the Gondwanan continent). In fact, a WAC-type basement locally crops out in the Western Moroccan Meseta: besides Cadomian rocks (see section 5.1), an Eburnean (≈ 2.05 Ga) meta-rhyolite has been described covered by Lower Cambrian sedimentary rocks (Pereira et al., 2015). This Moroccan Meseta Precambrian basement, if exposed during the Ordovician-Devonian, could have been an additional local source for the Ediacaran and Paleoproterozoic zircon grains of our samples.

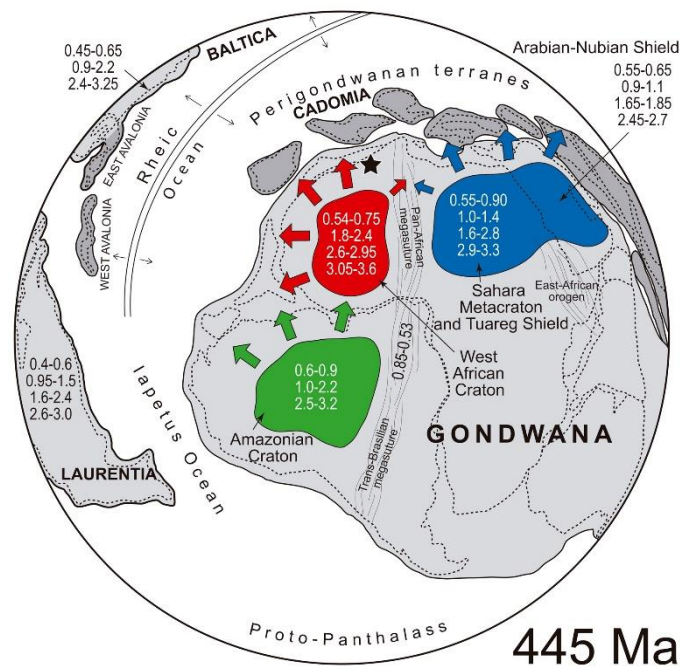


Figure 2.7. Palinspastic reconstruction of Gondwana, Laurentia, and Baltica (light grey) and Peri-Gondwanan terranes (dark grey) during Late Ordovician (about 445 Ma; modified from Bea et al., 2010; Linnemann et al., 2011; Naidoo et al., 2018). Ages are from Abati et al. (2010), Bea et al. (2010), Linnemann et al. (2011 and references therein), Naidoo et al. (2018), and Nance et al. (2008), and they are expressed in Ga. Colored arrows indicate the main transport directions of the sediments from the source areas within the northwestern Gondwanan continent. The black star indicates the approximate location of the area studied.

5.3. Tonian-Stenian population

Although all the samples show a dominant WAC affinity, the detrital zircon distribution patterns of a few of them diverge from the classical WAC signature, with secondary or minor detrital zircon populations of Tonian-Stenian age (Figure 2.8). In particular, the Late Ordovician samples from the Oujda area (OUJ2 and OUJ3) and the Late Ordovician samples from the Tazekka area (TAZ2 and TAZ3) include a Tonian-Stenian (about 1.0 Ga) population which reaches 30% of the analyses in the samples from Tazekka. Primary sources of that age are unknown in the WAC, but they are typical of the Grenville orogeny which affected Laurentia, Baltica, Avalonia, and the Amazonian Craton (Figure 2.7; Slagstad et al., 2017 and references therein), as well as the Arabian-Nubian shield and the Saharan Metacraton. Furthermore, because of the very small dimensions of the grains and their rounded morphology (particularly evident in samples TAZ2 and TAZ3; Figure 2.3), these zircons probably went through several cycles of erosion, transportation, and deposition, being finally deposited during the Late Ordovician glaciation that affected northern Gondwana (Ghienne et al., 2018; Le Heron et al., 2009). Consequently, it is possible that the Tonian-Stenian zircon grains analyzed in this work hailed from distant source areas that might be thousands of kilometers away from the current location of the sample sites.

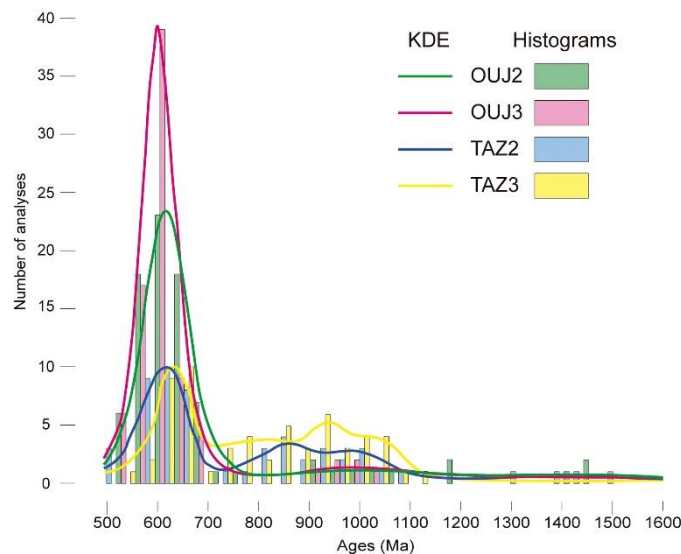


Figure 2.8. Summary Kernel Density Estimator (KDE, lines) and histograms (bars) combination of samples OUJ2 (n=85 of 126, in green), OUJ3 (n=83 of 135, in red), TAZ2 (n=53 of 65, in blue) and TAZ3 (n=59 of 88, in yellow) showing the different distribution patterns of data in the age range from 450 to 1600 Ma.

Laurentia, Baltica and Avalonian sources can be dismissed because they were separated from Gondwana by the Rheic Ocean at Ordovician to Late Devonian times (Figure 2.7). On the contrary, the Amazonian Craton was part of the Gondwana continent and it might be a plausible source area. However, zircon ages from this craton are continuous during all the Mesoproterozoic (1.0-1.6 Ga, and up to 2.2 Ga, Figure 2.7). Therefore, we would expect to find an analogous age pattern in detrital samples (Figure 2.9A) sourced from an Amazonian-type basement (for instance, the zircons described in

Bradley et al., 2015), but our samples only contain a few scattered Early to Middle Mesoproterozoic zircon grains (Figure 2.9B), thus suggesting a different source area. Actually, a more plausible source for the 1.0 Ga detrital zircons might be the Saharan Metacraton and/or the Arabian-Nubian Shield, which also contain zircons of that age (Figure 2.7). In this regard, northeastern African igneous sources were already suggested to explain the presence of Tonian-Stenian detrital zircon populations in samples from central and northern Iberia (Bea et al., 2010; Fernández-Suárez et al., 2014; Gutiérrez-Alonso et al., 2015; Pastor-Galán et al., 2013; Shaw et al., 2014; Talavera et al., 2012). Furthermore, such sources were previously claimed to explain minor Tonian-Stenian detrital zircon populations in samples from the Anti-Atlas (Avigad et al., 2012), High Atlas (Marzoli et al., 2017), and Middle Atlas (Ghienne et al., 2018; Pratt et al., 2015). However, Marzoli et al. (2017) and Pratt et al. (2015) studied post-Variscan rocks, which hampers provenance investigations because continental terranes with 1.0 Ga primary sources (*e.g.*, Avalonia, Baltica and Laurentia) were already amalgamated with Gondwana at the time of deposition of the studied samples. Accordingly, the above-mentioned authors proposed northeastern African sources as well as Amazonian or Avalonian provenance areas. However, the continuous Mesoproterozoic age distribution patterns in the Avalonian and Amazonian areas, in contrast to the pattern observed in the Moroccan samples (Figure 2.9), remains, in our opinion, the strongest point in favour of northeastern African sources. For the same reason, Ghienne et al. (2018) discarded the Amazonian Craton as a source area for Tonian-Stenian detrital zircons in the Tazekka area. According to these authors, 1.0 Ga grains in this area are found in sedimentary rocks deposited during a glacial maximum, making it possible that glaciers enhanced the transportation of detrital zircon grains from the northeastern regions of Africa (Saharan Metacraton and Arabian-Nubian Shield; Figure 2.7) to the Tazekka glacial depocenter. In this regard, the Ordovician age of samples OUI2, OUI3, TAZ2, and TAZ3 suggests that similar processes might be responsible for the accumulation of a Tonian-Stenian detrital zircon population in our samples.

Apart from the possibility of a very distant NE African source, it is possible that during the Ordovician, the Eastern Meseta was located in a closer position to the 1.0 Ga zircon sources of NE Africa. In this case, important regional faults, such as the SMF, would be necessary to explain the current position of the Eastern Meseta. Nevertheless, the SMF is characterized by dextral transpressional kinematics (Cerrina Feroni et al., 2010; Michard et al., 2010b), which is not congruent with the type of displacement needed to move the studied terranes from an original eastern position to their present day location. Moreover, the age and kinematic history of this structure is still a matter of discussion (Michard et al., 2010a; Simancas et al., 2009, 2010).

To conclude, the deposition of Tonian-Stenian detrital zircon grains probably occurred through long-travelled transportation from northeastern Africa, enhanced by Ordovician glaciation, and/or involving several cycles of erosion, transportation and sedimentation.

5.4. Cambro-Ordovician rifting in northern Gondwana

After the Ediacaran Cadomian subduction, the northern border of Gondwana was dominated, during the Early Paleozoic, by a rifting episode that preceded the opening of the Rheic Ocean (*e.g.*, Cambeses et al., 2017; Nance et al., 2010, 2012). Continental rift features, including very thick Cambrian and Ordovician sedimentary accumulations (up to 10 km) and copious Cambro-Ordovician rift-related plutonic and volcanic rocks (and the detrital zircon populations derived from them), are common in Variscan terranes now cropping out in central and southern Europe (*e.g.*, Cambeses et al., 2017; Demange, 1994; Linnemann et al., 2008 and references therein; Montero et al., 2009; Pastor-Galán et al., 2013; Pereira et al., 2012 and references therein; Pérez-Estaún et al., 1990).

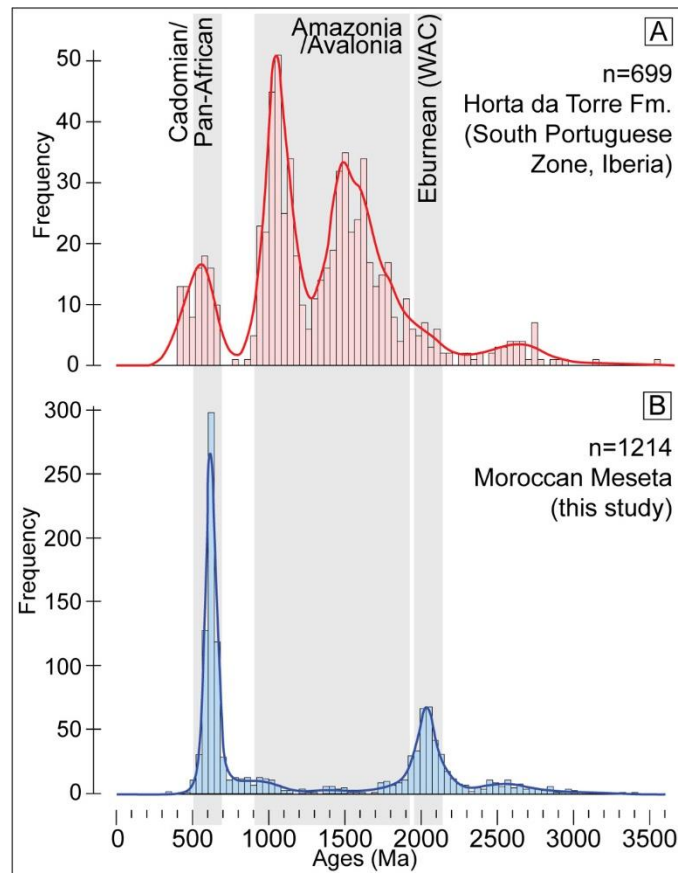


Figure 2.9. Comparison between Kernel Density Estimator (KDE) and histograms of U-Pb detrital zircon concordant ages: (A) data from the Devonian quartzites of the Horta da Torre Formation (Pulo do Lobo unit, South Portuguese Zone, SW Variscan Iberian Massif (Figure 2.1A); data compiled from Braid et al. (2011) and Pérez-Cáceres et al. (2017)), considered a typical example of Avalonian/Amazonian-derived sediments; (B) our data from the Eastern Meseta and Middle Atlas. Grey areas indicate the main crustal growth events in northern Gondwana.

In the Moroccan Meseta, evidence of Lower Paleozoic rifting is rather restricted in space and time. Sedimentary *grabens* have only been documented in the Middle Cambrian of the Coastal Block (Bernardin et al., 1988). Magmatic rocks are represented by discrete lenses of Cambrian mafic volcanics in the Coastal Block and rarely in the Central zone of the Western Moroccan Meseta (Poucllet et al., 2018 and references

therein). Cambro-Ordovician detrital zircon populations are almost missing, with the exception of a narrow unimodal zircon population centered at around 488 Ma recognized by Letsch et al. (2018) in a Lower Paleozoic greywacke from the Western Moroccan Meseta. A few Cambro-Ordovician detrital zircon ages were also obtained in Late Ordovician sandstones (Ghienne et al., 2018) and in Middle Jurassic sandstones (Pratt et al., 2015) from the Middle Atlas. As shown in Figures 2.4, 2.5, and 2.6, no Cambro-Ordovician detrital zircon populations were found in any of our samples from the Eastern Moroccan Meseta and Middle Atlas.

Based on the extent of the rift-related magmatism and detrital zircon content in Ordovician-Devonian rocks, it is generally accepted that Cambro-Ordovician rifting widely affected northern Gondwana-derived terranes, which are now exposed in Variscan massifs of central and southern Europe (*e.g.*, Cambeses et al., 2017; Linnemann et al., 2008; Montero et al., 2009; Pereira et al., 2012). Regarding the Moroccan Mesetas, we propose that Early Paleozoic rifting, accompanied by magmatism, partially affected the Western Meseta and aborted soon in late Cambrian time, but had no influence on the Eastern Meseta. Therefore, we suggest that the latter was located in a more inland position than the Western Meseta, and far from the rifted continental margin affected by rift-related magmatism (Iberia and central Europe correlatives).

6. Conclusion

The detrital zircon U-Pb dates obtained on Ordovician-Devonian rocks of the Eastern Moroccan Meseta (Oujda area) and Middle Atlas (Tazekka and Azrou areas) are similar to those obtained on other samples from the Western Meseta, attesting a strong WAC affinity, characterized by Ediacaran-Cryogenian, Paleoproterozoic, and minor Archean populations. Despite these similarities, it is worth highlighting that the samples studied in this work did not record Cambro-Ordovician magmatism (rifting phase preceding the opening of the Rheic Ocean that allowed the drift of peri-Gondwanan terranes). Such magmatism is locally evidenced in the Western Meseta, and widespread in southwestern Europe. This suggests that the Eastern Moroccan Meseta (and to some extent the Western Meseta) was located in northern Gondwana, relatively far from the portion of the continental margin affected by the rifting pulse.

The Late Ordovician samples from the Tazekka area and, to a lesser extent, the samples from the Oujda area, show an important (up to 30% of the data) Tonian-Stenian population which suggests the presence of exotic sources apart from the WAC, probably located in northeastern Africa (Saharan Metacraton and Arabian-Nubian Shield). The presence of this population in Ordovician samples from northwestern Africa sequences might be explained by the glaciation that occurred during the Late Ordovician in northern Gondwana. Furthermore, the small size and rounded morphology of the grains suggest that they experienced significant sedimentary recycling.

Acknowledgments

This study was funded by the Ministerio de Economía y Competitividad (MINECO) of Spain through the project CGL2015-71692-P and the Pre-Doctoral scholarship BES-2016-078168. Zircon analyses and imaging were carried out on the SHRIMP II, LA-ICPMS and SEM facilities at the John de Laeter Centre, Curtin University, with the financial support of the Australian Research Council (LE150100013) and Auscope NCRIS (AQ44 Australian Education Investment Fund program). The authors wish to thank Brad McDonald (Curtin University) for technical assistance regarding LA-ICPMS analyses, and Lorenzo Valetti for proof reading the manuscript. Constructive comments by two anonymous reviewers are greatly appreciated and helped to improve the manuscript.

References

- Abati, J., Mohsine Aghzer, A., Gerdes, A., Ennih, N., 2010. Detrital zircon ages of Neoproterozoic sequences of the Moroccan Anti-Atlas belt. *Precambrian Research* 181, 115–128. doi:10.1016/j.precamres.2010.05.018
- Avigad, D., Gerdes, A., Morag, N., Bechstädt, T., 2012. Coupled U-Pb-Hf of detrital zircons of Cambrian sandstones from Morocco and Sardinia: implications for provenance and Precambrian crustal evolution of North Africa. *Gondwana Research* 21, 690–703. doi:10.1016/j.gr.2011.06.005
- Avigad, D., Kolodner, K., McWilliams, M., Persing, H., Weissbrod, T., 2003. Origin of northern Gondwana Cambrian sandstone revealed by detrital zircon SHRIMP dating. *Geology* 31, 227. doi:10.1130/0091-7613(2003)031<0227:OONGCS>2.0.CO;2
- Bea, F., Montero, P., Talavera, C., Abu Anbar, M., Scarrow, J.H., Molina, J.F., Moreno, J.A., 2010. The palaeogeographic position of Central Iberia in Gondwana during the Ordovician: evidence from zircon chronology and Nd isotopes. *Terra Nova* 22, 341–346. doi:10.1111/j.1365-3121.2010.00957.x
- Berkhli, M., 1999. Sédimentologie, biostratigraphie et stratigraphie séquentielle du Nord-Est de la Méséta occidentale marocaine pendant le Carbonifère inférieur (Viséen-Serpoukhovien). Université Moulay-Ismaïl, Meknès, Maroc.
- Berkhli, M., Vachard, D., Paicheler, J.-C., Tahiri, A., 2000. Modèle sédimentaire et évolution géodynamique du Nord-Est de la Méséta occidentale marocaine au cours du Carbonifère inférieur. *Comptes Rendus de l'Académie des Sciences - Series IIA - Earth and Planetary Science* 331, 251–256. doi:10.1016/S1251-8050(00)01417-8
- Bernardin, C., Cornée, J.J., Corsini, M., Mayol, S., Muller, J., Tayebi, M., 1988. Variations d'épaisseur du Cambrien moyen en Meseta marocaine occidentale: signification géodynamique des données de surface et de subsurface. *Canadian Journal of Earth Science* 25, 2104–2117.

- Bouabdelli, M., 1982. Stratigraphie et évolution structurale du Paléozoïque d'Azrou. Université Louis Pasteur, Strasbourg.
- Bouabdelli, M., 1989. Tectonique et sédimentation dans un bassin orogénique : le sillon viséen d'Azrou-Khénifra (est du Massif Hercynien Central du Maroc). Université Louis Pasteur, Strasbourg.
- Bouabdelli, M., Cailleux, Y., Hoepffner, C., Michard, A., Pique, A., 1989. Le bassin dinantien d'Azrou et l'évolution de sa déformation hercynienne (Méséta marocaine nord-orientale). Notes et Mémoires du Service Géologique du Maroc 335, 221–227.
- Bradley, D.C., O'Sullivan, P., Cosca, M.A., Motts, H.A., Horton, J.D., Taylor, C.D., Beaudoin, G., Lee, G.K., Ramezani, J., Bradley, D.B., Jones, J.V., Bowring, S., 2015. Synthesis of geological, structural, and geochronologic data (phase V, deliverable 53), in: Taylor, C.D. (Ed.), Second Projet de Renforcement Institutionnel Du Secteur Minier de La République Islamique de Mauritanie (PRISM-II): U.S. Geological Survey Open-File Report 2013–1280-A. p. 328. doi:10.3133/ofr20131280
- Braid, J.A., Murphy, J.B., Quesada, C., Mortensen, J., 2011. Tectonic escape of a crustal fragment during the closure of the Rheic Ocean: U-Pb detrital zircon data from the Late Palaeozoic Pulo de Lobo and South Portuguese Zones, Southern Iberia. *Journal of the Geological Society of London* 168, 383-392. doi:10.1144/0016-76492010-104
- Cambeses, A., Scarrow, J.H., Montero, P., Lázaro, C., Bea, F., 2017. Palaeogeography and crustal evolution of the Ossa–Morena Zone, southwest Iberia, and the North Gondwana margin during the Cambro-Ordovician: a review of isotopic evidence. *International Geology Review* 59, 94–130. doi:10.1080/00206814.2016.1219279
- Cerrina Feroni, A., Ellero, A., Malusà, M.G., Musumeci, G., Ottria, G., Polino, R., Leoni, L., 2010. Transpressional tectonics and nappe stacking along the Southern Variscan front of Morocco. *International Journal of Earth Sciences* 99, 1111–1122. doi:10.1007/s00531-009-0449-x
- Chopin, F., Corsini, M., Schulmann, K., El Houicha, M., Ghienne, J.-F., Edel, J.-B., 2014. Tectonic evolution of the Rehamna metamorphic dome (Morocco) in the context of the Alleghanian-Variscan orogeny. *Tectonics* 33, 1154–1177. doi:10.1002/2014TC003539
- Choubert, G., Marçais, J., Suter, G., 1978. Carte géologique du Maroc - 1/500.000: Oujda. Royaume du Maroc, Ministère l'Énergie des Mines du Développement Durable.
- Demange, M., 1994. Antevvariscan evolution of the Montagne Noire (France): from a passive margin to a foreland basin. *Comptes Rendus l'Académie des Science de Paris* 318, 921–933.
- Desteucq, C., Fournier-Vinas, C., 1981. Présence d'Ordovicien dans la région d'Oujda. *Mines, Géologie et Énergie* 50.

- Destombe, J., 1971. L'Ordovicien au Maroc. Essai de synthèse stratigraphique. Mémoires du Bureau de Recherches Géologiques et Minières 73, 237–263.
- Dir. Geol. Maroc, 2005. Carte géologique du Maroc No461: Azrou - Échelle 1:50.000. Royaume du Maroc, Ministère l'Énergie des Mines du Développement Durable.
- Domènech, M., Stockli, D.F., Teixell, A., 2018. Detrital zircon U–Pb provenance and palaeogeography of Triassic rift basins in the Marrakech High Atlas. *Terra Nova* 30, 310–318. doi:10.1111/ter.12340
- Eddif, A., Gasquet, D., Hoepffner, C., Levresse, G., 2007. Age of the Wirgane granodiorite intrusions (Western High-Atlas, Morocco): New U–Pb constraints. *Journal of African Earth Science* 47, 227–231. doi:10.1016/j.jafrearsci.2007.02.003
- El Hadi, H., Simancas, J.F., Tahiri, A., Gonzalez-Lodeiro, F., Azor, A., Martinez-Poyatos, D., 2006. Comparative review of the Variscan granitoids of Morocco and Iberia: proposal of a broad zonation. *Geodinamica Acta* 19, 103–116. doi:10.3166/ga.19.103-116
- El Hassani, A., Tahiri, A., Walliser, O.H., 2003. The Variscan crust between Gondwana and Baltica. *CFS Courier Forschungsinstitut Senckenberg* 81–87.
- El Houicha, M., Pereira, M.F., Jouhari, A., Gama, C., Ennih, N., Fekkak, A., Ezzouhairi, H., El Attari, A., Silva, J.B., 2018. Recycling of the Proterozoic crystalline basement in the Coastal Block (Moroccan Meseta): new insights for understanding the geodynamic evolution of the northern peri-Gondwanan realm. *Precambrian Research* 306, 129–154. doi:10.1016/j.precamres.2017.12.039
- Fedo, C.M., Sircombe, K.N., Rainbird, R.H., 2003. Detrital zircon analysis of the sedimentary record. *Reviews in Mineralogy and Geochemistry* 53, 277–303. doi:10.2113/0530277
- Fernández-Suárez, J., Corfu, F., Arenas, R., Marcos, A., Martínez Catalán, J., García, F., Abati, J., Fernández, F., 2002. U–Pb evidence for a polyorogenic evolution of the HP-HT units of the NW Iberian Massif. *Contributions to Mineralogy and Petrology* 143, 236–253. doi:10.1007/s00410-001-0337-2
- Fernández-Suárez, J., Gutiérrez-Alonso, G., Pastor-Galán, D., Hofmann, M., Murphy, J.B., Linnemann, U., 2014. The Ediacaran–Early Cambrian detrital zircon record of NW Iberia: possible sources and paleogeographic constraints. *International Journal of Earth Sciences* 103, 1335–1357. doi:10.1007/s00531-013-0923-3
- Franke, W., Cocks, L.R.M., Torsvik, T.H., 2017. The Palaeozoic Variscan oceans revisited. *Gondwana Research* 48, 257–284. doi:10.1016/j.gr.2017.03.005
- Ghienne, J.F., Benvenuti, A., El Houicha, M., Girard, F., Kali, E., Khoukhi, Y., Langbour, C., Magna, T., Míková, J., Moscariello, A., Schulmann, K., 2018. The impact of the end-Ordovician glaciation on sediment routing systems: a case study from the Meseta

(northern Morocco). *Gondwana Research* 63, 169–178.
doi:10.1016/j.gr.2018.07.001

- Gutiérrez-Alonso, G., Fernández-Suárez, J., Pastor-Galán, D., Johnston, S.T., Linnemann, U., Hofmann, M., Shaw, J., Colmenero, J.R., Hernández, P., 2015. Significance of detrital zircons in Siluro-Devonian rocks from Iberia. *Journal of the Geological Society of London* 172, 309–322. doi:10.1144/jgs2014-118
- Hoepffner, C., 1977. Données nouvelles sur le Paléozoïques de la bordure occidentale du massif du Tazekka. *Comptes Rendus de l'Académie de Science de Paris* 284, 1635–1637.
- Hoepffner, C., 1981. Le complexe volcano-sédimentaire d'âge carbonifère dans le massif du Tazekka, sa place dans l'évolution hercynienne de la Méséta marocaine orientale. *Sciences Géologiques, bulletins et mémoires* 34, 97–106.
- Hoepffner, C., 1987. La tectonique hercynienne dans l'Est du Maroc. Université Louis Pasteur, Strasbourg.
- Hoepffner, C., 1989. L'évolution structurale hercynienne de la Méséta marocain orientale. Essai de mise au point. *Notes et Mémoires du Service Géologique du Maroc*.
- Hoepffner, C., Houari, M.R., Bouabdelli, M., 2006. Tectonics of the North African Variscides (Morocco, western Algeria): an outline. *Comptes Rendus - Géoscience* 338, 25–40. doi:10.1016/j.crte.2005.11.003
- Hoepffner, C., Soulaïmani, A., Piqué, A., 2005. The Moroccan Hercynides. *Journal of African Earth Sciences* 43, 144–165. doi:10.1016/j.jafrearsci.2005.09.002
- Horon, O., 1952. Contribution à l'étude du bassin de Djerada. *Notes et Mémoires du Protectorat de la République Française au Maroc* 89, 180.
- Houari, M.R., Hoepffner, C., 2003. Late Carboniferous dextral wrench-dominated transpression along the North African craton margin (Eastern High-Atlas, Morocco). *Journal of African Earth Sciences* 37, 11–24. doi:10.1016/S0899-5362(03)00085-X
- Huvelin, P., 1970. Chevauchements et écaillages précoces hercyniens des terrains antéviséens dans le domaine atlasique (Maroc). *Comptes Rendus de l'Académie des Sciences de Paris* 270, 2760–2763.
- Kharbouch, F., Juteau, T., Treuil, M., Joron, J.-L., Pique, A., Hoepffner, C., 1989. Le complexe volcano-sédimentaire hercynien de la Méséta marocaine nord-occidentale et orientale: étude pétrographique, géochimique et signification géodynamique. *Notes et Mémoires du Service Géologique du Maroc*.
- Khokhi, Y., Hamoumi, N., 2001. L'Ordovicien de la Meseta oriental (Maroc): stratigraphie génétique-contrôle géodynamique, climatique et eustatique. *African Geoscience Review* 8, 289–302.

- Lazreq, N., 1999. Biostratigraphie des conodontes du Givétien au Famennien du Maroc central: biofaciés et évènement Kellwasser. CFS Courier Forschungsinstitut Senckenberg 214.
- Le Heron, D.P., 2007. Late Ordovician glacial record of the Anti-Atlas, Morocco. *Sedimentary Geology* 201, 93–110. doi:10.1016/j.sedgeo.2007.05.004
- Le Heron, D.P., Craig, J., Etienne, J.L., 2009. Ancient glaciations and hydrocarbon accumulations in North Africa and the Middle East. *Earth-Science Reviews* 93, 47–76. doi:10.1016/j.earscirev.2009.02.001
- Letsch, D., El Houicha, M., von Quadt, A., Winkler, W., 2018. A missing link in the peri-Gondwanan terrane collage: the Precambrian basement of the Moroccan Meseta and its lower Paleozoic cover. *Canadian Journal of Earth Sciences* 55, 1–19. doi:10.1139/cjes-2017-0086
- Linnemann, U., McNaughton, N.J., Romer, R.L., Gehmlich, M., Drost, K., Tonk, C., 2004. West African provenance for Saxo-Thuringia (Bohemian Massif): did Armorica ever leave pre-Pangean Gondwana? - U-Pb-SHRIMP zircon evidence and the Nd-isotopic record. *International Journal of Earth Sciences* 93, 683–705. doi:10.1007/s00531-004-0413-8
- Linnemann, U., Ouzegane, K., Drareni, A., Hofmann, M., Becker, S., Gärtner, A., Sagawe, A., 2011. Sands of West Gondwana: an archive of secular magmatism and plate interactions - a case study from the Cambro-Ordovician section of the Tassili Ouan Ahaggar (Algerian Sahara) using U-Pb-LA-ICP-MS detrital zircon ages. *Lithos* 123, 188–203. doi:10.1016/j.lithos.2011.01.010
- Linnemann, U., Pereira, M.F., Jeffries, T.E., Drost, K., Gerdes, A., 2008. The Cadomian Orogeny and the opening of the Rheic Ocean: the diacrony of geotectonic processes constrained by LA-ICP-MS U-Pb zircon dating (Ossa-Morena and Saxo-Thuringian Zones, Iberian and Bohemian Massifs). *Tectonophysics* 461, 21–43. doi:10.1016/j.tecto.2008.05.002
- Marhoumi, M.R., 1984. Étude palynologique des séries dinantiennes de la Méséta marocaine. Conséquences stratigraphiques et structurales. Université Louis Pasteur, Strasbourg.
- Marhoumi, M.R., Doubinger, J., Rauscher, R., Hoepffner, C., 1989. Données nouvelles sur le Paléozoïque de la Méséta orientale marocaine. Apports de la palynologie. Notes et Mémoires du Service Géologique du Maroc.
- Marhoumi, M.R., Hoepffner, C., Doubinger, J., Rauscher, R., 1983. Données nouvelles sur l'histoire hercynienne de la Meseta orientale au Maroc: l'âge dévonien des schistes de Debdou et du Mekkam. *Comptes Rendus de l'Académie des Sciences de Paris* 297, 69–72.

- Marhoumi, M.R., Rauscher, R., 1984. Un plancton dévonien de la Meseta Orientale au Maroc. *Review of Palaeobotany and Palynology* 43, 237-253. doi:10.1016/0034-6667(84)90035-6
- Marie, P., 1931. Rapport sur les observations faites pendant le mois de Février 1931 dans la région de Debdou. Archives B.R.G.M., unpublished
- Marzoli, A., Davies, J.H.F.L., Youbi, N., Merle, R., Dal Corso, J., Dunkley, D.J., Fioretti, A.M., Bellieni, G., Medina, F., Wotzlaw, J.F., McHone, G., Font, E., Bensalah, M.K., 2017. Proterozoic to Mesozoic evolution of North-West Africa and Peri-Gondwana microplates: detrital zircon ages from Morocco and Canada. *Lithos* 278–281, 229–239. doi:10.1016/j.lithos.2017.01.016
- Matte, P., 2001. The Variscan collage and orogeny (480-290 Ma) and the tectonic definition of the Armorica microplate: a review. *Terra Nova* 13, 122–128. doi:10.1046/j.1365-3121.2001.00327.x
- Medioni, R., 1980. Mise au point stratigraphique sur les terrains carbonifères de la bordure septentrionale des Hauts-Plateaux marocains (massifs de Debdou, boutonnières de Lalla-Mimouna et du Mekam). *Notes du Service Géologique du Maroc* 285 (41), 25-37.
- Michard, A., 1976. *Éléments de géologie marocaine*. Notes et Mémoires du Service Géologique du Maroc 252, 408.
- Michard, A., Cailleux, Y., Hoepffner, C., 1989. L'orogène mésétien du Maroc: structure, déformation hercynienne et déplacement. Notes et Mémoires du Service Géologique du Maroc.
- Michard, A., Ouanaimi, H., Hoepffner, C., Soulaïmani, A., Baidder, L., 2010a. Comment on tectonic relationships of Southwest Iberia with the allochthons of Northwest Iberia and the Moroccan Variscides by J.F. Simancas et al. [*C. R. Géoscience* 341 (2009) 103-113]. *Comptes Rendus - Géoscience* 342, 170–174. doi:10.1016/j.crte.2010.01.008
- Michard, A., Saddiqi, O., Chalouan, A., Frizon de Lamotte, D., 2008. *Continental evolution: the geology of Morocco*. Springer. doi:10.1007/978-3-540-75761-0
- Michard, A., Soulaïmani, A., Hoepffner, C., Ouanaimi, H., Baidder, L., Rjijati, E.C., Saddiqi, O., 2010b. The south-western branch of the Variscan belt: evidence from Morocco. *Tectonophysics* 492, 1–24. doi:10.1016/j.tecto.2010.05.021
- Montero, P., Talavera, C., Bea, F., Lodeiro, F.G., Whitehouse, M.J., 2009. Zircon geochronology of the Ollo de Sapo Formation and the age of the Cambro-Ordovician rifting in Iberia. *The Journal of Geology* 117, 174-191. doi: 10.1086/595017
- Murphy, J. B., Fernández-Suárez, J., Keppie, J. D., Jeffries, T. E., 2004. Contiguous rather than discrete Paleozoic histories for the Avalon and Meguma terranes based on detrital zircon data. *Geology*, 32, 585-588. doi:10.1130/G20351.1

- Naidoo, T., Zimmermann, U., Vervoort, J., Tait, J., 2018. Evidence of early Archean crust in northwest Gondwana, from U–Pb and Hf isotope analysis of detrital zircon, in Ediacaran supracrustal rocks of northern Spain. *International Journal of Earth Sciences* 107, 409–429. doi:10.1007/s00531-017-1500-y
- Nance, R.D., Gutiérrez-Alonso, G., Keppie, J.D., Linnemann, U., Murphy, J.B., Quesada, C., Strachan, R.A., Woodcock, N.H., 2010. Evolution of the Rheic Ocean. *Gondwana Research* 17, 194–222. doi:10.1016/j.gr.2009.08.001
- Nance, R.D., Gutiérrez-Alonso, G., Keppie, J.D., Linnemann, U., Murphy, J.B., Quesada, C., Strachan, R.A., Woodcock, N.H., 2012. A brief history of the Rheic Ocean. *Geoscience Frontiers* 3, 125–135. doi:10.1016/j.gsf.2011.11.008
- Nance, R.D., Murphy, J.B., Strachan, R.A., Keppie, J.D., Gutiérrez-Alonso, G., Fernández-Suárez, J., Quesada, C., Linnemann, U., D’lemos, R., Pisarevsky, S.A., 2008. Neoproterozoic-early Palaeozoic tectonostratigraphy and palaeogeography of the peri-Gondwanan terranes: Amazonian v. West African connections. *Geological Society of London, Special Publication* 297, 345–383. doi:10.1144/SO297.17
- Ouabid, M., Ouali, H., Garrido, C.J., Acosta-Vigil, A., Román-Alpiste, M.J., Dautria, J.M., Marchesi, C., Hidas, K., 2017. Neoproterozoic granitoids in the basement of the Moroccan Central Meseta: correlation with the Anti-Atlas at the NW paleo-margin of Gondwana. *Precambrian Research* 299, 34–57. doi:10.1016/j.precamres.2017.07.007
- Pastor-Galán, D., Gutiérrez-Alonso, G., Murphy, J.B., Fernández-Suárez, J., Hofmann, M., Linnemann, U., 2013. Provenance analysis of the Paleozoic sequences of the northern Gondwana margin in NW Iberia: passive margin to Variscan collision and orocline development. *Gondwana Research* 23, 1089–1103. doi:10.1016/j.gr.2012.06.015
- Pereira, M.F., Chichorro, M., Johnston, S.T., Gutiérrez-Alonso, G., Silva, J.B., Linnemann, U., Hofmann, M., Drost, K., 2012. The missing Rheic Ocean magmatic arcs: provenance analysis of Late Paleozoic sedimentary clastic rocks of SW Iberia. *Gondwana Research* 22, 882–891. doi:10.1016/j.gr.2012.03.010
- Pereira, M.F., El Houicha, M., Chichorro, M., Armstrong, R., Jouhari, A., El Attari, A., Ennih, N., Silva, J.B., 2015. Evidence of a Paleoproterozoic basement in the Moroccan Variscan belt (Rehamna Massif, Western Meseta). *Precambrian Research* 268, 61–73. doi:10.1016/j.precamres.2015.07.010
- Pereira, M.F., Gutiérrez-Alonso, G., Murphy, J.B., Drost, K., Gama, C., Silva, J.B., 2017. Birth and demise of the Rheic Ocean magmatic arc(s): combined U-Pb and Hf isotope analyses in detrital zircon from SW Iberia siliciclastic strata. *Lithos* 278–281, 383–399. doi:10.1016/j.lithos.2017.02.009
- Pérez-Cáceres, I., Martínez Poyatos, D., Simancas, J.F., Azor, A., 2017. Testing the Avalonian affinity of the South Portuguese Zone and the Neoproterozoic evolution

of SW Iberia through detrital zircon populations. *Gondwana Research* 42, 177–192. doi:10.1016/j.gr.2016.10.010

Pérez-Estaún, A., Bastida, F., Martínez Catalán, J.R., Gutiérrez-Marco, J.C., Marcos, A., Pulgar, J.A., 1990. The West-Asturian Leonese zone. Stratigraphy, in: Dallmeyer, R.D., Martínez García, E. (Eds.), *Pre-Mesozoic Geology of Iberia*. Springer-Verlag, Berlin, pp. 92–102.

Piqué, A., 2001. *Geology of Northwest Africa*. Borntraeger, Berlin.

Piqué, A., Michard, A., 1981. Les zones structurales du Maroc hercynien. *Sciences Géologiques, bulletins et mémoires* 34, 135–146.

Piqué, A., Michard, A., 1989. Moroccan Hercynides: a synopsis. The Paleozoic sedimentary and tectonic evolution at the northern margin of West Africa. *American Journal of Science* 289, 286–330.

Poucllet, A., El Hadi, H., Álvaro, J.J., Bardintzeff, J.-M., Benharref, M., Fekkak, A., 2018. Review of the Cambrian volcanic activity in Morocco: geochemical fingerprints and geotectonic implications for the rifting of West Gondwana. *International Journal of Earth Sciences* 107, 2101–2123. doi:10.1007/s00531-018-1590-1

Pratt, J.R., Barbeau, D.L., Garver, J.I., Emran, A., Izykowski, T.M., 2015. Detrital zircon geochronology of Mesozoic sediments in the Rif and Middle Atlas belts of Morocco: provenance constraints and refinement of the West African signature. *The Journal of Geology* 123, 177–200. doi:10.1086/681218

Rauscher, R., Marhoumi, M.R., Vanguetaine, M., Hoepffner, C., 1982. Datation palynologique des schistes du Tazekka au Maroc. Hypothèse structurale sur le socle hercynien de la Meseta orientale. *Comptes Rendus de l'Académie de Science de Paris* 294, 1203–1206.

Said, I., Rodríguez, S., Berkli, M., Cózar, P., Gómez-Herguedas, A., 2010. Environmental parameters of a coral assemblage from the Akerchi Formation (Carboniferous), Adarouch area, central Morocco. *Journal of Iberian Geology* 36 (1), 7-19.

Shaw, J., Gutiérrez-Alonso, G., Johnston, S.T., Pastor Galán, D., 2014. Provenance variability along the Early Ordovician north Gondwana margin: paleogeographic and tectonic implications of U-Pb detrital zircon ages from the Armorican Quartzite of the Iberian Variscan belt. *Bulletin of the Geological Society of America* 126, 702–719. doi:10.1130/B30935.1

Simancas, J.F., Azor, A., Martínez-Poyatos, D., Tahiri, A., El Hadi, H., González-Lodeiro, F., Pérez-Estaún, A., Carbonell, R., 2009. Tectonic relationships of Southwest Iberia with the allochthons of Northwest Iberia and the Moroccan Variscides. *Comptes Rendus - Géoscience* 341, 103–113. doi:10.1016/j.crte.2008.11.003

- Simancas, J.F., Azor, A., Martínez-Poyatos, D., Tahiri, A., Hadi, H. El, González-Lodeiro, F., Pérez-Estaún, A., Carbonell, R., 2010. Reply to the comment by Michard et al. on “Tectonic relationships of Southwest Iberia with the allochthons of Northwest Iberia and the Moroccan Variscides.” *Comptes Rendus - Géoscience* 342, 175–177. doi:10.1016/j.crte.2010.01.007
- Simancas, J.F., Tahiri, A., Azor, A., Lodeiro, F.G., Martínez Poyatos, D.J., El Hadi, H., 2005. The tectonic frame of the Variscan-Alleghanian orogen in southern Europe and northern Africa. *Tectonophysics* 398, 181–198. doi:10.1016/j.tecto.2005.02.006
- Slagstad, T., Roberts, N.M.W., Kulakov, E., 2017. Linking orogenesis across a supercontinent; the Grenvillian and Sveconorwegian margins on Rodinia. *Gondwana Research* 44, 109–115. doi:10.1016/j.gr.2016.12.007
- Tahiri, A., Montero, P., El Hadi, H., Martínez Poyatos, D., Azor, A., Bea, F., Simancas, J.F., González Lodeiro, F., 2010. Geochronological data on the Rabat-Tiflet granitoids: their bearing on the tectonics of the Moroccan Variscides. *Journal of African Earth Sciences* 57, 1–13. doi:10.1016/j.jafrearsci.2009.07.005
- Tahiri, A., El Hadi, H., Pocelet, A., Martínez Poyatos, D.J., Azor, A., Lodeiro, F., Simancas, F., 2017. Ediacaran to Cambrian U-Pb ages of granite pebbles in the Lower Devonian conglomerate of Imouzzer Kandar (northwestern Middle Atlas, Morocco). In: *The First West African Craton and Margins International Workshop “WACMAr” (Abstract)*, Dakhla, Morocco.
- Talavera, C., Montero, P., Martínez Poyatos, D., Williams, I.S., 2012. Ediacaran to Lower Ordovician age for rocks ascribed to the Schist–Graywacke Complex (Iberian Massif, Spain): evidence from detrital zircon SHRIMP U–Pb geochronology. *Gondwana Research* 22, 928–942. doi:10.1016/j.gr.2012.03.008
- Valin, F., 1979. Stratigraphie du paléozoïque dans les monts d’Oujda (Maroc oriental). *Mines, Géologie et Énergie* 46, 79–81.
- Vermeesch, P., 2004. How many grains are needed for a provenance study? *Earth and Planetary Science Letters* 224, 441–451. doi:10.1016/j.epsl.2004.05.037
- Vermeesch, P., 2012. On the visualization of detrital age distributions. *Chemical Geology* 312–313, 190–194. doi:10.1016/j.chemgeo.2012.04.021
- Vermeesch, P., 2018. IsoplotR: a free and open toolbox for geochronology. *GeoscienceFrontiers* 9, 1479–1493. doi: 10.1016/j.gsf.2018.04.001.
- Vidal, J.C., Hoepffner, C., 1979. Carte géologique du Rif No282: Tahala - Échelle 1/50.000. Royaume du Maroc, Ministère l’Énergie des Mines du Développement Durable.
- Villeneuve, M., 2008. Review of the orogenic belts on the western side of the West African Craton: the Bassarides, Rokelides and Mauritanides. *Geological Society of London, Special Publications* 297, 169–201. doi:10.1144/SP297.8

- Walliser, O.H., El Hassani, A., Tahiri, A., 1995. Sur le Dévonien de la Meseta marocaine occidentale. Comparaisons avec le Dévonien allemand et évènements globaux. CFS Courier Forschungsinstitut Senckenberg 188, 21-30.
- Walliser, O.H., El Hassani, A., Tahiri, A., 2000. Mrirt: a key area for the Variscan Meseta of Morocco. Notes et Mémoires du Service Géologique du Maroc 399, 93-108.
- Wollen, I.D., 1974. Structure, stratigraphy and environmental analysis of the Lower Carboniferous rocks near Azrou. University of South Carolina.

Section II.2

Detrital zircon sources in the Ordovician metasedimentary rocks of the Moroccan Meseta: inferences for northern Gondwanan passive margin paleogeography

Cristina Accotto¹, David Martínez Poyatos¹, Antonio Azor¹, Cristina Talavera², Noreen J. Evans³, Antonio Jabaloy-Sánchez¹, Hassan El Hadi⁴, Abdelfatah Tahiri⁵

Accepted on:

GSA, in preparation

Special Publication

“New developments in the Appalachian-Caledonian-Variscan Orogen”

(Received: 11 August 2020; Accepted: 23 October 2020)

¹ Department of Geodynamics, University of Granada, Granada, Spain

² School of Geosciences, University of Edinburgh, Edinburgh, UK

³ School of Earth and Planetary Science, John the Laeter Centre, Curtin University, Perth, Australia

⁴ Laboratory of Geodynamics of Ancient Belts, Faculty of Science Ben M'Sik, Hassan II, University of Casablanca, Morocco

⁵ Laboratory of Geo-biodiversity and Natural Patrimony (GEOBIO), Scientific Institute; Geophysics, Natural Patrimony and Green Chemistry Research Center (GEOPAC), Mohammed V University in Rabat, Morocco

Abstract

Detrital zircon U-Pb geochronology has been widely used to constrain the pre-Carboniferous geography of the European and, to a lesser extent, the Moroccan Variscides. The latter have been generally considered as part of a long-lasting passive margin that characterized northern Gondwana from Ordovician to Devonian time, and was subsequently involved in the Late Paleozoic Variscan orogeny. We report detrital zircon ages for three Early to Late Ordovician samples from the Beni Mellala inlier in the northeastern part of the Western Moroccan Meseta in order to discuss the temporal evolution of the sources of sediments in this region. The detrital zircon spectra of these samples, characterized by two main populations with mean ages of 630-610 Ma and 2170-2060 Ma, are typical of Cambrian-Devonian rocks from the Moroccan Variscides and confirm their link to the West African Craton. A minor Stenian-Tonian population (peak at ca. 970 Ma) suggests the influence of a distant and intermittent NE-African source (Sahara Metacraton), which was probably interrupted after Ordovician time. Our data support previous interpretations of the Moroccan Meseta (and the entire northern Moroccan Variscides) as part of the northern Gondwana passive margin. The main sources of these sediments would have been the West African Craton in the western regions of the passive margin (Moroccan Meseta and central European Paleozoic massifs), and the Arabian-Nubian Shield and/or Sahara Metacraton in the eastern areas (Libya, Egypt, Jordan, central and NW Iberian zones during Paleozoic time) where the 1.0 Ga detrital zircon population is persistent throughout the Ordovician-Devonian time span.

1. Introduction

Zircon is an essential mineral in geochronological studies and paleogeographic reconstructions. Systematic dating and statistical analysis of detrital zircon ages in sedimentary clastic rocks (*e.g.*, Fedo et al., 2003; Gehrels, 2012) has particular value in pre-Alpine orogenies where plate reconstruction and kinematics cannot be based on direct seafloor magnetic stripe observations.

The Variscan orogeny is the result of the consumption of the Rheic Ocean and the collision between Gondwana, Laurussia, and a number of peri-Gondwanan terranes during Late Devonian-Permian time (*e.g.*, Franke et al., 2017; Matte, 2001; Simancas et al., 2005). The resulting Late Paleozoic Variscan belt in Europe has been extensively studied with detrital zircon geochronology during the last two decades (*e.g.*, Linnemann et al., 2004; Nance et al., 2008; Braid et al., 2011; Pereira et al., 2012a, 2017; Eckelmann et al., 2014; Fernández-Suárez et al., 2014; Shaw et al., 2014; Gutiérrez-Alonso et al., 2015; Franke and Dulce, 2017; Pérez-Cáceres et al., 2017). These studies enabled the identification of Gondwanan and Avalonian/Laurussian terranes incorporated into the Variscan belt, which have been interpreted as separated by the Paleozoic Rheic ocean from Late Cambrian to Early Devonian times (*e.g.*, Cocks and Fortey, 1982; Nance et al., 2010). However, along-strike differences in Gondwana-sourced detrital zircons and the

presence of putative second-order orogenic sutures still mask the regional paleogeographic picture (cf. Franke et al., 2017 and Stephan et al., 2019b).

An important portion of the Variscan belt crops out in NW Africa (Morocco and Mauritania) and represents the along-strike extension of the European segment, although the exact correlation is obliterated by the Alpine Betic-Rif orogenic system between the European and African plates (Figure 2.10A). Unfortunately, the number of studies devoted to detrital zircon systematics in the Paleozoic sequences of the NW African Variscides is still relatively small (Abati et al., 2010; Avigad et al., 2012; Gärtner et al., 2017, 2018; Pérez-Cáceres et al., 2017; El Houicha et al., 2018; Ghienne et al., 2018; Letsch et al., 2018; Accotto et al., 2019), while proposed paleogeographic correlation with other Variscan massifs has primarily been based on magmatic similarities and the apparent absence of orogenic sutures (*e.g.*, El Hadi et al., 2006; Simancas et al., 2009). This work focuses on the detrital zircon populations in the Ordovician sequence of the Beni Mellala inlier (Figure 2.10B), located in the northeastern part of the Western Moroccan Meseta. The Paleozoic succession in this inlier is paleontologically well dated (Charriere, 1990), allowing us to propose better characterization of the temporal variations of the putative sediment sources and compare them with other Paleozoic outcrops of similar age in Morocco and Europe.

2. Geological setting

The Paleozoic massifs in northern Morocco that were affected by the Variscan orogeny are collectively known as “northern Moroccan Variscides”. They crop out in different domains (Figure 2.10) that are separated by faults and/or tectonic lineaments (Hoepffner et al., 2006; Michard et al., 2010b), whose paleogeographic significance is still under debate (*e.g.*, Simancas et al., 2009, 2010; Michard et al., 2010a). To the north, the Sehouil Block is characterized by Caledonian deformation and magmatism (Simancas et al., 2005; Michard et al., 2010b; Tahiri et al., 2010) and is, therefore, considered as part of an allochthonous terrane, probably an Avalonian promontory (Simancas et al., 2005), juxtaposed during the Early Carboniferous with the Meseta Domain along the Rabat-Tiflet Fault Zone.

The Moroccan Meseta Domain is a vast area with variably deformed Cambrian to Carboniferous metasedimentary rocks intruded by Carboniferous-Permian Variscan granitoids, and partially covered by post-Variscan Mesozoic-Cenozoic sediments. This domain is subdivided into Eastern (EMM) and Western (WMM) Moroccan Mesetas, separated by the Tazekka-Bsabis-Bekrit Fault Zone. The WMM includes the Coastal Block to the west, the Central Zone, and the “Nappe Zone” to the east, separated by the Western Meseta Shear Zone and the Smaala-Oulmès Fault Zone, respectively (Michard et al., 2010b). The Paleozoic succession in the WMM is characterized by eastward-increasing deformation and low- to very-low grade metamorphism (Hoepffner et al., 2006). In contrast, the Paleozoic rocks of the EMM crop out in relatively small and isolated inliers affected by weak to intense deformation and low- to very low-grade

metamorphism (Hoepffner et al., 2006; Accotto et al., 2020). To the south, the Meseta Domain is juxtaposed with the Southern Zone along the South Meseta Fault Zone (Hoepffner et al., 2006). Farther to the south, the South Atlas Fault Zone separates the Southern Zone and the Sahara Domain (Anti-Atlas), the latter being characterized by almost no Variscan deformation and metamorphism, and hence considered to be part of the Gondwanan foreland of the Variscan Belt (Michard et al., 2010b).

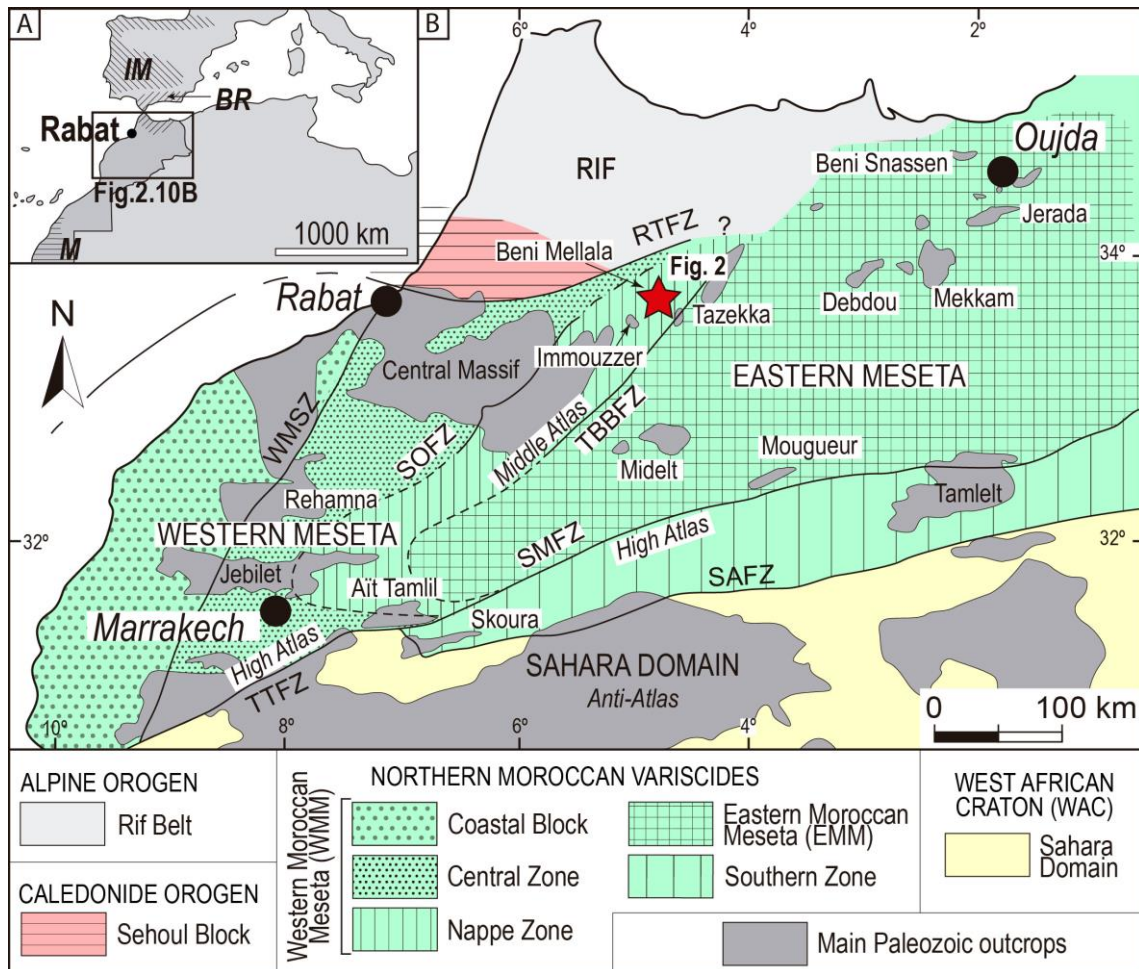


Figure 2.10 (previous page). Geographical and geological location of the studied area. A) Map of NW Africa and Iberia with the location of the northern Moroccan Variscides (rectangle); IM: Iberian Massif; BR: Betic-Rif Belt; M: Mauritanides. B) Geological map of the northern Moroccan Variscides (modified from Hoepffner et al., 2006; Michard et al., 2010b): RTFZ: Rabat-Tiflet Fault Zone; WMSZ: Western Meseta Shear Zone; SOFZ: Smaala-Oulmès Fault Zone; TBBFZ: Tazekka-Bsabis-Bekrit Fault Zone; TTFZ: Tizin'Test Fault Zone; SMFZ: South Meseta Fault Zone; SAFZ: South Atlas Fault Zone. The red star indicates the location of the studied area (Figure 2.11).

2.1. Stratigraphy of the Beni Mellala inlier

The Paleozoic succession of the WMM is roughly continuous from Cambrian to Viséan time (Hoepffner et al., 2005), and unconformably overlies a Neoproterozoic metaigneous basement exposed in a few small outcrops (Tahiri et al., 2010; Pereira et al., 2014, 2015; Ouabid et al., 2017; El Houicha et al., 2018; El Haïbi et al., 2020).

The Cambrian succession is characterized by carbonate sedimentation followed by shales and greywackes, and, locally (*e.g.*, in the Coastal Block; Pouclet et al., 2018), lenses of volcanic rocks (Hoepffner et al., 2005; Michard et al., 2008 and references therein), related to magmatism at the opening of the Rheic Ocean (Murphy et al., 2006; Schulz et al., 2008; Nance et al., 2010, 2012). The Ordovician-Devonian sedimentation defines a passive margin stage, characterized by shales and sandstones (Ordovician), black shales (Silurian), and a succession of quartzitic sandstones and shales passing upwards to limestones (Devonian) (Hoepffner et al., 2005; Michard et al., 2008 and references therein).

The syn-orogenic succession unconformably overlies the Cambrian-Devonian strata and consists of siliciclastic and volcanoclastic sediments deposited during an Early Carboniferous (“intra-Viséan”) extensional episode (Hoepffner et al., 2006) that predated the main Variscan compressional tectonic event (Hoepffner et al., 2005; Michard et al., 2010b).

The Beni Mellala inlier is characterized by gently folded Lower Ordovician-Silurian strata (Figures 2.11A and B; Baudelot et al., 1990; Charriere, 1990), unconformably overlain by an undeformed Mesozoic sequence (Charriere, 1990). The oldest outcropping rocks are the “Bsabis Shales” (Figure 2.11C; Charriere, 1990), which consist of a several hundred meter-thick sequence of black shales with a decameter-thick intercalation of quartzites in the lower part (sample SF3), and sporadic sandy intercalations, which become more common upwards (sample SF2); the uppermost part of the “Bsabis Shales” is made up of green shales. The black shales overlying the quartzite level were dated based on microfossil content as Arenig-Llanvirn (now Floian-Darriwillian, Early-Middle Ordovician; Ouarhache, 1987). These ages were also confirmed by the palynomorph content of several samples throughout the “Bsabis Shales” (Baudelot et al., 1990). As a whole, the “Bsabis Shales” are correlated with the Lower-Middle Ordovician succession of the northwestern sector of the Tazekka inlier (Hoepffner, 1977; Marhoumi et al., 1982; Rauscher et al., 1982; Chakir, 1983).

The “Microconglomeratic Shales” of Late Ordovician age (Upper Katian-Hirnantian; Figure 2.11C) conformably overlay the “Bsabis Shales”. They consist of a thick sequence of grey-greenish shales with a decametre-thick intercalation of black microconglomeratic quartzites (sample SF1; Figure 2.11C). These Upper Ordovician rocks also crop out in the nearby Immouzer inlier (Figure 2.10B), where two samples from the bottom and topmost part of the succession yielded fossils of Early Ashgill (now Katian, Late Ordovician) and earliest Llandovery (Early Silurian) ages, respectively (Charriere, 1990). The “Microconglomeratic Shales” were also recognized in other inliers of the Moroccan Variscides (Charriere, 1990 and references therein), for instance in the Tazekka area (Hoepffner, 1977; Ghienne et al., 2018), having been associated with the glaciation that widely affected Gondwana in the Late Ordovician (Le Heron, 2007; Le Heron et al., 2009, 2008).

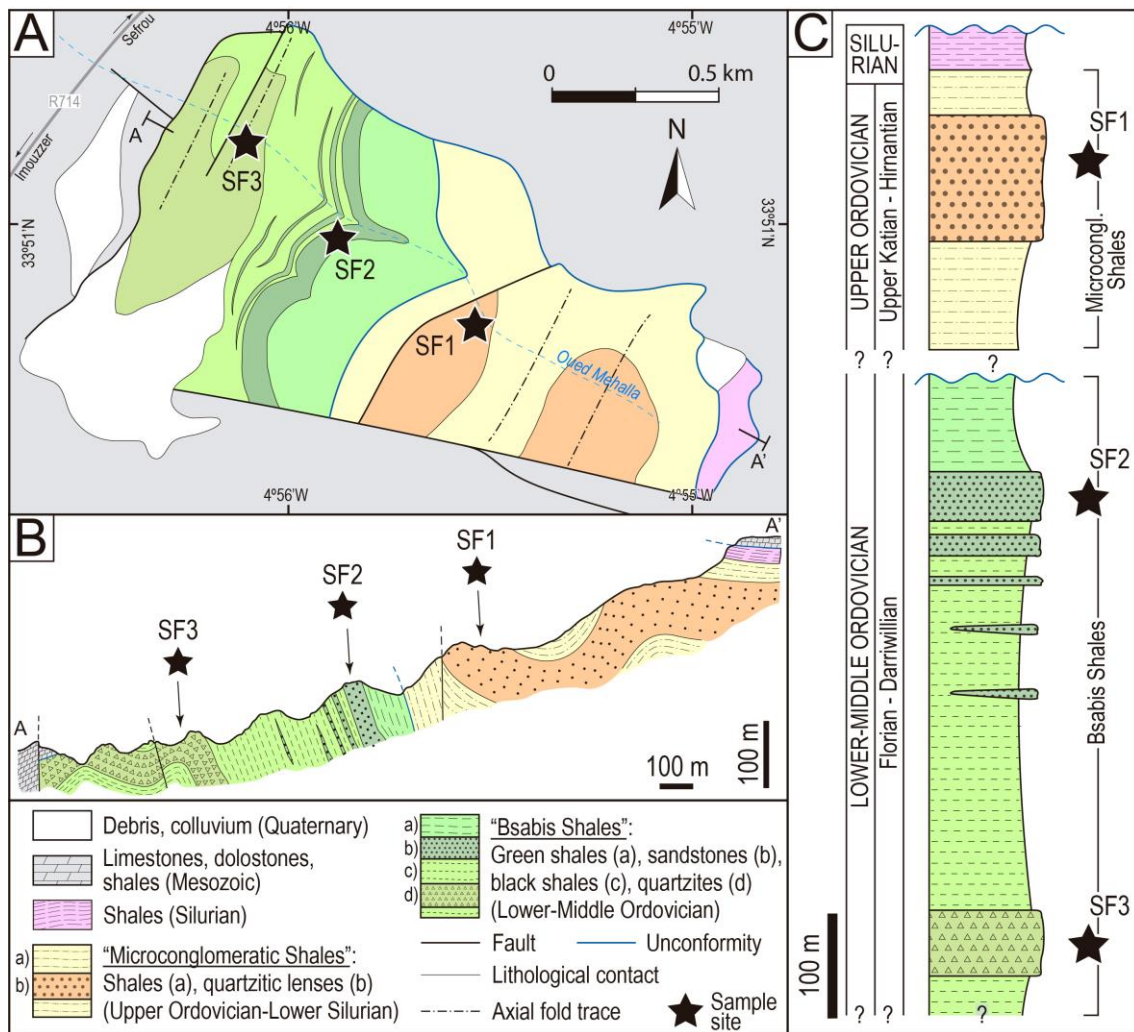


Figure 2.11. Geology of the Beni Mellala inlier (after Baudelot et al. (1990) and Charriere (1990)). (A) Schematic geological map with sample location; (B) Cross section and (C) stratigraphic column of the Paleozoic (Lower Ordovician-Silurian) succession.

Silurian black shales with graptolites (Figure 2.11C) crop out on top of the "Microconglomeratic Shales" (Horon, 1954; Charriere, 1990; Willefert and Charriere, 1990).

3. Sample and methods

During this study, three samples were collected in the Beni Mellala inlier (Figure 2.11). SF1 (IGSN: IEACC0006) was sampled from the black quartzite level, locally microconglomeratic, intercalated within the Upper Ordovician-Lower Silurian (Upper Katian-Lower Llandovery) "Microconglomeratic Shales" (Charriere, 1990). At the microscale, the sample is made up of > 90% rounded, medium-sized, mainly undeformed quartz grains with a few interstitial mica grains. SF2 (IGSN: IEACC0007) was collected from a meter-thick bed of sandstones within the upper part of the Lower-Middle Ordovician (Florian-Darriwilian) "Bsabis Shales" (Charriere, 1990). More than 80% of the sample is made up of angular, fine-sized, mainly undeformed quartz grains, with a

few interstitial oxide and mica grains. Finally, SF3 (IGSN: IEACC0008) was sampled from the quartzitic intercalation in the lower part of the “Bsabis Shales” (Charriere, 1990). At the microscale, the sample is made of > 90% angular, mainly undeformed quartz grains.

At each sample site, 4-5 kg of rock was collected and processed at the University of Granada (Spain). Detrital zircon grains were separated from each sample using mechanical smashing in a jaw-crusher, sorting by sieving, manual panning, and, finally, handpicking. Cathodoluminescence images (CL; Figure 2.12) of the zircon grains were taken with a Mira3 FESEM instrument at the John de Laeter Centre (JdLC), Curtin University (Perth, Australia) and Carl Zeiss SIGMA HD VP Field Emission SEM at the School of GeoSciences, University of Edinburgh (United Kingdom), in order to recognize zoning and alteration textures within the zircon grains.

Because of the variable size of the detrital zircon grains, U-Th-Pb analyses were conducted using laser ablation inductively coupled plasma mass spectrometry (LA-ICPMS, with a spot bin of c. 33 μm), sensitive high-resolution ion microprobe (SHRIMP), and secondary ion mass spectrometry (SIMS) techniques (both of them with a spot bin of c. 15 μm), as summarized in Table 2.3. LA-ICPMS and SHRIMP analyses were performed at the JdLC GeoHistory Facility (Curtin University, Perth, Australia); SIMS measurements were realized at the University of Edinburgh (UK). Details of the analytical methods are described in the Appendix A and the raw results are provided in Appendix D (Tables D.11 to D.13b) and in the Mendeley Dataset repository (doi: 10.17632/t69w5cwyrp.2)1.

Table 2.3. Details of the samples and analyses.

Sample	Location*		Lithology	Age	Zircon grains analyzed	Type of analyses	Number of analyses [§]
	X	Y					
SF1	321855	3746816	Quartzite	Late Ordovician	143	LA-ICPMS	150/ 139
SF2	321334	3747211	Quartzite	Early-Middle Ordovician	131	LA-ICMPS SIMS	80/ 64 52/ 47
SF3	320976	3747518	Quartzite	Early-Middle Ordovician	109	LA-ICPMS SHRIMP	65/ 54 51/ 42

[§]UTM coordinates, WGS84 ellipsoid, zone 30 S.

*Total number of analyses carried out with number of concordant ages (in bold).

All dates with a discordance higher than 10% were discarded. $^{206}\text{Pb}/^{238}\text{U}$ dates were used for zircon grains younger than 1.5 Ga. Due to the significant increase in error on $^{206}\text{Pb}/^{238}\text{U}$ dates for grains older than 1.5 Ga, the $^{207}\text{Pb}/^{206}\text{Pb}$ ratio was considered more appropriate for > 1.5 Ga material analyzed in this work (Spencer et al., 2016). The mean square weighted deviation (MSWD) of the youngest detrital zircon population was calculated using IsoplotR online (Vermeesch, 2018). Finally, Kernel Density Estimators (KDE) and histograms were realized using the software DensityPlotter 8.4 (Vermeesch, 2012), applying a KDE bandwidth and histogram bin of 20 Ma. Errors are expressed at 1 σ level.

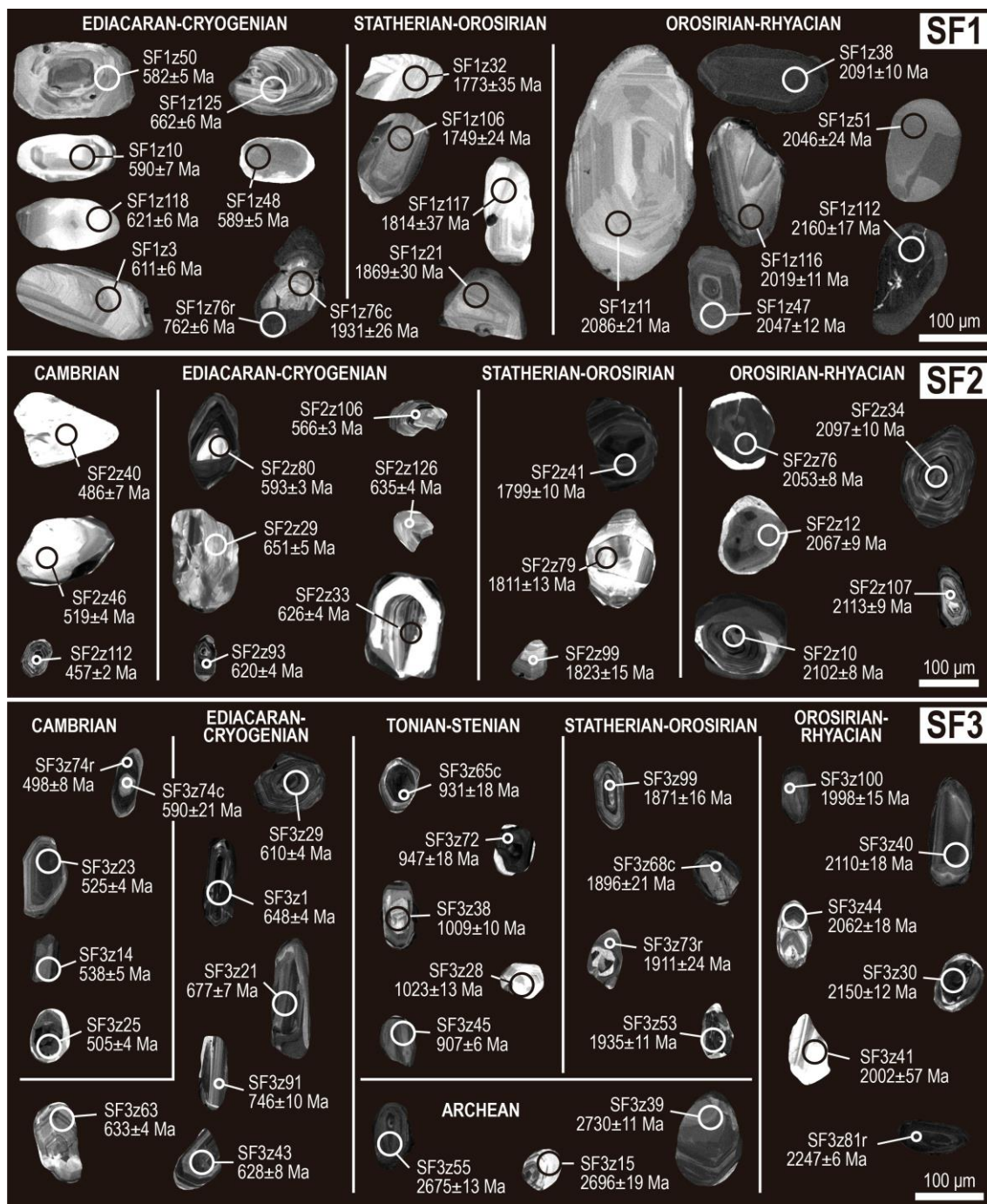


Figure 2.12 (previous page). Cathodoluminescence images of detrital zircon grains from the studied samples; high-U sectors of the crystals correspond to darker zones in the images.

4. Results

From sample SF1, we separated 250 detrital zircon grains with different degrees of roundness and whitish or yellowish color. Grains width vary between ca. 60 and 200 μm . The CL images show continuous oscillatory and sector zoning, and partially resorbed cores with thin overgrowths (Figure 2.12). One hundred and fifty LA-ICPMS analyses were performed, yielding 139 concordant dates (Table 2.3 and Figure 2.13A).

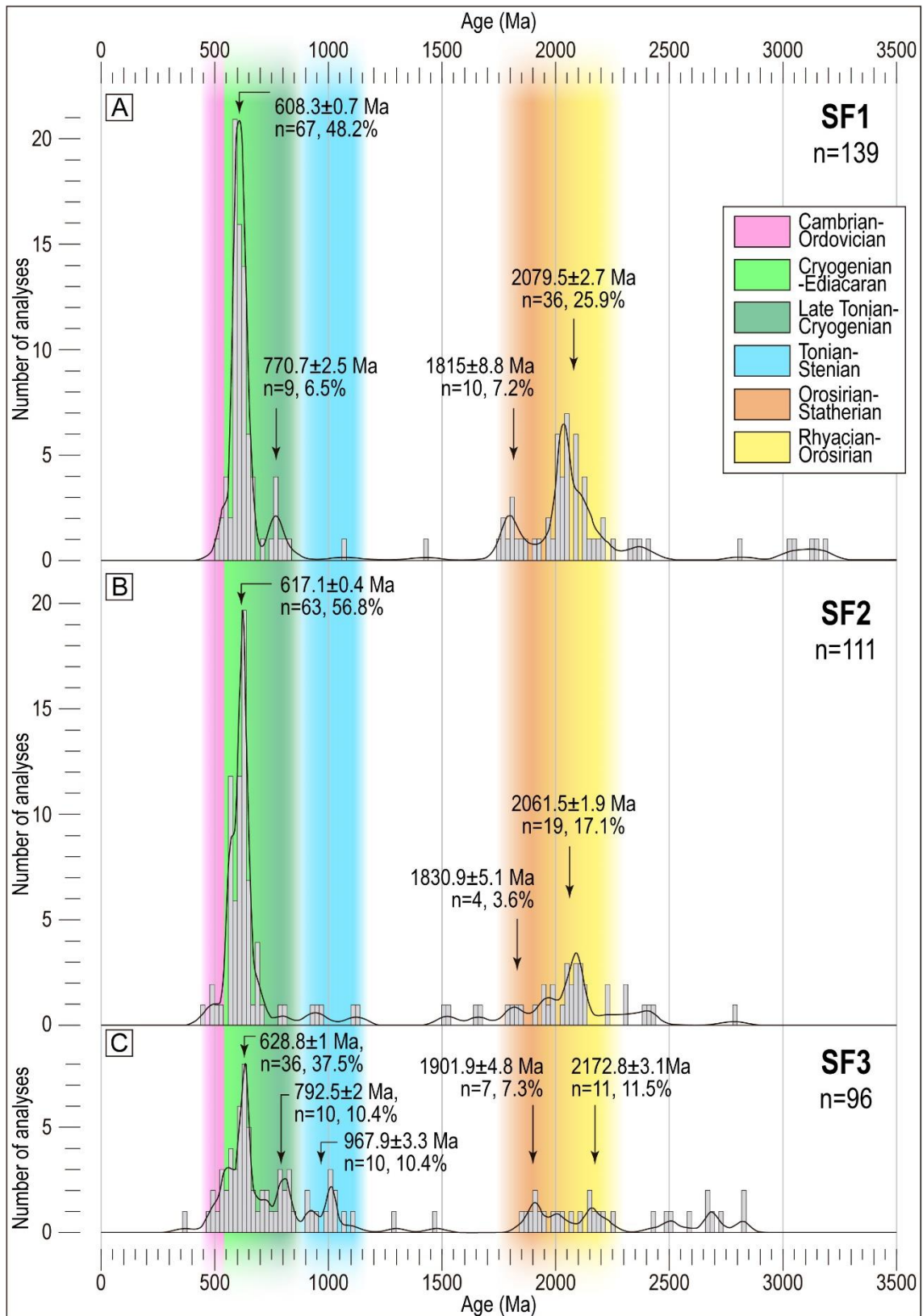


Figure 2.13. Results of U-Pb analyses of detrital zircon grains from the studied samples: combination of Kernel Density Estimates plots (KDE, black lines) and histograms (grey bars) based on $^{206}\text{Pb}/^{238}\text{U}$ (for grains < 1.5 Ga) and $^{207}\text{Pb}/^{206}\text{Pb}$ (for grains > 1.5 Ga) ages. Black arrows indicate the detrital zircon populations calculated with DensityPlotter 8.4 (Vermeesch, 2012); (A) sample SF1; (B) sample SF2; (C) sample SF3.

The most prominent detrital zircon population yielded an Ediacaran mean age of 608.3 ± 0.7 Ma, including 67 Cryogenian-Ediacaran dates (from ca. 668 to 544 Ma, 48.2% of the data). Another important population gave a Rhyacian age (2079.5 ± 2.7 Ma), comprising 36 Rhyacian-Orosirian ages from ca. 2239 to 1972 Ma (25.9% of the data). Minor detrital zircon populations yielded Orosirian-Statherian (mean age 1815 ± 8.8 Ma, 10 dates between ca. 1869 and 1749 Ma, 7.2% of the data) and Late Tonian-Early Cryogenian (mean age 770.7 ± 2.5 Ma, 9 dates from ca. 834 to 712 Ma, 6.5% of the data) ages. Three grains have Cambrian ages (between ca. 534 and 501 Ma), while two analyses yielded Mesoproterozoic ages (ca. 1424 and 1064 Ma), and a few grains gave ages between ca. 3188 and 2320 Ma. The youngest detrital zircon population, defined by 5 dates, yielded a Late Ediacaran age of 543.7 ± 2.5 Ma (MSWD = 1.15) compatible with the stratigraphic age of the sample (Late Ordovician).

Approximately 250 detrital zircons were separated from sample SF2. The grains are differently rounded, generally whitish or yellowish, and show continuous oscillatory or sector zoning with composite textures and overgrown high- or low-U rims (Figure 2.12). The grain size is highly variable (width between ca. 30 and 120 μm). Grains were generally small and only 80 LA-ICPMS analyses were carried out, while another 51 analyses were performed with SIMS (Table 2.3), yielding 64 and 47 concordant dates, respectively. The results were combined to obtain the age distribution shown in Figure 2.13B.

The most important detrital zircon population in sample SF2 yielded an Ediacaran mean age of 617.1 ± 0.4 Ma, including 63 dates with ages ranging from ca. 703 to 560 Ma (Cryogenian-Ediacaran, 56.8% of the data). Nineteen dates (17.1% of the data, dates ranging from ca. 2137 to 1940 Ma) are included in a Rhyacian detrital zircon population with a mean age of 2061.5 ± 1.9 Ma. Minor peaks gave Cambrian-Ordovician (5 dates from ca. 527 to 457 Ma, 4.5% of the data) and Orosirian (mean age 1830.9 ± 5.1 Ma, 4 dates from ca. 1857 to 1799 Ma, 3.6% of the data) ages. Scattered data yielded Statherian-Tonian (11 data with ages from ca. 1670 to 791 Ma) and Rhyacian-Neoproterozoic (8 data between ca. 2781 and 2223 Ma) ages. The youngest detrital zircon population includes 8 dates with an Ediacaran mean age of 562.7 ± 1.2 Ma (MSWD = 0.92), which is compatible with the stratigraphic age of this sample (Early Ordovician).

Two hundred and ten detrital zircons of variable size and color were separated from sample SF3. CL images show continuous oscillatory and sector zoning, as well as partially resorbed cores overgrown by low- or high-U rims (Figure 2.12). The width of the grains varies from ca. 30 to 100 μm . Only 65 LA-ICPMS analyses were performed, yielding 54 concordant results. An additional 42 concordant dates were obtained from 51 SHRIMP analyses (Table 2.3). All of the results were combined to obtain the age distribution shown in Figure 2.13C.

The most important detrital zircon population in sample SF3 has an Ediacaran mean age (628.8 ± 1 Ma) and includes 36 dates (37.5% of the data) ranging from ca. 746 to 541 Ma (Cryogenian-Ediacaran). A minor population (10.4% of the data), defined by 10 dates from ca. 847 to 779 Ma (Late Tonian-Cryogenian), gave a Late Tonian mean age of

792.5±2 Ma. Another 10 dates (10.4% of the data) define a Stenian-Tonian population ranging from ca. 1023 to 907 Ma, which yields an Early Tonian mean age of 967.9±3.3 Ma (with two minor peaks at 912.5±5.3 and 1000.3±4.3 Ma). The Rhyacian-Orosirian population includes only 11 dates (11.5% of the data) with ages from ca. 2247 to 1998 Ma and a Rhyacian mean age of 2172.8±3.1 Ma. Seven dates from ca. 1953 to 1848 Ma (Orosirian-Statherian) depict a minor Orosirian peak at 1901.9±4.8 Ma (7.3% of the data). Finally, 7 Cambrian-Ordovician dates (7.3% of the data) ranging from ca. 538 to 467 Ma can be differentiated from the dominant Cryogenian-Ediacaran population. Scattered grains yielded Late Devonian (ca. 371 Ma, incompatible with the stratigraphic age of the sample), Calymmian-Stenian (ca. 1475-1066 Ma) and Mesoarchean-Siderian (ca. 2828-2430 Ma) ages. The youngest detrital zircon population, including four data, gave a Late Ediacaran age of 543±2.2 Ma (MSWD = 1.38), which is consistent with the stratigraphic age of the sample (Early Ordovician).

In summary, the three samples from the Beni Mellala Ordovician rocks are characterized by a prominent (35-55% of the data) Cryogenian-Ediacaran detrital zircon population with mean ages between ca. 630 and 610 Ma. A second important peak is defined by a Rhyacian-Orosirian population with mean ages ranging from ca. 2170 to 2060 Ma (11-26% of the data). Minor populations found in all three samples define an Orosirian-Statherian peak (ca. 1910-1815 Ma, 4-7% of the data) and a variable number (2-7% of the data) of Cambrian-Ordovician grains have ages ranging between ca. 538 and 457 Ma. A Late Tonian-Cryogenian peak (6-10% of the data) is present in samples SF1 and SF3, with mean ages ranging from ca. 790 to 770 Ma. Sample SF3 is also characterized by a Stenian-Tonian population (ca. 970 Ma defined by 10% of the data), which is absent in the other two samples. The youngest detrital zircon population in all the samples is Ediacaran (ca. 563 Ma in sample SF2; ca. 543 Ma in samples SF1 and SF3).

5. Discussion

5.1. Detrital zircon-derived maximum depositional ages versus true depositional ages

Youngest detrital zircon populations are often used to constrain the maximum depositional ages (MDA) of sampled sedimentary rocks. True depositional ages (TDA), generally based on fossil content and/or direct geochronological dating of volcanic intercalations, can be coeval or slightly younger with respect to the MDA, or they can be separated by hundreds of millions of years (*e.g.*, Sharman and Malkowski, 2020). The time lapse between the MDA and TDA mainly depends on the geographical (*e.g.*, topography, size of drainage systems, etc.) and geological (*e.g.*, active vs passive margins, syn- vs pre-orogenic sequences, etc.) setting. In the case of the Beni Mellala inlier, the studied samples yielded a Late Ediacaran MDA, on average 100 Ma older than the

Ordovician TDA defined on the basis of paleontological and palynomorphic content (Ouarhache, 1987; Baudelot et al., 1990; Charriere, 1990).

Ediacaran MDA are dominant in Cambrian to Devonian rocks all over the Variscan belt (*e.g.*, Fernández-Suárez et al., 2002; Martínez Catalán et al., 2004; Díez Fernández et al., 2010; Avigad et al., 2012; Pereira et al., 2012b, 2012c; Linnemann et al., 2014; Gutiérrez-Alonso et al., 2015; Pérez-Cáceres et al., 2017; Ghienne et al., 2018; Accotto et al., 2019), confirming the spatial and temporal importance of Ediacaran (Pan-African/Cadomian) arc-related magmatism. Offsets between the TDA and the detrital zircon-based MDA vary between ca. 10 and 200 Ma. Therefore, the common assumption of approximating MDA to TDA must be used with caution, especially in passive margin settings such as the one recognized for the Upper Cambrian – Devonian successions all over the Gondwanan side of the Variscides. On the contrary, syn-orogenic successions usually reveal short temporal offsets between the detrital zircon-derived MDA and fossil-based TDA. This is the case for the uppermost Devonian – lowermost Carboniferous Debdou-Mekkan metasedimentary syn-orogenic rocks of the EMM (Accotto et al., 2020), but also of other syn-orogenic sequences in SW (Pereira et al., 2012a, 2017, 2020; Pérez-Cáceres et al., 2017) and NW Iberia (Martínez Catalán et al., 2004).

The presence of very scarce Cambrian (and even Lower Ordovician) detrital zircon grains in the studied samples is compatible with the TDA, and would attest to the very modest syn-rift magmatism at that time in the Moroccan Variscides (red line in Figure 2.14; *e.g.*, Ghienne et al., 2018; Accotto et al., 2019). In this regard, syn- and post-rift magmatism seems to be underrepresented in Ordovician-Devonian metasedimentary rocks in other transects of the Variscan belt with abundant Early Ordovician felsic magmatism (for instance the Central Iberian Zone in Spain; blue line in Figure 2.14; Gutiérrez-Alonso et al., 2015). The simplest explanation for this fact is that the Early Ordovician igneous rocks did not crop out until the collisional and/or post-collisional stages of the Variscan orogeny (*i.e.*, they would have only reached the surface during Carboniferous or even Permian times). However, the Cambrian-Ordovician detrital zircon populations are abundant in the central European Variscan massifs (*e.g.*, Armorican massif, French Central Massif, Saxothuringian Zone, and Moldanubian Zone; black line in Figure 2.14; Linnemann et al., 2004; Strnad and Mihaljevič, 2005; Bahlburg et al., 2010; Drost et al., 2011; Košler et al., 2014; Lin et al., 2016, 2019; Žák and Sláma, 2018; Szczepański et al., 2020). Unlike central/northern Iberia and northern Morocco, it is possible that during Ordovician-Devonian time, the northern Gondwanan passive margin in central European regions was affected by local tectonic activity that led to the exposure of the Cambrian-Ordovician magmatic rocks.

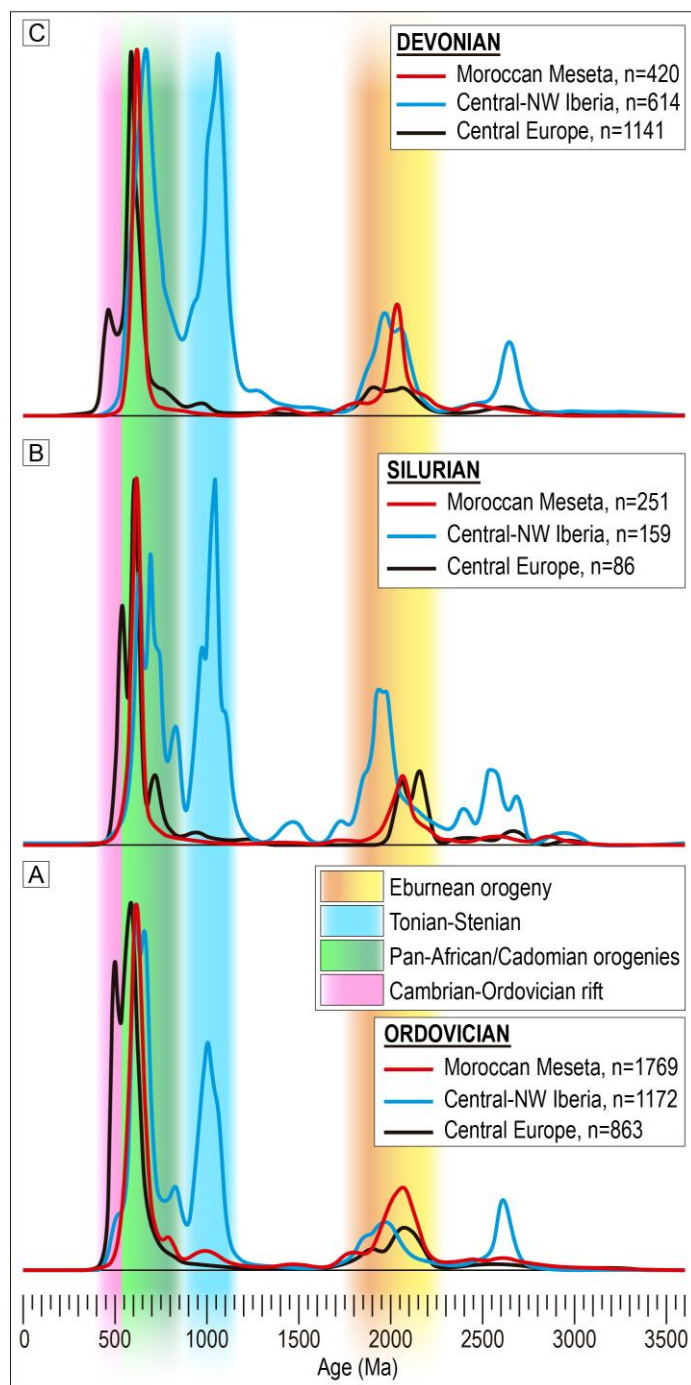


Figure 2.14. Combined KDE plots showing the detrital zircon populations observed in Ordovician-Devonian samples from the Moroccan Meseta (red lines), central and NW Iberia (blue lines), and central European Variscan massifs (Armorican massif, French Central Massif, Saxothuringian Zone, and Moldanubian Zone; black lines); A) Ordovician samples (Moroccan Meseta: Ghienne et al., 2018 and Accotto et al., 2019; central and NW Iberia: Shaw et al., 2014; central Europe: Linnemann et al., 2004; Bahlburg et al., 2010; Drost et al., 2011; Žák and Sláma, 2018; Szczepański et al., 2020); B) Silurian samples (Moroccan Meseta: Accotto et al., 2019; central and NW Iberia: Pastor-Galán et al., 2013 and Gutiérrez-Alonso et al., 2015; central Europe: Žák and Sláma, 2018); C) Devonian samples (Moroccan Meseta: Accotto et al., 2019; central and NW Iberia: Gutiérrez-Alonso et al., 2015; central Europe: Strnad and Mihaljevič, 2005; Košler et al., 2014; Lin et al., 2016, 2019; Žák and Sláma, 2018).

5.2. Stable detrital zircon sources throughout the Ordovician in the northern

Moroccan Variscides

Most of the U-Pb geochronological studies carried out on detrital zircons from the Cambrian to Triassic rocks of the northern Moroccan Variscides point out the prevalence of two main populations, also identified in the samples from the Beni Mellala inlier, with Cryogenian-Ediacaran (ca. 750-540 Ma; in light green in Figure 2.13) and Paleoproterozoic (ca. 2.25-1.95 Ga; in yellow in Figure 2.13) ages (*e.g.*, Abati et al., 2010; Avigad et al., 2012; Pratt et al., 2015; Marzoli et al., 2017; Pérez-Cáceres et al., 2017; Domènech et al., 2018; El Houicha et al., 2018; Ghienne et al., 2018; Letsch et al., 2018; Accotto et al., 2019). These two detrital zircon populations are generally attributed to the Pan-African/Cadomian and Eburnean orogenies (Nance et al., 2008 and references therein), and their presence, together with a significant Mesoproterozoic gap, is considered typical of sediments sourced from the West African Craton (WAC) and nearby areas (*e.g.*, Nance et al., 2008; Abati et al., 2010; Linnemann et al., 2011). We endorse this interpretation and consider the WAC and surrounding Pan-African/Cadomian arc magmatic rocks as the main sources of detrital zircon grains in the Moroccan Variscides. According to our data, these sources would have been stable throughout the Ordovician (at least 50 Ma) and would have supplied detritus to the northern Gondwanan passive margin, developed after Cambrian rifting and through the opening of the Rheic Ocean. However, the samples from Beni Mellala are also characterized by minor detrital zircon populations that deserve more discussion with regard to their potential sources.

A small number of grains (2-7% of the data in samples SF2 and SF3 and 3 grains in sample SF1) yielded Cambrian-Ordovician ages (ca. 538-457 Ma). Although this minor population does not form a real peak in the KDE diagrams (in pink in Figure 2.13), we separated it from the main Cryogenian-Ediacaran population because these data could represent a very different tectonic setting. In this regard, the Pan-African and Cadomian orogenies are considered to have ended by 615-580 Ma (Thomas et al., 2002; Inglis et al., 2004) and 545-540 Ma (Linnemann et al., 2008) respectively. Thus, the Cambrian-Ordovician detrital zircon grains found in our samples, might be related to the Cambrian-Ordovician rifting that preceded the opening of the Rheic Ocean (Linnemann et al., 2008; Schulz et al., 2008), marking the onset of the Variscan cycle. Detrital zircon grains of this age were only found in Early Ordovician samples from the Central Zone of the WMM (Letsch et al., 2018) and Late Ordovician rocks from the Middle Atlas (Ghienne et al., 2018). Cambrian eruptive centers are known in the Anti-Atlas, High Atlas, and Coastal Block, being volumetrically scarce and of basaltic composition (*e.g.*, Pouclet et al., 2018 and references therein). Thus, the scarcity or absence of Cambrian-Ordovician detrital zircon grains in the Ordovician sequence of the northern Moroccan Variscides might suggest that: (i) rifting only had a very local influence, (ii) zircon grains of that age were scarce due to the mafic composition of the parental magmas, and/or (iii) Cambrian magmatic rocks were not exposed at Ordovician time.

A minor Late Tonian-Cryogenian detrital zircon population is also present in samples SF1 and SF3 (790-770 Ma, in dark green in Figure 2.13). These detrital zircon grains

might be correlated with the earliest magmatic pulses of the Pan-African orogenic cycle characterized by the formation of an intra-oceanic volcanic arc (770-750 Ma; Soulaïmani and Hefferan, 2017) that followed the Rodinia supercontinent breakup (885-860 Ma; Ernst et al., 2008; Hefferan et al., 2014 and references therein; Soulaïmani and Hefferan, 2017 and references therein). Actually, a Pan-African oceanic suture was traced through the Anti-Atlas region (Bou Azzer inlier; El Hadi et al., 2010) and might have been the source of the subordinate Tonian-Cryogenian population transported through the same river catchments that brought the Paleoproterozoic and Ediacaran grains.

Stenian-Tonian (900-1100 Ma; 10% of sample SF3 and a few grains in the other samples) detrital zircon grains in the Paleozoic succession of the Moroccan Variscides have been noted in the Anti-Atlas (Avigad et al., 2012), High Atlas (Perez et al., 2019), Middle Atlas (WMM; Ghienne et al., 2018; Accotto et al., 2019), and EMM (Accotto et al., 2019; 2020), as well as in some Mesozoic rocks of the High Atlas (Marzoli et al., 2017), Middle Atlas (Pratt et al., 2015), and Rif (Azdimousa et al., 2019). Primary sources of this age are very common in areas affected by the Grenville orogeny (1.3-0.9 Ga; Ernst et al., 2008), such as Laurentia, Baltica, Avalonia, and Amazonia (Figure 2.15); nevertheless, they are unknown in regions near to the WAC, except in some Neoproterozoic metasedimentary samples from the Mauritanides (Figure 2.10A; Bradley et al., 2015). During Ordovician time, Laurentia, Baltica, and Avalonia were separated from Gondwana by the Rheic Ocean (Figure 2.15) and they cannot be considered primary sources for the Moroccan Ordovician metasedimentary rocks (Accotto et al., 2019). Furthermore, the zircon age spectra of all these Grenvillian terranes (*e.g.*, Drost et al., 2011; Linnemann et al., 2011 and references therein), as well as some of the samples from the Mauritanide orogen (*e.g.*, Bradley et al., 2015; Bea et al., 2020), are continuous throughout the Mesoproterozoic, while the Stenian-Tonian detrital zircon population so far described in Paleozoic rocks from the Moroccan Variscides is characterized by a single peak centered at *c.* 1.0 Ga (Avigad et al., 2012; Ghienne et al., 2018; Accotto et al., 2019; Perez et al., 2019; this work) with no ages older than 1.1-1.15 Ga. Considering this, and regardless of the paleogeographic setting, direct or recycled Amazonian, Laurentian, Baltian, and/or Avalonian sources were likely excluded in the Ordovician metasedimentary rocks of the northern Moroccan Variscides. Regarding the particular case of the Mauritanides, the absence of both *ca.* 1.0 Ga and 1.2-1.5 Ga detrital zircon populations in samples from areas located between the Mauritanides and the Moroccan Meseta, namely the Anti-Atlas (except a minor and very localized 1.0 Ga peak; Avigad et al., 2012), suggests that there were no drainage systems facilitating the direct transportation of sediments between these two regions (Mauritanides and northern Moroccan Variscides). Ghienne et al. (2018) proposed a *ca.* 1.0 Ga source located in an exotic Avalonian terrane remnant that did not drift apart from the main Gondwana continent during the Cambrian rifting and was accreted to the WAC during the Pan-African/Cadomian orogeny. The only evidence for the existence of such terrane is an obsolete charnockite K-Ar date from the Mazagan escarpment (offshore Morocco; Ruellan, 1985), recently re-dated with more reliable techniques at 1.95-1.64 Ga (zircon and monazite U-Pb; Kuiper, 2019; Kuiper et al., 2019). Therefore, the most widely

accepted explanation for the occurrence of a Stenian-Tonian detrital zircon population in samples from the northern Moroccan Variscides (Avigad et al., 2012; Accotto et al., 2019) is a distant source located in the Sahara Metacraton.

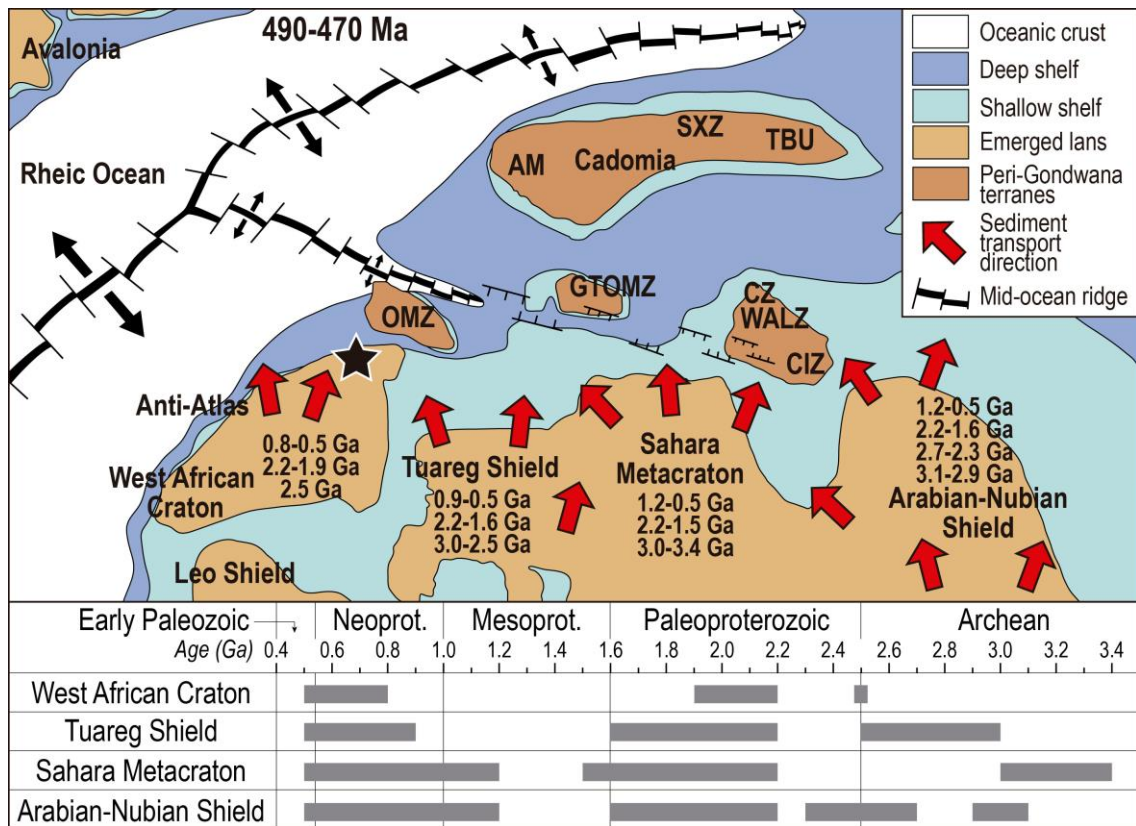


Figure 2.15. Paleogeographic reconstruction of northern Gondwana at Late Ordovician time (490-470 Ma) and distribution of magmatic zircon ages (expressed in Ga) in the main source areas (in map and graphical time scale). The black star locates the Moroccan Meseta. Central and NW Iberia: West-Asturian Leonese Zone (WALZ), Galicia-Tras-os-Montes Zone (GTOMZ), Central Iberian Zone (CIZ), Cantabrian Zone (CZ); SW Iberia: Ossa-Morena Zone (OMZ); Cadomia: Armorican Massif (AM), Saxo-Thuringian Zone (SXZ), Tepla-Barrandian Unit (TBU) (modified from Cambeses et al. (2017) and references therein).

The Sahara Metacraton, together with the Tuareg Shield (Figure 2.15), might also be the source of the Orosirian-Statherian (1.95-1.75 Ga) detrital zircon grains found in our samples. In fact, a zircon age source postdating the end of the Eburnean orogeny is unknown in the WAC, except some sets of bimodal dykes in the Anti-Atlas associated with the breakup of the Nuna/Columbia supercontinent and dated at 1.75 Ga (Lama et al., 1993; Gasquet et al., 2004; Youbi et al., 2013). Nevertheless, it is unlikely that these bimodal dykes yielded the volume of zircon grains of this age found in our samples and in other samples from the northern Moroccan Variscides (*e.g.*, Abati et al., 2010; Avigad et al., 2012; Ghienne et al., 2018; Letsch et al., 2018; Accotto et al., 2019, 2020).

Finally, a few scattered zircon grains in all the samples yielded Archean ages (2.5-3.2 Ga), possibly sourced from the Leonean-Liberian orogenies in central Africa (Hurley et al., 1971; Nance et al., 2008 and references therein), although the precise determination of the primary source areas of these grains has likely been obscured by sedimentary recycling.

In summary, based on the main detrital zircon populations observed in our samples we conclude that the principal source of sediments in this part of the WMM during the Ordovician was the WAC, in addition to some very subordinate Cambrian-Ordovician rift-related magmatic sources, probably located within the Moroccan Mesetas, and distant NE African sources that supplied the scarce Stenian-Tonian and Orosirian-Statherian detrital zircon grains.

5.3. Paleogeography of the northern Moroccan Variscides and correlation with European counterparts

Several attempts to reconstruct the paleogeographic evolution of the Moroccan Variscides have been carried out (*e.g.*, Michard, 1976; Michard et al., 1989, 2010a, 2010b; Piqué and Michard, 1989, 2018; Walliser et al., 1995, 2000; Piqué, 2001; El Hassani et al., 2003; Hoepffner et al., 2005, 2006; Simancas et al., 2005, 2009), proposing the affinity of the Meseta Domain with the northern Gondwanan (Sahara domain; Figure 2.10) based on stratigraphic similarities and the absence of suture-related units in-between (Simancas et al., 2009; Michard et al., 2010a, 2010b). The geochronological analyses of detrital zircon grains from the Paleozoic succession of the Anti-Atlas (Abati et al., 2010; Avigad et al., 2012), WMM (El Houicha et al., 2018; Ghienne et al., 2018; Letsch et al., 2018; Accotto et al., 2019; this study), and EMM (Accotto et al., 2019) confirm this paleogeographic picture and place the whole northern Moroccan Variscides (with the exception of the Sehoul Block with Avalonian affinity and its putative eastwards prolongation in the EMM; Accotto et al., 2020) close to the WAC throughout the Paleozoic (see previous sub-section).

From a tectonic point of view, all previously quoted reconstructions consider that the Moroccan Variscides as a whole represents a Cambrian-Devonian northern Gondwana passive margin, later inverted during the Variscan collision (*e.g.*, Hoepffner et al., 2005, 2006; Michard et al., 2010b; Accotto et al., 2020). Nevertheless, comparison of the detrital zircon distribution in the Ordovician-Devonian rocks of Morocco with the distribution seen in other paleogeographically well constrained northern Gondwanan sequences (*e.g.*, the central/northwestern Iberia and central Europe transects) yields remarkable differences. The most important of these concerns the ca. 1.0 Ga detrital zircon population (Figure 2.14). In this regard, a minor Stenian-Tonian detrital zircon population was described in some samples from the Cambrian-Ordovician succession of the Moroccan Variscides (Avigad et al., 2012; Ghienne et al., 2018; Accotto et al., 2019), but it generally represents less than 10-15% of the data (except in two samples from the Tazekka inlier with up to 30% Stenian-Tonian ages; Accotto et al., 2019). In contrast, the ca. 1.0 Ga population is always represented in samples from central and northwestern Iberia (*e.g.*, Bea et al., 2010; Talavera et al., 2012; Pastor-Galán et al., 2013; Fernández-Suárez et al., 2014; Shaw et al., 2014; Gutiérrez-Alonso et al., 2015) with abundances of up to 30-50% (red line in Figure 2.14). The detrital zircon age spectra for the Gondwana-derived central European Variscan massifs (*e.g.*, Armorican massif, French Central Massif, Saxothuringian Zone, and Moldanubian Zone; Linnemann et al., 2004; Strnad

and Mihaljevič, 2005; Bahlburg et al., 2010; Drost et al., 2011; Košler et al., 2014; Lin et al., 2016, 2019; Žák and Sláma, 2018; Szczepański et al., 2020) are very similar to those of the Moroccan Meseta (black line in Figure 2.14). Thus, the Stenian-Tonian detrital zircon population in these regions always represents less than 5% of the data. Accordingly, there is now consensus to place central and NW Iberian zones close to either the Arabian-Nubian Shield and/or the Sahara Metacraton (*e.g.*, Bea et al., 2010; Gutiérrez-Alonso et al., 2015) where primary Stenian-Tonian sources are common (Figure 2.15), while other central European massifs were probably located in more western areas. Thus, the northern Gondwana Paleozoic margin can be reconstructed as a several thousand km-long platform, with central and northern Iberia located in an eastern position and the Moroccan and central European Variscides in a western location, closer to the WAC (Figure 2.15). The differences between the Moroccan Paleozoic and the central and NW Iberian rocks seem to persist throughout the passive margin stage (ca. 200 Ma).

6. Conclusions

The detrital zircon content of the Beni Mellala Ordovician rocks in the EMM attests to a typical and temporally stable WAC source area (providing a ca. 750-540 Ma dominant population and a ca. 2250-1950 Ma subordinate one) with a distant -and maybe intermittent- influence from the Sahara Metacraton (minor population of ca. 970 Ma in an Early Ordovician sample). This detrital zircon spectrum is common in most of the Ordovician-Devonian rocks so far analyzed in the Moroccan Variscides. It has usually been interpreted, in combination with other geological data (especially the absence of suture-related rocks to the south (Variscan foreland)), as indicative of a northern Gondwana long-lasting passive margin stage. Therefore, the northern Gondwana margin have comprised a several thousand km-long and laterally continuous Ordovician-Devonian platform with diverse sediment routing systems (as shown by the detrital zircon content): Arabian-Nubian Shield and/or Saharan Metacraton sources would have dominated the eastern regions (including central and northwestern Iberia) throughout the passive margin stage, while WAC sources would have prevailed in western regions (Moroccan Variscides and central European massifs).

Acknowledgments

This work was funded by the Ministerio de Economía y Competividad (MINECO) of Spain through the project PANGEATOR (CGL2015-71692-P) and the Pre-Doctoral scholarship BES-2016-078168. We are indebted to Elain Millar, Mike Hall, and Brad McDonald for their assistance in the JdLC MMF, technical support on sample preparation, and the LA-ICPMS, respectively. The CL imaging was carried out on the Curtin University's Microscopy & Microanalysis Facility, whose instrumentation has been partially funded by the University, State and Commonwealth Governments, and the Scanning Electron Microscope (SEM) Facility at the University of Edinburgh. Laboratory

analyses on the detrital zircon grains were carried out on the JdLC SHRIMP II, supported by the Australian Research Council. Research in the JdLC GeoHistory Facility is enabled by AuScope (auscope.org.au) and the Australian Government via the National Collaborative Research Infrastructure Strategy (NCRIS). The SIMS analyses were performed at the NERC Ion Microprobe Facility of the University of Edinburgh (UK). The authors want to express their gratitude to Dr. Faouziya Haissen (Hassan II University of Casablanca, Morocco) and Dr. Douglas N. Reusch (University of Main, USA) as peer reviewers, and Dr. Yvette Kuiper (Colorado School of Mines, USA) as volume editor, for their constructive comments and suggestions that helped to improve the quality of the original manuscript.

References

- Abati, J., Mohsine Aghzer, A., Gerdes, A., and Ennih, N., 2010, Detrital zircon ages of Neoproterozoic sequences of the Moroccan Anti-Atlas belt: *Precambrian Research*, v. 181, p. 115–128, doi:10.1016/j.precamres.2010.05.018.
- Accotto, C., Martínez Poyatos, D.J., Azor, A., Jabaloy-Sánchez, A., Talavera, C., Evans, N.J., and Azdimousa, A., 2020, Tectonic evolution of the Eastern Moroccan Meseta: from Late Devonian fore-arc sedimentation to Early Carboniferous collision of an Avalonian promontory: *Tectonics*, v. 39, p. 1-29, doi: 10.1029/2019TC005976.
- Accotto, C., Martínez Poyatos, D.J., Azor, A., Talavera, C., Evans, N.J., Jabaloy-Sánchez, A., Azdimousa, A., Tahiri, A., and El Hadi, H., 2019, Mixed and recycled detrital zircons in the Paleozoic rocks of the Eastern Moroccan Meseta: paleogeographic inference: *Lithos*, v. 338–339, p. 73–86, doi:10.1016/j.lithos.2019.04.011.
- Avigad, D., Gerdes, A., Morag, N., and Bechstädt, T., 2012, Coupled U-Pb-Hf of detrital zircons of Cambrian sandstones from Morocco and Sardinia: implications for provenance and Precambrian crustal evolution of North Africa: *Gondwana Research*, v. 21, p. 690–703, doi:10.1016/j.gr.2011.06.005.
- Azdimousa, A., Jabaloy-Sánchez, A., Talavera, C., Asebriy, L., González-Lodeiro, F., and Evans, N.J., 2019, Detrital zircon U-Pb ages in the Rif Belt (northern Morocco): paleogeographic implications: *Gondwana Research*, v. 70, p. 133–150, doi:10.1016/j.gr.2018.12.008.
- Bahlburg, H., Vervoort, J.D., DuFrane, S.A., 2010. Plate tectonic significance of Middle Cambrian and Ordovician siliciclastic rocks of the Bavarian Facies, Armorican Terrane Assemblage, Germany - U-Pb and Hf isotope evidence from detrital zircons. *Gondwana Research*, 17, 223–235. doi:10.1016/j.gr.2009.11.007
- Baudelot, S., Charriere, A., Ouarhache, D., and Sabaoui, A., 1990, Données palynologiques nouvelles concernant l'Ordovicien et le Trias - Lias du Moyen-Atlas

(Maroc): *Géologie Méditerranéenne*, v. 17, p. 263–277, doi:10.3406/geolm.1990.1444.

- Bea, F., Montero, P., Haissen, F., Molina, J.F., Lodeiro, F.G., Mouttaqi, A., Kuiper, Y.D., Chaib, M., 2020. The Archean to Late-Paleozoic architecture of the Oulad Dlim Massif, the main Gondwanan indenter during the collision with Laurentia. *Earth-Science Reviews* 208 (103273). doi:10.1016/j.earscirev.2020.103273
- Bea, F., Montero, P., Talavera, C., Abu Anbar, M., Scarrow, J.H., Molina, J.F., and Moreno, J.A., 2010, The palaeogeographic position of Central Iberia in Gondwana during the Ordovician: Evidence from zircon chronology and Nd isotopes: *Terra Nova*, v. 22, p. 341–346, doi:10.1111/j.1365-3121.2010.00957.x.
- Black, L.P., Kamo, S.L., Williams, I.S., Mundil, R., Davis, D.W., Korsch, R.J., and Foudoulis, C., 2003, The application of SHRIMP to Phanerozoic geochronology; a critical appraisal of four zircon standards: *Chemical Geology*, v. 200, p. 171-188, doi: 10.1016/S0009-2541(03)00166-9.
- Bradley, D.C., O’Sullivan, P., Cosca, M.A., Motts, H.A., Horton, J.D., Taylor, C.D., Beaudoin, G., Lee, G.K., Ramezani, J., Bradley, D.B., Jones, J. V, Bowring, S.A., 2015. Synthesis of geological, structural, and geochronologic data (phase V, deliverable 53), chap. A of Taylor, C.D., ed., *Second projet de renforcement institution- nel du secteur minier de la République Islamique de Mauritanie (PRISM-II): U.S. Geological Sur.* doi:http://dx.doi.org/10.3133/ofr20131280.
- Braid, J.A., Murphy, J.B., Quesada, C., and Mortensen, J., 2011, Tectonic escape of a crustal fragment during the closure of the Rheic Ocean: U-Pb detrital zircon data from the Late Palaeozoic Pulo do Lobo and South Portuguese zones, southern Iberia: *Journal of the Geological Society of London*, v. 168, p. 383–392, doi:10.1144/0016-76492010-104.
- Cambeses, A., Scarrow, J.H., Montero, P., Lázaro, C., and Bea, F., 2017, Palaeogeography and crustal evolution of the Ossa–Morena Zone, southwest Iberia, and the North Gondwana margin during the Cambro-Ordovician: a review of isotopic evidence: *International Geology Review*, v. 59, p. 94–130, doi:10.1080/00206814.2016.1219279.
- Chakir, A., 1983, *Contribution à l’étude des Acritarches du massif du Tazekka (Maroc) [Ph.D. thesis]:* Department du Paléobotanique Paléopalynologie, Faculté de Science de la Université de Liège, Belgium, 154 p.
- Charriere, A., 1990. *Héritage hercynien et évolution géodynamique alpine d’une chaîne intracontinentale: le Moyen-Atlas au SE de Fes (Maroc) [Ph.D. thesis]:* Université de Toulouse 3, France.
- Chen, G., Robertson, A.H.F., and Ustaömer, T., 2019, U–Pb detrital zircon ages used to infer provenance and tectonic setting of Late Triassic–Miocene sandstones related to

- the Tethyan development of Cyprus: *Journal of the Geological Society of London*, v. 176, p. 863–884, doi:10.1144/jgs2018-207.
- Cherniak, D., and Watson, E., 2001, Pb diffusion in zircon: *Chemical Geology*, v. 172, p. 5–24, doi:10.1016/S0009-2541(00)00233-3.
- Claoué-Long, J.C, Compston, W., Roberts, J., and Fanning, C.M., 1995, Two Carboniferous ages: A comparison of SHRIMP zircon dating with conventional zircon ages and $^{40}\text{Ar}/^{39}\text{Ar}$ analysis. *Geochronology, Timescales and Global Stratigraphic Correlation*, in Berggren, W.A., Kint, D.V., Aubry, M.P. Hardenbol, J., Society for Sedimentary Geology, Special Publications 54, p. 3-21.
- Cocks, L.R.M., and Fortey, R.A., 1982, Faunal evidence for oceanic separations in the Palaeozoic of Britain: *Journal of the Geological Society London*, v. 139, p. 465–478, doi:10.1144/gsjgs.139.4.0465.
- Compston, W., Williams, I.S., and Meyer, C.E., 1984, U-Pb geochronology of zircons from lunar breccia 73217 using a sensitive high-mass resolution ion microprobe, in *Proceedings of the fourteenth Lunar and Planetary Science Conference, Par 2*, *Journal of Geophysical Research*, doi:10.1029/JB089iS02p0B525.
- De Laeter, J.R., and Kennedy, A.K., 1998, A double focusing mass spectrometer for geochronology: *International Journal of Mass Spectrometry*, v. 178, p. 43–50, doi:10.1016/S1387-3806(98)14092-7.
- Díez Fernández, R., Catalán, J.R.M., Gerdes, A., Abati, J., Arenas, R., and Fernández-Suárez, J., 2010, U–Pb ages of detrital zircons from the Basal allochthonous units of NW Iberia: Provenance and paleoposition on the northern margin of Gondwana during the Neoproterozoic and Paleozoic: *Gondwana Research*, v. 18, p. 385–399, doi:10.1016/j.gr.2009.12.006.
- Domènech, M., Stockli, D.F., and Teixell, A., 2018, Detrital zircon U–Pb provenance and palaeogeography of Triassic rift basins in the Marrakech High Atlas: *Terra Nova*, v. 30, p. 310–318, doi:10.1111/ter.12340.
- Drost, K., Gerdes, A., Jeffries, T., Linnemann, U., and Storey, C., 2011, Provenance of Neoproterozoic and early Paleozoic siliciclastic rocks of the Teplá-Barrandian unit (Bohemian Massif): evidence from U-Pb detrital zircon ages: *Gondwana Research*, v. 19, p. 213–231, doi:10.1016/j.gr.2010.05.003.
- Eckelmann, K., Nesbor, H.-D., Königshof, P., Linnemann, U., Hofmann, M., Lange, J.-M., and Sagawe, A., 2014, Plate interactions of Laurussia and Gondwana during the formation of Pangaea - Constraints from U-Pb LA-SF-ICP-MS detrital zircon ages of Devonian and Early Carboniferous siliciclastics of the Rhenohercynian zone, Central European Variscides: *Gondwana Research*, v. 25, p. 1484–1500, doi:10.1016/j.gr.2013.05.018.
- El Hadi, H., Simancas, J.F., Martínez-Poyatos, D., Azor, A., Tahiri, A., Montero, P., Fanning, C.M., Bea, F., and González-Lodeiro, F., 2010, Structural and

- geochronological constraints on the evolution of the Bou Azzer Neoproterozoic ophiolite (Anti-Atlas, Morocco): *Precambrian Research*, v. 182, p. 1–14, doi:10.1016/j.precamres.2010.06.011.
- El Hadi, H., Simancas, J.F., Tahiri, A., Gonzalez-Lodeiro, F., Azor, A., and Martinez-Poyatos, D., 2006, Comparative review of the Variscan granitoids of Morocco and Iberia: proposal of a broad zonation: *Geodinamica Acta*, v. 19, p. 103–116, doi:10.3166/ga.19.103-116.
- El Haibi, H., El Hadi, H., Tahiri, A., Martínez Poyatos, D., Gasquet, D., Pérez-Cáceres, I., González Lodeiro, and F., Mehdioui, S., 2020, Geochronology and isotopic geochemistry of Ediacaran high-K calc-alkaline felsic volcanism: an example of a Moroccan perigondwanan (Avalonian?) remnant in the El Jadida horst (Mazagonia): *Journal of African Earth Science*, v. 163, 103669, doi:10.1016/j.jafrearsci.2019.103669.
- El Hassani, A., Tahiri, A., and Walliser, O.H., 2003, The Variscan Crust between Gondwana and Baltica: *CFS Courier Forschungsinstitut Senckenberg*, n. 242, p. 81–87.
- El Houicha, M., Pereira, M.F., Jouhari, A., Gama, C., Ennih, N., Fekkak, A., Ezzouhairi, H., El Attari, A., and Silva, J.B., 2018, Recycling of the Proterozoic crystalline basement in the Coastal Block (Moroccan Meseta): new insights for understanding the geodynamic evolution of the northern peri-Gondwanan realm: *Precambrian Research*, v. 306, p. 129–154, doi:10.1016/j.precamres.2017.12.039.
- Ernst, R.E., Wingate, M.T.D., Buchan, K.L., and Li, Z.X., 2008, Global record of 1600–700 Ma Large Igneous Provinces (LIPs): implications for the reconstruction of the proposed Nuna (Columbia) and Rodinia supercontinents: *Precambrian Research*, v. 160, p. 159–178, doi:10.1016/j.precamres.2007.04.019.
- Fedo, C.M., Sircombe, K.N., and Rainbird, R.H., 2003, Detrital zircon analysis of the sedimentary record. *Reviews in Mineralogy and Geochemistry*, v. 53, p. 277–303, doi:10.2113/0530277.
- Fernández-Suárez, J., Alonso, G.G., Cox, R., and Jenner, G.A., 2002, Assembly of the Armorica microplate: a strike-slip terrane delivery? Evidence from U-Pb ages of detrital zircons. *The Journal of Geology*, v. 110, p. 619–626, doi:10.1086/341760.
- Fernández-Suárez, J., Gutiérrez-Alonso, G., Pastor-Galán, D., Hofmann, M., Murphy, and J.B., Linnemann, U., 2014, The Ediacaran–Early Cambrian detrital zircon record of NW Iberia: possible sources and paleogeographic constraint: *International Journal of Earth Sciences*, v. 103, p. 1335–1357, doi:10.1007/s00531-013-0923-3.
- Franke, W., Cocks, L.R.M., and Torsvik, T.H., 2017, The Palaeozoic Variscan oceans revisited: *Gondwana Research*, v. 48, p. 257–284, doi:10.1016/j.gr.2017.03.005.
- Franke, W., and Dulce, J.-C., 2017, Back to sender: tectonic accretion and recycling of Baltica-derived Devonian clastic sediments in the Rheno-Hercynian Variscides:

International Journal of Earth Sciences, v. 106, p. 377–386, doi:10.1007/s00531-016-1408-y.

- Franke, W., Huckriede, H., O’Sullivan, P., and Wemmer, K., 2019, Zircons to the front: accretionary history of the Rheno-Hercynian active margin (Variscides, Germany): Canadian Journal of Earth Sciences, v. 56, p. 1375–1397, doi:10.1139/cjes-2018-0255.
- Gärtner, A., Youbi, N., Villeneuve, M., Linnemann, U., Sagawe, A., Hofmann, M., Zieger, J., Mahmoudi, A., and Boumehdi, M.A., 2018, Provenance of detrital zircon from siliciclastic rocks of the Sebkhâ Gezmâyet unit of the Adrar Souttoug Massif (Moroccan Sahara) – Palaeogeographic implications.: Comptes Rendus - Geoscience, v. 350, p. 255–266, doi:10.1016/j.crte.2018.06.004.
- Gärtner, A., Youbi, N., Villeneuve, M., Sagawe, A., Hofmann, M., Mahmoudi, A., Boumehdi, M.A., and Linnemann, U., 2017, The zircon evidence of temporally changing sediment transport—the NW Gondwana margin during Cambrian to Devonian time (Aoucert and Smara areas, Moroccan Sahara): International Journal of Earth Sciences, v. 106, p. 2747–2769. doi:10.1007/s00531-017-1457-x.
- Gasquet, D., Chevremont, P., Baudin, T., Chalot-Prat, F., Guerrot, C., Cocherie, A., Roger, J., Hassenforder, B., and Cheilletz, A., 2004, Polycyclic magmatism in the Tagragra d’Akka and Kerdous–Tafeltast inliers (Western Anti-Atlas, Morocco): Journal of African Earth Science, v. 39, 267–275, doi:10.1016/j.jafrearsci.2004.07.062.
- Gehrels, G., 2012, Detrital zircon U-Pb geochronology: current methods and new opportunities, in Busby, C., and Azor, A., eds., Tectonics of sedimentary basins: recent advances, p. 45–62, Blackwell Publishing Ltd., doi:10.1002/9781444347166.ch2.
- Ghienne, J.F., et al., 2018, The impact of the end-Ordovician glaciation on sediment routing systems: a case study from the Meseta (northern Morocco): Gondwana Research, v. 63, p. 169–178, doi:10.1016/j.gr.2018.07.001.
- Gutiérrez-Alonso, G., Fernández-Suárez, J., Pastor-Galán, D., Johnston, S.T., Linnemann, U., Hofmann, M., Shaw, J., Colmenero, and J.R., Hernández, P., 2015, Significance of detrital zircons in Siluro-Devonian rocks from Iberia: Journal of the Geological Society London, v. 172, p. 309–322. doi:10.1144/jgs2014-118.
- Heaman, L.M., and LeCheminant, A.N., 1993, Paragenesis and U-Pb systematics of baddeleyite (ZrO₂): Chemical Geology, v. 110, p. 95–126, doi:10.1016/0009-2541(93)90249-I.
- Hefferan, K., Soullaimani, A., Samson, S.D., Admou, H., Inglis, J., Saquaque, A., Latifa, and C., Heywood, N., 2014, A reconsideration of Pan African orogenic cycle in the Anti-Atlas Mountains, Morocco: Journal of African Earth Science, v. 98, p. 34–46, doi:10.1016/j.jafrearsci.2014.03.007.

- Hoepffner, C., 1977, Données nouvelles sur le Paléozoïques de la bordure occidentale du massif du Tazekka: Comptes Rendus de l'Académie des Sciences de Paris, v. 284, p. 1635–1637.
- Hoepffner, C., Houari, M.R., and Bouabdelli, M., 2006, Tectonics of the North African Variscides (Morocco, western Algeria): an outline: Comptes Rendus - Geoscience, v. 338, p. 25–40, doi:10.1016/j.crte.2005.11.003.
- Hoepffner, C., Soullaimani, A., and Piqué, A., 2005, The Moroccan Hercynides: Journal of African Earth Science, v. 43, p. 144–165, doi:10.1016/j.jafrearsci.2005.09.002.
- Horon, O., 1954, Note sur la géologie des affleurements du Primaire de la région de Sefrou-Immouzer du Kandar, Rapport du Bureau de Recherche et de Participations Minières, n. 89, 180 p.
- Horstwood, M.S.A, et al., 2016, Community-derived standards for LA-ICP-MS U-(Th)-Pb geochronology – Uncertainty propagation, age interpretation and data reporting: Geostandards and Geoanalytical Research, v. 40, n. 3, p. 311-332, doi: 10.1111/j.1751-908X.2016.00379.x.
- Hurley, P.M., Leo, G.W., White, R.W., Fairbairn, H.W., 1971. Liberian age province (about 2,700 m.y.) and adjacent provinces in Liberia and Sierra Leone. GSA Bull. 82, 3483–3490.
- Inglis, J.D., MacLean, J.S., Samson, S.D., D’Lemos, R.S., Admou, H., and Hefferan, K., 2004, A precise U–Pb zircon age for the Bleïda granodiorite, Anti-Atlas, Morocco: implications for the timing of deformation and terrane assembly in the eastern Anti-Atlas: Journal of African Earth Science, v. 39, p. 277–283, doi:10.1016/j.jafrearsci.2004.07.041.
- Jackson, S.E., Pearson, N.J., Griffin, W.L., and Belousova, E., 2004, The application of laser ablation-inductively coupled plasma-mass spectrometry to in situ U-Pb zircon geochronology: Chemical Geology, v. 211, p. 47–69, doi:10.1016/j.chemgeo.2004.06.017.
- Kennedy, A.K., and De Laeter, J.R., 1994, The performance characteristics of the WA SHRIMP II ion microprobe, in Lanphere, M.A., Dalrymple, G.B., Turrin, B.D., eds., Abstracts of the Eighth International Conference on Geochronology, Cosmochronology, and Isotope Geology. U.S. Geological Survey Circular, Berkeley, California, USA, p. 166.
- Košler, J., Konopásek, J., Sláma, J., Vrána, S., 2014. U–Pb zircon provenance of Moldanubian metasediments in the Bohemian Massif. Journal of the Geological Society of London. 171, 83–95. doi:10.1144/jgs2013-059
- Kuiper, Y.D., 2019, An overview of middle to late Paleozoic connections between southeastern New England, USA, and Morocco, in, Eos Transactions, American Geophysical Union, Fall Meeting.

- Kuiper, Y.D., Michard, A., Ruellan, E., Holm-Denoma, C., and Crowley, J.L., 2019, U-Pb zircon and monazite results from granite and charnockite from the Mazagan escarpment, offshore Morocco, in, *GSA Abstracts with Programs*, Vol. 51, No. 2.
- Lama, C., Zimmermann, J.L., Mortaji, A., Macaudière, J., and Stussi, J.M., 1993, Age K–Ar protérozoïque moyen des leucogranites à deux micas de la Tagragra d’Akka (Anti Atlas occidental, Maroc): *Comptes Rendus de l’Académie des Sciences de Paris*, v. 317, p. 1601–1607.
- Le Heron, D.P., 2007, Late Ordovician glacial record of the Anti-Atlas, Morocco: *Sedimentary Geology*, v. 201, p. 93–110, doi:10.1016/j.sedgeo.2007.05.004.
- Le Heron, D.P., Craig, J., and Etienne, J.L., 2009, Ancient glaciations and hydrocarbon accumulations in North Africa and the Middle East. *Earth-Science Reviews*, v. 93, p. 47–76. doi:10.1016/j.earscirev.2009.02.001.
- Le Heron, D.P., Khoukhi, Y., Paris, F., Ghienne, J.F., and Le Herissé, A., 2008, Black shale, grey shale, fossils and glaciers: anatomy of the Upper Ordovician-Silurian succession in the Tazzeke Massif of eastern Morocco: *Gondwana Research*, v. 14, p. 483–496, doi:10.1016/j.gr.2008.02.006.
- Lee, J.K.W., Williams, I.S., and Ellis, D.J., 1997, Pb, U and Th diffusion in natural zircon: *Nature*, v. 390, p. 159–162, doi:10.1038/36554.
- Letsch, D., El Houicha, M., von Quadt, A., and Winkler, W., 2018, A missing link in the peri-Gondwanan terrane collage: the Precambrian basement of the Moroccan Meseta and its lower Paleozoic cover: *Canadian Journal of Earth Sciences*, v. 55, p. 1–19, doi:10.1139/cjes-2017-0086.
- in, W., Faure, M., Li, X.-H., Ji, W., 2019. Pre-Variscan tectonic setting of the south margin of Armorica: Insights from detrital zircon ages distribution and Hf isotopic composition of the St-Georges-sur-Loire Unit (S. Armorican Massif, France). *Tectonophysics* 766, 340–378. doi:10.1016/j.tecto.2019.06.015
- Lin, W., Faure, M., Li, X. hua, Chu, Y., Ji, W., Xue, Z., 2016. Detrital zircon age distribution from Devonian and Carboniferous sandstone in the Southern Variscan Fold-and-Thrust belt (Montagne Noire, French Massif Central), and their bearings on the Variscan belt evolution. *Tectonophysics* 677–678, 1–33. doi:10.1016/j.tecto.2016.03.032
- Linnemann, U., Gerdes, A., Hofmann, M., and Marko, L., 2014, The Cadomian Orogen: Neoproterozoic to Early Cambrian crustal growth and orogenic zoning along the periphery of the West African Craton-Constraints from U-Pb zircon ages and Hf isotopes (Schwarzburg Antiform, Germany): *Precambrian Research*, v. 244, p. 236–278, doi:10.1016/j.precamres.2013.08.007.
- Linnemann, U., McNaughton, N.J., Romer, R.L., Gehmlich, M., Drost, K., and Tonk, C., 2004, West African provenance for Saxo-Thuringia (Bohemian Massif): did Armorica ever leave pre-Pangean Gondwana? - U/Pb-SHRIMP zircon evidence and

- the Nd-isotopic record: *International Journal of Earth Sciences*, v. 93, p. 683–705, doi:10.1007/s00531-004-0413-8.
- Linnemann, U., Ouzegane, K., Drareni, A., Hofmann, M., Becker, S., Gärtner, A., and Sagawe, A., 2011, Sands of West Gondwana: an archive of secular magmatism and plate interactions - A case study from the Cambro-Ordovician section of the Tassili Ouan Ahaggar (Algerian Sahara) using U-Pb-LA-ICP-MS detrital zircon ages: *Lithos*, v. 123, p. 188–203, doi:10.1016/j.lithos.2011.01.010.
- Linnemann, U., Pereira, M.F., Jeffries, T.E., Drost, K., and Gerdes, A., 2008, The Cadomian Orogeny and the opening of the Rheic Ocean: the diachrony of geotectonic processes constrained by LA-ICP-MS U-Pb zircon dating (Ossa-Morena and Saxo-Thuringian Zones, Iberian and Bohemian Massifs): *Tectonophysics*, v. 461, p. 21–43, doi:10.1016/j.tecto.2008.05.002.
- Ludwig, K.R., 2003, Isoplot 3.0. A geochronological toolkit for Microsoft Excel: Berkeley Geochronology Center Special Publication, n. 4, 67p.
- Ludwig, K.R., 2009, SQUID 2: a user's manual (rev.12): Berkeley Geochronology Center Special Publication, n. 5.
- Maas, R., Kinny, P.D., Williams, I.S., Froude, D.O., and Compston, W., 1992, The Earth's oldest known crust: a geochronological and geochemical study of 3900–4200 Ma old detrital zircons from Mt. Narryer and Jack Hills, Western Australia: *Geochimica et Cosmochimica Acta*, v. 56, p. 1281–1300, doi:10.1016/0016-7037(92)90062-N.
- Marhoumi, M.R., Rauscher, R., and Vanguetaine, M., 1982, Les microfossiles (Chitinozoaires et Acritarches) des schistes du Tazekka au Maroc oriental: *Sciences Géologiques, bulletins et mémoires*, v. 35, p. 137–145.
- Martínez Catalán, J.R., Fernández-Suárez, J., Jenner, G.A., Belousova, E., and Díez Montes, A., 2004, Provenance constraints from detrital zircon U–Pb ages in the NW Iberian Massif: implications for Palaeozoic plate configuration and Variscan evolution: *Journal of the Geological Society London*, v. 161, p. 463–476, doi:10.1144/0016-764903-054.
- Marzoli, A., et al., 2017, Proterozoic to Mesozoic evolution of North-West Africa and Peri-Gondwana microplates: detrital zircon ages from Morocco and Canada: *Lithos*, v. 278–281, p. 229–239, doi:10.1016/j.lithos.2017.01.016.
- Matte, P., 2001. The Variscan collage and orogeny (480-290 Ma) and the tectonic definition of the Armorica microplate: a review. *Terra Nov.* 13, 122–128. doi:10.1046/j.1365-3121.2001.00327.x
- Michard, A., 1976. *Éléments de géologie marocaine: Notes et Memoires du Service Géologique du Maroc*, v. 252, 408 p.

- Michard, A., Cailleux, Y., and Hoepffner, C., 1989, L'orogène mésétien du Maroc: structure, déformation hercynienne et déplacement: Notes et Memoires du Service Géologique du Maroc, v. 335, p. 313-327.
- Michard, A., Ouanaimi, H., Hoepffner, C., Soulaïmani, A., and Baïdder, L., 2010a, Comment on Tectonic relationships of Southwest Iberia with the allochthons of Northwest Iberia and the Moroccan Variscides by J.F. Simancas et al. [C. R. Geoscience 341 (2009) 103-113]: Comptes Rendus - Geoscience, v. 342, p. 170–174, doi:10.1016/j.crte.2010.01.008.
- Michard, A., Saddiqi, O., Chalouan, A., and Frizon de Lamotte, D., 2008, Continental evolution: the geology of Morocco: Springer, 438 p., doi:10.1007/978-3-540-75761-0.
- Michard, A., Soulaïmani, A., Hoepffner, C., Ouanaimi, H., Baïdder, L., Rjimati, E.C., and Saddiqi, O., 2010b, The south-western branch of the Variscan Belt: evidence from Morocco: Tectonophysics, v. 492, p. 1–24, doi:10.1016/j.tecto.2010.05.021.
- Murphy, J.B., Gutiérrez-Alonso, G., Nance, R.D., Fernandez-Suarez, J., Keppie, J.D., Quesada, C., Strachan, R.A., and Dostal, J., 2006, Origin of the Rheic Ocean: rifting along a Neoproterozoic suture?: Geology, v. 34, p. 325–328, doi:10.1130/G22068.1.
- Nance, R.D., Gutiérrez-Alonso, G., Keppie, J.D., Linnemann, U., Murphy, J.B., Quesada, C., Strachan, R.A., and Woodcock, N.H., 2010, Evolution of the Rheic Ocean: Gondwana Research, v. 17, p. 194–222, doi:10.1016/j.gr.2009.08.001.
- Nance, R.D., Gutiérrez-Alonso, G., Keppie, J.D., Linnemann, U., Murphy, J.B., Quesada, C., Strachan, R.A., and Woodcock, N.H., 2012, A brief history of the Rheic Ocean: Geoscience Frontiers, v. 3, p. 125–135, doi:10.1016/j.gsf.2011.11.008.
- Nance, R.D., et al., 2008, Neoproterozoic-early Palaeozoic tectonostratigraphy and palaeogeography of the peri-Gondwanan terranes: Amazonian v. West African connections: Geological Society of London, Special Publication 297, p. 345–383, doi:10.1144/SP297.17.
- Ouabid, M., Ouali, H., Garrido, C.J., Acosta-Vigil, A., Román-Alpiste, M.J., Dautria, J.M., Marchesi, C., and Hidas, K., 2017, Neoproterozoic granitoids in the basement of the Moroccan Central Meseta: Correlation with the Anti-Atlas at the NW paleo-margin of Gondwana: Precambrian Research, v. 299, p. 34–57, doi:10.1016/j.precamres.2017.07.007.
- Ouarhache, D., 1987, Étude géologique dans le Paléozoïque et le Trias de la bordure NW du Causse Moyen Atlasique (S et SW de Fès, Maroc) [Ph.D. thesis]: Université de Toulouse, France.
- Pastor-Galán, D., Gutiérrez-Alonso, G., Murphy, J.B., Fernández-Suárez, J., Hofmann, M., and Linnemann, U., 2013, Provenance analysis of the Paleozoic sequences of the northern Gondwana margin in NW Iberia: passive margin to Variscan collision and

- orocline development: *Gondwana Research*, v. 23, p. 1089–1103, doi:10.1016/j.gr.2012.06.015.
- Paton, C., Hellstrom, J., Paul, B., Woodhead, J., and Hergt, J., 2011, Iolite: Freeware for the visualisation and processing of mass spectrometric data: *Journal of Analytical Atomic Spectrometry*, v. 26, 2508, doi:10.1039/c1ja10172b.
- Pereira, M.F., Chichorro, M., Johnston, S.T., Gutiérrez-Alonso, G., Silva, J.B., Linnemann, U., Hofmann, M., and Drost, K., 2012a, The missing Rheic Ocean magmatic arcs: provenance analysis of Late Paleozoic sedimentary clastic rocks of SW Iberia: *Gondwana Research*, v. 22, p. 882–891, doi:10.1016/j.gr.2012.03.010.
- Pereira, M.F., El Houicha, M., Aghzer, A., Silva, J.B., Linnemann, U., and Jouhari, A., 2014, New U-Pb zircon dating of Late Neoproterozoic magmatism in Western Meseta (Morocco): *Gondwana 15 - North meets South*, 133 p., doi:10.13140/2.1.2651.2641.
- Pereira, M.F., El Houicha, M., Chichorro, M., Armstrong, R., Jouhari, A., El Attari, A., Ennih, N., and Silva, J.B., 2015, Evidence of a Paleoproterozoic basement in the Moroccan Variscan Belt (Rehamna Massif, Western Meseta): *Precambrian Research*, v. 268, p. 61–73, doi:10.1016/j.precamres.2015.07.010.
- Pereira, M.F., Gama, C., Dias da Silva, Í., Silva, J., Hofmann, M., Linnemann, U., Gärtner, A., 2020. Chronostratigraphic framework and provenance of the Ossa-Morena Zone Carboniferous basins (SW Iberia). *Solid Earth Discussion* 1–34. doi:10.5194/se-2020-26
- Pereira, M.F., Gutiérrez-Alonso, G., Murphy, J.B., Drost, K., Gama, C., and Silva, J.B., 2017, Birth and demise of the Rheic Ocean magmatic arc(s): combined U–Pb and Hf isotope analyses in detrital zircon from SW Iberia siliciclastic strata: *Lithos*, v. 278–281, p. 383–399, doi:10.1016/j.lithos.2017.02.009.
- Pereira, M.F., Linnemann, U., Hofmann, M., Chichorro, M., Solá, A.R., Medina, J., and Silva, J.B., 2012b, The provenance of Late Ediacaran and Early Ordovician siliciclastic rocks in the Southwest Central Iberian Zone: constraints from detrital zircon data on northern Gondwana margin evolution during the late Neoproterozoic: *Precambrian Research*, v. 192–195, p. 166–189, doi:10.1016/j.precamres.2011.10.019.
- Pereira, M.F., Solá, A.R., Chichorro, M., Lopes, L., Gerdes, A., and Silva, J.B., 2012c, North-Gondwana assembly, break-up and paleogeography: U-Pb isotope evidence from detrital and igneous zircons of Ediacaran and Cambrian rocks of SW Iberia: *Gondwana Research*, v. 22, p. 866–881, doi:10.1016/j.gr.2012.02.010.
- Pérez-Cáceres, I., Martínez Poyatos, D., Simancas, J.F., and Azor, A., 2017, Testing the Avalonian affinity of the South Portuguese Zone and the Neoproterozoic evolution of SW Iberia through detrital zircon populations: *Gondwana Research*, v. 42, p. 177–192, doi:10.1016/j.gr.2016.10.010.

- Perez, N.D., Teixell, A., Gómez-Gras, D., and Stockli, D.F., 2019, Reconstructing extensional basin architecture and provenance in the Marrakech High Atlas of Morocco: implications for rift basins and inversion tectonics: *Tectonics*, v. 38, p. 1584–1608. doi:10.1029/2018TC005413.
- Piqué, A., 2001, *Geology of Northwest Africa*: Gebrüder Borntraeger, Berlin, 310 p.
- Piqué, A., and Michard, A., 1989, Moroccan Hercynides: a synopsis. The Paleozoic sedimentary and tectonic evolution at the northern margin of West Africa: *American Journal of Science*, v. 289, p. 286–330.
- Piqué, A., and Michard, A., 2018, Les zones structurales du Maroc hercynien, in *Science Géologiques, bulletin*, v. 34, n. 2, p. 135–146, doi:10.3406/sgeol.1981.1597
- Pouclet, A., El Hadi, H., Álvaro, J.J., Bardintzeff, J.-M., Benharref, M., and Fekkak, A., 2018, Review of the Cambrian volcanic activity in Morocco: geochemical fingerprints and geotectonic implications for the rifting of West Gondwana: *International Journal of Earth Sciences*, v. 107, p. 2101–2123, doi:10.1007/s00531-018-1590-1.
- Pratt, J.R., Barbeau, D.L., Garver, J.I., Emran, A., and Izykowski, T.M., 2015. Detrital zircon geochronology of Mesozoic sediments in the Rif and Middle Atlas belts of Morocco: provenance constraints and refinement of the West African signature: *The Journal of Geology*, v. 123, p. 177–200, doi:10.1086/681218.
- Rauscher, R., Marhoumi, M.R., Vanguetaine, M., and Hoepffner, C., 1982, Datation palynologique des schistes du Tazekka au Maroc. Hypothèse structurale sur la socle hercynien de la Meseta orientale: *Comptes Rendus de l'Académie des Sciences de Paris*, v. 294, p. 1203–1206.
- Rubatto, D., 2002, Zircon trace element geochemistry: partitioning with garnet and the link between U-Pb ages and metamorphism: *Chemical Geology*, v. 184, p. 123–138, doi:10.1016/S0009-2541(01)00355-2.
- Rubatto, D., 2017, Zircon: the metamorphic mineral: *Reviews in Mineralogy and Geochemistry*, v. 83, p. 261–295, doi:10.2138/rmg.2017.83.9.
- Ruellan, E., 1985, *Géologie des marges continentales passives: évolution de la marge atlantique du Maroc (Mazagan): étude par submersible, seabeam et sismique réflexion: comparaison avec la marge N.O. africain et la marge homologue E. américaine [Ph.D. thesis]*: University of Brest, France.
- Sharman, G.R., and Malkowski, M.A., 2020, Needles in a haystack: detrital zircon U Pb ages and the maximum depositional age of modern global sediment. *Earth-Science Reviews*, v. 203, p. 103-109, doi:10.1016/j.earscirev.2020.103109.
- Shaw, J., Gutiérrez-Alonso, G., Johnston, S.T., and Pastor Galán, D., 2014, Provenance variability along the Early Ordovician north Gondwana margin: paleogeographic and tectonic implications of U-Pb detrital zircon ages from the Armorican Quartzite of

- the Iberian Variscan belt, *Bulletin of the Geological Society of America*, v. 126, p. 702–719, doi:10.1130/B30935.1
- Schulz, K.J., Stewart, D.B., Tucker, R.D., Pollock, J.C., Ayuso, R.A., 2008. The Ellsworth terrane, coastal Maine: geochronology, geochemistry, and Nd-Pb isotopic composition--Implications for the rifting of Ganderia. *Geol. Soc. Am. Bull.* 120, 1134–1158. doi:10.1130/B26336.1
- Simancas, J.F., Azor, A., Martínez-Poyatos, D., Tahiri, A., El Hadi, H., González-Lodeiro, F., Pérez-Estaún, A., and Carbonell, R., 2009, Tectonic relationships of Southwest Iberia with the allochthons of Northwest Iberia and the Moroccan Variscides. *Comptes Rendus Geoscience*, v. 341, p. 103–113, doi:10.1016/j.crte.2008.11.003.
- Simancas, J.F., Azor, A., Martínez-Poyatos, D., Tahiri, A., Hadi, H. El, González-Lodeiro, F., Pérez-Estaún, A., and Carbonell, R., 2010, Reply to the comment by Michard et al. on “Tectonic relationships of Southwest Iberia with the allochthons of Northwest Iberia and the Moroccan Variscides.”: *Comptes Rendus Geoscience*, v. 342, p. 175–177, doi:10.1016/j.crte.2010.01.007.
- Simancas, J.F., Tahiri, A., Azor, A., Lodeiro, F.G., Martínez Poyatos, D.J., and El Hadi, H., 2005, The tectonic frame of the Variscan–Alleghanian orogen in Southern Europe and Northern Africa: *Tectonophysics*, v. 398, p. 181–198, doi:10.1016/j.tecto.2005.02.006.
- Sláma, J., et al., 2008, Plešovice zircon — A new natural reference material for U–Pb and Hf isotopic microanalysis: *Chemical Geology*, v. 249, p. 1–35, doi:10.1016/j.chemgeo.2007.11.005.
- Soulaimani, A., and Hefferan, K., 2017, Le Précambrien à la bordure nord du craton ouest-africain (Anti-Atlas et Haut Atlas, Maroc): *Géologues*, v. 194, p. 33–36.
- Spencer, C.J., Kirkland, C.L., Taylor, R.J.M., 2016. Strategies towards statistically robust interpretations of in situ U-Pb zircon geochronology. *Geosci. Front.* 7, 581–589. doi:10.1016/j.gsf.2015.11.006
- Stephan, T., Kroner, U., and Romer, R.L., 2019a, The pre-orogenic detrital zircon record of the Peri-Gondwanan crust: *Geological Magazine*, v. 156, p. 281–307, doi:10.1017/S0016756818000031.
- Stephan, T., Kroner, U., Romer, R.L., and Rösel, D., 2019b, From a bipartite Gondwanan shelf to an arcuate Variscan belt: the early Paleozoic evolution of northern Peri-Gondwana. *Earth-Science Reviews*, v. 192, p. 491–512, doi:10.1016/j.earscirev.2019.03.012.
- Stern, R.A., 2001, A new isotopic and trace-element standard for the ion microprobe: preliminary thermal ionization mass spectrometry (TIMS) U-Pb and electron-microprobe data; radiogenic age and isotopic studies: Geological Survey of Canada, Current Research 2001-F1, n. 14, 11 p.

- Stern, R.A., Bodorkos, S., Kamo, S.L., Hickman, A.H., and Corfu, F., 2009, Measurement of SIMS instrumental mass fractionation of Pb isotopes during zircon dating: *Geostandards and Geoanalytical Research*, v. 33, p. 145–168, doi:10.1111/j.1751-908X.2009.00023.x.
- Strnad, L., Mihaljevič, M., 2005. Sedimentary provenance of Mid-Devonian clastic sediments in the Teplá-Barrandian Unit (Bohemian Massif): U-Pb and Pb-Pb geochronology of detrital zircons by laser ablation ICP-MS. *Mineralogy and Petrology*. doi:10.1007/s00710-004-0057-1
- Szczepański, J., Turniak, K., Anczkiewicz, R., Gleichner, P., 2020. Dating of detrital zircons and tracing the provenance of quartzites from the Bystrzyckie Mts: implications for the tectonic setting of the Early Palaeozoic sedimentary basin developed on the Gondwana margin. *International Journal of Earth Science* 109, 2049–2079. doi:10.1007/s00531-020-01888-8
- Tahiri, A., Montero, P., El Hadi, H., Martínez Poyatos, D., Azor, A., Bea, F., Simancas, J.F., and González Lodeiro, F., 2010, Geochronological data on the Rabat-Tiflet granitoids: their bearing on the tectonics of the Moroccan Variscides: *Journal of African Earth Science*, v. 57, p. 1–13, doi:10.1016/j.jafrearsci.2009.07.005.
- Talavera, C., Montero, P., Martínez Poyatos, D., and Williams, I.S., 2012, Ediacaran to Lower Ordovician age for rocks ascribed to the Schist–Graywacke Complex (Iberian Massif, Spain): evidence from detrital zircon SHRIMP U–Pb geochronology: *Gondwana Research*, v. 22, p. 928–942, doi:10.1016/j.gr.2012.03.008.
- Thomas, R., et al., 2002, Precambrian evolution of the Sirwa Window, Anti-Atlas Orogen, Morocco: *Precambrian Research*, v. 118, p. 1–57, doi:10.1016/S0301-9268(02)00075-X.
- Vermeesch, P., 2012, On the visualisation of detrital age distributions: *Chemical Geology*, v. 312–313, p. 190–194, doi:10.1016/j.chemgeo.2012.04.021.
- Vermeesch, P., 2018, Dissimilarity measures in detrital geochronology: *Earth-Science Reviews*, v. 178, p. 310–321, doi:10.1016/j.earscirev.2017.11.027.
- Walliser, O.H., El Hassani, A., and Tahiri, A., 1995, Sur le Dévonien de la Meseta marocaine occidentale. Comparaisons avec le Dévonien allemand et événements globaux: *CFS Courier Forschungsinstitut Senckenberg*, v. 188, p. 21–30.
- Walliser, O.H., El Hassani, A., and Tahiri, A., 2000, Mrirt: a key area for the Variscan Meseta of Morocco: *Notes et Mémoires du Service Géologique du Maroc*, v. 399, p. 93–108.
- Wiedenbeck, M., Allé, P., Cordu, F., Griffin, W.L., Meier, M., Oberli, F., Quadt, A., Von Roddick, J.C., and Spiegel, W., 1995, Three natural zircon standards for U-Th-Pb, Lu-Hf, trace element and REE analyses: *Geostandards and Geoanalytical Research*, v. 19, p. 1–23, doi:10.1111/j.1751-908X.1995.tb00147.x.

- Willefert, S., and Charriere, A., 1990, Les formations à Graptolithes des boutonnières du Moyen-Atlas tabulaire (Maroc): *Géologie Méditerranéenne*, v. 17, p. 279–299, doi:10.3406/geolm.1990.1445.
- Youbi, N., et al., 2013, The 1750 Ma magmatic event of the West African Craton (Anti-Atlas, Morocco): *Precambrian Research*, v. 236, p. 106–123, doi:10.1016/j.precamres.2013.07.003.
- Žák, J., Sláma, J., 2018. How far did the Cadomian ‘terrane’ travel from Gondwana during early Palaeozoic? A critical reappraisal based on detrital zircon geochronology. *International Geology Review*, 60, 319–338. doi:10.1080/00206814.2017.1334599

Section II.3

Systematics of detrital zircon grains from Cambrian-Lower Devonian rocks of the Moroccan Mesetas

Cristina Accotto¹, David Martínez Poyatos¹, Antonio Azor¹, Cristina Talavera², Noreen J. Evans³, Antonio Jabaloy-Sánchez¹, Hassan El Hadi⁴, Abdelfatah Tahiri⁵, Ali Azdimousa⁶

Submitted to Earth Science Reviews

¹ Department of Geodynamics, University of Granada, Granada, Spain

² School of Geosciences, University of Edinburgh, Edinburgh, UK

³ School of Earth and Planetary Science, John the Laeter Centre, Curtin University, Perth, Australia

⁴ Laboratory of Geodynamics of Ancient Belts, Faculty of Science Ben M'Sik, Hassan II, University of Casablanca, Morocco

⁵ Laboratory of Geo-biodiversity and Natural Patrimony (GEOBIO), Scientific Institute; Geophysics, Natural Patrimony and Green Chemistry Research Center (GEOPAC), Mohammed V University in Rabat, Morocco

⁶ Faculté Pluridisciplinaire de Nador et Laboratoire des Géosciences Appliquées, Faculté des Sciences, Université Mohammed I, Oujda, Morocco

Abstract

The systematic acquisition of U-Pb geochronological data from detrital zircon grains has become an essential tool in tectonic studies focused on the reconstruction of the pre-Variscan geography of the early-middle Paleozoic northern Gondwanan passive margin. New detrital zircon ages of 16 samples from the Cambrian-Early Devonian succession of the Moroccan Mesetas are reported here. The obtained results, combined with previously published data, reassert the strong West African Craton affinity of the Paleozoic sedimentary rocks, characterized by dominant Cadomian/Pan-African (c. 850-540 Ma) and Eburnean (c. 2.2-1.9 Ga) detrital zircon populations, with a minor Leonian/Liberian (c. 2.5 Ga) one. Primary sources of these populations are well-known in the West African Craton located just to the south, but also in the Precambrian basement that locally crops out in the Moroccan Mesetas themselves. During the Cambrian-Early Ordovician, erosion dismantled preferentially Cadomian (c. 590-540 Ma) arc-derived rocks of the Gondwanan continental margin, while later on slightly older Pan-African (c. 650-600 Ma) basement became the main sediment source. In the studied samples, minor detrital zircon populations irregularly present suggest additional sediment provenance from secondary sources such as: (i) remote northeastern African cratons (*e.g.*, Sahara Metacraton and/or Arabian-Nubian Shield) that likely could have provided the c. 1.1-0.9 Ga and, possibly, the c. 1.9-1.7 Ga zircon grains, and (ii) rift-related Cambrian-Early Ordovician volcanic centers in the Moroccan Mesetas that supplied heterogeneously distributed - although locally dominant in small areas - sedimentary detritus before rift abortion and burial underneath the overlying passive margin sedimentary succession.

1. Introduction

The systematic U-Pb dating of detrital zircon grains is a powerful tool that in the last decades has been widely applied in sediment provenance studies and paleogeographic reconstructions (*e.g.*, Fedo et al., 2003; Gehrels, 2012). These studies have been fundamental in the recognition of the terranes involved in pre-Alpine orogenies, whose present-day field relationships are often complex and/or obliterated by superposed tectonics. In Europe, geochronology of detrital zircon grains is the basis of a good number of studies (*e.g.*, Braid et al., 2011; Eckelmann et al., 2014; Fernández-Suárez et al., 2014; Franke and Dulce, 2017; Gutiérrez-Alonso et al., 2015; Linnemann et al., 2004; Nance et al., 2008; Pereira et al., 2017, 2012; Pérez-Cáceres et al., 2017; Shaw et al., 2014) that allowed a better understanding of the late Paleozoic Variscan belt, which was formed by the closure of the Rheic Ocean and the subsequent collision between the Gondwanan and Laurussian supercontinents, with several minor peri-Gondwanan terranes (*e.g.*, Franke et al., 2017; Matte, 2001; Simancas et al., 2005).

The southward along-strike extension of the European Variscan belt, partially obliterated by younger orogenic systems (*e.g.*, Alpine Betic-Rif belt, Figure 2.16A), crops out in northern Morocco and western Mauritania. In Morocco, the areas affected by the Variscan orogeny are collectively referred to as the “Moroccan Variscides”, and have

been mainly investigated from the stratigraphic and tectonic points of view (*e.g.*, El Hassani et al., 2003; Hoepffner et al., 2006; Michard, 1976; Michard et al., 2010b, 2010a, 1989; Piqué, 1994; Piqué, 2001, 1981; Piqué and Michard, 1989; Simancas et al., 2009, 2005; Tahiri, 1991; Villeneuve et al., 2010; Walliser et al., 2000, 1995). Furthermore, the use of detrital zircon geochronological data has been recently incorporated into the study of this part of the Variscan belt, although the number of works dedicated to this technique is still relatively scarce (Abati et al., 2010; Accotto et al., 2019, 2020, 2021, in press; Avigad et al., 2012; El Houicha et al., 2018; Gärtner et al., 2017, 2018; Ghienne et al., 2018; Letsch et al., 2018; Pérez-Cáceres et al., 2017).

The northern Moroccan Variscides crop out in several domains (Figure 2.16B) separated by fault zones, whose paleogeographic importance is still a matter of debate (*e.g.*, Hoepffner et al., 2006; Michard et al., 2010a, 2010b; Simancas et al., 2009, 2010):

- The Sehoul Block is located north of the Rabat-Tiflet Fault Zone (RTFZ) and characterized by a lower-middle Cambrian siliciclastic succession that was deformed and metamorphosed before the intrusion of Devonian granitoids (Tahiri et al., 2010). This middle Paleozoic deformation has not been observed in any other part of the northern Moroccan Variscides and, hence, the Sehoul Block is considered to be part of a Caledonian exotic terrane (*i.e.*, Avalonian promontory; *e.g.*, Simancas et al., 2005) accreted to the northern margin of Gondwana during the Carboniferous (*e.g.*, Michard et al., 2010b and references therein; Tahiri et al., 2010).
- The Western Moroccan Meseta (WMM; see section 2.1) is limited by the RTFZ (to the north), the Tizin'Test Fault Zone (TTFZ, to the south), and the Tazekka-Bsabis-Bekrit Fault Zone (TBBFZ, to the east), and divided into Coastal Block, Central Zone and Nappe Zone, separated by the Western Meseta Shear Zone (WMSZ) and the Smaala-Oulmès Fault Zone (SOFZ), respectively.
- The Eastern Moroccan Meseta (EMM; see section 2.2) is located east of the TBBFZ and limited, to the south, by the South Meseta Fault Zone (SMFZ).
- The Southern Zone is bordered to the north by the SMFZ and to the south by the South Atlas Fault Zone (SAFZ), and characterized by a Cambrian-Carboniferous detrital succession slightly deformed and poorly metamorphosed.
- The Anti-Atlas is located south of the TTFZ and SAFZ, and considered to be the Gondwanan foreland of the Variscan belt; the Paleozoic succession of this domain is constituted by Cambrian-lower Carboniferous sedimentary rocks partially detached from the Precambrian basement and characterized by weak deformation, progressively decreasing southwards (Michard et al., 2010b and references therein).

With the exception of the Sehoul Block, all of the domains of the northern Moroccan Variscides are considered to have belonged to the northern Gondwanan passive margin during the Cambrian-Early Devonian time span. This is based on stratigraphic similarities and absence of ophiolite and/or high-pressure metamorphic belts between the different domains (*e.g.*, Michard et al., 2010b; Simancas et al., 2005).

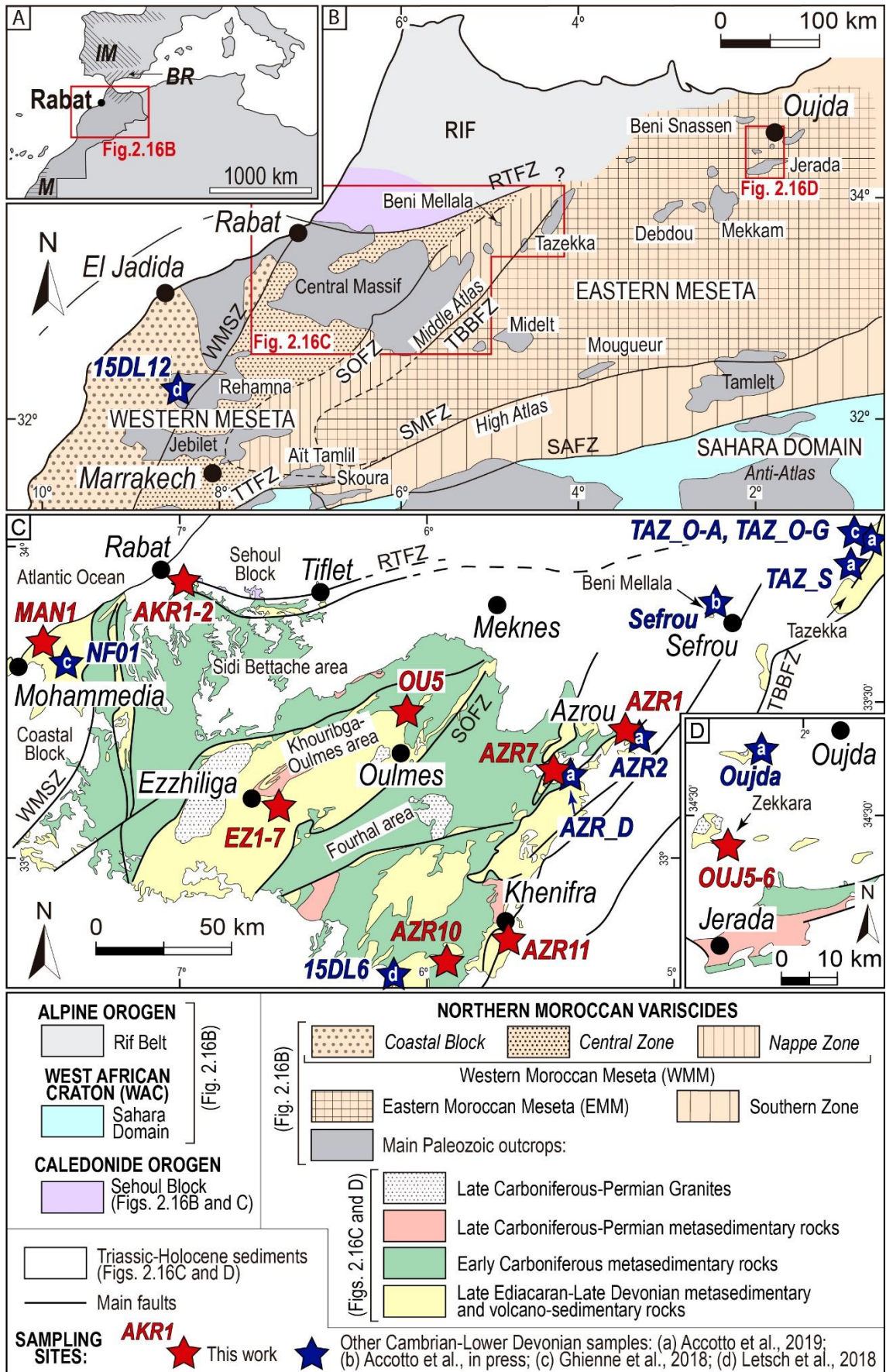


Figure 2.16 (previous page): Schematic geological maps of the Paleozoic inliers and structural domains in northern Morocco. A) Location of northern Morocco; IM: Iberian Massif; BR: Betic-Rif Belt; M: Mauritanides. B) Northern Moroccan Variscides (modified from Hoepffner et al., 2006; Michard et al., 2010b). C) Detail of the northern Western Moroccan Meseta (modified from Arboleya et al., 2004; Becker and El Hassani, 2020; Charriere, 1989). D) Detail of the Oujda-Zekkara area (modified from Muratet, 1995). RTFZ: Rabat-Tiflet Fault Zone; WMSZ: Western Meseta Shear Zone; SOFZ: Smaala-Oulmès Fault Zone; TBBFZ: Tazekka-Bsabis-Bekrit Fault Zone; TTFZ: Tizin’Test Fault Zone; SMFZ: South Meseta Fault Zone; SAFZ: South Atlas Fault Zone. Stars indicate the location of the samples studied in this work (in red) and other Cambrian-Early Devonian samples already published (in blue, see references in the Figure legend).

In this study, we collected 16 upper Cambrian-Lower Devonian (meta)sandstone samples from different areas of the Moroccan Mesetas (WMM and EMM; Figure 2.16) and carried out U-Pb geochronological analyses on detrital zircon grains in order to investigate the detrital sources that controlled the sedimentation in the northern Gondwanan passive margin. To do so, we have also considered the already published data from other coeval samples of the region, which are listed in Table 2.4.

Table 2.4: previously published results used in this work.

Original sample code	Codes used in this work	Age	Reference
<i>COASTAL BLOCK</i>			
15DL12	15DL12	Late Cambrian	Letsch et al., 2018
NF01	NF01	Late Ordovician	Ghienne et al., 2018
<i>NAPPE ZONE (KHENIFRA AREA)</i>			
15DL6	15DL6	Late Cambrian- Early Ordovician	Letsch et al., 2018
<i>NAPPE ZONE (AZROU AREA)</i>			
AZR2	AZR2	Late Ordovician	Accotto et al., 2019
AZR4, AZR5, AZR6	AZR_D	Early Devonian	
<i>NAPPE ZONE (SEFROU AREA)</i>			
SF1, SF2, SF3	Sefrou	Early-Late Ordovician	Accotto et al., in press
<i>NAPPE ZONE (TAZEKKA AREA)</i>			
TAZ2, TAZ3	TAZ_O-A	Late Ordovician	Accotto et al., 2019
TeB1, TeB2, TeB3, Tf1, Tf2, Tf3, Tf4, Tf5, Tf6	TAZ_O-G	Late Ordovician	Ghienne et al., 2018
TAZ5, TAZ6	TAZ_S	Silurian	Accotto et al., 2019
<i>EASTERN MOROCCAN MESETA (OUJDA AREA)</i>			
OUI2, OUI3	Oujda	Late Ordovician	Accotto et al., 2019

2. Geological setting

2.1. *The Western Moroccan Meseta*

The igneous Paleoproterozoic-Ediacaran basement of the northern Moroccan Variscides crops out locally in the WMM in the El Jadida (Coastal Block; El Haïbi et al., 2020; El Houicha et al., 2018), Tiflet (Central Zone; El Haïbi et al., 2021; Tahiri et al., 2010), and Rehamna areas (Central Zone; Baudin et al., 2003; Pereira et al., 2015). The unconformable Cambrian-Lower Devonian sedimentary succession is represented by siliciclastic passive margin deposits, locally intruded by Cambrian-Ordovician magmatic rocks (Pouclet et al., 2018 and references therein), and followed by a Devonian mainly carbonatic sequence. Local differences are showed in Figure 2.17 and described in the following subsections. After Late Devonian time, the synorogenic succession is mainly made up of siliciclastic rocks with a few carbonatic intercalations of early Carboniferous age. Unconformable late Carboniferous-Permian continental basins developed locally. The Paleozoic succession is intruded by upper Carboniferous-Permian Variscan dykes and granitoids (*e.g.*, El Hadi et al., 2006 and references therein; Kharbouch, 1994; Kharbouch et al., 1985), and unconformably overlain by post-orogenic Triassic volcano-sedimentary rocks (Destombe, 1987).

The Paleozoic succession of the WMM was deformed by late Carboniferous Variscan folding, coeval to low- to very low-grade metamorphism (Hoepffner et al., 2005; Michard et al., 2010b).

2.1.1. The Coastal Block

The Cambrian succession of the Coastal Block is characterized by siliciclastic deposits locally intruded by basalts and andesites (*e.g.*, Oued Rhebar – c. 40 km SW of Rabat – and Sidi Saïd Maâchou – c. 35 km E of El Jadida – volcanic centers; Pouclet et al., 2018 and references therein). The siliciclastic succession records an increase of grain size from a predominance of shales in the early-middle Cambrian (“Schistes à Paradoxides”) to mainly sandy sediments, which culminate in late Cambrian with the deposition of a thick and continuous level of quartzitic microconglomeratic sandstones and arkoses (“El Hank” Formation; Figure 2.17; Cailleux, 1994 and references therein). The base of the Ordovician is marked by a transgression. After a basal level of conglomerates and greywackes, the succession is mainly characterized by shales with an increase of sandy and microconglomeratic layers deposited at middle-late Ordovician time (Cailleux, 1994 and references therein). The Silurian succession is very similar in all of the Moroccan Mesetas and characterized by black shales with graptolites (Zahraoui, 1994 and references therein). A particularity of the Coastal Block is the presence of a few carbonatic layers, more common upwards, which appear interbedded with the shales. The deposition of shales continued during the Early Devonian with an increase of the

carbonatic beds, thus indicating the establishment of a carbonatic platform in this part of the Gondwanan passive margin.

2.1.2. The Central Zone

No Cambrian rocks have been recognized until now in the studied areas of the Central Zone (Oued Akreuch, Ezzhiliga and Oulmes areas). The Paleozoic succession (Figure 2.17) starts with the deposition of Ordovician shales with sandy and/or conglomeratic intercalations, more common during the Middle-Late Ordovician (*e.g.*, El Hassani, 1991; Tahiri and El Hassani, 1994). In the northwestern sector of this zone close to the Coastal Block (*e.g.*, Oued Akreuch area), basaltic and gabbroic intercalations are also common (El Hassani, 1991 and references therein). The Silurian is represented by black shales with graptolites and carbonatic beds, which are more common at late Silurian time and, in particular, in the Oued Akreuch area, where they can also be found in the lower Silurian succession (El Hassani, 1991 and references therein). The Lower Devonian deposition records the establishment of a carbonatic platform in the western sectors (*e.g.*, Oued Akreuch area), and more subsiding conditions in the eastern ones, which resulted in the prevalence of turbiditic deposits (*e.g.*, Ezzhiliga and Oulmes areas; Razin et al., 2001; Tahiri, 1991 and references therein).

2.1.3. The Nappe Zone

The Nappe Zone corresponds to the easternmost part of the WMM, and is characterized by Variscan thrust tectonics (Michard et al., 2010b and references therein) that was particularly relevant in the eastern part of the zone (Azrou-Khenifra areas; Figure 2.16C; Hoepffner et al., 2006).

To the southeast, the Khenifra nappe is made up of an upper Cambrian-Upper Ordovician succession of turbiditic shales, sandstones and subordinate conglomerates, followed by the Silurian black shales with graptolites and by Lower Devonian turbidites (Bouabdelli and Piqué, 1996).

In the Azrou area, three para-autochthonous units, characterized by an Upper Ordovician-upper Carboniferous succession, are overlain by an allochthonous nappe of Lower Devonian rocks (see sketched structural relationships in Figure 2.17; Bouabdelli et al., 1989). We only collected samples from the basal section of the Eastern (Upper Ordovician-lower Carboniferous) and Central (Lower Devonian-middle Carboniferous) para-autochthonous units. The Eastern unit is characterized by Upper Ordovician turbiditic microconglomeratic to shaly rocks, followed by a monotonous succession of Silurian black shales. The increase of carbonatic layers interbedded with the shales marks the establishment of an Early Devonian carbonatic platform (Bouabdelli, 1982). The correspondent Lower Devonian succession in the Central unit, on the contrary, is characterized by siliciclastic deposits, while the carbonatic sedimentation started Middle Devonian time (Walliser et al., 2000).

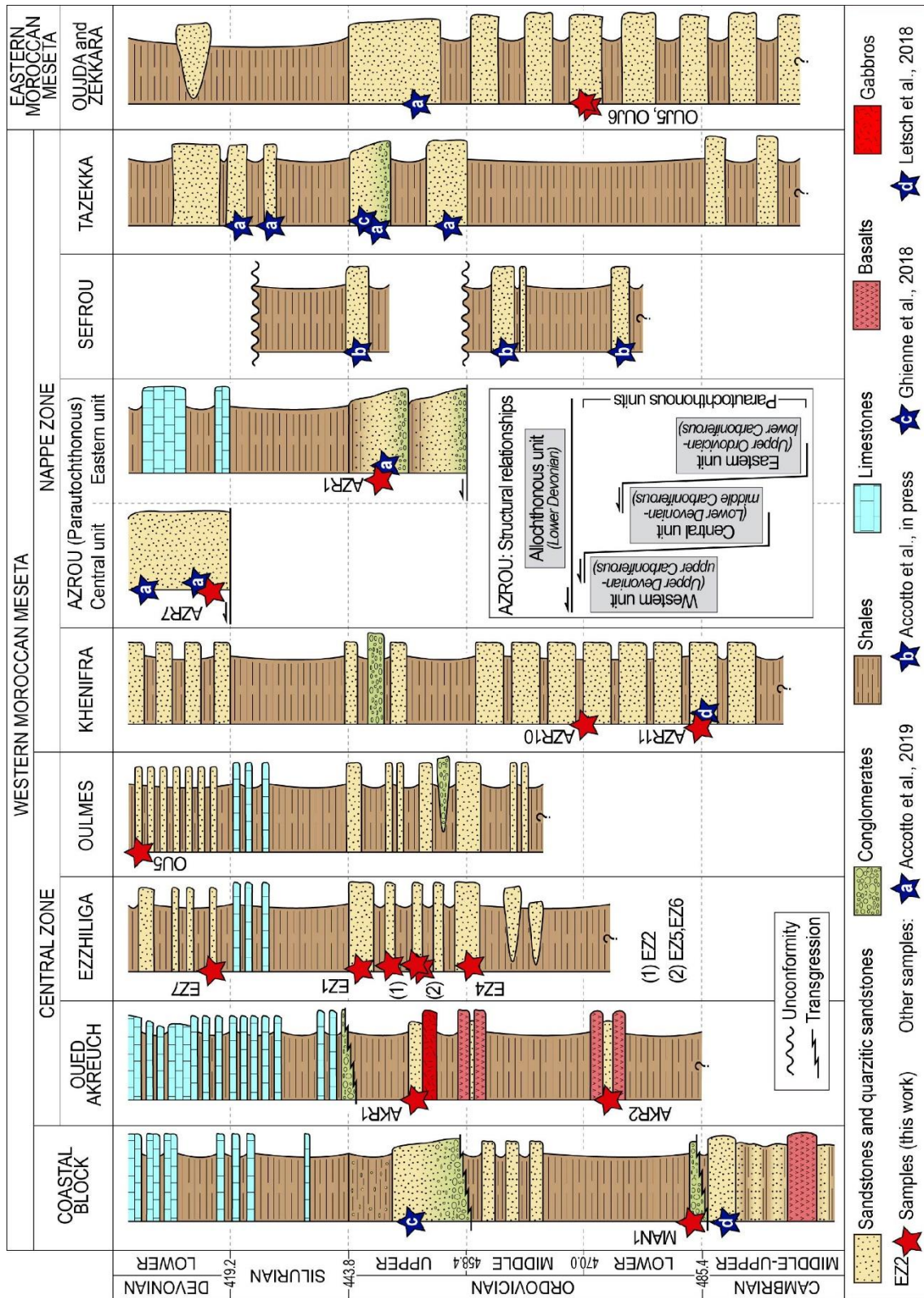


Figure 2.17: Schematic stratigraphic columns of the middle Cambrian-Lower Devonian successions of the northern Moroccan Variscides cropping out in the studied areas (Bouabdelli et al., 1989; Cailleux, 1994; Charriere, 1990; Choubert et al., 1978; El Hassani, 1991; Hoepffner, 1989; Horon, 1952; Marhoumi et al., 1989; Razin et al., 2001; Tahiri, 1991, 1994; Vidal and Hoepffner, 1979). Stars indicate the approximate location of the studied samples (in red) and other samples already published (in white, see references in the figure legend). Not to scale.

Towards the northeast, in the Sefrou and Tazekka areas the sedimentation is characterized by siliciclastic shales and sandstones during all the Cambrian-Devonian period (Charriere, 1990 and references therein; Hoepffner, 1987 and references therein). There are no evidences of carbonatic sedimentation during the Silurian and Devonian, although in the Sefrou area the stratigraphic sequence is incomplete (Charriere, 1990).

2.2. The Eastern Moroccan Meseta

The Paleozoic rocks of the EMM (Figure 2.16B, D) crops out in relatively small inliers below the Mesozoic-Cenozoic cover. The lower Paleozoic succession is a monotonous succession of shales, sandstones, and greywackes (Figure 2.17) attributed to the Cambrian-Ordovician (Desteucq and Fournier-Vinas, 1981; Hoepffner, 1989, 1977; Rauscher et al., 1982), which are followed by the Silurian black shales. The Lower Devonian is composed of siliciclastic sediments, mainly shales with a few sandy lenses that become more common during the Middle-Late Devonian and Tournaisian, and represent a subsident environment, in contrast with the coeval carbonatic platform that characterized most of the WMM. An upper Visean-Kasimovian succession unconformably overlies the Famennian-Tournaisian rocks (Médioni, 1979 and references therein); this second syn-orogenic succession is constituted by upper Visean volcano-sedimentary layers followed by siliciclastic turbidites and continental (limnic facies) sediments (*e.g.*, Jerada area).

Variscan metamorphism in the EMM is generally of low- to very low-grade (except in Midelt and northern Tamlet areas; Hoepffner, 1989) and deformation is variable: in some areas the Paleozoic succession recorded both Eovariscan (intense recumbent folding) and Variscan (upright folding) deformational events (*e.g.*, Debdou-Mekkam areas; Accotto et al., 2020), while others were only affected by the Variscan tectonic phase (*e.g.*, Jerada, Oujda, Beni Snassen areas; Figure 2.16B). The EMM was also intruded by upper Carboniferous-Permian granitoids (El Hadi et al., 2006a and references therein).

3. Samples and methods

During this study, we collected 16 sandstone samples in different areas of the Western and Eastern Moroccan Mesetas (Figure 2.16C and D). The location of the samples and other details are synthetized in Table 2.5.

Most of the samples are quartzites or quartzitic sandstones, with 90-99% of quartz grains of variable size: c. 0.05 mm in samples AKR1, EZ2, and AZR10, c. 0.1-0.3 mm in samples AKR1, AKR2, EZ1, EZ6, AZR10, and AZR1, and c. 0.4-1.0 mm in samples EZ4, EZ5, AZR10, AZR7. The quartz grains are usually sub-rounded and muscovite and/or oxides can be observed in fractures or interstitial positions. Samples EZ7, OU5, and AZR11 are sandstones with abundant sub-rounded quartz grains (diameters varying between c. 0.05 and c. 0.25 mm) and abundant phyllosilicates and oxides. Finally, samples MAN 1, OUI5 and OUI6 are greywackes characterized by a fine-grained matrix,

embedding c. 0.3-1.0 mm grains of quartz, shale, sandstone, plagioclase, volcanic rocks, oxides, and phyllosilicates.

3.1. U-Pb analyses

Each sample consisted in c. 4-5 kg of rock, which was mechanically smashed with a jaw-crusher and sorted by sieving in the laboratories of the University of Granada (Spain). Zircon grains were separated from the 0.3-0.05 mm fraction using magnetic separation and, finally, handpicking. The grains were then mounted in epoxy discs, polished, cleaned, gold-coated, and imaged by cathodoluminescence (CL) using a Mira3 Field Emission SEM instrument at the John the Laeter Centre (JdLC) of the Curtin University (Perth, Australia) and a Carl Zeiss SIGMA HD VP Field Emission SEM at the School of GeoSciences of the University of Edinburgh (United Kingdom). A selection of CL images for each sample is presented in Appendix C.

The U-Th-Pb analyses on most of the detrital zircon grains were performed at the JdLC GeoHistory Facility (Curtin University, Perth, Australia) using a laser ablation inductively coupled plasma mass spectrometry (LA-ICPMS) with a spot bin of c. 33 μm (Table 2.5). Nevertheless, because of the great variability of grain size in a few samples, sensitive high-resolution ion microprobe (SHRIMP) and secondary ion mass spectrometry (SIMS) techniques, both characterized by a spot bin of c. 15 μm , were performed (Table 2.5), respectively, at the JdLC GeoHistory Facility and at the University of Edinburgh. These analytical methods are explained in Appendix A and the results can be found in Appendix D.

LA-ICPMS, SHRIMP, and SIMS results were then combined to have a sufficient number of data to run statistical analyses (Vermeesch, 2004). Among the data, those with a discordance level exceeding 10% were discarded. The statistical analyses were performed using $^{206}\text{Pb}/^{238}\text{U}$ dates for ages younger than 1.5 Ga and $^{207}\text{Pb}/^{206}\text{Pb}$ dates for older ages (Spencer et al., 2016). The Kernel Density Estimators (KDE) and histograms were done by using DensityPlotter 8.4 software (Vermeesch, 2012) and applying a KDE bandwidth and a histogram bin width of 30 or 5 Ma (Figures 2.18 to 2.24). Each detrital zircon population was defined choosing age intervals that were statistically (i.e., peaks in the KDE diagrams) and geologically (i.e., ages of the main geological events; see legend in Figure 1 and section 5 for discussion) meaningful. The mean ages of the populations were calculated using the mixture-modelling tool in DensityPlotter 8.4. The youngest detrital zircon populations were calculated using the Isoplot software (Ludwig, 2003). All the errors are expressed at 1σ level.

Table 2.5: List and details of the studied samples. (*) total number of analyses performed vs concordant results (in bold).

Sample	IGSN (IEACC)	Location (UTM, NDAS 83)		Lithology	Stratigraphic age	U-Pb geochronology	
		Zone	Long. (m E)			Method	Analyses (*)
MAN1	0040	29S	3735681	Greywacke	Early Ordovician	LA-ICPMS	120/109
COASTAL BLOCK (EL MANSOURIA AREA)							
AKR1	0038	29S	3757672	Quartzitic sandstone	Late Ordovician	LA-ICPMS	150/124
AKR2	0039	29S	3757780	Quartzitic sandstone	Early Ordovician	LA-ICPMS	150/130
OUJED AKREUCH AREA							
EZ1	0032	29S	3682713	Quartzitic sandstone	Late Ordovician	LA-ICPMS SHRIMP	42/30 50/36
EZ2	0033	29S	3682624	Quartzitic sandstone	Late Ordovician	LA-ICPMS	75/68
EZ4	0034	29S	3682341	Quartzitic sandstone	Middle-Late Ordovician	LA-ICPMS	165/156
EZ5	0035	29S	3682849	Quartzitic sandstone	Late Ordovician	LA-ICPMS	180/167
EZ6	0036	29S	3684150	Quartzitic sandstone	Late Ordovician	LA-ICPMS	150/135
EZ7	0037	29S	3683869	Quartzitic sandstone	Early Devonian	LA-ICPMS SIMS	99/86 40/35
OULMES AREA							
OU5	0031	29S	3715910	Sandstone	Early Devonian	LA-ICPMS	150/135
KHENIFRA AREA							
AZR10	0029	30S	3633628	Quartzitic sandstone	Early-Middle Ordovician	LA-ICPMS	120/97
AZR11	0030	30S	3643326	Sandstone	Cambrian-Ordovician	LA-ICPMS SIMS	78/67 47/44
AZROU AREA							
AZR1	0023	30S	3821747	Quartzitic sandstone	Late Ordovician	LA-ICPMS SIMS	100/90 31/31
AZR7	0028	30S	3695342	Quartzitic sandstone	Early Devonian	LA-ICPMS	168/146
ZEKKARA AREA							
OUJ5	0021	30S	3821747	Greywacke	Cambrian-Ordovician	LA-ICPMS	145/143
OUJ6	0022	30S	3821747	Greywacke	Cambrian-Ordovician	LA-ICPMS	150/144

3.2. Hf isotopes analyses

Due to the peculiar U-Pb results obtained in sample AZR10 (see section 4), Hf analyses were performed on the detrital zircon grains of this sample that yielded concordant U-Pb results. These analyses were performed at the JdLC (Curtin University, Perth, Australia) using a Resonetics resolution M-50A excimer laser, coupled to a Nu Plasma II multi-collector inductively coupled plasma mass spectrometer (LA-MC-ICPMS). The detailed analytical methods are described in Appendix A; the results are listed in Appendix E. The statistical analysis was realized using an Excel® worksheet and errors are expressed at 2σ level.

4. Results

El Mansouria area

One hundred and nineteen zircon grains from a lower Ordovician sample (MAN1) were analyzed by LA-ICPMS, obtaining 120 ages, 109 of which yielded concordant results (Figure 2.18A). The main detrital zircon populations obtained in this sample are:

- Cambrian-Ordovician dates (c. 537-450 Ma, n=40, 36.7% of the data) with a Cambrian mean age (506.6 ± 0.7 Ma) and peaks at c. 460, 505 (main peak) and 530 Ma (Figure 2.18B); the grains of this population are generally euhedral or subhedral, with generally rounded edges and continuous oscillatory zoning.
- Ediacaran-Cryogenian dates (c. 660-551 Ma, n=50, 45.9% of the data) with a Late Ediacaran mean age (596.5 ± 0.8 Ma) and peaks at c. 575, 580 (main peak), 600, 630, and 660 Ma (Figure 2.18B); the grains are variable in shape and size, with common oscillatory zoning.
- Rhyacian-Orosirian dates (c. 2096-2010 Ma, n=12, 11% of the data) with a late Orosirian mean age (2048.7 ± 5.0 Ma); the shape and size of the grains are variable, usually with very rounded edges and variable internal zoning.

Scattered grains yielded early Orosirian (n=2, c. 1940 Ma) and late Rhyacian-Neoproterozoic (n=5, c. 2720-2260 Ma) ages. The youngest detrital zircon population of this sample comprises 28 dates and yielded a Cambrian age (506 ± 1 Ma, MSWD=1.05).

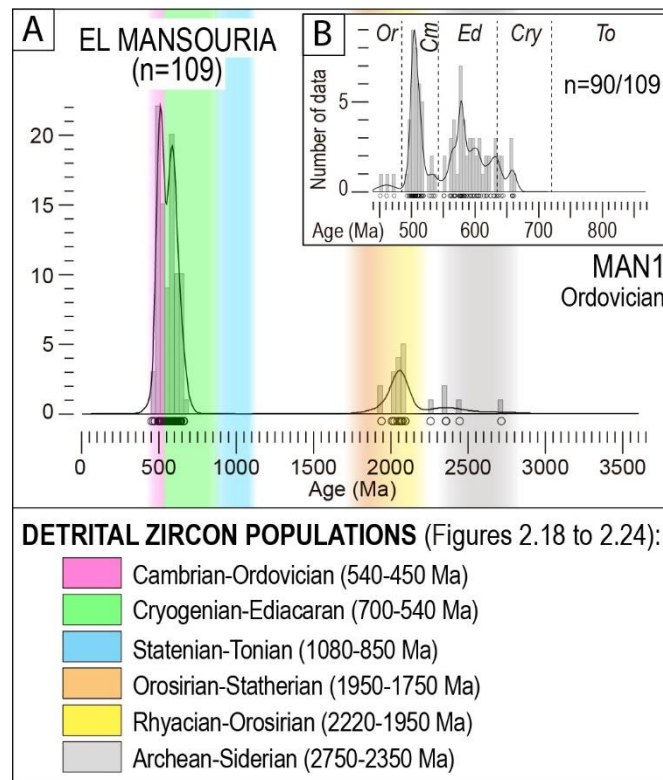


Figure 2.18: KDE (black lines) and histograms (grey bars) showing the U-Pb results in the El Mansouria area (Coastal Block, sample MAN1). (A) Detrital zircon age distribution; (B) window with the 440-870 Ma interval; Or: Ordovician; Cm: Cambrian; Ed: Ediacaran; Cry: Cryogenian; To: Tonian. The graphs were realized using DensityPlotter 8.4 (Vermeesch, 2012) with a KDE bandwidth and histogram bins of 30 Ma (A) and 5 Ma (B). Color bars indicate the most common detrital zircon populations recognized in all the samples.

Oued Akreuch area

On both Ordovician samples from this area, 150 LA-ICPMS analyses were carried out on detrital zircon grains (143 grains in AKR1 and 149 grains in AKR2), yielding 124 and 130 concordant results, respectively (Table 2.5). The age distribution is statistically identical on both samples, and the results have been combined in Figure 2.19. The main detrital zircon populations are as follows:

- Late Tonian-Ediacaran dates (c. 856-543 Ma, n=125, 49.2% of the data) with a late Cryogenian (639.2 ± 0.4 Ma) mean age. Main peaks appear at c. 600, 635 and 650 Ma. Secondary peaks have c. 550, 620, and 670 Ma (Figure 2.19B), while dates between c. 856 and c. 706 Ma appear more scattered. The detrital zircon grains included in this population are generally rounded to elongated, with common concentric oscillatory zoning and cores overgrown by rims.
- Stenian-early Tonian dates (c. 1119-891 Ma, n= 22, 8.7% of the data) with an early Tonian mean age (974.3 ± 1.4 Ma). This population is characterized by rounded to elongated grains showing sector or oscillatory zoning, as well as cores with overgrowth rims.

- Orosirian-Statherian dates (c. 1929-1766 Ma, n=19, 7.5% of the data) with a late Orosirian mean age (1836.0 ± 3.7 Ma). The grains have irregular shapes, sometimes elongated and always characterized by rounded edges; their internal structures show frequent cores with overgrown rims and sector zoning.
- Rhyacian-Orosirian dates (c. 2188-1941 Ma, n=53, 20.8% of the data) clustered in two peaks with Rhyacian (2143.5 ± 3.4 Ma) and early Orosirian (2018.1 ± 3.2 Ma) ages. The detrital zircon grains are generally rounded, with sector zoning or cores with overgrown rims.
- Siderian-Neoproterozoic dates (c. 2770-2404 Ma, n=19, 7.5% of the data) with a late Neoproterozoic mean age (2587.2 ± 2.9 Ma). The zircon grains of this populations are rounded to elongated and show variable internal structures.

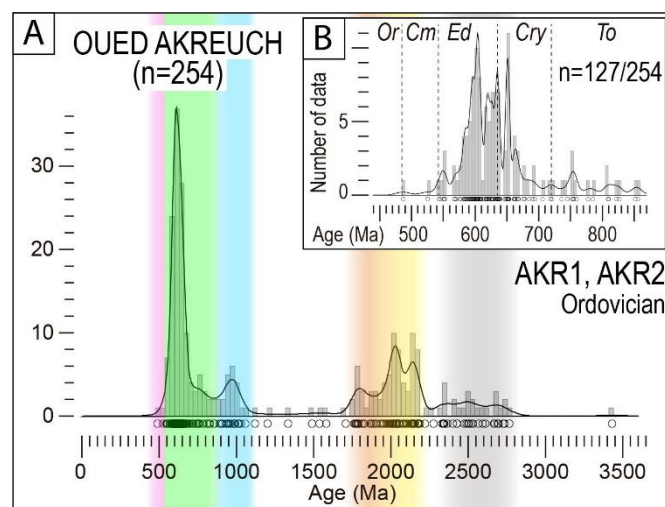


Figure 2.19: U-Pb results in the Oued Akreuch area (combined samples AKR1 and AKR2). Caption and legend as in Figure 2.18.

Scattered grains yielded Cambrian (c. 525-487 Ma, n=2), Statherian-Ectasian (c. 1707-1200 Ma, n=6), Rhyacian (c. 2366-2225 Ma, n=7), and Paleoproterozoic (c. 3437 Ma, n=1) ages. The youngest detrital zircon population of the two samples is late Ediacaran (549.6 ± 2.1 Ma, MSWD=0.59) and comprises 5 dates.

Ezzhiliga area

In this area, five Middle-Upper Ordovician samples and one Lower Devonian sample were collected (Figure 2.20A and C). Six hundred and sixty-two LA-ICPMS and SHRIMP analyses were carried out on a total of 628 zircon grains from the five Ordovician samples. Of these results, 592 yielded concordant dates. All the Ordovician samples show statistically identical results and, accordingly, they have been plotted together (Figure 2.20A). The following detrital zircon populations have been found:

- Cambrian-Ordovician dates (c. 539-476 Ma, n=16, 2.7% of the data) with a Cambrian mean age (519.9 ± 1.3 Ma) and a peak at c. 535 Ma (Figure 2.20B). The detrital zircon

grains of this population are generally rounded to elongate, with variable zoning and sometimes cores with overgrown rims.

- Late Tonian-Ediacaran dates (c. 853-541 Ma, n=332, 56.1% of the data) with an Ediacaran mean age (627.0 ± 0.3 Ma) and a main peak at c. 620 Ma. Second-order peaks appear at c. 560, 590, 630, and 650 Ma, while data between c. 853 and c. 694 Ma are more scarce and scattered (Figure 2.20B). Grains are usually elongate with more or less rounded edges, continuous oscillatory zoning, sector zoning and cores overgrown by rims.
- A very minor Stenian-Tonian population (c. 1049-875 Ma, n=11, 1.9% of the data), mainly concentrated in samples EZ1, EZ5, and EZ6. The mean age is early Tonian (991.7 ± 2.3 Ma) and the grains are elongate, with rounded edges, and in some cases have irregular shapes. The internal structures show oscillatory zoning and rims overgrowing cores.
- Orosirian-Statherian dates (c. 1902-1716 Ma, n=21, 3.5% of the data) with an early Statherian mean age (1815.8 ± 3.5 Ma). This population is characterized by rounded grains, sometimes slightly elongated, with variable internal structures.
- Rhyacian-Orosirian dates (c. 2210-1926 Ma, n=150, 25.3% of the data) with a late Rhyacian mean age (2069.3 ± 1.1 Ma). The detrital zircon grains in this range of ages are generally elongated with rounded edges; the internal structures are variable.
- Siderian-early Rhyacian dates (c. 2478-2291 Ma, n=27, 4.6%) yielding a Siderian mean age (2411.7 ± 2.7 Ma). The grains in this range of ages have variable shapes, usually with very rounded edges, and variable internal structures.

Scattered grains in the Ordovician samples yielded Calymmian-Stenian (c. 1584-1195 Ma, n=14) and Archean (c. 3608-2514 Ma, n=21) ages. The youngest detrital zircon population of the combined group of Ordovician samples is Early Cambrian (536.9 ± 1.5 Ma, MSWD=0.67) and includes 5 dates.

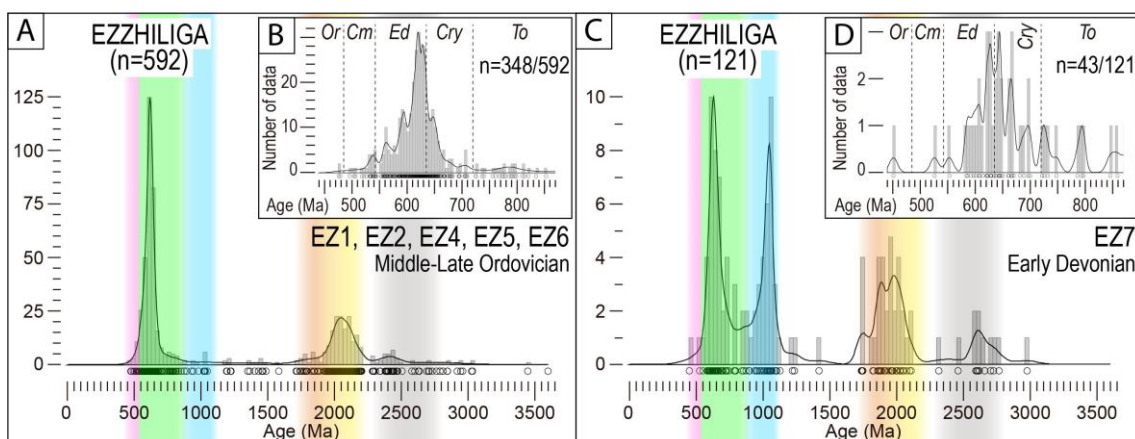


Figure 2.20: U-Pb results in the Ezzhiliga area. (A, B) Ordovician samples (combined EZ1, EZ2, EZ4, EZ5, and EZ6); (C, D) Devonian sample EZ7; Caption and legend as in Figure 2.18.

One hundred and thirty-six detrital zircon grains from the Devonian sample EZ7 were analyzed both with LA-ICPMS (99 grains) and SIMS (37 grains) techniques. These

analyses yielded a total of 121 concordant results (Table 2.5 and Figure 2.20C), clustered as follows:

- Late Tonian-Ediacaran dates (c. 845-553 Ma, n=40, 33.1% of the data) with a Cryogenian mean age (660.1 ± 0.6 Ma) and multiple peaks at c. 610, 630, 645, 665, 695, 725, and 795 Ma (Figure 2.20D). Detrital grains are subhedral with more or less rounded edges and frequent oscillatory zoning or rims overgrowing cores.
- Stenian-Tonian dates (c. 1133-858 Ma, n=33, 27.3% of the data), yielding a late Stenian mean age (1017.6 ± 1.0 Ma) and a main peak centered at c. 1050 Ma. The grains show irregular shapes and cores overgrown by rims.
- Orosirian-Statherian dates (c. 1925-1740 Ma, n=15, 12.4% of the data) clustered in two peaks at 1749.2 ± 8.9 Ma and 1901.9 ± 3.0 Ma (main peak). The detrital zircons show irregular shapes and variable internal structures.
- Rhyacian-Orosirian dates (c. 2117-1947 Ma, n=17, 14% of the data) with a late Rhyacian mean age (2067.3 ± 1.8) and a main peak centered at c. 1995 Ma. Grains are variably shaped, generally featuring sector zoning or cores overgrown by rims.
- Neoproterozoic dates (c. 2774-2600 Ma, n=8, 6.6% of the data) that give a mean age of 2662.2 ± 2.3 Ma. The detrital zircon grains with these ages are usually elongated but with very rounded edges; the internal structures are variable.

Scattered data yielded Cambrian (c. 526-451 Ma, n=2), Calymmian-Stenian (c. 1424-1222 Ma, n=3), Siderian (c. 2467-2325 Ma, n=2), and Mesoarchean (c. 2986 Ma, n=1) ages. The youngest detrital zircon population in this sample includes 4 dates and yielded an Ediacaran age (604.5 ± 1.8 Ma, MSWD=1.52).

Oulmes area

From the Early Devonian sample OU5, 148 detrital zircon grains were separated and 150 analyses were carried out, 135 of which yielded concordant results (Figure 2.21A). The main detrital zircon populations recognized in this sample are:

- Late Tonian-Ediacaran dates (c. 862-552 Ma, n=74, 54.8% of the data) with an early Ediacaran mean age (627.0 ± 0.3 Ma). This population is characterized by a main peak at c. 635 Ma and second order peaks at c. 565, 590, 610, 660, and 675 Ma; data between c. 862 and c. 692 Ma show a more scattered pattern (Figure 2.21B). Grains are generally subhedral to irregular, with more or less rounded edges. Among the internal structures, continuous oscillatory, sector zoning, and overgrown rims are the most common.
- Stenian-Tonian dates (c. 1101-922 Ma, n=9, 6.7% of the data) with a late Stenian mean age (1006.2 ± 2.1 Ma). The grains of this population show variable shape and internal structure.

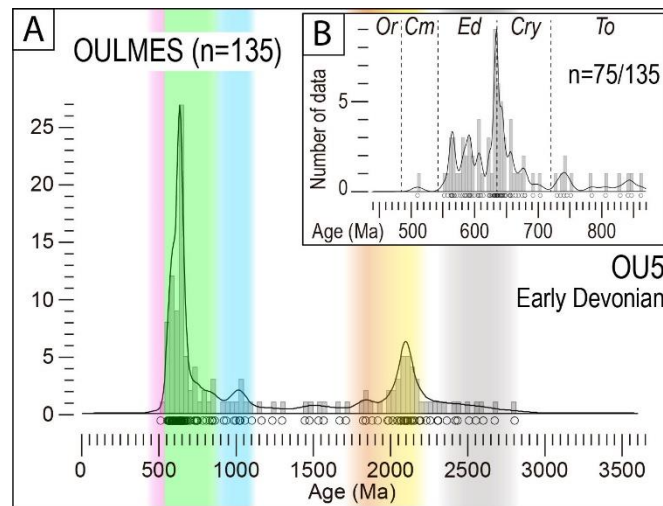


Figure 2.21: U-Pb results in the Oulmes area (sample OU5). Caption and legend as in Figure 2.18.

- A few Orosirian-Statherian dates (c. 1883-1824 Ma, n=4, 3% of the data) peaked at 1852.1 ± 5.5 Ma (Late Orosirian). The grains in this age range are rounded and lack internal structure.
- Rhyacian-Orosirian dates (c. 2198-1984 Ma, n=25, 18.5% of the data) characterized by a Rhyacian mean age (2107.6 ± 2.0 Ma). The grains of this population show variable shapes and continuous oscillatory zoning.

Scattered grains yielded Cambrian (c. 510 Ma, n=1), Statherian-Stenian (c. 1711-1163 Ma, n=9), Orosirian (c. 1922 Ma, n=1), and Mesoarchean-Rhyacian (c. 2810-2236 Ma, n=12) ages. The youngest detrital zircon population in this sample includes 7 dates that define a Late Ediacaran age (563.7 ± 1.4 Ma, MSWD=0.92).

Khenifra area

From the Cambrian-Ordovician sample (AZR11) collected in this area, only 78 detrital zircon grains could be analyzed with LA-ICPMS, yielding 67 concordant results. Other 47 grains, smaller in size, were analyzed with SIMS, having obtained 44 concordant results (Table 2.5). Combining all the concordant data (Figure 2.22A), the following detrital zircon populations have been recognized:

- Late Tonian-Ediacaran dates (c. 797-550 Ma, n=60, 54.1% of the data) with a late Ediacaran mean age (630.9 ± 0.4 Ma). Multiple peaks are distributed along the c. 550-690 age interval, and several scattered data are older than c. 728 Ma (Figure 2.22B). The shape of the grains is variable, from subhedral to elongate and irregular, with a variety of internal structures.
- Orosirian-Statherian dates (c. 1827-1761 Ma, n=6, 5.4% of the data) peaked at 1777.5 ± 4.9 Ma (Late Orosirian). The grains are rounded to irregularly shaped with variable internal zonation.

- Rhyacian-Orosirian dates (c. 2199-1907 Ma, n=26, 23.4% of the data) with a late Rhyacian mean age (2057.2 ± 1.5 Ma). The zircon grains of this age range are elongated to rounded, with common cores overgrown by rims.

Scattered data yielded Cambrian-Late Ordovician (c. 528-483 Ma, n=2), late Statherian-late Tonian (c. 1624-905 Ma, n=12, partially clustered at 1358.5 ± 2.6 Ma), and Mesoarchean-late Siderian (c. 2864-2371 Ma, n=5) ages. The youngest detrital zircon population in this sample is Late Ediacaran in age (551.6 ± 1.6 Ma, MSWD=0.09) and comprises 4 dates.

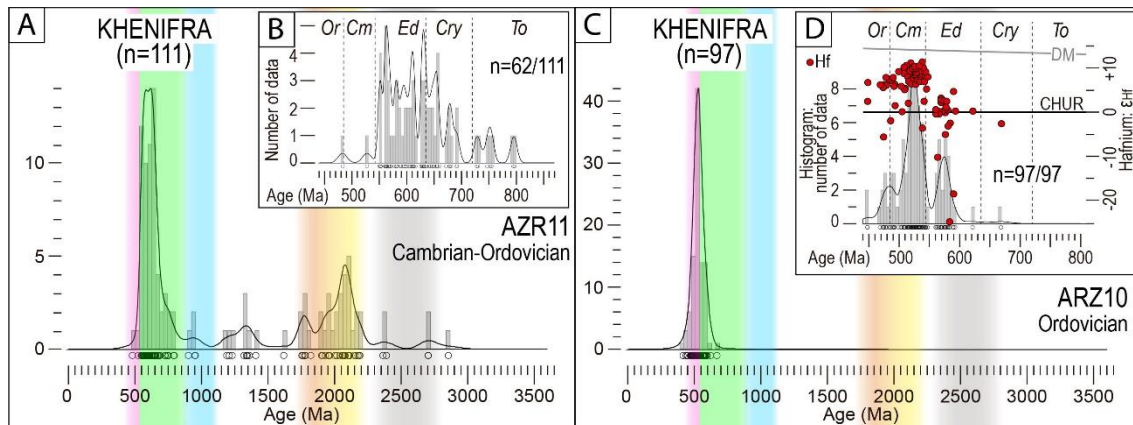


Figure 2.22: U-Pb results in the Khenifra area. (A, B) Cambrian-Ordovician sample AZR11; (C, D) Ordovician sample AZR10; (D) also shows the ϵ_{Hf} values (red circles); CHUR: Chondritic Uniform Reservoir (Iizuka et al., 2015); DM: depleted mantle (Chauvel et al., 2008). Caption and legend as in Figure 2.18.

One hundred and twenty zircon grains from the Ordovician sample (AZR10) were separated and analyzed, yielding 97 U/Pb concordant data. With the exception of two Silurian-Late Devonian (c. 434-412 Ma) and two Cryogenian-early Ediacaran (c. 669-622 Ma) scattered grains, all the data are clustered in a late Cambrian peak (531.5 ± 0.3 Ma; Figure 2.22C). A more careful observation of the detrital zircon spectrum shows the following age distribution (Figure 2.22D):

- Among the Cambrian-Ordovician dates (c. 541-448 Ma, n=66, 68% of the data), 50 ages are peaked at c. 524 Ma, while the other 16 are clustered around c. 479 Ma. The ϵ_{Hf} values associated with these ages are mainly positive and clustered between ϵ_{Hf} c. +5 and +11 (Figure 2.22D), with only a few sub-CHUR values (down to -5.6). The grains that constitute this detrital zircon population are generally euhedral to subhedral, with sharp to slightly rounded edges. Continuous oscillatory zoning is a very common feature.
- The Ediacaran dates (c. 593-541 Ma, n=29, 29.9% of the data) are peaked at 569.2 ± 0.6 Ma. The corresponding ϵ_{Hf} values are clustered between c. 0 and +5, with a few negative values (down to c. -25). These zircon grains have variable shapes and commonly oscillatory zoning.

The youngest detrital zircon population of this sample includes 5 dates that define an Early Ordovician mean age (476.3 ± 1.2 Ma, MSWD=0.87).

Azrou area

One hundred and thirty detrital zircon grains were separated from the Ordovician sample AZR1. One hundred of these grains were analyzed with LA-ICPMS; due to the small size of some of the zircons in this sample, 31 SIMS analyses were additionally performed in the 30 remaining grains. In total, we obtained 121 concordant results (90 LA-ICPMS and 31 SIMS) that are showed in Figure 2.23A. The main detrital zircon populations recognizable are:

- Late Tonian-Ediacaran dates (c. 828-541 Ma, n=63, 52.1% of the data), with a mean age of 631.3 ± 0.5 Ma (early Ediacaran) and peaks distributed along the c. 665-540 Ma interval, as well as scattered dates older than c. 680 Ma (Figure 2.23B). The grains within this population show a high variety of shapes and internal structures.
- Orosirian-Statherian dates (c. 1883-1765 Ma, n=6, 5% of the data) peaked at 1854.1 ± 9.9 Ma (late Orosirian). These zircon grains are characterized by rounded shapes with sector zoning.
- Rhyacian-Orosirian dates (c. 2195-1973 Ma, n=28, 23.1% of the data) with an Orosirian mean age (2081.4 ± 2.5 Ma). These grains show elongated to rounded shapes, oscillatory zoning and overgrown rims.

Scattered grains yielded Cambrian-Early Devonian (c. 538-415 Ma, n=2), Statherian-Stenian (c. 1745-1067 Ma, n=8, partially clustered around 1371.6 ± 3.2 Ma), and Archean-Siderian (c. 3335-2302 Ma, n=13) ages. The youngest detrital zircon population in this sample is late Ediacaran (542.4 ± 1.8 Ma, MSWD=1.15) and includes 4 dates.

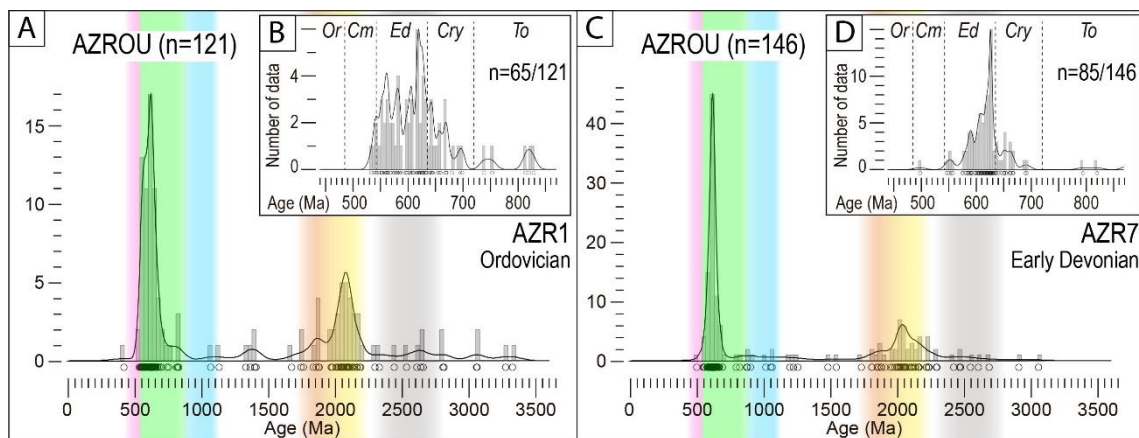


Figure 2.23: U-Pb results in the Azrou area. (A, B) Ordovician sample AZR1; (C, D) Devonian sample AZR7; Caption and legend as in Figure 2.18.

From the Devonian sample AZR7, we analyzed 153 zircon grains, yielding 168 analyses, 146 of which were concordant (Figure 2.23C). These data can be grouped in 3 detrital zircon populations:

- Cryogenian-Ediacaran dates (c. 692-546 Ma, n=82, 56.2% of the data) with an Ediacaran mean age (617.6 ± 0.3 Ma). These dates are clustered at c. 625 Ma (main peak), 550, 590, 610, and 655 Ma (secondary peaks; Figure 2.23D). The grains vary from subhedral to elongate, and their internal structure is variable (homogeneous, oscillatory zoning, cores overgrown by rims).
- Orosirian-Statherian dates (c. 1911-1851 Ma, n=5, 3.4% of the data) peaked at 1877.4 ± 5.6 Ma (Late Orosirian). This population is characterized by rounded grains with variable internal structure.
- Rhyacian-Orosirian dates (c. 2243-1955 Ma, n=32, 21.9% of the data) with a mean age of 2086.7 ± 0.7 Ma (Late Rhyacian). The grains in this age range are generally rounded and characterized by sector and oscillatory zoning.

One grain has a Cambrian age (c. 497 Ma), while scattered zircon grains yielded late Orosirian-late Tonian (c. 1814-795 Ma, n=16) and Mesoarchean-Rhyacian (c. 3064-2296 Ma, n=10) ages. The youngest detrital zircon population is late Ediacaran (589.2 ± 0.9 Ma, MSWD=1.1 n=8).

Zekkara area

From the two Cambrian-Ordovician samples collected in the Zekkara area (OUJ5 and OUJ6), 140 and 150 detrital zircon grains were separated, respectively. A total of 295 LA-ICPMS analyses were performed, yielding 287 concordant results (see details in Table 2.5). The detrital zircon populations recognized in both samples are statistically identical and have been plotted together (Figure 2.24A):

- Cambrian-Ordovician dates (c. 539-446 Ma, n=59, 20.6% of the data) with a Cambrian mean age (498.7 ± 0.3 Ma), a main peak at c. 505 Ma, and second order peaks at c. 460 and 495 Ma (Figure 2.24B). The grains within this age range are generally euhedral to subhedral, with frequent continuous oscillatory or sector zoning.
- Late Tonian-Ediacaran dates (c. 805-544 Ma, n=134, 46.9% of the data) with a mean age of 609.0 ± 0.3 Ma (Ediacaran). Excluding relatively scattered grains younger than c. 560 Ma or older than c. 644 Ma, most of the dates are clustered at c. 580 (main peak) and 615 Ma (Figure 2.24B). The grains are euhedral to subhedral, mainly characterized by continuous oscillatory zoning.
- Rhyacian-Late Orosirian dates (c. 2186-2002 Ma, n= 33, 11.5% of the data) with a late Rhyacian mean age (2103.4 ± 2.9 Ma). This population is characterized by rounded to elongated grains with variable internal structure.
- Neoaarchean-Siderian dates (c. 2694-2386 Ma, n=27, 9.4% of the data) with a late Siderian mean age (2552.9 ± 2.8 Ma). The grains are elongated with frequent oscillatory zoning and overgrown cores.

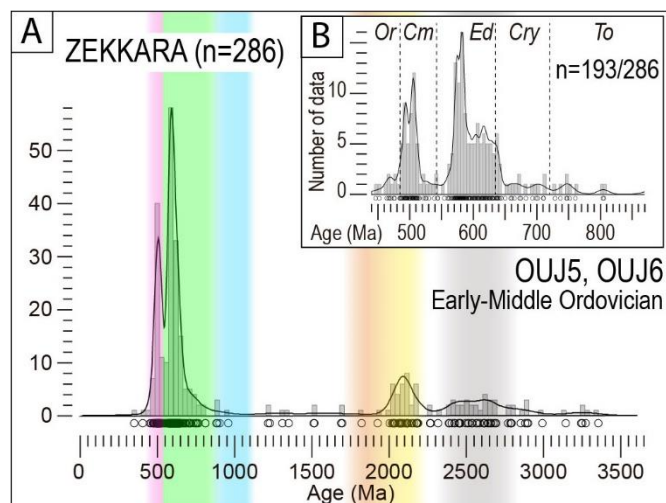


Figure 2.24: U-Pb results in the Zekkara area (samples Ouj5 and Ouj6). Caption and legend as in Figure 2.18.

Scattered grains yielded Early Devonian-early Carboniferous (c. 398-341 Ma, $n=2$), Orosirian-Tonian (c. 1923-875 Ma, $n=14$), Early Siderian-Rhyacian (c. 2315-2263 Ma, $n=3$), and Archean (c. 3357-2771 Ma, $n=14$) ages. The youngest detrital zircon population of the combined two samples includes 5 dates that define an Early-Middle Ordovician age (470.5 ± 1.3 Ma, $MSWD=1.4$), although, when taken separately, the two samples yield late Cambrian youngest detrital zircon population ages (495.4 ± 0.9 Ma for sample Ouj5 and 492.2 ± 1.0 Ma for Ouj6).

To sum up, with the exception of the peculiar results obtained in sample AZR10, the late Tonian-Ediacaran and Rhyacian-Orosirian populations are always dominant in our samples, representing 33-56% and 11-23% of the data, respectively. The occurrence of minor detrital zircon populations (Neoarchean-Siderian, Orosirian-Statherian, Tonian-Stenian, and Cambrian Ordovician) is very variable in time and space (Table 2.6).

Table 2.6 (next page): Summary of the detrital zircon populations recognized in the studied samples with approximate ages and percentage of occurrences.

	COASTAL BLOCK ORDOVICIAN	OUED AKREUCH ORDOVICIAN	EZZHILIGA ORDOVICIAN	DEVONIAN	OULMES DEVONIAN	KHENIFRA ORDOVICIAN	CAMBRIAN- ORDOVICIAN	AZROU ORDOVICIAN	DEVONIAN	ZEKKARA CAMBRIAN- ORDOVICIAN
YOUNGEST DETITAL ZIRCON POPULATION	506.1±0.9 Ma MSWD = 1.05 n = 29	549.6±2.1 Ma MSWD = 0.59 n = 5	536.9±1.5 Ma MSWD = 0.67 n = 14	604.5±1.8 Ma MSWD = 1.52 n = 4	563.7±1.4 Ma MSWD = 0.92 n = 7	476.3±1.2 Ma MSWD = 0.87 n = 5	551.6±1.6 Ma MSWD = 0.09 n = 4	542.4±1.8 Ma MSWD = 1.15 n = 4	589.2±0.9 Ma MSWD = 1.10 n = 8	470.5±1.3 Ma MSWD = 1.40 n = 5
CAMBRIAN- ORDOVICIAN ca. 540-450 Ma	c. 507 Ma 36.7%	-	c. 520 Ma 2.7%	-	-	c. 479 Ma c. 524 Ma 68%	-	-	-	c. 499 Ma 20.6%
LATE TONIAN- EDIACARAN ca. 850-540 Ma	c. 596 Ma 45.9%	c. 639 Ma 49.2%	c. 627 Ma 56.1%	c. 660 Ma 33.1%	c. 627 Ma 54.8%	c. 569 Ma 29.9%	c. 631 Ma 54.1%	c. 631 Ma 52.1%	c. 617 Ma 56.2%	c. 609 Ma 46.9%
STENIAN- EARLY TONIAN ca. 1080-850 Ma	-	c. 974 Ma 8.7%	c. 992 Ma 1.9%	c. 1015 Ma 26.4%	c. 1006 Ma 6.7%	-	-	-	-	-
OROSIRIAN- STATHERIAN ca. 1950-1750 Ma	-	c. 1836 Ma 7.5%	c. 1816 Ma 3.5%	c. 1749 Ma c. 1901 Ma 12.4%	c. 1852 Ma 3.0%	-	c. 1777 Ma 5.4%	c. 1854 Ma 5.0%	c. 1877 Ma 3.4%	-
RHYACIAN- OROSIRIAN ca. 2220-1950 Ma	c. 2049 Ma 11.0%	c. 2018 Ma c. 2143 Ma 20.8%	c. 2069 Ma 25.3%	c. 2067 Ma 14.0%	c. 2108 Ma 18.5%	-	c. 2057 Ma 23.4%	c. 2081 Ma 23.1%	c. 2087 Ma 21.9%	c. 2103 Ma 11.5%
NEOARCHEAN -SIDERIAN ca. 2800-2300 Ma	-	c. 2516 Ma 4.7%	c. 2412 Ma 4.6%	c. 2662 Ma 6.6%	-	-	-	-	-	c. 2467 Ma c. 2635 Ma 9.4%

5. Discussion

5.1. Maximum depositional ages

The analysis of detrital zircon ages in metasedimentary rocks is a powerful tool to ascertain the possible sources of sediments and constrain maximum depositional ages (MDA). MDA is defined by the youngest detrital zircon population made up of at least 4 dates in each sample, or group of statistically homogeneous samples. Thus, MDA might be virtually coeval or more commonly older (up to hundreds of millions of years; Sharman and Malkowski, 2020) than true depositional ages (TDA), these latter normally inferred from fossil content and/or geochronological dating of volcanic intercalations. The delay between MDA and TDA depends on the geographical and geological setting in which the sedimentary rocks were deposited, such as topography, drainage systems, basin configuration, tectonic setting, etc. In those cases in which TDA are poorly constrained, MDA might be taken as a rough approximation to the age of a sedimentary rock.

In the case of all the Cambrian-Lower Devonian samples studied in this work, TDA (constrained by the biostratigraphic knowledge of the sampled sections) are younger than MDA (Table 2.6). In most samples, the difference between MDA and TDA is between c. 100 and 200 Ma, which supports that sedimentation occurred in a passive continental margin free from the influence of magmatic activity. Nevertheless, in a few cases the delay between MDA and TDA is reduced to just a few tens of millions of years (*e.g.*, sample MAN1, Coastal Block) or even less (sample AZR10, Khenifra area, and samples OUI5 and OUI6, Zekkara area), suggesting the existence of some magmatic activity in the region at Cambrian-Ordovician time, although its relevance, as discussed in section 5.4.1, was probably minor and reduced to a local scale.

5.2. Main sediment source: West African Craton affinity

Provenance studies supported by statistical analysis of detrital zircon age distribution are based on the comparison among age spectra in detrital samples and those of potential source areas (*e.g.*, Fedo et al., 2003 and references therein). In the case of the Moroccan Variscides, the typical age spectrum of the West African Craton (WAC) accords quite well with the patterns found in Ediacaran to Carboniferous metasedimentary rocks (*e.g.*, Abati et al., 2010; Accotto et al., 2019, 2020, 2021, in press; Avigad et al., 2012; El Houicha et al., 2018; Ghienne et al., 2018; Letsch et al., 2018). This source area (WAC) is characterized by late Tonian-Ediacaran (c. 750-540 Ma) and Rhyacian-Orosirian (c. 2.2-1.95 Ga) ages (Figure 2.25), which are related to the Cadomian/Pan-African and Eburnean orogenies, respectively (Nance et al., 2008 and references therein). Furthermore, Neoproterozoic ages (c. 2.5 Ga) are also common in the WAC and have been generally associated with the Leonian-Liberian orogenies (Hurley et al.,

1971; Nance et al., 2008 and references therein). On the contrary, Mesoproterozoic magmatic sources are common in Baltica, Laurentia, Avalonia, Amazonia and other Grenvillian terranes (Ernst et al., 2008), but absent in the WAC.

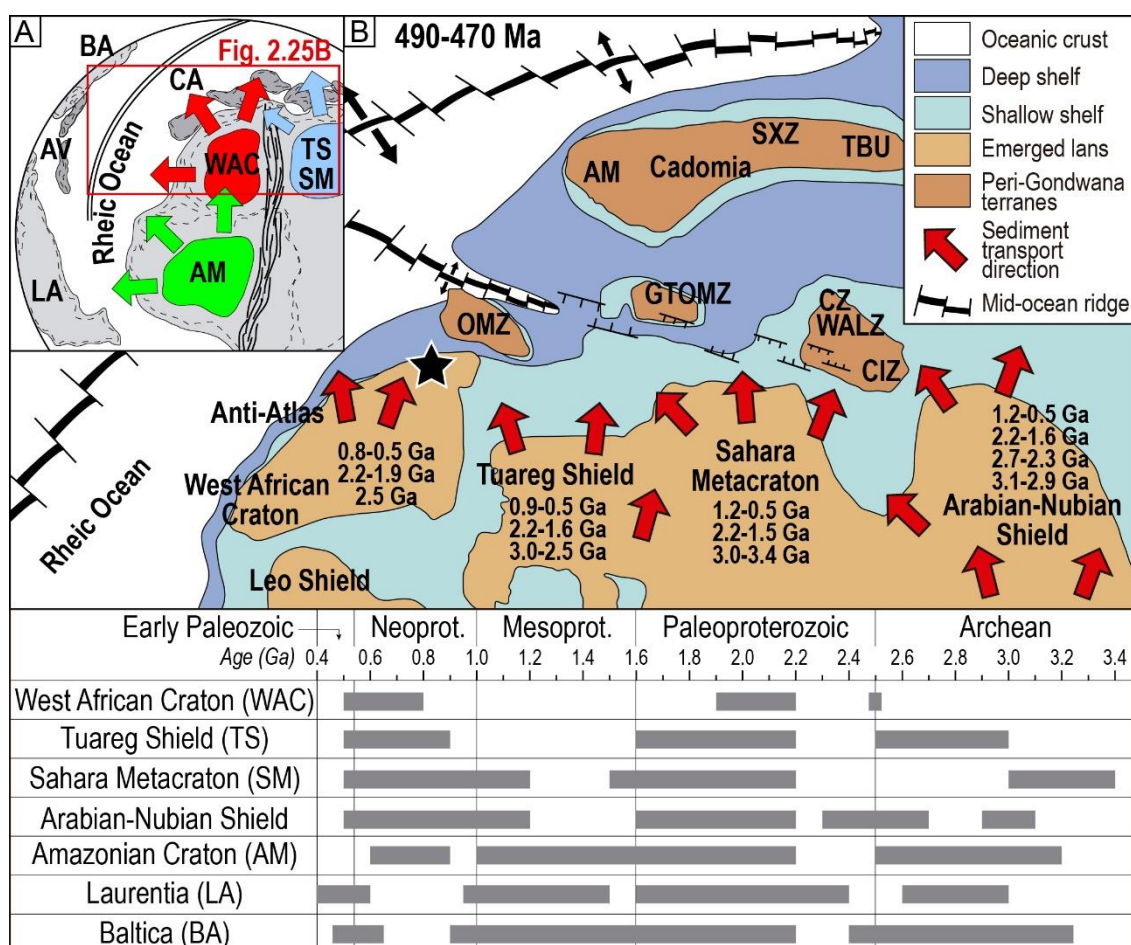


Figure 2.25: (A) Paleogeographic reconstruction of the northwestern margin of Gondwana and peri-Gondwanan terranes at Late Ordovician time (490-470 Ma); AM: Amazonia AV: Avalonia; BA: Baltica; CA: Cadomia; LA: Laurussia; TS-SM: Tuareg Shield and Sahara Metacraton; WAC: West African Craton; (B) A more detailed reconstruction with the different cratonic areas. The numbers in the map and the grey bars in the graphical time scale indicate the magmatic zircon age distribution in the main source areas. The studied area is located with a black star. AM: Armorican Massif; CIZ: Central Iberian Zone; CZ: Cantabrian Zone; GTOMZ: Galicia-Tras-os-Monte Zone; OMZ: Ossa Morena Zone; SXZ: Saxo-Thuringian Zone; TBU: Tepla-Barrandian Unit; WALZ: West-Leonese Zone. Modified from Díez Fernández et al. (2010) and Cambeses et al. (2017) and references therein.

Figure 2.26 shows a comparison among all the detrital zircon age spectra from lower Cambrian-Lower Devonian detrital metasedimentary rocks described in this work and in previous studies carried out in the Moroccan Mesetas (Accotto et al., 2019, in press; Ghienne et al., 2018; Letsch et al., 2018). This comparison clearly demonstrates that the main detrital zircon populations present in all of the samples are consistent with those that characterize the WAC and, therefore, features a WAC affinity for the studied rocks. The almost general lack of Mesoproterozoic detrital zircon grains can also be taken as evidence of WAC provenance. Furthermore, our new data are also consistent with the detrital zircon spectra from other Neoproterozoic-Early Paleozoic rocks from the High

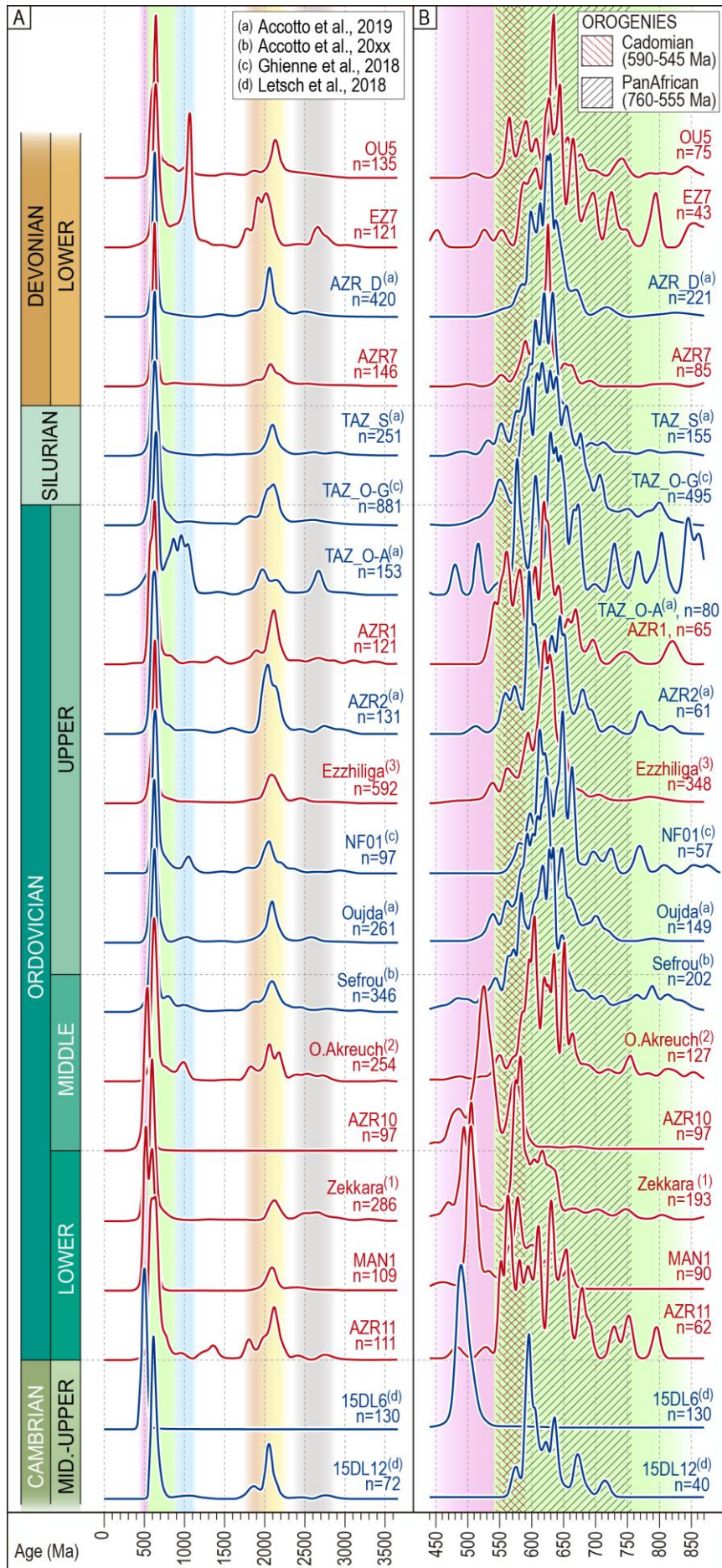
Atlas and Anti-Atlas (Abati et al., 2010; Avigad et al., 2012; Perez et al., 2019), unanimously supporting the common interpretation that the WAC represented the main source region for the sediments deposited in this part of the northern passive margin of Gondwana.

The (meta)igneous rocks that constitute the Precambrian basement of the Moroccan Mesetas could have also been the source of detrital zircon grains found in the overlying Paleozoic sedimentary succession. Though very small and scarce, some outcrops have revealed the existence of Eburnian (Pereira et al., 2015) and Cadomian (El Haïbi et al., 2020; El Haïbi et al., 2021; El Houicha et al., 2018; Letsch et al., 2018; Ouabid et al., 2017; Tahiri et al., 2010) basement in the Western Meseta. This basement might have been exposed and prone to erosion during the earliest Paleozoic rifting, prior to be covered by the passive margin sediments. Particularly, two metarhyolites from the Khenifra area yielded protholith ages of c. 564 Ma and c. 570 Ma (Letsch et al., 2018), that agree well with the c. 570 Ma detrital zircon population found in our nearby Cambrian-Ordovician samples AZR10 and AZR11 (Figure 2.22).

5.3. Discriminating between Pan-African and Cadomian sources

The Late Tonian-Ediacaran detrital zircon population is related to both the Cadomian (590-545 Ma; Linnemann et al., 2008 and references therein) and Pan-African (760-555 Ma; Hefferan et al., 2014 and references therein) orogenies, which partially overlap in time and space. The Pan-African orogeny is commonly considered responsible for the subductional/collisional tectonic events that assembled northern Africa along the Neoproterozoic, while the Cadomian orogeny refers to the Andean-type tectonic setting that was active in the North Gondwana margin at Ediacaran time. In the detailed KDE plots shown in Figure 2.26B we can observe that the highest peaks of the Late Tonian-Ediacaran population (green background) in the Lower Ordovician samples (AZR11, MAN1, OUI5 and OUI6, and AZR10) appear at c. 590 and c. 555 Ma, i.e., the period of time when the two orogenies overlap. On the contrary, in the Middle Ordovician-Upper Devonian samples, despite the presence of second- and/or third-order peaks at the 590-555 Ma interval, the highest ones are slightly older (c. 650-600 Ma). Accordingly, we suggest that during the early Paleozoic (Cambrian to Early Ordovician) the Moroccan Meseta sediments were sourced by both Cadomian and Pan-African rocks, i.e., from the neighboring and recently active subduction-related continental margin. Later on, from Middle Ordovician time onwards, continued subsidence at the continental now passive margin led to the burial of the remaining Cadomian magmatic arc, displacing the main sediment source to more inland and stable areas of the WAC where Pan-African older rocks cropped out.

Figure 2.26 (following page): Comparison among KDE plots from the Moroccan Mesetas; A) entire age spectra (3600-0 Ma); B) Late Tonian-Ordovician spectra (870-440 Ma). Red lines represent samples from this study; blue lines are data from previous works (see references in the figure). (1) Zekkara: OUI5 and OUI6; (2) Oued Akreuch: AKR1 and AKR2; (3) Ezzhiliga: EZ1, EZ2, EZ4, EZ5, and EZ6.



5.4. Minor detrital zircon populations and secondary sediment sources

5.4.1. Cambrian-Ordovician magmatism

Despite the predominance of Paleozoic sediments with WAC affinity in the Moroccan Mesetas, the occurrence of minor detrital zircon populations suggests the influence of additional secondary incomes from other terranes and/or local magmatic sources.

In this regard, the presence and distribution of a Cambrian-Ordovician (c. 525-480 Ma) detrital zircon population in the Moroccan Meseta deserves some consideration. All of the available tectonic reconstructions consider that a Cambrian-Ordovician rifting episode followed the conclusion of the Cadomian subduction, giving way to a new Wilson cycle during which the Rheic Ocean developed (Figure 2.25; *e.g.*, Cambeses et al., 2017; Nance et al., 2012, 2010). This rifting episode is well recognized in the Variscan massifs of central and southern Europe, where it is characterized by thick Cambrian-Ordovician sedimentary successions accompanied by rift-related magmatic rocks (*e.g.*, Álvaro et al., 2018 and references therein; Linnemann et al., 2007 and references therein; Sánchez-García et al., 2003). Detrital zircon grains of Cambrian-Ordovician age are also relatively common in the lower-middle Paleozoic (meta)sedimentary rocks of these regions (*e.g.*, Bahlburg et al., 2010; Drost et al., 2011; Košler et al., 2014; Lin et al., 2019, 2016; Linnemann et al., 2008; Montero et al., 2009; Pastor-Galán et al., 2013b; Pereira et al., 2012; Shaw et al., 2014; Strnad and Mihaljevič, 2005; Szczepański et al., 2020; Žák and Sláma, 2018).

In northern Morocco, the Cambrian-Ordovician rifting seems to have been aborted before reaching the oceanic phase (Bernardin et al., 1988; Ouali et al., 2003; Piqué, 2003, 1979; Piqué et al., 1995; Piqué and Michard, 1989). Paleogeographic studies allowed the reconstruction of this rift, extending from the western part of the Anti-Atlas to the northern part of the Coastal Block with a broadly NNE-SSW trend (Figure 2.27; *e.g.*, Álvaro et al., 2014; Bernardin et al., 1988; Ezzouhairi et al., 2008; Ouali et al., 2003; Piqué, 2003; Piqué et al., 1995; Piqué and Michard, 1989; Pouclet et al., 2018 and references therein). In the Anti-Atlas, Pouclet et al. (2018 and references therein) recognized 6 magmatic pulses related to the aborted rift, the youngest of which (c. 500-497 Ma) also affected the Western Moroccan Meseta in the northern part of the Coastal Block (El Hadi et al., 2006a) and the southern part of the Central Zone (Khenifra area; Figure 2.27; Ouabid et al., 2020; Ouali et al., 2003). Nevertheless, Cambrian-Ordovician detrital zircon grains are not common in the Cambrian-Devonian rocks of the Moroccan Mesetas, where they have been only reported locally and, except for an isolated case in the Khenifra area (sample 15DL6 by Letsch et al., 2018), in limited percentages (less than 5% of the data; Figure 2.27; Accotto et al., 2019, in press; Ghienne et al., 2018).

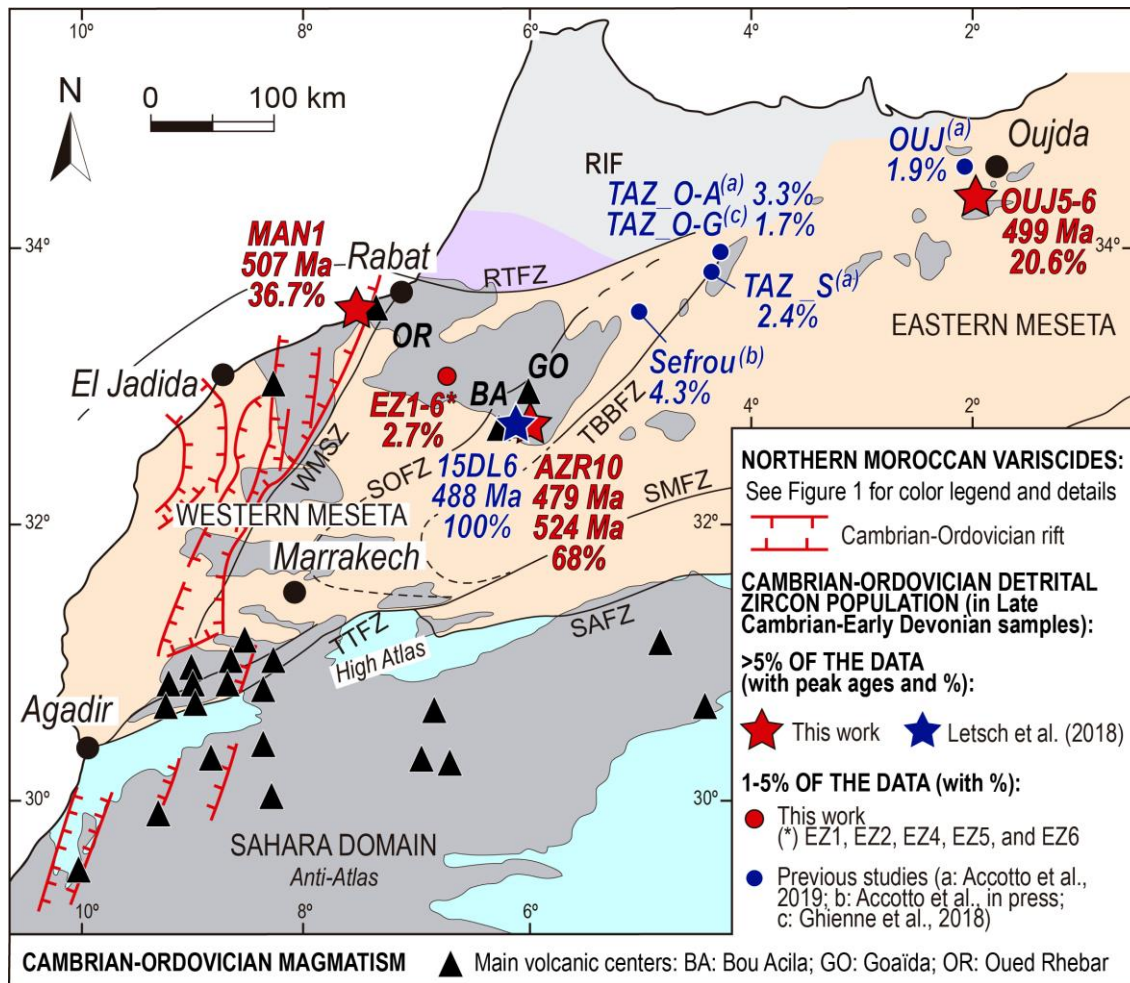


Figure 2.27: Distribution of the Cambrian-Ordovician rift and volcanic centers described in northern Morocco (after Pouclet et al., 2018 and references therein; Ouabid et al., 2020), with percentages of the Cambrian-Ordovician detrital zircon populations. See caption of Figure 2.16 for acronyms.

In the new data reported here, the Cambrian-Ordovician detrital zircon population is generally scarce, except in a few Lower-Middle Ordovician samples from the Coastal Block (MAN1), Khenifra (AZR10), and Zekkara (OUIJ5 and OUIJ6) areas (Figure 2.27). In the first two cases the samples were collected c. 10-15 km from the Oued Rhebar and Bou Acila volcanic centers (Pouclet et al., 2018 and references therein), respectively. In the Oued Rhebar sector, acid to intermediate trachyandesites (El Hadi et al., 2006b) yielded a geochronological date of 507 ± 5 Ma (U-Pb on magmatic zircon grains; El Attari et al., 2019), perfectly coincident with the average age of the Cambrian peak found in MAN1 (c. 507 Ma, 36.7% of the data). In the Bou Acila sector, at least two magmatic events poorly dated but separated by lower Cambrian limestones were recognized (Morin, 1960; Ouali et al., 2003; Pouclet et al., 2018; Verset, 1988). Interestingly, Letsch et al. (2018) published data from a sample of this sector (15DL6, Figures 2.26 and 2.27), which depicts a single late Cambrian (c. 488 Ma) detrital zircon peak; this sample suggests that at least one magmatic pulse in the Bou Acila sector occurred at late Cambrian time. Furthermore, our data from the nearby sample AZR10 show a main peak at c. 524 Ma (52% of the data) and a minor one at c. 479 Ma (16% of the data) (Figure 2.26B), both characterized by positive ε_{HF} values clustered between +5 and +11 (Figure 2.22D). These

peaks can be tentatively related to other magmatic pulses of the Bou Acila volcanic center. The positive ε_{Hf} values appear to confirm the juvenile nature of some of the magmas associated with the rifting episode.

In both the Coastal Block and Khenifra samples, however, the overall imprint of the Cambrian magmatism might have been limited, since other almost coeval samples collected c. 40 km away from the Oued Rhebar (AKR1 and AKR2, Lower-Upper Ordovician) and Bou Acila (AZR11, Cambrian-Ordovician) volcanic centers, as well as a slightly younger sample located very close to the Oued Rhebar sector (NF01, Upper Ordovician, Ben Slimane area; Ghienne et al., 2018) only contain a couple of scattered Cambrian grains or none (Figure 2.26B).

In the Eastern Moroccan Meseta, no Cambrian-Ordovician volcanic centers have been reported until now, but the samples from Zekkara (OUJ5 and OUJ6, Figures 2.16D, 2.16B and 2.27) yielded 20.6% of Cambrian-Ordovician ages (mean age c. 499 Ma), suggesting that at least one magmatic source of that age existed in that area. Nevertheless, other Late Ordovician samples from the nearby Oujda area (15 km NE from Zekkara) only yielded 1.9% of Cambrian ages (Accotto et al., 2019), which points to a rather very local influence of the claimed Cambrian-Ordovician EMM magmatic source.

The occurrence of Cambrian-Ordovician detrital zircon grains sensibly decreases in Middle Ordovician-Silurian samples ($\leq 5\%$ of the data), while in the Lower Devonian ones almost no Cambrian-Ordovician detrital zircon ages have been found (Figures 2.16B). These data suggest, therefore, that shortly after the rift abortion (Bernardin et al., 1988; Ouali et al., 2003; Piqué, 2003, 1979; Piqué et al., 1995; Piqué and Michard, 1989) and a brief erosional phase, the volcanic centers in the Moroccan Meseta were probably covered by the passive margin sedimentary sequence, mainly fed by erosion of the WAC and partial recycling of older sedimentary rocks.

5.4.2. Stenian-early Tonian detrital zircon ages

Another minor detrital zircon population already discussed by several authors in the northern Moroccan Variscides is the Stenian-early Tonian one (c. 1.0 Ga). This population has been described in middle Cambrian rocks from the Anti-Atlas (Avigad et al., 2012), a Lower Ordovician rock from the Coastal Block (WMM; sample NF01; Figure 11A; Ghienne et al., 2018), Lower-Middle Ordovician and Upper Ordovician-Silurian rocks from the Middle Atlas (WMM; Figures 2.26A; Accotto et al., 2019, in press; Ghienne et al., 2018), Upper Devonian rocks from the Central Zone (WMM; Accotto et al., 2021), and Upper Ordovician (Figures 2.26A) and middle-upper Carboniferous rocks from the EMM (Oujda and Jerada areas; Accotto et al., 2019, 2021). Among the samples analyzed in this study, we have identified the c. 1 Ga detrital zircon population in two Middle Ordovician rocks from the Oued Akreuch area (AKR1 and AKR2, 8.7% of the data), five Ordovician (EZ1, EZ2, EZ4, EZ5, and EZ6, 1.9%) and one Lower Devonian rocks from the Ezzhiliga area (EZ7, 26.4%), and one Lower Devonian rock from the Oulmes area (OU5, 6.7%). In the remaining samples, Mesoproterozoic ages

are absent or represented by scarce scattered grains that cannot be considered a proper detrital zircon population (Table 2.6).

Stenian-early Tonian sources are virtually unknown in the WAC, although a recent work (El Bouougri et al., 2020) pointed out the existence of a limited early Tonian (c. 883 Ma) magmatic activity in the Anti-Atlas related to an incipient phase of the Rodinia breakup. Nevertheless, even if this event would have been sufficiently widespread to provide zircon grains up to the Moroccan Meseta, it could only explain the youngest ages within the Stenian-early Tonian detrital zircon population found in our samples.

Ages ranging from c. 1.3 to c. 0.9 Ga are typical of the Grenvillian terranes (Ernst et al., 2008) that, before the opening of the Rheic Ocean at Cambrian-Ordovician time (Nance et al., 2012, 2010), were relatively close to the northern Gondwanan margin (*e.g.*, Amazonia). Nevertheless, these terranes are also characterized by other Mesoproterozoic sources in the range 1.7-1.1 Ga (Figures 2.25). Interestingly, detrital zircon age distributions compatible with Amazonian sources were found in Neoproterozoic metasedimentary rocks overlying the western WAC in Mauritania (Figures 2.16A; Bradley et al., 2015). On the contrary, all of the Neoproterozoic-Carboniferous metasedimentary rocks sampled from the Anti-Atlas (*e.g.*, Abati et al., 2010; Avigad et al., 2012) and, further north, in the High Atlas (Perez et al., 2019) and Moroccan Meseta (Accotto et al., 2019 2021, in press; El Houicha et al., 2018; Ghienne et al., 2018; Letsch et al., 2018; this work) did not record Mesoproterozoic ages older than c. 1.1 Ga (except for a very few scattered grains, *e.g.*, AZR11 and AZR1; Figures 2.23A). Therefore, it is very unlikely that Amazonian (c. 1.7-0.9 Ga) sources could have supplied the c. 1.0 Ga detrital zircon population that episodically is found in the northern Moroccan Variscides. As an exception, a statistically significant number of detrital zircon grains yielded ages between c. 1.7 and 1.1 Ga in a few lower Carboniferous samples from the Mohammedia (Coastal Block), Tiflet (northern Central Zone), and Debdou-Mekkam (EMM) areas (Figures 2.16; Accotto et al., 2020, 2021). In these specific cases, the authors invoked an Avalonian (Amazonia-derived) source only available since the early Variscan (Tournaisian-early Viséan) collision.

To explain the occurrences of c. 1.0 Ga detrital zircon ages in the pre-collisional succession of the northern Moroccan Variscides, several authors (Accotto et al., 2019, 2021, in press; Avigad et al., 2012; Ghienne et al., 2018) claimed for northeastern African sources (*e.g.*, Sahara Metacraton, Arabian-Nubian Shield; Figure 10). The age spectra of our samples containing the c. 1.0 Ga detrital zircon population are compatible with these northeastern African sources (Figures 2.26A).

The spatial and temporal distribution of samples containing Stenian-early Tonian dates is highly irregular, as well as the statistical relevance of this population (Figures 2.26A). In most of the cases, grains of these ages represent less than 10% of the data, but they locally reach c. 25% (*e.g.*, sample EZ7 from this work and the Ordovician samples from the Tazekka area in Accotto et al., 2019). This irregularity contrasts with other northern Gondwanan terranes cropping out in central and northwestern Iberia, where the c. 1.0 Ga detrital zircon population is very common and represents 30-50% of the data (Bea et al.,

2010; Fernández-Suárez et al., 2014; Gutiérrez-Alonso et al., 2015; Pastor-Galán et al., 2013a; Shaw et al., 2014; Talavera et al., 2012). Accordingly, we suggest that at Ordovician-Early Devonian time the Moroccan Mesetas belonged to the northern Gondwana passive margin, but was located in a more western and distal position than the current central/northwestern Iberian terranes (Figures 2.25), and, hence, the sedimentary incomes from northeastern African sources were distant and intermittent.

5.4.3. Orosirian-Statherian detrital zircon ages

The Orosirian-Statherian (c. 1.95-1.75 Ga) detrital zircon population found in NW Africa is considered by several authors to be related to the last pulses of the Eburnean orogeny (*e.g.*, Abati et al., 2012; Bessoles, 1977; Ghienne et al., 2018). Nevertheless, magmatic rocks related to this orogeny show ages not younger than c. 1.95 Ga (Rb/Sr, Sm/Nd, and U/Pb methods; Abouchami et al., 1990; Aït Malek et al., 1998; Boher et al., 1992; Hirdes et al., 1992; Liégeois et al., 1991; Schofield et al., 2006). Statherian (c. 1.75 Ga) bimodal dykes were described and dated in the Anti-Atlas, and considered to be the only remnants of a large igneous province developed during the breakup of the Nuna/Columbia supercontinent (Gasquet et al., 2004; Lama et al., 1993; Youbi et al., 2013) during the vanishing stages of the Eburnean orogeny. However, it is unlikely that volumetrically small dyke intrusions would have produced the amount of Orosirian-Statherian detrital zircon grains found in our samples (up to 12.4% of the data in sample EZ7; Table 2.6) and other Paleozoic samples from the northern Moroccan Variscides (*e.g.*, Abati et al., 2010; Accotto et al., 2019, 2020, 2021, in press; Avigad et al., 2012; Ghienne et al., 2018; Letsch et al., 2018).

Recent U-Pb dating on zircon grains in charnockites from the Mazagan escarpment, offshore the western Moroccan coast, highlighted crystallization ages varying from c. 1.95 to c. 1.75 Ga (Kuiper, 2019; Kuiper et al., 2019). These ages are compatible with those found in detrital samples from the northern Moroccan Variscides, including those studied in this work. However, the available data on the Mazagan escarpment are still scarce and, even if it is possible that at least part of the Orosirian-Statherian zircon grains were sourced in this terrane, the uncertainty still remains.

Other Orosirian-Statherian sources are known in Amazonia, Laurentia, and Baltica (Figures 2.25; Linnemann et al., 2011 and references therein; Nance et al., 2008). However, as previously discussed for the provenance of the Stenian-early Tonian detrital zircon population (see section 5.4.2), we exclude these terranes as possible sources because they would have provided also zircon grains in the range 1.75-1.2 Ga, which are generally absent in our samples. Alternatively, northeastern African sources (*e.g.*, Tuareg Shield, Sahara Metacraton, Arabian-Nubian Shield; Figures 2.25) might have provided both the Stenian-early Tonian and Orosirian-Statherian detrital zircon grains. If this were the case, we would expect a simultaneous occurrence of both detrital zircon populations, something that, on the contrary, does not always occur (Table 2.6 and Figures 2.26A).

To conclude, based on the data available we cannot define a unique source for the Orosirian-Statherian detrital zircon grains found in our samples and other rocks from the northern Moroccan Variscides (*e.g.*, Abati et al., 2010; Accotto et al., 2019, 2020, 2021, in press; Avigad et al., 2012; Ghienne et al., 2018; Letsch et al., 2018). Nonetheless, admitting that both the WAC and northeastern African cratons (*e.g.*, Sahara Metacraton) were the source of sediments on the passive margin of northern Gondwana during the Paleozoic, it is possible that the 1.95-1.75 Ga detrital zircon grains were actually sourced from different areas.

5.5. Relevance of the tectonic boundaries within the Moroccan Mesetas

The Moroccan Mesetas have been historically divided into several domains separated by fault zones (see section 1, Figure 2.16B). The tectonic relevance and significance of these boundaries is still under debate (*e.g.*, Hoepffner et al., 2006; Michard et al., 2010b, 2010a; Simancas et al., 2010, 2009).

According to some authors (*e.g.*, Hoepffner et al., 2006 and references therein; Michard et al., 2010a and references therein, 2010b), the faults bounding the different domains in the Moroccan Mesetas accommodated tens to hundreds of kilometers of displacement related to an important E-W oriented Variscan shortening. Nevertheless, the stratigraphic similarities between the Paleozoic successions within the Moroccan Mesetas and the Anti-Atlas (Piqué, 1994) suggest that there was a paleogeographic continuity between these regions. Furthermore, within the Moroccan Mesetas, our data on detrital zircon grains in the Cambrian-Lower Devonian successions from different areas also support this paleogeographic continuity. In particular, if the easternmost parts of the Moroccan Mesetas were located in a more eastern position, as suggested by Michard et al. (2010b and references therein), we would expect an increase of Stenian-early Tonian detrital zircon ages there. Nevertheless, the presence and distribution of this NE-African-sources is highly irregular and does not show an eastward systematic increase. Similarly, other minor detrital zircon populations found in samples from diverse areas and with different ages do not appear to be geographically controlled. The internal boundaries within the Moroccan Mesetas, therefore, seem to have had limited effects on the sedimentation in the different domains. Nonetheless, further tectono-metamorphic studies are needed to better constrain the tectonic relevance of the intra-Mesetas fault zones.

6. Conclusions

New U-Pb geochronological data on detrital zircon grains from 16 Cambrian-Lower Devonian samples from different zones of the Moroccan Mesetas show homogeneous age-frequency distributions. This similarity points to paleogeographical irrelevance of the proposed tectonic boundaries between the different zones/domains (with the exception of the Caledonian Sehoul Block) usually considered in the Moroccan Variscides, in accordance with other geological evidence (comparable stratigraphic successions, absence of ophiolite and/or high-pressure metamorphic belts). The main detrital zircon

populations common to our samples have late Tonian-Ediacaran (c. 850-540 Ma) and Rhyacian-Orosirian ages (c. 2220-1950 Ma), which suggest that the West African Craton was the main source of sediments for this part of the northern Gondwanan margin at early-middle Paleozoic time. Particularly, the Cadomian orogen (c. 590-540 Ma) constituted the main source during the Cambrian-Early Ordovician sedimentation, while erosion of slightly older Pan-African basement (c. 650-600 Ma) prevailed from the Middle Ordovician onwards. This change in the main sediment source during the Ordovician can be explained in terms of the progressive dismantling and burial of the Cadomian arc-related rocks at the continental margin, shifting the main source region to older areas located inland of the West African Craton.

The presence of additional minor detrital zircon populations suggests sediment income from other secondary sources:

- Cambrian-Early Ordovician (c. 540-450 Ma) zircon grains might have been sourced from active magmatic centers that developed in the Anti-Atlas and Western Moroccan Meseta in relation to the ongoing rifting process at that time. This detrital zircon population is only significant close to some of the known magmatic centers, and drastically reduces at Middle Ordovician time, probably due to rift cessation and burial underneath the ongoing passive margin sedimentation.
- Stenian-early Tonian ages (c. 1080-850 Ma) might have been sourced from northeastern African cratons, such as the Sahara Metacraton or the Arabian-Nubian Shield. The spatial distribution and statistical relevance of this detrital zircon population is variable, thus suggesting that this part of the northern Gondwanan passive margin was located in a relatively western position where the incomes from northeastern African sources were intermittent during Cambrian-Early Devonian time. A west Gondwana (Amazonia) source is excluded because it would also have provided other Mesoproterozoic ages (c. 1.7-1.1 Ga), which, on the contrary, are generally absent in our samples.
- Orosirian-Statherian (c. 1950-1750 Ma) detrital zircon grains are often present in our samples and a number of possible source areas are identified: (i) bimodal dykes in the Anti-Atlas related to the breakup of the Nuna/Columbia supercontinent, (ii) the Mazagan terrane offshore west Morocco, and/or (iii) northeastern African cratons that might have provided both the c. 1080-850 and 1950-1750 Ma zircon grains.

References

- Abati, J., Aghzer, A.M., Gerdes, A., Ennih, N., 2012. Insights on the crustal evolution of the West African Craton from Hf isotopes in detrital zircons from the Anti-Atlas belt. *Precambrian Res.* 212–213, 263–274. doi:10.1016/j.precamres.2012.06.005
- Abati, J., Mohsine Aghzer, A., Gerdes, A., Ennih, N., 2010. Detrital zircon ages of Neoproterozoic sequences of the Moroccan Anti-Atlas belt. *Precambrian Res.* 181, 115–128. doi:10.1016/j.precamres.2010.05.018

- Abouchami, W., Boher, M., Michard, A., Albarede, F., 1990. A major 2.1 Ga event of mafic magmatism in West Africa: an early stage of crustal accretion. *J. Geophys. Res.* 95, 17605–17629.
- Accotto, C., Martínez Poyatos, D., Azor, A., Jabaloy-Sánchez, A., Talavera, C., Evans, N.J., Azdimousa, A., 2020. Tectonic Evolution of the Eastern Moroccan Meseta: From Late Devonian Forearc Sedimentation to Early Carboniferous Collision of an Avalonian Promontory. *Tectonics* 39, 1–29. doi:10.1029/2019TC005976
- Accotto, C., Martínez Poyatos, D., Azor, A., Talavera, C., Evans, N.J., Jabaloy-Sánchez, A., Azdimousa, A., Tahiri, A., El Hadi, H., 2021. Syn-collisional detrital zircon source evolution in the northern Moroccan Variscides. *Gondwana Res.* 93, 73–88. doi:10.1016/j.gr.2021.02.001
- Accotto, C., Martínez Poyatos, D., Azor, A., Talavera, C., Evans, N.J., Jabaloy-Sánchez, A., El Hadi, H., Tahiri, A. (in press). Detrital zircon sources in the Ordovician metasedimentary rocks of the Moroccan Meseta: inferences for northern Gondwanan passive margin paleogeography. In: Kuiper, Y., Murphy, J.B., Nance, R.D., Strachan, R.A., Thompson, M.D. (Eds.), *New developments in the Appalachian-Caledonian-Variscan orogen*, GSA books, Special Publication
- Accotto, C., Martínez Poyatos, D.J., Azor, A., Talavera, C., Evans, N.J., Jabaloy-Sánchez, A., Azdimousa, A., Tahiri, A., El Hadi, H., 2019. Mixed and recycled detrital zircons in the Paleozoic rocks of the Eastern Moroccan Meseta: Paleogeographic inferences. *Lithos* 338–339, 73–86. doi:10.1016/j.lithos.2019.04.011
- Aït Malek, H., Gasquet, D., Bertrand, J.M., Leterrier, J., 1998. Eburnian and Panafrican granitoids from the Igherm, Kerdous and Bas-Drâa Proterozoic inliers (western Anti-Atlas, Morocco): U-Pb geochronology on zircon. *Comptes Rendus l'Académie des Sci. - Ser. IIA - Earth Planet. Sci.* 327, 819–826.
- Álvaro, J.J., Casas, J.M., Clausen, S., Quesada, C., 2018. Early Palaeozoic geodynamics in NW Gondwana. *J. Iber. Geol.* 44, 551–565. doi:10.1007/s41513-018-0079-x
- Álvaro, J.J., Pouclet, A., Ezzouhairi, H., Soulaïmani, A., Bouougri, E.H., Imaz, A.G., Fekkak, A., 2014. Early Neoproterozoic rift-related magmatism in the Anti-Atlas margin of the West African craton, Morocco. *Precambrian Res.* 255, 433–442. doi:10.1016/j.precamres.2014.10.008
- Arboleya, M.L., Teixell, A., Charroud, M., Julivert, M., 2004. A structural transect through the High and Middle Atlas of Morocco. *J. African Earth Sci.* 39, 319–327. doi:10.1016/j.jafrearsci.2004.07.036
- Avigad, D., Gerdes, A., Morag, N., Bechstädt, T., 2012. Coupled U-Pb-Hf of detrital zircons of Cambrian sandstones from Morocco and Sardinia: Implications for provenance and Precambrian crustal evolution of North Africa. *Gondwana Res.* 21, 690–703. doi:10.1016/j.gr.2011.06.005

- Bahlburg, H., Vervoort, J.D., DuFrane, S.A., 2010. Plate tectonic significance of Middle Cambrian and Ordovician siliciclastic rocks of the Bavarian Facies, Armorican Terrane Assemblage, Germany - U-Pb and Hf isotope evidence from detrital zircons. *Gondwana Res.* 17, 223–235. doi:10.1016/j.gr.2009.11.007
- Baudin, T., Chèvremont, P., Razin, P., Youbi, N., Andries, D., Hoepffner, C., Thiéblemont, D., Chihani, E.M., Tegye, M., 2003. Carte géologique du Maroc 1/50.000, feuille 435bis Skhour des Rehamna. Mémoire explicatif. Notes Mem. du Serv. Géologique du Maroc.
- Bea, F., Montero, P., Talavera, C., Abu Anbar, M., Scarrow, J.H., Molina, J.F., Moreno, J.A., 2010. The palaeogeographic position of Central Iberia in Gondwana during the Ordovician: Evidence from zircon chronology and Nd isotopes. *Terra Nov.* 22, 341–346. doi:10.1111/j.1365-3121.2010.00957.x
- Becker, R.T., El Hassani, A., 2020. Devonian to Lower Carboniferous stratigraphy and facies of the Moroccan Meseta: implications for palaeogeography and structural Interpretation - a project outline. *Front. Sci. Eng.* 10, 9–25.
- Bernardin, C., Cornée, J.J., Corsini, M., Mayol, S., Muller, J., Tayebi, M., 1988. Variations d'épaisseur du Cambrien moyen en Meseta marocaine occidentale: signification géodynamique des données de surface et de subsurface. *Can. J. Earth Sci.* 25, 2104–2117.
- Bessoles, B., 1977. Le Craton Ouest Africain. *Geologie de l'Afrique. Mémoires du Bur. Rech. Géologiques Minières* 88, 404.
- Boher, M., Abouchami, W., Michard, A., Albarede, F., Arndt, N.T., 1992. Crustal growth in West Africa at 2.1 Ga. *J. Geophys. Res.* 97, 345–369. doi:10.1029/91JB01640
- Bouabdelli, M., 1982. Stratigraphie et évolution structurale du Paléozoïque d'Azrou. Université Louis Pasteur, Strasbourg.
- Bouabdelli, M., Cailleux, Y., Hoepffner, C., Michard, A., Pique, A., 1989. Le bassin dinantien d'Azrou et l'évolution de sa déformation hercynienne (Méséta marocaine nord-orientale). *Notes Mem. du Serv. Géologique du Maroc* 335, 221–227.
- Bouabdelli, M., Piqué, A., 1996. Du bassin sur décrochement au bassin d'avant-pays: dynamique du bassin d'Azrou-Khénifra (Maroc hercynien central). *J. Africa* 23, 213–224.
- Bradley, D.C., O'Sullivan, P., Cosca, M.A., Motts, H.A., Horton, J.D., Taylor, C.D., Beaudoin, G., Lee, G.K., Ramezani, J., Bradley, D.B., Jones, J. V, Bowring, S.A., 2015. Second projet de renforcement institutionnel du secteur minier de la République Islamique de Mauritanie (PRISM-II). Synthesis of geological, structural, and geochronologic data: Phase V, Deliverable 53. doi:http://dx.doi.org/10.3133/ofr20131280.

- Braid, J.A., Murphy, J.B., Quesada, C., Mortensen, J., 2011. Tectonic escape of a crustal fragment during the closure of the Rheic Ocean: U-Pb detrital zircon data from the Late Palaeozoic Pulo do Lobo and South Portuguese zones, southern Iberia. *J. Geol. Soc. London.* 168, 383–392. doi:10.1144/0016-76492010-104
- Cailleux, Y., 1994. Introduction historique et structurale. (Le Massif central marocain et la Meseta orientale). *Bull. l'Institut Sci. Rabat* 18, 10–31.
- Cambeses, A., Scarrow, J.H., Montero, P., Lázaro, C., Bea, F., 2017. Palaeogeography and crustal evolution of the Ossa–Morena Zone, southwest Iberia, and the North Gondwana margin during the Cambro-Ordovician: a review of isotopic evidence. *Int. Geol. Rev.* 59, 94–130. doi:10.1080/00206814.2016.1219279
- Charriere, A., 1990. Héritage hercynien et évolution géodynamique alpine d'une chaîne intracontinentale: le Moyen-Atlas au SE de Fes (Maroc). Ph.D. Thesis, Université de Toulouse 3, France.
- Charriere, A., 1989. Carte géologique du Maroc No354: Sefrou - Echelle 1/100.000. Roy. du Maroc, Ministère l'Energie des Mines du Développement Durable.
- Chauvel, C., Lewin, E., Carpentier, M., Arndt, N.T., Marini, J.-C., 2008. Role of recycled oceanic basalt and sediment in generating the Hf–Nd mantle array. *Nat. Geosci.* 1, 64–67. doi:10.1038/ngeo.2007.51
- Choubert, G., Marçais, J., Suter, G., 1978. Carte géologique du Maroc - 1/500.000: Oujda. Roy. du Maroc, Ministère l'Energie des Mines du Développement Durable.
- Desteucq, C., Fournier-Vinas, C., 1981. Présence d'Ordovicien dans la région d'Oujda. *Mines, Géologie Energ.* 50.
- Destombe, J., 1987. Carte géologique du Maroc No350: Casablanca-Mohammedia - Echelle 1/100.000. Roy. du Maroc, Ministère l'Energie des Mines du Développement Durable.
- Díez Fernández, R., Catalán, J.R.M., Gerdes, A., Abati, J., Arenas, R., Fernández-Suárez, J., 2010. U–Pb ages of detrital zircons from the Basal allochthonous units of NW Iberia: Provenance and paleoposition on the northern margin of Gondwana during the Neoproterozoic and Paleozoic. *Gondwana Res.* 18, 385–399. doi:10.1016/j.gr.2009.12.006
- Drost, K., Gerdes, A., Jeffries, T., Linnemann, U., Storey, C., 2011. Provenance of Neoproterozoic and early Paleozoic siliciclastic rocks of the Teplá-Barrandian unit (Bohemian Massif): Evidence from U-Pb detrital zircon ages. *Gondwana Res.* 19, 213–231. doi:10.1016/j.gr.2010.05.003
- Eckelmann, K., Nesbor, H.-D., Königshof, P., Linnemann, U., Hofmann, M., Lange, J.-M., Sagawe, A., 2014. Plate interactions of Laurussia and Gondwana during the formation of Pangaea - Constraints from U-Pb LA-SF-ICP-MS detrital zircon ages of Devonian and Early Carboniferous siliciclastics of the Rhenohercynian zone,

Central European Variscides. *Gondwana Res.* 25, 1484–1500.
doi:10.1016/j.gr.2013.05.018

- El Attari, A., Pereira, M.F., Ezzouhairi, H., El Houicha, M., Jouhari, A., Berrada, I., Fekkak, A., Ennih, N., Hoepffner, C.H., Gama, C., Silva, J.B., 2019. Zircon U-Pb geochronology and geochemistry of Cambrian magmatism in the Coastal Block (Oued Rhebar volcanic complex, Moroccan Meseta): Implications for the geodynamic evolutionary model of North-Gondwana. *J. African Earth Sci.* 160, 103598. doi:10.1016/j.jafrearsci.2019.103598
- El Bouougri, H., Lahna, A.A., Tassinari, C.C.G., Basei, M.A.S., Youbi, N., Admou, H., Saquaque, A., Boumehdi, M.A., Maacha, L., 2020. Time constraints on Early Tonian Rifting and Cryogenian Arc terrane-continent convergence along the northern margin of the West African craton: Insights from SHRIMP and LA-ICP-MS zircon geochronology in the Pan-African Anti-Atlas belt (Morocco). *Gondwana Res.* 85, 169–188. doi:10.1016/j.gr.2020.03.011
- El Hadi, H., Simancas, J.F., Tahiri, A., Gonzalez-Lodeiro, F., Azor, A., Martinez-Poyatos, D., 2006a. Comparative review of the Variscan granitoids of Morocco and Iberia: proposal of a broad zonation. *Geodin. Acta* 19, 103–116. doi:10.3166/ga.19.103-116
- El Hadi, H., Simancas, J.F., Tahiri, A., González-Lodeiro, F., Azor, A., Martínez-Poyatos, D., 2006b. Comparative review of the Variscan granitoids of Morocco and Iberia: Proposal of a broad zonation. *Geodin. Acta* 19, 103–116. doi:10.3166/ga.19.103-116
- El Hadi, H., Tahiri, A., Simancas Cabrera, F., González Lodeiro, F., Azor Pérez, A., Jesús Martínez Poyatos, D., 2006c. An example of calc-alkaline, orogenic-type volcanism emplaced in a rift setting (Cambrian of Oued Rhebar, western Meseta, Morocco). *Comptes Rendus - Geosci.* 338, 229–236. doi:10.1016/j.crte.2005.12.006
- El Hadi, H., Tahiri, A., Simancas Cabrera, F., González Lodeiro, F., Azor Pérez, A., Jesús Martínez Poyatos, D., 2006d. Un exemple de volcanisme calco-alcalin de type orogénique mis en place en contexte de rifting (Cambrien de l’oued Rhebar, Meseta occidentale, Maroc). *Comptes Rendus Geosci.* 338, 229–236. doi:10.1016/j.crte.2005.12.006
- El Haïbi, H., El Hadi, H., Pesquera, A., Tahiri, A., Martínez Poyatos, D., Zahour, G., Mehdioui, S., Tahiri, M., 2021. Geochemical and Sr–Nd isotopic constraints on the petrogenesis of the Tiflet granitoids (Northwestern Moroccan Meseta): geological implications. *J. Iber. Geol.* doi:10.1007/s41513-020-00156-7
- El Haïbi, H., El Hadi, H., Tahiri, A., Martínez Poyatos, D., Gasquet, D., Pérez-Cáceres, I., González Lodeiro, F., Mehdioui, S., 2020. Geochronology and isotopic geochemistry of Ediacaran high-K calc-alkaline felsic volcanism: An example of a Moroccan perigondwanan (Avalonian?) remnant in the El Jadida horst (Mazagonia). *J. African Earth Sci.* 163, 103669. doi:10.1016/j.jafrearsci.2019.103669

- El Hassani, A., 1991. La Zone de Rabat-Tiflet: bordure nord de la Chaîne Calédono-Hercynienne du Maroc. Bull. l'Institut Sci.
- El Hassani, A., Tahiri, A., Walliser, O.H., 2003. The Variscan Crust between Gondwana and Baltica. CFS Cour. Forschungsinstitut Senckenb. 81–87.
- El Houicha, M., Pereira, M.F., Jouhari, A., Gama, C., Ennih, N., Fekkak, A., Ezzouhairi, H., El Attari, A., Silva, J.B., 2018. Recycling of the Proterozoic crystalline basement in the Coastal Block (Moroccan Meseta): New insights for understanding the geodynamic evolution of the northern peri-Gondwanan realm. *Precambrian Res.* 306, 129–154. doi:10.1016/j.precamres.2017.12.039
- Ernst, R.E., Wingate, M.T.D., Buchan, K.L., Li, Z.X., 2008. Global record of 1600-700 Ma Large Igneous Provinces (LIPs): Implications for the reconstruction of the proposed Nuna (Columbia) and Rodinia supercontinents. *Precambrian Res.* 160, 159–178. doi:10.1016/j.precamres.2007.04.019
- Ezzouhairi, H., Ribeiro, M.L., Ait Ayad, N., Moreira, M.E., Charif, A., Ramos, J.M.F., de Oliveira, D.P.S., Coke, C., 2008. The magmatic evolution at the Moroccan outboard of the West African craton between the Late Neoproterozoic and the Early Palaeozoic. *Geol. Soc. London, Spec. Publ.* 297, 329–343. doi:10.1144/SP297.16
- Fedo, C.M., Sircombe, K.N., Rainbird, R.H., 2003. Detrital Zircon Analysis of the Sedimentary Record. *Rev. Mineral. Geochemistry* 53, 277–303. doi:10.2113/0530277
- Fernández-Suárez, J., Gutiérrez-Alonso, G., Pastor-Galán, D., Hofmann, M., Murphy, J.B., Linnemann, U., 2014. The Ediacaran-Early Cambrian detrital zircon record of NW Iberia: Possible sources and paleogeographic constraints. *Int. J. Earth Sci.* 103, 1335–1357. doi:10.1007/s00531-013-0923-3
- Franke, W., Cocks, L.R.M., Torsvik, T.H., 2017. The Palaeozoic Variscan oceans revisited. *Gondwana Res.* 48, 257–284. doi:10.1016/j.gr.2017.03.005
- Franke, W., Dulce, J.-C., 2017. Back to sender: tectonic accretion and recycling of Baltica-derived Devonian clastic sediments in the Rheno-Hercynian Variscides. *Int. J. Earth Sci.* 106, 377–386. doi:10.1007/s00531-016-1408-y
- Gärtner, A., Youbi, N., Villeneuve, M., Linnemann, U., Sagawe, A., Hofmann, M., Zieger, J., Mahmoudi, A., Boumehdi, M.A., 2018. Provenance of detrital zircon from siliciclastic rocks of the Sebkhah Gezmayet unit of the Adrar Souttouf Massif (Moroccan Sahara) – Palaeogeographic implications. *Comptes Rendus - Geosci.* 350, 255–266. doi:10.1016/j.crte.2018.06.004
- Gärtner, A., Youbi, N., Villeneuve, M., Sagawe, A., Hofmann, M., Mahmoudi, A., Boumehdi, M.A., Linnemann, U., 2017. The zircon evidence of temporally changing sediment transport—the NW Gondwana margin during Cambrian to Devonian time (Aoucirt and Smara areas, Moroccan Sahara). *Int. J. Earth Sci.* 106, 2747–2769. doi:10.1007/s00531-017-1457-x

- Gasquet, D., Chevremont, P., Baudin, T., Chalot-Prat, F., Guerrot, C., Cocherie, A., Roger, J., Hassenforder, B., Cheilletz, A., 2004. Polycyclic magmatism in the Tagragra d' Akka and Kerdous–Tafeltast inliers (Western Anti-Atlas, Morocco). *J. African Earth Sci.* 39, 267–275. doi:10.1016/j.jafrearsci.2004.07.062
- Gehrels, G., 2012. Detrital Zircon U-Pb Geochronology: Current Methods and New Opportunities, in: Busby, C.J., Azor, A. (Eds.), *Tectonics of Sedimentary Basins*. John Wiley & Sons, Ltd, Chichester, UK, pp. 45–62. doi:10.1002/9781444347166.ch2
- Ghienne, J.F., Benvenuti, A., El Houicha, M., Girard, F., Kali, E., Khoukhi, Y., Langbour, C., Magna, T., Míková, J., Moscariello, A., Schulmann, K., 2018. The impact of the end-Ordovician glaciation on sediment routing systems: A case study from the Meseta (northern Morocco). *Gondwana Res.* 63, 169–178. doi:10.1016/j.gr.2018.07.001
- Gutiérrez-Alonso, G., Fernández-Suárez, J., Pastor-Galán, D., Johnston, S.T., Linnemann, U., Hofmann, M., Shaw, J., Colmenero, J.R., Hernández, P., 2015a. Significance of detrital zircons in Siluro-Devonian rocks from Iberia. *J. Geol. Soc. London.* 172, 309–322. doi:10.1144/jgs2014-118
- Gutiérrez-Alonso, G., Fernández-Suárez, J., Pastor-Galán, D., Johnston, S.T., Linnemann, U., Hofmann, M., Shaw, J., Colmenero, J.R., Hernández, P., 2015b. Significance of detrital zircons in Siluro-Devonian rocks from Iberia. *J. Geol. Soc. London.* 172, 309–322. doi:10.1144/jgs2014-118
- Hefferan, K., Soulaïmani, A., Samson, S.D., Admou, H., Inglis, J., Saquaque, A., Latifa, C., Heywood, N., 2014. A reconsideration of Pan African orogenic cycle in the Anti-Atlas Mountains, Morocco. *J. African Earth Sci.* 98, 34–46. doi:10.1016/j.jafrearsci.2014.03.007
- Hirdes, W., Davis, D.W., Eisenlohr, B.N., 1992. Reassessment of Proterozoic granitoid ages in Ghana on the basis of U/Pb zircon and monazite dating. *Precambrian Res.* 56, 89–96. doi:10.1016/0301-9268(92)90085-3
- Hoepffner, C., 1989. L'évolution structurale hercynienne de la Méséta marocain orientale. Essai de mise au point. Notes Mem. du Serv. Géologique du Maroc.
- Hoepffner, C., 1987. La tectonique hercynienne dans l'Est du Maroc. Université Louis Pasteur, Strasbourg.
- Hoepffner, C., 1977. Données nouvelles sur le Paléozoïques de la bordure occidentale du massif du Tazekka. *Comptes Rendus l'Académie des Sci. Paris* 284, 1635–1637.
- Hoepffner, C., Houari, M.R., Bouabdelli, M., 2006. Tectonics of the North African Variscides (Morocco, western Algeria): An outline. *Comptes Rendus - Geosci.* 338, 25–40. doi:10.1016/j.crte.2005.11.003

- Hoepffner, C., Soulaïmani, A., Piqué, A., 2005. The Moroccan Hercynides. *J. African Earth Sci.* 43, 144–165. doi:10.1016/j.jafrearsci.2005.09.002
- Horon, O., 1952. Contribution a l'étude du bassin de Djerada. *Notes Mem. du Prot. la Repub. Française au Maroc* 89, 180.
- Hurley, P.M., Leo, G.W., White, R.W., Fairbairn, H.W., 1971. Liberian age province (about 2,700 m.y.) and adjacent provinces in Liberia and Sierra Leone. *GSA Bull.* 82, 3483–3490. doi:10.1130/0016-7606(1971)82[3483:LAPAMA]2.0.CO;2
- Iizuka, T., Yamaguchi, T., Hibiya, Y., Amelin, Y., 2015. Meteorite zircon constraints on the bulk Lu-Hf isotope composition and early differentiation of the Earth. *Proc. Natl. Acad. Sci. U. S. A.* 112, 5331–5336. doi:10.1073/pnas.1501658112
- Kharbouch, F., 1994. Le volcanisme dévono-dinantien du Massif central et de la Meseta orientale. *Bull. l'Institut Sci. Rabat* 18, 192–200.
- Kharbouch, F., Juteau, T., Treuil, M., Joron, J.-L., Piqué, A., Hoepffner, C., 1985. Le volcanisme dinantien de la Meseta marocaine nord-occidentale et orientale. Caractères pétrographiques et géochimiques et implications géodynamiques. *Sci. Géol. Bull.* 38, 155–163.
- Košler, J., Konopásek, J., Sláma, J., Vrána, S., 2014. U–Pb zircon provenance of Moldanubian metasediments in the Bohemian Massif. *J. Geol. Soc. London.* 171, 83–95. doi:10.1144/jgs2013-059
- Kuiper, Y.D., 2019. An overview of middle to late Paleozoic connections between southeastern New England, USA, and Morocco, in: *Eos Transactions, American Geophysical Union, Fall Meeting.*
- Kuiper, Y.D., Michard, A., Ruellan, E., Holm-Denoma, C., Crowley, J.L., 2019. U-Pb zircon and monazite results from granite and charnockite from the Mazagan escarpment, offshore Morocco, in: *GSA Abstracts with Programs, Vol. 51, No. 2.*
- Lama, C., Zimmermann, J.L., Mortaji, A., Macaudière, J., Stussi, J.M., 1993. Age K–Ar protérozoïque moyen des leucogranites à deux micas de la Tagragra d'Akka (Anti Atlas occidental, Maroc). *Comptes Rendus l'Académie des Sci. Paris* 317, 1601–1607.
- Letsch, D., El Houicha, M., von Quadt, A., Winkler, W., 2018. A missing link in the peri-Gondwanan terrane collage: The Precambrian basement of the Moroccan Meseta and its lower Paleozoic cover. *Can. J. Earth Sci.* 55, 33–51. doi:10.1139/cjes-2017-0086
- Liégeois, J.P., Claessens, W., Camara, D., Klerkx, J., 1991. Short-lived Eburnian orogeny in southern Mali. *Geology, tectonics, U-Pb and Rb-Sr geochronology. Precambrian Res.* 50, 111–136.
- Lin, W., Faure, M., Li, X.-H., Ji, W., 2019. Pre-Variscan tectonic setting of the south margin of Armorica: Insights from detrital zircon ages distribution and Hf isotopic

- composition of the St-Georges-sur-Loire Unit (S. Armorican Massif, France). *Tectonophysics* 766, 340–378. doi:10.1016/j.tecto.2019.06.015
- Lin, W., Faure, M., Li, X. hua, Chu, Y., Ji, W., Xue, Z., 2016. Detrital zircon age distribution from Devonian and Carboniferous sandstone in the Southern Variscan Fold-and-Thrust belt (Montagne Noire, French Massif Central), and their bearings on the Variscan belt evolution. *Tectonophysics* 677–678, 1–33. doi:10.1016/j.tecto.2016.03.032
- Linnemann, U., Gerdes, A., Drost, K., Buschmann, B., 2007. The continuum between Cadomian orogenesis and opening of the Rheic Ocean: Constraints from LA-ICP-MS U-Pb zircon dating and analysis of plate-tectonic setting (Saxo-Thuringian zone, northeastern Bohemian Massif, Germany), in: *The Evolution of the Rheic Ocean: From Avalonian-Cadomian Active Margin to Alleghenian-Variscan Collision*. Geological Society of America, pp. 61–96. doi:10.1130/2007.2423(03)
- Linnemann, U., McNaughton, N.J., Romer, R.L., Gehmlich, M., Drost, K., Tonk, C., 2004. West African provenance for Saxo-Thuringia (Bohemian Massif): did Armorica ever leave pre-Pangean Gondwana? - U/Pb-SHRIMP zircon evidence and the Nd-isotopic record. *Int. J. Earth Sci.* 93, 683–705. doi:10.1007/s00531-004-0413-8
- Linnemann, U., Ouzegane, K., Drareni, A., Hofmann, M., Becker, S., Gärtner, A., Sagawe, A., 2011. Sands of West Gondwana: An archive of secular magmatism and plate interactions - A case study from the Cambro-Ordovician section of the Tassili Ouan Ahaggar (Algerian Sahara) using U-Pb-LA-ICP-MS detrital zircon ages. *Lithos* 123, 188–203. doi:10.1016/j.lithos.2011.01.010
- Linnemann, U., Pereira, M.F., Jeffries, T.E., Drost, K., Gerdes, A., 2008. The Cadomian Orogeny and the opening of the Rheic Ocean: The diacrony of geotectonic processes constrained by LA-ICP-MS U-Pb zircon dating (Ossa-Morena and Saxo-Thuringian Zones, Iberian and Bohemian Massifs). *Tectonophysics* 461, 21–43. doi:10.1016/j.tecto.2008.05.002
- Ludwig, K.R., 2003. *Isoplot 3.0. A geochronological toolkit for Microsoft Excel*. Berkeley Geochron, Cent. Spec. Publ. 4, 70.
- Marhoumi, M.R., Doubinger, J., Rauscher, R., Hoepffner, C., 1989. Données nouvelles sur le Paléozoïque de la Méséta orientale marocaine. Apports de la palynologie. *Notes Mem. du Serv. Géologique du Maroc*.
- Matte, P., 2001. The Variscan collage and orogeny (480-290 Ma) and the tectonic definition of the Armorica microplate: a review. *Terra Nov.* 13, 122–128. doi:10.1046/j.1365-3121.2001.00327.x
- Médioni, R., 1979. Carte géologique du Maroc au 1/100.000. Feuille Hassiane Ed Diab. Notice explicative. *Notes Mem. du Serv. Géologique du Maroc* 227, 64.

- Michard, A., 1976. *Éléments de géologie marocaine*. Notes Mem. du Serv. Géologique du Maroc 252, 408.
- Michard, A., Cailleux, Y., Hoepffner, C., 1989. L'orogène mésétien du Maroc: structure, déformation hercynienne et déplacement. Notes Mem. du Serv. Géologique du Maroc.
- Michard, A., Ouanaimi, H., Hoepffner, C., Soulaïmani, A., Baidder, L., 2010a. Comment on Tectonic relationships of Southwest Iberia with the allochthons of Northwest Iberia and the Moroccan Variscides by J.F. Simancas et al. [C. R. Geoscience 341 (2009) 103-113]. *Comptes Rendus - Geosci.* 342, 170–174. doi:10.1016/j.crte.2010.01.008
- Michard, A., Soulaïmani, A., Hoepffner, C., Ouanaimi, H., Baidder, L., Rjimati, E.C., Saddiqi, O., 2010b. The South-Western Branch of the Variscan Belt: evidence from Morocco. *Tectonophysics* 492, 1–24. doi:10.1016/j.tecto.2010.05.021
- Montero, P., Talavera, C., Bea, F., Lodeiro, F.G., Whitehouse, M.J., 2009. Zircon Geochronology of the Ollo de Sapo Formation and the Age of the Cambro-Ordovician Rifting in Iberia. *J. Geol.* 117, 174–191. doi:10.1086/595017
- Morin, P., 1960. Les marbres d'origine métamorphique du Maroc central (géologie et problèmes d'exploitation). *Mines et géologie* 11, 559–574.
- Muratet, B., 1995. Carte géologique du Maroc No364: Taourirt - Echelle 1/100.000. Roy. du Maroc, Ministère l'Energie des Mines du Développement Durable.
- Nance, R.D., Gutiérrez-Alonso, G., Keppie, J.D., Linnemann, U., Murphy, J.B., Quesada, C., Strachan, R.A., Woodcock, N.H., 2012. A brief history of the Rheic Ocean. *Geosci. Front.* 3, 125–135. doi:10.1016/j.gsf.2011.11.008
- Nance, R.D., Gutiérrez-Alonso, G., Keppie, J.D., Linnemann, U., Murphy, J.B., Quesada, C., Strachan, R.A., Woodcock, N.H., 2010. Evolution of the Rheic Ocean. *Gondwana Res.* 17, 194–222. doi:10.1016/j.gr.2009.08.001
- Nance, R.D., Murphy, J.B., Strachan, R.A., Keppie, J.D., Gutiérrez-Alonso, G., Fernández-Suárez, J., Quesada, C., Linnemann, U., D'lemos, R., Pisarevsky, S.A., 2008. Neoproterozoic-early Palaeozoic tectonostratigraphy and palaeogeography of the peri-Gondwanan terranes: Amazonian v. West African connections. *Geol. Soc. London, Spec. Publ.* 297, 345–383. doi:10.1144/SP297.17
- Ouabid, M., Garrido, C.J., Ouali, H., Harvey, J., Hidas, K., Marchesi, C., Acosta-Vigil, A., Dautria, J., El Messbahi, H., Román-Alpiste, M.J., 2020. Late Cadomian rifting of the NW Gondwana margin and the reworking of Precambrian crust – evidence from bimodal magmatism in the early Paleozoic Moroccan Meseta. *Int. Geol. Rev.* 00, 1–24. doi:10.1080/00206814.2020.1818301
- Ouabid, M., Ouali, H., Garrido, C.J., Acosta-Vigil, A., Román-Alpiste, M.J., Dautria, J.M., Marchesi, C., Hidas, K., 2017. Neoproterozoic granitoids in the basement of

- the Moroccan Central Meseta: Correlation with the Anti-Atlas at the NW paleo-margin of Gondwana. *Precambrian Res.* 299, 34–57. doi:10.1016/j.precamres.2017.07.007
- Ouali, H., Briand, B., Bouchardon, J.-L., Capiez, P., 2003. Le volcanisme cambrien du Maroc central: implications géodynamiques. *Comptes Rendus Geosci.* 335, 425–433. doi:10.1016/S1631-0713(03)00064-6
- Pastor-Galán, D., Gutiérrez-Alonso, G., Fernández-Suárez, J., Murphy, J.B., Nieto, F., 2013a. Tectonic evolution of NW Iberia during the Paleozoic inferred from the geochemical record of detrital rocks in the Cantabrian Zone. *Lithos* 182–183, 211–228. doi:10.1016/j.lithos.2013.09.007
- Pastor-Galán, D., Gutiérrez-Alonso, G., Murphy, J.B., Fernández-Suárez, J., Hofmann, M., Linnemann, U., 2013b. Provenance analysis of the Paleozoic sequences of the northern Gondwana margin in NW Iberia: Passive margin to Variscan collision and orocline development. *Gondwana Res.* 23, 1089–1103. doi:10.1016/j.gr.2012.06.015
- Pereira, M.F., Chichorro, M., Johnston, S.T., Gutiérrez-Alonso, G., Silva, J.B., Linnemann, U., Hofmann, M., Drost, K., 2012. The missing Rheic Ocean magmatic arcs: provenance analysis of Late Paleozoic sedimentary clastic rocks of SW Iberia. *Gondwana Res.* 22, 882–891. doi:10.1016/j.gr.2012.03.010
- Pereira, M.F., El Houicha, M., Chichorro, M., Armstrong, R., Jouhari, A., El Attari, A., Ennih, N., Silva, J.B., 2015. Evidence of a Paleoproterozoic basement in the Moroccan Variscan Belt (Rehamna Massif, Western Meseta). *Precambrian Res.* 268, 61–73. doi:10.1016/j.precamres.2015.07.010
- Pereira, M.F., Gutiérrez-Alonso, G., Murphy, J.B., Drost, K., Gama, C., Silva, J.B., 2017. Birth and demise of the Rheic Ocean magmatic arc(s): Combined U–Pb and Hf isotope analyses in detrital zircon from SW Iberia siliciclastic strata. *Lithos* 278–281, 383–399. doi:10.1016/j.lithos.2017.02.009
- Pérez-Cáceres, I., Martínez Poyatos, D., Simancas, J.F., Azor, A., 2017. Testing the Avalonian affinity of the South Portuguese Zone and the Neoproterozoic evolution of SW Iberia through detrital zircon populations. *Gondwana Res.* 42, 177–192. doi:10.1016/j.gr.2016.10.010
- Perez, N.D., Teixell, A., Gómez-Gras, D., Stockli, D.F., 2019. Reconstructing Extensional Basin Architecture and Provenance in the Marrakech High Atlas of Morocco: Implications for Rift Basins and Inversion Tectonics. *Tectonics* 38, 1584–1608. doi:10.1029/2018TC005413
- Piqué, A., 1994. Introduction historique et structurale. (Le Massif central marocain et la Meseta orientale). *Bull. l'Institut Sci. Rabat* 18, 1–2.
- Piqué, A., 2003. Evidence for an important extensional event during the Latest Proterozoic and Earliest Paleozoic in Morocco. *Comptes Rendus Geosci.* 335, 865–868. doi:10.1016/j.crte.2003.08.005

- Piqué, A., 2001. *Geology of Northwest Africa*. Gebrüder Borntraeger, Berlin.
- Piqué, A., 1994. *Géologie du Maroc*. éditions Pumag, Marrakech.
- Piqué, A., 1981. La chaîne hercynienne d'Europe occidentale et son prolongement dans le Nord-Ouest de l'Afrique. *Sci. Géologiques. Bull.* 34, 123–134. doi:10.3406/sgeol.1981.1596
- Piqué, A., 1979. *Évolution structurale d'un segment de la chaîne hercynienne: la Meseta marocaine nord-occidentale*. Ph.D. Thesis, Université de Strasbourg.
- Piqué, A., Bouabdelli, M., Darboux, J.-R., 1995. Le rift cambrien du Maroc occidental. *Comptes Rendus l'Académie des Sci. - Ser. IIA - Earth Planet. Sci.* 320, 1017–1024.
- Piqué, A., Michard, A., 1989. Moroccan Hercynides: a synopsis. The Paleozoic sedimentary and tectonic evolution at the northern margin of West Africa. *Am. J. Sci.* 289, 286–330.
- Poulet, A., El Hadi, H., Álvaro, J.J., Bardintzeff, J.-M., Benharref, M., Fekkak, A., 2018. Review of the Cambrian volcanic activity in Morocco: geochemical fingerprints and geotectonic implications for the rifting of West Gondwana. *Int. J. Earth Sci.* 107, 2101–2123. doi:10.1007/s00531-018-1590-1
- Rauscher, R., Marhomi, M.R., Vanguestaine, M., Hoepffner, C., 1982. Datation palynologique des schistes du Tazekka au Maroc. Hypothèse structurale sur la socle hercynien de la Meseta orientale. *Comptes Rendus l'Académie des Sci. Paris* 294, 1203–1206.
- Razin, P., Janjou, D., Baudin, T., Bensahal, A., Hoepffner, C., Chenakeb, M., Cailleux, Y., 2001. Carte géologique du Maroc No412: Sidi Matla' Ech Chams - Echelle 1/50.000. Roy. du Maroc, Ministère l'Energie des Mines du Développement Durable.
- Sánchez-García, T., Bellido, F., Quesada, C., 2003. Geodynamic setting and geochemical signatures of Cambrian–Ordovician rift-related igneous rocks (Ossa-Morena Zone, SW Iberia). *Tectonophysics* 365, 233–255. doi:10.1016/S0040-1951(03)00024-6
- Schofield, D.I., Horstwood, M.S.A., Pitfield, P.E.J., Crowley, Q.G., Wilkinson, A.F., Sidaty, H.C.O., 2006. Timing and kinematics of Eburnean tectonics in the central Reguibat Shield, Mauritania. *J. Geol. Soc. London.* 163, 549–560. doi:10.1144/0016-764905-097
- Sharman, G.R., Malkowski, M.A., 2020. Needles in a haystack: Detrital zircon U Pb ages and the maximum depositional age of modern global sediment. *Earth-Science Rev.* 203, 103–109. doi:10.1016/j.earscirev.2020.103109
- Shaw, J., Gutiérrez-Alonso, G., Johnston, S.T., Pastor Galán, D., 2014. Provenance variability along the Early Ordovician north Gondwana margin: Paleogeographic and tectonic implications of U-Pb detrital zircon ages from the Armorican Quartzite of the Iberian Variscan belt. *Bull. Geol. Soc. Am.* 126, 702–719. doi:10.1130/B30935.1

- Simancas, J.F., Azor, A., Martínez-Poyatos, D., Tahiri, A., El Hadi, H., González-Lodeiro, F., Pérez-Estaún, A., Carbonell, R., 2009. Tectonic relationships of Southwest Iberia with the allochthons of Northwest Iberia and the Moroccan Variscides. *Comptes Rendus Geosci.* 341, 103–113. doi:10.1016/j.crte.2008.11.003
- Simancas, J.F., Azor, A., Martínez-Poyatos, D., Tahiri, A., Hadi, H. El, González-Lodeiro, F., Pérez-Estaún, A., Carbonell, R., 2010. Reply to the comment by Michard et al. on “Tectonic relationships of Southwest Iberia with the allochthons of Northwest Iberia and the Moroccan Variscides.” *Comptes Rendus - Geosci.* 342, 175–177. doi:10.1016/j.crte.2010.01.007
- Simancas, J.F., Tahiri, A., Azor, A., Lodeiro, F.G., Martínez Poyatos, D.J., El Hadi, H., 2005. The tectonic frame of the Variscan–Alleghanian orogen in Southern Europe and Northern Africa. *Tectonophysics* 398, 181–198. doi:10.1016/j.tecto.2005.02.006
- Spencer, C.J., Kirkland, C.L., Taylor, R.J.M., 2016. Strategies towards statistically robust interpretations of in situ U-Pb zircon geochronology. *Geosci. Front.* 7, 581–589. doi:10.1016/j.gsf.2015.11.006
- Strnad, L., Mihaljevič, M., 2005. Sedimentary provenance of Mid-Devonian clastic sediments in the Teplá-Barrandian Unit (Bohemian Massif): U-Pb and Pb-Pb geochronology of detrital zircons by laser ablation ICP-MS. *Mineral. Petrol.* doi:10.1007/s00710-004-0057-1
- Szczepański, J., Turniak, K., Anczkiewicz, R., Gleichner, P., 2020. Dating of detrital zircons and tracing the provenance of quartzites from the Bystrzyckie Mts: implications for the tectonic setting of the Early Palaeozoic sedimentary basin developed on the Gondwana margin. *Int. J. Earth Sci.* 109, 2049–2079. doi:10.1007/s00531-020-01888-8
- Tahiri, A., 1994. Tectonique hercynienne de l’anticlinorium de Khouribga-Oulmès et du synclinorium de Fourhal. *Bull. l’Institut Sci. Rabat* 18, 125–144.
- Tahiri, A., 1991. Le Maroc central septentrional: stratigraphie, sedimentologie et tectonique du Paleozoïque; un exemple de passage des zones internes aux zones externes de la chaîne Hercynienne du Maroc. Ph.D. Thesis, Université de Bretagne Occidentale, Brest, France.
- Tahiri, A., El Hassani, A., 1994. L’Ordovicien du Maroc central septentrional. *Bull. l’Institut Sci. Rabat* 18, 32–37.
- Tahiri, A., Montero, P., El Hadi, H., Martínez Poyatos, D., Azor, A., Bea, F., Simancas, J.F., González Lodeiro, F., 2010. Geochronological data on the Rabat-Tiflet granitoids: their bearing on the tectonics of the Moroccan Variscides. *J. African Earth Sci.* 57, 1–13. doi:10.1016/j.jafrearsci.2009.07.005
- Talavera, C., Montero, P., Martínez Poyatos, D., Williams, I.S., 2012. Ediacaran to Lower Ordovician age for rocks ascribed to the Schist–Graywacke Complex (Iberian

- Massif, Spain): Evidence from detrital zircon SHRIMP U–Pb geochronology. *Gondwana Res.* 22, 928–942. doi:10.1016/j.gr.2012.03.008
- Vermeesch, P., 2012. On the visualisation of detrital age distributions. *Chem. Geol.* 312–313, 190–194. doi:10.1016/j.chemgeo.2012.04.021
- Vermeesch, P., 2004. How many grains are needed for a provenance study? *Earth Planet. Sci. Lett.* 224, 441–451. doi:10.1016/j.epsl.2004.05.037
- Verset, Y., 1988. Mémoire explicatif de la carte géologique du Maroc au 1:100.000, feuille de Qasbat-Tadla. *Notes Mem. du Serv. Géologique du Maroc.*
- Vidal, J.C., Hoepffner, C., 1979. Carte géologique du Rif No282: Tahala - Echelle 1/50.000. Roy. du Maroc, Ministère l’Energie des Mines du Développement Durable.
- Villeneuve, M., El Archi, A., Nzamba, J., 2010. Les chaînes de la marge occidentale du Craton Ouest-Africain, modèles géodynamiques. *Comptes Rendus - Geosci.* 342, 1–10. doi:10.1016/j.crte.2009.12.002
- Walliser, O.H., El Hassani, A., Tahiri, A., 2000. Mrirt: a key area for the Variscan Meseta of Morocco. *Notes Mémoires du Serv. Géologique du Maroc* 399, 93–108.
- Walliser, O.H., El Hassani, A., Tahiri, A., 1995. Sur le Dévonien de la Meseta marocaine occidentale. Comparaisons avec le Dévonien allemand et évènements globaux. *CFS Cour. Forschungsinstitut Senckenb.* 188, 21–30.
- Youbi, N., Kouyaté, D., Söderlund, U., Ernst, R.E., Soulaïmani, A., Hafid, A., Ikenne, M., El Bahat, A., Bertrand, H., Rkha Chaham, K., Ben Abbou, M., Mortaji, A., El Ghorfi, M., Zouhair, M., El Janati, M., 2013. The 1750Ma Magmatic Event of the West African Craton (Anti-Atlas, Morocco). *Precambrian Res.* 236, 106–123. doi:10.1016/j.precamres.2013.07.003
- Zahraoui, M., 1994. Le Silurien. *Bull. l’Institut Sci. Rabat* 18, 38–42.
- Žák, J., Sláma, J., 2018. How far did the Cadomian ‘terrane’ travel from Gondwana during early Palaeozoic? A critical reappraisal based on detrital zircon geochronology. *Int. Geol. Rev.* 60, 319–338. doi:10.1080/00206814.2017.1334599

Chapter III

Tectonic evolution of the Eastern Moroccan Meseta during the Eovariscan phase

The aim of this chapter is the reconstruction of the tectonic evolution of the Eastern Moroccan Meseta during the closure of the Rheic Ocean and the first phases of the collision between the northern margin of Gondwana and an Avalonian promontory (Tournaisian-Viséan).

Tectonic evolution of the Eastern Moroccan Meseta: from Late Devonian fore-arc sedimentation to Early Carboniferous collision of an Avalonian promontory

Cristina Accotto¹, David Martínez Poyatos¹, Antonio Azor¹, Antonio Jabaloy-Sánchez¹,
Cristina Talavera^{2,3}, Noreen J. Evans³, Ali Azdimousa⁴

Published on:

Tectonics, 2020

Volume 39 (7), Pages 1-29

doi: 10.1029/2019TC005976

(Received: 8 November 2019; Accepted: 14 April 2020; Available online: 20 April 2020)

¹ Department of Geodynamics, University of Granada, Granada, Spain

² School of Geosciences, University of Edinburgh, Edinburgh, UK

³ School of Earth and Planetary Science/John de Laeter Centre, Curtin University,
Bentley, Australia

⁴ Faculté Pluridisciplinaire de Nador et Laboratoire des Géosciences Appliquées,
Faculté des Sciences, Université Mohammed I, Oujda, Morocco

JCR: 3.543 (2019)

Key-Points

- The Debdou-Mekkam Metasediments deposited during the Late Devonian (Early Tournaisian?) closure of the Rheic Ocean on the N-Gondwanan margin
- An important input of Mesoproterozoic and Devonian detrital zircons points to Avalonian basement and arc sources
- The collision between an Avalonian promontory and N-Gondwana deformed the Debdou-Mekkam metasediments forming a SE-vergent fold belt

Abstract

The deformed Paleozoic succession of the Eastern Moroccan Meseta crops out in relatively small and isolated inliers surrounded by Mesozoic and Cenozoic rocks. Two of the largest inliers (Mekkam and Debdou) are characterized by a monotonous succession of slates and greywackes affected by polyphasic folding that occurred at low- to very low-grade metamorphic conditions. New U-Pb ages on detrital zircon grains from the Debdou-Mekkam Metasediments constrain the maximal depositional age as Late Devonian, interpreted to be close to the true sedimentation age. Furthermore, the ϵ_{Hf} values of the Devonian detrital zircons, together with the presence of a series of scattered zircon grains with ages between c. 0.9 and c. 1.9 Ga suggest provenance from a subduction related magmatic arc located on the Avalonian margin.

The Debdou-Mekkam massif is characterized by an Early Carboniferous first deformational event (D1), which gave way to a pervasive cleavage (S1) associated with plurikilometric-scale, tight to isoclinal, overturned to recumbent folds. Later events (Dc) occurred at Late Carboniferous time and generated variably developed crenulation cleavages (Sc) associated with variously oriented metric- to kilometer-scale folds, which complicate the pattern of both D1 intersection lineations (L1) and axial traces. The restoration of this pronounced curved pattern yields originally SW-NE oriented D1 fold axes with regional SE-vergence. This important Early Carboniferous shortening and SE-directed tectonic transport can be explained by closure of the Rheic Ocean and the first phases of the collision between the northern passive margin of Gondwana and an Avalonian promontory.

1. Introduction

The recognition of ophiolites in old collisional orogenic belts is the most valuable evidence of ancient oceanic closure and continental docking (*e.g.*, Dewey & Bird, 1971). However, the complete consumption of oceanic lithosphere is common in subduction zones, which makes many orogenic sutures appear as cryptic (*e.g.*, Pérez-Cáceres et al., 2015; Schulmann et al., 2014). In these cases, indirect lines of evidence (*e.g.*, recognition of paleogeographically exotic terranes and presence of high-pressure and/or intensely deformed belts) are usually employed to locate orogenic sutures and account for plate tectonic reconstructions (*e.g.*, Franke et al., 2017; Matte, 2001; Romer & Kroner, 2019; Van Hinsbergen et al., 2019).

The Late Paleozoic Variscan/Alleghanian Belt (Figure 3.1A) is frequently discussed in terms of the meaning and correlation of the orogenic sutures along the different transects (*e.g.*, Díez Fernández & Arenas, 2015; Faryad & Kachlik, 2013; Martínez Catalán et al., 2019; Pérez-Cáceres et al., 2015). The Variscan orogeny resulted from Rheic Ocean consumption and subsequent collision between Gondwana and Laurussia, with the final assembly of the Pangea supercontinent by the end of the Paleozoic (*e.g.*, Matte, 2001). Before that, Early Paleozoic rifting along the northern Gondwana margin gave way to the

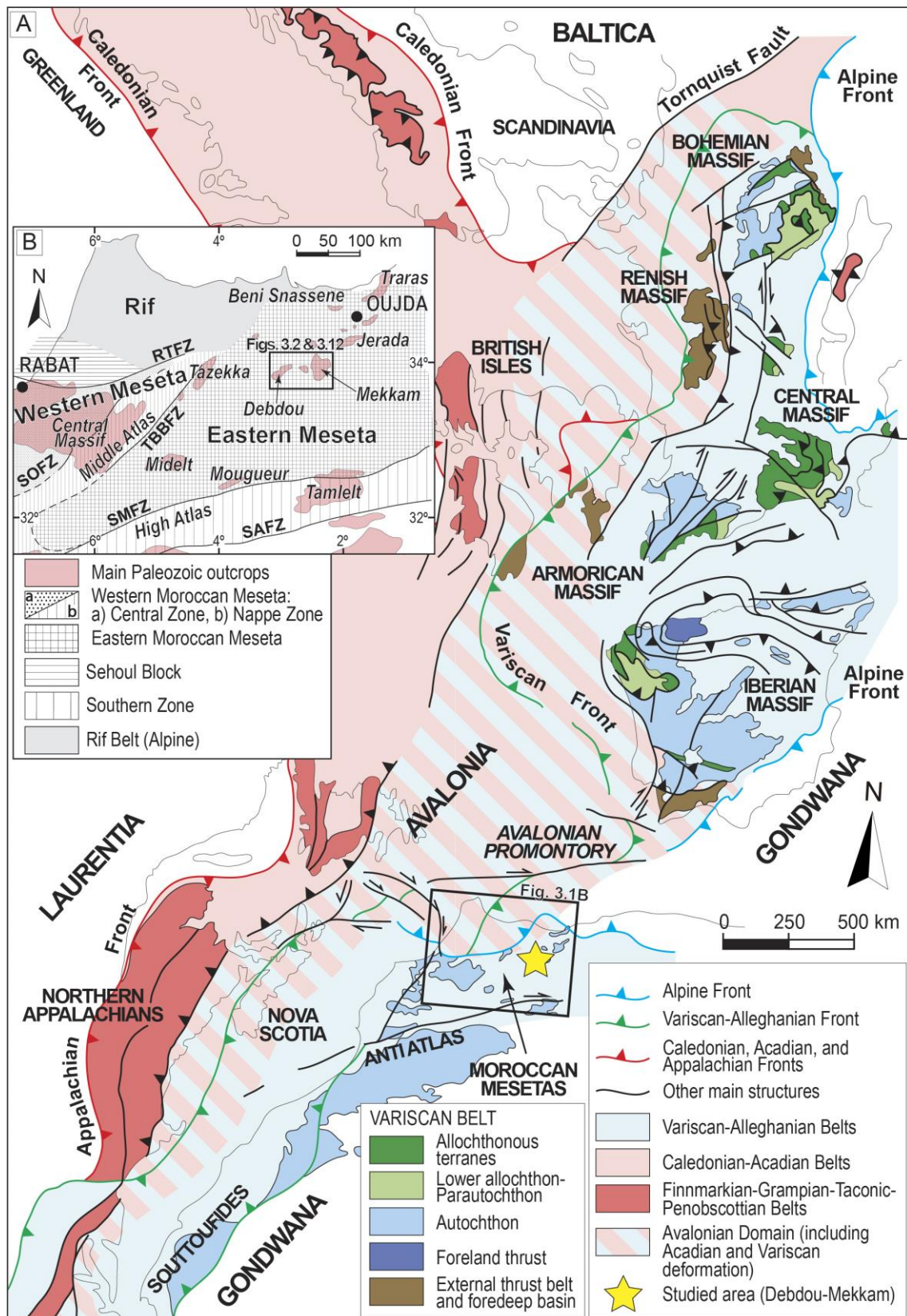


Figure 3.1. Large-scale geological setting of northern Morocco as part of the Variscan/Alleghanian Belt. (A) Reconstruction of the Variscan/Alleghanian and Caledonian belts at the end of the Paleozoic (modified from Martínez Catalán et al., 2002; Michard et al., 2010; Simancas et al., 2009). (B) Sketched geological map of the north-eastern Moroccan Variscides. RTFZ: Rabat-Tiflet Fault Zone; SOFZ: Smaala-Oulmès Fault Zone; TBBFZ: Tazekka-Bsabis-Bekrit Fault Zone; SMFZ: South Meseta Fault Zone; SAFZ: South Atlas Fault Zone (modified from Hoepffner et al., 2006; Michard et al., 2010).

opening of the Rheic Ocean during the drifting of continental domains (collectively called Avalonia) that were connected to the western part of northern Gondwana (Amazonia; Murphy et al., 2006) at Neoproterozoic time. On the other hand, Laurussia resulted from the amalgamation of Laurentia, Baltica and Avalonia during mid-Paleozoic time (Caledonian Orogeny s.l.).

Only a few of the sutures-related units recognized along the Variscan Belt preserve ophiolites, which were classically considered the remnants of the Rheic Ocean (*e.g.*, Matte, 2001) and were later reinterpreted as witnessing minor younger oceanic realms (*e.g.*, Arenas et al., 2014; Martínez Catalán et al., 2019; Shail & Leveridge, 2009). Thus, no direct relicts of the Rheic Ocean seem to crop out along the Variscides, which compromises all of the available paleogeographic reconstructions. Actually, the Rheic Ocean has been located based on indirect data derived from paleomagnetic, geochemical, and geochronological studies (*e.g.*, Gärtner et al., 2013; Villeneuve et al., 2015, in the SW Moroccan transect; Hoepffner et al., 2005; Michard et al., 2010; Simancas et al., 2005; Tahiri et al., 2010, in the NW Moroccan transect; Azor et al., 2008; Braid et al., 2011; Pérez-Cáceres et al., 2017, 2015, in the SW Iberian transect; Arenas et al., 2014; Martínez Catalán et al., 2019, in the NW Iberian transect; and Franke et al., 2017, in the central European transect).

The present-day dispersed configuration of the Variscan/Alleghanian Orogeny is the result of large-scale Late Carboniferous-Early Permian right-lateral wrenching, Pangea breakup and Alpine reworking. The Gondwanan side of the Variscan Belt crops out in a number of massifs distributed from western and central Europe to NW Africa (Figure 3.1A). In northern Morocco (Figure 3.1B), erosion of the Triassic-Cenozoic cover has exposed several deformed Paleozoic massifs (collectively known as the “Moroccan Variscides”) in the Moroccan Meseta and High Atlas; southwards, the front of the Variscan Belt can be traced through the almost undeformed Paleozoic series of the Anti-Atlas region. Previous regional tectonic studies (El Hassani et al., 2003; Hoepffner, 1987; Hoepffner et al., 2005, 2006; Michard et al., 2008, 2010; Piqué, 1994, 2001; Piqué & Michard, 1981, 1989; Simancas et al., 2005, 2009; Tahiri & Hoepffner, 1988) subdivided the Moroccan Variscides into different domains (Coastal Block, Western Moroccan Meseta, Eastern Moroccan Meseta, and High Atlas or Sub-Meseta Domain; Figure 3.1B) based on stratigraphic and tectonic differences that would have paleogeographic implications (Michard et al., 2010 and references therein). The boundaries between these domains are regional-scale fault zones that reactivated former narrow rifted areas (Hoepffner et al., 2005, 2006; Michard et al., 2010). Nevertheless, the paleogeographic relevance of these structures is unclear, since they do not include suture-related rocks (*e.g.*, ophiolites), and the Ordovician-Devonian stratigraphic successions in all the Moroccan Variscides, as well as in other zones of the northern margin of Gondwana, indicate deposition in a shared passive margin (Piqué, 1994; Simancas et al., 2009), suggesting that all the domains of the Moroccan Variscides remained attached to northern Gondwana throughout the Paleozoic. This paleogeographic affinity is also supported by the detrital zircon provenance studies performed to date (Abati et al., 2010; Accotto et al., 2019; Avigad et al., 2012; El Houicha et al., 2018; Ghienne et al., 2018; Letsch et al.,

2018), which suggest a Gondwanan provenance for the Cambrian to Devonian sediments of the Moroccan Variscides. The only exception would be the Sehou Block in the Western Moroccan Meseta (Figure 3.1B), which is thought to have an Avalonian derivation based on the presence of a mid-Paleozoic (i.e., Caledonian) deformation occurred before the emplacement of granites radiometrically dated at the Late Devonian (U-Pb on zircons; Tahiri et al., 2010).

This work aims to unravel the Late Paleozoic tectonic evolution of the complex and poorly known Debdou-Mekkam Massif in the Eastern Moroccan Meseta (Figure 3.1B). To do so, a detailed structural study of the metasedimentary Paleozoic rocks of this area was carried out, together with U-Pb geochronology and Hf isotope systematics on detrital zircon grains. This approach helped to constrain rock ages, provenance and tectonic evolution in the context of the Moroccan Variscides. On a broad scale, a new tectonic model emerges which highlights the close influence of the Rheic Ocean suture in the Eastern Moroccan Meseta, although the suture itself seems to be concealed and, hence, cryptic, as well as in many other transects of the Variscan Belt.

2. Geological setting

Paleozoic rocks are exposed in the Eastern Moroccan Meseta in relatively small (from a few square kilometers up to c. 1200 km²) and isolated inliers (Figure 3.1B), characterized by Cambrian-Permian successions deformed by Eovariscan (Late Devonian-Early Carboniferous) to Variscan (Carboniferous) events (Hoepffner, 1987). The Ediacaran basement that crops out in several areas of the Western Moroccan Meseta and Coastal Block (*e.g.*, El Haibi et al., 2020; El Houicha et al., 2018; Ouabid et al., 2017; Pereira et al., 2014, 2015; Tahiri et al., 2010) has not been reported in the Eastern Moroccan Meseta. Thus, the oldest sedimentary rocks described in this latter region are shales and schists attributed to the Cambrian-Ordovician in the Midelt Massif by correlation with similar facies in the Western Moroccan Meseta (Hoepffner, 1989). Only the highest levels of this succession were dated in Tazekka based on their paleontological and palynological content, which yielded Early Ordovician ages (Desteucq & Fournier-Vinas, 1981; Hoepffner, 1977; Rauscher et al., 1984). The overlying quartzitic sandstones, attributed to the Late Ordovician, reach maximum thickness at Tazekka (Hoepffner, 1989). The Silurian succession is characterized by black fine-grained quartzitic sandstones and shales with graptolites. Based on palynological content, the Devonian consists of slates followed by siliciclastic flysch sediments dated at Emsian (Marhoumi et al., 1983).

The Devonian flysch marks the change from a passive margin context, more or less continuous since the Cambrian, to a subsiding basin that preceded an “Eovariscan” tectonic event associated with the partial exhumation of the Moroccan Meseta (Hoepffner, 1987, 1989). In the Eastern Moroccan Meseta, the different inliers were variably affected by this “Eovariscan” deformation, which associated with very low-grade metamorphism, although greenschist to amphibolite facies conditions were locally

reached (Midelt and North Tamlet areas); the available ages point to the Late Devonian for the “Eovariscan” event: 366 ± 7 Ma obtained with Rb-Sr methods in the Midelt area (Clauer et al., 1980; Tisserant, 1977); 372.3 ± 8.1 and 368.3 ± 7.9 Ma obtained with the K-Ar method on syn-deformational illite grains from the Debdou and Mekkam Massifs, respectively (Huon et al., 1987). Hoepffner (1987) proposed that the “Eovariscan” tectonic event comprises two stages in the Midelt and Tamlet regions, both characterized by NW-SE trending isoclinal recumbent or overturned folds with W- to SW-vergences. The first of these stages would be associated with the development of a slaty cleavage, while the second would be related to a crenulation cleavage, horizontal shear and stretching lineation (Hoepffner, 1987; Hoepffner et al., 2006).

An “Intravisean” extensional phase (Hoepffner et al., 2006), associated with a transgression and the opening of volcano-clastic basins in the northern part of the Eastern Moroccan Meseta, was also described (*e.g.*, Debdou-Mekkam, Jerada, Traras basins, Figure 3.1B). The Late Visean sedimentary rocks were dated based on their fossil fauna content (Médioni, 1979 and references therein); they locally contain (*e.g.*, in the Mekkam region) a basal level of limestones and carbonatic breccias, which unconformably overlie the Cambrian-Devonian succession. The Late Visean volcanosedimentary deposition was accompanied by the emplacement of granitoids (El Hadi et al., 2006 and references therein).

The main Variscan event was described as responsible for E-W to ENE-WSW oriented, N-vergent folds (Hoepffner et al., 2006) that occurred at very low-grade metamorphic conditions during Late Carboniferous (*c.* 300 Ma; K-Ar methods on neoformed micas from the Tazekka Massif; Huon et al., 1987). This event was followed by the emplacement of several post-kinematic granitoids (*c.* 290 Ma; El Hadi et al., 2003, 2006 and references therein). Finally, Late Carboniferous-Early Permian tardi-Variscan events affected the Eastern Moroccan Meseta giving way to mainly compressional E-W, NW-SE, and N-S faults (Hoepffner et al., 2006).

The Permian post-orogenic continental red-beds that characterize the Western Moroccan Meseta and the Coastal Block (Hoepffner et al., 2005) have not been described in the Eastern Moroccan Meseta, where Lower Triassic red shales and basalts directly overlay in unconformity over the Carboniferous (Visean-Westphalian) volcano-sedimentary rocks.

2.1. The Debdou-Mekkam massifs

The Debdou-Mekkam massifs (comprising the Paleozoic outcrops in the Debdou and Mekkam areas, and a few smaller inliers between them; Figure 3.2) are characterized by a monotonous sequence of siliciclastic turbidites, previously called “Mekkam schists” (Hoepffner, 1987 and references therein). We prefer to refer to them as the “Debdou-Mekkam metasediments” (DMMS), because of the low-grade metamorphic imprint that these rocks underwent (as compared with the non-metamorphic overlying succession). The DMMS were originally dated as Tournaisian-Late Visean by Médioni (1980), based

on the presence of fragments of fossil plants. However, palynological data (Marhoumi, 1984; Marhoumi et al., 1983) yielded Middle-Late Devonian ages (Givetian-Frasnian).

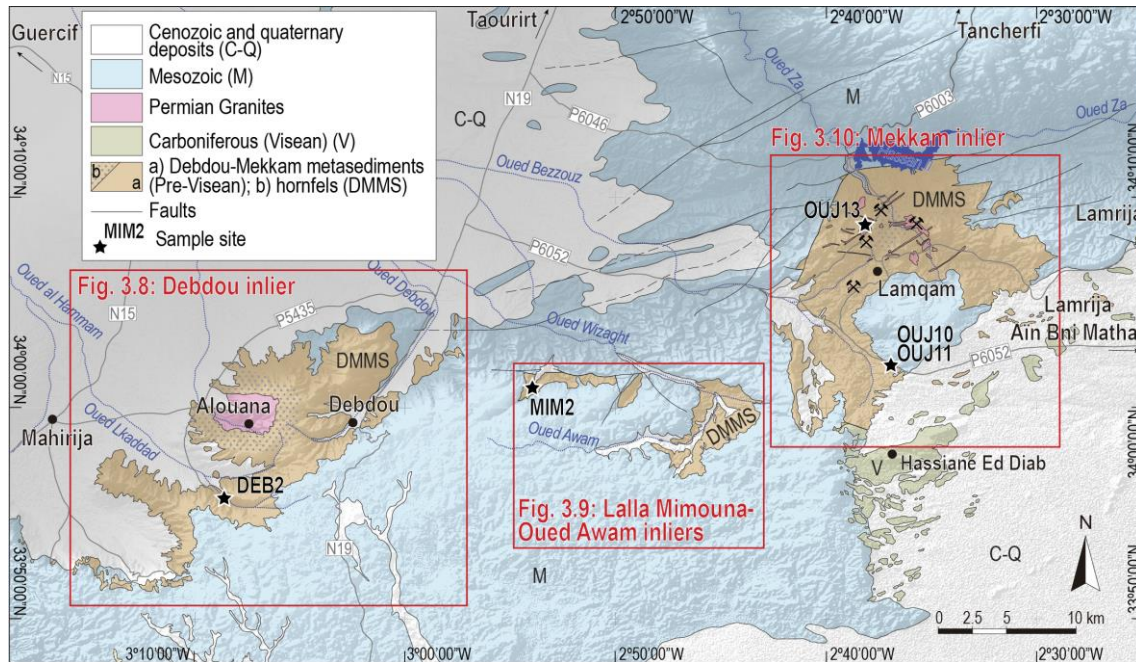


Figure 3.2. Paleozoic inliers in the Debdou-Mekkam region. The red squares refer to the detailed structural maps shown in Figures 3.8, 3.9, and 3.10. The topographic base is the Digital Earth Model SRTM 1 Arc-second Global (<https://earthexplorer.usgs.gov/>), with a superposed hillshade function to show altitude.

From a lithological point of view, the DMMS are an irregular alternation of slates and greywackes. The slates are particularly predominant in the minor inliers and, locally, in the Debdou and Mekkam areas; they are composed by very fine-grained sediments with abundant detrital mica (Figure 3.3A). The coarse-grained portion of the sequence is characterized by decimetric- to decametric-thick beds of greywackes with subordinate sandstones, quartzitic sandstones, arkoses, and, locally, microconglomerates (Figure 3.3B); under the microscope, these rocks show abundant quartz (often rounded), fragments of magmatic crystalline rocks, phyllosilicates (mica and clay), and oxides. The DMMS often show sedimentary structures, such as ripple laminations (Figure 3.3C) or graded bedding (Figure 3.3D), which were used in the field to identify the polarity of the sequence. The basal contact of the DMMS is not exposed in the region, hence its global thickness is unknown. The metamorphism is of very low- to low-grade with the phyllosilicate-rich rocks occurring as slates to phyllites.

The DMMS are unconformably overlain by a Visean succession, characterized by a basal breccia with carbonate cement and clasts of quartzitic sandstones and slates, probably reworked from the underlain sequence, and fragments of volcanites (Figure 3.3E), followed by limestones containing fragments of brachiopods and polyps of Late Visean age (Médioni, 1979 and references therein). The succession continues upwards with a 300 m-thick series of tuffs with interbedded rhyolites, trachyandesites and radiolarites, followed by a thick series of slates and sandstones, paleontologically dated at Late Visean (Médioni, 1979 and references therein). The Visean unconformity (Figure

3.3F) crops out in the southern zone of Mekkam area, NW of Hassiane Ed Diab (Figure 3.3), where is partially affected by a WNW-ESE trending fault (Section 4.4).

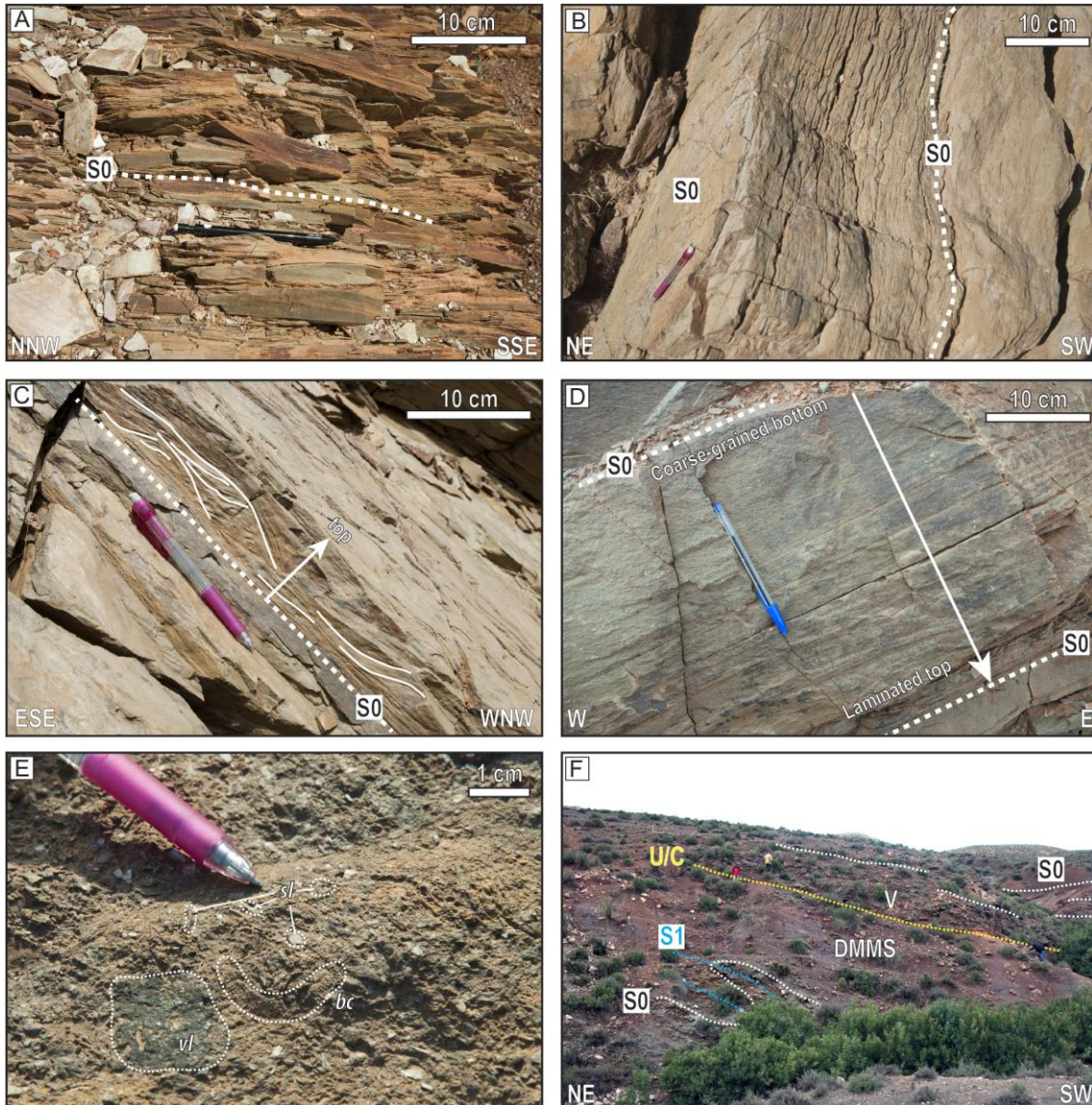


Figure 3.3. Main lithologies cropping out in the Debdou-Mekkam region: slates (A) and greywackes (B), which characterize the Debdou-Mekkam Metasediments (DMMS); cross-lamination in the slates (C) and graded bedding in a layer of greywackes (D) used as stratigraphic polarity criteria; (E) Upper Visean carbonate breccia with reworked clasts of DMMS slates (sl), volcanites (vl), and bioclasts (bc); (F) unconformity (U/C) between the previously deformed DMMS and the Visean succession (V) cropping out in the Hassiane Ed Diab area: S0, stratigraphic bedding; S1, main cleavage.

3. Detrital zircon geochronology

3.1. U-Pb analyses

Four to five kilograms of rock were collected from five outcrops of the DMMS (Figure 3.2). DEB2 (IGSN: IEACC0005) is a greywacke sampled in the Debdou inlier and made

up of abundant fine-sized (c. 0.1 mm in diameter) quartz and phyllosilicate grains, with subordinate altered feldspars and oxides. MIM2 (IGSN: IEACC0004) is a quartzitic sandstone sampled in the westernmost Lalla Mimouna-Oued Awam inliers, and composed of dominant medium-sized (c. 0.2 mm in diameter) quartz grains with subordinate phyllosilicates and oxides, which define the main cleavage. Samples OUI10 (IGSN: IEACC0001), OUI11 (IGSN: IEACC0002), and OUI13 (IGSN: IEACC0003) were collected in the Mekkam inlier. OUI10 is an arkose characterized by medium-sized (c. 0.2 mm in diameter) quartz grains, slightly oriented parallel to the main cleavage, which is defined by phyllosilicates. OUI11 was sampled not far from OUI10 (but in a different outcrop) and is a coarse-grained (c. 0.25-0.3 mm in diameter) arkose with abundant quartz and mica clasts; this latter is partially recrystallized, which suggests a slight metamorphic overprint. Finally, OUI13 is a quartz-rich sandstone with abundant phyllosilicate grains and the quartzitic clasts varying from fine to medium in size (diameter from c. 0.1 mm to c. 0.2 mm).

All the samples were processed in the laboratories of the University of Granada (Spain). They were crashed, and detrital zircon grains were separated using granulometric (sieves) and density (panning) separation procedures. Finally, 150-250 zircon grains were handpicked from each sample and sent to the John de Laeter Centre (JdLC) at Curtin University in Perth (Australia), where they were imaged by cathodoluminescence using a Mira3 FESEM instrument at the Microscopy and Microanalysis Facility (a selection of cathodoluminescence images of the most representative grains is included in the Appendix C, Figures C.13 to C.17), and then analyzed with Laser Ablation Inductively Coupled Plasma Mass Spectrometry (LA-ICPMS). In order to have a statistically significant amount of data (Vermeesch, 2004), a minimum of 146 analyses were carried out on each sample and the results that showed a discordance higher than 10% were considered anomalous and not accounted further. Given the increased errors associated with $^{206}\text{Pb}/^{238}\text{U}$ values observed for ages older than 1500 Ma, this ratio was only used to date younger grains; for ages older than 1500 Ma, the $^{207}\text{Pb}/^{206}\text{Pb}$ ratio was considered more appropriate. The detailed analytical methodology is provided in Appendix A. The statistical analysis of the data was carried out using DensityPlotter 8.4 software (Vermeesch, 2012). The histograms were created using a bin of 40 Ma, while an adaptive bandwidth of 40 Ma was applied for the Kernel Density Estimators (KDE). The youngest detrital zircon populations were calculated with IsoplotR online (Vermeesch, 2018). Errors are expressed at the 1σ level. The raw analytical results are listed in Tables D.30 to D.34 of the Appendix D.

3.1.1. Results

The zircon grains separated from the studied samples are between 100 μm and 300 μm in length. Most of the grains are yellowish or whitish; some of them are rounded, while others are euhedral; a few zircons are purple to pink, with a generally rounded shape. Cathodoluminescence images (Figures C.13 to C.17 in Appendix C) show continuous

oscillatory zoning, partially reabsorbed cores with low or high U overgrowth rims, sector zoning, or structureless grains.

From sample DEB2 (Figure 3.4A), 150 analyses were carried out on 147 detrital zircon grains, yielding 139 concordant results. Fifty-nine percent of the data ($n = 82$) range from c. 690 to c. 540 Ma and represent a main population with an Ediacaran mean age of 605.1 ± 0.4 Ma. Two minor detrital zircon populations yielded Paleoproterozoic mean ages, with two peaks at 2071.1 ± 2.7 Ma (c. 1.96-2.29 Ga, 16.5%) and 2458.8 ± 4.5 Ma (c. 2.49-2.43 Ga, 6.5%). A number of scattered data gave Cambrian ($n = 4$, c. 532-503 Ma), Tonian-Ectasian ($n = 11$, c. 1346-823 Ma), Orosirian ($n = 5$, c. 1938-1771 Ma), and Archean ($n = 3$, c. 3.0-2.7 Ga) ages. The youngest detrital zircon population in this sample ($n = 9$) yielded a Late Ediacaran weighted average age (549.6 ± 1.2 Ma, MSWD = 1.12); however, the 2 youngest detrital zircon grains gave Late Devonian (Late Frasnian) ages (374-375 Ma).

One hundred thirty-five detrital zircon grains from sample MIM2 were analyzed (Figure 3.4B) and 146 analyses were carried out, with 130 yielding concordant results. The main detrital zircon population has an Ediacaran mean age (616.3 ± 0.4 Ma; c. 786-547 Ma) and comprises the 50.8% of the data ($n = 66$). Furthermore, three minor populations can be defined: a Late Devonian population (average age of 369.6 ± 0.6 Ma; c. 380-357 Ma) that comprises 6.2% of the concordant data ($n = 8$), a c. 2013-2221 Ma Paleoproterozoic peak (2095.2 ± 3.8 Ma, 13.8%, $n = 18$), and a c. 2.43-2.6 Ga Siderian-Neoproterozoic population (mean age 2493.9 ± 4.2 Ma, 10%, $n = 13$). Scattered data gave Cambrian ($n = 2$, c. 523-501 Ma), Tonian-Orosirian ($n = 14$, c. 1940-873 Ma), and Mesoarchean ($n = 9$, c. 2.7-3.1 Ga) ages. The youngest detrital zircon population is Late Devonian (weighted average age 370.4 ± 0.9 Ma, MSWD = 1.28) and includes 4 data.

One hundred ninety detrital zircon grains from sample OUI10 were analyzed (Figure 3.4C) and 200 analyses were carried out, yielding 180 concordant results. The two main detrital zircon populations yielded mean ages of 615.9 ± 0.9 Ma (Ediacaran; c. 790-541 Ma, 39.4%, $n = 71$) and 371.4 ± 0.8 Ma (Late Devonian; c. 425-320 Ma, 19.4%, $n = 35$). Nine percent of the data ($n = 16$) are included in a minor Tonian-Stenian population (mean age of 1073.6 ± 2.9 Ma; c. 1215-847 Ma) and 12.2% in a Paleoproterozoic peak (mean age of 2078.1 ± 3.3 Ma; c. 2.23-1.94 Ga). Scattered data yielded Cambrian ($n = 7$, c. 538-514 Ma), Ectasian-Orosirian ($n = 19$, c. 1.28-1.9 Ga), and Siderian-Archean ($n = 10$, c. 2.44-2.83 Ga) ages. The youngest detrital zircon population in this sample is Late Devonian (weighted average age 361.7 ± 1.7 Ma, MSWD = 1.25) and includes 7 data.

From sample OUI11 (Figure 3.4D), 301 analyses were performed on 269 zircon grains, yielding 267 concordant results. The main detrital zircon populations yielded Ediacaran (mean age of 627.4 ± 0.8 Ma; c. 823-543 Ma, 39.3%) and Late Devonian (mean age of 376.9 ± 0.6 Ma; c. 426-343 Ma, 23.2%, $n = 62$) ages. Seventeen percent of the data ($n = 45$) can be grouped into a minor Paleoproterozoic population with a mean age of 2089 ± 2.5 Ma (c. 2.35-1.99 Ga). Scattered data yielded Cambrian ($n = 9$, c. 538-499 Ma), Tonian-Orosirian ($n = 35$, c. 1931-975 Ma), and Archean ($n = 11$, c. 3.37-2.47 Ga) ages.

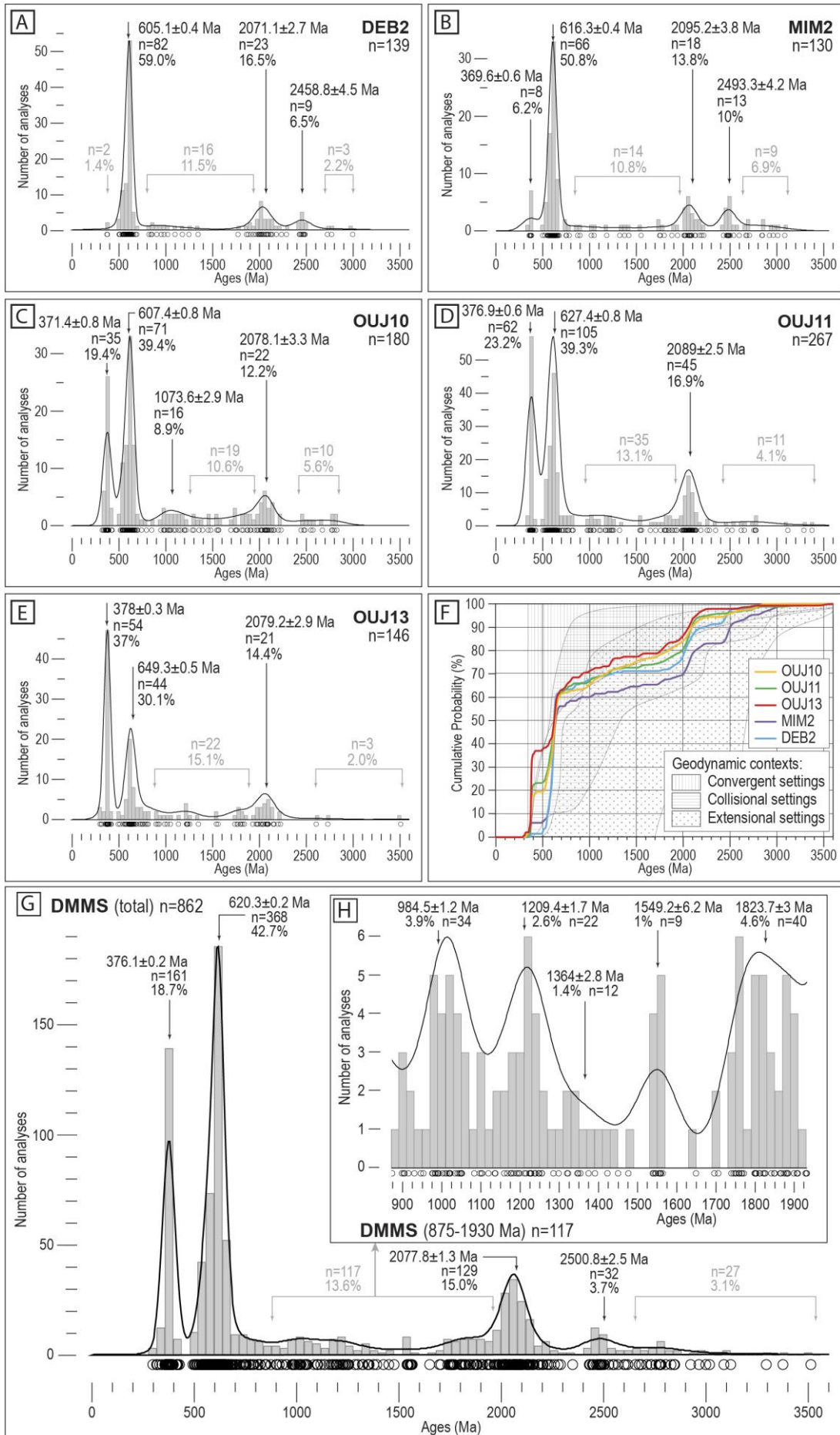


Figure 3.4 (previous page). U-Pb results. (A-E) KDE (Kernel Density Estimator; black solid lines) and histogram (grey bars) plots showing the results of the detrital zircon U-Pb geochronological analyses for each sample; (F) Cumulative probability plot showing the results of the 5 samples from the DMMS and the cumulative areas typical of different geodynamic contexts (Cawood et al., 2012); (G) Cumulative KDE (black solid lines) and histogram (grey bars) for the DMMS and (h) zoom for the ages ranging from c. 900 to c. 1900 Ma. All the plots were built using $^{206}\text{Pb}/^{238}\text{U}$ ages for dates < 1500 Ma, $^{207}\text{Pb}/^{206}\text{Pb}$ ages for dates > 1500 Ma, and errors expressed at the 1σ level. KDE and histograms were performed with DensityPlotter 8.4 (Vermeesch, 2012).

The youngest detrital zircon population is composed of 9 data with a Late Devonian weighted average age (362.3 ± 1.3 Ma, MSWD = 1.02).

Finally, from sample OUI13 (Figure 3.4E), 149 grains were analyzed yielding 150 results, 146 of which were concordant. Thirty-seven percent of the data ($n = 35$) are included in a main detrital zircon population with Late Devonian mean age (peak at 378 ± 0.3 Ma), with individual ages ranging from c. 417 Ma to c. 296 Ma. Another main population yielded a Cryogenian mean age of 649.3 ± 0.5 Ma (c. 811-543 Ma, 31.5%, $n = 44$). Fourteen percent of the data ($n = 21$) are included in a minor Paleoproterozoic peak with a mean age of 2079.2 ± 2.9 Ma and an age range of c. 2.23-1.93 Ga. Scattered analyses gave Cambrian ($n = 2$, c. 494-510 Ma), Tonian-Orosirian ($n = 22$, c. 1840-898 Ma), and Archean (c. 3.5-2.6 Ga, $n = 3$) ages. The youngest detrital zircon population ($n = 4$) yielded a Late Devonian age (weighted average age 360 ± 1.1 Ma, MSWD = 1.16).

In summary (Figure 3.4F and G), all samples are characterized by an important Ediacaran-Cryogenian detrital zircon population (peaked at c. 618 Ma and comprising c. 30-60% of the data) and by minor Paleoproterozoic-Archean populations (c. 2.1 Ga, c. 15%, and c. 2.5 Ga, c. 4%). Finally, a Devonian detrital zircon population (c. 375 Ma) can be dominant (OUI10, OUI11, and OUI13; 20-35%), secondary (MIM2, 6%), or almost absent (DEB2), thus pointing to a Late Devonian maximum depositional age for the DMMS. Scattered data with Tonian-Orosirian ages are common in all the samples (as highlighted in Figure 3.4H).

3.2. Hf isotope analyses

The four samples characterized by the Devonian detrital zircon population were analyzed for Hf isotopes with the aim of defining their isotopic signature. Therefore, Hf isotopes were not analyzed on sample DEB2, where only two Devonian zircons were found.

Hf isotopes in zircon were measured at the Geohistory facility in the JdLC, Curtin University (Australia). Previously dated zircon crystals were ablated using a Resonetics resolution M-50A excimer laser, coupled to a Nu Plasma II multi-collector inductively coupled plasma mass spectrometer (LA-MC-ICPMS). All isotopes (^{180}Hf , ^{179}Hf , ^{178}Hf , ^{177}Hf , ^{176}Hf , ^{175}Lu , ^{174}Hf , ^{173}Yb , ^{172}Yb , and ^{171}Yb) were counted on the Faraday collector array. Calculation of ϵ_{Hf} values employed the decay constant of Scherer et al. (2001) and the Chondritic Uniform Reservoir (CHUR) values of Blichert-Toft & Albarède (1997).

The detailed analytical methodology and results are included in Appendix A and E (Tables E.2 to E.5) respectively.

To calculate Hf model ages of the continental crust (T_{NC}) where the Devonian zircon grains were formed, the new continental crust composition of Dhuime et al. (2011) was used, which is more isotopically enriched than the depleted mantle and similar to the composition of island arc rocks.

3.2.1. Results

One hundred and twenty-nine analyses were carried out on detrital zircon grains from sample MIM2 (Figure 3.5A). The Devonian zircon population (mean age of 369.6 ± 0.6 Ma) is characterized by slightly negative (-6 to 0; $n = 8$) ϵ_{HF} values and T_{NC} between 1.2 Ga and 1.6 Ga. The Ediacaran detrital zircon population (mean age of 616.3 ± 0.4 Ma) is characterized by a very wide range of ϵ_{HF} values (from -24 to +12, $n = 68$), as is the Paleoproterozoic population (mean age of 2095.2 ± 3.8 Ma, ϵ_{HF} values from -13 to +6, plus an isolated value at +15, $n = 18$). The Siderian-Neoarchean peak (2493.3 ± 4.2 Ma) shows mostly negative ϵ_{HF} (from -10 to +3, $n = 12$). The scattered Tonian-Orosirian grains mainly yielded positive ϵ_{HF} values (from -10 to +11, $n = 14$), while the scattered Archean grains mostly displayed negative values (-17 to +2, $n = 9$).

On the detrital zircons from sample OUI10, 59 Hf isotope analyses were performed (Figure 3.5B). Ten grains from the Devonian population (mean age of 371.4 ± 0.8 Ma) were analyzed: nine yielded positive ϵ_{HF} values from +0 to +6, while one gave a ϵ_{HF} value of -4; T_{NC} varies between 0.7 Ga and 1.5 Ga. The Ediacaran peak (607.4 ± 0.8 Ma, $n = 27$) yielded a wide range of ϵ_{HF} values ranging from -21 to +10, while the Paleoproterozoic peak (2078.1 ± 3.3 Ma, $n = 7$) is characterized by mostly positive values (-1 to +5), with an isolated strongly negative result (-17). The scattered Tonian-Orosirian zircons yielded mostly positive ϵ_{HF} values (-2 to +3), with a couple of strongly negative data (-20 and -17). Two Archean grains gave negative values (-7 and -4).

One hundred and twenty-eight analyses were performed on detrital zircons from sample OUI11 (Figure 3.5C). Twenty-one Devonian zircons (peak at 376.9 ± 0.6 Ma) yielded mainly positive ϵ_{HF} values varying from -0.4 to +6 and T_{NC} varying from 0.6 Ga to 1.3 Ga. The ϵ_{HF} range increases for the Ediacaran peak (627.4 ± 0.8 Ma, $n = 56$, ϵ_{HF} from -24 to +12) and the Paleoproterozoic peak (2089 ± 2.5 Ma, $n = 27$, ϵ_{HF} from -2 to +9). The scattered Tonian-Orosirian zircons yielded variable values (from -20 to +7) with predominance of positive values, while the Archean zircons yielded negative values between -13 and -3.

Finally, 125 analyses were carried out on grains from sample OUI13 (Figure 3.5D). The Devonian detrital zircon population (mean age 378 ± 0.3 Ma) is characterized by mostly positive ϵ_{HF} values ranging from -1 to +8 ($n = 47$) and T_{NC} between 0.8 Ga and 1.2 Ga. The Ediacaran peak (649.3 ± 0.5 Ma, $n = 39$) yielded a very wide range of values (-25 to +12) and the Paleoproterozoic peak (2079.2 ± 2.9 Ma, $n = 17$) mostly gave positive values (-6 to +6), with an isolated strongly negative ϵ_{HF} value (-15). Twenty scattered

Tonian-Orosirian zircons yielded a wide range of values (-16 to +13). Two Archean data gave ϵ_{Hf} values of -3 and +3.

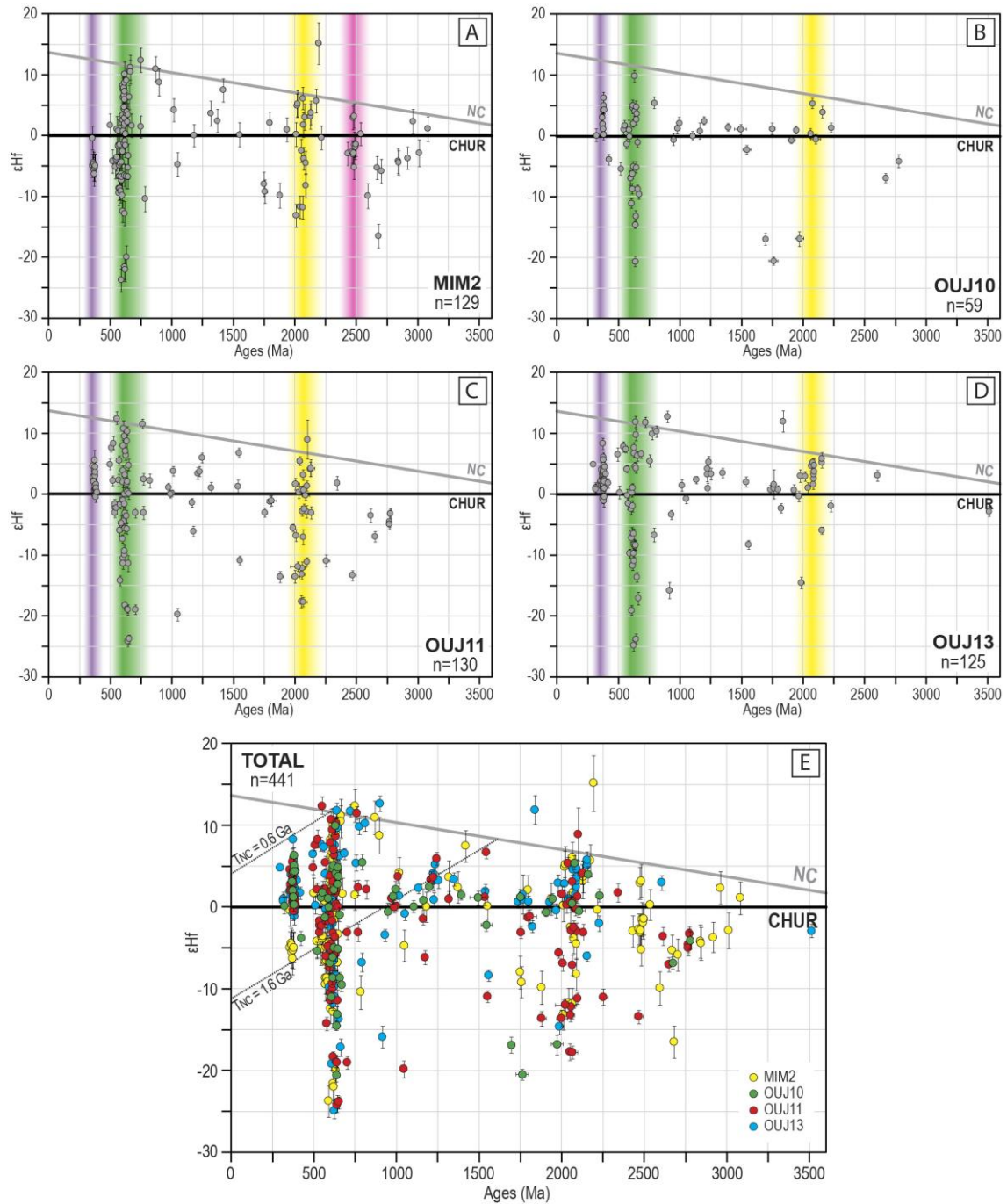


Figure 3.5. Mean ϵ_{Hf} values versus U-Pb ages plots for each sample (A-D) and cumulative (E). CHUR: Chondritic Uniform Reservoir (Bouvier et al., 2008); NC: new crust (Dhuime et al., 2011). The T_{NC} lines represent the bulk crust ($^{176}\text{Lu}/^{177}\text{Hf} = 0.015$) corresponding with the new crust ages of the Devonian detrital zircon population. Colors bands indicate the main detrital zircon populations described in section 3.1: Late Devonian (purple), Ediacaran-Cryogenian (green), Paleoproterozoic (yellow), and Archean (pink).

In summary (Figure 3.5E), the Devonian detrital zircon population is characterized by mostly (> 80% of the data) positive ϵ_{Hf} values ranging from -6 to +8, except for those in sample MIM2 which gave slightly negative values (between 0 and -6). The T_{NC} vary from

0.6 Ga to 1.6 Ga. The Ediacaran and Paleoproterozoic populations are characterized by a very wide range of ϵ_{Hf} values (-25 to +12, and -17 to +9, respectively). The scattered Tonian-Orosirian grains yielded mostly positive ϵ_{Hf} values, while the Siderian-Archean zircons gave mostly negative values.

4. Structural analysis

From a structural point of view, the Debdou-Mekkam Massif was previously described by Hoepffner (1987), who identified two “Eovariscan” deformational events. According to this author, the main deformation produced W-vergent structures related to an important shortening, though neither detailed structural maps, nor cross-sections of the inliers were provided.

Based on our field observations, the Debdou-Mekkam Massif is characterized by a polyphasic deformation. The first event (D1) is characterized by a pervasive cleavage (S1) associated with plurikilometric-scale SE-vergent folds. Later event (or events; Dc) generated variably developed crenulation cleavages (Sc) associated with differently oriented metric- to kilometric-scale folds. All of the cleavages observed are aligned with the axial-plane to the respective folding phase. Neither mineral/stretching lineations, nor structures indicative of simple shear deformation were observed. Some post-Variscan (post Dc) rectilinear fractures can locally limit the Paleozoic inliers (Figure 3.2). Our structural analysis focused on the D1 structures at outcrop scale and large-scale reconstruction.

4.1. Main tectonic fabrics

4.1.1. Early fabric

The earliest tectonic fabric recognizable is a foliation (S1) superimposed on the stratigraphic bedding (S0; Figure 3.3). Since overturned folds are present, a careful inspection of sedimentary polarity criteria was carried out, *e.g.*, graded bedding, basal erosive surfaces, geometry of sedimentary sets with cross lamination, and recognition of Bouma sequences (Figure 3.3C and D). S1 is a slaty (locally disjunctive) cleavage, well developed in phyllosilicate-rich beds, and less penetrative in coarse-grained layers, where refraction with respect to S0 is more intense (Figure 3.6). The obliquity between S0 and S1 usually defines a well-developed intersection lineation (L1). S1 represents the axial-planar cleavage of millimetric- to decametric-scale folds (Figure 3.6A, B, and E) and the orientation of L1 roughly indicates the hinge orientation. The folds are tight to isoclinal, inclined to recumbent, and often asymmetric. Fold asymmetry (S or Z shapes), together with local vergence (*i.e.*, S0-S1 relationships; Bell, 1981) (Figure 3.6C, D and F) and stratigraphic polarities (Figure 3.3C and D) were systematically examined in order to reconstruct the large-scale D1 structure in the Debdou-Mekkam Massif. When D1 folds

are not affected by later deformations, normal limbs are low-dipping and S1 is not very penetrative; on the contrary, overturned limbs show higher dips and more penetrative S1.

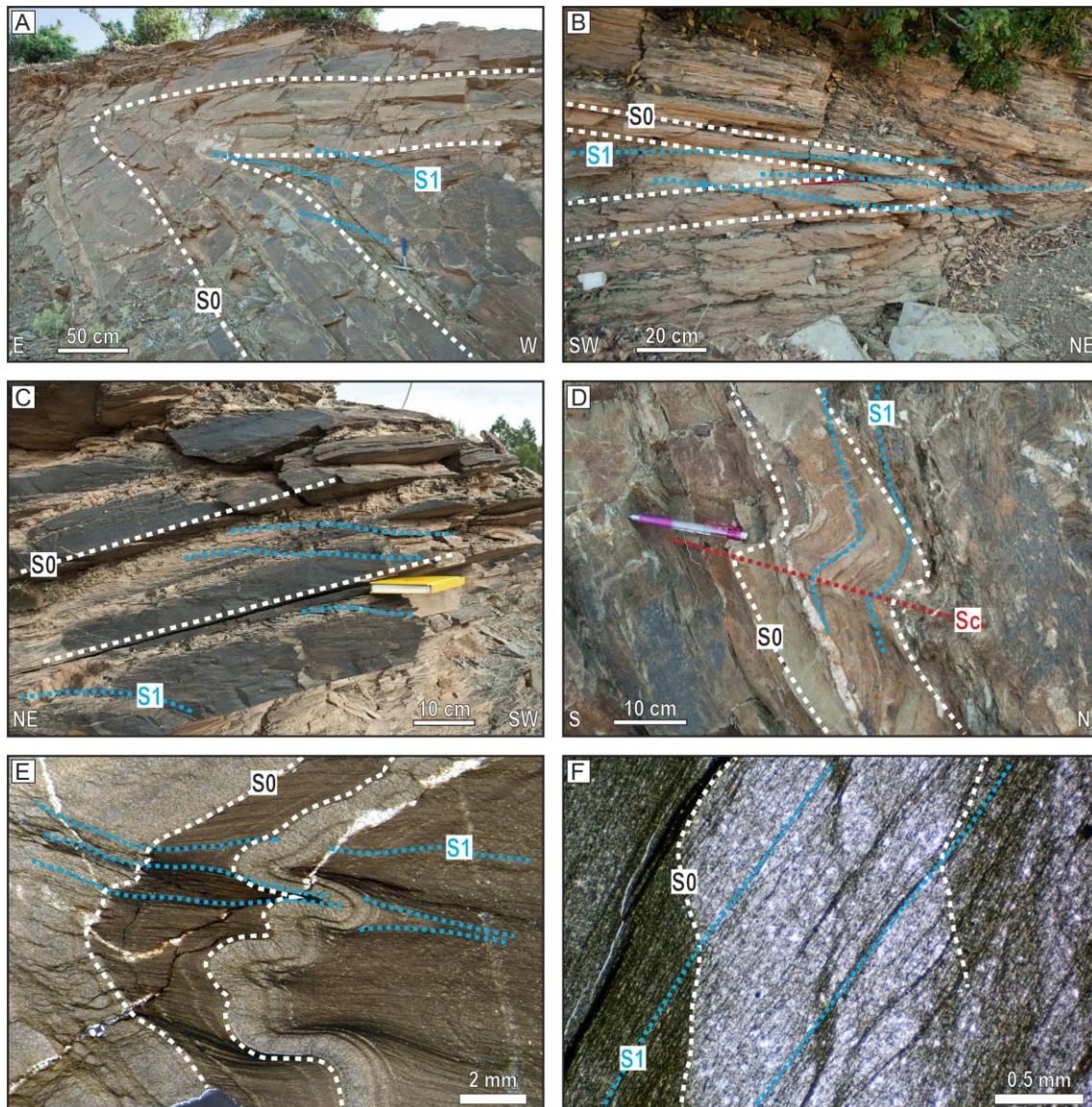


Figure 3.6. Field and microscopic images of bedding (S0) and principal cleavage (S1): mesoscale metric folds associated with S1 (A and B); S0/S1 relationships (C and D); microscale folds and axial plane cleavage, S1 (E); microscale relationships between S0 and S1 (F).

At microscopic scale, S1 is easily visible and defined by the sharp and continuous orientation of white mica, chlorite, and Fe-oxides (Figure 3.6E and F). In coarse-grained layers, S1 is a rough to anastomosing spaced cleavage, marked by the orientation of Fe-oxide concentrates, but less penetrative than within the fine-grained pelitic domains. When S1 presents an anastomosing geometry, it isolates sigmoidal-shaped quartz- and feldspar-rich domains.

4.1.2. Late fabrics

The late ductile deformational event (or events; Dc) generated folds with axial-planar cleavages (Sc) that refold and crenulate the previous structures (Figure 3.7A and E). The visible folds are, centimetric- to metric-scale (Figure 3.7B), open to tight, and they feature chevron or kink-band geometries. The orientation of the folds (and their corresponding axial-planar crenulation cleavages) is variable, and they can be grouped into three sets: two of them have steeply dipping to vertical axial planes trending NW-SE (Sc1) and NE-SW (Sc2) respectively; the third set (Sc3) is associated with low-dip to horizontal axial-plane kink-folds.

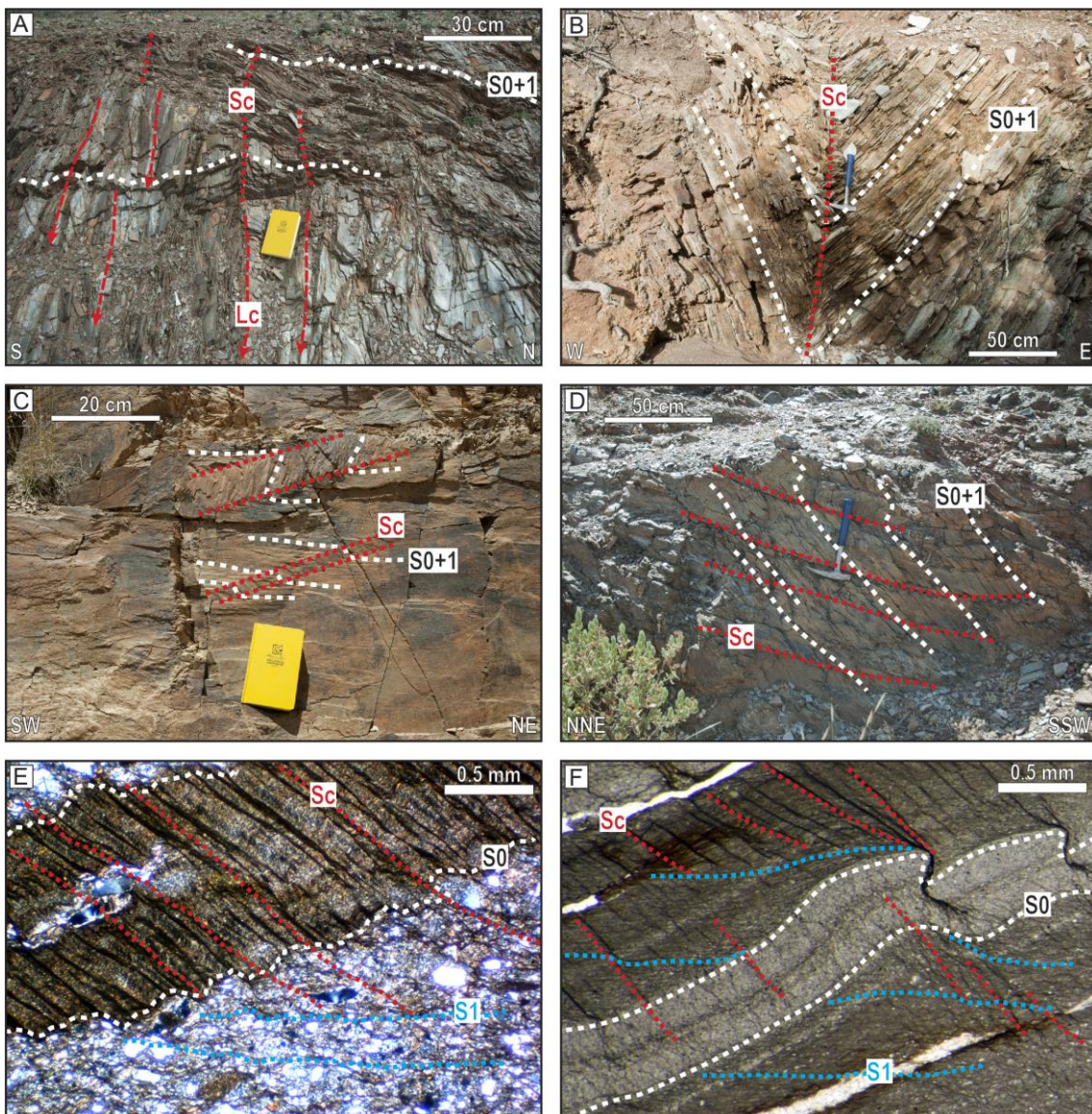


Figure 3.7. Late fabrics: crenulation cleavage (Sc) deforming S0 and S1 (A, B); incipient (C) and well developed (D) tectonic banding associated with a low-dipping crenulation cleavage; microscopic crenulation and its relationships with S0 and S1 (E, F).

At the outcrop scale, the penetrative nature of Sc varies from absent (only S0+S1 is observed), to spaced crenulation cleavage, to centimetric- to decimetric-scale tectonic

banding (Figure 3.7C and D). The distribution of Dc folds and related crenulation cleavages is heterogeneous across the Debdou-Mekkam Massif, and they rarely appear superposed at the outcrop scale, making the geometric and temporal relationships among the three sets unclear. Therefore, the interpretation of their genesis remains ambiguous: (i) they might be the result of successive deformational phases occurred under different regional stress orientations, or (ii) a unique deformational event resulted in different crenulation orientations due to local interference with the pre-existing, variably oriented, D1 structures (see section 5.3). Whatever the case, we have taken into account the geometry of the crenulation folds during the reconstruction of the D1 structures (the main purpose of our structural analysis), while the proposed tectonic evolution is restricted to the D1 event in order to avoid possible misinterpretations derived from the uncertain meaning of Dc structures.

At microscopic scale, Sc only appears in the phyllosilicate-rich layers as a spaced cleavage with anastomosing geometry defined by Fe-oxides (Figure 3.7E). Sometimes, Sc also deforms the previous S1 and S0 forming micro-kink bands (Figure 3.7F).

4.2. *The Debdou inlier*

The Debdou inlier has been divided into two sectors according to the orientation of S1 and L1. The southern sector (Figure 3.8) is characterized by variable trends of S1 (from NW-SE, through N-S, to NE-SW), with dominant low dips to the west and L1 mostly plunging to the south. In the R'chida area (western portion of cross-section A-A', Figure 3.8), a normal limb crops out, characterized by sub-horizontal S0 with a few indicators of normal polarity, and S1 gently dipping to the NW with L1 gently plunging to the SW. The local vergence of D1 is to the SE. A vertical E-W trending crenulation cleavage (Sc1) is present, though scarcely penetrative. In the eastern portion of cross-section A-A' (Figure 3.8), S1 and L1 trends rotate to NW-SE and a D1 hinge zone is observed. Similar L1 orientations are observed in the Galbi Al Hayyar area (cross-section B-B'; Figure 3.8), where S1 is sub-horizontal and S0 dips gently to the SW with reverse polarity. The local D1 vergence in this area is to the SW. To the SE, along cross-section B-B', the stratigraphic polarity is normal for a couple of kilometers, with S0 and S1 dipping to the SW, and showing the angular relationships typical of a normal limb. L1 is rotated with respect to the Galbi Al Hayyar area, being now oriented NE-SW and gently plunging to the SW. The asymmetry of the D1 parasitic folds and the relationships between S0 and S1 indicate local SE-vergence. In the remaining eastern portion of cross-section B-B' (Oulad Tayar area), S0 dips moderately to the west and repeated evidence of reverse polarity are observed (mainly graded bedding; Figure 3.3B). S1 and L1 are NE-SW to N-S trending, the cleavage dips gently to moderately to the west, and L1 plunges to the SSW. S0/S1 relationships and the asymmetry of the mesoscale D1 folds indicate local W-vergence. In one outcrop, a top-to-the-east, low-dipping thrust plane was observed crosscutting the S1 (cross-section B-B', Figure 3.8), which can be interpreted as a late-D1 brittle structure that contributed to shortening accommodated by D1 folds.

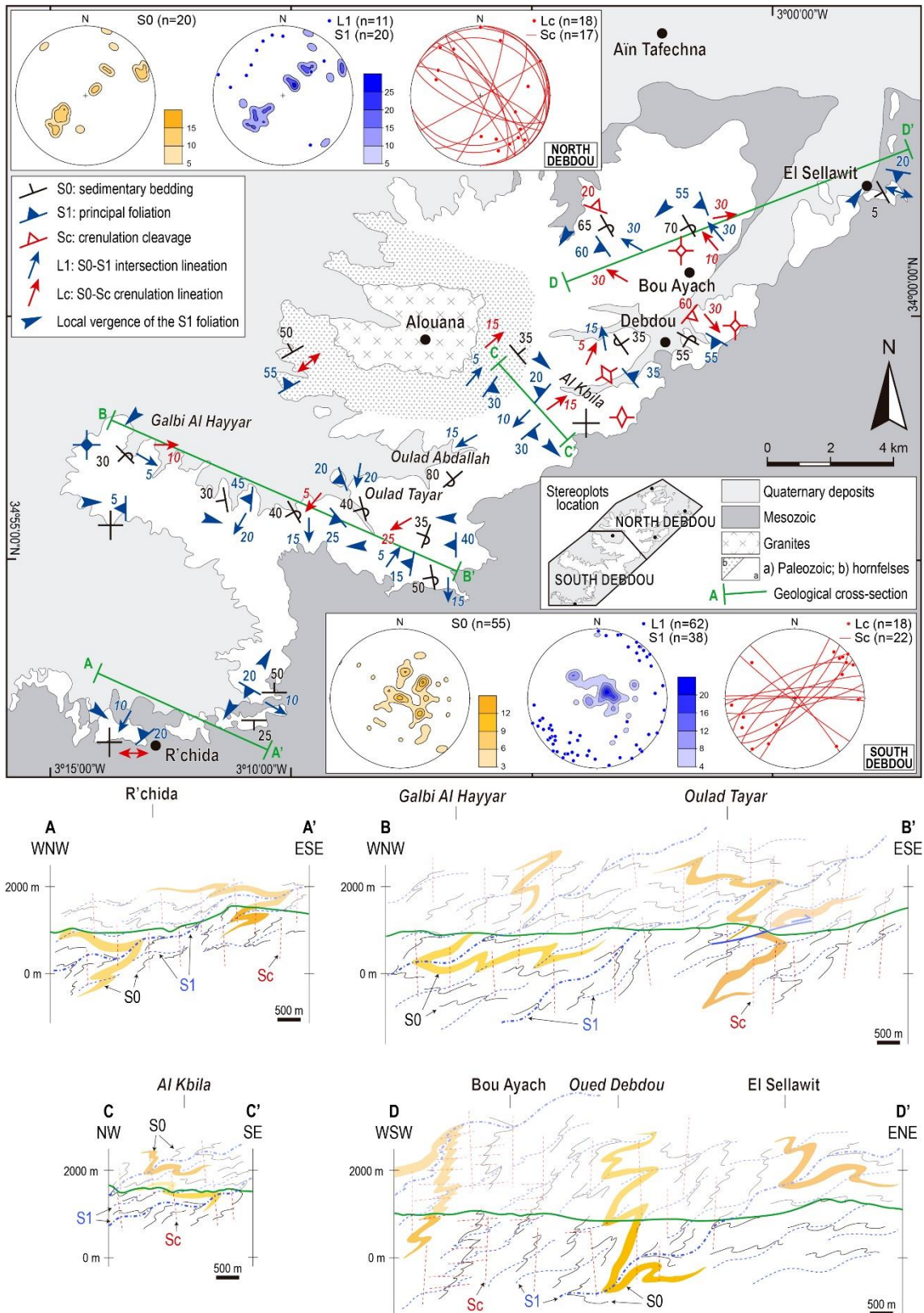


Figure 3.8. Structural map and cross-sections of the Debdou inlier. Colors for different structural elements in the cross-sections correspond to those in the map.

To the SE of Alouana, (Al Kbila area, cross-section C-C'; Figure 3.8), normal limb relationships dominate with NE-SW trending S0 and S1, and low-dips towards the NW

and SE due to Sc2 folds. L1 is NE-SW trending and sub-horizontal. D1 local vergence, defined mostly by the asymmetry of the mesoscale folds, is to the SE. Towards Alouana, the crenulation cleavage Sc2 (NE-SW trending and highly-dipping) intensifies, while contact metamorphism due to the nearby Alouana pluton obliterates the previous structures.

The northern sector of the Debdou inlier (cross-section D-D', Figure 3.8) is mostly characterized by NW-SE trending, SW-dipping S1, and L1 plunging to the NW. In the Debdou and Bou Ayach areas, S0 shows evidence of reverse polarity (cross-laminations and internal graded bedding). The crenulation cleavage is penetrative, with three different orientations: Sc1, with NW-SE trends and high dips, which is probably responsible for the dip variation of S0 and S1 from SW to NE; Sc2, with NE-SW trends, which is particularly prominent SW of Debdou; and Sc3, which is locally very penetrative east of Debdou and close to Bou Ayach, where Sc3 develops a sub-horizontal tectonic banding (Figure 3.7C and D). Finally, normal stratigraphic polarities were observed further NE, close to El Sellawit village, where S0 is sub-horizontal, S1 dips gently to the SSW and the local vergence is to the NE. No crenulation cleavages were observed in this area.

4.3. The Lalla Mimouna-Oued Awam inliers

These inliers extend from Lalla Mimouna to the valley of the Oued Awam, covering a sector in between the two large-scale Paleozoic outcrops of Debdou and Mekkam. In the westernmost inlier, the so called "Inlier 1" in Figure 3.9 (cross-sections E-E' and F-F'), S0 and S1 have NE-SW to ENE-WSW trends and dip gently to moderately both to the NW and SE as the result of late Dc open upright folds with E-W to ENE-WSW trends. The crenulation cleavage associated with these folds is locally penetrative and often obliterates the S0/S1 relationships. Where the S0/S1 relationships are preserved, they show dominant SE-vergences, although some NW-vergences suggest the presence of local overturned limbs related to parasitic D1 folds developed on a dominant normal limb (cross-sections E-E' and F-F'; Figure 3.9).

In the central inlier ("Inlier 2" in Figure 3.9), the trend of the D1 structures is WNW-ESE, with both S0 and S1 gently dipping to the NNE. The bedding polarity is generally normal, though reverse polarity is also found locally (cross-section G-G', Figure 3.9). Where the polarity is normal, S0/S1 relationships and the asymmetry of small-scale parasitic D1 folds indicate local vergence to the south. A N-S highly dipping crenulation cleavage locally affects the previous structures.

In the eastern inlier ("Inlier 3" in Figure 3.9), the D1 structures show similar orientation as in "Inlier 1": both S0, S1 and L1 are WSW-ENE trending. As showed in cross-section H-H' (Figure 3.9), S0 and S1 dip steeply to the NW and SE, due to Dc upright folding. The observed polarity is generally normal and the local vergence of D1 structures is to the SE. In the northern and central sectors of the inlier, the crenulation cleavage trends NE-SW (Sc2), while in the southern one it has NW-SE trends (Sc1).

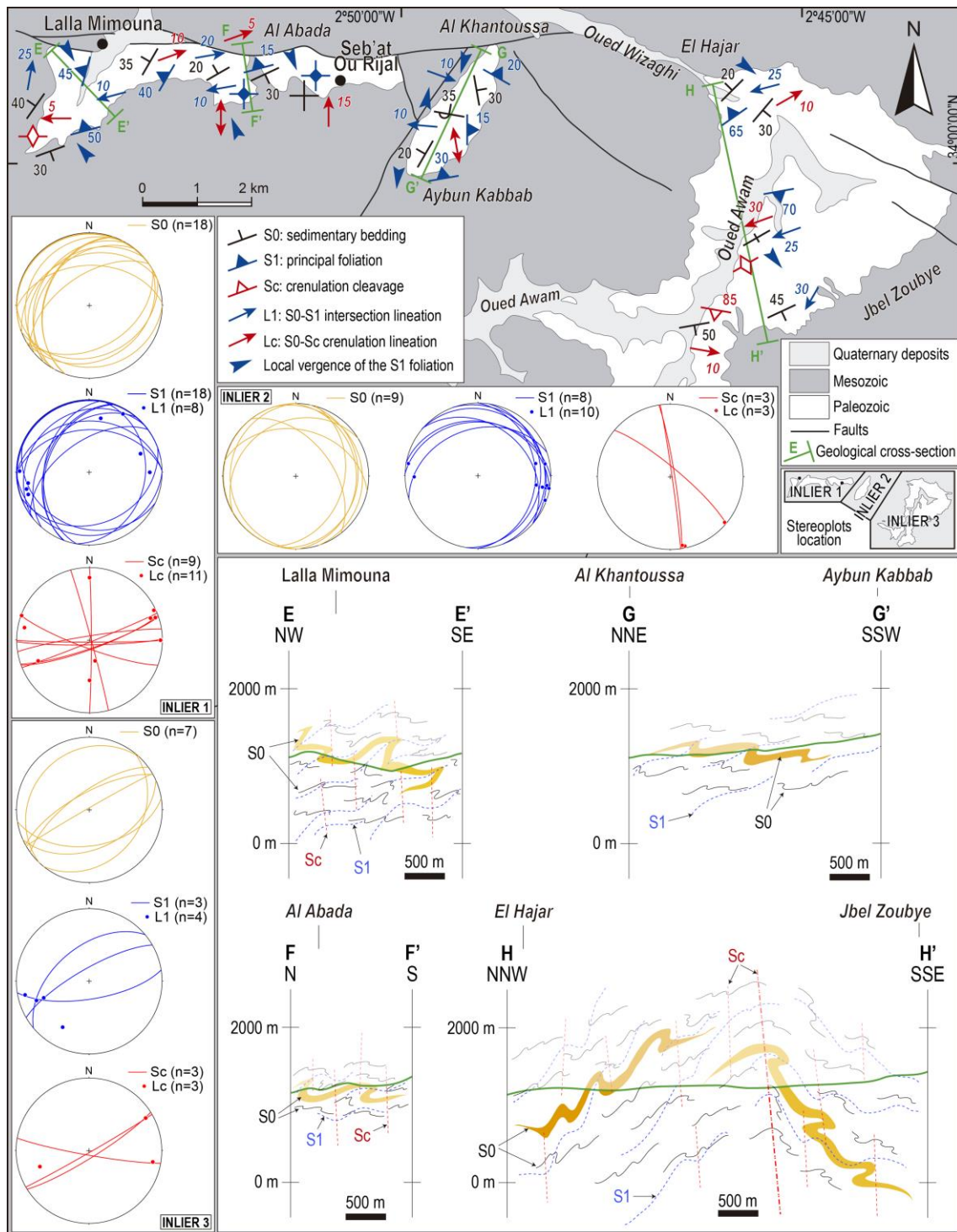


Figure 3.9. Structural map and cross-sections of the Lalla Mimouna-Oued Awam inliers. Colors for the different structural elements in the cross-sections correspond to those in the map.

4.4. The Mekkam inlier

In the Mekkam inlier, the dominant structural grain is NW-SE due to upright Dc folds (Sc1), with the exception of the southwestern and northwestern sectors where the dominant structural orientations are controlled by NE-SW trending Dc folds (Sc2) (Figure 3.10).

The southwestern sector of the Mekkam inlier (cross-section I-I'; Figures 3.10 and 3.11) is characterized by S0 and S1 trending NE-SW, with gentle to moderate dips to the NW and SE. The intersection lineation L1 trends mostly NW-SE. Along cross-section I-I', the polarity varies: clear reverse polarity criteria (graded bedding) were recognized in the Ayn Serraq area, where the S0/S1 relationships indicate west-vergences (western portion of cross-section I-I'); towards the SE, the opposite stratigraphic polarity and structural relationships were observed, with S0 and S1 folded by a Dc NE-SW trending upright synform (central portion of cross-section I-I'); further to the SE, in the corresponding Dc antiform, the dominant polarity is reverse and D1 structures show NW-vergence, although minor normal limbs locally crop out (eastern portion of cross-section I-I'). Besides the NE-SW highly-dipping crenulation cleavage associated with the macro-scale Dc folds, a second crenulation cleavage oriented NW-SE (Sc1) was also recognized.

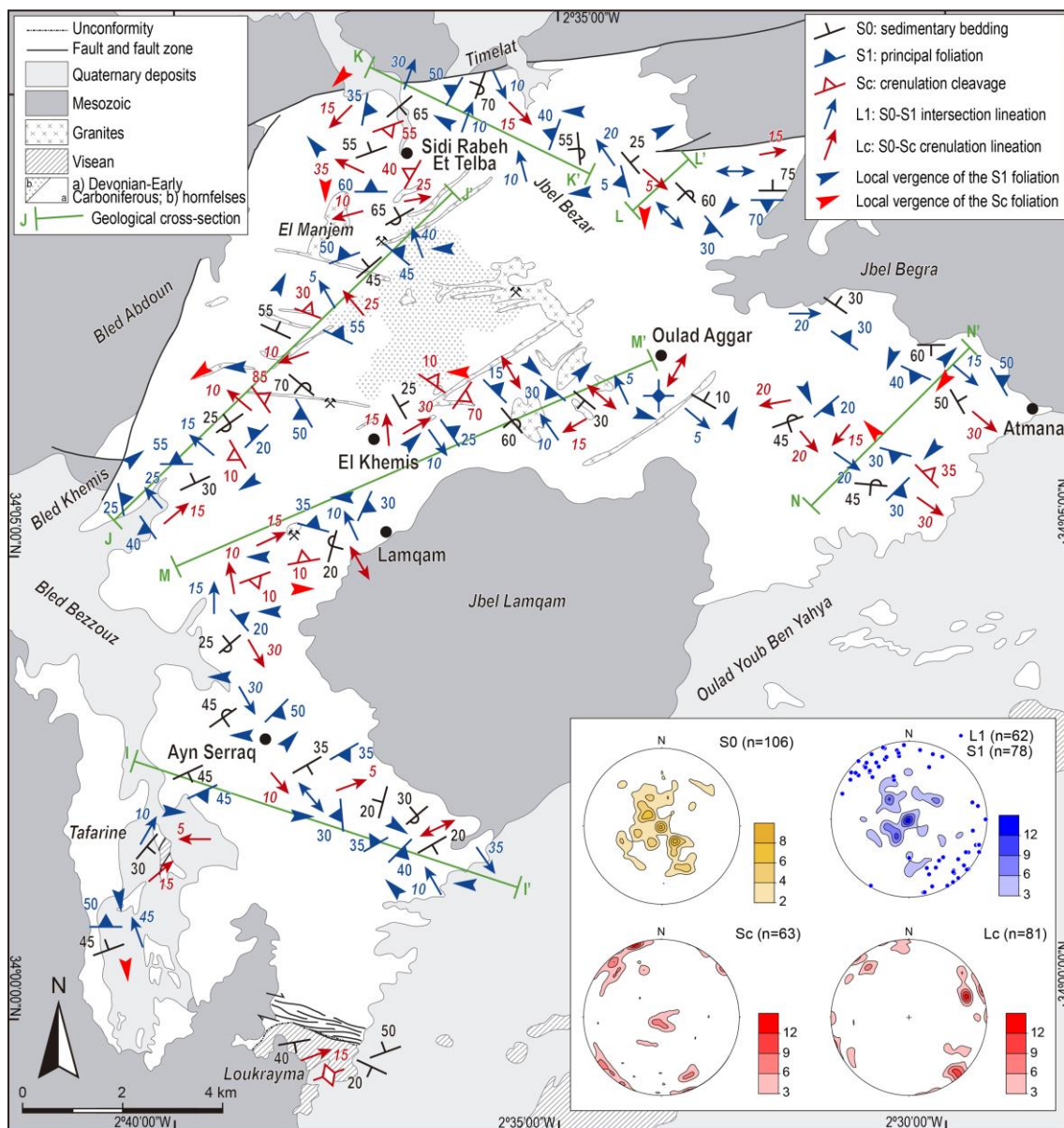


Figure 3.10. Structural map of the Mekkam inlier.

In the central and western sectors of the Mekkam inlier (cross-sections J-J' and M-M'; Figures 3.10 and 3.11), the S0 trend is variable and dip is usually low. Concerning the D1 folds, L1 is systematically oriented NW-SE, with gentle plunges towards the NW and SE. The western segment of cross-sections J-J' and M-M' is dominated by reverse polarities suggesting the presence of a kilometric-scale overturned D1 limb. Besides local rotations, S1 is generally NW-SE trending and its geometric relationships with S0, together with the asymmetry of the parasitic folds, indicate SW-vergences associated with the overturned limb; the scarce NE-vergences correspond to minor normal limbs. Towards the NE (eastern segment of cross-sections J-J' and M-M'), polarity and local vergence are dominantly the opposite, indicating a D1 normal limb (with NE-vergence). The three sets of crenulation cleavage (Sc1, Sc2, and Sc3; see Section appear variably (4.1.2 ,developed. The main structural trend (NW-SE) in controlled by Sc1 but in the northern segment of cross-section J-J', dip directions towards the NW were found due to the existence of a WSW-ENE oriented open antiform (Sc2) between El Manjem and El Khemis. The low-dip Sc3 cleavage can be locally very penetrative, especially in cross-section J-J' south of El Manjem mine and in the El Khemis area, where this cleavage often produces tectonic banding that partially obliterates the previous structures. As in other sectors of the region studied, the different sets of crenulation cleavages do not appear developed together, and, therefore, their mutual relationships are unclear.

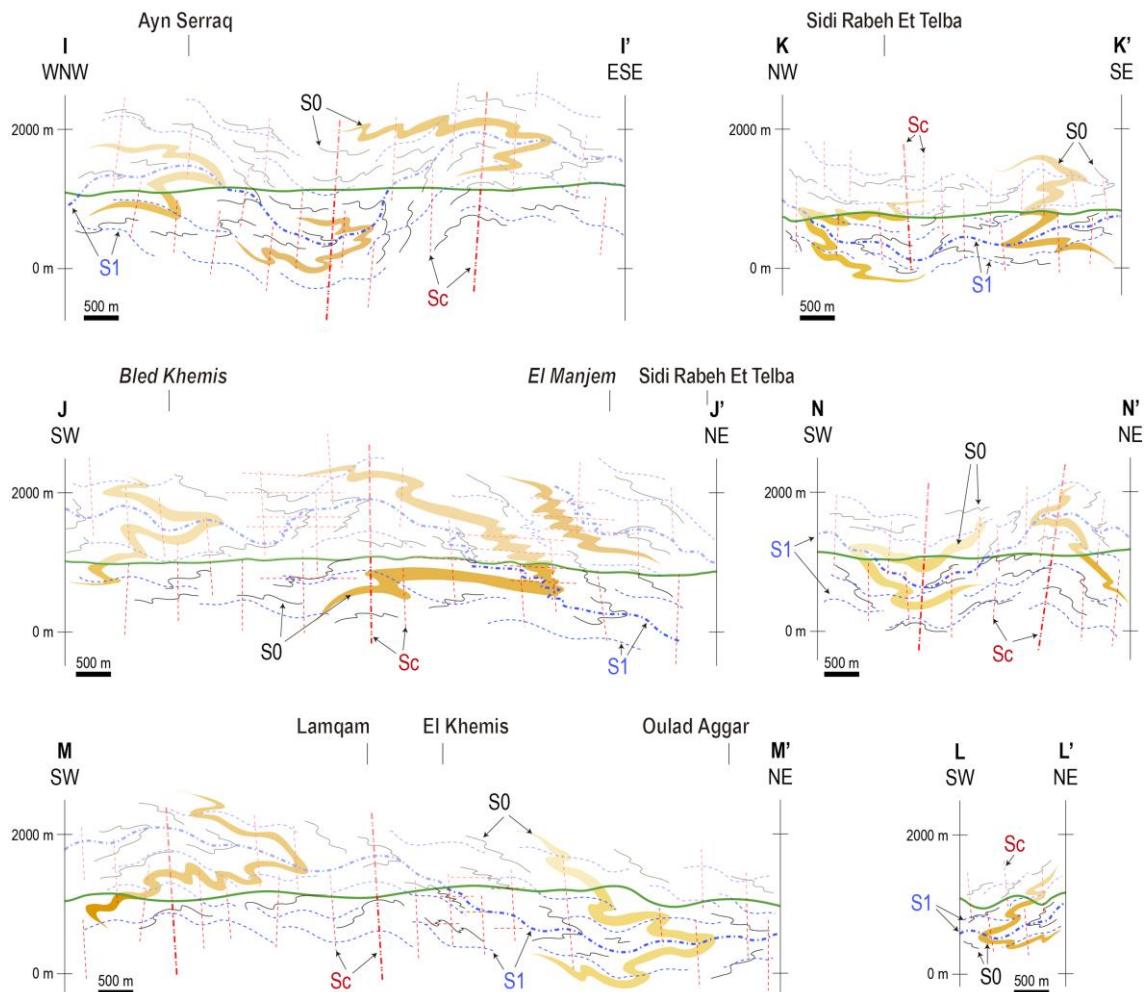


Figure 3.11 (previous page). Cross-sections of the Mekkam inlier. See location in Figure 3.10. Colors of the different structural elements in the cross-sections correspond to those in the map.

The structural trend in the northern sector of the Mekkam inlier (cross-sections K-K' and L-L'; Figures 3.10 and 3.11) is dominated by NE-SW (western part) and NW-SE (eastern part) crenulation upright folds. The S1/S0 relationships indicate west-vergences, which, together with reverse polarity criteria, suggest a dominant D1 overturned limb.

In the easternmost sector of the inlier (cross-section N-N', Figures 3.10 and 3.11), S0, S1, and L1 are mainly oriented NW-SE due to the presence of Sc1 crenulation folds. In the Dc synform, the stratigraphic polarity is reverse, which, together with the relationship between S1 and S0 showing local SW-vergence, indicates the presence of an overturned limb of a kilometric-scale D1 fold. Opposite relationships and polarities were observed in the corresponding Dc antiform (cross-section N-N', Figure 3.11).

The DMMS deformed by D1 are unconformably overlain by Viséan sediments cropping out in relatively small outcrops in the southern and southeastern parts of the Mekkam inlier (Figure 3.2). The angular unconformity is well exposed NW of Hassiane Ed Diab (Loukrayma area, Figures 3.3F and 3.10) and in a small and tectonized outcrop in the Tafarine area (Figure 3.10). In both outcrops, the D1 structures do not penetrate into the Viséan sediments, which, in turn, are only affected by the NE-SW trending crenulation cleavage (Sc2) observed in the DMMS.

In the Loukrayma area, the Viséan unconformity is partially affected by an important WNW-ESE trending semi-brittle shear zone with dextral strike-slip kinematics, which produced a tectonized band of at least 500 m-thick in the DMMS.

4.5. Building up a composite cross-section of the Debdou-Mekkam region

The above descriptions show that the Debdou-Mekkam region is characterized by a series of pre-Late Viséan tight to isoclinal, inclined to recumbent, plurikilometric D1 folds (Figure 3.12) with a related axial-planar main foliation S1. The L1 map delineated in Figure 3.12 shows important strike variations from NW-SE, through N-S, NE-SW, to E-W, being the relative regional vergence towards the NE, E, SE and S respectively.

In the Debdou inlier (cross-sections 1-1' to 4-4'; Figure 3.12), the folds are asymmetric with axial surfaces moderately dipping towards the west. The direction of D1 structures changes from NW-SE (cross-section 1-1') to NNE-SSW (cross-sections 2-2' and 3-3'), and then again to NW-SE (cross-section 4-4'). The regional vergence is towards the east, with the normal limbs dominated by normal polarities and local east-vergences while the overturned limbs show reverse polarities and local west-vergences. As a whole, this inlier is characterized by the regular alternation of normal and overturned limbs. The moderately inclined D1 folds in this inlier are scarcely affected by the later Dc deformations.

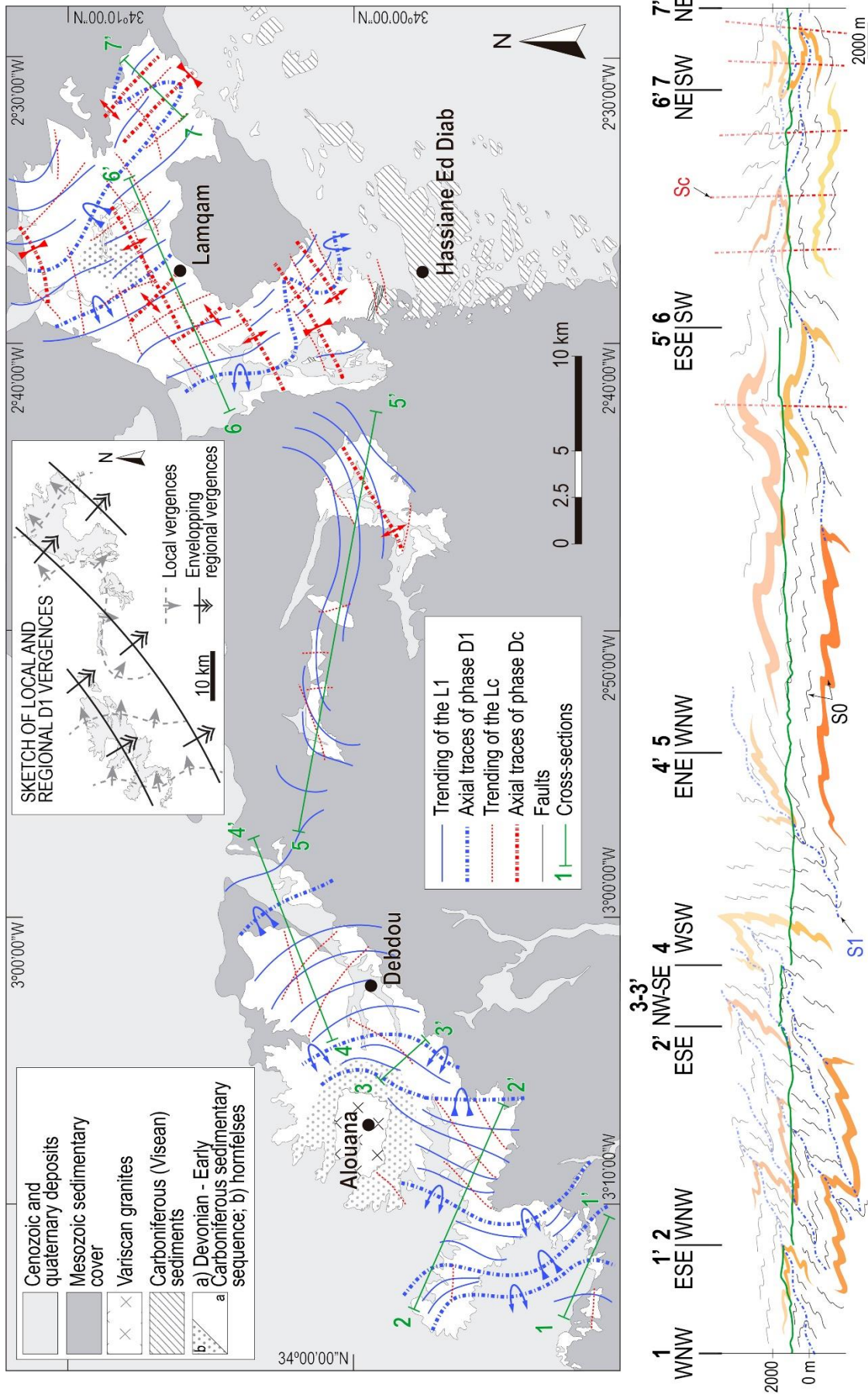


Figure 3.12 (previous page). Synthetic map and cross-sections of the Debdou-Mekkam region. Colors of the different structural elements in the cross-sections correspond to those in the map. Inset: sketch of the local and regional vergences of the D1 structures. See Figure 3.1B for a more general geological sketch with the location of the inliers.

The D1 Debdou fold train continues towards the east across the Lalla Mimouna-Oued Awam inliers. From the easternmost part of the Debdou inlier to the southwestern part of the Mekkam inlier, a D1 normal limb approximately 30 km-long is reconstructed (cross-section 5-5'; Figure 3.12). S0 and S1 are mostly subhorizontal, and the stratigraphic polarity dominantly normal. Toward the east, the SW-NE trending upright crenulation folds become more penetrative with a kilometric-scale antiform deforming the previous structures (cross-section 5-5' in Figure 3.12). Along this plurikilometric D1 normal limb, the structural trend is rotated, from west to east: in the western part L1 is rotated clockwise changing from NW-SE to E-W; on the contrary, in the eastern part, L1 trend rotates counterclockwise from E-W to NNW-SSE (Figure 3.12).

The axial surface of the D1 anticline whose c. 30 km-long normal limb crops out in the Lalla Mimouna-Oued Awam inliers, emerges in the SW sector of the Mekkam inlier, where it is folded by SW-NE trending upright crenulation folds (Dc). Here, the D1 normal limb crops out in the core of a Dc synform, and is underlain by a new overturned limb that appears in Dc antiforms located towards the SE and NW (Figure 3.11). L1 is crenulated by Dc folds and trends SE-NW. Towards the north, this overturned limb appears flat-lying in a wide area west of Lamqam village, maintaining the same L1 trend (western segment of cross-section 6-6', Figure 3.12). Moreover, just to the north of Lamqam, the axial surface of the D1 anticline dips towards the NE (refolded plunging anticline), thus causing the overlying normal limb to crop out again (eastern segment of cross-section 6-6', Figure 3.12). Further east, this normal limb is overlain by a new overturned limb, and the axial surface between them is deformed by NW-SE upright crenulation folds (cross-section 7-7', Figure 3.12). In that sector, L1 maintains the NW-SE trend but, towards the NW, it rotates to N-S and then to SW-NE due to WSW-ENE crenulation folds. Overall, the crenulation deformations are more penetrative in the Mekkam inlier than in the western inliers. Besides the variable development of the low-dipping crenulation cleavage, the occurrence of NE-SW and NW-SE trending upright crenulation folds forms a dome-and-basin-like interference pattern that makes the D1 structure in the Mekkam inlier to be, on average, flat-lying.

5. Discussion

5.1. Age of the Debdou-Mekkam Metasediments

Previous dating of the DMMS based on fossil plant fragments (Médioni, 1980) and palynomorphs (Marhoumi, 1984; Marhoumi et al., 1983) gave Early Carboniferous and Middle-Late Devonian biostratigraphic ages, respectively. Our detrital zircon geochronological study (Section 3.1) constrainsthe maximum depositionalage of the

DMMS at Late Devonian (more specifically Famennian) according to the youngest zircon population observed in four of the five samples. Therefore, our U-Pb data indicate that a younger putative age for the DMMS deposition would be compatible with the Early Carboniferous ages deduced from fossil plant fragments, but not with the Middle-Late Devonian ages suggested by palynomorphs, which would probably represent redeposited material. The real depositional age of the DMMS can be constrained by taking into account the series of subsequent events, specifically D1 deformation, emersion, partial erosion, renewed subsidence and unconformable sedimentation of the overlying Late Viséan succession, this latter well dated with brachiopods and polyps (Médioni, 1979 and references therein). In our preferred interpretation, the deposition of the DMMS occurred at Late Devonian time (Late Frasnian to Late Famennian), while D1 deformation likely occurred during Early Carboniferous (Tournaisian). Nonetheless, the presence of fossil plant fragments (Médioni, 1980) suggests that the deposition of the DMMS might have continued until the Early Carboniferous. In this case, the D1 deformational event, and the subsequent emersion/erosion would have occurred in a very short time span (1-5 Ma?), i.e., sedimentation would not cease until the Early Tournaisian, while D1 deformation would have occurred during Late Tournaisian-Early Viséan time.

A closer examination of the average maximum depositional ages suggests, not without uncertainty, an eastward younging direction (see Figure 3.2 for sample location): from 375 Ma (2 data from sample DEB2), to 370 Ma (4 data from sample MIM2), and c. 362 Ma ($n = 7, 9$ and 4 from samples OUI10, OUI11 and OUI13, respectively). This observation is in accordance with our interpretation that the DMMS represents a fore-arc basin fed by a close active magmatic (zircon-forming) arc, which was probably migrating towards the SE in relation to the subduction of the Rheic oceanic lithosphere underneath an Avalonian promontory (see Sections 5.2 and 5.4). In this scenario, the neo-formed zircons would have been rapidly incorporated into the neighboring fore-arc basin and, therefore, the zircon crystallization ages and the maximum depositional ages of the sediments would be almost coeval. Furthermore, if the sedimentation continued during the Early Tournaisian, the youngest part of the DMMS would have been deposited in a foreland basin fed by the dismantling of the already inactive Devonian magmatic arc.

5.2. Detrital zircon provenance in the Debdou-Mekkam Metasediments

With the exception of the Devonian population, the relevant old inherited detrital zircon populations in the DMMS samples are the prevalent Ediacaran peak (c. 620 Ma), a secondary middle Paleoproterozoic peak (c. 2.1 Ga), and sometimes a Neo-Archean minor population (c. 2.5 Ga; Figure 3.4). These populations are respectively related to primary sources of Cadomian/Pan-African, Eburnean and Liberian ages, which were formed by successive orogenies in northern Gondwana, and they are globally interpreted as indicative of West African Craton (WAC) affinity (e.g., Nance et al., 2008 and references therein). Recent U-Pb geochronological data on detrital zircons from the Ordovician-Devonian passive margin sequence of the para-autochthonous Eastern Moroccan Meseta (Accotto et al., 2019; Ghienne et al., 2018) highlighted the presence of

these detrital zircon populations and inferred their primary WAC affinity. In addition, these studies also found a Tonian-Stenian (c. 1 Ga) population, and a Mesoproterozoic (c. 1.7-1.1 Ga) gap which, considered together, point to NE-Africa secondary sources (Saharan Metacraton and/or Arabian-Nubian Shield), instead of Grenville (Amazonian) sources (Accotto et al., 2019; Ghienne et al., 2018). However, the new data provided in this study include a minor but remarkably continuous zircon content (up to 13.6%) in the c. 0.9-1.9 Ga time span (Figure 3.4H). Sources of these ages are virtually unknown in the WAC, unless in the Rokelides (De Waele et al., 2015; Villeneuve et al., 2015) and in the Bassarides (Brinckmann and Meinhold, 2007; Villeneuve et al., 2015). Nevertheless, these potential detrital zircon source areas (southern WAC) are a long way from the Eastern Moroccan Meseta and, more importantly, if they were the source of our Mesoproterozoic detrital zircon grains, similar ages would have been encountered also in detrital zircon grains from other Variscan domains located between the source regions and the studied area (*e.g.*, the Anti-Atlas region; Abati et al., 2010; Avigad et al., 2012), which is not the case. On the other hand, c. 0.9-1.9 Ga ages are typical of an Amazonian-type basement, which suggests that the Precambrian zircon inheritance in our samples is from both WAC and Amazonian-type basements, *i.e.*, they contain Gondwanan- and Avalonian-derived detrital zircons. The most plausible explanation for the presence of zircon grains derived from an Amazonian/Avalonian source resides in the commonly accepted paleogeographic attribution of Avalonia as part of northern Gondwana during Neoproterozoic-Cambrian time (Figure 3.13A), which is prior to its northward Early Paleozoic drift during the opening of the Rheic Ocean (Figure 3.13B). In fact, Avalonia is thought to have been located in a western position of the northern Gondwana margin during the Neoproterozoic-Cambrian time, and therefore connected not only to the WAC, but also to Amazonia (*e.g.*, Cocks & Fortey, 2009; Linnemann et al., 2012; Murphy et al., 2006).

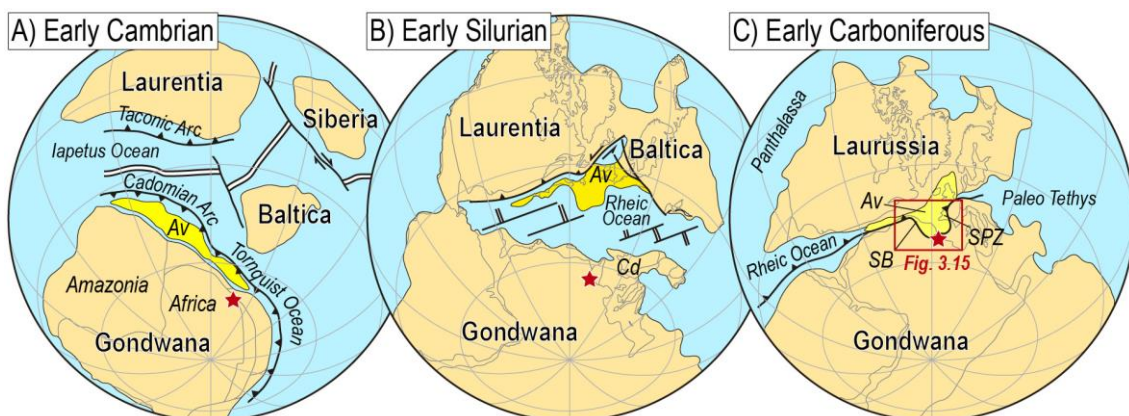


Figure 3.13. Paleogeographic reconstruction of the main continents during Early Cambrian (A), Early Silurian (B), and Early Carboniferous times (C). Av: Avalonia, Cd: Cadomia, SB: Sehouli Block, SPZ: South Portuguese Zone (after Murphy et al., 2016 and references therein; Nance et al., 2012 and references therein). Red stars indicate the approximate location of the studied area.

An outstanding feature of our zircon study is the presence of a Devonian detrital zircon population (c. 360-390 Ma, peak at c. 376 Ma; Figure 3.4). The content of Devonian

detrital zircons in the analyzed samples is very variable (1.4% in sample DEB2, up to 37% in sample OUI13), which can be taken as evidence of a nearby and immature (heterogeneous) source, instead of a homogeneous one. Furthermore, the generally almost idiomorphic morphology of the Devonian detrital zircon grains (see Appendix C) suggests a limited transportation of the sediments, in agreement with a relatively close source.

When considering a source for these Devonian zircon grains, the absence of outcropping igneous rocks of these ages in all NW-Africa must be stressed. The only exception is the Sehoul Block in Western Morocco (Figure 3.1; see Section 1), where Famennian (c. 367 Ma; U/Pb on igneous zircons) granites are exposed and postdate a presumably middle Paleozoic (Caledonian?) deformation (Tahiri et al., 2010). Just north of the Moroccan Variscides, in SW Iberia, Late Paleozoic metasediments from both the South Portuguese and Ossa-Morena Zones also provided Middle-Late Devonian detrital zircon populations, interpreted as derived from an unexposed magmatic arc, active along the Avalonian convergent margin during the Middle-Late Devonian subduction of the Rheic Ocean (Pereira et al., 2012, 2017; Pérez-Cáceres et al., 2017). Similarly, and based on the comparable ages of the Devonian detrital zircon populations and the paleogeographic vicinity between the Iberian and Moroccan Variscides, we interpret the DMMS as being primarily derived from a Devonian magmatic arc formed in the Avalonian margin, as a consequence of the northward subduction of the Rheic oceanic lithosphere. Furthermore, the hypothesis of a convergent/collisional geodynamic setting, in which the DMMS were deposited, is also supported by the comparison between the Cumulative Probability Plots of our samples and the areas defined by Cawood et al. (2012) for different geodynamic contexts (Figure 3.4F).

The Hf isotope analyses carried out on the Devonian zircons of the DMMS show a vertical ϵ_{Hf} array varying from +8.5 to -6.5, with T_{NC} ranging from c. 0.6 Ga to c. 1.6 Ga (Figure 3.5E). Despite this variability, most ϵ_{Hf} data are positive and suggest that these zircon grains formed from a magma generated by partial melting of Neoproterozoic continental crust. Nevertheless, some interaction with older Mesoproterozoic continental basement might also have occurred, which would account for the older model ages (T_{NC}) and the slight negative ϵ_{Hf} values recorded in MIM2. Very similar results were obtained by Pereira et al. (2017) in the Devonian zircon grains from SW Iberia (Figure 3.14A). Furthermore, the comparison between the Hf isotopic signature of our older data (> 450 Ma; Figure 3.14B) with those from Avalonian terranes (Henderson et al., 2018 and references therein) and the WAC (Abati et al., 2012; Avigad et al., 2012) shows similar distributions of the Ediacaran-Cryogenian (c. 620 Ma) and Paleoproterozoic (c. 2.1 Ga) main detrital zircon populations, suggesting that these terranes had a common evolution in North Gondwana (including both the Cadomian and Eburnean orogenies). The quite abundant Mesoproterozoic population in Avalonia, which is absent in the WAC (gap between c. 1.1 and 1.8 Ga), shows the majority of ϵ_{Hf} values between c. +10 and c. -10, being many of them slightly positive (from c. +5 to c. 0); a comparable distribution is found in our samples (Figure 3.14B), indicating that an Avalonia-type basement could have supplied detrital zircons to the DMMS.

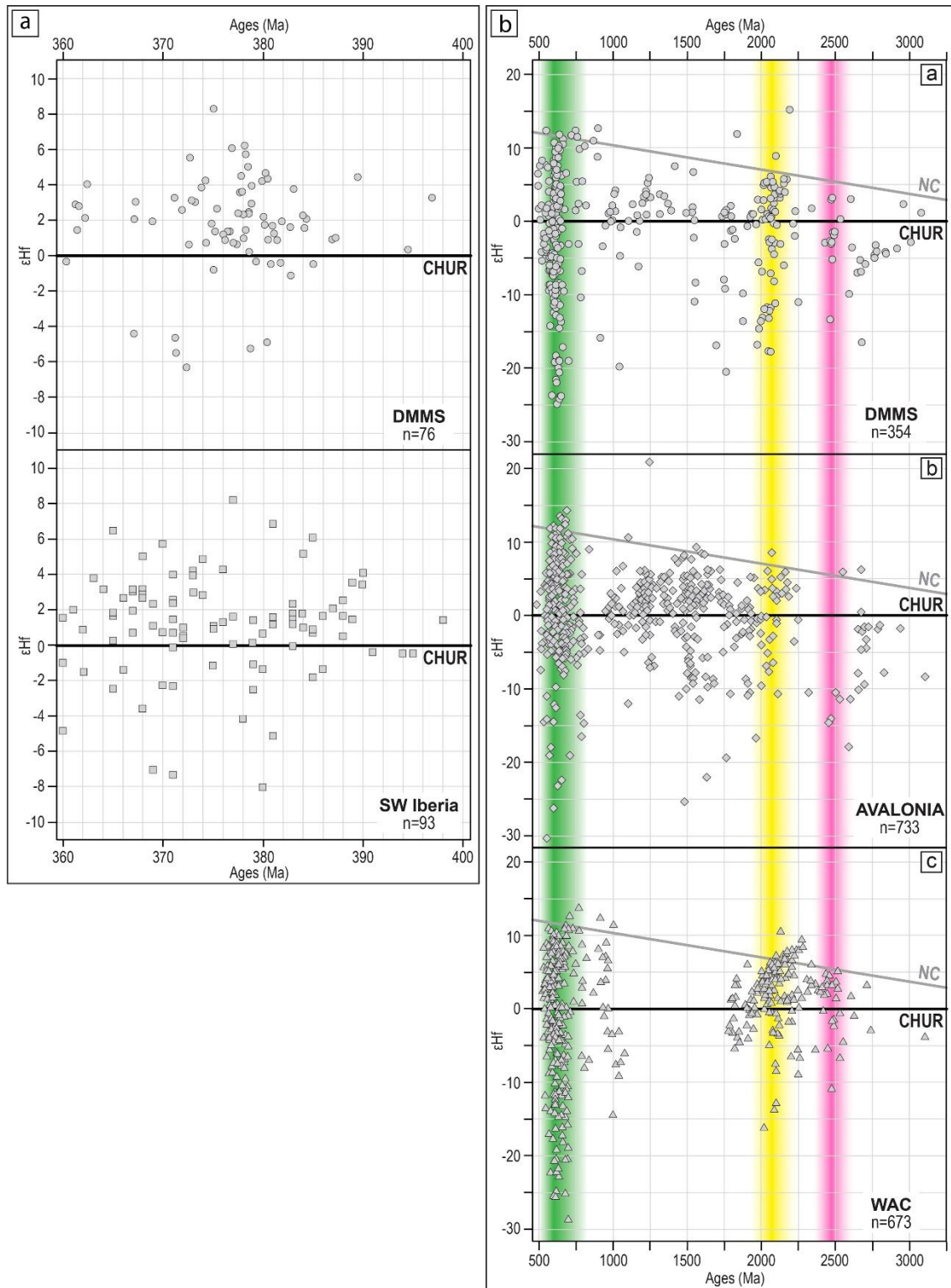


Figure 3.14. Comparison of Hf isotopic data of detrital zircon grains: (A) comparison between Devonian (400-360 Ma) data from DMMS (a: this work) and from SW Iberia (b: Pereira et al., 2017); (B) comparison among pre-Devonian (3250-450 Ma) data from DMMS (a: this work), Avalonian terranes (b: modified from Henderson et al., 2018 and references therein), and WAC (c: Abati et al., 2012; Avigad et al., 2012). Colors indicate some of the main detrital zircon populations identified in this work: Ediacaran-Cryogenian (green), Paleoproterozoic (yellow), and Archean (pink).

As a whole, our Hf isotope data provide additional evidence for the deposition of the DMMS in a fore-arc (and/or foreland) geological setting fed by both the north Gondwanan margin (WAC source) and a Devonian magmatic arc built on a Neoproterozoic crustal basement that included subordinate Mesoproterozoic Avalonia-derived igneous rocks. In this respect, both the Sehoul Block and the South Portuguese Zone are considered Avalonia-derived terranes (Michard et al., 2010; Pérez-Cáceres et al., 2017; Simancas et al., 2005; Tahiri et al., 2010 and references therein), i.e., they are nearby examples of a source type for the DMMS, which would include a Middle-Late Devonian continental magmatic arc with the Avalonian basement.

5.3. Original vergence of D1 folds

Our structural study focused on D1 folds across the investigated region (Section 4). The structural map in Figure 3.12 shows a complicated pattern for the trends of L1 intersection lineation (S0/S1) and the inferred axial traces of D1 folds (see Section 4.5 for a summary of D1 trends and Dc interference patterns). The simplified trend of D1 folds changes from NNW-SSE in the Debdou inlier, with ENE-vergence, to E-W in the Lalla Mimouna-Oued Awam inliers, with S-vergence, and, finally, to NW-SE in the Mekkam inlier, with NE-vergence, depicting an apparent clockwise rotation between the Debdou and Lalla Mimouna-Oued Awam inliers and a counterclockwise one between the latter and the Mekkam inlier (sketch in Figure 3.12). Accordingly, the local vergence on the D1 normal limbs is towards the ENE in the Debdou inlier, towards the south in the Lalla Mimouna-Oued Awam inliers, and towards the NE in the Mekkam inlier (grey arrows in the sketch in Figure 3.12). The pronounced curved trend of D1 folds, if restored to an original straight orientation, results in an average SW-NE trend with SE vergence on the normal limbs (sketch in Figure 3.12). We interpret that most of the present-day curvature of D1 folds is due to the post-Visean upright crenulation folds (Dc), as observed in some sectors of the Mekkam inlier (Figure 3.10). However, part of the curved trend of D1 folds might be primary, i.e., D1 folds could have been formed with an oscillatory trend that was later tightened by the upright crenulation folds. The reason for this putative primary undulated fold pattern is uncertain, although it can be speculated that the arcuate edge (at scale of tens of kilometers) of a southeastward-pushing crustal block could have formed a slightly curved D1 fold belt (see section 5.4).

5.4. Proposing a large-scale plate tectonic scenario

The Moroccan Variscides are generally viewed as an intracontinental part of the Variscan-Alleghanian orogenic system, developed on the northern Gondwanan margin and constituted by a number of tectonic domains bounded by crustal-scale strike-slip shear zones (*e.g.*, Hoepffner et al., 2005, 2006; Michard et al., 2010). The absence of ophiolitic rocks and high-pressure belts seems to support this interpretation. However, the presence of Devonian granites, which postdate the ductile (seemingly Caledonian) deformation observed in the Sehoul Block, suggests a non-Gondwanan origin for this domain and points to a cryptic suture, namely the Rheic Ocean suture, between itself and

the rest of the Moroccan Variscides (*e.g.*, Hoepffner et al., 2005; Michard et al., 2010 and references therein; Simancas et al., 2005; Tahiri et al., 2010). To the south, this cryptic suture has also been inferred in the Souttoufides (western Saharan belts; Figure 3.1A), by the recognition of “exotic” (Laurentian-derived) terranes (*e.g.*, Gärtner et al., 2013; Villeneuve et al., 2015), and in the Mauritanides (the southernmost outcropping transect of the Variscan-Alleghanian orogenic system in Africa; *e.g.*, Villeneuve, 2008; Villeneuve et al., 2010). To the north, the Rheic Ocean suture is masked in SW Iberia at the boundary between the Ossa Morena Zone and the South Portuguese Zone (*e.g.*, Braid et al., 2011; Pérez-Cáceres et al., 2015, 2017). Further north, the identification of the Rheic Ocean suture in the allochthonous complexes of NW Iberia is uncertain (*e.g.*, Arenas et al., 2014; Martínez Catalán et al., 2019).

The flysch nature (turbidites with coarse-grained greywackes), great thickness (more than 10 km according to an approximate restoration of our synthetic cross-section in Figure 3.12) and intense deformation (D1 folding accounting for important tectonic shortening) that characterize the Late Devonian-earliest Carboniferous DMMS have no equivalent in nearby Paleozoic inliers of the Eastern Moroccan Meseta. In this area (Beni Snassene, Oujda, and Jerada inliers; Figure 3.1B), a relatively thin pre-Carboniferous passive margin sequence is weakly deformed, together with the overlying Early Carboniferous succession, by E-W upright open folds. Furthermore, the deformation decreases to the west and southwest: in the Western Moroccan Meseta, NW- to NNE-trending upright folds associated with spaced cleavage and low- to very low-grade metamorphism were described, together with NNE-SSW transtensional basins, while the Coastal Block is characterized by NNE-trending upright open folds and no metamorphism (Hoepffner et al., 2006).

The Moroccan Meseta at Ordovician-Devonian time was part of the northwestern continental passive margin of Gondwana with the Rheic Ocean developed to the N and NW (Figure 3.13B). The counterpart was the Laurussia continental margin, which resulted from the middle Paleozoic Caledonian-Acadian collision between Avalonia and Laurentia-Baltica. The subduction of the Rheic Ocean began at Middle Devonian time and a magmatic arc formed along the Avalonian margin (Nance et al., 2010, 2012; Pereira et al., 2017). The subduction continued during Late Devonian (Figure 3.15A) with the partial closure of the Rheic Ocean at the frontal part of an Avalonian promontory (Simancas et al., 2005; Figure 3.15B). At the Famennian (and Tournaisian?) time, the Late Devonian magmatic arc and its Avalonian basement experienced denudation giving way to thick turbiditic flysch sedimentation (*e.g.*, DMMS) took place in a basin located in the fore-arc region, and likely attesting the oceanic trench that separated the Avalonian magmatic arc from the Gondwana continental passive margin (Figure 3.15B). The sediments were supplied mainly by erosion of the adjacent upper plate (Avalonian basement and its Middle-Late Devonian magmatic arc), but mature detritus could have also been provided from the WAC as pointed out by the presence of a relatively important Paleoproterozoic detrital zircon population, which is less abundant in Avalonian terranes. The advance of the Avalonian front towards the SE might have produced the coeval migration of the depocenter in the DMMS basin throughout the Famennian.

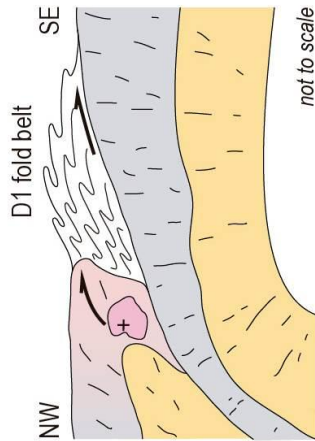
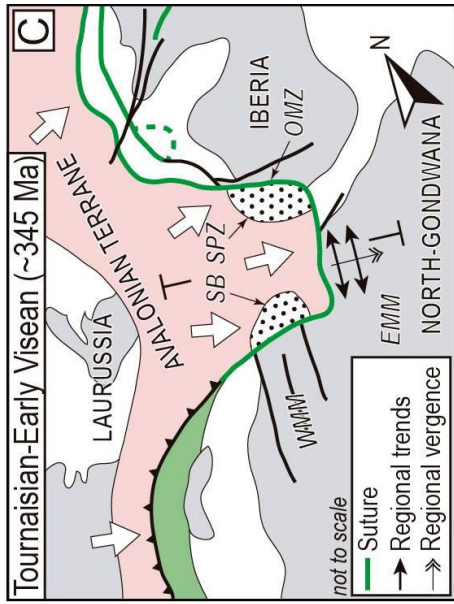
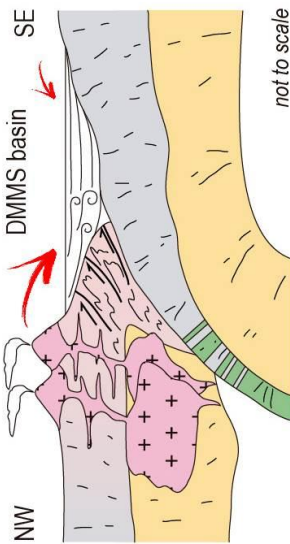
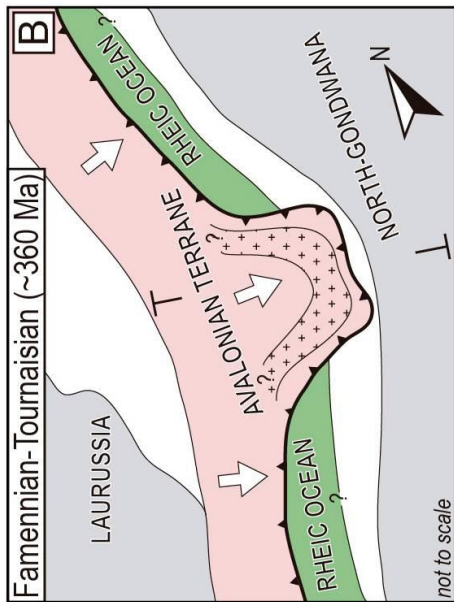
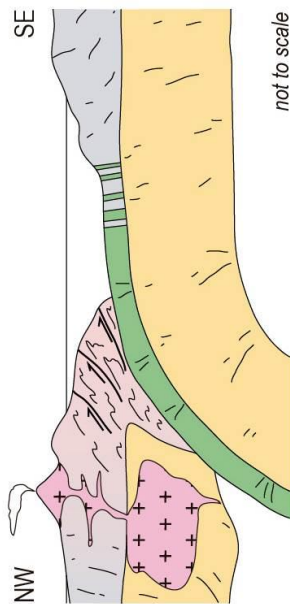
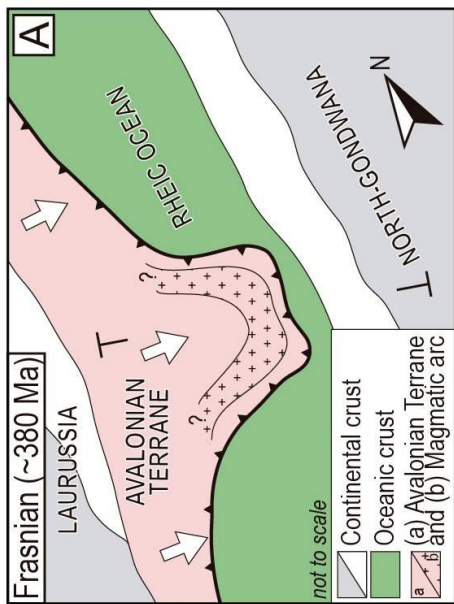


Figure 3.15 (previous page). Schematic large-scale evolution of the studied region between Frasnian and Tournaisian time. SH: Sehou Block; WMM: Western Moroccan Meseta; EMM: Eastern Moroccan Meseta; SPZ: South Portuguese Zone; OMZ: Ossa-Morena Zone (modified from Pereira et al. (2017) and Simancas et al. (2005)).

At Early Carboniferous time (Tournaisian-Early Viséan), continued convergence between the Avalonian promontory and Gondwana cut sediment supply to the DMMS basin and triggered compressive collisional deformation (D1 folding; Figure 3.15C). Thus, km-scale NE-SW trending SE-verging inclined to recumbent folds formed due to the south-eastward pushing of the overriding Avalonian promontory located to the NW of the DMMS basin. The geometry and outcropping (visible) size of the D1 fold belt (Figure 3.12) entails a considerable NW-SE shortening that implies the existence of a basal detachment between the folded belt and its relative para-autochthonous, which is the passive margin sequence of North Gondwana exposed in the neighbouring inliers (Beni Snassene, Oujda; Figure 3.1B). Unfortunately, the D1 deformation front and the transition to its relative Gondwanan foreland are not exposed.

The low- to very low-metamorphic grade of the DMMS suggests that these rocks never reached deep orogenic conditions and thus D1 deformation occurred at a relatively high structural level, i.e., the DMMS were not deeply underthrust below the Avalonian crust. Furthermore, the age of the Eo-Variscan metamorphic event proposed by Huon et al. (1987) based on K-Ar analyses of allegedly metamorphic illite grains from the Debdou and Mekkam inliers (372.3 ± 8.1 Ma and 368.3 ± 7.9 Ma, respectively) is overestimated according to our detrital zircon ages. These ages are older than, or coeval with, the maximum depositional ages of the DMMS deduced from the youngest detrital zircon population. We suggest that D1 occurred shortly after the deposition of the DMMS, in accordance with the proposed continued southeastwards advance of the adjacent Avalonian promontory. Furthermore, D1 occurred before the formation of the Viséan unconformity, since the Late Viséan sediments were not affected by this deformational event. Therefore, D1 should have occurred at Tournaisian-Early Viséan time.

Concerning the Avalonian nature of the continental promontory that collided with the Gondwanan margin (Figure 3.13C) to generate the SE-verging km-scale D1 folds in the Eastern Moroccan Meseta, the existence of neighbouring terranes interpreted as Avalonian derived supports our model. To the north, in SW Iberia, Devonian detrital zircons were interpreted as remnants of a missing subduction-related (Avalonian?) magmatic arc (Pereira et al., 2012), while the South Portuguese Zone is considered part of the Avalonian terrane (Pérez-Cáceres et al., 2017 and references therein), and its boundary with the adjacent Ossa-Morena Zone hides the Rheic suture (Pérez-Cáceres et al., 2015, 2016). The dominant left-lateral kinematics along the Ossa-Morena-South Portuguese Zone boundary agrees with the paleogeographic location of SW Iberia on the northern side of the Avalonian salient (Figure 3.15C). The southern side of that promontory would be represented by the Caledonian Sehou Block (Figure 3.15C; Simancas et al., 2005; Tahiri et al., 2010), where a Late Carboniferous brittle thrust would have obliterated previous right-lateral kinematics concomitant to the left-lateral one occurred in SW Iberia. In-between SW Iberia and the Sehou Block, the southeastwards

frontal impingement of the Avalonian promontory would have produced the km-scale SE-vergent recumbent folds in the Eastern Moroccan Meseta.

To sum up, the Early Carboniferous collisional deformation and detrital zircon isotopic data (U-Pb and Hf) recorded by the DMMS provide with indirect evidence on the location of a cryptic Rheic Ocean suture in the Eastern Moroccan Meseta, separating Avalonia and northern Gondwana (Figure 3.13C). In this context, correlations with other suture contacts can be proposed in an attempt to reconstruct the large-scale Variscan scenario. To the west of the Eastern Moroccan Meseta, the suture would continue concealed by the thrust of the Sehouf Block onto the Western Moroccan Meseta (Tahiri et al., 2010) and, further south, in the Souttoufides and, perhaps, the Mauritanides (Villeneuve et al., 2015). To the north of the Eastern Moroccan Meseta, the Rheic Ocean suture appears blurred in SW Iberia (Pérez-Cáceres et al., 2015), and prolongs between SW England and other European Variscan Massifs in France, Belgium, Germany and Czech Republic (*e.g.*, Franke et al., 2017; Martínez Catalán et al., 2019; Shail & Leveridge, 2009).

6. Conclusions

The DMMS constitutes a low- to very low-grade intensely deformed siliciclastic succession, previously attributed to either Middle-Late Devonian or Early Carboniferous ages. New U-Pb ages on detrital zircons constrain the maximal depositional age at Late Devonian and, therefore, are compatible with Early Carboniferous deposition. However, the fact that the DMMS underwent the main deformational event (D1) prior to the deposition of the unconformable Upper Viséan sediments, together with the euhedral morphologies of the Devonian detrital zircons, points to deposition at Late Devonian time (or no later than Early Tournaisian) and subsequent deformation at Early Carboniferous time (Tournaisian-Early Viséan).

Apart from the Late Devonian detrital zircon population, the DMMS shows the common presence of Ediacaran and Paleoproterozoic populations compatible with a northern WAC source. Furthermore, a conspicuous amount of scattered grains with ages between 1.9 Ga and 0.9 Ga evokes the possibility of an exotic source that might be found in the basement of an Avalonian promontory approaching the northern margin of Gondwana during the closure of the Rheic Ocean at Late Devonian time. These Avalonia-derived terranes crop out in the South Portuguese Zone in SW Iberia, and in the Sehouf Block in NW Morocco. Furthermore, the Hf isotopic signature of the Devonian detrital zircons suggests that they might be sourced in a subduction related magmatic arc located on the Avalonian margin, in which reworking of Neo- and Mesoproterozoic Avalonian crust would have occurred. Thus, the DMMS would represent turbiditic deposits in a fore-arc (and/or foreland) basin.

The deformational events that affected the Debdou-Mekkam massif are: (i) a main D1 event characterized by tight to isoclinal folds and slaty cleavage, with regional NE-SW trend and SE vergence, which occurred at Early Carboniferous (probably Tournaisian) time; and (ii) a late Dc event (or events) responsible for upright open to tight folds and

crenulation cleavage, which affected both the DMMS and the overlying Upper Visean succession. The main deformation D1 accounts for regional shortening that occurred during the first phases of the collision between the northern passive margin of Gondwana and an Avalonian promontory. In this scenario, the Avalonian block over-thrusted the Gondwanan margin, giving way to the SE-verging D1 structures. Therefore, the DMMS attests to sedimentation related to the denudation of a missing Late Devonian magmatic arc and subsequent Early Carboniferous collisional deformation triggered by an Avalonian promontory that approached the Gondwana margin after the consumption of the Rheic Ocean lithosphere. In this context, the DMMS might represent a syn-orogenic Eo-Variscan basin witnessing the cryptic oceanic suture between Avalonia and Gondwana in the Eastern Moroccan Meseta.

Acknowledgments

This study was funded by the Ministerio de Economía y Competitividad (MINECO) of Spain through the project PANGEATOR (CGL2015-71692-P) and the Doctoral scholarship BES-2016-078168. GeoHistory Facility instruments were funded via an Australian Geophysical Observing System grant provided to AuScope Pty Ltd. by the AQ44 Australian Education Investment Fund program. The NPII multi-collector was obtained via funding from the Australian Research Council LIEF program (LE150100013). The authors want to express their gratitude to Dr. Manuel Francisco Pereira (University of Évora, Portugal) and Dr. Michel Villeneuve (Centre Européen de Recherche et d'Enseignement des Géosciences de l'Environnement, France) for their constructive reviews that helped to improve the quality of the original manuscript. Special thanks to Brad McDonald (Curtin University, Australia) for technical assistance regarding LA-ICPMS and Hf analyses, Profs. Abdelfatah Tahiri (University Mohammed V of Rabat, Morocco) and Hassan El Hadi (University Hassan II of Casablanca, Morocco) for their support during field work, Prof. Yvette Kuiper (Colorado School of Mines, USA) for her precious hints about the interpretation of Hf data, and Dr. Lorenzo Valetti for proof reading the manuscript.

Supporting information can be obtained in Appendix A to E and in Mendeley Data: <http://dx.doi.org/10.17632/b8fdbykmbx.1> (<https://data.mendeley.com/datasets/b8fdbykmbx/draft?a=eaae2da0-8e22-4056-861b-4824984f1c10>).

References

- Abati, J., Aghzer, A.M., Gerdes, A., & Ennih, N. (2012). Insights on the crustal evolution of the West African Craton from Hf isotopes in detrital zircons from the Anti-Atlas belt. *Precambrian Research* 212–213, 263–274. doi:10.1016/j.precamres.2012.06.005

- Abati, J., Mohsine Aghzer, A., Gerdes, A., & Ennih, N. (2010). Detrital zircon ages of Neoproterozoic sequences of the Moroccan Anti-Atlas belt. *Precambrian Research*, 181(1–4), 115–128. <https://doi.org/10.1016/j.precamres.2010.05.018>
- Accotto, C., Martínez Poyatos, D. J., Azor, A., Talavera, C., Evans, N. J., Jabaloy-Sánchez, A., et al. (2019). Mixed and recycled detrital zircons in the Paleozoic rocks of the Eastern Moroccan Meseta: Paleogeographic inferences. *Lithos*. <https://doi.org/10.1016/j.lithos.2019.04.011>
- Avigad, D., Gerdes, A., Morag, N., & Bechstädt, T. (2012). Coupled U-Pb-Hf of detrital zircons of Cambrian sandstones from Morocco and Sardinia: Implications for provenance and Precambrian crustal evolution of North Africa. *Gondwana Research*, 21(2–3), 690–703. <https://doi.org/10.1016/j.gr.2011.06.005>
- Arenas, R., Díez Fernández, R., Sánchez Martínez, S., Gerdes, A., Fernández-Suárez, J., & Albert, R. (2014). Two-stage collision: Exploring the birth of Pangea in the Variscan terranes. *Gondwana Research*, 25(2), 756–763. <https://doi.org/10.1016/j.gr.2013.08.009>
- Azor, A., Rubatto, D., Simancas, J.F., González Lodeiro, F., Martínez Poyatos, D., Martín Parra, L.M., & Matas, J. (2008). Rheic Ocean ophiolitic remnants in southern Iberia questioned by SHRIMP U-Pb zircon ages on the Beja-Acebuches amphibolites. *Tectonics* 27, 1–11. doi:10.1029/2008TC002306
- Bell, A. M. (1981). Vergence: an evaluation. *Journal of Structural Geology*, 3(3), 197–202. [https://doi.org/10.1016/0191-8141\(81\)90015-8](https://doi.org/10.1016/0191-8141(81)90015-8)
- Blichert-Toft, J., & Albarède, F. (1997). The Lu-Hf isotope geochemistry of chondrites and the evolution of the mantle-crust system. *Earth and Planetary Science Letters*, 148(1–2), 243–258. [https://doi.org/10.1016/S0012-821X\(97\)00040-X](https://doi.org/10.1016/S0012-821X(97)00040-X)
- Brinckmann, J., & Meinhold, K.-D. (2007). La géologie de la Chaîne des Bassarides et des terrains environnants au Nord-Ouest de la Guinée: avec 16 tableaux, 5 annexes. Schweizerbart.
- Bouvier, A., Vervoort, J. D., & Patchett, P. J. (2008). The Lu–Hf and Sm–Nd isotopic composition of CHUR: Constraints from unequilibrated chondrites and implications for the bulk composition of terrestrial planets. *Earth and Planetary Science Letters*, 273(1–2), 48–57. <https://doi.org/10.1016/j.epsl.2008.06.010>
- Braid, J.A., Murphy, J.B., Quesada, C., & Mortensen, J. (2011). Tectonic escape of a crustal fragment during the closure of the Rheic Ocean: U-Pb detrital zircon data from the Late Palaeozoic Pulo do Lobo and South Portuguese zones, southern Iberia. *Journal of the Geological Society of London*. 168, 383–392. doi:10.1144/0016-76492010-104
- Cawood, P. A., Hawkesworth, C. J., & Dhuime, B. (2012). Detrital zircon record and tectonic setting. *Geology*, 40(10), 875–878. <https://doi.org/10.1130/G32945.1>

- Chu, N.-C., Taylor, R. N., Chavagnac, V., Nesbitt, R. W., Boella, R. M., Milton, J. A., et al. (2002). Hf isotope ratio analysis using multi-collector inductively coupled plasma mass spectrometry: an evaluation of isobaric interference corrections. *Journal of Analytical Atomic Spectrometry*, 17(12), 1567–1574. <https://doi.org/10.1039/b206707b>
- Clauer, N., Jeannette, D., & Tisserant, D. (1980). Datation isotopique des cristallisations successives d'un socle cristallin et cristallophyllien (Haute Moulouya, Moyen Maroc). *Geologische Rundschau*, 69(1), 63–83. <https://doi.org/10.1007/BF01869024>
- Cocks, L. R. M., & Fortey, R. A. (2009). Avalonia: a long-lived terrane in the Lower Palaeozoic? *Geological Society, London, Special Publications*, 325(1), 141–155. <https://doi.org/10.1144/SP325.7>
- Desteucq, C., & Fournier-Vinas, C. (1981). Présence d'Ordovicien dans la région d'Oujda. *Mines, Géologie et Energie*, 50.
- De Waele, B., Lacorde, M., Vergara, F., & Chan, G. (2015). New insights on proterozoic tectonics and sedimentation along the peri-Gondwanan West African margin based on zircon U–Pb SHRIMP geochronology. *Precambrian Research* 259, 156–175. doi:10.1016/j.precamres.2014.08.008
- Dewey, J., & Bird, J. (1971). Origin and emplacement of the ophiolite suite: Appalachian ophiolites in Newfoundland. *Journal of Geophysical Research*, 76(14), 3179–3206. <https://doi.org/10.1029/JB076i014p03179>
- Dhuime, B., Hawkesworth, C., & Cawood, P. (2011). When Continents Formed. *Science*, 331(6014), 154–155. <https://doi.org/10.1126/science.1201245>
- Díez Fernández, R., & Arenas, R. (2015). The Late Devonian Variscan suture of the Iberian Massif: a correlation of high-pressure belts in NW and SW Iberia. *Tectonophysics*, 654, 96–100. <https://doi.org/10.1016/J.TECTO.2015.05.001>
- El Hadi, H., Tahiri, A., & Reddad, A. (2003). Les granitoïdes hercyniens post-collisionnels du Maroc oriental: une province magmatique calco-alcaline à shoshonitique. *Comptes Rendus Geoscience*, 335(13), 959–967. <https://doi.org/10.1016/j.crte.2003.09.003>
- El Hadi, H., Simancas, J. F., Tahiri, A., Gonzalez-Lodeiro, F., Azor, A., & Martinez Poyatos, D. (2006). Comparative review of the Variscan granitoids of Morocco and Iberia: proposal of a broad zonation. *Geodinamica Acta*, 19(2), 103–116. <https://doi.org/10.3166/ga.19.103-116>
- El Haibi, H., El Hadi, H., Tahiri, A., Martínez Poyatos, D.J., Gasquet, D., Pérez-Cáceres, I., et al. (2020). Geochronology and isotopic geochemistry of Ediacaran high-K calc-alkaline felsic volcanism: An example of a Moroccan perigondwanan (Avalonian?) remnant in the El Jadida horst (Mazagonia). *Journal of African Earth Science*, doi:10.1016/j.jafrearsci.2019.103669

- El Hassani, A., Tahiri, A., & Walliser, O. H. (2003). The Variscan Crust between Gondwana and Baltica. *CFS Courier Forschungsinstitut Senckenberg*, (242), 81–87.
- El Houicha, M., Pereira, M. F., Jouhari, A., Gama, C., Ennih, N., Fekkak, A., et al. (2018). Recycling of the Proterozoic crystalline basement in the Coastal Block (Moroccan Meseta): new insights for understanding the geodynamic evolution of the northern peri-Gondwanan realm. *Precambrian Research*, 306(March 2017), 129–154. <https://doi.org/10.1016/j.precamres.2017.12.039>
- Faryad, S. W., & Kachlik, V. (2013). New evidence of blueschist facies rocks and their geotectonic implication for Variscan suture(s) in the Bohemian Massif. *Journal of Metamorphic Geology*, 31(1), 63–82. <https://doi.org/10.1111/jmg.12009>
- Franke, W., Cocks, L. R. M., & Torsvik, T. H. (2017). The Palaeozoic Variscan oceans revisited. *Gondwana Research*, 48, 257–284. <https://doi.org/10.1016/j.gr.2017.03.005>
- Gärtner, A., Villeneuve, M., Linnemann, U., El Archi, A., & Bellon, H. (2013). An exotic terrane of Laurussian affinity in the Mauritanides and Souttoufides (Moroccan Sahara). *Gondwana Research*, 24(2), 687–699. <https://doi.org/10.1016/j.gr.2012.12.019>
- Ghienne, J. F., Benvenuti, A., El Houicha, M., Girard, F., Kali, E., Khoukhi, Y., et al. (2018). The impact of the end-Ordovician glaciation on sediment routing systems: a case study from the Meseta (northern Morocco). *Gondwana Research*, 63, 169–178. <https://doi.org/10.1016/j.gr.2018.07.001>
- Henderson, B.J., Collins, W.J., Brendan Murphy, J., & Hand, M. (2018). A hafnium isotopic record of magmatic arcs and continental growth in the Iapetus Ocean: The contrasting evolution of Ganderia and the peri-Laurentian margin. *Gondwana Research* 58, 141–160. doi:10.1016/j.gr.2018.02.015
- Hoepffner, C. (1977). Données nouvelles sur le Paléozoïques de la bordure occidentale du massif du Tazekka. *Comptes Rendus de l'Académie des Sciences de Paris*, 284(D), 1635–1637.
- Hoepffner, C. (1987). La tectonique hercynienne dans l'Est du Maroc. Université Louis Pasteur, Strasbourg.
- Hoepffner, C. (1989). L'évolution structurale hercynienne de la Méséta marocain orientale. Essai de mise au point. Notes & Memoires Du Service Géologique Du Maroc.
- Hoepffner, C., Houari, M. R., & Bouabdelli, M. (2006). Tectonics of the North African Variscides (Morocco, western Algeria): an outline. *Comptes Rendus - Geoscience*, 338(1–2), 25–40. <https://doi.org/10.1016/j.crte.2005.11.003>

- Hoepffner, C., Soullaimani, A., & Piqué, A. (2005). The Moroccan Hercynides. *Journal of African Earth Sciences*, 43(1–3), 144–165. <https://doi.org/10.1016/j.jafrearsci.2005.09.002>
- Huon, S., Piqué, A., & Clauer, N. (1987). Étude de l'orogénèse hercynienne au Maroc par la datation K-Ar de l'évolution métamorphique de schistes ardoisiers. *Sciences Géologiques, bulletins et mémoires*, 40(3), 273–284.
- Jackson, S.E., Pearson, N.J., Griffin, W.L. & Belousova, E.A. (2004). The application of laser ablation-inductively coupled plasma-mass spectrometry to in situ U–Pb zircon geochronology. *Chemical Geology*, 211, 47–69. <https://doi.org/10.1016/j.chemgeo.2004.06.017>
- Letsch, D., El Houicha, M., von Quadt, A., & Winkler, W. (2018). A missing link in the peri-Gondwanan terrane collage: the Precambrian basement of the Moroccan Meseta and its lower Paleozoic cover. *Canadian Journal of Earth Sciences*, 55(1), 1–19. <https://doi.org/10.1139/cjes-2017-0086>
- Linnemann, U., Herbosch, A., Liégeois, J. P., Pin, C., Gärtner, A., & Hofmann, M. (2012). The Cambrian to Devonian odyssey of the Brabant Massif within Avalonia: A review with new zircon ages, geochemistry, Sm-Nd isotopes, stratigraphy and palaeogeography. *Earth-Science Reviews*, 112(3–4), 126–154. <https://doi.org/10.1016/j.earscirev.2012.02.007>
- Marhoumi, M. R. (1984). Etude palynologique des séries dinantiennes de la Méséta marocaine. Conséquences stratigraphiques et structurales. Université Louis Pasteur, Strasbourg.
- Marhoumi, M. R., Hoepffner, C., Doubinger, J., & Rauscher, R. (1983). Données nouvelles sur l'histoire hercynienne de la Meseta orientale au Maroc: l'âge dévonien des schistes de Debdou et du Mekkam. *Comptes Rendus de l'Académie Des Sciences de Paris*, 297(II), 69–72.
- Martínez Catalán, J.R., Collett, S., Schulmann, K., Aleksandrowski, P., & Mazur, S. (2019). Correlation of allochthonous terranes and major tectonostratigraphic domains between NW Iberia and the Bohemian Massif, European Variscan belt. *International Journal of Earth Science*. doi:10.1007/s00531-019-01800-z
- Martínez Catalán, J. R., Díaz García, F., Arenas, R., Abati, J., Castiñeiras, P., González Cuadra, P., et al. (2002). Thrust and Detachment systems in the Ordenes Complex (northwestern Spain): implications for the Variscan-Appalachian geodynamics. In J. R. Martínez Catalán, R. D. Hatcher Jr., R. Arenas, & F. Díaz García (Eds.), *Variscan-Appalachian dynamics: the building of the Late Paleozoic basement* (pp. 163–182). Geological Society of America, Special Paper 364.
- Matte, P. (2001). The Variscan collage and orogeny (480-290 Ma) and the tectonic definition of the Armorica microplate: a review. *Terra Nova*, 13(2), 122–128. <https://doi.org/10.1046/j.1365-3121.2001.00327.x>

- Médioni, R. (1979). Carte géologique du Maroc au 1/100.000. Feuille Hassiane Ed Diab. Notice explicative. Notes et Memoires Du Service Géologique Du Maroc, 227(bis), 64.
- Médioni, R. (1980). Mise au point stratigraphique sur les terrains carbonifères de la bordure septentrionale des Hauts-Plateaux marocains (massifs de Debdou, boutonnières de Lalla-Mimouna et du Mekam). Notes Du Service Géologique Du Maroc, 285(41), 25–37.
- Michard, A., Saddiqi, O., Chalouan, A., & Frizon de Lamotte, D. (2008). Continental evolution: the geology of Morocco. (S. Bhattacharji, H. J. Neugebauer, J. Reitner, & K. Stüwe, Eds.). Springer. <https://doi.org/10.1007/978-3-540-75761-0>
- Michard, A., Soulaïmani, A., Hoepffner, C., Ouanaimi, H., Baïdder, L., Rjimati, E. C., & Saddiqi, O. (2010). The South-Western Branch of the Variscan Belt: evidence from Morocco. *Tectonophysics*, 492(1–4), 1–24. <https://doi.org/10.1016/j.tecto.2010.05.021>
- Morel, M. L. A., Nebel, O., Nebel-Jacobsen, Y. J., Miller, J. S., & Vroon, P. Z. (2008). Hafnium isotope characterization of the GJ-1 zircon reference material by solution and laser-ablation MC-ICPMS. *Chemical Geology*, 255(1–2), 231–235. <https://doi.org/10.1016/j.chemgeo.2008.06.040>
- Murphy, J. B., Gutiérrez-Alonso, G., Nance, R. D., Fernandez-Suarez, J., Keppie, J. D., Quesada, C., et al. (2006). Origin of the Rheic Ocean: rifting along a Neoproterozoic suture? *Geology*, 34, 325–328. <https://doi.org/10.1130/G22068.1>
- Murphy, J.B., Quesada, C., Gutiérrez-Alonso, G., Johnston, S.T., & Weil, A. (2016). Reconciling competing models for the tectono-stratigraphic zonation of the Variscan orogen in Western Europe. *Tectonophysics* 681, 209–219. doi:10.1016/j.tecto.2016.01.006
- Nance, R. D., Gutiérrez-Alonso, G., Keppie, J. D., Linnemann, U., Murphy, J. B., Quesada, C., et al. (2010). Evolution of the Rheic Ocean. *Gondwana Research*, 17(2–3), 194–222. <https://doi.org/10.1016/j.gr.2009.08.001>
- Nance, R. D., Gutiérrez-Alonso, G., Keppie, J. D., Linnemann, U., Murphy, J. B., Quesada, C., et al. (2012). A brief history of the Rheic Ocean. *Geoscience Frontiers*, 3(2), 125–135. <https://doi.org/10.1016/j.gsf.2011.11.008>
- Nance, R. D., Murphy, J. B., Strachan, R. A., Keppie, J. D., Gutiérrez-Alonso, G., Fernández-Suárez, J., et al. (2008). Neoproterozoic-early Palaeozoic tectonostratigraphy and palaeogeography of the peri-Gondwanan terranes: Amazonian v. West African connections. *Geological Society, London, Special Publications*, 297(1), 345–383. <https://doi.org/10.1144/SP297.17>
- Ouabid, M., Ouali, H., Garrido, C.J., Acosta-Vigil, A., Román-Alpiste, M.J., Dautria, J.M., et al. (2017). Neoproterozoic granitoids in the basement of the Moroccan Central Meseta: Correlation with the Anti-Atlas at the NW paleo-margin of

- Gondwana. Precambrian Research, 299, 34–57.
doi:10.1016/j.precamres.2017.07.007
- Patchett, P. J., & Tatsumoto, M. (1980). Hafnium isotope variations in oceanic basalts. *Geophysical Research Letters*, 7(12), 1077–1080.
<https://doi.org/10.1029/GL007i012p01077>
- Paton, C., Hellstrom, J., Paul, B., Woodhead, J., & Hergt, J. (2011). Iolite: Freeware for the visualisation and processing of mass spectrometric data. *Journal of Analytical Atomic Spectrometry*, 26(12), 2508. <https://doi.org/10.1039/c1ja10172b>
- Pereira, M. F., Chichorro, M., Johnston, S. T., Gutiérrez-Alonso, G., Silva, J. B., Linnemann, U., et al. (2012). The missing Rheic Ocean magmatic arcs: provenance analysis of Late Paleozoic sedimentary clastic rocks of SW Iberia. *Gondwana Research*, 22(3–4), 882–891. <https://doi.org/10.1016/j.gr.2012.03.010>
- Pereira, M. F., El Houicha, M., Aghzer, A., Silva, J.B., Linnemann, U., & Jouhari, A., 2014. New U-Pb zircon dating of Late Neoproterozoic magmatism in Western Meseta (Morocco). *Gondwana*, 15 - North meets South 133.
doi:10.13140/2.1.2651.2641
- Pereira, M. F., El Houicha, M., Chichorro, M., Armstrong, R., Jouhari, A., El Attari, A., et al. (2015). Evidence of a Paleoproterozoic basement in the Moroccan Variscan Belt (Rehamna Massif, Western Meseta). *Precambrian Research*, 268, 61–73.
doi:10.1016/j.precamres.2015.07.01
- Pereira, M. F., Gutiérrez-Alonso, G., Murphy, J. B., Drost, K., Gama, C., & Silva, J. B. (2017). Birth and demise of the Rheic Ocean magmatic arc(s): Combined U–Pb and Hf isotope analyses in detrital zircon from SW Iberia siliciclastic strata. *Lithos*, 278–281, 383–399. <https://doi.org/10.1016/j.lithos.2017.02.009>
- Pérez-Cáceres, I., Martínez Poyatos, D., Simancas, J. F., & Azor, A. (2015). The elusive nature of the Rheic Ocean suture in SW Iberia. *Tectonics*, 34(12), 2429–2450.
<https://doi.org/10.1002/2015TC003947>
- Pérez-Cáceres, I., Martínez Poyatos, D., Simancas, J. F., & Azor, A. (2017). Testing the Avalonian affinity of the South Portuguese Zone and the Neoproterozoic evolution of SW Iberia through detrital zircon populations. *Gondwana Research*, 42, 177–192.
<https://doi.org/10.1016/j.gr.2016.10.010>
- Pérez-Cáceres, I., Simancas, J. F., Martínez Poyatos, D., Azor, A., & González Lodeiro, F. (2016). Oblique collision and deformation partitioning in the SW Iberian Variscides. *Solid Earth*, 7(3), 857–872. <https://doi.org/10.5194/se-7-857-2016>
- Piqué, A. (1994). *Géologie du Maroc*. Marrakech: éditions Pumag.
- Piqué, A. (2001). *Geology of Northwest Africa*. Berlin: Borntraeger.
- Piqué, A., & Michard, A. (1981). Les zones structurales du Maroc hercynien. *Sciences Géologiques, Bulletins et Mémoires*, 34(2), 135–146.

- Piqué, A., & Michard, A. (1989). Moroccan Hercynides: a synopsis. The Paleozoic sedimentary and tectonic evolution at the northern margin of West Africa. *American Journal of Science*, 289, 286–330.
- Rauscher, R., Marhoumi, R., Vanguetaine, M., & Hoepffner, C. (1984). Datation palynologique des schistes du Tazekka au Maroc. Hypothèse structurale sur la socle hercynien de la Meseta orientale. *Comptes Rendus de l'Académie Des Sciences de Paris*, 294(II), 1203–1206.
- Romer, R. L., & Kroner, U. (2019). First direct evidence for a contiguous Gondwana shelf to the south of the Rheic Ocean. *Geology*, 47(8), 767–770. <https://doi.org/10.1130/G46255.1>
- Scherer, E., Münker, C., & Mezger, K. (2001). Calibration of the Lutetium-Hafnium Clock. *Science*, 293(5530), 683–687. <https://doi.org/10.1126/science.1061372>
- Schulmann, K., Lexa, O., Janoušek, V., Lardeaux, J. M., & Edel, J. B. (2014). Anatomy of a diffuse cryptic suture zone: An example from the Bohemian Massif, European Variscides. *Geology*, 42(4), 275–278. <https://doi.org/10.1130/G35290.1>
- Shail, R.K. & Leveridge, B.E. (2009). The Rhenohercynian passive margin of SW England: Development, inversion and extensional reactivation. *Comptes Rendus Geoscience* 341, 140–155. doi:10.1016/j.crte.2008.11.002
- Simancas, J. F., Azor, A., Martínez Poyatos, D., Tahiri, A., El Hadi, H., González-Lodeiro, F., et al. (2009). Tectonic relationships of Southwest Iberia with the allochthons of Northwest Iberia and the Moroccan Variscides. *Comptes Rendus Geoscience*, 341(2–3), 103–113. <https://doi.org/10.1016/j.crte.2008.11.003>
- Simancas, J. F., Tahiri, A., Azor, A., Lodeiro, F. G., Martínez Poyatos, D. J., & El Hadi, H. (2005). The tectonic frame of the Variscan–Alleghanian orogen in Southern Europe and Northern Africa. *Tectonophysics*, 398(3–4), 181–198. <https://doi.org/10.1016/j.tecto.2005.02.006>
- Sláma, J., Košler, J., Condon, D. J., Crowley, J. L., Gerdes, A., Hanchar, J. M., et al. (2008). Plešovice zircon — A new natural reference material for U–Pb and Hf isotopic microanalysis. *Chemical Geology*, 249(1–2), 1–35. <https://doi.org/10.1016/j.chemgeo.2007.11.005>
- Stern, R.S., Bodorkos S., Kamo S. L., Hickman, A. H., & Corfu F. (2009). Measurement of SIMS instrumental mass fractionation of Pb-isotopes during zircon dating. *Geostandards and Geoanalytical Research*, 33, pp. 145–168. <https://doi.org/10.1111/j.1751-908X.2009.00023.x>
- Tahiri, A., & Hoepffner, C. (1988). Importance des mouvements distensifs au Dévonien supérieur en Meseta nord-occidentale (Maroc); les calcaires démantelés de Tiliouine et la ride d'Oulmès, prolongement oriental de la ride des Zaer. *Comptes Rendus de l'Académie Des Sciences de Paris*, 306, 223–226.

- Tahiri, A., Montero, P., El Hadi, H., Martínez Poyatos, D., Azor, A., Bea, F., et al. (2010). Geochronological data on the Rabat-Tiflet granitoids: their bearing on the tectonics of the Moroccan Variscides. *Journal of African Earth Sciences*, 57(1–2), 1–13. <https://doi.org/10.1016/j.jafrearsci.2009.07.005>
- Thirlwall, M. F., & Anczkiewicz, R. (2004). Multidynamic isotope ratio analysis using MC–ICP–MS and the causes of secular drift in Hf, Nd and Pb isotope ratios. *International Journal of Mass Spectrometry*, 235(1), 59–81. <https://doi.org/10.1016/j.ijms.2004.04.002>
- Tisserant, D. (1977). Les isotopes du strontium et l’histoire hercynienne du Maroc. Etude de quelques massifs atlasiques et mésétiens. Université Louis Pasteur, Strasbourg.
- Van Hinsbergen, D. J. J., Torsvik, T. H., Schmid, S. M., Mañenco, L. C., Maffione, M., Vissers, R. L. M., et al. (2019). Orogenic architecture of the Mediterranean region and kinematic reconstruction of its tectonic evolution since the Triassic. *Gondwana Research*, 97, 101145. <https://doi.org/10.1016/j.gr.2019.07.009>
- Vermeesch, P. (2004). How many grains are needed for a provenance study? *Earth and Planetary Science Letters*, 224(3–4), 441–451. <https://doi.org/10.1016/j.epsl.2004.05.037>
- Vermeesch, P. (2012). On the visualisation of detrital age distributions. *Chemical Geology*, 312–313, 190–194. <https://doi.org/10.1016/j.chemgeo.2012.04.021>
- Vermeesch, P. (2018). Dissimilarity measures in detrital geochronology. *Earth-Science Reviews*, 178(November 2017), 310–321. <https://doi.org/10.1016/j.earscirev.2017.11.027>
- Villeneuve, M. (2008). Review of the orogenic belts on the western side of the West African craton: the Bassarides, Rokelides and Mauritanides. Geological Society, London, Special Publications, 297(1), 169–201. <https://doi.org/10.1144/SP297.8>
- Villeneuve, M., El Archi, A., & Nzamba, J. (2010). Les chaînes de la marge occidentale du Craton Ouest-Africain, modèles géodynamiques. *Comptes Rendus - Geoscience*, 342(1), 1–10. <https://doi.org/10.1016/j.crte.2009.12.002>
- Villeneuve, M., Gärtner, A., Youbi, N., El Archi, A., Vernhet, E., Rjimati, E.-C., et al. (2015). The southern and central parts of the “Souttoufide” belt, Northwest Africa. *Journal of African Earth Science*, 112, 451–470. doi:10.1016/j.jafrearsci.2015.04.016
- Wiedenbeck, M., Allé, P., Cordu, F., Griffin, W. L., Meier, M., Oberli, F., et al. (1995). Three natural zircon standards for U-Th-Pb, Lu-Hf, trace element and REE analyses. *Geostandards and Geoanalytical Research*, 19(1), 1–23. <https://doi.org/10.1111/j.1751-908X.1995.tb00147.x>
- Woodhead, J., & Hergt, J. (2005). A Preliminary Appraisal of Seven Natural Zircon Reference Materials for In Situ Hf Isotope Determination. *Geostandards and*

Geoanalytical Research, 29(2), 183–195. <https://doi.org/10.1111/j.1751-908X.2005.tb00891.x>

Woodhead, J., Hergt, J., Shelley, M., Eggins, S., & Kemp, R. (2004). Zircon Hf-isotope analysis with an excimer laser, depth profiling, ablation of complex geometries, and concomitant age estimation. *Chemical Geology*, 209(1–2), 121–135. <https://doi.org/10.1016/j.chemgeo.2004.04.026>

Chapter IV

Evolution of the sedimentary sources during the Eovariscan phase in the Moroccan Mesetas

This chapter is a comparison among Late Devonian-late Carboniferous samples from the Moroccan Mesetas. Its objective is the study of the evolution of the sedimentary sources that fed this region during the first phases of the Variscan Orogeny.

Syn-collisional detrital zircon source evolution in the northern Moroccan Variscides

Cristina Accotto¹, David Martínez Poyatos¹, Antonio Azor¹, Cristina Talavera², Noreen J. Evans³, Antonio Jabaloy-Sánchez¹, Ali Azdimousa⁴, Abdelfatah Tahiri⁵, Hassan El Hadi⁶

Accepted on:

Gondwana Research, 2021

Volume 93, Pages 73-88

doi: 10.1016/j.gr.2021.02.001

(Received: 13 August 2020; Accepted: 2 February 2021; Available online: 5 February 2021)

¹ Departamento de Geodinámica, Universidad de Granada, Granada, Spain

² School of Geosciences, University of Edinburgh, Edinburgh, UK

³ School of Earth and Planetary Science, John de Laeter Centre, Curtin University, Bentley, Australia

⁴ Faculté Pluridisciplinaire de Nador et Laboratoire des Géosciences Appliquées, Faculté des Sciences, Université Mohammed I, Oujda, Morocco

⁵ Laboratory of Geo-biodiversity and Natural Patrimony (GEOBIO), Scientific Institut; Geophysics, Natural Patrimony and Green Chemistry Research Center (GEOPAC), Mohammed V University in Rabat, Morocco

⁶ Laboratory of Geodynamics of Ancient Belts, Faculty of Science Ben M'Sik, Hassan II, University of Casablanca, Morocco

JCR: 6.174 (2019)

Abstract

U-Pb dating and Hf isotopic analyses of detrital zircon grains from Cambrian-Devonian strata in the Moroccan Mesetas were undertaken in order to constrain its Paleozoic paleogeographic evolution. In this work, we analyzed 12 Late Devonian-Late Carboniferous samples of syn-collisional detrital rocks from the Western and Eastern Moroccan Mesetas. All our samples present significant Ediacaran (ca. 620 Ma) and Rhyacian (ca. 2.1 Ga) detrital zircon populations, suggesting that the West African Craton remained the main source of sediments for northern Morocco at least until the Late Carboniferous. Locally, a Stenian-Tonian (ca. 1.0 Ga) detrital zircon population is also present, probably fed from intermittent and distant source areas located in NE Africa (*e.g.*, Sahara Metacraton). The collisional evolution started with the approach of an Avalonian promontory to the northern Gondwana continental margin (latest Devonian - earliest Carboniferous), after the closure of the Rheic Ocean. This process entailed the former subduction of the Rheic oceanic lithosphere underneath the Avalonian continental terrane and the formation of a magmatic arc in the upper plate. In this scenario, the first syn-collisional sediments (Tournaisian; Tiflet and Debdou-Mekkam areas) are characterized by a Devonian detrital zircon population (ca. 370 Ma), presumably derived from the magmatic arc, and an increasing number of Mesoproterozoic dates, putatively also sourced from the continental crust of the Avalonian terrane. After the initial collision, only the Viséan samples located in areas close to the exotic terrane (*e.g.*, Ben Slimane area) displayed a minor Avalonian component. Finally, the Late Carboniferous samples from the Jerada area recorded an important Middle Carboniferous (ca. 330 Ma) detrital zircon population, probably sourced from Variscan granitoids emplaced in the Eastern Moroccan Meseta and attesting to crustal thickening and subsequent thermal maturation of the Gondwana continental crust in this area.

Highlights

- Robust detrital zircon ages for Late Paleozoic metasediments of the Moroccan Meseta
- The West African Craton was the main sediment source in the Moroccan Variscides
- Avalonia and Devonian arc provided additional detritus after Rheic ocean closure

Keywords

Detrital zircon provenance; Moroccan Mesetas; syn-collisional sediments; Avalonian magmatic arc.

1. Introduction

The study of syn-orogenic sediments is key to understanding collisional processes and orogenesis. In this regard, the age and distribution of syn-orogenic basins have traditionally been used to constrain the temporal and spatial evolution of the ongoing collision. Furthermore, the composition of the detrital fraction of syn-orogenic sediments can help to clarify which rocks were exhumed as a consequence of underthrusting (and/or extensional deformation) and concomitant mountain building/erosion. The possibility of dating some of the minerals included in the detrital fraction of syn-orogenic sediments has introduced a new dimension to the study of orogenesis and paleogeotectonic reconstructions. Thus, the systematic dating of minerals, especially zircon, is now used to track the continental terranes involved in collision, the successive input from originally deeper - and older - sources, and the contribution of syn-collisional neo-formed magmatic sources.

The Late Paleozoic Variscan belt constitutes an excellent opportunity to evaluate the role of systematic syn-orogenic sediment detrital zircon dating in elucidating orogenic evolution (*e.g.*, Pastor-Galán et al., 2013a, 2013b; Pereira et al., 2012, 2020a). This orogen resulted from Devonian-Permian complex collision between Gondwana and Laurussia, with a number of peri-Gondwanan terranes also involved in the process (*e.g.*, Franke et al., 2017; Matte, 2001; Simancas et al., 2005). In the Moroccan transects of the Variscan orogen, detrital zircon investigations have been focused on the pre-orogenic evolution (*e.g.*, Abati et al., 2010; Accotto et al., 2019, 2020; Avigad et al., 2012; Ghienne et al., 2018; Letsch et al., 2018; Pérez-Cáceres et al., 2017), but to date, no data have been reported on the syn-orogenic sediments, with the exception of a recent work on the Eastern Moroccan Meseta (Accotto et al., 2020). The present work provides a wide-scale study of U-Pb geochronological and Hf isotope detrital zircon analyses carried out on syn-collisional Late Devonian-Late Carboniferous samples from the Western and Eastern Moroccan Mesetas.

2. Geological setting

The Paleozoic successions of northwestern Africa (Figure 4.1A) crop out in different domains of the Moroccan Mesetas and surroundings (Figure 4.1B), having been variably affected by the Variscan orogeny. These domains are separated by putative regional fault zones, the paleogeographic importance of which is unclear and controversial (*e.g.*, Hoepffner et al., 2006; Michard et al., 2010a, 2010b; Simancas et al., 2009, 2010). The Rabat-Tiflet Fault Zone (RTFZ; Figure 4.1B) separates the Moroccan Mesetas domains from the Sehoul Block, located to the north and characterized by a Cambrian siliciclastic succession affected by Caledonian penetrative deformation and intruded by Devonian granites (Michard et al., 2010b; Simancas et al., 2005; Tahiri et al., 2010). Due to this Caledonian deformation, which did not affect any other domain of the Moroccan Variscides, the Sehoul Block is considered to be part of an exotic Avalonian promontory (Simancas et al., 2005), juxtaposed to the Moroccan Mesetas during the Carboniferous.

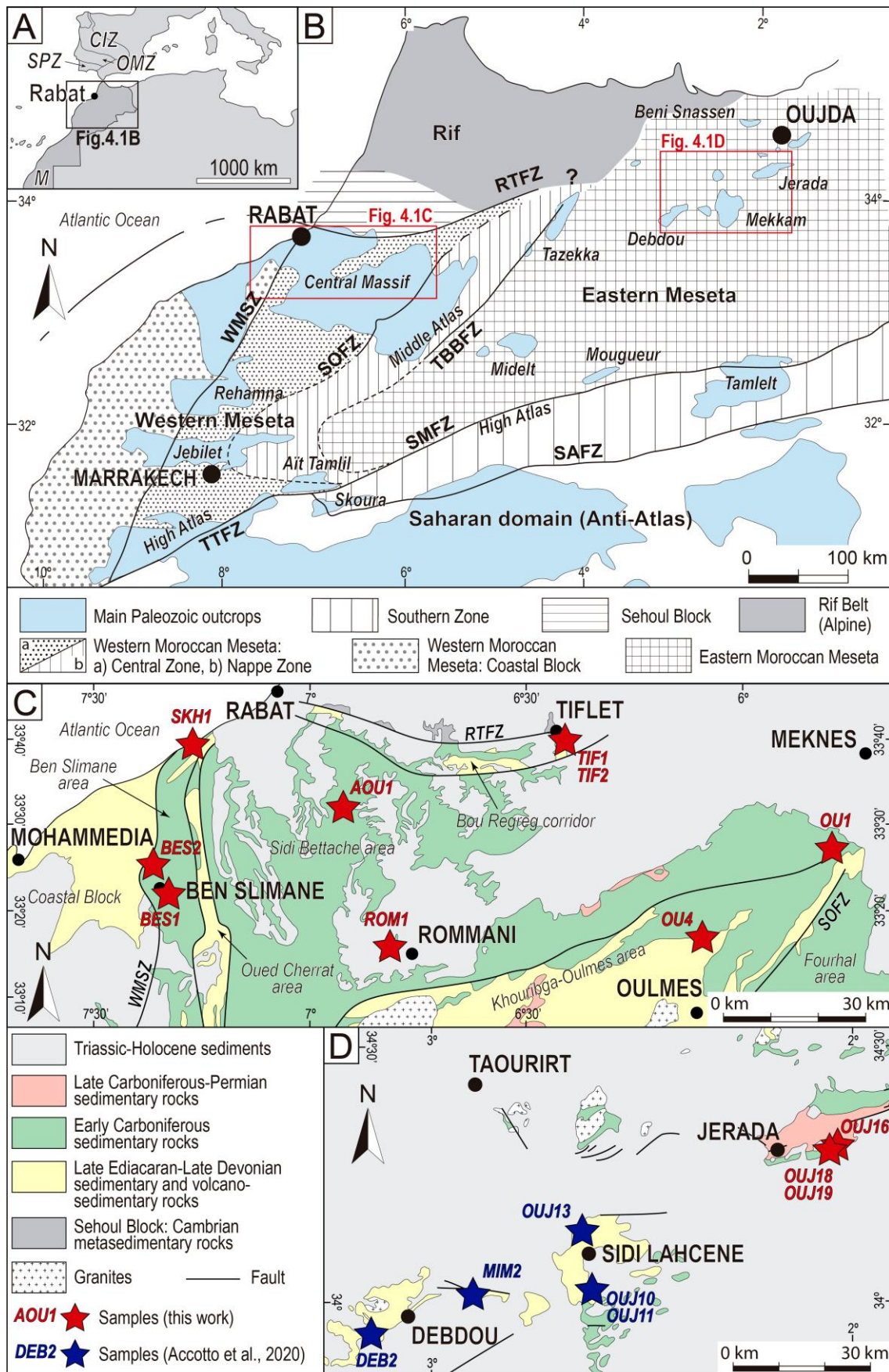


Figure 4.1. A) Schematic map of NW Africa and Iberia showing the location of the northern Moroccan Variscides (rectangle); SPZ: South Portuguese Zone; OMZ: Ossa-Morena Zone; M: Mauritanides; CIZ:

Central Iberian Zone; B) Geological map of the northern Moroccan Variscides (after Hoepffner et al., 2006; Michard et al., 2010b). RTFZ: Rabat-Tiflet Fault Zone; WMSZ: Western Meseta Shear Zone; SOFZ: Smaala-Oulmès Fault Zone; TBBFZ: Tazekka-Bsabis-Bekrit Fault Zone; TTFZ: Tizin'Test Fault Zone; SMFZ: South Meseta Fault Zone; SAFZ: South Atlas Fault Zone. C) Schematic geological map of part of the Western Moroccan Meseta (after Becker and El Hassani, 2020) with location of the studied samples. D) Schematic geological map of part of the Eastern Moroccan Meseta (after Muratet, 1988) with location of the studied samples.

South of the RTFZ, the Western Moroccan Meseta (WMM) is divided into three subdomains, namely the Coastal Block to the west, the Central Zone, and the so-called “Nappe Zone” to the east, separated by the Western Meseta Shear Zone (WMSZ) and the Smaala-Oulmès Fault Zone (SOFM), respectively (Figure 4.1B; Michard et al., 2010b). Eastwards, the Tazekka-Bsabis-Bekrit Fault Zone (TBBFZ) juxtaposes the WMM to the Eastern Moroccan Meseta (EMM). Finally, the South Meseta Fault Zone (Hoepffner et al., 2006) separates the Moroccan Mesetas from the Southern Zone, and, further south, the South Atlas and the Tizin'Test Fault Zones represent the limit of the Gondwanan foreland (Anti-Atlas; Michard et al., 2010b).

The igneous Precambrian basement of the northern Moroccan Variscides crops out in the WMM in relatively small and isolated areas of the Central Zone and Coastal Block (*e.g.*, El Haibi et al., 2020; El Houicha et al., 2018; Ouabid et al., 2017; Pereira et al., 2014, 2015; Tahiri et al., 2010). This basement is covered by a thick, more or less continuous, passive margin succession that is exposed in large areas of the WMM, and in more scarce and relatively small inliers of the EMM (Figure 4.1). The Cambrian-Silurian succession is mainly terrigenous, with the exception of local Lower Cambrian limestones in the WMM (Michard et al., 2010b and references therein); in the Coastal Block, this siliciclastic succession shows interbedded rift-related Cambrian-Ordovician basaltic lenses (Pouclet et al., 2018). During the Devonian, a carbonatic platform developed in the WMM (Michard et al., 2010b and references therein), while sedimentation in the EMM continued to be mainly terrigenous (Hoepffner, 1987; Marhoumi et al., 1983). The metamorphism affecting the whole Paleozoic succession is generally of low- to very low-grade and the tectonic deformation seems to increase eastwards (Hoepffner et al., 2006).

The studied samples were collected in the Upper Devonian – Upper Carboniferous successions from different parts of the Moroccan Mesetas (Figure 4.1C and D, Figure 4.2, and Table 4.1 for coordinates). These successions are described in detail in the following subsections.

2.1. Ben Slimane area

The Lower-Middle Devonian succession of the Coastal Block and Central Zone of the WMM is mainly characterized by limestones deposited in a shelf (Zahraoui, 1991). Locally, the carbonate succession changes laterally to carbonatic olistoliths or turbiditic sandstones and shales, deposited in deeper environments.

At Middle Devonian time, the Coastal Block and Central Zone regions were affected by a general uplift, which culminated in the emersion of some areas and the subsidence

of others (see subsection 2.2) during the Famennian. Thus, in the subsident Ben Slimane area (Figure 4.1C), transgressive turbiditic sandstones, shales and deltaic quartzitic sandstones (Piqué, 1979, 1984; Zahraoui, 1991) directly overlay the Lower-Middle Devonian carbonatic sequence. The turbiditic sedimentation continued until the Tournaisian with local hiatus (Figure 4.2; Zahraoui, 1991). A new subsiding phase started at Late Visean time (Izart, 1991) with the deposition of fossiliferous sandstones and shales with limestone intercalations (Destombe, 1987; Zahraoui, 1991).

The Triassic succession, characterized by red shales, conglomerates and basaltic lavas, unconformably overlays the Late Visean sediments (Figure 4.2; Destombe, 1987).

2.2. *Sidi Bettache area*

The Sidi Bettache area (Figure 4.1C) attests an allegedly pull-apart basin opened at Famennian-Tournaisian time (Piqué, 1979, 1984) in a regional contractive context (Fadli, 1990; Hoepffner, 1987; Piqué, 1979; Rolin et al., 1985). The opening of the basin triggered the deposition of turbiditic sequences dominated by quartzitic sandstones, conglomerates, and shales (Piqué et al., 1989), which transgressively overlie the Lower-Middle Devonian limestones (Figure 4.2; Destombe, 1987). Locally, along the main faults bounding the Sidi Bettache basin, limestone olistoliths were deposited (Piqué et al., 1989), while gabbroic dikes and, in a lesser amount, dolerite lavas were emplaced (Figure 4.2; Kharbouch, 1994; Kharbouch et al., 1989; Piqué, 1979).

Most of the Lower Visean succession, characterized by turbiditic deposits of sandstones and shales, was eroded during a period of subaerial emersion (Izart and Vieslet, 1988), with Middle-Upper Visean turbiditic sandstones, shales, and greywackes transgressively resting on the Tournaisian-lowermost Visean succession (Figure 4.2; Bouabdelli, 1989; Izart, 1991; Termier et al., 1975; Verset, 1983, 1985). Nonetheless, a recent review of the micropaleontological content of the Visean succession suggests that the Lower-Middle Visean sediments are absent in the Sidi Bettache basin (Cózar et al., 2020).

The terrigenous sedimentation continued in the Serpukhovian-Middle Bashkirian (corresponding to the former Namurian) with the deposition of turbiditic shales, greywackes, and carbonatic sandstones (Beauchamp and Izart, 1987; Chakiri and Tahiri, 2000; Izart, 1991; Piqué, 1984; Zahraoui, 1991). The Middle Bashkirian-Kasimovian (corresponding to the former Westphalian) is characterized by the deposition of alternating conglomerates and fossiliferous black limestones deposited in a lacustrine environment (Cailleux et al., 2001; Piqué, 1984).

The Permian succession, characterized by red conglomerates, shales, and sandstones with intercalations of volcanic ashes and rhyolitic lavas (El Wartiti, 1994), unconformably overlays the Middle Bashkirian-Kasimovian rocks (Figure 4.2). Finally, Triassic red shales and basaltic lavas unconformably overlay the Permian and pre-Permian successions (El Touhami, 1993).

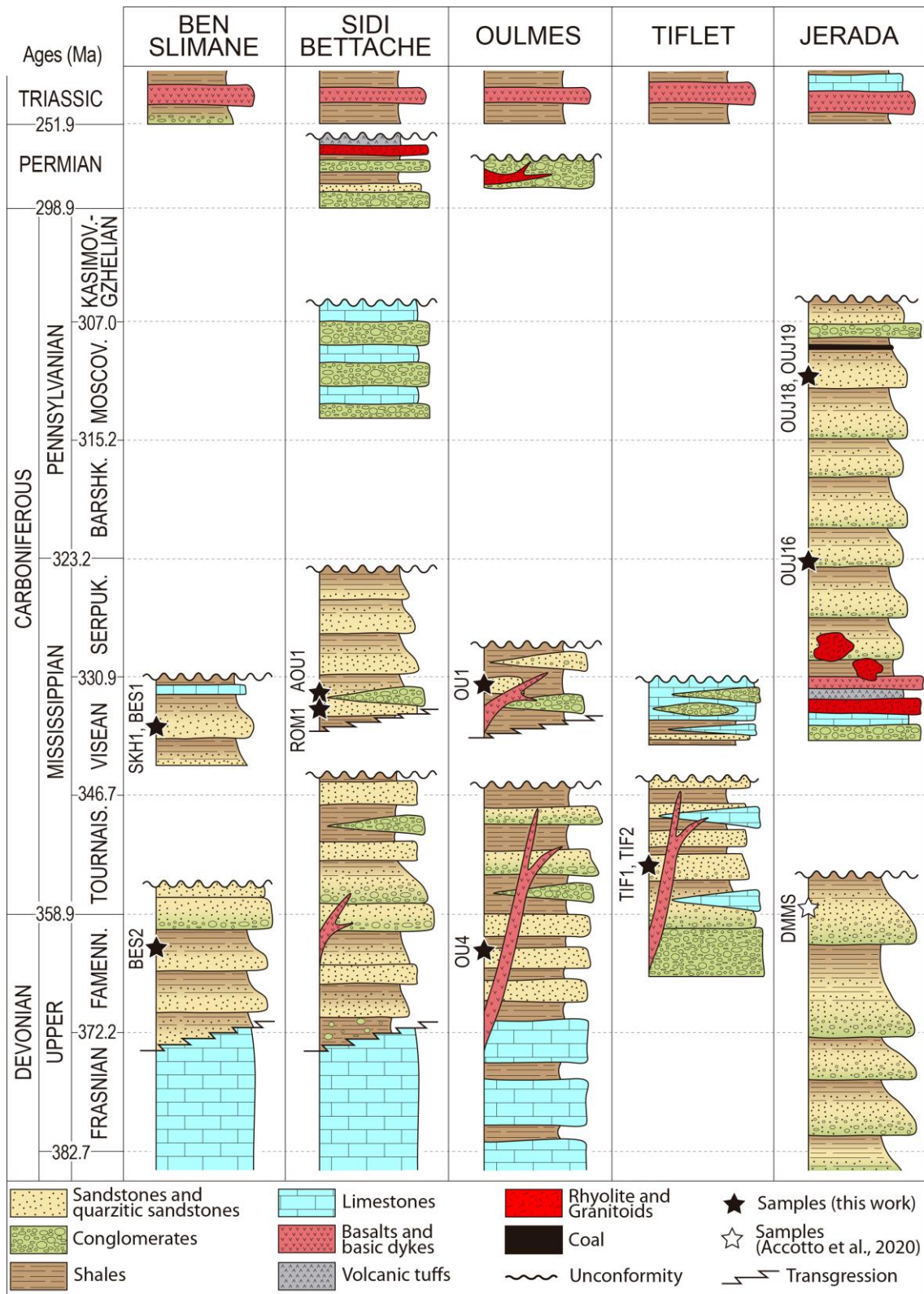


Figure 4.2. Schematic comparison among stratigraphic columns of the Upper Devonian-Triassic successions in different parts of the Moroccan Mesetas: Ben Slimane area (Destombe, 1987; Piqué, 1984; Zahraoui, 1991), Sidi Bettache area (Beauchamp and Izart, 1987; Cailleux et al., 2001; Chakiri and Tahiri, 2000; Cózar et al., 2020; El Wartiti, 1994; Izart, 1991; Kharbouch, 1994; Piqué, 1984; Razin et al., 2001; Vidal, 1989), Oulmes area (El Hassani et al., 2002; Izart et al., 2001; Kaiser et al., 2007), Tiflet area (Cózar et al., 2020; El Hassani, 1991, 1987; Kharbouch, 1994), and Jerada area (El Hadi et al., 2006; Hoepffner, 1989; Horon, 1952; Médioni, 1979, 1977; Muratet, 1988). Not to scale.

2.3. Oulmes area

The Oulmes area is part of a structural high separating the Sidi Bettache and Fourhal areas (Khouribga-Oulmes area in Figure 4.1C). The Upper Devonian succession is characterized by alternation of fossiliferous nodular limestones and shales, dated at the Frasnian-Famennian (Kaiser et al., 2007), passing upward to Upper Famennian quartzitic sandstones (Figure 4.2). During the Tournaisian, the deposition of shales was accompanied by local olistoliths of Middle Devonian limestones and beds of turbiditic sandstones (Izart et al., 2001). The Upper Visean- Serpukhovian shales with lenses of sandstones directly rest on the Tournaisian succession and are unconformably overlain by Permian continental conglomerates (El Hassani et al., 2002; Izart et al., 2001). The entire Upper Devonian-Carboniferous succession is cross-cut by basic and acid dykes (Izart et al., 2001; Kharbouch, 1994; Kharbouch et al., 1985) and intruded by Late Carboniferous-Permian granitoids (Izart et al., 2001). The Triassic red shales and basaltic lavas unconformably overlie the Permian conglomerates.

2.4. Tiflet area

To the south of the RTFZ, the Upper Famennian-Upper Visean succession of the Bou Regreg corridor (Figure 4.1C) unconformably overlies the Lower Devonian succession, the latter being characterized by black shales and black fossiliferous limestones of Lochkovian-Emsian age (Alberti, 1969; El Hassani, 1991). The Famennian period is characterized by deposition of conglomerates (Figure 4.2) with Ordovician-Devonian clasts (Lecointre and Delepine, 1933), dated by stratigraphic correlation with similar conglomerates cropping out in the Rabat area containing interbedded arkoses and shales with Famennian fossil plants (El Hassani, 1991 and references therein). The sedimentation continued with sandstones and shales interbedded with sporadic lenses of limestones containing Tournaisian fauna (Figure 4.2; Lecointre and Delepine, 1933). Upwards, a 400 m-thick succession of sandstones and shales with abundant limestone lenses was dated as Lower Visean (Izart and Vieslet, 1988; Lecointre and Delepine, 1933), although recent studies have re-dated it as Upper Visean based on a review of their foraminiferal content (Cózar et al., 2020). The entire Upper Devonian-Tournaisian succession is intruded by Permian basic dykes (Figure 4.2; Cailleux et al., 1983; Kharbouch, 1994). The Upper Visean sequence, characterized by oolitic limestones with conglomeratic lenses, unconformably overlies the Tournaisian (-Early Visean?) succession (El Hassani, 1991).

In this area, there is no record of Middle-Upper Carboniferous rocks, and the Triassic red shales and basalts unconformably overlie the Upper Visean succession (El Hassani et al., 2002).

2.5. Jerada area

Unlike the WMM, where the Devonian period was characterized by a carbonatic platform that was progressively fragmented, the EMM (Figure 4.1D) experienced more or less continuous sedimentation (*e.g.*, Debdou and Mekkam inliers) with a Devonian-Tournaisian thick siliciclastic turbiditic succession of shales, greywackes, and sandstones (Figure 4.2; Hoepffner, 1989), intensely deformed by a Tournaisian-Early Visean tectonic event induced by the collision between the northern margin of Gondwana and an Avalonian promontory (inferred as the eastern prolongation of the Sehouli Block; Accotto *et al.*, 2020).

After this tectonic event, sedimentation resumed during the Late Visean with the deposition of basal conglomerates in relatively small and fragmented basins, local and subordinate carbonatic platform deposits, and a thick volcano-sedimentary sequence with rhyolites, andesites, and tuffs (Izart, 1991; Kharbouch *et al.*, 1989; Médioni, 1979). The Serpukhovian-Middle Bashkirian succession in the Jerada area (Figure 4.2) is characterized by shales and sandstones, (Chellai *et al.*, 2011; Muratet, 1988), typical of deltaic environments (Izart, 1991). Deltaic sedimentation continued during the Middle Bashkirian-Kasimovian, but the environment became progressively more lacustrine, accompanied by deposition of fluvial conglomerates and coal levels (Figure 4.2; Chellai *et al.*, 2011).

After a Late Carboniferous Variscan tectonic event responsible for open ENE-WSW trending folds (*e.g.*, Hoepffner, 1989; Horon, 1952), Triassic red shales, basalts, and limestones unconformably overlay the Paleozoic succession (Figure 4.2; Muratet, 1988).

3. Samples and methods

This study is based on the U-Pb and Hf isotopic analysis of 12 samples collected in different areas of the Moroccan Mesetas (Figures 4.1 and 4.2). The samples are listed in Table 4.1, together with their location, lithology, stratigraphic age, as well as the number and kind of analyses carried out.

In the Ben Slimane area (Figure 4.1C), sample BES2 is a Famennian (Upper Devonian; Figure 4.2) white quartzitic sandstone collected a few kilometers north of Ben Slimane. At the microscope scale, it is composed of more than 90% of quartz grains with diameters between ca. 0.25 and 0.1 mm, not particularly rounded. Rare interstitial phyllosilicates are present. Samples BES1 and SKH1 are Visean (Figure 4.2) white quartzitic sandstones collected in Ben Slimane and along the coast, north of Ben Slimane. Both samples are characterized at the microscopic scale by more than 90% of angular quartz grains with diameters between ca. 0.2 and 0.1 mm. Interstitial phyllosilicates are very rare.

Table 4.1. List of samples and analyses carried out; (*) number of analyses and number of concordant results (in bold).

Sample	IGSN (IEACC)	Location (UTM, NDAS83)		Lithology	Age	U-Pb geochronology		Hf isotope analyses	
		Zone	Lat. (m N)			Long. (m E)	Method		Analyses (*)
BEN SLIMANE AREA									
BES1	0009	29S	3720500	674467	Quartzitic sandstone	Visean	LA-ICPMS	150/120	107
BES2	0010	29S	3724273	671847	Quartzitic sandstone	Famennian	LA-ICPMS	180/156	-
SKH1	0011	29S	3748316	678921	Quartzitic sandstone	Visean	SHRIMP LA-ICPMS	52/41 104/95	90
SIDI BETTACHE AREA									
ROM1	0012	29S	37122830	719745	Sandstone	Visean	SHRIMP LA-ICPMS	52/42 114/88	-
AOU1	0013	29S	3736131	708680	Sandstone	Visean	SIMS LA-ICPMS	28/26 84/72	-
OULMES AREA									
OU1	0014	30S	3731845	244382	Sandy shale	Late Visean	LA-ICPMS	124/104	-
OU4	0015	29S	3716170	777438	Quartzitic sandstone	Famennian	LA-ICPMS	150/134	-
TIFLET AREA									
TIF1	0016	29S	3752612	750380	Sandstone	Tournaisian	LA-ICPMS	100/73	66
TIF2	0017	29S	3752611	750354	Sandstone	Tournaisian	LA-ICPMS	120/89	88
JERADA AREA									
OUJ16	0018	30S	3796135	587342	Sandstone	Serpukhovian- Mid. Bashkirian	LA-ICPMS	150/128	128
OUJ18	0019	30S	3796505	587288	Sandstone	Mid. Bashkirian -Kasimovian	SIMS LA-ICPMS	70/58 50/46	46
OUJ19	0020	30S	3796474	587262	Sandstone	Mid. Bashkirian -Kasimovian	LA-ICPMS	130/120	106

From the Visean succession of the Sidi Bettache area we collected two samples (Figures 4.1C and 4.2). Sample ROM1 was sampled a few kilometers West of the city of Rommani. This sample is a reddish sandstone characterized by abundant quartz grains (about 75%) with very variable diameters from ca. 0.05 to 0.3 mm. Interstitial phyllosilicates and Fe-oxides are also frequent. Sample AOU1 was collected about 7 km SE of the city of Aïn El Aouda and it is a reddish Late Visean sandstone made up of \approx 70% of fine-grained quartz (ca. 0.05 mm in diameter) and abundant phyllosilicates and Fe-oxides.

Sample OU4 was collected about 14 km North of the city of Oulmes (Figure 4.1C). It is a quartzitic sandstone of Famennian age (Figure 4.2) composed of \approx 70% of quartz grains, mainly rounded and with a diameter between ca. 0.25 and 0.1 mm. Interstitial phyllosilicates and oxides are frequent. Sample OU1 was collected about 30 km SW of Meknes (Figure 4.1C), along the road connecting this city with Oulmes. It is an Upper Visean (Figure 4.2) sandy shale with a very heterogeneous texture characterized by zones with a fine-grained matrix (less than 0.03 mm); other portions of the sample are made up of \approx 80% of angular quartz clasts of ca. 0.05 mm in diameter, together with frequent interstitial phyllosilicates and Fe-oxides.

The two samples from the Tiflet area, TIF1 and TIF2, were collected 2 km East of Tiflet, along the Tiflet river (Figure 4.1C). They are Tournaisian sandstones (Figure 4.2) characterized by medium-sized (ca. 0.2-0.05 mm) grains of quartz (ca.70%), and abundant phyllosilicates and Fe-oxides.

Samples OUI16, OUI18, and OUI19 were collected about 10 km East of Jerada (Figure 4.1D), in the southern flank of the Jerada synform. Sample OUI16 is a Serpukhovian-Middle Bashkirian sandstone (Figure 4.2) characterized by a very variable grain-size. The matrix is mainly composed of 70% of rounded quartz grains with diameters of ca. 0.05 mm, interstitial phyllosilicates, and oxides. The clasts represent about 30% of the sample, have diameters of 0.3-0.8 mm, and comprise variable lithologies (*e.g.*, angular quartz grains, quartzitic sandstones, volcanic rocks, and foliated shales). Samples OUI18 and OUI19 were both collected from sandstone layers within the Middle Bashkirian-Kasimovian succession (Figure 4.2), being OUI18 stratigraphically younger than OUI19. They are both composed of abundant (ca. 65-70%) more or less rounded quartz grains with diameters varying between 0.05 and 0.2 mm. Phyllosilicates and oxides are also frequent, together with scarce glauconite.

For each sample, 4-5 kg of rock were collected and processed at the University of Granada (Spain). The separation processing of the detrital zircon grains included mechanical smashing with jaw- and ring-crusher, sorting with sieving, manual panning, and handpicking. A Mira3 VP-FESEM instrument at the John de Laeter Centre (JdLC) of Curtin University (Perth, Australia), and a Carl Zeiss SIGMA HD VP Field Emission SEM at the School of GeoSciences of the University of Edinburgh (United Kingdom) were used to obtain cathodoluminescence (CL) images of the zircon grains. A selection of these CL images is presented in Appendix C (Figures C.18 to C.29). Most of the detrital zircon grains were analyzed using laser ablation inductively coupled plasma mass

spectrometer (LA-ICPMS) at the JdLC GeoHistory Facility. Nevertheless, in some samples, the size of the zircon grains was very variable and sensitive high-resolution ion microprobe (SHRIMP) and secondary ion mass spectrometry (SIMS) analyses were performed to grant a statistically significant number of results in each sample (Vermeesch, 2004). SHRIMP measurements were carried out at the JdLC, while SIMS analyses were performed at the University of Edinburgh. A more detailed description of the analytical methods can be found in Appendix A.

All the raw U-Pb results are listed in Appendix D (Tables D.35 to D.46). Concordant (with a discordance level $\leq 10\%$) $^{206}\text{Pb}/^{238}\text{U}$ dates were used for grains with ages younger than 1.5 Ga; for older grains $^{207}\text{Pb}/^{206}\text{Pb}$ concordant dates were used, due to the significant increase in error on $^{206}\text{Pb}/^{238}\text{U}$ dates for > 1.5 Ga zircon grains. Kernel Density Estimators (KDE) and histograms of the concordant dates were made using DensityPlotter 8.4 (Vermeesch, 2012) applying a KDE bandwidth of 25 Ma and histogram bin of 20 Ma. Mean ages of the detrital zircon populations were calculated applying the mixture modelling tool in DensityPlotter 8.4 (Vermeesch, 2012) to groups of dates considered statistically (i.e., peaks in the KDE plots) and geologically (i.e., ages of the main geological events) meaningful. The ranges of dates used to calculate the mean ages of each population are detailed in section 4 (Results). The youngest age populations were calculated by using a weighted mean and assessed by the mean square weighted deviation (MSWD) within the software Isoplot (Ludwig, 2009, 2003) and IsoplotR (Vermeesch, 2018). Errors of mean ages and weighted mean ages are expressed at 1σ level.

Hf isotope analyses were run on those samples characterized by determinant detrital zircon populations (Carboniferous, Devonian, and Mesoproterozoic) in order to discriminate juvenile mantle-derived from recycled crustal-derived primary magmatic sources. These analyses were carried out at the JdLC on samples BES1, SKH1, TIF1, TIF2, OUI16, OUI18, and OUI19 (Table 4.1). The details of the analytical methods are described in Appendix A, while the results are listed in Appendix E (Tables E.6 to E.12). Errors are expressed at 2σ level.

4. Results

4.1. Ben Slimane area

One hundred and eighty LA-ICPMS analyses were performed on detrital zircon grains from Famennian sample BES2, yielding 156 concordant results. The KDE diagram in Figure 4.3A shows an important Cryogenian-Ediacaran population with an Ediacaran mean age of 612.8 ± 0.6 Ma (age range: ca. 701-542 Ma, $n=98$, 62.8% of the data). A second detrital zircon population yielded a Rhyacian mean age of 2062.7 ± 2.2 Ma (ca. 2207-1932 Ma, $n=37$, 23.7% of the data). A few scattered data have Archean-Rhyacian, Orosirian-Tonian, and Cambrian ages. The youngest detrital zircon population of this

sample defines an Early Cambrian age (538.9 ± 3.0 Ma, MSWD=1.38) and includes 4 dates.

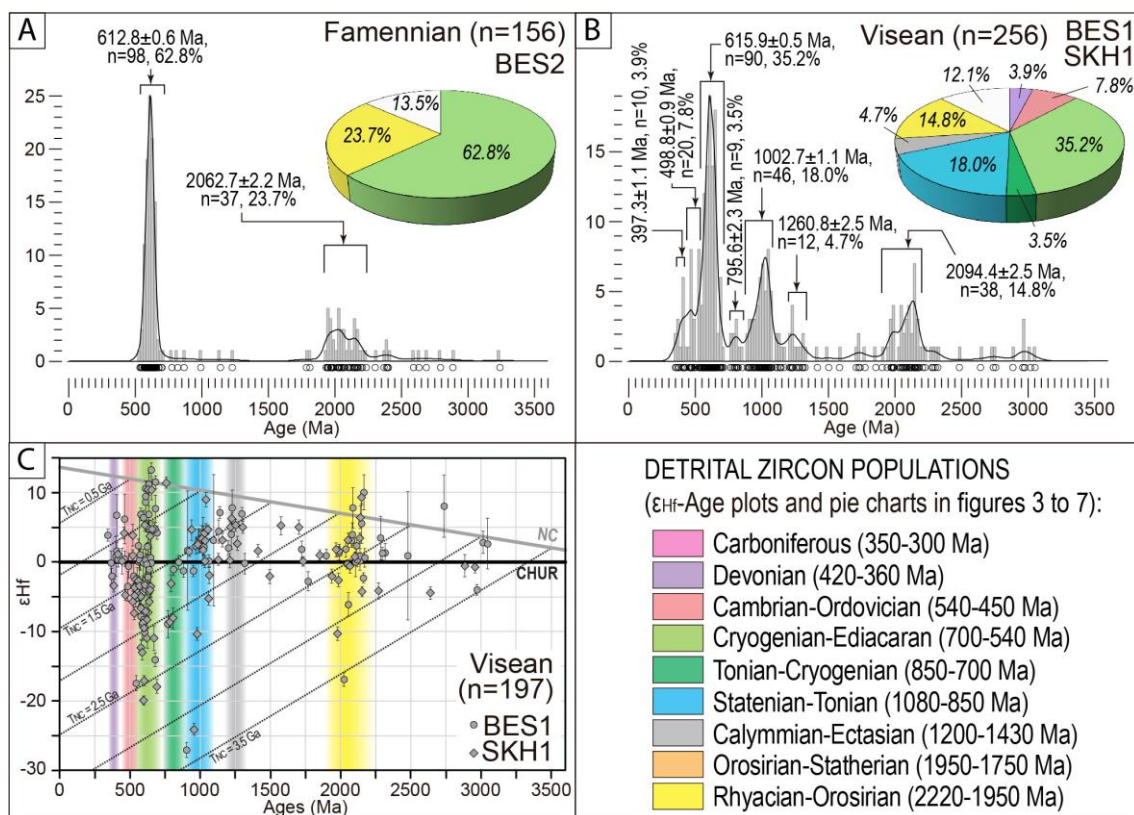


Figure 4.3. U-Pb and Hf results in the Ben Slimane area. A and B) Kernel Density Estimates (KDE, black lines), histograms (grey bars), and pie-charts (colors correspond to the different ages of the detrital zircon populations as in legend; white represents scattered data) showing the detrital zircon age distribution of Famennian (A) and Visean (B) samples. C) ϵ_{Hf} values versus U-Pb ages for the Ben Slimane samples (BES1 and SKH1); CHUR: Chondritic Uniform Reservoir (Bouvier et al., 2008); NC: new crust (Dhuime et al., 2011); dotted lines indicate the TNC new crust ages of the bulk crust ($^{176}\text{Lu}/^{177}\text{Hf} = 0.015$). Colors indicate the different detrital zircon populations used in the text.

The plot in Figure 4.3B represents a combination of the results from the two statistically identical Visean samples (BES1 and SHK1). Two hundred and fifty-four LA-ICPMS analyses were carried out on the two samples, yielding 215 concordant results. On sample SHK1, 52 SHRIMP measurements were also run, giving 41 concordant dates. Furthermore, 197 Hf isotope analyses were performed on detrital zircon grains from both samples, the results of which are shown in Figure 4.3C. The most outstanding feature of the resulting KDE/histogram plot (Figure 4.3B) is a Cryogenian-Ediacaran peak, which includes 35.2% of the data ($n=90$, ages from ca. 711 to 547 Ma) and yields an Ediacaran mean age of 615.9 ± 0.5 Ma. The ϵ_{Hf} values associated with this population ($n=71$) show considerable variability (-19.8 and +13.1). Second-order peaks gave Tonian-Stenian (1002.7 ± 1.1 Ma, ca. 1072-887 Ma, $n=46$, 18% of the data) and Rhyacian-Orosirian (2094.4 ± 2.5 Ma, ca. 2224-1932 Ma, $n=38$, 14.8% of the data) mean ages; both of these populations are characterized by mostly positive ϵ_{Hf} values, with a few scattered strongly negative ones (30 ϵ_{Hf} values between -26.9 and +8.9 for the Tonian-Stenian population, and 28 data from -16.8 to +9.9 for the Rhyacian-Orosirian one). Minor detrital zircon

populations are clustered at 1260.8 ± 2.5 Ma (ca. 1322-1206 Ma, $n=12$, 4.7%; 11 ϵ_{Hf} values between -0.3 and +7.8), 795.6 ± 2.3 Ma (ca. 852-764 Ma, $n=9$, 3.5%; 7 ϵ_{Hf} values between -8.9 and +11.3), 498.8 ± 0.9 Ma (ca. 538-450 Ma, $n=20$, 7.8%; 14 ϵ_{Hf} values between -7.4 and +6.1), and 397.3 ± 1.1 Ma (ca. 419-370 Ma, $n=10$, 3.9%; 7 ϵ_{Hf} values between -3.4 and +6.7). A few scattered dates have Archean-Rhyacian, Orosirian-Calymmian, and Stenian ages. The youngest detrital zircon populations of the Visean samples are Late Ediacaran (BES1: 578.3 ± 1.8 Ma, MSWD=1.32, $n=6$) and Early-Middle Ordovician (SKH1: 470.0 ± 2.3 Ma, MSWD=1.30, $n=5$); nonetheless, the youngest detrital zircon population of the combined two Visean samples is Early Devonian (409.7 ± 1.6 Ma, MSWD=0.85, $n=5$).

4.2. Sidi Bettache area

The results from the two Visean samples (ROM1 and AOU1) are represented in Figure 4.4. One hundred and ninety-eight LA-ICPMS analyses were carried out, together with 52 SHRIMP and 28 SIMS measurements, which yielded a total of 228 concordant results. The most important detrital zircon population is Cryogenian-Ediacaran (ca. 686-543 Ma), which yielded an Ediacaran mean age of 618.6 ± 0.5 Ma ($n=94$, 41.2% of the data). Another significant peak corresponds to the Rhyacian-Orosirian (ca. 2193-1902 Ma) population, with a mean age of 2052.3 ± 3.4 Ma ($n=49$, 21.5% of the data). Minor detrital zircon populations gave Statherian (1784.6 ± 6.2 Ma, ca. 1824-1689 Ma, $n=13$, 5.7% of the data) and Tonian (748.0 ± 1.8 Ma, ca. 808-716 Ma, $n=10$, 4.4% of the data) mean ages. Scattered data have Paleoarchean-Rhyacian, Calymmian-Tonian, and Cambrian-Carboniferous ages. The youngest detrital zircon populations in these two samples are Late Ediacaran (AOU1: 583.7 ± 1.7 Ma, MSWD=0.85, $n=6$) and Late Devonian (ROM1: 373.6 ± 1.9 Ma, MSWD=1.32, $n=4$). If the two statistically identical samples are considered together as representative of the Visean succession in the area, the youngest detrital zircon population is Late Devonian (373.6 ± 1.9 Ma, MSWD=1.32, $n=4$).

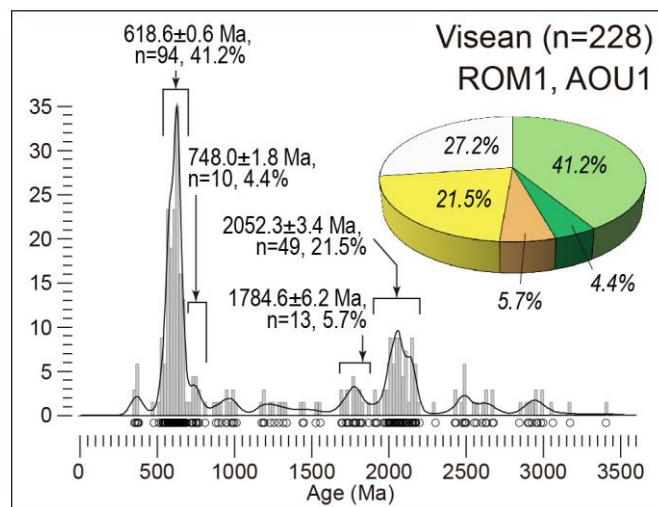


Figure 4.4. Kernel Density Estimates (KDE, black lines), histograms (grey bars), and pie-charts (colors correspond to detrital zircon populations as indicated in Figure 4.3; white represents scattered data)

showing the detrital zircon age distribution of two Visean samples (ROM1 and AOU1) from the Sidi Bettache area.

4.3. *Oulmes area*

One hundred and fifty LA-ICPMS analyses were carried out on the detrital zircon grains from Famennian sample OU4, which yielded 134 concordant results (Figure 4.5A). Three detrital zircon age populations can be identified in this sample, clustered at Cryogenian-Ediacaran (626.8 ± 0.5 Ma, ca. 717-549 Ma, $n=73$, 54.5% of the data), Tonian-Stenian (1010.6 ± 1.7 Ma, ca. 1078-923 Ma, $n=13$, 9.7% of the data) and Rhyacian-Orosirian (2049.4 ± 5.6 Ma, ca. 2133-2002 Ma, $n=14$, 10.4% of the data). Furthermore, twelve dates yielded Cambrian-Devonian ages, although they do not define a peak in the KDE diagram. Scattered dates gave Archean-Siderian, Orosirian-Stenian, and Tonian ages. The youngest detrital zircon population includes 5 dates that define a Late Ediacaran age of 558.7 ± 1.7 Ma (MSWD=1.04).

One hundred and twenty-four LA-ICPMS analyses were run on detrital zircon grains from the Visean sample OU1, yielding 104 concordant dates (Figure 4.5B). The main detrital zircon age populations observed in this sample are Cryogenian-Ediacaran (ca. 685-543 Ma), with an Ediacaran mean age of 619.8 ± 0.4 Ma ($n=53$, 51.0% of the data), and Rhyacian-Orosirian (ca. 2144-1940 Ma), with an Orosirian mean age of 2044.1 ± 1.8 Ma ($n=23$, 22.1% of the data). A few scattered dates yielded Paleoarchean-Rhyacian, Statherian-Tonian, and Late Devonian ages. The youngest detrital zircon population gave a Late Ediacaran mean age of 561.9 ± 1.5 Ma and includes 4 dates (MSWD=1.20).

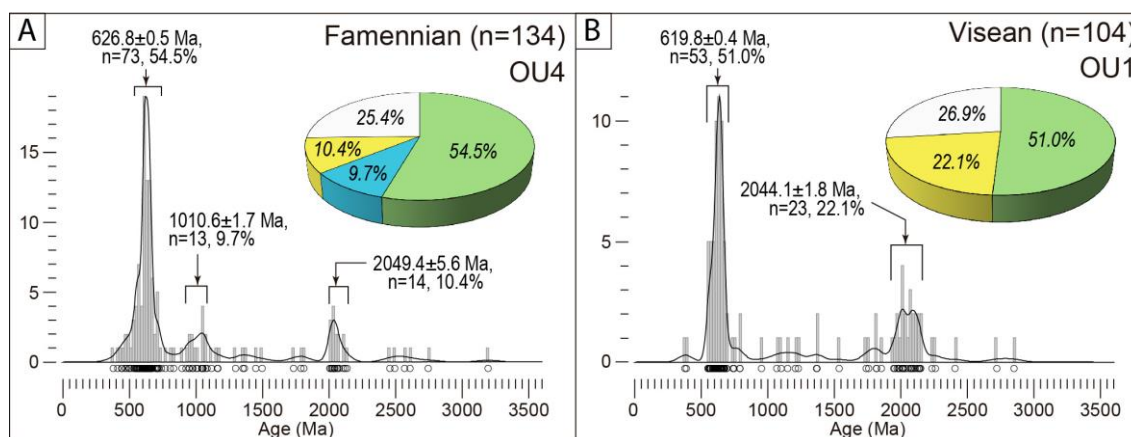


Figure 4.5. Kernel Density Estimates (KDE, black lines), histograms (grey bars), and pie-charts (colors correspond to detrital zircon populations as in legend indicated Figure 4.3; white represents scattered data) showing the detrital zircon age distribution of a Famennian (A; OU4) and a Visean (B; OU1) sample from the Oulmes area.

4.4. *Tiflet area*

The KDE diagram and histogram in Figure 4.6A show the results of the two Tournaisian samples (TIF1 and TIF2). Two hundred and twenty LA-ICPMS analyses

were carried out on detrital zircon grains from those samples, 162 of which yielded concordant results. Together with the U-Pb analyses, 154 Hf isotope analyses were performed. The results are shown in Figure 4.6B. Forty percent of the data are included in a Cryogenian-Ediacaran detrital zircon population (65 dates from ca. 713 Ma to ca. 544 Ma), which has an Ediacaran mean age of 614.5 ± 0.4 Ma and is characterized by a wide range of ϵ_{Hf} values (between -37.7 and +11.9, $n=64$). Secondary detrital zircon populations yielded Devonian (383.2 ± 0.6 Ma, ca. 415-361 Ma, $n=15$, 9.3% of the data; 15 ϵ_{Hf} values from -10.6 to +1.9), Stenian-Tonian (1005.7 ± 1.3 Ma, ca. 1058-970 Ma, $n=13$, 8% of the data; 11 ϵ_{Hf} values between -14.1 and +7.0), and Orosirian-Statherian (1783.1 ± 3.9 Ma, ca. 1814-1747 Ma, $n=10$, 6.2% of the data; 8 ϵ_{Hf} values between -17.0 and +3.2) mean ages. Minor populations are clustered around 1357.2 ± 2.9 Ma (Calymmian, ca. 1433-1280 Ma, $n=8$, 4.9% of the data; 8 ϵ_{Hf} values between -5.4 and +7.7) and 2097.7 ± 4.0 Ma (Rhyacian, ca. 2177-1965 Ma, $n=11$, 6.8% of the data; 11 ϵ_{Hf} values from -17.6 to +5.0). Scattered data have Mesoarchean-Rhyacian, Orosirian, Statherian-Calymmian, Ectasian-Stenian, Tonian, Cambrian-Ordovician, and Carboniferous ages. The youngest detrital zircon populations are Late Ediacaran in TIF1 (620.0 ± 1.5 Ma, MSWD=1.4, $n=6$) and Late Devonian in TIF2 (374.0 ± 1.5 Ma, MSWD=0.88, $n=4$). Combining both samples, the youngest detrital zircon population is Late Devonian and corresponds to the youngest detrital zircon population in TIF2.

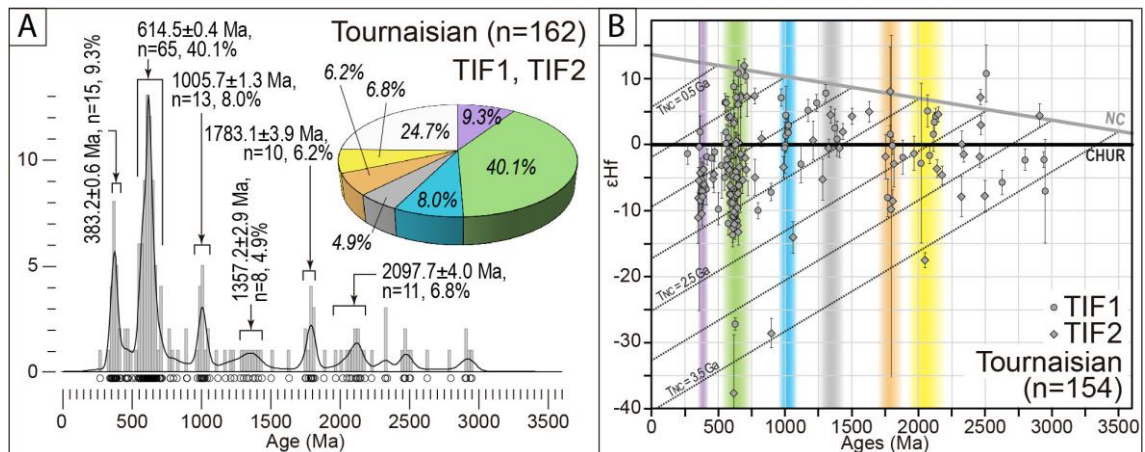


Figure 4.6. U-Pb and Hf results in the Tiflet area. A) Kernel Density Estimates (KDE, black lines), histograms (grey bars), and pie-charts (colors correspond to detrital zircon populations as indicated legend in Figure 4.3; white represents scattered data) showing the detrital zircon age distribution of two Tournaisian samples (TIF1 and TIF2). B) ϵ_{Hf} values versus U-Pb ages for samples TIF1 and TIF2; CHUR: Chondritic Uniform Reservoir (Bouvier et al., 2008); NC: new crust (Dhuime et al., 2011); dotted lines indicate the TNC new crust ages of the bulk crust ($^{176}\text{Lu}/^{177}\text{Hf} = 0.015$). Colors indicate the detrital zircon populations described in the text (see Figure 4.3 for legend).

4.5. Jerada area

One Serpukhovian-Middle Bashkirian (OUJ16) and two Middle Bashkirian-Kasimovian samples (OUJ18 and OUJ19) were collected in this area. The results are shown in Figure 4.7A, where all the concordant data have been plotted together, being the three samples statistically identical and representative of the Middle Carboniferous

succession in this area. Three hundred and thirty LA-ICMPS analyses were carried out, with 294 concordant results, 280 of which were then analyzed for Hf isotope signature (Figure 4.7B). Due to the variable size of zircon grains in sample OUI18, 70 additional SIMS analyses were run on this sample to reach a statistically representative number of data points; 58 of the SIMS analyses gave concordant dates. The most important detrital zircon age population in these samples is Cryogenian-Ediacaran, which yields a mean age of 615.3 ± 0.3 Ma (dates from ca. 685 to 543 Ma, $n=129$; 36.6% of the data); one hundred and three of these zircon spots were analyzed for Hf isotopes and yielded ϵ_{Hf} values varying between -30.1 and +9.0. Nineteen percent of the data ($n=66$) are clustered at Rhyacian-Orosirian ages (ca. 2218-1900 Ma) with a mean age of 2076.6 ± 2.5 Ma and a considerable variability in ϵ_{Hf} values (-16.9 to +5.9, $n=58$). Another important detrital zircon population yielded a Late Visean mean age (331.8 ± 0.3 Ma, dates from 351 to 297 Ma, $n=52$, 14.8% of the data). The ϵ_{Hf} values of this Carboniferous population are variable between -4.8 and +9.5 ($n=44$). Minor populations gave Cambrian (508.1 ± 1.0 Ma, ca. 538-478 Ma, $n=14$, 4% of the data; 8 ϵ_{Hf} values from -12.2 to +10.9), Late Tonian (754.0 ± 1.4 Ma, ca. 796-702 Ma, $n=12$, 3.4% of the data; 8 ϵ_{Hf} values from -14.5 to +11.3), Early Tonian (971.5 ± 1.1 Ma, ca. 1077-851 Ma, $n=33$, 9.4% of the data; 19 ϵ_{Hf} values between -19.7 and +12.2), and Orosirian (1847.8 ± 9.5 Ma, ca. 1895-1811 Ma, $n=8$, 2.3% of the data; 7 ϵ_{Hf} values between -17.0 and +3.2) mean ages. Very scattered data yielded Mesoarchean-Rhyacian, Statherian-Stenian, Tonian, and Middle Devonian ages. The youngest detrital zircon populations in the three samples are Serpukhovian-Middle Bashkirian (OUJ16: 323.0 ± 1.5 Ma, MSWD=1.4, $n=4$; OUJ18: 322.0 ± 2.5 Ma, MSWD=0.35, $n=4$) and Visean (OUJ19: 339.3 ± 0.7 Ma, MSWD=1.32, $n=7$). Combining the three samples, the youngest detrital zircon population includes 6 dates and yields an Early Bashkirian mean age (316.6 ± 0.9 Ma, MSWD=1.25).

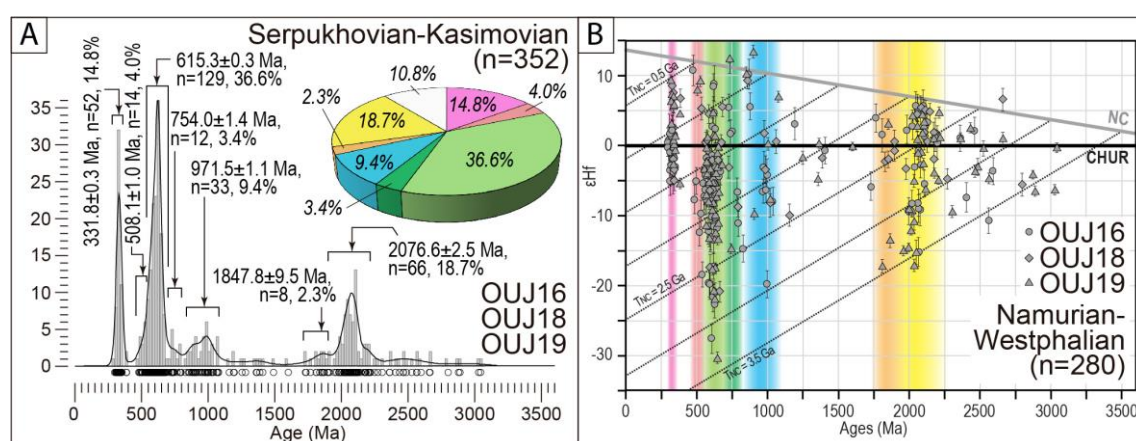


Figure 4.7. U-Pb and Hf results in the Jerada area. A) Kernel Density Estimates (KDE, black lines), histograms (grey bars), and pie-charts (colors correspond to detrital zircon populations as in legend indicated Figure 4.3; white represents scattered data) showing the detrital zircon age distribution of Serpukhovian-Middle Bashkirian (OUJ16) and Middle Bashkirian-Kasimovian (OUJ18 and OUJ19) samples. B) ϵ_{Hf} values versus U-Pb ages for samples OUJ16, OUJ18, and OUJ19; CHUR: Chondritic Uniform Reservoir (Bouvier et al., 2008); NC: new crust (Dhuime et al., 2011); dotted lines indicate the TNC new crust ages of the bulk crust ($^{176}\text{Lu}/^{177}\text{Hf} = 0.015$). Colors indicate the detrital zircon populations described in the text (see Figure 4.3 for legend).

To sum up, Cryogenian-Ediacaran and Rhyacian-Orosirian populations are always present in the studied Upper Devonian to Carboniferous samples, though at very different percentages. The Cryogenian-Ediacaran population encompasses 35-65% of the data, while the Rhyacian-Orosirian one represents 5-20% of the data. Taking into account all of the samples, up to seven minor detrital zircon populations can be defined: Orosirian-Statherian (ca. 1950-1750 Ma), Calymmian-Ectasian (ca. 1430-1200 Ma), Stenian-Tonian (ca. 1080-850 Ma), Tonian-Cryogenian (ca. 850-700 Ma), Cambrian-Ordovician (ca. 540-450 Ma), Devonian (ca. 420-360 Ma), and Carboniferous (ca. 350-300 Ma). The distribution of these populations in each area is summarized in Table 4.2.

5. Discussion

5.1. *Maximum depositional ages*

The youngest detrital zircon population in a sample is often used to define the maximum depositional age (MDA) of the rock (see Dickinson and Gehrels (2009) for methodology, and Sharman and Malkowski (2020) for discussion). This kind of data might be particularly useful to constrain the true depositional age (TDA) of the sediment, generally inferred either from the fossiliferous/palynological content or regional stratigraphic correlation. TDA can be coeval or younger than MDA (*e.g.*, Sharman and Malkowski, 2020) depending on the geodynamic and geographic setting in which the sediment was deposited.

All of the studied samples have MDA spanning from Late Ediacaran (ca. 585 Ma) to Late Carboniferous (ca. 315 Ma), which are coherent with the TDA based on palynomorphs/paleontological studies and/or regional stratigraphic correlation (Destombe, 1987; El Hassani, 1991 and references therein; Horon, 1952; Izart, 1991 and references therein; Kaiser et al., 2007; Muratet, 1988; Vidal, 1989; Zahraoui, 1991 and references therein). When considering groups of samples with similar TDA (see section 4; Figure 4.2), the Late Ediacaran youngest detrital zircon populations are replaced by Devonian to Late Carboniferous ones, thus suggesting that Devonian-Carboniferous magmatic rocks supplied detritus to all the Moroccan Mesetas, although in certain areas their impact is not noticeable in single samples. Our data show the necessity of exhaustive sampling and data density when trying to approximate MDA to TDA, especially in syn-orogenic settings, where high variability in the detrital zircon content is expected due to a combination of neo-formed with mixed and recycled sources.

Table 4.2. Summary of the detrital zircon populations identified in each area, with approximate mean ages, percentage of occurrence, and, when available, range of ϵ_{HF} values.

	BEN SLIMANE		SIDI BETTACHE VISEAN	OULMES		TIFLET TOURNAISIAN	JERADA SERPUKHOVIAN -BASHKIRIAN
	FAMENNIAN	VISEAN		FAMENNIAN	VISEAN		
CARBONIFEROUS ca. 350-300 Ma	-	-	-	-	-	-	ca. 330 Ma 14.8% $\epsilon_{\text{HF}} -4.8 / +9.5$
DEVONIAN ca. 420-360 Ma	-	ca. 400 Ma 3.9% $\epsilon_{\text{HF}} -3.4 / +6.7$	-	-	ca. 385 Ma 9.3% $\epsilon_{\text{HF}} -10.6 / +1.9$	-	-
CAMBRIAN- ORDOVICIAN ca. 540-450 Ma	-	ca. 500 Ma 7.8% $\epsilon_{\text{HF}} -7.4 / +6.1$	-	-	-	-	ca. 510 Ma 4.0% $\epsilon_{\text{HF}} -12.2 / +10.9$
CRYOGENIAN- EDIACARAN ca. 700-540 Ma	ca. 615 Ma 62.8%	ca. 615 Ma 35.2% $\epsilon_{\text{HF}} -19.8 / +13.1$	ca. 620 Ma 41.2%	ca. 630 Ma 54.5%	ca. 615 Ma 40.1% $\epsilon_{\text{HF}} -37.7 / +11.9$	ca. 615 Ma 36.6% $\epsilon_{\text{HF}} -30.1 / +9.0$	
TONIAN- CRYOGENIAN ca. 850-700 Ma	-	ca. 795 Ma 3.5% $\epsilon_{\text{HF}} -8.9 / +11.3$	ca. 750 Ma 4.4%	-	-	ca. 750 Ma 3.4% $\epsilon_{\text{HF}} -14.5 / +11.3$	
STENIAN- TONIAN ca. 1080-850 Ma	-	ca. 1000 Ma 18.0% $\epsilon_{\text{HF}} -26.9 / +8.9$	-	ca. 1010 Ma 9.7%	ca. 1005 Ma 8.0% $\epsilon_{\text{HF}} -14.1 / +7.0$	ca. 970 Ma 9.4% $\epsilon_{\text{HF}} -19.7 / +12.2$	
CALYMMIAN- ECTASIAN ca. 1430-1200 Ma	-	ca. 1260 Ma 4.7% $\epsilon_{\text{HF}} -0.3 / +7.8$	-	-	ca. 1355 Ma 4.9% $\epsilon_{\text{HF}} -5.4 / +7.7$	-	
OROSIRIAN- STATHERIAN ca. 1950-1750 Ma	-	-	ca. 1785 Ma 5.7%	-	ca. 1785 Ma 6.2% $\epsilon_{\text{HF}} -9.9 / +8.0$	ca. 1850 Ma 2.3% $\epsilon_{\text{HF}} -17.0 / +3.2$	
RHYACIAN- OROSIRIAN ca. 2220-1950 Ma	ca. 2065 Ma 23.7%	ca. 2095 Ma 14.8% $\epsilon_{\text{HF}} -16.8 / +9.9$	ca. 2055 Ma 21.5%	ca. 2050 Ma 10.4%	ca. 2100 Ma 6.8% $\epsilon_{\text{HF}} -17.6 / +5.0$	ca. 2075 Ma 18.7% $\epsilon_{\text{HF}} -16.9 / +5.9$	

5.2. Provenance of pre-Devonian detrital zircon grains

Geochronological studies on detrital zircon grains from Late Ediacaran-Early Carboniferous samples of the Moroccan Variscides have been carried out by several authors (Abati et al., 2010, 2012; Accotto et al., 2019, 2020; Avigad et al., 2012; Ghienne et al., 2018; Letsch et al., 2018; Pérez-Cáceres et al., 2017) with the aim of finding out the main sources of sediments that fed the northern Gondwanan margin during the Paleozoic. All of these authors agreed that the main source area of sediments in the Moroccan Variscides is the West African Craton (WAC; Figure 4.8), based on: (i) the recurrent presence of important Cryogenian-Ediacaran (ca. 0.6-0.75 Ga) and Paleoproterozoic (ca. 2.0 Ga) detrital zircon populations, which can be related to the Cadomian/Pan-African and Eburnean orogenic cycles, respectively (Nance et al., 2008 and references therein); and (ii) the absence of a significant Mesoproterozoic population, which is otherwise very common in areas affected by the Grenville orogeny (1.3-0.9 Ga; Ernst et al., 2008), such as Amazonia, Avalonia, and Baltica/Laurentia (Figure 4.8), and in some European Variscan zones fed from the Arabian-Nubian shield and/or the Saharan Metacraton (*e.g.*, Bea et al., 2010; Fernández-Suárez et al., 2014).

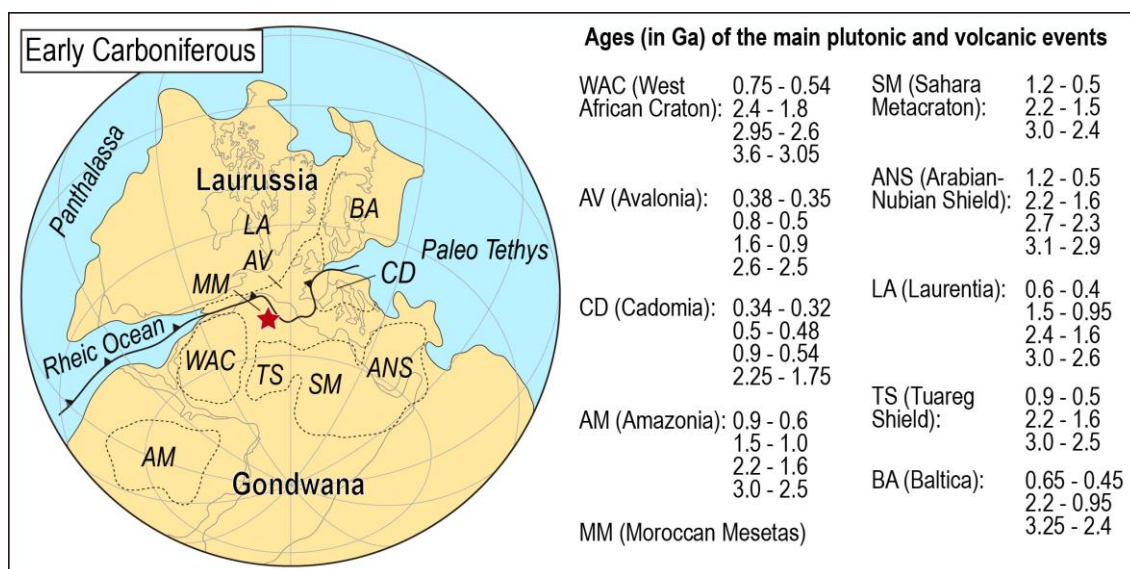


Figure 4.8. Paleogeographic reconstruction of Gondwana and Laurussia at Early Carboniferous time (after Murphy et al., 2016 and references therein; Nance et al., 2012 and references therein). Ages of the main magmatic events are from Abati et al. (2010), Bea et al. (2010), Cambeses et al. (2017) and references therein, Linnemann et al. (2011) and references therein, Marzoli et al., (2017) and references therein, Nance et al. (2008), Pereira et al. (2012, 2017), and Santos et al. (1987). The red star indicates the approximate location of the studied area.

In terms of detrital zircon populations, the magmatic input of Cambrian-Ordovician Rhenish Ocean rifting (Linnemann et al., 2008; Nance et al., 2012, 2010) in the Moroccan Variscides was scarce or negligible (Accotto et al., 2019, 2020; Ghienne et al., 2018; Letsch et al., 2018), except in a few, very localized areas (Letsch et al., 2018). In our samples, Cambrian-Ordovician zircon grains are rare (0-8% of the data). Cambrian mafic

magmatic rocks are known in the Coastal Block (Poulet et al., 2018), but they are restricted to volcanic focuses with limited spread. Therefore, we can infer that the Moroccan Variscides were only partially affected by the magmatism related to the Cambrian-Ordovician rifting, probably because of their more inland position in the Gondwana margin than other regions, such as the Ossa-Morena and Central Iberian Zones (Figure 4.1A), where this kind of magmatism was ubiquitous and Cambrian-Ordovician detrital zircon grains are usually present in syn-orogenic rocks (Martínez Catalán et al., 2008; Pastor-Galán et al., 2013b; Pereira et al., 2020b).

A Stenian-Tonian (ca. 1.0 Ga) detrital zircon population is identified in the Moroccan Variscides (up to 30% of the data) although it is not present everywhere. This population was found in Ediacaran-Late Devonian samples from the Anti-Atlas (Avigad et al., 2012) and the Moroccan Mesetas (Accotto et al., 2019, 2020; Ghienne et al., 2018). To explain the occurrence of these ages, the source of which is unknown in the WAC (Figure 4.8), a distal and probably intermittent NE African source (namely the Sahara Metacraton; Figure 4.8) was invoked.

5.3. Source evolution during Late Devonian-Carboniferous time

In this study, we analyzed two Famennian samples (BES2 and OU4 in the Ben Slimane and Oulmes areas, respectively), which have the same detrital zircon populations as those described by other authors in the Moroccan Variscides (Abati et al., 2010, 2012; Accotto et al., 2019, 2020; Avigad et al., 2012; Letsch et al., 2018; Pérez-Cáceres et al., 2017), thus suggesting that in Late Devonian times, this part of the northern margin of Gondwana was still mostly fed by the WAC (Eburnean and Cadomian/Pan-African orogenies), together with some minor and distant NE African (ca. 1.0 Ga) sources recorded in the Oulmes area (Figure 4.9A).

Slightly younger samples (Tournaisian) collected in the Tiflet area (TIF1 and TIF2) show a Devonian detrital zircon population, which could not have been supplied by the WAC. Very similar results were described by Accotto et al. (2020) in the Debdou-Mekkam area (EMM), and were interpreted as coming from a Devonian magmatic arc (Pereira et al., 2012), formed along the margin of an Avalonian terrane (*e.g.*, Simancas et al., 2005) during the closure of the Rheic ocean and the first collisional stages between this terrane and northern Gondwana (Tournaisian-Early Viséan; Accotto et al., 2020). This hypothesis is reinforced by the presence of Mesoproterozoic detrital zircon grains in these samples, which was also attributed to the approaching Avalonian block. Interestingly, the Tiflet area samples yielded a bimodal Mesoproterozoic detrital zircon population with peaks at ca. 1.0 and 1.35 Ga, which can be related to Grenvillian sources (*e.g.*, Ernst et al., 2008). Because of the location of the Tiflet area (*i.e.*, very close to the RTFZ separating the Moroccan Mesetas from the Caledonian Sehouli Block; Figure 4.1C), we claim that Tournaisian sedimentation in this area was partially fed from this exotic terrane (Figure 4.9B), which delivered zircon grains of Mesoproterozoic (Grenvillian orogeny) and Devonian (magmatic arc) ages; additionally, the WAC would

have provided the Cryogenian-Ediacaran and Paleoproterozoic detrital zircon grains. The similarities between the Tournaisian samples from Tiflet and Debdou-Mekkam areas also extend to the Hf isotope data (Figure 4.6B; Accotto et al., 2020). Actually, the Devonian ϵ_{Hf} range in the Tiflet samples (-10.6 to +1.9) is similar to that of sample MIM2 (-6 to 0) in the Debdou-Mekkam area. The new crustal ages (T_{NC} ; Dhuime et al., 2011) of the Tiflet samples range from ca. 1.0 to 2.0 Ga, which suggests that these zircon grains formed from partial melting of Mesoproterozoic and Paleoproterozoic crust, supporting the hypothesis of Avalonian sources for the Devonian detrital zircon population. Furthermore, the Stenian-Tonian and Ectasian detrital zircon populations are characterized by mostly positive ϵ_{Hf} values (-5.4 to +7.7, with the exception of only one more negative value at -14.1), a range compatible with that seen in the Debdou-Mekkam area (ca. -5 to +5; Accotto et al., 2020) and some Avalonian terranes (ca. -5 to +7; Henderson et al., 2018 and references therein). These mostly positive data might indicate that the magmas in which the zircon grains formed were generated from Late Paleoproterozoic-Mesoproterozoic crust. Based on these similarities and assuming that the Debdou-Mekkam region was a fore-arc basin located at the front of the Avalonian promontory (Accotto et al., 2020), we can infer that the Tournaisian sediments in the Tiflet area might have been deposited in an analogous context but in a more lateral position with respect to the frontal promontory. Moreover, the Devonian detrital zircon population in the Tiflet samples (ca. 385 Ma) is slightly older than in the EMM (ca. 376 Ma), which might support an eastward migration of the Avalonian promontory, as well as the accompanying magmatic arc, in Late Devonian times.

After the initial collision between Gondwana and Avalonia (Late Tournaisian-Early Visean; Accotto et al., 2020), the detrital zircon spectra in younger syn-orogenic sediments are characterized by a mix of Gondwanan (WAC) and non-Gondwanan (Avalonian-Grenvillian) sources (Figure 4.9C). This is particularly noticeable in a couple of samples from the Alborán Domain (Rif, Figure 4.1B) published by Azdimoussa et al. (2019), and in the Visean samples from the Ben Slimane area (BES1 and SKH1). All these samples, in fact, are characterized by a significant number of Mesoproterozoic dates. In particular, our samples include almost 5% of Ectasian (ca. 1.2-1.35 Ga) ages and, moreover, an Early Devonian (ca. 400 Ma) population that was not recorded in the Famennian sample (BES2). When looking at the Hf isotope signature, the ϵ_{Hf} values of the Devonian and Ectasian detrital zircon populations are very similar to those described in the Tiflet area. Therefore, we conclude that these zircon grains might have been sourced from the erosion of the Avalonian promontory already accreted to the northern Gondwana margin or its lateral continuation offshore of the Atlantic Moroccan coast. In this regards, further south in the Oulad Dlim Massif (SW Morocco), the existence of non-Gondwana-derived rocks with a Silurian-Devonian (Caledonian) tectono-magmatic imprint (Bea et al., 2020; Gärtner et al., 2013) suggests that the Rheic Ocean suture might be located close to the Atlantic coastline.

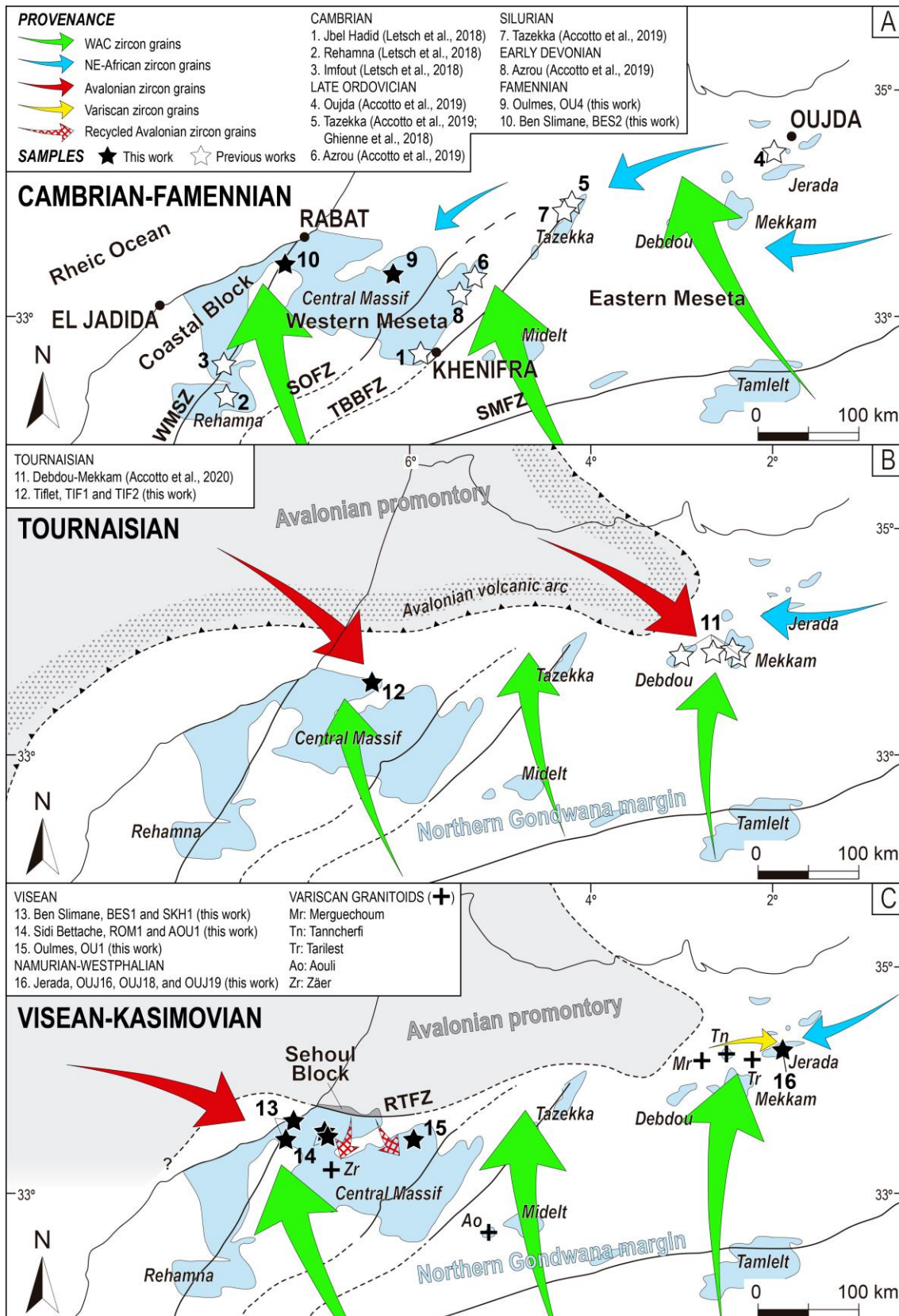


Figure 4.9. Evolutionary sketches showing the variation in detrital zircon sources in the Moroccan Mesetas. (A) Cambrian-Late Devonian, (B) Tournaisian, and (C) Visean-Kasimovian time.

In the Visean samples from the Sidi Bettache (ROM1, AOU1) and Oulmes areas (OU1), the influence of Avalonian sources seems to be minor as compared to the Ben Slimane area. In this regard, dates between ca. 1.6-1.05 Ga are scarce and very scattered in samples ROM1, AOU1 and OU1; combining the data of these three samples (Figures 4.4B and 4.5), the Mesoproterozoic data represents ca. 6% of the dates, although the rather scattered distribution precludes the individualization of any detrital zircon population of that age. Therefore, the influence of the Avalonian promontory in the Sidi Bettache and Oulmes areas appears to be minor with respect to the Ben Slimane, Tiflet, and Debdou-Mekkam areas, probably due to the longer distance from the exotic block. Furthermore, since these Visean samples postdate the Eo-Variscan collision between the Avalonian promontory and Gondwana, part of the Mesoproterozoic zircon grains might have been recycled from previous syn-orogenic sediments of Tournaisian-Early Visean ages deposited in areas close to the Avalonian terrane (i.e., Tiflet area; Figure 4.9C).

The Late Carboniferous samples from the Jerada area (OUJ16, OUJ18, and OUJ19) are characterized by detrital zircon spectra similar to older samples (i.e., Ordovician) from the Oujda EMM area (Accotto et al., 2019). Besides the Cryogenian-Ediacaran and Paleoproterozoic detrital zircon populations, the Oujda and Jerada samples are characterized by Stenian-Tonian dates clustered at ca. 0.95-0.97 Ga and representing 5-9% of the data. This similarity might suggest that the sources, at least in the eastern part of the EMM, did not change during the Ordovician-Carboniferous period. It is therefore plausible that the influence of the Avalonian promontory as a source of sediments only embraced the EMM to the Debdou-Mekkam area, while eastwards, the Oujda-Jerada region could have not received this input and represents a stable part of the northern Gondwana margin. Actually, the eastern part of the EMM (Beni Snassen, Oujda and Jerada areas) was not deformed during the initial collision between Avalonia and Gondwana (Accotto et al., 2020), and was principally fed by (primary or recycled) WAC sources during all of the Paleozoic and, to a lesser extent, by NE-African sources (e.g., Sahara Metacraton, Figure 4.8).

The Late Carboniferous samples from the Jerada area are also characterized by ca. 15% of the data clustered in a Middle Carboniferous (ca. 330 Ma) detrital zircon population, with ϵ_{HF} values ranging from -10 to +10, and T_{NC} from ca. 1.5 to 0.5 Ga. Variscan granitoids of Middle Carboniferous age are known in the EMM (e.g., Tarilest, Tanncherfi, and Merguechoum; El Hadi et al., 2006) and they probably represent the source of the detrital zircon grains with this age found in our samples. The crustal thickening originated by the collision between Avalonia and Gondwana (Accotto et al., 2020) probably induced an increase in the temperature within the Gondwanan crust, which, in turn, gave way to several middle Carboniferous igneous rocks, later exposed and partially eroded at Late Carboniferous times.

6. Conclusions

i) The systematic dating and Hf-isotopic characterization of Late Devonian-Late Carboniferous samples collected in several areas of the Moroccan Mesetas have allowed us to identify the influence of an allochthonous Avalonian promontory that approached and collided with the northern margin of Gondwana at Late Tournaisian-Early Visean time (Accotto et al., 2020). This Avalonian terrane is represented by the Sehoul Block, though it probably continues southwards offshore the Atlantic coastline.

ii) Before Late Devonian time, sediments in the Moroccan Variscides were sourced from the West African Craton, with a secondary and intermittent input from the distant Sahara Metacraton.

iii) The approaching and collision of the Avalonian promontory was recorded in Tournaisian samples from the Tiflet (this study) and Debdou-Mekkam (EMM; Accotto et al., 2020) areas, both characterized by a considerable number of Late Devonian (ca. 385-375 Ma) and Mesoproterozoic (ca. 1.6-1.0 Ga) zircon grains. The influence of this exotic terrane continued after its initial collision with Gondwana, delivering Devonian and Mesoproterozoic detrital zircon grains during the Visean in the adjacent areas to the Sehoul Block or its lateral prolongation offshore along the Moroccan Atlantic coastline.

iv) Among the Carboniferous samples analyzed, only those from the Ben Slimane are characterized by Mesoproterozoic and Devonian detrital zircon ages, while the samples from the Sidi Bettache, Oulmes, and Jerada areas did not record these dates or contain only a few (probably recycled) Mesoproterozoic grains.

v) The Late Carboniferous Jerada samples are characterized by a noteworthy Middle Carboniferous detrital zircon population sourced from syn-orogenic granites cropping out in the EMM and attesting the Early Variscan thickening and subsequent thermal maturation of the Gondwanan crust.

Acknowledgments

This study was funded by the Ministerio de Economía y Competitividad (MINECO) of Spain through the project PANGEATOR (CGL2015-71692) and the Pre-doctoral scholarship BES-2016-078168. The CL imaging was carried out in Curtin University's Microscopy & Microanalysis Facility, of which instrumentation has been partially funded by the University, State and Commonwealth Governments, and the Scanning Electron Microscope (SEM) Facility at the University of Edinburgh. Laboratory analyses on the detrital zircon grains were carried out on the SHRIMP II and GeoHistory Facility instruments of the JdLC, supported by AuScope (auscope.org.au) and the Australian Government via the National Collaborative Research Infrastructure Strategy (NCRIS). The NPII multi-collector in the GeoHistory Facility was obtained via funding from the Australian Research Council LIEF program (LE150100013). The SIMS analyses were performed at the NERC Ion Microprobe Facility of the University of Edinburgh (UK).

We are indebted to Mike Hall and Brad McDonald for their technical support on sample preparation and LA-ICPMS, respectively. The authors want to thank prof. R. Thomas Becker (University of Münster, Germany) for his insights into the Western Meseta stratigraphy. Reviews and comments by Dr. Gabriel Gutiérrez-Alonso, Prof. Dr. Ulf Linnemann, and Dr. Andrea Marzoli are warmly acknowledged.

Data availability

Supplementary material including the Appendix A, C, D, and E cited in the text might be found in Mendeley Datasets repository with the doi: 10.17632/x7zwsghnb.1 (<https://data.mendeley.com/datasets/x7zwsghnb/draft?a=4c930b1c-4108-449f-abcf-f8cb1b7e3cb7>)

References

- Abati, J., Aghzer, A.M., Gerdes, A., Ennih, N., 2012. Insights on the crustal evolution of the West African Craton from Hf isotopes in detrital zircons from the Anti-Atlas belt. *Precambrian Research* 212–213, 263–274. doi:10.1016/j.precamres.2012.06.005
- Abati, J., Mohsine Aghzer, A., Gerdes, A., Ennih, N., 2010. Detrital zircon ages of Neoproterozoic sequences of the Moroccan Anti-Atlas belt. *Precambrian Research* 181, 115–128. doi:10.1016/j.precamres.2010.05.018
- Accotto, C., Martínez Poyatos, D., Azor, A., Jabaloy-Sánchez, A., Talavera, C., Evans, N.J., Azdimousa, A., 2020. Tectonic Evolution of the Eastern Moroccan Meseta: From Late Devonian Forearc Sedimentation to Early Carboniferous Collision of an Avalonian Promontory. *Tectonics* 39, 1–29. doi:10.1029/2019TC005976
- Accotto, C., Martínez Poyatos, D.J., Azor, A., Talavera, C., Evans, N.J., Jabaloy-Sánchez, A., Azdimousa, A., Tahiri, A., El Hadi, H., 2019. Mixed and recycled detrital zircons in the Paleozoic rocks of the Eastern Moroccan Meseta: Paleogeographic inferences. *Lithos* 338–339, 73–86. doi:10.1016/j.lithos.2019.04.011
- Alberti, G.K.B., 1969. Trilobiten des jüngeren Silurium sowie des Unter- und Mitteldevons. I. Mit Beiträgen zur-Devon-Stratigraphie einiger Gebiete Marokko und Oberfranken. *Abh Senckenb Naturforsch Ges.*
- Avigad, D., Gerdes, A., Morag, N., Bechstäd, T., 2012. Coupled U-Pb-Hf of detrital zircons of Cambrian sandstones from Morocco and Sardinia: Implications for provenance and Precambrian crustal evolution of North Africa. *Gondwana Research* 21, 690–703. doi:10.1016/j.gr.2011.06.005
- Azdimousa, A., Jabaloy-Sánchez, A., Talavera, C., Asebriy, L., González-Lodeiro, F., Evans, N.J., 2019. Detrital zircon U-Pb ages in the Rif Belt (northern Morocco):

- Paleogeographic implications. *Gondwana Research* 70, 133–150. doi:10.1016/j.gr.2018.12.008
- Bea, F., Montero, P., Haissen, F., Molina, J.F., Lodeiro, F.G., Mouttaqi, A., Kuiper, Y.D., Chaib, M., 2020. The Archean to Late-Paleozoic architecture of the Oulad Dlim Massif, the main Gondwanan indenter during the collision with Laurentia. *Earth-Science Reviews* 103273. doi:10.1016/j.earscirev.2020.103273
- Bea, F., Montero, P., Talavera, C., Abu Anbar, M., Scarrow, J.H., Molina, J.F., Moreno, J.A., 2010. The palaeogeographic position of Central Iberia in Gondwana during the Ordovician: Evidence from zircon chronology and Nd isotopes. *Terra Nova* 22, 341–346. doi:10.1111/j.1365-3121.2010.00957.x
- Beauchamp, J., Izart, A., 1987. Early Carboniferous basins of the Atlas-Meseta domain (Morocco): sedimentary model and geodynamic evolution. *Geology* 15, 797–800. doi:10.1130/0091-7613(1987)15<797:ECBOTA>2.0.CO;2
- Becker, R.T., El Hassani, A., 2020. Devonian to Lower Carboniferous stratigraphy and facies of the Moroccan Meseta: implications for palaeogeography and structural Interpretation - a project outline. *Hassan II Accademy of Science and Technology, Frontiers in Science and Engineering* 10, 9–25.
- Bouabdelli, M., 1989. Tectonique et sédimentation dans un bassin orogénique: le sillon viséen d'Azrou-Khenifra (Est du Massif Hercynien Central du Maroc). Ph.D. Thesis. U.E.R. de Sciences de la vie et de la Terre, Institut de Géologie, Strasbourg, France.
- Bouvier, A., Vervoort, J.D., Patchett, P.J., 2008. The Lu–Hf and Sm–Nd isotopic composition of CHUR: Constraints from unequilibrated chondrites and implications for the bulk composition of terrestrial planets. *Earth and Planetary Science Letters* 273, 48–57. doi:10.1016/j.epsl.2008.06.010
- Cailleux, Y., Chevremont, P., Baudin, T., Razin, P., Chenakeb, M., Thieblemont, D., Hoepffner, C., Bensahal, A., Roger, J., Vaslet, D., 2001. Carte géologique du Maroc N°413: Ezzhiliga - Echelle 1/50.000. Royaume du Maroc, Ministère l'Énergie des Mines du Développement Durable.
- Cailleux, Y., Deloche, C., Gonord, H., Rolin, P., 1983. Les zones de cisaillement hercyniens en basse Meseta marocaine. *Notes et Memoires du Service Géologique du Maroc* 335, 199–209.
- Cambeses, A., Scarrow, J.H., Montero, P., Lázaro, C., Bea, F., 2017. Palaeogeography and crustal evolution of the Ossa–Morena Zone, southwest Iberia, and the North Gondwana margin during the Cambro-Ordovician: a review of isotopic evidence. *International Geology Review* 59, 94–130. doi:10.1080/00206814.2016.1219279
- Chakiri, S., Tahiri, A., 2000. La formation chaotique famenno-tournaisienne du Grou: témoin de la bordure orientale du bassin de Sidi Bettache (Meseta marocaine). *Bulletin de l'Institut Scientifique de Rabat* 22, 9–15.

- Chellai, H., Essamoud, R., Rjimati, E.C., 2011. Le bassin houiller de Jerada (Chaîne des Horsts, Maroc oriental), in: Mouttaqi, A., Rjimati, E.C., Maacha, L., Michard, A., Soulaïmani, A., Ibouh, H. (Eds.), *Nouveaux Guides Géologiques et Miniers Du Maroc. Volume 9: Les Principales Mines Du Maroc. Notes et Memoires Du Service Géologique Du Maroc*, 564. pp. 331–335.
- Cózar, P., Vachard, D., Izart, A., Said, I., Somerville, I., Rodríguez, S., Coronado, I., El Houicha, M., Ouarhache, D., 2020. Lower-middle Viséan transgressive carbonates in Morocco: Palaeobiogeographic insights. *Journal of African Earth Science* 168. doi:10.1016/j.jafrearsci.2020.103850
- Destombe, J., 1987. Carte géologique du Maroc No350: Casablanca-Mohammedia - Echelle 1/100.000. Roy. du Maroc, Ministère l’Energie des Mines du Développement Durable.
- Dhuime, B., Hawkesworth, C., Cawood, P., 2011. When Continents Formed. *Science*. 331, 154–155. doi:10.1126/science.1201245
- Dickinson, W.R., Gehrels, G.E., 2009. Use of U–Pb ages of detrital zircons to infer maximum depositional ages of strata: A test against a Colorado Plateau Mesozoic database. *Earth and Planetary Science Letters* 288, 115–125. doi:10.1016/j.epsl.2009.09.013
- El Hadi, H., Simancas, J.F., Tahiri, A., Gonzalez-Lodeiro, F., Azor, A., Martinez-Poyatos, D., 2006. Comparative review of the Variscan granitoids of Morocco and Iberia: proposal of a broad zonation. *Geodinamica Acta* 19, 103–116. doi:10.3166/ga.19.103-116
- El Haïbi, H., El Hadi, H., Tahiri, A., Martínez Poyatos, D., Gasquet, D., Pérez-Cáceres, I., González Lodeiro, F., Mehdioui, S., 2020. Geochronology and isotopic geochemistry of Ediacaran high-K calc-alkaline felsic volcanism: An example of a Moroccan perigondwanan (Avalonian?) remnant in the El Jadida horst (Mazagonia). *Journal of African Earth Science* 163, 103669. doi:10.1016/j.jafrearsci.2019.103669
- El Hassani, A., 1987. Les structures calédono-hercyniennes dans la zone de Rabat-Tiflet (Meseta Marocaine septentrionale). *Bulletin de l’Institut Scientifique de Rabat* 11, 47–58.
- El Hassani, A., 1991. La Zone de Rabat-Tiflet: bordure nord de la Chaîne Calédono-Hercynienne du Maroc. *Bulletin de l’Institut Scientifique de Rabat* 15, 1-34.
- El Hassani, A., Tahiri, A., Chakiri, S., Zouine, E.M., Fedan, B., El Fellah, B., 2002. Carte géologique du Maroc No398: Khemisset - Echelle 1/100.000. Royaume du Maroc, Ministère l’Energie des Mines du Développement Durable.
- El Houicha, M., Pereira, M.F., Jouhari, A., Gama, C., Ennih, N., Fekkak, A., Ezzouhairi, H., El Attari, A., Silva, J.B., 2018. Recycling of the Proterozoic crystalline basement in the Coastal Block (Moroccan Meseta): new insights for understanding the

- geodynamic evolution of the northern peri-Gondwanan realm. *Precambrian Research* 306, 129–154. doi:10.1016/j.precamres.2017.12.039
- El Touhami, M., 1993. Le Trias évaporitique du bassin de Khémisset (Maroc Central): Géométrie des dépôts, Evolution sédimentaire et géochimie. Ph.D. Thesis. University Claude Bernard, Lyon, France.
- El Wartiti, M., 1994. Le Permien. *Bulletin de l'Institut Scientifique de Rabat* 18, 84–92.
- Ernst, R.E., Wingate, M.T.D., Buchan, K.L., Li, Z.X., 2008. Global record of 1600-700 Ma Large Igneous Provinces (LIPs): Implications for the reconstruction of the proposed Nuna (Columbia) and Rodinia supercontinents. *Precambrian Research* 160, 159–178. doi:10.1016/j.precamres.2007.04.019
- Fadli, D., 1990. Evolution sédimentaire et structurale des massifs de Mdakra et du Khatouat: deux segments hercyniens de la Meseta marocaine nord-occidentale. Ph.D. Thesis. Université Mohammed V, Rabat.
- Fernández-Suárez, J., Gutiérrez-Alonso, G., Pastor-Galán, D., Hofmann, M., Murphy, J.B., Linnemann, U., 2014. The Ediacaran-Early Cambrian detrital zircon record of NW Iberia: Possible sources and paleogeographic constraints. 103, 1335–1357. doi:10.1007/s00531-013-0923-3
- Franke, W., Cocks, L.R.M., Torsvik, T.H., 2017. The Palaeozoic Variscan oceans revisited. *Gondwana Research* 48, 257–284. doi:10.1016/j.gr.2017.03.005
- Gärtner, A., Villeneuve, M., Linnemann, U., El Archi, A., Bellon, H., 2013. An exotic terrane of Laurussian affinity in the Mauritanides and Souttoufides (Moroccan Sahara). *Gondwana Research* 24, 687–699. doi:10.1016/j.gr.2012.12.019
- Ghienne, J.F., Benvenuti, A., El Houicha, M., Girard, F., Kali, E., Khoukhi, Y., Langbour, C., Magna, T., Míková, J., Moscariello, A., Schulmann, K., 2018. The impact of the end-Ordovician glaciation on sediment routing systems: a case study from the Meseta (northern Morocco). *Gondwana Research* 63, 169–178. doi:10.1016/j.gr.2018.07.001
- Henderson, B.J., Collins, W.J., Brendan Murphy, J., Hand, M., 2018. A hafnium isotopic record of magmatic arcs and continental growth in the Iapetus Ocean: The contrasting evolution of Ganderia and the peri-Laurentian margin. *Gondwana Research* 58, 141–160. doi:10.1016/j.gr.2018.02.015
- Hoepffner, C., 1987. La tectonique hercynienne dans l'Est du Maroc. Ph.D. Thesis. Université Louis Pasteur, Strasbourg.
- Hoepffner, C., 1989. L'évolution structurale hercynienne de la Méséta marocain orientale. Essai de mise au point. Notes et Memoires du Service Géologique du Maroc 335, 229-237.

- Hoepffner, C., Houari, M.R., Bouabdelli, M., 2006. Tectonics of the North African Variscides (Morocco, western Algeria): an outline. *Comptes Rendus - Geoscience* 338, 25–40. doi:10.1016/j.crte.2005.11.003
- Horon, O., 1952. Contribution a l'étude du bassin de Djerada. *Notes et Memoires du Protectorat de la Republique Française au Maroc* 89, 180.
- Izart, A., 1991. Les bassins carbonifères de la Méséta marocaine, étude sédimentologique et approche du contexte structural. Part de la tectonique et de l'eustatisme. *Géologie Méditerranéenne* 18, 61–72. doi:10.3406/geolm.1991.1452
- Izart, A., Tahiri, A., El Boursoumi, A., Chevremont, P., 2001. Carte géologique du Maroc no 411: Bouqachmir - echelle 1/50.000. Royaume du Maroc, Ministère l'Energie des Mines du Développement Durable.
- Izart, A., Vieslet, J.-L., 1988. Stratigraphie, sédimentologie et micropaléontologie du Faménnien, Tournaisien et Viséen du bassin de Sidi-Bettache et de ses bordures (Meseta marocaine nord-occidentale). *Notes et Mémoires du Service Géologique* 334, 7–41.
- Kaiser, S.I., Becker, R.T., El Hassani, A., 2007. Middle to Late Famennian successions at Ain Jemaa (Moroccan Meseta)—implications for regional correlation, event stratigraphy and synsedimentary tectonics of NW Gondwana. *Geological Society of London, Special Publication* 278, 237–260. doi:10.1144/SP278.11
- Kharbouch, F., 1994. Le volcanisme dévono-dinantien du Massif central et de la Meseta orientale. *Bulletin de l'Institut Scientifique de Rabat* 18, 192–200.
- Kharbouch, F., Juteau, T., Treuil, M., Joron, J.-L., Piqué, A., Hoepffner, C., 1985. Le volcanisme dinantien de la Meseta marocaine nord-occidentale et orientale. Caractères pétrographiques et géochimiques et implications géodynamiques. *Sciences Géologiques, bulletins et mémoires* 38, 155–163.
- Kharbouch, F., Juteau, T., Treuil, M., Joron, J.-L., Piqué, A., Hoepffner, C., 1989. Le complexe volcano-sédimentaire hercynien de la Méséta marocaine nord-occidentale et orientale: étude pétrographique, géochimique et signification géodynamique. *Notes et Memoires du Service Géologique du Maroc*.
- Lecointre, G., Delepine, G., 1933. Etudes géologiques dans la région paléozoïque comprise entre Rabat et Tiflet. *Notes et Memoires du Service Géologique du Maroc* 28, 7–52.
- Letsch, D., El Houicha, M., von Quadt, A., Winkler, W., 2018. A missing link in the peri-Gondwanan terrane collage: the Precambrian basement of the Moroccan Meseta and its lower Paleozoic cover. *Canadian Journal of Earth Science* 55, 1–19. doi:10.1139/cjes-2017-0086
- Linnemann, U., Ouzegane, K., Drareni, A., Hofmann, M., Becker, S., Gärtner, A., Sagawe, A., 2011. Sands of West Gondwana: an archive of secular magmatism and

- plate interactions - A case study from the Cambro-Ordovician section of the Tassili Ouan Ahaggar (Algerian Sahara) using U-Pb-LA-ICP-MS detrital zircon ages. *Lithos* 123, 188–203. doi:10.1016/j.lithos.2011.01.010
- Linnemann, U., Pereira, M.F., Jeffries, T.E., Drost, K., Gerdes, A., 2008. The Cadomian Orogeny and the opening of the Rheic Ocean: The diacrony of geotectonic processes constrained by LA-ICP-MS U-Pb zircon dating (Ossa-Morena and Saxo-Thuringian Zones, Iberian and Bohemian Massifs). *Tectonophysics* 461, 21–43. doi:10.1016/j.tecto.2008.05.002
- Ludwig, K.R., 2003. Isoplot 3.0. A geochronological toolkit for Microsoft Excel. Berkeley Geochron, Center Special Publication 4, 70.
- Ludwig, K.R., 2009. SQUID 2: a user's manual (rev.12).
- Marhoumi, M.R., Hoepffner, C., Doubinger, J., Rauscher, R., 1983. Données nouvelles sur l'histoire hercynienne de la Meseta orientale au Maroc: l'âge dévonien des schistes de Debdou et du Mekkam. *Comptes Rendus l'Académie des Science de Paris* 297, 69–72.
- Martínez Catalán, J.R., Fernández-Suárez, J., Meireles, C., González Clavijo, E., Belousova, E., Saeed, A., 2008. U–Pb detrital zircon ages in synorogenic deposits of the NW Iberian Massif (Variscan belt): interplay of Devonian–Carboniferous sedimentation and thrust tectonics. *Journal of the Geological Society of London* 165, 687–698. doi:10.1144/0016-76492007-066
- Marzoli, A., Davies, J.H.F.L., Youbi, N., Merle, R., Dal Corso, J., Dunkley, D.J., Fioretti, A.M., Bellieni, G., Medina, F., Wotzlaw, J.F., McHone, G., Font, E., Bensalah, M.K., 2017. Proterozoic to Mesozoic evolution of North-West Africa and Peri-Gondwana microplates: detrital zircon ages from Morocco and Canada. *Lithos* 278–281, 229–239. doi:10.1016/j.lithos.2017.01.016
- Matte, P., 2001. The Variscan collage and orogeny (480-290 Ma) and the tectonic definition of the Armorica microplate: a review. *Terra Nova* 13, 122–128. doi:10.1046/j.1365-3121.2001.00327.x
- Médioni, R., 1977. Carte géologique du Maroc au 1/100.000. Feuille Debdou. Notice explicative. *Notes et Memoires du Service Géologique du Maroc* 226, 63.
- Médioni, R., 1979. Carte géologique du Maroc au 1/100.000. Feuille Hassiane Ed Diab. Notice explicative. *Notes et Memoires du Service Géologique du Maroc* 227, 64.
- Michard, A., Ouanaimi, H., Hoepffner, C., Soulaïmani, A., Baïdier, L., 2010a. Comment on Tectonic relationships of Southwest Iberia with the allochthons of Northwest Iberia and the Moroccan Variscides by J.F. Simancas et al. [*C. R. Geoscience* 341 (2009) 103-113]. *Comptes Rendus - Geoscience* 342, 170–174. doi:10.1016/j.crte.2010.01.008

- Michard, A., Soulaïmani, A., Hoepffner, C., Ouanaimi, H., Baidder, L., Rjimati, E.C., Saddiqi, O., 2010b. The South-Western Branch of the Variscan Belt: evidence from Morocco. *Tectonophysics* 492, 1–24. doi:10.1016/j.tecto.2010.05.021
- Muratet, B., 1988. Carte géologique du Maroc No361: Aïn Bni Mathar - Echelle 1/100.000. Royame du Maroc, Ministère l’Energie des Mines du Développement Durable.
- Murphy, J.B., Quesada, C., Gutiérrez-Alonso, G., Johnston, S.T., Weil, A., 2016. Reconciling competing models for the tectono-stratigraphic zonation of the Variscan orogen in Western Europe. *Tectonophysics* 681, 209–219. doi:10.1016/j.tecto.2016.01.006
- Nance, R.D., Gutiérrez-Alonso, G., Keppie, J.D., Linnemann, U., Murphy, J.B., Quesada, C., Strachan, R.A., Woodcock, N.H., 2010. Evolution of the Rheic Ocean. *Gondwana Research* 17, 194–222. doi:10.1016/j.gr.2009.08.001
- Nance, R.D., Gutiérrez-Alonso, G., Keppie, J.D., Linnemann, U., Murphy, J.B., Quesada, C., Strachan, R.A., Woodcock, N.H., 2012. A brief history of the Rheic Ocean. *Geoscience Frontiers* 3, 125–135. doi:10.1016/j.gsf.2011.11.008
- Nance, R.D., Murphy, J.B., Strachan, R.A., Keppie, J.D., Gutiérrez-Alonso, G., Fernández-Suárez, J., Quesada, C., Linnemann, U., D’lemos, R., Pisarevsky, S.A., 2008. Neoproterozoic-early Palaeozoic tectonostratigraphy and palaeogeography of the peri-Gondwanan terranes: Amazonian v. West African connections. *Geological Society of London, Special Publication* 297, 345–383. doi:10.1144/SP297.17
- Ouabid, M., Ouali, H., Garrido, C.J., Acosta-Vigil, A., Román-Alpiste, M.J., Dautria, J.M., Marchesi, C., Hidas, K., 2017. Neoproterozoic granitoids in the basement of the Moroccan Central Meseta: Correlation with the Anti-Atlas at the NW paleo-margin of Gondwana. *Precambrian Research* 299, 34–57. doi:10.1016/j.precamres.2017.07.007
- Pastor-Galán, D., Gutiérrez-Alonso, G., Fernández-Suárez, J., Murphy, J.B., Nieto, F., 2013a. Tectonic evolution of NW Iberia during the Paleozoic inferred from the geochemical record of detrital rocks in the Cantabrian Zone. *Lithos* 182–183, 211–228. doi:10.1016/j.lithos.2013.09.007
- Pastor-Galán, D., Gutiérrez-Alonso, G., Murphy, J.B., Fernández-Suárez, J., Hofmann, M., Linnemann, U., 2013b. Provenance analysis of the Paleozoic sequences of the northern Gondwana margin in NW Iberia: Passive margin to Variscan collision and orocline development. *Gondwana Research* 23, 1089–1103. doi:10.1016/j.gr.2012.06.015
- Pereira, M.F., Chichorro, M., Johnston, S.T., Gutiérrez-Alonso, G., Silva, J.B., Linnemann, U., Hofmann, M., Drost, K., 2012. The missing Rheic Ocean magmatic arcs: provenance analysis of Late Paleozoic sedimentary clastic rocks of SW Iberia. *Gondwana Research* 22, 882–891. doi:10.1016/j.gr.2012.03.010

- Pereira, M.F., El Houicha, M., Aghzer, A., Silva, J.B., Linnemann, U., Jouhari, A., 2014. New U-Pb zircon dating of Late Neoproterozoic magmatism in Western Meseta (Morocco). *Gondwana 15 - North meets South* 133. doi:10.13140/2.1.2651.2641
- Pereira, M.F., El Houicha, M., Chichorro, M., Armstrong, R., Jouhari, A., El Attari, A., Ennih, N., Silva, J.B., 2015. Evidence of a Paleoproterozoic basement in the Moroccan Variscan Belt (Rehamna Massif, Western Meseta). *Precambrian Research* 268, 61–73. doi:10.1016/j.precamres.2015.07.010
- Pereira, M.F., Gama, C., Dias da Silva, Í., Fuenlabrada, J.M., Silva, J.B., Medina, J., 2020a. Isotope geochemistry evidence for Laurussian-type sources of South Portuguese Zone Carboniferous turbidites (Variscan Orogeny). *Geological Society of London, Special Publication SP503-2019–163*. doi:10.1144/SP503-2019-163
- Pereira, M.F., Gama, C., Dias da Silva, Í., Silva, J., Hofmann, M., Linnemann, U., Gärtner, A., 2020b. Chronostratigraphic framework and provenance of the Ossa-Morena Zone Carboniferous basins (SW Iberia). *Solid Earth Discuss.* 1–34. doi:10.5194/se-2020-26
- Pereira, M.F., Gutiérrez-Alonso, G., Murphy, J.B., Drost, K., Gama, C., Silva, J.B., 2017. Birth and demise of the Rheic Ocean magmatic arc(s): Combined U–Pb and Hf isotope analyses in detrital zircon from SW Iberia siliciclastic strata. *Lithos* 278–281, 383–399. doi:10.1016/j.lithos.2017.02.009
- Pérez-Cáceres, I., Martínez Poyatos, D., Simancas, J.F., Azor, A., 2017. Testing the Avalonian affinity of the South Portuguese Zone and the Neoproterozoic evolution of SW Iberia through detrital zircon populations. *Gondwana Research* 42, 177–192. doi:10.1016/j.gr.2016.10.010
- Piqué, A., 1979. Évolution structurale d'un segment de la chaîne hercynienne: la Meseta marocaine nord-occidentale. Ph.D. Thesis. Université de Strasbourg, France.
- Piqué, A., 1984. Faciès sédimentaire et évolution d'un bassin: le Bassin dévono-dinantien de Sidi-Bettache (Maroc nord-occidental). *Bulletin de l'Institut Scientifique de Rabat* 6, 1015–1023.
- Piqué, A., Cailleux, Y., Hoepffner, C., 1989. Plates-formes épicontinentales et sillons des flyschs au Paléozoïque dans la Méséta marocaine. Un domaine sédimentaire à la marge du craton saharien. *Notes et Memoires du Service Géologique du Maroc*.
- Pouclet, A., El Hadi, H., Álvaro, J.J., Bardintzeff, J.-M., Benharref, M., Fekkak, A., 2018. Review of the Cambrian volcanic activity in Morocco: geochemical fingerprints and geotectonic implications for the rifting of West Gondwana. *International Journal of Earth Sciences* 107, 2101–2123. doi:10.1007/s00531-018-1590-1
- Razin, P., Janjou, D., Baudin, T., Bensahal, A., Hoepffner, C., Chenakeb, M., Cailleux, Y., 2001. Carte géologique du Maroc No412: Sidi Matla' Ech Chams - Echelle 1/50.000. Roy. du Maroc, Ministère l'Énergie des Mines du Développement Durable.

- Rolin, P., Cailleux, Y., Deloche, C., Gonord, H., 1985. Décrochements fini-dévonien et ouverture de bassins de type pull-apart. Deux exemples comparés: les bassins de Sidi Bettache (Maroc septentrional) et de Chateaulin (Bretagne occidentale, France), in: *Géologie Africaine, Colloque, Congrès National Des Sociétés Savantes* 110. pp. 67–77.
- Santos, J.F.H.P., Mata, J., Goncalves, F., Munha, J., 1987. Contribuição para o conhecimento geológico-petroológico da região de Santa Susana: O complexo vulcano-sedimentar da Toca da Moura. *Comunicações dos Serviços Geológicos de Portugal* 73, 29–48.
- Sharman, G.R., Malkowski, M.A., 2020. Needles in a haystack: Detrital zircon U Pb ages and the maximum depositional age of modern global sediment. *Earth-Science Reviews* 203, 103–109. doi:10.1016/j.earscirev.2020.103109
- Simancas, J.F., Azor, A., Martínez-Poyatos, D., Tahiri, A., El Hadi, H., González-Lodeiro, F., Pérez-Estaún, A., Carbonell, R., 2009. Tectonic relationships of Southwest Iberia with the allochthons of Northwest Iberia and the Moroccan Variscides. *Comptes Rendus - Geoscience* 341, 103–113. doi:10.1016/j.crte.2008.11.003
- Simancas, J.F., Azor, A., Martínez-Poyatos, D., Tahiri, A., Hadi, H. El, González-Lodeiro, F., Pérez-Estaún, A., Carbonell, R., 2010. Reply to the comment by Michard et al. on “Tectonic relationships of Southwest Iberia with the allochthons of Northwest Iberia and the Moroccan Variscides.” *Comptes Rendus - Geoscience* 342, 175–177. doi:10.1016/j.crte.2010.01.007
- Simancas, J.F., Tahiri, A., Azor, A., Lodeiro, F.G., Martínez Poyatos, D.J., El Hadi, H., 2005. The tectonic frame of the Variscan–Alleghanian orogen in Southern Europe and Northern Africa. *Tectonophysics* 398, 181–198. doi:10.1016/j.tecto.2005.02.006
- Tahiri, A., Montero, P., El Hadi, H., Martínez Poyatos, D., Azor, A., Bea, F., Simancas, J.F., González Lodeiro, F., 2010. Geochronological data on the Rabat-Tiflet granitoids: their bearing on the tectonics of the Moroccan Variscides. *Journal of African Earth Science* 57, 1–13. doi:10.1016/j.jafrearsci.2009.07.005
- Termier, G., Termier, H., Vachard, D., 1975. Recherches micropaléontologiques dans le Paléozoïque supérieur du Maroc central. *Cahiers de micropaléontologie* 4, 1–90.
- Vermeesch, P., 2004. How many grains are needed for a provenance study? *Earth and Planetary Science Letters* 224, 441–451. doi:10.1016/j.epsl.2004.05.037
- Vermeesch, P., 2012. On the visualisation of detrital age distributions. *Chemical Geology* 312–313, 190–194. doi:10.1016/j.chemgeo.2012.04.021
- Vermeesch, P., 2018. IsoplotR: a free and open toolbox for geochronology. *Geoscience Frontiers*. doi:10.1016/j.gsf.2018.04.001

- Verset, Y., 1983. Geotransverse du Maroc hercynien (Zone Nord), Stratigraphie et aperçus tectoniques. Journées 4 et 6 de l'excursion B1. Livret Guid. l'excursion B1.
- Verset, Y., 1985. Carte géologique du Maroc au 1/100 000, feuille Quasbat-Tadla et Mémoire explicatif de la carte géologique. Notes Mémoires du Service Géologique du Maroc.
- Vidal, J.C., 1989. Carte géologique du Maroc No353: Rommani - Echelle 1/100.000. Royaume du Maroc, Ministère l'Energie des Mines du Développement Durable.
- Zahraoui, M., 1991. La plate-forme carbonatée dèvonienne du Maroc occidentale et sa dislocation hercynienne. Ph.D. Thesis. UBO, Brest, France.

Chapter V

Conclusions

This Ph.D. Thesis deals with the pre- and syn-orogenic paleogeographic reconstruction of the Moroccan Mesetas, as well as their Eo-Variscan tectonic evolution during the Paleozoic era. To achieve these objectives, an extensive study on the Paleozoic variation of sedimentary sources of this part of the Gondwana margin was carried out by using detrital zircon data from 46 sandstone samples. Furthermore, the Variscan structure of the Eastern Moroccan Meseta was investigated through a detailed structural analysis of the Debdou-Mekkam area, which is particularly significant for the understanding of the early Variscan deformations in this region. The main results and interpretations are summarized below, presented in geochronological order.

Cambrian-Devonian (passive margin phase)

Based on the detrital zircon content found in the siliciclastic Cambrian-Devonian rocks from the Moroccan Mesetas (Eastern – EMM – and Western – WMM – Moroccan Mesetas), the main sources of sediments in this part of the northern Gondwanan margin were the following:

- Nearby West African Craton (WAC).
This was the principal sediment source in the Moroccan Variscides, characterized by detrital zircon dates clustered in two main populations: a main Cryogenian-Ediacaran (c. 700-540 Ma) peak, and a secondary Rhyacian-Orosirian (c. 2.2-1.9 Ga) one, plus some Archean-early Paleoproterozoic zircon grains. These detrital zircon populations can be related to the Cadomian/Pan-African, Eburnean and Leonian/Liberian orogenies, respectively (e.g., Nance et al., 2008 and references therein).
- Distant northeast Africa (e.g., Sahara Metacraton, Arabian-Nubian Shield).
These sources have been invoked to explain the presence of Stenian-early Tonian (c. 1.1-0.9 Ga) detrital zircon ages and the almost systematic lack of older Mesoproterozoic ages. Nevertheless, the presence of this population in the Cambrian-Devonian samples of the Moroccan Mesetas is very irregular (geographically, in time, and in abundance), suggesting that this region was located in a distant position where paleocurrents from northeast Africa were intermittent.
- Local Cambrian-Ordovician rift magmatism.
Several volcanic centers formed during the Cambrian-Ordovician aborted rift in the Anti-Atlas and WMM (Poucllet et al., 2018) seem to have provided some detrital zircon grains to the studied samples. Cambrian-Ordovician (c. 540-450 Ma) detrital zircon ages are generally uncommon in the Cambrian-Devonian samples of the Moroccan Meseta. Nevertheless, Lower Ordovician samples collected in areas close to some of the known volcanic centers of the WMM contain important (c. 35-70%) Cambrian-Ordovician detrital zircon grains. In the EMM, the Ordovician samples from the Zekkara inlier also contain c. 20% of Cambrian-Ordovician zircon grains,

pointing to the existence of a nearby and unknown volcanic center. The effect of these sources was very local and limited in time.

Famennian-Tournaisian (Rheic Ocean closure)

Samples from these ages collected in the Tiflet (WMM) and Debdou-Mekkam (EMM) areas include the detrital zircon populations described above. Additionally, c. 10-35% of the data from these samples yielded Devonian (c. 420-360 Ma) ages (characterized by mostly positive ϵ_{HF} values) and an appreciable amount (c. 5-15%) of zircon grains gave Mesoproterozoic-late Paleoproterozoic ages. These ages are virtually unknown in the source areas invoked for the Cambrian-Devonian samples, but are common in Amazonian-type terranes such as Avalonia. Thus, the Devonian zircon populations might be sourced from a magmatic arc developed on the Avalonian margin during the subduction of the Rheic Ocean (Pereira et al., 2012), while the Mesoproterozoic-late Paleoproterozoic zircon grains might have come from the erosion of the Avalonian basement.

The presence of both sources (north Gondwanan and Avalonian) in the Famennian-Tournaisian samples suggests that the sedimentation in the northern Gondwanan margin was influenced by an approaching Avalonian volcanic arc active during the final stages of Rheic Ocean closure. The flysch-like lithologies and great thickness (thousands of meters) of the Famennian-Tournaisian Debdou-Mekkam metasedimentary rocks fully concord with this arc-related setting.

Tournaisian-early Visean (Eo-Variscan collision)

The approaching of the Avalonian promontory was followed by its collision with the northern Gondwanan margin (Eo-Variscan deformational event). In the Debdou-Mekkam area this collision is recorded by the presence of kilometric-scale inclined to recumbent folds associated with pervasive axial-planar cleavage formed at low-grade metamorphic conditions. These folds have variable trends at the scale of the single inlier (from NW-SE, through N-S, to E-W). Nevertheless, at a wider scale, an average NE-SW fold trend with SE-vergence is inferred, as a result of the southeastward-directed pushing of the Avalonian terrane. The related NW-SE shortening is considerable, but difficult to estimate due to the absence of stratigraphic markers in the deformed sequence.

In the Mekkam inlier, the upper Visean rocks unconformably overlie the Famennian-Tournaisian succession, and they are not deformed by the Eo-Variscan event, thus constraining the latter at Tournaisian-early Visean time.

The Eo-Variscan deformational front is unexposed, although its location can be roughly inferred between the inliers of Mekkam to the west, and those of Zekkara, Jerada, and Oujda to the east: the last three, in fact, are unaffected by the Eo-Variscan deformation.

The description and reinterpretation of the Eo-Variscan structure in this part of the EMM represents one of the most outstanding results of this Ph.D. Thesis. Previous studies in this area described NW-SE trending isoclinal recumbent to overturned folds with W-SW vergences (Hoepffner, 1987), although none of them provided detailed structural maps, cross-sections, nor geodynamic interpretations were provided.

Visean-Moscovian (Variscan s.s. deformation)

In the Debdou-Mekkam area, a second deformational event (Variscan s.s.) is responsible for the formation of metric- to kilometeric-scale upright open folds associated with axial-planar crenulation cleavage, which complicated the original Eo-Variscan fold trends. These structures deformed all the Paleozoic succession exposed in the Debdou-Mekkam area (Famennian-late Visean) and they have been described also in other inliers of the EMM (e.g., Jerada; Hoepffner, 1987).

The detrital zircon populations observed in samples from the post-Eo-Variscan sequence of the Moroccan Mesetas show similar characteristics to the Cambrian-Devonian pre-orogenic samples: strong WAC affinity (Cryogenian-Ediacaran and Rhyacian-Orosirian ages), variable occurrence of secondary northeastern African sources (Stenian-early Tonian ages), and scarce (probably recycled) Cambrian-Ordovician zircon grains. A few local features are summarized below:

- The westernmost Visean samples (Ben Slimane area) still recorded the effect of Avalonian sources, with a small but statistically significant number of Devonian (c. 4%) and Mesoproterozoic (c. 5%) detrital zircon grains.
- In other parts of the WMM (Sidi Bettache and Oulmes areas), the Visean samples appear to be unaffected by Avalonian sources, except a few scattered Devonian and Mesoproterozoic grains probably recycled from the Famennian-Tournaisian succession in the Tiflet area.
- In the EMM, Serpukhovian-Moscovian samples contain c. 15% of Carboniferous (c. 350-300 Ma) zircon grains. These grains were likely sourced by the granitoids that attest to the crustal thickening and thermal maturation of the Gondwanan crust resulting from the Variscan orogeny.

Open issues

The results of this Ph.D. Thesis represent an important contribution to the knowledge of the Paleozoic paleogeographic and tectonic evolution of the northern Moroccan Variscides. Nevertheless, a few issues remain open for further research. Some of the most significant of these open questions are indicated below:

- The northern Moroccan Variscides have been usually divided in domains (e.g., Eastern and Western Moroccan Mesetas, Southern Zone, Anti-Atlas) and sub-domains (Coastal Block, Central Zone, and Nappe Zone of the Western Moroccan

Meseta) separated by large-scale fault zones whose Variscan and pre-Variscan paleogeographic significance is still debated (e.g., Michard et al., 2010a; Simancas et al., 2010, 2009). Despite some proposals attributing offsets of hundreds of kilometers (e.g., Michard et al., 2010b and references therein) to these fault zones, the sedimentary successions do not show important differences between domains or sub-domains. Furthermore, the detrital zircon data described and discussed in this Ph.D. Thesis do not show significant variations among the sampled domains, suggesting that all the region belonged to the same passive margin fed by the same source areas. Nevertheless, more data are required from poorly sampled Paleozoic successions in other domains (e.g., Southern Zone and Anti-Atlas). Furthermore, detailed tectono-metamorphic studies focused on the boundaries among the different domains should not be excluded.

- The re-interpretation of the Eo-Variscan structures in the Debdou-Mekkam area, EMM, opens new questions on putative coeval structures in other parts of the Moroccan Mesetas, in particular those that are close to the WMM/EMM boundary. For instance, Hoepffner (1987) described refolded W-vergent Eo-Variscan structures in the Tazekka inlier, which they propose to be similar to those described in the Debdou-Mekkam area, in the same work. W-vergences were also described in the Azrou-Khenifra nappe area (Ben Abbou et al., 2001; Bouabdelli, 1989). To the west, in the Zaian area, Lahfid et al. (2019) described Eo-Variscan upright and recumbent folds. More detailed modern structural analyses are needed in these regions in order to understand how these supposedly W-vergent structures, if present, fit in the geodynamic model presented in this Ph.D. Thesis.
- The recognition of the Rheic suture and its correlation among different transects of the Variscan belt is an issue of the foremost importance. In central and southern Europe, the location of the Rheic suture is relatively clear, as it separates Avalonian terranes (Reno-Hercynian and South Portuguese Zones) from Gondwanan terranes, to the east. However, the features of the original suture were blurred by later strong Variscan imprint (e.g., Franke et al., 2017; Pérez-Cáceres et al., 2017). The prolongation of this orogenic suture in northwestern Africa (or eastern North America) is uncertain. In northwest Morocco, the Sehoul Block is considered to be part of an Avalonian promontory due to its Caledonian imprint (Tahiri et al., 2010), a feature that is absent in the remaining northern Moroccan Variscides. Therefore, the Rheic suture might be concealed along the limit between the Sehoul Block and the WMM, which is represented at present by a late Variscan thrust. The occurrence of Avalonian-derived sediments in the Tiflet and Debdou-Mekkam areas suggests an eastward continuation of the suture. Furthermore, the style of the Debdou-Mekkam Eo-Variscan structures suggests that the front of the Avalonian promontory (and hence the Rheic suture) might be located somewhere to the northwest of these inliers, although covered by younger sediments. Further north, the Rheic suture would continue in SW Iberia at the boundary between the Ossa-Morena (Gondwanan) and the South Portuguese (Avalonian) Zones (Pérez-Cáceres et al., 2015, 2017). The

southward prolongation of the Rheic suture remains uncertain between the Sehoul Block and the Souttoufides/Mauritanides. A possible location might be offshore the Moroccan Atlantic coast, based only on the recent findings of some Mesoproterozoic and late Paleoproterozoic zircon grains in magmatic rocks of the El Jadida coast and offshore in the Mazagan escarpment (El Haibi et al., 2020; Kuiper et al., 2019). As a corollary, the general lack of primary remnants of Rheic Oceanic crust (pre-Late Devonian ophiolites) in the whole Variscan belt has to be stressed, in light of the indirect nature of the evidences of this suture. Nevertheless, the uncertainties about the location of the Rheic suture are still high and need more studies.

- Last but not least, a concern worth pursuing would be deciphering whether the affinity of the Moroccan Mesetas Gondwanan basement is of WAC-type (which lacks Mesoproterozoic crust) or northeast African-type (which includes c. 1.0 Ga old crust, such as for instance the Sahara Metacraton). The Pan-African suture between both crust types can be precisely located in the Anti-Atlas (Bou-Azzer ophiolite; El Hadi et al., 2010), and it was suggested to continue northwards in Iberia (Pérez-Cáceres et al., 2017). Excluding the El Jadida area (see above), the scarce Precambrian outcrops in the WMM suggest a WAC-type basement (Ouabid et al., 2017; Pereira et al., 2015). The high variability of the c. 1.0 Ga detrital zircon population found in the Paleozoic Moroccan Mesetas and its possible long transport from distant sources (as suggested in this Ph.D. Thesis) complicates the attempt to unraveling this issue. A systematic study of the ages of xenocrystic zircon grains, and zircon cores in igneous rocks (in particular in Variscan granitoids) exposed in the Moroccan Mesetas, might be a more powerful tool to shed light on this issue, and perhaps leading to delineate the location of the Pan-African suture between the Anti-Atlas and Iberia.

References

- Ben Abbou, M., Soula, J.-C., Brusset, S., Roddaz, M., N'Tarmouchant, A., Driouch, Y., Christophoul, F., Bouabdelli, M., Majesté-Menjoulas, C., Béziat, D., Debat, P., Déramond, J., 2001. Contrôle tectonique de la sédimentation dans le système de bassins d'avant-pays de la Meseta marocaine. *Comptes Rendus l'Académie des Sci. - Ser. IIA - Earth Planet. Sci.* 332, 703–709. doi:10.1016/S1251-8050(01)01590-7
- Bouabdelli, M., 1989. Tectonique et sédimentation dans un bassin orogénique: le sillon viséen d'Azrou-Khenifra (Est du Massif Hercynien Central du Maroc). U.E.R. de Sciences de la vie et de la Terre, Strasbourg, France.
- El Hadi, H., Simancas, J.F., Martínez-Poyatos, D., Azor, A., Tahiri, A., Montero, P., Fanning, C.M., Bea, F., González-Lodeiro, F., 2010. Structural and geochronological constraints on the evolution of the Bou Azzer Neoproterozoic ophiolite (Anti-Atlas, Morocco). *Precambrian Res.* 182, 1–14. doi:10.1016/j.precamres.2010.06.011

- El Haibi, H., El Hadi, H., Tahiri, A., Martínez Poyatos, D., Gasquet, D., Pérez-Cáceres, I., González Lodeiro, F., Mehdioui, S., 2020. Geochronology and isotopic geochemistry of Ediacaran high-K calc-alkaline felsic volcanism: An example of a Moroccan perigondwanan (Avalonian?) remnant in the El Jadida horst (Mazagonia). *J. African Earth Sci.* 163, 103669. doi:10.1016/j.jafrearsci.2019.103669
- Franke, W., Cocks, L.R.M., Torsvik, T.H., 2017. The Palaeozoic Variscan oceans revisited. *Gondwana Res.* 48, 257–284. doi:10.1016/j.gr.2017.03.005
- Hoepffner, C., 1987. La tectonique hercynienne dans l'Est du Maroc. Université Louis Pasteur, Strasbourg.
- Kuiper, Y.D., Michard, A., Ruellan, E., Holm-Denoma, C., Crowley, J.L., 2019. U-Pb zircon and monazite results from granite and charnockite from the Mazagan escarpment, offshore Morocco, in: *GSA Abstracts with Programs*, Vol. 51, No. 2.
- Lahfid, A., Baidder, L., Ouanaimi, H., Soulaïmani, A., Hoepffner, C., Farah, A., Saddiqi, O., Michard, A., 2019. From extension to compression: high geothermal gradient during the earliest Variscan phase of the Moroccan Meseta; a first structural and RSCM thermometric study. *Eur. J. Mineral.* 31, 695–713. doi:10.1127/ejm/2019/0031-2882
- Michard, A., Ouanaimi, H., Hoepffner, C., Soulaïmani, A., Baidder, L., 2010a. Comment on Tectonic relationships of Southwest Iberia with the allochthons of Northwest Iberia and the Moroccan Variscides by J.F. Simancas et al. [*C. R. Geoscience* 341 (2009) 103-113]. *Comptes Rendus - Geosci.* 342, 170–174. doi:10.1016/j.crte.2010.01.008
- Michard, A., Soulaïmani, A., Hoepffner, C., Ouanaimi, H., Baidder, L., Rjimati, E.C., Saddiqi, O., 2010b. The South-Western Branch of the Variscan Belt: evidence from Morocco. *Tectonophysics* 492, 1–24. doi:10.1016/j.tecto.2010.05.021
- Nance, R.D., Murphy, J.B., Strachan, R.A., Keppie, J.D., Gutiérrez-Alonso, G., Fernández-Suárez, J., Quesada, C., Linnemann, U., D'lemos, R., Pisarevsky, S.A., 2008. Neoproterozoic-early Palaeozoic tectonostratigraphy and palaeogeography of the peri-Gondwanan terranes: Amazonian v. West African connections. *Geol. Soc. London, Spec. Publ.* 297, 345–383. doi:10.1144/SP297.17
- Ouabid, M., Ouali, H., Garrido, C.J., Acosta-Vigil, A., Román-Alpiste, M.J., Dautria, J.M., Marchesi, C., Hidas, K., 2017. Neoproterozoic granitoids in the basement of the Moroccan Central Meseta: Correlation with the Anti-Atlas at the NW paleo-margin of Gondwana. *Precambrian Res.* 299, 34–57. doi:10.1016/j.precamres.2017.07.007
- Pereira, M.F., Chichorro, M., Johnston, S.T., Gutiérrez-Alonso, G., Silva, J.B., Linnemann, U., Hofmann, M., Drost, K., 2012. The missing Rheic Ocean magmatic arcs: provenance analysis of Late Paleozoic sedimentary clastic rocks of SW Iberia. *Gondwana Res.* 22, 882–891. doi:10.1016/j.gr.2012.03.010
- Pereira, M.F., El Houicha, M., Chichorro, M., Armstrong, R., Jouhari, A., El Attari, A., Ennih, N., Silva, J.B., 2015. Evidence of a Paleoproterozoic basement in the Moroccan Variscan Belt (Rehamna Massif, Western Meseta). *Precambrian Res.* 268, 61–73. doi:10.1016/j.precamres.2015.07.010

- Pérez-Cáceres, I., Martínez Poyatos, D., Simancas, J.F., Azor, A., 2017. Testing the Avalonian affinity of the South Portuguese Zone and the Neoproterozoic evolution of SW Iberia through detrital zircon populations. *Gondwana Res.* 42, 177–192. doi:10.1016/j.gr.2016.10.010
- Pérez-Cáceres, I., Martínez Poyatos, D., Simancas, J.F., Azor, A., 2015. The elusive nature of the Rheic Ocean suture in SW Iberia. *Tectonics* 34, 2429–2450. doi:10.1002/2015TC003947
- Pouclet, A., El Hadi, H., Álvaro, J.J., Bardintzeff, J.-M., Benharref, M., Fekkak, A., 2018. Review of the Cambrian volcanic activity in Morocco: geochemical fingerprints and geotectonic implications for the rifting of West Gondwana. *Int. J. Earth Sci.* 107, 2101–2123. doi:10.1007/s00531-018-1590-1
- Simancas, J.F., Azor, A., Martínez-Poyatos, D., Tahiri, A., El Hadi, H., González-Lodeiro, F., Pérez-Estaún, A., Carbonell, R., 2009. Tectonic relationships of Southwest Iberia with the allochthons of Northwest Iberia and the Moroccan Variscides. *Comptes Rendus Geosci.* 341, 103–113. doi:10.1016/j.crte.2008.11.003
- Simancas, J.F., Azor, A., Martínez-Poyatos, D., Tahiri, A., Hadi, H. El, González-Lodeiro, F., Pérez-Estaún, A., Carbonell, R., 2010. Reply to the comment by Michard et al. on “Tectonic relationships of Southwest Iberia with the allochthons of Northwest Iberia and the Moroccan Variscides.” *Comptes Rendus - Geosci.* 342, 175–177. doi:10.1016/j.crte.2010.01.007
- Tahiri, A., Montero, P., El Hadi, H., Martínez Poyatos, D., Azor, A., Bea, F., Simancas, J.F., González Lodeiro, F., 2010. Geochronological data on the Rabat-Tiflet granitoids: their bearing on the tectonics of the Moroccan Variscides. *J. African Earth Sci.* 57, 1–13. doi:10.1016/j.jafrearsci.2009.07.005

APPENDIX

- Appendix A – Analytical methods
(all the chapters)*
- Appendix B – Description of the zircon grains
(Chapter II, Section II.1)*
- Appendix C – Cathodoluminescence images
(Chapter II, Section II.3; Chapter III; Chapter IV)*
- Appendix D – Results of the U-Pb analyses
(all the chapters)*
Only in the digital version of this Ph.D. Thesis (CD)
- Appendix E – Results of the Hf analyses
(Chapter II, Section II.3; Chapter III; Chapter IV)*
Only in the digital version of this Ph.D. Thesis (CD)

Appendix A

Analytical methods

LA-ICPMS Geochronology

LA-ICPMS geochronology was performed in the GeoHistory Facility, John de Laeter Centre (JdLC), Curtin University, Perth, Australia. Individual zircon grains (mounted and polished in 1” epoxy rounds) were ablated using a Resonetics RESolution M-50A-LR, incorporating a Compex 102 excimer laser. Following two cleaning pulses and 45 s of total baseline signal acquisition, ablations were undertaken at a 33 μm spot diameter with a 7 Hz laser repetition rate and on sample laser energy of 2 J cm^{-2} . Ultrahigh purity He (350 mL min^{-1}) and N₂ (3.8 mL min^{-1}) was used to flush the cell and high purity Ar was employed as the plasma carrier gas (flow rate 0.98 L min^{-1}). Isotopic intensities were measured on an Agilent 7700s quadrupole ICP-MS and for this work, the following isotopes were monitored for 0.03 s each: ²⁸Si, ²⁹Si, ⁴⁹Ti, ⁹¹Sr, ¹⁴⁷Sm, ²⁰²Hg, ²⁰⁴Pb, ²⁰⁶Pb, ²⁰⁷Pb, ²⁰⁸Pb, ²³²Th, and ²³⁸U.

The primary and secondary reference materials used in this study are listed in Table A.1. ²⁰⁶Pb/²³⁸U ages calculated for all zircon age standards, treated as unknowns, were found to be within 3% of the accepted value. The time-resolved mass spectra were reduced using the U_Pb_Geochronology3 data reduction scheme in Iolite (Paton et al, 2011 and references therein).

Table A.1. Recommended values for the standard materials used during the LA-ICPMS sessions

Zircon standard	Recommended values
91500	1062.4±0.4 Ma (Wiedenbeck et al., 1995)
Plešoviče	337.13±0.37 Ma (Sláma et al., 2008)
GJ-1	608.5±1.5 Ma (Jackson et a., 2004) 601.5±0.40 Ma (Horstwood et al., 2016)
OGC	3465.4±0.6 Ma (Stern et al., 2009)

SHRIMP analyses

The analytical procedures for the Curtin consortium SHRIMP II have been described by De Laeter and Kennedy (1998) and Kennedy and De Laeter (1994), and are similar to those described by Compston et al. (1984) and Williams (1998). Because of the small grain size, a 10-15 μm diameter spot was used, with a mass-filtered O_2^- -primary beam of ~ 1.1 - 1.3 nA. Data for each spot were collected in sets of five scans on the zircons through the mass range of $^{196}\text{Zr}_2\text{O}^+$, $^{204}\text{Pb}^+$, Background, $^{206}\text{Pb}^+$, $^{207}\text{Pb}^+$, $^{208}\text{Pb}^+$, $^{238}\text{U}^+$, $^{248}\text{ThO}^+$, and $^{254}\text{UO}^+$. The $^{206}\text{Pb}/^{238}\text{U}$ age standard and U-content standard used was BR266 (559 Ma and 903 ppm U; Stern, 2001). The $^{207}\text{Pb}/^{206}\text{Pb}$ standard used to monitor instrument induced mass fractionation is OGC zircon (3465 ± 3 Ma; Stern et al., 2009). The $^{207}\text{Pb}/^{206}\text{Pb}$ dates obtained on OGC zircons during the SHRIMP sessions matched the $^{207}\text{Pb}/^{206}\text{Pb}$ standard age within uncertainty and no fractionated correction was warranted. The common Pb correction was based on the measured ^{204}Pb -correction (Compston et al., 1984). The correction formula for Pb/U fractionation is:

$$^{206}\text{Pb}^+ / ^{238}\text{U}^+ = a(^{254}\text{UO}^+ / ^{238}\text{U}^+)^b$$

(Claoué-Long et al., 1995) using the parameter values of Black et al. (2003). The constant a was determined empirically from analyses of the standard during the analytical session. The program SQUID 2 (Ludwig, 2009) was used for data processing.

SIMS analyses

The zircon U-Th-Pb isotopic analyses were performed using a Cameca IMS1270 secondary ion mass spectrometer (SIMS) at the NERC Ion Microprobe Facility, University of Edinburgh, the United Kingdom, applying the procedures described by Chen et al. (2019).

A 10-15 μm diameter spot was used with a 3.5-5.4 nA O_2^- primary ion source on zircons from sample EZ7, AOU1, OUI18, AZR11, AZR1, and SF2. Data for each analysis was collected in 20 scans on the zircons over the following masses of interest: $^{196}(\text{Zr}_2\text{O})$, ^{204}Pb , 204.3 background, ^{206}Pb , ^{207}Pb , ^{208}Pb , $^{212}(\text{Zr}_2\text{O}_2)$, ^{238}U , $^{248}(\text{ThO})$, $^{254}(\text{UO})$, and $^{270}(\text{UO}_2)$. U/Pb ratios were calibrated against measurements of the Geostandards 91500 zircon (c. 1062.5 Ma; Wiedenbeck et al., 1995). Measurements over single ‘sessions’ gave a standard deviation on the $^{206}\text{Pb}/^{238}\text{U}$ ratio on single repeats of 91500 of about 1% (1σ). SL1 (Maas et al., 1992), OGC (Stern et al., 2009), and Phalaborwa baddeleyite (Heaman and LeCheminant, 1993) standards were run as a secondary standards to check on high U counts and the absolute mass fractionation of lead. Correction for in situ common Pb has been made using measured ^{204}Pb counts above that of detector background (0.03–0.08 c.p.s.; 0.2–1.5 ppb) and using modern day composition of common Pb. Uncertainty on this correction (typically, 15 ppb of ^{206}Pb) is included in the calculation of errors on the U/Pb and Pb/Pb ratios. Data were processed

offline using in-house data reduction spreadsheets (R. W. Hinton). Uncertainties on ages quoted in tables for single analyses (ratios and dates) are at the 1σ level. All uncertainties in calculated group age are reported at 95% confidence limits. Plots and age calculations have been made using ISOPLOT (Ludwig, 2003).

LA-ICPMS Hf isotope analyses

The Hf isotopic analysis of zircon was undertaken over five sessions at the GeoHistory facility, JdLC, Curtin University. Previously dated zircon crystals were ablated using a Resonetics RESOLUTION M-50A-LR, incorporating a Compex 102 excimer laser, coupled to a Nu Plasma II multi-collector inductively coupled plasma mass spectrometer (MC-ICPMS). Following two cleaning pulses and a 45 s period of background analysis, samples were spot ablated for 40 s at a 10 Hz repetition rate using a 50 μm beam and laser energy at the sample surface of 2.0 J cm^{-2} . An additional 15 s of baseline was collected after ablation. The sample cell was flushed with ultrahigh purity He (320 mL min^{-1}) and N_2 (1.2 mL min^{-1}) and high purity Ar was employed as the plasma carrier gas. All isotopes (^{180}Hf , ^{179}Hf , ^{178}Hf , ^{177}Hf , ^{176}Hf , ^{175}Lu , ^{174}Hf , ^{173}Yb , ^{172}Yb , and ^{171}Yb) were counted on the Faraday collector array. Time resolved data was baseline subtracted and reduced using Iolite (DRS after Woodhead et al., 2004), where ^{176}Yb and ^{176}Lu were removed from the 176 mass signal using $^{176}\text{Yb}/^{173}\text{Yb} = 0.7962$ (Chu et al., 2002) and $^{176}\text{Lu}/^{175}\text{Lu} = 0.02655$ (Chu et al., 2002) with an exponential law mass bias correction, assuming $^{172}\text{Yb}/^{173}\text{Yb} = 1.35274$ (Chu et al., 2002). An effective $^{176}\text{Yb}/^{173}\text{Yb}$ correction factor was determined for each session by iteratively adjusting the $^{176}\text{Yb}/^{173}\text{Yb}$ ratio until standard corrected ratios on both high Yb (e.g., R33, FC-1) and low Yb (e.g., 91500, GJ-1) zircon reference materials yielded values within the recommended range. No correlation was apparent between the abundance of interfering isotopes (Yb or Lu) and corrected $^{176}\text{Hf}/^{177}\text{Hf}$ ratios. The interference corrected $^{176}\text{Hf}/^{177}\text{Hf}$ was normalized to $^{179}\text{Hf}/^{177}\text{Hf} = 0.7325$ (Patchett and Tatsumoto, 1980) for mass bias correction. Zircons from the Mud Tank carbonatite locality were utilized as the primary reference material and analyzed together with secondary reference zircons Plešovič, 91500, GJ-1, and FC-1 zircons and samples in each session (Table A.2). The weighted mean $^{176}\text{Hf}/^{177}\text{Hf}$ ratio of the primary and secondary standards for these five sessions were within uncertainty of recommended values. The corrected $^{178}\text{Hf}/^{177}\text{Hf}$ ratio was calculated to monitor the accuracy of the mass bias correction and yielded the average values listed in Table A.3, which are within the range of values reported by Thirlwall and Anczkiewicz (2004). Calculation of ϵ_{Hf} values employed the decay constant of Scherer et al. (2001) and the Chondritic Uniform Reservoir (CHUR) values of Blichert-Toft and Albarède (1997).

Table A.2. Recommended values for the standard materials used during the Hf analyses

Zircon standard	Recommended $^{176}\text{Hf}/^{177}\text{Hf}$ ratios
Mud Tank	0.282505±0.000044 (Woodhead and Hergt, 2005)
Plešovice	0.252482±0.000013 (Sláma et al., 2008)
GJ-1	0.282000±0.000005 (Morel et al., 2008)
91500	0.282306±0.000311 (Woodhead et al., 2004)
FC1	0.282172±0.000042 (Woodhead and Hergt, 2005)

Table A.3. Average values of the corrected $^{178}\text{Hf}/^{177}\text{Hf}$ ratio calculated in each session.

Session	$^{178}\text{Hf}/^{177}\text{Hf}$ ratios	Samples
1st 14 th of October 2018	1.46723 ± 0.000014 (n=100)	OIJ10, OIJ11, BES1, SKH1
2nd 25 th of February 2019	1.46708 ± 17 (n=100)	MIM2, OIJ16, AZR10
3rd 28 th of February 2019	1.46721 ± 0.000011 (n=100)	OIJ13, OIJ19
4th 7 th of August 2019	1.46722 ± 0.0000087 (n=100)	TIF1, TIF2
5th 9 th of August 2019	1.46722 ± 0.0000061 (n=100)	OIJ18

REFERENCES

- Black, L.P., Kamo, S.L., Williams, I.S., Mundil, R., Davis, D.W., Korsch, R.J., Foudoulis, C., 2003. The application of SHRIMP to Phanerozoic geochronology; a critical appraisal of four zircon standards. *Chem. Geol.* 200, 171–188. doi:10.1016/S0009-2541(03)00166-9
- Blichert-Toft, J., Albarède, F., 1997. The Lu-Hf isotope geochemistry of chondrites and the evolution of the mantle-crust system. *Earth Planet. Sci. Lett.* 148, 243–258. doi:10.1016/S0012-821X(97)00040-X
- Chen, G., Robertson, A.H.F., Ustaömer, T., 2019. U–Pb detrital zircon ages used to infer provenance and tectonic setting of Late Triassic–Miocene sandstones related to the Tethyan development of Cyprus. *J. Geol. Soc. London.* 176, 863–884. doi:10.1144/jgs2018-207
- Chu, N.-C., Taylor, R.N., Chavagnac, V., Nesbitt, R.W., Boella, R.M., Milton, J.A., German, C.R., Bayon, G., Burton, K., 2002. Hf isotope ratio analysis using multi-collector inductively coupled plasma mass spectrometry: an evaluation of isobaric interference corrections. *J. Anal. At. Spectrom.* 17, 1567–1574. doi:10.1039/b206707b
- Claoué-Long, J.C., Compston, W., Roberts, J., Fanning, C.M., 1995. Two Carboniferous ages: a comparison of SHRIMP zircon dating with conventional zircon ages and

- 40Ar/39Ar analysis, in: Berggren, W.A., Kint, D.V., Aubry, M., Hardenbol, J. (Eds.), *Geochronology, Timescales and Global Stratigraphic Correlation*. Society for Sedimentary Geology, Special Publications 54, pp. 3–21.
- Compston, W., Williams, I.S., Meyer, C., 1984. U-Pb geochronology of zircons from lunar breccia 73217 using a sensitive high mass-resolution ion microprobe. *J. Geophys. Res.* 89, B525. doi:10.1029/JB089iS02p0B525
- De Laeter, J.R., Kennedy, A.K., 1998. A double focusing mass spectrometer for geochronology. *Int. J. Mass Spectrom.* 178, 43–50. doi:10.1016/S1387-3806(98)14092-7
- Heaman, L.M., and LeCheminant, A.N., 1993, Paragenesis and U-Pb systematics of baddeleyite (ZrO₂): *Chemical Geology*, v. 110, p. 95–126, doi:10.1016/0009-2541(93)90249-I.
- Jackson, S.E., Pearson, N.J., Griffin, W.L., Belousova, E.A., 2004. The application of laser ablation-inductively coupled plasma-mass spectrometry to in situ U–Pb zircon geochronology. *Chemical Geology*, 211, 47–69. <https://doi.org/10.1016/j.chemgeo.2004.06.017>
- Kennedy, A.K., De Laeter, J.R., 1994. The performance characteristics of the WA SHRIMP II ion microprobe, in: Lanphere, M.A., Dalrymple, G.B., Turrin, B.D. (Eds.), *Abstracts of the Eighth International Conference on Geochronology, Cosmochronology, and Isotope Geology*. U.S. Geological Survey Circular, Berkeley, California, USA, p. 166.
- Ludwig, K.R., 2009. SQUID 2: a user's manual (rev.12).
- Ludwig, K.R., 2003. Isoplot 3.0. A geochronological toolkit for Microsoft Excel. Berkeley Geochron, Cent. Spec. Publ. 4, 70.
- Maas, R., Kinny, P.D., Williams, I.S., Froude, D.O., Compston, W., 1992. The Earth's oldest known crust: A geochronological and geochemical study of 3900–4200 Ma old detrital zircons from Mt. Narryer and Jack Hills, Western Australia. *Geochim. Cosmochim. Acta* 56, 1281–1300. doi:10.1016/0016-7037(92)90062-N
- Morel, M.L.A., Nebel, O., Nebel-Jacobsen, Y.J., Miller, J.S., Vroon, P.Z., 2008. Hafnium isotope characterization of the GJ-1 zircon reference material by solution and laser-ablation MC-ICPMS. *Chem. Geol.* 255, 231–235. doi:10.1016/j.chemgeo.2008.06.040
- Nasdala, L., Hofmeister, W., Norberg, N., Martinson, J.M., Corfu, F., Dörr, W., Kamo, S.L., Kennedy, A.K., Kronz, A., Reiners, P.W., Frei, D., Kosler, J., Wan, Y., Götze, J., Häger, T., Kröner, A., Valley, J.W., 2008. Zircon M257 - a homogeneous natural reference material for the ion microprobe U-Pb analysis of zircon. *Geostand. Geoanalytical Res.* 32, 247–265. doi:10.1111/j.1751-908X.2008.00914.x

- Nasdala, L., Reiners, P.W., Garver, J.I., Kennedy, A.K., Stern, R.A., Balan, E., Wirth, R., 2004. Incomplete retention of radiation damage in zircon from Sri Lanka. *Am. Mineral.* 89, 219–231. doi:10.2138/am-2004-0126
- Patchett, P.J., Tatsumoto, M., 1980. Hafnium isotope variations in oceanic basalts. *Geophys. Res. Lett.* 7, 1077–1080. doi:10.1029/GL007i012p01077
- Paton, C., Hellstrom, J., Paul, B., Woodhead, J., Hergt, J., 2011. Iolite: Freeware for the visualisation and processing of mass spectrometric data. *J. Anal. At. Spectrom.* 26, 2508. doi:10.1039/c1ja10172b
- Scherer, E., Münker, C., Mezger, K., 2001. Calibration of the Lutetium-Hafnium Clock. *Science* (80-.). 293, 683–687. doi:10.1126/science.1061372
- Sláma, J., Košler, J., Condon, D.J., Crowley, J.L., Gerdes, A., Hanchar, J.M., Horstwood, M.S.A., Morris, G.A., Nasdala, L., Norberg, N., Schaltegger, U., Schoene, B., Tubrett, M.N., Whitehouse, M.J., 2008. Plešovice zircon — A new natural reference material for U–Pb and Hf isotopic microanalysis. *Chem. Geol.* 249, 1–35. doi:10.1016/j.chemgeo.2007.11.005
- Stern, R.A., 2001. A new isotopic and trace-element standard for the ion microprobe: preliminary thermal ionization mass spectrometry (TIMS) U-Pb and electron-microprobe data. *Ressources Nat. Canada. Geol. Surv. Canada.*
- Stern, R.A., Bodorkos, S., Kamo, S.L., Hickman, A.H., Corfu, F., 2009. Measurement of SIMS Instrumental Mass Fractionation of Pb Isotopes During Zircon Dating. *Geostand. Geoanalytical Res.* 33, 145–168. doi:10.1111/j.1751-908X.2009.00023.x
- Thirlwall, M.F., Anczkiewicz, R., 2004. Multidynamic isotope ratio analysis using MC–ICP–MS and the causes of secular drift in Hf, Nd and Pb isotope ratios. *Int. J. Mass Spectrom.* 235, 59–81. doi:10.1016/j.ijms.2004.04.002
- Wiedenbeck, M., Allé, P., Cordu, F., Griffin, W.L., Meier, M., Oberli, F., Quadt, A. VON, Roddick, J.C., Spiegel, W., 1995. Three natural zircon standards for U-Th-Pb, Lu-Hf, trace element and REE analyses. *Geostand. Geoanalytical Res.* 19, 1–23. doi:10.1111/j.1751-908X.1995.tb00147.x
- Williams, I.S., 1998. U-Th-Pb geochronology by ion microprobe, in: McKibben, M.A., Shanks, W.C., Ridely, W.I. (Eds.), *Applications of Microanalytical Techniques to Understanding Mineralizing Processes.*
- Woodhead, J., Hergt, J., 2005. A Preliminary Appraisal of Seven Natural Zircon Reference Materials for In Situ Hf Isotope Determination. *Geostand. Geoanalytical Res.* 29, 183–195. doi:10.1111/j.1751-908X.2005.tb00891.x
- Woodhead, J., Hergt, J., Shelley, M., Eggins, S., Kemp, R., 2004. Zircon Hf-isotope analysis with an excimer laser, depth profiling, ablation of complex geometries, and concomitant age estimation. *Chem. Geol.* 209, 121–135. doi:10.1016/j.chemgeo.2004.04.026

APPENDIX B

Description of the zircon grains (Chapter II, Section II.1)

Sample OIJ2

Zircon grain size in this sample varies from 80 to 200 μm , being 150 μm the average size. The grains are generally whitish or yellowish, with rounded or elongated shapes; their cathodoluminescence (CL) images show continuous oscillatory zoning; some grains present partially resorbed cores overgrown by high- or low-U rims. Normally, the cores are characterized by higher Th/U ratios than the rims.

Sample OIJ3

The majority of the zircons separated from this sample are elongated or rounded, with white, caramel, or violet colors. Their size varies from 80 to 240 μm , though most of them present a diameter of about 140 μm . Their CL images show continuous oscillatory zoning or partially resorbed cores overgrown by low- or high-U rims; at the same time, the rims generally show lower Th/U ratios than the cores. A few grains show sector zoning.

Sample TAZ2

Zircon grains are elongated or rounded, though most of them are broken and they generally have reddish or dark green colors. Their size varies from 40 to 100 μm , with an average size of 60 μm . CL images of these zircons show continuous oscillatory zoning or partially resorbed cores with low- or high-U rims overgrowth; several grains are unstructured.

Sample TAZ3

The zircon grains in this sample are elongated, though most of them appear broken. Their size varies between 50 and 130 μm , being 80 μm the average size; they are normally whitish or yellowish. CL images show that the internal structure of some of these grains is a continuous oscillatory zoning or consisting in partially resorbed cores overgrown by low- or high-U rims. Several grains are unstructured.

Sample TAZ5

Detrital zircon grains from this sample are variably colored (most of them are whitish or yellowish, but several grains are dark green or red colored); they are rounded and elongated, although some of them seem to be broken. The size varies from 90 to 190 μm , being 130 μm the average diameter. The most common internal structure showed up by the CL images is a continuous oscillatory zoning; nevertheless, there are also a few complex grains with partially resorbed cores overgrown by rims characterized by low- or high-U content and low Th/U ratios.

Sample TAZ6

The grain size of the detrital zircons in this sample varies from 70 to 200 μm , being 130 μm the average size. Under the microscope, the grains appear to be rounded or elongated, and mostly whitish or yellowish. CL images of them show continuous oscillatory zoning, sector zoning, or partially resorbed cores overgrown by low- or high-U rims. The rims are also characterized by lower Th/U values than the cores.

Sample AZR2

The zircons separated from this samples appear to have yellowish, reddish or pinkish colors. They are rounded or slightly elongated, the most equidimensional and rounded being generally the clearest. They have a grain size varying from 100 to 200 μm , with an average diameter of around 140 μm . CL images show continuous oscillatory zoning and some composite grains with cores overgrown by low- or high-U rims, also characterized by low Th/U ratios. A few grains appear to be unstructured or with sector zoning.

Sample AZR4

Most of the detrital zircons separated from sample AZR4 are characterized by violet and pink colors, although a few whitish and yellowish grains are also present. Their size varies from 100 to 200 μm , and the average diameter is around 150 μm . From a morphological point of view, they appear to be elongated and often broken. CL images of these zircons show continuous oscillatory zoning or partially resorbed cores with low- or high-U and lower Th/U rims. A few grains present sector zoning.

Sample AZR5

The detrital zircon grains from this sample have an average diameter of 180 μm , though their size varies from 100 to 260 μm . They are generally elongated and pinkish or yellowish in color. Their internal structure, imaged by CL, often presents continuous oscillatory zoning, but a few grains also appear to be composite with partially resorbed cores overgrown by rims with lower Th/U values. A few grains are also characterized by sector zoning.

Sample AZR6

This sample shows zircons generally elongated and whitish, yellowish or pinkish in color. Their size varies from 120 to 260 μm , being 160 μm the average diameter. CL images show that most of these zircons appear to be characterized by continuous oscillatory zoning or partially resorbed cores overgrown by low- or high-U rims; a few grains show however sector zoning. Where present, the rims are usually characterized by lower Th/U values than the cores.

Appendix C

Cathodoluminescence images

Chapter II, Section II.3

El Mansouria area

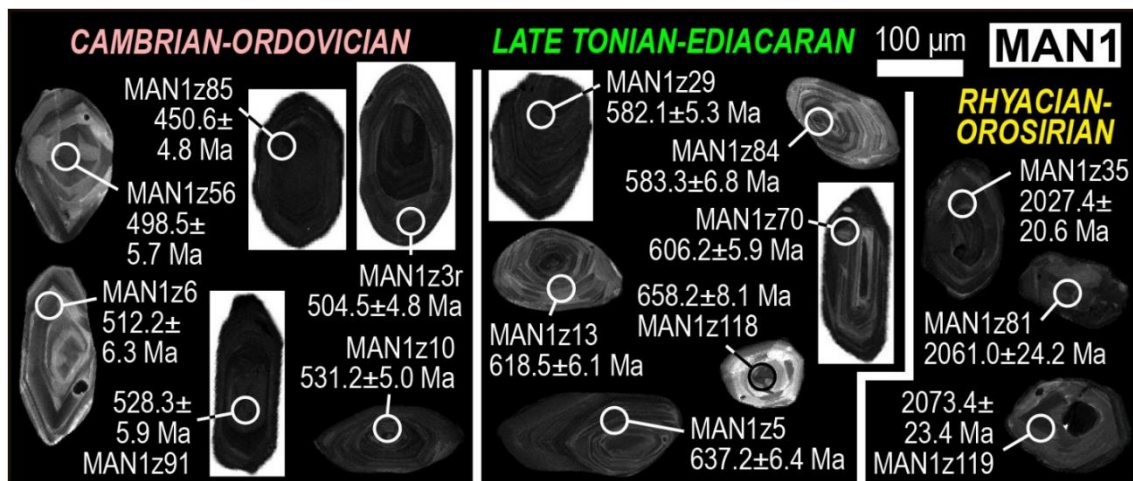


Figure C.1. Cathodoluminescence images of selected detrital zircon grains from the Early Ordovician sample MAN1 (IGSN: IEACC0040), accompanied by the result of the corresponding U-Pb analysis.

Oued Akreuch area



Figure C.2. Cathodoluminescence images of selected detrital zircon grains from the Late Ordovician samples AKR1 (IGSN: IEACC0038) and Early Ordovician sample AKR2 (IGSN: IEACC0039), accompanied by the result of the corresponding U-Pb analysis.

Ezzhiliga area



Figure C.3. Cathodoluminescence images of selected detrital zircon grains from the Late Ordovician samples EZ1 (IGSN: IEACC0032) and EZ2 (IGSN: IEACC0033), accompanied by the result of the corresponding U-Pb analysis.



Figure C.4. Cathodoluminescence images of selected detrital zircon grains from the Middle-Late Ordovician sample EZ4 (IGSN: IEACC0034) and Late Ordovician sample EZ5 (IGSN: IEACC0035), accompanied by the result of the corresponding U-Pb analysis.

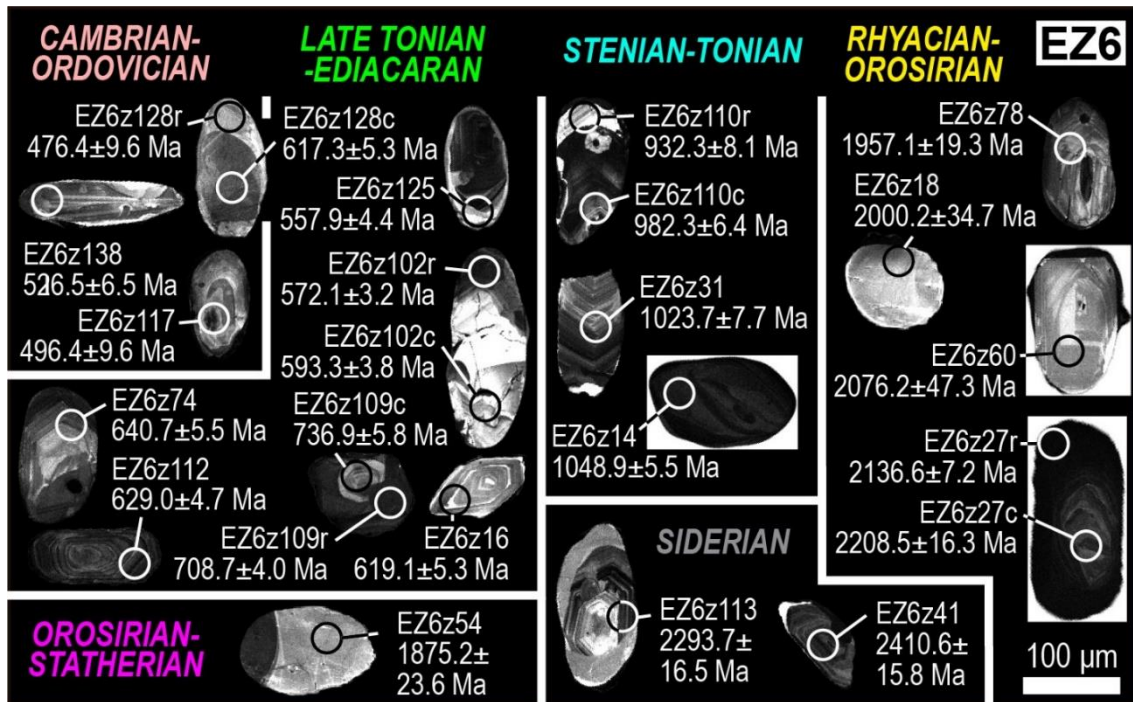


Figure C.5. Cathodoluminescence images of selected detrital zircon grains from the Late Ordovician sample EZ6 (IGSN: IEACC0036), accompanied by the result of the corresponding U-Pb analysis.

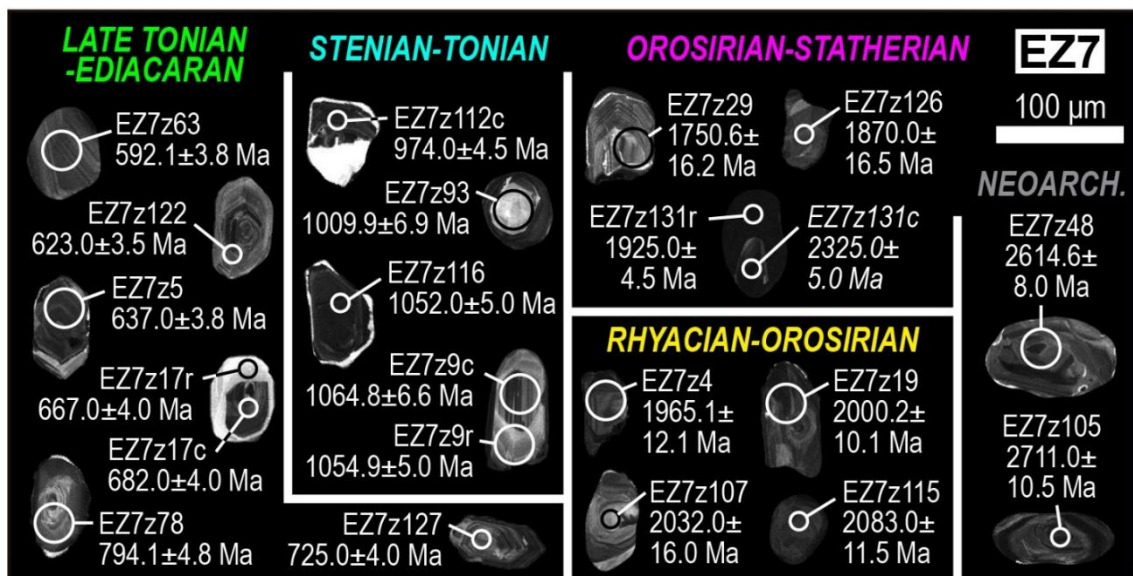


Figure C.6. Cathodoluminescence images of selected detrital zircon grains from the Early Devonian sample EZ7 (IGSN: IEACC0037), accompanied by the result of the corresponding U-Pb analysis.

Azrou area

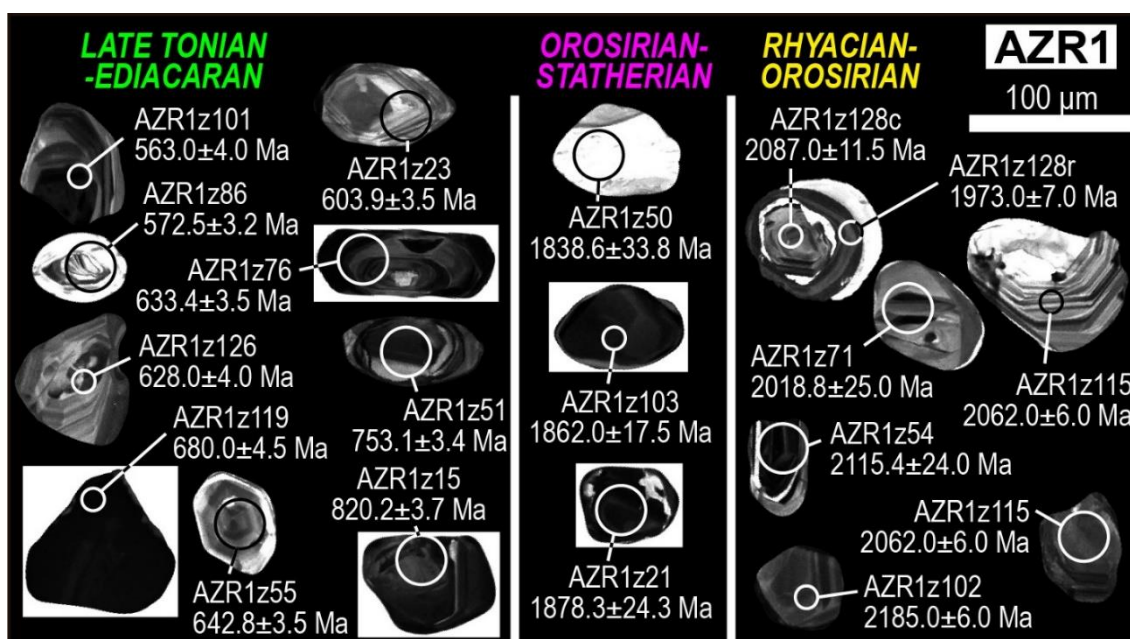


Figure C.7. Cathodoluminescence images of selected detrital zircon grains from the Late Ordovician sample AZR1 (IGSN: IEACC0023), accompanied by the result of the corresponding U-Pb analysis.

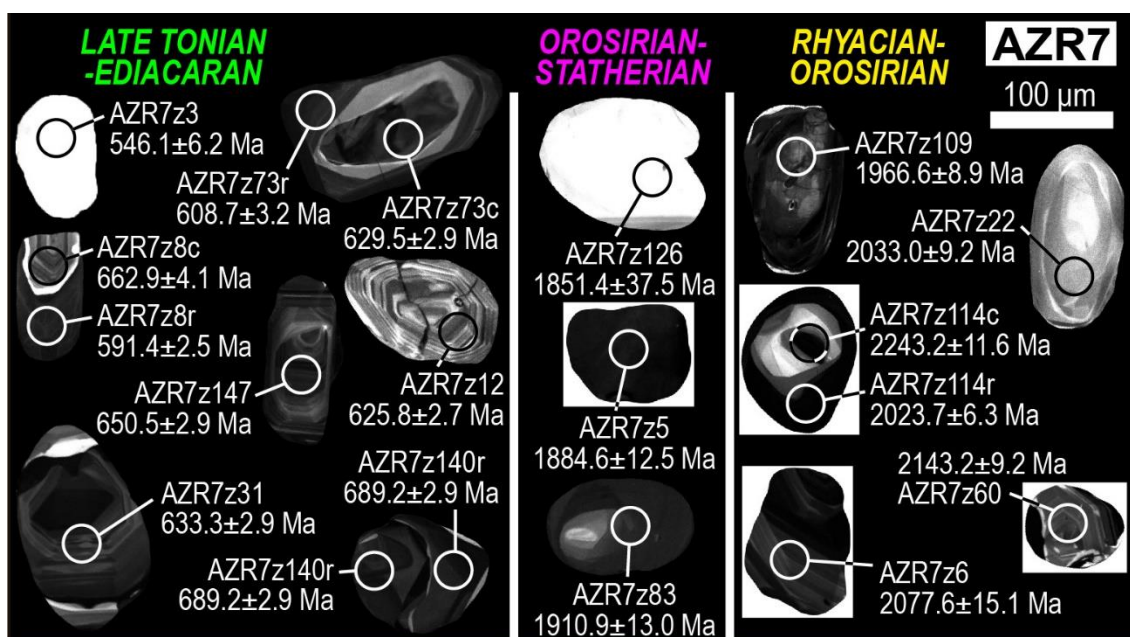


Figure C.8. Cathodoluminescence images of selected detrital zircon grains from the Early Devonian sample AZR7 (IGSN: IEACC0028), accompanied by the result of the corresponding U-Pb analysis.

Khenifra area

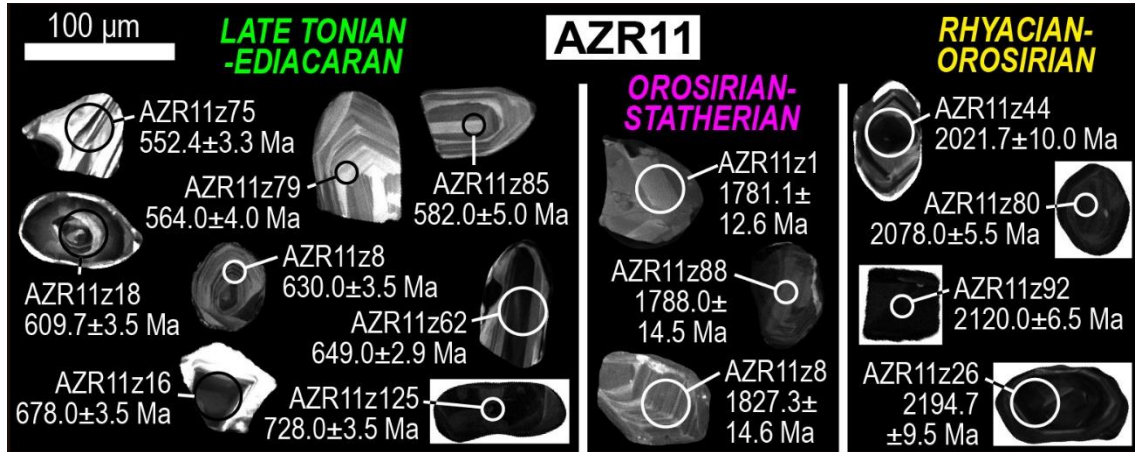


Figure C.9. Cathodoluminescence images of selected detrital zircon grains from the Cambrian-Ordovician sample AZR11 (IGSN: IEACC0030), accompanied by the result of the corresponding U-Pb analysis.

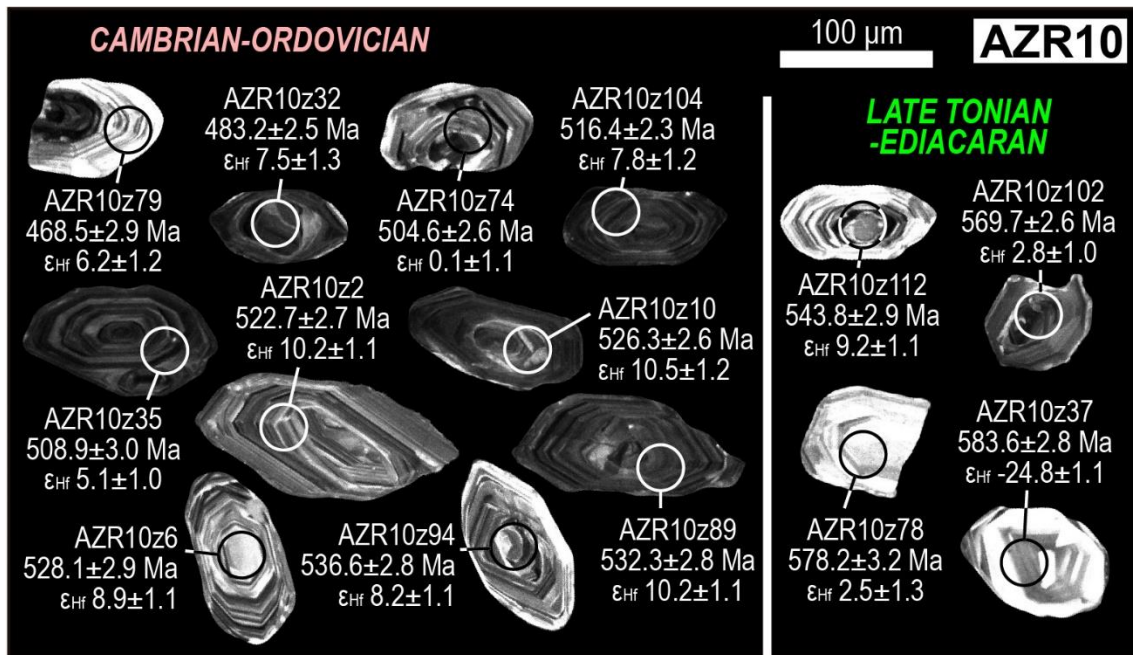


Figure C.10. Cathodoluminescence images of selected detrital zircon grains from the Early-Middle Ordovician sample AZR10 (IGSN: IEACC0029), accompanied by the result of the corresponding U-Pb and Hf analyses.

Zekkara area



Figure C.11. Cathodoluminescence images of selected detrital zircon grains from the Early-Middle Ordovician samples OUI5 (IGSN: IEACC0021) and OUI6 (IGSN: IEACC0022), accompanied by the result of the corresponding U-Pb analysis.

Oulmes area

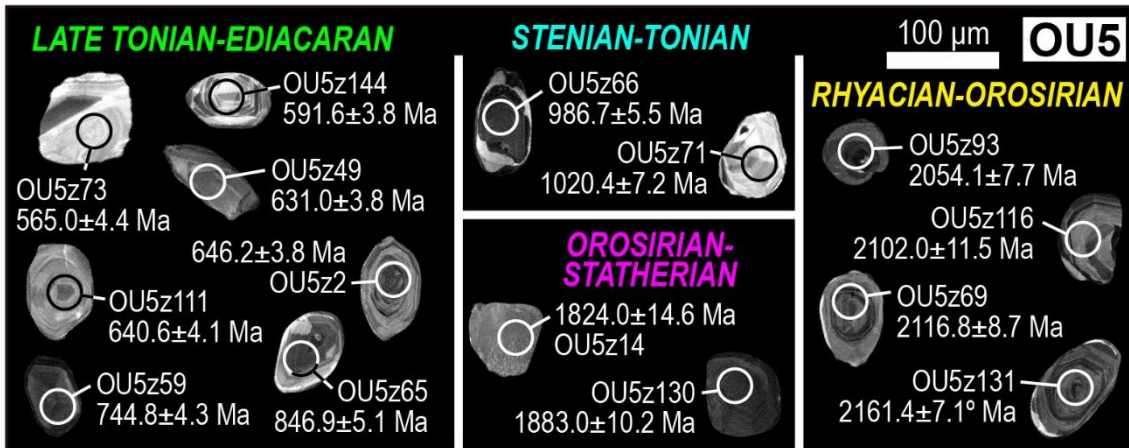


Figure C.12. Cathodoluminescence images of selected detrital zircon grains from the Early Devonian sample OU5 (IGSN: IEACC0031), accompanied by the result of the corresponding U-Pb analysis and, when available, Hf analyses.

Chapter III

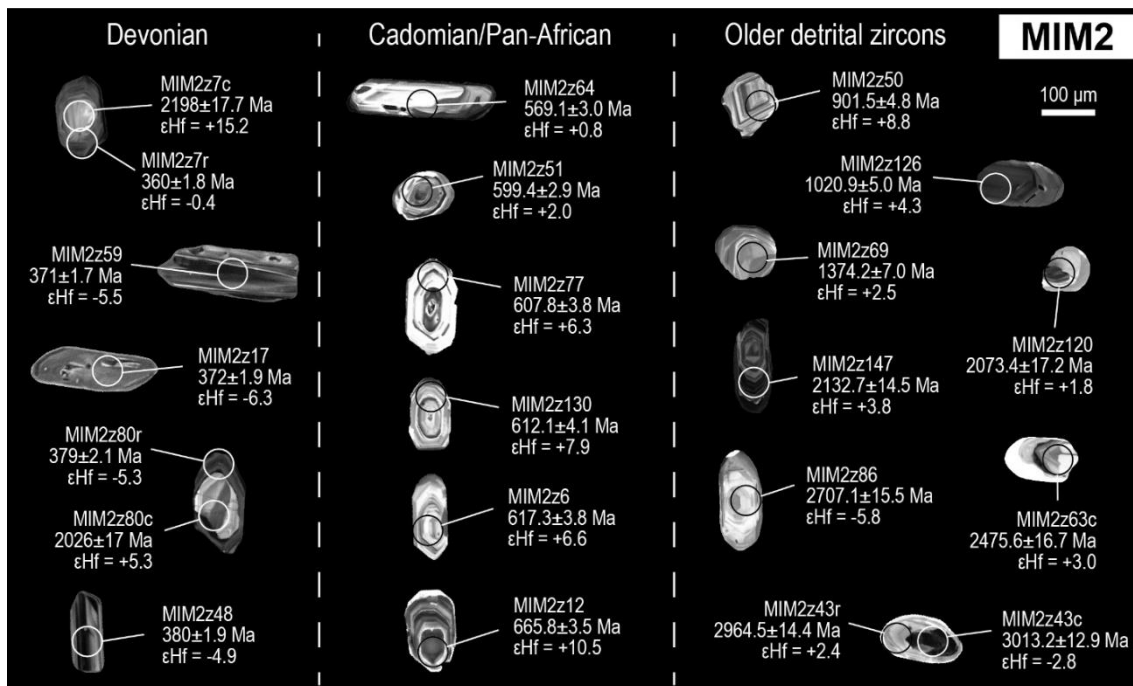


Figure C.13. Cathodoluminescence images of selected detrital zircon grains from sample MIM2 (IGSN: IEACC0004), accompanied by the result of the corresponding U-Pb and Hf analyses.

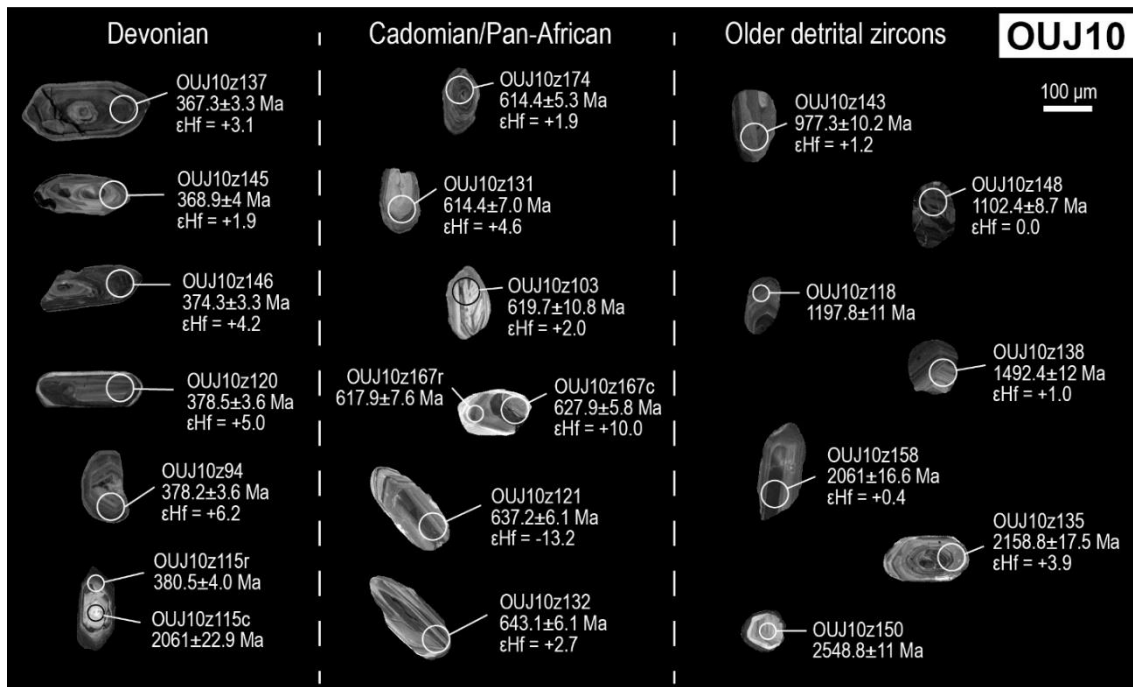


Figure C.14. Cathodoluminescence images of selected detrital zircon grains from sample OIJ10 (IGSN: IEACC0001), accompanied by the result of the corresponding U-Pb and, when available, Hf analyses.

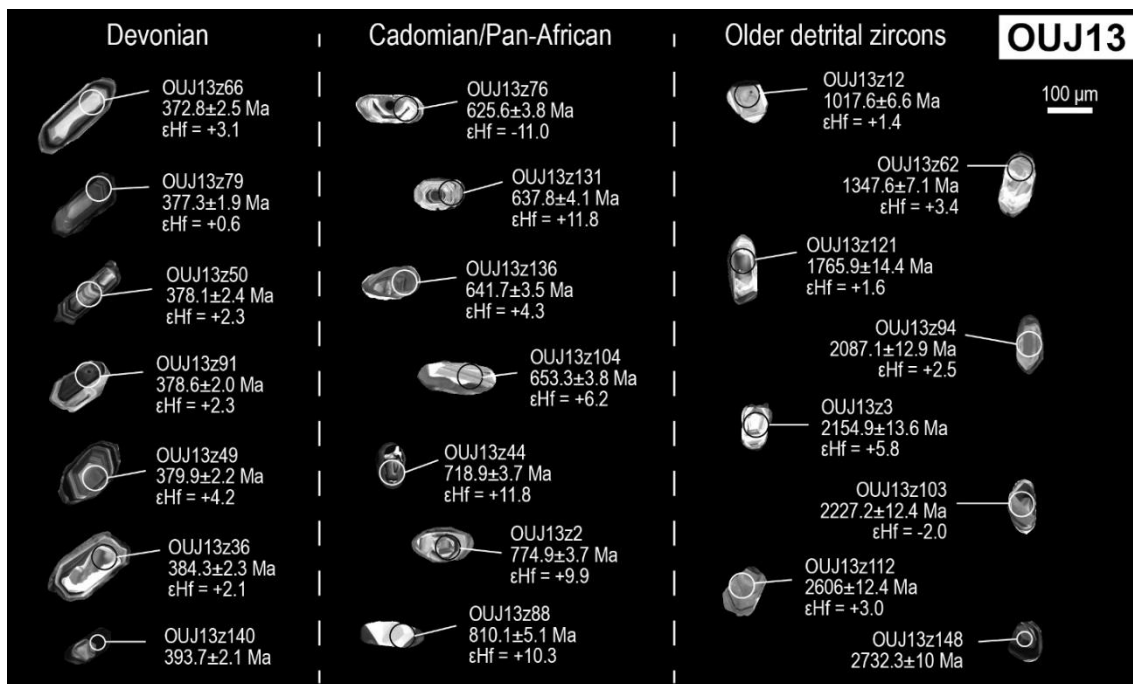


Figure C.15. Cathodoluminescence images of selected detrital zircon grains from sample OIJ11 (IGSN: IEACC0002), accompanied by the result of the corresponding U-Pb and Hf analyses.

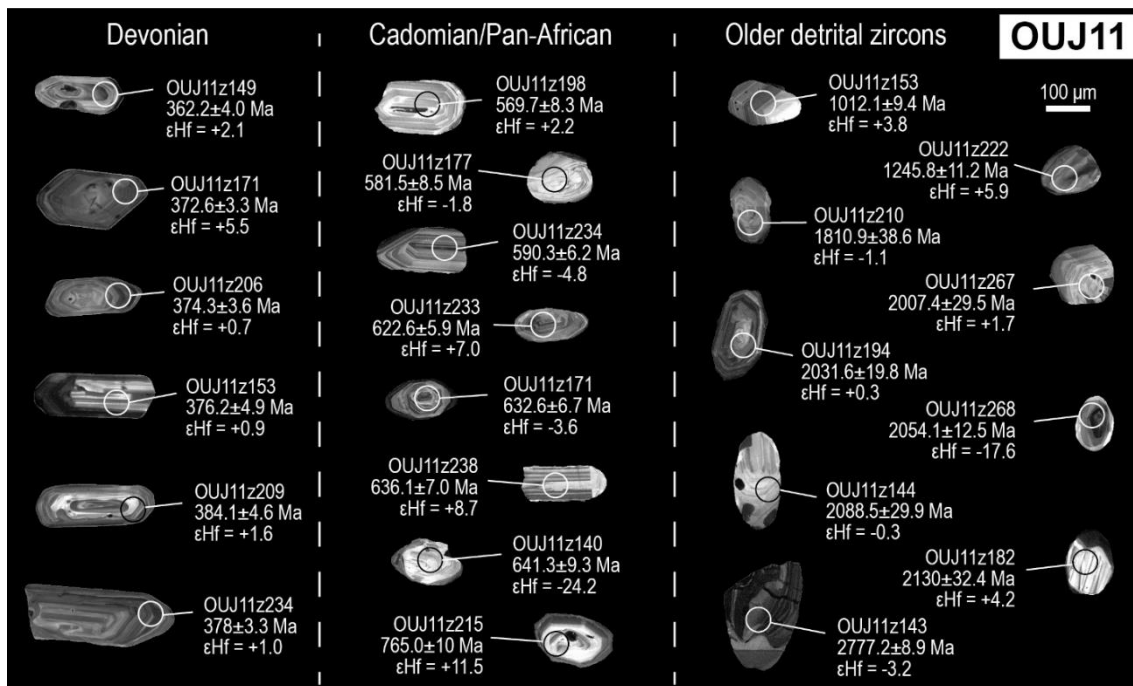


Figure C.16. Cathodoluminescence images of selected detrital zircon grains from sample OJJ13 (IGSN: IEACC0003), accompanied by the result of the corresponding U-Pb and Hf analyses.

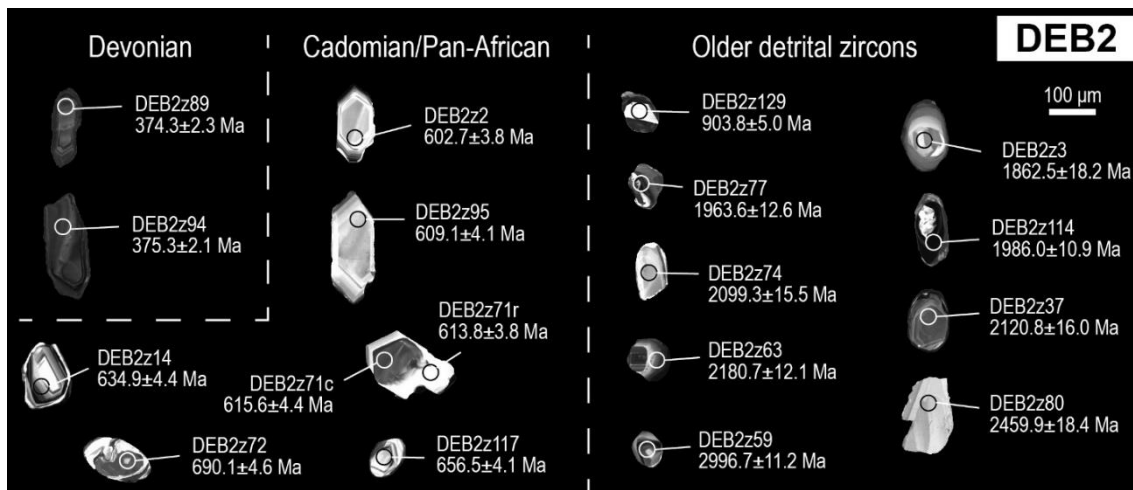


Figure C.17. Cathodoluminescence images of selected detrital zircon grains from sample DEB2 (IGSN: IEACC0005), accompanied by the result of the corresponding U-Pb analyses.

Chapter IV

Ben Slimane area

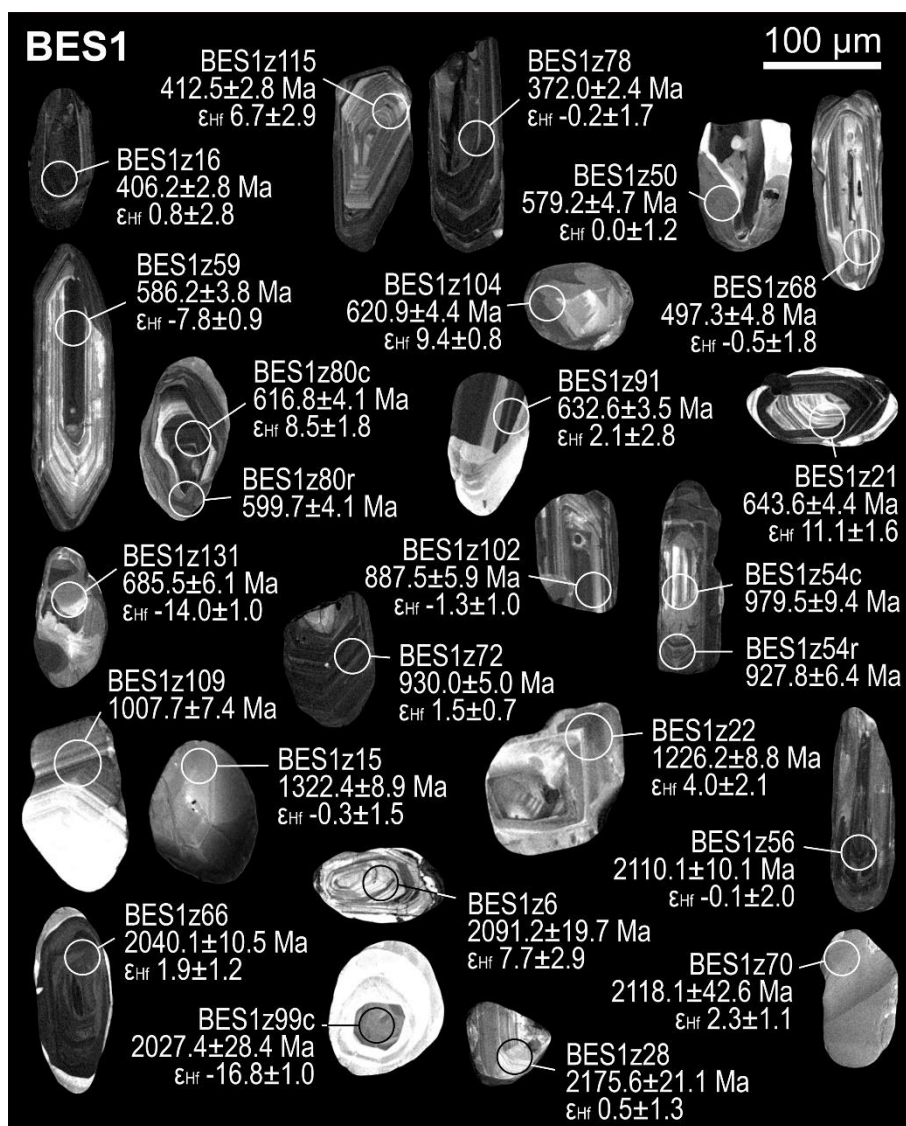


Figure C.18. Cathodoluminescence images of selected detrital zircon grains from the Visean sample BES1 (IGSN: IEACC0009), accompanied by the result of the corresponding U-Pb analyses and, when available, Hf analyses.



Figure C.19. Cathodoluminescence images of selected detrital zircon grains from the Visean sample SKH1 (IGSN: IEACC0011), accompanied by the result of the corresponding U-Pb analyses and, when available, Hf analyses.

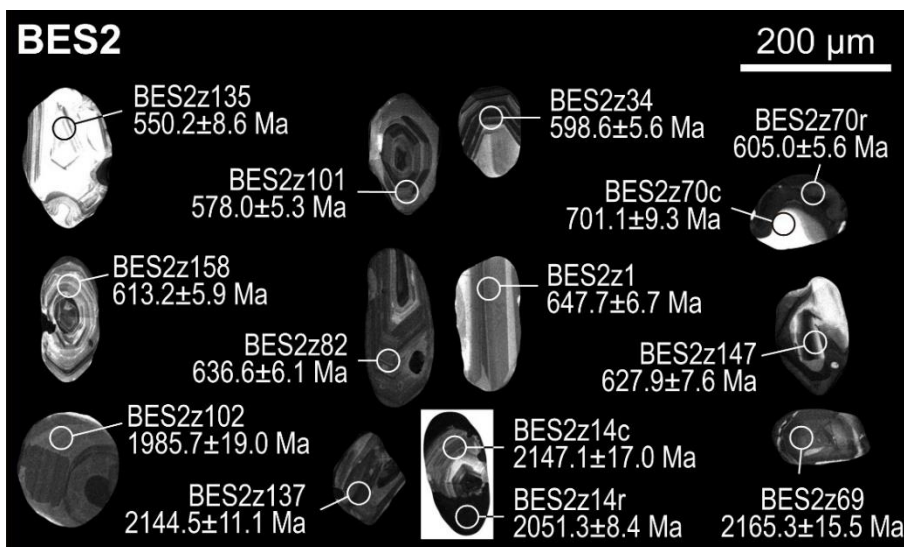


Figure C.20. Cathodoluminescence images of selected detrital zircon grains from the Famennian sample BES2 (IGSN: IEACC0010), accompanied by the result of the corresponding U-Pb analyses.

Sidi Bettache area

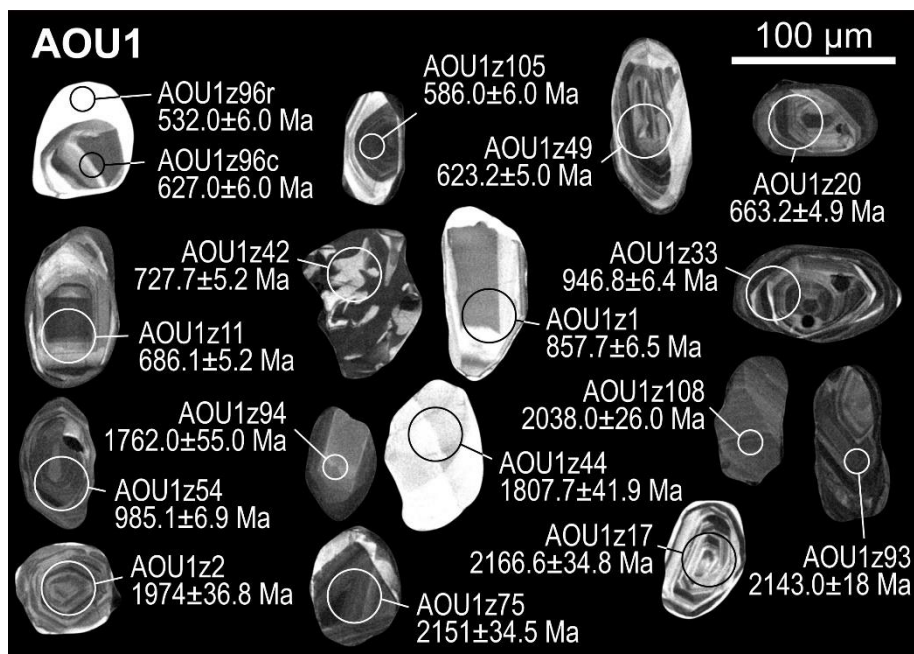


Figure C.21. Cathodoluminescence images of selected detrital zircon grains from the Visean sample AOU1 (IGSN: IEACC0013), accompanied by the result of the corresponding U-Pb analyses.

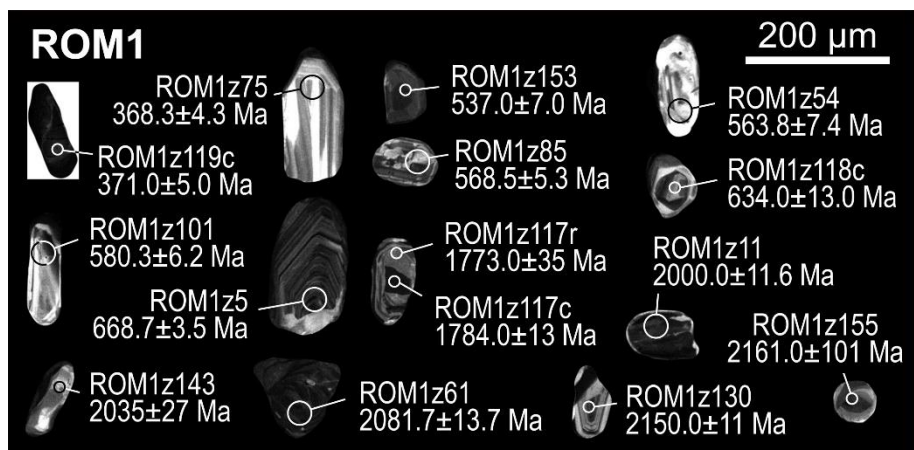


Figure C.22. Cathodoluminescence images of selected detrital zircon grains from the Visean sample ROM1 (IGSN: IEACC0012), accompanied by the result of the corresponding U-Pb analyses.

Tiflet area

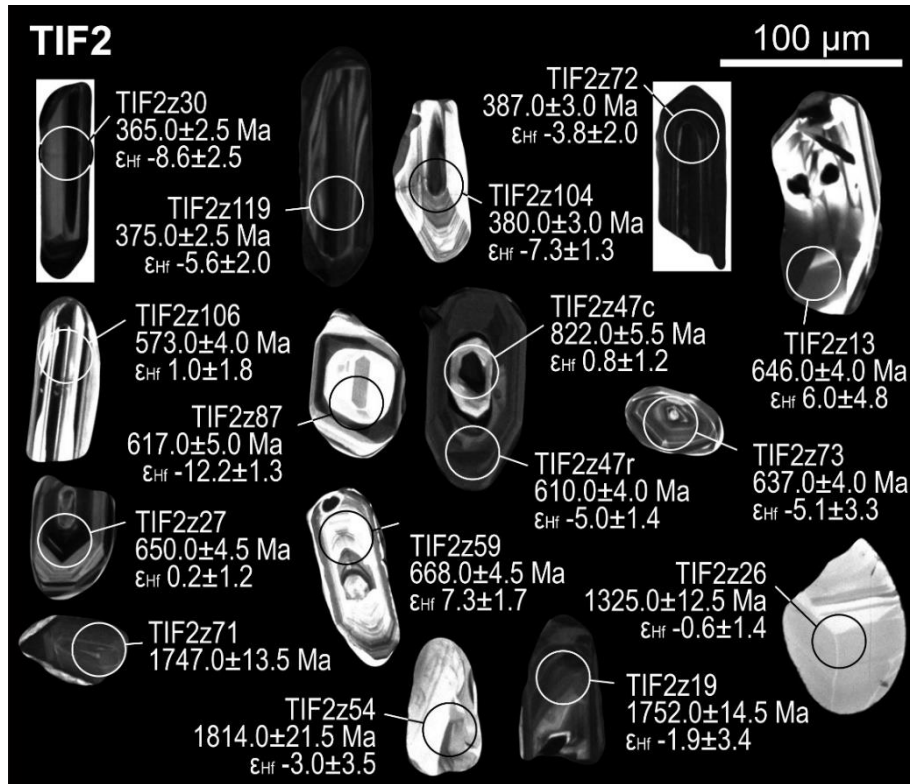


Figure C.23. Cathodoluminescence images of selected detrital zircon grains from the Tournaisian sample TIF2 (IGSN: IEACC0017), accompanied by the result of the corresponding U-Pb analyses and, when available, Hf analyses.

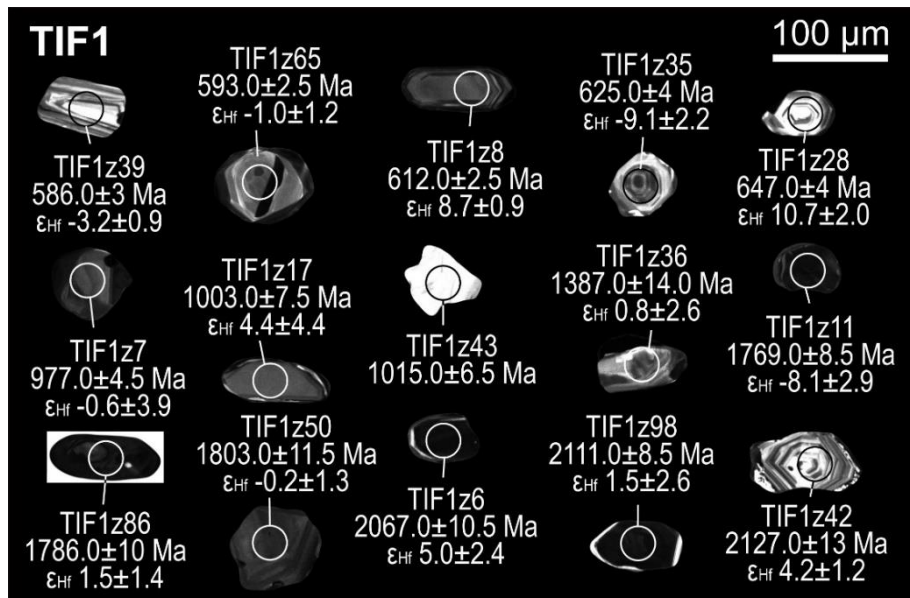


Figure C.24. Cathodoluminescence images of selected detrital zircon grains from the Tournaisian sample TIF1 (IGSN: IEACC0016), accompanied by the result of the corresponding U-Pb and Hf analyses.

Oulmes area

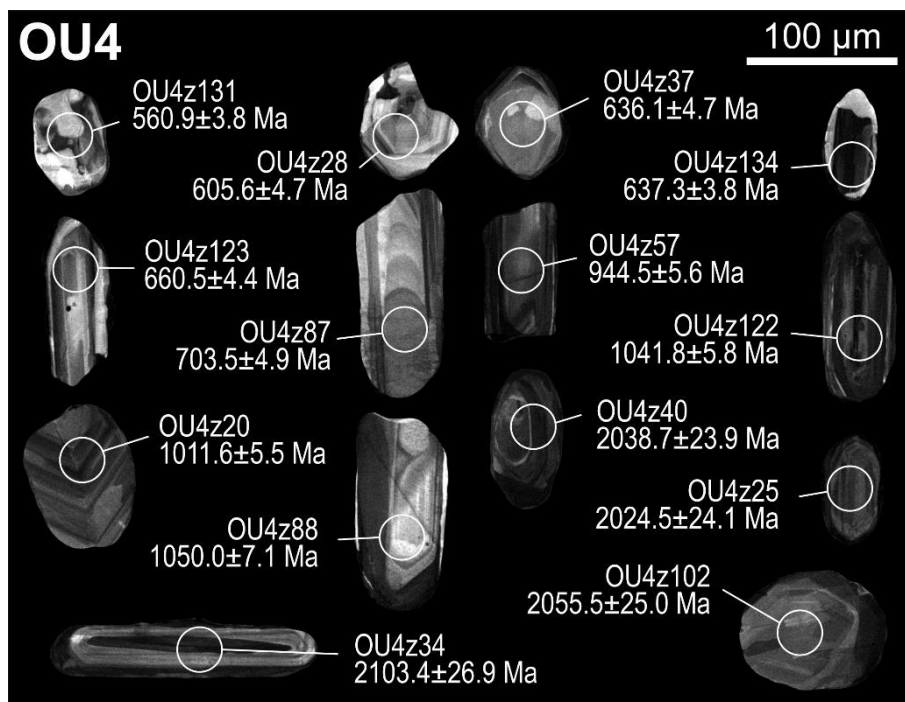


Figure C.25. Cathodoluminescence images of selected detrital zircon grains from the Famennian sample OU4 (IGSN: IEACC0015), accompanied by the result of the corresponding U-Pb analyses.

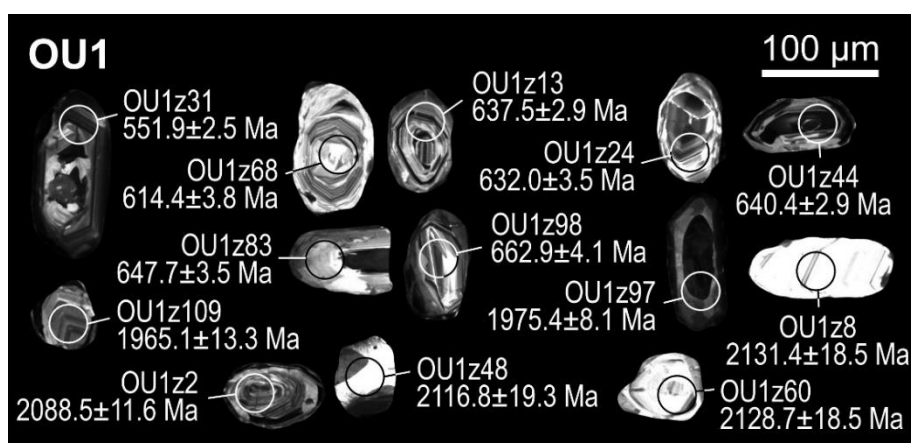


Figure BC.26. Cathodoluminescence images of selected detrital zircon grains from the Late Viséan sample OU1 (IGSN: IEACC0014), accompanied by the result of the corresponding U-Pb analyses.

Jerada area

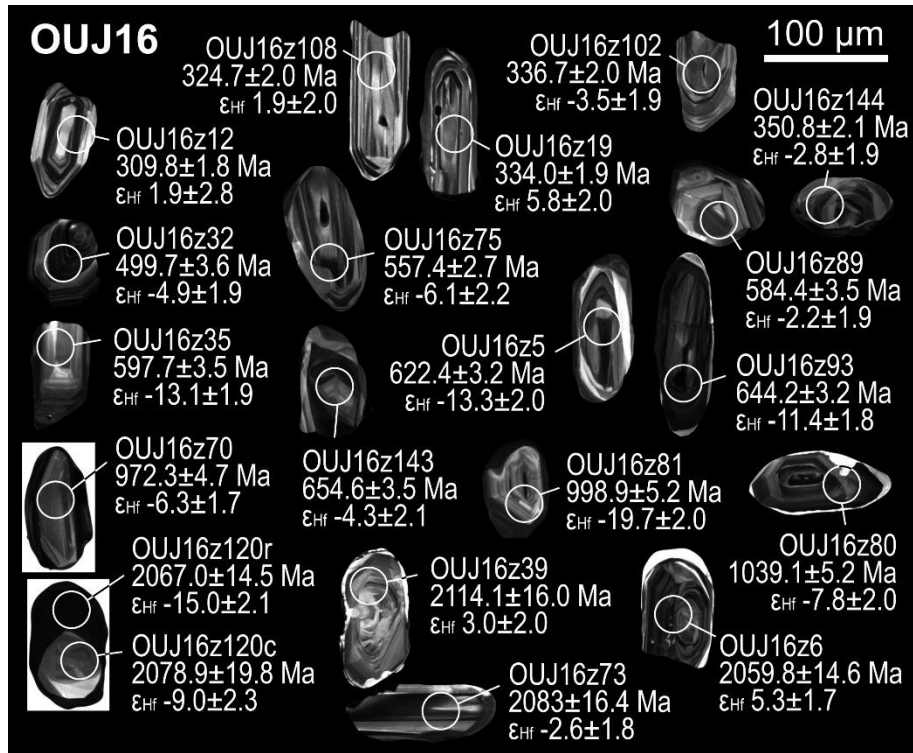


Figure C.27. Cathodoluminescence images of selected detrital zircon grains from the Middle Carboniferous sample OUI16 (IGSN: IEACC0018), accompanied by the result of the corresponding U-Pb and Hf analyses.

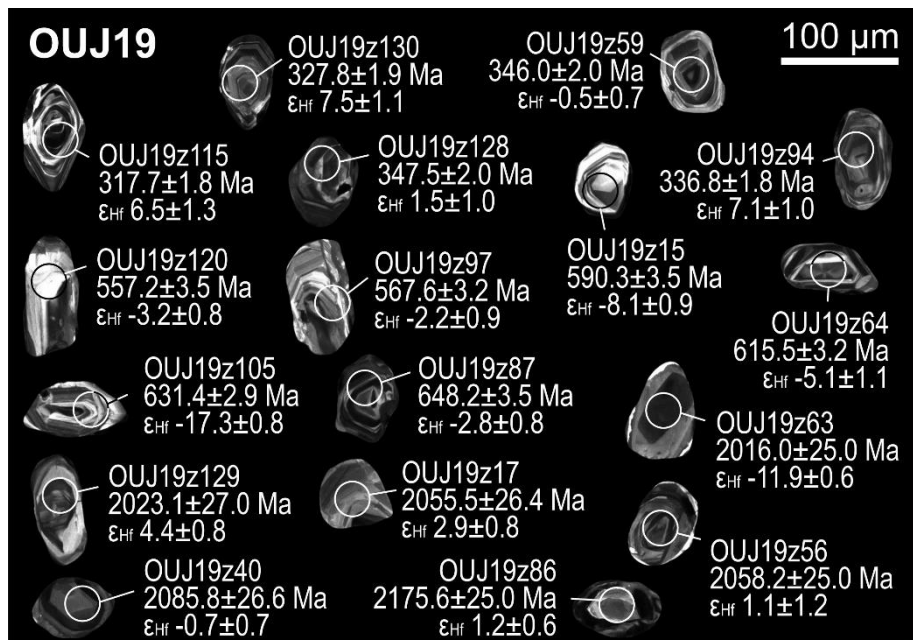


Figure C.28. Cathodoluminescence images of selected detrital zircon grains from the Late Carboniferous sample OUI19 (IGSN: IEACC0020), accompanied by the result of the corresponding U-Pb and Hf analyses.

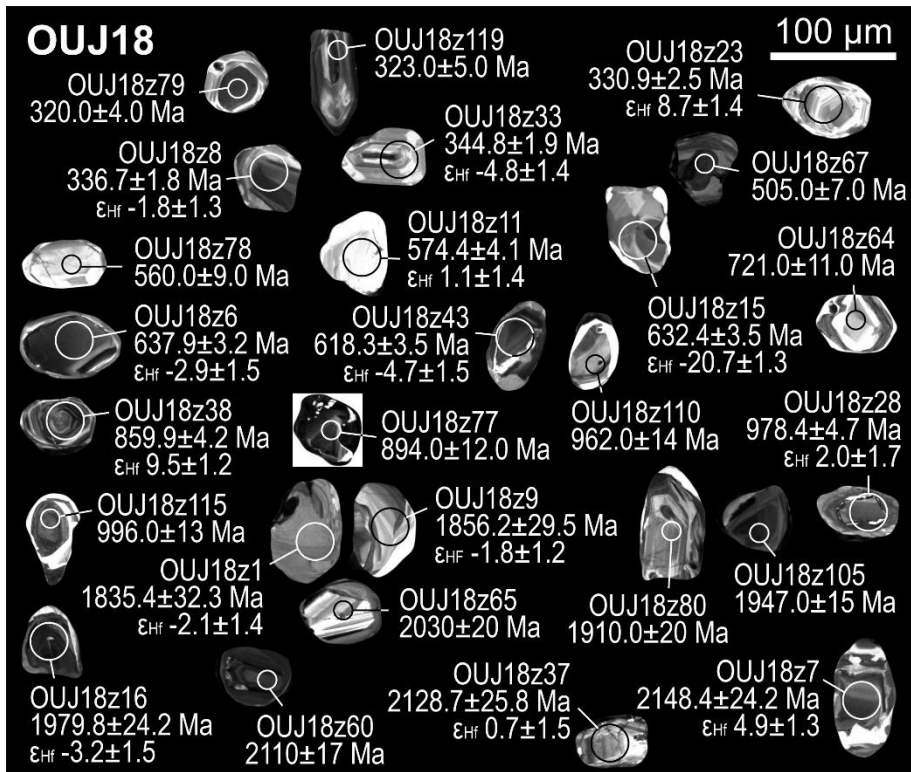


Figure C.29. Cathodoluminescence images of selected detrital zircon grains from the Late Carboniferous sample OJJ18 (IGSN: IEACC0019), accompanied by the result of the corresponding U-Pb analyses and, when available, Hf analyses.

Appendix D

Results of the U-Pb analyses

- Chapter II – Section II.1: Table D.1 to D.10*
Section II.2: Table D.11 to D.13b
Section II.3: Table D.14 to D.29
- Chapter III – Tables D.30 to D.34*
- Chapter IV – Tables D.35 to D.46*

ANALYSIS	U (ppm)	Th (ppm)	Pb (ppm)	Th/U	Ratios			Pb loss, high common Pb and/or discordant data			Ages (Ma)					Concordance (%)							
					$^{207}\text{Pb}/^{206}\text{Pb}$	2σ	$^{207}\text{Pb}/^{235}\text{U}$	2σ	$^{206}\text{Pb}/^{238}\text{U}$	2σ	Error correction	$^{207}\text{Pb}/^{206}\text{Pb}$	σ	2σ	$^{207}\text{Pb}/^{235}\text{U}$		σ	2σ	$^{206}\text{Pb}/^{238}\text{U}$	σ	2σ		
OUJ222	141.40	119.00	30.21	0.803	6.30E+04	4.90E+04	0.0531	0.0032	0.649	0.039	0.0906	0.0028	0.1715	310	65.0	130	505	12.0	24	559	8.0	16	111
OUJ223c	615.00	128.00	92.20	0.192	3.50E+05	4.00E+05	0.0822	0.0018	1.615	0.053	0.1437	0.0047	0.8202	1250	22.0	44	974	10.0	20	866	13.0	26	89
OUJ214	89.00	83.60	27.90	0.903	1.00E+05	3.20E+04	0.0782	0.0080	1.070	0.110	0.0109	0.0035	0.1939	1100	100.0	200	741	26.5	53	625	10.5	21	84
OUJ223	623.00	746.00	566.00	1.117	5.30E+05	1.70E+05	0.1551	0.0015	6.990	0.330	0.3260	0.0170	0.9739	2408	12.5	25	2100	21.0	42	1825	43.5	87	87
OUJ2250c	32.30	37.40	46.10	1.094	5.30E+04	4.20E+04	0.1520	0.0140	7.370	0.750	0.3518	0.0120	0.4718	2310	80.0	160	2124	45.0	90	1949	31.0	62	92
OUJ2252c	688.00	1360.00	287.00	1.916	1.32E+05	9.10E+04	0.0939	0.0034	0.932	0.033	0.0728	0.0025	0.2880	1498	35.0	70	672	8.5	17	453	7.5	15	67
OUJ2256	9.04	2.23	1.36	0.236	3.00E+04	1.20E+04	0.1100	0.0150	4.000	0.560	0.2590	0.0140	0.3026	1740	125.0	250	1630	60.0	120	1482	35.5	71	91
OUJ2267	750.00	281.00	149.40	0.364	8.00E+06	1.10E+06	0.1011	0.0015	2.847	0.048	0.2058	0.0057	0.5416	1640	17.0	34	1367	6.5	13	1206	15.0	30	88
OUJ2272c	123.00	77.30	66.40	0.617	1.00E+03	2.20E+05	0.2582	0.0049	12.620	0.320	0.3549	0.0110	0.6720	3245	17.0	34	2648	12.0	24	1958	26.0	52	74
OUJ2272r	443.00	60.90	55.50	0.131	5.00E+06	1.80E+06	0.2520	0.0025	15.040	0.480	0.4360	0.0160	0.9586	3200	12.0	24	2817	15.0	30	2328	35.5	71	83
OUJ2282	1545.00	1053.00	1250.00	0.645	1.43E+06	6.50E+05	0.1790	0.0230	6.200	0.990	0.2600	0.0130	0.6883	2480	100.0	200	1980	65.0	130	1489	33.0	66	75
OUJ2297c	417.00	115.00	70.60	0.276	1.30E+05	3.90E+05	0.1106	0.0023	3.240	0.200	0.2118	0.0110	0.9440	1823	17.5	35	1454	24.0	48	1236	30.0	60	85
OUJ22100	1176.00	709.00	598.80	0.585	3.10E+06	2.10E+06	0.1486	0.0014	6.607	0.088	0.3232	0.0093	0.7948	2301	12.5	25	2060	6.0	12	1805	23.0	46	88
OUJ22106	465.00	880.00	273.00	1.555	1.51E+05	8.30E+04	0.1031	0.0080	1.390	0.100	0.1001	0.0031	0.1877	1650	65.0	130	880	22.5	45	619	9.0	18	70
OUJ22110c	1025.00	215.00	155.50	0.208	4.50E+05	5.00E+05	0.0885	0.0025	1.648	0.061	0.1355	0.0040	0.6438	1398	28.0	56	986	11.5	23	819	11.5	23	83
OUJ22110r	747.00	109.00	187.10	0.145	1.29E+05	1.40E+04	0.1440	0.0044	2.260	0.110	0.1140	0.0040	0.8061	2273	26.0	52	1192	17.0	34	696	11.5	23	58
OUJ22112	1950.00	1051.00	153.00	0.541	5.80E+05	3.80E+05	0.0832	0.0016	0.613	0.034	0.0538	0.0031	0.9315	1267	19.0	38	483	10.5	21	338	9.5	19	70
OUJ22116	1181.00	404.00	377.00	0.270	1.60E+06	5.40E+06	0.1862	0.0019	10.570	0.190	0.4143	0.0120	0.6905	2689	12.0	24	2487	8.5	17	2234	27.0	54	90
OUJ22119c	835.00	79.00	87.00	0.085	7.00E+06	2.30E+06	0.1964	0.0015	12.170	0.200	0.4508	0.0130	0.8343	2782	12.5	25	2617	7.5	15	2398	29.0	58	92
OUJ22119f	88.00	38.20	14.00	0.469	6.00E+03	2.80E+05	0.1580	0.0110	8.300	1.300	0.3580	0.0430	0.9675	2400	65.0	130	2110	85.0	170	1940	105.0	210	92
OUJ22120c	189.00	92.20	109.80	0.491	2.00E+04	1.00E+06	0.2087	0.0032	13.940	0.320	0.4814	0.0150	0.7751	2880	15.0	30	2743	11.0	22	2532	31.5	63	92
OUJ22120r	44.20	27.60	85.00	0.581	3.35E+04	4.90E+03	0.3640	0.0280	12.800	1.500	0.2520	0.0210	0.8614	3700	70.0	140	2640	65.0	130	1450	55.0	110	55
OUJ22122r	266.10	117.80	48.00	0.446	2.60E+05	1.40E+05	0.0897	0.0056	1.180	0.070	0.0970	0.0029	0.3115	1410	60.0	120	785	16.5	33	597	8.5	17	76
OUJ22123c	172.20	168.00	119.00	0.958	1.68E+05	5.00E+04	0.1726	0.0076	3.040	0.160	0.1267	0.0040	0.6800	2585	36.0	72	1417	20.5	41	769	11.5	23	54

Footnotes:

. Analysis references: OUJ2z is zircon from sample OUJ2 (mount CT17-9), followed by grain number "c" or "r", meaning core or rim, respectively.

ANALYSIS	U (ppm)	Th (ppm)	Pb (ppm)	Th/U	Ratios			Ages (Ma)			Concordance (%)												
					$^{207}\text{Pb}/^{206}\text{Pb}$	$^{207}\text{Pb}/^{235}\text{U}$	$^{206}\text{Pb}/^{238}\text{U}$	$^{207}\text{Pb}/^{206}\text{Pb}$	$^{207}\text{Pb}/^{235}\text{U}$	$^{206}\text{Pb}/^{238}\text{U}$	σ	2σ	σ	2σ									
OUJ32117	115.70	14.79	5.09	0.127	-2.70E+06	1.60E+06	0.0630	0.0036	0.860	0.044	0.0994	0.0032	0.0032	660	65.0	130	627	12.0	24	611	9.5	19	97
OUJ32118	62.50	117.70	35.00	1.923	-1.10E+05	1.20E+05	0.0631	0.0066	0.861	0.084	0.1023	0.0043	0.0043	630	110.0	220	619	23.0	46	627	12.5	25	101
OUJ32119	49.50	37.50	9.35	0.760	8.00E+05	1.70E+05	0.0580	0.0073	0.678	0.084	0.0841	0.0034	0.0034	400	125.0	250	512	25.0	50	520	10.0	20	102
OUJ32120c	175.40	69.50	87.90	0.400	-4.00E+06	1.30E+06	0.0614	0.0026	13.040	0.200	0.4900	0.0140	0.0140	2763	15.0	30	2686	7.0	14	2570	29.5	59	96
OUJ32121	360.00	207.00	59.80	0.573	2.60E+05	6.10E+05	0.1674	0.0021	0.856	0.031	0.1002	0.0030	0.0030	643	37.0	74	629	8.5	17	616	8.5	17	88
OUJ32122c	110.40	111.40	29.80	1.014	-1.00E+06	1.70E+06	0.0600	0.0042	0.801	0.059	0.0961	0.0030	0.0030	560	75.0	150	591	17.0	34	591	9.0	18	100
OUJ32123	243.20	337.40	316.50	1.408	-6.00E+06	1.50E+06	0.1268	0.0020	6.252	0.098	0.3597	0.0110	0.0110	2051	17.5	35	2013	7.0	14	1980	25.0	50	98
OUJ32124	87.70	28.99	37.16	0.338	1.14E+06	6.70E+05	0.2251	0.0042	16.550	0.330	0.5347	0.0170	0.0170	3013	18.0	36	2907	9.5	19	2760	34.5	69	95
OUJ325	590.00	465.00	327.00	0.709	1.10E+05	2.40E+04	0.1890	0.0170	3.140	0.370	0.1215	0.0048	0.0048	2690	75.0	150	1454	43.0	86	739	13.5	27	51
OUJ329c	642.00	95.50	224.00	0.149	2.00E+05	3.30E+05	0.1630	0.0290	3.260	0.750	0.1374	0.0077	0.0077	2110	155.0	310	1360	85.0	170	829	21.5	43	61
OUJ329f	893.00	12.80	8.55	0.015	9.40E+05	9.50E+05	0.0850	0.0012	1.746	0.034	0.1454	0.0042	0.0042	1312	13.5	27	1025	6.5	13	875	12.0	24	86
OUJ340	716.00	214.00	243.00	0.287	2.90E+06	3.90E+06	0.1767	0.0017	10.030	0.200	0.4009	0.0130	0.0130	2636	125.0	250	2440	9.0	18	2172	29.5	59	89
OUJ346	43.20	101.60	29.80	0.390	-1.30E+05	1.20E+05	0.0530	0.0064	0.723	0.085	0.0992	0.0038	0.0038	240	125.0	250	547	26.0	52	612	10.5	21	112
OUJ372	911.00	476.00	374.00	0.532	2.60E+06	1.90E+06	0.1402	0.0017	6.730	0.120	0.2354	0.0100	0.0100	2236	14.5	29	2075	8.0	16	1905	25.0	50	92
OUJ387f	229.00	26.50	21.70	0.121	-9.30E+05	9.20E+05	0.1175	0.0023	3.850	0.120	0.3354	0.0030	0.0030	1919	16.5	33	1601	12.0	24	1362	21.0	42	85
OUJ389	1000.00	267.80	71.50	0.274	1.00E+06	1.10E+06	0.0915	0.0019	1.923	0.089	0.1480	0.0061	0.0061	1456	20.0	40	1084	15.5	31	889	17.0	34	82
OUJ398r	1020.00	1400.00	102.30	0.472	2.40E+06	4.50E+06	0.1323	0.0014	6.240	0.360	0.3350	0.0200	0.0200	2125	14.0	28	1995	25.5	51	1858	48.0	96	93
OUJ399f	20.37	16.14	4.43	0.793	2.50E+04	4.90E+04	0.0460	0.0110	0.610	0.140	0.0974	0.0043	0.0043	80	205.0	410	480	50.0	100	599	12.5	25	125
OUJ32112f	6.39	4.83	4.75	0.761	-2.20E+05	3.10E+05	0.1070	0.0170	5.720	0.880	0.3710	0.0230	0.0230	1720	165.0	330	1930	70.0	140	2027	55.0	110	105
OUJ32114	19.17	5.50	1.39	0.294	1.00E+04	3.80E+04	0.0520	0.0096	0.710	0.130	0.1026	0.0057	0.0057	130	175.0	350	536	39.5	79	629	16.5	33	117
OUJ32115	248.00	311.00	195.60	1.248	1.40E+05	8.50E+05	0.1233	0.0026	4.410	0.140	0.2587	0.0088	0.0088	1999	18.5	37	1714	12.5	25	1482	22.5	45	86
OUJ32120f	297.00	108.60	120.50	0.366	-6.00E+04	1.90E+06	0.1877	0.0028	10.690	0.170	0.4099	0.0120	0.0120	2721	15.5	31	2498	7.5	15	2214	27.5	55	89
OUJ32122f	29.20	12.87	3.78	0.454	-6.70E+04	4.20E+04	0.0730	0.0098	0.950	0.120	0.0982	0.0045	0.0045	870	145.0	290	677	35.5	71	604	13.0	26	89

Pb loss and discordant data

Footnotes: . . . Analysis references: OUJ3z is zircon from sample OUJ3 (mount CT17-9), followed by grain number "c" or "r", meaning core or rim, respectively.

ANALYSIS	U (ppm)	Th (ppm)	$^{232}\text{Th}/^{238}\text{U}$	% $^{206}\text{Pb}^c$	Ratios				Ages (Ma)				Discordance (%)						
					$^{204}\text{Pb}/^{206}\text{Pb}$	$^{207}\text{Pb}/^{206}\text{Pb}$	$^{207}\text{Pb}/^{235}\text{U}$	$^{208}\text{Pb}/^{238}\text{U}$	$^{207}\text{Pb}/^{238}\text{U}$	$^{206}\text{Pb}^*/^{238}\text{U}$	2σ	σ		2σ	σ				
TAZ2750	836	558	0.69	1.78	1.00E-03	15	0.067	3.6	0.53	3.8	1.1	0.3	361	4	8	832	75	150	58
TAZ2756C	833	68	0.08	0.02	1.60E-05	58	0.115	0.4	4.43	1.9	1.8	1.0	1593	26	52	1875	8	16	17
TAZ2764	45	122	2.79	3.55	2.30E-03	29	0.123	9.3	3.07	9.7	2.6	0.3	1072	26	52	2003	165	330	50
TAZ2766	428	102	0.25	0.05	3.00E-05	71	0.111	0.8	3.19	1.4	1.2	0.8	1223	13	26	1810	14	28	36
TAZ2771	284	184	0.67	0.08	5.10E-05	58	0.124	0.9	5.02	1.6	1.3	0.8	1655	19	76	2021	16	16	20

Footnotes:

- % $^{206}\text{Pb}^c$ is % of ^{206}Pb from common Pb
- Errors are 1-sigma
- Pb* indicates radiogenic Pb, corrected for common Pb.
- Analysis references: TAZ2z is zircon from sample TAZ2 (mount CT17-10), followed by grain number "c" or "r", meaning core or rim, respectively.
- Error in standard calibration was 0.23% (not included in above errors but required when comparing data from different mounts).

- Errors are 1-sigma
- Pb* indicates radiogenic Pb, corrected for common Pb.
- Analysis references: TAZ3 is zircon from sample TAZ3 (mount CT17-10), followed by grain number "c" or "r", meaning core or rim, respectively.
- Error in standard calibration was 0.23% (not included in above errors but required when comparing data from different mounts).

ANALYSIS	U (ppm)	Th (ppm)	Pb (ppm)	Th/U	Ratios		Ages (Ma)		Concordance (%)														
					$^{207}\text{Pb}/^{206}\text{Pb}$	$^{207}\text{Pb}/^{235}\text{U}$	$^{207}\text{Pb}/^{206}\text{Pb}$	$^{207}\text{Pb}/^{235}\text{U}$															
TAZ5z107	410.00	138.00	130.00	0.311	-8.00E+06	1.40E+06	0.1248	0.0053	6.058	0.320	0.3619	0.0085	0.6341	2029	11.5	23	1983	23.5	47	1991	20.0	40	100
TAZ5z108c	360.00	245.60	71.20	0.683	2.10E+05	2.10E+05	0.0603	0.0031	0.843	0.050	0.1023	0.0025	0.1076	627	55.0	110	620	14.0	28	628	7.5	15	101
TAZ5z109f	431.00	67.50	20.62	0.155	-3.10E+05	7.20E+05	0.0634	0.0031	0.865	0.050	0.1003	0.0023	0.3495	719	50.0	100	634	13.0	26	616	6.5	13	97
TAZ5z109c	274.00	209.00	68.60	0.746	8.30E+05	6.70E+05	0.0634	0.0034	1.026	0.063	0.1208	0.0028	0.1556	689	60.0	120	715	15.5	31	735	8.0	16	103
TAZ5z109f	83.40	49.20	16.10	0.585	-1.10E+04	5.50E+04	0.0608	0.0041	1.022	0.082	0.1254	0.0034	0.3512	600	75.0	150	714	20.0	40	750	9.5	19	105
TAZ5z110c	170.50	240.80	202.70	1.427	2.00E+05	3.20E+05	0.1179	0.0053	5.090	0.280	0.280	0.0077	0.5106	1924	17.5	35	1833	23.5	47	1777	19.0	38	97
TAZ5z110f	17.90	28.90	16.02	1.572	5.00E+04	3.10E+04	0.0975	0.0100	2.800	0.310	0.2107	0.0082	0.1207	1530	105.0	210	1324	41.0	82	1231	22.0	44	93
TAZ5z111c	176.50	128.00	33.70	0.651	-1.10E+05	1.00E+05	0.0636	0.0038	0.872	0.058	0.1034	0.0026	0.0348	693	65.0	130	637	16.5	33	634	7.5	15	100
TAZ5z111f	159.80	88.30	27.00	0.566	8.00E+05	1.80E+05	0.0629	0.0044	0.858	0.064	0.1016	0.0026	0.0499	690	75.0	150	634	18.5	37	624	7.5	15	98
TAZ5z112c	79.30	13.26	4.65	0.169	3.00E+05	1.00E+05	0.0664	0.0041	1.027	0.074	0.1137	0.0031	0.2096	800	70.0	140	713	18.5	37	694	9.0	18	97
TAZ5z112f	439.00	16.05	4.24	0.037	-8.00E+06	4.90E+06	0.0593	0.0029	0.765	0.044	0.0965	0.0022	0.2196	574	55.0	110	576	12.5	25	594	6.5	13	103
TAZ5z113c	171.00	84.70	101.60	0.484	3.20E+05	5.20E+05	0.1733	0.0076	11.430	0.630	0.4884	0.0120	0.7713	2594	14.5	29	2556	26.5	53	2563	26.0	52	100
TAZ5z113f	183.00	75.20	72.10	0.423	-3.70E+05	5.20E+05	0.1362	0.0062	6.970	0.410	0.3803	0.0039	0.7568	2178	18.5	37	2108	27.0	54	2077	23.0	46	99
TAZ5z114c	140.70	76.90	90.30	0.543	-9.00E+05	3.60E+05	0.1647	0.0071	10.470	0.570	0.4740	0.0120	0.4750	2506	12.5	25	2476	25.0	50	2500	25.5	51	101
TAZ5z114f	151.50	65.40	77.10	0.425	2.80E+05	6.40E+05	0.1600	0.0069	10.150	0.540	0.4697	0.0110	0.4221	2460	13.0	26	2448	24.5	49	2482	23.0	46	101
Discordant data																							
TAZ5z4	578.00	27.70	22.60	0.040	4.20E+06	4.40E+06	0.1111	0.0049	3.770	0.220	0.2405	0.0064	0.8363	1813	40.0	80	1583	13.0	48	1389	16.5	33	88
TAZ5z5	880.00	700.00	140.30	0.810	1.26E+06	3.70E+05	0.0812	0.0039	0.743	0.044	0.0654	0.0018	0.5730	1216	46.5	93	563	24.0	26	408	5.5	11	72
TAZ5z18	157.00	107.50	82.90	0.668	6.00E+05	5.30E+05	0.1095	0.0051	3.681	0.210	0.2417	0.0057	0.3205	1790	41.5	83	1565	22.5	45	1395	15.0	30	89
TAZ5z19f	532.00	189.10	172.00	0.354	1.60E+06	1.70E+06	0.1103	0.0059	4.230	0.290	0.2758	0.0057	0.8888	1805	29.5	59	1673	26.5	52	1570	17.0	34	94
TAZ5z31	48.00	55.90	15.95	1.125	-1.00E+05	1.10E+05	0.0709	0.0077	0.980	0.110	0.0987	0.0034	-0.0320	1010	115.0	230	701	29.0	58	607	10.0	20	87
TAZ5z38	861.00	969.00	209.00	1.100	6.20E+05	5.30E+05	0.0719	0.0032	0.761	0.042	0.0781	0.0020	0.4095	984	47.5	95	574	12.0	24	485	6.0	12	84
TAZ5z51	888.00	134.40	109.00	0.142	3.80E+06	2.30E+06	0.1206	0.0051	3.990	0.230	0.2411	0.0065	0.8948	1962	38.0	76	1630	22.5	45	1392	17.0	34	85
TAZ5z52f	5.50	0.92	0.28	0.169	-1.10E+04	1.10E+04	0.0890	0.0420	1.440	0.600	0.1158	0.0033	0.0540	520	480.0	960	1010	90.0	180	704	27.0	54	70
TAZ5z59c	531.00	655.00	135.30	1.242	4.00E+05	4.50E+05	0.0661	0.0033	0.693	0.043	0.0785	0.0029	0.5717	804	55.0	110	534	13.0	26	475	8.5	17	89
TAZ5z72	39.20	21.65	15.30	0.564	1.07E+05	8.20E+04	0.1040	0.0100	0.230	0.230	0.1474	0.0048	0.3723	1630	100.0	200	1120	38.0	76	886	13.5	27	79
TAZ5z90	2360.00	562.00	93.20	0.243	1.42E+06	6.20E+05	0.0796	0.0034	0.799	0.045	0.0745	0.0020	0.7383	1194	44.5	89	596	12.5	25	463	6.0	12	78
TAZ5z96f	255.00	339.00	1260.00	1.087	2.16E+04	4.50E+03	0.6230	0.0610	42.800	8.900	0.4460	0.0740	0.9925	4510	85.0	170	3450	160.0	320	2270	165.0	330	66
TAZ5z97c	469.00	145.00	106.60	0.305	1.00E+05	6.40E+05	0.1105	0.0049	3.427	0.200	0.2299	0.0058	0.6413	1802	41.5	83	1508	22.5	45	1334	15.0	30	88
TAZ5z100	544.00	622.00	244.00	1.164	1.52E+05	5.00E+04	0.1540	0.0120	2.130	0.200	0.1013	0.0024	0.7178	2390	65.0	130	1159	31.5	63	622	7.0	14	54

Footnotes: Analysis references: TAZ5z is zircon from sample TAZ5 (mount CT17-10), followed by grain number "c" or "f", meaning core or rim, respectively.

ANALYSIS	U (ppm)	Th (ppm)	Pb (ppm)	Th/U	Ratios				Error correction				Ages (Ma)				Concordance (%)						
					$^{206}\text{Pb}/^{208}\text{Pb}$	$^{207}\text{Pb}/^{208}\text{Pb}$	$^{207}\text{Pb}/^{235}\text{U}$	$^{206}\text{Pb}/^{238}\text{U}$	$^{206}\text{Pb}/^{208}\text{Pb}$	$^{207}\text{Pb}/^{208}\text{Pb}$	$^{207}\text{Pb}/^{235}\text{U}$	$^{206}\text{Pb}/^{238}\text{U}$	σ	2σ	σ	2σ		σ	2σ				
TAZ6z49r	460.00	63.70	100.00	0.132	3.80E+05	3.80E+05	0.1438	0.0069	7.550	0.530	0.3714	0.0110	0.8401	2264	21.5	43	2169	30.5	61	2034	26.5	53	94
TAZ6z50	257.40	130.30	134.00	0.495	2.90E+05	2.50E+05	0.1357	0.0066	6.490	0.400	0.3445	0.0086	0.4999	2162	23.0	46	2040	28.5	53	1911	20.0	40	94
TAZ6z53c	190.00	95.60	113.00	0.500	5.60E+04	2.30E+04	0.2260	0.0440	3.660	0.950	0.1146	0.0095	0.9820	2540	180.0	360	1440	110.0	220	697	27.0	54	48
TAZ6z53r	796.00	185.00	137.00	0.215	1.24E+05	1.70E+04	0.1077	0.0068	1.434	0.100	0.0945	0.0022	-0.1228	1742	55.0	110	899	20.5	41	582	6.5	13	65
TAZ6z56c	147.00	119.30	8200.00	0.803	8.31E+03	2.00E+02	0.7930	0.0350	318.000	59.000	2.7200	0.4800	0.9938	4944	17.5	35	5590	115.0	230	7890	445.0	890	141
TAZ6z61	620.00	400.00	155.00	0.418	1.90E+05	1.20E+05	0.0922	0.0074	1.404	0.120	0.1094	0.0033	0.0782	1400	75.0	150	882	24.5	49	669	9.5	19	76
TAZ6z65	483.00	189.00	125.50	0.375	5.50E+05	1.20E+05	0.1188	0.0052	4.100	0.280	0.2460	0.0130	0.9396	1934	39.0	78	1651	28.0	56	1414	33.5	67	86
TAZ6z64r	99.70	55.10	53.00	0.524	2.20E+05	2.90E+05	0.1739	0.0079	9.490	0.720	0.3940	0.0200	0.9195	2594	17.0	34	2370	36.0	72	2147	45.5	91	91
TAZ6z74c	431.00	647.00	250.40	1.307	6.70E+05	3.40E+05	0.1253	0.0055	4.590	0.380	0.2600	0.0170	0.9569	2034	38.0	76	1729	35.0	70	1485	43.0	86	86
TAZ6z74r	363.00	243.00	325.00	0.676	4.30E+05	2.20E+05	0.1535	0.0110	7.300	0.510	0.3428	0.0095	-0.2047	2342	48.5	97	2144	31.0	62	1899	23.0	46	89
TAZ6z76c	1150.00	1230.00	332.00	1.066	6.40E+04	7.80E+03	0.1479	0.0100	1.370	0.120	0.0643	0.0024	0.8293	2286	60.0	120	862	27.5	55	402	7.5	15	47
TAZ6z76r	987.00	414.00	298.20	0.425	4.42E+04	4.50E+03	0.2010	0.0110	2.091	0.130	0.0742	0.0017	-0.4988	2818	46.0	92	1143	21.5	43	461	5.0	10	40
TAZ6z78c	30.90	17.46	4.97	0.570	-2.00E+04	1.80E+04	0.0692	0.0091	1.050	0.130	0.1034	0.0042	0.0474	860	130.0	260	726	32.5	65	634	12.0	24	87
TAZ6z79c	81.20	313.00	371.90	3.747	1.08E+04	6.40E+02	0.5950	0.0280	23.500	1.600	0.2849	0.0110	0.8750	4486	16.5	33	3251	34.5	69	1614	26.5	53	50
TAZ6z80c	40.00	33.30	21.15	0.812	2.30E+04	5.80E+04	0.0964	0.0067	3.090	0.260	0.2236	0.0094	0.5715	1540	70.0	140	1431	33.5	67	1299	24.5	49	91
TAZ6z81	646.00	490.00	430.00	0.734	4.13E+04	6.10E+03	0.2090	0.0250	3.710	0.610	0.1221	0.0056	0.9613	2910	100.0	200	1520	60.0	120	742	16.0	32	49
TAZ6z92	817.00	494.00	652.00	0.600	1.28E+05	6.80E+03	0.1627	0.0068	7.260	0.390	0.3119	0.0075	0.7133	2476	9.0	18	2143	23.5	47	1750	18.5	37	82
TAZ6z94	314.00	716.00	214.50	2.259	-5.00E+05	1.10E+05	0.0797	0.0087	1.190	0.140	0.1017	0.0026	-0.3111	1150	105.0	210	787	30.5	61	625	7.5	15	79
TAZ6z100r	50.60	26.70	7.32	0.517	-3.00E+04	4.90E+04	0.0692	0.0058	0.970	0.088	0.0987	0.0030	0.0498	880	90.0	180	687	23.5	47	607	8.5	17	88
TAZ6z102	360.00	196.80	133.00	0.536	3.20E+04	8.60E+04	0.1380	0.0230	2.320	0.450	0.1119	0.0040	0.9409	1890	155.0	310	1130	70.0	140	683	11.5	23	60
TAZ6z103	159.00	66.30	54.40	0.415	1.90E+05	1.40E+05	0.1234	0.0078	5.450	0.700	0.3030	0.0280	0.9742	1964	49.0	98	1830	70.0	140	1710	70.0	140	93
TAZ6z106	81.00	93.00	29.50	1.174	5.00E+04	3.70E+04	0.0779	0.0066	1.154	0.110	0.1050	0.0028	0.2649	1080	85.0	170	776	24.0	48	644	8.5	17	83
TAZ6z112r	97.90	38.00	49.80	0.382	2.20E+05	1.20E+05	0.1557	0.0095	5.190	0.380	0.2360	0.0180	0.7072	2410	50.0	100	1846	31.0	62	1359	45.5	91	74
TAZ6z116	198.30	194.00	133.80	0.966	-1.10E+05	2.50E+05	0.1053	0.0048	3.717	0.210	0.2457	0.0062	0.6167	1720	43.0	86	1573	22.5	45	1416	16.0	32	90
TAZ6z121	380.00	301.00	116.20	0.791	1.35E+05	9.80E+04	0.0920	0.0120	1.360	0.230	0.0986	0.0032	0.9110	1370	115.0	230	831	43.0	86	606	9.5	19	73

Footnotes:
. Analysis references: TAZ6z is zircon from sample TAZ6 (mount CT17-10), followed by grain number "c" or "r", meaning core or rim, respectively.

ANALYSIS	U (ppm)			Th (ppm)			Pb (ppm)			Th/U			206Pb/208Pb			207Pb/208Pb			Ratios			Error correction			Ages (Ma)			Concordance (%)									
	U	Th	Pb	Th	Pb	Th/U	206Pb/208Pb	σ	207Pb/208Pb	σ	206Pb/238U	σ	207Pb/235U	σ	206Pb/238U	σ	207Pb/235U	σ	206Pb/238U	σ	207Pb/235U	σ	206Pb/238U	σ	207Pb/235U	σ	206Pb/238U	σ	207Pb/235U	σ							
AZR22122	45.40	43.30	13.02	0.963	-8.00E+05	1.10E+05	0.0566	0.0089	0.790	0.120	0.1007	0.0047	-0.0072	460	160.0	320	596	33.5	67	618	13.5	27	104														
AZR22123	187.20	77.20	46.90	0.415	4.90E+06	3.70E+06	0.0826	0.0053	2.435	0.140	0.2146	0.0061	0.1465	1243	65.0	130	1250	20.5	41	1253	16.0	32	100														
AZR22124	360.00	410.00	124.80	1.140	-1.90E+06	1.20E+06	0.0605	0.0040	0.893	0.055	0.1050	0.0031	0.2476	645	75.0	150	646	14.5	29	644	9.0	18	100														
AZR22125	153.60	99.00	31.94	0.644	2.80E+05	4.30E+05	0.0667	0.0055	1.101	0.084	0.1190	0.0038	0.0340	830	85.0	170	755	19.5	39	725	11.0	22	96														
AZR226	750.00	461.00	470.00	0.603	-1.80E+06	7.10E+06	0.1804	0.0100	10.430	0.530	0.4261	0.0130	0.8523	2657	111.5	23	2475	24.5	49	2288	29.5	59	92														
AZR227c	50.80	82.90	21.00	1.618	1.90E+04	5.20E+04	0.0648	0.0076	0.778	0.090	0.0857	0.0037	0.1544	780	125.0	250	601	26.0	52	530	11.0	22	88														
AZR2210	618.00	631.00	158.60	0.989	-8.20E+05	2.20E+05	0.0697	0.0045	0.808	0.046	0.0830	0.0034	0.2086	915	70.0	140	600	13.0	26	514	10.5	21	86														
AZR2240	407.00	430.00	185.80	1.073	-1.60E+06	6.80E+05	0.1355	0.0060	3.430	0.220	0.1831	0.0066	0.7662	2164	50.0	100	1504	25.0	50	1083	18.0	36	72														
AZR2244r	9.80	1.39	0.58	0.144	-4.00E+04	3.50E+04	0.0970	0.0220	1.690	0.370	0.1202	0.0084	0.0753	1370	220.0	440	990	65.0	130	738	25.5	51	75														
AZR2246	191.10	125.60	100.30	0.670	-1.70E+05	3.60E+05	0.1174	0.0071	3.880	0.240	0.2410	0.0095	0.7635	1907	55.0	110	1610	24.0	48	1391	24.5	49	86														
AZR2252	146.50	177.90	154.50	1.252	2.40E+05	8.10E+05	0.1321	0.0080	5.250	0.330	0.2874	0.0120	0.8136	2121	24.5	49	1860	27.0	54	1627	30.5	61	87														
AZR2262r	525.50	32.30	19.16	0.061	-8.00E+06	1.60E+06	0.0696	0.0046	0.781	0.045	0.0820	0.0027	-0.0989	912	70.0	140	585	12.5	25	508	8.0	16	87														
AZR2278	637.00	68.00	71.60	1.088	7.00E+07	1.30E+07	0.1818	0.0100	10.090	0.480	0.3995	0.0110	0.0559	2674	13.0	26	2443	22.0	44	2166	26.0	52	89														
AZR2287t	58.70	99.30	86.30	1.686	-2.60E+05	4.50E+05	0.1228	0.0082	4.820	0.300	0.2812	0.0093	0.3620	2012	35.5	71	1789	25.5	51	1597	23.5	47	89														
AZR2288c	92.20	52.20	68.50	0.577	-1.46E+06	9.00E+05	0.2418	0.0140	16.550	0.880	0.4898	0.0160	0.7032	3131	16.5	33	2912	24.0	48	2569	34.5	69	88														
AZR2288r	22.16	12.80	16.70	0.584	2.30E+05	3.40E+05	0.2187	0.0150	14.800	1.300	0.4880	0.0220	0.8069	2985	35.5	71	2801	41.0	82	2557	48.0	96	91														
AZR2289	710.00	149.70	150.50	0.219	-5.90E+06	6.10E+06	0.1413	0.0079	7.010	0.360	0.3608	0.0100	0.5346	2244	13.0	26	2114	23.0	44	1986	24.5	49	94														
AZR22106	1097.00	234.00	116.80	0.208	-6.40E+05	7.20E+05	0.0922	0.0054	1.387	0.074	0.1085	0.0032	0.4600	1473	55.0	110	866	16.5	33	670	9.0	18	76														
AZR22112r	1303.00	201.00	57.30	0.157	-3.10E+06	2.60E+06	0.1030	0.0058	1.762	0.093	0.1289	0.0045	0.7659	1677	50.0	100	1033	17.5	35	753	13.0	26	73														
AZR22115	816.00	154.70	29.80	0.191	-1.05E+06	8.10E+05	0.1034	0.0061	1.080	0.160	0.0770	0.0110	0.9890	1689	50.0	100	733	39.0	78	477	32.5	65	65														
AZR22120r	177.00	175.00	140.30	0.994	-3.40E+06	2.60E+06	0.1158	0.0069	3.770	0.410	0.2390	0.0260	0.9634	1885	55.0	110	1557	42.0	84	1370	65.0	130	88														

Footnotes:

. Analysis references: AZR22 is zircon from sample AZR2 (mount CT17-8), followed by grain number "c" or "r", meaning core or rim, respectively.

ANALYSIS	U (ppm)	Th (ppm)	Pb (ppm)	Th/U	Ratios			Ages (Ma)			Concordance (%)										
					$^{207}\text{Pb}/^{206}\text{Pb}$	$^{207}\text{Pb}/^{235}\text{U}$	$^{206}\text{Pb}/^{238}\text{U}$	$^{207}\text{Pb}/^{206}\text{Pb}$	$^{207}\text{Pb}/^{235}\text{U}$	$^{206}\text{Pb}/^{238}\text{U}$	σ	2σ	σ	2σ							
AZR4z111	95.40	118.80	29.00	1.248	1.50E+06	0.0060	0.686	0.074	0.0887	0.0033	0.3709	410	120.0	240	530	23.0	46	548	10.0	20	103
AZR4z112	105.50	75.60	19.90	0.678	-2.50E+05	0.0604	0.0057	0.775	0.0939	0.0031	0.1897	570	105.0	210	588	21.5	43	579	9.0	18	98
AZR4z114c	183.00	115.10	35.50	0.619	3.00E+06	0.0047	0.829	0.063	0.1027	0.0033	0.0551	550	90.0	180	620	18.0	36	630	10.0	20	102
AZR4z115	762.00	68.90	19.38	0.339	1.10E+06	0.0582	0.0064	0.860	0.1056	0.0040	-0.1472	560	120.0	240	636	23.5	47	647	11.5	23	102
AZR4z116	497.00	168.00	180.00	0.204	-1.40E+07	0.0037	0.807	0.044	0.0998	0.0029	-0.3777	542	70.0	140	600	12.5	25	613	8.5	17	102
AZR4z117	71.59	91.00	89.90	1.250	1.70E+06	0.0075	7.700	0.380	0.4150	0.0120	0.6351	2157	13.5	27	2195	22.5	45	2237	28.5	57	102
AZR4z118c	283.00	49.90	45.50	0.173	-2.60E+06	0.0075	6.510	0.360	0.3706	0.0110	0.2820	2053	23.0	46	2044	24.0	49	2032	25.5	51	99
AZR4z118r	326.00	17.07	5.24	0.051	9.00E+07	0.0072	6.020	0.300	0.3447	0.0099	0.2183	2043	18.0	36	1980	22.5	44	1909	24.0	48	96
AZR4z119	135.30	113.40	33.10	0.811	-8.00E+05	0.0047	0.793	0.054	0.1008	0.0031	0.0158	470	85.0	170	595	14.5	29	619	9.0	18	104
AZR4z120c	375.00	275.00	269.00	0.722	1.50E+07	0.0556	0.0070	0.320	0.3696	0.0110	0.5692	410	90.0	180	582	19.0	38	617	9.0	18	106
AZR4z120r	390.00	3.17	3.00	0.008	9.30E+06	0.1125	5.240	0.250	0.3358	0.0096	0.2353	2009	17.0	34	2007	21.0	42	2027	25.5	51	101
AZR4z121	237.00	211.00	222.30	0.881	-9.90E+06	0.0083	8.170	0.430	0.4109	0.0120	0.7963	1843	17.0	34	1859	20.5	41	1866	23.0	46	100
AZR4z122	45.50	56.60	64.20	1.232	-2.30E+05	0.1183	6.470	0.410	0.3952	0.0140	-0.1059	1919	48.0	96	2048	27.5	55	2146	31.5	63	105
AZR4z19	114.30	228.00	61.20	1.908	-4.80E+05	0.0530	0.655	0.057	0.0915	0.0032	0.1498	270	100.0	200	507	17.5	35	565	9.5	19	111
AZR4z21	323.00	326.00	158.00	0.977	1.50E+06	0.0072	2.830	0.170	0.1774	0.0068	0.6752	1962	50.0	100	1391	21.5	43	1052	18.5	37	76
AZR4z50	601.00	637.00	148.70	1.062	9.00E+06	0.0046	0.824	0.048	0.0825	0.0030	0.2961	962	70.0	140	609	13.5	27	511	9.0	18	84
AZR4z64c	530.00	282.00	271.00	0.513	-5.90E+06	0.1488	0.0982	0.380	0.3755	0.0100	0.5252	2340	12.0	24	2198	21.5	43	2055	24.5	49	93
AZR4z73c	35.50	63.10	17.98	1.764	1.30E+06	0.0800	1.160	0.140	0.1057	0.0042	0.0113	1110	145.0	290	774	34.0	68	647	12.5	25	94
AZR4z97c	118.40	126.70	42.30	1.060	1.70E+05	0.0795	1.140	0.150	0.1022	0.0038	0.6030	1080	125.0	250	753	34.0	68	627	11.0	22	83
AZR4z98c	195.00	87.00	91.00	0.410	7.00E+06	0.0100	8.910	0.550	0.3930	0.0140	0.7816	2503	24.5	49	2329	27.0	54	2133	33.5	67	92
AZR4z98r	189.00	106.70	108.00	0.548	1.40E+06	0.1780	10.190	0.600	0.4140	0.0170	0.8381	2640	20.0	40	2447	27.0	54	2232	38.0	76	91
AZR4z113	213.00	177.00	140.90	0.793	2.20E+06	0.1324	5.510	0.300	0.2996	0.0092	0.6909	2137	18.5	37	1899	23.0	46	1694	24.0	48	89

Footnotes:

. Analysis references: AZR4z is zircon from sample AZR4 (mount CT17-8), followed by grain number "c" or "r", meaning core or rim, respectively.

ANALYSIS	U (ppm)	Th (ppm)	Pb (ppm)	Th/U	Ratios			Error correction			Ages (Ma)			Concordance (%)								
					$^{207}\text{Pb}/^{206}\text{Pb}$	$^{207}\text{Pb}/^{235}\text{U}$	$^{206}\text{Pb}/^{238}\text{U}$	$^{207}\text{Pb}/^{206}\text{Pb}$	$^{207}\text{Pb}/^{235}\text{U}$	$^{206}\text{Pb}/^{238}\text{U}$	σ	2σ	σ		2σ	σ	2σ					
AZRSz117c	273.00	178.50	58.00	0.644	3.40E+06	0.0633	0.0042	0.940	0.059	0.1065	0.0034	0.6661	710	75.0	150	671	15.5	31	652	10.0	20	97
AZRSz117f	176.00	37.70	12.00	0.212	-8.30E+06	0.0586	0.0047	0.823	0.064	0.0999	0.0032	0.2684	580	90.0	180	606	18.0	36	613	9.5	19	101
AZRSz118	115.60	119.20	115.20	1.035	1.60E+06	0.1293	0.0079	6.520	0.360	0.3580	0.0110	0.2118	2098	26.5	53	2051	25.0	50	1977	26.5	53	96
AZRSz119c	79.00	58.00	18.45	0.725	3.20E+06	0.0643	0.0066	0.869	0.082	0.0994	0.0034	0.0171	720	110.0	220	642	22.0	44	610	10.0	20	95
AZRSz119f	488.00	40.10	16.20	0.082	-4.20E+06	0.0606	0.0039	0.847	0.048	0.1002	0.0030	0.1640	624	65.0	130	625	14.0	28	616	9.0	18	98
AZRSz120	86.00	52.20	14.94	0.609	7.00E+06	0.0656	0.0071	0.891	0.087	0.0986	0.0036	-0.1630	680	120.0	240	645	24.0	48	612	10.5	21	95
AZRSz121c	95.80	53.90	50.30	0.553	1.40E+06	0.1129	0.0071	5.430	0.320	0.3387	0.0100	0.3800	1855	32.0	64	1885	25.5	51	1885	25.0	50	100
AZRSz121f	135.90	84.50	78.60	0.612	-4.30E+06	0.1094	0.0069	5.120	0.280	0.3347	0.0097	0.0646	1808	30.0	60	1841	22.5	45	1861	23.5	47	101
AZRSz122	254.50	44.20	17.71	0.173	-5.00E+06	0.0655	0.0041	1.225	0.071	0.1347	0.0039	0.3105	788	70.0	140	810	16.0	32	815	11.0	22	101
AZRSz123	53.90	40.10	12.58	0.732	7.00E+06	0.0648	0.0078	0.910	0.110	0.0994	0.0037	0.1933	720	125.0	250	644	30.0	60	611	11.0	22	95
AZRSz124c	276.20	196.00	99.00	0.602	-2.00E+06	0.0752	0.0052	1.407	0.094	0.1361	0.0041	0.5720	1048	70.0	140	888	20.0	40	823	11.5	23	93
AZRSz125	247.00	61.10	16.80	0.242	-3.30E+06	0.0573	0.0041	0.773	0.051	0.0979	0.0030	0.0873	495	75.0	150	583	14.0	28	602	9.0	18	103
AZRSz126	36.50	29.00	29.10	0.773	1.40E+06	0.1336	0.0091	6.780	0.470	0.3706	0.0130	0.3508	2175	30.5	61	2082	30.0	60	2031	31.5	63	98
AZRSz127	106.10	270.10	110.90	2.511	1.11E+06	0.0644	0.0050	1.282	0.097	0.1429	0.0047	0.2541	760	80.0	160	832	21.5	43	861	13.0	26	103
AZRSz128	174.00	105.10	94.00	0.607	2.40E+06	0.1416	0.0087	6.740	0.360	0.3387	0.0110	-0.0737	2247	26.5	53	2076	23.5	47	1880	26.0	52	91
AZRSz129	327.00	55.90	21.11	0.169	3.60E+06	0.0644	0.0042	1.141	0.067	0.1297	0.0039	0.1802	737	70.0	140	771	16.0	32	786	11.0	22	102
Pb loss and discordant data																						
AZRSz29	21.12	0.82	0.23	0.031	4.90E+05	0.0730	0.0160	0.960	0.210	0.0952	0.0043	-0.0437	750	200.0	400	670	49.0	98	586	12.5	25	87
AZRSz42b	125.30	83.70	67.50	0.678	-1.90E+06	0.1122	0.0072	4.590	0.370	0.2980	0.0150	0.8721	1843	33.0	66	1756	33.5	67	1685	37.5	75	96
AZRSz97c	729.00	18.20	81.00	0.022	1.62E+07	0.1285	0.0075	4.870	0.310	0.2691	0.0097	0.9059	2088	18.5	37	1797	26.5	53	1535	24.5	49	85
AZRSz103c	434.30	422.10	493.00	0.963	-1.00E+05	0.1698	0.0095	9.320	0.510	0.3945	0.0130	0.8463	2561	14.0	28	2372	24.5	49	2148	30.0	60	91
AZRSz103f	334.00	62.40	77.00	0.139	6.60E+07	0.1310	0.0120	4.390	0.820	0.2220	0.0300	0.9880	2100	90.0	180	1570	90.0	180	1270	80.0	160	81
AZRSz105	40.20	139.80	12.80	3.597	5.90E+05	0.0630	0.0170	0.450	0.120	0.0479	0.0033	-0.1064	590	270.0	540	380	42.0	84	302	10.0	20	79
AZRSz124f	167.60	111.70	42.80	0.617	6.00E+06	0.0772	0.0073	1.211	0.110	0.1140	0.0036	-0.1319	1130	95.0	190	797	24.0	48	696	10.5	21	87

Footnotes:

. Analysis references: AZRSz is zircon from sample AZRS (mount CT17-8), followed by grain number "c" or "f", meaning core or rim, respectively.

ANALYSIS	U (ppm)	Th (ppm)	Pb (ppm)	Th/U	Ratios				Error correction	Ages (Ma)				Concordance (%)									
					$^{206}\text{Pb}/^{208}\text{Pb}$	$^{207}\text{Pb}/^{208}\text{Pb}$	$^{207}\text{Pb}/^{235}\text{U}$	$^{206}\text{Pb}/^{238}\text{U}$		$^{207}\text{Pb}/^{235}\text{U}$	σ	2σ	$^{206}\text{Pb}/^{238}\text{U}$		σ	2σ							
AZR6z121	64.00	29.20	8.45	0.442	2.10E+05	2.00E+05	0.0579	0.0068	0.827	0.088	0.1004	0.0042	-0.1156	570	125.0	250	611	24.0	48	616	12.0	24	101
AZR6z122	415.00	340.00	98.10	0.812	-4.00E+06	1.00E+06	0.0608	0.0039	0.880	0.050	0.1023	0.0030	0.1926	658	75.0	150	640	13.5	27	628	8.5	17	98
AZR6z123	89.00	67.80	60.20	0.758	2.00E+06	1.40E+06	0.1231	0.0076	6.220	0.340	0.3567	0.0110	0.1203	2022	27.5	55	2008	25.0	50	1971	26.5	53	98
AZR6z125	141.70	137.60	38.20	0.958	3.30E+05	6.50E+05	0.0600	0.0045	0.842	0.062	0.0987	0.0032	0.2800	580	80.0	160	622	17.5	35	612	9.5	19	98
AZR6z126	634.00	292.00	272.40	0.455	1.15E+07	7.90E+06	0.1235	0.0069	6.010	0.300	0.3530	0.0100	0.6984	2016	14.0	28	1979	22.5	45	1948	24.5	49	98
AZR6z127	62.10	57.40	17.23	0.920	-2.00E+06	1.00E+06	0.0623	0.0064	0.912	0.099	0.1056	0.0041	0.1955	630	115.0	230	665	26.0	52	647	12.0	24	97
AZR6z128	755.00	414.90	315.60	0.546	1.21E+07	5.10E+06	0.1069	0.0060	4.217	0.210	0.2886	0.0062	0.7311	1760	13.5	27	1679	20.0	40	1609	20.5	41	96
AZR6z129	270.10	273.90	81.10	1.004	9.00E+06	1.80E+06	0.0626	0.0045	0.918	0.060	0.1046	0.0032	0.1409	679	75.0	150	659	15.5	31	641	9.5	19	97
AZR6z130	198.80	141.70	117.00	0.707	1.80E+06	1.90E+06	0.1056	0.0062	4.648	0.230	0.3156	0.0091	-0.0088	1731	22.0	44	1757	21.0	42	1768	22.0	44	101
AZR6z131	112.60	96.20	94.90	0.839	7.00E+06	1.30E+06	0.1353	0.0079	7.920	0.440	0.4212	0.0140	0.8127	2174	19.5	39	2224	26.0	52	2265	32.5	65	102
Discordant data																							
AZR6z12c	687.00	522.00	304.00	0.755	8.80E+06	8.70E+06	0.1141	0.0065	3.053	0.150	0.1933	0.0058	0.4488	1862	50.0	100	1420	19.0	38	1139	15.5	31	80
AZR6z34	558.00	74.90	22.51	1.319	4.80E+05	3.80E+05	0.0670	0.0081	0.900	0.100	0.0957	0.0031	-0.0191	820	130.0	260	659	27.5	55	589	9.5	19	89
AZR6z50	1288.00	301.00	248.50	0.235	5.59E+05	4.50E+04	0.1692	0.0098	1.424	0.097	0.0606	0.0025	0.8944	2952	46.0	92	901	21.5	43	379	7.5	15	42
AZR6z51c	311.00	451.00	134.60	1.441	6.00E+04	1.40E+06	0.0708	0.0053	1.032	0.078	0.1038	0.0031	0.3798	974	70.0	140	715	19.5	39	637	9.0	18	89
AZR6z62	39.20	35.97	9.34	0.917	1.20E+05	1.80E+05	0.0529	0.0097	0.650	0.110	0.0897	0.0036	-0.2344	180	165.0	330	497	33.0	66	557	11.0	22	112
AZR6z65	1387.00	191.20	68.90	0.136	4.90E+06	1.20E+06	0.0708	0.0041	0.781	0.041	0.0783	0.0023	0.2414	952	60.0	120	588	11.0	22	486	7.0	14	83
AZR6z78	42.60	28.40	9.08	0.675	7.00E+05	1.20E+05	0.0980	0.0160	1.220	0.210	0.0893	0.0039	0.4176	1540	145.0	290	812	49.0	98	551	11.5	23	68
AZR6z100	215.00	106.90	170.00	0.495	1.13E+06	3.00E+05	0.1850	0.0170	8.470	1.000	0.3240	0.0170	0.7663	2670	55.0	110	2242	48.5	97	1803	40.5	81	80
AZR6z101f	105.90	63.60	23.80	0.581	-1.40E+05	2.40E+05	0.0920	0.0160	1.300	0.240	0.0999	0.0036	0.6489	1280	170.0	340	802	49.5	99	614	10.5	21	77
AZR6z112f	344.00	80.60	74.10	0.235	4.90E+06	4.00E+06	0.1117	0.0067	3.430	0.210	0.2202	0.0078	0.7847	1828	50.0	100	1512	25.0	50	1283	20.5	41	85
AZR6z114	21.39	31.40	8.80	1.412	8.00E+04	9.60E+04	0.0830	0.0160	1.220	0.230	0.1015	0.0055	-0.0980	1150	200.0	400	782	50.0	100	623	16.0	32	80
AZR6z124	42.80	25.80	11.40	0.610	-3.00E+05	1.80E+05	0.0920	0.0140	1.320	0.180	0.1072	0.0047	0.6333	1280	155.0	310	830	39.5	79	656	13.5	27	79

Footnotes:

. Analysis references: AZR6z is zircon from sample AZR6 (mount CT17-8), followed by grain number "c" or "f", meaning core or rim, respectively.

ANALYSIS	U (ppm)	Th (ppm)	Pb (ppm)	Th/U	²⁰⁶ Pb/ ²⁰⁸ Pb			Ratios			Ages (Ma)			Concordance (%)								
					2σ	²⁰⁷ Pb/ ²⁰⁸ Pb	²⁰⁷ Pb/ ²³⁵ U	2σ	²⁰⁶ Pb/ ²³⁸ U	Error correction	2σ	²⁰⁷ Pb/ ²⁰⁶ Pb	σ	2σ	²⁰⁶ Pb/ ²³⁸ U	σ	2σ					
SF1z134	151.10	126.90	380.00	0.856	2.30E+05	0.0625	0.0042	0.899	0.054	0.1045	0.0022	0.1790	691.3	71.7	143.3	651.2	14.4	28.8	640.7	6.4	12.8	98
SF1z135	147.90	200.30	540.00	1.366	-1.57E+06	0.0598	0.0038	0.791	0.046	0.0947	0.0019	0.0997	596.3	68.8	137.7	591.7	13.0	26.1	583.3	5.6	11.2	99
SF1z136	67.30	103.70	294.20	1.570	-1.70E+04	0.0606	0.0050	0.812	0.065	0.0971	0.0027	0.0928	625.1	88.9	177.9	603.6	18.2	36.4	597.4	7.9	15.9	99
SF1z137	112.90	123.50	1125.00	1.119	2.00E+05	0.1325	0.0025	6.560	0.290	0.3556	0.0062	0.3364	2131.4	16.5	33.0	2054.0	19.5	38.9	1961.3	14.7	29.5	95
SF1z138	60.60	60.10	179.20	0.988	-1.40E+05	0.0612	0.0042	0.890	0.060	0.1078	0.0026	0.2940	646.3	73.7	147.4	646.4	16.1	32.2	660.0	7.6	15.1	102
SF1z140	87.40	64.20	628.00	0.742	8.00E+05	0.1297	0.0029	6.990	0.320	0.3899	0.0076	0.2726	2093.9	19.6	39.3	2110.2	20.3	40.6	2122.4	17.6	35.2	101
SF1z141	55.84	120.90	322.00	2.211	8.00E+04	0.0584	0.0052	0.783	0.067	0.0963	0.0025	0.1551	544.8	97.3	194.6	587.2	19.1	38.1	592.7	7.4	14.7	101
SF1z142	57.70	67.70	195.00	1.153	8.90E+04	0.0643	0.0055	0.922	0.076	0.1040	0.0027	0.1772	751.5	90.3	160.6	663.4	20.1	40.1	637.8	7.9	15.8	96
SF1z143	299.50	117.00	1100.00	0.169	-1.40E+06	0.1253	0.0019	6.350	0.270	0.3648	0.0063	0.4132	2033.0	13.4	26.8	2025.4	18.6	37.3	2004.9	14.9	29.8	99
Discordant data																						
SF1z8	503.00	282.00	2280.00	0.528	1.60E+06	0.1362	0.0016	5.590	0.340	0.2960	0.0140	0.9721	2179	10.2	20.4	1915	26.2	52.3	1671	34.8	69.6	87
SF1z9	657.00	1002.00	6750.00	1.422	3.10E+06	0.1314	0.0064	4.700	0.270	0.2580	0.0110	0.9648	2117	42.7	85.4	1767	24.0	48.1	1480	28.2	56.4	84
SF1z11	816.00	45.80	316.10	0.052	-8.00E+07	0.1181	0.0057	4.161	0.170	0.2568	0.0045	0.6406	1928	43.2	86.5	1666	16.7	33.4	1473	11.5	23.1	88
SF1z13	67.50	71.80	244.00	0.985	2.10E+07	0.0768	0.0064	1.096	0.094	0.1033	0.0027	0.5499	1116	83.2	166.3	751	22.7	45.5	634	7.9	15.8	84
SF1z40	669.00	409.00	4210.00	0.558	4.00E+07	0.1370	0.0015	6.010	0.270	0.3148	0.0078	0.9129	2190	9.5	19.0	1977	19.5	39.1	1764	19.1	38.2	89
SF1z43	31.26	44.70	136.90	1.332	-6.00E+06	0.0518	0.0072	0.708	0.096	0.0986	0.0033	0.1286	277	159.2	318.3	544	28.5	57.0	606	9.7	19.4	112
SF1z56	278.10	84.00	334.00	0.272	2.20E+06	0.0913	0.0065	2.140	0.260	0.1640	0.0130	0.9686	1453	67.7	135.5	1162	42.0	84.0	979	36.0	72.0	84
SF1z86	735.00	586.00	2800.00	0.810	-2.62E+06	0.1053	0.0060	1.762	0.100	0.1198	0.0028	0.8442	1720	52.4	104.7	1032	18.4	36.7	1209	8.1	16.1	71
SF1z87	259.00	331.00	1228.00	1.211	-1.50E+06	0.1268	0.0064	3.640	0.220	0.2063	0.0094	0.9217	2054	44.6	89.1	1558	24.1	48.1	1209	25.1	50.2	78
SF1z127	461.00	349.20	2482.00	0.765	1.10E+06	0.1240	0.0016	4.746	0.200	0.2751	0.0047	0.4907	2015	11.4	22.9	1775	17.7	35.3	1567	11.9	23.8	88
SF1z139	2230.00	2050.00	2760.00	0.882	-3.52E+05	0.1287	0.0066	0.816	0.035	0.0470	0.0012	0.4887	2080	45.1	90.3	606	9.8	19.6	296	3.7	7.4	49

Footnotes:

. Analysis references: SF1z is zircon from sample SF1 (mount CT18-03), followed by grain number "c" or "r", meaning core or rim, respectively.

ANALYSIS	U (ppm)	Th (ppm)	Pb (ppm)	Th/U	Ratios					Ages (Ma)					Concordance (%)						
					$^{206}\text{Pb}/^{238}\text{U}$	2σ	$^{207}\text{Pb}/^{235}\text{U}$	2σ	$^{207}\text{Pb}/^{238}\text{U}$	2σ	$^{206}\text{Pb}/^{238}\text{U}$	2σ	$^{207}\text{Pb}/^{238}\text{U}$	σ		2σ					
					2σ	$^{207}\text{Pb}/^{206}\text{Pb}$	2σ	$^{207}\text{Pb}/^{206}\text{Pb}$	2σ	$^{206}\text{Pb}/^{238}\text{U}$	2σ	$^{207}\text{Pb}/^{238}\text{U}$	2σ	$^{206}\text{Pb}/^{238}\text{U}$		2σ					
SF2280	433.00	127.30	31.80	0.290	-2.40E+04	2.30E+04	0.0596	0.0022	0.787	0.025	0.0963	0.0009	0.0942	589	40.0	80.0	14.0	583	2.5	5.0	101
Discordant data																					
SF222	581.00	125.30	113.40	0.220	1.89E+06	8.30E+05	0.1454	0.0011	6.620	0.180	0.3301	0.0053	0.8658	2293	6.5	13.0	12.0	1839	13.0	13.0	89
SF225	687.20	481.00	244.80	0.700	1.86E+06	8.90E+05	0.1463	0.0048	4.091	0.130	0.2073	0.0039	0.6859	2303	28.0	56.0	13.0	1214	10.5	10.5	73
SF224	213.70	186.80	119.20	0.870	-4.80E+04	3.40E+04	0.1088	0.0035	3.382	0.090	0.2244	0.0021	0.2475	1779	29.5	59.0	10.5	1500	5.5	5.5	87
SF231	86.20	38.23	189.00	0.440	1.03E+04	5.50E+03	0.2870	0.0350	13.200	2.900	0.2730	0.0260	0.9970	3401	95.0	190.0	103.5	1556	66.0	66.0	58
SF237	315.90	1419.00	441.00	4.490	5.80E+04	1.40E+04	0.1189	0.0062	1.919	0.110	0.1155	0.0013	0.7305	1940	46.5	93.0	19.0	705	4.0	4.0	65
SF228	740.00	384.40	106.00	0.490	1.90E+04	9.30E+04	0.0615	0.0023	0.915	0.028	0.0992	0.0015	0.2980	657	40.0	80.0	8.0	610	4.5	4.5	101
SF245	1936.00	681.00	236.60	0.340	3.20E+05	1.10E+05	0.1312	0.0041	1.778	0.046	0.0897	0.0014	0.5589	2114	27.5	55.0	8.5	613	4.0	4.0	59
SF252	236.30	137.70	99.90	0.580	-9.60E+04	6.80E+04	0.1264	0.0014	4.918	0.120	0.2836	0.0030	0.6155	2048	10.0	20.0	10.5	1609	7.5	7.5	89
SF258	151.10	38.17	41.02	0.250	-2.90E+04	3.70E+04	0.1264	0.0018	4.618	0.120	0.2896	0.0026	0.2540	2048	12.5	25.0	11.0	1539	6.5	6.5	88
SF263	81.80	68.90	52.70	0.840	-1.90E+04	1.80E+04	0.1424	0.0025	5.383	0.150	0.2786	0.0034	0.2850	2257	15.0	30.0	12.0	1884	8.5	8.5	84
SF266	385.00	219.00	78.20	0.570	-1.50E+05	8.90E+04	0.1808	0.0016	7.470	0.350	0.3010	0.0120	0.9664	2660	7.5	15.0	21.0	1696	29.5	29.5	78
SF268	1405.00	527.00	152.00	0.380	9.00E+05	1.10E+05	0.0794	0.0028	0.822	0.026	0.0761	0.0017	0.4514	1182	35.0	70.0	7.0	473	5.0	5.0	78
SF270	949.00	1284.00	297.00	1.350	-9.96E+04	9.70E+04	0.0687	0.0026	0.751	0.025	0.0805	0.0016	0.4055	890	39.0	78.0	7.0	499	5.0	5.0	88
SF271	1765.00	812.00	158.40	0.460	-8.00E+05	1.40E+05	0.0684	0.0026	0.646	0.026	0.0702	0.0019	0.6542	881	39.5	79.0	8.0	437	5.5	5.5	86
SF273	1191.00	1427.00	898.00	1.200	2.40E+05	2.50E+05	0.1273	0.0013	4.970	0.170	0.2856	0.0076	0.8874	2061	9.0	18.0	14.5	1620	19.0	19.0	89
SF277	1310.00	465.50	229.90	0.380	1.38E+05	9.10E+04	0.0857	0.0028	2.007	0.062	0.1732	0.0025	0.5952	1331	31.5	63.0	10.5	1030	7.0	7.0	92

Footnotes:

. Analysis references: SF2z is zircon from sample SF2 (mounts CT18-11 and CT19-1), followed by grain number.

ANALYSIS	U (ppm)	Th (ppm)	Pb (ppm)	Th/U	Ratios				Ages (Ma)				Concordance (%)									
					$^{204}\text{Pb}/^{206}\text{Pb}$	$^{207}\text{Pb}/^{206}\text{Pb}$	$^{207}\text{Pb}/^{235}\text{U}$	$^{206}\text{Pb}/^{238}\text{U}$	2 σ	1 σ	2 σ	1 σ		$^{207}\text{Pb}/^{238}\text{U}$	$^{206}\text{Pb}/^{238}\text{U}$	2 σ	1 σ					
SF3z49	762.00	223.00	906.00	0.279	5.10E+05	0.0791	0.0016	1.192	0.026	0.1094	0.0016	0.4553	1174.6	20.0	40.0	796.9	6.0	12.0	669.3	4.6	9.3	84
SF3z54	502.00	627.00	2820.00	1.272	3.50E+05	0.1386	0.0028	2.697	0.062	0.1410	0.0017	0.5172	2209.8	17.5	35.1	1327.6	8.5	17.0	850.3	4.8	9.6	64
SF3z56	1217.00	110.80	783.00	0.089	4.78E+05	0.0914	0.0019	0.721	0.027	0.0573	0.0023	0.8367	1455.0	19.8	39.5	551.3	8.0	15.9	359.2	7.0	14.0	65
SF3z57	211.20	104.40	892.00	0.508	2.30E+05	0.1504	0.0023	6.980	0.160	0.3356	0.0063	0.7185	2350.5	13.1	26.1	2108.9	10.2	20.3	1865.5	15.2	30.4	88
SF3z58	504.00	251.00	769.00	0.510	7.50E+05	0.0745	0.0020	0.808	0.023	0.0783	0.0011	0.3172	1055.0	27.0	54.1	601.3	6.5	12.9	486.0	3.3	6.6	81

Footnotes:

. Analysis references: SF3z is zircon from sample SF3(mount CT18-03), followed by grain number "c" or "r", meaning core or rim, respectively.

ANALYSIS	U (ppm)	Th (ppm)	Th/U	% $^{206}\text{Pb}^c$	Ratios				Ages (Ma)				Discordance (%)								
					$^{206}\text{Pb}/^{208}\text{Pb}$	$\pm\%$	$^{207}\text{Pb}^*/^{208}\text{Pb}^*$	$\pm\%$	$^{207}\text{Pb}^*/^{235}\text{U}$	$\pm\%$	$^{206}\text{Pb}^*/^{238}\text{U}$	$\pm\%$		Error correction	$^{207}\text{Pb}/^{208}\text{Pb}$	σ	2σ	$^{206}\text{Pb}^*/^{238}\text{U}$	σ	2σ	
SF3z105	69.00	55.00	0.810	0.600	$3.50\text{E}-04$	$5.80\text{E}+01$	$\pm\%$	0.0590	10.1000	1.0600	13.7000	0.1300	9.3000	0.7000	567	220	440	789	69	138	-42
SF3z106	669.00	789.00	1.220	1.380	$7.60\text{E}-04$	$1.70\text{E}+01$	$\pm\%$	0.0640	3.2000	0.5100	3.4000	0.0570	1.1000	0.3000	798	67	134	388	4	8	54

Footnotes:

- . % $^{206}\text{Pb}^c$ is % of ^{206}Pb from common Pb
- . Errors are 1-sigma
- . Pb* indicates radiogenic Pb, corrected for common Pb
- . Analysis references: SF3z is zircon from sample SF3 (mount CT18-03), followed by grain number "c" or "r", meaning core or rim, respectively.
- . Error in standard calibration was 0.26% (not included in above errors but required when comparing data from different mounts).

ANALYSIS	U (ppm)	Th (ppm)	Pb (ppm)	Th/U	Ratios			Error correction	Ages (Ma)			Concordance (%)											
					$^{207}\text{Pb}/^{206}\text{Pb}$	$^{207}\text{Pb}/^{235}\text{U}$	$^{206}\text{Pb}/^{238}\text{U}$		$^{207}\text{Pb}/^{206}\text{Pb}$	$^{207}\text{Pb}/^{235}\text{U}$	$^{206}\text{Pb}/^{238}\text{U}$		σ	2σ	σ	2σ							
AKR1z17r	564.00	63.80	24.11	0.110	-1.00E+05	2.00E+05	0.0850	0.0019	1.319	0.1119	0.0024	0.8507	1316	21.5	43.0	18.0	854	9.0	18.0	684	7.0	14.0	80
AKR1z230	867.00	498.10	146.10	0.570	6.50E+05	4.10E+05	0.1500	0.0024	4.117	0.0043	0.0043	0.9008	2346	13.5	27.0	16.0	1658	8.0	16.0	1161	11.5	23.0	70
AKR1z31	410.00	573.00	112.00	1.400	1.35E+05	3.70E+04	0.1225	0.0051	1.108	0.026	0.0015	-0.3536	1993	37.0	74.0	13.0	757	6.5	13.0	410	4.5	9.0	54
AKR1z37	186.00	107.60	43.20	0.580	1.40E+04	5.70E+04	0.0816	0.0035	1.271	0.043	0.1114	-0.3483	1236	42.0	84.0	19.0	833	9.5	19.0	681	6.0	12.0	82
AKR1z41	715.00	163.80	71.80	0.230	3.40E+05	1.30E+05	0.0803	0.0015	1.013	0.016	0.0913	0.5020	1204	18.5	37.0	10.0	710	4.0	8.0	563	4.0	8.0	79
AKR1z43	275.70	272.00	202.20	0.990	3.40E+05	1.70E+05	0.1459	0.0023	6.706	0.100	0.3326	0.0065	2298	13.5	27.0	13.0	2073	6.5	13.0	1851	15.5	31.0	89
AKR1z48	735.00	446.70	323.00	0.610	1.15E+06	3.00E+05	0.1548	0.0021	6.320	0.077	0.2949	0.0045	2400	11.5	23.0	2021	5.5	11.0	1666	11.0	22.0	82	
AKR1z52	759.00	821.00	267.00	1.080	2.12E+05	5.20E+04	0.1321	0.0041	1.266	0.039	0.0716	0.0011	2126	27.0	54.0	831	8.5	17.0	446	3.5	7.0	54	
AKR1z60	284.60	641.00	192.30	2.250	-1.00E+04	4.50E+04	0.1321	0.0034	1.321	0.026	0.0728	-0.0548	2126	22.5	45.0	855	5.5	11.0	453	3.5	7.0	53	
AKR1z62	460.00	419.00	140.00	0.910	2.18E+05	6.40E+04	0.0942	0.0031	1.234	0.041	0.0946	0.0013	1512	31.0	62.0	816	9.5	19.0	582	4.0	8.0	71	
AKR1z64c	75.98	34.79	22.30	0.460	-1.10E+04	7.70E+04	0.1730	0.0042	8.830	0.300	0.3686	0.0076	2587	20.5	41.0	2321	15.5	31.0	2023	18.0	36.0	87	
AKR1z68	726.00	552.00	391.00	0.760	1.20E+05	7.10E+05	0.1432	0.0019	6.538	0.060	0.3292	0.0042	2266	11.5	23.0	2051	4.0	8.0	1835	10.0	20.0	89	
AKR1z80	586.00	794.00	237.30	1.350	1.30E+05	1.30E+05	0.0750	0.0016	1.086	0.019	0.1046	0.0016	1069	21.5	43.0	747	4.5	9.0	641	4.5	9.0	86	
AKR1z89	159.40	66.90	17.47	0.420	1.10E+04	2.30E+04	0.1084	0.0044	0.758	0.026	0.0547	0.0023	1773	37.0	74.0	573	7.5	15.0	343	7.0	14.0	60	
AKR1z95	1300.00	1570.00	2040.00	1.210	7.30E+04	2.10E+04	0.3860	0.0470	10.900	2.300	0.1170	0.0190	3855	92.0	184.0	2515	98.0	196.0	713	55.0	110.0	28	
AKR1z96	331.00	254.00	176.90	0.770	-3.20E+06	1.40E+06	0.1364	0.0020	5.402	0.066	0.2879	0.0042	2182	13.0	26.0	1885	5.0	10.0	1631	10.5	21.0	87	
AKR1z99	583.00	561.00	138.50	0.960	-3.80E+05	2.50E+05	0.0763	0.0017	0.899	0.017	0.0864	0.0017	1103	22.5	45.0	651	4.5	9.0	534	5.0	10.0	82	
AKR1z104	461.50	259.50	76.90	0.560	7.70E+04	9.50E+04	0.0710	0.0017	0.941	0.016	0.0977	0.0015	957	24.5	49.0	673	4.0	8.0	601	4.5	9.0	89	
AKR1z105	465.00	87.80	53.00	0.190	1.00E+06	1.10E+05	0.0833	0.0018	1.221	0.020	0.1063	0.0015	1276	21.0	42.0	810	4.5	9.0	651	4.5	9.0	80	
AKR1z116	650.00	580.00	168.30	0.890	2.78E+05	8.70E+04	0.0918	0.0021	1.152	0.019	0.0920	0.0013	1463	15.0	30.0	778	4.5	9.0	568	4.0	8.0	73	
AKR1z126	794.00	314.60	128.70	0.400	-3.00E+05	4.10E+05	0.1402	0.0024	3.179	0.048	0.1635	0.0026	2230	15.0	30.0	1452	6.0	12.0	976	7.0	14.0	67	
AKR1z136	285.50	83.80	97.70	0.290	-1.17E+06	5.80E+05	0.1968	0.0028	11.350	0.120	0.4176	0.0056	2800	11.5	23.0	2552	5.0	10.0	2250	12.5	25.0	88	
AKR1z137	587.70	76.24	39.60	0.130	-3.00E+05	1.30E+05	0.0890	0.0021	1.603	0.049	0.1299	0.0023	1404	22.5	45.0	971	9.5	19.0	787	6.5	13.0	81	
AKR1z138	166.80	226.20	111.80	1.360	3.60E+04	3.60E+04	0.1352	0.0055	2.209	0.090	0.1189	0.0018	2167	33.5	71.0	1184	14.0	28.0	724	5.0	10.0	61	

Footnotes:

. Analysis references: AKR1z is zircon from sample AKR1 (mount CT18-7), followed by grain number "c" or "r", meaning core or rim, respectively.

ANALYSIS	U (ppm)	Th (ppm)	Pb (ppm)	Th/U	Ratios				Error correction	Ages (Ma)				Concordance (%)								
					²⁰⁶ Pb/ ²⁰⁶ Pb	²⁰⁷ Pb/ ²⁰⁶ Pb	²⁰⁷ Pb/ ²³⁵ U	²⁰⁶ Pb/ ²³⁸ U		²⁰⁷ Pb/ ²⁰⁶ Pb	σ	²⁰⁷ Pb/ ²³⁵ U	σ		²⁰⁶ Pb/ ²³⁸ U	σ						
AKR22147	284.80	200.40	58.10	0.700	1.70E+05	1.00E+05	0.0601	0.0016	0.812	0.018	0.0980	0.0013	29.0	58.0	604	5.0	10.0	602	4.0	8.0	100	
AKR22148	106.90	128.40	37.05	1.200	5.40E+04	3.40E+04	0.0625	0.0021	0.853	0.028	0.0980	0.0015	36.0	72.0	626	7.5	15.0	603	4.5	9.0	96	
AKR22149	50.83	44.05	30.67	0.870	-1.60E+06	3.40E+06	0.1236	0.0030	5.780	0.120	0.3366	0.0049	21.5	43.0	1943	9.0	18.0	1870	12.0	24.0	96	
Discordant data																						
AKR226	566.70	157.10	160.90	0.280	-3.70E+05	6.80E+05	0.1768	0.0023	8.945	0.097	0.3674	0.0050	2623	11.0	2332	5.0	10.0	2017	12.0	24.0	86	
AKR2232	340.20	421.00	242.30	1.240	4.90E+05	3.20E+05	0.1495	0.0026	4.950	0.120	0.2407	0.0050	2340	15.0	30.0	1811	10.0	20.0	1380	13.0	26.0	77
AKR2237	920.30	1006.20	285.10	1.090	-1.61E+06	9.30E+05	0.0604	0.0011	0.806	0.011	0.0974	0.0013	619	19.5	39.0	600	3.0	6.0	599	4.0	8.0	100
AKR2238	417.00	59.40	20.50	1.130	-2.00E+05	1.00E+05	0.0686	0.0015	0.817	0.016	0.0665	0.0014	887	22.5	45.0	606	4.5	9.0	535	4.0	8.0	88
AKR2258	692.00	725.00	5800.00	1.050	6.90E+04	1.70E+04	0.4970	0.0340	49.200	8.100	0.5740	0.0730	4232	50.5	101.0	3976	82.0	164.0	2924	149.5	299.0	74
AKR2261	157.50	104.20	60.10	0.660	2.30E+04	5.80E+04	0.0868	0.0021	1.957	0.042	0.1636	0.0023	1356	23.5	47.0	1101	7.0	14.0	977	6.5	13.0	89
AKR2262	692.00	291.00	165.40	0.420	1.85E+05	6.60E+04	0.1050	0.0032	1.875	0.051	0.1299	0.0018	1714	28.0	56.0	1072	9.0	18.0	787	5.0	10.0	73
AKR2272	497.00	109.30	61.80	0.220	2.55E+05	9.80E+04	0.0963	0.0032	1.204	0.031	0.0911	0.0014	1554	31.0	62.0	802	7.0	14.0	562	4.0	8.0	70
AKR2277	606.00	113.80	62.20	0.190	7.90E+05	4.10E+05	0.0894	0.0022	1.386	0.038	0.1113	0.0018	1413	23.5	47.0	883	8.0	16.0	680	5.0	10.0	77
AKR2286	282.70	78.80	163.00	0.280	1.40E+05	1.10E+05	0.1972	0.0056	7.420	0.320	0.2669	0.0060	2803	23.0	46.0	2163	19.5	39.0	1525	15.5	31.0	70
AKR2295	425.40	391.70	275.60	0.920	3.90E+05	2.90E+05	0.1254	0.0022	4.450	0.110	0.2572	0.0052	2034	15.5	31.0	1722	10.0	20.0	1476	13.5	27.0	86
AKR2297	147.00	111.40	34.80	0.760	5.10E+04	3.20E+04	0.0734	0.0026	0.972	0.034	0.0960	0.0013	1025	36.0	72.0	689	8.5	17.0	591	4.0	8.0	86
AKR22115	432.00	522.00	172.60	1.210	1.51E+05	9.70E+04	0.0740	0.0018	1.123	0.026	0.1103	0.0016	1041	24.5	49.0	764	6.0	12.0	675	4.5	9.0	88
AKR22121	448.10	513.00	121.20	1.150	-6.40E+04	8.90E+04	0.0689	0.0015	0.840	0.015	0.0889	0.0012	896	22.5	45.0	619	4.0	8.0	549	3.5	7.0	89
AKR22124	938.00	450.00	550.00	0.480	6.90E+04	4.00E+03	0.2189	0.0061	3.391	0.081	0.1133	0.0015	2973	45.0	90.0	1502	9.5	19.0	692	4.5	9.0	46
AKR22133	0.00	0.00	67.43	#DIV/0!	no value	NAN	no value	NAN	no value	NAN	no value	NAN	#NUM!	#VALUE!	#VALUE!	#VALUE!	#VALUE!	#VALUE!	#VALUE!	#VALUE!	#VALUE!	#VALUE!
AKR22135	120.40	9.05	406.00	0.080	3.21E+04	5.50E+03	0.4390	0.0250	18.300	1.900	0.2680	0.0170	4048	42.5	85.0	3006	50.0	100.0	1531	43.0	86.0	51
AKR22139	520.00	196.10	195.60	0.380	1.85E+05	2.80E+04	0.1254	0.0028	2.418	0.037	0.1417	0.0020	2034	20.0	40.0	1248	5.5	11.0	854	5.5	11.0	68
AKR22140	567.70	508.10	162.20	0.900	-1.40E+06	2.10E+06	0.0724	0.0015	1.037	0.017	0.1036	0.0014	997	21.0	42.0	722	4.0	8.0	636	4.0	8.0	88
AKR22145	125.50	42.70	22.20	0.340	4.40E+04	2.80E+04	0.0809	0.0034	1.174	0.040	0.1035	0.0017	1219	41.5	83.0	789	9.5	19.0	635	5.0	10.0	81

Footnotes:

. Analysis references: AKR2z is zircon from sample AKR2 (mount CT18-7), followed by grain number "c" or "r", meaning core or rim, respectively.

ANALYSIS	U (ppm)	Th (ppm)	Pb (ppm)	Th/U	Ratios		Ratios		Ratios		Ages (Ma)		Ages (Ma)		Concordance (%)					
					$^{207}\text{Pb}/^{206}\text{Pb}$	$^{207}\text{Pb}/^{235}\text{U}$	$^{207}\text{Pb}/^{238}\text{U}$	$^{207}\text{Pb}/^{206}\text{Pb}$	$^{207}\text{Pb}/^{235}\text{U}$	$^{207}\text{Pb}/^{238}\text{U}$	σ	2σ	σ	2σ						
EZ2z64	336.50	75.70	106.80	0.230	-2.70E+06	2.60E+06	0.1896	0.0019	13.720	0.660	0.5166	0.0088	0.8976	2731	22.5	45.0	2685	18.5	37.0	98
EZ2z65	181.00	144.00	22.80	0.760	3.60E+05	2.70E+05	0.0622	0.0042	0.813	0.054	0.0933	0.0019	0.0900	604	15.0	30.0	575	5.5	11.0	95
EZ2z66	272.80	218.10	63.90	0.810	-7.40E+05	6.90E+05	0.0613	0.0039	0.854	0.049	0.1008	0.0019	-0.0339	627	13.5	27.0	619	5.5	11.0	99
EZ2z67	377.00	170.50	148.00	0.460	2.20E+06	2.50E+06	0.1131	0.0016	4.864	0.240	0.3084	0.0060	0.6638	1850	21.0	42.0	1733	15.0	30.0	96
EZ2z68	383.00	245.20	68.40	0.650	-1.19E+06	6.90E+05	0.0598	0.0038	0.790	0.047	0.0966	0.0018	0.0035	591	13.5	27.0	594	5.5	11.0	101
EZ2z69	108.40	68.00	21.80	0.630	9.00E+05	1.90E+05	0.0618	0.0048	0.877	0.061	0.1031	0.0024	-0.0441	667	83.0	166.0	633	7.0	14.0	99
EZ2z70	144.50	90.20	27.20	0.630	2.00E+05	1.30E+05	0.0585	0.0044	0.824	0.059	0.1015	0.0022	-0.0665	549	82.0	164.0	623	6.5	13.0	102
EZ2z71	51.30	35.30	15.22	0.670	-8.30E+04	7.60E+04	0.0688	0.0063	1.246	0.110	0.1314	0.0034	0.0479	893	94.5	189.0	796	9.5	19.0	97
Discordant data																				
EZ2z16	127.10	64.80	26.90	0.500	-3.00E+05	4.20E+05	0.0902	0.0110	1.250	0.160	0.1003	0.0022	0.5319	823	36.0	72.0	616	6.5	13.0	75
EZ2z26	187.60	99.60	42.50	0.530	-9.00E+06	2.00E+06	0.0779	0.0049	1.367	0.080	0.1276	0.0024	0.1249	875	17.0	34.0	774	7.0	14.0	88
EZ2z29	374.00	108.80	137.00	0.290	-4.20E+05	4.00E+05	0.1440	0.0190	2.590	0.400	0.1281	0.0037	0.9275	2276	113.5	227.0	1298	56.5	113.0	60
EZ2z38	61.66	64.40	51.20	1.050	2.10E+05	4.10E+05	0.1140	0.0087	3.600	0.250	0.2305	0.0058	0.1448	1864	69.0	138.0	1337	15.0	30.0	86
EZ2z61	931.00	199.00	119.60	0.220	-1.21E+06	3.10E+05	0.0927	0.0051	1.306	0.075	0.1013	0.0025	0.7205	1482	52.0	104.0	848	7.5	15.0	73
EZ2z72	423.00	300.00	95.00	0.750	-5.70E+05	6.10E+05	0.0768	0.0054	1.103	0.081	0.1038	0.0022	0.6190	1116	70.0	140.0	637	6.5	13.0	84
EZ2z73	164.00	96.90	36.50	0.610	6.80E+05	5.30E+05	0.0789	0.0066	1.213	0.110	0.1087	0.0024	0.4901	807	25.0	50.0	665	7.0	14.0	82

Footnotes:

. Analysis references: EZ2z is zircon from sample EZ2 (mount CT18-4), followed by grain number "c" or "r", meaning core or rim, respectively.

ANALYSIS	U (ppm)	Th (ppm)	Pb (ppm)	ThU	Ratios			Ages (Ma)			Concordance (%)												
					$^{207}\text{Pb}/^{206}\text{Pb}$	$^{207}\text{Pb}/^{235}\text{U}$	$^{206}\text{Pb}/^{238}\text{U}$	σ	$^{207}\text{Pb}/^{235}\text{U}$	σ	$^{206}\text{Pb}/^{238}\text{U}$	σ	2σ	2σ									
EZ4z129	505.00	171.50	53.30	0.339	2.00E+07	1.50E+07	0.0646	0.0036	0.932	0.1034	0.0022	0.3522	761	117.5	2055	21.4	42.9	634	6.4	12.9	95		
EZ4z130	72.80	45.70	47.70	0.616	1.90E+06	2.90E+06	0.1310	0.0036	7.300	0.3998	0.0080	0.3992	2111	24.1	48.2	607	19.5	39.0	2168	18.4	36.8	101	
EZ4z131	229.80	262.70	253.30	1.126	-7.60E+06	7.10E+06	0.1267	0.0021	6.570	0.3736	0.0066	0.3882	2053	14.6	29.3	799	15.2	30.5	2046	15.5	31.0	100	
EZ4z132	91.40	126.60	36.90	1.357	-6.00E+05	8.20E+05	0.0573	0.0050	0.819	0.1020	0.0026	0.1830	503	96.0	192.1	816	20.0	40.0	626	7.6	15.2	103	
EZ4z133c	326.60	64.30	23.75	0.194	-1.60E+06	2.60E+06	0.0659	0.0038	1.196	0.066	0.0024	0.2437	803	60.4	120.8	611	12.2	24.4	790	6.8	13.7	99	
EZ4z133r	446.00	24.90	7.77	0.055	3.00E+06	4.10E+06	0.0595	0.0033	0.826	0.044	0.0020	0.2588	585	60.2	120.4	513	17.4	34.9	613	5.9	11.7	100	
EZ4z134	101.90	50.70	18.66	0.494	-1.20E+06	1.10E+06	0.0664	0.0051	1.233	0.088	0.0022	0.0279	819	40.2	80.4	619	22.3	44.7	814	7.0	18.2	100	
EZ4z135	73.40	61.30	18.00	0.840	2.90E+05	8.90E+05	0.0601	0.0057	0.840	0.0996	0.0024	0.1561	607	102.5	205.1	632	18.0	35.9	612	7.0	14.1	99	
EZ4z136	198.10	45.10	10.90	0.403	-3.00E+06	1.50E+06	0.0560	0.0049	0.658	0.0843	0.0018	0.0963	452	97.1	208.8	240	48.0	48.0	522	5.4	10.7	102	
EZ4z137	98.20	102.50	29.30	1.031	3.60E+06	2.90E+06	0.0610	0.0047	0.863	0.1021	0.0027	0.3022	639	82.9	165.7	2731	22.7	45.5	627	7.9	15.8	99	
EZ4z138	105.60	83.11	80.20	0.773	2.00E+07	1.60E+07	0.1311	0.0037	6.820	0.3689	0.0072	0.2672	2173	24.7	49.5	702	18.3	37.0	2024	17.0	33.9	97	
EZ4z139	231.50	213.50	277.70	0.909	1.50E+07	4.40E+07	0.1832	0.0023	13.720	0.660	0.0087	0.4903	2770	9.8	19.5	642	13.5	27.6	2678	18.5	37.0	98	
EZ4z140	105.00	75.70	24.76	0.707	1.70E+07	1.20E+07	0.0632	0.0046	0.997	0.072	0.0025	0.2853	715	77.3	154.6	636	13.3	28.6	694	7.2	14.5	99	
EZ4z141	477.00	301.00	86.20	0.621	1.10E+09	2.20E+09	0.0627	0.0039	0.882	0.050	0.0018	-0.0226	698	66.2	132.5	3032	24.3	48.7	625	5.3	10.5	97	
EZ4z142	431.00	273.00	74.10	0.630	-4.40E+07	6.20E+07	0.0625	0.0037	0.871	0.049	0.0018	0.0778	691	63.1	126.2	1689	20.2	40.4	620	5.3	10.5	98	
EZ4z143	67.10	40.70	60.20	0.601	-6.60E+07	5.60E+07	0.2283	0.0045	18.800	0.950	0.0120	0.3863	3040	15.8	31.6	2034	21.2	42.4	3005	24.3	48.5	99	
EZ4z144	316.00	142.50	115.70	0.449	-2.40E+05	3.90E+05	0.1068	0.0020	4.279	0.210	0.0020	0.2243	1746	17.2	34.3	644	15.3	30.7	1630	12.8	25.5	96	
EZ4z145	314.80	278.70	264.00	0.879	-9.00E+05	9.10E+05	0.1280	0.0019	6.410	0.310	0.0022	0.0059	2071	26.2	51.9	2140	31.4	62.9	1969	14.0	28.0	97	
EZ4z146	139.10	178.50	52.00	1.280	6.00E+05	1.10E+05	0.0623	0.0042	0.885	0.057	0.0103	0.2069	684	72.0	143.9	1982	26.7	53.3	622	6.4	12.9	97	
EZ4z147	257.71	32.99	34.72	1.271	5.00E+04	4.10E+04	0.1366	0.0063	7.230	0.510	0.0022	0.6136	2185	40.1	80.2	2445	23.3	46.6	2106	23.3	46.5	98	
EZ4z148	207.70	102.90	94.90	0.491	2.70E+05	4.20E+05	0.1347	0.0026	6.040	0.370	0.0130	0.8701	2160	16.8	33.7	591	21.0	42.0	1799	31.7	63.4	91	
EZ4z149	109.20	19.40	21.90	0.169	1.40E+05	3.10E+05	0.1592	0.0032	10.110	0.510	0.0090	0.3886	2447	17.0	34.0	2148	28.1	56.3	2397	20.0	40.0	98	
EZ4z150	71.60	89.60	23.22	1.244	-7.70E+04	5.40E+04	0.0608	0.0059	0.789	0.074	0.0023	0.0107	632	104.5	209.0	624	19.2	38.4	569	6.8	13.6	96	
EZ4z152	28.70	36.56	36.50	1.255	2.90E+04	4.60E+04	0.1318	0.0049	7.290	0.460	0.0110	0.4480	2122	32.6	65.1	667	14.7	29.5	2154	25.4	50.8	100	
EZ4z153	95.20	115.80	33.75	1.206	-4.70E+04	4.00E+04	0.0595	0.0049	0.848	0.070	0.0101	0.0025	585	89.4	178.7	633	17.7	35.3	621	7.3	14.6	100	
EZ4z154	288.70	203.20	65.30	0.699	4.00E+05	2.40E+05	0.0619	0.0040	0.929	0.056	0.0021	0.1094	671	69.1	138.3	648	13.4	26.8	655	6.1	12.2	98	
EZ4z156	133.20	76.66	21.95	0.568	2.20E+04	8.20E+04	0.0616	0.0047	0.866	0.065	0.0021	0.1075	660	81.8	163.5	652	23.2	46.5	607	6.2	12.3	96	
EZ4z157	438.00	157.00	48.40	0.354	-1.10E+05	3.60E+05	0.0608	0.0035	0.893	0.050	0.1059	0.0020	0.3018	632	62.0	124.0	649	5.8	11.7	607	5.8	11.7	100
EZ4z158	81.10	69.50	20.47	0.840	-8.60E+04	6.90E+04	0.0625	0.0059	0.900	0.087	0.1017	0.0024	691	100.7	201.3	624	7.0	14.0	624	7.0	14.0	96	
Discordant data																							
EZ4z32	1015.00	210.30	124.60	0.208	1.70E+06	1.50E+06	0.1175	0.0059	2.985	0.160	0.1846	0.9363	1919	45.0	90.1	1404	20.4	40.7	1092	13.9	27.8	78	
EZ4z91	708.00	329.90	101.20	0.475	2.20E+05	8.00E+05	0.0719	0.0044	0.968	0.057	0.0973	0.0017	983	62.3	124.6	687	14.7	29.4	599	5.0	10.0	87	
EZ4z94c	70.00	37.00	610.00	0.498	1.90E+05	1.10E+05	0.4330	0.0270	80.000	13.000	0.1500	0.9882	4028	46.5	93.1	4462	81.4	162.8	5199	215.8	431.7	117	
EZ4z94f	14.84	5.69	1.47	0.375	-2.90E+04	2.70E+04	0.0500	0.0150	0.610	0.180	0.0092	-0.0190	195	348.7	697.3	484	56.7	113.4	610	15.2	30.5	126	
EZ4z97	52.70	19.10	5.49	0.371	1.20E+05	1.50E+05	0.0511	0.0061	0.696	0.078	0.0988	0.0027	245	137.5	274.9	536	20.3	46.7	607	7.9	15.8	113	
EZ4z108	158.60	68.20	25.70	0.428	1.40E+05	2.70E+05	0.0797	0.0067	1.017	0.081	0.0927	0.0019	1190	83.0	166.0	712	20.4	40.7	571	5.6	11.2	80	
EZ4z115	204.30	104.80	1250.00	0.483	-2.40E+05	4.20E+05	0.4430	0.0470	31.600	4.400	0.4750	0.9499	4062	79.0	158.0	3538	68.5	136.9	2505	56.8	113.6	71	
EZ4z151	98.70	92.10	38.70	0.940	7.00E+05	1.00E+05	0.0837	0.0075	1.950	0.130	0.1150	0.0029	1286	87.2	174.5	868	28.1	56.1	702	8.4	16.8	81	
EZ4z155	588.00	203.90	165.70	0.343	8.20E+05	8.50E+05	0.1476	0.0018	6.887	0.330	0.3350	0.0057	2318	10.5	20.9	2097	21.2	42.4	1863	13.8	27.5	89	

Footnotes:
 . Analysis references: EZ4z is zircon from sample EZ4 (mount CT18-4), followed by grain number "c" or "r", meaning core or rim, respectively.

Chapter II, Section II.3

Table D.20: Sample EZ5 (LA-ICPMS)

IGSN: IEAC00035

Coordinate UTM: Zone 29S, 737554 m E, 3682849 m N

ANALYSIS	U (ppm)	Th (ppm)	Pb (ppm)	Th/U	Ratios					Concordant data					Ages (Ma)					Concordance (%)		
					²⁰⁶ Pb/ ²⁰⁸ Pb	²⁰⁷ Pb/ ²⁰⁸ Pb	²⁰⁷ Pb/ ²³⁵ U	²⁰⁶ Pb/ ²³⁵ U	²⁰⁷ Pb/ ²³⁵ U	²⁰⁶ Pb/ ²³⁸ U	²⁰⁷ Pb/ ²³⁸ U	²⁰⁶ Pb/ ²³⁸ U	²⁰⁷ Pb/ ²³⁵ U	²⁰⁶ Pb/ ²³⁸ U	²⁰⁷ Pb/ ²³⁵ U	²⁰⁶ Pb/ ²³⁸ U	²⁰⁷ Pb/ ²³⁸ U	²⁰⁶ Pb/ ²³⁸ U	²⁰⁷ Pb/ ²³⁸ U			
					σ	σ	σ	σ	σ	σ	σ	σ	σ	σ	σ	σ	σ	σ	σ			
EZ5x1	61.40	77.60	22.76	1.290	1.40E+05	0.0576	0.0057	0.846	0.077	0.1014	0.0027	0.0971	515	108.7	217.4	622	21.2	42.3	623	7.9	15.8	100
EZ5x2	151.40	54.60	31.69	0.361	1.70E+05	0.0811	0.0045	2.282	0.120	0.2036	0.0035	0.0172	1224	54.5	109.0	1207	18.5	37.1	1195	9.4	18.7	99
EZ5x3	225.80	73.90	50.30	0.776	4.00E+04	0.0613	0.0037	0.840	0.048	0.0997	0.0021	0.3212	650	64.8	129.6	619	13.2	26.5	613	6.2	12.3	99
EZ5x4	517.00	94.00	79.60	1.182	7.30E+05	0.1219	0.0015	5.346	0.260	0.3176	0.0056	0.4272	1984	10.9	21.9	1876	20.8	41.6	1778	13.7	27.4	95
EZ5x5	228.20	111.10	101.80	0.481	1.60E+05	0.1269	0.0017	6.015	0.290	0.3433	0.0065	0.6167	2055	11.8	23.6	1978	21.0	41.9	1903	13.6	31.2	96
EZ5x6	584.20	43.30	41.30	0.075	3.00E+05	0.1241	0.0013	6.013	0.290	0.3506	0.0057	0.5901	2016	9.3	18.6	1978	21.0	42.0	1937	15.6	27.2	98
EZ5x7	392.00	226.80	91.20	0.581	1.50E+05	0.0673	0.0038	1.337	0.070	0.1454	0.0025	0.1562	859	58.3	116.5	862	15.2	30.4	875	7.0	14.1	102
EZ5x8	192.70	106.60	36.40	0.633	1.40E+05	0.0633	0.0044	0.871	0.059	0.1016	0.0019	0.1852	718	73.8	147.6	636	16.0	32.0	624	5.6	11.1	98
EZ5x9	502.00	665.00	177.70	1.330	7.00E+05	0.0572	0.0033	0.717	0.038	0.0903	0.0016	-0.0857	499	69.5	127.1	549	11.2	22.5	557	4.7	9.5	102
EZ5x10	586.00	237.10	69.70	0.403	2.90E+05	0.0617	0.0034	0.878	0.045	0.1032	0.0018	-0.0341	664	59.0	118.0	640	12.2	24.3	633	5.3	10.5	99
EZ5x11	297.00	235.20	63.00	0.796	3.00E+03	0.0595	0.0035	0.767	0.042	0.0935	0.0016	0.0212	585	63.8	127.7	578	12.1	24.1	576	4.7	9.4	100
EZ5x12	333.00	50.40	15.43	0.155	9.00E+05	0.0589	0.0036	0.839	0.048	0.1041	0.0020	0.2369	563	66.6	133.1	619	13.2	26.5	638	5.8	11.7	103
EZ5x13	68.20	29.80	33.40	0.436	6.80E+04	0.1332	0.0031	7.380	0.390	0.4024	0.0088	0.4842	2141	20.3	40.7	2159	23.6	47.2	2180	20.2	40.5	101
EZ5x14	399.00	159.00	136.50	0.397	6.00E+05	0.1269	0.0017	5.754	0.280	0.3213	0.0053	0.4826	2083	11.6	23.2	1940	21.0	42.1	1796	12.9	25.9	93
EZ5x15	140.10	79.10	110.20	0.565	1.50E+05	0.2035	0.0029	14.470	0.700	0.5204	0.0095	0.4307	2854	11.6	23.2	2781	23.0	45.9	2701	20.1	40.3	97
EZ5x16	323.50	3.81	1.01	0.012	9.60E+04	0.0592	0.0036	0.812	0.046	0.0996	0.0018	0.0544	574	66.1	132.2	604	12.9	25.8	612	5.3	10.6	101
EZ5x17	109.20	116.90	32.90	1.071	7.60E+04	0.0588	0.0044	0.958	0.062	0.1016	0.0022	0.1562	484	85.5	171.1	593	17.5	35.1	624	6.4	12.9	105
EZ5x18	53.10	34.20	11.84	0.665	6.00E+04	0.0677	0.0069	0.951	0.095	0.1041	0.0025	0.2091	859	105.8	211.5	679	24.7	49.4	638	7.3	14.6	94
EZ5x19	192.50	203.60	208.90	1.054	4.00E+05	0.1368	0.0020	7.270	0.360	0.3848	0.0071	0.5164	2187	12.7	25.4	2145	22.1	44.2	2099	16.5	33.1	98
EZ5x20	44.03	39.47	32.94	0.880	2.00E+04	0.1071	0.0038	4.840	0.280	0.3195	0.0076	0.1746	1751	32.5	64.9	1792	24.3	48.6	1787	18.6	37.1	100
EZ5x21	119.90	96.80	29.80	0.799	5.10E+04	0.0617	0.0042	0.892	0.061	0.1046	0.0023	0.3642	664	72.9	145.8	647	20.4	32.7	641	6.7	13.4	99
EZ5x22	934.00	184.50	150.60	1.197	8.70E+05	0.1224	0.0014	5.129	0.250	0.3059	0.0057	0.6790	1992	10.2	20.3	1841	16.7	41.4	1720	14.1	28.1	93
EZ5x23	119.00	65.90	37.90	0.542	4.10E+04	0.0824	0.0047	2.330	0.130	0.2040	0.0043	0.1858	1255	55.8	111.6	1221	19.8	39.6	1197	11.5	23.0	98
EZ5x24	282.10	192.30	55.80	0.688	4.80E+04	0.0594	0.0039	0.845	0.053	0.1090	0.0021	0.0873	582	71.3	142.6	622	14.6	29.1	632	6.1	12.3	102
EZ5x25	144.10	99.30	29.70	0.688	2.80E+04	0.0608	0.0044	0.852	0.055	0.1009	0.0023	-0.1233	632	77.9	155.8	626	15.1	30.1	620	6.7	13.5	99
EZ5x26	829.00	78.00	72.70	0.094	3.00E+06	0.1263	0.0013	6.416	0.300	0.3680	0.0060	0.4997	2047	9.1	18.2	2034	20.5	41.0	2020	14.1	28.3	99
EZ5x27	95.60	88.40	26.50	0.912	1.00E+04	0.0623	0.0053	0.896	0.074	0.1063	0.0024	0.1049	684	90.8	181.6	650	19.8	39.6	651	7.0	14.0	100
EZ5x28	402.00	289.00	276.00	0.715	3.70E+05	0.1233	0.0015	6.199	0.300	0.3688	0.0063	0.6216	2005	10.8	21.6	2024	21.1	42.3	2024	14.8	29.7	101
EZ5x29	200.80	98.70	87.80	0.326	1.80E+05	0.1337	0.0017	7.070	0.340	0.3845	0.0070	0.5818	2147	11.1	22.2	2120	21.4	42.7	2097	16.3	32.6	99
EZ5x30	343.00	283.90	245.10	1.154	7.00E+05	0.1135	0.0019	5.092	0.250	0.3273	0.0060	0.4545	1856	15.1	30.2	1635	20.8	41.6	1825	14.6	29.1	99
EZ5x31	349.00	259.00	97.90	0.734	8.00E+05	0.0671	0.0038	1.220	0.066	0.1388	0.0025	0.1659	841	58.9	117.9	810	15.1	30.2	810	7.1	14.2	100
EZ5x32	124.20	102.90	27.70	0.824	9.30E+04	0.0603	0.0042	0.818	0.054	0.0989	0.0022	0.0503	614	75.2	150.4	607	15.1	30.1	608	6.5	12.9	100
EZ5x33	50.00	43.90	10.71	0.870	1.00E+06	0.0620	0.0073	0.724	0.080	0.0878	0.0026	0.0008	674	125.9	251.8	553	23.5	47.1	543	7.7	15.4	98
EZ5x34	120.60	147.30	40.50	1.211	1.00E+05	0.0603	0.0044	0.788	0.055	0.0960	0.0022	0.0515	614	78.8	157.6	590	15.6	31.2	591	6.5	12.9	100
EZ5x35	46.90	34.10	32.60	0.718	1.80E+04	0.1289	0.0045	6.800	0.400	0.3848	0.0086	0.2978	2083	30.7	61.4	2086	26.0	52.0	2099	20.0	40.0	101
EZ5x36	106.40	241.10	67.30	2.227	1.40E+04	0.0609	0.0048	0.862	0.067	0.1029	0.0022	0.2408	636	84.8	169.6	631	18.3	36.5	631	6.4	12.9	100
EZ5x37	68.60	94.40	22.49	1.351	1.00E+04	0.0588	0.0059	0.694	0.068	0.0872	0.0019	0.1091	560	109.4	218.7	535	20.4	40.7	539	5.6	11.3	101
EZ5x38	591.00	189.50	173.80	0.315	5.40E+05	0.1258	0.0014	6.093	0.290	0.3522	0.0059	0.5517	2040	9.8	19.7	1989	20.7	41.5	1945	14.1	28.1	98
EZ5x39	115.10	137.00	164.60	1.167	3.00E+05	0.1558	0.0032	10.020	0.500	0.4664	0.0086	0.2705	2411	17.4	34.9	2437	23.0	46.0	2468	18.9	37.8	101
EZ5x40	92.50	84.20	22.89	0.886	7.20E+04	0.0606	0.0049	0.821	0.065	0.0982	0.0022	0.1672	625	87.2	174.3	609	18.1	36.2	604	6.5	12.9	99
EZ5x41	344.00	205.00	59.20	0.420	2.10E+05	0.0629	0.0036	0.964	0.053	0.1140	0.0021	0.1770	705	60.9	121.8	685	13.7	27.4	696	6.1	12.2	102
EZ5x42	75.00	18.04	20.08	0.744	1.40E+05	0.0577	0.0047	0.728	0.059	0.0909	0.0022	0.1988	518	89.4	178.8	555	17.3	34.6	561	6.5	13.0	101
EZ5x43	343.90	632.00	182.20	1.766	2.10E+05	0.0607	0.0035	0.852	0.048	0.1026	0.0020	0.2936	629	62.1	124.2	626	13.1	26.3	630	5.8	11.7	101
EZ5x44	134.10	174.40	50.30	1.282	1.30E+04	0.0573	0.0044	0.836	0.063	0.1049	0.0022	0.2361	503	84.5	169.0	617	17.4	34.8	643	6.4	12.8	104
EZ5x45	236.10	29.90	36.00	1.120	2.20E+05	0.1656	0.0024	10.330	0.520	0.4631	0.0087	0.6952	2514	12.2	24.4	2465	23.3	46.6	2409	19.3	38.6	98
EZ5x46	249.10	83.60	78.80	0.330	2.10E+05	0.1236	0.0016	6.242	0.300	0.3694	0.0063	0.5680	2009	11.5	24.0	2010	21.0	42.0	2027	14.8	29.7	101
EZ5x47	171.10	41.70	40.90	0.151	9.20E+05	0.1282	0.0016	6.750	0.330	0.3826	0.0068	0.6680	2073	11.0	22.0	2079	21.6	43.2	2088	15.9	31.7	100
EZ5x48	552.00	339.60	93.50	0.601	1.50E+05	0.0602	0.0034	0.834	0.045	0.1006	0.0017	0.2242	611	61.0	122.1	616	12.4	24.9	618	5.0	10.0	100
EZ5x49	106.00	68.40	20.08	0.631	2.60E+04	0.0656	0.0055	0.869	0.071	0.0970	0.0025	0.1601	794	87.9	175.9	635	19.3	38.5	597	7.3	14.7	94
EZ5x50	502.00	297.10	106.80	0.580	2.50E+05	0.0665	0.0038	1.173	0.063	0.1287	0.0023	0.1685	822	99.7	193.3	788	14.7					

ANALYSIS	U (ppm)		Th (ppm)		Pb (ppm)		ThU		²⁰⁶ Pb/ ²⁰⁸ Pb		²⁰⁷ Pb/ ²⁰⁸ Pb		Ratios		Error correction		Ages (Ma)		Concordance (%)			
	U	Th	Th	Pb	ThU	²⁰⁶ Pb/ ²⁰⁸ Pb	²⁰⁷ Pb/ ²⁰⁸ Pb	2σ	²⁰⁶ Pb/ ²³⁸ U	2σ	²⁰⁷ Pb/ ²³⁵ U	2σ	σ	²⁰⁶ Pb/ ²³⁸ U	2σ	σ	206Pb/208Pb	2σ	σ	Concordance (%)		
EZ5z64	104.30	125.20	36.42	1.171	1.171	3.30E+04	0.0613	0.0048	0.866	0.063	0.1044	0.0021	-0.0825	650	84.1	168.1	633	17.1	34.3	640	12.3	101
EZ5z66	286.40	128.40	137.90	0.440	0.440	2.30E+06	0.1620	0.0020	9.460	0.460	0.460	0.0072	0.6008	2477	10.3	20.8	2384	22.3	44.2	2270	16.3	95
EZ5z67	189.90	77.50	93.70	0.406	0.406	7.40E+05	0.1540	0.0024	9.840	0.480	0.4639	0.0082	0.3677	2391	13.3	26.5	2420	22.5	44.9	2457	18.1	102
EZ5z68	268.00	205.00	59.40	0.758	0.758	4.00E+05	0.0612	0.0039	0.844	0.051	0.1023	0.0018	0.1315	646	68.5	136.9	621	14.0	28.1	628	5.3	105
EZ5z69	232.00	186.00	46.60	0.764	0.764	3.00E+05	0.0612	0.0040	0.813	0.050	0.0985	0.0019	0.1818	646	70.2	140.4	604	14.0	28.0	606	5.6	111
EZ5z70	141.50	116.30	32.40	0.808	0.808	3.80E+04	0.0565	0.0042	0.787	0.056	0.1037	0.0025	0.2613	472	82.2	164.5	589	15.9	31.8	636	7.3	108
EZ5z71	639.00	38.40	60.40	0.059	0.059	7.50E+05	0.1257	0.0015	5.865	0.280	0.3400	0.0057	0.0920	2039	10.6	21.1	1956	20.7	41.4	1887	13.7	96
EZ5z72	711.90	217.00	62.10	0.275	0.275	3.70E+05	0.0600	0.0033	8.826	0.043	0.1007	0.0017	0.5742	604	59.5	119.0	611	11.9	23.9	618	5.0	100
EZ5z73	290.00	290.00	145.10	0.479	0.479	7.10E+05	0.1100	0.0014	4.848	0.230	0.2300	0.0053	0.3158	1799	11.6	22.0	1805	19.9	39.9	1805	12.9	101
EZ5z74	235.80	146.10	265.10	0.608	0.608	1.80E+06	0.1544	0.0020	9.140	0.460	0.4293	0.0030	0.6326	2395	11.0	22.0	2352	23.0	46.0	2303	18.0	98
EZ5z75	35.08	0.15	-0.21	-0.002	-0.002	1.00E+03	0.0572	0.0065	0.760	0.110	0.0923	0.0030	-0.1078	499	163.6	327.3	574	12.7	63.4	569	8.9	17.7
EZ5z76	415.80	334.00	93.00	0.795	0.795	1.31E+06	0.0594	0.0033	0.631	0.045	0.1019	0.0018	0.1839	582	60.3	120.7	614	12.5	24.9	626	5.3	105
EZ5z77	37.30	46.50	10.89	1.232	1.232	9.00E+04	0.0657	0.0079	0.792	0.091	0.0907	0.0029	0.1287	797	126.0	252.1	592	25.8	51.5	560	8.6	17.1
EZ5z79	366.40	478.00	138.90	1.291	1.291	2.30E+05	0.0639	0.0038	0.913	0.053	0.1015	0.0019	0.1118	722	63.6	127.2	659	14.1	28.1	644	5.5	11.1
EZ5z80	247.80	228.50	36.40	0.517	0.517	4.90E+05	0.0579	0.0035	0.804	0.046	0.1015	0.0018	0.0872	526	66.3	130.5	599	12.9	25.9	623	5.3	105
EZ5z81	96.60	79.60	22.88	0.822	0.822	2.00E+00	0.0591	0.0049	0.839	0.068	0.1033	0.0022	0.1238	571	90.2	180.4	619	18.8	37.5	634	6.4	12.9
EZ5z82	644.00	537.00	152.30	0.834	0.834	2.80E+05	0.0607	0.0034	0.845	0.044	0.1012	0.0018	0.1003	629	60.3	120.7	622	12.1	24.2	621	5.3	105
EZ5z83	186.30	73.30	69.80	0.388	0.388	3.00E+05	0.1251	0.0018	6.248	0.300	0.3661	0.0066	0.5179	2030	12.7	25.5	2011	21.0	42.0	2006	15.6	31.2
EZ5z84	870.00	242.80	238.60	0.277	0.277	2.80E+05	0.1276	0.0013	6.506	0.310	0.3713	0.0064	0.3723	2065	9.0	18.0	2047	20.9	41.9	2036	15.0	99
EZ5z85	700.00	115.20	108.90	0.199	0.199	-1.12E+06	0.1241	0.0014	6.232	0.300	0.3671	0.0062	0.3452	2016	10.0	20.0	2009	21.0	42.1	2016	14.6	100
EZ5z86	373.60	449.00	449.20	1.191	1.191	4.20E+05	0.0605	0.0016	6.660	0.330	0.3741	0.0069	0.6419	2095	10.8	21.7	2067	21.9	43.7	2049	16.2	99
EZ5z87	101.00	65.80	19.10	0.621	0.621	1.50E+04	0.0602	0.0055	0.857	0.078	0.1061	0.0026	0.3068	611	98.7	197.5	628	21.3	42.6	650	7.6	15.2
EZ5z88	80.30	73.40	21.00	0.911	0.911	6.80E+04	0.0547	0.0054	0.760	0.073	0.1023	0.0027	0.0547	400	110.6	221.2	574	21.0	42.1	628	7.9	15.8
EZ5z89	31.92	23.15	7.53	0.723	0.723	-2.10E+04	0.0622	0.0077	0.950	0.110	0.1112	0.0033	0.0355	681	132.2	264.4	678	28.6	57.2	680	9.6	19.1
EZ5z90	268.30	476.00	438.70	1.761	1.761	1.00E+05	0.1616	0.0035	10.000	0.520	0.3493	0.0092	0.5056	2472	18.3	36.6	2435	24.0	48.7	2409	20.4	99
EZ5z91	61.88	32.51	39.10	0.519	0.519	2.00E+05	0.1368	0.0033	7.350	0.380	0.3994	0.0080	0.2514	2187	21.0	42.0	2139	23.1	46.2	2139	18.5	99
EZ5z92	91.50	47.27	47.30	0.512	0.512	4.00E+05	0.1368	0.0033	7.350	0.380	0.3994	0.0080	0.2514	2187	21.0	42.0	2139	23.1	46.2	2139	18.5	99
EZ5z93	191.00	294.00	84.10	1.495	1.495	1.24E+05	0.0634	0.0039	0.841	0.054	0.1106	0.0026	0.0852	722	65.3	130.5	676	14.1	28.2	676	5.6	15.1
EZ5z94	298.00	204.00	56.80	1.686	1.686	5.00E+05	0.0584	0.0037	0.764	0.044	0.0952	0.0019	0.0970	545	69.2	138.5	576	12.7	25.3	586	7.5	11.2
EZ5z95	407.80	80.10	68.00	0.190	0.190	-2.50E+05	0.1247	0.0020	5.750	0.270	0.3400	0.0066	0.5917	2025	14.2	28.4	1939	21.6	43.6	1887	15.9	31.8
EZ5z96	677.00	133.20	116.40	0.196	0.196	-2.40E+06	0.140E+06	0.0014	5.656	0.290	0.3354	0.0057	0.5188	2006	10.1	20.1	1925	20.8	41.2	1865	13.8	97
EZ5z97	275.40	243.20	69.30	0.879	0.879	4.00E+05	0.0622	0.0038	0.856	0.050	0.1010	0.0018	0.0368	681	65.3	130.5	628	13.7	27.3	620	5.3	10.5
EZ5z98	97.30	101.90	25.94	1.040	1.040	8.10E+04	0.0580	0.0050	4.950	0.063	0.0942	0.0023	0.0356	550	94.4	188.9	571	18.2	36.4	580	6.8	13.6
EZ5z99	116.50	140.10	122.50	1.195	1.195	6.00E+05	0.1150	0.0029	4.790	0.250	0.3088	0.0064	0.3681	1880	22.7	44.5	1802	23.2	46.4	1795	15.8	31.5
EZ5z100	72.40	81.40	68.60	1.105	1.105	8.00E+05	0.1051	0.0031	4.490	0.250	0.3088	0.0069	0.4401	1716	21.1	54.2	1740	23.1	46.2	1740	17.0	34.0
EZ5z101	190.30	353.00	100.00	1.827	1.827	7.00E+04	0.0560	0.0042	0.781	0.055	0.1004	0.0020	0.3225	530	79.3	158.7	586	15.7	31.3	586	5.9	11.7
EZ5z102	67.00	79.00	23.38	1.185	1.185	-2.60E+04	0.0626	0.0058	0.837	0.077	0.1004	0.0029	0.0939	695	98.7	197.5	617	21.3	42.5	617	8.5	17.0
EZ5z103	149.40	149.80	43.20	0.994	0.994	2.20E+06	0.0603	0.0043	0.822	0.058	0.0998	0.0019	0.2189	614	77.0	154.0	609	16.1	32.3	613	5.6	11.1
EZ5z104	189.50	21.32	5.52	0.110	0.110	2.20E+04	0.0590	0.0039	0.733	0.048	0.0923	0.0017	0.1311	567	72.0	143.9	558	14.0	28.1	570	5.0	10.0
EZ5z105	169.60	105.10	31.20	0.621	0.621	5.10E+04	0.0609	0.0039	0.880	0.056	0.1035	0.0021	0.1522	636	69.9	137.8	641	15.1	30.2	634	6.1	12.3
EZ5z106	149.50	163.50	166.30	1.085	1.085	1.10E+05	0.0612	0.0020	6.740	0.330	0.3890	0.0071	0.4462	2057	13.9	27.8	2078	21.6	43.3	2118	16.5	33.0
EZ5z107	72.60	111.30	30.81	1.524	1.524	5.00E+04	0.0615	0.0055	0.821	0.070	0.0955	0.0024	-0.0641	657	95.9	191.8	609	19.5	39.0	588	7.1	14.1
EZ5z109c	359.60	320.60	288.50	0.891	0.891	1.30E+05	0.0615	0.0055	0.821	0.070	0.0955	0.0024	-0.0641	657	95.9	191.8	609	19.5	39.0	588	7.1	14.1
EZ5z109d	275.00	244.80	203.90	0.908	0.908	6.00E+05	0.1120	0.0017	4.795	0.240	0.3119	0.0064	0.5134	1832	13.8	27.5	1784	21.0	42.3	1874	15.4	30.8
EZ5z110	320.00	252.80	76.60	0.790	0.790	3.00E+05	0.0633	0.0037	0.821	0.050	0.1047	0.0020	0.3343	718	62.1	124.1	663	13.2	26.4	642	5.8	11.7
EZ5z111	210.40	380.90	407.90	1.811	1.811	-1.50E+05	0.1378	0.0021	7.550	0.370	0.4011	0.0070	0.4158	2200	13.2	26.5	2179	22.0	43.9			

Chapter II, Section II.3

Table D.21: Sample EZ6 (LA-ICPMS)

IGSN: IEAC00036

Coordinate UTM: Zone 29S, 739164 m E, 3684150 m N

ANALYSIS	U (ppm)	Th (ppm)	Pb (ppm)	Th/U	Ratios			Concordant data			Error correction	Ages (Ma)			Concordance (%)						
					²⁰⁷ Pb/ ²⁰⁶ Pb	²⁰⁷ Pb/ ²³⁵ U	²⁰⁷ Pb/ ²³⁸ U	2σ	2σ	2σ		σ	2σ	σ		2σ	σ	2σ			
EZ6z1	86.90	146.40	1163.00	1.672	0.1101	0.0030	4.960	0.130	0.3217	0.0053	0.3021	1801	24.8	49.6	1813	11.1	22.1	1798	12.9	25.9	99
EZ6z2	462.00	180.00	1490.00	0.631	0.0018	0.0018	0.754	0.021	0.0864	0.0014	0.2882	712	30.3	60.6	571	6.1	12.1	534	4.2	8.3	94
EZ6z3	45.70	89.40	702.00	1.972	0.0644	0.0065	0.808	0.080	0.0320	0.0031	0.0589	755	106.5	213.0	601	22.4	44.9	567	9.2	18.3	94
EZ6z4	616.80	245.10	2020.00	0.399	0.0644	0.0014	0.959	0.020	0.1079	0.0010	0.3037	755	22.9	45.9	683	5.2	10.4	661	2.9	5.8	97
EZ6z5	598.00	404.50	3493.00	0.687	0.1292	0.0011	6.405	0.074	0.3532	0.0043	0.6635	2067	7.5	15.0	2033	5.1	10.1	1950	7.6	15.2	96
EZ6z6	328.00	108.50	546.00	0.317	0.0017	0.0017	6.650	0.100	0.3154	0.0043	0.6877	2067	11.7	23.4	1924	7.6	15.3	1767	10.5	21.1	92
EZ6z7	353.00	157.00	1270.00	0.418	0.0021	0.0021	6.570	0.110	0.3725	0.0051	0.6806	2036	14.8	29.6	2055	10.1	20.1	2046	12.0	23.9	100
EZ6z8c	160.30	40.40	382.00	0.254	0.0020	0.0020	6.730	0.110	0.3823	0.0047	0.4807	2039	14.1	28.1	2077	7.2	14.4	2087	11.0	21.9	100
EZ6z8d	247.30	94.20	827.00	0.380	0.0016	0.0016	6.336	0.099	0.3672	0.0039	0.5598	2000	11.6	23.1	2023	6.8	13.7	2016	9.2	18.4	100
EZ6z9	242.70	52.20	494.00	0.161	0.0018	0.0018	6.930	0.100	0.3876	0.0042	0.4764	2067	12.4	24.8	2112	6.4	12.8	2112	6.8	19.5	100
EZ6z10	114.00	29.00	510.00	2.375	0.0037	0.0037	0.807	0.045	0.0871	0.0022	0.2234	841	57.4	114.8	601	12.6	25.3	538	6.5	13.0	90
EZ6z11	67.40	74.70	182.20	1.104	0.0050	0.0050	0.749	0.066	0.0925	0.0021	0.2602	545	93.6	187.1	568	19.1	38.3	570	6.2	12.4	100
EZ6z12	116.00	64.90	564.00	0.551	0.0028	0.0028	6.160	0.130	0.3610	0.0044	0.2313	1987	20.4	40.8	1999	9.2	18.4	1987	10.4	20.8	99
EZ6z13	180.10	111.50	1053.00	0.615	0.0022	0.0022	7.320	0.130	0.3779	0.0046	0.5176	2206	13.8	27.6	2151	7.9	15.9	2066	10.8	21.5	96
EZ6z14	238.50	153.90	691.00	0.638	0.0020	0.0020	1.850	0.051	0.1767	0.0020	0.2866	1082	26.6	53.1	1063	9.1	18.2	1049	5.5	11.0	99
EZ6z16	90.20	75.00	194.80	0.827	0.0038	0.0038	0.905	0.056	0.1008	0.0018	0.2044	745	62.7	125.3	654	14.9	29.8	619	5.3	10.5	95
EZ6z17	263.50	199.80	2324.00	0.752	0.0019	0.0019	11.820	0.140	0.4833	0.0051	0.5618	2608	9.0	18.1	2590	5.5	11.1	2542	11.1	22.2	98
EZ6z18	35.70	37.50	327.00	1.038	0.0048	0.0048	6.080	0.270	0.3532	0.0068	0.4572	2000	34.7	69.3	1987	19.3	38.7	1950	16.2	32.4	98
EZ6z19	397.00	382.00	1027.00	0.961	0.0019	0.0019	0.840	0.027	0.0986	0.0012	0.1419	632	33.6	67.3	619	7.4	14.9	613	2.9	5.9	99
EZ6z20	278.90	170.20	412.00	0.599	0.0016	0.0016	1.655+06	0.060	0.0608	0.0011	0.1163	660	38.3	76.6	634	9.0	17.9	621	2.9	5.7	98
EZ6z21	345.70	446.00	1247.00	1.279	0.0029	0.0029	0.887	0.028	0.1018	0.0012	0.2481	705	32.1	64.3	645	7.5	15.1	625	3.5	7.0	97
EZ6z22	112.70	105.50	779.00	0.898	0.0033	0.0033	6.680	0.130	0.3603	0.0052	0.2927	2142	16.4	32.8	2070	8.6	17.2	1984	12.3	24.6	96
EZ6z23	135.00	36.30	94.50	0.247	0.0026	0.0026	0.874	0.045	0.1011	0.0016	0.0211	695	57.9	115.8	638	12.2	24.4	621	4.7	9.4	97
EZ6z24	129.20	430.00	970.00	1.608	0.0052	0.0052	0.681	0.020	0.0896	0.0012	0.1419	537	56.4	112.8	527	11.2	22.3	518	3.6	7.1	98
EZ6z25	60.10	112.20	1142.00	1.838	0.0036	0.0036	8.100	0.220	0.4186	0.0064	0.4004	2205	22.6	45.2	2242	12.3	24.5	2254	14.5	29.1	101
EZ6z26	101.10	121.00	342.00	1.176	0.0043	0.0043	0.950	0.062	0.1063	0.0017	0.1774	752	66.7	131.4	678	16.1	32.3	651	5.0	9.9	96
EZ6z27c	133.50	111.90	1013.00	0.836	0.0026	0.0026	7.430	0.160	0.3836	0.0055	0.5350	2209	16.3	32.6	2165	9.6	19.3	2093	12.8	25.6	97
EZ6z27d	884.00	555.00	3553.00	0.624	0.0011	0.0011	6.600	0.095	0.3556	0.0053	0.8286	2137	7.2	14.5	2059	6.3	12.7	1961	12.6	25.2	95
EZ6z28	329.50	85.50	738.00	0.639	0.0027	0.0027	6.020	0.140	0.3551	0.0044	0.3863	1977	19.8	39.6	1979	10.1	20.2	1969	10.5	20.9	99
EZ6z29	31.25	43.08	864.00	0.902	0.0021	0.0021	0.837	0.028	0.0977	0.0010	0.1073	667	36.4	72.8	617	7.7	15.5	601	2.9	5.9	97
EZ6z30	31.25	43.08	864.00	0.902	0.0021	0.0021	0.837	0.028	0.0977	0.0010	0.1073	667	36.4	72.8	617	7.7	15.5	601	2.9	5.9	97
EZ6z31	73.70	35.60	169.10	0.480	0.0039	0.0039	1.809	0.098	0.1721	0.0028	0.2924	1092	51.5	102.9	1049	17.7	35.4	1024	7.7	15.4	98
EZ6z32	128.10	78.90	357.00	0.615	0.0021	0.0021	1.804	0.065	0.1729	0.0022	0.2002	1074	36.1	72.1	1047	11.8	23.0	1028	6.0	12.1	98
EZ6z33	115.30	10.20	36.40	0.015	0.0005	0.0005	0.863	0.057	0.0998	0.0016	0.1940	691	69.9	139.9	632	15.5	31.0	613	4.7	9.4	97
EZ6z34	258.10	289.90	762.00	1.179	0.0023	0.0023	0.865	0.031	0.0987	0.0013	-0.0480	695	39.2	78.3	633	8.4	16.9	613	3.8	7.6	97
EZ6z35	324.40	153.30	2301.00	0.476	0.0019	0.0019	16.950	0.230	0.5330	0.0052	0.7719	3035	6.7	13.4	2932	6.5	13.0	2754	10.9	21.9	94
EZ6z36	159.60	283.00	829.00	1.777	0.0047	0.0047	0.982	0.048	0.1092	0.0015	0.2306	765	50.5	101.0	695	12.3	24.6	668	4.4	8.7	96
EZ6z37	131.50	104.30	284.00	0.791	0.0032	0.0032	0.842	0.043	0.0980	0.0013	0.0970	678	55.1	110.1	620	11.8	23.7	603	3.8	7.6	97
EZ6z38	148.30	203.60	562.00	1.372	0.0028	0.0028	0.856	0.038	0.1022	0.0015	0.1197	643	49.3	98.5	628	10.4	20.8	627	4.4	8.8	100
EZ6z39	88.70	108.10	280.00	1.235	0.0045	0.0045	0.833	0.054	0.0936	0.0017	0.2934	816	70.9	141.9	615	14.9	29.9	577	5.0	10.0	94
EZ6z40	294.00	321.00	89.60	1.127	0.0021	0.0021	0.678	0.025	0.0772	0.0014	0.3336	718	35.2	70.4	526	7.6	15.1	479	4.2	8.4	91
EZ6z41	176.00	176.00	1437.00	0.158	0.0029	0.0029	8.390	0.190	0.3876	0.0070	0.6522	2411	15.8	31.6	2274	10.3	20.5	2112	16.3	32.5	93
EZ6z42	131.50	224.00	628.00	1.631	0.0030	0.0030	0.845	0.043	0.1044	0.0024	0.2430	556	55.7	111.5	622	11.8	23.6	640	7.0	14.0	103
EZ6z43	145.40	143.60	367.00	0.969	0.0034	0.0034	0.873	0.046	0.1022	0.0016	0.0510	671	58.8	117.5	637	12.5	24.9	627	4.7	9.4	98
EZ6z44	287.00	781.00	2071.00	2.753	0.0022	0.0022	0.818	0.031	0.0963	0.0011	0.3264	650	38.5	77.1	607	8.6	17.3	593	3.2	6.5	98
EZ6z45	232.70	221.10	1993.00	0.966	0.0020	0.0020	5.890	0.120	0.3434	0.0040	0.5902	2003	14.4	28.8	1960	8.8	17.7	1903	9.6	19.2	97
EZ6z46	266.00	52.90	614.00	0.200	0.0013	0.0013	7.990	0.030	0.3912	0.0085	0.8826	2291	24.3	48.5	2230	20.3	40.6	2128	19.7	39.4	95
EZ6z47	180.00	180.00	2700.00	1.395	0.0016	0.0016	0.826	0.019	0.0974	0.0011	0.2380	660	22.6	45.2	611	5.3	10.6	599	3.2	6.5	98
EZ6z48	284.80	147.70	414.00	0.640	0.0024	0.0024	0.819	0.033	0.1001	0.0013	0.1237	574	44.1	88.2	607	9.2	18.4	615	3.8	7.6	101
EZ6z51c	156.20	47.20	331.70	0.308	0.0024	0.0024	3.418	0.086	0.2586	0.0028	0.3007	752	23.3	46.7	1509	9.9	19.7	1467	7.2	14.4	97
EZ6z51d	54.70	62.20	170.00	1.134	0.0050	0.0050	0.871	0.068	0.0989	0.0022	0.0384	1522	83.7	167.3	636	18.4	36.9	614	6.4	12.9	96
EZ6z51e	70.20	45.80	122.90	0.657	0.0051	0.0051	0.772	0.064	0.0965	0.0021	-0.0443	537	95.9	191.7	581	18.3	36.6	594	6.2	12.3	102
EZ6z52	236.00	225.00	558.00	0.967	0.0027	0.0027	0.716	0.033	0.0875	0.0011	0.2740	698	45.9	91.7	575	9.5	19.0	541	3.3	6.5	94
EZ6z53a	905.00	143.20	224.50	1.161	0.0013	0.0013	0.731	0.018	0.0896	0.0010	0.4615	567	24.0	48.0	557	5.3	10.5	553	2.9	5.7	99
EZ6z54	58.40	85.10	746.0																		

ANALYSIS	U (ppm)	Th (ppm)	Pb (ppm)	ThU	Ratios					Ages (Ma)					Concordance (%)								
					$^{206}\text{Pb}/^{208}\text{Pb}$	$^{207}\text{Pb}/^{208}\text{Pb}$	$^{207}\text{Pb}/^{235}\text{U}$	$^{206}\text{Pb}/^{238}\text{U}$	$^{207}\text{Pb}/^{238}\text{U}$	Error correction	σ	$^{207}\text{Pb}/^{235}\text{U}$	σ	$^{206}\text{Pb}/^{238}\text{U}$		σ							
EZb260	23.64	28.00	264.00	1.212	-2.01E+06	9.70E+05	0.1284	0.0069	5.920	0.340	0.3410	0.0170	0.5938	2076	47.3	94.6	24.9	1964	49.8	40.9	81.7	96	
EZb261	198.80	76.50	500.00	0.398	2.20E+05	9.80E+05	0.0853	0.0018	2.758	0.060	0.2635	0.0025	0.2782	1322	20.4	40.9	1344	8.1	16.2	13.1	101	101	
EZb262	319.50	210.40	802.00	0.688	-5.60E+06	3.80E+06	0.1213	0.0018	4.840	0.110	0.2861	0.0038	0.7585	1975	13.2	26.4	1792	9.6	19.1	16.22	29.1	91	
EZb263	153.70	63.50	199.60	0.287	1.60E+06	1.00E+06	0.0616	0.0023	0.899	0.035	0.1056	0.0012	0.2066	660	40.0	80.0	651	9.3	18.7	6.47	3.5	7.0	99
EZb264	230.60	159.30	450.00	0.278	1.51E+06	9.40E+05	0.0600	0.0028	0.832	0.036	0.1163	0.0015	-0.0905	604	50.5	101.0	615	10.4	19.9	619	4.4	8.8	101
EZb265	189.70	164.80	552.00	0.910	-2.20E+06	1.30E+06	0.0617	0.0028	0.991	0.041	0.1163	0.0015	0.1088	664	45.1	90.3	699	10.4	20.9	709	4.3	8.7	101
EZb266	279.80	244.70	1330.00	2.024	-4.90E+05	7.40E+05	0.0616	0.0025	0.774	0.033	0.0909	0.0012	0.3503	660	43.5	84.0	582	9.4	18.9	561	3.5	7.1	96
EZb267	241.90	563.00	664.00	1.001	-7.70E+06	5.70E+06	0.0611	0.0024	0.874	0.035	0.1030	0.0013	0.2427	643	42.2	84.4	638	9.5	18.9	632	3.8	7.6	99
EZb270	113.40	121.00	1252.00	1.119	-1.10E+06	1.40E+06	0.1337	0.0028	7.040	0.180	0.3785	0.0055	0.5091	2147	18.3	30.6	2116	11.4	22.7	2060	12.9	25.8	97
EZb272	384.00	260.00	106.00	0.345	-3.90E+06	2.10E+06	0.0652	0.0025	0.787	0.034	0.0880	0.0030	0.5392	781	40.3	80.6	589	9.7	19.3	544	8.9	17.8	92
EZb273	164.20	72.10	231.70	0.464	-4.10E+05	5.60E+05	0.0610	0.0028	0.910	0.041	0.1089	0.0013	0.2084	639	49.4	98.7	657	10.9	21.8	666	3.8	7.6	101
EZb274	790.50	58.64	181.70	0.787	-3.30E+05	3.00E+05	0.0608	0.0037	0.876	0.054	0.1045	0.0019	0.1343	632	65.5	131.1	639	14.6	29.2	641	5.5	11.1	100
EZb275	296.00	207.00	1785.00	0.772	-8.20E+07	4.00E+07	0.1552	0.0022	8.520	0.130	0.3954	0.0044	0.4750	2404	12.0	24.1	2288	6.9	13.9	2148	10.2	20.3	94
EZb276	127.40	49.90	501.00	0.414	1.00E+06	1.10E+06	0.1206	0.0024	6.136	0.130	0.3653	0.0044	0.3610	1965	17.7	35.5	1995	9.2	18.5	2007	10.4	20.8	101
EZb277	201.40	8.82	32.00	0.046	1.34E+06	7.30E+05	0.0636	0.0027	0.946	0.040	0.1080	0.0013	0.1555	728	45.0	90.0	676	10.2	20.9	661	3.8	7.6	98
EZb278	96.40	159.80	1554.00	1.764	3.00E+05	1.20E+06	0.0637	0.0026	4.910	0.110	0.2942	0.0046	0.3837	1958	19.3	38.6	1804	9.4	18.9	1662	11.5	22.9	92
EZb279	110.30	118.20	330.00	1.135	-3.60E+05	3.40E+05	0.0544	0.0030	0.737	0.045	0.0949	0.0018	0.1586	388	61.9	123.8	561	13.1	26.3	584	5.3	10.6	104
EZb280	82.70	59.70	622.00	0.763	-1.10E+06	1.00E+06	0.1319	0.0028	7.020	0.180	0.3825	0.0051	0.5417	2123	18.6	37.2	2114	11.4	22.8	2088	11.9	23.8	99
EZb281	111.60	305.00	633.00	2.882	3.00E+06	1.30E+06	0.0617	0.0042	0.897	0.056	0.0985	0.0015	0.1298	862	64.3	128.5	650	15.0	29.9	594	4.4	8.8	91
EZb282	128.60	85.50	247.90	0.706	-2.60E+06	2.10E+06	0.0618	0.0034	0.818	0.043	0.0965	0.0014	-0.0346	664	59.0	118.0	607	12.0	24.0	594	4.1	8.2	98
EZb283	110.30	107.40	1096.00	1.032	-9.00E+06	1.40E+06	0.1203	0.0025	6.210	0.140	0.3712	0.0046	0.3553	1961	18.5	37.1	2006	9.8	19.7	2035	10.8	21.6	101
EZb284	407.00	102.90	831.00	0.268	-1.27E+07	7.50E+06	0.1209	0.0014	5.120	0.075	0.3042	0.0027	0.6244	1970	10.3	20.6	1839	6.2	12.4	1712	6.7	13.3	93
EZb285	90.90	75.10	244.20	0.876	-8.90E+05	6.00E+05	0.0637	0.0036	0.951	0.054	0.1077	0.0022	0.1806	732	59.9	119.7	679	14.0	28.1	659	6.4	12.8	97
EZb286	197.90	192.50	805.00	1.033	-8.90E+05	9.10E+05	0.0721	0.0041	1.300	0.074	0.1308	0.0020	0.1805	989	57.8	115.7	846	16.3	32.6	792	5.7	11.4	94
EZb288	106.90	145.00	1395.00	1.445	-3.80E+05	7.40E+05	0.1304	0.0027	6.150	0.140	0.3383	0.0051	0.4654	2103	18.2	36.3	1997	9.9	19.9	1883	12.3	24.5	94
EZb289	165.20	120.10	387.00	0.768	-1.04E+07	5.90E+06	0.0615	0.0024	0.906	0.035	0.1089	0.0015	0.2172	657	41.8	83.7	655	9.3	18.6	655	4.4	8.7	100
EZb291	35.00	24.48	77.00	0.737	5.00E+06	2.50E+06	0.0615	0.0055	0.879	0.081	0.1041	0.0031	0.1990	657	95.9	191.8	640	21.9	43.7	638	9.0	18.1	100
EZb292	68.20	86.70	274.30	1.346	-6.50E+05	4.20E+05	0.0600	0.0038	0.880	0.050	0.1036	0.0020	0.1318	604	68.5	137.0	619	13.8	27.6	635	5.8	11.7	103
EZb293	231.90	367.70	1120.00	1.688	-1.60E+06	1.20E+06	0.0615	0.0026	0.842	0.043	0.1014	0.0013	0.1975	657	45.3	90.7	626	9.6	19.2	623	3.8	7.6	99
EZb294	166.70	77.50	238.10	0.923	8.00E+05	4.70E+05	0.0605	0.0027	0.853	0.038	0.1024	0.0015	0.1730	630	62.6	104.0	626	10.4	20.8	628	4.4	8.8	100
EZb295	243.60	211.90	663.00	0.923	-2.00E+06	1.30E+06	0.0645	0.0026	0.928	0.037	0.1046	0.0013	0.1815	758	42.5	85.0	667	9.7	19.5	641	3.8	7.6	96
EZb296	32.20	35.86	118.20	1.170	-2.30E+05	2.30E+05	0.0648	0.0071	0.901	0.099	0.1018	0.0034	0.2053	768	115.4	230.8	652	26.4	52.8	625	9.9	19.9	96
EZb297	185.40	377.00	1027.00	2.114	1.25E+06	9.20E+05	0.0619	0.0029	0.738	0.035	0.0894	0.0024	0.2507	671	50.1	100.2	561	10.2	20.4	534	4.5	8.9	95
EZb298	311.00	233.00	2540.00	0.784	-7.90E+06	5.90E+06	0.1867	0.0015	12.740	0.160	0.4684	0.0057	0.7736	2713	6.6	13.2	2661	5.9	11.8	2577	12.3	24.6	97
EZb299	316.00	166.00	314.80	0.233	-5.80E+06	4.90E+06	0.1243	0.0017	6.000	0.080	0.3375	0.0038	0.5605	2019	12.1	24.2	1976	7.2	14.5	1923	9.1	18.2	99
EZb300	141.90	39.00	119.30	0.277	-1.80E+05	5.20E+05	0.0607	0.0030	0.806	0.040	0.0964	0.0013	0.2068	629	53.2	106.5	600	11.2	22.5	593	3.8	7.6	99
EZb301	346.70	121.10	85.00	0.331	-2.10E+07	1.40E+07	0.0620	0.0018	0.766	0.022	0.0928	0.0011	0.1507	611	32.3	64.6	577	6.3	12.6	572	3.2	6.5	99
EZb302	177.80	219.00	651.00	1.287	-1.90E+06	1.10E+06	0.0624	0.0022	0.900	0.034	0.1046	0.0017	0.2980	688	37.6	75.2	652	9.1	18.2	641	5.0	9.9	98
EZb303	425.90	124.80	400.00	0.305	5.10E+06	3.50E+06	0.0604	0.0018	0.842	0.027	0.1012	0.0010	0.3204	618	32.2	64.3	620	7.4	14.9	621	2.9	5.9	100
EZb304	63.10	87.50	240.00	1.429	-5.00E+05	2.40E+05	0.0606	0.0053	0.820	0.068	0.0988	0.0020	-0.0357	625	94.3	188.6	608	19.0	37.9	607	5.9	11.7	100
EZb305	193.00	226.90	636.00	1.239	-2.10E+06	1.40E+06	0.0619	0.0028	0.875	0.038	0.1030	0.0018	0.1680	671	49.4	96.8	632	10.3	20.6	632	5.3	10.5	99
EZb306	249.00	122.90	397.00	0.518	3.00E+06	1.10E+06	0.0630	0.0022	0.925	0.034	0.1068	0.0013	0.3051	708	37.1	74.3	665	9.0	17.9	654	3.8	7.6	98
EZb307	431.00	321.00	966.00	0.769	-1.50E+06	2.10E+06	0.0624	0.0016	0.883	0.022	0.1029	0.0011	0.1360	688	27.4	54.7	643	5.9	11.9	631	3.2	6.4	98
EZb308	51.20	62.20	672.00	1.271	-9.80E+05	8.10E+05	0.1314	0.0035	6.920	0.190	0.3804	0.0060	0.3350	2117	23.3	46.7	2101	12.2	24.3	2078	14.0	28.0	99
EZb309	137.90	82.80	279.00	0.613	1.80E+06	1.70E+06	0.0642	0.0032	1.067	0.053	0.1211	0.0020	0.1374	748	52.7	105.3	737	13.0	26.0	737	5.8	11.5	100
EZb310	216.10	110.90	588.00	0.532	4.00E+06	1.60E+06	0.0628	0.0025	0.996	0.039	0.1182	0.0014	0.2452	701	42.4	84.8	702	9.9	19.8	709	4.0	8.1	101
EZb311	121.40	118.90	616.00	1.006	4.60E+05	7.10E+05	0.0723	0.0024	1.536	0.058	0.1646	0.0023	0.2556	994	33.7	67.5	984	11.2	22.3	982	6.4	12.7	100
EZb312	127.10	93.80	395.00	0.774	-4.50E+05	9.10E+05	0.0764	0.0036	1.635	0.082	0.1566	0.0029	0.2914	1106	47.1	94.2	984	15.8	31.6	932	8.1	16.2	95
EZb313	530.00	310.80	876.00	0.610	-5.00E+06	2.10E+06	0.0609	0.0016	0.807	0.020	0.0965	0.0010	0.1276	636	28.3	56.5	601	5.6	11.2	594	2.9	5.9	101
EZb314	108.80	314.00	3325.00	2.991	-1.60E+06	1.80E+06	0																

ANALYSIS	U (ppm)	Th (ppm)	Pb (ppm)	Th/U	Ratios				Error correction	Ages (Ma)				Concordance (%)								
					$^{207}\text{Pb}/^{206}\text{Pb}$	$^{207}\text{Pb}/^{235}\text{U}$	$^{207}\text{Pb}/^{238}\text{U}$	$^{207}\text{Pb}/^{206}\text{Pb}$		$^{207}\text{Pb}/^{235}\text{U}$	$^{207}\text{Pb}/^{238}\text{U}$	σ	2σ		σ	2σ						
EZ6z130	278.00	287.00	822.00	1.036	1.60E+06	0.0611	0.0020	0.849	0.028	0.1013	0.0015	0.1251	643	35.2	70.4	624	7.7	15.4	622	4.4	8.8	100
EZ6z131	121.90	176.00	565.00	1.471	-3.20E+07	0.0598	0.0032	0.829	0.043	0.1014	0.0017	0.1346	586	58.0	115.9	613	11.9	23.9	623	5.0	9.9	102
EZ6z133	86.80	108.20	987.00	1.269	1.80E+06	0.1290	0.0026	6.720	0.200	0.3756	0.0084	0.6858	2084	17.7	35.5	2075	13.1	26.3	2056	19.7	39.4	99
EZ6z136	600.00	230.00	495.00	0.377	-6.80E+06	0.0622	0.0016	0.699	0.022	0.0817	0.0021	0.8281	681	27.5	54.9	538	6.6	13.1	506	6.3	12.5	94
EZ6z137	257.00	365.00	1045.00	1.479	-5.00E+06	0.0639	0.0021	0.905	0.034	0.1032	0.0015	0.4394	738	34.8	69.5	654	9.1	18.1	633	4.4	8.8	97
EZ6z138	104.30	315.00	532.00	3.049	1.18E+07	0.0650	0.0044	0.767	0.056	0.0851	0.0022	0.3201	774	71.2	142.4	578	16.1	32.2	528	6.5	13.1	91
EZ6z139	407.00	468.00	1237.00	1.171	-6.50E+06	0.0636	0.0019	0.885	0.028	0.1015	0.0013	0.3342	728	31.7	63.3	644	7.5	15.1	623	3.8	7.6	97
EZ6z140	118.20	222.00	821.00	1.299	3.90E+06	0.1306	0.0025	6.120	0.160	0.3400	0.0085	0.7116	2106	16.8	33.6	1993	11.4	22.8	1887	20.4	40.9	95
EZ6z15	189.30	151.40	382.00	0.801	-4.00E+05	0.0763	0.0027	1.269	0.049	0.1179	0.0023	0.4732	1154	34.2	68.4	832	11.0	21.9	718	6.6	13.3	86
EZ6z40c	125.00	185.00	614.00	1.389	1.23E+06	0.0948	0.0032	2.001	0.079	0.1516	0.0035	0.4745	1524	31.8	63.6	1116	13.4	26.7	910	9.8	19.6	82
EZ6z49	78.50	215.00	712.00	2.500	1.82E+07	0.1431	0.0049	4.820	0.330	0.2460	0.0130	0.8284	2265	29.5	59.1	1508	28.3	56.6	1418	33.6	67.3	79
EZ6z53c	687.00	626.00	811.00	0.929	4.00E+06	0.0720	0.0022	0.644	0.020	0.0650	0.0018	0.4820	986	31.1	62.2	505	6.2	12.3	406	5.4	10.9	80
EZ6z67	39.13	49.90	347.00	1.333	-7.10E+04	0.1890	0.0240	3.210	0.520	0.1162	0.0044	0.8297	2733	104.5	209.0	1460	62.7	125.3	709	12.7	25.4	49
EZ6z68	38.20	52.80	173.00	1.447	-3.20E+04	0.0777	0.0075	1.090	0.120	0.1027	0.0029	0.4951	1139	96.0	192.0	749	29.1	58.2	630	8.5	17.0	84
EZ6z71	486.00	227.00	1310.00	0.474	-9.00E+06	0.1356	0.0021	5.270	0.110	0.2779	0.0045	0.7489	2172	13.5	27.0	1864	8.9	17.8	1581	11.4	22.7	85
EZ6z87	60.60	49.10	152.80	0.861	-7.00E+05	0.0533	0.0047	0.756	0.064	0.1041	0.0023	-0.0538	342	99.8	199.6	572	18.5	37.0	638	6.7	13.4	112
EZ6z90	128.00	236.30	1020.00	1.974	-4.20E+05	0.1180	0.0210	2.070	0.480	0.1120	0.0046	0.9266	1926	159.4	318.9	1139	79.3	158.6	684	13.3	26.7	60
EZ6z98	228.20	201.50	1618.00	0.934	-3.00E+06	0.1301	0.0018	5.220	0.130	0.2897	0.0059	0.8272	2099	12.1	24.3	1856	10.6	21.2	1640	14.7	29.5	88
EZ6z99	190.70	283.00	2561.00	1.527	-1.00E+07	0.1723	0.0028	9.240	0.270	0.3844	0.0087	0.8449	2580	27.1	54.2	2362	13.4	26.7	2097	20.3	40.5	89
EZ6z118	47.20	130.80	114.80	2.825	1.08E+06	0.0806	0.0083	0.862	0.090	0.0780	0.0025	0.2818	1212	101.3	202.7	631	24.5	49.0	484	7.5	14.9	77
EZ6z132	291.00	682.00	1565.00	2.208	-8.20E+06	0.1253	0.0023	3.300	0.130	0.1922	0.0073	0.8913	2033	16.2	32.5	1481	15.3	30.7	1133	19.7	39.5	77
EZ6z134	77.90	182.80	904.00	2.445	-1.10E+06	0.1237	0.0038	4.750	0.140	0.2759	0.0060	0.4592	2010	27.3	54.5	1776	12.4	24.7	1571	15.2	30.3	88
EZ6z135	553.00	649.00	2980.00	1.215	3.90E+06	0.1188	0.0021	2.970	0.110	0.1818	0.0051	0.9398	1938	15.8	31.6	1400	14.1	28.1	1077	13.9	27.8	77

Discordant data

Footnotes:

. Analysis references: EZ6z is zircon from sample EZ6 (mount CT18-2), followed by grain number "c" or "r", meaning core or rim, respectively.

Chapter II, Section II.3

Table D.22a: Sample EZ7 (LA-1CPMS)

IGSN: IEAC00037

Coordinate UTM: Zone 29S, 735286 m E, 3683869 m N

ANALYSIS	U (ppm)	Th (ppm)	Pb (ppm)	Th/U	206Pb/208Pb		207Pb/208Pb		207Pb/205Pb		Ratios		Concordant data		Error correction	207Pb/206Pb		Ages (Ma)		206Pb/238U	σ	2 σ	Concordance (%)
					206Pb/208Pb	2 σ	207Pb/208Pb	2 σ	207Pb/205Pb	2 σ	207Pb/206Pb	σ	2 σ	207Pb/235U		σ	2 σ						
EZ71	39.33	16.36	7.31	0.420	1.71E+04	8.10E+03	0.0767	0.0037	1.660	0.081	0.1609	0.0026	0.1059	1113	48.0	96.0	993	15.5	31.0	962	7.0	14.0	97
EZ72	415.00	226.20	69.10	0.560	9.80E+04	5.10E+04	0.0629	0.0020	0.902	0.030	0.1040	0.0013	0.2148	705	34.0	68.0	653	8.0	16.0	638	4.0	8.0	98
EZ73	507.30	104.40	45.39	0.210	3.20E+05	1.00E+05	0.0690	0.0020	1.419	0.044	0.1501	0.0017	0.2286	899	30.0	18.0	897	9.0	18.0	902	5.0	10.0	101
EZ74	138.70	160.90	46.33	1.160	9.70E+04	4.50E+04	0.1206	0.0017	6.176	0.190	0.3686	0.0045	0.2144	1965	12.5	25.0	2001	13.5	27.0	2023	10.5	21.0	101
EZ75	237.80	300.70	91.80	1.260	5.40E+04	2.10E+04	0.0669	0.0025	0.847	0.037	0.1039	0.0013	0.0281	835	39.0	78.0	677	9.5	19.0	637	4.0	8.0	94
EZ76	289.10	175.20	89.60	0.610	1.66E+05	5.60E+04	0.0750	0.0023	1.849	0.061	0.1793	0.0021	0.2638	1069	31.0	62.0	1063	11.0	22.0	1063	5.5	11.0	100
EZ77	166.50	77.05	39.07	0.600	6.30E+05	2.00E+05	0.0859	0.0024	1.846	0.064	0.1807	0.0021	0.2208	1056	32.5	65.0	1062	11.5	23.0	1071	6.5	13.0	101
EZ78	319.20	277.00	146.80	0.870	4.30E+04	2.80E+04	0.0859	0.0026	1.938	0.062	0.1644	0.0021	0.2382	1336	29.5	59.0	1094	10.5	21.0	981	6.0	12.0	90
EZ79	110.30	48.30	25.17	0.440	7.20E+04	2.60E+04	0.0733	0.0025	1.793	0.064	0.1796	0.0024	0.2036	1022	34.5	69.0	1043	11.5	23.0	1065	6.5	13.0	102
EZ79	155.40	74.10	37.20	0.480	5.00E+04	2.90E+04	0.0763	0.0025	1.862	0.065	0.1778	0.0022	0.1273	1103	33.0	66.0	1068	11.5	23.0	1055	6.0	12.0	99
EZ710	148.70	195.30	93.90	1.330	8.70E+04	0.70E+04	0.0727	0.0026	1.683	0.062	0.1698	0.0023	0.0673	1006	36.5	73.0	1002	11.5	23.0	1011	6.5	13.0	101
EZ711	78.90	85.90	25.86	1.090	2.95E+04	9.70E+03	0.0621	0.0032	0.919	0.047	0.1079	0.0018	0.0475	678	55.0	110.0	662	12.5	25.0	661	5.0	10.0	100
EZ712	164.30	287.70	140.80	1.750	1.22E+05	5.10E+04	0.0738	0.0025	1.818	0.064	0.1779	0.0023	0.0674	1036	34.0	68.0	1055	11.5	23.0	1055	6.5	13.0	100
EZ713	390.10	7.58	2.68	0.020	3.10E+05	1.30E+05	0.0613	0.0020	0.964	0.033	0.1051	0.0015	0.1486	650	35.0	70.0	685	8.5	17.0	700	4.5	9.0	102
EZ714	179.70	157.50	48.40	0.880	2.60E+04	1.30E+04	0.0623	0.0023	0.906	0.035	0.1051	0.0017	0.1312	684	39.5	79.0	655	9.5	19.0	644	5.0	10.0	100
EZ715	77.40	67.33	33.10	0.870	9.40E+03	9.00E+03	0.0778	0.0029	1.914	0.075	0.1781	0.0025	0.2112	1142	37.0	74.0	1086	13.0	26.0	1057	7.0	14.0	97
EZ716	105.14	111.38	61.05	1.060	5.00E+04	1.00E+04	0.0795	0.0028	2.019	0.076	0.1921	0.0026	0.0445	1082	37.0	74.0	1122	13.0	26.0	1133	7.0	14.0	101
EZ717	385.30	154.00	75.80	0.400	2.20E+04	3.90E+04	0.0745	0.0021	1.829	0.057	0.1775	0.0021	0.0825	1055	28.5	57.0	1056	10.0	20.0	1053	5.5	11.0	100
EZ718	158.60	135.00	127.60	0.850	4.10E+04	5.70E+04	0.1194	0.0016	5.981	0.180	0.3599	0.0044	0.2674	1947	12.0	24.0	1973	13.0	26.0	1982	10.5	21.0	100
EZ719	178.10	110.20	116.30	0.630	4.30E+05	1.40E+05	0.1230	0.0014	6.494	0.200	0.3828	0.0045	0.3261	2000	10.0	20.0	2045	13.5	27.0	2089	10.5	21.0	102
EZ720	610.00	668.00	186.50	1.100	4.00E+07	1.00E+07	0.0608	0.0018	0.872	0.028	0.1033	0.0013	0.2371	631	32.0	64.0	637	7.5	15.0	634	4.0	8.0	100
EZ721	231.20	282.30	70.50	1.220	4.50E+05	4.40E+05	0.0610	0.0022	0.863	0.033	0.1000	0.0014	0.1900	639	38.0	78.0	626	9.0	18.0	614	4.0	8.0	100
EZ722	212.00	148.60	142.40	0.700	2.37E+05	7.80E+04	0.1239	0.0015	6.292	0.190	0.3689	0.0044	0.2344	2013	10.5	21.0	2017	13.0	26.0	2015	10.5	21.0	100
EZ723	152.10	115.30	115.50	0.760	3.00E+05	9.00E+05	0.1233	0.0016	6.578	0.190	0.3745	0.0047	0.2465	2005	11.5	23.0	2028	13.0	26.0	2051	11.0	22.0	101
EZ724	362.80	299.00	289.30	0.820	9.00E+06	2.00E+06	0.1272	0.0012	6.579	0.190	0.3757	0.0043	0.2858	2060	8.5	17.0	2057	12.5	25.0	2056	10.0	20.0	100
EZ725	250.30	225.40	167.00	0.900	6.60E+04	2.30E+04	0.0610	0.0022	0.870	0.033	0.1025	0.0013	-0.0723	639	39.0	78.0	636	9.0	18.0	629	4.0	8.0	99
EZ726	246.20	192.20	164.50	0.780	4.60E+05	1.60E+05	0.1069	0.0014	3.899	0.130	0.2649	0.0039	0.5827	1747	12.0	24.0	1613	13.5	27.0	1515	10.0	20.0	94
EZ727	140.90	101.20	41.10	0.720	4.80E+05	1.20E+05	0.0682	0.0025	1.323	0.050	0.1402	0.0018	-0.0007	875	38.0	76.0	856	11.0	22.0	846	5.0	10.0	99
EZ728	226.50	193.20	255.00	0.600	1.30E+07	1.70E+07	0.1752	0.0016	12.560	0.370	0.5178	0.0058	0.2879	2608	7.5	15.0	2647	14.0	28.0	2680	12.5	25.0	102
EZ729	128.10	144.60	119.90	1.150	1.80E+05	4.30E+05	0.1071	0.0019	4.071	0.130	0.2779	0.0035	0.2838	1751	16.0	32.0	1649	13.0	26.0	1581	9.0	18.0	96
EZ730	271.80	65.00	48.70	0.230	1.75E+05	7.70E+04	0.1065	0.0014	4.061	0.120	0.2779	0.0034	0.2332	1740	12.0	24.0	1647	12.0	24.0	1581	8.5	17.0	96
EZ731	151.80	66.60	21.90	0.440	1.60E+04	1.40E+04	0.0605	0.0023	0.917	0.036	0.1078	0.0015	0.0916	622	41.0	82.0	661	9.5	19.0	660	4.5	9.0	100
EZ732	304.60	122.00	163.90	0.400	9.60E+05	3.70E+05	0.1937	0.0017	13.870	0.410	0.5171	0.0064	0.4447	2774	7.0	14.0	2741	14.0	28.0	2687	13.5	27.0	98
EZ735	122.80	43.80	36.10	0.360	6.10E+04	3.90E+04	0.1116	0.0020	4.555	0.140	0.2943	0.0037	0.1228	1826	16.5	33.0	1741	13.0	26.0	1663	9.0	18.0	96
EZ736	66.50	53.10	23.82	0.800	1.23E+05	4.60E+04	0.0711	0.0034	1.409	0.070	0.1425	0.0025	0.3956	960	49.0	98.0	893	14.5	29.0	859	7.0	14.0	96
EZ737	212.30	70.90	64.00	0.330	2.00E+06	1.40E+06	0.1314	0.0017	6.771	0.210	0.3708	0.0051	0.4599	2117	11.5	23.0	2082	13.5	27.0	2033	12.0	24.0	98
EZ741	180.90	104.80	127.30	0.580	-1.80E+05	6.20E+05	0.1611	0.0017	9.703	0.290	0.4365	0.0051	0.4599	2467	9.0	18.0	2407	13.5	27.0	2385	11.5	23.0	97
EZ743	279.70	293.00	88.50	1.050	2.70E+05	1.20E+05	0.0610	0.0020	0.887	0.031	0.1060	0.0014	0.2903	639	35.5	71.0	645	8.5	17.0	650	4.0	8.0	101
EZ744	328.60	349.30	97.20	1.060	3.70E+04	2.60E+04	0.0580	0.0019	0.782	0.028	0.0977	0.0012	0.0653	530	30.0	60.0	587	8.0	16.0	601	3.5	7.0	102
EZ745	466.60	155.00	60.50	0.330	1.76E+05	8.60E+04	0.0716	0.0021	1.549	0.049	0.1569	0.0021	0.3353	975	30.0	60.0	950	10.0	20.0	940	6.0	12.0	99
EZ746	47.98	14.31	9.15	0.300	3.50E+04	1.40E+04	0.0801	0.0034	2.303	0.100	0.2115	0.0031	0.1696	1199	42.0	84.0	1213	15.5	31.0	1237	8.0	16.0	102
EZ747	206.50	163.10	47.60	0.790	4.00E+04	1.30E+04	0.0594	0.0023	0.829	0.033	0.1012	0.0014	0.1209	582	42.0	84.0	613	9.0	18.0	621	4.0	8.0	101
EZ748	175.90	406.00	501.70	2.300	5.40E+05	2.30E+05	0.1759	0.0017	11.810	0.340	0.4869	0.0057	0.2993	2615	8.0	16.0	2589	13.5	27.0	2557	12.5	25.0	99
EZ749	251.70	31.23	28.45	0.120	2.70E+05	1.10E+05	0.1121	0.0015	4.289	0.140	0.2783	0.0045	0.2893	1834	12.0	24.0	1691	13.5	27.0	1583	11.5	23.0	94
EZ750	238.20	214.30	63.50	0.900	6.70E+04	3.20E+04	0.0622	0.0023	0.873	0.033	0.1023	0.0013	0.1471	681	39.5	79.0	637	9.0	18.0	628	4.0	8.0	99
EZ751	123.50	135.80	122.50	1.100	8.10E+04	3.60E+04	0.0692	0.0018	1.159	0.041	0.1538	0.0014	0.1471	681	39.5	79.0	637	9.0	18.0	628	4.0	8.0	99
EZ752	84.00	70.50	24.85	0.840	2.24E+04	9.00E+03	0.0626	0.0026	1.037	0.044	0.1202	0.0020	0.1524	695	44.5	89.0	722	11.0	22.0	732	6.0	12.0	101
EZ753	427.00	154.80	229.20	0.360	-1.05E+06	4.20E+05	0.1254	0.0013	12.158	0.350	0.5066	0.0062	0.6036	2600	6.0	12.0	2617	13.5	27.0	2642	13.5	27.0	101
EZ754	143.30	70.45	70.90																				

ANALYSIS	U (ppm)	Th (ppm)	Pb (ppm)	Th/U	Ratios			Ages (Ma)			Concordance (%)									
					$^{207}\text{Pb}/^{206}\text{Pb}$	$^{207}\text{Pb}/^{235}\text{U}$	$^{206}\text{Pb}/^{238}\text{U}$	$^{207}\text{Pb}/^{235}\text{U}$	σ	$^{206}\text{Pb}/^{238}\text{U}$		σ								
AZR11269	64.18	44.11	13.92	0.690	-2.24E+04	8.90E+03	0.0587	0.0032	0.865	0.1071	0.0015	0.1182	556	633	12.0	24.0	656	4.5	9.0	104
AZR11271	267.70	329.00	322.00	1.230	-2.70E+04	7.10E+04	0.1203	0.0011	6.040	0.140	0.0029	0.2687	1961	8.0	16.0	2020	7.0	14.0	102	
AZR11273	95.60	51.70	15.91	0.540	-3.40E+04	2.00E+04	0.0600	0.0029	0.910	0.039	0.0016	-0.0023	604	52.5	105.0	21.0	681	4.5	9.0	104
AZR11274	147.00	250.70	68.50	1.710	1.69E+05	8.00E+04	0.0609	0.0028	0.818	0.034	0.0011	0.0318	636	49.5	99.0	19.0	604	3.0	6.0	100
AZR11275	91.80	28.80	7.23	0.310	-1.20E+04	1.00E+04	0.0576	0.0030	0.706	0.034	0.0085	0.0121	515	57.0	114.0	20.0	552	3.5	7.0	102
AZR11277	490.00	281.30	95.30	0.570	-1.80E+04	4.80E+04	0.0644	0.0022	0.934	0.026	0.0011	0.1788	755	36.0	72.0	14.0	650	3.0	6.0	97
AZR11278	46.12	33.95	10.34	0.740	-5.60E+03	4.80E+03	0.0631	0.0038	0.903	0.052	0.0015	0.1812	712	64.0	128.0	28.0	646	4.5	9.0	99
Discordant data																				
AZR11211	416.00	232.80	142.90	0.560	3.40E+06	1.40E+06	0.1273	0.0037	4.416	0.120	0.0043	0.7768	2061	25.5	51.0	22.0	1427	8.5	17.0	83
AZR11222	517.00	199.80	118.90	0.390	1.14E+05	3.00E+04	0.1427	0.0043	3.627	0.120	0.1858	0.8969	2260	26.0	52.0	26.0	1099	13.0	26.0	71
AZR11223	236.20	148.40	41.70	0.630	-3.80E+04	2.10E+04	0.0686	0.0036	0.774	0.032	0.0017	-0.2907	887	54.0	108.0	18.0	506	4.5	9.0	87
AZR11225	80.50	39.80	34.60	0.490	-6.60E+04	2.80E+04	0.1157	0.0021	4.240	0.140	0.2628	0.6608	1891	16.5	33.0	27.0	1504	11.5	23.0	89
AZR11228	208.00	54.30	19.00	0.260	-3.00E+04	1.40E+04	0.0715	0.0029	0.929	0.033	0.0934	0.1033	972	41.5	83.0	17.0	576	3.0	6.0	86
AZR11238	1025.00	396.00	152.00	0.390	5.70E+04	2.50E+04	0.1180	0.0035	2.454	0.064	0.1501	0.7830	1926	26.5	53.0	19.0	902	5.5	11.0	72
AZR11251	2436.00	1717.00	377.00	0.700	4.39E+02	3.80E+01	0.0936	0.0037	0.899	0.027	0.0697	0.0054	1500	37.5	75.0	14.0	434	3.5	7.0	67
AZR11255	415.00	248.00	97.70	0.600	1.71E+04	7.90E+03	0.0874	0.0034	1.125	0.034	0.0931	-0.2467	1369	37.5	75.0	16.0	574	3.5	7.0	75
AZR11270	223.50	275.00	60.60	1.230	-1.60E+04	1.50E+04	0.0789	0.0030	0.853	0.028	0.0790	0.1945	1170	37.5	75.0	15.0	490	5.0	10.0	78
AZR11272	318.00	170.80	60.70	0.540	-1.10E+04	2.80E+04	0.0748	0.0028	1.121	0.034	0.1075	-0.0721	1063	37.5	75.0	16.0	658	3.0	6.0	86
AZR11276	303.00	473.00	450.00	1.560	6.00E+04	7.40E+04	0.1353	0.0021	5.270	0.160	0.2876	0.8885	2168	13.5	27.0	28.0	1630	15.0	30.0	87

Footnotes:

. Analysis references: AZR11z is zircon from sample AZR11 (mounts CT18-11 and CT19-1), followed by grain number.

Chapter II, Section II.3

Table D.25: Sample AZR10 (LA-ICP/MS)

IGSN: IEAC00029

Coordinate UTM: Zone 30S, 233758 m E, 36333628 m N

ANALYSIS	U (ppm)	Th (ppm)	Pb (ppm)	Th/U	Ratios				Concordant data				Error correction				Ages (Ma)				Concordance (%)		
					$^{206}\text{Pb}/^{208}\text{Pb}$	$^{207}\text{Pb}/^{208}\text{Pb}$	$^{207}\text{Pb}/^{235}\text{U}$	$^{206}\text{Pb}/^{235}\text{U}$	2σ	$^{207}\text{Pb}/^{235}\text{U}$	2σ	$^{206}\text{Pb}/^{235}\text{U}$	2σ	2 σ	$^{207}\text{Pb}/^{235}\text{U}$	σ	2σ	$^{206}\text{Pb}/^{238}\text{U}$	σ	2σ			
					2σ	2σ	2σ	2σ	2σ	2σ	2σ	2σ	2σ	2σ	2σ	2σ	2σ	2σ	2σ	2σ			
AZR1021	1166.00	234.20	72.50	0.200	1.14E+05	6.80E+04	0.0639	0.0016	0.721	0.012	0.0819	0.0008	0.0569	738.0	26.5	53.0	551.0	3.5	7.0	508.0	2.5	5.0	92
AZR1022	487.20	96.20	23.31	0.200	-2.30E+04	2.50E+04	0.0572	0.0017	0.666	0.017	0.0845	0.0009	0.0609	499.0	32.5	65.0	518.0	5.0	10.0	523.0	2.5	5.0	101
AZR1023	1074.20	226.30	47.88	0.210	1.03E+05	3.40E+04	0.0596	0.0014	0.639	0.011	0.0792	0.0010	0.0362	590.0	25.5	51.0	502.0	3.5	7.0	491.0	3.0	6.0	98
AZR1024	936.00	210.00	58.50	0.220	7.00E+04	2.80E+04	0.0619	0.0016	0.699	0.013	0.0820	0.0009	0.0262	671.0	27.5	55.0	538.0	4.0	8.0	508.0	2.5	5.0	94
AZR1025	266.10	104.30	27.94	0.390	-2.30E+04	1.80E+04	0.0585	0.0022	0.783	0.025	0.0958	0.0011	0.0627	582.0	40.0	80.0	537.0	7.0	14.0	590.0	3.0	6.0	100
AZR1026	416.80	162.40	40.42	0.390	-3.60E+04	2.90E+04	0.0585	0.0017	0.690	0.013	0.0854	0.0010	0.0131	549.0	31.5	63.0	533.0	5.0	10.0	528.0	3.0	6.0	99
AZR1027	465.00	222.90	56.30	0.480	-1.00E+03	2.50E+04	0.0586	0.0018	0.707	0.018	0.0879	0.0009	0.0450	552.0	33.5	67.0	543.0	5.5	11.0	543.0	2.5	5.0	100
AZR1028	1093.00	196.40	46.60	0.180	-3.00E+04	5.50E+04	0.0588	0.0015	0.692	0.013	0.0862	0.0009	0.1041	560.0	26.0	56.0	534.0	4.0	8.0	533.0	2.5	5.0	100
AZR1029	781.00	172.90	41.60	0.220	8.00E+04	4.30E+04	0.0589	0.0015	0.690	0.013	0.0851	0.0009	0.1317	563.0	27.5	55.0	533.0	4.0	8.0	526.0	2.5	5.0	99
AZR10211	771.00	218.60	56.20	0.280	-1.37E+05	6.40E+04	0.0593	0.0015	0.745	0.013	0.0923	0.0009	0.1155	578.0	27.5	55.0	565.0	4.0	8.0	569.0	2.5	5.0	101
AZR10212	668.00	170.10	49.60	0.250	-4.20E+04	4.60E+04	0.0636	0.0017	0.758	0.014	0.0871	0.0010	0.0164	728.0	28.5	57.0	573.0	4.0	8.0	538.0	3.0	6.0	94
AZR10213	602.10	108.10	26.95	0.180	2.00E+04	2.90E+04	0.0679	0.0016	0.687	0.015	0.0856	0.0009	0.1014	526.0	30.5	61.0	491.0	4.5	9.0	530.0	2.5	5.0	100
AZR10214	1089.00	190.10	41.70	0.170	2.80E+04	3.90E+04	0.0575	0.0015	0.633	0.012	0.0765	0.0014	0.5479	620.0	27.0	54.0	498.0	3.5	7.0	475.0	4.0	8.0	95
AZR10215	1082.00	261.30	64.40	0.240	-1.56E+05	8.70E+04	0.0584	0.0014	0.697	0.013	0.0866	0.0008	0.0115	620.0	27.0	54.0	537.0	4.0	8.0	535.0	2.5	5.0	100
AZR10216	961.10	193.20	53.10	0.200	3.00E+04	4.00E+04	0.0626	0.0016	0.718	0.012	0.0832	0.0008	0.0115	695.0	26.0	52.0	549.0	3.5	7.0	515.0	2.5	5.0	94
AZR10217	711.50	289.50	81.00	0.410	-7.70E+04	4.50E+04	0.0590	0.0016	0.767	0.016	0.0942	0.0010	0.0624	567.0	29.5	59.0	578.0	4.5	9.0	580.0	3.0	6.0	100
AZR10218	665.00	154.80	38.97	0.230	1.10E+04	3.10E+04	0.0578	0.0017	0.692	0.015	0.0846	0.0008	0.0290	522.0	32.5	65.0	534.0	4.5	9.0	540.0	2.5	5.0	101
AZR10219	805.90	152.80	37.64	0.190	1.40E+04	4.20E+04	0.0579	0.0015	0.673	0.013	0.0846	0.0008	0.2104	526.0	28.5	57.0	523.0	4.0	8.0	523.0	2.5	5.0	100
AZR10220	539.20	129.40	32.28	0.240	1.00E+04	3.10E+04	0.0580	0.0016	0.696	0.015	0.0855	0.0009	0.0208	530.0	32.0	64.0	528.0	4.5	9.0	529.0	2.5	5.0	100
AZR10221	340.70	168.50	40.13	0.490	-4.80E+04	2.00E+04	0.0574	0.0019	0.661	0.018	0.0843	0.0009	0.0284	507.0	36.5	73.0	515.0	5.5	11.0	522.0	3.0	6.0	101
AZR10222	735.00	122.80	30.82	0.170	-9.95E+04	4.50E+04	0.0607	0.0017	0.698	0.016	0.0835	0.0009	0.2814	629.0	30.0	60.0	538.0	5.0	10.0	517.0	2.5	5.0	96
AZR10223	986.90	186.50	46.10	0.190	-1.14E+05	7.80E+04	0.0582	0.0014	0.685	0.011	0.0854	0.0008	0.1350	639.0	26.5	53.0	530.0	3.5	7.0	529.0	2.5	5.0	100
AZR10225	261.60	173.80	45.82	0.660	-5.00E+04	1.60E+04	0.0624	0.0021	0.801	0.024	0.0943	0.0011	0.1080	668.0	36.0	72.0	597.0	7.0	14.0	581.0	3.0	6.0	97
AZR10226	757.40	193.40	48.76	0.260	1.30E+04	3.70E+04	0.0584	0.0016	0.696	0.014	0.0863	0.0008	0.0286	545.0	30.0	60.0	576.0	4.0	8.0	534.0	2.5	5.0	100
AZR10227	340.30	160.00	40.90	0.470	-1.30E+04	1.60E+04	0.0594	0.0020	0.755	0.020	0.0918	0.0010	0.0623	582.0	36.5	73.0	531.0	6.0	12.0	566.0	3.0	6.0	99
AZR10230	598.00	131.50	35.30	0.340	-1.70E+04	2.00E+04	0.0589	0.0019	0.740	0.019	0.0908	0.0010	0.1585	596.0	34.5	69.0	562.0	5.5	11.0	560.0	3.0	6.0	100
AZR10238	598.00	147.20	39.10	0.250	-5.00E+04	3.30E+04	0.0599	0.0018	0.699	0.016	0.0852	0.0009	0.1817	600.0	32.5	65.0	538.0	5.0	10.0	527.0	2.5	5.0	98
AZR10239	371.00	73.20	15.85	0.200	1.00E+03	1.80E+04	0.0573	0.0019	0.659	0.019	0.0838	0.0012	0.2276	503.0	36.5	73.0	514.0	6.0	12.0	519.0	3.5	7.0	101
AZR10241	848.40	177.96	43.98	0.210	-7.00E+04	4.90E+04	0.0602	0.0015	0.647	0.011	0.0778	0.0008	0.0356	611.0	27.0	54.0	507.0	3.5	7.0	483.0	2.5	5.0	95
AZR10243	1210.00	343.00	81.50	0.280	5.40E+04	2.40E+04	0.0616	0.0014	0.673	0.011	0.0794	0.0010	0.4273	660.0	24.5	49.0	523.0	3.5	7.0	492.0	3.0	6.0	94
AZR10244	883.00	213.40	83.50	0.370	-1.10E+04	4.50E+04	0.0600	0.0015	0.769	0.013	0.0935	0.0009	0.1392	694.0	27.0	54.0	579.0	3.5	7.0	576.0	2.5	5.0	99
AZR10245	826.30	164.20	38.18	0.200	-1.60E+04	4.60E+04	0.0619	0.0015	0.689	0.012	0.0821	0.0010	0.3892	671.0	26.0	52.0	592.0	3.5	7.0	509.0	3.0	6.0	96
AZR10246	830.00	302.30	82.50	0.600	-3.70E+04	2.40E+04	0.0591	0.0016	0.771	0.016	0.0948	0.0010	0.1013	571.0	29.5	59.0	580.0	4.5	9.0	584.0	3.0	6.0	101
AZR10247	161.60	157.00	39.28	0.190	-1.30E+04	4.70E+04	0.0584	0.0015	0.696	0.014	0.0860	0.0009	0.0717	545.0	28.0	56.0	536.0	4.0	8.0	532.0	2.5	5.0	99
AZR10248	903.00	224.00	51.59	0.250	1.60E+04	5.00E+04	0.0580	0.0015	0.668	0.014	0.0839	0.0008	0.1604	530.0	28.5	57.0	519.0	4.0	8.0	519.0	2.5	5.0	100
AZR10249	542.90	201.30	54.10	0.370	-2.20E+05	2.60E+05	0.0592	0.0018	0.762	0.019	0.0932	0.0009	0.0581	574.0	33.0	66.0	575.0	5.5	11.0	574.0	3.0	6.0	100
AZR10242	1251.00	341.60	72.90	0.270	7.00E+04	2.10E+04	0.0602	0.0019	0.768	0.020	0.0925	0.0011	0.1266	611.0	34.0	68.0	579.0	5.5	11.0	571.0	3.0	6.0	99
AZR10243	826.30	164.20	38.18	0.200	-1.60E+04	3.90E+04	0.0582	0.0015	0.675	0.014	0.0839	0.0008	0.0578	537.0	28.5	56.0	524.0	4.0	8.0	479.0	2.5	5.0	96
AZR10245	830.00	160.20	35.40	0.190	-2.70E+04	3.70E+04	0.0599	0.0016	0.648	0.015	0.0789	0.0012	0.4060	590.0	29.0	58.0	507.0	4.5	9.0	490.0	3.5	7.0	97
AZR10246	631.00	691.00	190.60	0.910	4.00E+04	4.80E+04	0.0598	0.0015	0.791	0.014	0.0957	0.0009	0.1956	606.0	27.0	54.0	592.0	4.0	8.0	589.0	3.0	6.0	100
AZR10247	621.30	120.90	32.74	0.190	-8.80E+04	4.50E+04	0.0617	0.0018	0.718	0.018	0.0845	0.0008	0.1590	664.0	31.0	62.0	549.0	5.0	10.0	523.0	2.5	5.0	95
AZR10248	787.00	154.70	39.07	0.200	-4.10E+04	4.70E+04	0.0576	0.0015	0.679	0.013	0.0858	0.0009	0.1266	515.0	28.5	57.0	526.0	4.0	8.0	520.0	2.5	5.0	101
AZR10249	719.00	125.20	29.57	0.170	-2.10E+04	3.50E+04	0.0575	0.0016	0.672	0.014	0.0848	0.0009	0.1467	511.0	30.5	61.0	522.0	4.0	8.0	525.0	2.5	5.0	101
AZR10250	798.00	196.00	48.40	0.250	-3.00E+04	4.40E+04	0.0608	0.0016	0.686	0.014	0.0846	0.0009	0.3030	632.0	28.5	57.0	544.0	4.0	8.0	523.0	2.5	5.0	96
AZR10251	671.80	135.30	35.03	0.200	-7.60E+04	4.40E+04	0.0583	0.0016	0.686	0.015	0.0860	0.0009	0.2247	541.0	30.0	60.0	530.0	4.5	9.0	532.0	2.5	5.0	100
AZR10252	490.50	140.50	37.10	0.290	-5.70E+05	4.00E+05	0.0593	0.0019	0.724	0.019	0.0876	0.0009	0.0971	507.0	30.5	61.0	536.0	4.5	9.0	541.0	2.5	5.0	101
AZR10254	480.50	167.50	68.60	0.490	-5.20E+04	3.70E+04	0.0574																

ANALYSIS	U (ppm)	Th (ppm)	Pb (ppm)	ThU	Ratios				Ages (Ma)				Concordance (%)										
					²⁰⁷ Pb/ ²⁰⁶ Pb	²⁰⁷ Pb/ ²³⁵ U	²⁰⁷ Pb/ ²³⁸ U	²⁰⁶ Pb/ ²³⁸ U	σ	2σ	σ	2σ		σ	2σ								
AZR10272	544.10	198.50	51.81	0.360	6.00E+04	3.10E+04	0.0596	0.0017	0.749	0.016	0.0909	0.0009	0.1250	589.0	31.0	62.0	568.0	4.5	9.0	561.0	2.5	5.0	99
AZR10273	416.00	168.80	62.90	0.410	1.00E+05	2.20E+04	0.0732	0.0038	0.968	0.046	0.0975	0.0011	0.1250	589.0	31.0	62.0	568.0	4.5	9.0	561.0	2.5	5.0	99
AZR10274	749.00	142.20	36.80	0.190	8.20E+04	5.20E+04	0.0578	0.0016	0.682	0.014	0.0853	0.0009	0.1250	589.0	31.0	62.0	568.0	4.5	9.0	561.0	2.5	5.0	99
AZR10275	1099.00	354.00	88.00	0.470	4.90E+04	4.00E+04	0.0604	0.0018	0.682	0.016	0.0814	0.0009	0.1250	589.0	31.0	62.0	568.0	4.5	9.0	561.0	2.5	5.0	99
AZR10276	571.00	114.50	30.36	0.200	7.50E+04	6.00E+04	0.0596	0.0016	0.712	0.015	0.0864	0.0009	0.1250	589.0	31.0	62.0	568.0	4.5	9.0	561.0	2.5	5.0	99
AZR10277	988.00	208.30	50.40	0.210	4.90E+04	5.60E+04	0.0603	0.0015	0.644	0.016	0.0783	0.0017	0.1250	589.0	31.0	62.0	568.0	4.5	9.0	561.0	2.5	5.0	99
AZR10278	262.60	79.10	22.21	0.300	4.00E+04	1.70E+04	0.0609	0.0019	0.789	0.020	0.0938	0.0011	0.1250	589.0	31.0	62.0	568.0	4.5	9.0	561.0	2.5	5.0	99
AZR10279	458.00	148.10	40.93	0.320	4.80E+04	3.20E+04	0.0585	0.0019	0.613	0.015	0.0754	0.0010	0.1250	589.0	31.0	62.0	568.0	4.5	9.0	561.0	2.5	5.0	99
AZR10280	507.00	170.40	40.90	0.340	5.40E+04	3.10E+04	0.0598	0.0017	0.680	0.015	0.0847	0.0009	0.1250	589.0	31.0	62.0	568.0	4.5	9.0	561.0	2.5	5.0	99
AZR10281	732.00	147.40	43.86	0.240	2.60E+04	4.60E+04	0.0592	0.0017	0.714	0.015	0.0871	0.0009	0.1250	589.0	31.0	62.0	568.0	4.5	9.0	561.0	2.5	5.0	99
AZR10282	492.80	147.60	39.42	0.230	3.00E+04	2.30E+04	0.0586	0.0017	0.747	0.017	0.0924	0.0010	0.1250	589.0	31.0	62.0	568.0	4.5	9.0	561.0	2.5	5.0	99
AZR10284	990.10	288.50	68.10	0.290	5.60E+04	5.40E+04	0.0587	0.0014	0.686	0.011	0.0844	0.0009	0.1250	589.0	31.0	62.0	568.0	4.5	9.0	561.0	2.5	5.0	99
AZR10287	1388.00	391.90	86.80	0.280	9.10E+04	7.50E+04	0.0578	0.0014	0.647	0.010	0.0812	0.0011	0.1250	589.0	31.0	62.0	568.0	4.5	9.0	561.0	2.5	5.0	99
AZR10288	228.20	84.00	22.48	0.370	4.70E+04	2.10E+04	0.0595	0.0022	0.770	0.025	0.0937	0.0010	0.1250	589.0	31.0	62.0	568.0	4.5	9.0	561.0	2.5	5.0	99
AZR10289	1102.00	262.90	68.90	0.240	1.20E+05	7.20E+04	0.0609	0.0014	0.720	0.019	0.0861	0.0009	0.1250	589.0	31.0	62.0	568.0	4.5	9.0	561.0	2.5	5.0	99
AZR10290	215.00	111.90	30.18	0.520	1.90E+04	1.60E+04	0.0598	0.0025	0.784	0.029	0.0949	0.0012	0.1250	589.0	31.0	62.0	568.0	4.5	9.0	561.0	2.5	5.0	99
AZR10291	332.00	325.00	90.50	0.980	3.10E+04	3.00E+04	0.0593	0.0019	0.829	0.021	0.1012	0.0011	0.1250	589.0	31.0	62.0	568.0	4.5	9.0	561.0	2.5	5.0	99
AZR10292	973.00	328.70	84.00	0.340	7.80E+04	6.90E+04	0.0596	0.0015	0.726	0.013	0.0882	0.0009	0.1250	589.0	31.0	62.0	568.0	4.5	9.0	561.0	2.5	5.0	99
AZR10294	458.30	99.10	25.03	0.220	7.90E+04	3.40E+04	0.0576	0.0017	0.690	0.011	0.0868	0.0009	0.1250	589.0	31.0	62.0	568.0	4.5	9.0	561.0	2.5	5.0	99
AZR10295	1316.00	294.80	75.20	0.220	1.80E+05	1.80E+05	0.0602	0.0014	0.687	0.011	0.0835	0.0010	0.1250	589.0	31.0	62.0	568.0	4.5	9.0	561.0	2.5	5.0	99
AZR10298	237.60	138.20	37.57	0.580	2.40E+04	1.90E+04	0.0616	0.0024	0.778	0.026	0.0913	0.0012	0.1250	589.0	31.0	62.0	568.0	4.5	9.0	561.0	2.5	5.0	99
AZR10299	1228.00	353.00	81.70	0.290	8.00E+04	2.70E+04	0.0610	0.0015	0.662	0.013	0.0795	0.0011	0.1250	589.0	31.0	62.0	568.0	4.5	9.0	561.0	2.5	5.0	99
AZR10300	382.40	153.72	38.11	0.400	4.80E+04	1.60E+04	0.0602	0.0019	0.697	0.018	0.0852	0.0009	0.1250	589.0	31.0	62.0	568.0	4.5	9.0	561.0	2.5	5.0	99
AZR10302	551.00	216.90	57.60	0.390	1.00E+05	3.30E+04	0.0584	0.0017	0.743	0.017	0.0924	0.0009	0.1250	589.0	31.0	62.0	568.0	4.5	9.0	561.0	2.5	5.0	99
AZR10303	1150.00	579.00	146.90	0.500	1.80E+04	6.90E+04	0.0625	0.0015	0.747	0.013	0.0871	0.0013	0.1250	589.0	31.0	62.0	568.0	4.5	9.0	561.0	2.5	5.0	99
AZR10304	1279.00	299.30	70.20	0.230	1.90E+04	4.50E+04	0.0580	0.0013	0.667	0.009	0.0834	0.0008	0.1250	589.0	31.0	62.0	568.0	4.5	9.0	561.0	2.5	5.0	99
AZR10306	473.00	842.00	262.40	1.780	1.18E+05	5.00E+04	0.0620	0.0018	0.926	0.021	0.1093	0.0011	0.1250	589.0	31.0	62.0	568.0	4.5	9.0	561.0	2.5	5.0	99
AZR10307	830.00	175.40	46.30	0.210	4.30E+04	4.30E+04	0.0605	0.0015	0.688	0.012	0.0826	0.0008	0.1250	589.0	31.0	62.0	568.0	4.5	9.0	561.0	2.5	5.0	99
AZR10310	442.60	92.46	22.68	0.210	7.00E+04	2.20E+04	0.0590	0.0020	0.687	0.014	0.0844	0.0009	0.1250	589.0	31.0	62.0	568.0	4.5	9.0	561.0	2.5	5.0	99
AZR10311	962.00	302.80	66.80	0.310	8.60E+04	3.70E+04	0.0594	0.0016	0.626	0.018	0.0770	0.0008	0.1250	589.0	31.0	62.0	568.0	4.5	9.0	561.0	2.5	5.0	99
AZR10312	1255.00	304.00	58.80	0.240	5.90E+04	3.50E+04	0.0610	0.0015	0.607	0.010	0.0720	0.0008	0.1250	589.0	31.0	62.0	568.0	4.5	9.0	561.0	2.5	5.0	99
AZR103112	513.00	262.00	67.50	0.310	3.00E+05	1.60E+05	0.0583	0.0017	0.710	0.017	0.0880	0.0010	0.1250	589.0	31.0	62.0	568.0	4.5	9.0	561.0	2.5	5.0	99
AZR103113	863.00	229.80	61.60	0.270	4.00E+04	4.00E+04	0.0620	0.0016	0.714	0.014	0.0838	0.0010	0.1250	589.0	31.0	62.0	568.0	4.5	9.0	561.0	2.5	5.0	99
AZR103114	1536.00	471.00	100.80	0.310	8.60E+04	4.00E+04	0.0637	0.0015	0.666	0.011	0.0779	0.0010	0.1250	589.0	31.0	62.0	568.0	4.5	9.0	561.0	2.5	5.0	99
AZR103117	1345.00	421.00	79.90	0.310	5.00E+04	6.60E+04	0.0601	0.0014	0.663	0.013	0.0805	0.0010	0.1250	589.0	31.0	62.0	568.0	4.5	9.0	561.0	2.5	5.0	99
AZR103118	863.00	374.00	108.80	0.430	1.40E+04	6.30E+04	0.0603	0.0014	0.793	0.012	0.0963	0.0010	0.1250	589.0	31.0	62.0	568.0	4.5	9.0	561.0	2.5	5.0	99
AZR103119	1043.00	267.50	74.30	0.260	1.00E+06	2.50E+06	0.0660	0.0017	0.755	0.013	0.0983	0.0009	0.1250	589.0	31.0	62.0	568.0	4.5	9.0	561.0	2.5	5.0	99
AZR103120	922.00	208.00	49.80	0.230	1.10E+06	1.80E+06	0.0599	0.0016	0.679	0.014	0.0820	0.0011	0.1250	589.0	31.0	62.0	568.0	4.5	9.0	561.0	2.5	5.0	99
Discordant data																							
AZR1028	2415.00	352.00	68.70	0.150	6.00E+04	3.50E+04	0.0668	0.0016	0.329	0.006	0.0365	0.0007	0.4792	832.0	25.0	50.0	289.0	2.5	5.0	231.0	2.0	4.0	80
AZR10224	416.00	168.80	62.90	0.410	1.00E+05	2.20E+04	0.0732	0.0038	0.968	0.046	0.0975	0.0011	0.1250	589.0	31.0	62.0	568.0	4.5	9.0	561.0	2.5	5.0	99
AZR10229	1807.00	671.00	98.20	0.370	9.60E+04	2.80E+04	0.0678	0.0016	0.508	0.010	0.0545	0.0009	0.1250	589.0	31.0	62.0	568.0	4.5	9.0	561.0	2.5	5.0	99
AZR10236	1099.00	366.00	82.70	0.330	3.24E+04	9.00E+03	0.0693	0.0017	0.676	0.011	0.0713	0.0011	0.1250	589.0	31.0	62.0	568.0	4.5	9.0	561.0	2.5	5.0	99
AZR10244	2517.00	737.00	90.70	0.290	3.28E+04	4.90E+03	0.0735	0.0018	0.338	0.006	0.0338	0.0006	0.4840	1028.0	25.0	50.0	295.0	2.5	5.0	215.0	2.0	4.0	73
AZR10253	2764.00	1727.00	244.00	0.620	9.50E+04	2.80E+04	0.0789	0.0020	0.406	0.006	0.0376	0.0006	0.2488	1170.0	25.0	50.0	346.0	2.0	4.0	238.0	2.0	4.0	69
AZR10255	1802.00	349.00	51.60	0.190	4.20E+04	1.30E+04	0.0615	0.0016	0.374	0.007	0.0437	0.0005	0.2751	657.0	28.0	56.0	323.0	2.5	5.0	276.0	1.5	3.0	85
AZR10261	1082.00	272.80	80.30	0.250	7.90E+04	2.40E+04	0.0679	0.0025	0.676	0.011	0.0572	0.0011	0.0461	1369.0	27.5	55.0	524.0	3.5	7.0	359.0	3.5	7.0	86
AZR10262	1380.00	259.00	47.50	0.190	1.84E+05	6.70E+04	0.0679	0.0023	0.497	0.034	0.0572	0.0045	0.9320	866.0	35.0	70.0	410.0	11.5	23.0	359.0	13.5	27.0	88
AZR10264	1124.00	341.00	96.40	0.300	8.10E+04	3.90E+04	0.0778	0.0019	0.750	0.012	0.0705	0.0008	0.1108	1142.0	24.5	49.0	568.0	3.5	7.0	439.0	2.5	5.0	77
AZR10275	1534.00	619.00	91.00	0.400	4.50E+04	7.90E+04	0.0704	0.0017	0.545	0.012	0.0571	0.0010	0.5358	940.0	24.5	4							

Chapter II, Section II.3

Table D.26a: Sample AZR1 (LA-ICP/MS)

IGSN: IEACC0023

Coordinate UTM: Zone 30S, 295882 m E, 3705386 m N

ANALYSIS	U (ppm)	Th (ppm)	Pb (ppm)	Th/U	Ratios				Concordant data				Ages (Ma)				Concordance (%)						
					²⁰⁶ Pb/ ²⁰⁸ Pb	²⁰⁷ Pb/ ²⁰⁸ Pb	²⁰⁷ Pb/ ²³⁵ U	²⁰⁷ Pb/ ²³⁸ U	2σ	2σ	2σ	2σ	σ	σ	2σ	2σ		σ	σ				
					2σ	2σ	2σ	2σ	2σ	2σ	2σ	2σ	σ	σ	2σ	2σ		σ	σ				
AZR1Z1	628.20	408.20	106.70	0.650	3.50E+04	3.30E+04	0.0595	0.0016	0.778	0.017	0.0948	0.0010	0.1168	585.0	29.0	58.0	584.0	5.0	10.0	584.0	3.0	6.0	100
AZR1Z2	302.50	241.50	71.30	0.800	-3.10E+04	1.80E+04	0.0604	0.0019	0.877	0.023	0.1053	0.0011	0.1285	618.0	34.0	68.0	639.0	6.0	12.0	645.0	3.0	6.0	101
AZR1Z3	935.00	763.00	242.30	1.900	-4.70E+04	2.50E+04	0.0632	0.0019	0.948	0.023	0.1093	0.0012	0.2528	715.0	32.0	64.0	677.0	6.0	12.0	669.0	3.5	7.0	99
AZR1Z5	403.00	1066.00	586.20	1.140	-6.50E+04	9.70E+04	0.0766	0.0016	2.026	0.025	0.1921	0.0018	0.2834	1111.0	21.0	42.0	1124.0	4.0	8.0	1133.0	5.0	10.0	101
AZR1Z6	724.00	507.00	100.90	0.700	-2.20E+04	3.50E+04	0.0637	0.0017	0.752	0.014	0.0861	0.0014	-0.0314	732.0	28.5	57.0	569.0	4.0	8.0	592.0	3.0	6.0	94
AZR1Z7	371.60	188.00	173.80	0.510	-5.30E+04	5.60E+04	0.1324	0.0037	7.040	0.100	0.3884	0.0049	0.7220	2130.0	24.5	49.0	2116.0	6.5	13.0	2115.0	11.5	23.0	100
AZR1Z8	218.00	387.00	145.7	0.500	3.50E+03	5.20E+03	0.0601	0.0030	0.756	0.034	0.0916	0.0013	-0.0738	607.0	54.0	108.0	572.0	10.0	20.0	565.0	4.0	8.0	99
AZR1Z9	116.00	192.30	58.50	0.540	-8.00E+04	1.90E+04	0.0644	0.0020	0.896	0.024	0.1076	0.0011	0.1956	755.0	33.0	66.0	650.0	6.5	13.0	616.0	3.5	7.0	95
AZR1Z10	354.60	192.30	58.50	0.540	8.00E+04	1.90E+04	0.0617	0.0020	0.826	0.024	0.1076	0.0011	-0.0375	664.0	34.5	69.0	666.0	6.5	13.0	659.0	3.0	6.0	99
AZR1Z11	193.20	227.80	61.30	1.180	-9.00E+04	1.00E+04	0.0615	0.0023	0.635	0.026	0.0982	0.0012	0.1047	657.0	40.0	80.0	616.0	7.0	14.0	604.0	3.5	7.0	98
AZR1Z12	577.00	399.50	413.60	0.690	3.00E+05	1.70E+05	0.1264	0.0034	6.894	0.064	0.3938	0.0039	0.4249	2048.0	24.0	48.0	2098.0	4.0	8.0	2140.0	9.0	18.0	102
AZR1Z13	539.30	583.80	563.80	1.090	1.00E+06	1.20E+05	0.1296	0.0035	6.766	0.059	0.3786	0.0033	0.3180	2093.0	23.5	47.0	2081.0	4.0	8.0	2070.0	7.5	15.0	99
AZR1Z14	78.10	129.80	164.00	1.600	-1.60E+04	1.80E+04	0.1984	0.0059	12.930	0.200	0.4688	0.0056	0.4128	2813.0	24.5	49.0	2675.0	7.5	15.0	2478.0	12.5	25.0	93
AZR1Z15	436.00	792.00	298.00	1.820	-1.90E+04	2.98E+04	0.0665	0.0018	1.231	0.023	0.1357	0.0013	0.0583	822.0	28.5	57.0	815.0	5.0	10.0	820.0	3.5	7.0	101
AZR1Z16	369.60	315.50	326.00	0.850	-8.40E+04	8.10E+04	0.1491	0.0041	8.513	0.094	0.4146	0.0040	0.4703	2336.0	23.5	47.0	2287.0	5.0	10.0	2236.0	9.0	18.0	102
AZR1Z17	555.00	434.50	539.00	0.780	-1.80E+05	1.60E+05	0.1759	0.0047	12.020	0.110	0.4930	0.0047	0.5244	2615.0	22.0	44.0	2606.0	4.5	9.0	2584.0	10.0	20.0	99
AZR1Z18	261.60	363.10	81.40	1.390	-8.00E+04	1.20E+04	0.0655	0.0024	0.804	0.025	0.0895	0.0012	-0.0458	790.0	38.5	77.0	599.0	7.0	14.0	552.0	3.5	7.0	92
AZR1Z19	526.80	679.00	197.80	1.290	1.30E+04	3.20E+04	0.0597	0.0017	0.838	0.017	0.1021	0.0010	-0.0321	593.0	31.0	62.0	618.0	4.5	9.0	627.0	3.0	6.0	101
AZR1Z20	661.50	100.90	163.50	0.180	-2.70E+05	2.30E+05	0.2751	0.0073	24.630	0.180	0.6496	0.0068	0.4898	3335.0	21.0	42.0	3294.0	3.5	7.0	3227.0	11.5	23.0	98
AZR1Z21	813.40	767.90	702.60	0.940	1.20E+05	1.60E+05	0.1149	0.0031	5.319	0.048	0.3356	0.0030	0.2295	1878.0	24.5	49.0	1872.0	4.0	8.0	1865.0	7.0	14.0	100
AZR1Z22	117.90	52.77	57.40	0.450	-5.00E+04	2.10E+04	0.1339	0.0041	7.620	0.120	0.4115	0.0042	0.0991	2150.0	26.5	53.0	2107.0	7.0	14.0	2222.0	9.5	19.0	102
AZR1Z23	226.90	100.50	29.17	0.440	5.00E+04	1.0E+04	0.0604	0.0022	0.815	0.025	0.0982	0.0012	0.1338	618.0	38.5	79.0	605.0	7.0	14.0	604.0	3.5	7.0	100
AZR1Z24	292.60	162.70	201.70	0.560	-3.40E+04	7.70E+04	0.1792	0.0049	12.270	0.120	0.4982	0.0049	0.3734	2645.0	22.5	45.0	2625.0	4.5	9.0	2610.0	10.5	21.0	99
AZR1Z25	85.57	308.50	79.50	3.610	-5.60E+03	4.40E+03	0.0555	0.0038	0.956	0.044	0.0902	0.0013	-0.0165	432.0	76.5	153.0	536.0	13.0	26.0	557.0	4.0	8.0	104
AZR1Z26	275.80	315.00	96.70	1.140	8.00E+04	1.30E+04	0.0631	0.0022	0.890	0.027	0.1095	0.0012	-0.0499	712.0	37.0	74.0	678.0	7.0	14.0	670.0	3.5	7.0	99
AZR1Z27	124.40	56.40	17.42	0.450	-1.41E+04	7.90E+03	0.0614	0.0029	0.963	0.038	0.1073	0.0015	0.0307	653.0	50.5	101.0	653.0	10.0	20.0	657.0	4.5	9.0	101
AZR1Z28	141.80	87.70	31.16	0.580	-1.20E+04	7.40E+03	0.0612	0.0026	0.794	0.030	0.0949	0.0012	0.0307	646.0	45.5	91.0	593.0	8.5	17.0	584.0	3.5	7.0	98
AZR1Z29	439.80	528.00	585.80	1.270	1.25E+05	9.90E+04	0.1302	0.0036	7.206	0.067	0.4012	0.0038	0.1928	2101.0	24.5	49.0	2137.0	4.0	8.0	2175.0	8.5	17.0	102
AZR1Z30	519.90	348.00	498.50	0.630	3.00E+05	2.00E+05	0.2315	0.0062	17.840	0.240	0.5604	0.0075	0.8327	3062.0	21.5	43.0	2981.0	6.5	13.0	2663.0	15.5	31.0	96
AZR1Z31	341.80	246.70	72.70	0.720	-2.10E+04	2.00E+04	0.0600	0.0020	0.639	0.024	0.1016	0.0011	-0.0499	604.0	36.0	72.0	619.0	6.5	13.0	624.0	3.0	6.0	101
AZR1Z32	644.00	94.90	33.13	0.150	4.00E+04	4.10E+04	0.0648	0.0016	1.229	0.019	0.1371	0.0014	0.0573	768.0	52.0	104.0	814.0	4.5	9.0	828.0	4.0	8.0	92
AZR1Z33	591.00	199.50	302.00	1.850	-3.80E+04	3.10E+04	0.0614	0.0016	0.836	0.016	0.0988	0.0012	0.2571	653.0	28.0	56.0	617.0	4.5	9.0	607.0	3.5	7.0	98
AZR1Z34	154.80	87.73	53.94	0.570	-4.00E+04	1.90E+04	0.0884	0.0025	2.958	0.061	0.2443	0.0028	0.1048	1391.0	27.0	54.0	1367.0	8.0	16.0	1409.0	7.5	15.0	101
AZR1Z35	103.91	50.99	19.79	0.490	8.40E+03	6.30E+03	0.0611	0.0032	0.738	0.035	0.0896	0.0014	-0.0122	643.0	56.5	113.0	591.0	10.0	20.0	553.0	4.0	8.0	99
AZR1Z37	348.00	385.00	466.00	1.110	-6.50E+04	7.10E+04	0.1462	0.0040	9.252	0.091	0.4589	0.0045	0.3683	2302.0	23.5	47.0	2363.0	4.5	9.0	2435.0	10.0	20.0	103
AZR1Z38	117.80	168.80	51.00	0.400	5.00E+04	2.50E+04	0.0618	0.0018	0.824	0.021	0.1093	0.0011	0.1192	667.0	31.0	62.0	664.0	5.5	11.0	689.0	3.0	6.0	101
AZR1Z39	173.30	155.70	173.20	0.900	4.20E+04	2.50E+04	0.1289	0.0038	7.332	0.099	0.4105	0.0043	0.0824	2083.0	26.0	52.0	2153.0	6.0	12.0	2217.0	10.0	20.0	103
AZR1Z40	518.00	462.00	300.00	0.890	-2.40E+05	1.50E+05	0.0885	0.0019	2.798	0.036	0.2294	0.0022	0.1902	1393.0	20.5	41.0	1355.0	5.0	10.0	1331.0	6.0	12.0	98
AZR1Z41	119.00	127.40	87.90	1.070	4.00E+04	1.70E+04	0.0925	0.0027	3.096	0.073	0.2419	0.0026	0.1655	1478.0	27.5	55.0	1432.0	9.0	18.0	1397.0	6.5	13.0	98
AZR1Z43	179.60	110.30	37.86	0.610	-8.00E+04	1.20E+04	0.0619	0.0023	1.038	0.033	0.1213	0.0014	0.0513	671.0	40.0	80.0	723.0	6.0	12.0	738.0	4.0	8.0	102
AZR1Z44	334.00	301.00	91.00	0.900	2.90E+04	1.60E+04	0.0616	0.0019	0.889	0.022	0.1050	0.0012	0.0402	660.0	33.0	66.0	646.0	6.0	12.0	644.0	3.5	7.0	100
AZR1Z45	94.19	113.19	35.43	0.320	-6.00E+02	5.20E+03	0.0636	0.0032	0.899	0.044	0.1009	0.0015	0.1776	728.0	53.5	107.0	651.0	12.0	24.0	620.0	4.5	9.0	95
AZR1Z46	174.90	36.30	25.30	0.320	2.90E+04	2.80E+04	0.1212	0.0038	5.790	0.110	0.3448	0.0044	0.3475	1974.0	23.0	56.0	1945.0	8.0	16.0	1910.0	10.5	21.0	98
AZR1Z47	701.00	386.00	115.00	0.590	7.90E+04	9.60E+04	0.1304	0.0035	5.614	0.050	0.3121	0.0033	0.3725	2103.0	23.5	47.0	1918.0	4.0	8.0	1751.0	8.0	16.0	91
AZR1Z48	67.42	73.08	97.90	1.080	1.30E+04	2.00E+04	0.1812	0.0055	12.840	0.200	0.5116	0.0062	0.1507	2664.0	23.0	50.0	2668.0	7.5	15.0	2663.0	13.0	26.0	100
AZR1Z49	132.20	282.00	132.40	0.510	-3.30E+04	1.90E+04	0.1149	0.0036	5.281	0.099	0.3325	0.0034	0.2148	1878.0	28.0	56.0	1866.0	8.0	16.0	1850.0	8.0	16.0	99
AZR1Z50	59.60	103.90	91.30	1.740	1.00E+03	1.0E+04	0.0642	0.0042	1.028	0.030	0.0325	0.0039	0.0323										

ANALYSIS	U (ppm)	Th (ppm)	Pb (ppm)	ThU	Ratios				Error correction	Ages (Ma)				Concordance (%)								
					$^{206}\text{Pb}/^{208}\text{Pb}$	$^{207}\text{Pb}/^{206}\text{Pb}$	$^{207}\text{Pb}/^{235}\text{U}$	$^{206}\text{Pb}/^{238}\text{U}$		$^{207}\text{Pb}/^{206}\text{Pb}$	σ	$^{207}\text{Pb}/^{235}\text{U}$	σ	$^{206}\text{Pb}/^{238}\text{U}$	σ	2σ	2σ					
AZR1z64	406.00	288.50	277.40	0.710	7.80E+04	1.152	0.0032	5.576	0.054	0.3503	0.0033	0.2064	1883.0	25.0	50.0	1912.0	4.0	8.0	1936.0	8.0	16.0	101
AZR1z65	86.40	59.40	65.40	0.620	-1.50E+04	0.1680	0.0050	10.770	0.160	0.4616	0.0055	0.3351	2538.0	25.0	50.0	2503.0	7.0	14.0	2447.0	12.0	24.0	98
AZR1z67	727.00	168.60	148.40	0.230	-8.00E+05	0.1300	0.0035	6.795	0.057	0.3804	0.0036	0.3864	2098.0	23.5	47.0	2085.0	3.5	7.0	2078.0	8.5	17.0	100
AZR1z68	513.20	1097.00	320.50	2.140	-5.00E+04	0.0607	0.0018	0.852	0.020	0.1018	0.0011	0.0826	829.0	32.0	64.0	626.0	5.5	11.0	625.0	3.0	6.0	100
AZR1z69	380.20	87.70	34.59	0.230	-2.00E+04	0.0666	0.0018	1.228	0.024	0.1344	0.0014	0.1424	825.0	28.0	56.0	813.0	5.5	11.0	813.0	4.0	8.0	100
AZR1z70	200.30	241.30	71.80	1.200	-1.20E+04	0.0609	0.0024	0.852	0.029	0.1009	0.0013	0.1344	636.0	42.5	85.0	626.0	8.0	16.0	620.0	4.0	8.0	99
AZR1z71	219.00	459.00	452.00	2.100	1.10E+04	0.0035	0.0024	6.321	0.074	0.3683	0.0035	0.1226	2019.0	25.0	50.0	2021.0	5.0	10.0	2021.0	8.0	16.0	100
AZR1z72	595.80	384.00	97.00	1.480	1.20E+04	0.0591	0.0022	0.710	0.023	0.0871	0.0011	0.0737	571.0	40.5	81.0	545.0	7.0	14.0	538.0	3.5	7.0	99
AZR1z73	149.20	159.60	145.90	1.370	-8.00E+04	0.0038	0.0038	5.780	0.210	0.0087	0.0097	0.8934	2027.0	27.0	54.0	1943.0	15.5	31.0	1895.0	23.5	47.0	98
AZR1z75	229.20	313.30	96.10	1.070	3.00E+04	0.0612	0.0023	0.852	0.026	0.1010	0.0012	-0.0143	646.0	40.5	81.0	626.0	7.0	14.0	620.0	3.5	7.0	99
AZR1z76	632.30	146.70	47.81	0.230	-2.50E+04	0.0636	0.0016	0.902	0.018	0.1033	0.0012	0.4504	728.0	26.5	53.0	653.0	5.0	10.0	633.0	3.5	7.0	97
AZR1z77	119.70	197.90	53.50	1.650	-5.50E+03	0.0610	0.0032	0.787	0.036	0.0922	0.0015	-0.1429	639.0	56.5	113.0	589.0	10.0	20.0	574.0	4.5	9.0	97
AZR1z78	248.40	144.00	194.70	0.980	-2.60E+04	0.1351	0.0038	7.439	0.090	0.3962	0.0037	0.2794	2165.0	24.5	49.0	2166.0	5.5	11.0	2152.0	8.5	17.0	99
AZR1z79	184.70	326.00	283.40	1.770	-2.90E+04	0.1068	0.0032	4.643	0.068	0.3132	0.0034	0.2098	1746.0	27.5	55.0	1757.0	6.0	12.0	1756.0	8.5	17.0	100
AZR1z80	173.10	110.50	121.10	0.640	-9.00E+04	0.1374	0.0040	7.880	0.100	0.4148	0.0039	0.1175	2195.0	29.5	51.0	2217.0	5.5	11.0	2237.0	9.0	18.0	101
AZR1z81	210.40	105.60	29.06	0.500	-5.00E+04	0.0616	0.0023	0.777	0.026	0.0921	0.0011	0.1682	660.0	40.0	80.0	584.0	7.5	15.0	588.0	3.0	6.0	97
AZR1z82	681.00	288.40	86.30	0.420	3.10E+04	0.0624	0.0015	0.856	0.013	0.1003	0.0010	0.0417	688.0	25.5	51.0	628.0	3.5	7.0	616.0	3.0	6.0	98
AZR1z83	242.60	229.30	224.60	0.950	-3.40E+04	0.1217	0.0034	6.119	0.073	0.3641	0.0035	0.2258	1981.0	25.0	50.0	1993.0	5.0	10.0	2002.0	8.5	17.0	100
AZR1z84	331.00	337.00	99.10	1.020	-8.00E+04	0.0599	0.0019	0.852	0.023	0.1030	0.0012	0.0366	600.0	34.5	69.0	626.0	6.5	13.0	632.0	3.5	7.0	101
AZR1z85	408.70	238.40	190.40	0.980	3.70E+04	0.1263	0.0035	5.289	0.061	0.3035	0.0031	0.3282	2047.0	24.5	49.0	1867.0	5.0	10.0	1709.0	7.5	15.0	92
AZR1z86	222.00	94.10	25.75	0.420	-1.30E+04	0.0588	0.0022	0.748	0.025	0.0929	0.0011	0.0852	560.0	41.0	82.0	567.0	7.5	15.0	572.0	3.0	6.0	101
AZR1z87	144.90	271.00	45.18	1.870	-7.80E+03	0.0619	0.0028	0.769	0.031	0.0907	0.0012	0.0872	671.0	48.5	97.0	579.0	9.0	18.0	560.0	3.5	7.0	97
AZR1z89	165.79	86.40	128.60	0.520	-3.50E+05	0.1990	0.0055	14.710	0.150	0.5370	0.0032	0.2803	2818.0	22.5	45.0	2797.0	5.0	10.0	2771.0	11.0	22.0	99
AZR1z90	551.00	359.00	383.00	0.650	3.00E+05	0.1354	0.0037	7.607	0.066	0.4060	0.0038	0.3714	2169.0	24.0	48.0	2186.0	4.0	8.0	2197.0	8.5	17.0	100
AZR1z92	248.30	447.00	115.00	1.800	3.00E+04	0.0577	0.0023	0.704	0.024	0.0884	0.0010	0.0867	518.0	44.0	88.0	541.0	7.0	14.0	546.0	3.0	6.0	101
AZR1z94	590.00	893.00	245.60	1.510	-7.00E+04	0.0646	0.0017	0.858	0.017	0.0970	0.0013	0.2213	761.0	27.5	55.0	629.0	4.5	9.0	597.0	4.0	8.0	95
AZR1z97	1058.00	344.30	105.00	0.940	-1.90E+04	0.0606	0.0018	0.873	0.020	0.1045	0.0011	0.0973	625.0	32.0	64.0	637.0	5.5	11.0	640.0	3.0	6.0	101
AZR1z99	688.00	205.00	207.10	0.450	3.80E+05	0.1266	0.0034	5.166	0.041	0.2942	0.0030	0.4670	2051.0	23.5	47.0	1847.0	3.5	7.0	1662.0	7.5	15.0	90
AZR1z98	688.00	405.00	30.10	0.300	-1.50E+04	0.0683	0.0019	0.885	0.033	0.0972	0.0037	0.7906	878.0	29.0	58.0	644.0	9.0	18.0	598.0	11.0	22.0	93
AZR1z100	446.90	42.68	10.68	0.100	-1.00E+05	0.0580	0.0018	0.714	0.018	0.0893	0.0010	0.0533	530.0	34.0	68.0	547.0	5.5	11.0	552.0	3.0	6.0	101
Discordant data																						
AZR1z4	995.00	899.00	143.00	0.900	6.00E+04	0.0739	0.0019	0.941	0.015	0.0926	0.0012	0.2044	1039.0	26.0	52.0	673.0	4.0	8.0	571.0	3.5	7.0	85
AZR1z36	1181.00	800.00	201.00	0.680	4.10E+04	0.0776	0.0021	0.786	0.014	0.0746	0.0010	-0.0720	1137.0	27.0	54.0	589.0	4.0	8.0	464.0	3.0	6.0	79
AZR1z42	1012.00	1900.00	684.00	1.880	1.43E+05	0.1433	0.0029	3.702	0.036	0.1871	0.0022	0.5337	2267.0	17.5	35.0	1572.0	4.0	8.0	1106.0	6.0	12.0	70
AZR1z66	732.00	867.00	181.70	1.180	-3.00E+04	0.0794	0.0022	0.893	0.016	0.0828	0.0013	0.0522	1182.0	27.5	55.0	648.0	4.5	9.0	513.0	4.0	8.0	79
AZR1z74	290.30	252.90	42.50	0.870	-1.46E+04	0.0701	0.0023	0.844	0.022	0.0879	0.0011	-0.0171	931.0	33.5	67.0	621.0	6.0	12.0	543.0	3.5	7.0	87
AZR1z88	274.50	304.90	78.70	1.110	-1.70E+04	0.0675	0.0024	0.788	0.024	0.0860	0.0013	0.0852	853.0	37.0	74.0	596.0	7.0	14.0	532.0	4.0	8.0	89
AZR1z91	516.00	1045.00	244.20	2.030	-1.10E+04	0.0709	0.0023	0.885	0.017	0.0916	0.0018	-0.0289	965.0	33.0	66.0	644.0	4.5	9.0	585.0	4.0	8.0	89
AZR1z93	77.50	96.40	32.40	1.240	1.40E+03	0.0662	0.0071	1.114	0.099	0.0940	0.0021	0.5910	1343.0	79.5	159.0	760.0	24.0	48.0	579.0	6.0	12.0	76
AZR1z96	941.00	1978.00	510.00	2.100	2.80E+04	0.0953	0.0029	1.126	0.025	0.0873	0.0012	-0.0091	1534.0	28.5	57.0	766.0	6.0	12.0	540.0	3.5	7.0	70
AZR1z98	244.00	781.00	209.00	3.200	-5.00E+04	0.0771	0.0036	0.998	0.044	0.0951	0.0012	0.3176	1124.0	46.5	93.0	703.0	11.0	22.0	566.0	3.5	7.0	83

Footnotes:

Analysis references: AZR1z is zircon from sample AZR1 (mounts CT18-10b and CT19-3), followed by grain number.

Chapter II, Section II.3

Table D.26b: Sample AZR1 (SIMS)

IGSN: IEACC0023 Coordinate UTM: Zone 30S, 295882 m E, 3705386 m N

ANALYSIS	²³⁸ U (ppm)	²⁰⁶ Pb (ppm)	Th/U	²⁰⁴ Pb (ppb)	Concordant data					Ages (Ma)					Concordance (%)						
					²⁰⁷ Pb/ ²⁰⁶ Pb	σ	²⁰⁶ Pb/ ²⁰⁶ Pb	σ	Rho	²⁰⁷ Pb/ ²⁰⁶ Pb	σ	2σ	²⁰⁷ Pb/ ²⁰⁶ Pb	σ	2σ	²⁰⁶ Pb/ ²⁰⁶ Pb	σ	2σ			
AZR1z101	547.00	43.20	0.22	1.800	0.0571	0.0016	0.720	0.020	0.0900	0.0010	0.4368	63.0	126.0	126.0	549	14.0	28.0	563	8.0	16.0	102
AZR1z102	148.00	50.50	0.55	9.300	0.1367	0.0010	7.450	0.120	0.4000	0.0050	0.8567	12.0	24.0	32.0	2165	16.0	32.0	2147	25.0	50.0	92
AZR1z103	399.00	93.00	0.28	7.300	0.1139	0.0022	4.230	0.150	0.2700	0.0080	0.8302	35.0	70.0	58.0	1679	29.0	58.0	1539	40.0	80.0	99
AZR1z104	31.00	9.60	1.15	1.200	0.1257	0.0018	6.280	0.130	0.3600	0.0050	0.6874	25.0	50.0	40.0	2014	20.0	40.0	1992	25.0	50.0	99
AZR1z105	38.00	3.20	1.39	0.800	0.0681	0.0039	0.910	0.060	0.1000	0.0020	0.2755	120.0	240.0	64.0	656	32.0	64.0	595	10.0	20.0	91
AZR1z106	183.00	59.40	0.19	5.900	0.1282	0.0016	6.630	0.130	0.3800	0.0060	0.7622	22.0	44.0	36.0	2055	18.0	36.0	2055	26.0	52.0	100
AZR1z107	312.00	27.10	0.80	6.300	0.0564	0.0011	0.780	0.020	0.1000	0.0010	0.5029	41.0	82.0	26.0	585	13.0	26.0	616	8.0	16.0	105
AZR1z108	497.00	40.50	0.28	2.500	0.0554	0.0013	0.720	0.020	0.0900	0.0010	0.5083	52.0	104.0	24.0	550	12.0	24.0	580	8.0	16.0	106
AZR1z109	537.00	132.80	0.28	16.300	0.1028	0.0012	4.050	0.070	0.2900	0.0040	0.7642	21.0	42.0	32.0	1644	16.0	32.0	1621	20.0	40.0	99
AZR1z110	637.00	200.90	0.08	4.700	0.1278	0.0029	6.420	0.170	0.3600	0.0050	0.5406	40.0	80.0	48.0	2034	24.0	48.0	2002	25.0	50.0	98
AZR1z111	139.00	10.50	0.45	1.200	0.0607	0.0016	0.730	0.020	0.0900	0.0010	0.4712	57.0	114.0	28.0	541	14.0	28.0	541	8.0	16.0	97
AZR1z112	319.00	27.40	0.15	2.500	0.0588	0.0016	0.800	0.030	0.1000	0.0010	0.4687	58.0	116.0	30.0	589	15.0	30.0	609	9.0	18.0	102
AZR1z113	96.00	7.30	0.99	1.600	0.0618	0.0026	0.750	0.040	0.0900	0.0020	0.3516	91.0	182.0	44.0	567	22.0	44.0	543	9.0	18.0	96
AZR1z114	418.00	37.10	0.05	5.100	0.0591	0.0010	0.840	0.020	0.1000	0.0020	0.6439	38.0	76.0	24.0	617	12.0	24.0	630	10.0	20.0	102
AZR1z115	197.00	63.60	0.67	8.400	0.1274	0.0009	6.540	0.110	0.3700	0.0050	0.8742	12.0	24.0	30.0	2050	15.0	30.0	2040	25.0	50.0	100
AZR1z116	44.00	3.50	0.09	1.700	0.0622	0.0040	0.780	0.060	0.0900	0.0010	0.1793	136.0	272.0	72.0	586	36.0	72.0	562	8.0	16.0	96
AZR1z117	131.00	10.80	1.54	1.700	0.0675	0.0026	0.890	0.040	0.1000	0.0010	0.3423	79.0	158.0	42.0	645	21.0	42.0	587	8.0	16.0	91
AZR1z118	728.00	41.90	0.64	44.900	0.0566	0.0012	0.520	0.020	0.0700	0.0010	0.3629	47.0	94.0	28.0	424	14.0	28.0	415	6.0	12.0	98
AZR1z119	509.00	49.10	0.44	4.300	0.0612	0.0015	0.940	0.030	0.1100	0.0020	0.4981	64.0	128.0	30.0	672	14.0	30.0	680	9.0	18.0	101
AZR1z120	39.00	10.30	1.54	4.300	0.1080	0.0030	4.500	0.170	0.3000	0.0050	0.4827	50.0	100.0	62.0	1701	31.0	62.0	1701	26.0	52.0	98
AZR1z121	147.00	23.00	0.25	8.700	0.0743	0.0018	1.840	0.060	0.1800	0.0030	0.4388	104.0	208.0	44.0	1060	22.0	44.0	1067	14.0	28.0	101
AZR1z122	328.00	28.60	0.15	4.600	0.0568	0.0015	0.790	0.030	0.1000	0.0020	0.4769	48.0	96.0	30.0	590	15.0	30.0	619	9.0	18.0	105
AZR1z123	51.00	4.70	1.24	2.100	0.0593	0.0045	0.870	0.080	0.1100	0.0020	0.2362	57.0	114.0	34.0	636	16.0	34.0	654	13.0	26.0	103
AZR1z124	220.00	19.40	0.62	5.600	0.0588	0.0010	0.830	0.030	0.1000	0.0020	0.5037	39.0	78.0	28.0	611	14.0	28.0	625	9.0	18.0	102
AZR1z125	53.00	4.20	1.68	1.300	0.0565	0.0041	0.710	0.060	0.0900	0.0010	0.1982	162.0	324.0	70.0	542	35.0	70.0	560	9.0	18.0	103
AZR1z126	433.00	38.30	0.49	5.500	0.0640	0.0011	0.900	0.020	0.1000	0.0010	0.5786	74.0	148.0	24.0	652	12.0	24.0	628	8.0	16.0	96
AZR1z127	327.00	27.90	0.98	0.800	0.0607	0.0008	0.830	0.020	0.1000	0.0020	0.8070	27.0	54.0	20.0	606	10.0	20.0	606	10.0	20.0	99
AZR1z128c	246.00	79.80	0.69	4.300	0.1292	0.0017	6.680	0.130	0.3700	0.0050	0.7316	23.0	46.0	36.0	2068	18.0	36.0	2051	25.0	50.0	99
AZR1z128r	347.00	104.60	0.10	8.000	0.1212	0.0009	5.810	0.090	0.3500	0.0050	0.8719	14.0	28.0	30.0	1947	15.0	30.0	1925	24.0	48.0	99
AZR1z129	271.00	88.00	0.59	20.400	0.1309	0.0014	6.780	0.130	0.3800	0.0060	0.7937	18.0	36.0	36.0	2082	18.0	36.0	2057	26.0	52.0	99
AZR1z130	619.00	175.20	0.18	10.300	0.1237	0.0013	5.580	0.100	0.3300	0.0050	0.8378	18.0	36.0	34.0	1912	17.0	34.0	1825	25.0	50.0	95

Footnotes:

. Analysis references: AZR1z is zircon from sample AZR1 (mounts CT18-10b and CT19-3), followed by grain number "c" or "r", meaning core or rim, respectively.

. Pb* indicates radiogenic Pb, corrected for common Pb.

Chapter II, Section II.3

Table D.27: Sample AZR7 (LA-ICPMS)

IGSN: IEACC0028

Coordinate UTM: Zone 30S, 271 772 m E, 3695342 m N

ANALYSIS	U (ppm)	Th (ppm)	Pb (ppm)	Th/U	Ratios			Concordant data			Error correction	Ages (Ma)			2σ	σ	Concordance (%)									
					$^{207}\text{Pb}/^{206}\text{Pb}$	$^{207}\text{Pb}/^{235}\text{U}$	$^{207}\text{Pb}/^{238}\text{U}$	2σ	2σ	2σ		$^{207}\text{Pb}/^{235}\text{U}$	σ	2σ												
AZR7Z1	134.10	43.10	45.39	0.320	1.02E+05	5.90E+04	0.1352	0.0018	7.710	0.230	0.4108	0.0050	0.7543	2167.0	11.5	23.0	2198.0	13.5	27.0	2198.0	11.5	23.0	2219.0	11.5	23.0	101
AZR7Z2	83.20	73.80	62.10	0.890	2.00E+04	2.40E+04	0.1109	0.0018	4.847	0.130	0.3194	0.0032	0.3435	1814.0	14.5	23.0	1793.0	11.5	23.0	1793.0	11.5	23.0	1787.0	8.0	16.0	100
AZR7Z3	16.68	28.28	7.08	1.730	-1.70E+03	1.60E+03	0.0625	0.0068	0.739	0.077	0.0884	0.0021	0.0228	691.0	116.0	232.0	522.0	22.5	45.0	522.0	22.5	45.0	546.0	6.0	12.0	97
AZR7Z4	60.62	35.21	9.75	0.590	-4.40E+03	5.90E+03	0.0604	0.0034	0.846	0.044	0.1020	0.0011	0.0802	618.0	61.0	122.0	622.0	12.0	24.0	622.0	12.0	24.0	626.0	4.0	8.0	101
AZR7Z5	34.57	13.98	4.16	4.400	-9.10E+03	4.30E+03	0.0586	0.0040	0.861	0.056	0.1068	0.0017	0.0236	552.0	74.5	149.0	631.0	11.5	31.0	631.0	11.5	31.0	654.0	5.0	10.0	104
AZR7Z6	138.20	117.10	103.40	0.850	-8.70E+04	5.50E+04	0.1153	0.0016	5.114	0.130	0.3236	0.0031	0.2762	1885.0	12.5	25.0	1838.0	11.0	22.0	1838.0	11.0	22.0	1807.0	7.5	15.0	98
AZR7Z7	50.61	38.54	38.08	0.760	-5.50E+04	2.60E+04	0.1285	0.0022	6.850	0.190	0.3846	0.0038	0.2355	2078.0	15.0	30.0	2092.0	12.5	25.0	2092.0	12.5	25.0	2093.0	9.0	18.0	100
AZR7Z8	163.80	111.30	30.70	0.680	-5.20E+04	2.50E+04	0.0614	0.0026	0.811	0.031	0.1083	0.0014	0.1418	853.0	60.0	120.0	713.0	8.5	17.0	593.0	8.5	17.0	593.0	3.0	6.0	98
AZR7Z9	169.90	137.10	46.10	0.850	-2.10E+04	2.10E+04	0.0675	0.0039	1.018	0.069	0.1083	0.0014	0.8423	853.0	60.0	120.0	713.0	8.5	17.0	593.0	8.5	17.0	683.0	4.0	8.0	93
AZR7Z0	286.30	37.35	10.22	0.130	-1.88E+05	7.00E+04	0.0600	0.0021	0.793	0.025	0.0978	0.0009	0.0963	604.0	36.0	76.0	593.0	7.0	14.0	593.0	7.0	14.0	591.0	2.5	5.0	100
AZR7Z1	110.70	69.68	19.64	0.630	-3.00E+04	1.10E+04	0.0582	0.0026	0.784	0.032	0.0978	0.0011	0.1558	537.0	49.0	98.0	588.0	9.0	18.0	602.0	9.0	18.0	602.0	3.0	6.0	102
AZR7Z2	275.60	120.60	34.34	0.440	-1.15E+05	4.70E+04	0.0586	0.0021	0.818	0.026	0.1011	0.0009	0.0589	552.0	39.0	78.0	607.0	7.5	15.0	621.0	7.5	15.0	621.0	2.5	5.0	102
AZR7Z3	471.00	265.60	318.00	0.560	1.72E+05	8.20E+04	0.1696	0.0017	9.120	0.220	0.3917	0.0040	0.4472	2554.0	8.5	17.0	2350.0	11.0	22.0	2131.0	11.0	22.0	2131.0	9.5	19.0	91
AZR7Z4	342.60	257.50	74.60	0.750	-1.13E+05	6.10E+04	0.0611	0.0021	0.860	0.025	0.1019	0.0009	0.1422	643.0	37.0	74.0	630.0	7.0	14.0	626.0	7.0	14.0	626.0	2.5	5.0	99
AZR7Z5	228.50	193.20	203.40	0.850	-1.07E+05	8.00E+04	0.1330	0.0012	7.377	0.180	0.4018	0.0034	0.4360	2138.0	8.0	16.0	2158.0	11.0	22.0	2177.0	11.0	22.0	2177.0	8.0	16.0	101
AZR7Z6	51.56	42.18	12.44	0.820	-2.70E+03	5.50E+03	0.0578	0.0032	0.824	0.045	0.1023	0.0014	0.1283	522.0	60.5	121.0	610.0	12.5	25.0	628.0	12.5	25.0	628.0	4.0	8.0	103
AZR7Z7	841.00	598.00	598.70	0.710	2.60E+05	3.50E+05	0.1267	0.0008	6.719	0.150	0.3841	0.0027	0.4665	2052.0	5.5	11.0	2075.0	10.0	20.0	2095.0	10.0	20.0	2095.0	6.5	13.0	101
AZR7Z8	56.00	37.40	32.09	0.670	-4.00E+04	1.90E+04	0.1107	0.0025	4.830	0.150	0.3746	0.0033	0.0661	1811.0	20.5	41.0	1790.0	13.0	26.0	1778.0	13.0	26.0	1778.0	8.0	16.0	99
AZR7Z9	179.20	89.70	26.31	0.460	-4.00E+04	2.00E+04	0.0612	0.0024	0.858	0.029	0.1019	0.0010	0.0090	646.0	42.0	84.0	629.0	8.0	16.0	626.0	8.0	16.0	626.0	3.0	6.0	99
AZR7Z0	723.40	245.60	68.72	0.340	-9.30E+04	7.60E+04	0.0599	0.0018	0.791	0.020	0.0958	0.0008	0.2042	601.0	32.5	65.0	599.0	5.5	11.0	589.0	5.5	11.0	589.0	2.5	5.0	100
AZR7Z1	225.80	106.77	29.47	0.740	-8.50E+04	2.60E+04	0.0609	0.0022	0.793	0.026	0.1081	0.0009	0.1351	636.0	39.0	78.0	593.0	7.5	15.0	617.0	7.5	15.0	617.0	3.0	6.0	97
AZR7Z2	85.30	62.80	18.51	0.740	-4.30E+03	9.40E+03	0.0597	0.0028	0.850	0.026	0.1018	0.0012	0.0845	593.0	39.0	78.0	583.0	7.0	14.0	582.0	7.0	14.0	582.0	2.5	5.0	101
AZR7Z3	38.06	37.57	10.72	0.990	-3.70E+03	4.00E+03	0.0616	0.0042	0.788	0.051	0.0934	0.0016	0.0212	660.0	73.0	146.0	590.0	14.5	29.0	576.0	14.5	29.0	576.0	4.5	9.0	98
AZR7Z4	254.20	168.70	49.79	0.660	-1.30E+04	2.90E+04	0.0591	0.0021	0.828	0.026	0.1008	0.0009	0.1175	571.0	38.5	77.0	613.0	7.0	14.0	619.0	7.0	14.0	619.0	2.5	5.0	101
AZR7Z5	20.16	10.75	3.32	0.530	-1.88E+04	8.60E+03	0.0628	0.0063	0.862	0.072	0.1021	0.0020	0.0177	701.0	90.0	180.0	642.0	19.5	39.0	627.0	19.5	39.0	627.0	6.0	12.0	98
AZR7Z6	232.80	2.47	0.90	0.010	8.00E+04	1.90E+04	0.0596	0.0022	0.745	0.023	0.0904	0.0009	-0.0136	589.0	40.0	80.0	585.0	6.5	13.0	588.0	6.5	13.0	588.0	2.5	5.0	99
AZR7Z7	134.00	116.00	35.32	0.870	-3.80E+04	1.90E+04	0.0606	0.0026	0.858	0.033	0.1032	0.0010	-0.1552	625.0	46.5	93.0	629.0	9.0	18.0	633.0	9.0	18.0	633.0	3.0	6.0	101
AZR7Z8	12.33	11.10	3.25	0.900	-2.20E+03	1.60E+03	0.0667	0.0075	0.955	0.100	0.1026	0.0027	0.0099	828.0	117.5	235.0	681.0	26.0	52.0	630.0	26.0	52.0	630.0	8.0	16.0	92
AZR7Z9	106.60	50.71	53.59	0.480	-2.80E+05	1.10E+05	0.1396	0.0016	7.640	0.190	0.3955	0.0035	0.1830	2222.0	10.0	20.0	2190.0	11.0	22.0	2148.0	11.0	22.0	2148.0	8.0	16.0	98
AZR7Z0	291.80	191.30	53.50	0.900	-4.00E+05	1.20E+05	0.0595	0.0021	0.768	0.024	0.0933	0.0008	0.1264	585.0	38.5	77.0	579.0	7.0	14.0	575.0	7.0	14.0	575.0	2.5	5.0	99
AZR7Z1	31.70	28.65	26.63	0.600	-4.10E+03	9.80E+03	0.1155	0.0036	0.820	0.200	0.3289	0.0042	0.3410	1888.0	28.0	56.0	1856.0	16.5	33.0	1833.0	16.5	33.0	1833.0	10.0	20.0	99
AZR7Z2	205.20	72.90	73.40	0.360	-1.90E+05	1.00E+05	0.1296	0.0012	6.694	0.160	0.3753	0.0030	0.2395	2093.0	8.0	16.0	2072.0	10.5	21.0	2054.0	10.5	21.0	2054.0	7.0	14.0	99
AZR7Z3	187.00	162.40	161.60	0.870	-2.16E+05	9.80E+04	0.1310	0.0013	6.953	0.170	0.3849	0.0030	0.2959	2111.0	8.5	17.0	2105.0	11.0	22.0	2099.0	11.0	22.0	2099.0	7.0	14.0	100
AZR7Z4	213.30	104.70	31.86	0.490	6.00E+06	1.30E+06	0.0603	0.0022	0.876	0.027	0.1053	0.0010	0.0567	607.0	39.5	79.0	639.0	7.5	15.0	645.0	7.5	15.0	645.0	3.0	6.0	101
AZR7Z5	266.60	236.40	64.70	0.890	-3.70E+04	3.20E+04	0.0603	0.0022	0.744	0.023	0.0898	0.0009	0.0250	614.0	39.5	79.0	565.0	6.5	13.0	564.0	6.5	13.0	564.0	2.5	5.0	98
AZR7Z6	197.20	41.60	13.60	0.540	-1.10E+04	2.20E+04	0.0599	0.0023	0.800	0.027	0.0959	0.0009	0.1079	600.0	41.5	83.0	597.0	7.5	15.0	591.0	7.5	15.0	591.0	2.5	5.0	99
AZR7Z7	148.70	79.90	89.80	0.540	-1.28E+05	8.30E+04	0.1460	0.0015	8.456	0.200	0.4196	0.0035	0.3788	2300.0	9.0	18.0	2281.0	10.5	21.0	2259.0	10.5	21.0	2259.0	8.0	16.0	99
AZR7Z8	483.80	255.20	68.14	0.530	-2.45E+05	9.50E+04	0.0601	0.0020	0.785	0.022	0.0950	0.0008	0.1895	692.0	36.0	72.0	588.0	6.5	13.0	585.0	6.5	13.0	585.0	3.0	6.0	99
AZR7Z9	128.60	63.17	19.18	0.500	-1.90E+04	1.70E+04	0.0608	0.0025	0.867	0.073	0.1045	0.0010	0.1545	632.0	44.5	89.0	634.0	8.5	17.0	641.0	8.5	17.0	641.0	3.0	6.0	101
AZR7Z0	133.30	59.60	36.50	0.440	-2.50E+04	3.10E+04	0.0819	0.0028	2.419	0.069	0.2153	0.0018	0.0994	1243.0	33.5	67.0	1248.0	10.0	20.0	1257.0	10.0	20.0	1257.0	5.0	10.0	101
AZR7Z1	113.40	97.40	41.19	0.860	-3.20E+04	2.10E+04	0.0711	0.0025	1.471	0.045	0.1501	0.0014	0.1440	960.0	36.0	72.0	919.0	9.0	18.0	902.0	9.0	18.0	902.0	4.0	8.0	98
AZR7Z2	79.50	31.60	28.66	0.620	-5.30E+04	3.40E+04	0.1278	0.0019	6.131	0.160	0.3468	0.0032	0.1755	2068.0	13.0	26.0	1995.0	11.5	23.0	1919.0	11.5	23.0	1919.0	7.5	15.0	96
AZR7Z3	131.30	66.39	34.71	0.520	-5.90E+04	4.30E+04	0.0773	0.0028	1.891	0.059																

ANALYSIS	U (ppm)	Th (ppm)	Pb (ppm)	ThU	Ratios						Error correction			Ages (Ma)						Concordance (%)			
					²⁰⁶ Pb/ ²⁰⁸ Pb	²⁰⁷ Pb/ ²⁰⁸ Pb	²⁰⁷ Pb/ ²³⁵ U	²⁰⁶ Pb/ ²³⁸ U	²⁰⁷ Pb/ ²⁰⁶ Pb	²⁰⁶ Pb/ ²³⁸ U	σ	Error correction	σ	²⁰⁷ Pb/ ²⁰⁶ Pb	σ	²⁰⁶ Pb/ ²³⁸ U	σ	²⁰⁷ Pb/ ²³⁵ U	σ				
AZR7267	203.50	170.30	171.90	0.840	-1.53E+06	7.60E+05	0.1347	0.0015	7.177	0.3847	0.0035	0.3663	2160.0	9.5	19.0	2134.0	11.0	22.0	2098.0	8.0	16.0	98	
AZR7268	179.60	220.20	219.00	1.230	-2.49E+05	8.00E+04	0.1276	0.0017	6.700	0.3774	0.0034	0.2152	2085.0	11.5	23.0	2073.0	11.0	22.0	2064.0	8.0	16.0	100	
AZR7269	525.40	381.30	413.80	0.730	-7.40E+04	4.80E+04	0.0606	0.0021	0.867	0.1037	0.0009	0.1257	625.0	31.5	75.0	634.0	7.0	14.0	636.0	2.5	5.0	100	
AZR7270	368.70	287.40	162.30	0.780	5.70E+04	5.40E+04	0.0815	0.0026	2.294	0.2039	0.0018	0.2812	1294.0	31.5	63.0	1210.0	9.5	19.0	1196.0	5.0	10.0	99	
AZR7271	301.11	19.51	5.61	0.650	-1.77E+04	9.10E+03	0.0622	0.0054	0.822	0.067	0.0091	0.025	681.0	92.5	185.0	609.0	18.5	37.0	609.0	7.5	15.0	100	
AZR7272	348.30	501.30	136.60	1.440	-9.00E+04	2.10E+04	0.0604	0.0023	0.824	0.027	0.0384	0.009	618.0	41.0	82.0	610.0	7.5	15.0	605.0	3.0	6.0	99	
AZR7273	335.20	278.20	83.60	0.830	-1.90E+04	1.70E+04	0.0611	0.0025	0.871	0.031	0.0126	0.011	643.0	44.0	88.0	636.0	8.5	17.0	630.0	3.0	6.0	99	
AZR7273c	299.90	213.20	59.20	0.710	-2.00E+04	1.50E+04	0.0601	0.0025	0.824	0.031	0.0090	0.011	607.0	45.0	90.0	610.0	8.5	17.0	609.0	3.0	6.0	100	
AZR7274	1450.00	272.40	347.90	0.190	-2.30E+05	3.20E+05	0.1398	0.0011	7.705	0.190	0.3982	0.0035	2225.0	7.0	14.0	2197.0	11.0	22.0	2152.0	8.0	16.0	98	
AZR7275	82.00	68.81	18.65	0.840	-1.20E+05	3.80E+05	0.0564	0.0038	0.746	0.047	0.0975	0.0017	468.0	74.5	149.0	566.0	13.5	27.0	600.0	5.0	10.0	106	
AZR7276	37.42	27.37	22.82	0.730	2.50E+04	7.40E+04	0.1061	0.0040	4.630	0.190	0.3136	0.0053	1733.0	34.5	69.0	1736.0	17.5	35.0	1758.0	13.0	26.0	101	
AZR7277	148.40	191.00	54.80	1.540	5.30E+03	4.70E+03	0.0605	0.0034	0.830	0.044	0.1003	0.0014	622.0	60.5	121.0	614.0	12.0	24.0	616.0	4.0	8.0	100	
AZR7278	485.80	463.00	384.00	0.950	-2.30E+05	1.30E+05	0.1143	0.0039	4.042	0.110	0.2584	0.0025	1869.0	31.0	62.0	1843.0	11.0	22.0	1482.0	6.5	13.0	90	
AZR7280	213.00	381.00	110.30	1.780	-1.41E+05	6.70E+04	0.0591	0.0029	0.807	0.037	0.0996	0.0012	571.0	53.5	107.0	601.0	10.5	21.0	612.0	3.5	7.0	102	
AZR7281c	316.60	255.60	81.00	0.810	8.00E+04	6.30E+04	0.0602	0.0024	0.891	0.032	0.1080	0.0011	611.0	43.0	86.0	647.0	8.5	17.0	661.0	3.0	6.0	102	
AZR7281f	104.10	54.04	17.41	0.920	-3.00E+03	5.90E+03	0.0603	0.0037	0.891	0.053	0.1062	0.0014	625.0	66.0	132.0	628.0	14.0	28.0	651.0	4.0	8.0	101	
AZR7282	421.70	381.60	114.30	0.900	-1.05E+05	5.30E+04	0.0603	0.0024	0.857	0.029	0.1025	0.0010	614.0	43.0	86.0	647.0	8.0	16.0	629.0	3.0	6.0	100	
AZR7283	269.10	417.00	390.40	1.550	-1.70E+04	4.70E+04	0.1170	0.0017	5.625	0.140	0.3387	0.0027	1911.0	11.0	22.0	1904.0	11.0	22.0	1885.0	6.5	13.0	99	
AZR7284	64.10	88.90	25.03	1.390	-1.80E+03	3.70E+03	0.0644	0.0045	0.857	0.057	0.0972	0.0017	1143.0	73.5	147.0	625.0	15.5	31.0	598.0	5.0	10.0	95	
AZR7285	213.00	79.80	79.40	0.370	-3.80E+04	3.70E+04	0.1285	0.0020	5.229	0.140	0.2986	0.0033	2036.0	14.0	28.0	1857.0	11.5	23.0	1884.0	8.0	16.0	91	
AZR7286	304.40	241.20	73.00	0.790	-2.80E+04	2.00E+04	0.0585	0.0024	0.811	0.030	0.1011	0.0010	549.0	45.0	90.0	626.0	8.5	17.0	621.0	3.0	6.0	103	
AZR7287c	208.50	265.70	79.00	1.270	-2.30E+04	1.60E+04	0.0622	0.0029	0.852	0.035	0.0990	0.0010	609.0	50.0	100.0	603.0	9.5	19.0	609.0	3.0	6.0	97	
AZR7287f	178.50	232.30	69.50	1.300	-1.70E+05	1.40E+05	0.0609	0.0030	0.851	0.038	0.1001	0.0011	636.0	53.0	106.0	625.0	10.5	21.0	615.0	3.0	6.0	98	
AZR7288	528.00	523.00	149.40	0.990	-2.50E+04	3.00E+04	0.0592	0.0021	0.785	0.025	0.0960	0.0009	574.0	38.5	77.0	588.0	7.0	14.0	591.0	2.5	5.0	100	
AZR7289	71.00	43.51	12.73	0.610	-2.90E+04	1.20E+04	0.0617	0.0036	0.883	0.049	0.1018	0.0011	664.0	62.5	125.0	643.0	13.0	26.0	625.0	5.0	10.0	97	
AZR7290	186.70	175.20	52.30	0.940	-6.90E+04	4.80E+04	0.0632	0.0028	0.875	0.035	0.0989	0.0011	715.0	47.0	94.0	638.0	9.5	19.0	614.0	3.0	6.0	96	
AZR7291	235.40	356.30	356.30	1.510	-4.00E+05	2.10E+05	0.1247	0.0014	6.357	0.160	0.3647	0.0030	2025.0	10.0	20.0	2026.0	11.0	22.0	2004.0	7.0	14.0	99	
AZR7292	249.20	61.50	55.80	0.250	-1.40E+04	6.90E+04	0.1272	0.0014	5.869	0.160	0.3352	0.0043	0.7649	2060.0	9.5	19.0	1957.0	12.0	24.0	1864.0	10.5	21.0	95
AZR7293	76.10	66.90	67.50	0.880	-2.30E+04	2.30E+04	0.1239	0.0023	6.400	0.180	0.3701	0.0037	0.2685	2013.0	16.5	33.0	2030.0	12.5	25.0	2030.0	8.5	17.0	100
AZR7294	46.50	69.90	29.80	1.460	-5.40E+03	5.40E+03	0.0680	0.0041	1.362	0.076	0.1451	0.0021	869.0	62.5	125.0	873.0	16.5	33.0	873.0	6.0	12.0	100	
AZR7296	130.50	18.57	20.72	1.140	4.50E+05	7.30E+05	0.1323	0.0017	7.236	0.180	0.3916	0.0034	0.2296	2129.0	11.0	22.0	2130.0	8.0	16.0	2130.0	8.0	16.0	99
AZR7297c	276.30	162.40	51.02	0.590	-8.10E+04	4.00E+04	0.0619	0.0023	0.871	0.028	0.1017	0.0009	671.0	40.0	80.0	636.0	7.5	15.0	625.0	2.5	5.0	98	
AZR7297f	41.07	22.97	6.81	0.560	5.90E+03	3.40E+03	0.0645	0.0045	0.882	0.057	0.1008	0.0017	758.0	73.5	147.0	642.0	15.5	31.0	619.0	5.0	10.0	96	
AZR7300	449.20	59.80	59.00	0.130	-6.00E+05	2.20E+05	0.0689	0.0011	6.378	0.150	0.3670	0.0028	0.2987	2036.0	8.0	16.0	2029.0	10.5	21.0	2015.0	6.5	13.0	99
AZR7310	37.30	48.91	96.71	1.957	-2.30E+04	1.40E+04	0.0689	0.0030	1.281	0.049	0.1356	0.0014	0.0372	896.0	45.0	90.0	847.0	11.0	22.0	820.0	4.0	8.0	98
AZR7311	179.20	93.96	115.50	0.520	7.00E+06	2.10E+06	0.1621	0.0015	10.242	0.240	0.4541	0.0035	0.3751	2478.0	8.0	16.0	2413.0	8.0	16.0	2413.0	8.0	16.0	98
AZR7312	29.57	28.75	8.28	0.970	-4.60E+03	3.70E+03	0.0566	0.0047	0.868	0.060	0.0969	0.0018	-0.0199	476.0	92.0	184.0	573.0	17.5	35.0	596.0	5.5	11.0	104
AZR73102	537.70	518.00	162.00	0.960	-9.60E+04	6.50E+04	0.0615	0.0020	0.755	0.024	0.1021	0.0009	0.1568	675.0	35.0	70.0	633.0	6.5	13.0	627.0	2.5	5.0	99
AZR73105	336.20	151.80	160.90	0.450	5.30E+06	4.80E+06	0.1353	0.0010	7.163	0.170	0.3784	0.0027	0.3449	2168.0	6.5	13.0	2132.0	10.5	21.0	2069.0	6.5	13.0	97
AZR73107	101.00	42.96	54.72	0.420	-2.50E+05	1.30E+05	0.0755	0.0019	11.610	0.280	0.4782	0.0040	0.3203	2611.0	9.0	18.0	2573.0	11.5	23.0	2519.0	8.5	17.0	98
AZR73108	43.58	36.10	18.72	0.830	-1.35E+05	8.80E+04	0.0755	0.0036	1.879	0.083	0.1796	0.0021	0.0890	1082.0	49.0	96.0	1074.0	14.5	29.0	1065.0	5.5	11.0	99
AZR73109	57.90	45.20	14.51	0.780	-2.10E+04	1.30E+04	0.0652	0.0036	0.893	0.043	0.0989	0.0016	0.0840	781.0	58.0	116.0	648.0	11.5	23.0	608.0	4.5	9.0	94
AZR73111	124.80	39.05	36.73	0.310	-8.20E+04	8.80E+04	0.1221	0.0012	5.207	0.120	0.3090	0.0025	0.3153	1967.0	9.0	18.0	1854.0	10.0	20.0	1736.0	6.0	12.0	94
AZR73112	131.70	47.53	45.41	0.360	-1.78E+05	8.60E+04	0.1199	0.0015	6.043	0.150	0.3560	0.0029	0.3626	1987.0	11.0	22.0	1982.0	11.0	22.0	1963.0	7.0	14.0	99
AZR73113	94.90	157.30	50.05	1.660	-1.80E+04	1.80E+04	0.0653	0.0029	0.981	0.039	0.1092	0.0011	0.0882	784.0	46.5	93.0	694.0	10.0	20.0	668.0	3.0	6.0	96
AZR73114c	292.80	17.80	18.60	0.060	-2.28E+06	8.70E+05	0.1413	0.0019	7.990	0.250	0.4040	0.0047	0.8726	2243.0	11.5	23.0	2229.0	14.0	28.0	2187.0	11.0	22.0	98
AZR73114f	429.00	81.00	82.40	0.190	-7.10E+05	4.10E+05	0.1246	0.0009	6.635	0.150	0.3818	0.0030	0.5425	2024.0	6.5	13.0	2064.0	10.0	20.0	2085.0	7.0	14.0	101
AZR73115c	211.60	173.20	50.50	0.820	-7.50E+04	3.70E+04	0.0614	0.0022	0.849	0.026	0.1015	0.0010	0.1100	639.0	39.0	78.0	624.0	7.0	14.0	623.0	4.0	8.0	100
AZR73115f	66.25	43.14	13.07	0.650	-2.30E+04	1.30E+04	0.0610	0.0029	0.872	0.039	0.1019	0.0013	0.1540	653.0	50.5	101.0	637.0	10.5	21.0	626.0	3.0	6.0	98
AZR73116	141.80	123.10	36.44	0.8																			

ANALYSIS	U (ppm)	Th (ppm)	Pb (ppm)	ThU	Ratios			Ages (Ma)			Concordance (%)										
					²⁰⁷ Pb/ ²⁰⁶ Pb	²⁰⁷ Pb/ ²³⁵ U	²⁰⁷ Pb/ ²³⁸ U	σ	²⁰⁷ Pb/ ²³⁵ U	σ	²⁰⁷ Pb/ ²³⁸ U	σ	2σ	2σ							
AZR72136	46.89	14.93	15.28	0.320	0.1349	0.0027	7.540	0.3967	0.0040	0.1337	2163.0	17.5	35.0	2178.0	13.0	26.0	2154.0	9.0	18.0	99	
AZR72137	295.40	465.40	137.20	1.550	0.0637	0.0022	0.901	0.028	0.028	0.2718	732.0	36.5	73.0	652.0	7.5	15.0	626.0	7.5	15.0	96	
AZR72138	146.70	25.00	21.57	0.170	0.1269	0.0013	6.348	0.150	0.3582	0.3139	2055.0	9.0	18.0	2025.0	10.5	21.0	1974.0	7.5	15.0	97	
AZR72139	121.80	29.80	34.10	0.240	0.1843	0.0018	12.030	0.300	0.4685	0.0041	0.4585	2692.0	8.0	16.0	2607.0	11.5	23.0	2477.0	9.0	18.0	95
AZR72140c	271.20	84.61	32.06	0.310	0.0679	0.0024	1.063	0.032	0.1134	0.0010	0.1562	866.0	36.5	73.0	735.0	8.0	16.0	692.0	3.0	6.0	94
AZR72140t	273.30	25.67	8.70	0.090	0.0624	0.0021	0.978	0.028	0.1128	0.0010	0.3531	888.0	36.0	72.0	683.0	7.0	14.0	689.0	3.0	6.0	100
AZR72141	207.60	164.80	45.42	0.790	0.0615	0.0023	0.845	0.028	0.0982	0.0010	0.1290	657.0	40.0	80.0	622.0	7.5	15.0	604.0	2.5	5.0	97
AZR72142	221.70	57.00	17.31	0.260	0.0610	0.0023	0.890	0.029	0.1028	0.0009	0.0949	674.0	39.5	79.0	646.0	8.0	16.0	631.0	3.0	6.0	98
AZR72143	86.00	105.10	26.23	1.220	0.0596	0.0029	0.740	0.034	0.0981	0.0011	0.1485	596.0	53.0	106.0	562.0	10.0	20.0	550.0	3.5	7.0	98
AZR72144	323.00	329.20	367.10	1.020	0.0591	0.0011	8.538	0.100	0.4191	0.0031	0.3717	2296.0	6.5	13.0	2290.0	10.5	21.0	2256.0	7.0	14.0	99
AZR72145	122.60	117.67	33.96	0.960	0.0610	0.0026	0.871	0.033	0.1023	0.0011	0.0566	639.0	46.0	92.0	636.0	9.0	18.0	628.0	3.0	6.0	99
AZR72146	284.50	98.70	28.65	0.350	0.0615	0.0022	0.885	0.026	0.1039	0.0009	0.0530	657.0	38.5	77.0	644.0	7.0	14.0	637.0	2.5	5.0	99
AZR72147	205.60	130.20	38.66	0.640	0.0615	0.0024	0.910	0.031	0.1062	0.0010	0.1375	657.0	42.0	84.0	657.0	8.0	16.0	650.0	3.0	6.0	99
AZR72148	174.40	137.70	39.90	0.790	0.0601	0.0024	0.833	0.029	0.0993	0.0010	-0.0603	607.0	43.0	86.0	615.0	8.0	16.0	610.0	3.0	6.0	99
AZR72149	220.20	193.40	185.40	0.880	0.1237	0.0011	6.228	0.150	0.5998	0.0028	0.2570	2010.0	6.0	12.0	2008.0	10.5	21.0	1981.0	6.5	13.0	99
AZR72150	263.90	123.30	136.80	0.470	0.1573	0.0012	9.532	0.220	0.4327	0.0035	0.3645	2427.0	6.5	13.0	2391.0	10.5	21.0	2318.0	8.0	16.0	97
AZR72151	65.14	15.92	4.53	0.240	0.0595	0.0031	0.852	0.043	0.1022	0.0011	0.1252	585.0	56.5	113.0	626.0	12.0	24.0	627.0	3.0	6.0	100
AZR72152	112.00	62.60	91.40	0.560	0.2113	0.0019	16.750	0.390	0.5665	0.0047	0.3531	2916.0	7.5	15.0	2921.0	11.0	22.0	2889.0	9.5	19.0	99
AZR72153	185.50	124.40	34.56	0.670	0.0602	0.0024	0.814	0.029	0.0981	0.0010	0.1455	611.0	43.0	86.0	605.0	8.0	16.0	603.0	3.0	6.0	100
Discordant data																					
AZR7220	421.00	357.00	94.30	0.850	0.0684	0.0023	0.774	0.022	0.0825	0.0007	0.0902	881.0	35.0	70.0	582.0	6.5	13.0	511.0	2.0	4.0	88
AZR7234	717.00	98.30	43.00	0.140	0.1885	0.0019	9.340	0.260	0.5884	0.0061	0.8633	2729.0	8.5	17.0	2372.0	13.0	26.0	1975.0	14.5	29.0	83
AZR7236	1198.00	147.30	148.10	0.120	0.530E+05	2.70E+05	5.165	0.140	0.2807	0.0041	0.6867	2147.0	10.0	20.0	1847.0	11.5	23.0	1595.0	10.5	21.0	86
AZR7250r	54.15	19.55	7.25	0.360	0.0735	0.0044	1.033	0.053	0.1025	0.0022	-0.0361	1028.0	60.5	121.0	720.0	13.0	26.0	629.0	6.5	13.0	87
AZR7251	289.00	221.00	1180.00	0.760	0.3630	0.0500	8.200	2.100	0.1130	0.0140	0.9911	3782.0	104.5	209.0	2253.0	116.0	232.0	690.0	40.5	81.0	31
AZR7252c	33.91	20.39	13.46	0.600	0.148E+04	9.90E+03	0.1017	0.0047	0.1834	0.0031	0.2876	1655.0	43.0	86.0	1299.0	15.5	31.0	1086.0	8.5	17.0	84
AZR7256	168.80	348.20	121.40	0.660	0.0976	0.0068	2.670	0.130	0.1801	0.0044	0.2393	1859.0	46.0	92.0	1320.0	18.0	36.0	1068.0	12.0	24.0	81
AZR7259r	76.30	30.67	12.40	0.400	0.0827	0.0054	1.470	0.110	0.1057	0.0015	0.7126	1579.0	65.0	130.0	918.0	22.5	45.0	648.0	4.5	9.0	71
AZR7263c	2123.00	211.00	82.50	0.100	0.0034	0.0034	3.370	0.150	0.2177	0.0081	0.4488	1262.0	64.0	128.0	784.0	18.5	37.0	626.0	4.5	9.0	80
AZR7266	304.00	406.90	509.00	1.340	0.3200	0.0380	6.300	1.100	0.1133	0.0075	0.9841	3570.0	91.5	183.0	2018.0	76.5	153.0	1620.0	21.5	43.0	85
AZR7278	1704.00	443.20	270.80	0.260	0.1082	0.0032	3.288	0.078	0.2135	0.0018	0.5481	1770.0	27.0	54.0	1478.0	9.0	18.0	1279.0	5.0	10.0	87
AZR7299c	299.60	93.40	274.00	0.310	0.2040	0.0240	7.300	1.400	0.2610	0.0140	0.9570	2888.0	95.5	191.0	2149.0	85.5	171.0	1495.0	36.0	72.0	70
AZR7299r	2055.00	286.00	190.30	0.140	0.1099	0.0040	0.898	0.025	0.0597	0.0015	0.3609	1798.0	33.0	66.0	651.0	6.5	13.0	374.0	4.5	9.0	57
AZR72104	587.00	255.00	80.90	0.430	0.0727	0.0027	0.924	0.029	0.0925	0.0013	0.1511	1006.0	37.5	75.0	664.0	7.5	15.0	570.0	4.0	8.0	86
AZR72110	11.10	9.67	2.78	0.870	0.0687	0.0076	0.899	0.097	0.0943	0.0024	-0.0301	890.0	114.5	229.0	651.0	26.0	52.0	581.0	7.0	14.0	89
AZR72132	639.00	510.00	157.10	0.610	0.0632	0.0020	0.988	0.029	0.1129	0.0014	0.4923	714.0	33.5	67.0	698.0	7.5	15.0	690.0	4.0	8.0	99
AZR72134	2218.00	626.00	235.70	0.280	0.1240	0.0042	0.799	0.024	0.0484	0.0007	0.4157	2015.0	30.0	60.0	586.0	7.0	14.0	292.0	2.5	5.0	49

Footnotes:
. Analysis references: AZR7z is zircon from sample AZR7 (mount CT18-7), followed by grain number "c" or "r", meaning core or rim, respectively.

Chapter II, Section II.3

Table D.28: Sample OJL5 (LA-ICPMS)

IGSN: IEACC0021

Coordinate UTM: Zone 30S, 574362 m E, 3821747 m N

ANALYSIS	U (ppm)	Th (ppm)	Pb (ppm)	Th/U	Ratios			Concordant data			Error correction	Ages (Ma)			Concordance (%)								
					²⁰⁷ Pb/ ²⁰⁶ Pb	²⁰⁷ Pb/ ²³⁵ U	²⁰⁷ Pb/ ²³⁸ U	2σ	σ	2σ		σ	2σ	σ		2σ	σ	2σ					
OJL521	107.80	92.70	92.00	0.860	1.40E+05	1.40E+04	0.1274	0.0025	7.057	0.190	0.9347	0.0041	0.0349	2062.0	17.5	35.0	2119.0	12.0	24.0	2145.0	9.5	19.0	101
OJL522	111.50	101.90	102.00	0.480	3.80E+04	4.20E+04	0.1838	0.0030	13.670	0.360	0.5313	0.0050	0.3123	2687.0	13.5	27.0	2727.0	12.5	25.0	2747.0	10.5	21.0	101
OJL523	228.20	81.30	21.75	0.110	1.00E+05	1.90E+04	0.0667	0.0019	0.825	0.024	0.0980	0.0009	0.1572	630.0	33.5	67.0	611.0	6.5	13.0	609.0	2.5	5.0	100
OJL524	307.30	101.24	22.63	0.330	9.97E+03	7.10E+03	0.0509	0.0022	0.680	0.023	0.0824	0.0009	0.0810	488.0	42.5	85.0	502.0	7.0	14.0	511.0	2.5	5.0	102
OJL525	145.20	58.36	64.27	0.400	3.50E+04	1.70E+04	0.1473	0.0027	8.940	0.240	0.4333	0.0044	0.3116	2315.0	15.5	31.0	2332.0	12.0	24.0	2321.0	10.0	20.0	100
OJL526	767.40	262.50	68.83	0.340	1.60E+04	1.40E+04	0.6043	0.0019	0.778	0.020	0.0938	0.0009	0.2796	617.0	34.0	68.0	584.0	6.5	13.0	578.0	2.5	5.0	99
OJL527	887.70	41.31	11.06	0.470	4.20E+04	3.20E+03	0.0593	0.0032	0.777	0.040	0.0942	0.0013	0.0228	578.0	58.5	117.0	627.0	11.5	23.0	580.0	4.0	8.0	99
OJL528	108.77	158.34	43.67	1.460	3.80E+03	2.50E+03	0.0631	0.0028	0.855	0.036	0.0989	0.0013	-0.0228	712.0	47.0	94.0	562.0	10.0	20.0	608.0	4.0	8.0	97
OJL529	190.60	84.50	18.47	0.440	9.00E+02	2.30E+03	0.0566	0.0024	0.641	0.024	0.0809	0.0009	-0.0038	552.0	44.5	89.0	503.0	7.5	15.0	501.0	3.0	6.0	100
OJL530	269.20	73.48	19.74	0.270	5.30E+03	5.20E+03	0.0603	0.0022	0.798	0.028	0.0966	0.0011	0.0578	614.0	39.5	79.0	596.0	8.0	16.0	595.0	3.0	6.0	100
OJL531	104.20	34.89	7.85	0.330	2.80E+03	1.70E+03	0.0585	0.0027	0.641	0.030	0.0796	0.0011	0.1954	549.0	50.5	101.0	503.0	9.5	19.0	494.0	3.5	7.0	98
OJL532	260.00	113.40	42.10	0.440	4.60E+03	7.70E+03	0.0653	0.0022	1.187	0.038	0.1015	0.0015	0.0521	784.0	35.5	71.0	795.0	7.0	15.0	804.0	4.5	9.0	101
OJL533	111.00	816.00	117.10	0.730	9.30E+04	3.40E+04	0.0642	0.0020	0.653	0.025	0.0746	0.0024	0.9024	747.0	33.0	66.0	510.0	7.5	15.0	464.0	7.0	14.0	91
OJL534	655.20	33.60	39.20	0.050	9.50E+03	6.20E+03	0.0656	0.0025	1.039	0.036	0.1145	0.0013	-0.1001	794.0	40.0	80.0	723.0	9.0	18.0	699.0	4.0	8.0	97
OJL535	176.10	71.27	70.16	0.400	2.50E+04	2.10E+04	0.1241	0.0023	6.701	0.180	0.3834	0.0037	0.2682	2016.0	16.5	33.0	2073.0	12.0	24.0	2092.0	8.5	17.0	101
OJL536	225.00	46.10	83.60	0.200	3.50E+06	3.70E+04	0.2612	0.0046	22.970	0.670	0.6277	0.0072	0.8256	3254.0	14.0	28.0	3226.0	14.0	28.0	3140.0	14.5	29.0	97
OJL537	354.60	71.20	81.20	0.200	5.00E+06	2.70E+06	0.1682	0.0027	10.840	0.280	0.4602	0.0043	0.4030	2540.0	13.5	27.0	2510.0	12.0	24.0	2440.0	9.5	19.0	97
OJL538	918.00	34.00	27.54	0.310	3.00E+04	1.20E+04	0.0625	0.0022	0.835	0.027	0.0975	0.0010	0.0781	691.0	37.5	75.0	616.0	7.5	15.0	600.0	3.0	6.0	97
OJL539	318.00	34.32	7.73	0.360	2.50E+03	2.90E+03	0.0596	0.0032	0.652	0.033	0.0807	0.0011	0.0861	589.0	58.0	116.0	510.0	10.0	20.0	500.0	3.5	7.0	98
OJL540	19.41	22.15	24.80	1.140	1.88E+04	8.20E+03	0.1536	0.0043	9.710	0.320	0.4510	0.0055	0.0462	2386.0	24.0	48.0	2408.0	15.0	30.0	2400.0	12.0	24.0	100
OJL541	76.03	44.98	31.28	0.590	4.50E+04	2.00E+04	0.0935	0.0022	3.468	0.110	0.2641	0.0031	0.0596	1498.0	22.0	44.0	1520.0	12.5	25.0	1511.0	8.0	16.0	98
OJL542	130.60	97.30	100.80	0.750	7.00E+03	3.50E+05	0.1364	0.0025	7.836	0.210	0.4090	0.0043	0.2986	2182.0	16.0	32.0	2212.0	12.0	24.0	2210.0	10.0	20.0	100
OJL543	385.00	31.88	53.80	0.830	1.60E+04	1.70E+04	0.2084	0.0043	19.000	0.550	0.6427	0.0076	0.3442	2893.0	16.5	33.0	3042.0	14.0	28.0	3200.0	15.0	30.0	105
OJL544	155.90	30.20	7.18	0.190	1.50E+05	1.70E+05	0.0624	0.0024	0.645	0.025	0.0815	0.0009	0.0732	518.0	49.5	91.0	505.0	7.5	15.0	505.0	2.5	5.0	100
OJL545	276.90	177.50	45.42	0.640	1.24E+05	4.90E+04	0.0618	0.0023	12.776	0.370	0.0932	0.0011	0.0432	667.0	40.0	80.0	595.0	8.0	16.0	575.0	3.0	6.0	97
OJL546	33.65	68.20	85.00	2.030	6.10E+04	3.90E+04	0.1808	0.0039	0.770	0.280	0.5012	0.0063	0.2669	2660.0	18.0	36.0	2663.0	13.5	27.0	2619.0	13.5	27.0	98
OJL547	88.10	69.70	82.60	0.500	5.00E+04	2.40E+04	0.1713	0.0032	11.120	0.320	0.4669	0.0054	0.5566	2570.0	15.5	31.0	2533.0	13.5	27.0	2466.0	12.0	24.0	97
OJL548	1005.00	60.40	126.70	0.500	4.60E+05	3.70E+05	0.0605	0.0019	0.727	0.020	0.0880	0.0008	0.2344	620.0	34.0	68.0	555.0	6.0	12.0	544.0	2.5	5.0	98
OJL549	69.50	23.29	5.25	0.260	3.00E+05	2.30E+05	0.0570	0.0031	0.642	0.033	0.0804	0.0011	0.0431	492.0	60.0	120.0	504.0	10.0	20.0	499.0	3.5	7.0	99
OJL550	329.20	369.40	100.70	1.120	1.08E+05	8.40E+04	0.0614	0.0021	0.826	0.026	0.0979	0.0010	0.0377	653.0	36.5	73.0	615.0	7.0	14.0	602.0	3.0	6.0	98
OJL551	216.50	358.00	103.90	1.650	2.30E+04	4.90E+04	0.0602	0.0022	0.850	0.029	0.1027	0.0011	0.1538	611.0	39.5	79.0	625.0	8.0	16.0	630.0	3.0	6.0	101
OJL552	451.40	123.20	28.55	0.270	1.08E+05	8.40E+04	0.0571	0.0019	0.645	0.020	0.0823	0.0008	0.1361	495.0	36.5	73.0	505.0	6.0	12.0	510.0	2.5	5.0	101
OJL553	335.00	105.83	29.04	0.320	2.00E+05	1.00E+05	0.0612	0.0021	0.801	0.025	0.0951	0.0010	0.0132	646.0	37.0	74.0	597.0	7.0	14.0	585.0	3.0	6.0	98
OJL554	105.50	175.40	234.30	1.660	7.10E+05	3.70E+05	0.1958	0.0035	14.490	0.390	0.5317	0.0052	0.1555	2792.0	14.5	29.0	2782.0	13.0	26.0	2749.0	11.0	22.0	99
OJL555	49.24	39.88	41.05	0.810	6.60E+04	3.60E+04	0.1303	0.0030	7.010	0.220	0.3891	0.0046	0.3338	2102.0	20.0	40.0	2113.0	14.0	28.0	2119.0	10.5	21.0	100
OJL556	382.00	90.90	23.85	0.240	-1.90E+04	4.40E+04	0.0595	0.0020	0.749	0.024	0.0912	0.0010	0.3116	585.0	36.5	73.0	588.0	7.0	14.0	592.0	3.0	6.0	99
OJL557	278.10	348.30	102.20	1.250	4.70E+04	4.00E+04	0.0603	0.0021	0.847	0.027	0.1021	0.0010	0.2230	614.0	37.5	75.0	623.0	7.5	15.0	627.0	3.0	6.0	100
OJL558	326.10	46.48	42.10	0.140	4.00E+05	2.40E+05	0.2068	0.0034	14.070	0.380	0.4932	0.0056	0.7428	2881.0	13.5	27.0	2754.0	13.0	26.0	2585.0	12.0	24.0	94
OJL559	382.30	394.20	443.50	1.030	6.10E+05	3.40E+05	0.1593	0.0026	9.662	0.250	0.4406	0.0041	0.2846	2448.0	14.0	28.0	2403.0	12.0	24.0	2353.0	9.0	18.0	98
OJL560	938.00	393.00	103.70	0.420	4.00E+04	8.70E+04	0.0594	0.0018	0.774	0.022	0.0950	0.0009	0.1643	582.0	33.0	66.0	582.0	6.5	13.0	585.0	2.5	5.0	100
OJL561	801.00	282.00	213.30	0.350	1.50E+05	2.70E+05	0.1359	0.0022	6.010	0.170	0.3213	0.0048	0.8548	2175.0	14.0	28.0	1977.0	12.5	25.0	1796.0	11.5	23.0	91
OJL562	423.40	242.20	63.70	0.570	8.60E+04	5.00E+04	0.0591	0.0020	0.773	0.024	0.0941	0.0011	-0.0214	571.0	37.0	74.0	581.0	7.0	14.0	580.0	3.0	6.0	100
OJL563	247.70	250.70	71.40	1.010	1.07E+05	5.90E+04	0.0597	0.0021	0.834	0.028	0.1012	0.0011	0.1180	593.0	38.0	76.0	616.0	7.5	15.0	621.0	3.0	6.0	101
OJL564	411.90	497.90	147.90	1.210	3.60E+04	2.70E+04	0.0609	0.0020	0.782	0.025	0.0947	0.0009	0.0958	593.0	38.0	76.0	587.0	7.0	14.0	583.0	2.5	5.0	99
OJL565	388.20	408.00	90.60	1.050	1.22E+05	4.60E+04	0.0600	0.0021	0.702	0.023	0.0848	0.0010	0.0961	604.0	38.0	76.0	632.0	7.5	15.0	630.0	3.0	6.0	100
OJL566	424.00	117.70	31.22	0.280	5.00E+04	3.40E+04	0.0572	0.0019	0.798	0.026	0.1009	0.0011	0.2459	499.0	36.5	73.0	596.0	7.5	15.0	620.0	3.0	6.0	104
OJL567	247.90	86.80	23.23	0.350	7.40E+04	2.60E+04	0.0579	0.0022	0.769	0.027	0.0963	0.0011	0.1105	526.0	41.5	83.0	579.0	7.5	15.0	592.0	3.0	6.0	102
OJL568	451.80	192.90	51.99	0.430	6.40E+04	4.40E+04	0.0592	0.0020	0.780	0.024	0.0985	0.0010	0.1760	574.0	3								

ANALYSIS	U (ppm)	Th (ppm)	Pb (ppm)	ThU	Ratios				Ages (Ma)				Concordance (%)										
					$^{206}\text{Pb}/^{238}\text{U}$	$^{207}\text{Pb}/^{235}\text{U}$	$^{207}\text{Pb}/^{206}\text{Pb}$	$^{206}\text{Pb}/^{238}\text{U}$	2σ	Error correction	$^{207}\text{Pb}/^{235}\text{U}$	σ	2σ	$^{206}\text{Pb}/^{238}\text{U}$	σ	2σ	Concordance (%)						
OUJ5260	356.00	82.60	19.12	0.230	-2.40E+04	2.40E+04	0.0600	0.0021	0.750	0.025	0.0908	0.0010	0.0134	604.0	38.0	76.0	568.0	7.0	14.0	560.0	3.0	6.0	99
OUJ5261	311.80	148.00	157.30	0.470	1.70E+05	1.80E+05	0.1361	0.0023	7.675	0.200	0.4032	0.0038	0.2626	2178.0	14.5	29.0	2194.0	11.5	23.0	2184.0	8.5	17.0	100
OUJ5262	982.20	53.30	59.82	0.540	5.10E+04	5.80E+04	0.1434	0.0027	8.710	0.240	0.4349	0.0045	0.3078	2269.0	16.0	32.0	2308.0	12.5	25.0	2328.0	10.0	20.0	101
OUJ5263	165.90	99.28	33.44	0.600	-1.80E+04	1.80E+04	0.0637	0.0019	1.013	0.034	0.1165	0.0013	0.1024	732.0	38.0	76.0	710.0	8.5	17.0	710.0	4.0	8.0	100
OUJ5264	538.20	226.70	61.60	0.420	-4.90E+04	4.70E+04	0.0609	0.0013	0.794	0.024	0.0947	0.0010	0.3182	635.0	33.5	67.0	593.0	7.0	14.0	583.0	3.0	6.0	98
OUJ5265	113.16	175.40	51.60	1.550	-1.94E+04	7.20E+03	0.0623	0.0025	0.865	0.034	0.1000	0.0012	0.1448	684.0	43.0	86.0	633.0	9.0	18.0	615.0	3.5	7.0	97
OUJ5266	101.50	100.60	31.45	0.990	-2.30E+04	6.00E+03	0.0646	0.0027	0.959	0.037	0.1076	0.0013	0.1256	761.0	44.0	88.0	695.0	9.5	19.0	659.0	4.0	8.0	96
OUJ5267	229.50	91.44	25.80	0.490	-5.10E+04	1.30E+04	0.0609	0.0023	0.790	0.028	0.0952	0.0010	0.0131	611.0	41.5	83.0	591.0	8.0	16.0	586.0	3.0	6.0	99
OUJ5268	225.60	63.83	17.69	0.280	-2.80E+04	1.30E+04	0.0609	0.0023	0.800	0.028	0.0956	0.0011	0.1548	636.0	40.5	81.0	589.0	8.0	16.0	589.0	3.0	6.0	99
OUJ5270	192.90	56.20	13.96	0.300	-2.50E+04	1.70E+04	0.0583	0.0024	0.656	0.026	0.0827	0.0010	0.1670	541.0	45.0	90.0	512.0	8.0	16.0	512.0	3.0	6.0	100
OUJ5271	284.10	147.00	105.50	0.520	-4.40E+04	4.20E+04	0.0934	0.0017	3.426	0.093	0.2636	0.0025	0.2907	1496.0	17.0	34.0	1510.0	10.5	21.0	1508.0	6.5	13.0	100
OUJ5272	151.60	134.30	174.40	0.220	3.00E+05	2.20E+05	0.1802	0.0028	12.773	0.330	0.5048	0.0045	0.4190	2655.0	13.0	26.0	2634.0	12.0	24.0	2634.0	9.5	19.0	99
OUJ5273	362.50	93.40	25.09	0.260	-2.20E+04	1.80E+04	0.0597	0.0020	0.778	0.024	0.0940	0.0010	0.1590	593.0	36.5	73.0	584.0	7.0	14.0	579.0	3.0	6.0	99
OUJ5274	128.00	381.70	70.40	0.340	-4.40E+04	4.60E+04	0.0591	0.0018	0.959	0.017	0.0726	0.0007	0.3694	570.0	33.0	66.0	473.0	5.5	11.0	452.0	2.0	4.0	96
OUJ5275	247.90	359.00	109.10	1.450	1.00E+03	1.50E+04	0.0673	0.0027	0.681	0.036	0.1010	0.0011	0.3232	847.0	41.5	83.0	666.0	9.5	19.0	620.0	3.0	6.0	93
OUJ5276	278.00	368.00	90.30	1.320	1.90E+04	2.00E+04	0.0648	0.0022	0.887	0.030	0.0981	0.0013	0.3441	768.0	36.0	72.0	645.0	8.0	16.0	603.0	4.0	8.0	94
OUJ5277	59.42	28.01	12.72	0.470	-5.10E+03	4.80E+03	0.0582	0.0021	0.752	0.024	0.0930	0.0010	-0.0477	503.0	39.5	79.0	569.0	7.0	14.0	573.0	3.0	6.0	101
OUJ5278	218.50	73.00	17.87	0.330	-4.60E+03	9.20E+03	0.0581	0.0023	0.653	0.024	0.0816	0.0009	0.1369	534.0	43.5	87.0	510.0	7.5	15.0	505.0	2.5	5.0	99
OUJ5279	274.60	98.40	21.59	0.360	-1.88E+04	6.00E+03	0.0570	0.0022	0.600	0.022	0.0785	0.0008	0.0464	492.0	42.5	85.0	477.0	7.0	14.0	475.0	2.5	5.0	100
OUJ5280	377.00	183.00	46.70	0.490	-1.60E+04	1.30E+04	0.0601	0.0021	0.763	0.025	0.0923	0.0009	0.0813	607.0	38.0	76.0	576.0	7.0	14.0	569.0	2.5	5.0	99
OUJ5281	121.90	141.00	39.99	1.160	-4.10E+03	5.90E+03	0.0600	0.0025	0.821	0.032	0.0998	0.0012	0.0544	604.0	45.0	90.0	609.0	9.0	18.0	613.0	3.5	7.0	101
OUJ5282	105.90	59.60	50.60	0.510	1.00E+03	1.90E+04	0.1281	0.0026	6.542	0.190	0.3677	0.0039	0.1985	2072.0	18.0	36.0	2052.0	13.0	26.0	2019.0	9.0	18.0	98
OUJ5283	291.40	185.10	206.60	0.640	-2.70E+04	4.10E+04	0.1552	0.0025	9.249	0.240	0.4305	0.0042	0.4102	2404.0	13.5	27.0	2363.0	12.0	24.0	2303.0	9.5	19.0	98
OUJ5284	277.00	80.35	21.12	0.290	-1.73E+04	5.40E+03	0.0582	0.0021	0.752	0.024	0.0930	0.0010	-0.0477	503.0	39.5	79.0	569.0	7.0	14.0	573.0	3.0	6.0	101
OUJ5285	176.40	81.71	21.69	0.460	1.70E+04	1.0E+04	0.0593	0.0023	0.768	0.028	0.0941	0.0011	0.1115	578.0	42.0	84.0	579.0	8.0	16.0	580.0	3.0	6.0	100
OUJ5286	717.00	726.00	202.70	1.010	-4.00E+04	1.70E+04	0.0607	0.0019	0.828	0.023	0.0988	0.0009	0.0794	628.0	33.5	67.0	613.0	6.5	13.0	607.0	2.5	5.0	99
OUJ5287	162.40	218.70	61.40	1.350	9.50E+03	9.10E+03	0.0627	0.0025	0.855	0.033	0.0998	0.0012	0.1344	698.0	42.5	85.0	627.0	9.0	18.0	613.0	3.5	7.0	98
OUJ5288	143.10	106.86	111.40	0.750	6.00E+04	3.30E+04	0.1367	0.0026	7.675	0.210	0.4045	0.0041	0.1219	2186.0	16.5	33.0	2194.0	12.5	25.0	2190.0	9.5	19.0	100
OUJ5289	783.00	253.00	51.60	0.320	-4.70E+04	1.80E+04	0.0592	0.0019	0.601	0.019	0.0751	0.0014	0.0693	573.0	35.0	70.0	487.0	6.0	12.0	467.0	4.0	8.0	98
OUJ5290	390.80	115.95	29.60	0.300	-3.00E+04	1.0E+04	0.0570	0.0020	0.636	0.021	0.0807	0.0008	0.1171	492.0	38.5	77.0	500.0	6.5	13.0	500.0	2.5	5.0	100
OUJ5291	415.00	450.00	129.60	1.080	4.30E+04	2.0E+04	0.0603	0.0020	0.861	0.027	0.1037	0.0011	0.0942	614.0	36.0	72.0	631.0	7.5	15.0	636.0	3.0	6.0	101
OUJ5292	363.30	289.30	80.40	0.800	-2.30E+04	2.80E+04	0.0613	0.0021	0.849	0.026	0.1006	0.0010	-0.0030	650.0	37.0	74.0	624.0	7.0	14.0	618.0	3.0	6.0	99
OUJ5293	297.10	201.50	46.80	0.680	-3.00E+04	2.60E+04	0.0585	0.0021	0.663	0.023	0.0826	0.0008	0.0929	549.0	39.0	78.0	516.0	7.0	14.0	512.0	2.5	5.0	99
OUJ5294	512.00	195.30	43.00	0.380	1.00E+04	5.40E+04	0.0574	0.0019	0.629	0.019	0.0794	0.0008	0.0273	507.0	36.5	73.0	495.0	6.0	12.0	493.0	2.5	5.0	99
OUJ5295	351.00	143.60	40.40	0.410	-6.40E+04	1.90E+04	0.0690	0.0024	1.372	0.045	0.1454	0.0015	0.0970	899.0	36.0	72.0	875.0	9.5	19.0	875.0	3.0	6.0	100
OUJ5296	351.00	143.60	40.40	0.410	1.10E+05	1.0E+05	0.0602	0.0020	0.814	0.025	0.0978	0.0010	0.1914	611.0	36.0	72.0	605.0	7.0	14.0	601.0	3.0	6.0	99
OUJ5297	488.00	130.20	35.11	0.310	-3.29E+05	8.00E+04	0.0571	0.0019	0.651	0.020	0.0821	0.0008	0.1050	495.0	36.5	73.0	509.0	6.0	12.0	509.0	2.5	5.0	100
OUJ5298	497.70	154.30	22.28	0.270	-6.80E+05	5.20E+05	0.0592	0.0020	0.646	0.020	0.0798	0.0008	0.1399	574.0	36.5	73.0	506.0	6.0	12.0	495.0	2.5	5.0	98
OUJ5299	285.80	86.20	23.16	0.300	-1.70E+05	2.60E+05	0.0581	0.0021	0.738	0.025	0.0927	0.0010	0.0460	534.0	39.5	79.0	561.0	7.5	15.0	572.0	3.0	6.0	102
OUJ52101	217.90	158.30	144.00	0.730	3.20E+05	1.40E+05	0.1173	0.0021	5.700	0.150	0.3449	0.0033	0.1489	1923.0	16.0	32.0	1931.0	11.5	23.0	1910.0	8.0	16.0	99
OUJ52102	143.00	54.20	14.53	0.380	1.50E+04	2.50E+04	0.0623	0.0027	0.815	0.032	0.0949	0.0011	-0.1317	684.0	46.5	93.0	605.0	9.0	18.0	584.0	3.0	6.0	97
OUJ52103	835.00	352.90	81.15	0.420	2.00E+05	5.00E+04	0.0586	0.0019	0.656	0.019	0.0817	0.0008	0.0937	553.0	35.5	71.0	512.0	6.0	12.0	506.0	2.5	5.0	99
OUJ52104	140.50	42.51	45.10	0.300	1.10E+05	4.20E+04	0.1360	0.0025	7.724	0.210	0.4040	0.0040	0.2364	2177.0	16.0	32.0	2199.0	12.0	24.0	2187.0	9.0	18.0	99
OUJ52104c	258.90	213.20	62.90	0.820	-1.90E+04	2.80E+04	0.0614	0.0021	0.893	0.029	0.1024	0.0011	0.1678	653.0	36.5	73.0	647.0	8.0	16.0	644.0	3.0	6.0	100
OUJ52105	213.50	166.40	49.48	0.780	2.41E+04	8.20E+03	0.0619	0.0024	0.873	0.031	0.1024	0.0011	-0.0747	671.0	41.5	83.0	637.0	8.5	17.0	628.0	3.0	6.0	99
OUJ52106	367.30	86.00	20.15	0.230	-4.00E+04	2.20E+04	0.0578	0.0021	0.650	0.022	0.0825	0.0009	0.0514	522.0	40.0	80.0	508.0	7.0	14.0	511.0	2.5	5.0	101
OUJ52107c	307.00	210.60	246.80	0.690	1.28E+05	4.20E+04	0.1676	0.0028	11.002	0.290	0.4626	0.0046	0.3511	2534.0	14.0	28.0	2523.0	12.5	25.0	2451.0	10.0	20.0	97
OUJ52107f	234.40	79.92	70.70	0.340	-1.93E+05	8.00E+04	0.1231	0.0022	6.020	0.160	0.3444	0.0034	0.3274	2002.0	16.0	32.0	1979.0	11.5	23.0	1908.0	8.0	16.0	96
OUJ52108	121.70	95.80	95.60																				

ANALYSIS	U (ppm)	Th (ppm)	Pb (ppm)	Th/U	Ratios			Ages (Ma)			Concordance (%)										
					$^{207}\text{Pb}/^{206}\text{Pb}$	$^{207}\text{Pb}/^{235}\text{U}$	$^{206}\text{Pb}/^{238}\text{U}$	$^{207}\text{Pb}/^{206}\text{Pb}$	$^{207}\text{Pb}/^{235}\text{U}$	$^{206}\text{Pb}/^{238}\text{U}$	σ	2σ	σ	2σ							
OJJ5z126	1027.00	64.90	15.13	0.060	1.00E+05	0.0019	0.645	0.018	0.0785	0.0008	0.0713	569.0	35.0	70.0	505.0	5.5	11.0	487.0	2.5	5.0	96
OJJ5z127c	256.50	69.37	83.10	0.250	1.65E+05	0.0036	16.580	0.440	0.5222	0.0052	0.5483	2993.0	13.0	26.0	2911.0	12.5	25.0	2709.0	11.0	22.0	93
OJJ5z127f	174.10	61.34	14.98	0.350	1.88E+04	0.0295	0.686	0.029	0.0850	0.0010	0.0943	534.0	47.0	94.0	530.0	8.5	17.0	526.0	3.0	6.0	99
OJJ5z128	212.20	97.10	26.10	0.460	3.60E+04	0.0024	0.789	0.029	0.0945	0.0011	0.0142	604.0	43.5	87.0	591.0	8.0	16.0	582.0	3.0	6.0	99
OJJ5z129	148.20	97.70	119.40	0.670	1.15E+05	0.0029	10.980	0.300	0.4690	0.0047	0.4107	2495.0	15.0	30.0	2521.0	12.5	25.0	2479.0	10.5	21.0	98
OJJ5z130	187.30	87.40	88.90	0.470	1.18E+05	0.0024	7.060	0.190	0.3824	0.0036	0.1447	2083.0	16.5	33.0	2119.0	12.0	24.0	2087.0	8.5	17.0	99
OJJ5z131	1148.00	291.50	286.50	0.250	4.80E+05	0.0021	6.687	0.170	0.3499	0.0033	0.5373	2149.0	13.5	27.0	2071.0	11.0	22.0	1934.0	8.0	16.0	93
OJJ5z133c	96.72	20.75	4.78	0.210	9.60E+03	0.0029	0.628	0.031	0.0798	0.0010	-0.0281	484.0	56.5	113.0	495.0	9.5	19.0	495.0	3.0	6.0	100
OJJ5z133f	65.02	18.42	4.04	0.280	1.07E+04	0.0034	0.648	0.035	0.0812	0.0013	0.1234	556.0	63.0	126.0	507.0	11.0	22.0	503.0	4.0	8.0	99
OJJ5z134	383.60	160.10	44.08	0.420	1.90E+04	0.0022	0.813	0.027	0.0942	0.0009	-0.0449	671.0	38.0	76.0	604.0	7.5	15.0	580.0	2.5	5.0	96
OJJ5z135	204.90	131.01	35.38	0.640	3.50E+04	0.0023	0.789	0.028	0.0931	0.0010	0.0376	629.0	41.0	82.0	591.0	8.0	16.0	574.0	3.0	6.0	97
OJJ5z136	171.50	211.70	59.40	1.230	3.30E+04	0.0026	0.847	0.033	0.0997	0.0012	-0.0818	646.0	45.5	91.0	623.0	9.0	18.0	612.0	3.5	7.0	98
OJJ5z137	1018.00	718.00	164.40	0.710	1.00E+05	0.0019	0.715	0.021	0.0813	0.0012	0.8976	708.0	32.0	64.0	548.0	6.0	12.0	504.0	3.5	7.0	92
OJJ5z138	280.00	213.00	65.60	0.760	4.70E+04	0.0022	0.889	0.029	0.1099	0.0011	0.0761	667.0	38.0	76.0	646.0	8.0	16.0	637.0	3.0	6.0	99
OJJ5z139	184.90	65.60	14.38	0.350	2.40E+04	0.0025	0.637	0.027	0.0780	0.0009	0.1905	560.0	46.5	93.0	500.0	8.5	17.0	484.0	2.5	5.0	97
OJJ5z140	402.50	135.90	31.48	0.340	2.90E+04	0.0021	0.677	0.022	0.0819	0.0008	0.1296	596.0	38.0	76.0	525.0	6.5	13.0	508.0	2.5	5.0	97
Discordant data																					
OJJ5z104f	44.71	24.38	8.30	0.550	3.40E+03	0.0044	1.077	0.062	0.1073	0.0017	0.0687	1014.0	61.0	122.0	742.0	15.0	30.0	657.0	5.0	10.0	89
OJJ5z123	35.90	6.81	0.95	0.190	2.00E+02	0.0655	0.765	0.070	0.0825	0.0034	0.4921	790.0	88.0	176.0	577.0	20.0	40.0	511.0	10.0	20.0	89

Footnotes:

. Analysis references: OJJ5z is Zircon from sample OJJ5 (mount CT18-6), followed by grain number "c" or "f", meaning core or rim, respectively.

Chapter II, Section II.3

Table D.29: Sample OJL6 (LA-ICPMS)

IGSN: IEACC0022

Coordinate UTM: Zone 30S, 574362 m E, 3821747 m N

ANALYSIS	U (ppm)	Th (ppm)	Pb (ppm)	Th/U	206Pb/238Pb		207Pb/235U		Ratios		Concordant data		Error correction	207Pb/206Pb		Ages (Ma)		206Pb/238U	σ	2σ	Concordance (%)		
					206Pb/238Pb	σ	207Pb/235U	σ	207Pb/206Pb	σ	207Pb/235U	σ		207Pb/206Pb	σ	207Pb/235U	σ					207Pb/206Pb	σ
OJL621	125.52	55.18	56.15	0.440	1.70E+03	2.20E+03	0.1288	0.0025	6.849	0.190	0.3864	0.0039	0.1973	2082.0	17.0	34.0	2092.0	12.5	25.0	2106.0	9.0	18.0	101
OJL622	674.00	489.00	133.10	0.730	1.41E+04	6.90E+03	0.0601	0.0019	0.775	0.023	0.0935	0.0012	0.4272	607.0	34.0	68.0	583.0	6.5	13.0	576.0	3.5	7.0	99
OJL623	187.00	126.60	166.10	0.830	-9.60E+04	1.50E+04	0.1845	0.0031	13.300	0.350	0.5237	0.0051	0.5753	2694.0	14.0	28.0	2701.0	12.5	25.0	2715.0	11.0	22.0	101
OJL624	572.00	372.00	318.30	0.430	5.90E+03	8.90E+03	0.1308	0.0021	6.716	0.170	0.3741	0.0036	0.3721	2109.0	14.0	28.0	2075.0	11.0	22.0	2049.0	8.5	17.0	99
OJL625	67.60	51.20	18.77	0.760	-4.20E+02	2.30E+02	0.0690	0.0032	1.175	0.052	0.1237	0.0017	0.1179	899.0	48.0	96.0	789.0	12.0	24.0	752.0	5.0	10.0	95
OJL626	94.30	49.06	13.14	0.520	-1.40E+02	1.70E+02	0.0598	0.0028	0.771	0.035	0.0925	0.0013	0.1435	596.0	50.0	101.0	580.0	10.0	20.0	570.0	4.0	8.0	98
OJL627	104.65	62.11	18.71	0.740	4.00E+02	2.00E+02	0.0594	0.0028	0.858	0.038	0.1039	0.0014	-0.0378	582.0	51.0	102.0	629.0	10.5	21.0	637.0	4.0	8.0	101
OJL628	84.25	33.18	7.81	0.320	-6.30E+02	2.40E+02	0.0555	0.0026	0.611	0.028	0.0796	0.0011	0.0381	432.0	52.0	104.0	484.0	9.0	18.0	494.0	3.5	7.0	102
OJL629	930.00	688.00	569.50	0.740	1.50E+03	4.40E+03	0.1348	0.0021	5.831	0.150	0.3176	0.0036	0.2416	2162.0	13.5	27.0	1951.0	11.0	22.0	1779.0	9.0	18.0	91
OJL6210	249.90	231.60	66.90	0.930	-8.30E+02	4.60E+02	0.0600	0.0021	0.634	0.027	0.1005	0.0010	0.1143	604.0	36.0	76.0	616.0	7.5	15.0	617.0	3.0	6.0	100
OJL6211	461.60	451.50	124.40	0.980	-3.40E+03	1.00E+03	0.0579	0.0019	0.800	0.024	0.0999	0.0010	0.1234	526.0	36.0	72.0	597.0	7.0	14.0	614.0	3.0	6.0	103
OJL6212	372.60	321.10	92.90	0.860	1.23E+03	8.40E+02	0.0588	0.0019	0.839	0.026	0.1020	0.0011	0.0383	596.0	34.5	69.0	619.0	7.0	14.0	626.0	3.0	6.0	101
OJL6213	641.70	376.20	101.80	0.590	-2.13E+04	9.40E+03	0.0580	0.0018	0.762	0.022	0.0945	0.0009	0.2176	531.0	34.0	68.0	575.0	6.5	13.0	582.0	3.0	6.0	101
OJL6214	415.00	328.00	86.90	0.790	-5.20E+02	5.90E+02	0.0603	0.0020	0.809	0.025	0.0964	0.0010	0.0293	614.0	36.0	72.0	602.0	7.0	14.0	593.0	3.0	6.0	99
OJL6215	1014.00	595.00	145.20	0.590	-3.80E+03	5.90E+03	0.0598	0.0018	0.732	0.021	0.0881	0.0010	0.0344	597.0	32.5	65.0	558.0	6.0	12.0	544.0	3.0	6.0	98
OJL6216	148.90	197.70	55.26	1.330	1.30E+02	1.40E+02	0.0590	0.0025	0.802	0.032	0.0985	0.0011	0.1080	567.0	46.0	92.0	588.0	9.0	18.0	606.0	3.0	6.0	101
OJL6217	380.40	105.80	23.58	0.280	-4.50E+02	3.00E+02	0.0586	0.0021	0.617	0.021	0.0796	0.0008	-0.0191	476.0	41.0	82.0	488.0	6.5	13.0	488.0	2.5	5.0	100
OJL6218	93.75	79.70	35.80	0.850	5.00E+01	1.20E+02	0.0779	0.0030	1.626	0.059	0.1494	0.0018	0.1010	1144.0	38.5	77.0	980.0	11.5	23.0	898.0	5.0	10.0	92
OJL6219	272.80	106.10	23.30	0.390	-4.00E+02	2.10E+02	0.0561	0.0020	0.621	0.022	0.0793	0.0009	0.1931	456.0	39.5	79.0	490.0	7.0	14.0	492.0	2.5	5.0	100
OJL6220	274.30	75.80	95.20	0.280	-3.20E+03	2.20E+03	0.0596	0.0035	13.010	0.340	0.4574	0.0045	0.5148	2902.0	13.5	27.0	2680.0	12.5	25.0	2428.0	10.0	20.0	91
OJL6221	106.43	54.02	16.73	0.510	-3.40E+02	1.70E+02	0.0601	0.0027	0.899	0.039	0.1087	0.0013	0.1804	607.0	48.5	97.0	651.0	10.5	21.0	665.0	4.0	8.0	102
OJL6222	441.30	208.10	55.20	0.750	5.00E+04	1.10E+04	0.0580	0.0019	0.756	0.023	0.0899	0.0009	0.1418	530.0	36.0	72.0	572.0	6.5	13.0	584.0	3.0	6.0	101
OJL6223	297.90	160.30	35.51	0.540	-1.00E+02	5.10E+03	0.0559	0.0021	0.586	0.021	0.0757	0.0008	0.0156	448.0	41.5	83.0	468.0	6.5	13.0	470.0	2.5	5.0	100
OJL6224	206.50	145.40	41.48	0.700	-2.90E+03	4.70E+03	0.0600	0.0023	0.815	0.029	0.0978	0.0010	0.0295	604.0	41.5	83.0	605.0	8.0	16.0	602.0	3.0	6.0	99
OJL6225	347.00	352.60	102.10	1.020	-1.20E+03	5.80E+02	0.0620	0.0022	0.887	0.029	0.1031	0.0010	0.1151	674.0	38.0	76.0	645.0	8.0	16.0	633.0	3.0	6.0	98
OJL6226	141.30	27.79	38.17	0.200	-4.50E+03	2.50E+03	0.1951	0.0034	14.000	0.380	0.5284	0.0053	0.4045	2786.0	14.5	29.0	2750.0	13.0	26.0	2735.0	11.0	22.0	99
OJL6227	353.60	185.00	50.40	0.520	-7.30E+02	5.60E+02	0.0586	0.0021	0.770	0.026	0.0948	0.0010	-0.0646	552.0	39.0	78.0	580.0	7.5	15.0	584.0	3.0	6.0	101
OJL6228	636.00	279.80	73.00	0.440	-4.30E+03	2.00E+03	0.0580	0.0019	0.749	0.020	0.0930	0.0009	0.0869	530.0	36.0	72.0	568.0	6.5	13.0	573.0	2.5	5.0	101
OJL6229	227.20	231.90	243.00	1.020	2.40E+04	6.90E+04	0.1559	0.0026	8.514	0.230	0.4107	0.0042	0.4243	2390.0	14.5	29.0	2287.0	12.5	25.0	2218.0	9.5	19.0	97
OJL6230	119.50	51.20	12.56	0.430	-1.27E+03	5.30E+02	0.0576	0.0024	0.782	0.031	0.0967	0.0012	0.0174	350.0	46.0	90.0	587.0	9.0	18.0	595.0	3.5	7.0	101
OJL6231	401.13	77.50	21.33	1.930	-3.50E+02	1.60E+02	0.0619	0.0041	0.807	0.051	0.0958	0.0016	0.0358	671.0	71.0	142.0	601.0	14.5	29.0	590.0	4.5	9.0	98
OJL6232	337.40	102.60	24.20	0.300	2.05E+03	8.20E+02	0.0571	0.0019	0.650	0.020	0.0832	0.0009	0.1731	495.0	36.5	73.0	508.0	6.0	12.0	515.0	2.5	5.0	101
OJL6233	159.00	82.30	78.10	0.520	-3.90E+02	1.30E+03	0.0623	0.0023	6.141	0.170	0.3502	0.0036	0.3927	2090.0	15.5	31.0	1996.0	12.0	24.0	1936.0	8.5	17.0	97
OJL6234	156.10	484.50	139.50	3.100	-6.00E+02	5.90E+02	0.0618	0.0024	0.833	0.031	0.0979	0.0011	0.2270	667.0	41.5	83.0	615.0	8.5	17.0	602.0	3.0	6.0	98
OJL6235	124.10	99.40	26.93	0.800	-2.60E+03	1.10E+03	0.0588	0.0026	0.746	0.031	0.0930	0.0012	-0.0395	560.0	48.0	96.0	566.0	9.0	18.0	573.0	3.5	7.0	101
OJL6236	328.10	171.20	47.24	0.520	1.03E+04	4.50E+03	0.0588	0.0020	0.762	0.024	0.0945	0.0010	0.0643	560.0	37.0	74.0	575.0	7.0	14.0	582.0	3.0	6.0	101
OJL6237	314.20	114.00	17.54	0.360	2.90E+02	8.70E+02	0.0635	0.0024	0.621	0.024	0.0717	0.0012	0.4455	725.0	40.0	80.0	490.0	7.5	15.0	446.0	3.5	7.0	91
OJL6238	291.30	238.90	304.40	0.820	-1.69E+05	4.90E+04	0.1755	0.0029	11.365	0.290	0.4789	0.0044	0.4047	2611.0	14.0	28.0	2554.0	12.0	24.0	2522.0	9.5	19.0	99
OJL6239	424.40	11.15	8.76	0.030	-1.55E+05	5.30E+04	0.1279	0.0022	5.678	0.150	0.3306	0.0035	0.5027	2069.0	15.0	30.0	1928.0	11.5	23.0	1841.0	8.5	17.0	96
OJL6240	180.00	208.60	59.10	1.160	-1.16E+04	8.40E+03	0.0616	0.0023	0.823	0.028	0.0972	0.0011	0.1936	671.0	40.0	80.0	610.0	8.0	16.0	598.0	3.0	6.0	99
OJL6241	552.00	383.20	106.40	0.690	3.40E+05	1.40E+05	0.0619	0.0020	0.836	0.025	0.0992	0.0010	0.1179	660.0	35.0	70.0	617.0	7.0	14.0	610.0	3.0	6.0	99
OJL6242	406.70	207.30	46.50	0.650	1.38E+05	5.70E+04	0.0667	0.0020	0.604	0.020	0.0782	0.0008	0.0754	480.0	39.0	78.0	480.0	6.5	13.0	485.0	2.5	5.0	101
OJL6243	358.70	216.80	58.20	0.610	4.00E+04	2.20E+04	0.0600	0.0021	0.764	0.024	0.0934	0.0010	0.0602	604.0	38.0	76.0	576.0	7.0	14.0	576.0	3.0	6.0	100
OJL6244	191.20	94.90	25.41	0.500	3.80E+04	2.70E+04	0.0594	0.0023	0.752	0.028	0.0927	0.0010	0.0819	582.0	42.0	84.0	589.0	8.0	16.0	571.0	3.0	6.0	100
OJL6245	245.70	241.40	72.42	0.980	8.00E+04	3.00E+04	0.0623	0.0021	0.891	0.028	0.1041	0.0011	0.1426	684.0	36.0	72.0	647.0	7.5	15.0	638.0	3.0	6.0	99
OJL6246	547.20	316.60	382.00	0.580	5.00E+05	5.10E+05	0.1731	0.0027	10.087	0.260	0.4302	0.0043	0.6625	2588.0	13.0	26.0	2443.0	12.0	24.0	2307.0	9.5	19.0	94
OJL6247	62.60	47.77	48.26	0.760	1.36E+06	4.60E+05	0.1313	0.0028	6.800	0.200	0.3819	0.0042	0.2600	2193.0	18.5	37.0	2086.0	13.0	26.0	2085.0	10.0	20.0	100
OJL6248	349.00																						

ANALYSIS	U (ppm)	Th (ppm)	Pb (ppm)	ThU	Ratios				Ages (Ma)				Concordance (%)										
					$^{207}\text{Pb}/^{206}\text{Pb}$	$^{207}\text{Pb}/^{235}\text{U}$	$^{206}\text{Pb}/^{238}\text{U}$	$^{207}\text{Pb}/^{206}\text{Pb}$	$^{207}\text{Pb}/^{235}\text{U}$	$^{206}\text{Pb}/^{238}\text{U}$	σ	2σ											
OUJ6261	590.90	275.90	71.40	0.470	-4.10E-04	4.50E+04	0.0585	0.0019	0.736	0.021	0.0908	0.0009	0.0571	549.0	35.5	71.0	560.0	6.0	12.0	560.0	2.5	5.0	100
OUJ6262c	98.00	50.90	15.28	0.520	7.80E-04	5.70E+04	0.0612	0.0027	0.875	0.036	0.1041	0.0015	0.0778	646.0	47.5	95.0	638.0	9.5	15.0	638.0	4.5	9.0	100
OUJ6262r	279.50	139.50	40.65	0.500	-3.70E-04	2.70E+04	0.0601	0.0021	0.834	0.027	0.1008	0.0010	-0.0270	607.0	38.0	76.0	619.0	7.5	15.0	619.0	3.0	6.0	101
OUJ6263	340.20	143.60	39.91	0.420	-4.30E+05	0.56E+05	0.0587	0.0021	0.768	0.025	0.0950	0.0010	0.0850	566.0	39.0	78.0	579.0	7.0	14.0	585.0	3.0	6.0	101
OUJ6264	97.40	32.35	7.65	0.330	-4.20E-04	2.50E+04	0.0562	0.0029	0.622	0.030	0.0801	0.0011	-0.0483	460.0	57.0	114.0	491.0	9.5	19.0	486.0	3.5	7.0	101
OUJ6265	181.10	173.10	58.90	0.960	4.60E+04	4.50E+04	0.0638	0.0024	1.059	0.035	0.1196	0.0013	0.0002	735.0	40.0	80.0	733.0	8.5	17.0	728.0	3.5	7.0	99
OUJ6266	408.70	1350.00	370.00	3.300	3.90E+05	2.00E+05	0.0603	0.0021	0.806	0.026	0.0967	0.0010	0.2349	614.0	37.5	75.0	600.0	7.5	15.0	595.0	3.0	6.0	99
OUJ6267	657.60	322.00	87.10	0.490	-8.70E+06	8.20E+06	0.0583	0.0018	0.756	0.021	0.0934	0.0009	0.2241	541.0	33.5	67.0	571.0	6.0	12.0	575.0	2.5	5.0	101
OUJ6268	366.30	177.30	169.30	0.480	-1.23E+07	5.00E+06	0.1311	0.0029	6.810	0.180	0.3781	0.0040	0.5494	2113.0	14.5	29.0	2087.0	11.5	23.0	2067.0	9.5	19.0	99
OUJ6269	139.30	94.80	110.00	0.680	9.00E+05	2.00E+05	0.1570	0.0029	9.370	0.029	0.4309	0.0045	0.5195	2424.0	15.5	31.0	2375.0	12.5	25.0	2310.0	10.0	20.0	97
OUJ6270	280.00	146.20	237.00	0.520	4.20E+05	3.30E+05	0.2790	0.0045	24.840	0.640	0.6449	0.0062	0.3663	3357.0	12.5	25.0	3302.0	12.5	25.0	3208.0	12.0	24.0	97
OUJ6271	563.80	252.00	59.27	0.460	1.23E+05	6.80E+04	0.0567	0.0019	0.639	0.020	0.0817	0.0008	0.2610	480.0	37.0	74.0	502.0	6.0	12.0	506.0	2.5	5.0	101
OUJ6272	95.00	32.94	34.53	0.350	6.80E+04	6.20E+04	0.1314	0.0027	7.107	0.200	0.3910	0.0040	0.1769	2117.0	18.0	36.0	2123.0	12.5	25.0	2127.0	9.5	19.0	100
OUJ6273	25.50	38.68	37.47	1.520	9.10E+04	2.40E+04	0.1245	0.0037	6.500	0.220	0.3768	0.0050	0.1051	2022.0	28.5	53.0	2048.0	15.0	30.0	2061.0	11.5	23.0	101
OUJ6274	448.20	288.20	84.40	0.640	-5.70E+04	7.30E+04	0.0713	0.0023	1.152	0.035	0.1165	0.0012	0.2916	966.0	33.0	66.0	778.0	8.0	16.0	711.0	3.5	7.0	91
OUJ6275	364.79	203.70	63.07	2.090	-3.20E+04	1.40E+04	0.0592	0.0037	0.828	0.050	0.1017	0.0016	0.1359	624.0	68.0	136.0	613.0	14.0	28.0	624.0	4.5	9.0	102
OUJ6276	82.21	47.93	60.79	0.580	-9.50E+04	5.70E+04	0.1763	0.0034	12.320	0.340	0.4971	0.0052	0.2289	2637.0	16.0	32.0	2629.0	13.0	26.0	2601.0	11.0	22.0	99
OUJ6277	381.20	219.30	55.00	0.580	4.00E+04	1.70E+04	0.0589	0.0020	0.761	0.024	0.0916	0.0011	0.2841	600.0	36.0	72.0	575.0	7.0	14.0	565.0	3.0	6.0	98
OUJ6278	481.60	299.10	70.10	0.620	1.90E+04	1.60E+04	0.0575	0.0019	0.651	0.020	0.0818	0.0008	0.1375	511.0	36.5	73.0	509.0	6.0	12.0	507.0	2.5	5.0	100
OUJ6279	235.20	189.90	225.70	0.810	-2.90E+03	9.50E+03	0.1658	0.0028	10.733	0.280	0.4667	0.0045	0.3689	2516.0	14.0	28.0	2500.0	12.0	24.0	2469.0	10.0	20.0	99
OUJ6280	236.00	200.40	127.30	0.810	-1.37E+04	7.60E+03	0.1429	0.0024	8.009	0.210	0.4023	0.0038	0.3341	2283.0	14.5	29.0	2232.0	12.0	24.0	2180.0	8.5	17.0	98
OUJ6281	512.00	290.00	90.80	0.570	-6.70E+03	3.50E+03	0.0628	0.0020	0.953	0.028	0.1103	0.0011	0.2409	700.0	34.0	68.0	680.0	7.5	15.0	675.0	3.0	6.0	99
OUJ6282	332.70	483.40	117.40	1.450	2.60E+05	1.30E+05	0.0616	0.0021	0.789	0.025	0.0919	0.0011	0.2685	660.0	36.5	73.0	591.0	7.0	14.0	567.0	3.0	6.0	96
OUJ6283	140.30	121.70	39.90	0.870	3.10E+03	1.80E+03	0.0640	0.0027	1.066	0.041	0.1211	0.0014	0.0410	742.0	44.5	89.0	737.0	10.0	20.0	737.0	4.0	8.0	100
OUJ6284	197.80	64.80	64.80	0.330	2.30E+03	3.70E+03	0.1257	0.0022	6.709	0.180	0.3831	0.0037	0.3121	2039.0	15.5	31.0	2074.0	12.0	24.0	2091.0	8.5	17.0	101
OUJ6285	382.10	379.00	100.90	0.990	3.10E+03	1.70E+03	0.0613	0.0021	0.793	0.025	0.0939	0.0010	0.1266	650.0	37.0	74.0	583.0	7.0	14.0	578.0	3.0	6.0	98
OUJ6286	112.40	87.00	75.20	0.770	0.00E+00	1.30E+03	0.1112	0.0023	5.199	0.150	0.3345	0.0034	0.2464	1819.0	19.0	38.0	1852.0	12.5	25.0	1860.0	8.0	16.0	100
OUJ6287	529.70	255.80	68.30	0.430	8.70E+03	3.60E+03	0.0616	0.0020	0.800	0.024	0.0943	0.0009	0.2003	660.0	35.0	70.0	597.0	7.0	14.0	581.0	2.5	5.0	97
OUJ6288	239.80	103.80	104.70	0.480	6.30E+03	4.50E+03	0.1283	0.0023	6.999	0.190	0.3901	0.0042	0.3712	2075.0	16.0	32.0	2111.0	12.0	24.0	2123.0	9.5	19.0	101
OUJ6289	532.40	195.30	52.73	0.870	2.20E+03	1.80E+03	0.0594	0.0019	0.785	0.023	0.0962	0.0009	0.1817	592.0	34.5	69.0	588.0	6.5	13.0	592.0	3.0	6.0	101
OUJ6290	73.70	61.90	52.39	0.840	-5.00E-01	7.80E+02	0.1035	0.0027	4.611	0.140	0.3179	0.0034	0.0365	1683.0	24.0	48.0	1751.0	12.5	25.0	1779.0	8.5	17.0	102
OUJ6292	226.60	118.04	32.28	0.520	4.10E+02	6.80E+02	0.0609	0.0022	0.799	0.028	0.0957	0.0010	0.1855	636.0	38.0	78.0	596.0	7.0	14.0	599.0	3.0	6.0	99
OUJ6293	380.50	199.90	41.80	0.420	-7.70E+02	9.60E+02	0.0590	0.0021	0.760	0.025	0.0939	0.0010	0.1175	567.0	38.5	77.0	574.0	7.0	14.0	578.0	3.0	6.0	101
OUJ6294	487.00	193.40	303.00	0.400	-3.20E+03	8.10E+03	0.2599	0.0041	24.320	0.620	0.6665	0.0061	0.1019	653.0	33.0	66.0	625.0	12.5	25.0	3292.0	12.0	24.0	100
OUJ6296	207.40	168.60	174.00	0.810	1.50E+03	1.50E+03	0.0614	0.0019	0.864	0.025	0.1019	0.0011	0.2515	653.0	33.0	66.0	617.0	7.0	14.0	625.0	3.0	6.0	99
OUJ6297	691.00	450.00	120.30	0.650	2.70E+03	1.60E+03	0.0605	0.0019	0.789	0.022	0.0948	0.0009	0.1200	623.0	34.0	68.0	591.0	6.0	12.0	584.0	2.5	5.0	99
OUJ6298	305.10	124.00	28.56	0.410	-5.70E+02	4.90E+02	0.0574	0.0021	0.633	0.022	0.0801	0.0009	-0.0223	507.0	40.0	80.0	498.0	7.0	14.0	496.0	2.5	5.0	100
OUJ6299	180.30	130.10	42.40	0.720	3.80E+02	5.10E+02	0.0616	0.0025	0.956	0.036	0.1135	0.0012	0.0985	660.0	43.5	87.0	681.0	9.5	19.0	693.0	3.5	7.0	102
OUJ62101	1294.00	572.00	135.70	0.440	4.30E+03	2.70E+03	0.0599	0.0018	0.666	0.019	0.0815	0.0009	0.1410	803.0	33.0	66.0	518.0	6.0	12.0	505.0	2.5	5.0	97
OUJ62102	366.30	65.20	22.44	0.760	9.30E+02	4.80E+02	0.0559	0.0028	1.110	0.042	0.1230	0.0015	0.0329	583.0	44.5	89.0	758.0	10.0	20.0	748.0	4.5	9.0	99
OUJ62103	203.30	136.20	175.50	0.670	-4.60E+03	3.60E+03	0.1824	0.0032	12.950	0.350	0.5053	0.0052	0.4915	2675.0	14.5	29.0	2676.0	12.5	25.0	2637.0	11.0	22.0	99
OUJ62104	158.00	45.72	10.85	0.290	7.00E+02	6.90E+03	0.0569	0.0025	0.636	0.026	0.0816	0.0009	0.0641	488.0	48.5	97.0	500.0	8.0	16.0	505.0	3.0	6.0	101
OUJ62105	680.40	456.70	126.10	0.670	-1.30E+03	1.70E+03	0.0603	0.0019	0.792	0.023	0.0954	0.0009	0.1045	613.0	34.0	68.0	592.0	6.5	13.0	588.0	2.5	5.0	99
OUJ62106	142.30	94.30	27.46	0.660	-3.10E+02	4.60E+02	0.0628	0.0026	0.880	0.036	0.1010	0.0013	0.1401	701.0	44.0	88.0	641.0	9.5	19.0	620.0	4.0	8.0	97
OUJ62106	210.10	243.00	78.30	1.160	1.40E+03	1.10E+03	0.0638	0.0024	1.013	0.036	0.1149	0.0013	0.1310	735.0	40.0	80.0	710.0	9.0	18.0	701.0	4.0	8.0	99
OUJ62107	308.50	384.60	108.50	1.250	1.20E+03	1.20E+03	0.0626	0.0021	0.858	0.027	0.1001	0.0011	0.1974	695.0	35.5	71.0	629.0	7.5	15.0	615.0	3.0	6.0	98
OUJ62108	382.10	211.30	49.20	0.550	7.90E+03	2.90E+03	0.0571	0.0020	0.626	0.021	0.0792	0.0008	0.1972	495.0	38.5	77.0	494.0	6.5	13.0	491.0	2.5	5.0	100
OUJ62109	286.00	166.10	44.42	0.580	5.60E+03	2.40E+03	0.0591	0.0022	0.771	0.026	0.0950	0.0010	0.0039	571.0	40.5	81.0	580.0	7.5	15.0	585.0	3.0	6.0	101
OUJ62110	284.80	193.70	60.90	0.680</																			

ANALYSIS	U (ppm)	Th (ppm)	Pb (ppm)	Th/U	$^{206}\text{Pb}/^{208}\text{Pb}$		$^{207}\text{Pb}/^{209}\text{Pb}$		Ratios		$^{206}\text{Pb}/^{238}\text{U}$		$^{207}\text{Pb}/^{235}\text{U}$		Ages (Ma)		$^{206}\text{Pb}/^{238}\text{U}$	σ	Concordance (%)				
					2σ	2σ	2σ	2σ	$^{206}\text{Pb}/^{238}\text{U}$	2σ	$^{207}\text{Pb}/^{235}\text{U}$	σ	2σ	$^{207}\text{Pb}/^{235}\text{U}$	σ	2σ							
OJJ6z130	116.00	79.40	104.50	0.680	1.00E+04	2.50E+04	0.1765	0.0033	12.560	0.340	0.5156	0.0051	0.1699	2620.0	15.5	31.0	2647.0	12.5	25.0	2680.0	11.0	22.0	101
OJJ6z131	95.80	65.10	17.69	0.680	-7.20E+03	4.70E+03	0.0587	0.0030	0.740	0.036	0.0924	0.0013	0.0477	556.0	55.5	111.0	562.0	10.5	21.0	570.0	4.0	8.0	101
OJJ6z132	106.50	147.50	40.04	1.380	6.10E+03	7.80E+03	0.0608	0.0028	0.787	0.034	0.0946	0.0011	0.0120	632.0	49.5	99.0	589.0	9.5	19.0	583.0	3.0	6.0	99
OJJ6z133	100.96	127.12	36.85	1.260	-2.94E+04	9.60E+03	0.0608	0.0029	0.856	0.039	0.1028	0.0014	0.1345	632.0	51.5	103.0	628.0	10.5	21.0	631.0	4.0	8.0	100
OJJ6z134	640.70	196.00	44.75	0.310	5.70E+04	7.30E+04	0.0577	0.0019	0.645	0.019	0.0816	0.0008	0.1404	520.0	36.0	72.0	505.0	6.0	12.0	506.0	2.5	5.0	100
OJJ6z135	525.40	181.90	38.74	0.350	-8.00E+04	4.70E+04	0.0575	0.0020	0.824	0.020	0.0789	0.0009	0.2530	511.0	38.0	76.0	492.0	6.0	12.0	490.0	2.5	5.0	99
OJJ6z136	126.90	62.83	22.84	0.500	1.70E+04	2.90E+04	0.0658	0.0026	1.193	0.044	0.1331	0.0016	0.0831	800.0	41.5	83.0	797.0	10.0	20.0	806.0	4.5	9.0	101
OJJ6z137	177.30	110.40	31.53	0.620	1.70E+04	4.90E+04	0.0644	0.0025	0.887	0.033	0.1015	0.0012	0.1336	755.0	41.0	82.0	645.0	9.0	18.0	623.0	3.5	7.0	97
OJJ6z139	90.76	69.63	86.70	0.770	-1.73E+05	5.80E+04	0.1705	0.0032	11.610	0.330	0.4922	0.0049	0.3838	2563.0	15.5	31.0	2573.0	13.5	27.0	2580.0	10.5	21.0	100
OJJ6z140	322.00	154.00	136.20	0.480	-9.10E+04	8.00E+04	0.1252	0.0022	5.379	0.110	0.2245	0.0041	0.4163	2032.0	15.5	31.0	1882.0	12.0	24.0	1733.0	10.0	20.0	92
OJJ6z142	107.50	22.64	15.24	0.210	9.00E+04	1.10E+04	0.1040	0.0035	3.177	0.110	0.2245	0.0039	0.6353	1697.0	31.0	62.0	1452.0	13.5	27.0	1306.0	10.5	21.0	90
OJJ6z143	287.90	179.30	52.60	0.620	-3.00E+04	1.30E+04	0.0626	0.0023	0.901	0.031	0.1047	0.0011	0.1464	695.0	39.0	78.0	652.0	8.5	17.0	642.0	3.0	6.0	98
OJJ6z144	126.80	119.50	32.50	0.940	-1.10E+03	5.10E+03	0.0607	0.0026	0.834	0.035	0.1003	0.0012	0.0872	629.0	46.0	92.0	616.0	9.5	19.0	618.0	3.5	7.0	100
OJJ6z145	225.60	151.30	83.90	0.670	-5.20E+04	2.20E+03	0.0833	0.0027	2.365	0.069	0.2069	0.0020	0.0555	1276.0	31.5	63.0	1232.0	10.5	21.0	1212.0	5.5	11.0	98
OJJ6z146	158.80	316.30	86.40	1.990	-8.90E+03	6.00E+03	0.0627	0.0026	0.842	0.033	0.0984	0.0012	0.1195	698.0	44.0	88.0	620.0	9.0	18.0	605.0	3.5	7.0	98
OJJ6z147	342.90	209.80	157.30	0.610	-4.40E+04	3.10E+04	0.1039	0.0019	3.978	0.110	0.2743	0.0028	0.2846	1695.0	17.0	34.0	1630.0	11.0	22.0	1563.0	7.0	14.0	96
Discordant data																							
OJJ6z156	546.00	125.90	159.40	0.230	-8.90E+05	3.70E+05	0.2644	0.0041	18.740	0.480	0.5221	0.0049	0.6061	3273.0	12.0	24.0	3029.0	12.5	25.0	2708.0	10.5	21.0	89
OJJ6z125	1197.00	614.00	95.50	0.510	5.30E+04	2.90E+04	0.0630	0.0019	0.560	0.019	0.0643	0.0015	0.7648	709.0	32.0	64.0	482.0	6.0	12.0	402.0	4.5	9.0	89

Footnotes:

. Analysis references: OJJ6z is Zircon from sample OJJ6 (mount CT18-6), followed by grain number "c" or "r", meaning core or rim, respectively.

Chapter III

Table D.30: Sample DEB2 (LA-1CPMS)

Coordinate UTM: Zone 30S, 486835 m E, 3754573 m N

IGSN: IEACC0005

ANALYSIS	U (ppm)	Th (ppm)	Pb (ppm)	Th/U	Ratios				Concordant data				Error correction	Ages (Ma)				Concordance (%)					
					$^{207}\text{Pb}/^{206}\text{Pb}$	$^{207}\text{Pb}/^{235}\text{U}$	$^{206}\text{Pb}/^{238}\text{U}$	2σ	2σ	2σ	2σ	σ		2σ	σ	2σ	2σ		σ				
					$^{207}\text{Pb}/^{206}\text{Pb}$	$^{207}\text{Pb}/^{235}\text{U}$	$^{206}\text{Pb}/^{238}\text{U}$	2σ	2σ	2σ	2σ	σ		2σ	σ	2σ	2σ		σ				
DEB22	98.30	98.30	26.26	1.000	-1.00E+06	4.40E+06	0.0584	0.0027	0.786	0.036	0.0980	0.0013	0.1054	545	101	589	10.2	20	603	3.8	8	102	
DEB23	82.70	134.10	111.40	1.622	9.06E+06	4.90E+06	0.1139	0.0023	5.166	0.120	0.3305	0.0040	0.3419	1863	36	1847	9.9	20	1841	9.7	19	100	
DEB24	96.50	42.86	41.60	1.031	-3.20E+05	1.90E+05	0.0759	0.0024	1.652	0.049	0.1591	0.0020	0.1038	1092	58	990	9.4	19	952	5.6	11	96	
DEB25	415.60	219.90	51.10	0.529	-1.90E+05	1.30E+05	0.0596	0.0014	0.732	0.018	0.0892	0.0010	0.1587	589	25.5	51	558	5.3	11	551	3.0	6	99
DEB26	90.50	91.70	23.57	1.013	-3.70E+04	2.40E+04	0.0599	0.0027	0.812	0.036	0.0995	0.0014	0.0324	600	48.8	98	604	10.1	20	611	4.1	8	101
DEB27	112.70	108.60	28.74	0.946	-3.50E+04	3.20E+04	0.0608	0.0024	0.779	0.030	0.0935	0.0013	-0.0237	632	42.5	85	576	8.6	17	576	3.8	8	99
DEB28	20.83	12.33	12.99	1.024	-2.40E+03	8.60E+03	0.0361	0.0042	2.690	0.120	0.2322	0.0039	0.0154	1340	47.1	94	1326	16.5	33	1346	10.2	20	102
DEB29	115.50	102.10	28.97	0.884	-3.30E+04	2.80E+04	0.0622	0.0023	0.890	0.030	0.1028	0.0013	-0.0730	681	39.5	79	646	8.1	16	631	3.8	8	98
DEB210	148.20	293.40	332.90	1.980	-7.00E+05	1.30E+05	0.1630	0.0024	10.580	0.170	0.4694	0.0050	0.2469	2487	12.4	25	2487	7.4	15	2481	11.0	22	100
DEB211	235.60	165.40	44.80	0.706	-1.80E+04	4.00E+04	0.0597	0.0018	0.814	0.025	0.0990	0.0012	0.1095	593	32.7	65	605	7.0	14	609	3.5	7	101
DEB212	229.80	182.90	41.59	0.796	-4.40E+04	3.30E+04	0.0596	0.0017	0.701	0.020	0.0861	0.0011	0.0330	589	30.9	62	539	6.0	12	532	3.3	7	99
DEB213	70.87	34.81	8.47	0.491	7.30E+03	9.90E+03	0.0593	0.0030	0.719	0.037	0.0892	0.0014	0.0818	578	55.0	110	550	10.9	22	551	4.1	8	100
DEB214	66.60	44.20	12.17	0.664	-7.20E+03	8.00E+03	0.0615	0.0031	0.872	0.041	0.1035	0.0015	-0.1113	657	54.1	108	637	11.1	22	635	4.4	9	100
DEB215	99.00	69.90	57.20	0.706	3.50E+05	1.50E+05	0.1083	0.0021	4.738	0.092	0.3174	0.0036	0.2008	1771	17.7	35	1774	8.4	17	1777	8.8	18	100
DEB216	362.80	228.00	60.20	0.628	1.11E+05	5.30E+04	0.0598	0.0017	0.796	0.025	0.0965	0.0011	0.0910	596	62	62	595	6.2	12	594	3.2	6	100
DEB217	90.70	29.00	7.18	0.320	-1.30E+04	1.30E+04	0.0570	0.0026	0.707	0.032	0.0916	0.0013	0.1541	492	50.3	101	543	9.5	19	565	3.8	8	104
DEB218	94.80	93.10	24.01	0.962	-1.03E+04	9.90E+03	0.0580	0.0025	0.798	0.034	0.0998	0.0013	-0.1487	570	47.2	94	596	9.6	19	613	3.8	8	103
DEB219	569.60	439.40	105.10	0.771	6.20E+04	3.70E+04	0.0591	0.0013	0.724	0.016	0.0889	0.0010	0.1570	571	23.9	48	553	4.7	9	549	2.9	6	99
DEB220	16.72	179.20	78.40	10.718	-1.31E+04	6.30E+03	0.0798	0.0057	1.870	0.130	0.1714	0.0037	0.0218	1192	70.5	141	1071	23.0	46	1020	10.2	20	95
DEB222	304.90	151.00	173.70	0.495	-1.90E+05	1.40E+05	0.1614	0.0022	10.655	0.160	0.4809	0.0048	0.2209	2470	11.5	23	2494	7.0	14	2531	10.4	21	102
DEB223c	351.00	117.80	30.80	0.336	-4.90E+04	3.60E+04	0.0603	0.0011	0.773	0.021	0.0927	0.0010	0.1748	614	28.7	57	581	6.0	12	572	2.9	6	98
DEB223b	1472.00	493.20	120.20	0.335	-8.00E+04	1.20E+06	0.0593	0.0016	0.758	0.014	0.0927	0.0010	0.0880	578	20.2	40	573	4.0	8	571	2.8	6	100
DEB224	289.00	36.80	9.19	0.127	-6.00E+04	2.30E+04	0.0594	0.0016	0.767	0.021	0.0932	0.0011	0.1467	582	29.2	58	578	6.0	12	574	3.2	6	99
DEB225	624.00	594.00	219.40	0.952	-8.80E+05	3.20E+05	0.0672	0.0013	1.312	0.025	0.1411	0.0014	0.1457	844	20.1	40	851	5.5	11	851	4.0	8	100
DEB226	218.20	74.67	16.75	0.342	-5.50E+04	2.20E+04	0.0569	0.0019	0.638	0.021	0.0811	0.0010	0.0390	488	36.8	74	501	6.5	13	503	2.9	6	100
DEB227	505.60	422.40	326.70	0.835	-1.11E+06	4.30E+05	0.1293	0.0017	5.750	0.088	0.3235	0.0033	0.4747	2088	11.6	23	1939	6.6	13	1807	8.0	16	93
DEB228	211.50	82.50	21.95	0.390	-1.60E+04	1.30E+04	0.0604	0.0020	0.817	0.026	0.0984	0.0012	-0.0152	618	35.7	71	606	7.3	15	605	3.5	7	100
DEB229	843.00	313.50	299.00	0.914	8.00E+05	1.00E+05	0.1292	0.0018	6.981	0.110	0.3901	0.0040	0.1830	2087	12.3	25	2109	7.0	14	2123	9.3	19	101
DEB230	82.90	97.70	20.31	1.058	8.00E+03	9.40E+03	0.0557	0.0029	0.677	0.034	0.0886	0.0014	0.1010	440	57.9	116	625	10.3	21	547	4.1	8	104
DEB232	156.40	143.30	61.00	0.916	6.00E+02	9.70E+03	0.0715	0.0019	1.626	0.041	0.1649	0.0020	-0.0142	972	27.1	54	960	7.9	16	984	5.5	11	100
DEB233	158.50	183.20	49.99	1.156	2.00E+03	6.40E+03	0.0593	0.0022	0.804	0.028	0.0982	0.0012	0.0154	578	40.3	81	599	7.9	16	604	3.5	7	101
DEB234	311.00	181.90	96.20	0.585	-2.20E+05	1.40E+05	0.0808	0.0015	2.363	0.044	0.2136	0.0022	0.2101	1217	18.3	37	1231	6.6	13	1248	5.8	12	101
DEB236	245.00	247.80	65.70	1.011	-1.00E+04	1.60E+04	0.0605	0.0018	0.833	0.025	0.0996	0.0011	0.0508	621	32.1	64	615	6.9	14	612	3.2	6	99
DEB237	99.70	89.50	88.80	0.898	-2.60E+04	2.50E+04	0.1317	0.0024	7.210	0.150	0.3952	0.0046	0.4519	2122	16.0	32	2138	9.3	19	2147	10.6	21	100
DEB238	503.20	322.90	278.60	0.642	-3.00E+06	4.20E+06	0.1243	0.0017	6.159	0.091	0.3596	0.0036	0.2121	2018	12.1	24	1989	6.4	13	1980	8.5	17	99
DEB239	88.41	88.04	82.20	0.996	-6.00E+04	2.00E+04	0.1281	0.0024	6.708	0.130	0.3807	0.0043	0.1431	2072	16.5	33	2074	8.6	17	2080	10.0	20	100
DEB240	101.38	80.88	23.36	0.798	-3.00E+04	1.10E+04	0.0614	0.0024	0.839	0.026	0.1010	0.0014	0.1955	653	41.9	84	619	8.8	18	620	4.1	8	100
DEB242	200.80	185.40	52.20	0.923	-1.30E+04	1.20E+04	0.0599	0.0020	0.819	0.026	0.0990	0.0012	0.0373	600	36.1	72	607	7.3	15	608	3.5	7	99
DEB244	83.70	41.20	10.91	0.492	6.40E+03	5.20E+03	0.0598	0.0028	0.745	0.034	0.0909	0.0014	0.0943	596	50.7	101	565	9.9	20	561	4.1	8	100
DEB243	30.79	22.76	13.29	0.739	1.00E+02	3.90E+03	0.0789	0.0039	2.177	0.097	0.2003	0.0033	-0.0007	1170	48.9	98	1174	15.5	31	1177	8.9	18	100
DEB244	279.60	270.90	234.00	0.969	-9.40E+04	6.00E+04	0.1230	0.0018	5.251	0.088	0.3087	0.0032	0.3777	2000	13.0	26	1861	7.1	14	1734	7.9	16	93
DEB245	931.00	893.00	265.00	0.966	5.50E+04	3.60E+04	0.0654	0.0012	0.919	0.017	0.1017	0.0011	0.0123	786	19.3	39	662	4.5	9	624	3.2	6	94
DEB246	92.70	90.00	26.53	0.971	8.00E+04	2.60E+04	0.0567	0.0023	0.776	0.031	0.0987	0.0014	0.0564	480	44.8	90	563	8.9	18	607	4.1	8	104
DEB247	199.40	210.80	64.80	1.057	-2.00E+04	1.60E+04	0.0591	0.0018	0.840	0.026	0.1024	0.0014	0.0646	571	33.1	66	619	7.2	14	628	3.5	7	101
DEB249	70.00	26.90	8.20	0.384	8.00E+02	4.20E+03	0.0618	0.0032	0.806	0.041	0.0953	0.0014	-0.0159	667	55.4	111	600	9.5	23	587	4.1	8	98
DEB250	90.10	25.72	7.64	0.285	-1.64E+05	8.90E+04	0.0586	0.0026	0.719	0.031	0.0889	0.0012	0.0065	552	48.4	97	550	11.5	23	549	3.6	7	100
DEB251	720.00	790.00	256.10	1.097	-3.40E+04	4.40E+04	0.0604	0.0012	0.857	0.016	0.1022	0.0011	0.0316	618	21.4	43	628	4.4	9	627	3.2	6	100
DEB252	35.10	34.12	9.73	0.972	-4.00E+04	1.50E+04	0.0582	0.0043	0.725	0.049	0.0880	0.0017	0.0009	537	80.8	70	554	14.4	29	544	5.0	10	98
DEB253	179.40	122.00	38.35	0.680	-6.00E+04	1.20E+04	0.0591	0.0019	0.800	0.025	0.0981	0.0012	-0.0150	571	35.0	70	597	7.0	14	603	3.5	7	101
DEB254	85.40	126.00	39.50	1.489	-7.																		

ANALYSIS	U (ppm)	Th (ppm)	Pb (ppm)	Th/U	Ratios			Ages (Ma)			Concordance (%)												
					$^{207}\text{Pb}/^{206}\text{Pb}$	$^{207}\text{Pb}/^{238}\text{U}$	$^{206}\text{Pb}/^{238}\text{U}$	$^{207}\text{Pb}/^{238}\text{U}$	$^{206}\text{Pb}/^{238}\text{U}$	σ		2σ											
DEB2266	61.92	42.12	11.46	0.680	1.19E+04	6.50E+03	0.0570	0.0031	0.688	0.035	0.0874	0.0013	2.0	60.0	120	532	10.5	21	540	3.9	8	102	
DEB2267	42.15	51.47	65.32	1.221	4.70E+04	2.60E+04	0.1621	0.0034	10.330	0.230	0.4582	0.0058	1.786	2478	17.7	35	2465	10.3	21	2432	12.8	26	99
DEB2268	318.20	143.83	40.12	0.452	-2.90E+04	2.10E+04	0.0594	0.0015	0.769	0.020	0.0931	0.0011	0.1742	582	27.4	55	579	5.7	11	574	3.2	6	99
DEB2269	143.80	130.10	38.53	0.905	4.30E+03	8.70E+03	0.0614	0.0024	0.852	0.028	0.1004	0.0012	0.0545	653	35.0	70	626	7.7	15	616	3.5	7	99
DEB2270	102.90	137.50	40.17	1.336	2.00E+03	7.10E+03	0.0604	0.0024	0.837	0.032	0.0999	0.0013	0.0006	618	42.9	86	617	8.8	18	614	3.8	8	99
DEB2271c	100.40	65.90	19.40	0.656	-9.00E+02	5.90E+03	0.0593	0.0023	0.828	0.034	0.1002	0.0015	0.2954	578	42.1	84	613	9.4	19	616	4.4	9	101
DEB2271f	133.00	89.40	24.40	0.672	3.50E+03	7.40E+03	0.0578	0.0023	1.008	0.045	0.0999	0.0013	0.0070	522	43.6	87	596	9.3	19	614	3.8	8	103
DEB2272	71.40	178.70	57.30	2.503	-3.70E+03	5.30E+03	0.0854	0.0029	1.008	0.045	0.1130	0.0016	0.0021	787	46.6	93	708	11.4	23	690	4.6	9	107
DEB2273	122.60	64.10	17.11	0.523	2.60E+03	6.00E+03	0.0603	0.0026	0.832	0.035	0.0996	0.0013	-0.0441	614	46.6	93	615	6.1	19	616	3.8	8	100
DEB2274	130.30	154.90	148.30	1.189	-3.20E+04	2.90E+04	0.1301	0.0023	6.769	0.120	0.3779	0.0043	0.1500	2099	15.5	31	2032	7.8	16	2066	10.1	20	99
DEB2275	530.90	480.50	453.10	0.905	-1.60E+05	1.30E+05	0.1256	0.0016	6.391	0.094	0.3685	0.0036	0.2813	2037	11.3	23	2031	6.5	13	2022	8.5	17	100
DEB2276	62.89	71.90	81.90	1.143	4.00E+04	1.30E+04	0.1578	0.0030	10.250	0.210	0.4720	0.0056	0.1807	2432	16.1	32	2458	9.5	19	2492	12.0	24	101
DEB2277	312.40	25.82	23.76	0.063	-5.50E+04	6.70E+04	0.1205	0.0017	5.561	0.090	0.3334	0.0036	0.4018	1964	12.6	25	1910	7.0	14	1855	8.7	17	97
DEB2279	116.20	87.15	24.73	0.750	-8.80E+03	6.20E+03	0.0650	0.0034	0.912	0.052	0.1021	0.0016	0.4973	774	55.0	110	658	13.8	28	627	4.7	9	95
DEB2280	52.84	81.00	87.80	1.533	-1.70E+04	1.60E+04	0.1604	0.0034	10.160	0.220	0.4604	0.0055	0.1979	2460	18.4	37	2449	10.0	20	2441	12.1	24	100
DEB2281	766.80	584.00	147.10	0.762	-1.00E+05	4.90E+04	0.0600	0.0012	0.797	0.016	0.0964	0.0010	0.1079	602	21.7	43	595	4.5	9	593	2.9	6	100
DEB2282	693.90	458.80	122.30	0.658	-9.80E+04	4.80E+04	0.0596	0.0011	0.852	0.016	0.1030	0.0011	0.1205	589	20.0	40	626	4.4	9	593	2.9	6	100
DEB2283	155.20	154.10	168.40	0.993	-8.20E+04	4.70E+04	0.1592	0.0024	10.230	0.170	0.4663	0.0049	0.2854	2447	12.8	26	2456	7.7	15	2467	10.8	22	100
DEB2284	382.50	105.30	80.70	0.276	2.90E+04	7.30E+04	0.1188	0.0017	5.491	0.096	0.3357	0.0043	0.6216	1938	12.8	26	1899	7.5	15	1866	10.4	21	98
DEB2285	357.50	310.00	70.83	0.867	2.30E+04	1.20E+04	0.0577	0.0015	7.173	0.026	0.0889	0.0010	0.1790	518	28.5	57	547	5.9	12	549	3.0	6	100
DEB2286	824.00	299.60	374.30	0.364	-3.00E+05	2.50E+05	0.1934	0.0023	14.380	0.200	0.5391	0.0052	0.4481	2771	9.8	20	2775	6.6	13	2780	10.9	22	100
DEB2288	84.20	278.40	246.90	0.764	-1.16E+05	8.10E+04	0.1256	0.0017	6.224	0.097	0.3617	0.0037	0.2554	2037	12.0	24	2008	6.8	14	1990	8.8	18	99
DEB2289	463.50	118.20	197.75	0.255	-9.00E+04	1.50E+04	0.0557	0.0017	0.460	0.014	0.0598	0.0008	-0.0787	440	34.0	68	384	4.9	10	374	2.3	5	97
DEB2290	156.80	122.70	106.80	0.783	3.60E+04	2.10E+04	0.1167	0.0021	5.604	0.100	0.3453	0.0038	0.1554	1906	16.2	32	1917	7.7	15	1912	9.1	18	100
DEB2291	186.50	102.90	49.50	0.552	-2.60E+04	2.00E+04	0.0750	0.0018	1.916	0.048	0.1856	0.0021	0.1427	1069	24.1	48	1087	8.3	17	1097	5.7	11	101
DEB2292	82.90	35.17	37.98	0.424	-1.60E+04	2.00E+04	0.1451	0.0029	8.710	0.180	0.4365	0.0047	0.1238	2289	17.2	34	2308	9.4	19	2335	10.5	21	101
DEB2293	328.50	183.00	46.91	0.557	1.90E+04	1.20E+04	0.0576	0.0016	0.754	0.021	0.0940	0.0010	0.1008	515	30.5	61	571	6.1	12	579	2.9	6	102
DEB2294	530.00	92.03	15.46	0.174	-2.80E+04	1.90E+04	0.0529	0.0015	0.443	0.013	0.0600	0.0007	0.1157	325	32.2	64	372	4.6	9	375	2.1	4	101
DEB2295	92.70	81.40	22.03	0.878	-2.90E+03	4.90E+03	0.0586	0.0026	0.805	0.035	0.0991	0.0014	0.0322	552	48.4	97	600	9.8	20	609	4.1	8	102
DEB2296	118.20	172.20	166.80	1.024	-9.40E+04	3.80E+04	0.1280	0.0025	6.538	0.110	0.3718	0.0038	0.1466	2071	14.5	29	2051	7.4	15	2038	8.9	18	99
DEB2297	112.30	45.70	11.65	0.407	-1.00E+02	4.80E+03	0.0573	0.0021	0.715	0.031	0.0898	0.0013	0.0021	503	48.0	96	548	9.2	18	554	3.8	8	101
DEB2298	396.00	202.30	58.20	0.511	-3.60E+04	2.30E+04	0.0582	0.0014	0.793	0.019	0.0983	0.0010	0.1998	537	26.3	53	593	5.4	11	604	2.9	6	102
DEB2299	88.60	171.76	19.18	0.810	-3.50E+03	4.40E+03	0.0604	0.0026	0.788	0.043	0.0956	0.0013	0.1317	618	46.5	93	590	9.4	19	589	3.4	8	100
DEB22101	63.19	47.60	13.52	0.753	-4.20E+03	3.30E+03	0.0611	0.0031	0.841	0.043	0.0996	0.0015	0.0905	545	10.9	620	620	11.8	24	612	4.4	9	99
DEB22102	306.00	122.60	111.60	0.401	-1.50E+03	4.20E+03	0.0591	0.0028	0.821	0.037	0.0984	0.0014	-0.0601	571	51.5	103	609	10.3	21	605	4.1	8	99
DEB22103	152.20	125.60	122.40	0.825	-4.30E+04	2.80E+04	0.1244	0.0021	5.978	0.110	0.3476	0.0038	0.1476	2020	15.0	30	1973	8.0	16	1760	11.0	22	94
DEB22104	395.00	258.30	75.30	0.649	-3.00E+04	1.70E+04	0.0620	0.0015	0.880	0.021	0.1049	0.0011	0.0351	611	26.9	54	641	5.7	11	643	3.2	6	100
DEB22105	383.80	142.40	42.60	0.371	2.20E+04	2.20E+04	0.0597	0.0014	0.868	0.020	0.1045	0.0012	0.1415	593	25.4	51	634	5.4	11	641	3.5	7	101
DEB22106	218.00	127.00	35.35	0.583	-1.30E+03	9.60E+03	0.0601	0.0018	0.838	0.026	0.1011	0.0012	0.0992	607	32.4	65	618	7.2	14	621	3.5	7	100
DEB22107	95.70	59.00	16.80	0.617	-2.60E+03	4.50E+03	0.0590	0.0025	0.819	0.033	0.0999	0.0014	-0.0431	567	46.1	92	607	9.2	18	614	4.1	8	101
DEB22108	98.20	91.13	22.99	0.928	-9.50E+03	4.90E+03	0.0596	0.0026	0.747	0.031	0.0906	0.0013	0.0400	589	47.3	95	566	9.0	18	559	3.8	8	99
DEB22109	66.79	73.22	20.32	1.096	-6.10E+03	3.60E+03	0.0576	0.0026	0.804	0.039	0.1003	0.0017	0.2193	515	49.6	99	599	11.0	22	616	5.0	10	103
DEB22110	192.60	143.90	117.30	0.747	9.00E+04	2.60E+04	0.1151	0.0019	4.919	0.096	0.3090	0.0035	0.4595	1881	14.9	30	1806	8.2	16	1736	8.6	17	96
DEB22111	222.40	323.00	95.60	1.479	-1.60E+03	9.10E+03	0.0599	0.0018	0.871	0.026	0.1047	0.0013	0.1586	600	32.5	65	636	7.0	14	642	3.8	8	100
DEB22112	87.70	81.10	22.93	0.925	-6.40E+03	4.20E+03	0.0588	0.0028	0.803	0.037	0.1000	0.0015	0.0471	560	51.9	104	599	10.4	21	614	4.4	9	103
DEB22113	653.20	436.20	165.80	0.688	-2.60E+04	3.50E+04	0.0674	0.0013	1.306	0.024	0.1400	0.0015	0.0805	851	20.0	40	848	5.3	11	845	4.2	8	100
DEB22114	91.71	68.80	19.05	0.750	1.90E+03	3.00E+03	0.0622	0.0027	0.865	0.037	0.1004	0.0015	-0.0417	681	46.4	93	633	10.1	20	617	4.4	9	97
DEB22115	135.00	85.90	78.80	0.092	-1.30E+05	1.40E+05	0.1220	0.0015	5.874	0.086	0.3487	0.0035	0.4136	1986	10.9	22	1957	6.3	13	1928	8.4	17	99
DEB22116	938.20	113.40	29.62	0.821	1.20E+03	4.80E+03	0.0610	0.0024	0.827	0.031	0.0978	0.0012	0.0777	639	42.3	85	612	8.6	17	602	3.5	7	98
DEB22117	92.10	71.10	23.00	0.772	2.80E+03	3.40E+03	0.0590	0.0026	0.879	0.038	0.1072	0.0014	0.0361	567	48.0	96	640	10.3	21	656	4.1	8	103
DEB22118	321.90	213.30	64.47	0.663	-2.30E+04	1.60E+04	0.0821	0.0016	0.954	0.024	0.1026	0.0011	0.1097	622	21.4	43	630	4.9					

Chapter III

Table D.31: Sample MIM2 (LA-ICPMS)

IGSN: IEACC0004

Coordinate UTM: Zone 30S, 509359 m E, 3763408 m N

ANALYSIS	U (ppm)	Th (ppm)	Pb (ppm)	Th/U	Ratios			Concordant data			Error correction	Ages (Ma)			Concordance (%)								
					$^{207}\text{Pb}/^{206}\text{Pb}$	$^{207}\text{Pb}/^{235}\text{U}$	$^{206}\text{Pb}/^{238}\text{U}$	$^{207}\text{Pb}/^{206}\text{Pb}$	$^{207}\text{Pb}/^{235}\text{U}$	$^{206}\text{Pb}/^{238}\text{U}$		σ	2σ	σ		2σ	σ	2σ					
					2σ	2σ	2σ	2σ	2σ	2σ		σ	2σ	σ		2σ	σ	2σ					
MIM2z1	72.00	72.10	71.60	1.001	6.50E+03	6.40E+03	0.1239	0.0027	6.171	0.180	0.3663	0.0040	0.1142	2013	2000	12.7	25	2012	9.4	19	101		
MIM2z2	106.40	82.60	24.31	0.776	1.30E+03	2.70E+03	0.0613	0.0027	0.862	0.037	0.1023	0.0012	0.1278	650	631	10.1	20	628	3.5	7	99		
MIM2z4	406.20	183.20	161.20	0.456	-5.00E+04	5.00E+04	0.1999	0.0019	4.771	0.130	0.3194	0.0031	0.2978	1798	1780	11.4	23	1787	7.6	15	100		
MIM2z5	256.20	164.40	46.38	0.647	2.80E+04	3.20E+04	0.0624	0.0023	0.832	0.027	0.0971	0.0010	0.1609	688	615	7.5	15	597	2.9	6	97		
MIM2z6	89.30	70.84	21.07	0.793	-8.60E+03	4.60E+03	0.0603	0.0028	0.833	0.037	0.1005	0.0013	-0.0504	614	615	10.2	20	617	3.8	8	100		
MIM2z7c	78.20	43.62	46.18	0.558	-1.80E+04	1.90E+04	0.1377	0.0028	7.474	0.210	0.3990	0.0042	0.1937	2198	2170	12.6	25	2164	9.7	19	100		
MIM2z7r	539.40	180.70	31.41	0.335	-1.30E+04	2.00E+04	0.0544	0.0019	0.432	0.014	0.0575	0.0006	0.2065	388	392	8.0	10	360	1.8	4	99		
MIM2z8	199.70	163.90	52.06	0.846	-6.20E+04	2.60E+04	0.0609	0.0023	0.883	0.031	0.1054	0.0012	0.0562	636	643	5.4	17	646	3.5	7	101		
MIM2z9	1025.00	473.00	149.00	0.463	2.60E+05	1.60E+05	0.0608	0.0018	0.907	0.025	0.1075	0.0011	0.2261	631	64	6.7	13	658	3.2	6	100		
MIM2z10	258.00	340.40	334.50	1.319	-3.30E+05	2.20E+05	0.1262	0.0021	6.247	0.160	0.3640	0.0034	0.2876	2046	29	11.2	22	2001	8.0	16	100		
MIM2z11	206.10	130.20	36.10	0.626	-1.70E+05	1.60E+05	0.0605	0.0022	0.809	0.028	0.0968	0.0011	0.1397	622	78	7.9	16	596	3.2	6	99		
MIM2z12	245.00	188.40	59.90	0.769	3.00E+05	1.60E+05	0.0624	0.0025	0.941	0.031	0.1088	0.0012	0.1407	688	673	8.1	16	666	3.5	7	99		
MIM2z13	119.62	82.50	92.60	0.690	-1.13E+05	6.00E+04	0.1359	0.0025	7.431	0.200	0.4036	0.0041	0.3082	2176	2165	12.0	24	2186	9.4	19	101		
MIM2z14	164.10	84.20	93.10	0.513	6.50E+05	3.00E+05	0.1395	0.0025	7.805	0.210	0.4130	0.0040	0.2219	2221	31	22.09	12.1	24	2229	9.1	18	101	
MIM2z15	175.60	171.50	173.10	0.977	1.40E+05	1.90E+05	0.1377	0.0023	6.619	0.180	0.3822	0.0040	0.4069	2067	15.5	32	2062	12.0	24	2087	9.3	19	101
MIM2z16	631.00	180.10	208.00	0.285	-9.80E+05	3.30E+05	0.1579	0.0025	8.918	0.230	0.4173	0.0045	0.7383	2433	13.4	27	2330	11.8	24	2248	10.2	20	97
MIM2z17	564.80	120.80	19.48	0.214	-3.00E+04	2.00E+04	0.0533	0.0019	0.441	0.014	0.0595	0.0006	-0.0108	342	371	4.9	10	372	1.9	4	100		
MIM2z18	194.80	180.00	52.00	0.909	-2.00E+04	1.00E+04	0.0591	0.0022	0.819	0.028	0.1001	0.0011	0.0593	571	607	7.8	16	615	3.2	6	101		
MIM2z19f	434.90	19.75	5.95	0.045	-2.00E+05	1.00E+05	0.0593	0.0019	0.802	0.023	0.0982	0.0010	0.0691	578	598	6.5	13	604	2.8	6	101		
MIM2z20	74.80	79.70	22.60	1.066	-1.00E+03	1.00E+03	0.0620	0.0032	0.859	0.041	0.1008	0.0016	0.0667	674	630	11.2	22	619	4.7	9	98		
MIM2z21	293.40	483.50	141.70	1.648	2.40E+04	1.00E+04	0.0602	0.0021	0.841	0.026	0.1011	0.0011	0.0201	611	620	7.2	14	621	3.2	6	100		
MIM2z22c	197.70	125.20	38.43	0.633	3.90E+03	3.00E+03	0.0605	0.0021	0.881	0.030	0.1057	0.0012	0.2099	622	647	8.0	16	648	3.5	7	100		
MIM2z22f	278.40	30.69	8.59	0.110	1.70E+03	1.00E+03	0.0591	0.0020	0.760	0.024	0.0927	0.0010	0.0256	571	574	6.9	14	571	2.9	6	100		
MIM2z23	201.10	165.80	49.20	0.824	7.60E+03	3.90E+03	0.0598	0.0022	0.839	0.030	0.1009	0.0011	0.1215	596	619	8.3	17	620	3.2	6	100		
MIM2z24	404.70	312.20	449.60	0.771	3.30E+04	1.70E+04	0.2025	0.0032	15.495	0.400	0.5602	0.0052	0.4517	2846	26	28.46	12.3	25	2867	10.7	21	101	
MIM2z25	215.00	288.00	358.70	1.340	-2.40E+04	1.50E+04	0.1639	0.0028	10.716	0.280	0.4765	0.0044	0.3151	2496	14.4	29	2499	12.1	24	2512	9.6	19	101
MIM2z26	631.30	274.10	204.00	0.434	1.30E+04	1.00E+04	0.0963	0.0016	3.611	0.096	0.2734	0.0028	0.4612	1553	15.6	31	1552	10.6	21	1558	7.1	14	100
MIM2z27	128.10	24.17	30.10	0.355	-2.60E+04	2.40E+04	0.1683	0.0024	11.910	0.360	0.5162	0.0078	0.6652	2541	15.9	32	2597	14.1	28	2683	16.6	33	103
MIM2z28	68.00	55.62	58.60	0.435	-4.90E+03	2.60E+03	0.1289	0.0024	6.734	0.180	0.3813	0.0038	0.1854	2083	16.4	33	2077	11.8	24	2082	8.9	18	100
MIM2z29	414.00	70.60	19.20	0.171	-1.60E+03	2.10E+03	0.0609	0.0020	0.850	0.026	0.1010	0.0010	0.1023	636	625	7.1	14	620	2.9	6	99		
MIM2z30	12.81	10.41	2.71	0.813	-5.40E+01	4.70E+01	0.0567	0.0070	0.755	0.090	0.0927	0.0027	0.0553	480	571	26.0	52	595	7.9	16	104		
MIM2z31	65.30	55.10	15.80	0.844	6.30E+03	2.60E+03	0.0601	0.0030	0.768	0.036	0.0927	0.0013	0.1499	607	579	10.3	21	571	3.8	8	99		
MIM2z32	1125.00	280.5	27.38	0.025	6.00E+04	1.50E+04	0.1283	0.0019	6.082	0.160	0.3449	0.0032	0.5481	2075	17.7	19.88	11.5	23	1910	7.7	15	96	
MIM2z33	370.50	349.40	91.50	0.943	1.20E+03	1.30E+03	0.0577	0.0019	0.717	0.022	0.0900	0.0009	0.0711	518	549	6.5	13	555	2.6	5	101		
MIM2z35	188.56	108.94	30.06	0.578	1.30E+03	7.80E+02	0.0603	0.0023	0.802	0.028	0.0956	0.0011	0.0276	614	609	7.9	16	589	3.2	6	98		
MIM2z36	170.00	124.60	34.52	0.733	-5.20E+02	4.20E+02	0.0607	0.0024	0.822	0.031	0.0981	0.0011	0.0405	629	609	8.6	17	603	3.2	6	99		
MIM2z37	236.10	223.30	257.50	0.946	3.80E+03	3.10E+03	0.1629	0.0027	9.391	0.240	0.4151	0.0040	0.3026	2486	14.0	28	2377	12.2	24	2238	9.1	18	94
MIM2z38	79.40	52.97	15.13	0.667	5.40E+02	3.50E+02	0.0632	0.0030	0.855	0.040	0.0990	0.0013	0.0872	715	50.4	101	627	10.9	22	609	3.8	8	97
MIM2z39f	106.70	79.60	67.55	0.746	2.10E+03	1.50E+03	0.1076	0.0023	4.566	0.130	0.3070	0.0031	0.0797	1759	19.5	31	1743	11.8	24	1726	7.6	15	99
MIM2z41	190.80	156.20	145.10	0.819	2.20E+04	1.10E+04	0.1270	0.0024	6.134	0.170	0.3496	0.0038	0.3847	2057	16.7	33	1995	12.1	24	1933	9.1	18	97
MIM2z42	150.90	113.20	104.40	0.783	-7.10E+03	4.40E+03	0.1151	0.0022	5.255	0.150	0.3300	0.0033	0.3013	1881	17.2	34	1862	12.2	24	1838	8.0	16	99
MIM2z43c	278.00	185.60	273.00	0.672	6.00E+04	6.90E+04	0.2245	0.0036	17.840	0.460	0.5747	0.0054	0.4714	3013	12.9	26	2981	12.4	25	2927	11.1	22	96
MIM2z43f	106.10	46.02	69.00	0.434	-2.60E+04	1.10E+04	0.2178	0.0039	17.840	0.460	0.5917	0.0063	0.5068	2964	14.4	29	2981	13.2	26	2996	12.8	26	101
MIM2z44	110.40	141.60	39.20	1.283	-4.80E+02	5.30E+02	0.0609	0.0028	0.819	0.036	0.0963	0.0011	0.0496	636	607	10.0	20	593	3.2	6	98		
MIM2z46	160.90	234.90	60.90	1.460	1.10E+03	1.20E+03	0.0574	0.0022	0.705	0.026	0.0885	0.0010	0.0425	507	542	7.7	15	547	2.9	6	101		
MIM2z47	120.20	183.50	50.80	1.527	6.20E+02	9.40E+02	0.0604	0.0020	0.814	0.033	0.0978	0.0013	0.1535	618	605	9.2	18	602	3.8	8	99		
MIM2z48	498.90	207.70	37.42	0.416	3.90E+03	2.90E+03	0.0557	0.0026	0.468	0.016	0.0608	0.0006	0.1138	440	390	5.5	11	380	1.9	4	98		
MIM2z49	168.30	70.80	16.52	0.421	-1.30E+03	1.50E+03	0.0568	0.0023	0.637	0.024	0.0809	0.0009	0.1172	484	44.7	89	500	7.4	15	501	2.8	6	100
MIM2z50	119.40	44.00	19.94	0.869	4.30E+03	3.40E+03	0.0669	0.0026	1.429	0.051	0.1501	0.0017	0.0765	896	78	901	10.7	21	902	4.8	10	100	
MIM2z51	220.10	176.10	49.70	0.800	1.15E+04	5.50E+03	0.0606	0.0023	0.811	0.028	0.0975	0.0010	0.1126	625	603	7.8	16	599	2.9	6	99		
MIM2z52	157.10	55.43	16.52	0.752	2.00E+03	1.60E+03	0.0624	0.0031	0.875	0.040	0.1001	0.0014	0.1138	688	53.0	106	638	11.4	23	615	4.1	8	96
MIM2z54	73.70	141.00	140.00	0.895	-2.00E+04	1.30E																	

ANALYSIS	U (ppm)	Th (ppm)	Pb (ppm)	Th/U	Ratios			Error correction			Ages (Ma)			Concordance (%)									
					$^{207}\text{Pb}/^{206}\text{Pb}$	$^{207}\text{Pb}/^{238}\text{U}$	$^{207}\text{Pb}/^{235}\text{U}$	2σ	2σ	2σ	σ	2σ	2σ		σ								
MIM2263c	83.58	23.09	22.47	0.276	-1.20E+04	1.10E+04	0.1619	0.0032	9.310	0.260	0.4153	0.0044	0.1445	2476	16.7	33	2389	12.8	26	2239	10.0	20	95
MIM2264	158.40	93.60	25.10	0.591	2.46E+04	7.40E+03	0.0695	0.0023	0.770	0.028	0.0923	0.0010	0.0007	622	41.0	82	569	8.0	16	569	3.0	6	98
MIM2265	148.80	107.80	34.56	0.724	2.54E+04	7.10E+03	0.0696	0.0029	0.957	0.038	0.1005	0.0012	0.0014	917	42.9	86	682	9.8	20	617	3.5	7	91
MIM2266	480.00	175.40	33.19	0.368	9.50E+03	2.90E+03	0.0596	0.0021	0.467	0.015	0.0570	0.0006	0.0793	589	38.2	76	589	5.2	10	357	1.9	4	92
MIM2268	184.00	150.20	40.81	0.814	-6.70E+04	2.90E+04	0.0593	0.0023	0.775	0.028	0.0944	0.0011	0.0018	578	42.1	84	583	8.0	16	582	3.2	6	100
MIM2269	65.82	36.22	23.81	0.550	-3.00E+04	5.10E+04	0.0908	0.0032	2.931	0.096	0.2376	0.0027	0.1621	1442	33.6	67	1390	12.4	25	1374	7.0	14	99
MIM2271	112.90	25.29	30.91	0.224	3.80E+04	2.30E+04	0.1627	0.0028	10.726	0.280	0.4709	0.0045	0.2456	2484	14.5	29	2500	12.1	24	2488	9.9	20	100
MIM2274	45.00	33.30	9.86	0.740	1.80E+04	1.80E+04	0.0600	0.0037	0.861	0.050	0.1060	0.0017	0.0781	604	66.7	133	631	13.6	27	649	5.0	10	100
MIM2275	305.00	237.90	252.20	0.670	1.59E+06	6.50E+05	0.1743	0.0031	9.900	0.310	0.4058	0.0057	0.8919	2599	14.3	29	2426	14.4	29	2196	13.1	26	91
MIM2276	419.00	42.60	12.60	0.104	-7.00E+04	2.00E+04	0.0618	0.0021	0.872	0.027	0.1028	0.0010	0.0015	667	36.4	73	637	7.3	15	631	2.9	6	99
MIM2277	93.20	95.90	27.01	1.029	-6.50E-03	4.10E+03	0.0695	0.0026	0.804	0.033	0.0969	0.0013	-0.0293	585	47.9	95	599	9.3	19	608	3.8	8	101
MIM2278	749.00	474.90	140.20	0.634	-2.20E+04	1.80E+04	0.0618	0.0019	0.881	0.025	0.1031	0.0010	0.2075	669	32.9	66	642	6.7	13	632	2.9	6	99
MIM2279	115.46	57.72	16.90	0.500	-3.20E+03	2.70E+03	0.0598	0.0026	0.845	0.036	0.1011	0.0012	0.0504	596	47.1	94	622	9.9	20	621	3.5	7	100
MIM2280	184.00	108.70	90.10	0.591	-2.20E+04	1.20E+04	0.1248	0.0024	5.131	0.140	0.2955	0.0031	0.3175	2026	17.0	34	1841	11.6	23	1669	7.7	15	91
MIM2281	371.50	117.50	20.18	0.316	-1.30E+04	1.00E+04	0.0566	0.0021	4.478	0.017	0.0605	0.0007	0.0881	476	41.0	82	397	5.8	12	379	2.1	4	95
MIM2282	55.82	37.08	11.21	0.664	-1.30E+03	1.10E+03	0.0618	0.0031	0.896	0.043	0.1052	0.0016	0.1559	667	53.7	107	650	11.5	23	645	4.7	9	99
MIM2282	63.40	48.10	14.74	0.759	-5.30E+02	9.00E+02	0.0607	0.0030	0.904	0.044	0.1067	0.0017	0.0830	629	53.2	106	654	11.7	23	665	4.9	10	102
MIM2283	105.20	33.82	22.63	0.321	-7.30E+03	5.00E+03	0.0602	0.0030	3.094	0.096	0.2468	0.0027	0.1147	1430	31.7	63	1431	11.9	24	1422	7.0	14	99
MIM2284	84.00	53.65	15.42	0.639	2.05E+04	7.00E+03	0.0616	0.0029	0.862	0.039	0.1016	0.0013	0.1856	660	50.5	101	631	10.6	21	624	3.8	8	99
MIM2284	1101.00	648.00	890.00	0.589	7.50E+04	7.00E+04	0.2121	0.0033	16.358	0.420	0.5512	0.0050	0.6395	2922	12.6	25	2898	12.3	25	2830	10.4	21	98
MIM2286	79.20	60.90	75.40	0.769	-1.09E+04	5.90E+03	0.1860	0.0035	12.540	0.340	0.4810	0.0050	0.2964	2707	15.5	31	2646	12.7	25	2532	10.9	22	96
MIM2287	38.46	30.27	14.79	0.787	-1.03E+03	6.60E+02	0.0752	0.0038	1.835	0.091	0.1771	0.0024	0.1883	1074	50.7	101	1058	16.3	33	1051	6.6	13	99
MIM2288	269.20	181.30	211.70	0.673	3.00E+02	7.50E+03	0.1625	0.0027	10.713	0.280	0.4718	0.0045	0.4113	2482	14.0	28	2491	12.1	24	2491	9.9	20	100
MIM2289	51.43	49.99	48.35	0.972	-2.70E+03	1.80E+03	0.1240	0.0031	6.390	0.190	0.3671	0.0042	-0.0136	2015	22.2	44	2031	13.0	26	2016	9.9	20	99
MIM2291	386.30	242.20	84.07	0.627	3.00E+03	2.40E+03	0.0655	0.0021	1.124	0.034	0.1235	0.0012	0.1046	790	33.6	67	765	8.1	16	751	3.4	7	98
MIM2292	89.10	116.20	148.20	1.304	1.20E+03	3.30E+03	0.1819	0.0032	12.910	0.350	0.5113	0.0053	0.3466	2670	14.6	29	2673	12.8	26	2662	11.3	23	100
MIM2293	443.30	191.90	50.81	0.433	8.00E+02	2.80E+03	0.0587	0.0019	0.772	0.024	0.0942	0.0009	0.1605	556	35.3	71	581	6.9	14	581	2.7	5	100
MIM2294	170.40	120.20	34.22	0.705	-2.30E+03	1.40E+03	0.0617	0.0025	0.857	0.033	0.1005	0.0012	0.0255	664	43.4	87	628	9.0	18	618	3.5	7	98
MIM2295	177.60	308.80	348.90	1.741	-3.70E+04	1.70E+04	0.1622	0.0028	9.201	0.240	0.4109	0.0042	0.2660	2479	14.6	29	2358	11.9	24	2219	9.6	19	94
MIM2296	283.10	193.20	179.10	0.704	1.70E+03	4.90E+03	0.1189	0.0021	5.545	0.150	0.3375	0.0033	0.2188	1940	15.8	32	1908	11.6	23	1875	8.0	16	98
MIM2297	378.46	41.06	12.18	1.084	-2.30E+03	1.00E+03	0.0591	0.0040	0.861	0.056	0.1035	0.0018	-0.0643	571	73.6	147	631	15.3	31	635	5.3	11	101
MIM2298	23.84	22.74	32.13	0.954	5.00E+04	2.30E+04	0.2019	0.0046	14.970	0.440	0.5371	0.0071	0.1126	2842	18.6	37	2813	14.0	28	2771	14.9	30	99
MIM2299	62.77	65.46	78.44	1.043	-1.00E+05	1.00E+05	0.1611	0.0033	10.220	0.300	0.4604	0.0051	0.3332	2467	17.3	35	2455	13.6	27	2441	11.3	23	99
MIM2300	132.70	257.70	307.80	1.942	-1.33E+04	1.00E+03	0.1613	0.0029	10.407	0.280	0.4701	0.0047	0.2006	2469	15.2	30	2472	12.5	25	2484	10.3	21	100
MIM2310	75.47	65.29	18.44	0.865	-9.60E+02	9.10E+02	0.0587	0.0030	0.823	0.041	0.1009	0.0013	0.1086	556	55.7	111	610	11.4	23	620	3.8	8	102
MIM2311	192.00	185.00	47.50	0.964	-8.80E+03	3.90E+03	0.0642	0.0025	0.813	0.029	0.0925	0.0013	0.0167	748	41.1	82	604	8.1	16	570	3.8	8	94
MIM2312	314.40	298.30	304.60	0.949	5.00E+04	1.50E+04	0.1324	0.0022	7.018	0.180	0.3888	0.0036	0.3641	2130	14.5	29	2114	11.4	23	2117	8.4	17	100
MIM2313	108.50	129.30	37.94	1.182	-2.10E+03	1.70E+03	0.0590	0.0029	0.837	0.038	0.1033	0.0016	-0.0836	567	53.5	107	617	10.5	21	634	3.8	8	103
MIM2314	65.12	45.03	12.93	0.691	5.00E+02	1.10E+03	0.0563	0.0030	0.783	0.039	0.1011	0.0016	0.0290	464	59.0	118	587	11.1	22	621	4.7	9	106
MIM2315	229.00	363.00	105.50	1.585	-3.40E+03	5.30E+03	0.0591	0.0021	0.834	0.027	0.1019	0.0011	0.0535	571	38.7	77	516	7.5	15	625	3.2	6	102
MIM2316	619.60	236.00	64.63	0.381	-5.20E+04	2.40E+04	0.0587	0.0018	0.795	0.023	0.0982	0.0009	0.1657	556	33.4	67	594	6.5	13	604	2.7	5	102
MIM2317	73.40	73.10	21.25	0.996	1.50E+03	1.30E+03	0.0608	0.0029	0.847	0.039	0.1006	0.0014	0.1030	632	51.4	103	623	10.7	21	618	4.1	8	99
MIM2318	521.00	79.96	21.55	0.153	2.00E+04	3.20E+04	0.0577	0.0019	0.727	0.022	0.0905	0.0010	0.1148	518	36.1	72	555	6.5	13	558	2.8	6	101
MIM2319	592.00	88.40	19.22	0.149	-5.40E+04	2.40E+04	0.0585	0.0020	0.685	0.021	0.0845	0.0008	0.0903	549	37.3	75	530	6.3	13	523	2.5	5	99
MIM2320	363.00	76.60	28.80	0.211	-1.28E+06	7.90E+05	0.0645	0.0021	1.166	0.035	0.1297	0.0013	-0.0180	758	34.3	69	785	8.2	16	786	3.7	7	100
MIM2321	356.00	122.30	24.07	0.344	-1.01E+04	9.60E+03	0.0578	0.0021	0.471	0.016	0.0566	0.0007	0.1507	522	39.9	80	382	5.5	11				

ANALYSIS	U (ppm)	Th (ppm)	Pb (ppm)	Th/U	Ratios				Ages (Ma)				Concordance (%)							
					$^{206}\text{Pb}/^{238}\text{U}$	$^{207}\text{Pb}/^{235}\text{U}$	$^{207}\text{Pb}/^{206}\text{Pb}$	$^{206}\text{Pb}/^{238}\text{U}$	$^{207}\text{Pb}/^{235}\text{U}$	$^{207}\text{Pb}/^{206}\text{Pb}$	$^{206}\text{Pb}/^{238}\text{U}$	$^{207}\text{Pb}/^{206}\text{Pb}$								
MIM22133	203.00	88.48	50.35	0.436	0.026	2.216	0.065	0.2014	0.0020	0.0631	1192	32.2	64	1186	10.3	21	1183	5.4	11	100
MIM22134	214.30	85.84	23.20	0.401	0.024	0.781	0.029	0.0946	0.0010	-0.0679	614	43.0	86	586	8.3	17	582	2.9	6	99
MIM22135	97.00	27.95	27.84	0.288	0.025	6.417	0.180	0.3687	0.0039	0.2379	2020	17.8	36	2035	12.3	25	2023	9.2	18	99
Discordant data																				
MIM223	985.00	586.00	188.70	0.595	0.059	4.780	0.160	0.1638	0.0039	0.9566	2907	22.7	45	1781	14.0	28	978	10.8	22	55
MIM2219c	629.00	680.00	623.30	1.061	0.025	7.521	0.200	0.3523	0.0040	0.7614	2434	13.4	27	2175	11.9	24	1946	9.5	19	89
MIM2232	2170.00	1780.00	297.40	0.820	0.058	3.650	0.380	0.1300	0.0130	0.9961	2833	23.6	47	1561	41.5	83	788	37.1	74	50
MIM2240	1335.00	384.00	145.30	0.288	0.058	0.058	0.066	0.0585	0.0017	0.9004	1652	53.0	106	617	18.2	36	366	5.2	10	59
MIM2245	417.00	332.00	207.00	0.796	0.034	9.470	0.570	0.3200	0.0170	0.9903	2929	12.9	26	2385	27.6	55	1790	41.5	83	75
MIM2253	284.90	38.05	23.22	0.134	0.027	1.820	0.053	0.1521	0.0018	0.4214	1347	30.2	60	1053	9.5	19	913	5.0	10	87
MIM2258	780.00	882.00	625.00	1.131	0.019	4.416	0.120	0.2668	0.0032	0.7399	1946	14.2	28	1715	11.2	22	1525	8.1	16	89
MIM2263r	17.57	13.99	3.49	0.796	0.074	0.832	0.084	0.0849	0.0024	0.1019	949	107.1	214	615	23.3	47	525	7.1	14	85
MIM2267	618.30	430.00	210.00	0.695	0.032	3.058	0.110	0.2024	0.0059	0.9445	1803	26.4	53	1422	13.7	27	1188	15.8	32	84
MIM2270	1001.00	629.00	202.60	0.628	0.044	3.896	0.120	0.1837	0.0032	0.9293	2401	24.1	48	1613	12.4	25	1087	8.7	17	67
MIM2272	1134.00	295.70	61.45	0.261	0.023	4.498	0.014	0.0507	0.0005	-0.0928	972	32.8	66	410	4.7	9	319	1.6	3	78
MIM2273r	163.60	66.82	55.12	0.408	0.025	4.980	0.160	0.2837	0.0039	0.7711	2030	17.7	35	1816	13.6	27	1610	9.8	20	89
MIM22732	1168.00	238.20	48.30	0.204	0.022	4.459	0.013	0.0482	0.0005	0.1951	917	32.5	65	384	4.5	9	303	1.5	3	79
MIM2290	316.40	548.00	352.00	1.732	0.046	5.248	0.160	0.2414	0.0038	0.9189	2413	25.0	50	1860	13.0	26	1394	9.9	20	75
MIM22112	596.00	223.90	243.90	0.376	0.034	12.940	0.370	0.4364	0.0065	0.9063	2946	12.8	26	2675	13.5	27	2335	14.6	29	87
MIM22119	640.00	58.81	58.70	0.092	0.020	4.543	0.130	0.2652	0.0038	0.7759	1992	14.5	29	1739	11.9	24	1516	9.7	19	87

Footnotes:

. Analysis references: MIM2z is zircon from sample MIM2 (mount CT18-6), followed by grain number "c" or "r", meaning core or rim, respectively.

Chapter III

Table D.32: Sample OJU10 (LA-ICRMS)

Coordinate UTM: Zone 30S, 536550 m E, 3764944 m N

IGSN: IEACC0001

ANALYSIS	U (ppm)	Th (ppm)	Pb (ppm)	Th/U	Ratios				Concordant data				Error correction	Ages (Ma)				Concordance (%)					
					²⁰⁷ Pb/ ²⁰⁶ Pb	²⁰⁷ Pb/ ²³⁵ U	²⁰⁷ Pb/ ²⁰⁶ Pb	²⁰⁷ Pb/ ²³⁵ U	²⁰⁶ Pb/ ²⁰⁶ Pb	²⁰⁶ Pb/ ²³⁸ U	2σ	2σ		2σ	2σ	σ	2σ		2σ	σ	2σ	2σ	
OJU1021	87.90	25.10	12.75	0.289	1.00E+05	3.90E+05	0.0759	0.0037	1.819	0.086	0.1739	0.0057	0.2277	1070	50.0	100	1047	15.5	31	1033	16.0	32	99
OJU1023	106.90	44.10	7.98	0.413	9.96E+05	9.00E+05	0.0844	0.0061	0.444	0.050	0.0585	0.0022	0.0421	340	125.0	250	370	18.5	37	366	6.5	13	99
OJU1024	226.50	119.30	33.00	0.491	1.50E+05	6.90E+05	0.0634	0.0028	0.909	0.040	0.1038	0.0032	0.0753	690	50.0	100	658	10.0	20	637	9.5	19	97
OJU1025	90.00	87.20	25.40	0.981	2.00E+05	1.50E+05	0.0690	0.0053	0.786	0.070	0.0959	0.0033	0.0482	500	95.0	190	581	19.5	39	590	10.0	20	102
OJU1026	243.00	163.30	31.60	0.671	1.80E+05	2.60E+05	0.0601	0.0038	0.501	0.032	0.0603	0.0019	0.2011	630	65.0	130	409	8.0	22	377	5.5	11	92
OJU1027	269.20	262.20	87.70	0.980	2.80E+05	6.10E+05	0.0603	0.0021	0.942	0.031	0.1129	0.0038	0.4063	618	36.5	73	672	11.0	22	690	11.0	22	103
OJU1028	141.00	156.00	39.90	1.112	2.00E+05	3.40E+05	0.0541	0.0043	0.654	0.049	0.0863	0.0028	0.0478	340	85.0	170	506	15.0	30	533	8.0	16	95
OJU1029	433.00	140.10	68.10	0.322	-1.20E+06	2.50E+06	0.0754	0.0014	1.774	0.039	0.1711	0.0050	0.5152	1081	19.0	38	1035	7.0	14	1018	13.5	27	98
OJU10210	706.00	203.00	68.90	0.290	3.90E+06	4.70E+06	0.0732	0.0011	1.238	0.050	0.1220	0.0053	0.8915	1014	16.0	32	815	11.5	23	741	15.5	31	91
OJU10211	300.00	131.00	65.50	0.435	-1.40E+07	1.40E+07	0.0793	0.0021	1.996	0.060	0.1823	0.0060	0.5891	1178	24.5	49	1115	10.5	21	1082	16.5	33	97
OJU10212a	230.10	160.40	220.60	0.697	4.90E+06	4.10E+06	0.1947	0.0018	14.430	0.220	0.5367	0.0150	0.6525	2773	12.0	24	2780	7.0	14	2769	32.0	64	100
OJU10212b	196.00	219.00	284.00	0.724	2.90E+07	2.10E+07	0.1965	0.0025	14.570	0.200	0.5408	0.0160	0.5110	2826	13.5	27	2787	6.5	13	2786	33.0	66	100
OJU10213	268.00	120.20	95.70	0.734	2.16E+06	8.90E+05	0.1126	0.0026	4.520	0.120	0.2943	0.0110	0.6307	1825	23.0	46	1731	11.0	22	1662	26.5	53	96
OJU10214	199.80	92.20	51.20	0.458	3.70E+06	1.30E+06	0.0807	0.0027	2.313	0.085	0.2074	0.0061	0.4668	1206	32.0	64	1212	13.0	26	1215	16.0	32	100
OJU10215	651.00	423.00	110.20	0.678	3.70E+06	2.20E+06	0.0692	0.0028	0.903	0.043	0.0853	0.0061	0.7807	893	41.0	82	595	12.5	25	532	18.0	36	89
OJU10217	135.40	120.00	29.80	0.826	1.50E+05	2.70E+05	0.0573	0.0051	0.669	0.060	0.0860	0.0030	0.3070	470	90.0	180	524	18.0	36	532	9.0	18	102
OJU10218	462.00	1020.00	143.00	2.028	-1.30E+06	1.70E+06	0.0561	0.0020	0.416	0.017	0.0544	0.0017	0.2765	467	43.0	86	353	6.0	12	341	5.5	11	97
OJU10219	371.00	480.00	145.90	1.292	2.20E+06	2.10E+06	0.0604	0.0020	0.877	0.028	0.1047	0.0030	-0.0013	634	38.0	76	638	7.5	15	642	8.5	17	101
OJU10220	120.60	104.50	31.70	0.860	-3.00E+05	4.40E+05	0.0619	0.0040	0.998	0.062	0.1038	0.0037	0.1302	720	65.0	130	660	16.0	32	637	10.5	21	97
OJU10221	180.00	200.90	61.80	1.091	-7.30E+05	4.60E+05	0.0623	0.0030	0.934	0.043	0.1091	0.0031	-0.0335	689	47.0	94	671	11.0	22	668	9.0	18	100
OJU10223a	332.00	208.00	57.10	0.634	4.40E+06	3.20E+06	0.0602	0.0022	0.839	0.028	0.1021	0.0029	0.1071	615	38.5	77	620	8.0	16	627	8.5	17	101
OJU10223b	87.30	66.00	22.90	0.695	2.50E+05	4.10E+05	0.0615	0.0049	0.989	0.069	0.1142	0.0043	0.0988	650	75.0	150	696	18.0	36	697	12.5	25	100
OJU10223c	287.00	180.00	51.00	0.415	1.80E+06	2.00E+06	0.0664	0.0029	0.948	0.038	0.1043	0.0034	0.0452	822	47.0	94	681	10.5	21	639	10.0	20	94
OJU10224	201.80	143.30	132.90	0.699	-1.30E+06	2.00E+06	0.1171	0.0035	4.520	0.098	0.2802	0.0086	0.2457	1898	23.0	46	1736	9.5	19	1592	21.5	43	92
OJU10225	313.20	169.20	29.00	0.537	-2.00E+06	2.10E+06	0.0553	0.0028	0.431	0.025	0.0568	0.0023	0.0828	400	65.0	130	362	9.0	18	356	7.0	14	98
OJU10226a	174.60	112.60	33.20	0.635	8.00E+05	7.80E+05	0.0627	0.0030	0.903	0.037	0.1050	0.0034	-0.1829	680	50.0	100	654	9.5	19	644	10.0	20	98
OJU10226b	273.70	211.50	58.40	0.765	-1.10E+07	1.10E+07	0.0594	0.0024	0.802	0.029	0.0361	0.0031	0.2814	589	40.5	81	596	10.0	20	603	9.0	18	101
OJU10227	64.10	58.60	17.49	0.919	7.00E+05	1.80E+05	0.0636	0.0058	0.890	0.079	0.1004	0.0033	-0.0246	650	100.0	200	636	21.5	43	617	9.5	19	97
OJU10228	409.00	327.40	89.10	0.808	9.00E+06	1.60E+06	0.0607	0.0020	0.826	0.027	0.0991	0.0028	0.0914	622	35.0	70	613	7.5	15	609	8.5	17	99
OJU10229	88.10	116.40	32.30	1.318	-1.10E+05	4.20E+05	0.0623	0.0039	0.870	0.052	0.1018	0.0032	0.1119	690	70.0	140	637	13.5	27	623	9.0	18	98
OJU10230	95.20	103.80	96.80	1.080	2.50E+06	3.00E+06	0.1165	0.0037	5.710	0.180	0.3605	0.0110	0.3574	1872	29.0	58	1939	14.0	28	1984	26.0	52	102
OJU10232	209.60	76.50	24.60	0.367	5.60E+05	6.80E+05	0.0634	0.0031	0.942	0.045	0.1065	0.0033	0.1880	710	55.0	110	671	12.0	24	652	9.5	19	97
OJU10233	103.00	214.00	35.20	0.279	5.00E+04	1.70E+06	0.0565	0.0017	0.438	0.015	0.0366	0.0018	0.0850	471	35.5	71	370	5.0	10	355	5.5	11	96
OJU10234	86.30	72.30	48.30	0.847	-1.09E+06	6.80E+05	0.0673	0.0034	2.817	0.099	0.2336	0.0078	0.0803	1344	38.5	77	1361	13.0	26	1353	19.0	38	99
OJU10235c	341.60	143.50	25.50	0.424	1.80E+05	6.70E+05	0.0537	0.0024	0.431	0.022	0.0591	0.0018	0.2681	350	47.5	95	363	8.0	16	370	5.5	11	102
OJU10235f	320.00	147.10	25.70	0.439	3.00E+06	3.20E+06	0.0540	0.0023	0.447	0.019	0.0601	0.0018	0.0410	364	49.0	98	374	6.5	13	376	5.5	11	101
OJU10237	60.10	53.90	15.35	0.902	8.00E+05	2.00E+05	0.0605	0.0065	0.780	0.079	0.0936	0.0036	-0.1299	560	110.0	220	583	21.5	43	579	11.0	22	99
OJU10238	947.00	160.80	138.70	0.168	6.00E+06	9.00E+06	0.1304	0.0013	6.899	0.090	0.3863	0.0110	0.8056	2088	13.5	27	2098	5.5	11	2105	26.0	52	100
OJU10239	587.00	13.31	15.41	0.023	-1.10E+08	1.30E+08	0.2007	0.0018	13.590	0.120	0.4929	0.0140	0.5080	2800	12.0	24	2721	4.2	8	2586	28.5	57	95
OJU10240	371.00	191.00	194.00	0.522	-4.50E+06	5.10E+06	0.1311	0.0017	6.930	0.110	0.3849	0.0110	0.6097	2077	15.5	31	2107	7.5	15	2099	29.5	51	100
OJU10241a	324.00	91.00	14.70	0.254	6.00E+06	1.10E+06	0.0559	0.0029	0.447	0.020	0.0582	0.0017	-0.1790	450	55.0	110	374	7.0	14	365	5.5	11	97
OJU10241b	240.00	62.00	10.18	0.249	-8.10E+06	5.50E+06	0.0605	0.0035	0.512	0.029	0.0617	0.0019	0.0133	570	65.0	130	418	9.5	19	386	6.0	12	92
OJU10242c	41.00	7.60	2.21	-0.007	6.00E+05	2.80E+05	0.0592	0.0056	0.823	0.078	0.1017	0.0042	0.0956	570	105.0	210	588	22.5	45	624	12.5	25	104
OJU10242f	146.00	21.90	6.30	0.103	1.30E+06	1.70E+06	0.0602	0.0044	0.533	0.057	0.1002	0.0032	-0.0481	590	75.0	150	610	16.0	32	616	9.5	19	101
OJU10243	1332.00	69.30	12.10	0.051	6.30E+0																		

ANALYSIS	U (ppm)	Th (ppm)	Pb (ppm)	Th/U	Ratios			Error correction			Ages (Ma)			Concordance (%)						
					$^{207}\text{Pb}/^{235}\text{U}$	$^{207}\text{Pb}/^{238}\text{U}$	$^{207}\text{Pb}/^{206}\text{Pb}$	2σ	2σ	2σ	$206\text{Pb}/^{238}\text{U}$	$207\text{Pb}/^{238}\text{U}$	2σ							
OUJ10260	69.30	72.20	22.80	1.044	0.0075	0.947	0.098	0.0987	0.0036	0.3179	900	105.0	210	210	26.0	10.5	21	90		
OUJ10261	179.00	348.00	304.00	1.962	0.0027	5.460	0.139	0.3262	0.0096	0.2584	1983	22.0	44	1903	10.5	21	1820	23.0	46	96
OUJ10262	256.00	271.00	267.00	1.050	0.0020	6.950	0.139	0.3819	0.0100	0.3033	2123	16.5	33	2107	6.5	13	2085	24.0	48	99
OUJ10263	103.70	198.00	38.50	0.953	0.0035	4.495	0.034	0.0674	0.0023	0.0334	340	80.0	160	405	11.5	23	421	7.0	14	104
OUJ10264	237.70	90.90	65.00	0.725	0.0027	3.163	0.096	0.2521	0.0073	0.2870	1457	28.0	56	1445	11.5	23	1449	14.0	38	100
OUJ10265	504.00	70.20	38.90	0.136	0.0017	1.847	0.037	0.1759	0.0050	0.1573	1097	21.5	43	1082	6.5	13	1044	14.0	28	98
OUJ10266	345.00	212.40	140.90	0.612	0.0022	3.040	0.110	0.2205	0.0081	0.1627	1627	20.0	40	1413	14.5	29	1284	21.0	42	91
OUJ10267	810.00	520.00	122.00	0.627	0.0018	0.798	0.021	0.0883	0.0026	0.5584	835	27.0	54	595	6.0	12	546	8.0	16	92
OUJ10268	394.00	231.00	58.40	0.681	0.0031	0.762	0.052	0.0909	0.0058	0.6883	670	55.0	110	570	15.0	30	560	17.0	34	98
OUJ10270	172.60	210.00	54.50	1.205	0.0031	0.448	0.015	0.0604	0.0017	0.4092	370	38.5	77	376	5.5	11	378	5.5	11	100
OUJ10271	256.00	40.90	18.10	0.157	0.0022	1.674	0.047	0.1645	0.0048	0.3656	780	47.0	94	633	12.0	24	601	11.0	22	95
OUJ10272	198.00	89.10	82.10	0.559	0.0024	7.960	0.150	0.3994	0.0120	0.4128	1062	29.0	58	997	9.0	18	982	13.0	26	98
OUJ10273	419.00	247.00	40.30	0.538	0.0022	0.440	0.019	0.0610	0.0019	0.1555	271	47.0	94	369	6.5	13	382	6.0	12	103
OUJ10274	151.10	139.50	38.10	0.896	0.0034	0.726	0.040	0.0912	0.0028	0.1352	550	60.0	120	569	11.0	22	562	8.5	17	101
OUJ10275	325.00	261.00	50.80	0.778	0.0022	0.587	0.020	0.0683	0.0035	0.4208	657	43.0	86	470	6.5	13	425	10.5	21	90
OUJ10278	640.00	228.20	40.70	0.356	0.0021	0.461	0.016	0.0611	0.0017	0.0327	422	41.0	82	384	5.5	11	382	5.0	10	100
OUJ10279	266.80	495.00	146.60	1.828	0.0028	0.894	0.041	0.1007	0.0030	0.3906	771	46.0	92	652	11.0	22	618	8.5	17	95
OUJ10280	191.50	345.00	105.00	1.812	0.0036	0.887	0.047	0.1043	0.0031	0.1673	620	65.0	130	645	12.5	25	639	9.0	18	99
OUJ10281	619.00	280.00	48.10	0.450	0.0020	0.437	0.015	0.0615	0.0018	0.2739	295	41.5	83	368	5.5	11	385	5.5	11	105
OUJ10282	126.50	130.00	41.90	0.935	0.0042	0.797	0.051	0.0945	0.0031	0.1438	670	70.0	140	596	14.0	28	582	9.0	18	98
OUJ10286	171.10	85.60	62.00	0.501	0.0029	3.474	0.096	0.2617	0.0076	0.0851	1563	29.5	59	1522	10.5	21	1498	19.5	39	98
OUJ10287	866.00	191.00	24.70	0.219	0.0018	0.415	0.013	0.0528	0.0015	0.1271	507	32.0	64	354	4.5	9	331	4.6	9	94
OUJ10288	115.00	332.00	95.10	0.791	0.0022	0.959	0.031	0.1040	0.0035	0.4342	862	31.5	63	661	8.0	16	638	10.0	20	94
OUJ10289	400.00	235.20	208.80	0.589	0.0018	6.070	0.120	0.3484	0.0100	0.7916	2084	16.5	33	1987	9.5	19	1927	24.5	49	97
OUJ10290	866.00	143.70	25.50	0.182	0.0018	0.796	0.027	0.0906	0.0032	0.6047	758	30.0	60	596	8.0	16	559	9.5	19	94
OUJ10291	192.60	105.40	92.30	0.549	0.0028	5.040	0.110	0.3248	0.0094	0.2398	1866	25.0	50	1824	9.5	19	1813	23.0	46	99
OUJ10292	432.30	50.70	14.50	0.112	0.0018	0.834	0.026	0.0971	0.0028	0.1948	705	30.5	61	617	7.0	14	597	8.0	16	97
OUJ10293	96.00	116.60	1326.00	1.229	0.0030	9.810	0.430	0.4447	0.0084	0.5186	2443	16.0	32	2417	20.2	40	2372	18.7	37	98
OUJ10294	356.00	163.90	292.00	0.473	0.0032	0.453	0.025	0.0604	0.0012	0.2529	358	67.2	134	379	8.7	17	378	6.6	7	100
OUJ10295	115.00	203.00	596.00	1.840	0.0047	0.932	0.062	0.1052	0.0022	0.0680	752	77.2	154	669	16.3	33	645	6.4	13	96
OUJ10296	36.80	26.70	76.90	0.728	0.0070	0.760	0.085	0.0966	0.0034	0.0991	522	132.8	266	574	24.5	49	594	10.0	20	104
OUJ10297	166.20	216.60	2800.00	1.307	0.0026	13.420	0.570	0.5021	0.0093	0.6260	2776	11.0	22	2710	20.1	40	2623	20.0	40	97
OUJ10298	192.60	105.40	92.30	0.549	0.0028	5.040	0.110	0.3248	0.0094	0.2398	1866	25.0	50	1824	9.5	19	1813	23.0	46	99
OUJ10299	249.00	150.10	383.00	0.606	0.0037	0.687	0.038	0.0834	0.0016	0.1148	596	67.0	134	364	11.4	23	316	4.8	10	103
OUJ10300	96.30	63.30	504.00	0.657	0.0027	4.470	0.210	0.3005	0.0058	0.3333	1749	23.1	46	1725	19.5	39	1694	14.4	29	98
OUJ10310	217.00	32.70	308.00	0.156	0.0021	6.350	0.270	0.3657	0.0064	0.5166	2027	14.9	30	2025	16.6	37	2009	15.1	30	99
OUJ10313	43.89	36.50	94.60	0.801	0.0071	0.858	0.094	0.1009	0.0037	0.0880	678	122.2	244	629	25.7	51	620	10.8	22	99
OUJ10314	177.80	104.60	1010.00	0.583	0.0020	6.370	0.280	0.3638	0.0066	0.5148	2053	13.9	28	2028	19.3	39	2000	15.6	31	99
OUJ10315	39.50	28.89	85.70	0.727	0.0059	4.790	0.280	0.1887	0.0035	0.2146	480	115.0	230	638	23.5	47	665	10.2	20	104
OUJ10316	37.50	56.90	476.00	1.515	0.0041	4.790	0.280	0.1887	0.0035	0.2146	480	115.0	230	638	23.5	47	665	10.2	20	104
OUJ10317	358.00	87.30	742.00	0.242	0.0016	6.127	0.260	0.3546	0.0061	0.6394	2020	11.4	23	1994	18.5	37	1957	14.5	29	98
OUJ10318	95.00	287.00	477.00	3.003	0.0059	0.556	0.052	0.0674	0.0031	0.3456	688	100.9	202	449	17.0	34	420	9.4	19	94
OUJ10319	147.60	294.00	830.00	1.996	0.0040	0.856	0.051	0.1031	0.0021	0.1699	618	71.5	143	628	13.9	28	633	6.1	12	101
OUJ10320	339.00	2095.00	2095.00	0.694	0.0018	6.355	0.270	0.3412	0.0056	0.4745	2148	11.7	23	2026	18.6	37	1892	13.5	27	93
OUJ10321	232.00	124.10	1192.00	0.525	0.0019	6.330	0.270	0.3653	0.0064	0.4448	2009	13.6	27	2023	18.7	37	2007	15.1	30	99
OUJ10322	218.40	65.60	598.00	0.300	0.0017	5.561	0.230	0.3360	0.0055	0.3576	1944	12.7	25	1910	17.8	36	1867	13.3	27	98
OUJ10323	183.00	264.00	744.00	1.374	0.0037	0.830	0.046	0.0993	0.0020	0.1834	632	65.5	131	614	12.8	26	610	5.9	12	99
OUJ10324	203.30	553.00	1630.00	2.716	0.0035	0.917	0.047	0.1070	0.0019	0.1376	678	60.2	120	661	12.4	25	655	5.5	11	99
OUJ10325	67.20	33.55	330.80	0.501	0.0033	6.060	0.280	0.3399	0.0068	0.2586	2061	22.9	46	1985	20.1	40	1886	16.4	33	95
OUJ10326	450.90	102.60	174.10	0.229	0.0032	0.492	0.026	0.0608	0.0013	0.6485	552	59.6	119	406	8.8	18	380	4.0	8	94
OUJ10327	228.30	255.30	632.00	1.129	0.0041	0.736	0.043	0.0861	0.0019	0.1110	701	69.5	139	560	12.6	25	522	5.6	11	95
OUJ10328	202.70	470.00	1273.00	2.326	0.0035	0.812	0.044	0.0962	0.0019	0.2830	596	63.4	127	604	12.3	25	592	5.6	11	98
OUJ10329	126.20	67.40	391.00	0.620	0.0046	2.999	0.120	0.2042	0.0041	0.3557	1329	52.0	104	1242	17.9	36	1198	11.0	22	96
OUJ10330	67.30	62.40	533.00																	

ANALYSIS	U (ppm)	Th (ppm)	Pb (ppm)	Th/U	Ratios		Ratios		Ratios		Ages (Ma)		Ages (Ma)		Concordance (%)						
					$^{206}\text{Pb}/^{238}\text{U}$	$^{207}\text{Pb}/^{235}\text{U}$	$^{206}\text{Pb}/^{238}\text{U}$	$^{207}\text{Pb}/^{235}\text{U}$	$^{206}\text{Pb}/^{238}\text{U}$	$^{207}\text{Pb}/^{235}\text{U}$	$^{206}\text{Pb}/^{238}\text{U}$	$^{207}\text{Pb}/^{235}\text{U}$	$^{206}\text{Pb}/^{238}\text{U}$	$^{207}\text{Pb}/^{235}\text{U}$		$^{206}\text{Pb}/^{238}\text{U}$	$^{207}\text{Pb}/^{235}\text{U}$				
OUJ10z142	671.00	457.00	3759.00	0.686	8.50E+05	0.1839	0.0019	8.598	0.350	0.3374	0.0059	0.6432	2688	17	2296	18.5	37	1874	14.2	28	82
OUJ10z149	43.40	88.80	229.00	2.038	2.20E+04	0.0723	0.0071	0.955	0.086	0.0957	0.0029	0.1359	994	200	681	22.3	45	589	8.5	17	87
OUJ10z154	129.10	137.30	1120.00	1.063	1.90E+04	0.1880	0.0360	3.210	0.760	0.1180	0.0069	0.9664	2725	315	1460	91.6	183	719	19.9	40	49
OUJ10z166	684.00	127.90	486.00	0.189	-3.40E+05	0.1239	0.0061	3.010	0.140	0.1753	0.0049	0.8604	2013	87	1410	17.7	35	1041	13.4	27	74
OUJ10z180	3010.00	660.00	3350.00	0.236	-4.00E+05	0.1277	0.0062	1.673	0.070	0.0956	0.0018	0.7726	2067	86	998	13.3	27	589	5.3	11	59
OUJ10z182	30.40	34.80	102.60	1.164	5.00E+04	0.0734	0.0086	1.060	0.120	0.1044	0.0044	0.1672	1025	237	734	29.5	59	640	12.8	26	87
OUJ10z187	696.00	308.40	598.00	0.445	2.50E+06	0.0648	0.0036	0.589	0.029	0.0661	0.0014	0.3258	768	117	470	9.3	19	413	4.2	8	88

Footnotes:

. Analysis references: OUJ10z is zircon from sample OUJ10 (mounts CT17-9 and CT18-5), followed by grain number "c" or "r", meaning core or rim, respectively.

Chapter III

Table D.33: Sample OJ11 (LA-ICP/MS)

Coordinate UTM: Zone 30S, 536550 m E, 376494.4 m N

IGSN: IEACC0002

ANALYSIS	U (ppm)	Th (ppm)	Pb (ppm)	Th/U	Ratios					Concordant data					Error correction	Ages (Ma)					Concordance (%)		
					$^{207}\text{Pb}/^{206}\text{Pb}$	2σ	$^{207}\text{Pb}/^{235}\text{U}$	2σ	$^{206}\text{Pb}/^{238}\text{U}$	2σ	$^{207}\text{Pb}/^{206}\text{Pb}$	σ	$^{207}\text{Pb}/^{235}\text{U}$	2σ		$^{206}\text{Pb}/^{238}\text{U}$	σ	$^{207}\text{Pb}/^{235}\text{U}$	2σ	$^{206}\text{Pb}/^{238}\text{U}$		σ	
OJ11z1	455.00	261.00	46.50	0.573	-4.00E-04	4.20E+06	0.0533	0.0025	0.449	0.021	0.0620	0.0018	0.1873	340	50.0	100	375	7.5	388	5.5	11	103	
OJ11z2	284.00	77.70	12.59	0.271	3.00E-06	5.20E+06	0.0560	0.0024	0.452	0.021	0.0594	0.0017	0.1276	425	47.0	94	377	7.5	372	5.5	11	90	
OJ11z3	753.00	86.10	15.80	0.111	2.20E+06	3.80E+06	0.0546	0.0017	0.464	0.013	0.0616	0.0019	0.0862	359	36.5	73	387	4.6	385	5.5	11	100	
OJ11z4	85.40	30.90	30.90	1.124	-6.00E-06	1.20E+06	0.0631	0.0048	0.955	0.071	0.1089	0.0038	-0.1200	860	80.0	160	679	17.5	668	10.5	21	98	
OJ11z5	798.00	152.00	35.80	0.186	-5.30E-06	4.10E+06	0.0614	0.0023	0.498	0.018	0.0591	0.0017	0.1963	640	39.5	79	410	6.0	370	5.0	10	90	
OJ11z6	583.00	807.00	822.10	1.371	-2.11E-07	6.80E+06	0.1344	0.0012	6.878	0.071	0.3717	0.0017	0.5513	2187	13.0	26	2097	4.4	2037	24.5	49	97	
OJ11z7	65.00	65.00	18.25	0.914	-4.90E-05	6.90E+05	0.0594	0.0049	0.772	0.059	0.0947	0.0032	-0.0905	520	85.0	170	575	17.0	583	9.5	19	101	
OJ11z8c	72.10	38.30	10.54	0.787	-4.20E-05	2.80E+05	0.0636	0.0060	0.822	0.084	0.0931	0.0036	0.0306	680	100.0	200	605	24.5	574	10.5	21	95	
OJ11z9	172.00	103.90	18.70	0.601	7.00E-06	1.50E+06	0.0534	0.0052	0.423	0.039	0.0660	0.0021	0.0153	250	100.0	200	366	14.5	376	6.5	13	103	
OJ11z10	55.00	31.00	22.10	0.544	9.00E+06	1.50E+06	0.1003	0.0045	3.710	0.170	0.2666	0.0081	0.1359	1648	45.0	90	1566	18.5	37	1923	20.5	41	97
OJ11z11c	221.20	282.40	232.50	1.263	2.30E+06	3.40E+06	0.1114	0.0021	4.890	0.095	0.3038	0.0086	0.3970	1849	20.0	40	1764	8.5	17	1710	21.5	43	97
OJ11z11r	591.00	49.00	8.49	0.082	-2.60E-06	4.20E+06	0.0547	0.0019	0.443	0.014	0.0593	0.0017	0.0668	381	39.0	78	375	5.0	371	5.0	10	99	
OJ11z12r	128.70	157.90	40.40	1.205	-8.20E-05	8.20E+05	0.0621	0.0044	0.790	0.054	0.0926	0.0030	-0.1231	680	75.0	150	597	15.5	31	18	96		
OJ11z13c	374.80	132.80	23.04	0.345	-6.10E-05	9.70E+05	0.0541	0.0026	0.444	0.020	0.0599	0.0018	0.0035	360	50.0	100	371	7.0	375	5.5	11	101	
OJ11z13r	434.00	141.30	24.60	0.324	7.50E-06	6.50E+06	0.0533	0.0030	0.444	0.025	0.0603	0.0017	0.0996	340	65.0	130	371	9.0	377	5.0	10	102	
OJ11z14	516.00	88.20	15.34	0.188	-7.00E+06	2.80E+06	0.0543	0.0022	0.464	0.019	0.0626	0.0018	0.0372	356	46.0	92	386	6.5	392	5.5	11	101	
OJ11z15c	33.50	28.70	25.18	0.855	1.20E+06	1.30E+06	0.1149	0.0037	5.170	0.026	0.3255	0.0110	-0.0498	1950	42.5	85	1846	17.5	1816	27.5	55	98	
OJ11z15r	190.00	49.70	8.76	0.287	-2.30E-05	4.30E+05	0.0588	0.0036	0.543	0.037	0.0660	0.0021	0.2322	550	75.0	150	437	12.0	24	412	6.5	13	94
OJ11z17c	609.00	268.00	72.50	0.437	-2.40E+07	2.80E+07	0.0583	0.0019	0.768	0.026	0.0952	0.0027	0.2807	539	32.5	65	580	7.5	586	8.0	16	101	
OJ11z17r	79.50	40.00	10.33	0.506	-1.11E+06	9.60E+05	0.0626	0.0048	0.816	0.065	0.0941	0.0033	0.3307	610	85.0	170	598	18.5	37	580	9.5	19	97
OJ11z18c	148.00	114.00	59.00	0.685	-7.90E-06	4.90E+06	0.0753	0.0019	1.986	0.068	0.1894	0.0059	0.6205	1078	23.0	46	1108	11.5	23	1118	16.0	32	101
OJ11z18r	97.20	61.70	36.60	0.639	5.00E+05	6.30E+05	0.0800	0.0030	2.249	0.086	0.2031	0.0063	0.3371	1199	37.5	75	1192	13.5	27	1191	17.0	34	100
OJ11z19	330.00	189.00	47.40	0.543	-1.60E+06	2.80E+06	0.0564	0.0026	0.677	0.035	0.0869	0.0027	0.3543	430	50.0	100	529	10.0	537	8.0	16	102	
OJ11z20	255.00	111.50	19.50	0.422	-5.00E+05	8.30E+05	0.0569	0.0032	0.468	0.023	0.0616	0.0019	-0.0489	460	65.0	130	395	8.5	385	6.0	12	98	
OJ11z21	250.90	326.00	97.80	1.306	6.00E-06	1.40E+06	0.0582	0.0024	0.840	0.035	0.1048	0.0031	0.1811	537	42.5	85	617	9.5	642	9.0	18	104	
OJ11z22	123.90	88.90	31.70	0.709	1.90E+05	9.90E+05	0.0621	0.0035	1.050	0.050	0.1228	0.0039	0.2857	690	50.0	100	734	11.5	23	747	11.0	22	102
OJ11z23	149.70	42.40	20.22	0.282	1.60E+06	1.30E+06	0.0743	0.0020	1.752	0.058	0.1693	0.0049	0.1793	1033	34.0	68	1029	10.0	20	1008	13.5	27	98
OJ11z24	75.80	30.10	27.20	1.175	4.50E+05	2.60E+05	0.0583	0.0053	0.828	0.075	0.1039	0.0038	0.0117	500	95.0	190	609	21.0	42	637	11.0	22	105
OJ11z25	360.20	139.30	23.70	0.378	1.70E+05	7.10E+05	0.0513	0.0026	0.418	0.020	0.0588	0.0017	0.2796	230	55.0	110	354	7.0	368	5.5	11	104	
OJ11z26	431.30	96.40	17.00	0.224	5.20E+06	4.20E+06	0.0547	0.0026	0.446	0.020	0.0592	0.0017	0.2825	400	50.0	100	373	7.5	377	5.5	11	99	
OJ11z27	220.00	75.30	13.40	0.337	-3.00E+05	7.20E+05	0.0553	0.0035	0.456	0.027	0.0614	0.0019	0.2261	390	65.0	130	380	9.5	384	5.5	11	101	
OJ11z28r	109.80	56.70	15.54	0.518	5.00E+05	5.10E+05	0.0575	0.0044	0.733	0.054	0.0928	0.0032	0.0769	480	80.0	160	553	16.0	32	572	9.5	19	103
OJ11z29	427.00	50.90	10.58	0.118	-7.80E+06	4.70E+06	0.0573	0.0028	0.473	0.020	0.0600	0.0018	-0.0590	510	50.0	100	395	9.0	376	5.5	11	95	
OJ11z30	376.00	214.80	62.10	0.561	-7.50E+05	8.50E+05	0.0608	0.0021	0.867	0.035	0.1029	0.0031	0.3700	626	39.0	78	632	9.5	631	9.0	18	100	
OJ11z31	466.00	263.00	255.70	0.569	-9.80E+06	5.90E+06	0.1243	0.0016	6.360	0.110	0.3688	0.0110	0.6801	2023	15.5	31	2026	7.5	2023	25.5	51	100	
OJ11z32	42.50	28.10	8.80	0.588	8.00E+05	2.30E+05	0.0607	0.0052	0.952	0.075	0.1108	0.0048	0.0602	640	95.0	190	678	20.5	677	14.0	28	100	
OJ11z33	283.00	202.00	180.00	0.711	1.10E+06	4.10E+06	0.1658	0.0026	9.730	0.190	0.4268	0.0120	0.5646	2522	16.5	33	2408	9.0	18	2291	28.0	56	99
OJ11z34	86.60	71.70	23.50	0.789	-5.20E+06	4.40E+06	0.0649	0.0040	1.107	0.068	0.1225	0.0039	0.1200	710	70.0	140	750	16.5	33	745	11.5	23	96
OJ11z35	264.00	118.70	103.60	0.439	8.20E+06	8.50E+06	0.1237	0.0021	5.800	0.100	0.3363	0.0098	0.4332	2017	17.5	35	1945	8.0	16	1869	23.5	47	99
OJ11z36	257.00	28.10	5.20	0.114	1.00E+07	1.10E+06	0.0568	0.0026	0.466	0.023	0.0593	0.0019	0.2902	450	50.0	100	388	8.0	371	5.5	11	96	
OJ11z37c	277.00	122.20	23.20	0.437	8.40E+05	7.90E+05	0.0548	0.0028	0.456	0.024	0.0595	0.0017	0.0381	380	55.0	110	380	8.0	373	5.0	10	98	
OJ11z38	136.30	46.30	12.44	0.352	-4.30E+05	3.10E+05	0.0566	0.0026	0.489	0.025	0.0633	0.0019	0.2908	500	55.0	110	413	8.0	395	5.5	11	96	
OJ11z39	473.00	157.30	26.80	0.330	-3.10E+06	2.90E+06	0.0519	0.0020	0.435	0.018	0.0602	0.0018	0.4611	505	45.5	91	388	6.5	377	5.5	11	102	
OJ11z40c	372.00	189.00	185.00	0.490	-7.00E+06	3.60E+06	0.1255	0.0016	6.593	0.091	0.3775	0.0110	0.4537	2044	15.0	30	2060	6.5	13	2067	24.5	49	100
OJ11z40r	488.40	85.90	15.21	0.175	-5.00E+06	1.30E+06	0.0530	0.0022	0.460	0.019	0.0546	0.0020	0.0640	318	46.5	93	383	6.5	388	5.5	11	101	
OJ11z41	521.00	267.00	38.80	0.383	-1.00E+07	1.10E+06	0.0571	0.0025	0.438	0.017	0.0546	0.0020	0.0640	465	60.0	120	522	6.0	534	6.0	12	93	100
OJ11z42	345.00	130.00	31.90	0.364	-6.10E+05	9.70E+05	0.0565	0.0030	0.676	0.034	0.0864	0.0026	-0.0297	460	46.0	92	370	6.0	370	5.5	11	102	
OJ11z43	46.60	32.90	27.99	0.697	2.40E+05	8.00E+05	0.1142	0.0045	5.120	0.180	0.3310	0.0110	0.1133	1878	38.0	76	1844	15.5	31	1842	26.5	53	100
OJ11z44c	122.80	63.80	107.60	0.518	-1.00E+06	2.10E+06	0.0571	0.0045	25.910	0.380	0.6640	0.0190	0.4904	3373	13.0	26	3342	7.5	15	3282	37.0	74	98
OJ11z44r	573.00	194.30	34.80	0.374	-1.07E+06	6.00E+05	0.0523	0.0023	0.455	0.019	0.0619	0.0018	-0.0005	287	48.0	96	380	6.5	387	5.5	11	102	

ANALYSIS	U (ppm)	Th (ppm)	Pb (ppm)	Th/U	Ratios				Errors			Ages (Ma)				Concordance (%)				
					$^{206}\text{Pb}/^{238}\text{U}$	$^{207}\text{Pb}/^{235}\text{U}$	$^{207}\text{Pb}/^{206}\text{Pb}$	2σ	2σ	2σ	2σ	Error correction	$^{207}\text{Pb}/^{238}\text{U}$	2σ	$^{206}\text{Pb}/^{238}\text{U}$		2σ			
OUJ11z256	235.50	218.50	52.00	0.922	0.922	0.029	0.035	0.0879	0.0026	-0.3236	57.0	55.0	110	562	10.0	20	543	8.0	16	97
OUJ11z257	392.00	46.70	9.41	0.129	-3.10E+05	5.70E+05	0.0530	0.0615	0.0019	0.2869	318	43.5	87	383	6.5	13	385	5.5	11	101
OUJ11z258	263.10	51.90	14.56	0.196	2.10E+05	8.00E+05	0.0599	0.0435	0.0031	0.1898	560	630	100	630	11.5	23	630	9.0	18	101
OUJ11z259	549.00	69.00	12.40	0.120	-1.20E+06	1.10E+06	0.0516	0.0607	0.0018	0.0137	262	48.5	97	368	6.5	13	380	5.5	11	103
OUJ11z263	425.00	143.80	41.90	0.348	-3.10E+06	1.90E+06	0.0601	0.818	0.025	0.4485	593	31.0	62	608	7.5	15	600	8.5	17	99
OUJ11z264	71.10	78.60	64.20	1.085	-3.20E+05	5.20E+05	0.1111	4.940	0.160	0.3197	1848	28.5	57	1815	14.5	29	1788	25.0	50	99
OUJ11z265	74.10	96.40	27.00	1.307	-1.70E+05	2.00E+05	0.0841	0.889	0.059	0.3576	710	65.0	130	646	16.5	33	619	10.0	20	96
OUJ11z266	227.20	144.50	88.00	0.630	-2.90E+05	6.70E+05	0.0811	0.222	2.388	0.2119	1222	25.5	51	1243	9.0	18	1239	16.0	32	100
OUJ11z267	617.00	273.00	52.30	0.385	-9.30E+06	1.40E+06	0.0559	0.485	0.025	-0.0586	540	60.0	120	403	8.5	17	367	5.0	11	91
OUJ11z268	791.00	268.00	47.40	0.384	1.30E+06	6.10E+06	0.0393	0.477	0.017	0.6068	440	37.5	75	395	10.0	20	411	5.5	11	96
OUJ11z269	581.00	122.00	38.70	0.149	-6.00E+06	7.00E+06	0.0616	0.918	0.033	0.7104	649	27.0	54	660	8.5	17	655	10.5	21	99
OUJ11z270a	202.00	113.00	65.20	0.551	1.80E+05	7.60E+05	0.0785	0.0221	2.372	0.068	1163	27.0	55	1232	10.5	21	1255	18.0	36	102
OUJ11z70a	202.00	32.30	10.49	0.563	-7.00E+05	1.10E+05	0.0950	0.899	0.089	0.0379	390	105.0	210	647	23.5	47	704	13.0	26	109
OUJ11z71	242.00	40.30	7.71	0.160	-6.30E+05	9.00E+05	0.0553	0.452	0.030	0.0573	480	65.0	130	380	10.0	20	359	5.5	11	95
OUJ11z73	653.00	120.10	309.00	1.799	-5.00E+06	1.20E+06	0.0585	0.753	0.021	0.0917	555	27.0	54	573	6.0	12	566	8.0	16	99
OUJ11z75	179.70	105.00	90.00	0.572	-1.00E+07	1.00E+06	0.1088	4.880	0.110	0.3190	1802	22.5	45	1801	9.0	18	1785	23.5	47	99
OUJ11z76	126.00	246.00	268.00	1.927	-4.00E+06	1.10E+06	0.0423	8.320	0.150	0.4164	2277	18.5	37	2265	8.5	17	2244	28.0	56	99
OUJ11z77	61.00	59.10	17.69	0.968	-5.00E+05	1.60E+05	0.0549	0.0621	0.776	0.080	410	110.0	220	605	23.0	46	644	12.0	24	106
OUJ11z78	247.00	208.10	107.00	0.831	-1.60E+05	6.90E+05	0.0727	1.891	0.061	0.1862	1011	30.5	61	1075	11.0	22	1101	14.5	29	102
OUJ11z79	81.20	88.90	24.30	1.091	-9.00E+05	1.80E+05	0.0644	0.048	0.881	0.067	690	80.0	160	648	17.5	35	623	11.0	22	96
OUJ11z80	236.00	121.30	20.00	0.499	1.50E+05	2.00E+05	0.0578	0.035	0.496	0.032	480	70.0	140	410	10.5	21	380	5.5	11	93
OUJ11z81c	79.40	210.50	80.30	2.687	7.00E+06	1.10E+06	0.0652	1.190	0.088	0.1337	690	80.0	160	792	12.0	24	809	12.0	24	102
OUJ11z81f	465.00	551.00	208.30	1.179	-4.60E+05	8.50E+05	0.0648	0.018	1.253	0.033	765	28.0	56	824	7.5	15	822	11.5	23	100
OUJ11z82	299.00	291.60	87.00	0.984	1.10E+06	1.60E+06	0.0597	0.853	0.038	0.1045	601	48.5	97	640	10.5	21	641	8.5	17	100
OUJ11z83	191.00	141.50	24.31	0.485	-3.00E+05	4.60E+05	0.0561	0.032	0.461	0.026	470	60.0	120	383	9.0	18	360	5.5	11	94
OUJ11z84	137.00	103.10	27.60	0.689	-1.00E+05	1.40E+05	0.0691	0.035	0.741	0.044	540	65.0	130	560	12.5	25	555	9.0	18	99
OUJ11z85	151.00	517.00	146.20	3.367	-5.00E+05	2.30E+05	0.0592	0.027	0.788	0.035	500	50.0	100	591	10.5	21	598	9.0	18	101
OUJ11z86	117.00	174.00	32.60	0.192	-8.00E+05	7.20E+05	0.0550	0.020	0.461	0.017	389	41.5	83	384	6.0	12	375	5.0	10	98
OUJ11z88	417.00	111.00	88.00	0.229	-1.10E+06	1.50E+06	0.0572	0.038	0.710	0.046	440	70.0	140	546	14.0	28	560	8.0	16	103
OUJ11z89	285.00	507.00	123.00	1.689	1.20E+05	5.00E+05	0.0605	0.028	0.756	0.036	603	49.5	99	569	10.5	21	549	8.0	16	97
OUJ11z90	232.80	95.30	15.45	0.402	-6.00E+05	1.70E+05	0.0520	0.024	0.442	0.026	300	55.0	110	370	9.0	18	371	6.0	12	100
OUJ11z90c	305.10	102.90	18.42	0.337	-5.90E+05	4.70E+05	0.0545	0.028	0.475	0.025	390	55.0	110	393	8.5	17	390	5.5	11	99
OUJ11z91	231.00	121.30	20.50	0.512	-6.00E+05	3.00E+05	0.0560	0.033	0.468	0.026	440	70.0	140	388	9.0	18	377	5.5	11	97
OUJ11z92	73.10	60.70	21.61	0.822	-3.00E+05	1.80E+05	0.0651	0.036	1.080	0.057	810	60.0	120	745	14.5	29	726	11.0	22	97
OUJ11z93	129.00	140.60	25.34	0.610	-5.00E+05	2.80E+05	0.0516	0.032	0.466	0.030	450	65.0	130	386	10.5	21	398	6.5	13	103
OUJ11z95	181.00	78.30	20.51	0.610	-1.90E+05	1.50E+05	0.0572	0.038	0.710	0.046	440	70.0	140	546	14.0	28	560	8.0	16	103
OUJ11z96	78.60	24.00	11.33	0.304	-6.20E+05	8.90E+05	0.0700	0.0421	1.720	0.100	910	65.0	130	1015	19.5	39	1040	15.5	31	102
OUJ11z97	576.00	69.60	12.45	0.120	-1.30E+05	6.60E+05	0.0526	0.021	0.452	0.019	335	48.0	96	380	6.5	13	380	5.5	11	100
OUJ11z99	295.00	74.90	13.33	0.250	4.00E+05	3.90E+05	0.0502	0.031	0.439	0.029	190	65.0	130	367	10.0	20	366	5.5	11	105
OUJ11z100	589.00	1014.00	933.00	1.705	1.00E+05	8.70E+06	0.1225	0.013	5.990	0.074	1989	14.0	28	1975	5.0	10	1939	24.0	48	98
OUJ11z100c	109.80	97.50	37.50	0.883	-6.40E+05	3.60E+05	0.0550	0.028	6.420	0.180	2009	24.5	49	2031	12.5	25	2034	24.5	49	100
OUJ11z102	229.00	95.60	18.80	0.416	1.04E+06	7.40E+05	0.0550	0.034	0.518	0.031	360	70.0	140	421	10.5	21	427	6.0	12	101
OUJ11z102	313.00	122.80	22.49	0.394	-3.40E+05	2.40E+05	0.0567	0.025	0.484	0.022	450	50.0	100	399	7.5	15	384	5.5	11	96
OUJ11z103	582.00	44.20	39.30	0.078	-3.90E+06	4.10E+06	0.1166	0.017	5.392	0.065	1908	16.0	32	1885	5.0	10	1842	22.0	44	98
OUJ11z104c	337.00	203.10	61.00	0.598	1.90E+05	4.50E+05	0.0609	0.019	0.904	0.028	649	33.5	67	655	7.5	15	643	9.0	18	98
OUJ11z104f	409.00	237.00	73.10	0.601	-1.85E+07	9.05E+06	0.0599	0.021	0.845	0.027	578	37.0	74	621	7.5	15	625	9.0	18	101
OUJ11z106	288.00	292.00	80.70	0.983	-8.40E+05	4.50E+05	0.0598	0.026	0.809	0.039	560	50.0	100	607	11.0	22	614	8.5	17	101
OUJ11z108	117.70	72.80	22.09	0.613	1.60E+05	2.40E+05	0.0551	0.040	0.788	0.059	480	80.0	160	584	16.5	33	627	9.0	18	107
OUJ11z109	123.00	98.40	27.10	0.801	1.00E+05	1.30E+05	0.0638	0.035	0.836	0.047	730	55.0	110	613	13.0	26	586	9.0	18	96
OUJ11z110c	219.00	137.20	37.80	0.625	2.90E+05	6.30E+05	0.0635	0.030	0.820	0.036	726	47.5	95	606	10.0	20	606	8.5	17	93
OUJ11z110f	117.20	52.40	15.30	0.429	1.50E+05	1.70E+05	0.0589	0.039	0.848	0.057	580	70.0	140	629	15.5	31	637	10.5	21	101
OUJ11z111c	133.00	114.60	30.40	0.847	-3.40E+05	3.00E+05	0.0570	0.033	0.737	0.044	450	65.0	130	562	13.5	27	577	8.5	17	103
OUJ11z111f	538.00	769.00	202.50	1.417	-1.80E+06	1.10E+06	0.0577	0.016	0.747	0.021	521	31.0	62	566	6.0	12	568	8.0	16	100
OUJ11z111r	26.42	24.15	7.02	0.898	9.00E+04	2.50E+04	0.0612	0.0094	0.850	0.130	460	155.0	310	619	38.0	76	622	12.5	25	100
OUJ11z113c	305.50	298.70	302.10	0.977	1.11E+07	8.40E+06	0.1298	0.016	6.932	0.091	2089	15.0	30	2102	6.0	12	2094	25.0	50	100
OUJ11z113f	106.10	87.50	92.40	0.811	6.00E+06	1.20E+06	0.1262	0.030	6.900	0.190	2035	23.0	46	2095	12.0	24	2143	28.0	56	102
OUJ11z113r	145.00	106.00	33.40	0.726	6.00E+05	3.10E+05	0.0630	0.037	0.911	0.052	700	60.0	120	668	13.5	27	643	10.0	20	97
OUJ11z114f	53.40	141.20	41.80	2.634	1.70E+04	3.40E+04	0.0620	0.052	0.858	0.081	320	95.0	190	634						

ANALYSIS	U (ppm)	Th (ppm)	Pb (ppm)	Th/U	Ratios			Agnes (Ma)				Concordance (%)							
					²⁰⁷ Pb/ ²⁰⁶ Pb	²⁰⁷ Pb/ ²³⁵ U	²⁰⁷ Pb/ ²⁰⁶ Pb	σ	²⁰⁷ Pb/ ²³⁵ U	σ	²⁰⁶ Pb/ ²³⁸ U		σ						
					2σ	2σ	2σ	σ	2σ	σ	2σ		σ						
OJ1112121c	269.10	262.00	74.20	0.970	0.024	0.802	0.031	0.0979	0.0029	42.5	85	596	9.0	18	602	8.5	17	101	
OJ1112121r	110.90	100.80	26.40	0.835	0.057	0.808	0.058	0.0888	0.0044	80.0	160	602	17.0	34	548	13.0	26	91	
OJ1112122c	689.00	754.00	746.00	1.078	0.010	7.200	0.099	0.3915	0.0110	12.0	24	2136	6.0	12	2782	23.0	52	100	
OJ1112122r	502.00	107.50	112.50	0.215	0.017	6.861	0.080	0.3855	0.0110	13.5	27	2083	5.0	10	2102	25.0	50	100	
OJ1112123c	262.00	123.40	103.80	0.498	0.0012	4.209	0.088	0.2915	0.0084	17.05	18.0	1649	7.5	15	1649	21.0	42	98	
OJ1112123r	18.97	13.89	12.21	0.721	0.0687	4.910	0.290	0.3217	0.0130	65.0	130	1807	27.0	54	1796	31.5	63	99	
OJ1112124r	331.60	107.80	99.70	0.318	0.0022	5.880	0.150	0.3211	0.0110	17.0	34	1929	11.5	23	1794	25.5	51	93	
OJ1112125r	158.20	97.60	69.00	0.617	0.0030	6.470	0.290	0.3693	0.0070	20.40	42	2042	19.7	39	2026	16.5	33	99	
OJ1112126r	118.50	75.70	235.00	0.639	0.0051	9.815	0.059	0.1039	0.0023	81.7	163	660	15.6	31	637	6.7	13	97	
OJ1112128c	186.00	97.50	1276.00	0.529	0.0024	13.810	0.580	0.5127	0.0090	10.2	20	2737	19.9	40	2668	19.2	38	97	
OJ1112128r	97.00	39.50	486.00	0.414	0.0031	13.080	0.570	0.4844	0.0098	13.2	26	2686	20.5	41	2646	21.3	43	95	
OJ1112129r	180.00	140.10	390.00	0.789	0.0041	8.857	0.050	0.0971	0.0020	74.8	135	628	13.7	27	597	5.9	12	95	
OJ1112130r	117.90	79.10	739.00	0.674	0.0025	6.490	0.290	0.3646	0.0061	17.2	34	2045	19.6	39	2004	14.4	29	98	
OJ1112131r	216.30	277.00	775.00	1.247	0.0039	8.867	0.048	0.0983	0.0020	63.4	128	634	13.0	26	604	5.9	12	95	
OJ1112132c	302.00	227.00	633.00	0.730	0.0034	8.851	0.041	0.1004	0.0018	11.2	22	617	11.2	22	617	5.3	11	99	
OJ1112134r	242.30	75.90	570.00	0.320	0.0059	3.659	0.160	0.2708	0.0047	18.6	37	1562	17.4	35	1545	11.9	24	99	
OJ1112135r	121.00	70.30	668.00	0.588	0.0027	6.260	0.290	0.3605	0.0066	20.12	39	2013	20.3	41	1985	15.6	31	99	
OJ1112136c	55.40	62.10	179.40	1.130	0.0064	8.942	0.083	0.1012	0.0027	98.3	197	674	21.7	43	621	7.9	16	92	
OJ1112137c	193.30	55.50	205.00	0.281	0.0040	1.171	0.064	0.1274	0.0024	83.8	124	787	15.0	30	773	6.9	14	98	
OJ1112137r	410.00	86.80	295.00	0.185	0.0039	8.868	0.041	0.0932	0.0025	88.1	118	634	11.1	22	574	7.4	15	91	
OJ1112138r	105.50	92.80	164.60	0.873	0.0060	6.519	0.052	0.0631	0.0018	59.3	118	424	17.4	35	394	5.5	11	93	
OJ1112139r	162.00	48.40	87.50	0.301	0.0043	4.880	0.034	0.0595	0.0014	80.5	161	398	11.7	23	373	4.3	9	94	
OJ1112140r	45.50	58.10	179.70	1.287	0.0064	9.913	0.088	0.1046	0.0032	73.2	106.4	213	65.9	23.3	47	641	9.3	19	97
OJ1112141r	158.90	30.26	284.00	0.615	0.0044	8.853	0.058	0.0979	0.0021	74.1	148	626	15.9	32	602	6.2	12	96	
OJ1112142r	58.10	30.26	168.30	0.519	0.0059	2.360	0.140	0.1984	0.0051	66.0	132	1231	21.1	42	1167	13.7	27	95	
OJ1112143r	327.20	100.40	1206.00	0.311	0.0021	12.800	0.530	0.4753	0.0081	8.9	18	2665	19.5	39	2507	17.7	35	94	
OJ1112144r	39.20	69.30	687.00	1.743	0.0044	6.760	0.350	0.3739	0.0099	29.9	60	2082	22.8	46	2048	23.2	46	98	
OJ1112146r	155.60	276.60	750.00	1.741	0.0041	8.870	0.060	0.0988	0.0020	67.8	141	630	14.5	29	607	5.9	12	96	
OJ1112147r	98.70	84.80	178.50	0.674	0.0054	6.643	0.043	0.0842	0.0019	42.8	82.5	504	13.3	27	521	5.4	11	103	
OJ1112148r	169.00	116.00	310.00	0.672	0.0040	4.900	0.040	0.0915	0.0018	58.2	73.1	146	57.2	13.9	28	564	5.6	11	99
OJ1112150r	137.50	137.20	224.80	0.992	0.0051	4.476	0.037	0.0601	0.0016	95.0	190	395	12.7	25	376	4.9	10	95	
OJ1112151r	88.60	137.40	381.00	1.558	0.0059	8.872	0.074	0.1056	0.0023	88.4	94.2	188	39.5	40	618	6.7	13	97	
OJ1112152r	26.63	30.90	101.90	1.171	0.0055	1.160	0.150	0.1156	0.0045	97.7	140.7	281	78.2	35.2	70	705	13.0	26	90
OJ1112153r	136.10	53.70	275.80	0.397	0.0048	1.834	0.094	0.1700	0.0034	61.4	123	1058	16.8	34	1012	9.4	19	96	
OJ1112154r	125.50	111.90	290.00	0.888	0.0042	6.771	0.052	0.0927	0.0019	58.9	76.4	153	58.0	14.9	30	571	5.6	11	98
OJ1112155r	180.70	272.30	1467.00	1.490	0.0043	2.217	0.110	0.2000	0.0037	119.2	106	1186	17.3	35	91	18	99		
OJ1112155r	107.20	90.70	291.00	0.853	0.0054	4.900	0.240	0.3309	0.0064	20.4	41	1802	20.6	41	1843	16.2	32	102	
OJ1112157r	174.20	293.00	820.00	1.727	0.0045	8.784	0.055	0.0936	0.0019	60.8	162	588	15.6	31	577	5.6	11	98	
OJ1112159r	307.00	147.10	258.00	0.477	0.0037	4.461	0.028	0.0604	0.0012	436	74.1	148	38.5	19	378	3.6	7	98	
OJ1112159r	60.95	89.50	266.70	1.468	0.0061	9.904	0.081	0.1044	0.0027	72.2	102.1	240	65.4	43	640	7.9	16	98	
OJ1112160r	33.41	59.10	564.00	1.751	0.0030	6.160	0.330	0.3644	0.0092	33.2	66	1999	23.4	47	2003	21.7	43	100	
OJ1112161r	84.70	84.00	770.00	0.997	0.0030	6.330	0.290	0.3571	0.0074	205.8	20.8	42	2023	20.1	40	1968	17.6	35	97
OJ1112163r	56.00	88.50	842.00	1.577	0.0045	6.380	0.330	0.3573	0.0065	206.9	31.0	62	2030	22.7	45	1969	20.2	40	97
OJ1112164r	166.70	201.10	577.00	1.193	0.0044	8.842	0.056	0.1007	0.0021	65.7	76.7	153	62.0	31	619	6.1	12	100	
OJ1112165r	229.80	157.50	876.00	0.676	0.0043	2.365	0.110	0.2096	0.0036	51.3	103	1232	16.6	33	1227	9.6	19	100	
OJ1112166r	247.10	93.50	164.70	0.362	0.0039	3.458	0.029	0.0586	0.0010	49.5	75.3	151	38.3	10.1	20	367	3.0	6	96
OJ1112167r	115.20	149.30	518.00	1.285	0.0050	1.198	0.083	0.1273	0.0026	87.5	75.9	152	80.0	19.2	38	772	7.4	15	97
OJ1112168r	327.10	132.90	225.70	0.403	0.0034	4.447	0.027	0.0595	0.0011	416	68.9	138	37.5	9.5	19	373	3.3	7	99
OJ1112169r	365.00	303.00	2566.00	0.839	0.0017	5.399	0.230	0.3022	0.0050	206.7	11.7	23	1885	18.2	36	1702	12.4	25	90
OJ1112170c	168.00	76.50	734.00	0.469	0.0026	6.990	0.320	0.3902	0.0092	17.8	36	2110	20.3	41	2124	21.3	43	101	
OJ1112170c	154.10	160.50	1597.00	1.025	0.0049	8.840	0.290	0.3864	0.0068	13.0	26	2104	18.5	37	2106	15.8	32	100	
OJ1112171r	142.90	210.70	574.00	1.466	0.0014	8.863	0.057	0.1031	0.0023	65.3	76.9	154	63.2	31	633	6.7	13	100	
OJ1112172r	450.00	314.40	2213.00	0.688	0.0015	3.544	0.150	0.2639	0.0044	14.6	29	1537	16.7	33	1510	11.2	22	98	
OJ1112173r	76.00	164.90	451.00	2.154	0.0059	8.853	0.075	0.0980	0.0028	66.4	102.4	205	62.6	20.5	41	603	8.2	16	96
OJ1112175r	233.60	280.70	818.00	1.091	0.0033	8.823	0.040	0.1019	0.0018	60.9	122	610	11.1	22	626	5.3	11	103	
OJ1112176r	620.00	21.70	169.20	0.033	0.0013	6.566	0.270	0.3640	0.0062	8.8	18	2055	18.1	36	2001	14.7	29	97	
OJ1112177r	49.40	60.60	156.50	1.218	0.0071	0.782	0.085	0.0944	0.0029	61.1	127.4	255	58.2	48	582	8.5	17	99	
OJ1112177r	131.50	170.00	477.00	1.288	0.0047														

ANALYSIS	U (ppm)	Th (ppm)	Pb (ppm)	Th/U	207Pb/206Pb		207Pb/206Pb		Ratios		207Pb/206Pb		Error correction		Ages (Ma)		Concordance (%)						
					2σ	σ	σ	σ	2σ	σ	2σ	σ	σ	σ	σ	σ	σ	σ	σ	σ	σ		
OUJ11z186	53.70	63.90	624.00	1.147	-6.50E+04	8.50E+04	0.1321	0.0037	7.120	0.370	0.3909	0.0097	0.6091	2126	2127	23.1	46	2127	22.5	45	100		
OUJ11z187	80.20	90.50	265.00	1.106	7.40E+04	7.40E+04	0.0689	0.0059	0.1034	0.076	0.1034	0.0026	0.6091	896	696	20.2	40	696	7.6	15	91		
OUJ11z188C	151.70	196.90	544.00	1.272	-2.70E+05	1.30E+05	0.0658	0.0046	0.984	0.059	0.0797	0.0022	0.0444	800	646	15.0	30	602	6.5	13	93		
OUJ11z188R	74.60	60.00	171.20	0.789	1.00E+04	0.0662	0.0058	0.906	0.074	0.1008	0.0025	0.1021	813	655	19.7	39	619	7.3	15	95			
OUJ11z189	269.60	176.90	2092.00	0.665	-1.90E+05	4.60E+05	0.1739	0.0022	12.500	0.520	0.5015	0.0086	0.6292	2652	10.1	20	2643	19.5	39	2620	18.5	37	99
OUJ11z190	456.00	213.00	1857.00	0.482	4.00E+05	5.80E+05	0.1221	0.0016	5.753	0.240	0.3400	0.0058	0.6101	1987	11.7	23	1939	18.0	36	1887	14.0	28	97
OUJ11z191	249.00	480.00	1265.00	1.901	-3.90E+05	2.80E+05	0.0610	0.0037	0.832	0.045	0.0984	0.0020	0.2282	639	65	130	615	25	25	605	5.9	12	98
OUJ11z192	187.50	106.00	252.00	0.575	-6.20E+04	6.00E+04	0.0630	0.0043	0.732	0.046	0.0852	0.0016	0.2060	708	72.6	145	558	13.5	27	527	4.8	10	95
OUJ11z193	90.90	32.20	162.00	0.352	3.00E+04	3.70E+04	0.0778	0.0058	1.750	0.110	0.1632	0.0030	-0.0961	1142	70.3	141	1027	20.3	41	975	8.9	18	95
OUJ11z194	139.50	75.20	667.00	0.523	-1.80E+05	2.70E+05	0.1252	0.0028	6.070	0.280	0.3471	0.0070	0.4920	2032	19.8	40	1986	20.1	40	1921	16.7	33	97
OUJ11z195	156.00	210.20	527.00	1.331	1.20E+04	5.30E+04	0.0822	0.0043	0.740	0.048	0.0870	0.0019	0.2948	681	73.8	148	562	14.0	28	538	5.6	11	96
OUJ11z196	106.70	51.90	97.40	0.495	1.00E+05	1.80E+04	0.0585	0.0053	0.485	0.042	0.0608	0.0015	0.1462	549	98.9	198	401	14.3	29	380	4.6	9	95
OUJ11z197	280.00	175.00	798.00	0.620	1.20E+05	2.40E+05	0.0742	0.0039	1.722	0.081	0.1681	0.0032	0.3589	1047	53.0	106	1017	15.1	30	1002	8.8	18	99
OUJ11z198	49.00	51.60	139.50	1.022	1.00E+05	2.10E+04	0.0649	0.0065	0.880	0.082	0.0924	0.0028	0.2727	771	105.4	211	570	12.7	25	617	5.3	11	96
OUJ11z199	309.40	343.10	965.00	1.089	9.00E+05	1.30E+05	0.0638	0.0038	0.802	0.047	0.1005	0.0018	0.2383	728	63.3	127	642	12.7	25	617	5.3	11	96
OUJ11z200	172.00	27.00	89.00	0.833	-8.00E+04	1.10E+04	0.0619	0.0075	0.802	0.099	0.0987	0.0036	0.0070	671	129.6	259	598	27.9	56	554	10.6	21	93
OUJ11z201	291.00	52.20	90.70	0.180	5.90E+04	6.70E+04	0.0571	0.0045	0.476	0.035	0.0598	0.0012	-0.0934	495	395	12.0	24	374	3.6	7	95		
OUJ11z202	82.40	101.50	304.00	1.222	4.00E+04	8.60E+04	0.0642	0.0049	0.920	0.068	0.1052	0.0026	0.3016	748	80.6	161	662	18.0	36	645	7.6	15	97
OUJ11z203	134.30	91.00	163.40	0.671	8.20E+04	5.00E+04	0.0613	0.0054	0.512	0.044	0.0614	0.0015	0.2399	650	94.6	189	420	14.8	30	384	4.6	9	92
OUJ11z204	53.10	312.00	312.00	0.573	3.00E+05	1.80E+05	0.1424	0.0040	7.410	0.370	0.3710	0.0091	0.3892	2257	24.2	48	2162	25.3	45	2034	21.4	43	94
OUJ11z205	288.00	316.20	894.00	1.068	-1.18E+05	7.40E+04	0.0605	0.0034	0.815	0.042	0.0979	0.0017	0.2796	622	60.6	121	605	11.7	23	602	5.0	10	99
OUJ11z206	57.80	166.90	899.00	0.899	6.00E+04	2.60E+04	0.0655	0.0073	0.878	0.099	0.1072	0.0034	-0.0069	790	116.9	234	693	25.4	51	656	9.9	20	95
OUJ11z208	17.00	25.70	262.00	1.517	7.40E+04	1.40E+04	0.1249	0.0090	5.890	0.520	0.3630	0.0180	0.4047	2027	63.8	128	1960	38.3	77	1996	42.6	85	102
OUJ11z209	272.00	123.60	913.00	0.457	-5.40E+05	4.60E+05	0.0955	0.0017	3.632	0.160	0.2711	0.0047	0.2944	1538	16.7	33	1557	17.5	35	1546	11.9	24	99
OUJ11z210	45.70	39.70	338.00	0.850	4.40E+04	3.90E+04	0.1107	0.0047	4.840	0.270	0.3184	0.0085	0.3089	1811	38.6	77	1792	23.5	47	1782	20.8	42	99
OUJ11z211	92.50	108.80	271.00	1.122	1.00E+04	5.60E+04	0.0624	0.0058	0.855	0.078	0.0977	0.0043	0.0772	688	99.2	198	626	21.4	43	601	12.6	25	96
OUJ11z212	65.30	78.30	230.60	1.193	-3.00E+04	2.10E+04	0.0668	0.0062	0.926	0.082	0.0999	0.0030	0.2319	832	96.7	193	666	21.6	43	614	8.8	18	92
OUJ11z214	75.60	122.30	1082.00	1.590	4.50E+05	3.20E+05	0.1273	0.0035	6.010	0.300	0.3426	0.0069	0.3559	2061	24.2	48	1977	21.7	43	1899	16.6	33	96
OUJ11z215	68.10	46.90	158.00	0.673	2.60E+04	3.20E+04	0.0692	0.0059	1.197	0.100	0.1260	0.0035	0.1974	905	87.9	176	799	23.1	46	765	10.0	20	96
OUJ11z216	434.00	286.00	459.00	0.637	3.20E+04	9.50E+04	0.0555	0.0037	0.442	0.026	0.0373	0.0012	-0.1125	432	43.2	149	372	9.1	18	361	3.7	7	97
OUJ11z218	83.00	97.70	985.00	1.148	7.20E+05	5.40E+05	0.1271	0.0031	6.620	0.320	0.3753	0.0061	0.3205	2058	21.5	43	2082	21.3	43	2045	19.0	38	99
OUJ11z219	121.30	64.90	231.00	0.454	-1.60E+04	2.50E+04	0.0865	0.0092	1.230	0.140	0.1017	0.0026	0.1903	1349	102.6	205	814	31.8	64	624	7.6	15	77
OUJ11z222	120.40	83.30	481.00	0.684	-3.20E+05	2.20E+05	0.0817	0.0047	2.423	0.120	0.2132	0.0042	0.0212	1238	56.4	113	1249	17.8	36	1246	11.2	29	100
OUJ11z223	336.00	450.00	4140.00	1.314	1.20E+05	2.50E+05	0.1297	0.0018	6.426	0.270	0.3536	0.0060	0.4218	2094	12.2	24	2036	18.4	37	1952	14.3	29	96
OUJ11z224	422.60	134.50	261.00	0.318	1.30E+04	5.50E+04	0.0575	0.0035	0.481	0.027	0.0604	0.0011	0.2662	511	66.9	134	399	9.2	18	378	3.3	7	95
OUJ11z225	232.80	136.00	327.00	0.543	6.20E+04	3.90E+04	0.0587	0.0041	0.663	0.046	0.0804	0.0017	0.3151	556	76.2	152	516	14.0	28	499	5.1	10	97
OUJ11z226	56.50	48.90	239.00	0.851	3.90E+04	2.40E+04	0.0816	0.0058	1.876	0.120	0.1656	0.0043	0.2046	1236	69.7	139	1073	21.2	42	988	11.9	24	92
OUJ11z227	195.50	264.20	786.00	1.344	3.40E+04	9.20E+04	0.0645	0.0040	0.936	0.052	0.1053	0.0020	-0.2173	758	65.4	131	671	13.6	27	645	5.8	12	96
OUJ11z228	119.90	70.70	419.00	0.589	1.00E+06	1.00E+05	0.0821	0.0046	2.346	0.110	0.2065	0.0040	0.1919	1248	54.8	110	1226	16.7	33	1210	10.7	21	99
OUJ11z229	161.80	137.00	352.00	0.846	2.00E+04	4.60E+04	0.0618	0.0045	0.738	0.051	0.0868	0.0021	0.2876	667	77.9	156	561	14.9	30	537	6.2	12	96
OUJ11z230	61.60	52.30	440.00	0.841	8.40E+04	6.90E+04	0.1100	0.0032	4.760	0.240	0.3133	0.0070	0.3814	1799	26.5	53	1778	21.1	42	1757	17.2	34	99
OUJ11z231	198.50	54.20	536.00	0.262	-6.00E+05	2.20E+05	0.1280	0.0024	6.870	0.300	0.3812	0.0068	0.3561	2071	16.5	33	2095	19.3	39	2082	15.9	32	99
OUJ11z232	137.60	158.50	1549.00	1.147	-6.00E+03	1.10E+05	0.1328	0.0027	6.940	0.310	0.3764	0.0070	0.4350	2135	17.8	36	2104	19.8	40	2059	16.4	33	98
OUJ11z233	182.00	307.00	873.00	1.678	-7.00E+05	3.30E+05	0.0629	0.0038	0.876	0.046	0.1014	0.0020	0.2055	705	64.3	129	639	12.4	25	623	5.9	12	97
OUJ11z234	163.10	134.30	364.00	0.816	-1.70E+04	3.10E+04	0.0620	0.0041	0.822	0.050	0.0959	0.0021	0.2389	674	70.7	141	609	13.9	28	590	6.2	12	97
OUJ11z235	255.10	115.50	377.00	0.451	5.00E+06	2.40E+06	0.0632	0.0035	0.997	0.051	0.1157	0.0023	0.3179	715	58.8	118	702	13.0	26	706	6.6	13	100
OUJ11z236	87.00	68.90	129.80	0.779	-1.40E+04	1.30E+04	0.0489	0.0057	0.420	0.049	0.0610	0.0015	0.2115	143	196.8	274	356	17.5	35	382	4.6	9	107
OUJ11z237	193.80	20.43	143.10	0.104	1.20E+04	8.70E+04	0.0886	0.0047	2.791	0.130	0.2272	0.0042	0.2024	1396	50.9	102	1353	17.4	35	1320	11.0	22	98
OUJ11z238	131.50	158.00	473.00	1.211	2.50E+05	2.10E+05	0.0651	0.0050	0.931	0.066	0.1037	0.0024	0.0389	778	80.8	162	668	17.3	35	636	7.0	14	95
OUJ11z239	145.10	155.00	1723.00	1.064	-4.00E+05	1.10E+05	0.1500	0.0024	8.590	0.360	0.4114	0.0077	0.4886	2346	13.7	27	2295	19.0	38	2221	17.6	35	9

ANALYSIS	U (ppm)	Th (ppm)	Pb (ppm)	Th/U	Ratios					Error correction	Ages (Ma)				Concordance (%)								
					$^{206}\text{Pb}/^{238}\text{U}$	$^{207}\text{Pb}/^{235}\text{U}$	$^{207}\text{Pb}/^{206}\text{Pb}$	$^{206}\text{Pb}/^{238}\text{U}$	$^{207}\text{Pb}/^{235}\text{U}$		$^{207}\text{Pb}/^{238}\text{U}$	σ	2σ	σ		2σ	$^{206}\text{Pb}/^{238}\text{U}$	σ	2σ				
Discordant data																							
OUJ11283	27.60	43.90	226.00	1.592	1.56E+05	9.40E+04	0.0771	0.0065	1.890	0.150	0.1765	0.0051	0.0727	1124	84.0	168	1078	26.3	53	1048	14.0	28	97
OUJ11284	242.10	84.20	861.00	0.353	-7.10E+05	3.80E+05	0.1301	0.0020	6.900	0.3784	0.0070	0.0065	0.0727	2099	13.5	27	2099	19.3	39	2069	16.4	33	99
OUJ11285	70.40	150.20	1313.00	2.129	-8.90E+04	4.90E+04	0.1152	0.0033	5.140	0.250	0.3223	0.0065	0.1391	1883	25.8	52	1843	20.7	41	1801	15.8	32	98
OUJ11286	274.60	186.30	334.00	0.689	4.50E+04	4.60E+04	0.0552	0.0038	0.470	0.029	0.0605	0.0012	-0.0150	420	76.8	154	391	10.0	20	379	3.6	7	97
OUJ11287	48.20	63.20	401.00	1.330	-1.70E+05	1.20E+05	0.1235	0.0041	5.690	0.290	0.3267	0.0076	0.3744	2007	29.5	59	1930	23.0	44	1822	18.5	37	94
OUJ11288	342.00	9.86	111.00	0.028	1.60E+05	3.90E+05	0.1268	0.0018	6.320	0.270	0.3558	0.0061	0.5364	2054	12.5	25	2021	18.7	37	1962	14.5	29	97
OUJ11289	910.00	177.90	32.20	0.193	-5.50E+06	3.00E+06	0.0667	0.0028	0.494	0.017	0.0541	0.0016	-0.3545	813	47.0	94	409	6.0	12	340	5.0	10	83
OUJ11290	643.00	171.00	32.60	0.240	-1.70E+06	1.40E+06	0.0680	0.0025	0.542	0.030	0.0597	0.0020	0.4295	870	41.5	83	439	6.5	13	374	6.0	12	85
OUJ11291	1240.00	776.00	195.00	0.623	-6.39E+05	5.40E+04	0.1213	0.0028	0.978	0.020	0.0584	0.0020	0.7183	1970	18.5	37	691	7.5	15	366	6.0	12	53
OUJ11292	487.00	273.00	85.70	0.542	-4.00E+06	1.20E+06	0.1162	0.0035	1.965	0.096	0.1218	0.0074	0.8560	1887	27.5	55	1108	15.0	31	741	11.5	23	67
OUJ11293	131.00	101.00	24.80	0.894	-2.70E+05	3.50E+05	0.0750	0.0140	0.790	0.100	0.7078	0.0074	0.1589	1150	160.0	320	602	30.0	60	439	22.5	45	73
OUJ11294	352.00	111.70	24.90	0.313	-2.20E+06	1.70E+06	0.0643	0.0030	0.896	0.030	0.0669	0.0023	0.2615	750	50.0	100	476	9.5	19	417	7.0	14	88
OUJ11295	73.60	37.10	11.39	0.506	1.20E+05	1.30E+05	0.0695	0.0048	0.967	0.058	0.1017	0.0095	-0.0427	880	75.0	150	703	17.0	34	624	10.0	20	89
OUJ11296	138.00	70.10	19.24	1.364	-4.00E+05	1.20E+05	0.0532	0.0060	0.732	0.078	0.1022	0.0045	0.0119	260	105.0	210	563	22.5	45	627	13.0	26	111
OUJ11297	546.00	35.40	0.396	0.396	9.00E+06	1.10E+06	0.0804	0.0022	2.798	0.086	0.2466	0.0074	0.3164	1205	26.0	52	1352	11.5	23	1421	19.0	38	105
OUJ11298	250.00	215.00	44.30	0.863	-1.20E+05	1.70E+05	0.0893	0.0025	0.519	0.019	0.0526	0.0017	0.1744	923	38.0	76	424	6.5	13	331	5.0	10	78
OUJ11299	656.00	81.50	49.30	0.120	-5.00E+06	1.40E+06	0.1138	0.0077	2.780	0.160	0.1750	0.0110	0.9466	1856	14.0	28	1352	21.0	42	1035	31.5	63	77
OUJ11300	924.00	302.00	77.20	0.326	-7.00E+05	4.70E+05	0.0815	0.0018	0.896	0.018	0.0600	0.0021	0.5534	1254	21.5	43	535	5.5	11	375	6.5	13	70
OUJ11301	591.00	113.40	0.589	0.637	-7.30E+05	2.40E+05	0.0794	0.0031	0.564	0.017	0.0514	0.0017	-0.1059	1160	39.0	78	457	6.0	12	323	5.0	10	71
OUJ11302	820.00	530.00	86.90	0.637	-2.70E+05	4.90E+05	0.0640	0.0026	0.507	0.019	0.0571	0.0018	0.0810	743	43.0	86	418	7.0	14	358	5.5	11	86
OUJ11303	1149.00	199.00	55.30	0.169	-7.70E+05	2.00E+05	0.0725	0.0016	0.574	0.015	0.0570	0.0018	0.4369	1010	23.5	47	460	4.9	10	357	5.5	11	78
OUJ11304	1517.00	948.00	585.00	0.622	-2.53E+06	5.30E+05	0.1321	0.0012	4.210	0.220	0.2310	0.0150	0.9797	2127	8.5	17	1665	25.5	45	1336	38.5	77	80
OUJ11305	753.00	160.70	406.00	0.215	-6.00E+05	1.60E+05	0.0835	0.0035	0.512	0.025	0.0587	0.0011	0.2191	725	58.4	117	420	8.4	17	368	3.3	7	88
OUJ11306	105.00	95.80	105.70	0.531	5.00E+04	1.80E+04	0.0627	0.0060	0.548	0.047	0.0632	0.0018	-0.1061	698	101.9	204	444	15.4	31	395	5.5	11	89
OUJ11307	60.90	54.70	102.80	0.901	2.10E+04	3.00E+04	0.0770	0.0120	0.619	0.089	0.0633	0.0026	0.0436	1121	155.4	311	489	27.9	56	396	7.9	16	81
OUJ11308	137.20	180.00	311.00	1.314	2.50E+04	2.80E+04	0.0636	0.0086	0.516	0.067	0.0596	0.0015	-0.0223	728	143.3	287	422	22.4	45	373	4.6	9	88
OUJ11309	100.10	55.00	333.00	0.550	-5.50E+04	4.30E+04	0.0887	0.0059	2.120	0.150	0.1734	0.0048	0.7635	1398	63.8	128	1155	24.4	49	1031	13.2	26	89
OUJ11310	170.90	120.50	214.40	0.697	-2.40E+04	2.30E+04	0.0655	0.0061	0.550	0.045	0.0605	0.0018	-0.1562	790	97.7	195	445	14.7	29	379	5.5	11	85
OUJ11311	91.20	56.70	167.00	0.602	-4.60E+04	4.20E+04	0.0718	0.0061	0.987	0.073	0.0991	0.0025	-0.1207	980	86.5	173	697	18.6	37	609	7.3	15	87
OUJ11312	50.90	22.39	49.40	0.426	4.00E+04	1.30E+04	0.0810	0.0110	0.709	0.090	0.0635	0.0026	-0.0249	1221	133.4	267	544	26.7	53	397	7.9	16	73
OUJ11313	42.50	37.20	128.30	0.864	-1.80E+04	1.80E+04	0.0845	0.0097	1.280	0.140	0.1063	0.0043	-0.0718	1304	111.5	223	837	31.1	62	651	12.5	25	78
OUJ11314	77.40	26.80	87.20	0.340	9.90E+04	3.20E+04	0.0709	0.0075	0.985	0.100	0.1005	0.0031	0.0763	955	108.2	216	696	25.6	51	617	9.1	18	89
OUJ11315	15.93	19.30	71.70	1.188	-1.80E+04	1.60E+04	0.1070	0.0200	1.680	0.290	0.1192	0.0089	-0.0394	1749	171.1	342	1001	54.9	110	726	25.6	51	73
OUJ11316	81.00	56.70	97.70	0.694	-1.40E+04	1.10E+04	0.0612	0.0058	0.600	0.048	0.0583	0.0015	0.2034	646	101.8	204	412	16.2	32	365	4.6	9	89
OUJ11317	208.00	181.00	288.00	0.870	1.00E+04	3.40E+04	0.0645	0.0061	0.511	0.046	0.0578	0.0014	0.2439	758	99.7	199	419	15.4	31	362	4.3	9	86
OUJ11318	612.00	363.00	523.00	0.575	-9.98E+04	5.40E+04	0.0726	0.0043	0.468	0.026	0.0471	0.0014	0.3614	1003	60.1	120	390	9.0	18	297	4.3	9	76
OUJ11319	22.05	40.90	117.00	1.883	-2.90E+03	5.60E+03	0.0640	0.0150	1.110	0.200	0.0964	0.0045	-0.1028	1293	173.7	347	758	48.1	96	593	13.2	26	78
OUJ11320	377.00	162.00	319.00	0.450	7.10E+04	7.70E+04	0.0701	0.0050	0.505	0.032	0.0652	0.0014	-0.1440	931	73.2	146	415	10.8	22	328	4.3	9	79
OUJ11321	334.00	158.10	1713.00	0.478	6.10E+06	3.80E+06	0.2090	0.0026	10.960	0.470	0.3777	0.0075	0.7706	2898	10.1	20	2520	19.9	40	2066	17.5	35	82

Footnotes: . . . Analysis references: OUJ11z is zircon from sample OUJ11 (mounts CT17-9 and CT18-5), followed by grain number "c" or "r", meaning core or rim, respectively.

ANALYSIS	U (ppm)	Th (ppm)	Pb (ppm)	Th/U	Ratios					Ages (Ma)					Concordance (%)								
					$^{207}\text{Pb}/^{206}\text{Pb}$	$^{207}\text{Pb}/^{238}\text{U}$	$^{207}\text{Pb}/^{235}\text{U}$	$^{206}\text{Pb}/^{238}\text{U}$	2σ	Error correction	$^{207}\text{Pb}/^{238}\text{U}$	σ	2σ	$^{206}\text{Pb}/^{238}\text{U}$		σ	2σ						
OUJ13z59	878.00	300.00	34.90	0.342	-1.50E+06	0.0599	0.0012	0.399	0.012	0.0499	0.0015	0.7397	601	21.7	43	341	9	4.4	9	314	4.6	9	92
OUJ13z60	205.30	603.00	225.20	0.990	7.20E+06	0.1379	0.0019	7.980	0.130	4.138	0.0043	0.2986	2201	12.0	24	2217	14	6.9	14	2232	9.8	20	101
OUJ13z61	70.50	263.00	62.10	0.894	7.20E+06	4.40E+06	0.1258	6.820	0.130	0.3809	0.0043	0.0565	2040	17.6	35	2062	8.7	17	2080	10.0	20	101	
OUJ13z62	80.60	37.47	24.33	0.485	9.30E+05	6.90E+05	0.0876	2.779	0.063	0.2325	0.0027	0.1732	1374	20.9	42	1350	17	8.5	17	1348	7.1	14	100
OUJ13z63	291.60	149.00	108.00	0.497	-2.30E+06	1.80E+06	0.0956	3.646	0.058	0.2763	0.0028	0.3902	1374	15.8	28	1560	13	6.3	13	1573	7.1	14	101
OUJ13z64	575.00	367.00	219.30	0.638	1.00E+07	1.40E+06	0.0814	3.322	0.038	0.2089	0.0022	0.3684	1231	13.7	31	1219	5.8	10	1223	5.9	12	100	
OUJ13z65	484.00	293.60	51.00	0.619	4.20E+05	3.70E+05	0.0547	0.452	0.012	0.0602	0.0006	-0.0774	400	30.7	61	379	4.2	8	377	1.9	4	100	
OUJ13z66	195.70	34.89	5.78	0.178	6.00E+04	6.30E+04	0.0564	0.452	0.015	0.0595	0.0008	0.0673	468	39.3	79	378	5.2	10	373	2.5	5	99	
OUJ13z68	277.50	112.50	31.38	0.405	3.50E+05	2.30E+05	0.0606	0.813	0.021	0.0984	0.0011	0.1266	625	26.7	53	604	5.9	12	605	3.2	6	100	
OUJ13z69	571.00	121.10	20.71	0.212	1.07E+06	4.60E+05	0.0549	0.459	0.011	0.0609	0.0007	0.1516	625	26.7	53	604	5.9	12	605	3.2	6	100	
OUJ13z70	247.50	132.60	22.52	0.536	-1.20E+05	1.10E+05	0.0556	0.465	0.015	0.0610	0.0008	0.0896	436	36.0	72	382	3.8	8	381	2.0	4	99	
OUJ13z71	528.40	133.40	82.39	0.252	-8.00E+03	2.70E+05	0.1125	4.118	0.063	0.2661	0.0027	0.4380	1840	12.1	24	1658	6.2	12	1521	6.9	14	92	
OUJ13z72	237.40	142.40	58.44	0.600	-9.00E+05	1.30E+05	0.0717	1.519	0.031	0.1551	0.0017	0.1882	977	19.9	40	938	6.2	12	929	4.7	9	99	
OUJ13z73	632.00	284.10	68.60	0.450	1.40E+05	1.50E+05	0.0594	0.663	0.015	0.0824	0.0012	0.3024	582	23.8	48	516	4.6	9	510	3.6	7	99	
OUJ13z74	925.70	387.00	55.60	0.418	-1.10E+06	1.40E+06	0.0558	0.011	0.338	0.019	0.0577	0.0007	0.3231	442	21.9	44	369	3.4	7	361	2.0	4	98
OUJ13z75	275.90	215.60	60.88	0.785	1.31E+05	8.50E+04	0.0621	0.918	0.023	0.1083	0.0012	0.0165	678	27.5	55	661	6.1	12	663	3.5	7	100	
OUJ13z76	116.00	161.70	43.80	1.394	-3.20E+04	3.20E+04	0.0663	0.927	0.034	0.1019	0.0013	0.1596	816	37.8	76	666	8.9	18	626	3.8	8	94	
OUJ13z77	38.22	69.70	61.70	1.824	1.40E+04	3.20E+04	0.1220	6.240	0.160	0.3703	0.0050	0.1459	1986	24.1	48	2010	11.2	22	2031	11.8	24	101	
OUJ13z78	178.10	159.60	27.03	0.952	8.00E+04	2.90E+04	0.0565	0.467	0.019	0.0605	0.0008	-0.0335	472	43.1	86	389	6.6	13	379	2.3	5	97	
OUJ13z79	434.50	140.80	23.18	0.324	4.00E+04	5.90E+04	0.0541	0.444	0.011	0.0603	0.0006	0.0951	375	29.1	58	373	3.9	8	377	1.9	4	101	
OUJ13z80	171.90	158.40	133.40	0.921	4.10E+05	2.50E+05	0.1181	0.020	0.5603	0.100	0.3449	0.2608	1928	15.2	30	1917	7.7	15	1910	8.6	17	100	
OUJ13z81	1007.00	142.00	23.96	0.141	-8.90E+04	9.40E+04	0.0554	0.011	0.450	0.010	0.0596	0.0006	0.3061	428	22.1	44	373	3.4	7	373	1.9	4	99
OUJ13z82	170.50	44.10	6.97	0.259	2.30E+04	2.30E+04	0.0542	0.447	0.018	0.0599	0.0008	0.0817	379	45.6	91	375	6.3	13	375	2.3	5	100	
OUJ13z83	276.00	89.80	13.87	0.325	2.50E+04	3.20E+04	0.0547	0.461	0.016	0.0614	0.0008	0.2496	400	38.9	78	385	5.6	11	384	2.3	5	100	
OUJ13z84	128.90	71.80	10.89	0.557	2.00E+04	1.00E+04	0.0542	0.444	0.020	0.0602	0.0010	0.1122	379	51.9	104	373	7.0	14	377	2.6	5	101	
OUJ13z85	202.90	125.60	15.48	0.619	-1.50E+04	1.90E+04	0.0542	0.466	0.017	0.0623	0.0008	0.1257	379	43.6	87	388	5.9	12	389	2.4	5	100	
OUJ13z86	1049.00	213.00	25.90	0.203	-3.20E+05	2.00E+05	0.0575	0.013	0.379	0.024	0.0502	0.0011	0.6479	511	24.8	50	326	4.4	9	316	4.9	10	97
OUJ13z87	166.50	243.60	57.70	1.463	3.80E+04	2.50E+04	0.0603	0.758	0.012	0.0932	0.0011	0.1363	614	34.0	68	573	6.9	14	574	3.2	6	100	
OUJ13z88	28.62	16.93	6.70	0.592	1.47E+04	7.50E+03	0.0887	1.432	0.074	0.1495	0.0025	0.1091	890	54.1	108	902	15.4	31	888	7.0	14	100	
OUJ13z89	91.40	99.90	33.30	1.093	1.00E+04	1.90E+04	0.0660	0.025	1.213	0.045	0.1339	0.0018	-0.0146	806	39.6	79	807	10.3	21	810	5.1	10	100
OUJ13z90	55.10	62.50	15.48	1.134	8.40E+03	9.20E+03	0.0573	0.797	0.042	0.3796	0.0038	0.2294	2087	12.9	26	2077	7.2	14	2074	8.9	18	100	
OUJ13z91	427.00	879.00	45.50	0.385	2.00E+05	1.20E+05	0.0613	0.014	0.870	0.017	0.1041	0.0010	0.1144	650	21.0	42	636	4.6	9	638	2.9	6	100
OUJ13z92	152.20	81.12	64.06	0.533	4.70E+04	7.30E+04	0.1101	4.996	0.087	0.3281	0.0034	0.0833	432	32.1	64	384	4.5	9	379	2.0	4	99	
OUJ13z93	72.20	31.50	5.54	0.436	-7.00E+03	8.50E+03	0.0516	0.032	0.926	0.0615	0.0009	-0.0448	268	71.1	142	370	9.2	18	385	2.8	6	104	
OUJ13z94	194.60	128.20	120.80	0.659	-7.00E+05	1.10E+05	0.1292	0.019	6.734	0.110	0.3796	0.0038	0.2294	2087	12.9	26	2077	7.2	14	2074	8.9	18	100
OUJ13z95	432.90	84.11	9.00	0.257	2.40E+04	1.80E+04	0.0542	0.447	0.017	0.0604	0.0007	-0.0726	379	43.6	87	375	6.0	12	378	2.2	4	101	
OUJ13z96	498.00	264.40	149.60	0.611	-5.00E+06	1.90E+06	0.0821	0.014	2.416	0.041	0.2150	0.0022	0.1455	1248	16.7	33	1247	6.1	12	1255	5.8	12	101
OUJ13z97	334.50	114.80	101.20	0.343	3.90E+05	2.60E+05	0.1242	0.018	5.758	0.088	0.3379	0.0037	0.2906	2017	12.8	26	1940	6.6	13	1877	8.9	18	97
OUJ13z98	215.20	66.67	30.19	0.310	-2.00E+06	1.50E+06	0.0741	0.016	1.676	0.038	0.1660	0.0018	0.1922	1044	21.8	44	999	7.2	14	990	5.0	10	99
OUJ13z99	504.00	288.00	45.50	0.571	-5.90E+04	6.00E+04	0.0573	0.445	0.011	0.0569	0.0009	0.3334	503	26.9	54	373	3.9	8	357	2.6	5	95	
OUJ13z100	326.50	121.20	95.60	0.371	-1.00E+05	9.20E+04	0.1207	0.017	5.010	0.083	0.2999	0.0035	0.5771	1967	12.6	25	1821	7.0	14	1691	8.7	17	93
OUJ13z101	179.80	129.90	120.80	0.722	4.00E+05	2.40E+05	0.1215	0.088	6.088	0.100	0.3634	0.0038	0.2047	1978	13.9	28	1989	7.2	14	1988	9.0	18	100
OUJ13z102	144.90	114.70	97.30	0.792	8.50E+04	7.30E+04	0.1100	0.019	4.957	0.088	0.3263	0.0034	0.1855	1799	15.7	31	1812	7.5	15	1820	8.3	17	100
OUJ13z103	133.70	135.10	146.80	1.010	1.50E+05	1.90E+05	0.1400	0.020	8.073	0.130	0.4197	0.0043	0.1828	2227	12.4	25	2239	7.3	15	2259	9.8	20	101
OUJ13z104	161.80	112.40	34.70	0.695	-3.50E+05	2.60E+05	0.0616	0.898	0.027	0.1067	0.0013	0.0045	660	31.3	63	651	7.2	14	653	3.8	8	100	
OUJ13z105	142.10	99.40	101.10	0.700	-1.90E+05	1.30E+05	0.1290	0.020	6.785	0.110	0.3819	0.0040	0.2983	2084	13.6	27	2084	7.2	14	2085	9.3	19	100
OUJ13z106	57.84	54.30	15.69	0.939	1.60E+04	1.40E+04	0.0613	0.026	0.865	0.035	0.1021	0.0015	-0.2526	650	45.5	91	633	9.5	19	627	4.4	9	99
OUJ13z107	534.70	187.90	34.35	0.351	2.70E+05	1.20E+05	0.0549	0.456	0.010	0.0607	0.0007	0.1366	400	24.5	49	381	3.5	7	380	2.0	4	100	
OUJ13z108	634.00	34.80	33.30	0.150	-2.00E+05	1.20E+05	0.1295	0.019	5.918	0.093	0.3329	0.0036	0.2857	2091	12.9	26	1984	6.8	14	1852	8.7	17	94
OUJ13z109	684.00	160.70	84.45	-4.00E+03	1.10E+05	0.0583	0.011	0.730	0.013	0.0921	0.0009	0.1182	541	20.6	41	557	3.8	8	588	2.7	5	102	
OUJ13z110	97.80	83.30	17.00	0.852	-1.90E+04	1.80E+04	0.0776	0.048	0.670	0.044	0.0635	0.0010	0.3177	1137	61.5	123	521	13.4	27	397	2.9	6	76
OUJ13z111	91.00	34.00	6.92	0.374	1.60E+04	1.20E+04	0.0545	0.026	0.454	0.022	0.0610	0.0008	0.1290	392	53.5	107	380	7.7	15	381	2.6	5	

ANALYSIS	U (ppm)	Th (ppm)	Pb (ppm)	Th/U	Ratios				Ages (Ma)				Concordance (%)										
					$^{207}\text{Pb}/^{206}\text{Pb}$	$^{207}\text{Pb}/^{238}\text{U}$	$^{206}\text{Pb}/^{238}\text{U}$	Error correction	$^{207}\text{Pb}/^{238}\text{U}$	σ	$^{207}\text{Pb}/^{238}\text{U}$	σ		$^{206}\text{Pb}/^{238}\text{U}$	σ								
OUI13z124	66.10	28.83	34.20	0.436	1.00E+07	1.341	0.0025	7.110	0.140	0.3881	0.0042	0.1006	2152	16.3	33	2125	8.8	18	2105	9.8	20	99	
OUI13z125	273.60	182.40	172.70	0.667	1.47E+07	7.30E+06	0.1064	4.490	0.074	0.3072	0.0032	0.3580	1739	13.8	28	1727	6.8	14	1727	7.9	16	100	
OUI13z126	257.30	92.30	51.00	0.359	1.60E+05	0.0732	0.0014	1.761	0.034	0.1770	0.0018	0.1177	1019	19.4	39	1031	6.2	12	1050	4.9	10	102	
OUI13z127	219.30	94.10	18.44	0.429	6.00E+04	4.60E+04	0.0553	0.0018	0.462	0.0612	0.0007	-0.0628	424	36.3	73	386	5.2	10	383	2.2	4	99	
OUI13z128	56.78	46.73	13.84	0.823	3.80E+04	3.00E+04	0.0561	0.0025	0.712	0.0942	0.0013	0.0046	456	49.4	99	546	8.9	18	580	3.8	8	106	
OUI13z129c	38.17	12.10	8.08	0.317	1.02E+05	4.90E+04	0.0835	0.0026	2.390	0.074	0.2093	0.0752	1281	30.3	61	1240	11.1	22	1225	7.5	15	99	
OUI13z129r	117.90	36.71	23.55	0.311	-4.40E+04	6.40E+04	0.0812	2.353	0.053	0.2113	0.0024	0.1664	1226	21.8	44	1228	8.0	16	1236	6.4	13	101	
OUI13z130	339.40	95.50	19.05	0.281	8.30E+05	3.80E+05	0.0542	0.0016	0.443	0.013	0.0603	0.0007	0.2033	379	33.2	66	372	4.6	9	378	2.1	4	101
OUI13z131	82.99	55.42	18.47	0.688	-2.00E+04	3.40E+04	0.0604	0.0024	0.866	0.034	0.1040	0.0014	-0.0069	618	42.9	86	633	9.2	18	638	4.1	8	101
OUI13z132	182.40	82.30	94.80	0.451	2.60E+05	3.20E+05	0.1342	0.0019	7.511	0.120	0.4063	0.0041	0.1819	2154	12.4	25	2174	7.2	14	2198	9.4	19	101
OUI13z133	459.00	128.30	26.70	0.280	8.10E+05	3.10E+05	0.0549	0.0014	0.452	0.011	0.0602	0.0007	-0.1042	408	28.5	57	378	3.8	8	377	2.0	4	100
OUI13z134	311.10	60.65	22.80	0.195	1.45E+06	4.70E+05	0.0652	0.0013	1.103	0.237	0.0013	0.2920	781	21.0	42	755	5.5	11	752	3.7	7	100	
OUI13z135	209.00	132.30	24.50	0.633	2.00E+06	3.60E+06	0.0556	0.0019	0.463	0.016	0.0612	0.0008	0.2006	436	38.0	76	386	5.5	11	383	2.3	5	99
OUI13z136	188.17	81.10	26.16	0.431	2.20E+06	1.00E+06	0.0615	0.0017	0.871	0.023	0.1047	0.0012	-0.0972	657	29.6	59	636	6.2	12	642	3.5	7	101
OUI13z137	175.80	30.80	12.06	0.175	1.60E+05	1.40E+05	0.0663	0.0017	1.189	0.031	0.1308	0.0015	0.0808	816	26.8	54	795	7.2	14	793	4.3	9	100
OUI13z138	92.10	52.91	16.43	0.574	8.30E+04	8.90E+04	0.0591	0.0023	0.856	0.034	0.1040	0.0014	0.0644	571	42.3	85	628	9.3	19	638	4.1	8	102
OUI13z139	153.60	193.00	57.60	1.257	1.10E+05	1.20E+05	0.0607	0.0020	0.831	0.027	0.0984	0.0012	0.1641	629	35.5	71	614	7.5	15	611	3.5	7	99
OUI13z140	52.00	54.71	10.95	0.099	4.60E+05	3.30E+05	0.0532	0.0014	0.461	0.012	0.0630	0.0007	0.1038	337	29.8	60	385	4.2	8	384	2.1	4	102
OUI13z142	152.70	260.00	84.80	1.703	4.00E+05	3.60E+05	0.0627	0.0017	0.962	0.024	0.1117	0.0013	0.1533	698	28.9	58	684	6.2	12	682	3.8	8	100
OUI13z143	456.00	199.00	35.20	0.436	-9.00E+06	2.10E+06	0.0563	0.0016	0.468	0.014	0.0612	0.0007	0.1271	464	31.5	63	390	4.8	10	383	2.1	4	98
OUI13z144	1198.00	60.80	10.63	0.051	-4.00E+07	2.20E+07	0.0544	0.0010	0.441	0.008	0.0594	0.0006	0.0000	386	20.7	41	371	3.0	6	372	1.8	4	100
OUI13z145	412.20	452.70	123.20	1.098	3.00E+06	4.00E+06	0.0614	0.0014	0.838	0.018	0.0953	0.0011	0.0757	653	24.5	49	618	5.0	10	610	3.2	6	99
OUI13z146	259.60	123.80	21.82	0.500	-8.00E+05	4.90E+05	0.0550	0.0017	0.457	0.014	0.0603	0.0007	0.1019	412	34.6	69	382	4.9	10	378	2.1	4	99
OUI13z147	190.80	267.00	96.70	1.399	9.90E+05	6.10E+05	0.0654	0.0017	1.209	0.032	0.1341	0.0015	0.1177	787	27.3	55	805	7.3	15	811	4.3	9	101
OUI13z148	656.80	196.20	242.10	0.299	-1.03E+07	5.30E+06	0.1889	0.0023	12.996	0.190	0.4996	0.0049	0.4467	2732	10.0	20	2679	6.9	14	2612	10.5	21	97
Discordant data																							
OUI13z38	69.20	45.80	9.77	0.662	-2.40E+04	1.40E+04	0.0729	0.0051	0.614	0.046	0.0616	0.0010	0.2779	1011	70.9	142	466	14.5	29	385	3.0	6	79
OUI13z67	81.50	167.00	44.60	2.049	1.12E+05	7.30E+04	0.0702	0.0032	0.886	0.041	0.0915	0.0013	0.0662	934	46.8	94	644	11.0	22	584	3.8	8	88
OUI13z122	388.00	173.20	111.40	0.446	1.46E+06	6.50E+05	0.1157	0.0018	3.716	0.069	0.2346	0.0032	0.6840	1891	14.0	28	1575	7.4	15	1359	8.4	17	86
OUI13z141	2659.00	227.70	52.90	0.086	5.60E+06	2.00E+06	0.0797	0.0014	0.270	0.006	0.0245	0.0005	0.7601	1190	17.3	35	243	2.5	5	156	1.5	3	64

Footnotes:
 . Analysis references: OUI13z is zircon from sample OUI13 (mount CT1 8-8), followed by grain number "c" or "r", meaning core or rim, respectively.

Chapter IV

Table D.35: Sample BES1 (L.A-ICPMS)

IGSN: IEACCC0009 Coordinate UTM: Zone 29S, 3720500 m N, 674467 m E

ANALYSIS	U (ppm)	Th (ppm)	Pb (ppm)	Th/U	Ratios			Concordance			Error correction			Ages (Ma)			Concordance (%)						
					$^{207}\text{Pb}/^{235}\text{U}$	2σ	$^{207}\text{Pb}/^{206}\text{Pb}$	2σ	$^{206}\text{Pb}/^{238}\text{U}$	2σ	Error correction	$^{207}\text{Pb}/^{235}\text{U}$	σ	2σ	$^{207}\text{Pb}/^{235}\text{U}$	σ		2σ					
																			2σ	2σ	2σ	σ	2σ
BES121	411.90	59.50	306.00	0.147	-1.46E+07	8.90E+06	0.0742	0.0015	1.754	0.040	0.1754	0.0022	0.0166	20.4	40.8	1028.6	7.4	14.7	1024.8	4.4	8.8	100	
BES123	180.40	111.80	592.00	0.575	9.00E+06	5.50E+05	0.0720	0.0020	1.711	0.048	1.735	0.0022	0.0168	28.3	56.5	1012.7	9.0	18.0	1031.4	6.0	12.1	102	
BES124	103.00	92.10	287.00	0.953	-8.90E+05	8.30E+05	0.0620	0.0034	0.832	0.042	0.0982	0.0020	0.1468	55.2	110.4	614.7	11.6	23.3	603.9	5.9	11.7	98	
BES125	88.30	50.30	341.50	0.587	-9.00E+06	1.40E+06	0.0864	0.0034	2.650	0.110	0.2240	0.0033	0.2067	38.0	76.0	1314.6	15.3	30.6	1303.0	8.7	17.4	99	
BES126	115.10	72.10	762.00	0.841	-8.00E+06	3.50E+06	0.1295	0.0029	6.160	0.140	0.3437	0.0042	0.2883	39.4	78.8	1998.8	9.9	19.8	1904.4	10.1	20.1	95	
BES127	169.00	96.40	563.00	0.565	-2.00E+04	2.40E+06	0.0771	0.0026	2.054	0.075	0.1943	0.0027	0.4130	33.6	67.2	1133.6	12.5	24.9	1144.6	7.3	14.6	101	
BES128	597.00	572.00	4190.00	0.984	-1.20E+07	1.20E+07	0.1333	0.0014	6.519	0.099	0.3532	0.0043	0.7236	9.2	18.4	2048.5	6.7	13.4	1949.9	10.2	20.5	95	
BES129	212.20	153.70	747.00	0.739	2.00E+06	1.30E+06	0.0662	0.0028	0.580	0.029	0.0754	0.0043	0.1617	55.2	110.5	464.5	9.3	18.6	468.6	3.6	7.2	101	
BES1211	62.10	77.20	276.00	1.238	-1.70E+06	1.40E+06	0.0844	0.0044	2.050	0.130	0.1806	0.0045	0.5968	50.6	101.3	1132.3	21.6	43.2	1070.3	12.3	24.6	95	
BES1212	23.90	33.60	266.00	1.021	-4.20E+05	7.90E+05	0.1292	0.0059	6.960	0.360	0.3900	0.0101	0.4652	2087.1	40.2	80.3	2106.3	22.9	45.9	2122.8	23.2	46.4	101
BES1213	311.00	341.00	2630.00	1.043	-1.00E+07	1.60E+07	0.2297	0.0023	15.990	0.710	0.5030	0.0210	0.9769	3050.0	8.0	16.0	2876.2	21.2	42.4	2626.7	45.0	90.1	91
BES1214	167.00	379.00	916.00	2.358	-3.30E+06	2.20E+06	0.0652	0.0033	0.772	0.040	0.0866	0.0019	0.3001	780.8	53.2	106.4	580.9	11.5	22.9	535.4	5.6	11.3	92
BES1215	91.10	61.50	412.00	0.685	6.70E+06	3.80E+06	0.0886	0.0027	2.768	0.095	0.2277	0.0034	0.4486	1395.5	29.2	58.4	1347.0	12.8	25.6	1322.4	8.9	17.9	98
BES1216	481.00	273.00	544.00	0.583	-5.00E+06	2.80E+06	0.0572	0.0024	5.054	0.019	0.0650	0.0009	-0.1361	493.3	46.2	92.4	414.4	6.4	12.8	406.2	2.8	5.6	98
BES1217	336.00	92.70	747.00	0.279	1.20E+07	1.50E+07	0.1225	0.0018	5.451	0.083	0.3224	0.0038	0.4628	1993.0	13.1	26.1	1892.9	6.5	13.1	1801.4	9.3	18.5	95
BES1219	118.90	135.80	810.00	1.155	-5.90E+06	4.50E+06	0.0769	0.0028	2.022	0.071	0.1927	0.0024	0.1986	1118.6	36.3	72.6	1122.9	11.9	23.8	1136.0	6.5	13.0	101
BES1220	65.60	89.20	428.00	1.357	-2.80E+06	1.90E+06	0.0790	0.0037	2.020	0.100	0.1864	0.0048	0.5417	1172.1	46.4	92.7	1122.3	16.8	33.6	1101.8	13.0	26.1	98
BES1221	142.40	177.60	594.00	1.259	1.42E+07	8.60E+06	0.0691	0.0031	0.849	0.045	0.1050	0.0015	0.1685	570.8	57.1	114.1	624.1	12.3	24.7	643.6	4.4	8.8	103
BES1222	87.50	48.33	314.60	0.553	4.20E+06	3.20E+06	0.0811	0.0029	2.331	0.089	0.2095	0.0033	0.3714	1223.9	35.1	70.2	1221.8	13.6	27.1	1226.2	8.8	17.6	100
BES1223	182.10	216.30	680.00	1.189	4.80E+06	2.80E+06	0.0594	0.0023	0.845	0.033	0.1038	0.0014	0.1430	581.8	42.0	84.1	621.9	9.1	18.1	636.6	4.1	8.2	102
BES1226	306.00	280.00	745.00	0.900	1.90E+06	3.80E+06	0.0872	0.0027	2.036	0.085	0.1710	0.0035	0.7583	1364.9	29.8	59.6	1127.6	14.2	28.4	1017.6	9.6	19.3	90
BES1227	288.40	278.00	727.00	0.912	-4.30E+06	5.00E+06	0.0659	0.0021	1.013	0.031	0.1125	0.0019	0.2079	803.2	33.4	66.7	710.4	7.8	15.6	687.3	5.5	11.0	97
BES1228	66.30	61.20	674.00	0.892	-1.60E+06	4.70E+06	0.1359	0.0033	7.800	0.190	0.4047	0.0037	0.3426	2175.6	21.1	42.3	2184.9	11.2	22.4	2190.6	13.1	26.2	100
BES1229	21.63	37.10	153.00	1.572	-5.60E+05	6.70E+05	0.0665	0.0083	1.360	0.170	0.1495	0.0059	0.2030	822.2	130.3	260.6	625.2	21.9	43.8	613.8	7.6	15.2	98
BES1231C	46.60	67.50	200.00	1.351	2.30E+05	4.60E+05	0.0615	0.0660	0.851	0.080	0.0999	0.0026	-0.0542	656.8	104.6	209.2	625.2	21.9	43.8	613.8	7.6	15.2	98
BES1232	104.20	179.30	368.00	0.972	-6.40E+06	3.70E+06	0.0540	0.0029	0.501	0.020	0.0677	0.0011	0.2182	371.0	60.5	120.9	412.4	9.5	18.9	422.3	3.3	6.6	102
BES1233	175.40	97.40	1160.00	0.892	-4.30E+06	3.00E+06	0.0748	0.0038	1.389	0.077	0.1348	0.0030	0.3958	1063.1	51.1	102.2	884.3	16.3	32.7	815.2	8.5	17.0	92
BES1234	79.46	84.50	246.90	0.966	3.00E+07	1.10E+07	0.0616	0.0021	0.883	0.031	0.1045	0.0012	0.1794	680.3	36.5	73.1	642.6	8.4	16.7	640.7	3.5	7.0	100
BES1236	428.00	455.00	1362.00	0.966	5.00E+04	5.70E+06	0.0618	0.0023	0.898	0.036	0.1068	0.0012	0.1335	667.2	39.8	79.7	650.7	9.6	19.2	684.1	5.0	9.9	101
BES1240	120.40	70.90	416.00	0.531	1.50E+07	1.00E+07	0.0823	0.0023	2.322	0.063	0.2057	0.0029	0.2492	1252.7	22.3	44.7	1219.0	9.6	19.2	1205.9	7.8	15.5	99
BES1242	842.00	2052.00	5270.00	2.182	-2.40E+08	1.10E+08	0.0586	0.0012	0.739	0.017	0.0918	0.0010	0.4389	552.3	22.3	44.7	561.8	5.0	9.9	566.4	2.8	5.6	101
BES1243	134.00	92.70	273.00	0.400	-1.10E+07	1.50E+07	0.0716	0.0024	1.713	0.063	0.1736	0.0026	0.3230	974.6	34.2	68.4	1013.4	11.8	23.6	1031.9	7.1	14.3	102
BES1245C	155.80	92.30	240.00	0.493	-5.30E+07	2.90E+07	0.0689	0.0033	0.756	0.043	0.0934	0.0014	0.2224	563.4	61.0	122.1	571.7	12.4	24.8	575.6	4.1	8.3	101
BES1245F	205.40	169.40	474.00	0.729	2.00E+07	2.90E+07	0.0628	0.0025	0.865	0.033	0.1004	0.0014	0.1128	701.5	42.4	84.8	632.8	9.0	18.0	616.8	4.1	8.2	97
BES1246	49.90	39.60	191.00	0.703	7.60E+06	7.10E+06	0.0722	0.0046	1.660	0.100	0.1670	0.0040	0.0700	991.6	64.8	129.6	993.4	19.1	38.1	995.6	11.0	22.1	100
BES1247	248.00	145.20	399.00	0.501	-6.00E+07	4.30E+07	0.0613	0.0024	0.879	0.034	0.1046	0.0040	0.0921	649.8	42.0	84.1	640.4	9.2	18.4	641.3	3.8	7.6	100
BES1249	383.90	252.00	504.00	0.567	-8.30E+07	7.30E+07	0.0583	0.0020	0.630	0.022	0.0788	0.0013	0.3649	541.1	37.5	75.0	496.1	6.8	13.7	489.0	3.9	7.8	99
BES1250	134.30	120.30	256.00	0.790	-3.50E+08	1.90E+08	0.0654	0.0033	0.843	0.043	0.0940	0.0016	0.2209	787.2	53.0	105.9	620.8	11.8	23.7	579.2	4.7	9.4	93
BES1251	49.20	89.40	170.40	1.592	1.60E+07	6.80E+07	0.0612	0.0061	0.792	0.078	0.0948	0.0022	0.1721	646.3	107.1	214.1	592.3	22.1	44.2	583.9	6.5	13.0	99
BES1252	16.96	28.20	62.00	1.385	2.40E+08	1.30E+08	0.0720	0.0120	1.030	0.160	0.1075	0.0041	-0.1168	985.9	169.6	339.2	718.9	40.0	80.0	658.2	11.9	23.9	92
BES1253	98.40	299.00	3090.00	2.620	3.00E+07	2.90E+07	0.1479	0.0031	8.450	0.190	0.4145	0.0059	0.4044	2321.8	18.0	35.9	2280.6	10.2	20.4	2235.5	13.4	26.9	98
BES1254C	88.90	113.00	481.00	1.042	-7.30E+07	4.20E+07	0.0748	0.0034	1.868	0.082	0.1641	0.0034	0.3556	1063.1	45.7	91.4	1004.0	15.5	30.9	979.5	9.4	18.8	98
BES1254F	150.90	117.00	478.00	0.693	4.60E+07	3.20E+07	0.0699	0.0031	1.488	0.059	0.1548	0.0023	-0.0867	925.4	45.6	91.1	925.5	12.0	24.1	927.8	6.4	12.8	100
BES1255	268.30	419.00	677.00	1.379	-1.40E+07	1.40E+07	0.0666	0.0022	0.868	0.030	0.0948	0.0014	0.3642	825.3	34.5	68.9	634.5	8.1	16.3	583.9	4.1	8.2	92
BES1256	393.00	280.00	2880.00	0.611	8.70E+07	7.30E+07	0.1309	0.0015	6.770	0.110	0.3741	0.0047	0.6675	2110.1	20.1	20.1	2081.8	7.2	14.4	2048.7	11.0	22.0	98
BES1257	175.00	170.40	749.00	0.276	-8.40E+06	7.10E+06	0.0707	0.0030	1.550	0.061	0.1600	0.0023	-0.0285	948.8	43.4	86.9	950.5	12.1	24.3	956.8	6.4	12.8	101
BES1258	419.00	366.00	1076.00	0.662	7.40E+07	5.20E+07	0.1352	0.0016	6.270	0.150	0.3356	0.0029	0.8712	2166.6	10.3	20.6	2014.3	10.5	20.9	1885.5	19.1	38.1	93
BES1259																							

ANALYSIS	U (ppm)	Th (ppm)	Pb (ppm)	Th/U	Ratios				Error correction				Ages (Ma)				Concordance (%)						
					²⁰⁶ Pb/ ²⁰⁸ Pb	²⁰⁷ Pb/ ²⁰⁸ Pb	²⁰⁷ Pb/ ²³⁵ U	²⁰⁶ Pb/ ²³⁸ U	σ	²⁰⁷ Pb/ ²⁰⁶ Pb	σ	²⁰⁷ Pb/ ²³⁵ U	σ	²⁰⁶ Pb/ ²³⁸ U	σ	²⁰⁷ Pb/ ²³⁵ U		σ					
BESI272	335.00	270.90	933.00	0.773	4.00E+06	7.30E+06	0.0774	0.0020	1.651	0.043	0.1552	0.0018	0.1499	1131.5	25.7	51.5	989.9	8.2	16.5	930.0	5.0	10.0	94
BESI273	267.40	226.80	1857.00	0.816	1.10E+07	1.05E+07	0.1057	0.0016	4.404	0.068	0.3018	0.0030	0.3742	1713.1	13.9	27.8	1713.1	6.4	12.8	1700.2	7.4	14.9	99
BESI274	230.40	435.80	1342.00	1.828	1.40E+07	8.50E+06	0.0639	0.0021	0.932	0.032	0.1054	0.0013	0.1396	738.3	34.8	69.5	668.7	8.4	16.8	646.0	3.8	7.6	97
BESI275	134.90	78.90	803.00	0.560	9.30E+07	4.40E+07	0.1318	0.0021	7.190	0.160	0.3949	0.0069	0.7030	2122.1	14.0	27.9	2135.3	9.5	19.8	2145.5	15.9	31.9	100
BESI276	114.50	90.60	243.00	0.768	9.00E+06	1.20E+06	0.0585	0.0029	0.724	0.046	0.0906	0.0013	0.2580	548.5	72.8	145.6	515.0	13.5	27.1	559.1	3.8	7.7	101
BESI277	568.00	430.00	751.00	0.727	7.90E+06	7.50E+06	0.0853	0.0015	0.874	0.025	0.0972	0.0019	0.5934	784.0	24.1	48.3	637.7	6.8	13.5	598.0	5.6	11.2	94
BESI278	439.00	278.00	418.00	0.627	1.60E+06	3.70E+06	0.0563	0.0025	0.460	0.020	0.0594	0.0008	0.2084	464.2	49.2	98.4	384.3	6.9	13.9	372.0	2.4	4.9	97
BESI279	99.80	79.70	282.00	0.777	2.60E+06	1.40E+06	0.0634	0.0041	0.933	0.060	0.1073	0.0008	0.2282	761.2	68.6	137.2	665.2	15.7	31.5	657.0	5.2	10.5	98
BESI280C	291.00	349.00	410.00	1.227	6.70E+06	3.30E+06	0.0623	0.0024	0.861	0.033	0.1004	0.0014	0.1309	684.4	41.1	82.4	630.7	9.0	18.0	616.8	4.1	8.2	98
BESI280T	189.00	158.00	400.00	0.831	-1.60E+07	7.10E+06	0.0599	0.0029	0.802	0.041	0.0975	0.0014	0.2087	600.0	52.4	104.8	593.0	11.5	23.1	599.7	4.1	8.2	100
BESI281	576.00	56.60	282.00	0.094	8.00E+07	1.80E+07	0.1266	0.0015	5.676	0.094	0.3246	0.0038	0.6903	2051.3	10.5	20.9	1927.7	7.1	14.3	1812.2	9.2	18.5	94
BESI282	185.70	111.70	577.00	0.608	2.00E+06	3.50E+06	0.0739	0.0024	1.786	0.056	0.1765	0.0019	0.1375	1038.7	32.8	65.6	1040.4	10.2	20.4	1047.8	5.2	10.4	101
BESI283	96.10	107.20	219.50	1.112	2.40E+05	6.00E+05	0.0534	0.0052	0.480	0.045	0.0662	0.0014	0.0462	345.8	110.1	220.3	398.1	15.4	30.8	413.2	4.2	8.5	104
BESI284	230.40	285.50	865.00	1.262	2.30E+06	1.90E+06	0.0607	0.0019	0.819	0.027	0.0974	0.0012	0.1734	628.6	33.7	67.4	607.5	15.1	30.8	599.2	3.5	7.0	99
BESI285	250.80	97.80	484.00	0.398	5.00E+06	4.20E+06	0.0729	0.0024	1.693	0.057	0.1686	0.0020	0.2447	1011.2	33.4	66.7	1005.9	10.7	21.5	1004.4	5.5	11.0	100
BESI287	42.60	30.70	106.80	0.737	3.50E+05	5.00E+05	0.0628	0.0060	0.966	0.086	0.1125	0.0024	-0.1771	701.5	101.7	203.4	686.4	22.2	44.4	687.3	7.0	13.9	100
BESI288	171.30	167.00	531.00	0.995	-1.80E+05	8.30E+05	0.0637	0.0027	0.921	0.039	0.1051	0.0014	0.1105	731.7	44.9	89.8	662.9	10.3	20.6	644.2	4.1	8.2	97
BESI289T	250.00	55.00	76.90	0.224	-9.00E+06	1.80E+06	0.0635	0.0026	0.782	0.032	0.0895	0.0014	0.1667	725.0	43.4	86.8	585.6	9.1	18.2	552.6	4.1	8.3	94
BESI290	107.10	126.00	728.00	1.166	-6.40E+06	4.20E+06	0.0873	0.0031	2.532	0.092	0.2107	0.0039	0.2975	1367.1	34.2	68.4	1281.3	13.2	28.4	1232.5	10.4	20.8	96
BESI291	408.00	405.00	1233.00	1.005	4.00E+06	3.60E+06	0.0593	0.0016	0.843	0.024	0.1031	0.0012	0.2997	578.1	29.3	58.6	620.8	6.6	13.2	632.6	3.5	7.0	102
BESI292	107.50	79.70	654.00	0.762	-1.70E+06	2.70E+06	0.0709	0.0023	1.439	0.042	0.1476	0.0021	0.0754	954.5	33.2	66.3	905.3	8.7	17.5	887.5	5.9	11.8	98
BESI293	190.40	258.40	615.00	1.403	8.00E+06	1.10E+06	0.0590	0.0027	0.622	0.029	0.3397	0.0048	0.5340	2059.6	17.3	34.7	1965.6	9.5	19.0	1885.2	11.5	23.1	96
BESI294	106.80	53.10	276.50	0.515	1.60E+06	1.60E+06	0.0735	0.0027	1.757	0.028	0.1737	0.0029	0.2401	1027.8	101.7	74.3	1029.7	12.0	23.9	1032.5	8.0	15.9	100
BESI296	321.10	355.50	1031.00	1.145	-2.80E+06	2.70E+06	0.0604	0.0021	0.800	0.028	0.0961	0.0014	0.2068	612.9	37.5	75.1	596.8	7.9	15.8	591.5	4.1	8.2	99
BESI299C	77.10	89.90	926.00	1.252	6.00E+06	1.60E+06	0.1249	0.0040	6.300	0.340	0.3650	0.0140	0.4562	2027.4	28.4	56.7	2018.5	23.6	47.3	2005.8	33.1	66.1	99
BESI299T	103.20	115.10	1183.00	1.147	-1.40E+06	2.40E+06	0.1333	0.0027	7.010	0.150	0.3830	0.0037	0.4562	2141.9	17.7	35.4	2112.7	9.5	19.0	2090.3	13.3	26.6	99
BESI300T	216.10	409.50	1236.00	1.962	7.20E+06	3.60E+06	0.0633	0.0027	0.889	0.038	0.1020	0.0014	0.2022	718.3	45.3	90.6	645.8	10.2	20.4	626.1	4.1	8.2	97
BESI301	204.80	388.90	1675.00	1.964	3.00E+04	1.90E+06	0.0709	0.0026	1.439	0.042	0.1476	0.0021	0.0754	954.5	33.2	66.3	905.3	8.7	17.5	887.5	5.9	11.8	98
BESI3103	412.00	1070.00	1610.00	0.697	9.00E+06	1.50E+06	0.0576	0.0026	0.442	0.019	0.0557	0.0010	0.1132	514.6	49.6	99.2	371.7	13.4	34.9	444.4	3.1	6.1	94
BESI3104	132.80	88.60	275.50	0.691	1.79E+06	6.80E+05	0.0749	0.0042	0.842	0.045	0.1011	0.0015	0.1911	621.5	57.1	114.1	620.2	12.4	24.8	620.9	4.4	8.8	100
BESI3105	50.80	54.70	245.60	1.111	7.90E+06	8.60E+05	0.0749	0.0042	0.842	0.045	0.1011	0.0015	0.1911	621.5	57.1	114.1	620.2	12.4	24.8	620.9	4.4	8.8	100
BESI3106	55.70	20.07	95.60	0.372	1.90E+06	1.40E+06	0.0702	0.0038	1.620	0.091	0.1676	0.0033	0.2334	934.2	55.5	111.0	973.0	17.6	35.2	998.9	9.1	18.2	102
BESI3107	120.00	61.30	302.50	0.529	-1.10E+06	1.00E+06	0.0750	0.0030	1.745	0.068	0.1704	0.0023	0.1918	648.8	40.2	80.4	1025.3	12.6	25.1	1014.3	6.3	12.7	99
BESI3108	312.50	22.00	47.50	0.046	-1.10E+06	1.90E+06	0.0613	0.0028	0.780	0.036	0.0925	0.0015	0.1698	669.8	49.0	98.1	585.5	10.3	20.5	570.3	4.4	8.9	97
BESI3109	99.80	80.20	434.00	0.824	5.60E+05	7.10E+05	0.0803	0.0048	1.900	0.120	0.1692	0.0027	0.0555	1204.4	58.9	117.8	1081.1	13.9	27.9	1007.7	7.4	14.9	93
BESI3110	90.70	95.00	309.00	0.967	9.00E+05	5.40E+05	0.0683	0.0032	0.930	0.053	0.1146	0.0022	0.2091	541.1	60.0	120.0	667.6	13.9	27.9	699.4	6.4	12.7	105
BESI3111	147.00	212.00	1095.00	1.460	-8.00E+06	1.80E+06	0.1165	0.0026	4.470	0.110	0.2784	0.0062	0.6710	1903.2	20.0	40.1	1725.4	13.0	26.0	1583.3	15.6	31.3	92
BESI3112	345.00	268.00	2684.00	0.799	1.80E+07	1.10E+07	0.1309	0.0016	6.920	0.110	0.3833	0.0042	0.6003	2110.1	10.7	21.4	2091.2	7.0	14.1	2091.7	9.8	19.6	100
BESI3113	179.00	185.00	1577.00	1.042	7.80E+06	5.00E+06	0.1320	0.0028	6.540	0.180	0.3592	0.0051	0.6161	2124.7	18.6	37.1	2051.3	12.1	24.2	1978.4	14.5	28.9	96
BESI3114	533.00	463.90	1266.00	0.904	1.30E+07	6.30E+06	0.0646	0.0017	0.836	0.026	0.0939	0.0012	0.3021	761.3	27.7	55.5	619.9	6.4	12.7	578.6	3.5	7.1	94
BESI3115	172.70	112.10	209.10	0.669	6.90E+05	5.80E+05	0.0547	0.0009	0.497	0.023	0.0661	0.0009	0.0931	400.0	59.4	118.8	400.0	59.4	118.8	412.5	2.8	5.6	101
BESI3116	201.00	141.80	408.00	0.723	-4.20E+05	8.30E+05	0.0608	0.0027	0.816	0.037	0.0974	0.0016	0.2732	632.2	47.8	95.6	605.8	10.3	20.7	599.2	4.4	8.8	99
BESI3117	332.90	233.70	3354.00	0.717	-2.90E+07	1.60E+07	0.2250	0.0020	18.760	0.190	0.6045	0.0056	0.5582	3016.8	7.1	14.3	3029.6	4.9	9.8	3047.9	11.2	22.5	101
BESI3118	380.00	305.00	1920.00	0.823	2.20E+06	8.10E+06	0.1916	0.0025	12.440	0.300	0.4699	0.0070	0.5524	2755.9	10.7	21.4	2638.2	11.3	22.6	2483.1	15.3	30.7	94
BESI3119	89.60	71.40	1025.00	0.820	2.20E+06	8.10E+06	0.2190	0.0033	16.970	0.300	0.5620	0.0069	0.5298	2973.4	12.1	24.3	2933.1	8.5	16.9	2874.9	14.2	28.5	98
BESI3120	269.00	200.00	2040.00	0.747	-1.20E+06	3.90E+06	0.1341	0.0018	7.050	0.130	0.3810	0.0049	0.6429	2152.3	11.7	23.4	2117.8	8.2	16.4	2081.0	11.4	22.9	98
BESI3121	154.90	195.00	1874.00	1.106	-2.20E+07	1.60E+07	0.1896	0.0049	11.600	0.230	0.4470	0.0150	0.6484	2738.7	21.3	42.5	2572.7	9.3	18.5	2381.9	33.4	66.8	98
BESI3123	50.10	29.77	159.30	0.602	6.40E+05	6.10E+05	0																

ANALYSIS	U (ppm)	Th (ppm)	Pb (ppm)	Th/U	Ratios			Error correction			Ages (Ma)			Concordance (%)									
					$^{206}\text{Pb}/^{238}\text{U}$	$^{207}\text{Pb}/^{235}\text{U}$	$^{207}\text{Pb}/^{206}\text{Pb}$	$^{206}\text{Pb}/^{238}\text{U}$	$^{207}\text{Pb}/^{235}\text{U}$	$^{207}\text{Pb}/^{206}\text{Pb}$	$^{207}\text{Pb}/^{235}\text{U}$	$^{207}\text{Pb}/^{206}\text{Pb}$	$^{206}\text{Pb}/^{238}\text{U}$		σ	2σ							
BES1231r	20.80	27.95	77.40	1.272	2.60E+06	1.10E+06	0.0760	0.0110	0.930	0.130	0.0908	0.0031	0.0024	1095.1	144.9	289.8	667.6	34.2	68.3	560.3	9.2	18.3	84
BES1235	88.50	177.00	642.00	1.825	-1.69E+08	8.20E+07	0.1040	0.0040	2.470	0.110	0.1735	0.0044	0.4629	1696.7	35.4	70.9	1263.3	16.1	32.2	1031.4	12.1	24.2	82
BES1238	396.00	132.10	891.00	0.299	-1.30E+07	1.50E+07	0.1232	0.0019	3.733	0.091	0.2206	0.0040	0.7907	2003.1	13.7	27.4	1578.5	9.8	19.5	1285.0	10.6	21.1	81
BES1239	157.60	373.00	1350.00	1.842	-4.30E+06	2.10E+06	0.1500	0.0300	2.410	0.650	0.0978	0.0057	0.9763	2345.9	171.0	342.0	1245.6	96.7	193.4	601.5	16.7	33.5	48
BES1241	588.00	311.00	658.00	0.433	-1.71E+08	9.09E+07	0.1223	0.0012	4.666	0.083	0.2763	0.0046	0.7943	1980.0	8.7	17.4	1761.2	7.4	14.9	1572.7	11.6	23.2	89
BES1244	189.10	280.80	552.00	1.344	2.80E+06	9.50E+06	0.0712	0.0034	0.867	0.041	0.0890	0.0016	0.1832	983.2	48.8	97.5	633.9	11.1	22.3	549.6	4.7	9.5	87
BES1248	1217.00	3300.00	918.00	2.404	-3.60E+07	2.10E+07	0.0851	0.0033	0.281	0.010	0.0242	0.0006	0.1299	1317.8	37.6	75.2	251.5	3.8	7.6	154.3	1.8	3.5	61
BES1265	84.40	82.30	2250.00	0.884	2.80E+05	4.00E+05	0.3430	0.0490	10.000	1.900	0.1740	0.0200	0.4803	3676.2	109.0	218.1	2434.8	87.6	175.2	1034.1	54.9	109.8	42
BES1286c	61.90	52.90	254.00	0.848	2.83E+06	8.40E+05	0.1902	0.0023	5.680	0.067	0.2168	0.0019	0.3444	2743.9	9.9	19.9	1928.3	5.1	10.2	1264.9	5.0	10.1	66
BES1295	106.80	348.00	498.00	2.976	3.30E+06	1.80E+06	0.0725	0.0056	0.530	0.041	0.0546	0.0022	0.3050	1000.0	78.4	156.9	431.8	13.6	27.2	342.7	6.7	13.4	79
BES1297	504.00	90.30	630.00	0.184	3.20E+06	8.30E+06	0.1182	0.0014	4.021	0.089	0.2485	0.0042	0.8491	1929.2	10.6	21.2	1638.5	9.0	18.0	1420.4	10.9	21.7	87
BES1299r	673.00	685.00	4630.00	1.063	4.00E+07	1.50E+07	0.2036	0.0015	12.330	0.280	0.4391	0.0087	0.9367	2855.3	6.0	12.0	2629.9	9.9	19.8	2346.6	19.5	39.0	89
BES12107c	48.30	147.90	1071.00	3.211	-1.30E+05	5.10E+05	0.1123	0.0049	3.710	0.160	0.2428	0.0071	0.4856	1837.0	39.5	79.0	1573.5	17.2	34.5	1401.2	18.4	36.8	89
BES12122	60.60	75.50	241.00	1.287	-8.40E+05	5.10E+05	0.0699	0.0032	1.290	0.180	0.1202	0.0085	0.9676	1052.3	73.1	146.2	841.3	39.9	79.7	731.7	24.5	48.9	87
BES12128	513.00	774.00	2860.00	1.538	4.00E+06	4.80E+06	0.2211	0.0034	9.140	0.690	0.2950	0.0190	0.9850	2988.7	12.4	24.7	2352.1	34.5	69.0	1686.5	47.3	94.6	71
BES12124	269.00	203.70	839.00	0.754	-1.90E+06	2.60E+06	0.1250	0.0023	4.760	0.180	0.2752	0.0090	0.8610	2028.8	16.3	32.6	1777.9	15.9	31.7	1567.1	22.7	45.5	88
BES12126	98.90	121.60	304.00	1.236	1.50E+05	2.90E+05	0.0787	0.0040	1.099	0.054	0.1018	0.0020	0.1532	1164.6	50.4	100.7	752.9	13.0	26.1	624.9	5.9	11.7	83
BES12128	121.60	154.00	351.00	1.021	3.00E+05	4.70E+05	0.0877	0.0099	1.200	0.110	0.1033	0.0024	-0.3442	1375.9	108.5	217.1	800.6	25.4	50.7	633.7	7.0	14.0	79
BES12132	93.20	181.00	600.00	1.764	2.10E+05	7.30E+05	0.1358	0.0040	5.000	0.280	0.2690	0.0150	0.8824	2174.3	25.7	51.3	1819.3	23.7	47.3	1535.7	38.1	76.2	84
BES12133	570.00	853.00	747.00	1.468	9.00E+06	1.20E+06	0.0768	0.0024	0.791	0.025	0.0750	0.0016	0.3116	1116.0	31.2	62.4	591.7	7.1	14.2	466.2	4.8	9.6	79
BES12134	923.00	258.00	1240.00	0.272	6.00E+07	1.00E+07	0.1832	0.0021	6.691	0.070	0.2660	0.0027	0.2570	2682.1	9.5	19.0	2071.4	4.6	9.2	1520.5	6.9	13.7	73
BES12141	62.80	204.00	674.00	2.268	3.00E+05	6.00E+05	0.1301	0.0044	4.960	0.260	0.2780	0.0120	0.7922	2099.3	29.7	59.4	1812.5	22.1	44.3	1581.3	30.3	60.5	87

Footnotes:

. Analysis references: BES1z is zircon from sample BES1 (mount CT18-2), followed by grain number "c" or "r", meaning core or rim, respectively.

Chapter IV

Table D.36: Sample BES2 (LA-ICP/MS)

IGSN: IEACC00010 Coordinate UTM: Zone 28S, 3724273 m N, 671847 m E

Table with columns: ANALYSIS, U (ppm), Th (ppm), Pb (ppm), Th/U, 206Pb/208Pb, 207Pb/208Pb, 207Pb/238U, Ratios (207Pb/235U), 206Pb/238U, Error correction, Concordant data (207Pb/206Pb, 206Pb/238U, 207Pb/235U, 206Pb/238U), Ages (Ma) (207Pb/235U, 206Pb/238U), Concordance (%). Rows include samples BESZ21 through BESZ62.

ANALYSIS	U (ppm)	Th (ppm)	Pb (ppm)	Th/U	Ratios					Error correction					Ages (Ma)					Concordance (%)		
					$^{207}\text{Pb}/^{235}\text{U}$	$^{207}\text{Pb}/^{238}\text{U}$	$^{207}\text{Pb}/^{206}\text{Pb}$	$^{207}\text{Pb}/^{235}\text{U}$	$^{207}\text{Pb}/^{238}\text{U}$	$^{207}\text{Pb}/^{206}\text{Pb}$	2σ	correction	2σ	$^{207}\text{Pb}/^{235}\text{U}$	$^{207}\text{Pb}/^{238}\text{U}$	$^{207}\text{Pb}/^{206}\text{Pb}$	σ	2σ	$^{207}\text{Pb}/^{235}\text{U}$		$^{207}\text{Pb}/^{238}\text{U}$	$^{207}\text{Pb}/^{206}\text{Pb}$
BESZ263	80.70	30.24	31.13	0.376	0.0029	0.1306	0.0029	7.060	0.370	0.3853	0.0076	0.391	2106.0	19.5	39.0	2119.0	19.5	46.6	2101.0	17.7	35.4	99
BESZ264	178.50	119.40	33.57	0.667	0.0031	0.0597	0.0031	0.801	0.051	0.0964	0.0020	0.744	597.4	74.4	148.9	597.4	74.4	28.7	593.3	5.9	11.8	99
BESZ265	109.20	45.00	43.30	0.408	0.0040	0.1276	0.0040	6.680	0.340	0.3731	0.0067	6.072	2065.2	20.7	41.5	2070.0	20.7	44.9	2044.0	15.7	31.5	99
BESZ266	556.00	709.00	189.50	1.244	0.0032	0.0625	0.0032	0.769	0.040	0.0939	0.0017	0.558	2053.0	59.5	118.9	2053.0	59.5	22.9	2053.0	5.0	10.0	100
BESZ267	29.03	57.15	16.16	1.946	0.0031	0.0625	0.0031	0.880	0.110	0.1016	0.0032	0.137	691.3	138.2	276.4	641.0	138.2	52.9	623.8	9.4	18.7	97
BESZ268	151.00	87.50	89.80	0.577	0.0024	0.1351	0.0024	7.430	0.370	0.3887	0.0072	0.207	2165.3	15.5	31.0	2164.6	15.5	44.5	2116.8	16.7	33.4	98
BESZ270c	53.40	38.90	12.00	0.296	0.0035	0.0604	0.0035	0.949	0.090	0.1149	0.0032	0.203	617.9	105.4	209.9	677.6	105.4	46.8	701.1	9.3	18.5	100
BESZ270f	409.00	127.30	36.30	0.296	0.0035	0.0604	0.0035	0.812	0.046	0.0984	0.0019	0.124	567.1	64.6	129.2	603.6	64.6	25.8	605.0	5.3	10.5	100
BESZ271	469.00	343.00	98.00	0.763	0.0033	0.0609	0.0033	0.866	0.047	0.1025	0.0018	0.236	635.7	56.3	116.6	633.4	56.3	25.6	629.0	5.3	10.5	98
BESZ272	85.00	36.25	86.60	0.661	0.0046	0.2586	0.0046	23.040	1.400	0.6300	0.0180	0.970	3238.2	14.0	28.0	3228.6	14.0	59.1	3149.6	35.6	71.2	98
BESZ273	292.00	317.00	88.20	1.081	0.0036	0.0598	0.0036	0.835	0.049	0.1009	0.0019	0.208	596.3	65.2	130.4	616.4	65.2	27.1	619.7	5.6	11.1	101
BESZ274	79.80	42.90	42.20	0.511	0.0027	0.1326	0.0027	7.370	0.370	0.3963	0.0078	0.380	2192.7	17.8	35.6	2157.3	17.8	44.8	2152.0	18.0	36.0	100
BESZ275	107.80	120.90	33.38	1.122	0.0047	0.0648	0.0047	0.866	0.059	0.0963	0.0022	0.126	767.8	76.4	152.8	633.4	76.4	32.1	592.7	6.5	12.9	94
BESZ276	222.80	240.80	235.30	1.088	0.0021	0.1264	0.0021	6.640	0.330	0.3753	0.0069	0.3467	2048.5	14.7	29.3	2064.7	14.7	43.8	2054.3	16.2	32.3	99
BESZ277	98.60	127.50	36.14	1.292	0.0043	0.0594	0.0043	0.849	0.061	0.1024	0.0021	0.1507	581.8	78.6	157.2	624.1	78.6	33.5	628.5	6.1	12.3	101
BESZ281	343.00	161.90	180.30	0.472	0.0019	0.1733	0.0019	11.590	0.560	0.4778	0.0023	0.6483	2589.8	9.1	18.3	2571.9	9.1	45.1	2517.7	18.1	36.2	98
BESZ282	168.20	87.90	26.50	0.522	0.0042	0.0599	0.0042	0.850	0.058	0.1038	0.0021	0.1482	600.0	75.9	151.8	624.6	75.9	31.8	636.6	6.1	12.3	102
BESZ283	81.90	75.60	24.61	0.925	0.0045	0.0600	0.0045	0.950	0.074	0.1108	0.0025	0.266	603.6	81.1	162.3	678.1	81.1	38.5	677.4	7.3	14.5	100
BESZ284	144.50	15.30	5.88	0.105	0.0043	0.0605	0.0043	0.937	0.065	0.1099	0.0023	0.136	621.5	76.7	153.3	671.3	76.7	34.0	672.2	6.7	13.4	100
BESZ285f	218.00	71.80	62.10	0.331	0.0017	0.1207	0.0017	5.631	0.260	0.3351	0.0058	0.289	1966.6	12.6	25.1	1920.9	12.6	42.8	1863.1	14.0	28.0	97
BESZ286	152.40	56.20	62.80	0.367	0.0023	0.1538	0.0023	9.310	0.460	0.4350	0.0079	0.5343	2388.6	12.7	25.5	2369.0	12.7	45.3	2328.2	17.7	35.5	98
BESZ287	787.00	156.70	47.70	0.202	0.0034	0.0627	0.0034	0.917	0.046	0.1060	0.0018	0.1799	698.1	57.8	115.5	660.8	57.8	24.3	649.7	5.2	10.5	98
BESZ289	499.00	72.50	20.06	1.146	0.0028	0.0628	0.0028	0.035	0.048	0.1133	0.0018	0.2697	701.5	59.3	118.7	635.0	59.3	25.5	645.3	5.2	10.5	98
BESZ292	81.80	54.00	14.92	0.657	0.0060	0.0645	0.0060	0.869	0.076	0.1004	0.0023	0.0782	758.1	98.1	196.2	655.0	98.1	41.3	616.8	6.7	13.5	97
BESZ293	115.70	81.70	24.10	0.711	0.0045	0.0614	0.0045	0.902	0.062	0.1052	0.0023	0.1114	653.3	78.6	157.3	652.8	78.6	33.1	644.8	6.7	13.4	99
BESZ294	346.30	283.20	264.50	0.818	0.0015	0.1212	0.0015	6.094	0.290	0.3604	0.0060	0.231	1974.0	11.0	22.1	1989.4	11.0	41.5	1984.1	14.2	28.4	100
BESZ295	338.00	185.30	53.40	0.553	0.0036	0.0604	0.0036	0.861	0.049	0.1024	0.0018	0.276	617.9	64.3	128.7	630.7	64.3	26.7	628.5	5.3	10.5	100
BESZ296	637.00	162.10	43.20	0.256	0.0025	0.0607	0.0025	0.788	0.041	0.0935	0.0016	0.1664	628.6	56.6	117.0	590.0	56.6	23.3	576.4	4.7	9.4	98
BESZ297	283.70	240.00	238.60	0.850	0.0015	0.1213	0.0015	6.231	0.300	0.3703	0.0063	0.4578	1975.4	12.5	25.0	2008.8	12.5	42.1	2030.8	14.8	29.6	101
BESZ298	178.20	102.30	29.68	0.571	0.0043	0.0673	0.0043	0.930	0.061	0.1025	0.0025	0.4026	847.1	66.4	132.9	667.6	66.4	30.2	1833.5	7.3	14.6	96
BESZ299	23.63	84.45	29.70	1.456	0.0052	0.1194	0.0052	5.500	0.450	0.3290	0.0180	0.8618	1947.3	38.9	77.8	1900.6	38.9	72.1	2029.5	43.7	87.3	94
BESZ2100	116.40	77.70	95.30	0.683	0.0028	0.1776	0.0028	11.880	0.590	0.4828	0.0092	0.4680	2630.6	13.1	26.2	2595.0	13.1	46.5	2538.5	20.0	40.0	98
BESZ2101	334.10	179.20	47.70	0.540	0.0036	0.0621	0.0036	0.810	0.044	0.0938	0.0018	0.0594	677.6	62.0	123.9	602.5	62.0	24.7	578.0	5.3	10.6	96
BESZ2102	112.60	34.20	32.30	0.307	0.0026	0.1220	0.0026	6.020	0.310	0.3549	0.0070	0.3947	1985.7	19.0	37.9	1978.7	19.0	44.8	1958.0	16.7	33.3	99
BESZ2103	714.00	232.90	98.50	0.328	0.0037	0.0699	0.0037	1.407	0.070	0.1439	0.0024	0.1642	925.4	54.4	108.7	89.9	54.4	29.5	866.7	6.8	13.5	97
BESZ2104	1023.00	24.19	44.80	0.024	0.0011	0.1316	0.0011	6.501	0.310	0.3546	0.0060	0.7322	2119.2	7.3	14.7	2046.0	7.3	41.9	1956.5	14.3	28.6	96
BESZ2105	154.20	40.37	10.71	0.262	0.0039	0.0838	0.0039	0.838	0.058	0.1010	0.0019	0.1055	581.8	71.3	142.6	618.0	71.3	29.8	620.3	5.6	11.1	100
BESZ2106	64.20	28.13	8.41	0.442	0.0052	0.0589	0.0052	0.836	0.078	0.1015	0.0028	0.2894	563.4	114.7	229.3	616.9	114.7	43.1	623.2	8.2	16.4	101
BESZ2107c	138.00	100.60	95.70	0.732	0.0025	0.1244	0.0025	6.330	0.320	0.3642	0.0067	0.3831	2020.3	17.8	35.6	2022.6	17.8	44.3	2002.1	15.8	31.7	99
BESZ2107d	105.20	84.30	82.90	0.810	0.0045	0.1248	0.0045	6.250	0.310	0.3651	0.0065	0.2991	2026.0	17.0	34.1	2011.5	17.0	43.4	2006.3	15.3	30.7	100
BESZ2108	426.80	42.57	11.55	0.101	0.0035	0.0632	0.0035	0.851	0.046	0.0976	0.0017	0.3115	588	117.6	235.8	625.2	117.6	58.8	600.5	5.0	10.0	96
BESZ2109	47.30	70.80	20.40	1.486	0.0058	0.0655	0.0058	0.961	0.085	0.1059	0.0030	0.1744	790.4	92.9	185.8	683.8	92.9	44.0	648.9	8.7	17.5	95
BESZ2110	285.00	49.70	14.04	0.175	0.0038	0.0612	0.0038	0.882	0.055	0.1030	0.0019	0.2653	646.3	66.7	133.4	642.1	66.7	29.6	632.0	5.6	11.1	98
BESZ2111	143.70	241.10	72.30	0.771	0.0036	0.0610	0.0036	0.898	0.049	0.1069	0.0019	0.1013	639.2	63.5	126.9	650.7	63.5	26.2	654.7	5.5	11.1	101
BESZ2112	146.30	197.00	53.00	1.366	0.0041	0.0584	0.0041	0.769	0.053	0.0956	0.0019	0.1212	544.8	76.7	153.4	579.2	76.7	30.4	588.6	5.6	11.2	102
BESZ2114	53.00	30.30	8.14	0.575	0.0064	0.0621	0.0064	0.837	0.080	0.0972	0.0023	0.0193	677.6	110.1	220.3	617.5	110.1	44.2	588.0	6.8	13.5	97
BESZ2115	84.70	57.50	17.48	0.684	0.0049	0.0648	0.0049	0.901	0.065	0.1030	0.0023	0.0982	767.8	79.6	159.3	652.3	79.6	34.7	632.0	6.7	13.4	97
BESZ2116	158.20	189.10	49.70	1.209	0.0041	0.0582	0.0041	0.742	0.051	0.0922	0.0019	0.1121	537.3	77.1	154.1	563.6	77.1	29.7	568.5	5.6	11.2	101
BESZ2117	128.00	88.20	23.34	0.697	0.0045	0.0657	0.0045	0.719	0.060	0.0934	0.0022	0.2851	440.4	83.4	166.8	676.0	83.4	36.5	575.6	6.5	13.0	105
BESZ2118	100.80	142.50	47.30	1.420	0.0047	0.0607	0.0047	0.946	0.070	0.1137	0.0024	0.2273	638.6	83.4	166.8	639.0	83.4	36.5	694.2	6.9	13.9	103
BESZ2119c	143.70	22.30	22.08</																			

ANALYSIS	U (ppm)		Th (ppm)	Pb (ppm)	Th/U	$^{206}\text{Pb}/^{208}\text{Pb}$		$^{207}\text{Pb}/^{208}\text{Pb}$		Ratios		Error correction		Ages (Ma)		Concordance (%)						
	2σ	2σ				2σ	2σ	2σ	2σ	2σ	2σ	2σ	2σ	2σ	2σ	2σ	2σ	2σ	2σ			
BESZ2137	305.00	154.60	160.90	0.510	0.1335	0.0017	0.6780	0.3330	0.3660	0.0065	0.5011	2144.5	11.1	22.3	2083.1	11.1	43.0	2010.6	15.3	30.7	97	
BESZ2138	29.10	22.45	5.86	0.782	0.0584	0.0079	0.682	0.068	0.0879	0.0029	0.2896	544.8	147.8	295.6	528.0	147.8	56.1	543.1	8.6	17.2	103	
BESZ2140	72.50	19.70	5.38	0.274	0.0543	0.0052	0.683	0.093	0.0916	0.0025	0.1155	383.5	107.6	215.2	531.0	107.6	40.9	565.0	7.4	14.8	106	
BESZ2141	157.40	136.10	157.30	0.882	0.1519	0.0028	9.300	0.470	0.4395	0.0080	0.4489	2367.4	15.7	31.4	2368.0	15.7	46.3	2348.4	17.9	35.8	99	
BESZ2142	58.70	39.90	36.30	0.702	0.0039	0.0039	5.310	0.330	0.3178	0.0087	0.5062	1932.2	29.5	59.0	1870.5	29.5	53.1	1778.0	21.3	42.6	95	
BESZ2143	323.30	151.90	50.90	0.474	0.0685	0.0041	0.934	0.055	0.1004	0.0019	-0.0706	822.2	64.4	128.7	669.7	64.4	28.8	616.8	5.6	11.1	92	
BESZ2144c	291.80	254.10	78.60	0.662	0.108E+06	0.0617	0.906	0.052	0.1058	0.0019	-0.0564	663.7	64.2	128.5	654.9	64.2	27.7	648.3	5.5	11.1	99	
BESZ2144E	250.00	163.40	50.80	0.889	0.0057	0.0041	0.875	0.056	0.1046	0.0021	0.0796	592.7	74.4	148.8	638.3	74.4	30.3	641.3	6.1	12.3	100	
BESZ2145c	178.50	38.10	11.27	0.216	0.0611	0.0040	0.823	0.054	0.0977	0.0020	0.2345	642.8	70.4	140.7	609.7	70.4	29.5	600.9	5.9	11.7	99	
BESZ2146	157.60	63.80	18.03	0.407	0.0610	0.0042	0.833	0.054	0.0988	0.0021	0.0325	639.2	74.0	148.1	615.3	74.0	29.9	607.4	6.2	12.3	99	
BESZ2147	281.70	230.00	61.30	0.796	0.0616	0.0040	0.820	0.052	0.0966	0.0022	0.3752	660.3	69.6	139.2	608.0	69.6	29.0	594.5	6.5	12.9	96	
BESZ2147c	110.50	92.00	29.30	0.798	0.0626	0.0046	0.900	0.070	0.1023	0.0026	0.4246	694.7	78.3	156.6	651.7	78.3	37.4	627.9	7.6	15.2	96	
BESZ2148	116.60	71.20	19.38	0.616	0.0599	0.0046	0.767	0.058	0.0914	0.0020	0.2117	600.0	83.1	166.3	578.0	83.1	33.3	563.8	5.9	11.8	98	
BESZ2149	29.80	32.40	9.53	1.101	0.0052	0.0039	0.750	0.130	0.1017	0.0037	0.0854	289.8	201.7	403.5	568.2	201.7	75.4	624.4	10.8	21.6	110	
BESZ2150	135.90	86.30	123.90	0.639	0.2073	0.0028	16.050	0.800	0.5569	0.0110	0.7153	2884.6	11.0	21.9	2879.8	11.0	47.6	2853.8	22.8	45.5	99	
BESZ2151	292.00	261.00	77.70	0.906	0.0590	0.0036	0.851	0.050	0.1052	0.0020	0.0835	567.1	66.4	132.8	618.0	66.4	27.4	644.8	5.8	11.7	100	
BESZ2153	45.40	31.30	9.17	0.693	0.0615	0.0031	0.838	0.093	0.1002	0.0029	0.1223	656.8	123.8	247.6	625.0	123.8	51.3	615.6	8.5	17.0	100	
BESZ2154	528.00	148.00	41.40	0.279	0.0593	0.0034	0.783	0.043	0.0954	0.0017	0.1184	578.1	62.3	124.6	587.2	62.3	24.5	578.0	5.0	10.0	100	
BESZ2155	333.50	237.50	71.30	0.717	0.0618	0.0036	0.858	0.049	0.0993	0.0019	0.1846	667.2	62.4	124.7	629.0	62.4	26.8	610.3	5.6	11.1	97	
BESZ2156	109.30	112.00	32.85	1.030	0.0612	0.0045	0.877	0.065	0.1026	0.0023	0.3329	646.3	79.0	158.0	629.6	79.0	35.1	629.6	6.7	13.4	97	
BESZ2157	44.70	23.09	5.87	0.514	0.0609	0.0067	0.859	0.088	0.1002	0.0031	-0.1424	635.7	118.4	236.8	629.6	118.4	48.0	615.6	9.1	18.2	98	
BESZ2158	184.30	152.10	45.10	0.824	0.0626	0.0042	0.878	0.058	0.0998	0.0020	0.1309	694.7	71.5	143.0	639.9	71.5	31.3	613.2	5.9	11.7	96	
BESZ2159	115.50	74.80	95.00	0.662	0.1835	0.0037	12.820	0.680	0.4987	0.0095	0.5246	2684.8	16.7	33.3	2666.5	16.7	49.9	2608.2	20.4	40.9	98	
BESZ2160	39.40	54.50	15.84	1.389	0.0591	0.0075	0.850	0.110	0.1006	0.0035	0.2062	570.8	138.1	276.1	624.6	138.1	60.3	617.9	10.3	20.5	99	
BESZ2161	369.00	317.00	290.00	0.719	0.1481	0.0018	7.630	0.400	0.3713	0.0090	0.8732	2300.8	10.6	21.2	2188.4	10.6	47.0	2035.5	21.2	42.3	93	
BESZ2162c	332.00	87.30	98.20	0.289	0.1340	0.0018	7.840	0.370	0.4053	0.0069	0.4179	2151.0	11.7	23.5	2189.6	11.7	43.4	2193.4	15.8	31.7	100	
BESZ2163	223.20	206.00	59.30	0.925	0.0594	0.0039	0.814	0.051	0.0996	0.0019	-0.0566	591.8	71.3	142.6	604.7	71.3	28.5	612.1	5.6	11.1	101	
BESZ2164	160.30	130.30	47.90	0.818	0.0644	0.0042	1.134	0.072	0.1274	0.0023	0.1850	754.8	68.8	137.6	769.7	68.8	34.2	773.0	6.6	13.2	100	
BESZ2165	100.30	29.13	27.23	0.029	0.1248	0.0002	5.906	0.280	0.3384	0.0055	0.6301	2026.0	8.5	17.0	1962.1	8.5	41.1	1879.0	13.2	26.5	96	
BESZ2172	726.00	54.70	14.40	0.075	0.0608	0.0033	0.839	0.042	0.0979	0.0016	0.0150	632.2	58.4	116.9	618.6	58.4	23.2	601.8	4.7	9.4	97	
BESZ2173	3720.00	268.00	480.00	0.074	0.2105	0.0110	0.985	0.051	0.0336	0.0015	0.8280	2909.4	42.3	84.7	686.2	42.3	26.1	213.0	4.7	9.4	31	
BESZ2286	230.50	219.00	85.50	0.933	0.0930	0.0130	1.450	0.230	0.1078	0.0028	0.8262	1487.9	132.4	264.7	909.9	132.4	95.2	660.0	8.1	16.3	73	
BESZ2288	754.00	92.50	216.00	0.123	0.1489	0.0083	3.560	0.200	0.1740	0.0039	0.5518	2333.3	47.7	95.4	1540.7	47.7	22.2	1034.1	10.7	21.4	67	
BESZ230	722.00	1190.00	319.00	1.590	0.0631	0.0034	0.837	0.043	0.0953	0.0017	0.3787	711.6	57.3	114.5	617.5	57.3	23.7	586.8	5.0	10.0	95	
BESZ233	1820.00	76.40	80.10	0.043	0.0909	0.0048	0.672	0.034	0.0529	0.0015	0.6134	1444.5	50.3	100.6	521.9	50.3	20.6	332.3	4.6	9.2	64	
BESZ244	86.90	111.30	55.80	1.280	0.0956	0.0060	2.494	0.150	0.1847	0.0040	0.1705	1539.9	59.0	118.0	1270.3	59.0	43.6	1092.6	10.9	21.8	86	
BESZ250	419.00	89.60	47.90	0.208	0.0787	0.0042	2.098	0.110	0.1914	0.0036	0.3549	1164.6	52.9	105.7	1148.2	52.9	36.0	1128.0	9.7	19.5	88	
BESZ267	1037.00	103.20	87.00	0.101	0.1166	0.0059	3.850	0.230	0.2372	0.0094	0.8686	1904.7	45.4	90.9	1603.3	45.4	48.1	1372.1	24.5	49.0	86	
BESZ278	4.04	86.20	25.89	21.277	0.0960	0.0340	1.520	0.530	0.1229	0.0096	0.2701	1547.8	332.7	665.4	938.5	332.7	213.4	747.2	27.6	55.1	80	
BESZ279	233.80	46.00	43.50	0.196	0.1256	0.0017	6.415	0.310	0.3627	0.0064	0.5196	2037.3	12.0	23.9	2034.3	12.0	42.4	1995.0	15.1	30.3	98	
BESZ280	1420.00	128.60	187.20	0.091	0.1382	0.0069	4.307	0.210	0.2238	0.0046	0.7932	2204.8	43.3	86.7	1694.7	43.3	40.1	1301.9	12.1	24.2	77	
BESZ285c	312.00	49.90	38.90	0.170	0.1897	0.0024	10.360	0.520	0.3894	0.0083	0.7583	2739.6	10.4	20.8	2467.5	23.2	46.4	2120.0	19.3	38.5	86	
BESZ287	161.80	165.90	56.80	1.029	0.0744	0.0051	1.137	0.077	0.1107	0.0022	0.2399	1052.3	69.1	138.1	771.1	69.1	18.3	676.8	6.4	12.8	88	
BESZ288	851.00	388.00	934.00	0.457	0.2810	0.0200	8.430	0.760	0.2114	0.0079	0.9435	3688.5	55.5	111.1	2278.4	40.9	81.8	1236.3	21.0	42.0	54	
BESZ291	829.00	74.30	65.00	0.089	0.1191	0.0060	3.701	0.180	0.2250	0.0043	0.7810	1942.8	45.0	90.1	1571.6	45.0	38.8	1306.2	11.3	22.6	83	
BESZ2110c	155.40	197.60	74.70	1.263	0.0792	0.0052	1.247	0.082	0.1132	0.0023	0.3341	1177.1	64.9	129.9	822.1	64.9	37.0	691.3	6.7	13.3	84	
BESZ2110r	634.00	420.40	199.00	0.670	0.0990	0.0080	1.530	0.130	0.1113	0.0022	0.9304	1605.4	75.3	150.7	942.5	75.3	52.1	680.3	6.4	12.8	72	
BESZ2124	450.00	257.00	91.40	0.571	0.1048	0.0077	1.261	0.100	0.0873	0.0021	0.6890	1710.8	67.6	135.2	828.4	67.6	22.4	539.5	6.2	12.5	65	
BESZ2134	685.00	482.00	148.60	0.709	0.0783	0.0042	1.045	0.052	0.0980	0.0019	0.1982	1154.5	53.2	106.4	726.4	53.2	25.8	602.7	5.6	11.2	83	
BESZ2136	145.90	74.20	51.60	0.511	0.1150	0.0190	1.710	0.320	0.1084	0.0033	0.8038	1879.9	148.8	297.7	1012.3	148.8	59.9	119.8	683.4	9.6	19.2	66
BESZ2139	907.00	439.00	181.00	0.516	0.1451	0.0023	6.310	0.320	0.3084	0.0057	0.4193	2300.8	13.5	27.0	2019.8	13.5	44.4	1732.8	14.0	28.1	66	
BESZ2152	581.00	227.90	67.30	0.397	0.0607	0.0033	0.872	0.046	0.1026	0.0019	-0.0566	628.6	58.6	117.1	636.7	58.6	12.5	629.6	5.6	11.1	99	
BESZ2162r	1010.00	108.30	111.50	0.108	0.1344	0.0068	4.423	0.220	0.2374	0.0059	0.9010	2156.2	44.1	88.3	1716.7	44.1	20.6	1373.2	15.4	30.7	80	

Footnotes: Analysis references: BESZ2 is zircon from sample BES2 (mount CT118-4), followed by grain number "c" or "r

Chapter IV

Table D.37a: Sample SKH1 (LA-ICP/MS)

IGSN: IEACC00011 Coordinate UTM: Zone 28S, 3748316 m N, 678921 m E

ANALYSIS	U (ppm)	Th (ppm)	Pb (ppm)	Th/U	Ratios			Concordant data			Error correction			Ages (Ma)			Concordance (%)						
					$^{206}\text{Pb}/^{238}\text{U}$	$^{207}\text{Pb}/^{235}\text{U}$	$^{207}\text{Pb}/^{206}\text{Pb}$	$^{206}\text{Pb}/^{238}\text{U}$	$^{207}\text{Pb}/^{235}\text{U}$	$^{207}\text{Pb}/^{206}\text{Pb}$	$^{206}\text{Pb}/^{238}\text{U}$	$^{207}\text{Pb}/^{235}\text{U}$	$^{207}\text{Pb}/^{206}\text{Pb}$	$^{206}\text{Pb}/^{238}\text{U}$	$^{207}\text{Pb}/^{235}\text{U}$	$^{207}\text{Pb}/^{206}\text{Pb}$	σ	2σ	σ	2σ	σ	2σ	
					2σ	2σ	2σ	2σ	2σ	2σ	2σ	2σ	2σ	2σ	2σ	2σ	2σ	2σ	2σ	2σ	2σ	2σ	2σ
SHK121	245.80	179.20	526.00	0.750	7.30E+05	5.00E+05	0.0592	0.0020	0.853	0.033	0.1034	0.0012	0.4254	574.5	36.7	73.5	626.3	9.0	18.1	634.3	3.5	7.0	101
SHK122	69.10	159.20	470.00	2.355	1.70E+05	1.00E+05	0.0641	0.0055	0.868	0.075	0.0992	0.0027	0.1391	744.9	90.7	181.4	634.5	20.4	40.7	609.7	7.9	15.8	96
SHK123	35.78	14.11	65.30	0.404	5.40E+04	7.10E+04	0.0744	0.0060	1.730	0.130	0.2251	0.0038	-0.0247	1052.3	81.2	162.5	634.5	24.2	48.3	1012.7	10.5	20.9	99
SHK124	162.70	151.90	991.00	0.960	8.00E+05	3.50E+05	0.0844	0.0023	2.618	0.076	0.1750	0.0028	0.3304	1301.8	26.5	52.9	1305.7	10.7	21.3	1310.3	7.4	14.7	100
SHK125	74.20	56.40	324.00	0.776	9.00E+05	0.0784	0.0038	0.0030	2.240	0.110	0.2079	0.0033	0.1777	1157.0	48.1	96.2	1193.7	17.2	34.6	1217.6	8.8	17.6	102
SHK126	47.40	22.85	111.90	0.492	1.40E+05	1.10E+05	0.0758	0.0038	1.790	0.120	0.1713	0.0033	0.2589	1089.8	66.1	132.2	1041.8	21.8	43.6	1019.3	9.1	18.2	98
SHK127	117.50	51.20	238.00	0.444	4.00E+05	1.80E+05	0.0737	0.0029	1.782	0.064	0.1752	0.0027	0.0980	1033.3	39.8	79.5	1038.9	11.7	23.5	1040.7	7.4	14.8	100
SHK128	66.70	46.10	141.90	0.699	1.14E+05	9.20E+04	0.0629	0.0049	0.919	0.071	0.1062	0.0021	0.2363	704.9	82.9	165.8	661.8	18.8	37.5	650.6	6.1	12.2	98
SHK129C	42.80	93.40	292.00	2.218	2.80E+05	2.00E+05	0.0600	0.0036	0.923	0.082	0.1143	0.0029	0.1248	603.6	101.0	202.0	663.9	21.6	43.3	697.7	8.4	16.8	105
SHK1211	381.00	182.40	1250.00	0.487	1.18E+06	7.40E+05	0.0890	0.0047	2.360	0.140	0.1923	0.0021	0.5767	1404.2	50.6	101.2	1230.6	21.1	42.3	1139.8	5.7	11.4	92
SHK1212	118.90	91.20	226.40	0.787	1.70E+05	1.60E+05	0.0635	0.0036	0.760	0.045	0.0870	0.0016	0.3285	725.0	60.1	120.2	574.0	13.0	25.9	537.8	4.7	9.5	94
SHK1213	297.00	130.80	626.00	0.444	2.60E+06	0.0735	0.0018	1.796	0.047	0.1768	0.020	0.2629	0.2629	1027.8	24.8	49.5	1044.0	8.5	17.1	1049.5	5.5	11.0	101
SHK1214	115.20	50.30	240.30	0.441	2.70E+05	2.40E+05	0.0630	0.0028	1.663	0.067	0.1755	0.0026	0.2109	898.7	41.9	83.7	994.5	12.8	25.5	1042.3	7.1	14.3	105
SHK1215C	122.10	141.40	392.80	1.164	-2.00E+05	0.0606	0.0034	0.880	0.052	0.1052	0.0018	-0.0756	0.3953	625.1	58.7	117.4	641.0	14.0	28.1	644.8	5.2	10.5	101
SHK1215F	241.80	102.90	285.90	0.425	2.70E+05	3.10E+05	0.0612	0.0024	0.889	0.032	0.1054	0.0012	-0.0756	646.3	42.1	84.3	645.8	8.6	17.2	646.0	3.5	7.0	100
SHK1216	85.70	82.50	229.80	0.984	-2.00E+04	0.0575	0.0044	0.755	0.059	0.0952	0.0016	0.2001	0.2001	510.8	84.1	168.2	571.1	17.1	34.1	586.2	4.7	9.4	103
SHK1217	149.10	183.20	432.00	1.222	5.10E+06	2.70E+06	0.0587	0.0028	0.689	0.034	0.0854	0.0013	0.3151	556.0	52.0	104.0	522.2	10.2	20.4	528.3	3.9	7.7	99
SHK1219	274.00	143.80	673.00	0.514	-3.00E+05	4.30E+05	0.0752	0.0017	1.847	0.046	0.1786	0.0020	0.3957	1073.9	22.7	45.4	1062.4	8.2	16.4	1059.3	5.5	10.9	100
SHK1220	49.40	35.20	133.00	0.617	-1.07E+05	7.30E+04	0.0626	0.0048	0.951	0.071	0.1114	0.0030	0.0528	694.7	81.7	163.4	678.6	18.5	36.9	680.9	8.7	17.4	100
SHK1221	175.30	172.40	819.00	0.970	6.00E+05	3.20E+05	0.0750	0.0021	1.845	0.049	0.1738	0.0023	0.2430	1068.5	28.1	56.3	1061.6	8.7	17.5	1065.9	6.3	12.6	100
SHK1222	79.70	248.00	587.00	1.103	3.10E+05	2.70E+05	0.0617	0.0027	0.746	0.031	0.0885	0.0012	0.1125	663.7	46.9	93.7	565.9	9.0	18.0	546.7	3.6	7.1	97
SHK1223	80.60	80.60	228.00	0.989	5.60E+04	8.00E+04	0.0636	0.0038	0.945	0.059	0.1069	0.0020	0.2383	728.4	63.3	126.6	675.5	15.4	30.8	654.7	5.8	11.6	97
SHK1224	136.70	183.70	474.00	1.312	1.20E+05	1.50E+05	0.0632	0.0036	0.824	0.048	0.0949	0.0013	0.1877	715.0	60.5	121.0	610.3	13.3	26.7	584.5	3.8	7.7	96
SHK1225	103.30	129.80	529.00	1.228	5.00E+05	4.70E+06	0.0729	0.0032	1.611	0.072	0.1608	0.0028	0.2897	1011.2	44.5	89.0	974.5	14.2	28.4	961.2	7.8	15.5	99
SHK1226	412.50	426.40	721.00	1.003	-2.20E+05	2.80E+05	0.0557	0.0026	0.481	0.022	0.0630	0.0009	0.0196	440.4	51.9	103.9	398.8	7.5	15.1	393.8	2.8	5.6	99
SHK1227	81.40	90.70	237.50	1.082	-4.60E+05	2.50E+05	0.0635	0.0044	0.924	0.064	0.1061	0.0018	0.1423	725.0	73.5	147.0	664.5	16.9	33.7	650.1	5.2	10.5	98
SHK1228	41.44	218.7	100.80	0.507	-7.30E+05	4.80E+05	0.0750	0.0051	1.860	0.130	0.1810	0.0032	0.1068	1068.5	68.3	136.7	1067.0	23.1	46.1	1072.4	8.7	17.5	101
SHK1230	683.00	144.00	335.00	0.192	2.00E+05	5.50E+05	0.0620	0.0015	0.877	0.024	0.1029	0.0011	0.4800	674.1	25.9	51.7	639.4	6.5	13.0	631.4	3.2	6.4	99
SHK1231	60.30	34.78	397.20	0.555	3.00E+05	2.50E+05	0.1336	0.0038	7.360	0.190	0.3997	0.0070	0.2789	2145.8	24.8	49.7	2156.1	11.5	23.1	2167.7	16.1	32.2	101
SHK1232	441.00	184.40	2091.00	0.403	9.00E+06	4.70E+06	0.1788	0.0015	12.180	0.130	0.4915	0.0044	0.6472	2641.8	70.0	13.9	2618.4	5.0	10.0	2577.2	9.5	19.0	98
SHK1233	203.90	228.70	549.00	1.044	1.40E+05	1.70E+05	0.0627	0.0027	0.792	0.035	0.0937	0.0016	0.2590	656.8	47.1	94.2	592.3	9.9	19.8	577.4	4.7	9.4	97
SHK1234	189.50	99.50	246.70	0.677	2.30E+05	4.70E+05	0.0615	0.0024	0.831	0.083	0.2837	0.0035	0.2318	1580.7	23.0	46.0	1599.3	8.7	17.4	1610.0	8.8	17.6	101
SHK1235	174.00	147.00	729.00	0.826	-1.70E+05	5.70E+05	0.1392	0.0049	6.980	0.290	0.3660	0.0055	0.5908	2204.8	30.8	61.5	2108.9	18.4	36.9	2010.6	13.0	26.0	95
SHK1236	65.70	57.30	605.00	0.802	-2.00E+05	2.30E+05	0.1439	0.0034	8.750	0.230	0.4354	0.0068	0.5030	2274.7	20.4	40.7	2312.3	12.0	23.9	2330.0	15.3	30.5	101
SHK1237	222.00	132.90	721.00	0.571	2.50E+05	4.20E+05	0.0804	0.0018	2.410	0.057	0.1282	0.0022	0.2574	1206.8	23.0	44.1	1245.6	8.5	17.0	1272.4	5.8	11.6	102
SHK1238	257.60	164.20	323.00	0.610	-1.60E+05	2.00E+05	0.0613	0.0037	0.569	0.038	0.0672	0.0012	0.4301	649.8	64.8	129.6	457.4	12.3	24.6	419.3	3.6	7.2	92
SHK1239	467.00	62.80	145.00	0.130	1.80E+05	4.40E+05	0.0606	0.0018	0.846	0.024	0.1018	0.0012	0.0921	625.1	35.0	64.0	622.5	6.6	13.2	624.9	3.5	7.0	100
SHK1240	38.60	260.00	2034.00	5.952	1.00E+06	1.20E+05	0.1218	0.0052	0.680	0.250	0.3609	0.0071	0.1368	1982.8	38.0	76.0	1987.4	17.9	35.8	1986.4	16.8	33.6	100
SHK1241	241.00	46.93	437.00	0.187	2.90E+06	2.30E+06	0.1343	0.0019	6.997	0.090	0.3747	0.0039	0.3769	2154.9	11.7	23.4	2111.0	5.7	11.4	2051.5	9.1	18.3	97
SHK1242	275.70	536.00	1485.00	1.863	1.70E+05	2.60E+05	0.0595	0.0019	0.876	0.029	0.1071	0.0013	0.3143	585.4	34.7	69.3	638.8	7.8	15.7	655.9	3.8	7.6	103
SHK1243	116.60	232.00	453.00	1.862	-2.40E+05	1.40E+05	0.0563	0.0039	0.584	0.042	0.0746	0.0015	0.1292	464.2	76.7	153.5	467.0	13.4	26.9	463.8	4.5	9.0	99
SHK1244	114.00	72.30	368.00	0.615	6.00E+05	3.70E+05	0.0824	0.0027	2.246	0.077	0.1978	0.0026	0.3490	1255.0	32.0	64.1	1195.5	12.0	24.1	1163.5	7.0	14.0	97
SHK1245	285.70	110.50	484.00	0.371	9.00E+05	3.70E+05	0.0715	0.0017	1.612	0.036	0.1635	0.0019	0.1989	971.7	24.2	48.5	974.9	7.0	14.0	976.2	5.3	10.5	100
SHK1246	115.80	80.30	746.00	0.666	6.00E+06	2.50E+06	0.1270	0.0027	6.840	0.150	0.3875	0.0047	0.3632	2056.9	18.8	37.5	2090.9	9.7	19.4	2111.2	10.9	21.8	101
SHK1247	360.80	929.00	2285.00	2.470	-6.00E+05	2.50E+05	0.0617	0.0020	0.772	0.027	0.0911	0.0015	0.4746	663.7	34.7	69.4	580.9	7.7	15.5	562.0	4.4	8.9	97
SHK1248	143.60	108.60	259.20	0.730	-2.00E+05	1.50E+05</																	

ANALYSIS	U (ppm)	Th (ppm)	Pb (ppm)	Th/U	Ratios			Error correction			Ages (Ma)			Concordance (%)					
					$^{207}\text{Pb}/^{206}\text{Pb}$	$^{207}\text{Pb}/^{235}\text{U}$	$^{206}\text{Pb}/^{238}\text{U}$	$^{207}\text{Pb}/^{206}\text{Pb}$	$^{207}\text{Pb}/^{235}\text{U}$	$^{206}\text{Pb}/^{238}\text{U}$	$^{207}\text{Pb}/^{206}\text{Pb}$	$^{207}\text{Pb}/^{235}\text{U}$	$^{206}\text{Pb}/^{238}\text{U}$	σ	2σ				
SHK1263	188.40	343.00	760.00	1.799	1.30E+05	0.0028	0.656	0.034	0.0855	0.0013	0.2278	512.2	10.4	20.8	528.9	3.9	7.7	103	
SHK1264	104.00	240.40	626.00	2.328	8.90E+04	0.0035	0.843	0.046	0.0998	0.0017	0.0647	620.8	12.7	25.3	613.2	5.0	10.0	99	
SHK1265	135.70	36.69	201.30	2.827	1.70E+05	0.0024	2.372	0.081	0.2104	0.0034	0.3883	1234.2	12.2	24.4	1230.9	9.1	18.1	100	
SHK1266	68.50	78.00	200.40	1.140	8.10E+05	0.0050	0.786	0.067	0.0932	0.0035	0.2046	588.9	19.0	38.1	574.4	5.6	11.2	98	
SHK1267	43.50	47.90	167.90	1.096	4.50E+05	0.0057	1.210	0.100	0.1315	0.0035	0.1471	840.9	88.4	176.8	796.4	10.0	19.9	99	
SHK1268	215.00	202.00	427.00	0.928	6.00E+05	0.0025	0.916	0.037	0.1034	0.0016	0.3057	660.2	9.8	19.6	634.3	4.7	9.3	96	
SHK1270	143.60	167.40	1472.00	1.176	5.00E+05	0.0027	6.020	0.140	0.3544	0.0048	0.3288	1980.0	19.6	39.3	1978.7	11.4	22.8	99	
SHK1271	308.00	350.00	921.00	1.152	2.40E+05	0.0033	8.805	0.040	0.0986	0.0014	0.3626	599.6	11.2	22.5	606.2	4.1	8.2	101	
SHK1273	96.70	80.00	1077.00	0.835	5.00E+05	0.0035	16.600	0.360	0.5743	0.0075	0.6170	2912.0	10.4	20.8	2925.5	15.4	30.7	100	
SHK1274	123.90	67.10	163.80	0.553	4.90E+04	0.0059	0.717	0.042	0.0887	0.0017	0.1161	548.9	12.4	24.8	547.8	5.0	10.1	100	
SHK1275	524.00	440.00	1037.00	0.853	2.50E+06	0.0593	0.694	0.021	0.0850	0.0010	0.2680	535.2	6.3	12.6	526.1	3.0	5.9	96	
SHK1276	174.80	210.00	488.00	1.178	9.70E+05	0.0056	0.710	0.036	0.0869	0.0013	-0.0107	544.7	10.7	21.4	537.2	3.9	7.7	99	
SHK1278	106.80	132.60	343.60	1.271	2.20E+05	0.0058	0.749	0.040	0.0964	0.0016	-0.0228	472.1	11.6	23.2	593.3	4.7	9.4	105	
SHK1279	112.90	36.42	282.20	0.332	1.60E+05	0.0027	4.380	0.110	0.3011	0.0039	0.2342	1709.1	23.7	47.5	1708.6	10.4	20.7	1696.8	
SHK1280	173.40	116.90	310.00	0.693	3.00E+05	0.0026	0.865	0.037	0.1007	0.0015	0.1138	674.1	44.8	89.7	692.8	10.1	20.1	618.5	
SHK1282	163.10	102.40	814.00	0.623	5.00E+05	0.0024	6.600	0.220	0.3570	0.0100	0.8403	2153.6	15.6	31.2	1967.9	23.8	47.5	95	
SHK1283	116.90	114.90	1114.00	0.985	7.70E+05	0.0029	6.940	0.160	0.3873	0.0050	0.2404	2070.7	10.2	20.4	2110.3	11.6	23.2	100	
SHK1284	247.00	190.20	386.00	0.793	7.00E+05	0.0025	0.565	0.025	0.0724	0.0009	0.2456	460.3	49.3	98.6	454.8	8.1	16.2	5.7	
SHK1285	173.40	72.50	633.00	0.427	5.00E+05	0.0021	5.390	0.110	0.3495	0.0040	0.4361	1856.2	16.7	33.4	1838.3	8.7	17.5	1936.7	
SHK1286	94.60	74.50	201.00	1.676	1.10E+04	0.0036	0.787	0.048	0.0999	0.0019	0.1018	506.9	69.0	137.9	589.5	13.6	27.3	613.8	
SHK1287	128.50	18.67	109.70	0.150	2.20E+05	0.0024	2.369	0.071	0.2084	0.0038	0.3009	1259.8	28.4	56.8	1233.3	10.7	21.4	1220.3	
SHK1288	24.40	13.98	45.60	0.587	5.00E+04	0.0096	1.040	0.130	0.1077	0.0040	0.1066	937.1	140.0	280.0	723.9	32.3	64.6	659.4	
SHK1289	170.20	106.70	476.00	0.633	7.40E+05	0.0025	1.688	0.056	0.1661	0.0019	0.0512	1030.5	34.3	68.7	1004.0	10.6	21.1	990.6	
SHK1290	78.80	62.30	196.00	0.800	1.30E+05	0.0050	0.997	0.074	0.1088	0.0025	0.0548	834.7	77.9	155.7	702.3	18.8	37.6	665.8	
SHK1291	318.00	148.30	1233.00	0.485	1.00E+07	0.0016	5.237	0.092	0.3109	0.0041	0.8415	1972.5	11.8	23.5	1858.7	7.5	15.0	1745.1	
SHK1292	167.90	128.50	347.00	0.791	2.20E+05	0.0028	0.791	0.039	0.0936	0.0012	0.3739	642.8	49.3	98.5	591.7	11.0	22.1	576.8	
SHK1293	147.00	274.00	790.00	1.215	5.80E+05	0.0040	0.963	0.064	0.1108	0.0024	0.2474	684.4	68.5	137.1	684.8	16.5	33.1	677.4	
SHK1294	18.20	30.00	143.00	1.653	6.90E+05	0.0078	1.900	0.210	0.1805	0.0073	0.2753	1141.8	113.7	227.4	1081.1	36.7	73.5	1069.7	
SHK1296	146.40	47.10	222.30	0.333	1.07E+06	0.0029	1.758	0.069	0.1725	0.0024	0.2243	1038.7	39.6	79.2	1030.1	12.7	25.4	1025.9	
SHK1297	73.20	36.00	110.20	0.325	5.60E+05	0.0025	1.291	0.046	0.1343	0.0021	0.2003	922.5	36.8	73.6	841.7	10.2	20.4	812.3	
SHK1298	118.10	65.50	600.00	0.574	3.20E+05	0.0025	1.763	0.097	0.1579	0.0048	0.0368	1245.5	62.1	124.2	1032.0	17.8	35.6	945.1	
SHK1299	98.10	124.30	550.00	1.314	1.20E+05	0.0039	1.855	0.076	0.3602	0.0050	0.4166	1941.3	18.8	37.6	1970.0	9.5	18.9	1983.1	
SHK12100	172.30	80.90	649.00	0.494	2.90E+04	0.0022	4.526	0.098	0.3061	0.0039	-0.1324	1033.3	53.5	106.9	991.5	14.5	29.0	985.1	
SHK12101	124.80	152.50	1467.00	1.258	7.80E+05	0.0026	6.970	0.130	0.3772	0.0048	0.3853	2141.9	17.0	34.1	2107.6	8.3	16.5	2063.2	
SHK129r	20.60	27.44	91.30	1.351	3.10E+04	0.0025	0.800	0.130	0.1155	0.0042	0.1815	307.2	186.6	373.1	596.8	36.6	73.3	704.6	
SHK1210	142.10	143.40	514.00	1.026	5.00E+05	0.0086	1.140	0.130	0.1089	0.0019	0.5015	1121.2	107.5	215.0	772.5	30.8	61.6	666.4	
SHK1218	200.20	158.80	696.00	0.778	2.50E+05	0.1057	1.440	0.120	0.0971	0.0017	0.5366	1743.8	67.8	135.6	905.7	24.9	49.9	597.4	
SHK1229	743.00	201.00	1350.00	0.262	5.02E+03	0.1119	2.530	0.072	0.1642	0.0030	0.7448	1850.5	17.0	34.0	1280.7	10.3	20.7	980.1	
SHK1261	319.80	396.00	3278.00	1.230	4.70E+05	0.2185	0.0023	1.140	0.200	0.3656	0.0050	81.37	2969.7	8.5	17.0	2534.9	8.4	16.7	2008.7
SHK1269	198.30	120.70	1034.00	0.604	2.37E+05	0.1378	3.530	0.180	0.1856	0.0024	0.4168	2199.7	40.3	80.7	1534.0	20.2	40.3	1097.5	
SHK1272	341.00	312.00	2960.00	0.930	3.60E+05	0.2260	0.0053	11.880	0.380	0.3770	0.0060	0.7142	3023.9	18.8	37.6	2595.0	15.0	29.9	2062.3
SHK1277	246.00	342.00	853.00	1.416	1.80E+05	0.1070	1.150	0.200	0.0778	0.0014	0.6814	1748.9	145.4	290.9	777.2	47.2	94.4	483.0	
SHK1281	795.00	834.00	2900.00	1.081	4.40E+05	0.1482	0.0025	2.571	0.068	0.1282	0.0040	2301.9	14.7	29.4	1292.4	9.7	19.3	777.6	
SHK128r	142.10	143.40	514.00	1.026	5.00E+05	0.0086	1.140	0.130	0.1089	0.0019	0.5015	1121.2	107.5	215.0	772.5	30.8	61.6	666.4	
SHK1218	200.20	158.80	696.00	0.778	2.50E+05	0.1057	1.440	0.120	0.0971	0.0017	0.5366	1743.8	67.8	135.6	905.7	24.9	49.9	597.4	
SHK1229	743.00	201.00	1350.00	0.262	5.02E+03	0.1119	2.530	0.072	0.1642	0.0030	0.7448	1850.5	17.0	34.0	1280.7	10.3	20.7	980.1	
SHK1261	319.80	396.00	3278.00	1.230	4.70E+05	0.2185	0.0023	1.140	0.200	0.3656	0.0050	81.37	2969.7	8.5	17.0	2534.9	8.4	16.7	2008.7
SHK1269	198.30	120.70	1034.00	0.604	2.37E+05	0.1378	3.530	0.180	0.1856	0.0024	0.4168	2199.7	40.3	80.7	1534.0	20.2	40.3	1097.5	
SHK1272	341.00	312.00	2960.00	0.930	3.60E+05	0.2260	0.0053	11.880	0.380	0.3770	0.0060	0.7142	3023.9	18.8	37.6	2595.0	15.0	29.9	2062.3
SHK1277	246.00	342.00	853.00	1.416	1.80E+05	0.1070	1.150	0.200	0.0778	0.0014	0.6814	1748.9	145.4	290.9	777.2	47.2	94.4	483.0	
SHK1281	795.00	834.00	2900.00	1.081	4.40E+05	0.1482	0.0025	2.571	0.068	0.1282	0.0040	2301.9	14.7	29.4	1292.4	9.7	19.3	777.6	
SHK128r	142.10	143.40	514.00	1.026	5.00E+05	0.0086	1.140	0.130	0.1089	0.0019	0.5015	1121.2	107.5	215.0	772.5	30.8	61.6	666.4	
SHK1218	200.20	158.80	696.00	0.778	2.50E+05	0.1057	1.440	0.120	0.0971	0.0017	0.5366	1743.8	67.8	135.6	905.7	24.9	49.9	597.4	
SHK1229	743.00	201.00	1350.00	0.262	5.02E+03	0.1119	2.530	0.072	0.1642	0.0030	0.7448	1850.5	17.0	34.0	1280.7	10.3	20.7	980.1	
SHK1261	319.80	396.00	3278.00	1.230	4.70E+05	0.2185	0.0023	1.140	0.200	0.3656	0.0050	81.37	2969.7	8.5	17.0	2534.9	8.4	16.7	2008.7
SHK1269	198.30	120.70	1034.00	0.604	2.37E+05	0.1378	3.530	0.180	0.1856	0.0024	0.4168	2199.7	40.3	80.7	1534.0	20.2	40.3	1097.5	
SHK1272	341.00	312.00	2960.00	0.930	3.60E+05	0.2260	0.0053	11.880	0.380	0.3770	0.0060	0.7142	3023.9	18.8	37.6	2595.0	15.0	29.9	2062.3
SHK1277	246.00	342.00	853.00	1.416	1.80E+05	0.1070	1.150	0.200	0.0778	0.0014	0.6814	1748.9	145.4	290.9	777.2	47.2	94.4	483.0	
SHK1281	795.00	834.00	2900.00	1.081	4.40E+05	0.1482	0.0025	2.571	0.068	0.1									

ANALYSIS	U (ppm)	Th (ppm)	$^{232}\text{Th}/^{238}\text{U}$	% $^{206}\text{Pb}^c$	Ratios				Ages (Ma)				Discordant (%)							
					$^{201}\text{Pb}/^{206}\text{Pb}$	$\pm\%$	$^{207}\text{Pb}/^{206}\text{Pb}^*$	$\pm\%$	$^{207}\text{Pb}/^{235}\text{U}$	$\pm\%$	$^{206}\text{Pb}/^{238}\text{U}$	$\pm\%$		Error correction	$^{207}\text{Pb}/^{206}\text{Pb}$	σ	2σ	σ	2σ	
SKH1z139	486.00	572.00	1.210	0.230	$1.50\text{E}-04$	$1.80\text{E}+01$	0.2060	0.3000	10.7200	2.1000	0.3770	2.1000	1.0000	2876	6	12	2062	37	74	33

Footnotes:

- . $^{206}\text{Pb}^c$ is % of ^{206}Pb from common Pb
- . Errors are 1-sigma
- . Pb* indicates radiogenic Pb, corrected for common Pb.
- . Analysis references: SKH1z is zircon from sample SKH1 (mount CT18-03), followed by grain number "c" or "r", meaning core or rim, respectively.
- . Error in standard calibration was 0.26% (not included in above errors but required when comparing data from different mounts).

ANALYSIS	U (ppm)	Th (ppm)	Pb (ppm)	Th/U	Ratios				Error correction	Ages (Ma)				Concordance (%)								
					$^{206}\text{Pb}/^{208}\text{Pb}$	$^{207}\text{Pb}/^{208}\text{Pb}$	$^{207}\text{Pb}/^{238}\text{U}$	$^{206}\text{Pb}/^{238}\text{U}$		$^{207}\text{Pb}/^{235}\text{U}$	$^{207}\text{Pb}/^{238}\text{U}$	$^{206}\text{Pb}/^{238}\text{U}$	σ									
AOU1z73	101.40	58.20	19.18	0.570	-3.80E+03	2.00E+03	0.0617	3.10E-03	1.017	0.047	0.1186	0.0020	683.7	53.8	107.6	712.4	11.8	23.6	722.5	5.8	11.5	101
AOU1z74	239.30	255.00	71.70	1.070	-1.09E+04	4.90E+03	0.0625	2.80E-03	0.854	0.036	0.0980	0.0016	691.3	47.8	95.5	626.8	9.8	19.7	602.9	4.7	9.4	96
AOU1z75	264.30	132.70	130.00	0.500	-5.10E+04	2.40E+04	0.1340	5.30E-03	6.985	0.240	0.3698	0.0053	2151.0	34.5	69.1	2107.0	15.3	30.6	2028.5	12.5	24.9	96
AOU1z76	177.00	85.20	62.10	0.480	-7.90E+03	7.60E+03	0.0948	3.90E-03	3.530	0.130	0.2656	0.0039	1524.1	38.8	77.5	1534.0	14.6	29.1	1518.4	9.9	19.9	99
AOU1z77	130.30	108.80	90.40	0.830	-1.80E+04	9.90E+03	0.1059	4.40E-03	4.601	0.170	0.3108	0.0046	1730.0	38.1	76.3	1749.4	15.4	30.8	1744.6	11.3	22.6	100
AOU1z78	103.92	40.01	45.50	0.390	-2.60E+04	1.30E+04	0.1339	5.60E-03	7.510	0.280	0.4045	0.0062	2143.7	36.5	73.0	2174.2	16.7	33.4	2189.7	14.2	28.5	101
AOU1z79	91.30	69.82	43.59	0.760	-7.90E+03	8.00E+03	0.0888	3.70E-03	2.799	0.110	0.2299	0.0035	1356.1	41.1	82.2	1355.3	14.7	29.4	1334.0	9.2	18.3	98
AOU1z80	386.40	396.60	110.90	1.030	-4.20E+04	1.90E+04	0.0604	2.50E-03	0.844	0.033	0.1003	0.0015	617.9	44.7	89.3	621.4	9.1	18.2	616.4	4.4	8.8	99
AOU1z81	270.90	258.00	69.40	0.950	-3.00E+04	2.60E+04	0.0618	2.80E-03	0.828	0.035	0.0969	0.0015	667.2	48.5	97.0	612.5	9.7	19.4	596.0	4.4	8.8	97
AOU1z82	217.90	136.70	141.00	0.630	-1.12E+06	5.40E+05	0.1270	5.10E-03	6.966	0.240	0.3937	0.0059	2056.9	35.4	70.9	2107.1	15.3	30.6	2140.0	13.6	27.3	102
AOU1z83	334.30	165.70	45.20	0.500	1.70E+05	6.80E+04	0.0594	2.50E-03	0.799	0.031	0.0975	0.0015	581.8	45.7	91.4	596.3	8.7	17.5	599.7	4.4	8.8	101
AOU1z84	238.50	230.90	222.60	0.970	2.80E+04	5.10E+04	0.1226	4.90E-03	6.227	0.220	0.3666	0.0054	1994.4	35.5	71.0	2008.2	15.4	30.9	2013.4	12.7	25.5	100
Discordant data																						
AOU1z8	342.00	841.70	298.50	2.460	-1.06E+05	5.20E+04	0.0773	3.30E-03	1.270	0.053	0.1193	0.0018	1128.9	42.5	85.0	832.4	11.8	23.7	726.4	5.2	10.4	87
AOU1z15	776.00	504.00	402.00	0.650	3.60E+05	5.80E+04	0.1524	6.00E-03	5.650	0.200	0.2746	0.0050	2373.0	33.6	67.1	1923.8	15.3	30.5	1564.1	12.6	25.3	81
AOU1z28	590.00	484.00	87.40	0.820	3.20E+03	8.30E+03	0.0782	3.10E-03	0.759	0.029	0.0699	0.0012	1152.0	39.3	78.7	573.4	8.4	16.7	435.4	3.6	7.2	76
AOU1z30	413.00	268.00	132.30	0.650	1.30E+04	2.60E+04	0.1328	5.20E-03	5.300	0.230	0.2952	0.0094	0.9360	34.2	68.5	1868.9	18.5	37.0	1667.5	23.4	46.8	89
AOU1z41	173.70	313.00	182.80	1.800	9.00E+04	1.20E+04	0.1230	5.30E-03	4.920	0.210	0.2823	0.0090	2084.4	36.1	72.3	1805.7	18.0	36.0	1602.9	22.6	45.2	89
AOU1z43	344.90	367.73	32.03	0.110	6.40E+04	3.10E+04	0.1227	4.90E-03	4.384	0.150	0.2644	0.0038	1995.9	35.5	71.0	1709.3	14.1	28.3	1523.3	9.7	19.4	88
AOU1z55	564.00	385.00	139.20	0.680	-1.30E+05	7.20E+04	0.0836	3.20E-03	1.574	0.058	0.1355	0.0025	1283.3	37.3	74.6	960.0	11.4	22.9	819.2	7.1	14.2	85
AOU1z56	502.00	359.00	243.00	0.720	-2.10E+05	1.30E+05	0.2096	8.20E-03	9.240	0.340	0.3248	0.0065	2894.7	31.9	63.8	2362.1	16.8	33.7	1813.1	15.8	31.6	77
AOU1z62	129.00	117.80	33.40	0.910	-5.30E+03	3.20E+03	0.0757	4.30E-03	0.891	0.047	0.0863	0.0024	1087.1	56.9	113.9	646.9	12.6	25.2	533.6	7.1	14.2	82
AOU1z65	911.00	700.00	205.80	0.770	-5.60E+04	2.30E+04	0.1791	6.70E-03	3.865	0.150	0.1548	0.0033	2644.6	31.0	62.1	1806.4	15.6	31.3	927.8	9.2	18.4	58
AOU1z67	436.00	375.00	131.20	0.860	-2.30E+04	1.00E+04	0.0741	3.90E-03	1.058	0.056	0.1040	0.0017	1044.2	53.1	106.2	732.8	13.8	27.6	637.8	5.0	9.9	87
AOU1z70	575.00	67.80	28.60	0.120	-1.27E+04	7.00E+03	0.0708	2.80E-03	0.855	0.032	0.0873	0.0014	951.6	40.5	80.9	627.4	8.8	17.5	539.7	4.2	8.3	86

Footnotes:

. Analysis references: AOU1z is zircon from sample AOU1 (mount CT19-1), followed by grain number "c" or "r", meaning core or rim, respectively.

ANALYSIS	U (ppm)	Th (ppm)	Pb (ppm)	Th/U	Ratios				Error correction	Ages (Ma)				Concordance (%)							
					$^{206}\text{Pb}/^{208}\text{Pb}$	$^{207}\text{Pb}/^{208}\text{Pb}$	$^{207}\text{Pb}/^{238}\text{U}$	$^{206}\text{Pb}/^{238}\text{U}$		2σ	$^{207}\text{Pb}/^{235}\text{U}$	σ	2σ		$^{206}\text{Pb}/^{208}\text{U}$	σ	2σ				
OU42139	290.20	354.70	92.80	1.220	-1.44E+05	9.50E+04	0.0590	0.028	0.0909	0.0012	0.1773	529.8	37.8	75.5	568.8	8.1	16.2	560.7	3.5	7.1	99
OU42141	326.00	369.00	97.80	1.130	1.00E+05	1.00E+05	0.0644	0.033	0.0983	0.0013	0.1913	754.8	36.1	72.1	650.1	8.8	17.6	604.6	3.8	7.6	93
OU42142	106.50	64.60	39.30	0.610	8.90E+04	7.00E+04	0.0857	0.033	0.2222	0.0029	0.1673	1331.4	32.7	65.5	1324.6	13.3	26.7	1293.5	7.6	15.3	98
OU42143	798.00	1860.00	121.80	2.330	4.00E+05	3.60E+05	0.0772	0.055	0.1624	0.0025	0.6388	1126.9	27.1	54.2	1030.5	10.1	20.2	970.1	6.9	13.9	94
OU42144	365.00	248.00	56.60	0.700	1.50E+05	1.20E+05	0.0574	0.025	0.0857	0.0012	0.2669	506.9	36.4	72.8	535.2	7.5	15.0	530.1	3.6	7.1	99
OU42147	566.00	216.60	58.10	0.390	1.30E+05	1.70E+05	0.0608	0.026	0.0894	0.0010	0.2100	632.2	33.6	67.3	576.3	7.5	15.0	551.9	3.0	5.9	96
OU42148	456.00	194.10	49.99	0.430	1.50E+05	2.00E+05	0.0726	0.051	0.1484	0.0024	0.6312	1002.8	29.4	58.7	934.4	10.3	20.6	892.0	6.7	13.5	95
Discordant data																					
OU424	802.00	122.10	96.50	0.150	4.00E+05	2.10E+05	0.1050	0.084	0.1803	0.0026	0.8425	1714.3	25.4	50.8	1291.6	11.9	23.9	1068.6	7.1	14.2	83
OU4212	456.00	444.00	129.70	0.970	2.00E+05	1.30E+05	0.0695	0.033	0.0912	0.0012	0.4434	913.6	35.5	71.1	629.0	9.0	18.0	562.3	3.5	7.1	89
OU4223	332.40	657.90	344.30	1.980	4.60E+05	2.40E+05	0.1169	0.110	0.2165	0.0033	0.7106	1909.4	24.6	49.1	1527.7	12.4	24.8	1263.4	8.7	17.5	83
OU4224	1123.00	597.00	117.70	0.530	-1.48E+06	7.00E+05	0.1279	0.096	0.1809	0.0027	0.7754	2063.7	23.4	46.8	1453.8	11.6	23.3	1071.9	7.4	14.7	84
OU4238f	149.40	72.40	17.83	0.480	2.40E+04	4.70E+04	0.0831	0.069	0.1280	0.0030	0.7020	1271.6	36.4	72.8	914.4	14.2	28.4	776.4	8.6	17.1	85
OU4264	120.20	40.70	53.10	0.340	1.28E+05	6.30E+04	0.1471	0.110	0.1448	0.0019	0.3528	2312.5	28.6	57.2	1383.2	14.3	28.6	871.7	5.3	10.7	63
OU4271	154.50	72.30	35.62	0.470	8.00E+05	1.70E+05	0.1015	0.088	0.1927	0.0025	0.2271	1651.7	28.3	56.6	1324.3	12.1	24.2	1136.0	6.8	13.5	86
OU4293	503.00	579.00	217.20	1.150	6.00E+06	1.30E+06	0.1579	0.160	0.1373	0.0050	0.9882	2433.3	24.1	48.3	1397.4	20.5	41.0	829.4	14.2	28.3	59
OU42104	1368.00	2400.00	154.50	1.750	-6.00E+06	1.20E+06	0.0759	0.021	0.0574	0.0016	0.7897	1092.4	29.0	58.1	471.5	6.7	13.4	359.8	4.9	9.8	76
OU42117	264.50	348.00	83.80	1.370	-3.50E+05	4.90E+05	0.1140	0.140	0.2443	0.0052	0.6153	1864.1	26.9	53.8	1602.6	14.7	29.3	1409.0	13.5	26.9	88
OU42133	320.90	152.50	30.00	0.480	8.00E+04	9.20E+04	0.0656	0.024	0.0666	0.0009	0.3270	793.6	35.2	70.3	503.4	7.4	14.8	427.8	2.7	5.4	85
OU42137	811.00	1213.00	365.00	1.500	-4.70E+05	3.70E+05	0.1148	0.085	0.1656	0.0023	0.7463	1876.7	24.3	48.7	1329.6	11.6	23.3	987.8	6.4	12.7	74
OU42140	903.00	857.00	90.00	0.950	-1.80E+05	1.30E+05	0.0972	0.027	0.0577	0.0011	0.4096	1571.1	30.8	61.7	596.8	7.6	15.2	361.6	3.4	6.7	61
OU42145	683.00	121.10	35.80	0.180	8.00E+05	2.10E+05	0.0702	0.032	0.1044	0.0013	0.2934	934.2	30.7	61.4	718.9	8.0	16.0	640.1	3.8	7.6	89
OU42146	845.00	282.40	58.02	0.330	-1.00E+05	1.60E+05	0.0646	0.021	0.0689	0.0009	0.3950	761.3	32.6	65.3	493.0	6.6	13.1	429.5	2.8	5.6	87
OU42149	941.00	1461.00	198.00	1.550	-1.30E+05	1.90E+05	0.0723	0.024	0.0717	0.0012	0.5302	984.4	29.5	59.0	556.6	7.0	14.1	446.4	3.6	7.2	80

Footnotes:

. Analysis references: OU4z is zircon from sample OU4 (mount CT19-1), followed by grain number "c" or "r", meaning core or rim, respectively.

ANALYSIS	U (ppm)	Th (ppm)	Pb (ppm)	Th/U	Ratios				Error correction			Ages (Ma)				Concordance (%)					
					²⁰⁶ Pb/ ²⁰⁸ Pb	²⁰⁷ Pb/ ²⁰⁸ Pb	²⁰⁷ Pb/ ²³² Th	²⁰⁶ Pb/ ²³⁸ U	2σ	σ	#NUM!	#VALUE!	²⁰⁶ Pb/ ²³⁸ U	2σ	σ	#NUM!	#VALUE!	2σ	σ		
TiF2278	86.90	94.90	89.70	1.080	-1.80E+05	1.30E+05	0.1206	2.30E-03	0.096	0.3596	0.0050	17.0	34.0	1977.7	6.9	13.9	1980.3	11.9	23.7	100	
TiF2279	487.00	118.20	94.40	0.250	-7.30E+05	4.90E+05	0.1103	1.60E-03	0.058	0.3303	0.0046	13.2	26.4	1826.4	4.9	9.7	1839.8	11.1	22.3	101	
TiF2280	562.00	455.00	124.50	0.800	4.00E+05	2.00E+05	0.0630	1.20E-03	0.014	0.1043	0.0003	20.2	40.5	709.2	3.7	7.5	654.9	4.4	8.8	98	
TiF2281	97.40	173.30	35.06	1.270	4.20E+04	4.30E+04	0.0602	2.30E-03	0.842	0.3014	0.0015	-0.0471	82.6	620.2	8.3	16.5	615.2	4.4	8.8	99	
TiF2282	692.00	173.00	54.30	0.250	1.00E+05	2.10E+05	0.0665	1.50E-03	0.932	0.1001	0.0014	0.1628	883.7	3.7	7.4	607.0	4.1	8.2	91		
TiF2283	307.60	195.80	203.80	0.640	-6.80E+05	4.10E+05	0.1480	2.10E-03	8.676	0.100	0.4243	0.0057	6.256	2322.9	12.2	24.3	2304.6	12.9	25.8	99	
TiF2284	115.80	98.10	42.32	0.850	5.00E+04	7.30E+04	0.0685	2.00E-03	1.414	0.037	0.1091	0.0021	0.2399	863.7	30.2	60.4	894.8	7.8	15.5	100	
TiF2285	179.40	168.60	59.20	1.050	-1.50E+04	6.40E+04	0.0592	1.80E-03	0.867	0.1068	0.0015	0.1368	574.5	33.1	66.1	654.1	4.4	8.7	103		
TiF2286	55.77	141.20	39.80	2.550	1.10E+04	2.90E+04	0.0559	2.80E-03	0.793	0.039	0.1005	0.0017	0.0896	448.4	55.6	111.3	617.3	5.0	10.0	104	
TiF2288	318.10	221.10	322.80	0.700	1.07E+06	9.20E+05	0.2103	2.80E-03	16.530	0.150	0.5699	0.0072	0.4179	2907.9	10.8	21.6	2908.0	4.3	8.7	100	
TiF2289	326.20	214.00	122.20	0.640	4.00E+05	2.50E+05	0.0824	1.60E-03	2.359	0.034	0.2063	0.0027	0.2881	1250.3	5.1	10.3	1209.1	7.2	14.4	98	
TiF2290	441.90	284.00	228.20	0.640	5.30E+05	5.10E+05	0.1097	1.50E-03	4.369	0.052	0.2873	0.0040	0.6071	1793.9	12.5	24.9	1705.7	4.9	9.8	95	
TiF2294	74.70	35.80	16.89	0.430	-2.60E+04	4.50E+04	0.0709	2.0E-03	1.620	0.047	0.1656	0.0024	0.1609	954.5	31.7	63.5	978.0	9.1	18.2	101	
TiF2295	308.00	440.00	119.00	1.430	-4.00E+05	1.10E+05	0.0592	1.60E-03	0.778	0.1016	0.0953	0.0013	-0.0564	574.5	29.4	58.8	584.3	4.6	9.1	100	
TiF2296	429.70	400.90	190.20	0.930	-1.30E+05	2.90E+05	0.0780	1.80E-03	1.934	0.038	0.1783	0.0025	0.6032	1146.9	20.4	40.8	1092.9	6.6	13.1	97	
TiF2297	326.00	498.00	103.70	1.530	-1.30E+04	7.90E+04	0.0560	1.50E-03	0.979	0.014	0.0748	0.0011	0.2100	462.4	29.7	59.5	463.8	4.5	9.0	100	
TiF2298	130.20	19.34	6.39	0.150	2.00E+04	4.90E+04	0.0614	2.10E-03	0.928	0.030	0.1086	0.0016	0.1535	653.3	36.7	73.4	666.6	7.9	15.8	100	
TiF2299	711.00	228.90	1.080	2.70E+05	2.40E+05	0.0629	1.20E-03	0.911	0.014	0.1048	0.0014	0.3864	705.9	20.3	40.6	657.6	3.7	7.4	98		
TiF2300	779.00	574.00	159.60	0.740	2.00E+05	2.70E+05	0.0606	1.10E-03	0.822	0.011	0.0979	0.0012	0.2705	624.7	19.6	39.1	609.2	3.1	6.1	99	
TiF2301	207.10	110.10	62.00	0.530	-2.40E+05	1.90E+05	0.0930	1.80E-03	3.213	0.052	0.2490	0.0034	0.5001	1487.9	18.3	36.7	1463.3	8.8	17.5	98	
TiF2302	411.50	173.80	54.80	0.420	1.20E+05	1.70E+05	0.0615	1.40E-03	0.941	0.017	0.1110	0.0015	0.1588	667.8	24.4	48.8	673.4	4.4	8.9	101	
TiF2304	162.40	108.60	17.91	0.670	-3.90E+04	4.10E+04	0.0541	2.20E-03	0.455	0.018	0.0808	0.0010	-0.0213	375.2	45.8	91.5	380.8	5.9	11.9	100	
TiF2306	275.00	140.00	34.70	0.510	-4.80E+04	8.80E+04	0.0586	1.50E-03	0.751	0.019	0.0930	0.0013	0.2110	582.3	27.9	55.9	568.8	5.2	10.4	101	
TiF2310	625.40	355.80	58.27	0.570	-1.80E+05	1.40E+05	0.0571	1.40E-03	0.440	0.009	0.0550	0.0009	0.2953	495.4	27.0	54.0	369.9	3.3	6.6	93	
TiF2311	148.90	95.40	63.20	0.640	-6.00E+05	1.40E+05	0.0898	1.90E-03	3.035	0.052	0.2439	0.0032	0.2227	1421.3	20.2	40.4	1416.5	6.5	13.1	99	
TiF2312	524.00	190.40	30.80	0.360	-3.00E+05	1.00E+05	0.0600	1.60E-03	0.465	0.010	0.0556	0.0008	-0.0139	603.6	28.9	57.7	348.8	2.3	4.6	90	
TiF2315	173.20	65.10	18.97	0.380	-4.60E+04	6.70E+04	0.0607	1.90E-03	0.842	0.025	0.0959	0.0014	0.1387	628.6	33.7	67.4	620.2	6.9	13.8	99	
TiF2319	557.00	147.00	25.90	0.260	1.10E+05	1.30E+05	0.0554	1.30E-03	0.460	0.009	0.0399	0.0008	0.0436	428.4	26.2	52.3	383.9	3.1	6.2	98	
TiF2322	66.60	75.30	26.09	1.130	3.30E+04	3.00E+04	0.1469	9.90E-03	1.730	0.130	0.0819	0.0018	0.7068	2310.1	57.8	115.7	1019.8	24.2	48.3	50	
TiF2324	0.00	0.00	-0.01	#DIV/0!	no value	no value	no value	no value	no value	no value	no value	no value	no value	no value	no value	no value	no value	no value	no value	no value	50
TiF2325	28.86	36.73	12.90	1.270	2.50E+04	1.30E+04	0.0869	9.90E-03	1.330	0.240	0.0952	0.0028	0.9287	1358.3	109.8	219.6	859.9	52.2	104.5	68	
TiF2316	1950.00	377.00	95.70	0.910	3.00E+05	1.20E+05	0.1105	3.10E-03	0.271	0.007	0.0180	0.0003	0.0657	1807.7	25.5	51.0	243.5	2.7	5.3	47	
TiF2317	1743.00	1674.00	264.70	0.960	3.14E+05	6.80E+04	0.1435	2.80E-03	0.736	0.010	0.0371	0.0006	0.3778	2269.9	16.8	33.6	559.9	2.9	5.8	42	
TiF2322	0.00	0.02	0.02	#DIV/0!	no value	no value	no value	no value	no value	no value	no value	no value	no value	no value	no value	no value	no value	no value	no value	no value	42
TiF2321	1127.00	247.60	37.70	0.220	-4.00E+05	1.90E+05	0.0618	1.30E-03	0.412	0.007	0.0485	0.0006	0.1196	667.2	22.5	45.0	350.4	2.5	5.0	87	
TiF2329	1375.00	1625.00	197.00	1.180	6.70E+05	2.80E+05	0.1522	2.60E-03	1.384	0.028	0.0658	0.0012	0.8704	2370.8	14.6	29.1	882.1	6.0	11.9	47	
TiF2323	3.84	21.12	31.18	5.500	1.20E+04	1.20E+04	0.7590	2.50E-02	42.000	1.400	0.4170	0.0120	0.2965	4846.7	23.5	47.1	3819.1	16.5	33.0	59	
TiF2326	0.00	0.00	0.00	#DIV/0!	no value	no value	no value	no value	no value	no value	no value	no value	no value	no value	no value	no value	no value	no value	no value	no value	59
TiF2339	101.90	57.78	33.76	0.570	8.10E+04	8.00E+04	0.1143	2.70E-03	3.440	0.075	0.2183	0.0033	0.4273	1868.9	21.3	42.6	1513.6	8.6	17.1	84	
TiF2346	0.00	0.00	11.48	#DIV/0!	no value	no value	no value	no value	no value	no value	no value	no value	no value	no value	no value	no value	no value	no value	no value	no value	84
TiF2250	770.00	418.50	213.00	0.540	1.04E+06	5.20E+05	0.1890	3.70E-03	4.450	0.260	0.1682	0.0083	0.9864	2735.5	16.1	32.2	1721.7	24.2	48.4	58	
TiF2257	1096.00	499.00	82.00	0.460	4.00E+05	1.60E+05	0.0705	1.50E-03	0.487	0.008	0.0501	0.0007	0.3160	943.0	21.8	43.6	403.0	2.9	5.7	78	
TiF2260	1263.00	1503.00	172.60	1.180	2.08E+05	3.90E+05	0.1758	3.70E-03	0.710	0.012	0.0299	0.0006	0.3703	2613.6	17.5	35.0	544.7	3.6	7.1	35	
TiF2262	1210.00	834.00	89.60	0.690	2.00E+05	1.90E+05	0.0687	1.40E-03	0.382	0.007	0.0403	0.0007	0.5570	869.4	21.1	42.1	328.3	2.7	5.4	78	
TiF2277	587.00	468.00	173.40	0.790	1.70E+05	7.80E+05	0.2096	2.80E-03	10.700	0.150	0.3673	0.0061	0.8374	2902.5	10.8	21.7	2497.4	6.5	13.0	81	
TiF2285	1413.00	165.00	60.00	0.120	2.90E+05	1.50E+05	0.0927	1.90E-03	0.487	0.009	0.0379	0.0008	0.5918	1481.8	19.4	38.8	402.7	2.9	5.8	60	
TiF2291	16.15	141.80	99.40	8.780	2.68E+04	6.30E+03	0.6220	1.70E-02	22.890	0.810	0.2679	0.0084	0.7181	4560.2	19.8	39.6	3222.3	17.2	34.4	47	
TiF2292	815.00	321.00	148.40	0.390	2.90E+05	4.40E+05	0.0985	1.60E-03	2.164	0.029	0.1594	0.0024	0.7369	1595.9	15.2	30.3	1169.6	4.6	9.3	82	
TiF2293	159.10	79.50	85.70	0.500	-1.40E+05	1.80E+05	0.1328	2.30E-03	5.326	0.080	0.2899	0.0039	0.4332	2135.3	15.1	30.3	1873.0	6.4	12.8	88	
TiF22103	1071.00	554.00	172.80	0.520	9.50E+05	9.10E+05	0.1637	2.60E-03	5.743	0.086	0.2552	0.0048	0.8793	2494.2	13.4	26.8	1937.9	6.5	12.9	76	
TiF22107	499.00	579.00	147.30	1.160	6.00E+05	1.50E+05	0.0851	1.80E-03	1.083	0.007	0.0394	0.0007	0.1419	940.0	24.7	49.5	329.2	2.4	4.8	76	
TiF22105	485.00	445.00	177.20	1.060	1.50E+05	1.50E+05	0.0682	1.80E-03	1.083	0.017	0.0930	0.0015	0.3165	1317.8	20.5	41.0	748.1	4.1	8.3	77	
TiF22108	970.00	601.00	64.10	0.660	-9.00E+05	1.20E+05	0.0647	1.80E-03	0.489	0.010	0.0552	0.0010	0.3876	780.8	24.2	48.4	404.1	3.4	6.7	86	
TiF22111	518.00	214.00	36.40	0.370	3.00E+05	1.10E+05	0.0655	1.80E-03	0.496	0.009	0.0488	0.0008	0.2897	764.6	29.3	58.6	362.0	3.1	6.1	85	
TiF22114	1082.00	832.00	155.80	0.770	5.10E+05	1.60E+05	0.1300	2.20E-03	1.201	0.031	0.0669	0.0018	0.9154	2096.0							

Chapter IV

Table D 44: Sample OUU16 (LA-ICPMS)

IGSN: IEACC00018 Coordinate UTM: Zone 30S, 3796135 m N, 587342 m E

ANALYSIS	U (ppm)	Th (ppm)	Pb (ppm)	Th/U	Ratios					Error correction	Ages (Ma)					Concordance (%)				
					$^{207}\text{Pb}/^{235}\text{U}$		$^{206}\text{Pb}/^{238}\text{U}$		2σ		σ	2σ	σ	2σ	σ		2σ	σ		
					2σ	σ	2σ	σ											2σ	σ
OUU16z1	213.20	230.40	243.80	1.080	2.40E-03	0.1367	7.594	0.200	0.3961	0.0034	0.1829	2185.8	15.3	30.5	2184.2	11.8	23.6	2151.1	9.0	18.0
OUU16z2	59.70	44.20	45.50	0.740	3.00E-03	0.1378	7.700	0.220	0.3992	0.0047	0.2391	2199.7	18.9	37.8	2196.6	12.8	25.7	2185.4	10.8	21.7
OUU16z3	168.80	111.20	171.80	0.680	2.80E-03	0.0545	0.399	0.020	0.0534	0.0007	0.0136	391.8	57.6	115.3	340.9	7.3	14.5	335.1	2.1	4.2
OUU16z4	268.00	266.10	277.00	0.990	2.20E-03	0.0625	0.864	0.027	0.1014	0.0011	0.1317	694.7	37.5	74.9	632.3	7.3	14.7	622.4	3.2	6.4
OUU16z5	430.40	189.50	184.70	0.440	2.10E-03	0.1272	6.622	0.170	0.3728	0.0035	0.3538	2059.6	14.6	29.1	2062.3	11.3	22.6	2042.6	8.2	16.4
OUU16z6	290.50	37.54	37.54	0.180	2.20E-03	0.1272	6.700	0.180	0.3779	0.0039	0.3713	2059.6	15.3	29.7	2072.6	11.9	23.7	2066.5	9.1	18.2
OUU16z7	283.60	179.90	57.45	0.680	2.20E-03	0.0639	0.963	0.031	0.1096	0.0012	0.1873	738.3	36.4	72.9	684.8	8.0	16.0	670.1	3.5	7.0
OUU16z8	395.00	383.00	54.70	0.970	2.10E-03	0.0534	0.368	0.014	0.0503	0.0006	0.0871	345.8	44.5	89.0	318.2	5.2	10.4	316.3	1.8	3.6
OUU16z9	496.20	328.30	50.30	0.660	2.10E-03	0.0554	0.400	0.014	0.0527	0.0008	0.0892	428.4	42.3	84.5	341.6	5.1	10.1	331.3	1.7	3.4
OUU16z10	422.00	64.50	25.77	0.150	2.40E-03	0.0750	1.336	0.056	0.1300	0.0036	0.8871	1068.5	32.2	64.3	861.5	12.2	24.3	787.9	10.3	20.5
OUU16z11	259.10	137.00	19.95	0.530	2.50E-03	0.0545	1.362	0.015	0.0492	0.0006	0.1273	391.7	51.5	102.9	313.7	5.6	11.2	309.8	1.8	3.7
OUU16z12	239.80	145.83	43.19	0.610	2.10E-03	0.0600	0.840	0.028	0.1018	0.0011	0.2255	603.6	37.9	75.7	619.1	7.7	15.4	624.7	3.2	6.4
OUU16z13	124.00	124.60	32.10	1.000	2.90E-03	0.0610	0.766	0.034	0.0914	0.0012	0.0870	639.2	51.1	102.3	577.5	9.8	19.5	563.8	3.5	7.1
OUU16z14	257.70	330.20	88.10	1.280	2.30E-03	0.0634	0.774	0.026	0.0889	0.0010	0.1632	721.7	38.5	77.0	582.1	7.4	14.9	549.0	2.9	5.9
OUU16z15	213.60	156.70	43.13	0.730	2.40E-03	0.0615	0.818	0.036	0.0962	0.0010	0.2020	656.8	41.8	83.7	592.3	8.4	16.7	592.3	2.9	5.9
OUU16z16	223.30	100.30	28.96	0.450	2.40E-03	0.0627	0.902	0.032	0.1050	0.0011	0.1115	698.1	40.8	81.5	652.8	8.5	17.1	643.5	3.2	6.4
OUU16z17	322.60	298.50	48.20	0.890	2.20E-03	0.0556	0.408	0.015	0.0532	0.0006	0.0710	436.4	44.0	88.1	347.4	5.4	10.8	334.0	1.9	3.7
OUU16z18	224.60	179.40	74.10	0.800	3.90E-03	0.0696	1.317	0.043	0.1372	0.0014	0.2675	916.6	35.5	70.9	853.2	9.4	18.8	828.8	4.0	7.9
OUU16z19	1038.00	164.20	21.35	0.160	1.90E-03	0.0566	0.371	0.011	0.0483	0.0006	0.2755	476.0	37.1	74.2	320.1	4.1	8.1	303.8	2.0	3.9
OUU16z20	889.00	480.00	55.00	0.540	1.90E-03	0.0550	0.350	0.011	0.0471	0.0009	0.4155	412.2	38.6	77.2	304.4	4.1	8.3	296.8	2.6	5.3
OUU16z21	214.70	202.50	55.27	0.940	2.00E-03	0.0598	0.792	0.028	0.0962	0.0011	0.1047	596.3	39.9	79.7	592.3	7.9	15.9	591.8	3.2	6.5
OUU16z22	98.10	75.00	76.20	0.760	2.80E-03	0.1288	6.756	0.126	0.3813	0.0039	0.1871	2081.3	17.8	35.5	2080.0	12.4	24.9	2082.4	9.1	18.2
OUU16z23	25.16	20.82	20.82	0.750	3.50E-03	0.1060	4.450	0.170	0.3048	0.0039	0.0980	1731.7	30.3	60.6	1721.7	15.8	31.6	1715.1	9.6	19.3
OUU16z24	271.00	155.40	22.16	0.570	2.40E-03	0.0517	0.363	0.016	0.0499	0.0006	-0.0704	272.2	53.2	106.4	314.5	6.0	11.9	314.2	1.9	3.7
OUU16z25	114.00	114.10	91.90	0.990	2.40E-03	0.1107	4.666	0.140	0.3074	0.0034	0.2187	1810.9	19.7	39.4	1761.2	12.5	25.1	1727.9	8.4	16.8
OUU16z26	271.00	245.00	292.10	1.350	2.80E-03	0.1740	10.820	0.320	0.4488	0.0067	0.9237	2896.5	13.4	26.8	2807.8	13.7	27.5	2389.9	14.9	29.8
OUU16z27	63.85	89.97	26.42	0.410	2.70E-03	0.0588	0.810	0.041	0.1011	0.0015	0.1530	593.3	59.3	118.6	602.5	11.5	23.0	620.9	4.4	8.8
OUU16z28	413.00	259.00	54.40	0.630	3.60E-03	0.0576	0.612	0.020	0.0770	0.0008	0.1586	514.6	38.1	76.3	484.8	6.3	12.6	478.0	2.3	4.6
OUU16z29	137.80	64.64	66.63	0.470	4.70E-03	0.1312	7.100	0.190	0.3927	0.0041	0.2138	1141.1	16.0	32.1	1214.0	11.9	23.8	2135.3	9.5	19.0
OUU16z30	466.60	414.60	126.80	0.890	2.00E-03	0.0618	0.922	0.027	0.1085	0.0011	0.0226	667.2	34.6	69.3	663.4	7.1	14.3	663.8	3.2	6.4
OUU16z31	38.54	15.52	15.26	0.400	3.50E-03	0.1294	6.760	0.220	0.3828	0.0045	-0.0385	2048.5	24.5	48.9	2080.5	14.4	28.8	2089.4	10.5	21.0
OUU16z32	374.70	523.70	150.50	1.400	2.90E-03	0.0617	0.851	0.027	0.1000	0.0010	0.1368	663.7	36.5	72.9	625.2	7.4	14.8	614.2	2.9	5.9
OUU16z33	399.70	170.80	47.10	0.500	1.00E-04	0.0592	0.759	0.025	0.0929	0.0010	0.0083	574.5	38.6	77.1	573.4	7.2	14.4	572.7	2.8	5.6
OUU16z34	702.20	429.10	66.49	0.610	1.09E-05	0.0557	0.411	0.013	0.0539	0.0006	0.1839	440.4	37.9	75.9	349.7	4.7	9.3	338.7	1.7	3.4
OUU16z35	181.00	76.20	21.70	0.420	2.40E-04	0.0607	0.824	0.031	0.0986	0.0011	-0.0587	628.6	42.6	85.2	628.6	8.6	17.2	606.0	3.2	6.5
OUU16z36	233.80	107.70	15.60	0.460	8.70E-04	0.0535	0.375	0.023	0.0540	0.0007	0.0583	350.1	50.7	101.4	323.4	5.9	11.8	321.6	1.9	3.9
OUU16z37	99.90	99.90	15.44	0.710	2.55E-04	0.0539	0.849	0.031	0.1034	0.0013	0.0443	366.9	64.8	129.6	345.7	8.3	16.6	339.3	2.3	4.5
OUU16z38	102.30	86.77	25.92	0.850	8.00E-05	0.0588	0.849	0.031	0.1034	0.0013	0.0443	366.9	64.8	129.6	345.7	8.3	16.6	339.3	2.3	4.5
OUU16z39	176.10	191.60	56.40	1.090	1.89E-04	0.0628	0.873	0.031	0.1020	0.0012	0.0712	701.5	40.7	81.4	631.2	8.4	16.8	626.3	3.5	7.0
OUU16z40	227.50	157.00	29.39	0.690	1.77E-05	0.0525	0.392	0.016	0.0540	0.0006	-0.0646	307.2	52.1	104.1	335.8	9.3	18.6	338.8	1.9	3.7
OUU16z41	154.10	104.40	29.36	0.680	1.47E-04	0.0589	0.803	0.033	0.0978	0.0012	-0.0368	583.4	48.1	96.2	598.5	5.8	11.7	601.7	3.5	7.0
OUU16z42	196.13	93.40	23.48	0.480	3.70E-03	0.0598	0.750	0.027	0.0907	0.0011	0.1649	596.3	39.9	79.7	568.2	7.8	15.7	559.6	3.3	6.5
OUU16z43	244.50	139.70	164.90	0.570	1.10E-04	0.1608	10.286	0.270	0.4554	0.0044	0.2747	2464.1	14.2	28.4	2460.8	12.1	24.3	2419.2	9.7	19.5
OUU16z44	103.30	100.30	26.64	0.970	2.21E-03	0.0637	0.874	0.039	0.0991	0.0013	0.1113	731.7	48.2	96.4	637.7	10.6	21.1	609.1	3.8	7.6
OUU16z45	276.30	53.99	15.60	0.200	1.30E-05	0.0616	0.876	0.028	0.1034	0.0011	0.1400	660.3	36.5	73.1	638.8	7.6	15.1	634.2	3.2	6.4
OUU16z46	254.50	129.50	20.72	0.510	4.90E-03	0.0559	0.418	0.018	0.0539	0.0006	0.0665	448.4	49.7	99.4	354.6	6.4	12.9	338.2	1.9	3.9
OUU16z47	347.00	308.70	87.11	0.890	1.12E-04	0.0597	0.807	0.025	0.0985	0.0010	0.1153	592.7	36.3	72.6	600.8	7.0	14.0	605.5	2.9	5.9
OUU16z48	14.58	12.02	4.14	0.820	6.00E-03	0.0724	1.187	0.100	0.1198	0.0028	0.2883	997.2	91.2	182.4	794.6	23.2	46.4	729.4	8.1	16.1
OUU16z49	598.00	345.00	84.60	0.580	2.40E-04	0.0642	0.944	0.023	0.0844	0.0011	0.3943	748.2	34.6	69.1	565.9	6.7	13.4	522.6	3.3	6.5
OUU16z50																				

ANALYSIS	U (ppm)	Th (ppm)	Pb (ppm)	Th/U	$^{207}\text{Pb}/^{206}\text{Pb}$	$^{208}\text{Pb}/^{206}\text{Pb}$	$^{207}\text{Pb}/^{238}\text{U}$	$^{206}\text{Pb}/^{238}\text{U}$	Error correction	$^{207}\text{Pb}/^{206}\text{Pb}$	$^{207}\text{Pb}/^{235}\text{U}$	$^{207}\text{Pb}/^{235}\text{U}$	$^{206}\text{Pb}/^{238}\text{U}$	σ	Ages (Ma)	σ	Concordance (%)							
OUJ16273	177.80	319.00	329.00	1.790	-9.30E+03	5.80E+03	7.081	0.190	0.3887	0.0038	0.0038	0.0038	0.0038	16.4	2083.0	16.4	2121.7	11.9	23.9	2116.8	8.8	17.6	100	
OUJ16274	284.40	84.90	79.90	0.320	-1.30E+04	1.20E+04	5.880	0.160	0.3427	0.0033	0.0033	0.0033	0.0033	16.0	1958.3	16.0	1958.3	11.8	23.6	1899.6	7.9	15.8	97	
OUJ16275	311.50	311.70	80.00	1.000	4.00E+04	1.90E+04	0.770	0.026	0.0903	0.0009	0.0009	0.0009	0.0009	38.4	656.7	38.4	579.8	7.5	14.9	557.4	2.7	5.5	96	
OUJ16276	591.00	692.00	163.10	0.770	6.90E+04	6.06E7	0.806	0.024	0.0878	0.0012	0.0012	0.0012	0.0012	32.9	600.2	32.9	600.2	6.7	13.5	542.7	3.6	7.1	90	
OUJ16277	504.00	472.10	64.40	0.790	-4.10E+04	1.90E+04	0.863	0.015	0.0494	0.0013	0.0013	0.0013	0.0013	43.4	480.3	43.4	329.2	5.5	11.0	310.8	4.0	8.0	94	
OUJ16278	435.00	97.90	61.35	0.230	2.43E+04	7.90E+03	3.195	0.092	0.2442	0.0034	0.0034	0.0034	0.0034	28.0	1514.1	28.0	1456.0	11.1	22.2	1408.5	8.8	17.6	97	
OUJ16279	77.50	106.30	30.80	1.370	-3.50E+03	4.20E+03	0.890	0.042	0.1008	0.0015	0.0015	0.0015	0.0015	52.4	104.9	52.4	646.4	11.3	22.5	619.1	4.4	8.8	96	
OUJ16280	37.01	42.35	12.01	1.140	-5.20E+02	3.20E+02	0.869	0.053	0.1024	0.0017	0.0017	0.0017	0.0017	67.1	67.6	67.1	635.0	14.4	28.8	628.5	5.0	9.9	99	
OUJ16281	150.40	109.60	61.05	0.800	-9.00E+02	1.00E+03	1.812	0.057	0.1749	0.0019	0.0019	0.0019	0.0019	34.9	1065.8	34.9	1049.8	10.3	20.6	1039.1	5.2	10.4	99	
OUJ16282	98.90	109.80	50.20	1.110	6.00E+04	1.80E+04	1.715	0.060	0.1676	0.0019	0.0019	0.0019	0.0019	38.2	76.5	38.2	1014.2	11.2	22.4	998.9	5.2	10.5	98	
OUJ16283	220.80	193.60	48.10	0.800	-1.80E+03	1.20E+03	0.804	0.029	0.0912	0.0010	0.0010	0.0010	0.0010	41.3	741.6	41.3	593.1	8.2	16.2	562.7	3.0	5.9	94	
OUJ16284	337.20	338.30	90.80	1.000	4.80E+03	3.20E+03	0.782	0.026	0.0945	0.0010	0.0010	0.0010	0.0010	38.0	76.1	38.0	586.6	7.1	14.2	582.2	2.9	5.8	99	
OUJ16285	298.10	235.30	105.70	0.780	7.70E+03	3.90E+03	1.824	0.048	0.1637	0.0016	0.0016	0.0016	0.0016	32.5	965.3	32.5	973.9	9.3	18.6	977.0	4.4	8.9	100	
OUJ16286	249.40	212.50	59.40	0.850	1.00E+03	1.70E+03	0.893	0.029	0.0995	0.0011	0.0011	0.0011	0.0011	40.9	81.8	40.9	611.7	8.0	16.1	611.7	3.2	6.4	99	
OUJ16287	26.94	32.89	32.72	1.220	-8.00E+02	1.00E+03	6.650	0.230	0.3791	0.0051	0.0051	0.0051	0.0051	20.7	2066.0	20.7	2066.0	15.3	30.5	2072.1	11.9	23.8	100	
OUJ16288	325.50	94.40	18.54	0.290	2.94E+04	8.80E+03	0.619	0.022	0.0785	0.0009	0.0009	0.0009	0.0009	40.6	81.2	40.6	483.2	6.9	13.8	487.0	2.6	5.1	100	
OUJ16289	117.80	113.10	32.43	0.960	4.30E+03	2.40E+03	0.867	0.035	0.0949	0.0012	0.0012	0.0012	0.0012	46.1	92.2	46.1	633.9	9.5	19.0	584.4	3.5	7.1	92	
OUJ16290	248.00	164.50	48.10	0.660	4.30E+04	1.80E+04	0.838	0.029	0.1012	0.0010	0.0010	0.0010	0.0010	41.6	83.1	41.6	618.0	8.0	16.0	621.5	2.9	5.9	101	
OUJ16291	223.40	195.20	56.10	0.870	-2.00E+02	2.30E+03	0.844	0.030	0.1025	0.0011	0.0011	0.0011	0.0011	41.7	83.3	41.7	83.3	8.3	16.5	629.2	3.2	6.4	101	
OUJ16292	106.70	109.12	30.17	1.020	-9.97E+03	3.30E+03	0.842	0.038	0.0983	0.0012	0.0012	0.0012	0.0012	50.2	100.5	50.2	62.0	10.5	20.9	604.3	3.5	7.0	97	
OUJ16293	328.00	475.00	138.20	1.450	-2.10E+04	1.40E+04	0.896	0.029	0.1051	0.0011	0.0011	0.0011	0.0011	38.4	76.7	38.4	649.6	7.8	15.5	644.2	3.2	6.4	98	
OUJ16294	188.60	115.10	136.40	0.610	1.42E+05	6.10E+04	10.78	0.290	0.4658	0.0044	0.0044	0.0044	0.0044	14.2	28.5	14.2	2521.3	12.3	24.6	2465.1	9.7	19.4	99	
OUJ16295	425.60	258.60	117.70	0.610	1.28E+05	6.00E+04	1.644	0.046	0.1661	0.0016	0.0016	0.0016	0.0016	31.2	62.3	31.2	987.2	8.8	17.7	990.4	4.4	8.8	100	
OUJ16296	204.50	141.80	22.23	0.690	-9.00E+02	1.70E+03	0.391	0.019	0.0540	0.0006	0.0006	0.0006	0.0006	11.6	335.1	6.9	339.0	6.9	13.9	339.0	1.9	3.9	101	
OUJ16297	394.00	203.20	33.61	0.630	5.10E+03	3.20E+03	0.430	0.016	0.0549	0.0006	0.0006	0.0006	0.0006	44.1	88.1	44.1	363.2	5.7	11.4	344.4	1.8	3.6	95	
OUJ16298	99.10	49.90	16.89	0.500	1.05E+03	2.40E+03	1.080	0.044	0.1217	0.0015	0.0015	0.0015	0.0015	45.9	91.8	45.9	743.6	10.7	21.5	740.3	4.3	8.6	100	
OUJ16299	276.80	111.60	30.54	0.400	-1.70E+03	4.90E+03	0.814	0.028	0.0986	0.0010	0.0010	0.0010	0.0010	39.5	79.0	39.5	604.7	7.8	15.7	606.4	2.9	5.9	100	
OUJ16300	175.90	177.50	91.70	0.700	1.01E+03	7.40E+02	1.820	0.110	0.1676	0.0030	0.0030	0.0030	0.0030	119.7	1179.6	119.7	1052.7	19.8	39.6	998.9	8.3	16.6	95	
OUJ16301	255.30	141.30	22.72	0.740	5.00E+03	2.30E+03	0.394	0.019	0.0536	0.0006	0.0006	0.0006	0.0006	59.2	118.3	59.2	337.3	6.9	13.8	336.7	2.0	3.9	100	
OUJ16302	189.70	115.00	48.76	0.360	7.30E+04	4.90E+04	1.205	0.036	0.1315	0.0013	0.0013	0.0013	0.0013	84.0	9.3	84.0	802.9	8.3	16.6	796.2	3.7	7.4	99	
OUJ16303	128.30	95.45	28.87	0.740	-1.20E+05	1.70E+05	0.928	0.036	0.1065	0.0012	0.0012	0.0012	0.0012	43.1	66.3	43.1	666.6	9.5	18.9	652.6	3.5	7.0	98	
OUJ16304	190.00	26.75	27.05	0.140	-2.50E+05	1.0E+05	6.976	0.190	0.3667	0.0038	0.0038	0.0038	0.0038	16.1	210.1	16.1	32.2	2108.4	12.1	24.2	2107.5	8.8	17.7	100
OUJ16305	89.49	71.62	70.87	0.800	-3.30E+04	1.80E+04	6.813	0.190	0.3782	0.0039	0.0039	0.0039	0.0039	18.2	36.4	18.2	208.4	12.3	24.7	2087.9	9.1	18.2	99	
OUJ16306	521.50	291.10	45.57	0.560	-3.00E+04	1.00E+04	0.392	0.013	0.0530	0.0006	0.0006	0.0006	0.0006	379.4	41.5	83.0	335.9	4.7	9.5	333.0	1.7	3.4	99	
OUJ16307	886.80	155.90	22.88	0.540	-6.80E+04	2.60E+04	0.375	0.016	0.0517	0.0006	0.0006	0.0006	0.0006	315.9	49.6	315.9	323.4	5.9	11.8	324.7	2.0	3.9	100	
OUJ16308	757.30	231.20	34.63	0.310	-2.10E+04	5.60E+04	0.377	0.012	0.0510	0.0005	0.0005	0.0005	0.0005	398.7	382.7	398.7	324.7	4.4	8.8	320.5	1.6	3.1	99	
OUJ16309	115.10	77.50	31.50	0.670	-4.20E+04	4.40E+04	1.393	0.046	0.1462	0.0017	0.0017	0.0017	0.0017	37.0	74.0	37.0	886.0	9.8	19.5	879.6	4.8	9.6	99	
OUJ16310	67.18	57.30	16.83	0.850	-4.30E+05	2.40E+05	0.916	0.044	0.1008	0.0014	0.0014	0.0014	0.0014	51.5	103.0	51.5	660.2	11.6	23.3	619.1	4.1	8.2	94	
OUJ16311	78.20	22.25	73.00	0.580	1.90E+05	1.0E+05	0.815	0.034	0.1011	0.0012	0.0012	0.0012	0.0012	48.9	97.8	48.9	605.3	9.5	19.0	621.0	3.5	7.0	103	
OUJ16312	55.13	31.88	32.71	0.750	-2.80E+05	1.90E+05	7.150	0.220	0.3950	0.0045	0.0045	0.0045	0.0045	19.5	39.0	19.5	2130.3	13.7	27.4	2146.0	10.4	20.8	101	
OUJ16313	411.30	288.60	83.70	0.580	-1.25E+05	9.20E+04	0.863	0.026	0.1010	0.0010	0.0010	0.0010	0.0010	34.7	69.4	34.7	626.3	7.1	14.2	620.4	2.9	5.9	99	
OUJ16314	188.90	225.50	67.74	1.190	-5.00E+05	2.00E+05	0.608	0.032	0.1044	0.0012	0.0012	0.0012	0.0012	42.5	85.0	42.5	637.2	8.7	17.3	640.3	3.5	7.0	100	
OUJ16315	45.65	55.63	53.12	1.220	4.00E+02	8.90E+03	6.090	0.190	0.3574	0.0043	0.0043	0.0043	0.0043	22.4	44.8	22.4	1988.8	13.6	27.2	1969.8	10.2	20.4	99	
OUJ16316	240.50	138.30	21.98	0.580	-3.00E+04	1.50E+04	0.404	0.017	0.0546	0.0007	0.0007	0.0007	0.0007	48.6	97.2	48.6	344.5	6.1	12.3	342.5	2.0	4.0	99	
OUJ16317	35.69	56.70	16.35	1.590	3.00E+02	1.50E+03	0.911	0.062	0.1028	0.0018	0.0018	0.0018	0.0018	75.4	150.8	75.4	657.6	16.5	32.9	630.8	5.3	10.5	96	
OUJ16318	71.41	35.37	35.23	0.500	-4.90E+03	9.80E+03	6.780	0.200	0.3785	0.0040	0.0040	0.0040	0.0040	19.8	39.7	19.8	2083.1	13.0	26.1	2089.3	9.4	18.7	99	
OUJ16319	519.60	227.40	203.30	0.440	-3.60E+05	1.70E+05	6.477	0.170	0.3624	0.0034	0.0034	0.0034	0.0034	14.5	29.0	14.5	2042.8	11.5	23.1	1983.5	8.0	16.1	98	
OUJ16320	828.00	446.00	115.90	0.540	1.50E+04	1.70E+04	0.785	0.023	0.0959	0.0009	0.0009	0.0009	0.0009	33.6	67.1	33.6	583.3	6.5	13.1	531.4	2.7	5.4	90	
OUJ16321	204.90	118.90	119.90	0.580	7.80E																			

ANALYSIS	U (ppm)	Th (ppm)	Pb (ppm)	Th/U	Ratios				Error correction	Ages (Ma)				Concordance (%)									
					$^{206}\text{Pb}/^{208}\text{Pb}$	$^{207}\text{Pb}/^{208}\text{Pb}$	$^{206}\text{Pb}/^{238}\text{U}$	$^{207}\text{Pb}/^{238}\text{U}$		$^{206}\text{Pb}/^{208}\text{Pb}$	$^{207}\text{Pb}/^{208}\text{Pb}$	$^{207}\text{Pb}/^{238}\text{U}$	$^{206}\text{Pb}/^{238}\text{U}$		σ	2σ	σ	2σ					
OJJ16z146	237.70	106.90	108.30	0.450	-3.80E+05	3.50E+05	0.1258	2.20E-03	6.646	0.180	0.3824	0.0037	0.4719	2040.1	15.5	30.9	2065.5	11.9	23.9	2087.5	8.6	17.3	101
Discordant data																							
OJJ16z3	1322.00	635.00	44.90	0.480	-1.32E+05	8.80E+04	0.0608	2.00E-03	0.364	0.012	0.0429	0.0011	0.7246	632.2	35.4	70.8	307.5	4.5	9.0	270.8	3.4	6.8	88
OJJ16z18	751.00	395.00	315.50	0.530	7.30E+04	3.10E+04	0.1340	2.10E-03	5.356	0.140	0.2892	0.0027	0.4912	2150.4	13.7	27.4	1877.8	11.2	22.3	1637.5	6.8	13.5	87
OJJ16z21	705.00	839.00	97.00	1.190	2.40E+03	1.60E+03	0.0652	2.30E-03	0.371	0.012	0.0412	0.0005	0.2120	780.8	37.1	74.1	320.6	4.4	8.9	260.0	1.5	3.0	81
OJJ16z23	421.00	349.00	59.80	0.830	-8.10E+03	3.70E+03	0.0624	2.60E-03	0.364	0.017	0.0431	0.0013	0.5512	687.8	44.5	88.9	315.2	6.3	12.6	272.0	4.0	8.0	86
OJJ16z30	230.20	92.20	84.50	0.400	-1.30E+03	2.50E+03	0.1532	2.70E-03	7.163	0.190	0.3402	0.0035	0.3135	2882.0	15.0	30.0	2131.9	11.8	23.6	1887.6	8.4	16.8	89
OJJ16z63	192.40	48.90	39.68	0.250	-5.30E+03	9.10E+03	0.0917	3.20E-03	1.793	0.062	0.1428	0.0020	0.5388	1461.2	33.2	66.3	1042.9	11.3	22.5	860.5	5.6	11.3	83
OJJ16z67	546.70	271.50	199.00	0.500	-3.90E+04	1.70E+04	0.1189	1.90E-03	4.563	0.120	0.2712	0.0025	0.3913	1939.0	14.3	28.6	1740.7	11.0	21.9	1546.9	6.3	12.7	89
OJJ16z82	1152.00	189.20	68.10	0.160	1.01E+04	6.50E+03	0.1045	3.10E-03	1.285	0.052	0.0887	0.0025	0.9204	1705.5	27.3	54.6	839.1	11.5	23.1	547.8	7.4	14.8	65
OJJ16z121	285.60	211.70	37.38	0.720	6.20E+04	2.70E+04	0.0668	3.40E-03	0.501	0.026	0.0544	0.0007	0.3691	831.5	53.1	106.1	412.4	8.8	17.6	341.5	2.2	4.3	83
OJJ16z124	579.00	224.10	202.30	0.390	4.70E+04	3.90E+04	0.1496	2.70E-03	5.710	0.240	0.2695	0.0073	0.9627	2341.4	15.4	30.9	1932.9	18.1	36.3	1538.3	16.5	37.1	80
OJJ16z130	259.10	156.80	29.76	0.610	-3.00E+04	4.80E+04	0.0671	2.80E-03	0.501	0.020	0.0535	0.0006	0.0478	840.9	43.4	86.9	412.4	6.8	13.5	335.9	1.9	3.9	81

Footnotes:

. Analysis references: OJJ16z is zircon from sample OJJ16 (mount CT18-6), followed by grain number "c" or "r", meaning core or rim, respectively.

Chapter IV

Table D.45a: Sample OUJ18 (LA-ICPMS)

IGSN: IEACC00019 Coordinate UTM: Zone 30S, 3796505 m N, 587288 m E

ANALYSIS	U (ppm)	Th (ppm)	Pb (ppm)	Th/U	²⁰⁶ Pb/ ²⁰⁸ Pb		²⁰⁷ Pb/ ²³⁵ U		Ratios		Error correction		Ages (Ma)				Concordance (%)						
					2 σ	²⁰⁶ Pb/ ²⁰⁸ Pb	2 σ	²⁰⁷ Pb/ ²³⁵ U	2 σ	²⁰⁷ Pb/ ²³⁵ U	2 σ	²⁰⁶ Pb/ ²³⁸ U	2 σ	²⁰⁷ Pb/ ²³⁵ U	σ	2 σ		²⁰⁶ Pb/ ²³⁸ U	σ	2 σ			
OUJ182-1	73.90	84.50	71.60	1.140	7.00E+04	1.20E+04	0.1122	4.00E-03	5.300	0.130	0.3421	0.0041	1.6354	32.3	64.6	1868.9	10.5	20.9	1896.8	9.8	19.7	101	
OUJ182-2	666.00	437.50	433.00	0.670	2.10E+05	1.50E+05	0.1302	3.60E-03	7.165	0.066	0.4030	0.0039	0.4015	24.3	48.6	2132.2	4.1	8.2	2182.8	9.0	17.9	102	
OUJ182-3	753.00	414.00	516.00	0.550	-1.00E+05	1.70E+05	0.1957	5.20E-03	14.350	0.170	0.5337	0.0074	0.8634	21.6	43.3	2773.1	5.6	11.2	2757.0	15.6	31.1	99	
OUJ182-4	56.60	64.21	31.05	1.130	7.50E+03	6.30E+03	0.0781	3.60E-03	2.099	0.085	0.1964	0.0027	0.0174	45.8	91.5	1148.5	13.9	27.8	1156.0	7.3	14.5	101	
OUJ182-5	31.90	1.490	1.90E+04	0.0592	1.90E+04	1.90E+04	0.0592	1.90E-03	0.842	0.020	0.1040	0.0011	0.0329	34.9	69.8	620.2	5.5	11.0	637.9	3.2	6.4	103	
OUJ182-6	356.20	528.00	258.10	0.770	-2.20E+04	6.00E+04	0.1338	3.70E-03	7.342	0.074	0.3980	0.0037	0.1790	2148.4	48.3	2153.9	4.5	9.0	2159.8	8.5	17.1	100	
OUJ182-7	341.00	262.10	38.80	0.550	1.00E+04	1.30E+04	0.0524	1.90E-03	3.988	0.102	0.0336	0.0006	0.0616	302.9	41.3	332.9	4.4	8.8	336.7	1.8	3.5	101	
OUJ182-8	484.80	102.10	108.75	89.20	1.70E+04	1.30E+04	0.1135	3.70E-03	5.330	0.100	0.3320	0.0035	0.3840	2119.4	47.9	2099.7	4.6	9.1	1886.2	8.9	17.8	101	
OUJ182-9	367.60	337.30	309.50	0.920	-2.80E+04	7.00E+04	0.1316	3.60E-03	6.908	0.071	0.3820	0.0035	0.3840	2119.4	47.9	2099.7	4.6	9.1	2085.6	8.2	16.3	99	
OUJ182-10	85.70	55.98	13.66	0.650	-5.00E+02	3.80E+03	0.0590	3.50E-03	0.767	0.042	0.0932	0.0014	0.0393	587.1	64.6	129.2	578.0	12.1	24.1	574.4	4.1	8.3	98
OUJ182-11	401.80	501.40	130.20	1.250	-3.00E+04	1.80E+04	0.0610	1.90E-03	0.819	0.021	0.0971	0.0010	0.1237	639.2	33.5	67.0	607.5	5.9	11.7	597.2	2.9	5.8	98
OUJ182-12	120.40	148.00	40.98	1.210	-3.70E+03	5.10E+03	0.0567	3.00E-03	0.782	0.039	0.0998	0.0014	0.0293	479.9	58.5	116.9	586.6	11.1	22.2	613.2	4.1	8.2	105
OUJ182-13	278.10	122.50	38.90	0.440	9.00E+04	1.20E+04	0.0648	2.20E-03	0.928	0.025	0.1031	0.0012	-0.0351	767.8	71.5	666.6	6.6	13.2	632.4	3.5	7.0	95	
OUJ182-14	835.00	585.00	482.70	0.700	1.00E+05	1.30E+05	0.1216	3.30E-03	5.346	0.052	0.3185	0.0032	0.4707	1979.8	24.2	48.3	1876.2	4.2	8.3	1782.4	7.8	15.6	95
OUJ182-15	446.00	1203.00	1256.00	2.700	-3.40E+04	8.40E+04	0.1360	3.70E-03	7.732	0.067	0.4129	0.0040	0.4015	2176.9	23.7	47.4	2200.3	3.9	7.8	2228.2	9.1	18.3	101
OUJ182-16	312.00	418.30	121.90	1.340	-2.00E+04	1.30E+04	0.0615	2.00E-03	0.928	0.023	0.1102	0.0012	-0.0558	656.8	34.9	69.7	666.6	6.1	12.1	673.6	3.5	7.0	101
OUJ182-17	365.00	68.40	68.70	0.190	1.60E+04	7.00E+04	0.1294	3.60E-03	7.143	0.090	0.3993	0.0042	0.5034	2089.8	24.5	48.9	2129.4	5.6	11.2	2165.8	9.7	19.3	102
OUJ182-18	299.00	240.00	35.97	0.800	1.00E+04	7.90E+03	0.0531	2.60E-03	0.402	0.019	0.0546	0.0007	0.0999	333.1	55.5	111.0	343.1	6.9	13.7	342.7	2.1	4.3	100
OUJ182-19	181.00	279.00	239.30	0.990	1.90E+04	4.30E+04	0.1163	3.40E-03	5.517	0.066	0.3459	0.0039	0.0701	1900.1	26.3	52.5	1903.2	5.1	10.3	1915.0	9.3	18.7	101
OUJ182-20	185.60	137.30	23.62	0.740	-2.70E+03	5.10E+03	0.0659	3.60E-03	0.476	0.027	0.0527	0.0008	0.2212	803.2	57.2	114.4	395.3	9.3	18.6	330.9	2.5	5.0	84
OUJ182-21	744.00	285.60	50.90	0.380	-2.00E+04	2.30E+04	0.0621	1.80E-03	0.492	0.014	0.0614	0.0008	0.2469	570.8	33.1	66.3	406.3	4.8	9.5	384.1	2.5	5.0	95
OUJ182-22	264.60	308.60	97.50	1.160	0.00E+00	1.50E+04	0.0621	2.10E-03	1.020	0.028	0.1192	0.0013	0.0095	677.6	36.1	72.3	713.9	7.0	14.1	726.0	3.7	7.5	102
OUJ182-23	491.50	358.60	101.70	0.730	8.00E+04	2.80E+04	0.0605	1.70E-03	0.889	0.020	0.1063	0.0011	0.1589	621.5	30.3	60.6	645.8	5.4	10.7	651.0	3.2	6.4	101
OUJ182-24	132.80	198.50	51.50	1.490	0.00E+00	5.50E+03	0.0573	2.90E-03	0.718	0.032	0.0918	0.0013	-0.1309	503.1	55.7	111.4	549.5	9.4	18.9	566.2	3.8	7.7	103
OUJ182-25	486.00	528.70	232.70	1.080	5.00E+04	3.90E+04	0.0702	1.70E-03	1.581	0.025	0.1639	0.0017	0.1210	934.2	24.8	49.7	962.8	4.9	9.8	978.4	4.7	9.4	102
OUJ182-26	497.00	973.00	281.80	1.960	-2.50E+04	3.10E+04	0.0611	1.70E-03	0.878	0.018	0.1051	0.0011	0.1342	642.8	29.9	59.8	639.9	4.9	9.7	644.1	3.2	6.4	101
OUJ182-27	304.00	304.00	60.40	0.210	3.60E+04	5.20E+04	0.0668	1.90E-03	1.201	0.025	0.1309	0.0013	0.1466	831.5	29.6	59.3	801.0	5.8	11.5	792.7	3.7	7.4	99
OUJ182-28	929.00	195.50	60.40	0.210	1.60E+04	9.40E+04	0.0617	1.50E-03	0.951	0.015	0.1121	0.0011	0.2314	664.4	26.0	52.1	678.6	3.9	7.8	684.7	3.2	6.4	101
OUJ182-29	377.00	377.00	58.70	1.000	1.30E+03	9.40E+03	0.0562	2.30E-03	0.426	0.016	0.0549	0.0006	0.0873	480.3	45.4	90.7	360.3	5.7	11.4	344.8	1.9	3.7	96
OUJ182-30	518.00	149.70	161.60	0.290	1.50E+05	1.30E+05	0.1436	3.90E-03	8.630	0.110	0.4365	0.0052	0.7640	2271.1	23.4	46.8	2299.7	5.8	11.6	2385.0	11.7	23.3	96
OUJ182-31	508.00	329.50	50.20	0.640	8.00E+04	1.40E+04	0.0561	2.10E-03	0.405	0.033	0.0529	0.0007	0.1317	456.3	41.5	83.1	345.3	4.7	9.4	332.4	2.2	4.3	96
OUJ182-32	291.00	257.50	229.30	0.880	8.30E+04	5.40E+04	0.1160	3.30E-03	5.995	0.069	0.3498	0.0035	0.2811	1895.5	25.6	51.2	1915.3	5.3	10.6	1933.6	8.4	16.7	101
OUJ182-33	257.00	126.50	107.70	0.490	4.00E+04	3.80E+04	0.1323	3.90E-03	5.507	0.096	0.3037	0.0047	0.6331	2128.7	25.8	51.6	1901.7	7.5	15.0	1709.6	11.6	23.2	90
OUJ182-34	566.00	712.00	250.90	1.260	1.09E+05	5.00E+04	0.0722	1.80E-03	1.404	0.027	0.1427	0.0015	0.1569	991.6	25.3	50.7	890.6	5.7	11.4	859.9	4.2	8.5	97
OUJ182-35	1961.00	207.50	57.10	0.110	-6.80E+04	8.70E+04	0.0595	1.30E-03	0.783	0.011	0.0954	0.0011	0.4575	585.1	23.7	47.4	587.2	3.1	6.3	587.3	3.2	6.5	100
OUJ182-36	677.00	171.00	128.80	0.250	-3.00E+04	7.60E+04	0.1015	2.10E-03	3.329	0.059	0.2403	0.0026	0.6307	1651.7	19.2	38.3	1487.9	6.2	12.4	1388.3	6.8	13.5	93
OUJ182-37	467.40	1233.00	316.60	2.640	-9.00E+04	2.20E+04	0.0639	1.70E-03	0.852	0.018	0.0970	0.0013	0.4237	738.3	28.2	56.3	625.7	4.9	9.9	596.8	3.8	7.6	95
OUJ182-38	584.50	239.60	230.20	0.420	3.00E+05	1.20E+05	0.1271	3.50E-03	6.710	0.075	0.3817	0.0039	0.5207	2058.2	24.3	48.6	2073.9	4.9	9.9	2084.2	9.1	18.2	100
OUJ182-39	687.00	193.20	2.310	2.00E+04	1.50E+04	0.0615	2.00E-03	0.851	0.024	0.1007	0.0012	0.1904	656.8	34.9	69.7	625.2	6.6	13.2	618.3	3.5	7.0	99	
OUJ182-40	35.95	36.35	8.86	1.010	-2.00E+02	1.50E+03	0.0602	5.50E-03	0.699	0.061	0.0871	0.0019	-0.0124	610.8	98.7	197.5	538.2	18.2	36.4	538.4	5.6	11.3	100
OUJ182-41	388.00	215.20	211.00	0.550	5.40E+04	7.00E+04	0.1358	3.80E-03	6.755	0.075	0.3612	0.0035	0.3122	2174.3	24.4	48.7	2079.8	4.9	9.8	1987.9	8.3	16.6	96
OUJ182-42	585.00	302.40	116.90	0.520	6.60E+04	3.80E+04	0.0772	1.80E-03	1.755	0.026	0.1660	0.0017	0.1298	1128.4	23.2	46.5	1029.0	4.8	9.6	990.0	4.7	9.4	96
OUJ182-43	312.90	237.80	117.10	0.760	1.00E+05	2.90E+04	0.0748																

Chapter IV

Table D.45b: Sample OJU18 (SIMS)

IGSN: IEACC00019 Coordinate UTM: Zone 30S, 3796505 m N, 587288 m E

ANALYSIS	²³⁸ U (ppm)	²⁰⁶ Pb (ppm)	Th/U	²⁰⁴ Pb (ppb)	Ratios			Concordant data			Ages (Ma)			Concordance (%)							
					²⁰⁷ Pb/ ²³⁸ U	σ	σ	²⁰⁶ Pb/ ²³⁸ U	σ	Rho	²⁰⁷ Pb/ ²⁰⁶ Pb	σ	2 σ	²⁰⁷ Pb/ ²³⁵ U	σ	2 σ	²⁰⁶ Pb/ ²³⁸ U	σ	2 σ		
OJU18z51	131.00	20.70	0.58	3.400	0.0736	0.0015	1.850	0.050	0.1800	0.0030	0.5639	1030	40.0	80.0	1061	19.0	36.0	1077	16.0	32.0	102
OJU18z52	296.00	13.80	1.00	2.400	0.0495	0.0020	0.370	0.020	0.0500	0.0010	0.3282	170	95.0	190.0	318	13.0	26.0	338	5.0	10.0	107
OJU18z53	142.00	12.50	0.52	0.400	0.0596	0.0023	0.840	0.030	0.1000	0.0020	0.3953	590	82.0	164.0	618	19.0	36.0	626	10.0	20.0	101
OJU18z54	94.00	7.90	0.40	0.900	0.0579	0.0026	0.780	0.040	0.1000	0.0020	0.3460	526	98.0	196.0	584	22.0	44.0	599	10.0	20.0	103
OJU18z55	74.00	6.30	0.48	1.400	0.0657	0.0027	0.890	0.040	0.1000	0.0020	0.3399	798	85.0	170.0	647	24.0	48.0	605	10.0	20.0	94
OJU18z56	661.00	49.50	0.08	0.400	0.0578	0.0012	0.690	0.020	0.0900	0.0010	0.5725	520	47.0	94.0	532	11.0	22.0	535	8.0	16.0	101
OJU18z57	287.00	36.60	0.53	0.900	0.0696	0.0008	1.410	0.030	0.1500	0.0020	0.8066	916	23.0	46.0	894	12.0	24.0	886	13.0	26.0	99
OJU18z58	266.00	23.70	0.71	0.000	0.0593	0.0013	0.840	0.020	0.1000	0.0020	0.6734	578	38.0	76.0	620	11.0	22.0	631	10.0	20.0	102
OJU18z60	315.00	104.20	0.22	0.500	0.1309	0.0013	6.900	0.020	0.3800	0.0050	0.8227	2110	17.0	34.0	2097	16.0	32.0	2086	25.0	50.0	99
OJU18z61	570.00	47.50	0.85	5.000	0.0614	0.0012	0.820	0.020	0.1000	0.0010	0.5656	653	43.0	86.0	605	12.0	24.0	593	8.0	16.0	98
OJU18z62	258.00	22.60	0.70	2.200	0.0590	0.0016	0.820	0.030	0.1000	0.0020	0.4680	567	58.0	116.0	610	15.0	30.0	621	9.0	18.0	102
OJU18z63	795.00	106.90	0.10	15.300	0.0684	0.0010	1.480	0.030	0.1600	0.0020	0.6667	881	30.0	60.0	923	13.0	26.0	942	12.0	24.0	102
OJU18z64	109.00	11.20	0.80	1.600	0.0635	0.0020	1.040	0.040	0.1200	0.0020	0.4238	724	88.0	136.0	721	20.0	40.0	721	11.0	22.0	100
OJU18z65	215.00	65.00	0.74	1.300	0.1251	0.0014	6.020	0.110	0.3500	0.0050	0.7778	2030	20.0	40.0	1977	17.0	34.0	1930	24.0	48.0	98
OJU18z66	329.00	51.50	0.89	2.400	0.0746	0.0014	1.860	0.040	0.1800	0.0030	0.6071	1057	38.0	76.0	1066	16.0	32.0	1070	14.0	28.0	100
OJU18z67	834.00	58.80	0.13	26.900	0.0567	0.0014	0.640	0.020	0.0800	0.0010	0.4450	478	54.0	108.0	500	13.0	26.0	505	7.0	14.0	101
OJU18z68	116.00	12.70	0.52	0.000	0.0696	0.0022	1.210	0.040	0.1300	0.0020	0.4509	916	65.0	130.0	805	20.0	40.0	766	11.0	22.0	95
OJU18z69	875.00	51.80	0.32	7.600	0.0698	0.0012	1.540	0.040	0.1600	0.0030	0.6522	923	36.0	72.0	946	16.0	32.0	956	15.0	30.0	101
OJU18z70	311.00	115.40	0.19	5.200	0.0742	0.0011	1.680	0.040	0.1600	0.0020	0.6785	1046	31.0	62.0	1001	14.0	28.0	981	13.0	26.0	98
OJU18z71	500.00	34.10	0.05	15.800	0.0612	0.0014	0.660	0.020	0.0800	0.0010	0.4671	645	51.0	102.0	517	14.0	28.0	489	7.0	14.0	95
OJU18z73	58.00	7.60	0.76	1.900	0.0728	0.0023	1.530	0.060	0.1500	0.0020	0.3962	1009	63.0	126.0	942	25.0	50.0	914	14.0	28.0	97
OJU18z74	390.00	27.70	0.64	2.800	0.0591	0.0010	0.670	0.020	0.0800	0.0010	0.6414	570	38.0	76.0	519	11.0	22.0	508	8.0	16.0	98
OJU18z75	181.00	13.50	0.64	4.300	0.0584	0.0014	0.700	0.030	0.0900	0.0010	0.4139	544	53.0	106.0	537	16.0	32.0	535	8.0	16.0	100
OJU18z76	161.00	21.50	0.45	5.500	0.0682	0.0017	1.460	0.050	0.1500	0.0030	0.4843	873	53.0	106.0	912	21.0	42.0	928	14.0	28.0	102
OJU18z77	689.00	88.70	0.57	14.500	0.0712	0.0007	1.460	0.030	0.1500	0.0020	0.7669	962	20.0	40.0	913	11.0	22.0	894	12.0	24.0	98
OJU18z78	122.00	9.60	1.61	4.300	0.0589	0.0015	0.740	0.040	0.0900	0.0020	0.3546	562	64.0	128.0	560	21.0	42.0	560	9.0	18.0	100
OJU18z79	738.00	32.50	1.00	1.600	0.0531	0.0015	0.370	0.010	0.0500	0.0010	0.4337	332	64.0	128.0	321	9.0	18.0	320	4.0	8.0	100
OJU18z80	221.00	61.40	1.44	0.300	0.1169	0.0013	5.190	0.100	0.3200	0.0050	0.7904	1910	20.0	40.0	1849	17.0	34.0	1798	23.0	46.0	97
OJU18z82	502.00	46.80	0.31	1.200	0.0613	0.0009	0.910	0.020	0.1100	0.0020	0.6888	651	31.0	62.0	657	10.0	20.0	659	9.0	18.0	100
OJU18z85	151.00	33.90	0.28	1.200	0.0991	0.0026	3.550	0.120	0.2600	0.0050	0.6134	1607	48.0	96.0	1538	27.0	54.0	1490	27.0	54.0	97
OJU18z86	159.00	13.70	0.39	3.800	0.0585	0.0016	0.800	0.030	0.1000	0.0010	0.3825	547	61.0	122.0	598	17.0	34.0	612	9.0	18.0	102
OJU18z87	283.00	23.80	0.85	1.700	0.0611	0.0016	0.820	0.030	0.1000	0.0010	0.4515	642	58.0	116.0	606	15.0	30.0	597	8.0	16.0	99
OJU18z89	130.00	10.80	0.47	1.200	0.0599	0.0019	0.790	0.030	0.1000	0.0020	0.4154	600	70.0	140.0	592	17.0	34.0	590	9.0	18.0	100
OJU18z92	507.00	22.70	1.07	41.800	0.0526	0.0007	0.380	0.020	0.0500	0.0010	0.2172	313	32.0	64.0	324	18.0	36.0	326	4.0	8.0	101
OJU18z94	189.00	16.10	0.67	3.800	0.0548	0.0018	0.740	0.030	0.1000	0.0010	0.3627	405	75.0	150.0	564	18.0	36.0	605	9.0	18.0	107
OJU18z95	228.00	21.80	0.51	4.100	0.0628	0.0018	0.950	0.030	0.1100	0.0020	0.4275	695	61.0	122.0	678	18.0	36.0	673	10.0	20.0	99
OJU18z96	288.00	89.50	0.65	15.600	0.1284	0.0012	6.350	0.110	0.3600	0.0050	0.8193	2075	17.0	34.0	2024	17.0	34.0	1976	24.0	48.0	98
OJU18z98	288.00	28.70	0.38	6.100	0.0601	0.0009	0.950	0.020	0.1200	0.0020	0.5833	606	33.0	66.0	679	13.0	26.0	702	10.0	20.0	103
OJU18z99	455.00	40.90	0.55	14.700	0.0650	0.0006	0.930	0.020	0.1000	0.0020	0.6337	773	21.0	42.0	667	12.0	24.0	637	9.0	18.0	95
OJU18z100	391.00	17.30	0.14	1.300	0.0526	0.0016	0.370	0.010	0.0500	0.0010	0.4307	312	68.0	136.0	321	10.0	20.0	322	5.0	10.0	100
OJU18z101	684.00	31.50	0.55	2.400	0.0527	0.0012	0.390	0.010	0.0500	0.0010	0.5087	313	53.0	106.0	331	8.0	16.0	334	5.0	10.0	101
OJU18z102	708.00	106.20	0.34	6.200	0.0731	0.0006	1.750	0.030	0.1700	0.0020	0.8352	1017	18.0	36.0	1026	12.0	24.0	1031	5.0	10.0	100
OJU18z104	146.00	13.20	0.63	0.000	0.0592	0.0021	0.630	0.030	0.1000	0.0020	0.4054	575	76.0	152.0	625	18.0	36.0	639	9.0	18.0	102
OJU18z105	171.00	48.20	0.56	10.600	0.1194	0.0010	5.370	0.090	0.3300	0.0050	0.8113	1947	15.0	30.0	1878	16.0	32.0	1818	22.0	44.0	97
OJU18z106	99.00	12.60	1.06	1.900	0.0717	0.0026	1.460	0.060	0.1500	0.0030	0.4255	976	75.0	150.0	914	26.0	52.0	889	15.0	30.0	97
OJU18z107	858.00	67.00	0.71	33.000	0.0609	0.0005	0.760	0.020	0.0900	0.0010	0.6257	637	17.0	34.0	573	10.0	20.0	557	8.0	16.0	97
OJU18z108	247.00	21.80	0.04	5.100	0.0604	0.0009	0.850	0.030	0.1000	0.0010	0.4449	616	52.0	104.0	623	10.0	20.0	626	9.0	18.0	100
OJU18z110	122.00	17.00	0.34	2.000	0.0732	0.0010	1.620	0.040	0.1600	0.0030	0.6984	1018	27.0	54.0	979	15.0	30.0	962	14.0	28.0	98
OJU18z111	251.00	32.60	0.62	5.500	0.0661	0.0009	1.370	0.030	0.1500	0.0020	0.6527	808	74.0	148.0	874	14.0	28.0	901	12.0	24.0	103
OJU18z112	291.00	13.70	0.68	0.000	0.0572	0.0030	0.430	0.020	0.0500	0.0010	0.3175	497	114.0	228.0	362	17.0	34.0	342	6.0	12.0	94
OJU18z113	167.00	13.10	1.30	1.500	0.0582	0.0016	0.880	0.030	0.0900	0.0010	0.4455	536	62.0	124.0	552	15.0	30.0	557	9.0	18.0	101
OJU18z114	193.00	17.10	1.29	1.500	0.0623	0.0022	0.880	0.040	0.1000	0.0020	0.3891	683	77.0	154.0	641	19.0	38.0	629	9.0	18.0	98
OJU18z115	666.00	96.30	0.64	11.300	0.0739	0.0011	1.700	0.040	0.1700	0.0020	0.6537	1039	31.0	62.0	1009	14.0	28.0	996	13.0	26.0	99
OJU18z116	45.00	15.90	0.12	1.500	0.1416	0.0026	7.910	0.200	0.4100	0.0060	0.6444	2246	32.0	64.0	2219	24.0	48.0	2192	30.0	60.0	99
OJU18z118	965.00	66.90</																			

ANALYSIS	²³⁸ U (ppm)	²⁰⁶ Pb (ppm)	Th/U	²⁰⁴ Pb (ppb)	Ratios			Ages (Ma)			Concordance (%)						
					²⁰⁷ Pb/ ²⁰⁶ Pb	²⁰⁷ Pb/ ²³⁵ U	²⁰⁶ Pb/ ²³⁸ U	Rho	²⁰⁷ Pb/ ²⁰⁶ Pb	²⁰⁷ Pb/ ²³⁵ U	²⁰⁶ Pb/ ²³⁸ U	σ	2σ	σ	2σ		
OUJ18z119	182.00	8.10	0.43	0.800	0.0517	0.0028	0.370	0.020	0.0500	0.0010	0.2731	316	16.0	32.0	5.0	10.0	102
OUJ18z120	56.00	14.70	0.97	0.000	0.1059	0.0029	4.250	0.130	0.2900	0.0040	0.4680	1682	26.0	52.0	21.0	42.0	98
OUJ18z59	35.00	5.90	0.28	0.000	0.0972	0.0054	2.580	0.160	0.1900	0.0060	0.4845	1294	46.0	92.0	32.0	64.0	88
OUJ18z72	1177.00	164.80	0.56	28.400	0.1271	0.0007	2.840	0.080	0.1600	0.0040	0.9755	1364	21.0	42.0	24.0	48.0	71
OUJ18z81	319.00	28.50	0.54	472.500	-0.0289	-0.0019	-0.410	-0.170	0.1000	0.0090	0.2277	-538	-337.0	-674.0	55.0	110.0	-118
OUJ18z83	1058.00	200.00	0.20	21.900	0.1388	0.0039	4.180	0.130	0.2200	0.0030	0.4515	1669	27.0	54.0	17.0	34.0	76
OUJ18z84	77.00	3.90	1.11	14.700	0.0423	0.0013	0.340	0.090	0.0600	0.0010	0.0993	294	64.0	128.0	36.2	72.4	123
OUJ18z88	900.00	356.20	0.69	49.800	0.3089	0.0010	19.480	0.280	0.4600	0.0060	0.9736	3064	16.0	32.0	24.28	28.0	56.0
OUJ18z90	26.00	2.40	1.18	1.300	0.0716	0.0049	1.040	0.090	0.1100	0.0030	0.3257	722	46.0	92.0	18.0	36.0	89
OUJ18z91	1879.00	108.90	1.26	214.200	0.0645	0.0006	0.600	0.020	0.0700	0.0010	0.5387	474	12.0	24.0	4.18	7.0	14.0
OUJ18z97	1039.00	123.30	0.16	35.700	0.0921	0.0007	1.740	0.030	0.1400	0.0020	0.8523	1024	13.0	26.0	8.29	12.0	24.0
OUJ18z103	581.00	34.60	0.98	66.200	0.0676	0.0010	0.640	0.030	0.0700	0.0010	0.3370	503	19.0	38.0	4.29	7.0	14.0
OUJ18z109	721.00	130.50	0.06	6.200	0.1096	0.0014	3.160	0.060	0.2100	0.0030	0.7788	1447	16.0	32.0	12.24	18.0	36.0
OUJ18z117	332.00	100.50	0.66	4.000	0.1634	0.0017	7.890	0.200	0.3500	0.0080	0.9064	2217	24.0	48.0	38.0	76.0	87

Footnotes:

. Analysis references: OUJ18z is zircon from sample OUJ18 (mounts CT18-10b and CT19-3), followed by grain number.

. Pb* indicates radiogenic Pb, corrected for common Pb.

Chapter IV

Table D.46: Sample OLU19 (LA-ICP/MS)

IGSN: IEACC00020 Coordinate UTM: Zone 30S, 3796474 m N, 587262 m E

ANALYSIS	U (ppm)	Th (ppm)	Pb (ppm)	Th/U	Ratios				Error correction				Ages (Ma)				Concordance (%)				
					$^{206}\text{Pb}/^{208}\text{Pb}$	$^{207}\text{Pb}/^{208}\text{Pb}$	$^{206}\text{Pb}/^{238}\text{U}$	$^{207}\text{Pb}/^{238}\text{U}$	2σ	2σ	2σ	2σ	2σ	2σ	2σ	2σ		2σ	2σ		
					2σ	2σ	2σ	2σ	2σ	2σ	2σ	2σ	2σ	2σ	2σ	2σ		2σ	2σ	2σ	
OLU1921	973.00	60.10	56.00	0.060	2.00E-03	1.224	0.026	0.1221	0.0012	-0.0610	1002.8	28.0	55.9	811.6	5.9	11.9	742.9	3.4	6.9	92	
OLU1923	682.00	701.00	111.10	1.060	2.00E-03	0.449	0.014	0.0545	0.0006	-0.1077	610.8	39.5	79.0	376.6	4.9	9.8	341.8	1.7	3.5	91	
OLU1924	125.86	495.90	476.60	3.940	3.90E-03	6.490	0.110	0.3741	0.0039	0.1256	2049.9	27.2	14.9	2048.7	7.4	14.9	2048.7	9.1	18.3	100	
OLU1925	194.10	128.80	18.53	0.650	2.00E-03	0.382	0.019	0.0507	0.0007	0.1060	404.1	59.2	118.5	328.5	7.0	13.9	319.1	2.1	4.2	97	
OLU1926	139.50	117.40	48.90	0.840	2.00E-03	1.317	0.040	0.1411	0.0018	-0.0035	880.7	37.8	75.6	853.2	8.8	17.5	850.9	5.1	10.2	100	
OLU1927	243.50	557.70	152.60	2.290	2.00E-03	0.821	0.023	0.0996	0.0012	-0.1375	596.3	39.9	79.7	608.6	6.4	12.8	612.3	3.5	7.0	101	
OLU1928	83.80	338.00	310.40	4.030	4.00E-04	6.280	0.130	0.3606	0.0044	0.1807	2068.2	29.7	59.4	2015.7	9.1	18.1	1985.0	10.4	20.8	98	
OLU1929	210.70	220.00	63.60	1.040	1.07E-04	8.40E-03	0.028	0.0997	0.0013	0.0769	708.2	40.5	81.7	637.7	7.6	15.2	612.7	3.8	7.6	96	
OLU19210	269.50	70.91	96.40	0.260	1.03E-05	7.00E-04	0.2287	0.160	0.5731	0.0053	3043.0	21.7	43.4	2992.9	4.3	8.5	2920.5	10.9	21.7	98	
OLU19211	235.50	119.20	140.30	0.510	7.00E-04	4.10E-04	0.1668	0.100	0.4643	0.0045	2828.8	23.2	46.3	2494.8	4.3	8.7	2488.5	9.9	19.8	99	
OLU19212	206.40	126.10	72.60	0.610	1.60E-04	1.80E-04	0.0894	0.050	0.2143	0.0021	1278.6	28.0	56.1	1251.7	7.3	14.7	1251.7	5.6	11.1	99	
OLU19213	906.90	917.40	140.60	1.010	2.00E-04	1.70E-04	0.0551	0.010	0.0541	0.0006	416.3	32.4	64.9	350.3	3.6	7.2	339.9	1.7	3.4	97	
OLU19214	407.80	251.70	125.60	0.620	5.10E-04	2.90E-04	0.0745	0.030	0.1818	0.0018	1055.0	24.3	48.7	1064.9	5.3	10.7	1076.8	4.9	9.8	101	
OLU19215	181.00	255.20	66.70	1.410	3.30E-04	1.50E-04	0.0591	0.030	0.0959	0.0012	-0.0279	570.8	47.9	95.7	586.6	8.5	17.1	590.3	3.5	7.1	101
OLU19216	287.20	361.00	174.00	1.260	8.30E-04	3.10E-04	0.0735	0.035	0.1759	0.0019	1027.8	26.1	52.3	1021.6	6.5	13.0	1022.6	5.2	10.5	100	
OLU19217	165.20	106.30	106.70	0.640	6.50E-04	3.50E-04	0.1289	0.100	0.3919	0.0043	2055.5	26.4	52.9	2088.3	6.5	13.0	2131.6	10.0	19.9	102	
OLU19218	243.90	224.80	33.90	0.920	1.19E-04	6.10E-03	0.0532	0.015	0.0536	0.0008	0.0948	337.3	51.1	102.2	333.6	5.5	11.0	336.8	2.3	4.6	101
OLU19219	146.10	133.50	135.70	0.910	5.10E-04	3.60E-04	0.1297	0.110	0.3993	0.0043	2093.9	26.4	52.8	2135.3	6.8	13.6	2165.8	9.9	19.8	101	
OLU19220	12.23	16.06	4.29	1.310	4.40E-02	4.40E-02	0.0623	0.120	0.0960	0.0033	0.0149	684.4	159.3	318.7	596.8	33.8	67.6	590.9	9.7	19.4	99
OLU19221	232.40	187.70	220.70	0.810	-1.60E+04	5.30E+04	0.1609	0.120	0.4744	0.0044	2465.1	23.6	47.2	2483.4	5.3	10.5	2502.8	9.6	19.2	101	
OLU19222	64.30	38.95	40.72	0.600	8.50E-04	4.00E-04	0.1369	0.160	0.4085	0.0018	2213.5	29.3	58.7	2205.9	9.2	18.5	2208.1	11.2	22.4	100	
OLU19223	282.20	160.40	143.80	0.570	2.80E-04	3.20E-04	0.1256	0.081	0.3320	0.0040	2037.3	25.3	50.7	1937.0	6.1	12.2	1848.1	9.7	19.4	95	
OLU19224	927.00	792.00	224.60	0.850	3.00E+04	3.90E-04	0.0597	0.012	0.1013	0.0009	592.4	25.4	50.8	615.2	3.3	6.7	621.8	2.7	5.3	102	
OLU19225	270.00	147.80	52.30	0.550	1.00E+03	1.60E-04	0.0619	0.028	0.1209	0.0013	0.0318	31.9	61.7	719.4	7.0	14.0	735.6	3.7	7.5	102	
OLU19226	291.30	397.70	124.30	1.370	1.70E+04	1.30E-03	0.0633	0.022	0.1109	0.0011	678.3	31.6	63.7	683.3	5.7	11.4	677.7	3.2	6.4	99	
OLU19227	146.10	133.50	135.70	0.910	5.10E-04	3.60E-04	0.1297	0.110	0.3993	0.0043	2093.9	26.4	52.8	2135.3	6.8	13.6	2165.8	9.9	19.8	101	
OLU19228	109.20	81.20	78.70	0.740	-4.00E+04	2.00E+04	0.1312	0.110	0.3916	0.0040	-0.0161	2114.1	27.4	54.9	1978.6	6.0	12.0	1996.9	8.7	17.5	101
OLU19229	117.80	111.50	26.37	0.950	9.00E-03	5.80E-03	0.0584	0.034	0.0919	0.0013	0.0980	544.8	54.3	108.5	564.7	9.9	19.8	566.8	3.8	7.7	100
OLU19230	357.00	63.19	18.32	0.180	1.90E+04	2.10E-04	0.0610	0.021	0.1022	0.0011	1.1188	639.2	31.7	63.5	623.6	5.8	11.5	627.5	3.2	6.4	101
OLU19231	475.00	360.00	445.00	0.760	9.00E+05	1.80E-05	0.1811	0.100	0.4940	0.0044	0.3280	2693.0	22.4	44.8	2632.9	3.8	7.6	2588.0	9.5	19.0	98
OLU19232	214.20	165.50	46.85	0.770	-1.40E+05	1.80E+05	0.0616	0.025	0.1035	0.0013	0.1080	660.3	34.8	69.6	691.7	6.7	13.5	634.9	3.8	7.6	99
OLU19233	394.10	242.40	221.20	0.620	-2.70E+05	1.50E+05	0.1230	0.076	0.3196	0.0041	0.5719	2000.2	24.6	49.1	1891.7	6.0	12.0	1787.8	10.0	20.0	95
OLU19234	159.70	113.00	33.68	0.710	8.10E+03	8.00E+03	0.0622	0.033	0.1040	0.0014	0.0079	681.0	44.6	89.3	644.2	8.9	17.8	637.8	4.1	8.2	99
OLU19235	201.00	384.00	104.80	0.910	7.30E-03	8.20E+03	0.0620	0.029	0.0981	0.0014	0.0672	674.1	43.1	86.2	619.1	8.0	16.0	603.3	4.1	8.2	97
OLU19236	131.10	125.30	36.77	0.960	1.19E-04	8.00E-03	0.0594	0.037	0.1054	0.0013	0.0803	581.8	53.0	106.0	631.2	10.1	20.2	646.0	3.8	7.6	102
OLU19237	224.60	73.10	20.19	0.330	-1.00E+03	1.10E-04	0.0609	0.025	0.1024	0.0013	-0.0187	635.7	38.9	77.7	626.5	6.8	13.7	628.5	3.8	7.6	100
OLU19238	654.00	181.30	171.20	0.280	1.50E+05	1.30E-05	0.1305	0.062	0.3974	0.0038	0.4376	2104.8	23.5	47.1	2127.4	3.9	7.7	2157.1	8.8	17.5	101
OLU19239	534.80	174.60	220.20	0.330	2.60E+05	2.40E+05	0.2077	0.150	0.5286	0.0053	0.6370	2887.7	21.9	43.8	2825.3	4.7	9.4	2735.6	11.2	22.4	97
OLU19240	137.90	126.40	130.20	0.920	-2.00E+04	2.20E+04	0.1291	0.110	0.4010	0.0039	0.1719	2085.8	26.6	53.1	2136.5	6.8	13.6	2173.6	9.0	17.9	102
OLU19241	143.10	120.70	35.24	0.840	4.10E+03	6.60E+03	0.0605	0.035	0.1035	0.0014	0.0516	621.5	48.1	96.3	633.4	9.5	19.0	634.9	4.1	8.2	100
OLU19242	305.20	627.00	177.80	2.050	2.70E+04	1.60E+04	0.0606	0.023	0.1027	0.0012	0.0196	625.1	35.6	71.2	627.9	6.3	12.6	630.4	3.5	7.0	100
OLU19243	291.70	291.00	78.70	1.260	6.50E+04	3.90E-04	0.0597	0.024	0.0942	0.0011	0.1582	592.7	39.9	79.9	578.6	6.9	13.8	580.6	3.2	6.5	100
OLU19244	305.40	241.50	100.10	0.790	4.20E+04	3.40E-04	0.0696	0.026	0.1505	0.0016	0.2938	916.6	28.1	56.2	906.1	6.0	12.1	903.8	4.5	9.0	100
OLU19245	233.90	142.20	37.27	0.610	-2.40E+03	8.40E+03	0.0584	0.026	0.0950	0.0012	0.1506	544.8	41.2	82.3	578.0	7.5	14.9	585.2	3.5	7.1	101
OLU19246	296.80	175.90	28.41	0.590	1.00E+03	7.60E+03	0.0538	0.034	0.0543	0.0007	-0.0037	362.7	50.3	100.6	344.5	5.4	10.8	340.9	2.1	4.3	99
OLU19247	275.50	220.80	225.30	0.800	2.10E+04	3.70E-04	0.1314	0.077	0.3899	0.0036	0.2721	2116.8	24.7	49.4	2115.4	4.9	9.7	2122.4	8.3	16.7	100
OLU19248	195.30	147.30	37.50	0.750	1.03E+04	9.00E+03	0.0604	0.030	0.0918	0.0012	0.0394	617.9	46.5	92.9	576.9	8.6	17.2	565.9	3		

ANALYSIS	U (ppm)	Th (ppm)	Pb (ppm)	Th/U	Ratios				Ages (Ma)				Concordance (%)						
					$^{207}\text{Pb}/^{235}\text{U}$		$^{206}\text{Pb}/^{238}\text{U}$		$^{207}\text{Pb}/^{235}\text{U}$		$^{206}\text{Pb}/^{238}\text{U}$								
					2σ	2σ	2σ	2σ	2σ	2σ	2σ	2σ							
OJ19265	332.50	224.90	104.50	0.680	1.90E-03	0.0727	1.679	0.031	0.1687	0.0017	0.0225	1000.6	5.9	11.7	1004.9	4.7	9.4	100	
OJ19266	486.00	301.00	72.70	0.620	1.80E-03	0.0591	0.674	0.018	0.0822	0.0009	0.0251	570.8	6.5	10.9	509.4	2.7	5.5	97	
OJ19267	301.40	279.00	252.90	0.930	3.00E+05	0.1142	5.202	0.082	0.3362	0.0042	0.6273	1867.3	35.3	13.4	1868.4	10.1	20.3	101	
OJ19268	392.30	307.70	315.40	0.780	4.40E+04	0.1393	7.833	0.077	0.4098	0.0037	0.3209	2218.5	35.6	47.3	2214.0	8.5	16.9	100	
OJ19269	142.60	148.10	60.58	1.020	-5.20E+03	0.0716	1.481	0.044	0.1513	0.0018	0.1676	974.6	36.1	9.0	908.2	5.0	10.1	98	
OJ19270	537.00	269.20	45.50	0.500	-1.00E+04	0.0553	0.467	0.014	0.0615	0.0008	0.2711	424.4	36.3	72.6	389.1	2.4	4.9	99	
OJ19271	510.20	32.39	32.39	0.220	3.40E+04	0.0619	0.889	0.018	0.1049	0.0011	0.0160	670.7	29.4	58.8	642.9	3.2	6.4	100	
OJ19272	525.00	127.10	36.70	0.240	1.00E+04	0.0617	0.893	0.017	0.1050	0.0010	0.0128	663.7	27.8	55.6	648.0	2.9	5.8	99	
OJ19273	320.40	328.40	97.50	1.020	1.00E+04	0.0583	0.854	0.021	0.1060	0.0011	-0.0307	541.1	33.8	67.5	626.8	3.2	6.4	104	
OJ19274	103.30	154.90	42.60	1.500	4.80E+03	0.0672	3.50E-03	0.039	0.0946	0.0016	-0.1675	844.0	5.7	11.5	649.5	3.2	6.4	104	
OJ19275	1461.00	1116.00	1050.00	0.760	6.00E+05	0.1464	7.084	0.067	0.3524	0.0036	0.7263	2304.8	22.9	45.7	1946.0	8.6	17.2	92	
OJ19276	383.40	136.10	85.80	0.350	5.30E+04	0.0857	2.773	0.037	0.2360	0.0022	0.1150	1331.4	22.6	45.2	1365.9	5.7	11.5	101	
OJ19277	723.00	612.00	95.70	0.850	-1.80E+04	0.0518	1.70E-03	0.381	0.010	0.0634	0.0006	0.0218	278.6	37.6	75.2	335.3	1.7	3.4	102
OJ19278	622.00	520.00	377.20	0.840	-3.60E+04	0.0937	3.045	0.035	0.2348	0.0028	0.3750	1502.1	20.2	40.3	1419.0	4.4	8.8	96	
OJ19279	988.00	1458.00	407.00	1.510	1.08E+05	0.0611	0.843	0.015	0.1012	0.0010	0.4681	643.1	24.6	49.2	620.8	4.1	8.3	100	
OJ19280	273.80	232.30	70.10	0.850	-2.40E+04	0.0592	2.00E-03	0.873	0.025	0.1066	0.0012	1.807	574.5	36.7	73.5	652.9	3.5	7.0	102
OJ19281	235.40	8.68	2.34	0.040	3.60E+04	0.0595	0.716	0.028	0.0887	0.0010	0.0519	585.4	47.4	94.8	548.3	2.9	5.9	100	
OJ19282	130.50	118.30	31.78	0.910	3.90E+03	0.0586	0.775	0.030	0.0961	0.0012	0.0177	582.6	48.4	96.8	582.6	3.5	7.1	101	
OJ19283	254.90	153.00	154.00	0.600	5.00E+04	0.1363	7.421	0.087	0.3956	0.0038	0.2889	2180.7	24.9	49.8	2148.7	8.8	17.6	99	
OJ19284	145.00	135.60	36.62	0.940	1.38E+04	0.0592	2.70E-03	0.751	0.031	0.0929	0.0013	-0.0386	574.5	49.6	99.2	572.7	3.8	7.7	101
OJ19285	861.00	44.40	43.50	0.050	1.50E+05	0.1258	5.640	0.058	0.3245	0.0032	0.5173	2040.1	23.9	47.8	1811.7	7.8	15.6	94	
OJ19286	253.70	131.10	136.40	0.520	-5.40E+04	0.1359	3.90E-03	7.570	0.091	0.4053	0.0039	1.608	2175.6	25.0	50.0	2183.4	8.9	17.9	101
OJ19287	340.30	488.80	142.90	1.440	5.20E+04	0.0597	2.00E-03	0.868	0.024	0.1058	0.0012	0.904	634.5	6.5	13.0	648.2	3.5	7.0	102
OJ19288	379.10	195.60	195.60	0.520	1.00E+04	0.1256	6.550	0.073	0.3767	0.0037	0.2883	2027.3	24.6	49.3	2052.6	4.9	9.8	100	
OJ19289	924.00	877.00	259.30	0.950	1.30E+04	0.0614	0.908	0.015	0.1073	0.0011	0.1152	654.0	26.2	52.4	657.2	3.2	6.4	100	
OJ19290	157.70	94.60	51.80	0.600	6.00E+04	0.0819	2.277	0.056	0.2029	0.0024	0.1361	1243.1	31.1	62.2	1190.9	6.4	12.9	99	
OJ19291	38.46	14.56	12.48	0.380	6.80E+03	0.1143	4.80E-03	5.150	0.170	0.3287	0.0045	0.1149	1868.9	37.9	75.8	1844.4	14.0	28.0	99
OJ19292	325.20	105.40	25.39	0.320	9.00E+04	0.0578	0.680	0.019	0.0852	0.0010	0.1528	522.2	38.0	75.9	526.8	5.7	11.5	100	
OJ19293	560.00	412.20	124.30	0.740	4.10E+04	0.1066	1.50E-03	0.863	0.015	0.1031	0.0013	0.4166	625.1	26.7	53.4	632.5	2.9	5.9	100
OJ19294	537.80	380.00	57.40	0.710	2.00E+04	0.0543	1.90E-03	0.399	0.021	0.0536	0.0006	0.767	383.5	39.3	78.6	340.9	4.4	8.7	99
OJ19295	535.20	355.70	331.00	0.660	1.60E+05	0.1217	6.185	0.054	0.3683	0.0035	0.2772	1981.3	24.1	48.3	2002.3	3.8	7.6	101	
OJ19297	223.00	213.50	55.95	0.960	5.90E+03	0.0620	2.40E-03	0.779	0.028	0.0920	0.0011	0.1757	674.1	41.4	82.8	584.9	8.0	16.0	97
OJ19298	601.10	40.10	32.10	0.070	5.00E+05	0.0987	2.70E-03	4.041	0.043	0.2978	0.0029	0.3271	1599.3	25.5	51.1	1642.5	4.3	8.7	102
OJ19299	786.00	759.00	111.90	0.970	3.20E+04	0.0543	0.409	0.010	0.0543	0.0006	0.1990	383.5	33.1	66.2	340.7	1.7	3.4	98	
OJ192102	230.10	330.60	288.80	1.450	-2.50E+04	0.1243	6.037	0.086	0.3530	0.0039	0.3391	2018.8	25.7	51.3	1981.2	6.2	12.4	98	
OJ192103	478.10	158.60	47.66	0.330	1.80E+04	0.0634	1.70E-03	0.974	0.020	0.1111	0.0012	0.1133	721.7	28.4	56.9	690.5	5.1	10.3	98
OJ192104	351.30	194.20	51.01	0.550	2.40E+04	0.0606	2.00E-03	0.790	0.021	0.0953	0.0011	0.0875	625.1	35.6	71.2	591.2	6.0	11.9	98
OJ192105	357.50	241.00	69.40	0.670	1.00E+00	0.0654	1.90E-03	0.928	0.023	0.1029	0.0010	0.1041	787.2	30.5	61.0	666.6	6.1	12.1	95
OJ192107	276.90	210.40	205.90	0.760	-5.80E+04	0.1295	3.60E-03	7.052	0.078	0.3938	0.0038	0.3153	2091.2	24.4	48.9	2118.0	4.9	9.8	101
OJ192108	692.60	221.80	59.00	0.320	1.00E+03	0.0605	1.90E-03	0.838	0.015	0.1007	0.0010	0.1052	621.5	26.7	53.5	618.6	2.9	5.7	100
OJ192109	59.38	75.60	62.50	1.270	-9.60E+03	0.1107	3.50E-03	5.190	0.120	0.3372	0.0045	0.1019	1810.9	32.0	64.0	1851.0	9.8	19.7	101
OJ192110	113.70	111.90	27.87	0.980	3.30E+03	0.0573	3.10E-03	0.744	0.039	0.0937	0.0014	0.1187	503.1	59.5	119.1	564.7	11.3	22.7	102
OJ192111	892.00	429.00	406.00	0.480	1.20E+05	0.1133	3.10E-03	5.123	0.048	0.3270	0.0033	0.4691	1852.8	24.7	49.5	1839.9	4.0	8.0	99
OJ192112	625.30	288.80	271.80	0.460	1.20E+05	0.1304	6.800	0.048	0.3785	0.0033	0.0991	2103.4	23.6	47.1	2085.7	3.1	6.2	97	
OJ192113	695.30	288.80	271.80	0.460	1.20E+05	0.1304	6.800	0.048	0.3785	0.0033	0.0991	2103.4	23.6	47.1	2085.7	3.1	6.2	97	
OJ192114	830.00	222.00	231.80	0.270	2.40E+05	0.1579	4.20E-03	9.051	0.077	0.4155	0.0044	0.5791	2433.3	22.5	45.1	2343.2	3.9	7.8	96
OJ192115	846.00	866.00	126.30	1.020	1.70E+04	0.0598	1.70E-03	0.417	0.010	0.0505	0.0006	0.1954	596.3	30.8	61.6	357.7	1.8	3.6	90
OJ192116	927.00	679.00	645.00	0.730	7.00E+05	0.1228	3.30E-03	6.167	0.048	0.3643	0.0034	0.3599	1997.7	23.9	47.7	1999.8	3.4	6.8	100
OJ192117	785.00	396.10	498.00	0.500	-2.10E+05	0.2266	6.10E-03	16.370	0.140	0.5231	0.0048	0.5964	3028.2	21.6	43.2	2898.7	4.1	8.2	94
OJ192118	545.60	621.00	158.50	1.140	3.00E+04	0.0585	1.80E-03	0.757	0.020	0.0939	0.0010	0.1251	548.5	33.6	67.2	572.3	5.8	11.5	101
OJ192119	190.20	351.70	407.80	1.850	1.90E+05	0.1628	4.50E-03	10.600	0.120	0.4734	0.0045	0.4174	2485.0	23.3	46.6	2488.7	9.2	19.7	100
OJ192120	144.20	321.00	76.70	2.230	4.00E+02	0.0602	2.90E-03	0.756	0.033	0.0903	0.0012	-0.0582	610.8	52.1	104.1	571.7	5.5	11.1	95
OJ192121	372.00	188.40	164.00	0.510	3.10E+04	0.1306	3.70E-03	6.040	0.150	0.3591	0.0085	0.8779	2106.0	24.9	49.7	1981.6	10.8	21.6	97
OJ192122	673.00	776.00	214.10	1.150	1.10E+04	0.0634	1.50E-03	0.878	0.015	0.1018	0.0010	0.2285	721.7	25.1	50.2	639.9	4.1	8.1	98
OJ192123	130.50	152.90	146.90	1.170	1.10E+04	0.1244	4.00E-03	5.700	0.120	0.3301	0.0048	0.4908	2020.3	28.5	57.0	1931.4	9.1	18.2	95
OJ192124	110.20	70.60	34.20	2.340	2.70E+03	0.0673	3.20E-03	0.921	0.040	0.1001	0.0014	0.1473	847.1	49.4	98.9	662.9	10.6	21.1	93
OJ192127	171.10	294.90	383.30	1.720	-2.90E+04	0.2063	5.70E-03	15.160	0.210	0.5301	0.0059	0.6246	2876.7	22.4	44.9	2825.3	6.6	13.2	97
OJ192128	460.30	335.00	50.29	0.730	-7.40E+03	0.0547	2.00E-03	0.416	0.013	0.0554	0.0006	-0.1231	400.0	41.0	81.9	353.2	4.7	9.3	98
OJ192129	133.20	83.10	76.90	0.620	-4.00E+04	0.1246	3.80E-03	6.449	0.098	0.3754	0.0043	0.1482	2023.1						

ANALYSIS	U (ppm)	Th (ppm)	Pb (ppm)	Th/U	$^{207}\text{Pb}/^{206}\text{Pb}$		Ratios		$^{207}\text{Pb}/^{238}\text{U}$		Error correction		$^{207}\text{Pb}/^{206}\text{Pb}$		Ages (Ma)		$^{206}\text{Pb}/^{238}\text{U}$		Concordance (%)		
					2σ	2σ	2σ	2σ	2σ	2σ	2σ	2σ	2σ	2σ	2σ	2σ	2σ	2σ		2σ	2σ
OJJ19z101	551.00	860.00	263.80	1.560	5.00E+04	2.10E+04	0.0876	2.80E-03	1.201	0.024	0.1003	0.0016	1373.7	30.7	61.5	801.0	5.5	11.1	616.2	4.7	9.4
OJJ19z106	277.50	106.20	22.30	0.380	9.20E+03	7.50E+03	0.0734	4.00E-03	0.540	0.029	0.0532	0.0007	1025.0	55.1	110.3	438.4	9.6	19.1	334.1	2.1	4.2
OJJ19z125	1025.00	321.00	162.80	0.310	1.40E+05	1.10E+05	0.1449	2.80E-03	4.778	0.079	0.2399	0.0041	2286.6	16.6	33.3	1781.0	6.9	13.9	1386.2	10.7	21.3
OJJ19z126	1836.00	1249.00	738.00	0.680	3.45E+04	3.10E+03	0.2178	5.20E-03	2.275	0.035	0.0756	0.0009	2964.5	19.2	38.5	1204.6	5.4	10.8	469.6	2.6	5.2

Footnotes:

. . . Analysis references: OJJ19z is zircon from sample OJJ19 (mount CT18-10b), followed by grain number.

Appendix E

Results of the Hf analyses

Chapter II – Section II.3: Table E.1

Chapter III – Tables E.2 to E.5

Chapter IV – Tables E.6 to E.12

Chapter II, Section II.3

Table E.1: Sample AZR10

IGSN: IEACC0029

Coordinate UTM: Zone 30S, 233758 m E, 3633628 m N

GRAIN	Age (Ma)	σ	2σ	Concordia	$^{176}\text{Lu}/^{177}\text{Hf}$	2σ	$^{176}\text{Hf}/^{177}\text{Hf}$	2σ	$(^{176}\text{Hf}/^{177}\text{Hf})_{\text{init}}$	2σ	ϵ_{Hf}	2σ
AZR10z1	507.5	2.4	4.8	92	0.0006041	0.0000036	0.282739	0.000058	0.000058000	0.000058	9.8	2.0522
AZR10z2	522.7	2.7	5.4	101	0.0004031	0.0000016	0.282739	0.000061	0.000061000	0.000061	10.2	2.15915
AZR10z3	491.3	3.0	6.0	98	0.0011660	0.0000270	0.282642	0.000060	0.000060000	0.000060	5.8	2.11535
AZR10z4	507.8	2.5	5.1	94	0.0005166	0.0000034	0.282707	0.000056	0.000056000	0.000056	8.7	1.98146
AZR10z5	589.6	3.2	6.5	100	0.0009260	0.0000140	0.282548	0.000064	0.000064000	0.000064	4.7	2.26077
AZR10z6	528.1	2.9	5.8	99	0.0005187	0.0000080	0.282700	0.000063	0.000063000	0.000063	8.9	2.22773
AZR10z7	542.9	2.7	5.3	100	0.0006120	0.0000170	0.282674	0.000069	0.000069000	0.000069	8.3	2.43692
AZR10z9	533.0	2.5	5.0	100	0.0006840	0.0000120	0.282743	0.000059	0.000059000	0.000059	10.5	2.08469
AZR10z10	526.3	2.6	5.3	99	0.0004964	0.0000047	0.282747	0.000069	0.000069000	0.000069	10.5	2.44132
AZR10z11	569.1	2.6	5.3	101	0.0010260	0.0000180	0.282519	0.000064	0.000064000	0.000064	3.2	2.25935
AZR10z12	538.1	2.8	5.6	94	0.0005207	0.0000052	0.282764	0.000059	0.000059000	0.000059	11.4	2.0871
AZR10z13	529.6	2.6	5.1	100	0.0005184	0.0000094	0.282661	0.000061	0.000061000	0.000061	7.6	2.15643
AZR10z14	475.2	4.2	8.4	95	0.0010144	0.0000086	0.282662	0.000061	0.000061000	0.000061	6.2	2.15676
AZR10z15	535.3	2.5	4.9	100	0.0005640	0.0000030	0.282708	0.000056	0.000056000	0.000056	9.3	1.98166
AZR10z16	515.4	2.4	4.7	94	0.0008060	0.0000200	0.282654	0.000063	0.000063000	0.000063	6.9	2.22364
AZR10z17	580.3	2.8	5.6	100	0.0009210	0.0000110	0.282436	0.000071	0.000071000	0.000071	0.5	2.50983
AZR10z18	539.8	2.6	5.2	101	0.0006090	0.0000110	0.282727	0.000063	0.000063000	0.000063	10.1	2.22665
AZR10z19	523.4	2.5	4.9	100	0.0004748	0.0000020	0.282652	0.000061	0.000061000	0.000061	7.1	2.15901
AZR10z20	528.6	2.6	5.2	100	0.0004980	0.0000150	0.282656	0.000058	0.000058000	0.000058	7.4	2.04825
AZR10z21	521.9	2.8	5.6	101	0.0004762	0.0000063	0.282695	0.000061	0.000061000	0.000061	8.6	2.15751
AZR10z22	516.9	2.7	5.4	96	0.0005430	0.0000054	0.282722	0.000060	0.000060000	0.000060	9.4	2.12241
AZR10z23	528.5	2.4	4.8	100	0.0007640	0.0000360	0.282671	0.000065	0.000065000	0.000065	7.8	2.28871
AZR10z25	581.0	3.2	6.5	97	0.0006870	0.0000230	0.282329	0.000060	0.000060000	0.000060	-3.1	2.1157
AZR10z26	533.8	2.4	4.9	100	0.0005473	0.0000078	0.282639	0.000058	0.000058000	0.000058	6.9	2.05077
AZR10z27	566.1	3.0	5.9	99	0.0009070	0.0000260	0.282435	0.000071	0.000071000	0.000071	0.2	2.50422
AZR10z28	560.4	3.0	5.9	100	0.0011450	0.0000320	0.282455	0.000078	0.000078000	0.000078	0.7	2.74991
AZR10z30	527.1	2.7	5.5	98	0.0007940	0.0000095	0.282629	0.000063	0.000063000	0.000063	6.3	2.22721
AZR10z31	518.8	3.6	7.1	101	0.0002991	0.0000023	0.282767	0.000057	0.000057000	0.000057	11.2	2.01727
AZR10z32	483.2	2.5	4.9	95	0.0006339	0.0000068	0.282689	0.000073	0.000073000	0.000073	7.5	2.58215
AZR10z33	492.3	3.0	6.0	94	0.0006900	0.0000100	0.282653	0.000066	0.000066000	0.000066	6.4	2.3333
AZR10z34	576.0	2.7	5.3	99	0.0006841	0.0000060	0.282418	0.000061	0.000061000	0.000061	-0.1	2.15766
AZR10z35	508.9	3.0	6.0	96	0.0006640	0.0000100	0.282606	0.000057	0.000057000	0.000057	5.1	2.01464
AZR10z37	583.6	2.8	5.6	101	0.0010120	0.0000210	0.281719	0.000064	0.000064000	0.000064	-24.8	2.25808
AZR10z38	531.7	2.5	5.0	99	0.0007175	0.0000038	0.282650	0.000065	0.000065000	0.000065	7.1	2.30002
AZR10z39	519.4	2.3	4.6	100	0.0007641	0.0000081	0.282635	0.000061	0.000061000	0.000061	6.3	2.15689
AZR10z40	574.2	2.8	5.5	100	0.0009375	0.0000019	0.282498	0.000060	0.000060000	0.000060	2.6	2.12381
AZR10z41	570.5	3.2	6.5	99	0.0010760	0.0000280	0.282432	0.000061	0.000061000	0.000061	0.1	2.14932
AZR10z42	478.7	2.4	4.8	96	0.0008160	0.0000120	0.282653	0.000054	0.000054000	0.000054	6.1	1.90787
AZR10z43	519.5	2.5	5.0	99	0.0009089	0.0000081	0.282660	0.000057	0.000057000	0.000057	7.2	2.01527
AZR10z45	489.6	3.6	7.2	97	0.0006690	0.0000230	0.282696	0.000056	0.000056000	0.000056	7.9	1.97506
AZR10z46	589.3	2.8	5.5	100	0.0035266	0.0000086	0.281922	0.000067	0.000067000	0.000067	-18.5	2.36911
AZR10z47	522.9	2.5	4.9	95	0.0007038	0.0000023	0.282702	0.000057	0.000057000	0.000057	8.8	2.01728
AZR10z48	530.5	2.6	5.3	101	0.0009469	0.0000026	0.282683	0.000063	0.000063000	0.000063	8.2	2.22963
AZR10z49	524.7	2.6	5.2	101	0.0010800	0.0000210	0.282727	0.000059	0.000059000	0.000059	9.6	2.08158
AZR10z50	523.3	2.7	5.5	96	0.0009713	0.0000060	0.282675	0.000062	0.000062000	0.000062	7.7	2.19302
AZR10z51	531.7	2.6	5.2	100	0.0010800	0.0000120	0.282676	0.000060	0.000060000	0.000060	7.9	2.1201
AZR10z52	541.4	2.7	5.5	101	0.0014070	0.0000260	0.282644	0.000065	0.000065000	0.000065	6.9	2.29208
AZR10z54	547.4	2.7	5.4	99	0.0011375	0.0000085	0.282671	0.000066	0.000066000	0.000066	8.1	2.33376
AZR10z56	514.5	2.4	4.8	98	0.0017290	0.0000360	0.282526	0.000059	0.000059000	0.000059	2.0	2.07655
AZR10z57	474.0	3.6	7.2	94	0.0026060	0.0000300	0.282342	0.000066	0.000066000	0.000066	-5.6	2.32704
AZR10z58	540.9	2.7	5.4	101	0.0015470	0.0000160	0.282521	0.000064	0.000064000	0.000064	2.5	2.26026
AZR10z59	485.7	2.7	5.4	95	0.0016070	0.0000310	0.282431	0.000062	0.000062000	0.000062	-1.9	2.18493
AZR10z60	576.1	2.9	5.9	100	0.0030220	0.0000330	0.282302	0.000060	0.000060000	0.000060	-5.1	2.11192
AZR10z63	575.8	2.6	5.2	98	0.0021500	0.0000390	0.282456	0.000072	0.000072000	0.000072	0.7	2.53454
AZR10z65	509.4	2.8	5.6	92	0.0012380	0.0000130	0.282620	0.000064	0.000064000	0.000064	5.4	2.26146
AZR10z66	412.2	2.4	4.8	94	0.0011303	0.0000058	0.282609	0.000058	0.000058000	0.000058	3.0	2.0514
AZR10z67	525.8	2.4	4.8	99	0.0011289	0.0000050	0.282665	0.000061	0.000061000	0.000061	7.4	2.15797
AZR10z68	473.3	2.5	4.9	96	0.0012070	0.0000110	0.282646	0.000065	0.000065000	0.000065	5.6	2.29762
AZR10z69	565.6	3.5	7.1	100	0.0017430	0.0000130	0.282426	0.000061	0.000061000	0.000061	-0.4	2.15502
AZR10z71	434.3	3.0	5.9	92	0.0010470	0.0000170	0.282708	0.000062	0.000062000	0.000062	7.0	2.18978
AZR10z72	560.8	2.6	5.1	99	0.0013110	0.0000170	0.282424	0.000059	0.000059000	0.000059	-0.4	2.08274
AZR10z73	527.6	2.5	5.0	100	0.0008790	0.0000140	0.282735	0.000062	0.000062000	0.000062	10.0	2.19022
AZR10z74	504.6	2.6	5.1	96	0.0016880	0.0000260	0.282476	0.000062	0.000062000	0.000062	0.1	2.18631
AZR10z76	534.4	2.5	5.0	98	0.0005872	0.0000047	0.282649	0.000066	0.000066000	0.000066	7.2	2.33512
AZR10z77	486.0	5.1	10.2	96	0.0009355	0.0000090	0.282680	0.000059	0.000059000	0.000059	7.1	2.08582
AZR10z78	578.2	3.2	6.5	98	0.0008239	0.0000028	0.282491	0.000076	0.000076000	0.000076	2.5	2.69003
AZR10z79	468.5	2.9	5.9	97	0.0007810	0.0000140	0.282662	0.000066	0.000066000	0.000066	6.2	2.33209
AZR10z81	524.1	2.6	5.1	99	0.0007180	0.0000069	0.282651	0.000060	0.000060000	0.000060	7.0	2.1219
AZR10z82	538.2	2.5	5.0	98	0.0008435	0.0000052	0.282686	0.000063	0.000063000	0.000063	8.5	2.22873
AZR10z83	569.5	2.8	5.6	101	0.0011990	0.0000230	0.282493	0.000067	0.000067000	0.000067	2.2	2.36368
AZR10z84	522.0	2.5	5.1	98	0.0006470	0.0000230	0.282704	0.000064	0.000064000	0.000064	8.9	2.25794
AZR10z87	503.0	3.3	6.6	99	0.0006860	0.0000130	0.282632	0.000071	0.000071000	0.000071	5.9	2.5093
AZR10z88	577.3	2.9	5.9	100	0.0007552	0.0000039	0.282455	0.000076	0.000076000	0.000076	1.2	2.6896
AZR10z89	532.3	2.8	5.5	97	0.0009370	0.0000200	0.282660	0.000057	0.000057000	0.000057	7.4	2.01106
AZR10z90	584.2	3.5	7.1	99	0.0004397	0.0000060	0.282344	0.000065	0.000065000	0.000065	-2.5	2.2993
AZR10z91	621.6	3.2	6.4	101	0.0007230	0.0000150	0.282399	0.000067	0.000067000	0.000067	0.2	2.36645
AZR10z92	544.6	2.7	5.4	98	0.0007484	0.0000052	0.282589	0.000059	0.000059000	0.000059	5.3	2.08711
AZR10z94	536.6	2.8	5.5	101	0.0005844	0.0000045	0.282674	0.000060	0.000060000	0.000060	8.2	2.12276
AZR10z95	516.8	3.0	5.9									

GRAIN	Age (Ma)	σ	2σ	Concordia	$^{176}\text{Lu}/^{177}\text{Hf}$	2σ	$^{176}\text{Hf}/^{177}\text{Hf}$	2σ	$(^{176}\text{Hf}/^{177}\text{Hf})_{\text{int}}$	2σ	ϵHf	2σ
AZR10z104	516.4	2.3	4.5	100	0.0009170	0.0000210	0.282680	0.000069	0.000069000	0.000069	7.8	2.43571
AZR10z106	668.8	3.2	6.4	100	0.0016700	0.0001400	0.282304	0.000061	0.000061000	0.000061	-2.6	2.09815
AZR10z107	511.7	2.4	4.8	96	0.0007105	0.0000039	0.282759	0.000062	0.000062000	0.000062	10.6	2.19373
AZR10z108	522.0	2.7	5.4	98	0.0006740	0.0000260	0.282733	0.000060	0.000060000	0.000060	9.9	2.11529
AZR10z110	478.0	2.3	4.6	97	0.0008110	0.0000160	0.282704	0.000059	0.000059000	0.000059	7.9	2.08361
AZR10z111	448.0	2.4	4.8	93	0.0010970	0.0000190	0.282692	0.000063	0.000063000	0.000063	6.7	2.2245
AZR10z112	543.8	2.9	5.8	100	0.0007011	0.0000051	0.282700	0.000065	0.000065000	0.000065	9.2	2.29959
AZR10z113	518.5	2.9	5.7	95	0.0007400	0.0000200	0.282756	0.000056	0.000056000	0.000056	10.6	1.97577
AZR10z114	447.6	4.2	8.4	93	0.0016420	0.0000790	0.282577	0.000073	0.000073000	0.000073	2.5	2.56067
AZR10z117	498.9	3.0	6.0	97	0.0009740	0.0000150	0.282729	0.000062	0.000062000	0.000062	9.1	2.19002
AZR10z118	592.7	2.9	5.8	100	0.0017010	0.0000260	0.282430	0.000067	0.000067000	0.000067	0.3	2.36226
AZR10z119	514.3	2.6	5.1	90	0.0008840	0.0000110	0.282685	0.000072	0.000072000	0.000072	7.9	2.54535
AZR10z120	508.2	3.3	6.6	97	0.0009340	0.0000260	0.282752	0.000078	0.000078000	0.000078	10.2	2.75273

Chapter III

Table E.2: Sample MIM2

IGSN: IEACC0004

Coordinate UTM: Zone 30S, 509359 m E, 3763408 m N

GRAIN	Age (Ma)	σ	2σ	Concordia	$^{176}\text{Lu}/^{177}\text{Hf}$	2σ	$^{176}\text{Hf}/^{177}\text{Hf}$	2σ	$(^{176}\text{Hf}/^{177}\text{Hf})_{\text{int}}$	2σ	ϵ_{Hf}	2σ
MIM2z1	2013.1	19.3	38.7	101	0.0010745	0.0000061	0.281550	0.000055	0.281508891	0.000055	0.3	2.0
MIM2z2	627.6	3.5	7.0	99	0.0005429	0.0000076	0.282396	0.000051	0.282389608	0.000051	0.3	1.8
MIM2z4	1797.7	15.7	31.5	100	0.0012340	0.0000470	0.281741	0.000050	0.281698925	0.000050	2.1	1.8
MIM2z5	597.4	2.9	5.9	97	0.0017260	0.0000100	0.282297	0.000056	0.282277663	0.000056	-4.3	2.0
MIM2z6	617.3	3.8	7.6	100	0.0011330	0.0000120	0.282588	0.000061	0.282574880	0.000061	6.6	2.2
MIM2z7c	2198.5	17.7	35.3	100	0.0012550	0.0000920	0.281862	0.000092	0.281809473	0.000092	15.2	3.4
MIM2z7r	360.3	1.8	3.7	99	0.0013640	0.0000300	0.282547	0.000054	0.282537804	0.000054	-0.4	1.9
MIM2z8	645.9	3.5	7.0	101	0.0010490	0.0000210	0.282192	0.000055	0.282179287	0.000055	-6.7	2.0
MIM2z9	658.2	3.2	6.4	100	0.0028660	0.0000340	0.282576	0.000056	0.282540601	0.000056	6.3	2.0
MIM2z10	2045.7	14.7	29.4	100	0.0015240	0.0000470	0.281210	0.000051	0.281150733	0.000051	-11.7	1.9
MIM2z11	595.7	3.2	6.5	99	0.0006790	0.0000540	0.282217	0.000058	0.282209414	0.000058	-6.8	2.1
MIM2z12	665.8	3.5	7.0	99	0.0030950	0.0000800	0.282692	0.000054	0.282653331	0.000054	10.5	1.9
MIM2z13	2175.6	16.0	32.0	101	0.0006493	0.0000058	0.281586	0.000055	0.281559113	0.000055	5.8	2.0
MIM2z14	2221.0	15.5	31.1	101	0.0006091	0.0000076	0.281385	0.000055	0.281359240	0.000055	-0.3	2.0
MIM2z15	2066.6	15.9	31.8	101	0.0003960	0.0000300	0.281152	0.000052	0.281136440	0.000052	-11.8	1.9
MIM2z16	2433.4	13.4	26.8	97	0.0004140	0.0000140	0.281167	0.000054	0.281147779	0.000054	-2.9	1.9
MIM2z17	372.3	1.9	3.9	100	0.0008570	0.0000440	0.282368	0.000055	0.282362028	0.000055	-6.3	2.0
MIM2z18	615.2	3.2	6.4	101	0.0007640	0.0000200	0.282444	0.000052	0.282435184	0.000052	1.6	1.8
MIM2z19r	603.9	2.8	5.6	101	0.0004390	0.0000077	0.282474	0.000053	0.282469028	0.000053	2.6	1.9
MIM2z20	619.1	4.7	9.4	98	0.0008850	0.0000250	0.282643	0.000052	0.282632722	0.000052	8.7	1.9
MIM2z21	620.9	3.2	6.4	100	0.0015400	0.0000370	0.282571	0.000052	0.282553063	0.000052	5.9	1.9
MIM2z22c	647.7	3.5	7.0	100	0.0010300	0.0000430	0.282232	0.000052	0.282219482	0.000052	-5.3	1.9
MIM2z22r	571.5	2.9	5.8	100	0.0007066	0.0000071	0.282158	0.000058	0.282150429	0.000058	-9.4	2.1
MIM2z23	619.6	3.2	6.4	100	0.0015007	0.0000083	0.282458	0.000051	0.282440559	0.000051	1.9	1.8
MIM2z24	2846.5	12.9	25.7	101	0.0008000	0.0000170	0.280881	0.000055	0.280837383	0.000055	-4.4	2.0
MIM2z25	2496.3	14.4	28.8	101	0.0007505	0.0000086	0.281173	0.000056	0.281137234	0.000056	-1.9	2.0
MIM2z26	1553.4	15.6	31.2	100	0.0012800	0.0001200	0.281839	0.000053	0.281801374	0.000053	0.2	2.0
MIM2z27	2540.8	15.9	31.9	103	0.0004480	0.0000030	0.281191	0.000052	0.281169280	0.000052	0.3	1.9
MIM2z28	2083.0	16.4	32.8	100	0.0018540	0.0000380	0.281617	0.000060	0.281543558	0.000060	3.1	2.2
MIM2z29	620.0	2.9	5.9	99	0.0008710	0.0000250	0.282213	0.000051	0.282202870	0.000051	-6.5	1.8
MIM2z30	595.0	7.9	15.9	104	0.0008660	0.0000140	0.282206	0.000054	0.282196336	0.000054	-7.3	1.9
MIM2z31	571.5	3.8	7.7	99	0.0008440	0.0000180	0.282181	0.000054	0.282171956	0.000054	-8.7	1.9
MIM2z33	2075.4	13.7	27.4	96	0.0011220	0.0000110	0.281360	0.000052	0.281355185	0.000052	-3.8	1.9
MIM2z34	555.5	2.6	5.3	101	0.0067100	0.0001500	0.282526	0.000059	0.282456125	0.000059	1.1	2.1
MIM2z35	588.6	3.2	6.5	98	0.0030090	0.0000360	0.282182	0.000054	0.282148785	0.000054	-9.1	1.9
MIM2z36	603.1	3.2	6.5	99	0.0035530	0.0000150	0.282364	0.000056	0.282323808	0.000056	-2.6	2.0
MIM2z37	2486.0	14.0	27.9	94	0.0017352	0.0000057	0.281133	0.000054	0.281050656	0.000054	-5.2	1.9
MIM2z38	608.5	3.8	7.6	97	0.0017510	0.0000290	0.282434	0.000055	0.282414014	0.000055	0.7	2.0
MIM2z39c	1759.2	19.5	39.1	99	0.0015690	0.0000460	0.281459	0.000052	0.281406670	0.000052	-9.2	1.9
MIM2z39r	1751.5	15.4	30.7	98	0.0022200	0.0000610	0.281519	0.000054	0.281445285	0.000054	-8.0	2.0
MIM2z41	2056.9	16.7	33.4	97	0.0006802	0.0000042	0.281431	0.000053	0.281404400	0.000053	-2.5	1.9
MIM2z42	1881.5	17.2	34.4	99	0.0066800	0.0000360	0.281548	0.000056	0.281309444	0.000056	-9.8	2.0
MIM2z43c	3013.2	12.9	25.7	98	0.0034700	0.0001200	0.280974	0.000055	0.280773413	0.000055	-2.8	2.2
MIM2z43r	2964.5	14.4	28.9	101	0.0012250	0.0000098	0.281021	0.000056	0.280951365	0.000056	2.4	2.0
MIM2z44	592.6	3.2	6.5	98	0.0005382	0.0000045	0.281739	0.000054	0.281733019	0.000054	-23.7	1.9
MIM2z46	546.8	2.9	5.7	101	0.0031700	0.0001500	0.282319	0.000053	0.282286505	0.000053	-5.1	1.9
MIM2z47	601.5	3.8	7.6	99	0.0025210	0.0000330	0.282149	0.000062	0.282120560	0.000062	-9.8	2.2
MIM2z48	380.4	1.9	3.8	98	0.0025400	0.0001000	0.282415	0.000052	0.282396918	0.000052	-4.9	1.9
MIM2z49	501.5	2.8	5.5	100	0.0025430	0.0000940	0.282532	0.000052	0.282508104	0.000052	1.7	1.9
MIM2z50	901.5	4.8	9.5	100	0.0020950	0.0000370	0.282493	0.000063	0.282457478	0.000063	8.8	2.3
MIM2z51	599.4	2.9	5.9	99	0.0009370	0.0000140	0.282467	0.000052	0.282456466	0.000052	2.0	1.8
MIM2z52	615.0	4.1	8.2	96	0.0010980	0.0000330	0.282366	0.000051	0.282353334	0.000051	-1.3	1.8
MIM2z54	2091.2	16.3	32.6	99	0.0012900	0.0001500	0.281272	0.000051	0.281220695	0.000051	-8.2	2.0
MIM2z55	638.1	3.2	6.4	93	0.0018590	0.0000370	0.282507	0.000056	0.282484745	0.000056	3.9	2.0
MIM2z56	551.8	3.0	5.9	99	0.0003460	0.0000100	0.282323	0.000056	0.282319421	0.000056	-3.9	2.0
MIM2z57	619.4	2.9	5.8	101	0.0004630	0.0000180	0.282031	0.000056	0.282025620	0.000056	-12.8	2.0
MIM2z59	371.2	1.7	3.3	98	0.0019200	0.0001400	0.282400	0.000053	0.282386660	0.000053	-5.5	1.9
MIM2z60	595.2	2.9	5.8	101	0.0001151	0.0000019	0.282226	0.000068	0.282224715	0.000068	-6.3	2.4
MIM2z61	2682.1	14.9	29.8	101	0.0004310	0.0000100	0.280628	0.000055	0.280605893	0.000055	-16.5	2.0
MIM2z62	626.1	4.4	8.8	100	0.0009110	0.0000210	0.282349	0.000057	0.282338300	0.000057	-1.5	2.0
MIM2z63c	2475.6	16.7	33.4	95	0.0010450	0.0000420	0.281336	0.000054	0.281286621	0.000054	3.0	2.0
MIM2z64	569.1	3.0	5.9	98	0.0009040	0.0000100	0.282450	0.000055	0.282440355	0.000055	0.8	2.0
MIM2z65	617.2	3.5	7.0	91	0.0008490	0.0000370	0.282521	0.000060	0.282511171	0.000060	4.4	2.1
MIM2z66	357.1	1.9	3.7	92	0.0012270	0.0000320	0.282419	0.000054	0.282410801	0.000054	-4.9	1.9
MIM2z68	581.6	3.2	6.5	100	0.0003920	0.0000170	0.282371	0.000055	0.282366725	0.000055	-1.5	2.0
MIM2z69	1374.2	7.0	14.1	99	0.0004873	0.0000019	0.281992	0.000054	0.281979350	0.000054	2.5	1.9
MIM2z71	2483.9	14.5	29.0	100	0.0005229	0.0000042	0.281313	0.000056	0.281288207	0.000056	3.2	2.0
MIM2z74	649.5	5.0	9.9	103	0.0003692	0.0000088	0.282278	0.000055	0.282273501	0.000055	-3.3	2.0
MIM2z75	2599.4	14.3	28.7	91	0.0009760	0.0000630	0.280893	0.000054	0.280844520	0.000054	-9.9	2.0
MIM2z76	630.7	2.9	5.8	99	0.0008430	0.0000270	0.282494	0.000052	0.282484025	0.000052	3.7	1.9
MIM2z77	607.8	3.8	7.6	101	0.0005561	0.0000054	0.282577	0.000052	0.282570661	0.000052	6.3	1.8
MIM2z78	632.3	2.9	5.8	99	0.0006811	0.0000031	0.282197	0.000055	0.282188920	0.000055	-6.7	1.9
MIM2z79	621.0	3.5	7.0	100	0.0005200	0.0000260	0.282473	0.000054	0.282466942	0.000054	2.9	1.9
MIM2z80c	2026.0	17.0	34.1	91	0.0008470	0.0000320	0.281675	0.000059	0.281642385	0.000059	5.3	2.1
MIM2z80r	378.7	2.1	4.2	95	0.0009453	0.0000080	0.282395	0.000063	0.282388299	0.000063	-5.3	2.2
MIM2z81	644.8	4.7	9.3	99	0.0006620	0.0000014	0.282443	0.000058	0.282434991	0.000058	2.3	2.1
MIM2z82	665.2	4.9	9.9	102	0.0006820	0.0000370	0.282683	0.000057	0.282674487	0.000057	11.2	2.0
MIM2z83	1422.0	7.0	14.0	99	0.0009104	0.0000099	0.282116	0.000054	0.282091534	0.000054	7.5	1.9
MIM2z84	623.6	3.8	7.6	99	0.0005939	0.0000015	0.282367	0.000054	0.282360053	0.000054	-0.8	1.9
MIM2z85	2921.6	12.6	25.2	96	0.0015910	0.0000150	0.280899	0.000051	0.280809905	0.000051	-3.7	1.8
MIM2z86	2707.1	15.5										

GRAIN	Age (Ma)	σ	2σ	Concordia	$^{176}\text{Lu}/^{177}\text{Hf}$	2σ	$^{176}\text{Hf}/^{177}\text{Hf}$	2σ	$(^{176}\text{Hf}/^{177}\text{Hf})_{\text{int}}$	2σ	ϵHf	2σ
MIM2z96	1939.8	15.8	31.6	98	0.0008240	0.0000290	0.281608	0.000055	0.281577645	0.000055	1.0	2.0
MIM2z97	634.9	5.3	10.5	101	0.0017170	0.0000250	0.281834	0.000052	0.281813549	0.000052	-19.9	1.9
MIM2z98	2841.6	18.6	37.1	99	0.0001842	0.0000008	0.280858	0.000058	0.280847976	0.000058	-4.2	2.1
MIM2z100	2469.3	15.2	30.4	100	0.0008350	0.0000190	0.281172	0.000052	0.281132646	0.000052	-2.7	1.9
MIM2z101	619.7	3.8	7.6	102	0.0011530	0.0000460	0.282606	0.000054	0.282592597	0.000054	7.3	1.9
MIM2z102	570.3	3.8	7.7	94	0.0013470	0.0000420	0.282385	0.000060	0.282370597	0.000060	-1.6	2.1
MIM2z103	2130.0	14.5	29.1	100	0.0021500	0.0000480	0.281603	0.000057	0.281515872	0.000057	3.2	2.1
MIM2z104	633.7	3.8	7.6	103	0.0018940	0.0000120	0.282657	0.000057	0.282634482	0.000057	9.1	2.0
MIM2z105	620.9	4.7	9.4	106	0.0008290	0.0000078	0.282680	0.000058	0.282670345	0.000058	10.1	2.1
MIM2z106	625.3	3.2	6.4	102	0.0016200	0.0001100	0.281781	0.000055	0.281761997	0.000055	-22.0	2.0
MIM2z107	603.6	2.7	5.5	102	0.0007607	0.0000069	0.282054	0.000051	0.282045389	0.000051	-12.4	1.8
MIM2z108	617.9	4.1	8.2	99	0.0010000	0.0000300	0.281789	0.000056	0.281777409	0.000056	-21.6	2.0
MIM2z109c	558.3	2.8	5.6	101	0.0045500	0.0001600	0.282372	0.000054	0.282324375	0.000054	-3.5	2.0
MIM2z109r	523.0	2.5	4.9	99	0.0041460	0.0000680	0.282369	0.000054	0.282328359	0.000054	-4.2	1.9
MIM2z110	786.0	3.7	7.4	100	0.0032410	0.0000370	0.282036	0.000059	0.281988138	0.000059	-10.4	2.1
MIM2z111c	367.1	2.0	4.0	94	0.0020660	0.0000250	0.282433	0.000053	0.282418807	0.000053	-4.4	1.9
MIM2z111r	371.2	1.8	3.7	97	0.0026890	0.0000580	0.282429	0.000053	0.282410321	0.000053	-4.6	1.9
MIM2z113	2502.4	15.9	31.7	101	0.0005175	0.0000034	0.281170	0.000054	0.281145275	0.000054	-1.4	1.9
MIM2z114	2092.1	14.2	28.5	90	0.0022640	0.0000120	0.281416	0.000053	0.281325916	0.000053	-4.4	1.9
MIM2z115c	577.4	3.8	7.7	93	0.0011600	0.0000290	0.282288	0.000053	0.282275441	0.000053	-4.9	1.9
MIM2z115r	572.0	2.7	5.4	99	0.0024330	0.0000390	0.282253	0.000056	0.282226908	0.000056	-6.7	2.0
MIM2z116	606.2	5.3	10.6	96	0.0014441	0.0000086	0.282625	0.000056	0.282608581	0.000056	7.6	2.0
MIM2z117	2067.9	17.9	35.9	100	0.0004167	0.0000089	0.281656	0.000051	0.281639615	0.000051	6.1	1.8
MIM2z118	3085.7	13.2	26.5	100	0.0016470	0.0000230	0.280935	0.000055	0.280837436	0.000055	1.1	2.0
MIM2z120	2073.4	17.2	34.4	100	0.0005280	0.0000150	0.281534	0.000057	0.281513183	0.000057	1.8	2.0
MIM2z121	873.4	4.8	9.6	99	0.0013940	0.0000190	0.282559	0.000057	0.282536106	0.000057	11.0	2.0
MIM2z122	2489.1	19.1	38.2	99	0.0007600	0.0000280	0.281189	0.000057	0.281152888	0.000057	-1.5	2.1
MIM2z123	1322.4	6.0	12.1	100	0.0024560	0.0000440	0.282108	0.000056	0.282046674	0.000056	3.7	2.0
MIM2z124	585.5	3.5	7.1	96	0.0007745	0.0000019	0.282288	0.000056	0.282279496	0.000056	-4.5	2.0
MIM2z125	753.0	4.6	9.2	101	0.0007690	0.0000710	0.282664	0.000056	0.282653125	0.000056	12.4	2.0
MIM2z126	1020.9	5.0	9.9	99	0.0030810	0.0000470	0.282313	0.000052	0.282253775	0.000052	4.3	1.9
MIM2z127	677.5	3.2	6.4	99	0.0037860	0.0000510	0.282445	0.000053	0.282396863	0.000053	1.7	1.9
MIM2z128	646.9	2.9	5.8	99	0.0017880	0.0000450	0.282488	0.000053	0.282466297	0.000053	3.4	1.9
MIM2z129	605.1	3.5	7.0	99	0.0008330	0.0000150	0.282499	0.000059	0.282489546	0.000059	3.3	2.1
MIM2z130	612.1	4.1	8.2	100	0.0011390	0.0000170	0.282626	0.000056	0.282612924	0.000056	7.9	2.0
MIM2z131	605.0	3.5	7.0	96	0.0010120	0.0000320	0.282640	0.000057	0.282628516	0.000057	8.3	2.0
MIM2z132	2132.7	14.5	29.0	101	0.0015640	0.0000310	0.281594	0.000054	0.281530539	0.000054	3.8	2.0
MIM2z133	1182.8	5.4	10.7	100	0.0009200	0.0000190	0.282053	0.000051	0.282032479	0.000051	0.0	1.8
MIM2z134	582.4	2.9	5.9	99	0.0006250	0.0000170	0.282172	0.000053	0.282165175	0.000053	-8.6	1.9
MIM2z135	2020.3	17.8	35.6	99	0.0007247	0.0000011	0.281665	0.000053	0.281637174	0.000053	5.0	1.9

Chapter III

Table E.3: Sample OJJ10

IGSN: IEACC0001

Coordinate UTM: Zone 30S, 536550 m E, 3764944 m N

GRAIN	Age (Ma)	σ	2σ	Concordia	$^{176}\text{Lu}/^{177}\text{Hf}$	2σ	$^{176}\text{Hf}/^{177}\text{Hf}$	2σ	$(^{176}\text{Hf}/^{177}\text{Hf})_{\text{int}}$	2σ	ϵHf	2σ
OJJ10z94	378.2	3.6	7.3	100	0.0017780	0.0000980	0.282726	0.000025	0.282713415	0.000025	6.2	0.9
OJJ10z95	644.8	6.4	12.8	96	0.0018820	0.0000660	0.282247	0.000026	0.282224231	0.000026	-5.2	0.9
OJJ10z96	594.5	10.0	20.0	104	0.0009902	0.0000087	0.282217	0.000034	0.282205961	0.000034	-6.9	1.2
OJJ10z97	2776.4	11.0	22.0	97	0.0008400	0.0001300	0.280936	0.000024	0.280891360	0.000024	-4.1	1.1
OJJ10z98	645.4	10.5	21.0	103	0.0007205	0.0000028	0.282482	0.000030	0.282473275	0.000030	3.7	1.1
OJJ10z99	516.4	4.8	9.5	97	0.0013800	0.0000400	0.282311	0.000029	0.282297646	0.000029	-5.4	1.0
OJJ10z100	1748.9	23.1	46.2	98	0.0023370	0.0000330	0.281782	0.000026	0.281704516	0.000026	1.2	1.0
OJJ10z103	619.7	10.8	21.7	99	0.0006630	0.0000190	0.282451	0.000017	0.282443293	0.000017	2.0	0.6
OJJ10z108	420.5	9.4	18.7	94	0.0028300	0.0001900	0.282423	0.000025	0.282400720	0.000025	-3.9	0.9
OJJ10z109	632.6	6.1	12.3	101	0.0019470	0.0000410	0.282517	0.000024	0.282493895	0.000024	4.1	0.9
OJJ10z112	1944.3	12.7	25.5	98	0.0004670	0.0000180	0.281590	0.000017	0.281572756	0.000017	0.9	0.6
OJJ10z113	610.3	5.9	11.7	99	0.0004790	0.0000200	0.282222	0.000025	0.282216517	0.000025	-6.2	0.9
OJJ10z114	655.3	5.5	11.1	99	0.0015130	0.0000340	0.282353	0.000024	0.282334396	0.000024	-1.0	0.9
OJJ10z119	1906.3	30.0	60.0	99	0.0010670	0.0000150	0.281590	0.000017	0.281551383	0.000017	-0.7	0.6
OJJ10z120	378.5	3.6	7.3	101	0.0025200	0.0001800	0.282696	0.000042	0.282678149	0.000042	5.0	1.5
OJJ10z121	637.2	6.1	12.3	96	0.0059400	0.0002400	0.282074	0.000024	0.282002987	0.000024	-13.2	1.0
OJJ10z122	1694.9	18.6	37.3	95	0.0016400	0.0001000	0.281282	0.000025	0.281229331	0.000025	-16.9	1.0
OJJ10z123	380.4	3.6	7.3	102	0.0023000	0.0000700	0.282674	0.000019	0.282657626	0.000019	4.3	0.7
OJJ10z125	618.5	7.9	15.8	102	0.0009130	0.0000770	0.282255	0.000023	0.282244407	0.000023	-5.0	0.8
OJJ10z128	2102.0	39.8	79.5	97	0.0010380	0.0000640	0.281470	0.000020	0.281428500	0.000020	-0.6	0.8
OJJ10z129	612.7	6.4	12.9	102	0.0005070	0.0000180	0.282151	0.000024	0.282145174	0.000024	-8.7	0.9
OJJ10z130	541.3	6.2	12.4	102	0.0022800	0.0001800	0.282489	0.000022	0.282465865	0.000022	1.1	0.8
OJJ10z131	614.4	7.0	14.1	99	0.0006240	0.0000500	0.282527	0.000025	0.282519809	0.000025	4.6	0.9
OJJ10z132	643.1	6.1	12.3	98	0.0016310	0.0000980	0.282468	0.000026	0.282448322	0.000026	2.7	1.0
OJJ10z133	789.6	8.6	17.1	100	0.0006090	0.0000220	0.282441	0.000026	0.282431966	0.000026	5.4	0.9
OJJ10z134	604.4	6.2	12.3	96	0.0006243	0.0000021	0.282090	0.000022	0.282082923	0.000022	-11.1	0.8
OJJ10z135	2158.8	17.5	35.0	97	0.0013090	0.0000650	0.281571	0.000024	0.281517221	0.000024	3.9	0.9
OJJ10z137	367.3	3.3	6.7	99	0.0014409	0.0000099	0.282640	0.000017	0.282630096	0.000017	3.1	0.6
OJJ10z138	1492.4	12.0	24.0	98	0.0008561	0.0000040	0.281887	0.000024	0.281862837	0.000024	1.0	0.9
OJJ10z139	376.0	3.3	6.7	100	0.0024090	0.0000290	0.282589	0.000022	0.282572048	0.000022	1.2	0.8
OJJ10z141	945.7	8.1	16.1	100	0.0007798	0.0000042	0.282178	0.000028	0.282164125	0.000028	-0.6	1.0
OJJ10z143	977.3	10.2	20.5	98	0.0008474	0.0000075	0.282212	0.000027	0.282196413	0.000027	1.2	1.0
OJJ10z145	368.9	4.0	7.9	99	0.0018180	0.0000520	0.282610	0.000026	0.282597448	0.000026	1.9	0.9
OJJ10z146	374.3	3.3	6.7	103	0.0016750	0.0000230	0.282671	0.000022	0.282659267	0.000022	4.2	0.8
OJJ10z147	1195.2	9.6	19.3	100	0.0008006	0.0000015	0.282111	0.000019	0.282092954	0.000019	2.5	0.7
OJJ10z148	1102.4	8.7	17.4	96	0.0008480	0.0000200	0.282099	0.000022	0.282081385	0.000022	0.0	0.8
OJJ10z151	1759.2	35.7	71.4	99	0.0011150	0.0000380	0.281123	0.000018	0.281085812	0.000018	-20.6	0.7
OJJ10z152	636.1	9.1	18.1	90	0.0013020	0.0000330	0.281979	0.000016	0.281963463	0.000016	-14.6	0.6
OJJ10z155	642.5	5.8	11.7	97	0.0016200	0.0001600	0.282526	0.000028	0.282506472	0.000028	4.8	1.1
OJJ10z156	1391.4	10.4	20.8	100	0.0008680	0.0000180	0.281962	0.000017	0.281939181	0.000017	1.4	0.6
OJJ10z157	2074.8	17.2	34.3	100	0.0008365	0.0000069	0.281645	0.000023	0.281611997	0.000023	5.3	0.8
OJJ10z158	2061.0	16.6	33.3	94	0.0009800	0.0000490	0.281520	0.000021	0.281481597	0.000021	0.4	0.8
OJJ10z159	585.6	6.8	13.5	93	0.0009600	0.0001700	0.282446	0.000043	0.282435457	0.000043	1.0	1.6
OJJ10z163	653.0	7.0	14.0	99	0.0019320	0.0000330	0.282142	0.000018	0.282118328	0.000018	-8.7	0.7
OJJ10z165	378.6	3.6	7.3	94	0.0011390	0.0000370	0.282551	0.000024	0.282542929	0.000024	0.2	0.9
OJJ10z167c	627.9	5.8	11.7	94	0.0006500	0.0001200	0.282671	0.000026	0.282663466	0.000026	9.8	1.0
OJJ10z169	634.9	6.1	12.3	98	0.0021560	0.0000620	0.281820	0.000024	0.281794320	0.000024	-20.6	0.9
OJJ10z170	991.7	12.2	24.3	101	0.0008290	0.0000720	0.282227	0.000028	0.282211525	0.000028	2.1	1.0
OJJ10z171	1969.5	35.4	70.8	101	0.0001626	0.0000033	0.281060	0.000035	0.281053916	0.000035	-16.9	1.2
OJJ10z174	614.4	5.3	10.5	98	0.0013190	0.0000560	0.282546	0.000026	0.282530799	0.000026	5.0	0.9
OJJ10z176	1543.9	32.4	64.7	99	0.0011540	0.0000200	0.281771	0.000020	0.281737290	0.000020	-2.3	0.7
OJJ10z177	2672.1	14.1	28.2	96	0.0013210	0.0000200	0.280948	0.000021	0.280880501	0.000021	-6.9	0.8
OJJ10z178	320.1	2.9	5.9	93	0.0030100	0.0002600	0.282594	0.000029	0.282575977	0.000029	0.1	1.1
OJJ10z179	563.8	5.9	11.8	102	0.0032400	0.0001600	0.282417	0.000021	0.282382751	0.000021	-1.4	0.8
OJJ10z184	586.8	5.0	10.0	100	0.0004600	0.0000250	0.282409	0.000027	0.282403938	0.000027	-0.1	1.0
OJJ10z186	1159.2	8.9	17.8	98	0.0010440	0.0000130	0.282091	0.000038	0.282068184	0.000038	0.8	1.4
OJJ10z188	2229.7	13.0	25.9	91	0.0004840	0.0000200	0.281421	0.000021	0.281400449	0.000021	1.4	0.8
OJJ10z189	550.8	5.3	10.7	103	0.0011020	0.0000160	0.282489	0.000023	0.282477621	0.000023	1.7	0.8
OJJ10z190	665.2	6.1	12.2	99	0.0006420	0.0000300	0.282095	0.000023	0.282086986	0.000023	-9.6	0.8

Chapter III

Table E.4: Sample OUI1

IGSN: IEACC0002

Coordinate UTM: Zone 30S, 536550 m E, 3764944 m N

GRAIN	Age (Ma)	σ	2σ	Concordia	$^{176}\text{Lu}/^{177}\text{Hf}$	2σ	$^{176}\text{Hf}/^{177}\text{Hf}$	2σ	$(^{176}\text{Hf}/^{177}\text{Hf})_{\text{int}}$	2σ	ϵHf	2σ
OUI1z125	2040.1	21.1	42.2	99	0.0008010	0.0000180	0.281668	0.000019	0.281636937	0.000019	5.4	0.7
OUI1z126	637.2	6.7	13.4	97	0.0005872	0.0000021	0.281849	0.000019	0.281841980	0.000019	-18.9	0.7
OUI1z127	549.6	11.5	23.1	90	0.0005320	0.0000012	0.282371	0.000029	0.282365519	0.000029	-2.3	1.0
OUI1z128c	2771.3	10.2	20.4	97	0.0021020	0.0000210	0.280983	0.000024	0.280871502	0.000024	-5.0	0.9
OUI1z128r	2768.7	13.2	26.3	95	0.0013400	0.0001600	0.280955	0.000018	0.280883989	0.000018	-4.6	0.9
OUI1z129	597.4	5.9	11.8	95	0.0019450	0.0000560	0.282394	0.000025	0.282372209	0.000025	-1.0	0.9
OUI1z130	2069.3	17.2	34.4	98	0.0006522	0.0000021	0.281579	0.000024	0.281553338	0.000024	3.1	0.9
OUI1z131	604.4	5.9	11.7	95	0.0011930	0.0000680	0.282632	0.000026	0.282618475	0.000026	7.9	0.9
OUI1z132	616.8	5.3	10.5	99	0.0014400	0.0001100	0.282357	0.000026	0.282340341	0.000026	-1.7	1.0
OUI1z134	1545.8	18.6	37.2	99	0.0006140	0.0000130	0.282009	0.000021	0.281991041	0.000021	6.7	0.8
OUI1z135	2011.7	19.3	38.7	99	0.0000220	0.0000003	0.281312	0.000027	0.281311159	0.000027	-6.8	1.0
OUI1z136	621.4	7.9	15.8	92	0.0002490	0.0000180	0.281871	0.000018	0.281868097	0.000018	-18.3	0.6
OUI1z137c	773.0	6.9	13.7	98	0.0007300	0.0001700	0.282213	0.000028	0.282202400	0.000028	-3.1	1.1
OUI1z138	394.5	5.5	10.9	93	0.0025030	0.0000600	0.282555	0.000027	0.282536519	0.000027	0.3	1.0
OUI1z139	372.6	4.3	8.5	94	0.0014757	0.0000065	0.282569	0.000020	0.282558710	0.000020	0.6	0.7
OUI1z140	641.3	9.3	18.7	97	0.0010600	0.0000940	0.281702	0.000022	0.281689246	0.000022	-24.2	0.8
OUI1z141	602.1	6.2	12.3	96	0.0000112	0.0000007	0.282100	0.000020	0.282099874	0.000020	-10.5	0.7
OUI1z142	1166.7	13.7	27.4	95	0.0006221	0.0000026	0.282016	0.000020	0.282002315	0.000020	-1.4	0.7
OUI1z143	2777.2	8.9	17.7	94	0.0007880	0.0000680	0.280959	0.000021	0.280917110	0.000021	-3.2	0.9
OUI1z144	2088.5	29.9	59.8	98	0.0004990	0.0000110	0.281466	0.000022	0.281446180	0.000022	-0.3	0.8
OUI1z146	607.4	5.9	11.7	96	0.0004827	0.0000027	0.282272	0.000026	0.282266501	0.000026	-4.5	0.9
OUI1z147	521.1	5.4	10.7	103	0.0008760	0.0000300	0.282518	0.000022	0.282509444	0.000022	2.2	0.8
OUI1z150	376.2	4.9	9.7	95	0.0028000	0.0002000	0.282583	0.000036	0.282563284	0.000036	0.9	1.3
OUI1z151	617.9	6.7	13.5	97	0.0014300	0.0001200	0.282315	0.000025	0.282298425	0.000025	-3.1	0.9
OUI1z152	705.2	13.0	26.0	90	0.0007002	0.0000027	0.281806	0.000022	0.281796730	0.000022	-19.0	0.8
OUI1z153	1012.1	9.4	18.7	96	0.0011969	0.0000067	0.282268	0.000023	0.282245193	0.000023	3.8	0.8
OUI1z154	571.5	5.6	11.2	98	0.0010285	0.0000063	0.282583	0.000021	0.282571979	0.000021	5.5	0.7
OUI1z155	1175.3	9.1	18.3	99	0.0006420	0.0000110	0.281878	0.000025	0.281863772	0.000025	-6.1	0.9
OUI1z156	1757.5	20.4	40.8	102	0.0006557	0.0000016	0.281602	0.000021	0.281580152	0.000021	-3.0	0.7
OUI1z157	576.8	5.6	11.2	98	0.0019780	0.0000640	0.282266	0.000026	0.282244607	0.000026	-6.0	0.9
OUI1z158	377.8	3.6	7.3	98	0.0015210	0.0000340	0.282675	0.000023	0.282664245	0.000023	4.5	0.8
OUI1z159	640.1	7.9	15.8	98	0.0019780	0.0000310	0.282407	0.000023	0.282383244	0.000023	0.4	0.8
OUI1z160	2003.1	33.2	66.3	100	0.0004805	0.0000012	0.281145	0.000029	0.281126710	0.000029	-13.6	1.0
OUI1z161	2058.2	20.8	41.6	97	0.0007471	0.0000060	0.281131	0.000022	0.281101764	0.000022	-13.2	0.8
OUI1z163	2069.3	31.0	62.0	97	0.0019250	0.0000170	0.281043	0.000022	0.280967257	0.000022	-17.7	0.8
OUI1z164	618.5	6.1	12.3	100	0.0005154	0.0000026	0.282233	0.000021	0.282227020	0.000021	-5.7	0.7
OUI1z165	1226.7	9.6	19.2	100	0.0007120	0.0000073	0.282125	0.000024	0.282108523	0.000024	3.7	0.9
OUI1z166	367.1	3.0	6.1	96	0.0012890	0.0000160	0.282611	0.000025	0.282602145	0.000025	2.1	0.9
OUI1z167	772.4	7.4	14.9	97	0.0006750	0.0000340	0.282369	0.000026	0.282359206	0.000026	2.4	0.9
OUI1z168	372.6	3.3	6.7	99	0.0023000	0.0004100	0.282713	0.000045	0.282696960	0.000045	5.5	1.7
OUI1z169	2066.6	11.7	23.5	90	0.0009940	0.0000410	0.281307	0.000034	0.281267942	0.000034	-7.1	1.3
OUI1z170c	2076.2	17.8	35.7	101	0.0015340	0.0000420	0.281454	0.000019	0.281393437	0.000019	-2.4	0.7
OUI1z171	632.6	6.7	13.4	100	0.0009940	0.0000480	0.282287	0.000027	0.282275204	0.000027	-3.6	1.0
OUI1z172	1555.6	14.6	29.2	98	0.0016485	0.0000097	0.281536	0.000020	0.281487474	0.000020	-10.9	0.7
OUI1z173	602.7	8.2	16.4	96	0.0009310	0.0000210	0.282086	0.000027	0.282075477	0.000027	-11.4	1.0
OUI1z175	625.5	5.3	10.5	103	0.0006530	0.0000100	0.282569	0.000021	0.282561337	0.000021	6.3	0.7
OUI1z176	2098.0	8.8	17.6	97	0.0006710	0.0000370	0.281511	0.000020	0.281484225	0.000020	1.3	0.8
OUI1z177	581.5	8.5	17.1	99	0.0016200	0.0000870	0.282378	0.000019	0.282360335	0.000019	-1.8	0.7
OUI1z178	617.3	6.4	12.9	95	0.0012030	0.0000970	0.282401	0.000030	0.282387069	0.000030	0.0	1.1
OUI1z179	2102.0	17.5	35.0	100	0.0050100	0.0006600	0.281896	0.000064	0.281695695	0.000064	8.9	3.2
OUI1z180	512.2	5.4	10.7	96	0.0029391	0.0000082	0.282696	0.000020	0.282667789	0.000020	7.6	0.7
OUI1z181	2061.0	17.3	34.6	97	0.0005508	0.0000026	0.281413	0.000023	0.281391416	0.000023	-2.8	0.8
OUI1z182	2130.0	32.4	64.8	98	0.0007380	0.0000930	0.281575	0.000036	0.281545093	0.000036	4.2	1.4
OUI1z183	378.3	4.0	7.9	92	0.0017540	0.0000280	0.282590	0.000020	0.282577581	0.000020	1.4	0.7
OUI1z184	649.5	6.7	13.4	95	0.0008610	0.0000540	0.282379	0.000024	0.282368508	0.000024	0.0	0.9
OUI1z185r	536.0	8.3	16.6	91	0.0018500	0.0002400	0.282395	0.000021	0.282376414	0.000021	-2.2	0.8
OUI1z186	2126.1	24.5	49.0	100	0.0008120	0.0000200	0.281576	0.000033	0.281543156	0.000033	4.1	1.2
OUI1z187	634.3	7.6	15.2	91	0.0015060	0.0000230	0.282444	0.000026	0.282426079	0.000026	1.7	0.9
OUI1z188c	602.1	6.5	12.9	93	0.0015720	0.0000590	0.282524	0.000020	0.282506249	0.000020	3.9	0.7
OUI1z188r	619.1	7.3	14.6	95	0.0012190	0.0000420	0.282489	0.000024	0.282474844	0.000024	3.1	0.9
OUI1z189	2651.9	10.1	20.3	99	0.0011020	0.0000180	0.280948	0.000023	0.280892126	0.000023	-7.0	0.9
OUI1z190	1987.1	11.7	23.3	97	0.0001934	0.0000007	0.281369	0.000017	0.281361697	0.000017	-5.6	0.6
OUI1z191	605.0	5.9	11.7	98	0.0034870	0.0000650	0.282490	0.000023	0.282450431	0.000023	2.0	0.8
OUI1z192	527.1	4.8	9.5	95	0.0022100	0.0001600	0.282701	0.000028	0.282679168	0.000028	8.3	1.0
OUI1z193	974.5	8.9	17.7	95	0.0003930	0.0000230	0.282202	0.000019	0.282194792	0.000019	1.1	0.7
OUI1z194	2031.6	19.8	39.6	97	0.0015020	0.0000590	0.281557	0.000027	0.281498998	0.000027	0.3	1.0
OUI1z195	537.8	5.6	11.3	96	0.0011450	0.0000140	0.282402	0.000022	0.282390459	0.000022	-1.7	0.8
OUI1z196	380.5	4.6	9.1	95	0.0018130	0.0000150	0.282574	0.000021	0.282561089	0.000021	0.9	0.7
OUI1z197	1001.6	8.8	17.7	99	0.0009390	0.0000230	0.282168	0.000016	0.282150294	0.000016	0.2	0.6
OUI1z198	569.7	8.3	16.5	95	0.0015300	0.0001700	0.282497	0.000026	0.282480657	0.000026	2.2	1.0
OUI1z199	617.3	5.3	10.5	96	0.0007560	0.0000032	0.282664	0.000022	0.282655246	0.000022	9.5	0.8
OUI1z200	553.8	10.6	21.3	93	0.0024500	0.0001800	0.282803	0.000028	0.282777566	0.000028	12.4	1.1
OUI1z201	374.3	3.6	7.3	95	0.0018940	0.0000520	0.282572	0.000025	0.282558733	0.000025	0.7	0.9
OUI1z202	644.8	7.6	15.2	97	0.0006878	0.0000043	0.281842	0.000023	0.281833679	0.000023	-19.0	0.8
OUI1z203	384.1	4.6	9.1	92	0.0018320	0.0000560	0.282591	0.000026	0.282577828	0.000026	1.6	0.9
OUI1z204	2256.6	24.2	48.5	94	0.0006210	0.0000160	0.281063	0.000027	0.281036307	0.000027	-11.0	1.0
OUI1z205	602.1	5.0	10.0	99	0.0012500	0.0000460	0.282382	0.000074	0.282367885	0.000074	-1.0	2.6
OUI1z206	656.5	9.9	19.8	95	0.0004230	0.0000210	0.281696	0.000020	0.281690789	0.000020	-23.8	0.7
OUI1z208	2027.4	63.8	127.6	102	0.0008270	0.0000150	0.281189	0.000022	0.281157132	0.000022	-11.9	0.8
OUI1z209	1538.0	16.7	33.5	99	0.0010170	0.0000180						

GRAIN	Age (Ma)	σ	2σ	Concordia	$^{176}\text{Lu}/^{177}\text{Hf}$	2σ	$^{176}\text{Hf}/^{177}\text{Hf}$	2σ	$(^{176}\text{Hf}/^{177}\text{Hf})_{\text{int}}$	2σ	ϵHf	2σ
OUJ11z224	378.0	3.3	6.7	95	0.0023900	0.0001800	0.282581	0.000018	0.282564092	0.000018	1.0	0.7
OUJ11z225	498.5	5.1	10.1	97	0.0021530	0.0000650	0.282619	0.000024	0.282598890	0.000024	4.9	0.9
OUJ11z226	987.8	11.9	23.8	92	0.0011920	0.0000120	0.282176	0.000018	0.282153836	0.000018	0.0	0.6
OUJ11z227	645.4	5.8	11.7	96	0.0032580	0.0000630	0.282088	0.000036	0.282048548	0.000036	-11.4	1.3
OUJ11z228	1210.1	10.7	21.4	99	0.0011161	0.0000085	0.282135	0.000028	0.282109524	0.000028	3.4	1.0
OUJ11z229	536.6	6.2	12.5	96	0.0015510	0.0000490	0.282367	0.000022	0.282351401	0.000022	-3.1	0.8
OUJ11z230	1799.4	26.5	52.9	99	0.0005483	0.0000053	0.281622	0.000027	0.281603287	0.000027	-1.3	1.0
OUJ11z231	2070.7	16.5	33.0	99	0.0009920	0.0000280	0.281522	0.000021	0.281482941	0.000021	0.6	0.8
OUJ11z232	2135.3	17.8	35.6	98	0.0009545	0.0000068	0.281376	0.000029	0.281337221	0.000029	-3.1	1.0
OUJ11z233	622.6	5.9	11.7	97	0.0029460	0.0000470	0.282617	0.000021	0.282582593	0.000021	7.0	0.8
OUJ11z234	590.3	6.2	12.4	97	0.0015300	0.0001100	0.282285	0.000037	0.282268062	0.000037	-4.8	1.4
OUJ11z235	705.8	6.6	13.3	100	0.0016190	0.0000210	0.282266	0.000022	0.282244549	0.000022	-3.1	0.8
OUJ11z236	381.7	4.6	9.1	107	0.0026310	0.0000380	0.282541	0.000024	0.282522204	0.000024	-0.4	0.9
OUJ11z237	1319.8	11.0	22.1	98	0.0000165	0.0000016	0.281973	0.000028	0.281972589	0.000028	1.0	1.0
OUJ11z238	636.1	7.0	14.0	95	0.0046600	0.0002300	0.282676	0.000049	0.282620392	0.000049	8.7	1.8
OUJ11z239	2345.9	13.7	27.4	97	0.0007850	0.0000530	0.281372	0.000029	0.281336893	0.000029	1.8	1.1
OUJ11z242	823.1	7.7	15.3	93	0.0020360	0.0000750	0.282351	0.000031	0.282319503	0.000031	2.2	1.1
OUJ11z243	581.8	4.7	9.4	99	0.0011120	0.0000290	0.282020	0.000023	0.282007868	0.000023	-14.2	0.8
OUJ11z246	387.2	3.6	7.3	95	0.0021910	0.0000880	0.282576	0.000031	0.282560120	0.000031	1.0	1.1
OUJ11z247	357.4	3.4	6.7	96	0.0016110	0.0000220	0.282691	0.000023	0.282680226	0.000023	4.6	0.8
OUJ11z248	652.4	7.3	14.6	100	0.0021860	0.0000590	0.282526	0.000027	0.282499240	0.000027	4.7	1.0
OUJ11z249	2469.3	27.2	54.4	95	0.0009260	0.0000590	0.280875	0.000020	0.280831358	0.000020	-13.4	0.8
OUJ11z251	373.8	4.0	7.9	97	0.0016840	0.0000950	0.282661	0.000030	0.282649219	0.000030	3.9	1.1
OUJ11z253	2617.4	8.5	17.0	99	0.0030400	0.0001800	0.281164	0.000022	0.281011921	0.000022	-3.5	1.1
OUJ11z254	637.8	5.8	11.7	94	0.0020900	0.0001500	0.282457	0.000051	0.282431991	0.000051	2.0	1.9
OUJ11z255	362.2	4.0	7.9	100	0.0022960	0.0000660	0.282623	0.000030	0.282607437	0.000030	2.1	1.1
OUJ11z256	377.7	3.6	7.3	97	0.0022200	0.0002000	0.282654	0.000024	0.282638307	0.000024	3.6	0.9
OUJ11z257	634.9	5.3	10.5	100	0.0012870	0.0000280	0.282230	0.000023	0.282214671	0.000023	-5.7	0.8
OUJ11z258	637.2	9.6	19.3	99	0.0007800	0.0000560	0.282675	0.000020	0.282665675	0.000020	10.3	0.7
OUJ11z259	607.4	5.6	11.1	99	0.0012930	0.0000250	0.282711	0.000038	0.282696270	0.000038	10.7	1.4
OUJ11z260	617.3	6.2	12.3	100	0.0013490	0.0000150	0.282122	0.000022	0.282106379	0.000022	-10.0	0.8
OUJ11z261	379.3	4.9	9.7	90	0.0023100	0.0002300	0.282543	0.000014	0.282526602	0.000014	-0.3	0.6
OUJ11z262	361.6	4.3	8.5	98	0.0019670	0.0000530	0.282639	0.000025	0.282625689	0.000025	2.8	0.9
OUJ11z263	1047.8	14.0	27.9	97	0.0010500	0.0001600	0.281579	0.000026	0.281558279	0.000026	-19.8	1.0
OUJ11z264	2099.3	13.5	27.0	99	0.0000853	0.0000006	0.281136	0.000019	0.281132594	0.000019	-11.1	0.7
OUJ11z265	1883.0	25.8	51.6	98	0.0009674	0.0000076	0.281237	0.000025	0.281202423	0.000025	-13.6	0.9
OUJ11z266	378.8	3.6	7.3	97	0.0031200	0.0001900	0.282642	0.000020	0.282619881	0.000020	2.9	0.8
OUJ11z267	2007.4	29.5	58.9	94	0.0011260	0.0000100	0.281595	0.000026	0.281552046	0.000026	1.7	0.9
OUJ11z268	2054.1	12.5	25.1	97	0.0008220	0.0000580	0.281011	0.000026	0.280978900	0.000026	-17.6	1.0

Chapter III

Table E.5: Sample OUJ13

IGSN: IEACC0003

Coordinate UTM: Zone 30S, 533485 m E, 3775692 m N

GRAIN	Age (Ma)	σ	2σ	Concordia	$^{176}\text{Lu}/^{177}\text{Hf}$	2σ	$^{176}\text{Hf}/^{177}\text{Hf}$	2σ	$(^{176}\text{Hf}/^{177}\text{Hf})_{\text{initial}}$	2σ	ϵ_{Hf}	2σ
OUJ13z1	378.2	2.0	4.0	102	0.0026270	0.0000760	0.282716	0.000024	0.282697403	0.000024	5.7	0.9
OUJ13z2	774.9	3.7	7.4	100	0.0027200	0.0001300	0.282608	0.000025	0.282568405	0.000025	9.9	1.0
OUJ13z3	2154.9	13.6	27.3	101	0.0031800	0.0001300	0.281704	0.000024	0.281573594	0.000024	5.8	1.0
OUJ13z5	628.2	3.8	7.6	100	0.0009685	0.0000055	0.282606	0.000025	0.282594587	0.000025	7.6	0.9
OUJ13z6	591.5	2.9	5.9	103	0.0020800	0.0001100	0.282151	0.000019	0.282127927	0.000019	-9.8	0.7
OUJ13z7	2092.5	12.2	24.4	99	0.0013870	0.0000740	0.281639	0.000029	0.281583801	0.000029	4.7	1.1
OUJ13z8	607.0	3.2	6.5	99	0.0000258	0.0000009	0.281854	0.000023	0.281853706	0.000023	-19.1	0.8
OUJ13z10	381.1	2.0	4.0	101	0.0048100	0.0000940	0.282605	0.000022	0.282570691	0.000022	1.3	0.8
OUJ13z11	376.5	2.0	4.0	100	0.0007350	0.0000600	0.282582	0.000020	0.282576821	0.000020	1.4	0.7
OUJ13z12	1017.6	6.6	13.2	100	0.0012160	0.0000150	0.282198	0.000026	0.282174702	0.000026	1.4	0.9
OUJ13z13	375.2	2.3	4.6	101	0.0028090	0.0000690	0.282596	0.000026	0.282576275	0.000026	1.3	0.9
OUJ13z14	661.6	3.8	7.6	101	0.0019400	0.0002300	0.281900	0.000027	0.281875915	0.000027	-17.1	1.1
OUJ13z15	386.9	2.5	5.1	103	0.0035100	0.0003600	0.282583	0.000025	0.282557584	0.000025	0.9	1.0
OUJ13z16	378.8	2.0	4.1	101	0.0021600	0.0000970	0.282663	0.000018	0.282647684	0.000018	3.9	0.7
OUJ13z17	1822.7	13.0	26.1	101	0.0023710	0.0000500	0.281640	0.000019	0.281558016	0.000019	-2.3	0.7
OUJ13z19	562.6	3.8	7.7	99	0.0017480	0.0000310	0.282649	0.000015	0.282630562	0.000015	7.4	0.5
OUJ13z20	624.8	3.5	7.0	102	0.0012810	0.0000190	0.281695	0.000025	0.281679985	0.000025	-24.9	0.9
OUJ13z21	756.5	3.7	7.5	99	0.0009360	0.0000190	0.282467	0.000027	0.282453701	0.000027	5.4	1.0
OUJ13z22	623.5	3.2	6.4	101	0.0005830	0.0000280	0.282206	0.000023	0.282199181	0.000023	-6.5	0.8
OUJ13z23	380.2	2.3	4.6	99	0.0024310	0.0000500	0.282602	0.000029	0.282584702	0.000029	1.7	1.0
OUJ13z24	380.0	1.9	3.9	100	0.0029360	0.0000530	0.282619	0.000022	0.282598119	0.000022	2.2	0.8
OUJ13z25	913.8	5.0	10.1	86	0.0021030	0.0000320	0.281791	0.000037	0.281754851	0.000037	-15.8	1.3
OUJ13z26	3511.4	9.3	18.5	101	0.0004902	0.0000009	0.280477	0.000023	0.280443821	0.000023	-2.9	0.8
OUJ13z27	359.3	2.0	3.9	90	0.0059500	0.0001700	0.282649	0.000032	0.282608995	0.000032	2.1	1.2
OUJ13z28	643.1	3.8	7.6	100	0.0007520	0.0000250	0.282655	0.000026	0.282645927	0.000026	9.7	0.9
OUJ13z29	1764.3	13.5	27.1	101	0.0010820	0.0000110	0.281724	0.000022	0.281687806	0.000022	0.9	0.8
OUJ13z30	2066.6	18.6	37.3	101	0.0007520	0.0000160	0.281627	0.000021	0.281597451	0.000021	4.6	0.8
OUJ13z31	2078.9	15.1	30.1	100	0.0006317	0.0000062	0.281629	0.000020	0.281604027	0.000020	5.1	0.7
OUJ13z32	493.8	3.3	6.6	100	0.0028990	0.0000310	0.282675	0.000031	0.282648179	0.000031	6.5	1.1
OUJ13z34	380.7	2.0	4.1	101	0.0018720	0.0000370	0.282534	0.000019	0.282520660	0.000019	-0.5	0.7
OUJ13z35	641.7	3.8	7.6	104	0.0005623	0.0000075	0.281706	0.000023	0.281699230	0.000023	-23.8	0.8
OUJ13z36	384.3	2.3	4.7	104	0.0018630	0.0000660	0.282605	0.000025	0.282591599	0.000025	2.1	0.9
OUJ13z37	296.1	4.6	9.2	89	0.0042800	0.0002200	0.282749	0.000022	0.282725301	0.000022	4.9	0.8
OUJ13z39	417.1	3.3	6.6	100	0.0014600	0.0000530	0.282574	0.000021	0.282562599	0.000021	1.8	0.8
OUJ13z40	375.4	2.4	4.8	102	0.0015580	0.0000710	0.282624	0.000024	0.282613054	0.000024	2.6	0.9
OUJ13z41	375.1	3.0	6.1	97	0.0010200	0.0000160	0.282523	0.000021	0.282515840	0.000021	-0.8	0.7
OUJ13z42	634.0	3.5	7.0	100	0.0007556	0.0000039	0.282514	0.000020	0.282505013	0.000020	4.5	0.7
OUJ13z43	362.4	2.2	4.4	98	0.0018500	0.0001500	0.282673	0.000031	0.282660453	0.000031	4.0	1.1
OUJ13z44	718.9	3.7	7.5	101	0.0009840	0.0000380	0.282670	0.000022	0.282656718	0.000022	11.8	0.8
OUJ13z45	649.7	3.2	6.4	101	0.0009130	0.0000170	0.281992	0.000022	0.281980871	0.000022	-13.7	0.8
OUJ13z46	374.9	2.1	4.3	99	0.0025520	0.0000860	0.282608	0.000025	0.282590094	0.000025	1.8	0.9
OUJ13z48	625.9	3.2	6.4	101	0.0005780	0.0000830	0.282154	0.000021	0.282147214	0.000021	-8.3	0.8
OUJ13z49	379.9	2.2	4.5	102	0.0017830	0.0000280	0.282668	0.000020	0.282655323	0.000020	4.2	0.7
OUJ13z50	378.1	2.4	4.8	99	0.0015020	0.0000280	0.282613	0.000020	0.282602372	0.000020	2.3	0.7
OUJ13z51	608.0	4.1	8.2	98	0.0003757	0.0000046	0.282194	0.000021	0.282189716	0.000021	-7.2	0.7
OUJ13z52	686.2	3.5	7.0	100	0.0008918	0.0000087	0.282541	0.000019	0.282529514	0.000019	6.6	0.7
OUJ13z53	371.2	2.0	4.1	99	0.0022940	0.0000600	0.282650	0.000022	0.282634064	0.000022	3.3	0.8
OUJ13z54	1134.9	5.4	10.8	100	0.0006482	0.0000059	0.282141	0.000017	0.282127134	0.000017	2.3	0.6
OUJ13z55	1557.5	16.5	33.1	100	0.0006260	0.0000100	0.281577	0.000020	0.281558549	0.000020	-8.3	0.7
OUJ13z56	2089.3	11.6	23.1	100	0.0008500	0.0000270	0.281577	0.000025	0.281543226	0.000025	3.2	0.9
OUJ13z57	1227.8	5.9	11.7	102	0.0007178	0.0000049	0.282047	0.000024	0.282030375	0.000024	1.0	0.9
OUJ13z59	313.9	4.6	9.2	92	0.0020200	0.0001500	0.282618	0.000022	0.282606139	0.000022	1.0	0.8
OUJ13z61	2040.1	17.6	35.1	101	0.0007290	0.0000220	0.281541	0.000023	0.281512729	0.000023	1.0	0.8
OUJ13z62	1347.6	7.1	14.1	100	0.0008850	0.0000054	0.282046	0.000022	0.282023476	0.000022	3.4	0.8
OUJ13z63	1539.7	13.8	27.5	101	0.0008702	0.0000078	0.281886	0.000023	0.281860649	0.000023	2.0	0.8
OUJ13z64	1223.0	5.9	11.7	100	0.0011510	0.0000490	0.282123	0.000031	0.282096446	0.000031	3.2	1.1
OUJ13z65	376.8	1.9	3.9	100	0.0027500	0.0001500	0.282728	0.000020	0.282708605	0.000020	6.0	0.7
OUJ13z66	372.8	2.5	4.9	99	0.0015300	0.0001600	0.282639	0.000021	0.282628324	0.000021	3.1	0.8
OUJ13z68	605.3	3.2	6.5	100	0.0003380	0.0000110	0.282329	0.000025	0.282325163	0.000025	-2.5	0.9
OUJ13z69	380.9	2.0	4.1	99	0.0017340	0.0000400	0.282595	0.000020	0.282582638	0.000020	1.7	0.7
OUJ13z70	381.8	2.3	4.6	98	0.0014340	0.0000190	0.282599	0.000026	0.282588752	0.000026	1.9	0.9
OUJ13z71	1840.4	12.1	24.1	92	0.0002293	0.0000082	0.281957	0.000049	0.281948993	0.000049	11.9	1.8
OUJ13z72	929.4	4.7	9.5	99	0.0006794	0.0000032	0.282107	0.000021	0.282095121	0.000021	-3.4	0.7
OUJ13z73	510.2	3.6	7.1	99	0.0022900	0.0000780	0.282484	0.000029	0.282462106	0.000029	0.3	1.1
OUJ13z74	361.4	2.0	4.1	98	0.0020670	0.0000760	0.282602	0.000022	0.282588022	0.000022	1.4	0.8
OUJ13z76	625.6	3.8	7.6	94	0.0005850	0.0000640	0.282080	0.000016	0.282073135	0.000016	-11.0	0.6
OUJ13z77	1985.7	24.1	48.1	101	0.0005471	0.0000045	0.281129	0.000026	0.281108359	0.000026	-14.6	0.9
OUJ13z78	378.6	2.3	4.7	97	0.0016430	0.0000400	0.282617	0.000029	0.282605358	0.000029	2.4	1.0
OUJ13z79	377.3	1.9	3.9	101	0.0014620	0.0000270	0.282565	0.000023	0.282554675	0.000023	0.6	0.8
OUJ13z80	1927.7	15.2	30.3	100	0.0008610	0.0000230	0.281606	0.000025	0.281574483	0.000025	0.6	0.9
OUJ13z81	373.3	1.9	3.8	99	0.0021910	0.0000780	0.282640	0.000022	0.282624695	0.000022	3.0	0.8
OUJ13z82	375.1	2.3	4.6	100	0.0010580	0.0000670	0.282781	0.000025	0.282773572	0.000025	8.3	0.9
OUJ13z83c	384.0	2.3	4.6	100	0.0016620	0.0000510	0.282609	0.000027	0.282597054	0.000027	2.3	1.0
OUJ13z83r	376.7	2.6	5.2	101	0.0012532	0.0000064	0.282586	0.000023	0.282577164	0.000023	1.4	0.8
OUJ13z84	389.5	2.4	4.7	100	0.0021740	0.0000410	0.282671	0.000034	0.282655151	0.000034	4.4	1.2
OUJ13z85	315.7	4.9	9.8	97	0.0034050	0.0000990	0.282619	0.000022	0.282598890	0.000022	0.8	0.8
OUJ13z86	574.5	3.2	6.5	100	0.0043100	0.0001400	0.282454	0.000027	0.282407573	0.000027	-0.2	1.0
OUJ13z87	898.2	7.0	14.0	100	0.0010620	0.0000370	0.282587	0.000026	0.282569061	0.000026	12.7	0.9
OUJ13z88	810.1	5.1	10.2	100	0.0006830	0.0000170	0.282567	0.000026	0.282556603	0.000026	10.3	0.9
OUJ13z89	614.4	4.7	9.4									

GRAIN	Age (Ma)	σ	2σ	Concordia	$^{176}\text{Lu}/^{177}\text{Hf}$	2σ	$^{176}\text{Hf}/^{177}\text{Hf}$	2σ	$(^{176}\text{Hf}/^{177}\text{Hf})_{\text{init}}$	2σ	ϵ_{Hf}	2σ
OUJ13z100	1966.6	12.6	25.1	93	0.0001009	0.0000055	0.281525	0.000024	0.281521231	0.000024	-0.4	0.9
OUJ13z101	1978.4	13.9	27.8	100	0.0002480	0.0000130	0.281617	0.000028	0.281607679	0.000028	3.0	1.0
OUJ13z103	2227.2	12.4	24.7	101	0.0007527	0.0000081	0.281340	0.000026	0.281308076	0.000026	-2.0	0.9
OUJ13z104	653.3	3.8	7.6	100	0.0016200	0.0000290	0.282561	0.000023	0.282541140	0.000023	6.2	0.8
OUJ13z105	2084.4	13.6	27.3	100	0.0004564	0.0000037	0.281517	0.000022	0.281498909	0.000022	1.5	0.8
OUJ13z106	626.7	4.4	8.8	99	0.0005682	0.0000086	0.282576	0.000017	0.282569320	0.000017	6.6	0.6
OUJ13z107	380.1	2.0	4.1	100	0.0010330	0.0000320	0.282676	0.000020	0.282668651	0.000020	4.7	0.7
OUJ13z108	2091.2	12.9	25.8	94	0.0006590	0.0000270	0.281581	0.000020	0.281554791	0.000020	3.7	0.7
OUJ13z109	568.1	2.7	5.5	102	0.0012790	0.0000270	0.282548	0.000017	0.282534376	0.000017	4.1	0.6
OUJ13z110	396.9	2.9	5.8	76	0.0008370	0.0000340	0.282624	0.000029	0.282617782	0.000029	3.3	1.0
OUJ13z111	381.4	2.6	5.1	100	0.0009660	0.0000810	0.282567	0.000021	0.282560104	0.000021	0.9	0.8
OUJ13z112	2606.0	12.4	24.8	101	0.0010790	0.0000280	0.281258	0.000024	0.281204262	0.000024	3.0	0.9
OUJ13z113	377.0	2.6	5.3	103	0.0015950	0.0000380	0.282568	0.000027	0.282556745	0.000027	0.7	1.0
OUJ13z115	622.3	3.2	6.4	101	0.0006019	0.0000034	0.282116	0.000023	0.282108974	0.000023	-9.8	0.8
OUJ13z116	615.0	5.0	10.0	97	0.0004840	0.0000190	0.282063	0.000023	0.282057417	0.000023	-11.7	0.8
OUJ13z118	542.7	2.8	5.7	99	0.0023150	0.0000180	0.282677	0.000025	0.282653450	0.000025	7.8	0.9
OUJ13z120	635.5	4.1	8.2	102	0.0010071	0.0000054	0.282147	0.000023	0.282134993	0.000023	-8.5	0.8
OUJ13z121	1765.9	14.4	28.8	97	0.0004410	0.0000600	0.281720	0.000065	0.281705234	0.000065	1.6	2.4
OUJ13z123	614.4	3.5	7.0	100	0.0010431	0.0000094	0.282431	0.000019	0.282418979	0.000019	1.0	0.7
OUJ13z124	2152.3	16.3	32.5	99	0.0006270	0.0000560	0.281584	0.000022	0.281558320	0.000022	5.2	0.9
OUJ13z125	1738.6	13.8	27.6	100	0.0012115	0.0000097	0.281737	0.000022	0.281697073	0.000022	0.7	0.8
OUJ13z126	1050.3	4.9	9.9	102	0.0003121	0.0000017	0.282099	0.000022	0.282092826	0.000022	-0.8	0.8
OUJ13z127	382.8	2.2	4.4	99	0.0013680	0.0000400	0.282512	0.000027	0.282502199	0.000027	-1.1	1.0
OUJ13z128	580.3	3.8	7.7	106	0.0005258	0.0000082	0.282371	0.000028	0.282365278	0.000028	-1.6	1.0
OUJ13z129c	1225.1	7.5	14.9	99	0.0005310	0.0000110	0.282133	0.000029	0.282120728	0.000029	4.1	1.0
OUJ13z129r	1235.7	6.4	12.8	101	0.0006187	0.0000060	0.282161	0.000025	0.282146576	0.000025	5.3	0.9
OUJ13z131	637.8	4.1	8.2	101	0.0008760	0.0000081	0.282719	0.000026	0.282708518	0.000026	11.8	0.9
OUJ13z132	2153.6	12.4	24.7	101	0.0006913	0.0000018	0.281271	0.000016	0.281242668	0.000016	-6.0	0.6
OUJ13z135	383.0	2.3	4.7	99	0.0017320	0.0000360	0.282653	0.000027	0.282640583	0.000027	3.8	1.0
OUJ13z136	641.7	3.5	7.0	101	0.0008515	0.0000092	0.282503	0.000023	0.282492749	0.000023	4.3	0.8
OUJ13z137	792.6	4.3	8.6	100	0.0011900	0.0001200	0.282105	0.000030	0.282087279	0.000030	-6.7	1.1
OUJ13z139	610.7	3.5	7.0	99	0.0008700	0.0001800	0.282408	0.000018	0.282398034	0.000018	0.2	0.7
OUJ13z143	382.7	2.1	4.1	98	0.0012690	0.0000390	0.282588	0.000024	0.282578909	0.000024	1.6	0.9
OUJ13z144	371.9	1.8	3.7	100	0.0031930	0.0000860	0.282635	0.000024	0.282612779	0.000024	2.5	0.9
OUJ13z145	610.4	3.2	6.5	99	0.0006360	0.0000220	0.282218	0.000026	0.282210719	0.000026	-6.4	0.9
OUJ13z146	377.5	2.1	4.3	99	0.0019570	0.0000670	0.282619	0.000028	0.282605173	0.000028	2.4	1.0

Chapter IV

Table E.6: Sample BES1

IGSN: IEACC0009

Coordinate UTM: Zone 29S, 3720500 m N, 674467 m E

GRAIN	Age (Ma)	σ	2σ	Concordia	$^{176}\text{Lu}/^{177}\text{Hf}$	2σ	$^{176}\text{Hf}/^{177}\text{Hf}$	2σ	$(^{176}\text{Hf}/^{177}\text{Hf})_{\text{init}}$	2σ	ϵ_{Hf}	2σ
BES1z1	1024.8	4.4	8.8	100	0.0005890	0.0000340	0.282225	0.000096	0.282213635	0.000096	2.9	3.4
BES1z3	1031.4	6.0	12.1	102	0.0009180	0.0000740	0.282206	0.000033	0.282188171	0.000033	2.2	1.2
BES1z4	603.9	5.9	11.7	98	0.0008681	0.0000055	0.282170	0.000043	0.282160168	0.000043	-8.4	1.5
BES1z5	1303.0	8.7	17.4	99	0.0020380	0.0000260	0.282199	0.000025	0.282148869	0.000025	6.9	0.9
BES1z6	2091.2	19.7	39.4	95	0.0015300	0.0001100	0.281729	0.000077	0.281668150	0.000077	7.7	2.9
BES1z8	1144.6	7.3	14.6	101	0.0007200	0.0001200	0.282270	0.000021	0.282254465	0.000021	7.0	0.8
BES1z9	2141.9	9.2	18.4	95	0.0015230	0.0000800	0.281483	0.000032	0.281420930	0.000032	0.1	1.3
BES1z10	468.6	3.6	7.2	101	0.0018800	0.0000260	0.282670	0.000100	0.282653498	0.000100	6.1	3.5
BES1z11	1070.3	12.3	24.6	95	0.0011940	0.0000870	0.282131	0.000023	0.282106928	0.000023	0.2	0.9
BES1z12	2087.1	40.2	80.3	101	0.0011240	0.0000460	0.281609	0.000044	0.281564386	0.000044	3.9	1.6
BES1z13	3050.0	8.0	16.0	91	0.0024400	0.0002000	0.281045	0.000090	0.280902185	0.000090	2.6	3.6
BES1z14	535.4	5.6	11.3	92	0.0021150	0.0000380	0.282401	0.000059	0.282379776	0.000059	-2.1	2.1
BES1z15	1322.4	8.9	17.9	98	0.0008163	0.0000074	0.281956	0.000041	0.281935617	0.000041	-0.3	1.5
BES1z16	406.2	2.8	5.6	98	0.0024000	0.0001600	0.282559	0.000079	0.282540749	0.000079	0.8	2.8
BES1z17	1993.0	13.1	26.1	95	0.0009720	0.0000260	0.281585	0.000034	0.281548192	0.000034	1.2	1.2
BES1z19	1136.0	6.5	13.0	101	0.0012480	0.0000740	0.282210	0.000045	0.282183278	0.000045	4.3	1.7
BES1z20	1101.8	13.0	26.1	98	0.0082000	0.0036000	0.282340	0.000190	0.282169752	0.000190	3.1	9.4
BES1z21	643.6	4.4	8.8	103	0.0028700	0.0002300	0.282719	0.000042	0.282684341	0.000042	11.1	1.6
BES1z22	1226.2	8.8	17.6	100	0.0022710	0.0000720	0.282168	0.000058	0.282115469	0.000058	4.0	2.1
BES1z23	636.6	4.1	8.2	102	0.0030500	0.0002400	0.282429	0.000041	0.282392570	0.000041	0.6	1.6
BES1z27	687.3	5.5	11.0	97	0.0026300	0.0001600	0.282593	0.000052	0.282559074	0.000052	7.6	1.9
BES1z28	2175.6	21.1	42.3	100	0.0009510	0.0000340	0.281452	0.000035	0.281412620	0.000035	0.5	1.3
BES1z31c	613.8	7.6	15.2	98	0.0003650	0.0000220	0.282107	0.000024	0.282102798	0.000024	-10.2	0.9
BES1z32	422.3	3.3	6.6	102	0.0012700	0.0000270	0.282528	0.000029	0.282517959	0.000029	0.3	1.0
BES1z33	2289.0	14.8	29.6	100	0.0044000	0.0005600	0.281612	0.000062	0.281420101	0.000062	3.4	3.1
BES1z34	815.2	8.5	17.0	92	0.0007000	0.0000280	0.282244	0.000025	0.282233276	0.000025	-1.1	0.9
BES1z36	640.7	3.5	7.0	100	0.0029700	0.0001200	0.282542	0.000032	0.282506297	0.000032	4.7	1.2
BES1z37	654.1	5.0	9.9	101	0.0088200	0.0005400	0.282490	0.000068	0.282381740	0.000068	0.6	2.6
BES1z40	1205.9	7.8	15.5	99	0.0007250	0.0000330	0.282088	0.000029	0.282071510	0.000029	1.9	1.1
BES1z42	566.4	2.8	5.6	101	0.0025630	0.0000240	0.282511	0.000028	0.282483782	0.000028	2.3	1.0
BES1z43	1031.9	7.1	14.3	102	0.0006160	0.0000110	0.282199	0.000036	0.282187030	0.000036	2.1	1.3
BES1z45c	575.6	4.1	8.3	101	0.0022100	0.0001400	0.282448	0.000038	0.282424147	0.000038	0.4	1.4
BES1z45r	616.8	4.1	8.2	97	0.0015270	0.0000950	0.282702	0.000029	0.282684334	0.000029	10.5	1.1
BES1z46	995.6	11.0	22.1	100	0.0007990	0.0000340	0.282249	0.000047	0.282234026	0.000047	3.0	1.7
BES1z47	641.3	3.8	7.6	100	0.0015010	0.0000320	0.282583	0.000034	0.282564940	0.000034	6.8	1.2
BES1z49	489.0	3.9	7.8	99	0.0046400	0.0002400	0.282411	0.000057	0.282368494	0.000057	-3.5	2.1
BES1z50	579.2	4.7	9.4	93	0.0009730	0.0000240	0.282423	0.000035	0.282412434	0.000035	0.0	1.2
BES1z51	583.9	6.5	13.0	99	0.0019470	0.0000790	0.282246	0.000064	0.282224683	0.000064	-6.5	2.3
BES1z52	658.2	11.9	23.9	92	0.0028240	0.0000250	0.282768	0.000029	0.282733120	0.000029	13.1	1.0
BES1z53	2321.8	18.0	35.9	98	0.0020660	0.0000710	0.281431	0.000034	0.281339574	0.000034	1.3	1.3
BES1z55	583.9	4.1	8.2	92	0.0014640	0.0000440	0.282616	0.000025	0.282599971	0.000025	6.8	2.0
BES1z56	2110.1	10.1	20.1	98	0.0013220	0.0000750	0.281490	0.000054	0.281436938	0.000054	-0.1	2.0
BES1z57	956.8	6.4	12.8	101	0.0008760	0.0000280	0.282153	0.000022	0.282137228	0.000022	-1.3	0.8
BES1z58	2166.6	10.3	20.6	93	0.0030810	0.0000780	0.281465	0.000017	0.281337957	0.000017	-2.3	0.7
BES1z59	586.2	3.8	7.7	100	0.0016000	0.0001600	0.282203	0.000025	0.282185411	0.000025	-7.8	0.9
BES1z60	623.2	5.0	9.9	101	0.0017860	0.0000600	0.282395	0.000041	0.282374121	0.000041	-0.3	1.5
BES1z61	2300.8	13.5	27.0	99	0.0009010	0.0000440	0.281389	0.000023	0.281349497	0.000023	1.2	0.9
BES1z62	1772.7	19.4	38.7	102	0.0010990	0.0000970	0.281615	0.000035	0.281578059	0.000035	-2.8	1.4
BES1z63	907.7	5.0	10.1	94	0.0016370	0.0000760	0.281474	0.000029	0.281446052	0.000029	-26.9	1.1
BES1z64	375.6	3.0	6.1	97	0.0019510	0.0000660	0.282494	0.000032	0.282480284	0.000032	-2.1	1.1
BES1z66	2040.1	10.5	21.1	95	0.0006900	0.0000480	0.281564	0.000032	0.281537241	0.000032	1.9	1.2
BES1z67	2083.0	19.1	38.2	99	0.0014770	0.0000230	0.281600	0.000026	0.281541492	0.000026	3.0	1.0
BES1z68	497.3	4.8	9.5	97	0.0021300	0.0001200	0.282467	0.000049	0.282447152	0.000049	-0.5	1.8
BES1z69	619.1	5.0	10.0	99	0.0012820	0.0000960	0.282407	0.000052	0.282392112	0.000052	0.2	1.9
BES1z70	2118.1	42.6	85.3	100	0.0006660	0.0000510	0.281527	0.000029	0.281500165	0.000029	2.3	1.1
BES1z71	852.0	11.3	22.6	92	0.0006470	0.0000200	0.282248	0.000028	0.282237637	0.000028	-2.3	1.0
BES1z72	930.0	5.0	10.0	94	0.0027600	0.0001400	0.282281	0.000017	0.282232709	0.000017	1.5	0.7
BES1z73	1726.5	13.9	27.8	99	0.0010890	0.0000330	0.281771	0.000032	0.281735364	0.000032	1.8	1.2
BES1z74	646.0	3.8	7.6	97	0.0039900	0.0008200	0.282387	0.000062	0.282338640	0.000062	-1.1	2.5
BES1z75	2122.1	14.0	27.9	100	0.0014830	0.0000540	0.281496	0.000022	0.281436131	0.000022	0.2	0.9
BES1z76	559.1	3.8	7.7	101	0.0011540	0.0000950	0.282367	0.000044	0.282354904	0.000044	-2.4	1.6
BES1z77	598.0	5.6	11.2	94	0.0011010	0.0000220	0.282291	0.000028	0.282278653	0.000028	-4.3	1.0
BES1z78	372.0	2.4	4.9	97	0.0016040	0.0000280	0.282547	0.000049	0.282535834	0.000049	-0.2	1.7
BES1z79	657.0	5.2	10.5	98	0.0018710	0.0000980	0.282382	0.000057	0.282358932	0.000057	-0.1	2.1
BES1z80c	616.8	4.1	8.2	98	0.0033700	0.0004000	0.282667	0.000046	0.282628013	0.000046	8.5	1.8
BES1z81	2051.3	10.5	20.9	94	0.0004090	0.0000350	0.281483	0.000017	0.281467050	0.000017	-0.4	0.7
BES1z82	1047.8	5.2	10.4	101	0.0005316	0.0000076	0.282248	0.000033	0.282237509	0.000033	4.3	1.2
BES1z83	413.2	4.2	8.5	104	0.0019900	0.0001400	0.282575	0.000032	0.282559605	0.000032	1.6	1.2
BES1z84	599.2	3.5	7.0	99	0.0012520	0.0000340	0.282322	0.000029	0.282307931	0.000029	-3.2	1.0
BES1z85	1004.4	5.5	11.0	100	0.0003010	0.0000240	0.282218	0.000029	0.282212309	0.000029	2.4	1.0
BES1z87	687.3	7.0	13.9	100	0.0004964	0.0000073	0.282671	0.000026	0.282664597	0.000026	11.4	0.9
BES1z88	644.2	4.1	8.2	97	0.0016200	0.0000500	0.282267	0.000036	0.282247419	0.000036	-4.4	1.3
BES1z89r	552.6	4.1	8.3	94	0.0058100	0.0002100	0.281998	0.000028	0.281937815	0.000028	-17.4	1.1
BES1z90	1232.5	10.4	20.8	96	0.0021000	0.0001000	0.282268	0.000069	0.282219168	0.000069	7.8	2.5
BES1z91	632.6	3.5	7.0	102	0.0026000	0.0004300	0.282468	0.000073	0.282437146	0.000073	2.1	2.8
BES1z92	2059.6	17.3	34.7	96	0.0008600	0.0002400	0.281334	0.000038	0.281300323	0.000038	-6.1	1.7
BES1z93	469.8	3.3	6.6	96	0.0013800	0.0002600	0.282504	0.000028	0.282491855	0.000028	4.4	1.1
BES1z94	1032.5	8.0	15.9	100	0.0015400	0.0001600	0.282272	0.000025	0.282242059	0.000025	0.1	1.0
BES1z96	591.5	4.1	8.2	99	0.0012520	0.0000510	0.282162	0.000063	0.282148112	0.000063	-9.1	2.3
BES1z99c	2027.4	28.4	56.7	99	0.0003500	0.0000170	0.281033	0.000027	0.281019513	0.000027	-16.8	1.0
BES1z100	2141.9	17.7	35.4	99								

GRAIN	Age (Ma)	σ	2 σ	Concordia	$^{176}\text{Lu}/^{177}\text{Hf}$	2 σ	$^{176}\text{Hf}/^{177}\text{Hf}$	2 σ	$(^{176}\text{Hf}/^{177}\text{Hf})_{\text{init}}$	2 σ	ϵHf	2 σ
BES1z107r	570.3	4.4	8.9	97	0.0004570	0.0000360	0.282420	0.000190	0.282415113	0.000190	-0.1	6.7
BES1z110	699.4	6.4	12.7	105	0.0010890	0.0000410	0.282468	0.000026	0.282453702	0.000026	4.2	0.9
BES1z111	1903.2	20.0	40.1	92	0.0017190	0.0000210	0.281657	0.000026	0.281594889	0.000026	0.8	1.0
BES1z114	578.6	3.5	7.1	94	0.0018400	0.0001000	0.282461	0.000024	0.282441039	0.000024	1.0	0.9
BES1z115	412.5	2.8	5.6	101	0.0015940	0.0000910	0.282716	0.000082	0.282703690	0.000082	6.7	2.9
BES1z116	599.2	4.4	8.8	99	0.0014320	0.0000490	0.282292	0.000028	0.282275909	0.000028	-4.4	1.0
BES1z117	3016.8	7.1	14.3	101	0.0009860	0.0000210	0.280986	0.000043	0.280928934	0.000043	2.8	1.6
BES1z118c	2973.4	12.1	24.3	98	0.0008397	0.0000054	0.280814	0.000021	0.280766121	0.000021	-4.0	0.8
BES1z119	600.3	5.3	10.6	98	0.0026400	0.0002200	0.282425	0.000051	0.282395276	0.000051	-0.1	1.9
BES1z120	2152.3	11.7	23.4	98	0.0013860	0.0000800	0.281623	0.000075	0.281566233	0.000075	5.5	2.8
BES1z121	2738.7	21.3	42.5	93	0.0008450	0.0000920	0.281300	0.000120	0.281255719	0.000120	8.0	4.4
BES1z125	916.1	13.4	26.8	98	0.0008190	0.0000220	0.282260	0.000240	0.282245887	0.000240	1.6	8.5
BES1z130	604.4	7.9	15.8	105	0.0014130	0.0000330	0.282591	0.000028	0.282574981	0.000028	6.4	1.0
BES1z131	685.5	6.1	12.2	104	0.0012520	0.0000520	0.281965	0.000027	0.281948891	0.000027	-14.0	1.0
BES1z135	633.7	3.2	6.4	98	0.0011670	0.0000820	0.282330	0.000032	0.282316126	0.000032	-2.2	1.2
BES1z136	623.2	4.7	9.4	101	0.0019270	0.0000990	0.282551	0.000023	0.282528473	0.000023	5.1	0.9
BES1z137	775.9	5.4	10.9	98	0.0026400	0.0001500	0.282075	0.000052	0.282036521	0.000052	-8.9	1.9
BES1z138	634.3	6.1	12.3	96	0.0022500	0.0000420	0.282469	0.000071	0.282442225	0.000071	2.3	2.5
BES1z139	2482.9	17.6	35.3	99	0.0048000	0.0027000	0.281450	0.000130	0.281222506	0.000130	0.9	9.2
BES1z140	2169.2	19.3	38.6	92	0.0024500	0.0001500	0.281781	0.000065	0.281679853	0.000065	9.9	2.5

Chapter IV

Table E.7: Sample SKH1

IGSN: IEACC00011

Coordinate UTM: Zone 29S, 3748316 m N, 678921 m E

GRAIN	Age (Ma)	σ	2σ	Concordia	$^{176}\text{Lu}/^{177}\text{Hf}$	2σ	$^{176}\text{Hf}/^{177}\text{Hf}$	2σ	$(^{176}\text{Hf}/^{177}\text{Hf})_{\text{init}}$	2σ	ϵHf	2σ
SHK1z1	634.3	3.5	7.0	101	0.0006497	0.0000056	0.282676	0.000021	0.282668269	0.000021	10.3	0.7
SHK1z2	609.7	7.9	15.8	96	0.0008230	0.0000190	0.281921	0.000021	0.281911588	0.000021	-17.0	0.7
SHK1z3	1012.7	10.5	20.9	99	0.0008600	0.0000290	0.282246	0.000026	0.282229604	0.000026	3.2	0.9
SHK1z4	1310.3	7.4	14.7	100	0.0016110	0.0000420	0.282129	0.000025	0.282089145	0.000025	4.9	0.8
SHK1z5	1217.6	8.8	17.6	102	0.0005850	0.0000140	0.282027	0.000029	0.282013563	0.000029	0.1	1.0
SHK1z6	1019.3	9.1	18.2	98	0.0004260	0.0000140	0.282238	0.000033	0.282229825	0.000033	3.4	1.2
SHK1z7	1040.7	7.4	14.8	100	0.0006650	0.0000110	0.282136	0.000024	0.282122967	0.000024	0.1	0.8
SHK1z8	650.6	6.1	12.2	98	0.0007700	0.0000250	0.282481	0.000023	0.282471600	0.000023	3.7	0.8
SHK1z9c	697.7	8.4	16.8	105	0.0008380	0.0000120	0.281845	0.000028	0.281834025	0.000028	-17.8	1.0
SHK1z11	1133.8	5.7	11.4	92	0.0013400	0.0000180	0.282100	0.000025	0.282071363	0.000025	0.3	0.9
SHK1z12	537.8	4.7	9.5	94	0.0014890	0.0000240	0.282347	0.000018	0.282331991	0.000018	-3.7	0.6
SHK1z13	1049.5	5.5	11.0	101	0.0013590	0.0000410	0.282394	0.000030	0.282367139	0.000030	8.9	1.0
SHK1z14	1042.3	7.1	14.3	105	0.0005513	0.0000075	0.282214	0.000022	0.282203178	0.000022	2.9	0.8
SHK1z15c	644.8	5.2	10.5	101	0.0000760	0.0000110	0.282212	0.000018	0.282211081	0.000018	-5.6	0.6
SHK1z15r	646.0	3.5	7.0	100	0.0001330	0.0000005	0.282266	0.000026	0.282264389	0.000026	-3.7	0.9
SHK1z16	586.2	4.7	9.4	103	0.0003754	0.0000038	0.282223	0.000032	0.282218873	0.000032	-6.7	1.1
SHK1z17	528.3	3.9	7.7	99	0.0008960	0.0000110	0.282477	0.000023	0.282468129	0.000023	0.9	0.8
SHK1z19	1059.3	5.5	10.9	100	0.0005432	0.0000045	0.282250	0.000018	0.282239162	0.000018	4.6	0.6
SHK1z20	680.9	8.7	17.4	100	0.0012740	0.0000430	0.282499	0.000022	0.282482719	0.000022	4.8	0.8
SHK1z21	1065.9	6.3	12.6	100	0.0033200	0.0002500	0.282024	0.000032	0.281957342	0.000032	-5.2	1.0
SHK1z22	546.7	3.6	7.1	97	0.0027590	0.0000350	0.282312	0.000035	0.282283728	0.000035	-5.2	1.2
SHK1z24	584.5	3.8	7.7	96	0.0008470	0.0000480	0.282072	0.000032	0.282062717	0.000032	-12.2	1.1
SHK1z25	961.2	7.8	15.5	99	0.0016520	0.0000150	0.281525	0.000024	0.281495118	0.000024	-24.0	0.8
SHK1z26	393.8	2.8	5.6	99	0.0016240	0.0000380	0.282443	0.000026	0.282431029	0.000026	-3.4	0.9
SHK1z30	631.4	3.2	6.4	99	0.0028800	0.0002200	0.282105	0.000044	0.282070887	0.000044	-10.9	1.5
SHK1z31	2145.8	24.8	49.7	101	0.0023300	0.0003500	0.281691	0.000059	0.281595864	0.000059	6.4	1.6
SHK1z32	2641.8	7.0	13.9	98	0.0008070	0.0000180	0.281010	0.000026	0.280969244	0.000026	-4.5	0.9
SHK1z33	577.4	4.7	9.4	97	0.0017620	0.0000220	0.282334	0.000026	0.282314924	0.000026	-3.5	0.9
SHK1z34	1580.7	23.0	46.0	101	0.0013480	0.0000270	0.281964	0.000037	0.281923670	0.000037	5.1	1.3
SHK1z36	2274.7	20.4	40.7	101	0.0007870	0.0000270	0.281250	0.000033	0.281215895	0.000033	-4.2	1.1
SHK1z37	1272.4	5.8	11.6	102	0.0012600	0.0000790	0.282079	0.000030	0.282048743	0.000030	2.6	1.0
SHK1z38	419.3	3.6	7.2	92	0.0012500	0.0000290	0.282551	0.000022	0.282541188	0.000022	1.1	0.8
SHK1z39	624.9	3.5	7.0	100	0.0008080	0.0000530	0.282156	0.000021	0.282146527	0.000021	-8.4	0.7
SHK1z40	1982.8	38.0	76.0	100	0.0001310	0.0000110	0.281237	0.000028	0.281232065	0.000028	-10.3	1.0
SHK1z41	2154.9	11.7	23.4	97	0.0016600	0.0001200	0.281358	0.000025	0.281289926	0.000025	-4.3	0.7
SHK1z42	655.9	3.8	7.6	103	0.0011800	0.0000860	0.282277	0.000044	0.282262477	0.000044	-3.6	1.5
SHK1z43	463.8	4.5	9.0	99	0.0010690	0.0000210	0.282609	0.000024	0.282599713	0.000024	4.1	0.8
SHK1z44	1163.5	7.0	14.0	97	0.0014190	0.0000450	0.282163	0.000029	0.282131872	0.000029	3.1	1.0
SHK1z45	976.2	5.3	10.5	100	0.0007420	0.0000270	0.282241	0.000034	0.282227367	0.000034	2.3	1.2
SHK1z46	2056.9	18.8	37.5	101	0.0009680	0.0000250	0.281598	0.000030	0.281560146	0.000030	3.1	1.0
SHK1z47	562.0	4.4	8.9	97	0.0009300	0.0001200	0.282354	0.000021	0.282344200	0.000021	-2.8	0.7
SHK1z48	596.2	4.4	8.8	101	0.0011794	0.0000092	0.282165	0.000019	0.282151813	0.000019	-8.8	0.7
SHK1z49	1993.0	16.7	33.4	98	0.0010550	0.0000250	0.281598	0.000020	0.281558049	0.000020	1.5	0.7
SHK1z50	606.2	6.7	13.5	101	0.0005310	0.0000140	0.281841	0.000019	0.281834963	0.000019	-19.8	0.7
SHK1z51r	653.0	5.0	9.9	96	0.0009030	0.0000340	0.282260	0.000026	0.282248936	0.000026	-4.1	0.9
SHK1z52	535.4	4.2	8.3	98	0.0021110	0.0000600	0.282323	0.000029	0.282301816	0.000029	-4.9	1.0
SHK1z53	2960.0	8.2	16.3	92	0.0018500	0.0000540	0.280971	0.000026	0.280865999	0.000026	-0.8	0.8
SHK1z54	2106.0	25.5	51.1	103	0.0006980	0.0000200	0.281491	0.000019	0.281463039	0.000019	0.7	0.6
SHK1z55	763.9	7.2	14.3	103	0.0016850	0.0000750	0.282640	0.000024	0.282615824	0.000024	11.3	0.8
SHK1z56	1499.6	7.9	15.8	100	0.0008383	0.0000059	0.281795	0.000029	0.281771543	0.000029	-2.5	1.0
SHK1z57	1043.4	7.1	14.3	99	0.0004321	0.0000024	0.282212	0.000021	0.282203509	0.000021	3.0	0.7
SHK1z58	1417.0	32.0	64.0	103	0.0012660	0.0000250	0.281961	0.000025	0.281927097	0.000025	1.6	0.9
SHK1z59	793.0	4.0	8.0	101	0.0018280	0.0000660	0.282062	0.000023	0.282034764	0.000023	-8.6	0.8
SHK1z60	1257.5	8.2	16.4	100	0.0003480	0.0000150	0.282139	0.000024	0.282130742	0.000024	5.2	0.8
SHK1z62	475.2	4.2	8.4	99	0.0018690	0.0000640	0.282361	0.000021	0.282344362	0.000021	-4.7	0.7
SHK1z63	528.9	3.9	7.7	103	0.0015300	0.0001400	0.282297	0.000043	0.282281834	0.000043	-5.7	1.5
SHK1z64	613.2	5.0	10.0	99	0.0028870	0.0000740	0.282571	0.000024	0.282537792	0.000024	5.2	0.8
SHK1z65	1230.9	9.1	18.1	100	0.0008470	0.0000370	0.282196	0.000023	0.282176330	0.000023	6.2	0.8
SHK1z66	574.4	5.6	11.2	98	0.0005680	0.0000130	0.282286	0.000025	0.282279882	0.000025	-4.8	0.9
SHK1z67	796.4	10.0	19.9	99	0.0006872	0.0000032	0.282198	0.000035	0.282187717	0.000035	-3.1	1.2
SHK1z68	634.3	4.7	9.3	96	0.0014060	0.0000460	0.282191	0.000019	0.282174269	0.000019	-7.2	0.7
SHK1z70	1990.0	19.6	39.3	99	0.0000600	0.0000030	0.281446	0.000027	0.281443731	0.000027	-2.6	1.0
SHK1z71	606.2	4.1	8.2	101	0.0007700	0.0000150	0.282135	0.000019	0.282126245	0.000019	-9.5	0.7
SHK1z73	2886.9	13.7	27.4	100	0.0005670	0.0000250	0.280951	0.000046	0.280919636	0.000046	-0.6	1.6
SHK1z74	547.8	5.0	10.1	100	0.0019210	0.0000730	0.282379	0.000022	0.282359272	0.000022	-2.5	0.8
SHK1z75	526.1	3.0	5.9	98	0.0098100	0.0003500	0.282649	0.000047	0.282552277	0.000047	3.8	1.5
SHK1z76	537.2	3.9	7.7	99	0.0008430	0.0000770	0.282238	0.000026	0.282229512	0.000026	-7.4	0.9
SHK1z78	593.3	4.7	9.4	105	0.0010860	0.0000310	0.282048	0.000029	0.282035917	0.000029	-13.0	1.0
SHK1z79	1709.1	23.7	47.5	99	0.0018710	0.0000180	0.281897	0.000029	0.281836404	0.000029	5.0	1.0
SHK1z80	618.5	4.4	8.8	98	0.0005708	0.0000084	0.282194	0.000029	0.282187378	0.000029	-7.1	1.0
SHK1z82	2153.6	15.6	31.2	95	0.0011290	0.0000380	0.281717	0.000027	0.281670730	0.000027	9.2	0.9
SHK1z83	2070.7	20.0	39.9	100	0.0006600	0.0000190	0.281473	0.000029	0.281447013	0.000029	-0.6	1.0
SHK1z84	450.5	2.8	5.7	99	0.0010510	0.0000910	0.282504	0.000053	0.282495133	0.000053	0.1	1.8
SHK1z85	1856.2	16.7	33.4	101	0.0009270	0.0000220	0.281661	0.000022	0.281628347	0.000022	0.9	0.8
SHK1z86	613.8	5.6	11.1	104	0.0021850	0.0000690	0.282319	0.000040	0.282293843	0.000040	-3.4	1.4
SHK1z87	1220.3	10.1	20.3	99	0.0004860	0.0000140	0.282158	0.000025	0.282146813	0.000025	4.9	0.9
SHK1z88	659.4	11.6	23.3	91	0.0011400	0.0000330	0.282666	0.000043	0.282651894	0.000043	10.3	1.5
SHK1z89	990.6	5.3	10.5	99	0.0007810	0.0000330	0.282241	0.000019	0.282226437	0.000019	2.6	0.7
SHK1z90	665.8	7.3	14.5	95	0.0024300	0.0001700	0.282520	0.000035	0.282489639	0.000035	4.7	1.2
SHK1z91	1972.5	11.8	23.5	94	0.0002564	0.0000092	0.281586	0.000029	0.2815763			

GRAIN	Age (Ma)	σ	2σ	Concordia	$^{176}\text{Lu}/^{177}\text{Hf}$	2σ	$^{176}\text{Hf}/^{177}\text{Hf}$	2σ	$(^{176}\text{Hf}/^{177}\text{Hf})_{\text{init}}$	2σ	ϵHf	2σ
SHK1z97	945.1	13.4	26.7	92	0.0004490	0.0000160	0.282317	0.000041	0.282309016	0.000041	4.5	1.4
SHK1z98	1941.3	18.8	37.6	101	0.0013470	0.0000230	0.281540	0.000029	0.281490339	0.000029	-2.0	1.0
SHK1z99	985.1	7.2	14.4	99	0.0007649	0.0000081	0.281880	0.000025	0.281865818	0.000025	-10.3	0.9
SHK1z100	1736.9	19.0	37.9	99	0.0018480	0.0000900	0.281741	0.000022	0.281680157	0.000022	0.0	0.7
SHK1z101	2141.9	17.0	34.1	98	0.0010460	0.0000520	0.281557	0.000023	0.281514370	0.000023	3.4	0.7

Chapter IV

Table E.8: Sample TIF1

IGSN: IEACC00016

Coordinate UTM: Zone 29S, 3752612 m N, 750380 m E

GRAIN	Age (Ma)	σ	2σ	Concordia	$^{176}\text{Lu}/^{177}\text{Hf}$	2σ	$^{176}\text{Hf}/^{177}\text{Hf}$	2σ	$(^{176}\text{Hf}/^{177}\text{Hf})_{\text{init}}$	2σ	ϵHf	2σ
TIF1z1	1116.0	5.5	11.0	99	0.0005930	0.0000110	0.282000	0.000079	0.281987528	0.000079	-3.1	2.8
TIF1z3	593.0	2.5	5.0	91	0.0003570	0.0000420	0.282370	0.000110	0.282366030	0.000110	-1.3	3.9
TIF1z6	2067.0	10.5	21.0	97	0.0006228	0.0000080	0.281633	0.000068	0.281608523	0.000068	5.0	2.4
TIF1z7	997.0	4.5	9.0	99	0.0003850	0.0000370	0.282140	0.000110	0.282132774	0.000110	-0.6	3.9
TIF1z8	612.0	2.5	5.0	98	0.0002270	0.0000190	0.282639	0.000026	0.282636394	0.000026	8.7	0.9
TIF1z10	1234.0	4.5	9.0	100	0.0007264	0.0000081	0.282191	0.000036	0.282174089	0.000036	6.2	1.3
TIF1z11	1769.0	8.5	17.0	98	0.0006436	0.0000075	0.281451	0.000081	0.281429412	0.000081	-8.1	2.9
TIF1z12	1017.0	5.5	11.0	97	0.0002964	0.0000088	0.282198	0.000048	0.282192325	0.000048	2.0	1.7
TIF1z17	1003.0	7.5	15.0	97	0.0006000	0.0001600	0.282280	0.000120	0.282268671	0.000120	4.4	4.4
TIF1z19	1026.0	3.5	7.0	100	0.0006090	0.0000170	0.282223	0.000042	0.282211235	0.000042	2.9	1.5
TIF1z20	448.0	2.0	4.0	97	0.0007010	0.0000560	0.282438	0.000058	0.282432118	0.000058	-2.2	2.1
TIF1z22	523.0	3.5	7.0	93	0.0005108	0.0000024	0.282360	0.000140	0.282354993	0.000140	-3.2	5.0
TIF1z23	2507.0	11.5	23.0	99	0.0003570	0.0000160	0.281500	0.000120	0.281482912	0.000120	10.7	4.3
TIF1z25	1880.0	13.5	27.0	92	0.0004025	0.0000042	0.281545	0.000072	0.281530637	0.000072	-2.0	2.6
TIF1z26	547.0	2.5	5.0	99	0.0010830	0.0000120	0.282620	0.000038	0.282608895	0.000038	6.3	1.3
TIF1z28	647.0	4.0	8.0	98	0.0012860	0.0000570	0.282687	0.000055	0.282671388	0.000055	10.7	2.0
TIF1z29	2627.0	7.5	15.0	91	0.0004418	0.0000083	0.280964	0.000052	0.280941816	0.000052	-5.8	1.9
TIF1z31	498.0	3.0	6.0	96	0.0016220	0.0000490	0.282200	0.000068	0.282184865	0.000068	-9.8	2.4
TIF1z34	637.0	2.5	5.0	95	0.0004370	0.0000300	0.282050	0.000044	0.282044777	0.000044	-11.7	1.6
TIF1z35	625.0	4.0	8.0	96	0.0002763	0.0000026	0.282129	0.000062	0.282125761	0.000062	-9.1	2.2
TIF1z36	1387.0	14.0	28.0	95	0.0006570	0.0000150	0.281941	0.000074	0.281923783	0.000074	0.8	2.6
TIF1z38	2019.0	13.5	27.0	100	0.0000890	0.0000140	0.281420	0.000340	0.281416585	0.000340	-2.9	12.1
TIF1z39	586.0	3.0	6.0	93	0.0006850	0.0000140	0.282323	0.000026	0.282315473	0.000026	-3.2	0.9
TIF1z40	1302.0	7.0	14.0	102	0.0006687	0.0000015	0.282189	0.000038	0.282172564	0.000038	7.7	1.3
TIF1z41c	580.0	3.0	6.0	97	0.0007160	0.0000650	0.282205	0.000048	0.282197213	0.000048	-7.6	1.7
TIF1z41r	584.0	4.0	8.0	95	0.0006570	0.0000340	0.282165	0.000057	0.282157805	0.000057	-8.9	2.0
TIF1z42	2127.0	13.0	26.0	100	0.0004677	0.0000077	0.281565	0.000034	0.281546074	0.000034	4.2	1.2
TIF1z44	607.0	3.0	6.0	98	0.0005440	0.0000200	0.282012	0.000051	0.282005807	0.000051	-13.7	1.8
TIF1z45	620.0	2.5	5.0	98	0.0003790	0.0000260	0.282491	0.000032	0.282486592	0.000032	3.6	1.1
TIF1z46	1005.0	4.0	8.0	100	0.0012800	0.0000320	0.282205	0.000068	0.282180782	0.000068	1.3	2.4
TIF1z47	471.0	2.5	5.0	95	0.0010960	0.0000620	0.282454	0.000039	0.282444330	0.000039	-1.2	1.4
TIF1z49	628.0	4.5	9.0	97	0.0009010	0.0000560	0.282272	0.000058	0.282261385	0.000058	-4.2	2.1
TIF1z50	1803.0	11.5	23.0	99	0.0006940	0.0000120	0.281654	0.000037	0.281630267	0.000037	-0.2	1.3
TIF1z51	620.0	2.5	5.0	99	0.0000205	0.0000008	0.282025	0.000037	0.282024762	0.000037	-12.8	1.3
TIF1z54	2950.0	9.0	18.0	91	0.0047000	0.0014000	0.280960	0.000140	0.280964172	0.000140	-7.1	7.8
TIF1z55	415.0	2.0	4.0	97	0.0008480	0.0000270	0.282464	0.000033	0.282457411	0.000033	-2.0	1.2
TIF1z56	970.0	3.5	7.0	100	0.0010160	0.0000570	0.282383	0.000036	0.282364453	0.000036	7.0	1.3
TIF1z57	1019.0	4.0	8.0	99	0.0005860	0.0000400	0.282194	0.000043	0.282182757	0.000043	1.7	1.6
TIF1z58	573.0	3.0	6.0	94	0.0013460	0.0000100	0.282091	0.000050	0.282076539	0.000050	-12.0	1.8
TIF1z60	624.0	2.5	5.0	98	0.0010430	0.0000190	0.281626	0.000026	0.281613791	0.000026	-27.3	0.9
TIF1z64	2798.0	7.0	14.0	99	0.0004310	0.0000190	0.280950	0.000044	0.280926912	0.000044	-2.4	1.6
TIF1z65	593.0	2.5	5.0	94	0.0002150	0.0000140	0.282378	0.000034	0.282375609	0.000034	-1.0	1.2
TIF1z66	361.0	2.0	4.0	99	0.0020720	0.0000650	0.282615	0.000067	0.282601003	0.000067	1.9	2.4
TIF1z68	998.0	4.0	8.0	100	0.0009810	0.0000300	0.282162	0.000034	0.282143570	0.000034	-0.2	1.2
TIF1z69	796.0	3.5	7.0	99	0.0025400	0.0001400	0.282029	0.000032	0.281991011	0.000032	-10.1	1.2
TIF1z70	268.0	1.5	3.0	102	0.0022500	0.0001700	0.282576	0.000044	0.282564726	0.000044	-1.4	1.6
TIF1z71	544.0	3.5	7.0	94	0.0042000	0.0005100	0.282333	0.000049	0.282290172	0.000049	-5.1	1.9
TIF1z73	618.0	3.0	6.0	99	0.0031100	0.0002300	0.282110	0.000092	0.282073948	0.000092	-11.1	3.4
TIF1z74	556.0	2.5	5.0	99	0.0033400	0.0003200	0.282464	0.000029	0.282429186	0.000029	0.1	1.1
TIF1z76	701.0	4.0	8.0	94	0.0014900	0.0000840	0.282645	0.000028	0.282625392	0.000028	10.3	1.0
TIF1z78	561.0	3.5	7.0	98	0.0022130	0.0000270	0.282378	0.000061	0.282354725	0.000061	-2.4	2.2
TIF1z79	2938.0	10.0	20.0	99	0.0006472	0.0000025	0.280872	0.000033	0.280835548	0.000033	-2.4	1.2
TIF1z81	556.0	5.0	10.0	108	0.0016000	0.0001000	0.282493	0.000032	0.282476323	0.000032	1.8	1.2
TIF1z82	408.0	2.0	4.0	97	0.0017090	0.0000290	0.282338	0.000067	0.282324946	0.000067	-6.8	2.4
TIF1z84	2082.0	15.5	31.0	100	0.0025000	0.0001200	0.281509	0.000032	0.281410017	0.000032	-1.7	1.3
TIF1z85	654.0	3.0	6.0	102	0.0018410	0.0000420	0.282209	0.000047	0.282186408	0.000047	-6.3	1.7
TIF1z86	1786.0	10.0	20.0	99	0.0015100	0.0001200	0.281740	0.000034	0.281688857	0.000034	1.5	1.4
TIF1z87	986.0	3.5	7.0	99	0.0011410	0.0000940	0.282078	0.000043	0.282056824	0.000043	-3.5	1.6
TIF1z88	2119.0	18.5	37.0	92	0.0021080	0.0000630	0.281612	0.000039	0.281527025	0.000039	3.3	1.5
TIF1z89	1372.0	5.5	11.0	98	0.0016220	0.0000510	0.282021	0.000081	0.281978961	0.000081	2.4	2.9
TIF1z90	1172.0	4.5	9.0	99	0.0016340	0.0000840	0.282218	0.000045	0.282181891	0.000045	5.1	1.7
TIF1z91	632.0	2.5	5.0	100	0.0012600	0.0000310	0.282174	0.000064	0.282159061	0.000064	-7.8	2.3
TIF1z92	673.0	4.5	9.0	97	0.0008390	0.0000330	0.282306	0.000040	0.282295403	0.000040	-2.0	1.4
TIF1z93	893.0	10.0	20.0	91	0.0005070	0.0000250	0.282018	0.000037	0.282009485	0.000037	-7.3	1.3
TIF1z94	572.0	2.0	4.0	101	0.0042500	0.0002300	0.282575	0.000087	0.282529419	0.000087	4.0	3.2
TIF1z98	2111.0	8.5	17.0	99	0.0007550	0.0000730	0.281510	0.000069	0.281479683	0.000069	1.5	2.6

Chapter IV

Table E.9: Sample TIF2

IGSN: IEACC00017

Coordinate UTM: Zone 29S, 3752611 m N, 750354 m E

GRAIN	Age (Ma)	σ	2σ	Concordia	¹⁷⁶ Lu/ ¹⁷⁷ Hf	2σ	¹⁷⁶ Hf/ ¹⁷⁷ Hf	2σ	(¹⁷⁶ Hf/ ¹⁷⁷ Hf) _{init}	2σ	εHf	+2σ
TIF2z1	707.0	4.5	9.0	100	0.0022810	0.0000340	0.282250	0.000027	0.282219725	0.000027	-4.0	1.0
TIF2z3	376.0	2.5	5.0	99	0.0034100	0.0001500	0.282264	0.000050	0.282240004	0.000050	-10.6	1.8
TIF2z5	1280.0	9.0	18.0	98	0.0013850	0.0000640	0.281852	0.000086	0.281818539	0.000086	-5.4	3.1
TIF2z6	585.0	4.0	8.0	101	0.0019900	0.0000350	0.282252	0.000066	0.282230170	0.000066	-6.3	2.4
TIF2z7	616.0	5.0	10.0	98	0.0012310	0.0000420	0.282113	0.000045	0.282098776	0.000045	-10.3	1.6
TIF2z8	2498.0	12.0	24.0	100	0.0025800	0.0002000	0.281090	0.000059	0.280966960	0.000059	-7.9	2.4
TIF2z9	629.0	4.5	9.0	102	0.0009190	0.0000520	0.282591	0.000032	0.282580156	0.000032	7.1	1.2
TIF2z10	1340.0	8.0	16.0	100	0.0015170	0.0000360	0.282095	0.000034	0.282056611	0.000034	4.4	1.2
TIF2z11	1486.0	15.5	31.0	100	0.0041340	0.0000980	0.282073	0.000031	0.281956828	0.000031	4.2	1.2
TIF2z12	612.0	4.0	8.0	102	0.0020400	0.0002900	0.282099	0.000038	0.282075582	0.000038	-11.2	1.5
TIF2z13	646.0	4.0	8.0	101	0.0115900	0.0004100	0.282680	0.000130	0.282539520	0.000130	6.0	4.8
TIF2z14	1788.0	16.5	33.0	100	0.0014590	0.0000340	0.281920	0.000190	0.281870528	0.000190	8.0	6.8
TIF2z17	554.0	3.5	7.0	91	0.0021400	0.0001100	0.282358	0.000036	0.282335775	0.000036	-3.2	1.3
TIF2z19	1752.0	14.5	29.0	100	0.0014770	0.0000410	0.281665	0.000093	0.281615942	0.000093	-1.9	3.4
TIF2z20	647.0	4.0	8.0	100	0.0022910	0.0000610	0.282020	0.000055	0.281992188	0.000055	-13.3	2.0
TIF2z21	389.0	2.5	5.0	96	0.0024640	0.0000690	0.282372	0.000043	0.282354059	0.000043	-6.2	1.5
TIF2z23	577.0	6.0	12.0	96	0.0012840	0.0000800	0.282318	0.000031	0.282304108	0.000031	-3.8	1.1
TIF2z24	2339.0	12.0	24.0	99	0.0019650	0.0000320	0.281335	0.000031	0.281247385	0.000031	-1.6	1.2
TIF2z25	371.0	2.5	5.0	96	0.0022450	0.0000790	0.282361	0.000035	0.282345413	0.000035	-6.9	1.3
TIF2z26	1325.0	12.5	25.0	99	0.0004936	0.0000688	0.281936	0.000038	0.281923651	0.000038	-0.6	1.4
TIF2z27	650.0	4.5	9.0	100	0.0026600	0.0001000	0.282406	0.000034	0.282373558	0.000034	0.2	1.2
TIF2z28	459.0	3.0	6.0	99	0.0018030	0.0000290	0.282352	0.000037	0.282336499	0.000037	-5.3	1.3
TIF2z30	365.0	2.5	5.0	96	0.0017400	0.0001500	0.282315	0.000070	0.282303115	0.000070	-8.6	2.5
TIF2z32	701.0	4.5	9.0	99	0.0014200	0.0001700	0.282292	0.000039	0.282273314	0.000039	-2.2	1.5
TIF2z34	2457.0	17.0	34.0	101	0.0003970	0.0000110	0.281180	0.000046	0.281161385	0.000046	-1.9	1.7
TIF2z35	772.0	5.0	10.0	100	0.0013600	0.0001000	0.282168	0.000076	0.282148277	0.000076	-5.0	2.7
TIF2z37	355.0	3.0	6.0	95	0.0015500	0.0001400	0.282550	0.000700	0.282539704	0.000700	-0.4	24.8
TIF2z38	387.0	2.5	5.0	98	0.0032000	0.0001600	0.282383	0.000089	0.282359820	0.000089	-6.1	3.2
TIF2z40	558.0	4.0	8.0	99	0.0025910	0.0000770	0.282262	0.000029	0.282598895	0.000029	6.2	1.1
TIF2z41	575.0	3.5	7.0	101	0.0009900	0.0000180	0.282390	0.000027	0.282379326	0.000027	-1.2	1.0
TIF2z42	364.0	2.5	5.0	91	0.0019300	0.0001300	0.282435	0.000064	0.282421853	0.000064	-4.4	2.3
TIF2z43	2147.0	17.0	34.0	100	0.0003586	0.0000050	0.281556	0.000032	0.281541350	0.000032	4.5	1.1
TIF2z44	713.0	4.5	9.0	104	0.0006510	0.0000410	0.282539	0.000086	0.282530286	0.000086	7.2	3.1
TIF2z45	1630.0	15.0	30.0	99	0.0003660	0.0000370	0.281896	0.000043	0.281884703	0.000043	4.9	1.6
TIF2z47c	822.0	5.5	11.0	97	0.0006970	0.0000720	0.282292	0.000032	0.282281232	0.000032	0.8	1.2
TIF2z47r	610.0	4.0	8.0	98	0.0004980	0.0000160	0.282258	0.000038	0.282252302	0.000038	-5.0	1.4
TIF2z48	598.0	4.0	8.0	99	0.0008680	0.0000350	0.282222	0.000049	0.282212265	0.000049	-6.6	1.7
TIF2z49	373.0	2.5	5.0	99	0.0016240	0.0000640	0.282400	0.000076	0.282388663	0.000076	-5.4	2.7
TIF2z51	640.0	4.5	9.0	97	0.0014640	0.0000250	0.282043	0.000035	0.282025421	0.000035	-12.3	1.3
TIF2z52	631.0	4.5	9.0	101	0.0009390	0.0000160	0.282404	0.000034	0.282392884	0.000034	0.5	1.2
TIF2z53	2048.0	16.0	32.0	102	0.0000999	0.0000066	0.280988	0.000032	0.280984110	0.000032	-17.6	1.1
TIF2z54	1814.0	21.5	43.0	98	0.0005500	0.0000220	0.281564	0.000098	0.281545075	0.000098	-3.0	3.5
TIF2z55	379.0	2.5	5.0	99	0.0016900	0.0001500	0.282347	0.000078	0.282335012	0.000078	-7.1	2.8
TIF2z56	772.0	5.0	10.0	99	0.0002019	0.0000080	0.282499	0.000034	0.282496072	0.000034	7.3	1.2
TIF2z58	349.0	3.0	6.0	92	0.0017600	0.0001900	0.282411	0.000056	0.282399507	0.000056	-5.5	2.0
TIF2z59	668.0	4.5	9.0	101	0.0015890	0.0000560	0.282583	0.000047	0.282563080	0.000047	7.3	1.7
TIF2z61	612.0	4.0	8.0	101	0.0025300	0.0000510	0.282110	0.000065	0.282080958	0.000065	-11.0	2.3
TIF2z63	624.0	4.5	9.0	102	0.0005390	0.0000110	0.282094	0.000048	0.282087691	0.000048	-10.5	1.7
TIF2z64	2139.0	13.0	26.0	100	0.0009520	0.0000490	0.281355	0.000036	0.281316255	0.000036	-3.7	1.4
TIF2z65	2177.0	13.0	26.0	98	0.0010740	0.0000180	0.281308	0.000039	0.281263497	0.000039	-4.7	1.4
TIF2z66	625.0	4.0	8.0	96	0.0008080	0.0000250	0.282388	0.000055	0.282378527	0.000055	-0.1	2.0
TIF2z67	381.0	2.5	5.0	103	0.0004530	0.0000150	0.282312	0.000044	0.282308770	0.000044	-8.0	1.6
TIF2z68	664.0	5.0	10.0	98	0.0012049	0.0000091	0.282330	0.000250	0.282314986	0.000250	-1.5	8.9
TIF2z69	694.0	5.5	11.0	102	0.0011190	0.0000460	0.282689	0.000029	0.282674423	0.000029	11.9	1.0
TIF2z70	589.0	5.5	11.0	96	0.0018980	0.0000430	0.282542	0.000041	0.282521036	0.000041	4.1	1.5
TIF2z72	387.0	3.0	6.0	91	0.0022900	0.0001200	0.282440	0.000056	0.282423412	0.000056	-3.8	2.0
TIF2z73	637.0	4.0	8.0	101	0.0005050	0.0000960	0.282237	0.000093	0.282230965	0.000093	-5.1	3.3
TIF2z74	2464.0	14.5	29.0	98	0.0004620	0.0000460	0.281432	0.000030	0.281410274	0.000030	7.1	1.2
TIF2z75	2467.0	13.0	26.0	100	0.0009140	0.0000950	0.281332	0.000036	0.281288965	0.000036	2.9	1.4
TIF2z76	2325.0	13.5	27.0	98	0.0009330	0.0000370	0.281342	0.000054	0.281300654	0.000054	0.0	2.0
TIF2z78	1965.0	17.0	34.0	100	0.0009470	0.0000760	0.281528	0.000070	0.281492651	0.000070	-1.4	2.6
TIF2z79	1804.0	13.0	26.0	101	0.0031300	0.0001500	0.281500	0.000043	0.281392901	0.000043	-8.6	1.7
TIF2z80	640.0	4.5	9.0	98	0.0007660	0.0000310	0.282112	0.000037	0.282102802	0.000037	-9.6	1.3
TIF2z81	615.0	4.5	9.0	99	0.0006010	0.0000190	0.281330	0.000250	0.281323067	0.000250	-37.7	8.9
TIF2z82	607.0	4.0	8.0	91	0.0004810	0.0000480	0.282041	0.000063	0.282035524	0.000063	-12.7	2.3
TIF2z83	2323.0	12.0	24.0	99	0.0007500	0.0000660	0.281111	0.000084	0.281077793	0.000084	-8.0	3.1
TIF2z84	896.0	6.0	12.0	100	0.0003113	0.0000095	0.281410	0.000063	0.281404754	0.000063	-28.6	2.2
TIF2z86	654.0	4.5	9.0	103	0.0005270	0.0000430	0.282272	0.000053	0.282265533	0.000053	-3.5	1.9
TIF2z87	617.0	5.0	10.0	104	0.0003043	0.0000059	0.282047	0.000037	0.282043478	0.000037	-12.2	1.3
TIF2z88	2908.0	11.0	22.0	100	0.0009150	0.0000260	0.281094	0.000048	0.281043005	0.000048	4.3	1.8
TIF2z89	1209.0	7.0	14.0	98	0.0005760	0.0000120	0.282043	0.000083	0.282029865	0.000083	0.5	3.0
TIF2z90	1794.0	12.5	25.0	95	0.0007700	0.0000460	0.281390	0.000740	0.281363801	0.000740	-9.9	26.3
TIF2z94	988.0	6.5	13.0	101	0.0007900	0.0001300	0.282071	0.000043	0.282056308	0.000043	-3.5	1.6
TIF2z95	587.0	4.0	8.0	100	0.0007200	0.0001400	0.282198	0.000053	0.282190074	0.000053	-7.7	1.9
TIF2z96	1058.0	7.0	14.0	97	0.0008860	0.0000650	0.281729	0.000067	0.281711344	0.000067	-14.1	2.4
TIF2z97	465.0	3.5	7.0	100	0.0019240	0.0000390	0.282370	0.000077	0.282353242	0.000077	-4.6	2.7
TIF2z98	665.0	4.5	9.0	100	0.0000336	0.0000062	0.282557	0.000086	0.282556581	0.000086	7.0	3.0
TIF2z99	642.0	4.0	8.0	98	0.0002720	0.0000170	0.282166	0.000047	0.282162724	0.000047	-7.4	1.7
TIF2z100	602.0	3.5	7.0	99	0.0008940	0.0000710	0.282155	0.000049	0.282144906	0.000049	-8.9	1.8
TIF2z101	1433.0	9.0	18.0	98	0.0014300	0.0001000	0.281964	0.000031	0.281925267	0.000031	1.9	1.2
TIF2z102	679.0	4.5	9.0	101	0.000							

Chapter IV

Table E.10: Sample OJJ16

IGSN: IEACC00018

Coordinate UTM: Zone 30S, 3796135 m N, 587342 m E

GRAIN	Age (Ma)	σ	2σ	Concordia	$^{176}\text{Lu}/^{177}\text{Hf}$	2σ	$^{176}\text{Hf}/^{177}\text{Hf}$	2σ	$(^{176}\text{Hf}/^{177}\text{Hf})_{\text{init}}$	2σ	ϵ_{Hf}	2σ
OJJ16z1	2185.8	15.3	30.5	98	0.0017200	0.0001100	0.281517	0.000064	0.281445428	0.000064	2.0	2.1
OJJ16z2	2199.7	18.9	37.8	99	0.0005705	0.0000060	0.281422	0.000068	0.281398106	0.000068	0.6	2.4
OJJ16z4	335.1	2.1	4.2	98	0.0013490	0.0000350	0.282437	0.000054	0.282428545	0.000054	-4.8	1.9
OJJ16z5	622.4	3.2	6.4	98	0.0014170	0.0000740	0.282026	0.000057	0.282009467	0.000057	-13.3	2.0
OJJ16z6	2059.8	14.6	29.1	99	0.0011420	0.0000470	0.281665	0.000050	0.281620272	0.000050	5.3	1.7
OJJ16z7	2059.6	15.3	30.5	100	0.0010240	0.0000460	0.281669	0.000056	0.281628893	0.000056	5.6	1.9
OJJ16z8	670.1	3.5	7.0	98	0.0008780	0.0000510	0.282267	0.000056	0.282255960	0.000056	-3.5	2.0
OJJ16z9	316.3	1.8	3.6	99	0.0024470	0.0000910	0.282576	0.000061	0.282561536	0.000061	-0.5	2.1
OJJ16z10	331.3	1.7	3.4	97	0.0018510	0.0000600	0.282484	0.000054	0.282472538	0.000054	-3.3	1.9
OJJ16z11	787.9	10.3	20.5	91	0.0011030	0.0000320	0.282116	0.000056	0.282099670	0.000056	-6.4	2.0
OJJ16z12	309.8	1.8	3.7	99	0.0033500	0.0002200	0.282652	0.000080	0.282632576	0.000080	1.9	2.8
OJJ16z13	624.7	3.2	6.4	101	0.0013580	0.0000096	0.282122	0.000053	0.282106078	0.000053	-9.8	1.9
OJJ16z14	563.8	3.5	7.1	98	0.0007900	0.0000200	0.282318	0.000056	0.282309646	0.000056	-3.9	2.0
OJJ16z15	549.0	2.9	5.7	94	0.0024810	0.0000240	0.282311	0.000059	0.282285467	0.000059	-5.1	2.1
OJJ16z16	592.3	2.9	5.9	98	0.0011200	0.0000250	0.282095	0.000056	0.282082566	0.000056	-11.4	2.0
OJJ16z17	643.5	3.2	6.4	99	0.0002756	0.0000045	0.282210	0.000055	0.282206675	0.000055	-5.8	1.9
OJJ16z19	334.0	1.9	3.7	96	0.0019910	0.0000430	0.282741	0.000057	0.282728559	0.000057	5.8	2.0
OJJ16z20	828.8	4.0	7.9	97	0.0016730	0.0000280	0.281871	0.000055	0.281844933	0.000055	-14.5	1.9
OJJ16z22	303.8	2.0	3.9	95	0.0046600	0.0000530	0.282604	0.000063	0.282577505	0.000063	-0.2	2.2
OJJ16z24	296.8	2.6	5.3	97	0.0031210	0.0000940	0.282624	0.000059	0.282606665	0.000059	0.7	2.1
OJJ16z25	591.8	3.2	6.5	100	0.0008570	0.0000340	0.281864	0.000059	0.281854486	0.000059	-19.4	2.1
OJJ16z26	2081.7	17.8	35.5	100	0.0008740	0.0000180	0.281639	0.000059	0.281604396	0.000059	5.2	2.1
OJJ16z27	1731.7	30.3	60.6	100	0.0008280	0.0000310	0.281551	0.000058	0.281523817	0.000058	-5.6	2.0
OJJ16z28	314.2	1.9	3.7	100	0.0048970	0.0000620	0.282469	0.000059	0.282440239	0.000059	-4.8	2.1
OJJ16z29	1810.9	19.7	39.4	98	0.0020480	0.0000240	0.281748	0.000068	0.281677647	0.000068	1.6	2.4
OJJ16z31	594.7	3.5	7.1	100	0.0013700	0.0000200	0.281865	0.000064	0.281849713	0.000064	-19.5	2.3
OJJ16z32	499.7	3.6	7.2	95	0.0014630	0.0000600	0.282337	0.000055	0.282323294	0.000055	-4.9	1.9
OJJ16z33	2361.8	14.7	29.3	99	0.0004145	0.0000025	0.281330	0.000053	0.281311333	0.000053	1.2	1.9
OJJ16z34	324.1	1.6	3.2	99	0.0055700	0.0001500	0.282534	0.000056	0.282500241	0.000056	-2.5	1.9
OJJ16z35	597.7	3.5	7.1	97	0.0011480	0.0000150	0.282044	0.000055	0.282031125	0.000055	-13.1	1.9
OJJ16z36	2596.5	13.4	26.8	95	0.0013960	0.0000110	0.281097	0.000054	0.281027749	0.000054	-3.5	1.9
OJJ16z37	620.9	4.4	8.8	103	0.0011994	0.0000071	0.281919	0.000055	0.281905028	0.000055	-17.0	1.9
OJJ16z38	478.0	2.3	4.6	99	0.0013210	0.0000130	0.282795	0.000061	0.282783171	0.000061	10.9	2.2
OJJ16z39	2114.1	16.0	32.1	101	0.0008310	0.0000210	0.281556	0.000057	0.281522582	0.000057	3.0	2.0
OJJ16z40	663.8	3.2	6.4	100	0.0007550	0.0000370	0.282278	0.000061	0.282268592	0.000061	-3.2	2.1
OJJ16z41	2048.5	24.5	48.9	100	0.0005875	0.0000051	0.281667	0.000057	0.281644126	0.000057	5.9	2.0
OJJ16z42	614.2	2.9	5.9	98	0.0030600	0.0000470	0.282276	0.000056	0.282240758	0.000056	-5.3	2.0
OJJ16z44	572.7	2.8	5.6	100	0.0022200	0.0001400	0.282395	0.000054	0.282371149	0.000054	-1.6	1.9
OJJ16z45	338.7	1.7	3.4	97	0.0015360	0.0000220	0.282619	0.000057	0.282609258	0.000057	1.7	2.0
OJJ16z46	606.0	3.2	6.5	99	0.0006651	0.0000032	0.282249	0.000056	0.282241440	0.000056	-5.4	2.0
OJJ16z47	321.6	1.9	3.9	99	0.0016140	0.0000250	0.282627	0.000054	0.282617278	0.000054	1.6	1.9
OJJ16z48	339.3	2.3	4.5	98	0.0008490	0.0000120	0.282565	0.000058	0.282559615	0.000058	-0.1	2.0
OJJ16z49	634.3	3.8	7.6	102	0.0009930	0.0000100	0.282102	0.000059	0.282090189	0.000059	-10.2	2.1
OJJ16z50	626.3	3.5	7.0	98	0.0017500	0.0001800	0.282209	0.000064	0.282188449	0.000064	-6.9	2.2
OJJ16z51	338.8	1.9	3.7	101	0.0005725	0.0000096	0.282559	0.000053	0.282555369	0.000053	-0.2	1.9
OJJ16z52	601.7	3.5	7.0	101	0.0008550	0.0000170	0.282047	0.000057	0.282037347	0.000057	-12.7	2.0
OJJ16z54	559.6	3.3	6.5	98	0.0032700	0.0001400	0.282362	0.000062	0.282327669	0.000062	-3.4	2.1
OJJ16z55	2464.1	14.2	28.4	98	0.0011550	0.0000130	0.281329	0.000055	0.281274685	0.000055	2.3	1.9
OJJ16z56	609.1	3.8	7.6	96	0.0008586	0.0000085	0.281629	0.000060	0.281619193	0.000060	-27.4	2.1
OJJ16z57	634.2	3.2	6.4	99	0.0009350	0.0000170	0.282462	0.000058	0.282450879	0.000058	2.6	2.0
OJJ16z59	338.2	1.9	3.9	95	0.0015760	0.0000520	0.282588	0.000059	0.282578034	0.000059	0.6	2.1
OJJ16z60	605.5	2.9	5.9	101	0.0020400	0.0002100	0.282282	0.000075	0.282258852	0.000075	-4.8	2.6
OJJ16z61	729.4	8.1	16.1	92	0.0014730	0.0000510	0.282497	0.000055	0.282476837	0.000055	5.6	1.9
OJJ16z65	522.6	3.3	6.5	92	0.0009820	0.0000560	0.282112	0.000056	0.282102375	0.000056	-12.2	2.0
OJJ16z66	625.9	3.2	6.4	98	0.0012080	0.0000160	0.282650	0.000072	0.282635814	0.000072	9.0	2.5
OJJ16z68	329.4	1.8	3.6	97	0.0019870	0.0000180	0.282648	0.000059	0.282635771	0.000059	2.4	2.1
OJJ16z69	1767.6	17.7	35.5	99	0.0010270	0.0000260	0.281809	0.000058	0.281774572	0.000058	4.1	2.0
OJJ16z70	972.3	4.7	9.4	98	0.0025600	0.0001300	0.282033	0.000051	0.281986170	0.000051	-6.3	1.7
OJJ16z71	552.6	4.1	8.3	96	0.0036800	0.0001700	0.282266	0.000056	0.282227850	0.000056	-7.1	1.9
OJJ16z72	2066.6	15.2	30.4	96	0.0010340	0.0000890	0.281282	0.000058	0.281241361	0.000058	-8.0	1.9
OJJ16z73	2083.0	16.4	32.8	100	0.0012370	0.0000670	0.281433	0.000054	0.281383999	0.000054	-2.6	1.8
OJJ16z74	1985.7	16.0	32.1	97	0.0008260	0.0000130	0.281620	0.000057	0.281588832	0.000057	2.5	2.0
OJJ16z75	557.4	2.7	5.5	96	0.0019228	0.0000085	0.282273	0.000062	0.282252922	0.000062	-6.1	2.2
OJJ16z76	542.7	3.6	7.1	90	0.0016970	0.0000370	0.281937	0.000051	0.281919727	0.000051	-18.2	1.8
OJJ16z77	310.8	4.0	8.0	94	0.0022000	0.0001000	0.282499	0.000063	0.282486203	0.000063	-3.3	2.2
OJJ16z78	1408.5	8.8	17.6	97	0.0028360	0.0000330	0.281949	0.000054	0.281873543	0.000054	-0.5	1.9
OJJ16z79c	619.1	4.4	8.8	96	0.0011110	0.0000310	0.281795	0.000063	0.281782100	0.000063	-21.4	2.2
OJJ16z79r	628.5	5.0	9.9	99	0.0007360	0.0000120	0.281753	0.000054	0.281744329	0.000054	-22.5	1.9
OJJ16z80	1039.1	5.2	10.4	99	0.0011310	0.0000150	0.281925	0.000057	0.281902871	0.000057	-7.8	2.0
OJJ16z81	998.9	5.2	10.5	98	0.0015390	0.0000500	0.281622	0.000056	0.281593058	0.000056	-19.7	2.0
OJJ16z83	562.7	3.0	5.9	94	0.0026100	0.0001100	0.282239	0.000066	0.282211451	0.000066	-7.4	2.3
OJJ16z84	582.2	2.9	5.8	99	0.0021900	0.0001800	0.282095	0.000056	0.282071100	0.000056	-12.0	1.9
OJJ16z85	977.0	4.4	8.9	100	0.0016970	0.0000430	0.282111	0.000065	0.282079795	0.000065	-2.9	2.3
OJJ16z86	611.7	3.2	6.4	99	0.0019050	0.0000770	0.282189	0.000054	0.282167132	0.000054	-7.9	1.9
OJJ16z87	2067.9	27.6	55.2	100	0.0008234	0.0000047	0.281251	0.000056	0.281218623	0.000056	-8.8	2.0
OJJ16z88	487.0	2.6	5.1	100	0.0044200	0.0001000	0.282298	0.000059	0.282257672	0.000059	-7.5	2.1
OJJ16z89	584.4	3.5	7.1	92	0.0022090	0.0000230	0.282371	0.000055	0.282346809	0.000055	-2.2	1.9
OJJ16z90	621.5	2.9	5.9	101	0.0017340	0.0000720	0.282543	0.000065	0.282522801	0.000065	4.9	2.3
OJJ16z91	629.2	3.2	6.4	101	0.0023960	0.0000530	0.282086	0.000061	0.282057727	0.000061	-11.4	2.1
OJJ16z92	604.3	3.5	7.0	97	0.0009990	0.0000340	0.282127	0.000060	0.282115683	0.000060	-9.9	

GRAIN	Age (Ma)	σ	2σ	Concordia	$^{176}\text{Lu}/^{177}\text{Hf}$	2σ	$^{176}\text{Hf}/^{177}\text{Hf}$	2σ	$(^{176}\text{Hf}/^{177}\text{Hf})_{\text{init}}$	2σ	ϵHf	2σ
OJJ16z101	998.9	8.3	16.6	95	0.0028830	0.0000470	0.282090	0.000064	0.282035782	0.000064	-4.0	2.2
OJJ16z102	336.7	2.0	3.9	100	0.0011651	0.0000056	0.282471	0.000053	0.282463654	0.000053	-3.5	1.9
OJJ16z103	796.2	3.7	7.4	99	0.0032260	0.0000420	0.282014	0.000051	0.281965751	0.000051	-11.0	1.8
OJJ16z104	652.6	3.5	7.0	98	0.0015750	0.0000460	0.282281	0.000057	0.282261702	0.000057	-3.7	2.0
OJJ16z105	2110.1	16.1	32.2	100	0.0000402	0.0000019	0.281481	0.000052	0.281479387	0.000052	1.4	1.8
OJJ16z106	2100.7	18.2	36.4	99	0.0014530	0.0000270	0.281669	0.000064	0.281610936	0.000064	5.9	2.2
OJJ16z107	333.0	1.7	3.4	99	0.0018170	0.0000330	0.282653	0.000054	0.282641680	0.000054	2.7	1.9
OJJ16z108	324.7	2.0	3.9	100	0.0022150	0.0000360	0.282636	0.000057	0.282622534	0.000057	1.9	2.0
OJJ16z109	320.5	1.6	3.1	99	0.0041860	0.0000580	0.282636	0.000057	0.282610943	0.000057	1.3	2.0
OJJ16z110	879.6	4.8	9.6	99	0.0005499	0.0000089	0.282395	0.000054	0.282385901	0.000054	5.8	1.9
OJJ16z111	619.1	4.1	8.2	94	0.0004332	0.0000034	0.282254	0.000059	0.282248970	0.000059	-4.9	2.1
OJJ16z112	621.0	3.5	7.0	103	0.0005955	0.0000054	0.282633	0.000054	0.282626063	0.000054	8.5	1.9
OJJ16z113	2106.0	19.5	39.0	101	0.0005547	0.0000094	0.281599	0.000056	0.281576780	0.000056	4.8	2.0
OJJ16z114	620.4	2.9	5.9	99	0.0010920	0.0000340	0.282243	0.000054	0.282230300	0.000054	-5.5	1.9
OJJ16z116	640.3	3.5	7.0	100	0.0012825	0.0000057	0.282207	0.000057	0.282191600	0.000057	-6.4	2.0
OJJ16z117	1998.7	22.4	44.8	99	0.0011320	0.0000350	0.281295	0.000055	0.281252001	0.000055	-9.2	1.9
OJJ16z118	342.5	2.0	4.0	99	0.0011050	0.0000053	0.282518	0.000060	0.282510929	0.000060	-1.7	2.1
OJJ16z119	630.8	5.3	10.5	96	0.0007064	0.0000080	0.282237	0.000057	0.282228638	0.000057	-5.3	2.0
OJJ16z120c	2078.9	19.8	39.7	99	0.0004787	0.0000019	0.281226	0.000065	0.281207075	0.000065	-9.0	2.3
OJJ16z120r	2067.0	14.5	29.0	98	0.0005660	0.0000320	0.281067	0.000060	0.281044755	0.000060	-15.0	2.1
OJJ16z122	531.4	2.7	5.4	90	0.0006492	0.0000090	0.282179	0.000054	0.282172539	0.000054	-9.5	1.9
OJJ16z123	2130.0	15.2	30.4	100	0.0010084	0.0000041	0.281567	0.000055	0.281526136	0.000055	3.5	1.9
OJJ16z125	2069.3	15.8	31.7	100	0.0006810	0.0000520	0.281479	0.000063	0.281452209	0.000063	-0.5	2.2
OJJ16z126	612.1	3.2	6.4	96	0.0007880	0.0000180	0.282484	0.000058	0.282474954	0.000058	3.0	2.0
OJJ16z127	2020.3	15.7	31.3	99	0.0003060	0.0000019	0.281280	0.000054	0.281268252	0.000054	-8.1	1.9
OJJ16z128	590.5	3.5	7.1	98	0.0029270	0.0000760	0.282291	0.000058	0.282258560	0.000058	-5.2	2.0
OJJ16z129	871.7	5.3	10.7	99	0.0006765	0.0000081	0.282532	0.000060	0.282520908	0.000060	10.4	2.1
OJJ16z132	2107.4	15.4	30.9	99	0.0003583	0.0000050	0.281308	0.000054	0.281293640	0.000054	-5.3	1.9
OJJ16z133	570.7	2.8	5.6	98	0.0011560	0.0000280	0.282219	0.000061	0.282206624	0.000061	-7.4	2.1
OJJ16z134	329.2	2.0	3.9	91	0.0013680	0.0000380	0.282531	0.000061	0.282522580	0.000061	-1.6	2.2
OJJ16z136	624.6	2.8	5.7	98	0.0010240	0.0000150	0.282083	0.000067	0.282070994	0.000067	-11.0	2.4
OJJ16z137	2028.8	15.6	31.2	99	0.0008248	0.0000039	0.281606	0.000053	0.281574191	0.000053	2.9	1.9
OJJ16z138	647.1	4.1	8.2	96	0.0007140	0.0000089	0.282289	0.000062	0.282280332	0.000062	-3.1	2.2
OJJ16z139	622.1	3.2	6.4	99	0.0004278	0.0000075	0.282164	0.000057	0.282159008	0.000057	-8.0	2.0
OJJ16z140	587.2	3.2	6.5	100	0.0002004	0.0000023	0.282390	0.000063	0.282387794	0.000063	-0.7	2.2
OJJ16z141	1194.1	5.6	11.2	100	0.0007390	0.0000210	0.282134	0.000065	0.282117359	0.000065	3.3	2.3
OJJ16z142	307.7	1.8	3.6	100	0.0022450	0.0000520	0.282619	0.000061	0.282606067	0.000061	0.9	2.1
OJJ16z143	654.6	3.5	7.0	100	0.0005389	0.0000045	0.282250	0.000060	0.282243377	0.000060	-4.3	2.1
OJJ16z144	350.8	2.1	4.3	97	0.0006200	0.0000170	0.282478	0.000055	0.282473928	0.000055	-2.8	1.9
OJJ16z145	2406.2	14.2	28.4	98	0.0010280	0.0000130	0.281092	0.000059	0.281044821	0.000059	-7.2	2.1
OJJ16z146	2040.1	15.5	30.9	101	0.0006500	0.0000110	0.281430	0.000055	0.281404794	0.000055	-2.8	1.9

Chapter IV

Table E.11: Sample OJJ18

IGSN: IEACC00019

Coordinate UTM: Zone 30S, 3796505 m N, 587288 m E

GRAIN	Age (Ma)	σ	2σ	Concordia	$^{176}\text{Lu}/^{177}\text{Hf}$	2σ	$^{176}\text{Hf}/^{177}\text{Hf}$	2σ	$(^{176}\text{Hf}/^{177}\text{Hf})_{\text{init}}$	2σ	ϵHf	2σ
OJJ18z1	1835.4	32.3	64.6	101	0.0005362	0.0000096	0.281575	0.000039	0.281556332	0.000039	-2.1	1.4
OJJ18z2	2100.7	24.3	48.6	102	0.0006349	0.0000057	0.281529	0.000033	0.281503628	0.000033	2.1	1.2
OJJ18z3	2799.0	21.6	43.3	99	0.0009420	0.0000340	0.280892	0.000044	0.280841520	0.000044	-5.4	1.6
OJJ18z4	1156.0	7.3	14.5	101	0.0005020	0.0000220	0.281784	0.000044	0.281773060	0.000044	-9.8	1.6
OJJ18z6	637.9	3.2	6.4	103	0.0013930	0.0000390	0.282309	0.000042	0.282292326	0.000042	-2.9	1.5
OJJ18z7	2148.4	24.2	48.3	100	0.0013790	0.0000460	0.281610	0.000034	0.281553636	0.000034	4.9	1.3
OJJ18z8	336.7	1.8	3.5	101	0.0007130	0.0000310	0.282515	0.000037	0.282510505	0.000037	-1.8	1.3
OJJ18z9	1856.2	29.5	58.9	101	0.0006172	0.0000078	0.281574	0.000033	0.281552262	0.000033	-1.8	1.2
OJJ18z10	2119.4	24.0	47.9	99	0.0005650	0.0000100	0.281606	0.000037	0.281583224	0.000037	5.3	1.3
OJJ18z11	574.4	4.1	8.3	99	0.0006170	0.0000190	0.282451	0.000038	0.282444359	0.000038	1.1	1.4
OJJ18z12	597.2	2.9	5.8	98	0.0004590	0.0000230	0.281921	0.000050	0.281915861	0.000050	-17.2	1.8
OJJ18z13	613.2	4.1	8.2	105	0.0005566	0.0000088	0.282344	0.000037	0.282337600	0.000037	-1.9	1.3
OJJ18z15	632.4	3.5	7.0	95	0.0001936	0.0000037	0.281795	0.000037	0.281792705	0.000037	-20.7	1.3
OJJ18z16	1979.8	24.2	48.3	95	0.0002000	0.0000340	0.281441	0.000041	0.281433477	0.000041	-3.2	1.5
OJJ18z18	2176.9	23.7	47.4	101	0.0011690	0.0000480	0.281395	0.000051	0.281346561	0.000051	-1.8	1.9
OJJ18z19	673.6	3.5	7.0	101	0.0005970	0.0000210	0.282376	0.000032	0.282368448	0.000032	0.6	1.1
OJJ18z20	2089.8	24.5	48.9	102	0.0002580	0.0000510	0.281622	0.000037	0.281611745	0.000037	5.7	1.4
OJJ18z21	342.7	2.1	4.3	100	0.0007230	0.0000130	0.282472	0.000041	0.282467360	0.000041	-3.2	1.5
OJJ18z22	1900.1	26.3	52.5	101	0.0010440	0.0000350	0.281594	0.000038	0.281556343	0.000038	-0.6	1.4
OJJ18z23	330.9	2.5	5.0	84	0.0012060	0.0000120	0.282821	0.000040	0.282813532	0.000040	8.7	1.4
OJJ18z24	384.1	2.5	5.0	95	0.0006880	0.0000230	0.282734	0.000037	0.282729055	0.000037	6.9	1.3
OJJ18z25	726.0	3.7	7.5	102	0.0012070	0.0000170	0.282255	0.000044	0.282238546	0.000044	-2.9	1.6
OJJ18z26	651.0	3.2	6.4	101	0.0007040	0.0000300	0.282324	0.000037	0.282315401	0.000037	-1.8	1.3
OJJ18z27	566.2	3.8	7.7	103	0.0011430	0.0000260	0.282451	0.000039	0.282438871	0.000039	0.7	1.4
OJJ18z28	978.4	4.7	9.4	102	0.0015700	0.0001100	0.282246	0.000047	0.282217101	0.000047	2.0	1.7
OJJ18z30	644.1	3.2	6.4	101	0.0004460	0.0000410	0.282180	0.000140	0.282174611	0.000140	-6.9	5.0
OJJ18z31	792.7	3.7	7.4	99	0.0011600	0.0001100	0.282052	0.000038	0.282034717	0.000038	-8.6	1.4
OJJ18z32	684.7	3.2	6.4	101	0.0000201	0.0000033	0.282506	0.000039	0.282505742	0.000039	5.7	1.4
OJJ18z33	344.8	1.9	3.7	96	0.0014860	0.0000510	0.282431	0.000040	0.282421408	0.000040	-4.8	1.4
OJJ18z34	2271.1	23.4	46.8	102	0.0009870	0.0000430	0.281251	0.000039	0.281208299	0.000039	-4.5	1.5
OJJ18z35	332.4	2.2	4.3	96	0.0039700	0.0002400	0.282811	0.000039	0.282786342	0.000039	7.8	1.4
OJJ18z36	1895.5	25.6	51.2	101	0.0012280	0.0000580	0.281645	0.000043	0.281600824	0.000043	0.8	1.6
OJJ18z37	2128.7	25.8	51.6	90	0.0014260	0.0000140	0.281505	0.000041	0.281447240	0.000041	0.7	1.5
OJJ18z38	859.9	4.2	8.5	97	0.0022770	0.0000290	0.282539	0.000032	0.282502185	0.000032	9.5	1.2
OJJ18z39	587.3	3.2	6.5	100	0.0020140	0.0000600	0.282561	0.000037	0.282538831	0.000037	4.7	1.3
OJJ18z40	1388.3	6.8	13.5	93	0.0004470	0.0000150	0.281871	0.000044	0.281859278	0.000044	-1.5	1.6
OJJ18z41	596.8	3.8	7.6	95	0.0038900	0.0001400	0.282267	0.000046	0.282223447	0.000046	-6.3	1.7
OJJ18z42	2058.2	24.3	48.6	100	0.0012140	0.0000330	0.281652	0.000043	0.281604499	0.000043	4.7	1.6
OJJ18z43	618.3	3.5	7.0	99	0.0029400	0.0001500	0.282289	0.000041	0.282254918	0.000041	-4.7	1.5
OJJ18z44	538.4	5.6	11.3	100	0.0038900	0.0004200	0.282631	0.000042	0.282591772	0.000042	5.5	1.6
OJJ18z45	2174.3	24.4	48.7	96	0.0017170	0.0000160	0.281526	0.000041	0.281454954	0.000041	2.0	1.5
OJJ18z46	990.0	4.7	9.4	96	0.0021700	0.0002900	0.282102	0.000051	0.282061562	0.000051	-3.3	2.0
OJJ18z47	1061.5	5.2	10.4	100	0.0018400	0.0001100	0.282166	0.000045	0.282129193	0.000045	0.8	1.7
OJJ18z48	2662.1	22.0	43.9	97	0.0006500	0.0000490	0.281304	0.000043	0.281270915	0.000043	6.7	1.6
OJJ18z49	665.8	7.0	14.0	101	0.0013800	0.0001100	0.281790	0.000041	0.281772752	0.000041	-20.7	1.5
OJJ18z50	1019.8	4.7	9.4	101	0.0004600	0.0000330	0.281919	0.000058	0.281910166	0.000058	-7.9	2.1

Chapter IV

Table E.12: Sample OJJ19

IGSN: IEACC00020

Coordinate UTM: Zone 30S, 3796474 m N, 587262 m E

GRAIN	Age (Ma)	σ	2σ	Concordia	$^{176}\text{Lu}/^{177}\text{Hf}$	2σ	$^{176}\text{Lu}/^{177}\text{Hf}$	2σ	$(^{176}\text{Lu}/^{177}\text{Hf})_{\text{int}}$	2σ	ϵHf	2σ
OJJ19z1	742.9	3.4	6.9	92	0.0000381	0.0000048	0.281899	0.000020	0.281898468	0.000020	-14.5	0.7
OJJ19z3	341.8	1.7	3.5	91	0.0008270	0.0000310	0.282577	0.000030	0.282571708	0.000030	0.4	1.1
OJJ19z4	2049.9	27.2	54.5	100	0.0002820	0.0000180	0.281065	0.000049	0.281054010	0.000049	-15.1	1.7
OJJ19z5	319.1	2.1	4.2	97	0.0011530	0.0000130	0.282850	0.000022	0.282843120	0.000022	9.5	0.8
OJJ19z6	850.9	5.1	10.2	100	0.0009528	0.0000041	0.282549	0.000029	0.282533757	0.000029	10.4	1.0
OJJ19z7	612.3	3.5	7.0	101	0.0003710	0.0000180	0.282139	0.000019	0.282134741	0.000019	-9.1	0.7
OJJ19z8	2065.2	29.7	59.4	98	0.0002373	0.0000035	0.281454	0.000029	0.281444683	0.000029	-0.8	1.0
OJJ19z9	612.7	3.8	7.6	96	0.0004761	0.0000038	0.282533	0.000022	0.282527526	0.000022	4.9	0.8
OJJ19z10	3043.0	21.7	43.4	98	0.0005880	0.0000430	0.280864	0.000022	0.280829665	0.000022	-0.1	0.7
OJJ19z11	2525.8	23.2	46.3	99	0.0006700	0.0001100	0.281196	0.000035	0.281163681	0.000035	-0.2	1.1
OJJ19z12	1251.7	5.6	11.1	99	0.0005595	0.0000027	0.281957	0.000027	0.281943782	0.000027	-1.6	1.0
OJJ19z13	339.9	1.7	3.4	97	0.0011020	0.0000340	0.282731	0.000026	0.282723990	0.000026	5.8	0.9
OJJ19z14	1076.8	4.9	9.8	101	0.0005301	0.0000037	0.282311	0.000022	0.282300245	0.000022	7.2	0.8
OJJ19z15	590.3	3.5	7.1	101	0.0008100	0.0000150	0.282185	0.000025	0.282176038	0.000025	-8.1	0.9
OJJ19z16	1022.6	5.2	10.5	100	0.0008800	0.0000180	0.281938	0.000021	0.281921049	0.000021	-7.5	0.7
OJJ19z17	2055.5	26.4	52.9	102	0.0001946	0.0000041	0.281565	0.000023	0.281557397	0.000023	2.9	0.8
OJJ19z18	336.8	2.3	4.6	101	0.0006276	0.0000095	0.282566	0.000022	0.282562043	0.000022	0.0	0.8
OJJ19z19	2093.9	26.4	52.8	101	0.0006597	0.0000085	0.281605	0.000023	0.281578727	0.000023	4.6	0.8
OJJ19z20	590.9	9.7	19.4	99	0.0004173	0.0000048	0.282037	0.000031	0.282032375	0.000031	-13.2	1.1
OJJ19z21	2465.1	23.6	47.2	101	0.0003230	0.0000120	0.281127	0.000025	0.281111804	0.000025	-3.5	0.9
OJJ19z22	2213.5	29.3	58.7	100	0.0007648	0.0000074	0.281543	0.000023	0.281510760	0.000023	4.9	0.8
OJJ19z23	2037.3	25.3	50.7	95	0.0008750	0.0000330	0.281383	0.000027	0.281349119	0.000027	-4.9	0.9
OJJ19z24	621.8	2.7	5.3	102	0.0017200	0.0000760	0.282452	0.000019	0.282431931	0.000019	1.7	0.6
OJJ19z25	735.6	3.7	7.5	102	0.0006590	0.0000170	0.282640	0.000021	0.282630892	0.000021	11.3	0.7
OJJ19z26	677.7	3.2	6.4	99	0.0016000	0.0000330	0.282294	0.000028	0.282273640	0.000028	-2.7	1.0
OJJ19z27	1962.2	25.9	51.9	101	0.0002615	0.0000057	0.281126	0.000021	0.281116254	0.000021	-14.9	0.7
OJJ19z29	566.8	3.8	7.7	100	0.0004850	0.0000120	0.282229	0.000031	0.282223844	0.000031	-6.9	1.1
OJJ19z30	627.5	3.2	6.4	101	0.0001342	0.0000096	0.281768	0.000021	0.281766419	0.000021	-21.8	0.7
OJJ19z31	2663.0	22.4	44.8	98	0.0009450	0.0000540	0.281162	0.000028	0.281113882	0.000028	1.2	0.9
OJJ19z32	634.9	3.8	7.6	99	0.0013120	0.0000260	0.282434	0.000028	0.282418370	0.000028	1.5	1.0
OJJ19z33	2000.2	24.6	49.1	95	0.0029900	0.0001000	0.281373	0.000026	0.281259367	0.000026	-8.9	0.8
OJJ19z34	637.8	4.1	8.2	99	0.0016780	0.0000410	0.282287	0.000022	0.282266915	0.000022	-3.8	0.8
OJJ19z35	603.3	4.1	8.2	97	0.0028700	0.0001200	0.282339	0.000030	0.282306542	0.000030	-3.2	1.0
OJJ19z37	628.5	3.8	7.6	100	0.0019100	0.0000420	0.282123	0.000024	0.282100498	0.000024	-9.9	0.7
OJJ19z38	2104.8	23.5	47.1	101	0.0032130	0.0000500	0.281672	0.000024	0.281543355	0.000024	3.6	0.8
OJJ19z39	2887.7	21.9	43.8	97	0.0026800	0.0001100	0.280905	0.000026	0.280756694	0.000026	-6.3	0.7
OJJ19z40	2085.8	26.6	53.1	102	0.0016870	0.0000480	0.281501	0.000022	0.281434076	0.000022	-0.7	0.7
OJJ19z42	630.4	3.5	7.0	100	0.0036500	0.0001000	0.282149	0.000026	0.282105861	0.000026	-9.7	0.9
OJJ19z43	580.6	3.2	6.5	100	0.0039110	0.0000210	0.282386	0.000023	0.282343391	0.000023	-2.4	0.8
OJJ19z44	903.8	4.5	9.0	100	0.0047620	0.0000450	0.282634	0.000026	0.282553034	0.000026	12.2	0.9
OJJ19z47	2116.8	24.7	49.4	100	0.0023000	0.0001100	0.281358	0.000029	0.281265375	0.000029	-6.0	0.9
OJJ19z48	565.9	3.5	7.1	98	0.0016960	0.0000410	0.282121	0.000031	0.282103002	0.000031	-11.2	1.1
OJJ19z49	2362.9	23.7	47.3	98	0.0013412	0.0000035	0.281370	0.000022	0.281309572	0.000022	1.2	0.8
OJJ19z50	2207.3	24.5	48.9	97	0.0024700	0.0001700	0.281347	0.000022	0.281243212	0.000022	-4.8	0.5
OJJ19z51	649.2	3.5	7.0	96	0.0026860	0.0000770	0.281551	0.000022	0.281518292	0.000022	-30.1	0.7
OJJ19z53	322.8	2.0	4.0	93	0.0069100	0.0001700	0.282703	0.000022	0.282661249	0.000022	3.2	0.7
OJJ19z54	653.5	2.9	5.8	100	0.0034530	0.0000200	0.282098	0.000023	0.282055691	0.000023	-11.0	0.8
OJJ19z55	2565.5	41.6	83.2	100	0.0004790	0.0000110	0.281042	0.000022	0.281018529	0.000022	-4.5	0.8
OJJ19z56	2058.2	25.0	50.0	95	0.0015000	0.0001100	0.281562	0.000038	0.281503308	0.000038	1.1	1.2
OJJ19z59	346.0	2.0	4.0	99	0.0034650	0.0000770	0.282564	0.000020	0.282541568	0.000020	-0.5	0.7
OJJ19z60	337.4	1.7	3.3	99	0.0032650	0.0000950	0.282511	0.000025	0.282490415	0.000025	-2.6	0.9
OJJ19z63	2016.0	25.0	50.0	101	0.0022500	0.0001600	0.281250	0.000023	0.281163793	0.000023	-11.9	0.9
OJJ19z64	615.5	3.2	6.4	102	0.0058130	0.0000590	0.282311	0.000033	0.282243943	0.000033	-5.1	1.1
OJJ19z65	1004.9	4.7	9.4	100	0.0045590	0.0000650	0.282242	0.000027	0.282155744	0.000027	0.4	0.9
OJJ19z66	509.4	2.7	5.5	97	0.0041280	0.0000560	0.282726	0.000024	0.282686627	0.000024	8.2	0.8
OJJ19z68	2218.5	23.6	47.3	100	0.0029850	0.0000340	0.281532	0.000019	0.281405876	0.000019	1.3	0.6
OJJ19z69	908.2	5.0	10.1	98	0.0054080	0.0000780	0.282027	0.000023	0.281934640	0.000023	-9.6	0.8
OJJ19z70	384.8	2.4	4.9	99	0.0040460	0.0000540	0.282414	0.000022	0.282384844	0.000022	-5.2	0.8
OJJ19z71	642.9	3.2	6.4	100	0.0022050	0.0000390	0.282198	0.000017	0.282171399	0.000017	-7.1	0.6
OJJ19z72	643.8	2.9	5.8	99	0.0015140	0.0000590	0.282362	0.000020	0.282343706	0.000020	-1.0	0.7
OJJ19z73	649.5	3.2	6.4	104	0.0023150	0.0000450	0.282023	0.000023	0.281994766	0.000023	-13.2	0.8
OJJ19z74	582.7	4.7	9.4	92	0.0020240	0.0000400	0.282210	0.000020	0.282187873	0.000020	-7.8	0.7
OJJ19z75	2304.8	22.9	45.7	92	0.0021450	0.0000280	0.281148	0.000025	0.281053780	0.000025	-9.2	0.8
OJJ19z76	1365.9	5.7	11.5	101	0.0021820	0.0000810	0.281986	0.000021	0.281929697	0.000021	0.5	0.7
OJJ19z77	335.3	1.7	3.4	102	0.0044240	0.0000430	0.282753	0.000022	0.282725273	0.000022	5.7	0.8
OJJ19z78	1359.6	7.3	14.6	96	0.0032930	0.0000250	0.281874	0.000027	0.281789408	0.000027	-4.6	0.9
OJJ19z79	621.6	2.9	5.9	100	0.0050400	0.0001700	0.281865	0.000026	0.281806194	0.000026	-20.5	0.9
OJJ19z80	652.9	3.5	7.0	102	0.0039860	0.0000930	0.282413	0.000029	0.282364160	0.000029	0.0	1.0
OJJ19z82	591.3	3.5	7.1	101	0.0021130	0.0000160	0.282284	0.000023	0.282260581	0.000023	-5.1	0.8
OJJ19z83	2180.7	24.9	49.8	99	0.0020200	0.0000740	0.281372	0.000023	0.281288141	0.000023	-3.8	0.7
OJJ19z84	572.7	3.8	7.7	101	0.0023870	0.0000490	0.282439	0.000020	0.282413355	0.000020	-0.1	0.7
OJJ19z85	2040.1	23.9	47.8	94	0.0006910	0.0000310	0.281035	0.000026	0.281008204	0.000026	-16.9	0.9
OJJ19z86	2175.6	25.0	50.0	101	0.0060900	0.0002200	0.281682	0.000025	0.281429770	0.000025	1.2	0.6
OJJ19z87	648.2	3.5	7.0	102	0.0045200	0.0001200	0.282344	0.000024	0.282289043	0.000024	-2.8	0.8
OJJ19z88	2037.3	24.6	49.3	100	0.0006750	0.0000260	0.281210	0.000033	0.281183863	0.000033	-10.8	1.1
OJJ19z89	657.2	3.2	6.4	100	0.0045300	0.0002100	0.282233	0.000021	0.282177152	0.000021	-6.6	0.7
OJJ19z91	1868.9	37.9	75.8	99	0.0007180	0.0000180	0.281243	0.000029	0.281217531	0.000029	-13.4	1.0
OJJ19z92	527.3	2.9	5.9	100	0.0032810	0.0000170	0.282740	0.000022	0.282707594	0.000022	9.3	0.8
OJJ19z93	632.5	3.8	7.6	100	0.0030160	0.0000670	0.282067	0.000019	0.282031241	0.000019	-12.3	0.6
OJJ19z94	336.8	1.8	3.6	99	0.0035510	0.0000600	0.282786	0.000029	0.282763612			

GRAIN	Age (Ma)	σ	2 σ	Concordia	$^{176}\text{Lu}/^{177}\text{Hf}$	2 σ	$^{176}\text{Hf}/^{177}\text{Hf}$	2 σ	$(^{176}\text{Hf}/^{177}\text{Hf})_{\text{int}}$	2 σ	ϵHf	2 σ
OJJ19z108	618.6	2.9	5.7	100	0.0010000	0.0000540	0.282171	0.000021	0.282159389	0.000021	-8.0	0.7
OJJ19z109	1810.9	32.0	64.0	101	0.0014930	0.0000280	0.281203	0.000029	0.281151712	0.000029	-17.0	1.0
OJJ19z110	577.4	4.1	8.3	102	0.0016980	0.0000065	0.282324	0.000023	0.282305629	0.000023	-3.8	0.8
OJJ19z111	1852.8	24.7	49.5	99	0.0026840	0.0000590	0.281790	0.000023	0.281695624	0.000023	3.2	0.7
OJJ19z112	613.6	2.8	5.7	97	0.0021060	0.0000720	0.281919	0.000023	0.281894745	0.000023	-17.5	0.8
OJJ19z113	2103.4	23.6	47.1	99	0.0025550	0.0000230	0.281478	0.000023	0.281375799	0.000023	-2.4	0.8
OJJ19z114	2433.3	22.5	45.1	96	0.0013110	0.0000290	0.281368	0.000022	0.281307143	0.000022	2.7	0.7
OJJ19z115	317.7	1.8	3.6	90	0.0047600	0.0001800	0.282786	0.000038	0.282757686	0.000038	6.5	1.3
OJJ19z116	1997.7	23.9	47.7	100	0.0021290	0.0000920	0.281187	0.000018	0.281106171	0.000018	-14.4	0.5
OJJ19z117	3028.2	21.6	43.2	94	0.0025700	0.0000800	0.280820	0.000025	0.280670690	0.000025	-6.1	0.7
OJJ19z118	578.4	2.9	5.9	101	0.0016690	0.0000330	0.282467	0.000025	0.282448911	0.000025	1.3	0.9
OJJ19z119	2485.0	23.3	46.6	100	0.0014200	0.0000200	0.281184	0.000035	0.281116641	0.000035	-2.9	1.2
OJJ19z120	557.2	3.5	7.1	97	0.0016460	0.0000200	0.282353	0.000024	0.282335812	0.000024	-3.2	0.8
OJJ19z121	2106.0	24.9	49.7	95	0.0019920	0.0000210	0.281606	0.000021	0.281526204	0.000021	3.0	0.7
OJJ19z122	624.7	2.9	5.9	98	0.0019740	0.0000350	0.282260	0.000022	0.282236856	0.000022	-5.2	0.8
OJJ19z127	2876.7	22.4	44.9	97	0.0013800	0.0001100	0.280905	0.000021	0.280828932	0.000021	-4.0	0.5
OJJ19z128	347.5	2.0	3.9	98	0.0021650	0.0000520	0.282612	0.000029	0.282597944	0.000029	1.5	1.0
OJJ19z129	2023.1	27.0	54.0	101	0.0017770	0.0000430	0.281689	0.000024	0.281620675	0.000024	4.4	0.8
OJJ19z130	327.8	1.9	3.9	100	0.0031900	0.0001100	0.282800	0.000032	0.282780426	0.000032	7.5	1.1